Rapporter och meddelanden 141

Geology of the Northern Norrbotten ore province, northern Sweden

Editor: Stefan Bergman

SGU
Sveriges geologiska undersökning
Geological Survey of Sweden

Rapporter och meddelanden 141

Geology of the Northern Norrbotten ore province, northern Sweden

Editor: Stefan Bergman

Sveriges geologiska undersökning
2018

ISSN 0349-2176
ISBN 978-91-7403-393-9

Changes made on November 15, 2018

Pages 10–11

New text: Mafic pyroclastic deposits are overlain by volcaniclastic rocks interlayered with carbonate rock, graphite schist, skarn-related iron oxide deposits, banded iron formation and chert (Martinsson 1993, Martinsson et al. 2018b, Lynch et al. 2018b). Most of these rocks were deposited before 2.14 Ga, and only minor assimilation of older continental crust occurred during magma ascent or storage (Lynch et al. 2018b).

Original text: Mafic pyroclastic deposits are overlain by volcaniclastic rocks interlayered with carbonate rock, graphite schist, skarn-related iron oxide deposits, banded iron formation and chert (Martinsson 1993, Martinsson et al. 2018b, Lynch et al. 2018b) show that most of these rocks were deposited before 2.14 Ga, and that only minor assimilation of older continental crust occurred during magma ascent or storage.

Cover photos:
Upper left: View of Torneälven, looking north from Sakkaravaara, northeast of Kiruna. ***Photographer:*** Stefan Bergman.
Upper right: View (looking north-northwest) of the open pit at the Aitik Cu-Au-Ag mine, close to Gällivare. The Nautanen area is seen in the background. ***Photographer:*** Edward Lynch.
Lower left: Iron oxide-apatite mineralisation occurring close to the Malmberget Fe-mine. ***Photographer:*** Edward Lynch.
Lower right: View towards the town of Kiruna and Mt. Luossavaara, standing on the footwall of the Kiruna apatite iron ore on Mt. Kiirunavaara, looking north. ***Photographer:*** Stefan Bergman.

Head of department, Mineral Resources: Kaj Lax
Editor: Stefan Bergman

Layout: Tone Gellerstedt och Johan Sporrong, SGU
Print: Elanders Sverige AB

Geological Survey of Sweden
Box 670, 751 28 Uppsala
phone: 018-17 90 00
fax: 018-17 92 10
e-mail: sgu@sgu.se
www.sgu.se

Table of Contents

Introduktion (in Swedish) **6**

Introduction **7**

1. Regional geology of northern Norrbotten County **9**
References 14

2. Geology, lithostratigraphy and petrogenesis of c. 2.14 Ga greenstones in the Nunasvaara and Masugnsbyn areas, northernmost Sweden **19**
Abstract 19
Introduction 20
Regional setting of Norrbotten greenstone belts 21
Geology of the Nunasvaara and Masugnsbyn greenstone successions 23
Petrogenesis of the greenstones: Preliminary U-Pb geochronology, lithogeochemistry and Sm-Nd isotopic results 52
Summary and conclusions 68
Acknowledgements 69
References 70

3. Stratigraphy and ages of Palaeoproterozoic metavolcanic and metasedimentary rocks at Käymäjärvi, northern Sweden **79**
Abstract 79
Introduction 80
General geology 80
Structure and stratigraphy of the Käymäjärvi area 81
Sample description 89
Analytical methods 90
Analytical results 91
Discussion 96
Conclusions 100
Acknowledgements 101
References 101

4. Petrological and structural character of c. 1.88 Ga meta-volcanosedimentary rocks hosting iron oxide-copper-gold and related mineralisation in the Nautanen–Aitik area, northern Sweden **107**
Abstract 107
Introduction 108
Regional setting 108
Geology of the Nautanen–Aitik area 110
Structural geology and deformation 132
Summary and Conclusions 144
Acknowledgements 144
References 145

5. Age and lithostratigraphy of Svecofennian volcanosedimentary rocks at Masugnsbyn, northernmost Sweden – host rocks to Zn-Pb-Cu- and Cu ±Au sulphide mineralisations **151**
Abstract 151
Introduction 152
Geological overview 153
Discussion and preliminary conclusions 194
Acknowledgements 197
References 198

6. Folding observed in Palaeoproterozoic supracrustal rocks in northern Sweden **205**
Abstract 205
Introduction 205
Geological setting 207
Structural geological models 209
Geophysical data 212
Discussion and Conclusions 251
References 255

7. The Pajala deformation belt in northeast Sweden:
Structural geological mapping and 3D modelling around Pajala **259**
Abstract 259
Geological setting 259
Structural analysis 263
2D regional geophysical modelling and geological interpretation 272
Local and semi-regional 3D models 274
Discussion 280
Conclusions 283
ReferenceS 284

8. The Vakko and Kovo greenstone belts north of Kiruna:
Integrating structural geological mapping and geophysical modelling **287**
Abstract 287
Introduction 287
Geological setting 289
Geophysical surveys 291
Results 296
Discussion 306
Conclusions 308
References 309

9. Geophysical 2D and 3D modelling in the areas around
Nunasvaara and Masugnsbyn, northern Sweden **311**
Abstract 311
Nunasvaara 312
2D modelling of profile 1 and 2 316
Masugnsbyn 321
Regional modelling 329
Conclusion 338
References 339

10. Imaging deeper crustal structures by 2D and 3D modelling of geophysical data.
Examples from northern Norrbotten **341**
Abstract 341
Introduction 341
Methodology 342
Geological setting 342
Results 345
Conclusion 358
Outlook 358
Acknowledgements 358
References 359

11. Early Svecokarelian migmatisation west of the Pajala deformation belt, northeastern Norrbotten province, northern Sweden 361
Abstract 361
Introduction 362
Geology of the Masugnsbyn area 362
Discussion 372
Conclusions 374
Acknowledgements 375
References 376

12. Age and character of late-Svecokarelian monzonitic intrusions in northeastern Norrbotten, northern Sweden 381
Abstract 381
Introduction 381
Geological setting 382
Analytical methods 387
Analytical results 388
Discussion 393
Conclusions 396
Acknowledgements 396
References 397

13. Till geochemistry in northern Norrbotten – regional trends and local signature in the key areas 401
Abstract 401
Introduction 401
Glacial geomorphology and quaternary stratigraphy of Norrbotten 403
Samples and methods 406
Results and discussion 407
Conclusions 426
Acknowledgements 427
References 427

Introduktion

Stefan Bergman & Ildikó Antal Lundin

Den här rapporten presenterar de samlade resultaten från ett delprojekt inom det omfattande tvärvetenskapliga Barentsprojektet i norra Sverige. Projektet initierades av Sveriges geologiska undersökning (SGU) som ett första led i den svenska mineralstrategin. SGU fick ytterligare medel av Näringsdepartementet för att under en fyraårsperiod (2012–2015) samla in nya geologiska, geofysiska och geokemiska data samt för att förbättra de geologiska kunskaperna om Sveriges nordligaste län. Det statligt ägda gruvbolaget LKAB bidrog också till finansieringen. Projektets strategiska mål var att, genom att tillhandahålla uppdaterad och utförlig geovetenskaplig information, stödja prospekterings- och gruvindustrin för att förbättra Sveriges konkurrenskraft inom mineralnäringen. Ny och allmänt tillgänglig geovetenskaplig information från den aktuella regionen kan hjälpa prospekterings- och gruvföretag att minska sina risker och prospekteringskostnader och främjar därigenom ekonomisk utveckling. Dessutom bidrar utökad geologisk kunskap till en effektiv, miljövänlig och långsiktigt hållbar resursanvändning. All data som har samlats in i projektet lagras i SGUs databaser och är tillgängliga via SGU.

Syftet med det här delprojektet var att få en djupare förståelse för den stratigrafiska uppbyggnaden och utvecklingen av de mineraliserade ytbergarterna i nordligaste Sverige. Resultaten, som är en kombination av ny geologisk kunskap och stora mängder nya data, kommer att gynna prospekterings- och gruvindustrin i regionen i många år framöver.

Norra Norrbottens malmprovins står för en stor del av Sveriges järn- och kopparmalmsproduktion. Här finns fyra aktiva metallgruvor (mars 2018) och mer än 500 dokumenterade mineraliseringar. Fyndigheterna är av många olika slag, där de viktigaste typerna är stratiforma kopparmineraliseringar, järnformationer, apatitjärnmalm av Kirunatyp och epigenetiska koppar-guldmineraliseringar. En vanlig egenskap hos de flesta malmer och mineraliseringar i Norr- och Västerbotten är att de har paleoproterozoiska vulkaniska och sedimentära bergarter som värdbergart. För undersökningarna valdes ett antal nyckelområden med bästa tillgängliga blottningsgrad. De utvalda områdena representerar tillsammans en nästan komplett stratigrafi i ytbergarter inom åldersintervallet 2,5–1,8 miljarder år.

Rapporten består av tretton kapitel och inleds med en översikt över de geologiska förhållandena, som beskriver huvuddragen i de senaste resultaten. Översikten följs av fyra kapitel (2–5) som huvudsakligen handlar om litostratigrafi och åldersbestämningar av ytbergarterna. Huvudämnet för de därpå följande fem kapitlen (6–10) är 3D-geometri och strukturell utveckling. Därefter kommer två kapitel (11–12) som fokuserar på U-Pb-datering av en metamorf respektive intrusiv händelse. Rapporten avslutas med en studie av geokemin hos morän i Norra Norrbottens malmprovins (kapitel 13).

Introduction

Stefan Bergman & Ildikó Antal Lundin

This volume reports the results from a subproject within the Barents Project, a major programme in northern Sweden. The multidisciplinary Barents Project was initiated by SGU as the first step in implementing the Swedish National Mineral Strategy. SGU obtained additional funding from the Ministry of Enterprise and Innovation to gather new geological, geophysical and till geochemistry data, and generally enhance geological knowledge of northern Sweden over a four-year period (2012–2015). The state-owned iron mining company LKAB also helped to fund the project. The strategic goal of the project was to support the exploration and mining industry, so as to improve Sweden's competitiveness in the mineral industry by providing modern geoscientific information. Geological knowledge facilitates sustainable, efficient and environmentally friendly use of resources. New publicly available geoscientific information from this region will help exploration and mining companies to reduce their risks and exploration costs, thus promoting economic development. All data collected within the project are stored in databases and are available at SGU.

This subproject within the Barents Project aims to provide a deeper understanding of the stratigraphy and depositional evolution of mineralised supracrustal sequences in northernmost Sweden. The combined results in the form of new geological knowledge and plentiful new data will benefit the exploration and mining industry in the region for many years to come.

The Northern Norrbotten ore province is a major supplier of iron and copper ore in Sweden. There are four active metal mines (March 2018) and more than 500 documented mineralisations. A wide range of deposits occur, the most important types being stratiform copper deposits, iron formations, Kiruna-type apatite iron ores and epigenetic copper-gold deposits. A common feature of most deposits is that they are hosted by Palaeoproterozoic metavolcanic or metasedimentary rocks. A number of key areas were selected across parts of the supracrustal sequences with the best available exposure. The areas selected combine to represent an almost complete stratigraphic sequence.

This volume starts with a brief overview of the geological setting, outlining some of the main recent achievements. This is followed by four papers (2–5) dealing mainly with lithostratigraphy and age constraints on the supracrustal sequences. 3D geometry and structural evolution are the main topics of the next set of five papers (6–10). The following two contributions (11–12) focus on U-Pb dating of a metamorphic event and an intrusive event, respectively. The volume concludes with a study of the geochemical signature of till in the Northern Norrbotten ore province (13).

Author, paper 1:
Stefan Bergman
Geological Survey of Sweden,
Department of Mineral Resources,
Uppsala, Sweden

1. Regional geology of northern Norrbotten County

Stefan Bergman

The Precambrian bedrock in northernmost Sweden, including the Northern Norrbotten ore province, is part of the 2.0–1.8 Ga old Svecokarelian orogen. The orogen comprises both pre-orogenic rocks formed in the Archaean and early Palaeoproterozoic, as well as rocks formed during the orogeny itself. All the rocks were deformed and metamorphosed to variable degrees at different stages during the orogenic evolution. To the west the Precambrian rocks are overlain by Ediacaran–Cambrian platformal sedimentary cover rocks and nappes of the Caledonian orogen (Fig. 1).

The geology of northern Norrbotten County was first described by Fredholm (1886) and Svenonius (1900). More detailed work by Lundbohm (1910), Sundius (1915), Geijer (1931), Ödman (1939, 1957) and Eriksson (1954) followed these brief outlines. Summaries were presented by Witschard (1984), Bergman et al. (2001, 2007), Martinsson (2004), Martinsson & Wanhainen (2013) and Martinsson et al. (2016). A short summary is given here, including preferred nomenclature (Table 1), with reference to some of the main results from the papers in this volume.

The oldest rocks were formed in the Archaean and belong to the Råstojaure complex. The main component is gneissic granitoid of mainly tonalitic to granodioritic composition, which shows intrusive relationships with paragneiss, amphibolite and, locally, banded orthogneiss interpreted as metaandesitic to dacitic tuff. Bodies consisting of non-migmatitic metamorphosed granite are common in the east. Age determinations suggest crystallisation of granitoids at 2.8–2.7 Ga, and a regional metamorphic event is constrained at 2.7 Ga (Skiöld 1979, Skiöld & Page 1998, cf. Martinsson et al. 1999).

Layered mafic-ultramafic intrusions with an age of 2.5–2.4 Ga occur locally within the Råstojaure complex; more common are mafic dykes and felsic–mafic intrusions related to later events. A metamorphosed volcano-sedimentary sequence, deposited before 2.0 Ga and unconformably overlying the Archaean basement is commonly referred to as the Karelian supracrustal rocks (see also Gaál and Gorbatschev 1987). The lowermost unit in the Kiruna area is the Kovo group, which is composed of a basal clastic sequence of metamorphosed conglomerate and quartzite, overlain by tholeiitic metabasalt and metamorphosed calc-alkaline volcaniclastic rocks of andesitic composition. The eastern part of the Råstojaure complex is overlain by the Tjärro quartzite, along with subordinate metamorphosed conglomerate and phyllite. Locally, metavolcanic rocks of andesitic to dacitic composition occur below

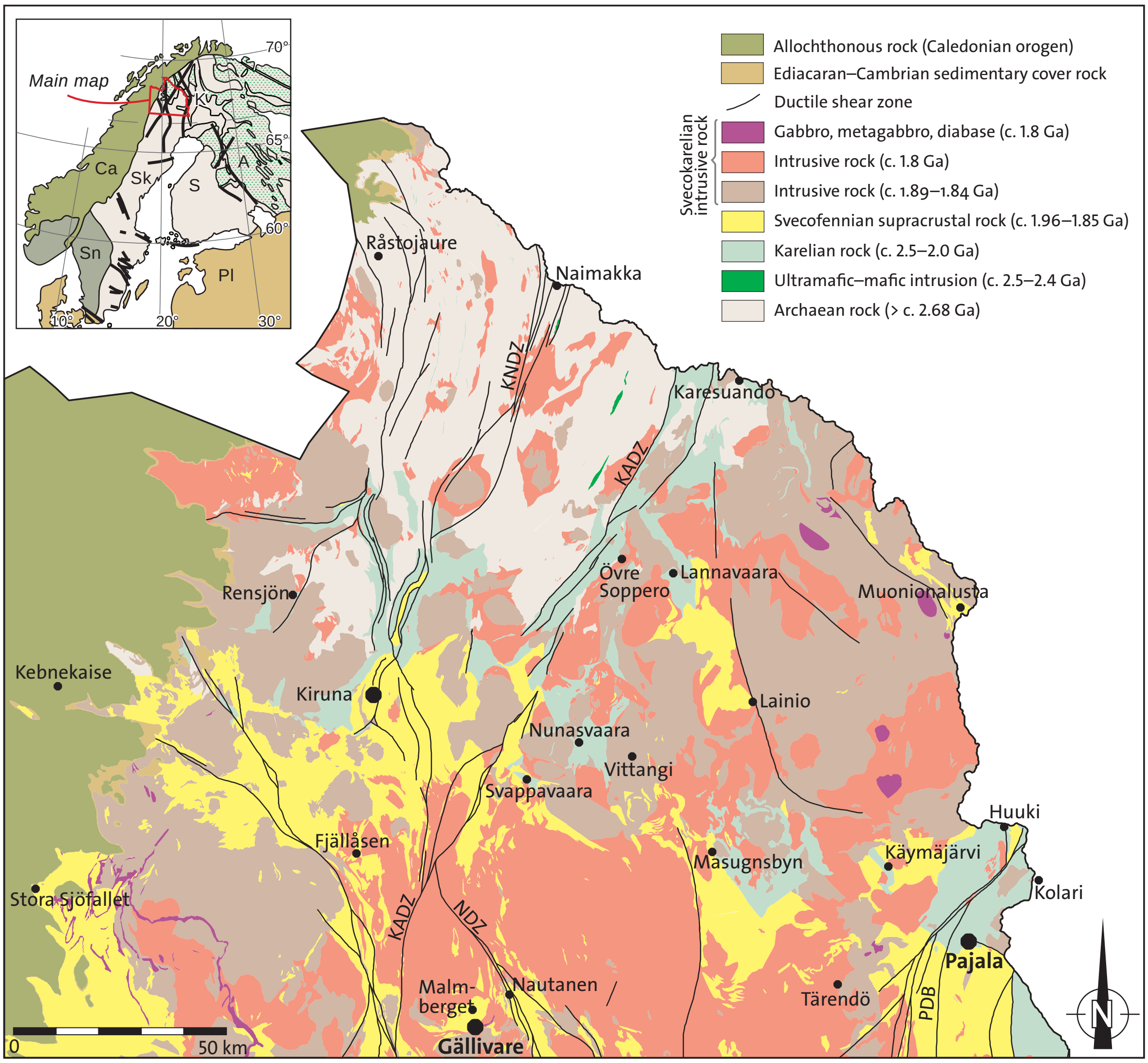

Figure 1. Simplified bedrock map of northern Norrbotten County, modified from Bergman et al. (2001). KNDZ = Kiruna–Naimakka deformation zone, KADZ = Karesuando–Arjeplog deformation zone, NDZ = Nautanen deformation zone, PDB = Pajala deformation belt. Inset map: Sk = Svecokarelian orogen, Sn = Sveconorwegian orogen, Ca = Caledonian orogen, Pl = Platformal sedimentary cover rocks, A (green ornament) = Archaean rocks in part reworked in the Palaeoproterozoic, K (grey ornament) = Karelian rocks, S (without ornament) = Svecofennian supracrustal rocks and Svecokarelian intrusive rocks; thick lines are major deformation zones.

the quartzite. Metasandstone, quartzite and quartzo-feldspathic gneiss in the Pajala area and to the south are spatially associated with both Karelian and younger metavolcanic rocks. The presence of several originally clastic units, with distinctly different detrital zircon age populations, is confirmed by recent results of Lahtinen et al. (2015).

In the Kiruna area the Kovo group is overlain by the Kiruna greenstone group, which predominantly comprises metamorphosed, tholeiitic basalt lava flows, including pillow lava, less important komatiitic lava, tholeiitic tuff and andesitic to dacitic tuffaceous rocks, and minor conglomerate, black schist and carbonate rock (Martinsson 1997). The Viscaria Cu-rich sulphide deposit is hosted by metamorphosed volcaniclastic and associated sedimentary rocks belonging to the Kiruna greenstone group. The stratigraphic sequence is similar but less complete in the area between Kiruna and Pajala, where mainly the upper parts are exposed in the Veikkavaara greenstone group. Mafic pyroclastic

Table 1. Lithostratigraphic and lithodemic unit names preferred in this volume.

Approximate age (Ga)	Lithostratigraphic units	
< 1.88	Snavva-Sjöfallet group[1]	
		Hauki quartzite[2] Maattavaara quartzite[3]
1.89–1.87	Kiirunavaara group[4]	Matojärvi formation[4] Luossavaara formation[4] Hopukka formation[4]
1.89–1.88	Porphyrite group[5]	
		Kurravaara conglomerate[6]
	Pahakurkio group[7] Sakarinpalo suite[20] Kalixälv group[7] Muorjevaara group[8]	
	Sammakkovaara group[4]	Hosiovaara formation[4] Hosiokangas formation[4] Muotkamaa formation[4]
2.3–2.0	Kiruna greenstone group[9]	Linkaluoppal formation[9] Peuravaara formation[9] Viscaria formation[9] Pikse formation[9] Ädnamvare formation[9] Såkevaratjah formation[9]
	Vittangi greenstone group[3]	Nunasvaara member[21]
	Veikkavaara greenstone group[7]	*West:* Masugnsbyn formation[21] Tuorevaara greenstone formation[21] Suinavaara formation[21] Nokkokorvanrova greenstone formation[21] *East:* Vinsa formation[10] Käymäjärvi formation[10]
2.7–2.3		Tjärro quartzite[12]
	Kovo group[9]	Harrejaure formation[11] Rautojaure formation[11]
	Lithodemic units	
1.80–1.79	Edefors suite[13]	Nabrenjarka diabase[14]
1.81–1.78	Lina suite[15]	
1.86–1.85	Jyryjoki granite[16]	
1.88–1.86	Perthite monzonite suite[17]	
1.89–1.88	Haparanda suite[18]	
>2.7	Råstojaure complex[19]	

[1]Ödman (1957), [2]Lundbohm (1898), [3]Eriksson & Hallgren (1975), [4]Martinsson (2004), [5]Offerberg (1967), [6]Sundius (1912), [7]Padget (1970), [8]Zweifel (1976), [9]Martinsson (1997), [10]Martinsson & Wanhainen (2013), [11]Martinsson (1999a), [12]Ödman (1939), [13]Öhlander & Skiöld (1994), [14]Witschard (1975), [15]Holmqvist (1906), [16]Witschard (1970), [17]Witschard (1984), [18]Ödman et al. (1949), [19]Martinsson (1999b), [20]Hellström et al. (2018), [21]Lynch et al. (2018b).

deposits are overlain by volcaniclastic rocks interlayered with carbonate rock, graphite schist, skarn-related iron oxide deposits, banded iron formation and chert (Martinsson 1993, Martinsson et al. 2018b, Lynch et al. 2018b). Most of these rocks were deposited before 2.14 Ga, and only minor assimilation of older continental crust occurred during magma ascent or storage (Lynch et al. 2018b).

Svecofennian supracrustal rocks, recording the onset of the Svecokarelian orogeny, unconformably to disconformably overlie the Kiruna greenstone group and related units. The lower part of the sequence is characterised by calc-alkaline, metavolcanic rocks of andesitic composition. On a regional scale, these rocks show extensive interlayering, with metamorphosed, siliciclastic sedimentary rocks. They contain both Palaeoproterozoic and Archaean detrital zircons (Hellström et al. 2018), consistent with their origin in both local and remote source areas (Martinsson 2004). Metavolcanic and metasedimentary rocks are traditionally included in the Porphyrite group, defined in the low-grade rocks southwest of Kiruna. Equivalent units occur in other areas; see Table 1. Available age determinations show crystallisation ages of 1.89–1.88 Ga (Edfelt et al. 2006, Martinsson et al. 2018b, Hellström et al. 2018, Lynch et al. 2018a).

The Kiirunavaara group stratigraphically overlies the Kurravaara conglomerate in the Kiruna area and the Porphyrite group to the southwest of Kiruna. In Kiruna metamorphosed andesitic to trachyandesitic lava flows comprise the footwall of the Kiruna apatite iron oxide ore deposit. This deposit is overlain by porphyritic metadacite of pyroclastic origin (Martinsson 2004). The age of the host rocks is 1.89–1.87 Ga, and the ore has been dated at 1.88–1.87 Ga (Westhues et al. 2016). The uppermost unit in the Kiirunavaara group mainly consists of metamorphosed ignimbritic tuff, basalt and siliciclastic sedimentary rock. Southwest of Kiruna a thick sequence of metamorphosed, high-Ti and high-Zr tholeiitic basaltic lava is overlain by a unit predominantly comprising pyroclastic metadacite. There are subordinate intercalations of metamorphosed andesite, locally ignimbritic rhyolite, conglomerate, sandstone and siltstone (Offerberg 1967, Perdahl & Martinsson 1995, Martinsson 2004).

The youngest supracrustal unit consists of sandstone with subordinate conglomerate and mudstone, and in some areas basaltic intercalations. The sequence is best developed in the Snavva–Sjöfallet group, where it exceeds a thickness of 6 000 ms (Witschard & Zachrisson 1995), resting on metavolcanic rocks similar to the Kiirunavaara group. Although the contacts are tectonic in most other areas, including the Hauki quartzite in the Kiruna area, there is a locality northwest of Vittangi where a metaconglomerate rests unconformably on a metadiorite (Ödman 1939). The metadiorite is 1.88 Ga old (Bergman et al. 2002a), representing the maximum age of the clastic deposition in this area.

The more or less gneissic rocks in the Haparanda suite are commonly grey and medium-grained, but fine-grained types are also present; porphyritic varieties are uncommon. Magma mingling textures are common in some areas. According to published modal data (Ödman 1957, Bergman et al. 2001), there is a wide spectrum of rock types, from predominantly gabbroid and dioritoid, through quartz monzonite, tonalite and granodiorite, to subordinate granite.

The intrusive rocks in the Perthite monzonite suite, formed between 1.88 and 1.86 Ga, mainly occur in the westernmost part of the area. Quartz-poor rocks, including monzonite, quartz monzonite and quartz monzodiorite, predominate over granite. Many large intrusions of gabbro and diorite, inferred to belong to this suite, are also present. Magmatic layering has been observed in some of these bodies, and several show a concentric, banded magnetic pattern. Ultramafic rocks such as pyroxenite and serpentinite are present in some areas. Perthite-bearing granite is commonly red and medium- to coarse-grained. Enclaves and hybridisation phenomena show that magma mingling and mixing processes were prevalent. The rocks in the Perthite monzonite suite are typically isotropic but there are also areas where a tectonic fabric is prominent. Witschard (1975, 1984) pointed out the geochemical similarity between the Perthite monzonite suite and the Kiirunavaara group, suggesting that the former was emplaced under sub-volcanic conditions. The rock types in the Perthite monzonite suite are similar to those in the Haparanda suite, but have traditionally been considered separate on the basis of several lines of evidence, including field relationships and lithogeochemical characteristics.

A suite of granite and granodiorite that has yielded an age of c. 1.85 Ga (Bergman et al. 2006, Hellström & Bergman 2016), the Jyryjoki granite, occurs in a large area east of Lainio (Fig. 1). The granitoids are spatially associated with pegmatite, and in many places contain biotite-rich seams and partly assimilated remnants of older rocks. The granitoids are porphyritic, have an unequigranular matrix and are weakly foliated.

Large bodies of intrusive rocks belonging to the Lina suite, which formed around 1.8 Ga (Skiöld 1988, Bergman et al. 2002b), are common throughout the area, and dykes or veins of rocks belonging to this suite commonly cut older rocks. The Lina suite is mainly composed of greyish-red, medium-grained and weakly porphyritic granite; red, fine-grained and equigranular varieties are also common.

The granite is usually weakly foliated, associated with pegmatite, and fragments of assimilated country rock are common. Dykes or veins in older rocks consist of granite, pegmatite or aplite. A suite of intrusive rocks consisting of gabbro to granite, with quartz monzonite, monzonite, quartz monzodiorite and monzodiorite as intermediate members is found in the east of the area. Syenite has been reported from southwest of Kiruna. They have ages close to 1.8 Ga (Romer et al. 1994, Martinsson et al. 2018a) and the latter authors suggest a genetic relationship to ring-shaped gabbroic intrusions. The Nabrenjarka diabase, west of Gällivare, is a conspicuous, flat-lying, bowl-shaped and sill-like intrusion with an exposed length of more than 50 km. It intrudes the Lina suite and is 1.8 Ga or younger.

Ductile deformation includes several phases of folding and the formation of major crustal-scale shear zones. The metamorphic grade within the region varies from greenschist facies to upper amphibolite facies, and the intensity of deformation varies from strong penetrative foliation to texturally and structurally well-preserved rocks, both on a regional and local scale. Firm control of the geometry of folds, shear zones and other structures, as well as structural evolution is essential to correctly interpret stratigraphic sequences. The major structures in the Kiruna–Vittangi–Masugnsbyn areas have been modelled in 2D and 3D using a range of geophysical data (Bastani et al. 2018, Jönberger et al. 2018) and evaluation of existing geological data and models. This has provided a broad structural framework for more local studies. Grigull et al. (2018) describe the styles of folds and folding phases, concluding that the Kiruna area only experienced one major ductile deformation phase, whereas the deformation history further east is more complex. Up to four separate phases of deformation have been identified in the east (Grigull et al. 2018, Lynch et al. 2018b). New kinematic data, 3D models and a reconstructions of the deformation history of the Pajala deformation belt and the Vakko and Kovo zones north of Kiruna are provided by Luth et al. (2018a, 2018b). Together, these contributions provide new insights into the three-dimensional structural geometry, as well as a refined view of the structural evolution.

An event of deformation and metamorphism at c. 1.88 Ga, previously inferred from local field observations and indirect dating (e.g. Skiöld & Öhlander 1989, Bergman et al. 2001), has now been confirmed by U-Pb zircon dating of a migmatite in the Masugnsbyn area (Hellström 2018). A younger metamorphic event at 1.86–1.85 Ga is recorded by monazite ages from the same area (Bergman et al. 2006). A protracted event or several separate events during the time interval 1.83–1.78 Ga (Bergman et al. 2001, 2006, Lahtinen et al. 2015, Hellström & Bergman 2016), including movement along the Pajala deformation belt, concluded the ductile deformation in the region.

The most important types of mineralisation are stratiform copper deposits, iron formations, Kiruna-type apatite iron ores and epigenetic copper-gold deposits. Hydrothermal alterations are both of regional character and spatially associated with mineralisations. The most characteristic alteration products are scapolite and albite, but skarn, biotite, carbonate, K-feldspar, sericite, tourmaline, epidote and chlorite are also common (e.g. Bergman et al. 2001, Martinsson et al. 2016, Lynch et al. 2018a). The geochemical composition of till overlying the bedrock reflects these alterations as enrichment in e.g. Ba, Ca, Cl, K, Na, Sr, La, Rb and P (Ladenberger et al. 2018a). New age determinations show that major mineralisation events occurred at 1.88–1.86 Ga and 1.79–1.74 Ga (Martinsson et al. 2016), i.e. close in time to major phases of magmatism, deformation and metamorphism.

REFERENCES

Bastani, M., Antal Lundin, I., Wang, S. & Bergman, S., 2018: Imaging deeper crustal structures by 2D and 3D modelling of geophysical data. Examples from northern Norrbotten. *In:* Bergman, S. (ed): Geology of the Northern Norrbotten ore province, northern Sweden. *Rapporter och Meddelanden 141,* Sveriges geologiska undersökning. This volume pp 341–359.

Bergman, S., Kübler, L. & Martinsson, O., 2001: Description of regional geological and geophysical maps of northern Norrbotten County (east of the Caledonian orogen). *Sveriges geologiska undersökning Ba 56*, 110 pp.

Bergman, S., Martinsson, O. & Persson, P.-O., 2002a: U-Pb zircon age of a metadiorite of the Haparanda suite, northern Sweden. In S. Bergman (ed.): *Radiometric dating results 5. Sveriges geologiska undersökning C 834*, 6–11.

Bergman, S., Persson, P.-O. & Kübler, L., 2002b: U-Pb titanite and zircon ages of the Lina granite at the type locality NW of Gällivare, northern Sweden. In S. Bergman (ed.): *Radiometric dating results 5. Sveriges geologiska undersökning C 834*, 12–17.

Bergman, S., Billström, K., Persson, P.-O., Skiöld, T. & Evins, P., 2006: U-Pb age evidence for repeated Palaeoproterozoic metamorphism and deformation near the Pajala shear zone in the northern Fennoscandian Shield. *GFF 128*, 7–20.

Bergman, S., Weihed, P., Martinsson, O., Eilu, P. & Iljina, M., 2007: Geological and tectonic evolution of the northern part of the Fennoscandian Shield. In V.J. Ojala, P. Weihed, P. Eilu & M. Iljina (eds.): Metallogeny and tectonic evolution of the Northern Fennoscandian Shield: Field trip guidebook. *Geological Survey of Finland, Guide 54*, 6–15.

Edfelt, Å., Sandrin, A., Evins, P., Jeffries, T., Storey, C., Elming S.-Å. & Martinsson O., 2006: Stratigraphy and tectonic setting of the host rocks to the Tjårrojåkka Fe-oxide Cu-Au deposits, Kiruna area, northern Sweden. *GFF 128*, 221–232.

Eriksson, B. & Hallgren, U., 1975: Beskrivning till berggrundskartbladen Vittangi NV, NO, SV, SO. *Sveriges geologiska undersökning Af 13–16*, 203 pp.

Eriksson, T., 1954: Pre-Cambrian geology of the Pajala district, northern Sweden. *Sveriges geologiska undersökning C 522*, 38 pp.

Fredholm, K.A., 1886: Öfversigt af Norrbottens geologi inom Pajala, Muonionalusta och Tärändö socknar. *Sveriges geologiska undersökning C 83*, 39 pp.

Gaál, G., & Gorbatschev, R., 1987: An outline of the Precambrian evolution of the Baltic shield. *Precambrian Research 35*, 15–52.

Geijer, P., 1931: Berggrunden inom malmtrakten Kiruna–Gällivare–Pajala. *Sveriges geologiska undersökning C 366*, 225 pp.

Grigull, S., Berggren, R., Jönberger, J., Jönsson, C., Hellström, F.A. & Luth, S., 2018: Folding observed in Palaeoproterozoic supracrustal rocks in northern Sweden. *In:* Bergman, S. (ed): Geology of the Northern Norrbotten ore province, northern Sweden. *Rapporter och Meddelanden 141,* Sveriges geologiska undersökning. This volume pp 205–257.

Hellström, F.A., 2018: Early Svecokarelian migmatisation west of the Pajala Deformation Belt, northeastern Norrbotten Province, northern Sweden. *In:* Bergman, S. (ed): Geology of the Northern Norrbotten ore province, northern Sweden. *Rapporter och Meddelanden 141,* Sveriges geologiska undersökning. This volume pp 361–379.

Hellström, F. & Bergman, S., 2016: Is there a 1.85 Ga magmatic event in northern Norrbotten? – U-Pb SIMS zircon dating of the Pingisvaara metagranodiorite and the Jyryjoki granite, northern Sweden, *GFF, DOI: 10.1080/11035897.2016.1171254.*

Hellström, F.A., Kumpulainen, R., Jönsson, C., Thomsen, T.B., Huhma, H. & Martinsson, O., 2018: Age and lithostratigraphy of Svecofennian volcanosedimentary rocks at Masugnsbyn, northernmost Sweden – host rocks to Zn-Pb-Cu- and Cu ±Au sulphide mineralisations. *In:* Bergman, S. (ed): Geology of the

Northern Norrbotten ore province, northern Sweden. *Rapporter och Meddelanden 141,* Sveriges geologiska undersökning. This volume pp 151–203.

Holmqvist, P.J., 1906, Studien über die granite von Schweden: *Bulletin of the Geological Institution of the University of Upsala VII*, 77–269.

Jönberger, J., Jönsson, C. & Luth, S., 2018: Geophysical 2D and 3D modeling in the areas around Nunasvaara and Masugnsbyn, northern Sweden. *In:* Bergman, S. (ed): Geology of the Northern Norrbotten ore province, northern Sweden. *Rapporter och Meddelanden 141,* Sveriges geologiska undersökning. This volume pp 311–339.

Ladenberger, A., Andersson, M., Smith, C. & Carlsson, M., 2018: Till geochemistry in northern Norrbotten – regional trends and local signature in the key areas. *In:* Bergman, S. (ed): Geology of the Northern Norrbotten ore province, northern Sweden. *Rapporter och Meddelanden 141,* Sveriges geologiska undersökning. This volume pp 401–428.

Lahtinen, R., Huhma, H., Lahaye, Y, Jonsson, E., Manninen, T., Lauri, L.S., Bergman, S., Hellström, F., Niiranen, T. & Nironen, M., 2015: New geochronological and Sm-Nd constraints across the Pajala shear zone of northern Fennoscandia: Reactivation of a Paleoproterozoic suture. *Precambrian Research 256*, 102–119.

Lundbohm, H. , 1898. Kirunavara-traktens geologi. *Geologiska Föreningens i Stockholm Förhandlingar 20*, 68–78.

Lundbohm, H., 1910: Sketch of the geology of the Kiruna district. *Geologiska Föreningens i Stockholm Förhandlingar 32*, 751–788.

Luth, S., Jönberger, J. & Grigull, S., 2018a: The Vakko and Kovo greenstone belts north of Kiruna: Integrating structural geological mapping and geophysical modelling. *In:* Bergman, S. (ed): Geology of the Northern Norrbotten ore province, northern Sweden. *Rapporter och Meddelanden 141,* Sveriges geologiska undersökning. This volume pp 287–309.

Luth, S., Jönsson, C., Jönberger, J., Grigull, S., Berggren, R., van Assema, B., Smoor, W. & Djuly, T., 2018b: The Pajala Deformation Belt in northeast Sweden: Structural geological mapping and 3D modelling around Pajala. *In:* Bergman, S. (ed): Geology of the Northern Norrbotten ore province, northern Sweden. *Rapporter och Meddelanden 141,* Sveriges geologiska undersökning. This volume pp 259–285.

Lynch, E.P., Bauer, T.E., Jönberger, J., Sarlus, Z., Morris, G.A. & Persson, P.-O., 2018a: Petrology and deformation of c. 1.88 Ga meta-volcanosedimentary rocks hosting iron oxide-copper-gold and related mineralisation in the Nautanen-Gällivare area, northern Sweden. *In:* Bergman, S. (ed): Geology of the Northern Norrbotten ore province, northern Sweden. *Rapporter och Meddelanden 141,* Sveriges geologiska undersökning. This volume pp 107–149.

Lynch, E.P., Hellström, F.A., Huhma, H., Jönberger, J., Persson, P.-O. & Morris, G.A., 2018b: Geology, lithostratigraphy and petrogenesis of c. 2.14 Ga greenstones in the Nunasvaara and Masugnsbyn areas, northernmost Sweden. *In:* Bergman, S. (ed): Geology of the Northern Norrbotten ore province, northern Sweden. *Rapporter och Meddelanden 141,* Sveriges geologiska undersökning. This volume pp 19–77.

Martinsson, O., 1993: Stratigraphy of greenstones in the eastern part of northern Norrbotten. In O. Martinsson, J.-A. Perdahl & J. Bergman: Greenstone and porphyry hosted ore deposits in northern Norrbotten, *NUTEK Project nr 92-00752P*, 1–5.

Martinsson, O., 1997: Paleoproterozoic greenstones at Kiruna in northern Sweden: a product of continental rifting and associated mafic-ultramafic volcanism. In O. Martinsson: *Tectonic setting and metallogeny of the Kiruna greenstones. Doctoral thesis 1997:19, Paper I,* 1–49. Luleå University of Technology.

Martinsson, O., 1999a: Berggrundskartan 30J Rensjön SO, skala 1:50 000. *Sveriges geologiska undersökning Ai 133*.

Martinsson, O., 1999b: Berggrundskartan 31J Råstojaure SV/SO, skala 1:50 000. *Sveriges geologiska undersökning Ai 135.*

Martinsson, O., 2004: Geology and Metallogeny of the Northern Norrbotten Fe-Cu-Au Province. In R.L. Allen, O. Martinsson & P. Weihed (eds.): Svecofennian Ore-Forming Environments: Volcanic-Associated Zn-Cu-Au-Ag, Intrusion-Associated Cu-Au, Sediment-Hosted Pb-Zn, and Magnetite-Apatite Deposits of Northern Sweden. *Society of Economic Geologists, Guidebook Series 33*, 131–148.

Martinsson, O. & Wanhainen, C., 2013: The Northern Norrbotten ore district. In O. Martinsson & C. Wanhainen (eds.): Fe oxide and Cu-Au deposits in the northern Norrbotten ore district. Excursion guidebook SWE5, 12th Biennial SGA Meeting, Uppsala, Sweden, 19–28.

Martinsson, O., Vaasjoki, M. & Persson, P.-O., 1999: U-Pb ages of Archaean to Palaeoproterozoic granitoids in the Torneträsk-Råstojaure area, northern Sweden. In S. Bergman (ed.): Radiometric dating results 4. *Sveriges geologiska undersökning C 831*, 70–90

Martinsson, O. Billström, K., Broman, C., Weihed, P. & Wanhainen, C., 2016: Metallogeny of the Northern Norrbotten Ore Province, northern Fennoscandian Shield with emphasis on IOCG and apatite-iron ore deposits. *Ore Geology Reviews,* doi: 10.1016/j.oregeorev.2016.02.011.

Martinsson, O., Bergman, S., Persson, P.-O. & Hellström, F.A., 2018a: Age and character of late-Svecokarelian monzonitic intrusions in north-eastern Norrbotten, northern Sweden. *In:* Bergman, S. (ed): Geology of the Northern Norrbotten ore province, northern Sweden. *Rapporter och Meddelanden 141,* Sveriges geologiska undersökning. This volume pp 381–399.

Martinsson, O., Bergman, S., Persson, P.-O., Schöberg, H., Billström, K. & Shumlyanskyy, L., 2018b: Stratigraphy and ages of Palaeoproterozoic metavolcanic and metasedimentary rocks at Käymäjärvi, northern Sweden. *In:* Bergman, S. (ed): Geology of the Northern Norrbotten ore province, northern Sweden. *Rapporter och Meddelanden 141,* Sveriges geologiska undersökning. This volume pp 79–105.

Ödman, O. H., 1939: Urbergsgeologiska undersökningar inom Norrbottens län. *Sveriges geologiska undersökning C 426,* 100 pp.

Ödman, O. H., 1957: Beskrivning till berggrundskarta över urberget i Norrbottens län. *Sveriges geologiska undersökning Ca 41*, 151 pp.

Ödman, O. H., Härme, M., Mikkola, A. & Simonen, A., 1949: Den svensk-finska geologiska exkursionen i Tornedalen sommaren 1948. *Geologiska Föreningens i Stockholm Förhandlingar 71*, 113–126.

Offerberg, J., 1967: Beskrivning till berggrundskartbladen Kiruna NV, NO, SV, SO. *Sveriges geologiska undersökning Af 1–4*, 147 pp.

Öhlander, B. & Skiöld, T., 1994: Diversity of 1.8 Ga potassic granitoids along the edge of the Archaean craton in northern Scandinavia: a result of melt formation at various depths and from various sources. *Lithos 33*, 265–283.

Padget, P., 1970: Beskrivning till berggrundskartbladen Tärendö NV, NO, SV, SO. *Sveriges geologiska undersökning Af 5–8*, 95 pp.

Perdahl, J.-A. & Martinsson, O., 1995: Paleoproterozoic flood basalt magmatism in the Kiruna area, northern Sweden. In J.-A. Perdahl: *Svecofennian volcanism in northern Sweden, Doctoral thesis 1995:169D, Paper V,* 1–10. Luleå University of Technology.

Romer, R.L., Martinsson, O. & Perdahl, J.-A., 1994: Geochronology of the Kiruna iron ores and hydrothermal alterations. *Economic Geology 89*, 1249–1261.

Skiöld, T., 1979: Zircon ages from an Archean gneiss province in northern Sweden. *Geologiska Föreningens i Stockholm Förhandlingar 101*, 169–171.

Skiöld, T., 1986: On the age of the Kiruna Greenstones, northern Sweden. *Precambrian Research 32*, 3544.

Skiöld, T., 1988: Implications of new U-Pb zircon chronology to early Proterozoic crustal accretion in northern Sweden. *Precambrian Research 38*, 147–164.

Skiöld, T. & Öhlander, B., 1989: Chronology and geochemistry of late Svecofennian processes in northern Sweden. *Geologiska Föreningens i Stockholm Förhandlingar 111*, 347–354.

Skiöld, T. & Page, R., 1998: SHRIMP and isotope dilution zircon ages on Archaean basement–cover rocks in northern Sweden. 23. *Nordiske geologiske vintermøde, Aarhus 13–16 January 1998,* Abstracts, 273.

Sundius, N., 1912: Pebbles of magnetite-syenite-porphyry in the Kurravaara conglomerate. *Geologiska Föreningens i Stockholm Förhandlingar 34*, 703–726.

Sundius, N., 1915: *Beiträge zur Geologie des südlichen Teils des Kirunagebiets.* Vetenskapliga och praktiska undersökningar i Lappland, arrangerade av Luossavaara–Kiirunavaara Aktiebolag, Uppsala, 237 pp.

Svenonius, F., 1900. Öfversikt af Stora Sjöfallets och angränsande fjälltrakters geologi. *Geologiska Föreningens i Stockholm Förhandlingar 22*, 273–322.

Westhues, A., Hanchar, J.M., Whitehouse, M.J. & Martinsson, O., 2016: New constraints on the timing of host-rock emplacement, hydrothermal alteration, and iron oxide-apatite mineralization in the Kiruna district, Norrbotten, Sweden. *Economic Geology, 111*, 1595–1618.

Witschard, F., 1970: Description of the geological maps Lainio NV, NO, SV, SO. *Sveriges geologiska undersökning Af 9–12*, 116 pp.

Witschard, F., 1975: Description of the geological maps Fjällåsen NV, NO, SV, SO. *Sveriges geologiska undersökning Af 17–20*, 125 pp.

Witschard, F., 1984: The geological and tectonic evolution of the Precambrian of northern Sweden a case for basement reactivation? *Precambrian Research 23*, 273–315.

Witschard, F., & Zachrisson, E., 1995: Berggrundskartan 28I Stora Sjöfallet SO, 1:50 000, *Sveriges geologiska undersökning Ai 91.*

Zweifel, H., 1976, Aitik: geological documentation of a disseminated copper deposit – A preliminary Investigation: *Sveriges geologiska undersökning C 720*, 80 pp.

Authors, paper 2:
Edward P. Lynch
Geological Survey of Sweden
Department of Mineral Resources
Uppsala, Sweden

Fredrik A. Hellström
Geological Survey of Sweden
Department of Mineral Resources
Uppsala, Sweden

Hannu Huhma
Geological Survey of Finland,
Espoo, Finland

Johan Jönberger
Geological Survey of Sweden
Department of Mineral Resources
Uppsala, Sweden

Per-Olof Persson
Swedish Museum of Natural History,
Department of Geosciences,
Stockholm, Sweden

George A. Morris
Geological Survey of Sweden
Department of Mineral Resources
Uppsala, Sweden

2. Geology, lithostratigraphy and petrogenesis of c. 2.14 Ga greenstones in the Nunasvaara and Masugnsbyn areas, northernmost Sweden

Edward P. Lynch, Fredrik A. Hellström, Hannu Huhma, Johan Jönberger,
Per-Olof Persson & George A. Morris

ABSTRACT

Two Palaeoproterozoic greenstone successions in the Nunasvaara and Masugnsbyn areas of north-central Norrbotten (northernmost Sweden) have been investigated to (1) characterise their primary depositional features; (2) establish lithostratigraphic correlations between both areas; and (3) gain insights into the petrogenesis of greenstone-type volcano-sedimentary successions in this sector of the Fennoscandian Shield.

In the Nunasvaara area (*Vittangi greenstone group*), a partly conformable, polydeformed, approximately 2.4 km thick greenstone sequence mainly consists of basaltic (tholeiitic) metavolcanic and metavolcaniclastic rocks (amygdaloidal lava, laminated tuff). Intercalated metasedimentary units include graphite-bearing black schist, and pelite. The uppermost part consists of amphibolitic pelite with intercalated metacarbonate layers and rare meta-ironstone, metachert and meta-ultrabasic horizons. Numerous metadoleritic sills occur throughout the package.

In the Masugnsbyn area (*Veikkavaara greenstone group*) a relatively conformable approximately 3.4 km thick greenstone sequence displays lithological, geochemical and geophysical characteristics similar to that at Nunasvaara. This succession consists of a dominant basaltic metatuff sequence overlain by metasedimentary units towards the top (e.g. meta-ironstone, metachert, amphibolitic schist, calcitic and dolomitic marbles). Minor metadolerite sills occur in the metatuffs. Near the base of the metatuff package, a graphitic black schist horizon occupies a similar stratigraphic position to a prominent black schist layer at Nunasvaara (here named the *Nunasvaara member*). This unit is a key marker horizon providing lateral correlation between both successions and also acts as a useful strain marker for reconstructing deformational events.

Both greenstone successions record the effects of overprinting syn- to late-orogenic (Svecokarelian) tectonothermal events. These include complex, polyphase ductile deformation (D1 to D3 events at Nunasvaara, forming the *Nunasvaara dome*), peak amphibolite facies metamorphism, metasomatic-hydrothermal alteration and late-stage retrogression and brittle faulting (composite D4 at Nunasvaara). Locally, these overprinting processes formed metamorphic graphite, skarn-related Fe ± Cu and hydrothermal Cu ± Pb ± Mo mineralisation.

U-Pb SIMS zircon dating of a metadolerite dyke from Nunasvaara and a metadolerite sill from Masugnsbyn have yielded mean weighted $^{207}Pb/^{206}Pb$ ages of 2144 ±5 Ma (2σ, *n* = 10) and 2139 ±4 Ma (2σ, *n* = 5) Ma, respectively. These precise dates constrain the timing of hypabyssal mafic magmatism, provide a minimum age for the deposition of the volcanic and sedimentary rocks, and identify a new approximetly 2.14 Ga episode of tholeiitic magmatism in this sector of the Fennoscandian Shield. Whole-rock initial εNd values for greenstone meta-igneous units range from +0.4 to +4.0 at Nunasvaara (*n* = 11) and +0.4 to +3.7 at Masugnsbyn (*n* = 7). These data indicate a juvenile depleted to partly enriched mantle (asthenospheric or lithospheric) as a major source of the tholeiitic melts. Corresponding trace element systematics have enriched mid-ocean ridge (E-MORB)-type signatures, and indicate minor assimilation of Archaean continental crust (i.e. Norrbotten craton) during magma ascent and storage. Overall, the combined geological, geochemical and isotopic characteristics of the greenstones are consistent with protolith formation within an incipient oceanic basin (epieric *Norrbotten Seaway*) during approximetly 2.14 Ga rifting and sagging of the Norrbotten craton.

INTRODUCTION

The Palaeoproterozoic bedrock of northernmost Sweden (i.e. northern Norrbotten) predominantly comprises supracrustal and intrusive rocks formed 1.90–1.78 Ga during the composite Svecokarelian orogeny (the name *Svecofennian* is also used). Historically, geological investigations in northern Norrbotten have focused on synorogenic rocks (and associated structures), since these preserve evidence of Palaeoproterozoic orogenesis and crustal accretion (e.g. Skiöld et al. 1993, Talbot & Koyi 1995, Wikström et al. 1996, Öhlander et al. 1999, Talbot 2001, Bergman et al. 2006, Lahtinen et al. 2015). Similarly, metallogenic studies of Svecokarelian-related supracrustal and intrusive rocks have been favoured because they preferentially host economically important mineral deposits, including "Kiruna-type" iron oxide-apatite (IOA), iron oxide-copper-gold (IOCG) and "modified" or "hybrid" deposits such as the Aitik porphyry Cu + IOCG and Tjårrojåkka IOA + IOCG systems (e.g. Cliff et al. 1990, Romer et al. 1994, Edfelt et al. 2005, Smith et al. 2007, Smith et al. 2009, Billström et al. 2010, Wanhainen et al. 2012).

In contrast, supracrustal and intrusive rocks in northern Norrbotten formed before the Svecokarelian orogeny (i.e. "Karelian" successions and associated mafic-ultramafic intrusions > c. 2.0 Ga) have received less attention in terms of their petrographic, geochemical, structural or metallogenic characteristics (cf. Martinsson 1997). Consequently, knowledge about the petrogenesis and subsequent modification of these rocks remains limited, particularly when compared with analogous successions in other sectors of Fennoscandia (cf. Hanski & Huhma 2005, Hanski 2012, Melezhik & Hanski 2012). Additionally, given that Karelian rocks in northern Finland, Sweden and Norway host known Fe, Cr, Ni, Cu, PGE, Au and graphite mineralisation (e.g. Bergman et al. 2001, Weihed et al. 2005, Eilu 2012, Sandstad et al. 2012), geological studies of Karelian greenstone belts in northern Norrbotten may enhance the prospectivity of these units for undiscovered base, precious and critical raw materials (cf. Sarapää et al. 2015).

In this account we present an investigation of two Palaeoproterozoic greenstone successions (i.e. metamorphosed mafic volcanic-sedimentary sequences) located in the Nunasvaara and Masugnsbyn areas, north-central Norrbotten. Field mapping, structural measurements and geophysical investigations have been integrated with U-Pb SIMS zircon dating, lithogeochemistry and Sm-Nd isotopic analysis to reassess the lithostratigraphy of both successions, establish lateral correlations, review deformation and mineralisation events, and provide constraints for greenstone petrogenesis as part of the broader Palaeoproterozoic evolution of the Fennoscandia Shield.

A note on Norrbotten greenstone nomenclature

Various informal geographical, geological and stratigraphic names (or a combination of them) have been used to label and subdivide greenstone-type volcanic-sedimentary successions in Norrbotten, either collectively or for individual sequences. Numerous local names exist for individual successions or belts (e.g. Bergman et al. 2001, Table 2), often designated at the stratigraphic "group" level and typically subdivided into informal formations (e.g. Eriksson & Hallgren 1975; cf. Öhlander et al. 1992). Examples of informal collective names include *Greenstone group* (Frietsch 1984, Witschard 1984, Bergman et al. 2001) *Norrbotten greenstone belt* (Gustafsson 1993) and *Kiruna greenstone group* (Martinsson 2004, Martinsson et al. 2016). The latter name, or simply *Kiruna greenstones*, has also been used in a local sense for greenstones in the immediate Kiruna area (e.g. Ambros 1980, Skiöld 1986, Martinsson 1997, Masurel 2011; cf. Fig. 1B). Additional collective names applied in a broader, regional sense have included *Nordkalott tholeiitic province* (Pharoh et al. 1987) and *Karelian supracrustal rocks* (Welin 1987). Thus, a clearly defined, formally adopted and consistently used stratigraphic or descriptive nomenclature for the greenstones is somewhat lacking. Likewise, rigorous application of stratigraphic principles has been hampered by relatively poor exposure, the effects of multiple deformation events, a lack of marker horizons to establish lateral correlations, and apparent minimal formal stratigraphic oversight.

In this chapter we retain the previously established informal stratigraphy and unit names for the Nunasvaara and Masugnsbyn successions, with some modification mainly at the "formation" stratigraphic level, in particular for the latter area (cf. Padget 1970, Eriksson & Hallgren 1975). Our approach provides a degree of continuity with the previously established systems and aims to minimise the introduction of new unit names without clear geological or practical justification. Additionally, we use the name *Norrbotten greenstone belts* (without any stratigraphic connotation) to refer collectively to all greenstone-related rocks in Norrbotten (cf. Gustafsson 1993).

REGIONAL SETTING OF NORRBOTTEN GREENSTONE BELTS

Palaeoproterozoic greenstone belts occur only in the most northerly and northeasterly parts of Norrbotten (Fig. 1; Bergman et al. 2001, 2012). Compared with analogous belts in Norway and Finland, greenstone successions in northern Sweden tend to form smaller, disconnected "inlier" domains enclosed by younger Palaeoproterozoic rocks (Fig. 1A). Collectively, the greenstones combine to form an approximately 100 × 400 km northwest-trending discontinuous zone comprised of individual north–northeast and north–northwest-orientated, 5–15 km wide, curvilinear zones (Fig. 1B).

From a regional perspective, the Norrbotten greenstone belts represent the northwestern margin of a major northwest–southeast-trending, approximately 800 × 1,500 km lithotectonic domain stretching from Tromsö (Norway) in the northwest to beyond Petrozavodsk (Russia) in the southeast (Fig. 1A). This domain mainly consists of mafic-ultramafic rocks formed during lithospheric-scale intraplate rifting and break-up of the composite Fennoscandian Shield between approximetly 2.5 and 2.0 Ga (e.g. Lahtinen et al. 2008, Melezehik & Hanski 2012, Melezhik et al. 2012). Before this major phase of continental dispersal, the Fennoscandian Shield formed part of a composite supercontinent called Kenorland (e.g. Reddy & Evans 2009, Melezhik et al. 2012).

In northern Norrbotten, greenstone belts and other Palaeoproterozoic metasupracrustal rocks are underlain by the *Norrbotten craton* (Lahtinen et al. 2005), a partly hidden Meso- to Neoarchaean continental basement terrane extending roughly from Luleå in the south to Sweden's northernmost border (e.g. Öhlander et al. 1987b, Mellqvist et al. 1999). The greenstones are typically separated by younger syn- to late-orogenic metasupracrustal and intrusive rocks (Fig. 1B), while isolated greenstone blocks are also known from the northernmost Swedish Caledonides (e.g. Romer & Boundy 1988).

Lithologically, the greenstone sequences predominantly comprise basaltic (tholeiitic) metavolcanic and meta-intrusive rocks (e.g. Pharaoh & Pearce 1984, Pharaoh & Brewer 1990, Martinsson 1997).

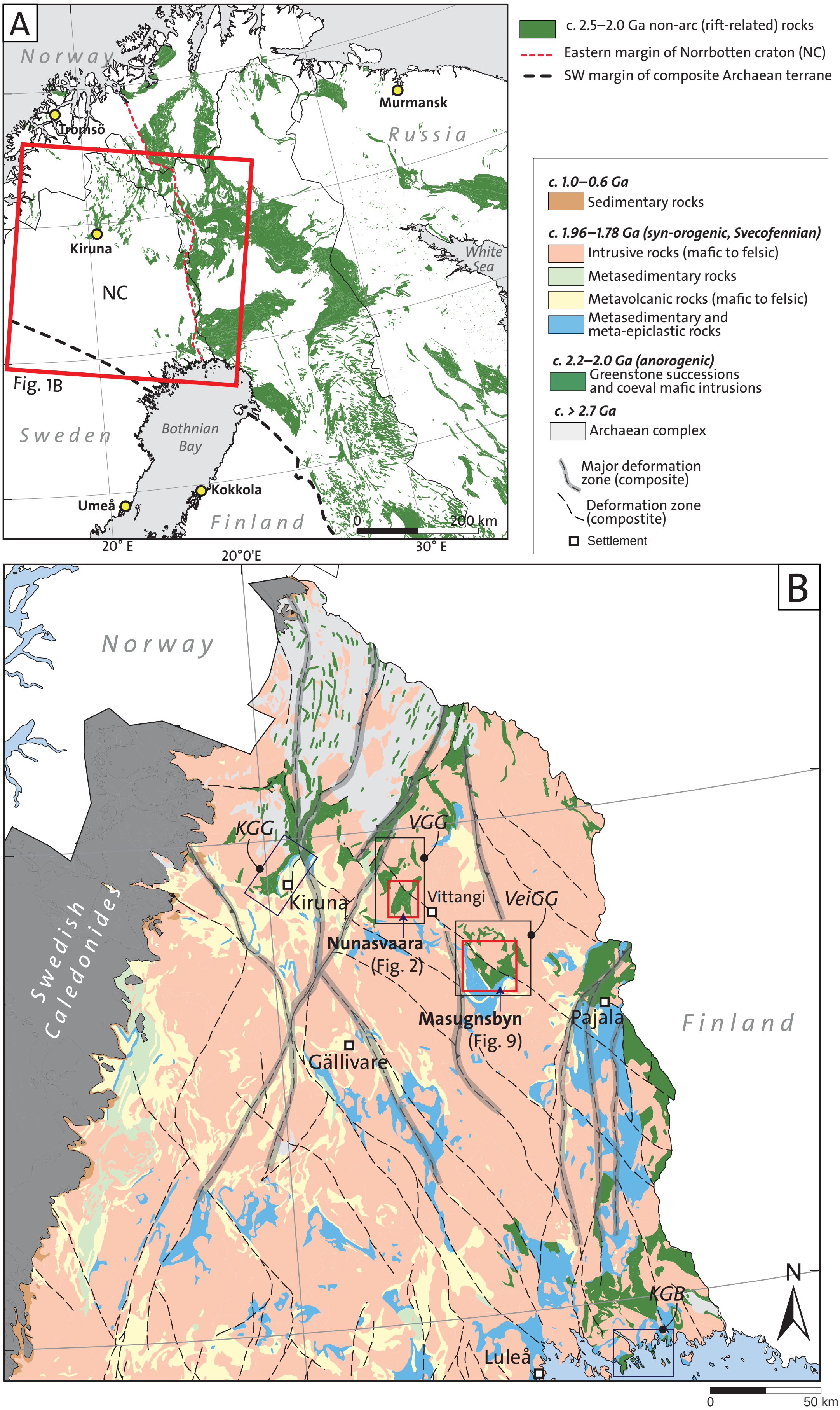
A
Norway
Tromsø
Murmansk
Russia
Kiruna
NC
White Sea
Fig. 1B
Sweden
Bothnian Bay
Umeå
Kokkola
Finland
0
200 km
20° E
20°0'E
30° E
c. 2.5–2.0 Ga non-arc (rift-related) rocks
Eastern margin of Norrbotten craton (NC)
SW margin of composite Archaean terrane
c. 1.0–0.6 Ga
Sedimentary rocks
c. 1.96–1.78 Ga (syn-orogenic, Svecofennian)
Intrusive rocks (mafic to felsic)
Metasedimentary rocks
Metavolcanic rocks (mafic to felsic)
Metasedimentary and meta-epiclastic rocks
c. 2.2–2.0 Ga (anorogenic)
Greenstone successions and coeval mafic intrusions
c. > 2.7 Ga
Archaean complex
Major deformation zone (composite)
Deformation zone (compostite)
Settlement
B
Norway
Swedish Caledonides
68°0'N
KGG
Kiruna
VGG
Vittangi
VeiGG
Nunasvaara (Fig. 2)
Masugnsbyn (Fig. 9)
Pajala
Finland
Gällivare
KGB
N
66°0'N
Luleå
0
50 km

◀ Figure 1. **A.** Map of northern Fennoscandia highlighting the distribution of undifferentiated volcanic, sedimentary and intrusive rocks associated with continental rifting events that affected the composite Archaean craton between c. 2.5 and 2.0 Ga. Base geology is taken from Koistinen et al. (2001). NC = Norrbotten craton. **B.** Precambrian geology of northernmost Sweden (Norrbotten), showing the location of the Nunasvaara and Masugnsbyn areas (red rectangles). Geology modified from Bergman et al. (2012). Major deformation zones (grey) are taken from Bergman et al. (2001). Black rectangles outline the approximate location of major greenstone successions discussed in the main text. KGG = Kiruna greenstone group, VGG = Vittangi greenstone group, VeiGG = Veikkavaara greenstone group, KGB = Kalix greenstone belt.

Most of these rocks contain intercalations of metasedimentary rocks such as amphibolitic pelite to schist, marble, black schist and banded meta-ironstones. In some areas, greenstone-related metasedimentary rocks are more abundant than metavolcanic units (e.g. the Pajala area and Kalix greenstone belt, northeastern Norrbotten, Fig. 1B; Gustafsson 1993, Martinsson 1993, Wanke & Melezhik 2005). This feature may reflect facies variation, stratigraphic position or erosional level (cf. Martinsson 2004).

Greenstone-related mafic intrusions mainly consist of doleritic to gabbroic dykes and sills, and their orientation tends to mimic the trends of the main greenstone belts. Details about the character and age of these intrusive units and their genetic association with mafic extrusive suites are presently lacking (cf. Bergman et al. 2001). In the Kiruna area (*Kiruna greenstone group*), komatiitic lavas occur in the lower part of the greenstone sequence (e.g. Martinsson 1997).

From a stratigraphic perspective, Norrbotten greenstone successions represent the upper part of a 2.4–2.1 Ga Karelian metasupracrustal sequence resting unconformably on the Norrbotten craton (Bergman et al. 2001). The basal part of the Karelian sequence is mainly represented by continental-derived flysch deposits (metaconglomerate, meta-arenite) formed during early continental rifting (e.g. *Kovo group,* Martinsson 1997). More abundant 1.9–1.8 Ga (syn-orogenic) metavolcanic and metasedimentary sequences lie unconformably above the greenstones (Fig. 1B). Regionally, the Norrbotten greenstones mostly correlate with Jatulian (Rhyacian) 2.3–2.06 Ga volcanic-sedimentary successions located to the north and east in northern Finland and Norway, and in northwest Russia (e.g. Hanski 2012, Bingen et al. 2016).

GEOLOGY OF THE NUNASVAARA AND MASUGNSBYN GREENSTONE SUCCESSIONS

Previous geological descriptions and reviews of the studied areas have been presented by Eriksson (1969), Padget (1970), Eriksson & Hallgren (1975), Lynch et al. (2014) and Hellström & Jönsson (2014, 2015).

The lithostratigraphic descriptions that follow present new minimum thicknesses for the various stratigraphic units. These estimates are based on the thickness of steeply dipping (0–90°) volcanic-sedimentary units (excluding hypabyssal rocks) occurring along profiles X–X’ and Y–Y’ at Nunasvaara (Fig. 2A–B), and profiles A and B at Masugnsbyn (Fig. 9A–B). In general, estimating exact true thicknesses of the stratigraphic units in both successions is complicated by (1) the polydeformed nature of the bedrock; (2) the presence of metadoleritic intrusions (often emplaced concordantly along unit boundaries); (3) the truncation of both packages by younger intrusions; and (4) likely preservation and exposure gaps (cf. Gustafsson 1993).

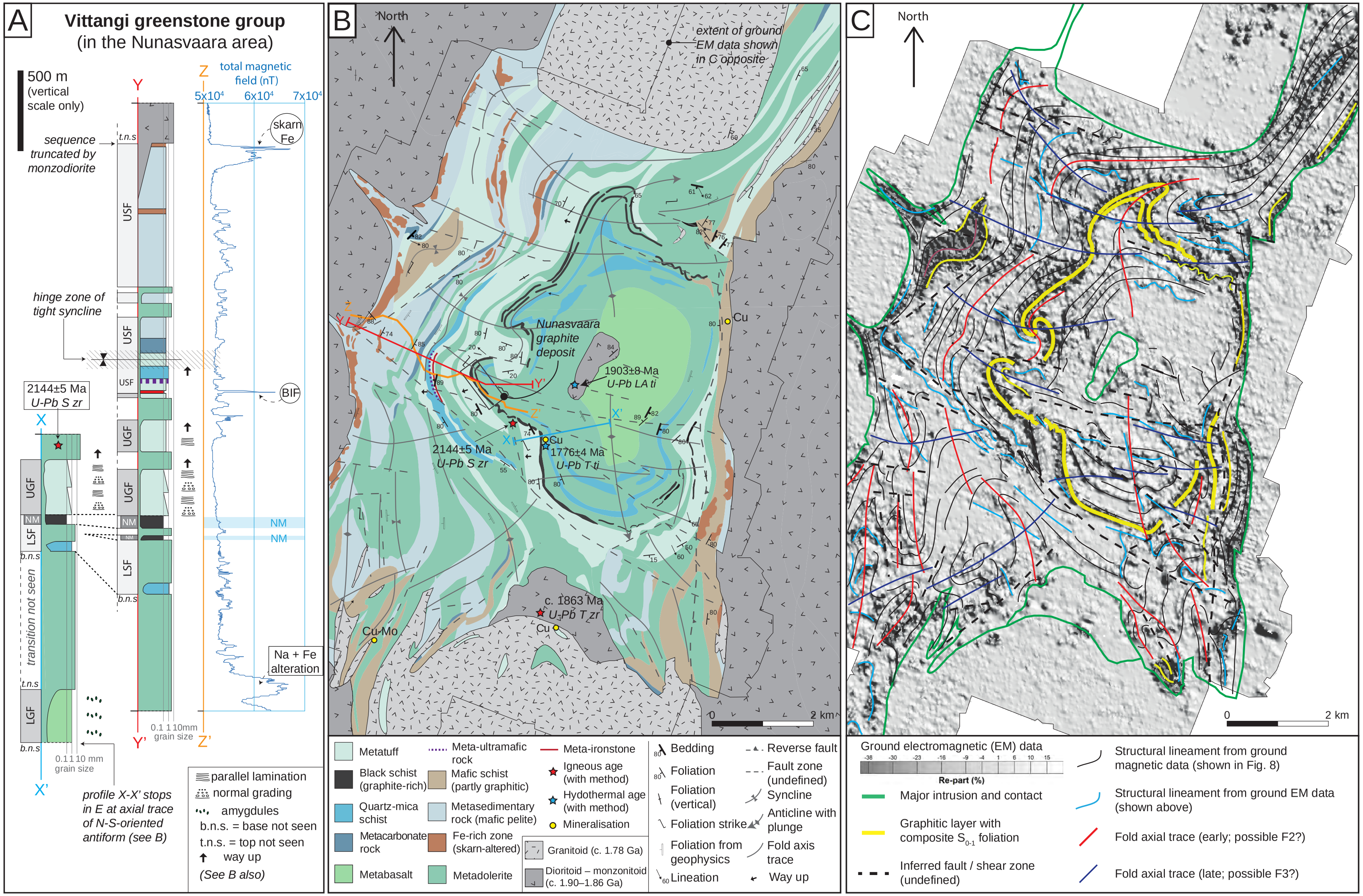
A
Vittangi greenstone group
(in the Nunasvaara area)
500 m
(vertical scale only)
sequence truncated by monzodiorite
hinge zone of tight syncline
2144±5 Ma
U-Pb S zr
total magnetic field (nT)
5x10⁴
6x10⁴
7x10⁴
skarn Fe
BIF
NM
Na + Fe alteration
USF
UGF
LSF
LGF
t.n.s
b.n.s
transition not seen
0.1 1 10mm
grain size
profile X-X' stops in E at axial trace of N-S-oriented antiform (see B)
parallel lamination
normal grading
amygdules
b.n.s. = base not seen
t.n.s. = top not seen
way up
(See B also)
B
North
extent of ground EM data shown in C opposite
Nunasvaara graphite deposit
1903±8 Ma
U-Pb LA ti
2144±5 Ma
U-Pb S zr
1776±4 Ma
U-Pb T ti
c. 1863 Ma
U-Pb T zr
Cu
Cu-Mo
0
2 km
Metatuff
Black schist (graphite-rich)
Quartz-mica schist
Metacarbonate rock
Metabasalt
Meta-ultramafic rock
Mafic schist (partly graphitic)
Metasedimentary rock (mafic pelite)
Fe-rich zone (skarn-altered)
Metadolerite
Meta-ironstone
Igneous age (with method)
Hydrothermal age (with method)
Mineralisation
Granitoid (c. 1.78 Ga)
Dioritoid – monzonitoid (c. 1.90–1.86 Ga)
Bedding
Foliation
Foliation (vertical)
Foliation strike
Foliation from geophysics
Lineation
Reverse fault
Fault zone (undefined)
Syncline
Anticline with plunge
Fold axis trace
Way up
C
North
0
2 km
Ground electromagnetic (EM) data
Re-part (%)
Major intrusion and contact
Graphitic layer with composite S_{0-1} foliation
Inferred fault / shear zone (undefined)
Structural lineament from ground magnetic data (shown in Fig. 8)
Structural lineament from ground EM data (shown above)
Fold axial trace (early; possible F2?)
Fold axial trace (late; possible F3?)

◀ Figure 2. Geology of the Nunasvaara area (part of Vittangi greenstone group). **A.** Schematic stratigraphy of the Nunasvaara area based on profile lines X–X', Y–Y' and Z–Z' shown in B. LGF = Lower greenstone formation, LSF = Lower sedimentary formation, NM = Nunasvaara member (of the LSF), UGF = Upper greenstone formation, USF = Upper sedimentary formation. Unit thicknesses represent minimum estimates. **B.** Geological map highlighting greenstone-related lithologies (based on Eriksson & Hallgren 1975, with additional mapping from this study). Radiometric age sources are: Skiöld 1981 for U-Pb TIMS zircon age (U-Pb T zr), Smith et al. 2009 for U-Pb LA-ICP-MS titanite age (U-Pb LA ti) and Martinsson et al. 2016 for U-Pb TIMS titanite age (U-Pb T ti). U-Pb SIMS zircon age (U-Pb S zr) is from this study. C. Ground-based electromagnetic (slingram) map (in-phase, real component) showing anomalous zones of relatively high conductivity (darker shade) corresponding to graphite-rich layers, fracture zones and skarn-related alteration. Additional structural lineaments (black lines) are based on magnetic anomalies shown in Figure 8A. Fold axial traces from C are also plotted in B and suggest at least two folding events.

Geology and lithostratigraphy at Nunasvaara (Vittangi greenstone group)

The Nunasvaara area is located about 10 km west of Vittangi village (Fig. 1). Here, a polydeformed succession of mafic metavolcanic rocks, hypabyssal intrusions (metadoleritic sills, minor dykes) and metasedimentary rocks form a rectangular, approximately 9 × 11 km, north-northeast-orientated, metasupracrustal inlier (Fig. 2). The sequence extends a further 9 km or so from the northeastern corner of the study area, along a narrow, linear belt toward the north-northeast (cf. Eriksson & Hallgren 1975). In the study area, important examples of skarn-related iron and metamorphic graphite mineralisation occur (e.g. Frietsch 1997, Pearce et al. 2015).

At Nunasvaara the greenstone succession is bordered and truncated by extensive syn- to late-orogenic intrusions (Fig. 2B–C). These consist of (1) generally deformed c. 1.89 Ga gabbros, dioritoids and granitoids assigned to the regional *Haparanda suite*; (2) less abundant c. 1.87 Ga syenitoids and granitoids belonging to the regional *Perthite-monzonite suite*; and (3) weakly deformed to massive c. 1.80 Ga granitic plutons, stocks and dykes assigned to the regional *Lina suite* (cf. Ahl et al. 2001).

Stratigraphically, the greenstones form part of the *Vittangi greenstone group* (VGG, Fig. 1B; Eriksson & Hallgren 1975, Gustafsson 1993). Historically, the VGG has been subdivided into five informal formations (see Eriksson & Hallgren 1975, p. 5). For our study (and in the interests of consistency), we retain the informal stratigraphic subdivisions and unit names proposed by Eriksson & Hallgren (1975), with some minor modifications. A schematic stratigraphic column for the sequence is presented in Figure 2A.

The lowermost stratigraphic unit of the VGG, named the *Tjärro quartzite formation* (TQF), has not been seen at Nunasvaara and is not considered further in this account. In their regional compilation, Bergman et al. (2001) re-assigned the TQF to the regionally extensive and inferred stratigraphically lower *Kovo group*, based on lithological considerations (cf. Kumplulainen 2000).

Lower greenstone formation

The lowermost VGG unit occurring at Nunasvaara is the *Lower greenstone formation* (LGF, Fig. 2A). Contact between the LGF and its bounding formations are not preserved in the area. Thus, a tentative minimum thickness of approximately 300 m is estimated for this unit (Profile X–X', Fig 2A). In contrast, Gustafsson (1993) indicated a minimum thickness of approximately 900 m, while Eriksson & Hallgren (1975) reported a thickness of approximately 5 km for a more completely exposed section about 35 km to the northwest of Nunasvaara (Saivo–Leppäkoski area).

The LGF predominantly consists of effusive mafic metavolcanic rock (*basaltic lava* of Eriksson & Hallgren 1975). Rare ultramafic dykes (Mg-rich, olivine-bearing serpentinite) have also been assigned to this unit (Eriksson & Hallgren 1975). The metabasalt is dark grey to greenish-grey, aphanitic (< 0.5 mm) and locally amygdaloidal. It crops out across several flat-lying exposures in the centre of the study area (Figs. 2 & 3A). In general, it is massive to weakly foliated, without conspicuous banding or layering and consists of granoblastic hornblende and plagioclase feldspar, with minor biotite, clinopyroxene (diopside?), titanite, magnetite and late-stage epidote.

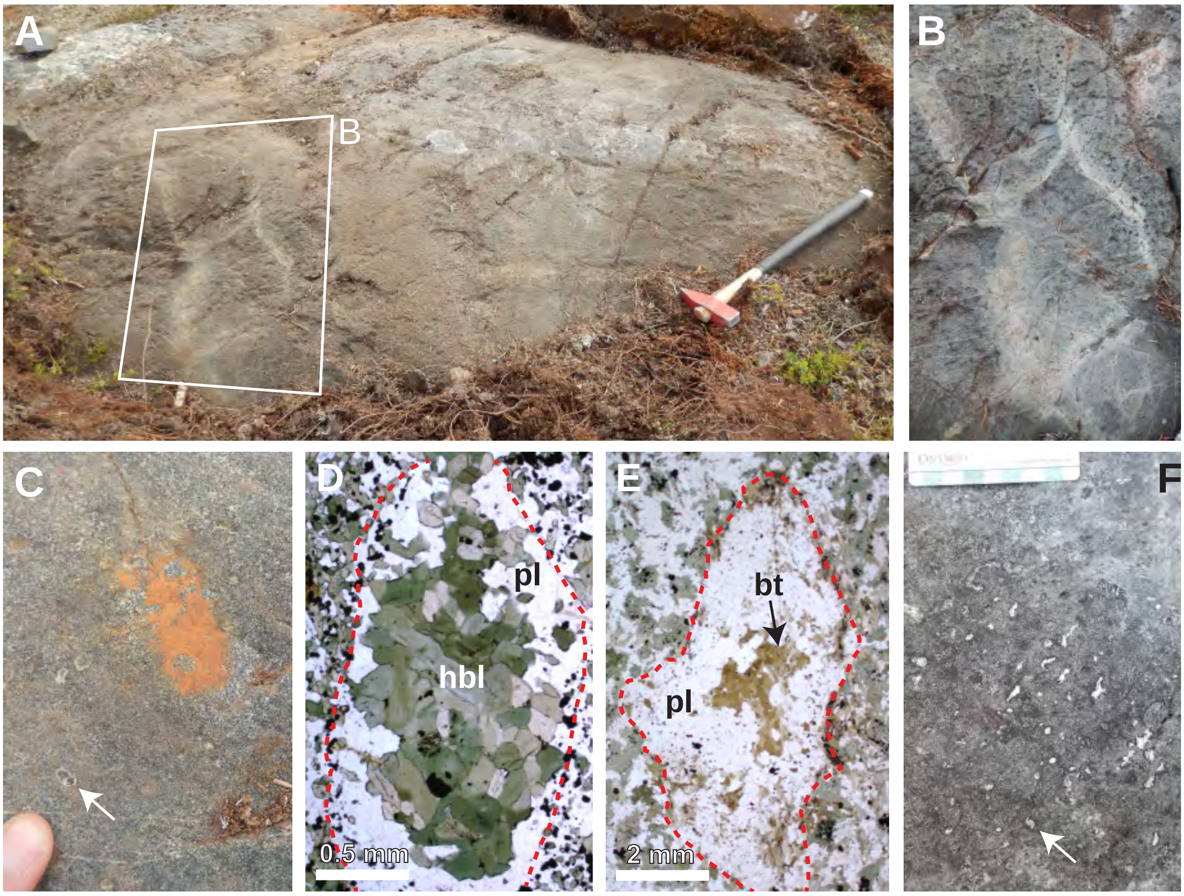

Figure 3. **A.** Outcrop view of metabasalt (orthoamphibolite) of the Lower greenstone formation, Nunasvaara. The hammer head is 15 cm long. **B.** Close-up view from A showing possible cross-section through a deformed tube-like structure (i.e. tube-fed pahoehoe lava flow). Curvilinear, pale green zones (actinolite-chlorite altered?) delineate the outer rim of the lobe. **C.** Oblate, hornblende-rich amygdales (arrow) in metabasalt. **D.** Thin section, plane polarised light (PPL) view of an amygdale (dashed outline), with an outer zone of plagioclase (pl) and a core of hornblende (hbl). **E.** PPL view of irregular and stretched amygdale with an outer zone of plagioclase (pl) and a core of biotite (bt). **F.** Outcrop view of elongate-irregular (pipe vesicle?) amygdales in metabasalt (arrow).

Although bedding contacts are not well exposed, some outcrops display bulbous, tabular forms, suggesting flow bed thicknesses of 0.7–2 m. Rare polygonal shapes, delineated by curvilinear, pale green bands (actinolite ± chlorite?), may represent cross-sectional views of tube-like flow lobes or deformed pillows (Fig. 3A–B). Where present, these structures consist of dense, vesicle-free interiors, which grade outwards to an external vesicular zone (1–3 cm wide), and then to an outermost rind or margin (1–2 cm wide), typically devoid of vesicles. These features are suggestive of the types of flow lobes and channels associated with pahoehoe-type lava extrusion (e.g. Self et al. 1998, Oze & Winter 2005). Thicker and better preserved sequences of pillowed metabasalt occur to the northwest of Nunasvaara (cf. Eriksson & Hallgren 1975).

A more conspicuous feature of the metabasalt at Nunasvaara is the variable presence of amygdales, which impart a spotted, variolitic appearance to the rock (Fig. 3C–F). Amygdales are generally oblate to elongate or irregular and typically range from 0.2 cm to 1.5 cm in length. They mainly contain hornblende or biotite cores with plagioclase ± scapolite rims (Fig. 3C–E). Examples of sericite-altered K-feldspar cores that grade into plagioclase margins also occur. Locally, some cores have a pale green appearance, suggesting chlorite ± actinolite replacement, while fine-grained subhedral magnetite may be disseminated around rims (Fig. 3E). Rarely, amygdales consist of creamy white scapolite ± albite without the darker amphibole-rich cores (Fig. 3F).

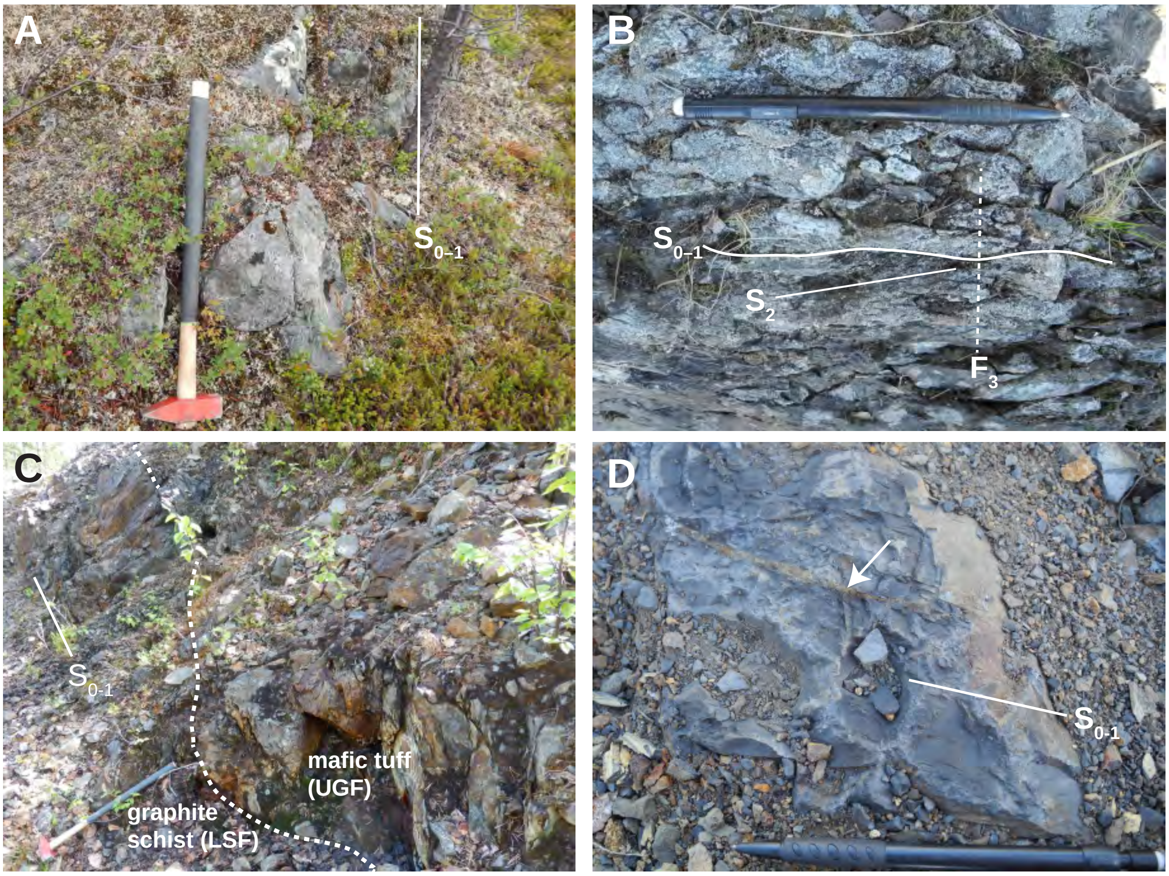

Figure 4. Lower sedimentary formation rocks at Nunasvaara. **A.** Along-strike view to the north of sub-vertical, mafic to intermediate metasedimentary rock (amphibole-mica schist). The hammer head is 15 cm long. **B.** Horizontal surface view to the east–north-east of Nunasvaara member graphite schist. The rock displays a weak S-C-fabric with a crenulation cleavage formed at an acute angle (approximately < 15°) to the main schistosity. The schist is also affected by east-northeast-orientated and steeply plunging gentle F2 folds. The pencil is 15 cm long. **C.** View to the southeast of the hanging wall contact zone at the Nunasvaara graphite deposit showing steeply southwest-dipping graphite-rich schist (LSF, left) overlain by metatuff of the Upper greenstone formation (UGF, right). **D.** Horizontal surface view to the southwest of graphite-rich schist at the Nunasvaara deposit (Nunasvaara member). A weak S0–1 foliation is developed. The arrow indicates a weathered, sulphide-bearing veinlet. The pencil is 15 cm long.

Lower sedimentary formation

The next overlying stratigraphic unit at Nunasvaara is the *Lower sedimentary formatio*n (LSF, Fig. 2A). It consists of basal quartz-mica schist and an uppermost graphitic black schist horizon (Fig. 4). The lower contact with the underlying LGF is not seen in the Nunasvaara area. The top of the LSF is marked by a distinctive, graphite-rich schist horizon (*graphite schist* of Eriksson & Hallgren 1975). This layer hosts the Nunasvaara graphite deposit and several other named graphite prospects along strike (cf. Shaikh 1972). A minimum thickness estimate for the LSF is 200 m. Gustafsson (1993) reports a minimum thickness of 450 m for this formation.

The lithologically distinctive nature of the black schist layer (relatively abundant flake and amorphous graphite), its stratified, semi-continuous character, and its potential use as a strain marker, provide a basis for this unit to act as a correlative stratigraphic horizon in the Nunasvaara and broader north-central Norrbotten areas. We therefore formally introduce the name *Nunasvaara member* for this graphitic black schist horizon. A brief, systematic description of this unit now follows.

The Nunasvaara member (NM) refers to a 10–50 m thick graphite schist horizon (black schist) that forms the stratigraphically uppermost part of the Lower sedimentary formation of the Vittangi greenstone group at Nunasvaara (Vittangi area, northern Norrbotten). A suggested stratotype locality is the old Nunasvaara quarry (Nunasvaara graphite deposit; SWEREF99 TM: N7524309, E0770109, and general area). Here, the unit is in conformable contact with an overlying laminated metatuff (i.e. Upper greenstone formation, Fig. 4C). The basal contact with underlying mafic to intermediate schist is not exposed and is intruded by a metadoleritic sill, which locally entrains the graphite schist, creating two sub-parallel horizons (e.g. Shaikh 1972). The NM extends along strike toward the northeast and southwest and intermittently continues as a polydeformed, discontinuous, sub-circular horizon with a total length of approximately 14 km.

In general, the graphite schist is dark grey, fine-grained (0.01–1 mm) and foliated, containing lepidoblastic feldspar, amphibole (actinolite-tremolite), scapolite, graphite, mica, titanite and pyrite. Locally, microcrystalline graphite abundances are relatively high (25–45 modal %; Shaikh 1972, Bergström 1987). The schist has a dark metallic blue-grey appearance and is massive to weakly foliated (Fig. 4D). Historical lithogeochemical analyses indicate that graphitic carbon concentrations for the NM range 10–45 wt. % (e.g. Shaikh 1972, Eriksson & Hallgren 1975, Bergström 1987; cf. Table 3).

Stable carbon isotope analysis of Nunasvaara graphite has yielded $\delta^{13}C_{graphite}$ values within a narrow range of approximately -23 to -22‰ that are consistent with a biogenic source for the precursor carbonaceous material (Pearce et al. 2015; cf. Luque et al. 2012). These data are similar to $\delta^{13}C_{graphite}$ values from the "C zone" black schist horizon of the *Viscaria formation* (Kiruna greenstone group), located southwest of Kiruna (Martinsson et al. 1997). They also fall within the range of approximately -27.0 to -19.2‰ for graphite-bearing metasedimentary rocks from elsewhere in north-central Norrbotten (Gavelin 1957). Deposition of an inferred black shale protolith for the Nunasvaara graphitic schist at c. 2.14 Ga corresponds with a known global increase in organic carbon production and burial at c. 2.1 Ga during a major period of continental dispersal (Condie et al. 2001).

Upper greenstone formation

The next overlying unit in the sequence is the *Upper greenstone formation* (UGF, Fig. 2A). It predominantly consists of fine-grained, laminated, mafic metavolcaniclastic rock (*amphibolitic tuff* of Eriksson & Hallgren 1975). The upper and lower contacts of the UGF and its bounding formations appear to be transitional-conformable. At Nunasvaara, the UGF has a minimum thickness of approximately 600 m. Gustafsson (1993) indicated a minimum thickness of approximately 800 m for this unit. About 30 km to the northwest (Sautusvaara area) the UGF comprises intercalated mafic metavolcaniclastic and effusive metavolcanic rocks (including local pillowed horizons in the latter), with subordinate meta-epiclastic and marble layers (Eriksson & Hallgren 1975).

In general, UGF metatuff is dark grey to medium grey, fine- to medium-grained (0.1–2 mm) and forms parallel, laterally continuous and planar, thin to medium beds (approximately 3 cm and 50 cm thick, Fig. 5A). Within individual beds, the metatuff has a stratified appearance and contains planar to wavy, parallel to sub-parallel, laterally continuous, 0.1–1 cm thick laminae (Fig 5B). Locally, it contains thicker (2–10 cm), alternating mafic and intermediate bands, resulting in an overall interlayered, compositionally variable volcaniclastic sequence (Fig. 4C–D). Likewise, relatively thin argillaceous seams (often micaceous and iron oxide-stained) occur, suggesting variable input of terrigeneous sedimentary material (Fig. 5C–D). Higher in the sequence, the metatuff is more crystalline (hornfelsed?) with a non-laminated appearance.

Along the mapped profile Y–Y' shown in Figure 2A & B UGF metatuffs dip steeply (80–90°) towards the west-southwest and contain laminated, fining upward sequences (i.e. normal grading), which indicate younging toward the southwest (Fig. 5E; cf. Eriksson & Hallgren 1975). Rarely, lensoidal, channel-like features are also developed, indicative of sub-aqueous, climbing ripple deposition (Fig. 5F).

Mineralogically, the metatuff consists of lepidoblastic hornblende (± actinolite) and plagioclase, with minor biotite, muscovite, magnetite, pyrite and garnet (e.g. Fig. 5E–G). The latter mineral is generally subhedral to euhedral, dark red to greyish-red (almandine), fine- to medium-grained (0.2–0.8 cm) and appears to occur preferentially within darker brown to rust-brown horizons with a more clay-like

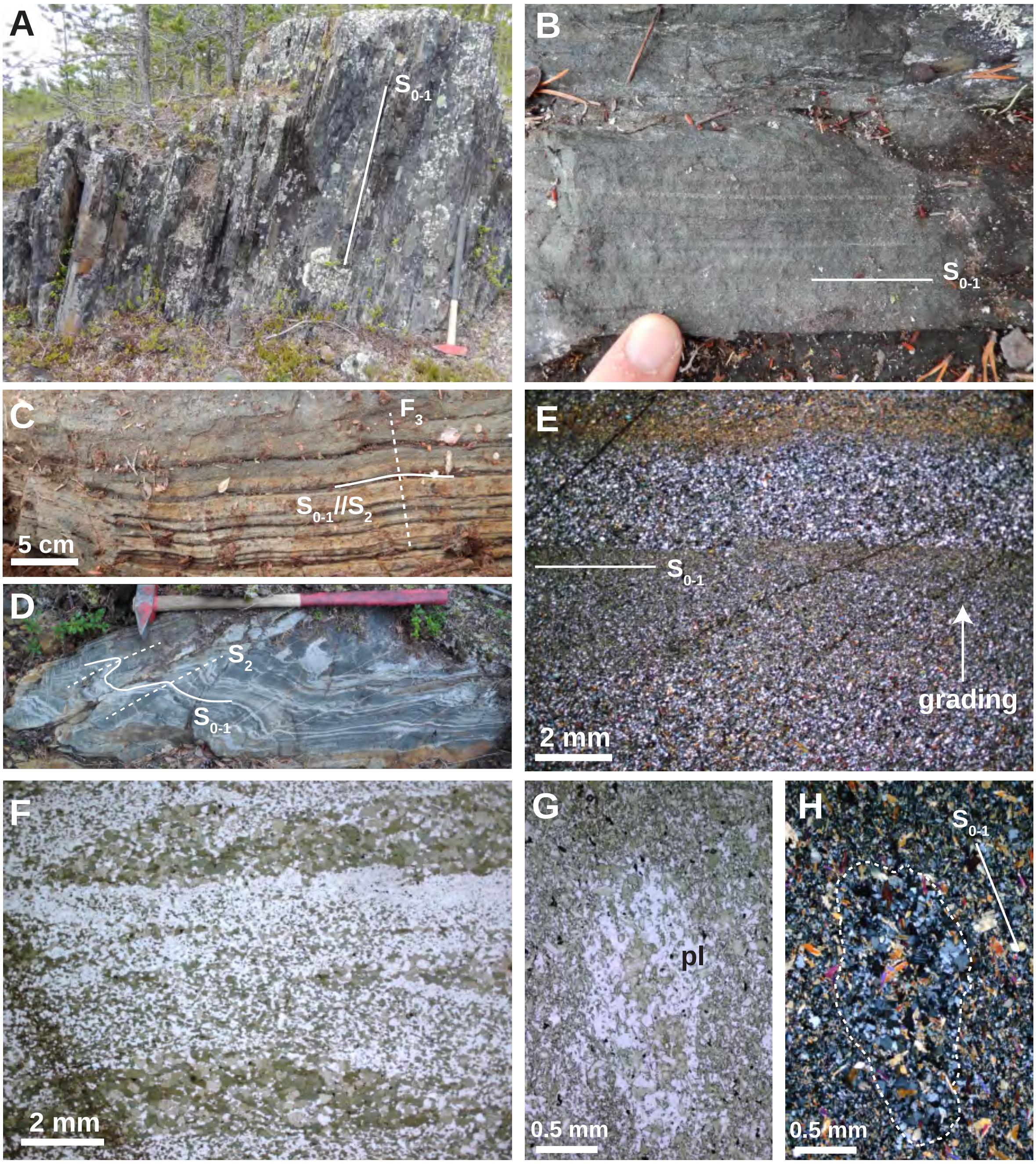

Figure 5. Mafic metatuff of the Upper greenstone formation at Nunasvaara. **A.** Outcrop view to the northwest of steeply southwest-dipping, medium- to thickly-bedded, metatuff. This sequence forms part of the hanging wall rocks of the Nunasvaara graphite deposit. The hammer is 65 cm long. **B.** Sub-horizontal, bedding orthogonal view (to the southwest) of fine-grained and well-sorted laminated tuff. **C.** Sub-horizontal view (to the southwest) of thin- to medium-bedded, compositionally banded metatuff. Locally, bands and laminae display gentle, steeply southwest-plunging upright F2 folds, typically orientated orthogonally to a composite So-1 foliation. **D.** Sub-horizontal view (to the northeast) of compositionally banded and folded metatuff. The hammer is 65 cm long. **E.** Thin section cross-polarised light (XPL) view of fine-grained, well-sorted, laminated metatuff, displaying fining upwards, normal grading, indicating younging toward the west-southwest. **F.** Thin section plane polarised light (PPL) view of lensoidal, channel-like features in metatuff. **G and H.** PPL and XPL views (respectively) of a possible remnant lithic clast in metatuff (dashed outline). The clast consists of an aggregate of relatively coarse plagioclase feldspar (pl) and amphibole and is stretched parallel to the main So-1 foliation.

appearance. Other features of the metatuff include the presence of chert-like nodules and bands, and granular lapilli-like horizons, with elongate, sub-rounded to oblate feldspar aggregates, possibly representing previously consolidated volcaniclastic material (i.e. lithic metatuff, Fig. 5G–H).

Upper sedimentary formation

The uppermost stratigraphic unit at Nunasvaara is the *Upper sedimentary formation* (USF, Fig. 2A). It consists of intercalated mafic to intermediate pelite to schist (Fig. 6A–B), graphitic black schist (Fig. 6C), metacarbonate rocks (Fig. 6E–F), minor banded quartz-rich horizons (metachert, Fig. 6G) and laminated iron-rich seams (meta-ironstone or BIF, Fig. 6H). In the last-mentioned unit, magnetite grains display fining upward textures that indicate younging toward the west-northwest (Fig. 6I).

A prominent feature of the USF at Nunasvaara is the occurrence of curvilinear zones of metasomatised, iron-rich and locally sulphide-bearing "skarn-"-altered rocks (i.e. amphibole + pyroxene + magnetite ± sulphide horizons, e.g. Frietsch 1997). These areas, locally containing relatively abundant stratabound iron mineralisation, are typically associated with upper metacarbonate and metasedimentary layers. The skarn metasomatic alteration zones also appear to be spatially focused along the margins of c. 1.89 Ga mafic to intermediate intrusions in the west and east of the study area (Fig. 2B).

Gustafsson (1993) reported that the UGF–USF contact is not preserved in the general Vittangi area. For this study, we have assigned the base of the USF to a thin seam (< 1 m) of banded meta-ironstone located approximately 985 m west-northwest of the Nunasvaara graphite deposit (Fig. 2A–B). Although poorly exposed, this laminated, magnetite-rich horizon is identifiable using ground-based magnetic measurements, and is illustrated in Figure 2A as a relatively narrow and intense (approximately 6.4×10^4 nT) magnetic anomaly on profile Z–Z'.

The basal part of the USF is inferred to represent the hinge zone of a northeast-trending upright syncline (Fig. 2A–B). Here, the greenstone sequence has mixed metasedimentary-metavolcanic characteristics, marking a transitional (conformable?) zone between the UGF and USF. The area contains intercalations of mafic metatuff and a rare, relatively thin (approximately < 5 m), meta-ultramafic horizon with a picritic geochemical signature (Table 3, Fig. 15C). A similar meta-ultramafic unit occurs in the Masugnsbyn area.

The stratigraphic top of the USF is not exposed in the study area and in the west the formation is truncated by an inferred c. 1.89 Ga quartz monzodiorite (Fig. 2A–B; e.g. Lynch et al. 2014). An estimated minimum thickness of the USF at Nunasvaara is approximately 1.3 km, similar to that indicated by Gustafsson (1993).

In summary, Palaeoproterozoic greenstones at Nunasvaara represent a discontinuous, partly conformable sequence of predominantly basaltic metavolcanic, metavolcaniclastic and metasedimentary rocks. The entire package may be divided into four informal lithostratigraphic formations (including one member), which have an estimated total minimum thickness of approximately 2.4 km (cf. Martinsson 1993, Gustafsson 1993).

Greenstone-related mafic intrusions at Nunasvaara

Metadoleritic intrusions occur throughout the volcanic-sedimentary sequence at Nunasvaara (*metadiabase* of Eriksson & Hallgren 1975). Typically, they form discontinuous, sub-parallel to lenticular sills, ranging 25–150 m maximum thickness (locally up to approximately 450 m, Fig. 2A–B). Minor discordant dykes (apophyses) associated with larger bodies also occur (Eriksson & Hallgren 1975). While distinct intrusive contacts are only rarely exposed, their sub-volcanic nature is most apparent from intrusive contacts seen in drill cores and their general petrographic characteristics (cf. Eriksson 1969, Gerdin et al. 1990).

Metadolerite at Nunasvaara is typically dark greenish-grey, fine- to medium-grained (0.3–4 mm), weakly to moderately foliated, and displays an intergranular (granoblastic) texture (Fig. 7A–C). Scapolite ± albite alteration commonly imparts a medium grey speckled or knobbly appearance to exposed surfaces (Fig. 7A). Mineralogically, they consist of ophitic hornblende and plagioclase feldspar (andesine to labradorite; Eriksson & Hallgren 1975), with minor biotite, zircon, titanite and magnetite (Fig. 7C–D). The latter mineral may be relatively abundant (10–15 vol. %) and is typically associated with disseminated pyrite,

Figure 6. Upper sedimentary formation rocks at Nunasvaara. **A.** Argillaceous layer (arrow) in mica schist. The hammer head is 15 cm long. **B.** Sub-vertical, bedding plane view of fine-grained, mafic metasedimentary rock (possible greywacke). **C.** Sub-vertical, along-strike view of graphitic schist. The pencil is 15 cm long. **D.** Sub-vertical, along-strike view of approximately 20 cm thick, planar to undulose metacarbonate horizon (calc-silicate rock) in a metasedimentary rock. **E.** Sub-vertical view of laminated meta-carbonate rock showing a composite S0-2 foliation. **F.** Sub-vertical view of bedding plane surface (approximately orthogonal to strike) shown in E with L3 intersection lineations. **G.** Hand specimen of laminated meta-ironstone. **H**. Thin section plane polarised light view of laminated meta-ironstone showing grading. **I.** Hand specimen view of amphibole and sulphide-bearing quartz-rich horizon (possible metachert).

chalcopyrite and titanite, or occurs in hornblende ± actinolite veinlets (Figs. 7C & 7E). Rarely, relict clino-pyroxene occurs, typically as anhedral and fragmented crystals, enclosed or partly replaced by hornblende aggregates (Fig. 7E). Plagioclase is commonly replaced by scapolite (Figs. 7B & 7D) while late-stage (retro-gressive) minerals include chlorite (replacing hornblende), sericite (replacing plagioclase) and hematite (replacing magnetite). Irregular amphibole ± magnetite veinlets are also a fairly common feature (Fig. 7A).

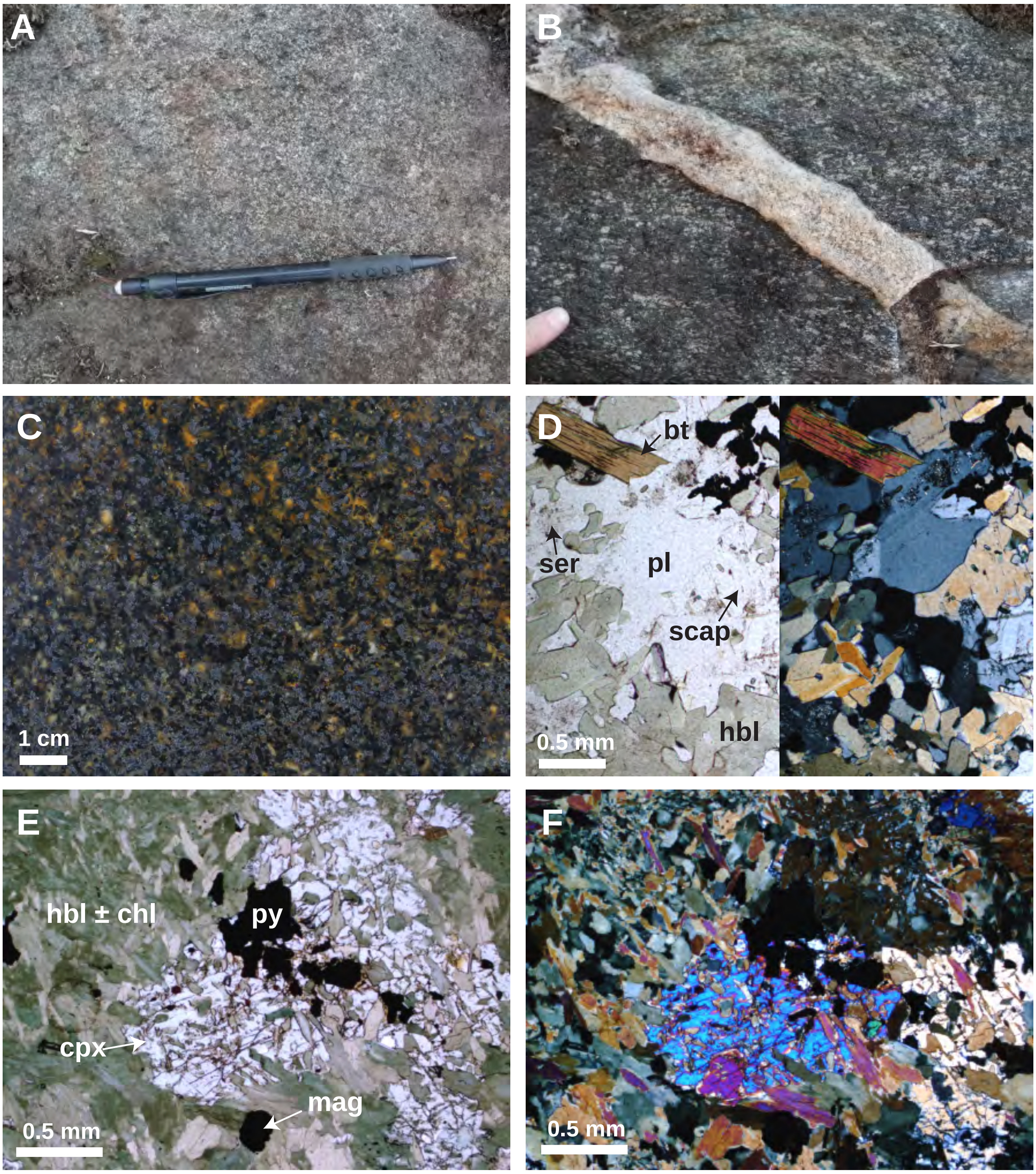

Figure 7. Metadolerite at Nunasvaara. **A.** Outcrop view of weakly foliated, weakly to moderately scapolite ± albite-altered, metadolerite. Dark grey, amphibole-rich veinlets also seen. The pencil is 15 cm long. **B.** Outcrop view of a foliated metadolerite cut by an aplite dyke. **C.** Cut hand sample surface showing medium-grained, intergranular (granoblastic), amphibole-plagioclase feldspar matrix with abundant disseminated magnetite (medium grey, anhedral grains). Patchy orange staining is fine-grained hematite (after magnetite) overprinting plagioclase. **D.** Split thin section plane-polarised light (PPL, left) and cross-polarised light (XPL, right) views of ophitic and xenoblastic hornblende–plagioclase feldspar matrix. Subhedral biotite (top left) may be a late metasomatic phase (replacing hornblende?). **E and F.** Thin section PPL and XPL views of granoblastic to decussate hornblende associated with relict clinopyroxene grain (second-order blue, purple). Mineral abbreviations: bt = biotite, chl = chlorite, hbl = hornblende, mag = magnetite, pl = plagioclase feldspar, py = pyrite, cpx = clinopyroxene, scap = scapolite, ser = sericite.

Throughout the sequence the metadolerite sills are variably deformed and display folding patterns that conform to the general ductile deformation trends seen across the area (Fig. 2B). Based on magnetic anomaly data, folded sills partly correspond to curvilinear zones, with relatively high magnetic signatures (Fig. 8A). In general, the folded nature of the sills attests to their emplacement as part of the broader greenstone sequence before the onset of Svecokarelian-cycle orogenesis and deformation.

Based on geological and petrographic considerations, Eriksson & Hallgren (1975) considered the metadolerite to represent the hypabyssal equivalent of *Vittangi greenstone group* mafic metavolcanic rocks. Alternatively, the prevalence of sill-like bodies crosscutting the volcanic-sedimentary sequence suggests that the metadolerite may represent a compositionally similar but younger phase of mafic magmatism. However, given the lack of chilled margins in the sills, the comparable mineralogy of both units, their close spatial proximity and similar deformation history, a comagmatic link between the metadolerite and mafic metavolcanic rocks seems plausible (e.g. Eriksson & Hallgren 1975). Lithogeochemical and isotopic results reported here support the contention that both units form part of a broadly contemporaneous suite of tholeiitic mafic magmatism.

Deformation and structures at Nunasvaara

The greenstone sequence at Nunasvaara has been affected by episodic, polyphase deformation (Eriksson 1969, Eriksson & Hallgren 1975). Overprinting folding events have imparted a striking "basin and dome"-type pattern, indicative of refold interference (cf. Thiessien 1986). Asymmetric fold patterns, localised shearing and strain partitioning of structurally incompetent layers has developed a broad, roughly northeast-trending ductile shear zone, in which meta-volcanosedimentary units "wrap around" a central, relatively more competent mainly meta-igneous core. In addition, numerous crosscutting fault and fracture zones suggest one or more episodes of late-stage brittle or brittle-ductile deformation.

The most commonly observed structure in the Nunasvaara area is a penetrative planar fabric (S1) in layered metavolcanic and metasedimentary rocks that locally parallels inferred bedding (S0). Based on this premise and the general observation that layered rocks display large-scale folding patterns formed by subsequent deformation events, the composite bedding–foliation fabric (S0-1) is inferred to represent the earliest deformation event in the area (i.e. D1) and to have formed before the major folding episodes.

Two major folding systems are recognised at Nunasvaara (cf. Eriksson & Hallgren 1975). These are (1) asymmetric, approximately north-northwest to north-northeast-orientated, moderate to tight, gently to moderately-plunging, upright folds; and (2) symmetric, east-southeast to east-northeast-orientated, open to gentle, steeply plunging (sub-vertical) folds (Fig. 8). Eriksson & Hallgren (1975) tentatively suggested the latter folds represent the earlier phase of folding. Based on refold patterns derived from structural lineament analysis of reprocessed ground geophysical data and outcrop structural features (Fig. 8A–E), we preliminarily interpret the north-trending folds as the earlier fold system, here designated F2 (D2 event), whereas the gentler, east-trending and steeply plunging folds formed later (F3 folds during D3). However, the possibility that F2 folds have refolded earlier, approximately E–W-aligned, upright and horizontal F1 folds, is suggested by the domical, non-cylindrical nature of some F2 folds (Fig. 8B–C). Overall, the interaction and overprinting of F2 and F3 folds (and potential earliest F1 folds) developed numerous fold interference patterns across the area. The largest expression of this is an approximately 5 × 6 km, antiformal domical structure, here named the *Nunasvaara dome* (Fig. 8A).

The Nunasvaara dome has an elongate, north–south-orientated oblate form, centred on a doubly-plunging, non-cylindrical, F2 antiform (Figs. 2 & 8). The domical outline is clearly delineated by folding patterns on geophysical anomaly maps and is reinforced by compositional and rheological contrasts between metasedimentary and meta-igneous rock layers (e.g. Figs. 2C & 8A). In particular, the graphite schist horizon hosting the Nunasvaara graphite deposit (i.e. *Nunasvaara member*) acts as an important strain "marker horizon", which discontinuously curves around the domical body, highlighting its oblate form (Fig. 8A). Moreover, moderately to steeply plunging F2 and F3 fold axes and mineral lineations from across the study area highlight how linear structures generally record axial-type symmetry, concomitant with a radiating, dome-like pattern following fold interference (Fig. 8C).

Locally, the domical shape is disrupted in the west and north by distinct refold patterns (Figs. 2 & 8).

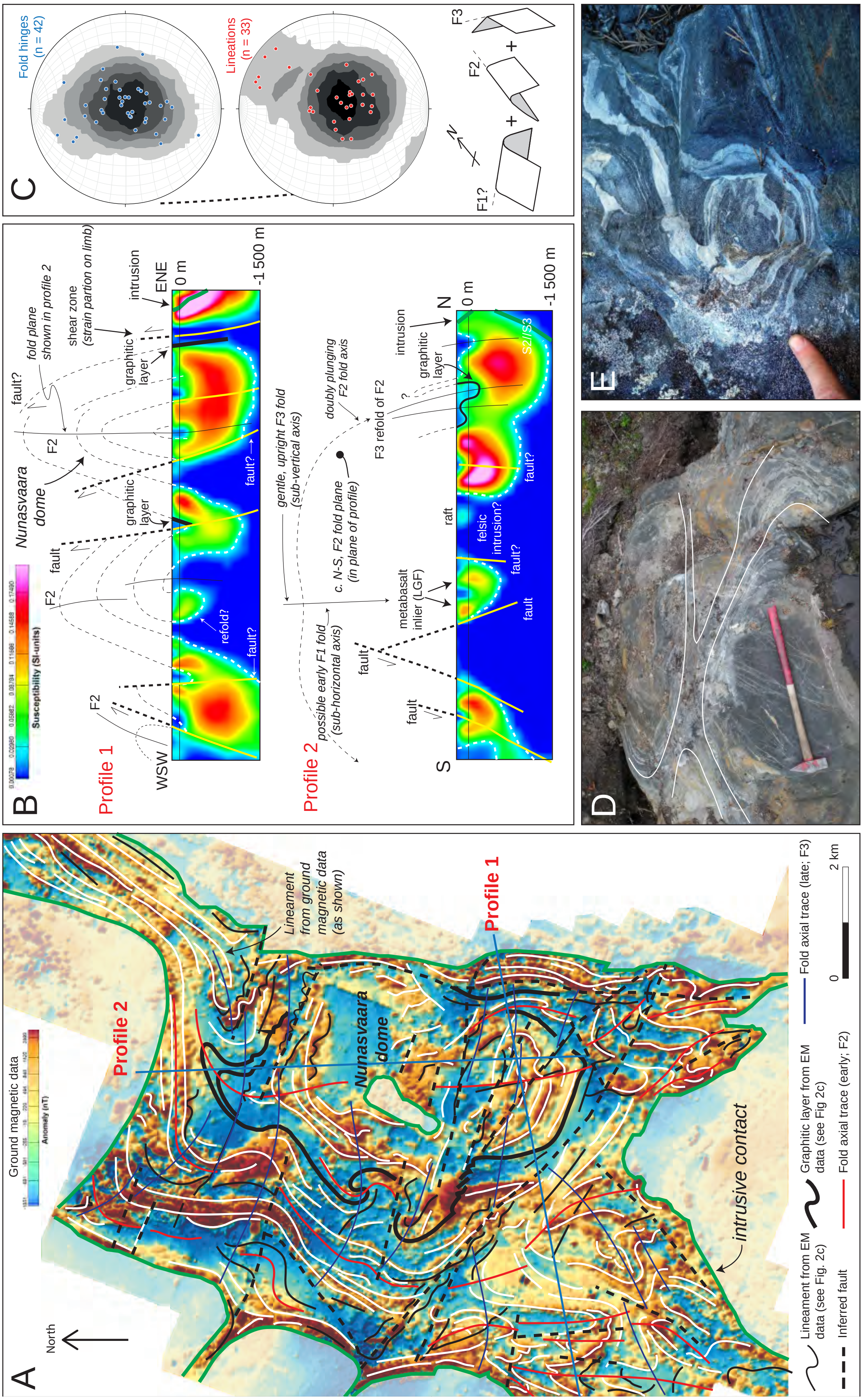

A
North
Ground magnetic data
Anomaly (nT)
Profile 2
Profile 1
Lineament from ground magnetic data (as shown)
Nunasvaara dome
intrusive contact
Lineament from EM data (see Fig. 2c)
Inferred fault
Graphitic layer from EM data (see Fig 2c)
Fold axial trace (early; F2)
Fold axial trace (late; F3)
0
2 km
B
Susceptibility (SI-units)
Profile 1
WSW
ENE
0 m
-1 500 m
F2
fault
fault?
refold?
graphitic layer
Nunasvaara dome
fold plane shown in profile 2
shear zone (strain partion on limb)
intrusion
gentle, upright F3 fold (sub-vertical axis)
c. N-S, F2 fold plane (in plane of profile)
doubly plunging F2 fold axis
F3 refold of F2
possible early F1 fold (sub-horizontal axis)
Profile 2
S
N
metabasalt inlier (LGF)
raft
felsic intrusion?
S2//S3
C
Fold hinges (n = 42)
Lineations (n = 33)
F1?
F2
F3
D
E

◀ Figure 8. Structural geology of the Nunasvaara area. **A.** Ground magnetic anomaly map with interpreted structural lineaments. Solid black lines and graphitic layers are derived from the slingram data shown in Figure 2C. **B.** Two-dimensional magnetic susceptibility models along profiles lines 1 and 2 (shown in A), with associated structural interpretations. Profile 2 highlights the position of metabasaltic rocks of the Lower greenstone formation (LGF) in the core of an approximately N–S-aligned, antiformal dome-type structure. **C.** Equal-area stereonets with plotted points for fold axis and lineation orientations from across the study area. These data, displaying axial-like symmetry, corroborate the presence of non-cylindrical, domical structures, formed by the interaction of two or three overprinting folding events (sketch). **D.** Outcrop view to the south-southeast of an "egg box"-type fold interference pattern in a laminated metatuff. The hammer head is 15 cm long. E. View of dome-like pattern preserved in a laminated metatuff. Top is to the northeast.

In the west, a west-northwest-orientated, steeply west to northwest-plunging F2 fold hosts the Nunasvaara graphite deposit along its hinge area and southwest limb (Fig. 8A). In the north, the axis of a northward-plunging F2 fold is deflected towards the northeast by an east-trending F3 fold. Beyond the tightening hinge zone of the refolded F2 fold, the greenstones become stretched and transposed into a curvilinear, northeast-trending composite deformation zone (Fig. 8A–B). Overall, bedding appears squeezed and channelled between two large intrusions, while locally, bedding and F2 fold traces appear deflected, indented and locally truncated by a c. 1.8 Ga granite (Figs. 2B & 8A). In contrast, F3 fold traces tend to curve parallel to the contact with the granitoid. This suggests F3 folding may have been synchronous with, or slightly predate, the c. 1.8 Ga phase of granitic magmatism. Further refolding patterns are evident in the southwest of the study area (e.g. Type I of McClay 1987) from structural lineament patterns derived from magnetic anomalies (Fig. 8A).

The layered greenstone sequence (including metadoleritic sills) extends outward along the western and eastern flanks of the Nunasvaara dome. On the western limb, the most continuous stratigraphic sequence is preserved (corresponding to the stratigraphy determined along profile lines X–X', Y–Y' and Z–Z', Fig. 2A–B). In contrast, the eastern limb is truncated by a steeply east-dipping, north to north-northeast-trending, composite deformation zone (Fig. 8A–B). Here, shearing and faulting have juxtaposed a narrow zone of graphitic schist (*Upper sedimentary formation*) against a tapering slice of metatuff (*Upper greenstone formation*). This apparent superimposition, combined with asymmetric lineament patterns and magnetic anomaly dip orientations (Fig. 8A–B), indicates mainly top-to-the-west thrusting, with a possible dextral-oblique component (i.e. reverse-oblique shearing or faulting). Strain partitioning along the eastern limb of the dome may have contributed to the focused deformation occurring along this relatively narrow, localised zone. An additional aspect is how bedding on the eastern limb is intruded and partly deflected by a foliated, c. 1.9 Ga, gabbroic to dioritic pluton (Fig. 8A). Syn-tectonic emplacement of this intrusion may have contributed to focused zones of deformation along its western margin.

Magnetic susceptibility inversion modelling (to a depth of 1.5 km) and structural lineament analysis of geophysical anomaly data have facilitated further assessment of the nature and geometry of the Nunasvaara dome (Fig. 8A–B). A preliminary interpretation of Profile 1 (west-southwest-aligned, Fig. 8A) indicates steeply east-northeast-dipping anomalies in the east and steeply west-southwest-dipping anomalies in the west. Correspondingly, the southern part of the dome consists of an asymmetric, weakly west-verging, upright F2 fold. In contrast, at the western end of the profile, lower amplitude upright F2 folds verge to the east. The narrow deformation zone along the eastern limb of the Nunasvaara dome is steeply east-dipping (Fig. 8B, Profile 1).

Profile 2 (north-aligned, Fig. 8A) transects the length of the Nunasvaara dome, sub-parallel to a major F2 axial plane. This profile highlights fold interference patterns in the north, where an F2 fold is refolded and transposed into a composite S2-3 foliation (Fig. 8B, Profile 2). Where the profile transects the central part of the dome, a fault-bounded anomaly corresponds to an inlier block of mafic metavolcanic rocks (metabasalt), and is inferred to represent the base of the stratigraphy at Nunasvaara (i.e. *Lower greenstone formation*). Two adjacent zones of low magnetic susceptibility (that have no known surface exposures) may represent intermediate to felsic intrusions in this central area (Fig. 8B, Profile 2).

In summary, ductile deformation patterns observed across the study area suggest the succession forms part of a broader, roughly northeast-trending composite shear zone. Locally, asymmetric F2 folding of layered units indicates shearing was mainly dextral-oblique. A conspicuous feature of the deformation geometry is the strongly distorted and partly sinuous nature of areas underlain by layered meta-volcanosedimentary rocks. These units appear to "wrap around" the core of the Nunasvaara dome, imparting a large-scale, somewhat "augen"-type pattern to the sequence. This geometry suggests the core of the dome (mainly comprising metadolerite and metabasalt) may have acted as a more competent or rigid block within the larger shear zone.

Numerous faults and fracture zones transect the Nunasvaara area, and represent a composite phase of brittle deformation (i.e. D4 event, Fig. 2A). The faults are mainly west-northwest-aligned, are subvertical, and their general orientation parallels the roughly east–west trace of F3 fold axes. Locally, D4 faults displace and truncate both F2 and F3 axial traces (e.g. southwest study area, Fig. 8). Based on structural lineament patterns (Figs. 2B & 8A), lateral fault displacements are not strongly developed and the steeply dipping faults may have facilitated mainly vertical displacements.

A major northwest-trending fault zone occurs to the south of the Nunasvaara graphite deposit and transects the southern part of the Nunasvaara dome (Fig. 2B). A fault splay of this zone trends close to and partly overlaps the southeastern extension of the Nunasvaara graphite deposit. Given that numerous graphite-bearing veins occur within the deposit, localised brittle or brittle-ductile deformation may have played an important role in enhancing the degree of graphite mineralisation at Nunasvaara (cf. Pearce et al. 2015).

Structural analysis of similar graphite mineralisation in northern Norway (Western Troms Basement Complex) indicates that complex folding and composite brittle-ductile shearing and faulting are important controls on graphite mineralisation in Palaeoproterozoic metasupracrustal rocks (Henderson & Kendrik 2003).

Geology and lithostratigraphy at Masugnsbyn (Veikkavaara greenstone group)

The Masugnsbyn area is located approximately 90 km east-southeast of Kiruna and approximately 60 km northwest of Pajala (Fig. 1B). Here, greenstones of the *Veikkavaara greenstone group* are overlain by a package of Svecofennian metasedimentary and subordinate metavolcanic rocks assigned to the *Pahakurkio* and *Kalixälv groups* (Padget 1970). The supracrustal sequence is folded into large scale anticlinal and synclinal structures. The area is best known for its skarn-type iron mineralisation and dolomite, which occur in the uppermost part of Veikkavaara greenstone group. Minor Cu-Zn-Pb, Cu-Au and graphite mineralisation also occurs in the Masugnsbyn area (e.g. Geijer 1929, Padget 1970, Witschard et al. 1972, Grip & Frietsch 1973, Niiniskorpi 1986, Frietsch 1997, Martinsson et al. 2013, 2016, Zaki 2015).

Rocks of the Veikkavaara greenstone group, predominantly consisting of mafic volcaniclastic rocks, form a V-shaped area between the villages of Masugnsbyn, Saittarova and Junosuando (Fig. 9). This distinctive pattern developed on the opposing limbs of a large-scale, roughly north-trending, upright fold, named the Saitajärvi anticline (Padget 1970). Additional folding and faulting with variable orientations developed across the area during protracted, polyphase deformation (cf. Grigull et al. 2018).

Outcrop exposure of greenstone-related units at Masugnsbyn is generally poor (< 1% by area). The greenstone sequence is clearly outlined as a high-magnetic and banded sequence on the aeromagnetic map (Fig. 10A). The alternating high and low magnetic anomalies probably reflect depositional features, further accentuated by secondary-growth magnetite in distinct layers, associated with overprinting metamorphic and metasomatic alteration events.

Low-resistivity, graphite-bearing horizons in the greenstones are discernible from airborne electromagnetic measurements (Fig. 10B). A relatively conductive graphitic horizon at the stratigraphic top of the sequence marks the contact zone with overlying Svecofennian rocks, and can be traced continuously around the V-shaped structure (Fig. 8B). Locally, the graphitic horizons coincide with stratiform Masugnsbyn skarn iron mineralisation. The iron mineralisation north of Masugnsbyn forms a relatively continuous, approximately 8 km long curvilinear zone, coinciding with the uppermost part of the greenstone stratigraphy (e.g. Witschard et al. 1972, Frietsch 1997).

Supracrustal rocks at Masugnsbyn are intruded by c. 1.88 Ga early and 1.80 Ga late orogenic intrusions of mainly granitic to syenitic composition. At Masugnsbyn village a perthitic granite is in direct contact with skarn iron mineralisation (Fig. 9, Padget 1970). In the central part of the Veikkavaara greenstones a homogeneous, low-conductive rectangular area is inferred to represent intrusive rocks of gabbroic composition (Figs. 9 & 10).

The stratigraphy of the Veikkavaara greenstone group has previously been assessed by Padget (1970). In that account, three broad, informal subdivisions were proposed. They are (1) a lowermost approximately 2000 m thick unit of massive, basaltic greenstones (named Unit 1a); (2) an approximately 100 m thick middle unit comprising pelitic schist and quartzite (Unit 1b); and (3) an uppermost, approximately 1500 m thick composite unit of basaltic tuffs with overlying graphite schist and metacarbonate horizons (Unit 1c). Given the lack of exposure and degree of deformation, the thickness estimates proposed by Padget (1970) are probably approximations.

As part of this study, we have reassessed the stratigraphy of the Veikkavaara greenstone group. Detailed geological mapping along two profiles that equate to approximately 2000 m of stratigraphy provides the basis for our re-examination (Profiles A and B, Fig. 9). Additionally, new interpretations of reprocessed airborne magnetic and electromagnetic data (Fig. 10A–B) have been integrated with geological observations to construct a new composite stratigraphy for the area.

In summary, four new subdivisions at the stratigraphic formation level are recognised for the Veikkavaara greenstone group at Masugnsbyn. Detailed descriptions of these units incorporating new minimum thickness estimates are presented in the following subsections. As part of this work, we officially abandon the alphanumeric names used by Padget (1970) for subunits of the Veikkavaara greenstone group, and here propose new informal names that combine geographical (i.e. stratotype location) and stratigraphic unit or rank components. This approach is more consistent with formal stratigraphic nomenclature and procedures (e.g. Salvador 1994). Two of the proposed informal names retain geological qualifiers, however. The lowermost unit (previously 1a) is referred to as the *Nokkokorvanrova greenstone formation*, the middle unit (1b) as the *Suinavaara formation*; while the uppermost unit (1c) is now split into the lower *Tuorevaara greenstone formation* and upper *Masugnsbyn formation*.

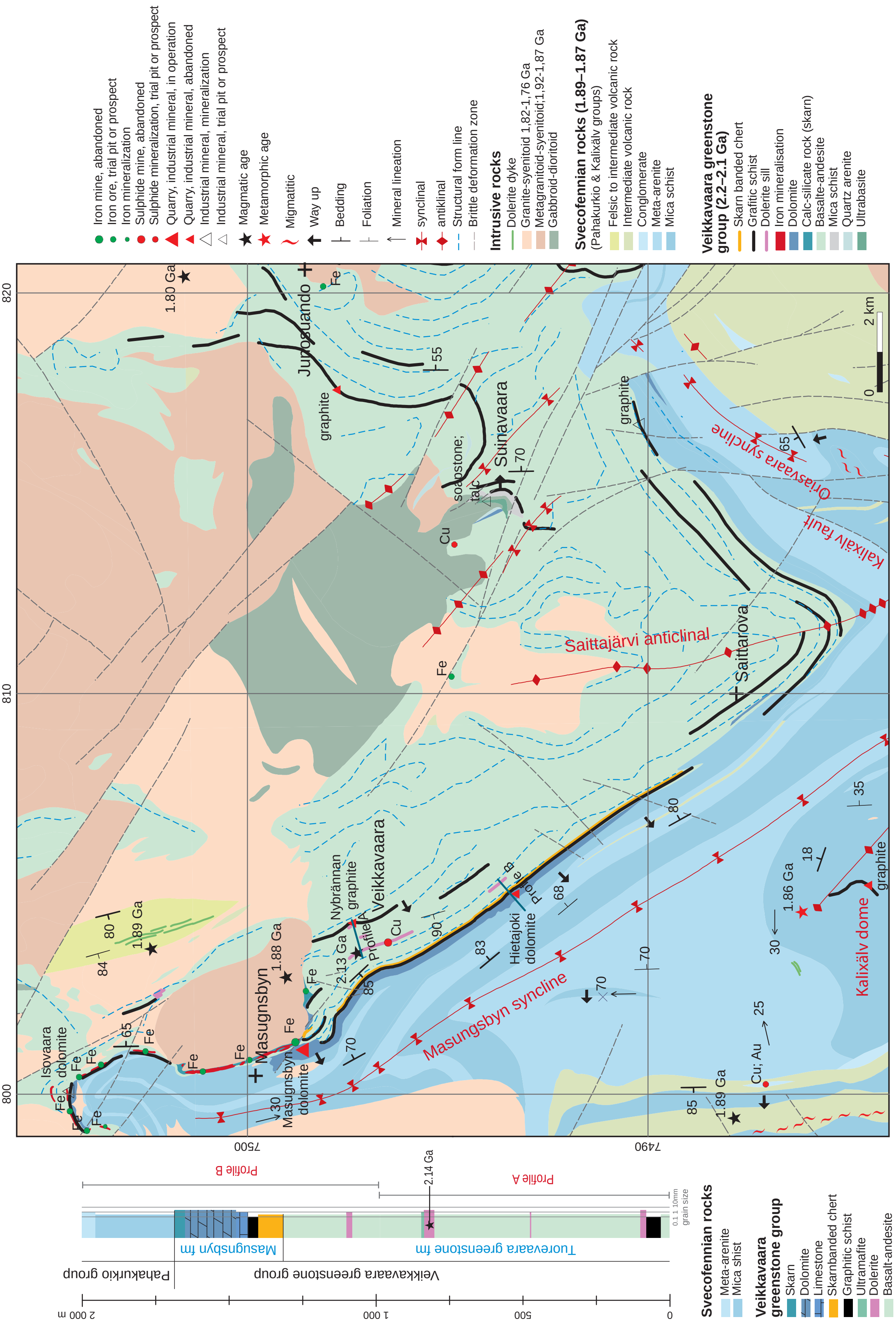

Figure 9. Geology of the Masugnsbyn area with a composite schematic stratigraphy of the Veikkavaara greenstone group, based on profiles A and B. Radiometric age determinations are from Bergman et al. (2001, 2006), Hellström et al. (2018), and this study.

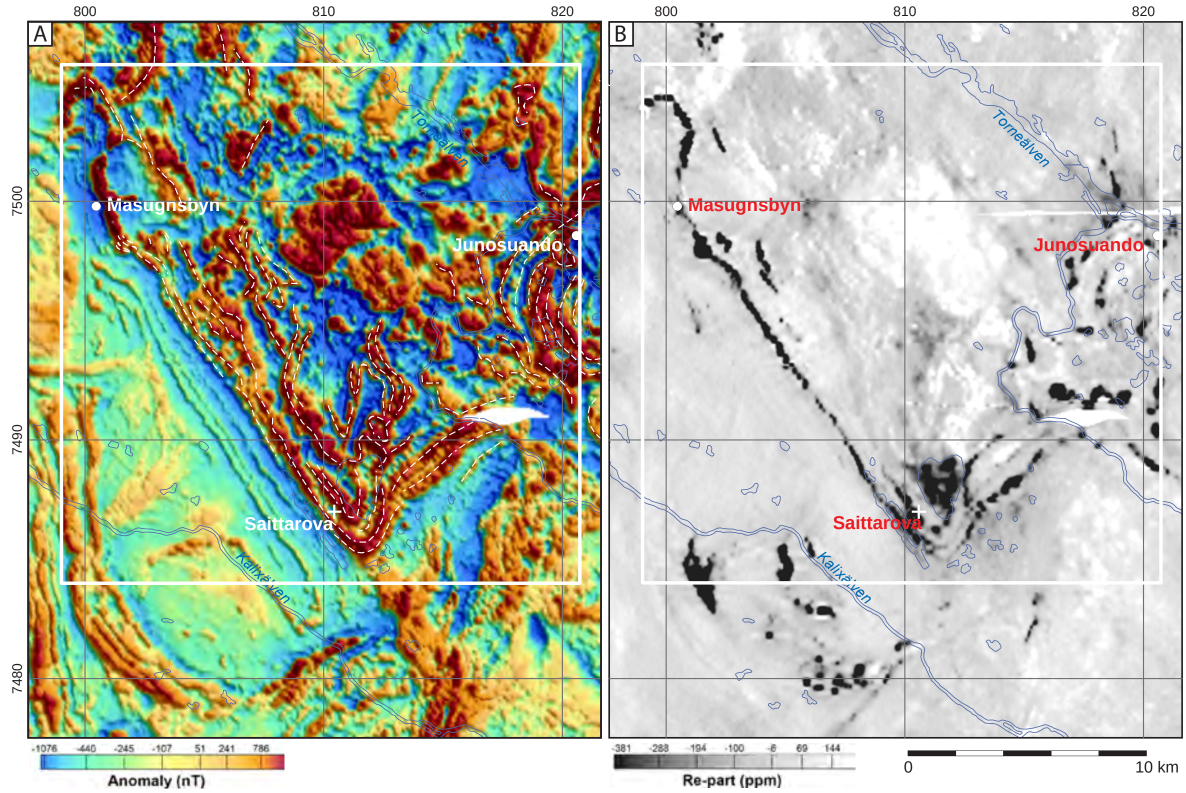

Figure 10. **A.** Airborne magnetic anomaly map for the Masugnsbyn area. It is suggested that structural form lines (broken white lines) in the Veikkavaara greenstones represent bedding in the basaltic tuffs. The white rectangle shows the extent of the geological map in Figure 9. **B.** Grey-scale, airborne electromagnetic (slingram) anomaly map (in-phase, real component) of the Masugnsbyn area. Black areas represent relatively conductive, graphite- and sulphide-rich rocks. The white rectangle shows the extent of the geological map in Figure 9.

Nokkokorvanrova greenstone formation

Mafic rocks assigned to the Nokkokorvanrova greenstone formation (NGF) are only exposed north of Suinavaara (eastern Masugnsbyn area), along the banks of the river Tärendöälven (Fig. 9, unit 1a of Padget 1970). This area represents the eastern limb of the Saitajärvi anticline. This lowermost formation predominantly consists of dark green, fine-grained, massive units, resembling mafic lavas or possibly intrusive rocks.

Banded magnetic anomaly patterns seen on the Masugnsbyn aeromagnetic map (Fig 10A) suggest the NGF extends to the west and north of Tärendöälven, but no outcrops are known from that area. Based on this interpretation, Padget (1970) estimated the (minimum) thickness of the NGF to be approximately 2 km. But a homogenous, low-conductive area in the core of the Saitajärvi anticline (Fig. 10B) suggests that parts of the core area may consist of intrusive rocks, highlighting a degree of uncertainty about the thickness estimate.

Suinavaara formation

Padget (1970) described an approximately 100 m thick metasedimentary sequence at Suinavaara (unit 1b, eastern Masugnsbyn area, Fig. 9). The sequence mainly consists of a clastic quartzite horizon with lesser pelite and metacarbonate rocks. The pelitic rocks (partly graphitic) occur at the same horizon or slightly above the quartzite. Locally, at Suinavaara, the quartzite is in contact with a marble horizon (Padget 1970).

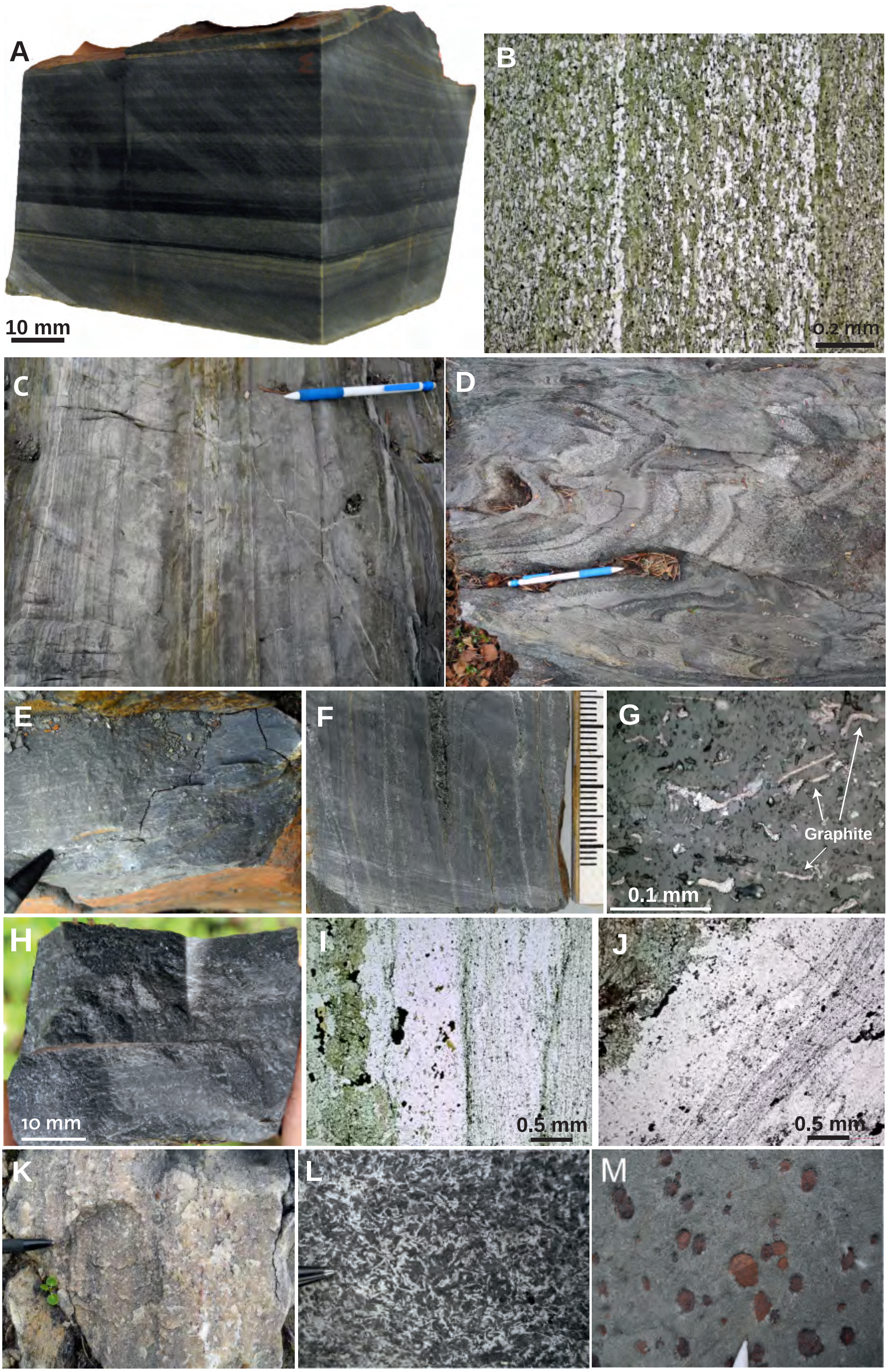

A
10 mm
B
0.2 mm
C
D
E
F
G
Graphite
0.1 mm
H
10 mm
I
0.5 mm
J
0.5 mm
K
L
M

◀ Figure 11. Rock types of the Veikkavaara greenstone group. **A.** Sawn rock sample of laminated metatuff taken from the western wall rock of the Veikkavaara Cu prospect (Tuorevaara greenstone formation) (7496490/803773). **B.** Thin section plane-polarised light (PPL) view of the laminated metatuff shown in A, predominantly consisting of layered amphibole and plagioclase feldspar. **C.** Outcrop showing the laminated to layered character of Tuorevaara greenstone formation metatuff. The pen is 15 cm long (7497085/803714). **D.** Folded mafic metatuff at Suinavaara (Tuorevaara greenstone formation), from the eastern limb of the Saitajärvi anticline (7494094/815621). **E.** Graphite schist at the Nybrännan graphite quarry, basal part of the Tuorevaara greenstone formation (7497394/804271). **F.** Graphitic schist of the Masugnsbyn formation (7498403/801505). **G.** Thin section reflected-light view of graphitic schist shown in F. **H.** Skarn-banded chert with very fine-grained, dark quartz bands alternating with diopside-rich bands (Masugnsbyn formation). **I.** Thin section cross-polarised light view of skarn-banded chert. Granular quartz (grey, right) is variably very fine- to fine-grained. **J.** PPL view of skarn-banded chert. Band of green diopside (left), alternating with quartz bands (colourless, right). **K.** Dolomitic marble from the Hietajoki quarry (7493321/805002, Masugnsbyn formation). **L.** Fine- to medium-grained metadolerite with relict subophitic texture (7497276/803517). **M.** Ultramafite with orthopyroxene megacrysts in an amphibole-rich matrix (7497209/803517). Coordinates are given in SWEREF99 TM.

Stratigraphically, the metasedimentary sequence at Suinavaara, here named the Suinavaara formation (equivalent to Unit 1b of Padget 1970), has been placed between the Nokkokorvanrova greenstone formation and Tuorevaara greenstone formation (Padget 1970). Cross-bedding in the basaltic tuffs above the Suinavaara formation indicates way-up to the east and thus support this stratigraphic interpretation (Padget 1970). Occurrence of marble and graphitic schist is otherwise a characteristic feature of the uppermost part of the Veikkavaara greenstone group. Complex folding of the metatuffs at Suinavaara probably complicates the interpretation of way-up indicators in the sequence (e.g. Fig. 11D).

Tuorevaara greenstone formation

The Tuorevaara greenstone formation (TGF) is primarily exposed in the Veikkavaara–Tuorevaara area and forms the western limb of the Saitajärvi anticline (Fig. 9). Here, the sequence mainly consists of mafic metatuffs with minor graphitic schist and metadolerite sills. The formation has an estimated thickness of approximately 1 km (cf. Padget 1970).

The metatuffs typically display planar, parallel laminae or compositionally variable layering at the mm- to cm-scale (Fig. 11A–D). Locally, subordinate cm- to m-scale layers have a more massive appearance and resemble lava flows or mafic intrusive rocks. While cross-bedded tuffaceous rocks are known at Suinavaara in the eastern Masugnsbyn area (Padget 1970), metatuffs at Veikkavaara are predominantly planar, with a parallel, laminated structure. Locally, grain size grading indicates way-up to the west-southwest.

Mineralogically, the metatuffs consist of plagioclase feldspar (An_{10-50}, Padget 1970) and green, pleochroic hornblende. Locally, elongate actinolite-tremolite crystals are the predominant amphibole phase. Minor and accessory minerals include brown, pleochroic biotite, and magnetite, pyrite, chalcopyrite and rare quartz.

Intercalated graphitic schist horizons are known from the TGF, primarily from electromagnetic surveys and exploration trenching. At Veikkavaara (Fig. 9), a layer of graphite schist is exposed at the Nybrännan graphite quarry in the easternmost part of the mapping profile at Veikkavaara (Figs. 9 & 11E). This unit possibly constitutes the same stratigraphic level as the Suinavaara formation, thus forming the upper part of a predominantly metasedimentary sequence. This interpretation provides a correlation between the graphite schist at Nybrännan and the Nunasvaara member of the Lower sedimentary formation at Nunasvaara. East of the Nybrännan quarry there are no known outcrops, but the banded magnetic anomaly pattern suggests that the greenstones continue for approximately 3 km (Fig. 10A).

The Nybrännan graphitic schist unit, estimated to be at least 50 m thick, is bordered by an approximately 20 m thick dolerite sill to the west. Locally, the horizon is inter-layered with plagioclase-rich light grey tuffite containing subordinate biotite, pale green actinolite and accessory titanite and pyrrhotite. Gerdin et al. (1990) describe the graphite-rich horizon at Nybrännan as an approximately 20 m thick, northwest-trending and sub-vertical layer containing up to approximately 40% graphite. Graphite is typically very fine-grained (approximately 0.005 mm, amorphous) and disseminated within a groundmass of microcline, quartz, plagioclase, biotite, titanite and rutile. Locally, graphite occurs in aggregates and veins of more variable grain size. Amphibole porphyroblasts (0.5–2 mm) also occur. No greenstone-type outcrops are known east of Nybrännan.

Masugnsbyn formation

The Masugnsbyn formation constitutes the uppermost part of the Veikkavaara greenstone group in the Masugnsbyn area. It mainly consists of chemically deposited metasedimentary rocks such as skarn-banded metachert (BIF-related) and calcitic to dolomitic marble with lesser graphitic schist. The thickness of the formation is estimated to be 370 m (see Profile B, Fig. 9).

The stratigraphically lowest rock unit is an approximately 80 m thick skarn-banded chert. It is dark grey and consists of alternating bands of very fine-grained to fine-grained polygonal quartz and fine- to medium-grained clinopyroxene or amphibole (Fig. 11H–J). Relatively abundant disseminated pyrrhotite and pyrite also occur (2.4 wt % S, Table 3), which are coarser within skarn bands. Minor magnetite and flakey graphite are disseminated in quartz-rich zones and locally enriched in thin seams, imparting a banded appearance. The whole-rock iron content is 17.5 wt. % Fe_2O_3t (Table 3).

A 20–30 m thick graphitic schist horizon occurs above the skarn-banded chert (Fig. 9). The unit does not crop out along Profile B (Fig. 9), but is known from electromagnetic measurements (slingram), historical exploration trenching (Fig. 10B, e.g. Gerdin et al. 1990), recent core drilling at Masugnsbyn (Zaki 2015) and a newly discovered outcrop east of the Masugnsbyn quarry. Based on these data, the graphitic unit forms a fairly continuous, approximately 10 km long, conductive layer from the Masugnsbyn dolomite quarry in the north to the village of Saittarova to the southeast (Figs. 9 & 10). Sulphide minerals and graphite associated with the underlying chert horizon may also contribute to this geophysical anomaly. In general, the graphitic schist is very fine-grained and laminated, and locally contains veins of coarser quartz, mica and amphibole, as well as thin calcite layers (Fig. 11F). It predominantly consists of quartz, feldspar, biotite, muscovite and amphibole. Accessory minerals include graphite, carbonates, Fe-oxides, sulphides and titanite. Graphite typically occurs as disseminated, very fine flakes (Fig. 11G). Historical geochemical analyses indicate whole-rock C and S concentrations ranging from 1.1 to 5.1 wt % and 1.8 to 5.2 wt %, respectively (Gerdin et al. 1990). Fairly thin layers of calcitic marble occur locally within the graphitic schist (Zaki 2015).

Stratigraphically above the graphitic schist lies a 150–250 m thick metacarbonate unit (dolomitic marble, Fig. 11K), which is exposed along Profile B at the Hietajoki dolomite quarry (e.g. Bida 1979). This unit marks the top of the Veikkavaara greenstone group. It is suggested that it forms a more or less continuous layer from Hietajoki northwards to the Masugnsbyn dolomite quarry (Fig. 9). In the latter area the dolomite horizons widens to approximately 300 m, possibly due the effects of folding (Zaki 2015). Further to the north, at Isovaara, the dolomitic horizon also crops out (Fig. 9). To the west, above the carbonate rocks, there is an andalusite-bearing mica schist of the *Pahakurkio group*, which seems to be concordant with the carbonate rocks.

At Hietajoki (Fig. 9) the metacarbonate sequence from east to west consists of (1) a 20–25 m thick lowermost unit of fine- to medium-grained calcitic marble with intercalations of fine-grained schist and skarn bands; (2) a 150–200 m thick dolomitic marble; and (3) an uppermost 30–40 m wide skarn-altered rock with tremolite and calcite. In general, bedding strikes northwest and dips steeply to the east (80–85°). The dolomitic marble is pinkish or yellowish to greyish-white. Some layers are dark grey, attributable to disseminated graphite. Mineralogically, the dolomitic marble consists of medium- to coarse-grained, polygonal to granular dolomite with minor quartz, tremolite, pyrite and limonite (after pyrite). Rare diopside, sericite, chlorite, serpentine and scapolite also occur (Bida 1979). Late-stage calcite fills fractures. The main components of the dolomite are rather constant, with 21 wt. % MgO and 30 wt. % CaO, together with some impurities resulting in 0.5–3.0 wt % SiO_2 and 0.5–1.5 wt % Fe_2O_3 (Bida 1979).

Andalusite-bearing mica schist assigned to the Svecofennian Pahakurkio group occurs to the west at Hietajoki (Fig. 9), stratigraphically above the metacarbonate rocks of the Masugnsbyn formation. In general, the attitude and orientation of this younger supracrustal sequence is concordant with the Masugnsbyn formation (cf. Hellström et al. 2018).

In summary, a mainly mafic metavolcaniclastic sequence occurs at Masugnsbyn, containing subordinate metasedimentary horizons located predominantly near the top of the stratigraphy. The package may be divided into four informal formations, and has a total thickness of approximately 3.4 km.

Greenstone-related mafic intrusions at Masugnsbyn

Like Nunasvaara, metadoleritic rocks form part of the greenstone sequence at Masugnsbyn and most commonly occur as relatively thin sills, concordant to bedding in the Tuorevaara greenstone formation (Fig. 9). Typically, they are fine- to medium-grained (0.5–5 mm), and are variably deformed and altered. Locally, metadolerites are isotropic and display relict igneous, intergranular to subophitic textures (Fig. 11L). They predominantly consist of uralitic hornblende aggregates, which fill the interstices between randomly orientated plagioclase laths. The latter are commonly recrystallised into a polygonal granoblastic texture. Subordinate minerals include biotite, magnetite and quartz.

The largest known metadolerite sill at Masugnsbyn occurs approximately 800 m along Profile A and is estimated to be 35–40 m thick (Fig. 9). Within this body, a medium-grained (1–5 mm) gabbroic pegmatite pod occurs, which was sampled for U-Pb geochronology. At the western margin of the doleritic sill, an approximately 10 m wide meta-ultramafic rock occurs. This rock consists of rounded, up to 2 cm orthopyroxene megacrysts in a fine-grained, amphibole-rich (anthophyllite) matrix (Fig. 11M). The relationship between the metadolerite and the meta-ultramafic rock is unclear.

Deformation and structures at Masugnsbyn

Metasupracrustal rocks at Masugnsbyn preserve large-scale, upright folds and steeply dipping fault zones, which mainly have northeast or northwest trends (Fig. 9, Padget 1970). A detailed assessment of geological structures and deformation events in the Masugnsbyn area is presented by Grigull et al. (2018). Hence, only a brief outline of some key structural features is given here.

In general, fold axial planes have northwest to north-northwest orientations, are steeply inclined to upright, and verge toward the west (Fig. 9). One exception is the northeast-orientated and east-verging Oriasvaara syncline, which is bounded to the northwest by the parallel-trending Kalixälv fault. Dip-slip movements along the Kalixälv fault have down-thrown the southeastern block, resulting in a major tectonic contact between the Pahakurkio and Kalixälv groups.

In the Kalixälv dome (Fig. 9), inferred bedding has low to moderate dips, which increase progressively outwards from the centre of the structure. The dome is thought to have formed by the interaction and overprinting of at least two folding events (Padget 1970, Grigull et al., 2018). Insights into polyphase folding at Masugnsbyn are best derived from magnetic anomaly patterns, which reveal a complexly folded internal structure for both the Veikkavaara greenstones and younger Svecofennian rocks (Fig. 10A). Tight to isoclinal folding, with mainly north-northwest-orientated axial planes within the Veikkavaara greenstones may possibly represent an earlier phase of folding.

Metamorphism and metasomatism

The greenstone successions in both study areas have undergone peak regional metamorphism to approximately lower amphibolite facies conditions, based on observed metamorphic mineral assemblages (cf. Padget 1970, Eriksson & Hallgren 1975). Green, pleochroic hornblende is ubiquitous in metamorphosed mafic rocks and typically forms granoblastic, blasto-ophitic and lepidoblastic intergrowths with plagioclase feldspar ± biotite (Fig. 12A–C). Commonly, it is retrogressed to actinolite, chlorite and oxyhornblende (Fig. 12B–C).

In mafic metatuffs, subhedral almandine porphyroblasts with randomly orientated inclusions (muscovite) occur locally as disseminated seams in more biotite-rich (argillaceous?) layers (Fig. 12D). Individual garnets symmetrically deflect a composite S_{0-1} fabric, while weakly developed asymmetric tails indicate limited sinistral-oblique lateral shearing and suggest overall pre- to syn-tectonic garnet growth (Fig. 12E). Additionally, compositionally banded metatuff alternates locally between darker, hornblende- or biotite-rich layers and lighter, cummingtonite ± actinolite-bearing zones (Fig. 12F).

Other key metamorphic minerals include porphyroblastic andalusite, sillimanite and cordierite in more micaceous metasedimentary units (e.g. Lower sedimentary formation, Nunasvaara; cf. Eriksson & Hallgren 1975), while carbonaceous horizons (black schist) record locally significant graphitisation (Fig. 12G). Partial dolomitisation of metalimestone horizons is probably a by-product of syn-deformation metasomatic effects as well.

At Masugynsbyn, Svecofennian meta-volcanosedimentary rocks also contain porphyroblasts of andalusite, sillimanite and cordierite consistent with lower to mid amphibolite facies metamorphism (Padget 1970). However, localised zones of migmatitic paragneiss in the south of the area suggest that possible upper amphibolite facies conditions existed locally. Here, the timing of migmatitisation is constrained to 1878 ±3 Ma (U-Pb SIMs zircon dating), and coincides with the emplacement of voluminous, mafic to felisic, syn-orogenic Svecokarelian intrusive rocks (Hellström 2018).

Quantitative metamorphic pressure-temperature (PT) modelling has not been conducted either at Nunasvaara or Masugnsbyn. However, Bergman et al. (2001) reported PT estimates for several greenstone-related units from across the region, albeit without corresponding metamorphic age constraints. A mafic metatuff (approximately 35 km northwest of Nunasvaara, *Vittangi greenstone group*) yielded PT values of 2.6 ± 0.5 kbars and 510 ± 35°C, while a meta-argillite (approximately 40 km east of Masugnsbyn, Veikkavaara greenstone group) gave values of 3.6 ± 0.6 kbars and 570 ± 20°C. Recently, Pearce et al. (2015) obtained a peak temperature range of 400–500°C for graphitisation at the Nunasvaara graphite deposit, consistent with the regional prograde burial path and the expected thermal regime for successful conversion of carbonaceous matter to graphite (e.g. Buseck & Beyssac 2014).

Overprinting metasomatic alteration affects the greenstones in a variety of styles and with varying degrees of intensity (Lynch et al. 2014). In general, a fairly early (metasomatic) sodic ± calcic assemblage (scapolite ± albite ± actinolite-tremolite) is pervasively developed in broad zones, thin bands and irregular patches and disseminations (Fig. 13). In mafic metatuffs, disseminated and aggregate scapolite porphyroblasts (≤ approximately 1 cm), associated with matrix actinolite, form planar, conformable seams, parallel to primary laminae and bedding (Fig. 13A–B). Relatively intense amphibole + clinopyroxene (diopside) ± garnet alteration (skarn) associated with stratiform–stratabound magnetite-rich horizons and metacarbonate layers is found within the upper stratigraphy (Fig. 13H).

Sodic ± calcic alteration of metadoleritic bodies locally imparts a leucocratic, speckled appearance to the rock, defining a pseudomorphic igneous texture, with scapolite typically replacing plagioclase (Fig. 13C). In extreme cases, the obliteration of primary features has produced monomineralic albitites (*leuco-diabase* of Eriksson & Hallgren 1975). Adjacent to metadoleritic bodies, breccia-like zones containing albitised wall-rock clasts in a fine-grained, magnetite + amphibole ± albite matrix are locally developed (Fig. 13D). In mafic metatuffs these features are associated with more massive (non-laminated), hornfelsed wall rock and suggest mobilisation of magnetite during localised fluid-rock interaction.

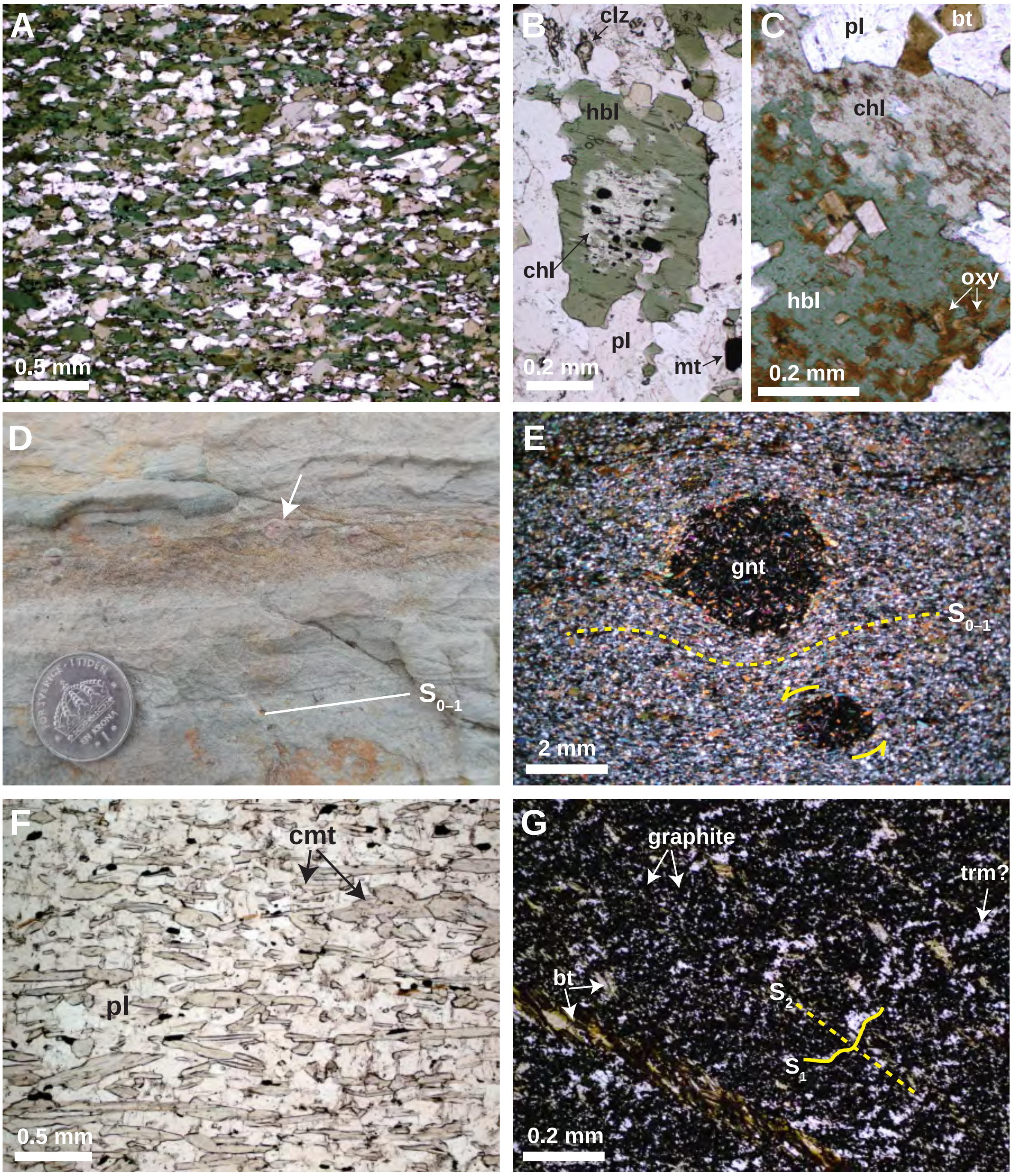

Figure 12. Representative metamorphic minerals (amphibolite facies) in greenstone units. **A.** Thin section plane-polarised light (PPL) view of lepidoblastic hornblende-plagioclase matrix in mafic metavolcanic rock. **B.** PPL view of hornblende crystaloblast retrogressed to chlorite in amphibolitic lava. **C.** PPL view of granoblastic hornblende-plagioclase ± biotite matrix in metadoleritic intrusion. Hornblende is retrogressed to chlorite and oxyhornblende. **D.** Outcrop view (orthogonal to bedding) of laminated, mafic metatuff containing almandine porphyroblasts (arrow). The coin is 25 mm in diameter. **E.** Thin section cross-polarised light view of almandine porphyroblasts in a mafic metatuff. Deflection of a composite S_{0-1} fabric indicates pre- to syn-tectonic garnet growth with a weak sinistral-oblique rotation. **F.** PPL view of lepidoblastic cummingtonite-plagioclase matrix from a more leucocratic band of a metatuff. **G.** PPL view of graphite-rich black schist cut by a biotite veinlet (bottom left corner). Biotite occurs preferentially along an S_2 crenulation cleavage that steeply transects an earlier S_1 foliation. Mineral abbreviations: bt = biotite, chl = chlorite, clz = clinozoisite, cmt = cummingtonite, hbl = hornblende, mt = magnetite, oxy = oxyhornblende, pl = plagioclase feldspar, gnt = garnet, trm = tremolite, amf = amphibole.

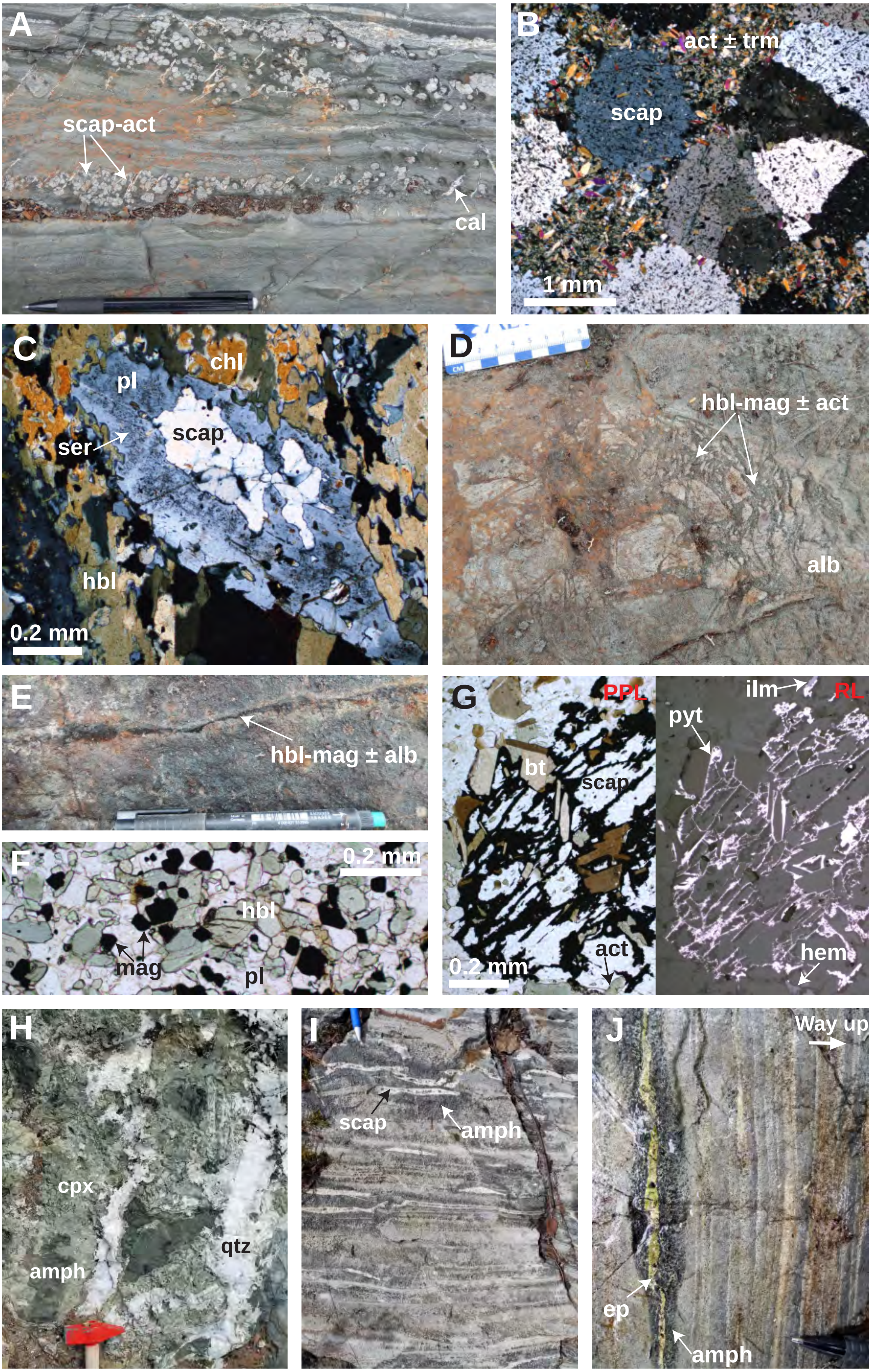
A
scap-act
cal
B
act ± trm
scap
1 mm
C
chl
pl
ser
scap
hbl
0.2 mm
D
hbl-mag ± act
alb
E
hbl-mag ± alb
F
0.2 mm
hbl
mag
pl
G
PPL
bt
scap
act
0.2 mm
ilm
RL
pyt
hem
H
cpx
amph
qtz
I
scap
amph
J
Way up
ep
amph

◀ Figure 13. Representative metasomatic alteration features. **A.** Pervasive, scapolite + actinolite ± albite alteration in a laminated mafic tuffite (Nunasvaara). Locally, scapolite forms relatively coarse, sub-rounded porphyroblasts. Calcite veinlets fill late, high-angle fractures subparallel to an earlier, spaced crenulation cleavage. The pencil is 14 cm long. **B.** Thin section plane polarised light (PPL) view of sub-rounded, scapolite porphyroblasts associated with fine-grained actinolite ± tremolite in a mafic tuffite (Nunasvaara). **C.** PPL view of anhedral scapolite replacing sericitised plagioclase feldspar in a metadolerite (Nunasvaara). **D.** Hornblende + magnetite ± actinolite ± albite breccia in an amphibolitic metatuff near the contact with a metadoleritic intrusion (Nunasvaara). **E.** Hornblende + magnetite veinlet with albite halo in a metabasalt (Nunasvaara). The pen is 14 cm long. **F.** PPL view of subhedral to euhedral hydrothermal magnetite overprinting the hornblende-plagioclase matrix of a mafic tuffite (Nunasvaara). **G.** Split PPL-reflected light views (left and right sides, respectively), showing a pyrite breccia associated with biotite, ilmenite and magnetite (replaced by hematite) in a scapolite ± actinolite-altered metabasalt (Nunasvaara). **H.** Skarn-type amphibole + pyroxene alteration associated with late quartz veins (Masugnsbyn). The hammer head is 15 cm long. **I.** Scapolite veinlets associated with amphibole in a mafic tuff (Masugnsbyn). The pencil is 1 cm thick. **J.** Epidote veinlet (late?) associated with amphibole in a laminated mafic tuff (Masugnsbyn). The pencil is 3 cm long in this view. Abbreviations: act = actinolite, alb = albite, amph = amphibole, bt = biotite, cal = calcite, chl = chlorite, cpx = clinopyroxene, ep = epidote, hem = hematite, hbl = hornblende, ilm = ilmenite, mag = magnetite, pl = plagioclase feldspar, pyt = pyrite, qtz = quartz, scap = scapolite, ser = sericite, trm = tremolite.

The sodic ± calcic assemblage also forms veins and vein-related alteration haloes across both study areas. For example, mafic metavolcanic rocks at Nunasvaara (Lower greenstone formation) contain fairly common hornblende-magnetite ± actinolite veins, with discontinuous albite ± scapolite haloes (Fig. 13E). Locally, these veins grade into relatively intense stockwork and breccia zones. Scapolite ± albite bands and veinlets are particularly abundant in mafic metatuff at Masugnsbyn (Veikkavaara upper greenstone formation). Here they trend parallel to primary laminae or are slightly discordant with en enchelon orientations and local folding, suggesting pre- to syn-tectonic formation (Fig. 13I). Late-stage epidote veins bordered by patchy amphibole haloes also occur in mafic metatuffs (Fig. 13J).

A later (overprinting) potassic ± sodic alteration (biotite + magnetite + pyrite + chalcopyrite + titanite ± K-feldspar ± carbonate) also affects the greenstone successions, although it is less pervasively developed than the sodic ± calcic assemblage. It typically occurs as overprinting disseminations or is associated with sulphide-bearing fractures, veins and narrow breccia zones and with thin aplitic veinlets and granitic dykes (Fig. 13F–G). Biotite is typically tabular and subhedral where associated with sulphide and may fill high-angle crenulation cleavages (cf. Fig. 12G). Magnetite is subhedral to euhedral and is locally martitised along irregular fracture planes.

Recent geochronology results provide a temporal framework for the overprinting metasomatism and alteration. For example, Smith et al. (2009) constrained the timing of sodic ± calcic metasomatism at Nunasvaara to 1903 ± 8 Ma (U-Pb LA-ICP-MS method) by dating titanite from a scapolitised metadioritic intrusion (e.g. Fig. 2B). Trace element analysis of the titanite revealed chondrite-normalised REE patterns (LREE-enriched with [Ce/Lu]N ≈ 8–20, negative Eu anomalies with $[Eu/Eu^*]_N \approx 0.5–0.9$), similar to those for 1.90–1.87 Ga, intermediate to felsic syn-orogenic volcanic and intrusive suites in northern Norrbotten (e.g. Blake 1990, Wanhainen et al. 2006, Edfelt et al. 2006).

Younger metasomatic-hydrothermal events are also recorded in the Nunasvaara and Masugnsbyn areas, suggesting that metasomatism-alteration was both protracted and episodic during orogenesis. For example, Bergman et al. (2006) obtained a U-Pb monazite cooling age of c. 1.86 Ga for Svecofennian andalusite mica schist at Masugnsbyn, while Martinsson et al. (2016) report U-Pb TIMS titanite ages of 1.80–1.77 Ga for sodic ± carbonate alteration associated with epigenetic-style Cu mineralisation in both areas (cf. Billström et al. 2002).

The predominant sodic ± calcic assemblage affecting the greenstones is representative of the regionally pervasive scapolite ± albite alteration that preferentially overprints mafic and intermediate metasupracrustal rocks across northern Norrbotten (e.g. Frietsch et al. 1997). The broad footprint of this hydrothermal event(s) is also manifested by positive Na, Ba, Cl and Ca anomalies in the glacial overburden (Ladenberger et al. 2012). In general, extensive sodic ± calcic metasomatism is interpreted to have formed via the circulation of halogen-rich, high-salinity basinal ± magmatic brines during early 1.90–1.87 Ga tectonothermal events (Frietsch et al. 1997, Smith et al. 2009, Smith et al. 2013). Subsequent hydrothermal activity during later orogenic stages probably led to additional magmatic and metamorphic-related alteration (cf. Bergman et al. 2006).

At deposit scales in northern Norrbotten, sodic alteration is associated with skarn-related stratabound iron, volcanic-exhalative Cu, Kiruna-type iron oxide-apatite, and hydrothermal Cu-Au mineralisation (e.g. Frietsch 1997, Martinsson et al. 1997, Masurel 2011, Nordstrand 2012). In contrast, potassic alteration is most typically associated with hydrothermal Cu-Au mineralisation (IOCG-style), particularly where links with relatively high-strain deformation zones and related structures have developed (e.g. Edfelt et al. 2005, Smith et al. 2007, Wanhainen et al. 2012, Lynch et al. 2015, Lynch et al. 2018).

Greenstone-hosted mineralisation

Four major types of mineralisation are hosted by greenstone-related rocks in the Nunasvaara and Masugnsbyn areas. These are

1. *Black schist-hosted graphite mineralisation* (e.g. Nunasvaara graphite deposit, Bergström 1987; Nybrännan graphite mineralisation at Veikkavaara, Gerdin et al. 1990).
2. *Stratiform–stratabound iron mineralisation ± sulphides* (e.g. Masugnsbyn iron deposits, Geijer 1929, Witschard et al. 1972, Frietsch 1997; Kuusi Nunasvaara iron deposit, Frietsch 1997).
3. *Stratiform dolomite* (e.g. Masugnsbyn and Hietajoki dolomite deposits; Bida 1979, Zaki 2015).
4. *Hydrothermal vein- and breccia-hosted Cu ± Pb ± Mo mineralisation* (e.g. Jälketkurkkio and Veikkavaara prospects, Martinsson et al. 2016).

(1) Graphite mineralisation: Stratiform black schist horizons containing variable graphite mineralisation form an integral part of the volcanic–sedimentary successions in both study areas. The most important example is the Nunasvaara graphite deposit in west-central Nunasvaara (Fig. 2B). A recent JORC-compliant indicated and inferred resource estimate for this deposit (using a 10% cut-off) is 9.8 Mt grading 25.3 wt. % graphitic carbon (Talga Resources 2016). Based on this assessment, graphite minerlisation at Nunasvaara is considered to be one of the world's highest grade metamorphic graphite deposit (Scogings et al. 2015).

Graphite mineralisation at the Nunasvaara deposit occurs within two subparallel, black schist horizons that form part of the hinge zone and southern limb of an approximately northwest-aligned, subvertical and upright fold (cf. Bergström 1987). The graphitic horizons dip steeply toward the southwest (75–90°) and extend laterally beyond the deposit, forming part of the Nunasvaara member (Fig. 2B). Along the limb section, both graphitic seams are weakly foliated and contain a steeply southwest-dipping, spaced S_1 fracture cleavage that tends to parallel the approximately SE-striking bedding (Fig. 14A–B). Locally, a discordant S_2 crenulation cleavage is also observed (cf. Fig. 12G).

In general, the stratigraphically upper black schist horizon is thicker and more graphite-rich compared to the lower horizon. At the deposit, both seams are divided by a metadolerite sill, which also represents the footwall unit. Where exposed, the contact between the upper black schist horizon and hanging wall mafic metatuffs appears conformable-sedimentary. Finally, a set of apparently younger (Sveckokarelian-related?) mafic dykes of uncertain origin also crosscuts the area.

In general, the mineralisation consists of dark grey, semi-massive to massive (25–50 vol. %), disseminated microcrystalline graphite (< approximately 0.08 mm, or "amorphous"-grade; cf. Taylor 2006), in a granoblastic amphibole-scapolite ± feldspar ± biotite ± pyrite matrix. Typically, graphite has a metallic, dullish blue-grey colour, is well-sorted and forms sub-rounded and tabular anhedral grains (Fig. 14C). Beyond the high-grade zone elsewhere along the Nunasvaara member, slightly coarser (0.08–0.15 mm) disseminated graphite with a flake-like morphology has developed (Fig. 14D). Relatively abundant graphite-bearing veinlets also occur at the Nunasvaara deposit (Fig. 14C; cf. Pearce et al. 2015). Their presence suggests remobilisation of graphite, producing several depositional generations and that deformation and hydrothermal events may have facilitated secondary enrichment (upgrading) of the deposit (Fig. 14C; cf. Henderson & Kendrick 2003, Pearce et al. 2015). Future research should focus on testing this hypothesis.

At the Nunasvaara deposit, minor pyrite, pyrrhotite and chalcopyrite also occur in amphibole-mica-scapolite ± feldspar ± graphite veinlets and fractures (cf. Fig. 4D). Rarely, pyrite also forms fine-grained nodular disseminations in thin, stringer-like bands. The presence of accessory sulphides associated with metasedimentary graphite mineralisation provides petrographic evidence for a relatively reduced (anoxic to euxinic) depositional environment (e.g. Mitchell 1993, Tice & Lowe 2006).

Graphite mineralisation in the Masugnsbyn area is exemplified by the Nybrännan deposit (e.g. Gerdin et al. 1990). Here, an approximately 20 m thick, roughly northwest-orientated and sub-vertical graphite schist horizon occurs and has similar characteristics to the Nunasvaara deposit (Figs. 9 & 10). The mineralisation consists of stratiform, semi-massive, fine-grained (approximately 0.005 mm) disseminated graphite, or occurs as aggregates and veins of more variable grain size.

(2) Banded and skarn-related iron: Banded iron formations occur in the stratigraphically upper parts of the Masugnsbyn and Nunasvaara greenstones, and contain iron-rich silicates or iron oxide alternating with layers of chert (Frietsch 1997, Martinsson 2004). In places these typically grade into Mg-rich iron zones, traditionally referred to as "skarn iron ores", with Mg-rich silicates typical as gangue minerals (e.g. Grip & Frietsch 1973). The close association between the banded iron formations and Mg-rich skarn iron suggests that the latter represents metamorphosed banded iron (e.g. Frietsch 1997). From a resource perspective, the skarn-style mineralization tends to be more iron-rich than the banded iron-style (Frietsch 1997). The Tornefors iron deposit at Junosuando is one example, where a Mg-rich skarn horizon containing 25–35 wt % Fe is overlain by typical BIF mineralisation with 15–25 wt % Fe (Martinsson et al. 2016). At Tornefors layers of magnetite alternate with layers of actinolite–tremolite diopside and layers of dense, very fine-grained "quartzitic" chert (cf. Damberg et al. 1974).

In general, the skarn-related mineralisation consists of massive stratabound magnetite lenses, layers and seams associated with banded and disseminated amphibole + pyroxene + pyrite + chalcopyrite ± garnet alteration (Fig. 14E–F & H). The Masugnsbyn iron mineralisation occurs in an approximately 8 km long zone, apparently concordant with the stratigraphy in the uppermost part of the Veikkavaara greenstones next to the overlying Svecofennian metasedimentary rocks (Witschard et al. 1972, Frietsch 1997). The southern iron deposits are classified as skarn iron ores, whereas Fe mineralisations to the north have more sedimentary characteristics including mm- to cm-wide, quartz + calc-silicate + magnetite, banded iron indicative of an exhalative origin (Fig. 14G). The southern skarn iron mineralisations, including the Junosuando deposit, contain concentrations of economic interest and were discovered in 1644, the first such discovery in Norrbotten (Geijer 1929, Witschard et al. 1972). The Junosuando deposit has a JORC-compliant indicated and inferred resource of 112 Mt grading 28.6% Fe (Talga Resources 2014).

A significant difference between Fe mineralisations is that the southern part is bordered by a thick dolomitic marble layer and granite, whereas no spatial association with granite or carbonate is present in the north. The close spatial connection between skarn iron ores and granite suggests that the intrusion is responsible for the skarn formation and remobilisation of iron, with higher grade and coarser grain size of the magnetite ore in the footwall next to the granite (cf. Frietsch 1997, Hellström 2018). In the southern ores, skarn minerals are intimately associated with magnetite in a steeply dipping, 70–100 m wide zone with diopside, tremolite-actinolite and phlogopite, and more rarely serpentine and chondrodite (Fig. 14F). Magnetite is irregularly distributed, but tends to be concentrated in bands. Chalcopyrite is a minor constituent, and uranium-bearing fractures are found locally (Padget 1970, Witschard et al. 1972).

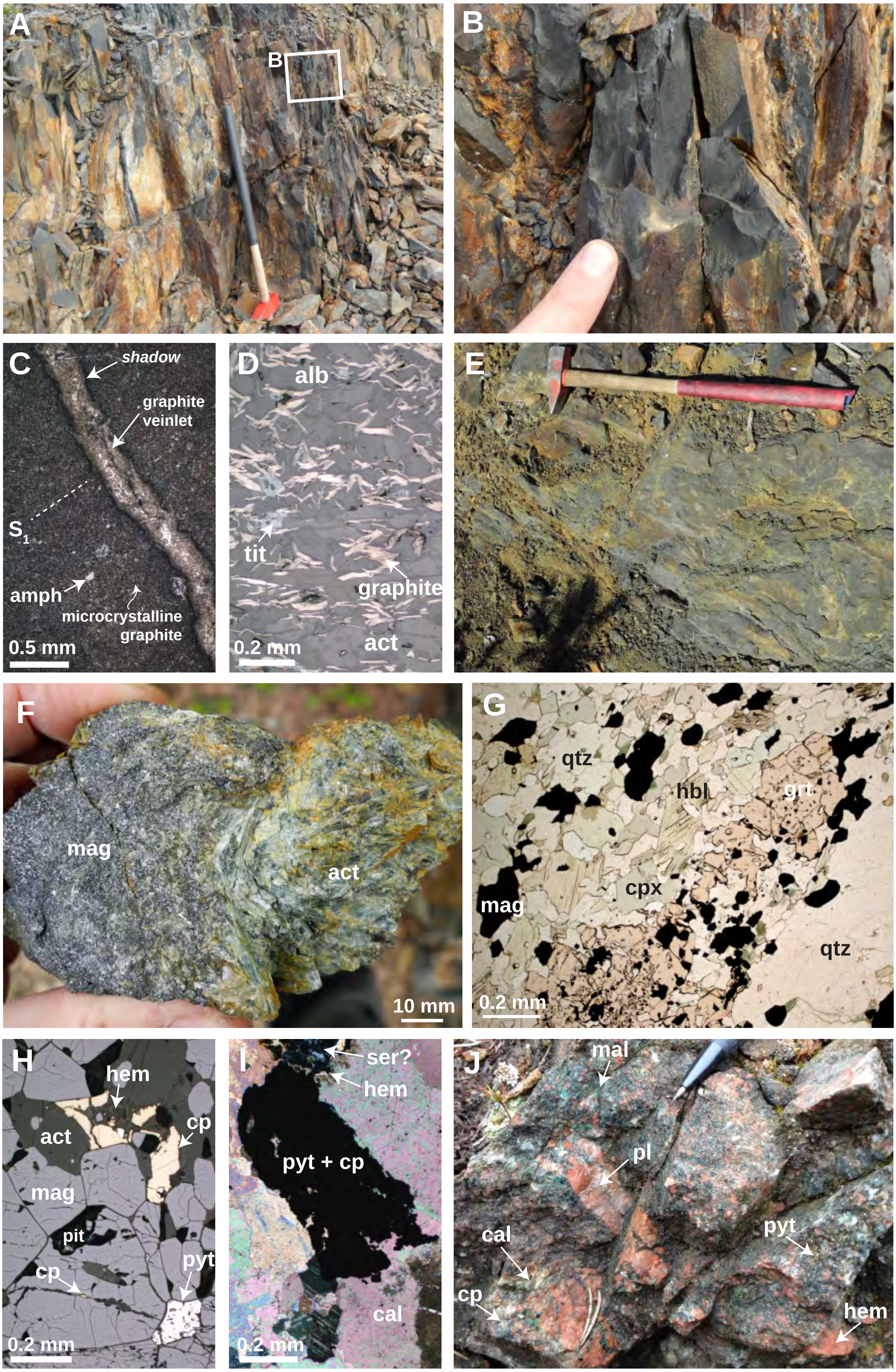
A
B
B
C
shadow
graphite veinlet
S1
amph
microcrystalline graphite
0.5 mm
D
alb
tit
graphite
0.2 mm
act
E
F
mag
act
10 mm
G
qtz
hbl
grt
cpx
mag
qtz
0.2 mm
H
hem
act
cp
mag
pit
cp
pyt
0.2 mm
I
ser?
hem
pyt + cp
cal
0.2 mm
J
mal
pl
cal
pyt
cp
hem

◀ Figure 14. Main mineralisation types in the study areas. **A and B.** Semi-massive, stratiform graphite mineralisation at the Nunasvaara deposit. Both views are toward the southeast (i.e. along strike), and show steeply southwest-dipping, graphite-rich black schist with a well-developed, composite S_{0-1} fracture cleavage. **C.** Thin section reflected light (RL) view of a graphite veinlet crosscutting a massive, fine-grained (typically < 0.05 mm), graphite mineralisation at Nunasvaara. A weak S_1 foliation has developed in the graphite. **D.** RL view of coarser, flake graphite in amphibole-feldspar-biotite schist (Nunasvaara). **E.** Semi-massive, skarn-type, stratiform magnetite associated with amphibole + clinopyroxene (Nunasvaara). Outcrop shows abundant hematite-goethite weathering. The hammer head is 15 cm long. **F.** Skarn-type iron mineralisation (magnetite) associated with intense and pervasive amphibole alteration (Masugnsbyn). **G.** Thin section PPL view of a quartz-banded iron mineralisation at the Välivaara ore field in the northern part of the Masugnsbyn iron ores, which may represent a metamorphosed banded iron formation. Bands of quartz alternate with bands rich in clinopyroxene, hornblende, garnet, magnetite ± quartz (SWEREF99 TM: 7504207/800423). **H.** RL view of granular magnetite associated with pyrite and chalcopyrite from a skarn horizon similar to that in E and F. **I.** Thin section cross-polarised light view of a calc-silicate rock (metacarbonate), showing opaque pyrite grain with minor chalcopyrite. **J.** Example of breccia-style, hydrothermal Cu mineralisation (Nunasvaara). Feldspar grains and aggregate feldspathic clasts show 'red rock'-type hematite staining. Pencil length shown is approximately 2.5 cm. Abbreviations: act = actinolite, alb = albite, amph = amphibole, cal = calcite, cp = chalcopyrite, cpx = clinopyroxene, grt = garnet, hbl = hornblende, hem = hematite, mag = magnetite, mal = malachite, pit = polish pit, pl = plagioclase, pyt = pyrite, qtz = quartz, ser = sericite, tit = titanite.

At Nunasvaara skarn-related Fe mineralisation is spatially concentrated within amphibolitic metasedimentary sequences containing minor metacarbonate layers, and occurs close to the margins of intrusive rocks (e.g. Figs. 2 & 9). While primary mineralisation is considered to have formed through exhalative processes (e.g. Frietsch 1997; cf. Klein & Beukes 1992), the close spatial association between the Fe ± sulphide mineralisation, metacarbonate rocks and granitoid intrusions suggests that exoskarn-type magmatic-hydrothermal processes have facilitated Fe ± Cu remobilisation during later, overprinting tectonothermal events (e.g. Fig. 14I; cf. Frietsch 1997).

(3) Dolomite: A marble unit at the top of the Veikkavaara greenstone group is an important dolomite resource and is currently mined by LKAB at Masugnsbyn village. The dolomite is used as an additive in iron ore pellet production. According to Zaki (2015), the total production up to 2015 has been approximately 4 Mt, with an annual production of about 0.2 Mt. The estimated resource is 28.3 Mt of first-quality dolomite (SiO_2 ≤ 3 wt %) and 3.4 Mt of second-quality dolomite (SiO_2 3–10 wt %). Geochemically, the dolomite contains fairly constant MgO and CaO concentrations (approximately 21 wt % and 30 wt %, respectively), with variable impurities resulting in elevated amounts of SiO_2 and Fe_2O_3.

(4) Hydrothermal Cu ± Pb and Mo mineralisation: Minor hydrothermal Cu ± Pb and Mo mineralisation occurs sporadically within the greenstones. For example, at the Jälketkurkkio showing in the central Nunasvaara area an approximately 25 m wide, north-trending sodic + calcic + carbonate alteration zone at the contact between a metadolerite and black schist contains minor breccia- and vein-hosted Cu-Pb mineralisations (Fig. 2B). Here, disseminated pyrite, chalcopyrite and minor galena are found in a matrix- to clast-supported, carbonate-amphibole ± magnetite breccia. In addition, minor chalcopyrite occurs in planar carbonate-amphibole veinlets. Locally, the mineralised breccia contains reddish-pink, angular clasts (volcanic?) that are hematite-stained (Fig. 14J). The clasts are typically barren and are cut by thin amphibole-carbonate veinlets similar to the breccia matrix. Breccia clasts of a more doleritic composition are also seen. In general, the breccia has a somewhat crushed and disrupted appearance, suggesting fragmentation within a zone of higher permeability.

The Veikkavaara Cu prospect (Masugnsbyn area, Fig. 9) occurs at the western border of a 30–40 m thick mafic sill that has intruded laminated metatuff of the Tuorevaara greenstone formation. Pyrrhotite and minor chalcopyrite form disseminations and patches in a pyroxene-amphibole ± biotite ± scapolite-altered zone (Martinsson et al. 2016). In the southern Nunasvaara area, minor molybdenite ± chalcopyrite in quartz veins and pegmatitic zones occur near the margins of several Lina-type granites (e.g. Äijärova showing).

PETROGENESIS OF THE GREENSTONES: PRELIMINARY U-PB GEOCHRONOLOGY, LITHOGEOCHEMISTRY AND Sm-Nd ISOTOPIC RESULTS

This section contains preliminary analytical results relating to the greenstone successions at Nunasvaara and Masugnsbyn. New U-Pb SIMS zircon ages for two metadoleritic intrusions from both areas are presented. This dating is the first application of U-Pb SIMS geochronology to Palaeoproterozoic greenstone-related rocks in northern Sweden, and the new dates currently represent the most precise and robust absolute time constraints for "Karelian" mafic magmatism in this sector of the Fennoscandian Shield. New lithogeochemical results for the various rock units from both successions are also shown. These data facilitate preliminary rock classification and lithostratigraphic comparisons. Finally, new whole-rock Sm-Nd isotopic results for the major rock units in both study areas are presented and discussed.

U-Pb SIMS zircon geochronology

U-Pb SIMS zircon dating of greenstone-related metadolerite was conducted to establish age constraints on the formation of the greenstone sequences. At Nunasvaara, a metadolerite sample (ELH130004A) was collected from a discordant body (dyke-like) intruding hanging wall metatuff close to the Nunasvaara graphite deposit (i.e. Upper greenstone formation; e.g. Fig. 2A–B). At Masugnsbyn, a metadoleritic to metagabbroic sill intruding the Tuorevaara greenstone formation metatuff was sampled and dated (FHM140006A, Fig. 9).

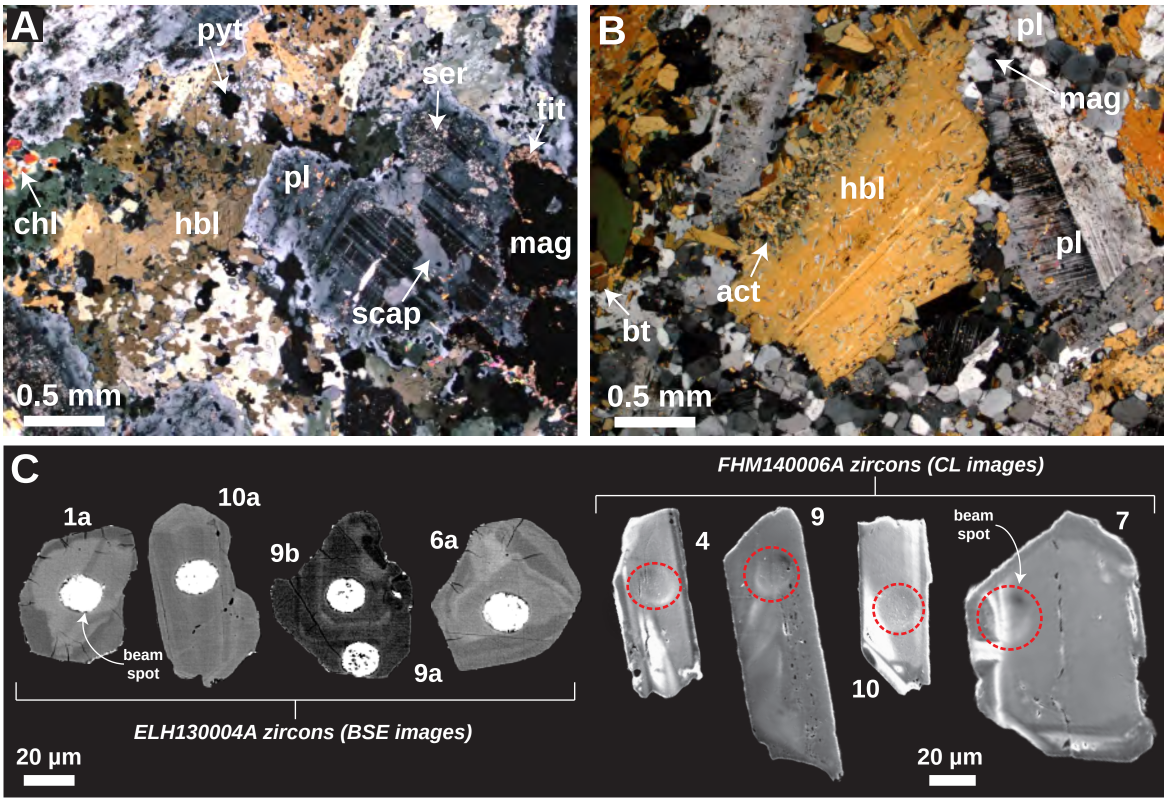

Figure 15. **A and B.** Representative thin section cross-polarised light views of metadolerite samples (ELH130004A and FHM140006A, respectively) used for U-Pb SIMS zircon dating. **C.** Back scattered electron (BSE) and cathodoluminescence (CL) images of representative zircon grains obtained from the dated samples. SIMS beam spot locations are highlighted. The adjacent numbers refer to the analytical spot numbers listed in Table 2 (final digits only). Mineral abbreviations: act = actinolite, bt = biotite, chl = chlorite, hbl = hornblende, mag = magnetite, pl = plagioclase, pyt = pyrite, scap = scapolite, ser = sericite, tit = titanite.

A summary description of the dated samples and their associated zircon fractions is presented in Table 1; representative photomicrographs and images of the dated samples and zircons are shown in Figure 15. The results of the U-Pb SIMS zircon dating are presented in Table 2, while a summary of the analytical method is presented below. Related U-Pb concordia and mean $^{207}Pb/^{206}Pb$ weighted age plots are shown in Figure 16.

Table 1. Summary descriptions of the metadolerite samples used for U-Pb SIMS zircon dating.

Sample	Setting	Brief description	Zircon characteristics
ELH130004A	Metadolerite dyke intruding mafic metatuff of the Upper greenstone formation (Vittangi greenstone group) at Nunasvaara (Fig. 2A–B).	Fine- to medium-grained (0.5–4 mm), granoblastic to blasto-ophitic, massive to weakly foliated, metadolerite. Essential minerals are plagioclase and hornblende, with minor biotite, clinopyroxene, ilmenite, zircon and magnetite (Fig. 15A–a). Alteration: (1) earlier, weak to moderate, patchy and disseminated scapolite + actinolite ± albite; and (2) later, moderate, disseminated and fracture-related amphibole + biotite + magnetite + pyrite + chalcopyrite + titanite ± K-feldspar ± carbonate alteration. Late chlorite and sericite replace hornblende and plagioclase, respectively.	Fine-grained (< 1 mm), anhedral to subhedral, tabular, colourless (Fig. 15C). Some grains show broad domainal to oscillatory zoning, and may have thin bright rims in CL images.
FHM140006A	Gabbro-pegmatitic pod in central part of 40 m wide dolerite sill intruding mafic metatuff of the Tuorevaara greenstone formation at Masugnsbyn (Fig. 9)	Relict igneous, medium-grained, isotropic texture with aggregates of green uralitic hornblende filling the interstices between randomly orientated plagioclase laths, which are in part re-crystallised into finer-grained polygonal, granoblastic texture (Fig. 15B). Minor to accessory minerals are biotite, actinolite (after hornblende), magnetite, quartz and zircon.	Subhedral to euhedral, prismatic zircon; many are fragmented (Fig. 15C). Most are metamict with inclusions. Homogeneous to oscillatory as well as patchy or irregular zoned crystals.

Table 2. SIMS U-Pb-Th zircon data for the dated metadolerite samples.

Spot #	U ppm	Th ppm	Pb ppm	Th/U calc[1]	$^{238}U/^{206}Pb$	±σ %	$^{207}Pb/^{206}Pb$	±σ %	Disc. % conv.[2]	Disc. % 2σ lim.[3]	$^{207}Pb/^{206}Pb$	±σ Ma	$^{206}Pb/^{238}U$	±σ Ma	$^{206}Pb/^{204}Pb$ measured	f206 %[4]
Sample ELH130004A (metadolerite, Nunasvaara)																
n5166_01a	233	215	132	0.96	2.463	1.09	0.1333	0.32	3.0	0.4	2141	6	2197	20	811639	{0.00}
n5166_02a	52	54	30	1.07	2.515	1.09	0.1332	0.68	1.0		2140	12	2158	20	80777	{0.02}
n5166_03a	318	305	181	1.00	2.480	0.96	0.1333	0.28	2.3		2143	5	2184	18	336375	{0.01}
n5166_04a	94	51	48	0.57	2.504	1.02	0.1336	0.64	1.1		2146	11	2166	19	>1e6	{0.00}
n5166_05a	79	63	43	0.81	2.535	1.13	0.1334	0.55	0.0		2144	10	2144	21	87077	{0.02}
n5166_06a	127	55	65	0.46	2.475	1.10	0.1338	0.43	2.2		2148	8	2188	20	177782	{0.01}
n5166_07a	118	125	67	1.08	2.510	1.03	0.1337	0.45	0.8		2147	8	2161	19	80717	{0.02}
n5166_08a	159	195	94	1.23	2.512	1.10	0.1335	0.39	0.9		2145	7	2160	20	70724	{0.03}
~~n5166_09a~~	~~109~~	~~3~~	~~39~~	~~0.02~~	~~3.128~~	~~1.12~~	~~0.1069~~	~~0.71~~	~~2.7~~		~~1747~~	~~13~~	~~1788~~	~~17~~	~~4852~~	~~0.39~~
~~n5166_09b~~	~~133~~	~~3~~	~~48~~	~~0.02~~	~~3.119~~	~~1.06~~	~~0.1098~~	~~0.55~~	~~-0.2~~		~~1797~~	~~10~~	~~1793~~	~~17~~	~~>1e6~~	~~{0.00}~~
~~n5166_10a~~	~~132~~	~~12~~	~~62~~	~~0.08~~	~~2.472~~	~~0.91~~	~~0.1333~~	~~0.68~~	~~2.7~~		~~2142~~	~~12~~	~~2190~~	~~17~~	~~94769~~	~~{0.02}~~
n5166_11a	268	175	147	0.72	2.426	1.06	0.1338	0.46	4.2	1.2	2149	8	2225	20	13651	0.14
SAMPLE FHM140006A (metadolerite, Masugnsbyn)																
~~n5407-01~~	~~501~~	~~1505~~	~~410~~	~~3.26~~	~~2.4662~~	~~0.90~~	~~0.1317~~	~~0.36~~	~~4.1~~	~~1.6~~	~~2121~~	~~6~~	~~2194~~	~~17~~	~~75314~~	~~0.02~~
~~n5407-02~~	~~540~~	~~2566~~	~~539~~	~~4.95~~	~~2.5196~~	~~0.90~~	~~0.1325~~	~~0.28~~	~~1.3~~		~~2131~~	~~5~~	~~2155~~	~~17~~	~~13521~~	~~0.14~~
~~n5407-03~~	~~326~~	~~141~~	~~137~~	~~0.44~~	~~2.9403~~	~~0.89~~	~~0.1145~~	~~0.38~~	~~0.9~~		~~1872~~	~~7~~	~~1887~~	~~15~~	~~78188~~	~~{0.02}~~
n5407-04	186	198	108	1.10	2.4862	0.96	0.1333	0.46	2.1		2142	8	2179	18	43476	{0.04}
n5407-05	134	143	78	1.08	2.4538	0.97	0.1331	0.55	3.5	0.4	2140	10	2204	18	34258	{0.05}
n5407-06	131	111	73	0.87	2.4786	0.97	0.1326	0.53	2.9		2133	9	2185	18	54715	{0.03}
n5407-07	143	133	80	0.93	2.5013	0.96	0.1330	0.51	1.7		2138	9	2168	18	19901	0.09
n5407-08	96	90	54	0.94	2.4958	1.04	0.1321	0.66	2.5		2126	11	2172	19	5741	0.33
~~n5407-09~~	~~454~~	~~985~~	~~318~~	~~2.21~~	~~2.4816~~	~~0.89~~	~~0.1321~~	~~0.28~~	~~3.1~~	~~0.9~~	~~2126~~	~~5~~	~~2183~~	~~17~~	~~78465~~	~~0.02~~
n5407-10	123	119	70	0.99	2.4888	0.98	0.1332	0.54	2.0		2141	9	2177	18	40051	{0.05}

Isotope values are common Pb-corrected using modern common Pb composition (Stacey & Kramers 1975) and measured ^{204}Pb.
Data rows with strikethrough lines were excluded from the concordia and mean weighted age determinations
[1] Th/U ratios calculated from $^{208}Pb/^{206}Pb$ and $^{207}Pb/^{206}Pb$ ratios, assuming a single stage of closed U-Th-Pb evolution
[2] Age discordance in conventional concordia space. Positive numbers are reverse discordant.
[3] Age discordance at closest approach of error ellipse to concordia (2σ level).
[4] Figures in curly brackets are given when no correction has been applied, and indicate a value calculated assuming present-day Stacey-Kramers common Pb.

U-Pb SIMS dating method: Zircons were obtained from a density separate of a crushed rock sample using a Wilfley water table. The magnetic minerals were removed by hand magnet. Handpicked crystals were mounted in transparent epoxy resin together with chips of reference zircon 91500. The zircon mounts were polished and, after gold coating, examined by back-scattered electron (BSE) and Cathodoluminescence (CL) imaging using electron microscopy at EBC, Uppsala University and the Swedish Museum of Natural History in Stockholm. High-spatial resolution secondary ion mass spectrometer (SIMS) analysis was carried out in November and December 2014 using the Cameca IMS 1280 at the Nordsim facility at the Swedish Museum of Natural History in Stockholm. Detailed descriptions of the analytical procedures are given in Whitehouse et al. (1997, 1999), and Whitehouse & Kamber (2005). An approximately 6 nA O^{2-} primary ion beam was used, yielding spot sizes of approximately 15 µm. U/Pb ratios, elemental concentrations and Th/U ratios were calibrated relative to the Geostandards zircon 91500 reference, which has an age of c. 1 065 Ma (Wiedenbeck et al. 1995, 2004). Common Pb-corrected isotope values were calculated using modern common Pb composition (Stacey & Kramers 1975), and measured ^{204}Pb in cases of a ^{204}Pb count rate above the detection limit. Decay constants follow the recommendations of Steiger & Jäger (1977). Diagrams and age calculations of isotopic data were made using Isoplot 4.15 software (Ludwig 2012). All age uncertainties are presented at the 2σ or 95% confidence level. After recoating with carbon, electron microscopy imaging of the dated zircons was performed to confirm the spot locations.

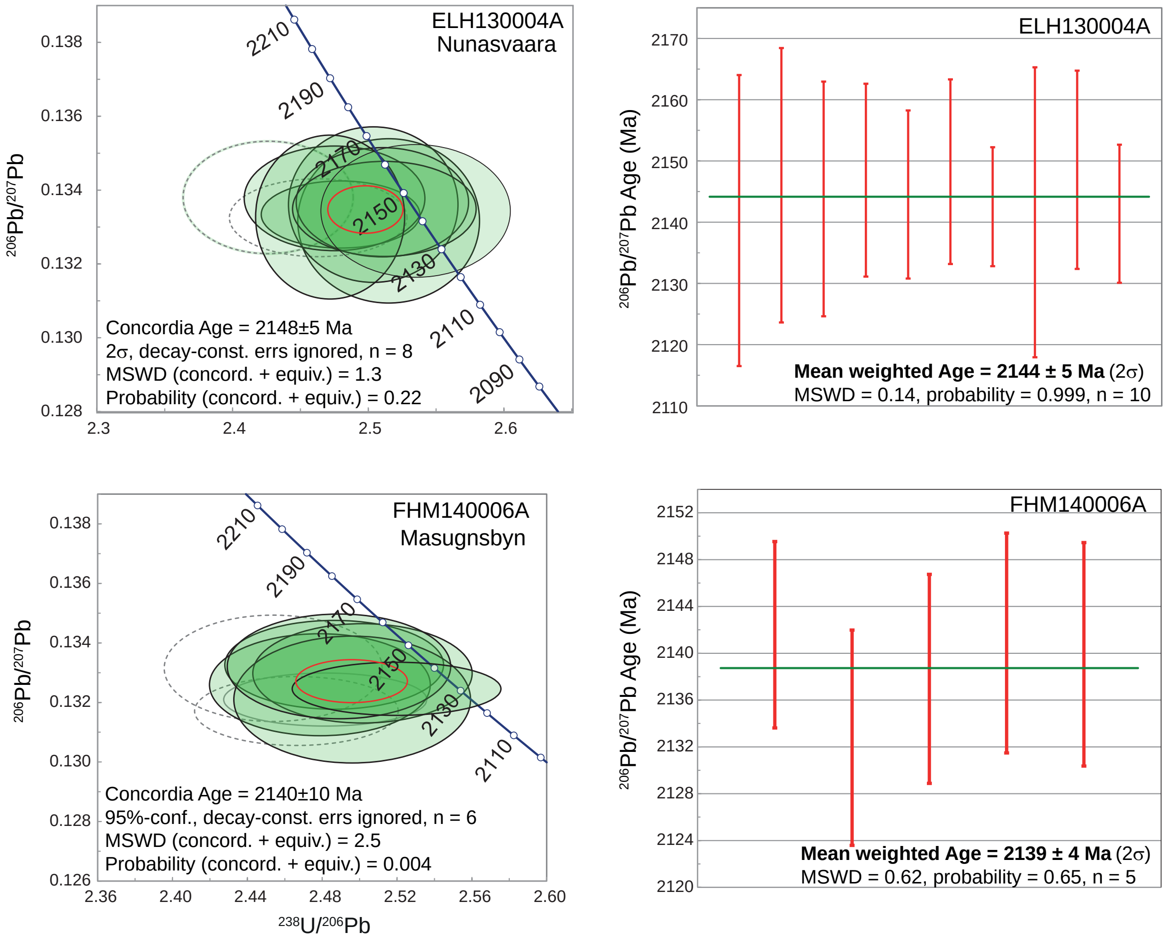

Figure 16. Tera-Wasserburg concordia diagrams (left) and mean weighted $^{207}Pb/^{206}Pb$ age plots (right) showing U-Pb SIMS zircon dating results for metadolerite samples ELH130004A (Nunasvaara) and FHM140006A (Masugnsbyn). In the concordia diagrams discordant analyses are shown with broken lines. The red ovals represent the calculated U-Pb concordia ages and associated uncertainties. See main text for discussion.

For the Nunasvaara sample (ELH130004A), 12 zircons were analysed in total. All the analyses overlap or plot close to concordia and contain fairly low amounts of uranium (52 to 318 ppm, Table 2). 10 zircons form a coherent group with apparent $^{207}Pb/^{206}Pb$ ages of 2.15–2.14 Ga and Th/U ratios of 0.46–1.23 (except spot 10a, which has a Th/U ratio of 0.08, Fig. 15C). Eight of these 10 analyses are concordant at the 2σ level and yield a U-Pb concordia age of 2 148 ± 5 Ma (2σ, n = 8, MSWD = 1.3, probability = 0.22, Fig. 16). Taken together, the mean $^{207}Pb/^{206}Pb$ weighted age for the 10 zircons is 2144 ± 5 Ma (2σ, n = 10, MSWD = 0.14, probability = 0.999). This date overlaps within error of the concordia age and is chosen as the crystallisation age of the dolerite protolith (cf. Lynch et al. 2016).

Two analyses (09a, 09b) from one of the Nunasvaara zircons record younger apparent $^{207}Pb/^{206}Pb$ ages (1.80–1.75 Ga) compared to the other 10 analyses and have relatively low Th/U ratios of 0.02 (Table 2). Analytical spot 9b is from the core domain displaying a broad oscillatory zonation, and has an apparent age of 1797 ± 20 Ma (Fig. 15C). Analytical spot 9a is from the rim domain showing a homogenous CL-grey level, and has an apparent age of 1 746 ± 26 Ma (Fig. 15C). Both dates overlap at the 2σ level. While the apparent age of the rim domain (9a) suggests a slightly younger event, this analysis yielded a relatively high amount of common lead and is thus less reliable (Table 2; e.g. Williams 1998).

The 1.80–1.75 Ga apparent ages are clearly distinct from the c. 2.14 Ga dates obtained for the rest of the zircon fraction, and may record a younger geological process. The younger ages overlap with a mixed-fraction U-Pb TIMS zircon age of 1 794 ± 24 Ma obtained from two Lina-type granites, located to the southeast of Nunasvaara (Skiöld 1988). They also coincide with 1.81–1.77 Ga U-Pb TIMS titanite ages determined for hydrothermal amphibole ± albite ± carbonate alteration in the general Nunasvaara area (Martinsson et al. 2016; cf. Smith et al. 2009).

For the metadolerite at Masugnsbyn (FMH140006A), a total of 10 zircons were analysed. These data are concordant or close to concordant at c. 2.15 Ga, except one analysis (5407-3), which records a younger age of c. 1.87 Ga (not shown in Fig. 16). This analysis has a lower Th/U ratio of 0.44, compared with 0.87 to 4.95 for the other nine spots (Table 2). Uranium concentrations for all 10 analyses range between 96 and 540 ppm (Table 2). Two analyses (5407-1, 2), placed in CL-dark grey unzoned crystals, have relatively high Th values (1 505 and 2 566 ppm, respectively), and also high Th/U ratios (3.26 and 4.95, respectively; Table 2). Additionally, analytical spot no. 9, partly placed in a CL-dark inclusion-rich domain, has a relatively high Th concentration (985 ppm). All three analyses give slightly younger $^{207}Pb/^{206}Pb$ ages (2.13–2.12 Ga) compared with the remaining six analyses, which may be attributed to Pb loss. Spots 1 and 9 also plot discordantly at the 2σ level (Fig. 16).

The six remaining zircon analyses, representing a texturally and geochemically coherent group, are concordant at the 2σ level and record a U-Pb concordia age of 2 140 ± 10 Ma (2σ, n = 6, MSWD of concordance + equivalence = 2.5, probability of conc. + equiv. = 0.004, Fig. 16). Three of these analyses are close to reversely discordant, plotting to the left side of the concordia line, which accounts for the rather poor MSWD of concordance. Excluding analytical spot 8, which has an elevated value for common Pb (f_{206}% = 0.33, Table 2), the mean weighted $^{207}Pb/^{206}Pb$ age for the metadolerite is 2 139 ± 4 Ma (2σ, n = 5, MSWD = 0.62, probability = 0.65, Fig. 16). This mean weighted age overlaps the concordia age and is chosen as the best age estimate for crystallisation of the dolerite protolith.

The new U-Pb SIMS zircon dates for the metadoleritic bodies at Nunasvaara and Masugnsbyn are geologically identical at c. 2.14 Ga, and provide minimum age constraints for the deposition of the two greenstone volcanic-sedimentary sequences. Since both successions display key lithostratigraphic similarities, are comparable in terms of their overall thicknesses, and occur relatively close to each other (based on their present-day positions), the older mean weighted age of c. 2 144 Ma represents the best estimate of a minimum age for both successions. However, the length of time between the deposition of volcanic and sedimentary material and the emplacement of the mafic hypabyssal bodies remains uncertain.

The new ages of 2 144 ± 5 Ma (Nunasvaara) and 2 139 ± 4 Ma (Masugnsbyn) for the metadolerites overlap at the 2σ precision level and thus identify a coeval mafic magmatic event in both areas. Given that the dated bodies have similar petrological, mineralogical and geochemical characteristics, the geochronology results confirm a spatially and temporally focused episode of mafic magmatism at c. 2.14 Ga in this sector of the Fennoscandian Shield (e.g. Table 1, Fig. 15A–B). This newly identified magmatic event in Norrbotten coincides with a known epoch of correlative 2.15–2.11 Ga mafic magmatism in the Finnish sector of the craton (e.g. Hanski & Huhma 2005, Huhma et al. 2013, Huhma et al. 2016). Additionally, the new dates represent the most robust and precise ages obtained thus far for greenstone-related rocks in northern Norrbotten (cf. Skiöld & Cliff 1984, Skiöld 1986). In this regard, our results highlight the utility of U-Pb SIMS zircon dating of Palaeoproterozoic hypabyssal mafic rocks to bracket volcanic and sedimentary depositional events, and its potential use in aiding stratigraphic correlations between disconnected greenstone belts in Norrbotten and across Fennoscandia.

Lithogeochemistry

Lithogeochemical analysis of representative whole-rock samples was conducted at ALS Minerals in Piteå, Sweden. Sample crushing and milling, powder digestion and measurement of major and trace element concentrations using several methods followed standard analytical procedures (see ALS methodology factsheets, www.alsglobal.com). A brief summary of the analytical techniques for the various elements is listed at the bottom of Table 3. Geochemical diagrams were plotted using GCD-Kit 3.0 (Janoušek et al. 2006).

Lithogeochemical results for visually and geochemically screened "weakly altered" greenstone-related rocks are listed in Table 3. Where more than one sample was analysed per unit, the mean value is shown. In total, 51 analyses of seven rock types from Nunasvaara and 20 analyses of nine rock units from Masugnsbyn were made. A "graphite schist" and "skarn-altered chert" sample from Masugnsbyn represent "mineralised" varieties (Table 3).

Figure 17 presents several geochemical classification plots for selected greenstone-related rock types. For the purpose of plotting, the units have been subdivided into two broad categories: coherent meta-igneous rocks (i.e. mafic metavolcanic lava, metadolerite sills and meta-ultramafic rocks), and metavolcaniclastic rocks (i.e. metatuff). Inferred metasedimentary rocks (black schist, amphibolitic pelite to schist, metacarbonate rocks, quartzite, etc.) have not been plotted.

Using the immobile trace element ratio diagram of Pearce (1996), mafic metavolcanic and metadolerite rocks from both areas form a relatively tight cluster within the sub-alkali basalt field (Fig. 17A; cf. Lager & Loberg 1990, pp. 4–5). In contrast, two meta-ultramafic rock samples fall close to the basalt-alkali basalt boundary, reflecting elevated concentrations of "incompatible" Nb relative to the other meta-igneous units (7.7 & 9.4 ppm, respectively; Table 3). For the metavolcaniclastic rocks (metatuff), all data points plot in the sub-alkali basalt field forming a relatively narrow cluster, albeit with slightly more Nb/Y variation (Fig. 17B).

► Figure 17. Lithogeochemical characteristics of Nunasvaara (green) and Masugnsbyn (blue) greenstone-type units. Data points in plots A–D represent individual analyses (not means). **A and B.** Trace element classification plot (Pearce 1996, based on Winchester and Floyd 1977) for coherent meta-igneous and metavolcaniclastic rocks, respectively. **C and D.** Jensen cation plot (Jensen 1976) for coherent meta-igneous and metavolcaniclastic rocks, respectively. **E.** Chondrite-normalised rare earth element (REE) diagram for average coherent meta-igneous rocks (cf. Table 3). Ultramafic rock patterns are based on one analysis only (as highlighted). Normalising values are from Boynton (1984). Representative REE patterns for "normal mid-ocean ridge basalt" (N-MORB) and "enriched mid-ocean ridge basalt" (E-MORB) also plotted for comparison (values from Sun & McDonough 1989). **F.** Chondrite-normalised REE diagram for average metavolcaniclastic and metasedimentary rock units. Six of the patterns from the Masugnsbyn area (highlighted) are based on one analysis only (Table 3).

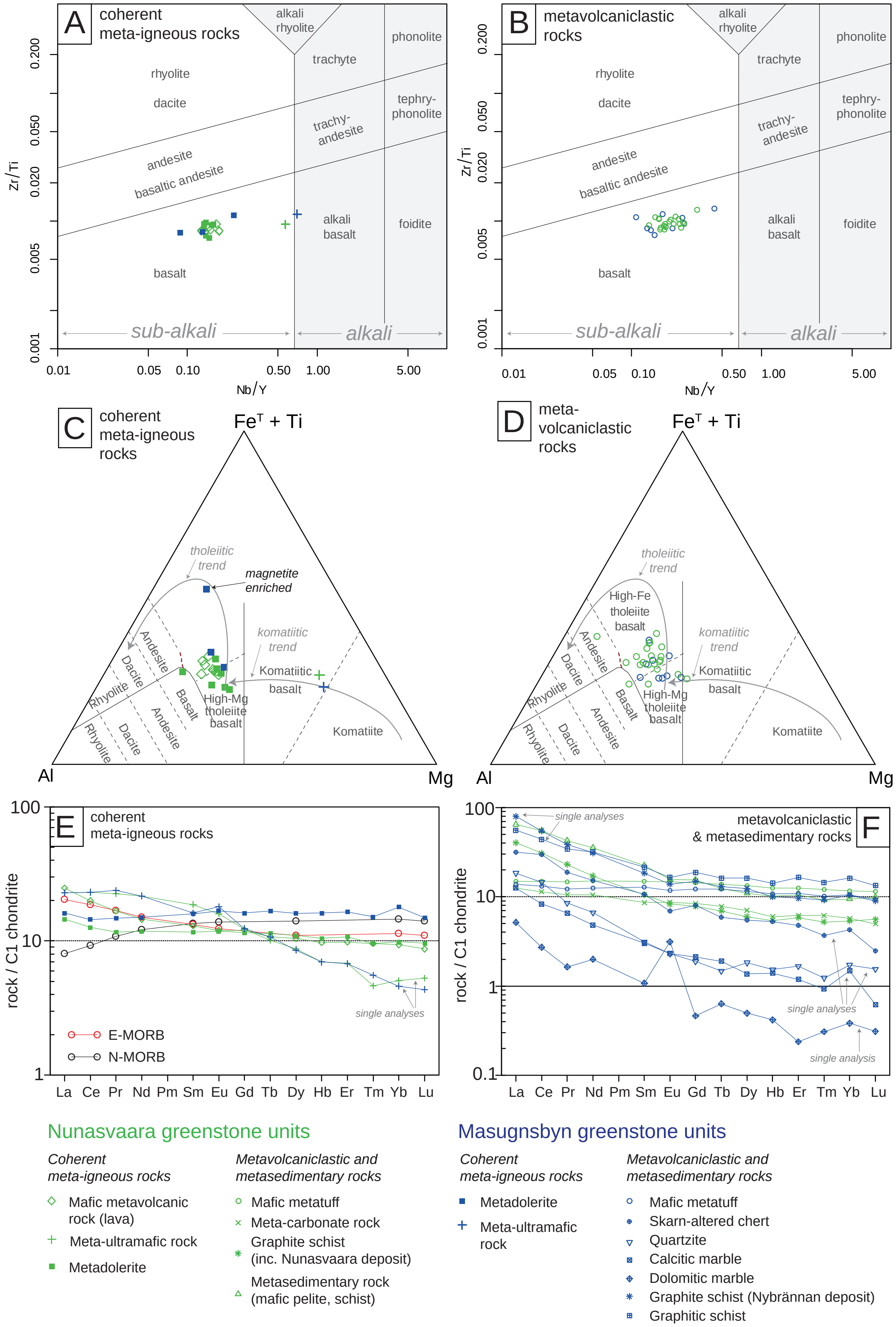
A
coherent meta-igneous rocks
B
metavolcaniclastic rocks
alkali rhyolite
phonolite
trachyte
rhyolite
dacite
tephry-phonolite
trachy-andesite
andesite
basaltic andesite
alkali basalt
foidite
basalt
sub-alkali
alkali
Zr/Ti
Nb/Y
C
coherent meta-igneous rocks
D
meta-volcaniclastic rocks
Fe^T + Ti
Al
Mg
tholeiitic trend
magnetite enriched
High-Fe tholeiite basalt
komatiitic trend
Komatiitic basalt
High-Mg tholeiite basalt
Komatiite
Rhyolite
Dacite
Andesite
Basalt
E
coherent meta-igneous rocks
F
metavolcaniclastic & metasedimentary rocks
rock / C1 chondrite
single analyses
single analysis
E-MORB
N-MORB
La Ce Pr Nd Pm Sm Eu Gd Tb Dy Hb Er Tm Yb Lu
Nunasvaara greenstone units
Coherent meta-igneous rocks
Mafic metavolcanic rock (lava)
Meta-ultramafic rock
Metadolerite
Metavolcaniclastic and metasedimentary rocks
Mafic metatuff
Meta-carbonate rock
Graphite schist (inc. Nunasvaara deposit)
Metasedimentary rock (mafic pelite, schist)
Masugnsbyn greenstone units
Coherent meta-igneous rocks
Metadolerite
Meta-ultramafic rock
Metavolcaniclastic and metasedimentary rocks
Mafic metatuff
Skarn-altered chert
Quartzite
Calcitic marble
Dolomitic marble
Graphite schist (Nybrännan deposit)
Graphitic schist

Table 3. Summary of lithogeochemical data for greenstone-related rock units at Nunasvaara and Masugnsbyn.

	Nunasvaara area							Masugnsbyn area								
Rock type	**Mafic metavolcanic rock** (lava)	**Graphite schist**	**Meta-tuff**	**Meta-ultramafic rock**	**Metasedimentary rock**	**Meta-carbonate rock**	**Meta-dolerite**	**Quartzite**	**Meta-tuff**	**Meta-ultramafic rock**	**Graphite schist**	**Graphitic schist**	**Skarn-banded chert**	**Calcitic marble**	**Dolomitic marble**	**Meta-dolerite**
Formation	LGF	LSF	UGF	USF	USF	USF		SF	TGF	TGF	TGF (Nybrännan)	MF	MF	MF	MF	
Quantity	*mean (n = 8)*	*mean (n = 8)*	*mean (n = 21)*	*(n = 1)*	*mean (n = 4)*	*mean (n = 2)*	*mean (n = 7)*	*(n = 1)*	*mean (n = 9)*	(n = 1)	*(n = 1)*	*(n = 1)*	*(n = 1)*	*(n = 1)*	*mean (n = 2)*	*mean (n = 3)*
wt. %																
SiO_2	47.8	45.6	50.1	42.7	59.1	33.7	47.5	98.1	51.9	41.8	26.4	62.1	64.5	5.5	0.63	48.4
Al_2O_3	13.94	11.02	13.57	6.30	16.16	6.96	14.24	0.79	14.13	7.62	6.65	14.20	2.61	1.02	0.07	12.57
Fe_2O_3t	13.19	1.86	14.30	14.05	9.49	9.66	12.19	0.55	14.31	14.05	13.35	1.23	17.45	0.91	0.88	18.05
CaO	9.22	2.98	8.26	12.75	3.12	21.58	10.97	0.03	6.08	10.20	7.39	3.97	7.56	50.80	32.30	8.70
MgO	6.59	3.00	6.61	16.30	3.93	10.73	7.42	0.99	7.87	20.00	4.43	3.56	2.85	1.58	21.20	5.86
Na_2O	4.98	3.85	3.71	0.77	4.70	1.53	3.36	0.05	3.47	0.78	1.84	1.29	1.52	0.23	0.01	3.24
K_2O	0.84	1.54	0.37	0.23	1.27	0.76	0.69	0.06	0.18	0.35	0.18	6.15	0.01	0.16	<0.01	0.66
Cr_2O_3	0.04	0.02	0.03	0.19	0.04	0.12	0.03	<0.01	0.03	0.20	0.03	0.03	0.01	0.01	<0.01	0.02
TiO_2	1.05	1.08	1.34	1.38	0.90	1.16	1.02	0.02	1.13	1.56	0.51	1.24	0.20	0.07	0.01	1.44
MnO	0.08	0.03	0.21	0.24	0.09	0.26	0.16	<0.01	0.24	0.33	0.06	0.07	1.26	0.15	0.08	0.28
P_2O_5	0.07	0.05	0.09	0.10	0.17	0.12	0.07	0.01	0.07	0.13	2.49	0.22	0.19	0.09	0.02	0.10
SrO	0.02	0.01	0.02	<0.01	0.02	<0.01	0.01	0.01	0.01	<0.01	<0.01	<0.01	<0.01	<0.01	<0.01	<0.01
BaO	0.01	0.03	0.01	0.01	0.05	0.03	0.01	<0.01	0.01	<0.01	<0.01	0.05	0.01	0.03	<0.01	0.02
LOI	0.70	28.28	1.20	1.33	0.76	13.36	0.98	1.12	0.64	2.10	36.40	4.97	2.98	38.80	46.50	0.30
Total	98.50	99.36	99.84	96.35	99.76	99.94	98.63	101.73	100.03	99.12	99.73	99.08	101.15	99.33	101.70	99.61
wt. %																
C	0.11	22.65	0.25	0.47	0.02	3.41	0.16	0.01	0.21	0.08	33.30	2.60	0.82	10.40	12.65	0.02
S	0.07	0.27	0.09	0.03	0.03	0.24	0.06	0.01	0.03	0.15	6.02	0.35	2.39	<0.01	0.09	0.03
Cl	0.75	0.25	0.17	0.04	0.07	0.03	0.61	NA	0.07	0.04	0.02	0.04	0.03	0.06	0.05	0.38
ppm																
Ag*	0.01	0.06	0.01	0.02	0.04	<0.01	<0.01	NA	NA	NA	NA	NA	NA	NA	NA	NA
As*	0.2	5.7	0.4	0.6	0.20	1.2	0.5	NA	NA	NA	NA	NA	NA	NA	NA	NA
Ba	62.7	248.0	61.2	70.7	330	138.5	85.4	4.6	47.5	23.9	14.4	392	58.1	283	9.5	120
Bi*	0.01	0.71	0.04	0.03	0.01	0.04	0.05	<0.01	NA	NA	NA	NA	NA	NA	NA	NA
Co**	42	4	46	78	27	56	41	1	48	93	77	6	69	4	5	51
Cr	283	156	210	1400	143	970	203	20	248	1530	190	230	30	20	10	93
Cs	0.32	1.70	0.29	0.02	0.46	0.13	0.70	<0.01	0.12	0.04	0.1	1.4	0.79	0.03	0.04	0.32
Cu**	46	36	61	137	56	101	55	2	78	102	372w	19	364	7	7	84
Ga	17.8	14.6	17.9	12.1	20	12.2	15.8	2.4	18.2	15.5	9.4	22.4	7.8	1.6	0.3	18.7
Hf	1.9	3.1	2.3	2.5	3.7	2.1	1.6	1.0	2.0	2.9	2.0	4.3	0.8	0.3	<0.2	2.2
Hg*	0.007	<0.005	0.014	<0.005	0.005	<0.005	0.005	NA	NA	NA	NA	NA	NA	NA	NA	NA
Mo**	<1	20	<1	<1	<1	<1	<1	<1	<1	<1	18	1	1	<1	<1	<1
Nb	2.9	8.7	4.5	7.7	8.6	6.0	2.9	0.2	3.9	9.4	4.9	10.4	3.6	0.8	0.8	4.2

Table 3. Continues.

	Nunasvaara area							Masugnsbyn area								
Rock type	**Mafic metavolcanic rock** (lava)	**Graphite schist**	**Meta-tuff**	**Meta-ultramafic rock**	**Metasedimentary rock**	**Meta-carbonate rock**	**Meta-dolerite**	**Quartzite**	**Meta-tuff**	**Meta-ultramafic rock**	**Graphite schist**	**Graphitic schist**	**Skarn-banded chert**	**Calcitic marble**	**Dolomitic marble**	**Meta-dolerite**
Formation	LGF	LSF	UGF	USF	USF	USF		SF	TGF	TGF	TGF (Nybrännan)	MF	MF	MF	MF	
Quantity	*mean (n = 8)*	*mean (n = 8)*	*mean (n = 21)*	*(n = 1)*	*mean (n = 4)*	*mean (n = 2)*	*mean (n = 7)*	*(n = 1)*	*mean (n = 9)*	(n = 1)	*(n = 1)*	*(n = 1)*	*(n = 1)*	*(n = 1)*	*mean (n = 2)*	*mean (n = 3)*
Ni**	91	11	90	888	62	596	96	4	98	1040	487	16	36	5	<1	44
Rb	24.6	48.5	9.9	0.6	38.8	22.3	24.5	2.5	4.9	2.6	11.1	173.0	5.3	2.4	0.5	15.6
Sb*	0.09	0.37	0.09	0.1	0.15	0.09	0.07	NA	NA	NA	NA	NA	NA	NA	NA	NA
Sc**	40	18	41	22	21	23	41	<1	38	25	20	23	3	2	<1	44
Se*	0.5	4.0	0.7	0.3	0.4	0.5	0.4	NA	NA	NA	NA	NA	NA	NA	NA	NA
Sn	1	1	1	<1	2	1	1	<1	1.00	2.00	<1	<1	<1	<1	2	<1
Sr	138.6	96.9	89.2	42.3	171.0	40.7	113	1.8	66.2	35.9	34.7	48.7	15.5	74.3	22.9	91.8
Ta	0.2	0.6	0.3	0.5	0.5	0.4	0.2	0.1	0.33	0.70	0.6	0.8	0.20	<0.1	<0.1	0.27
Te*	0.02	0.50	0.16	0.03	0.08	0.2	0.05	NA	NA	NA	NA	NA	NA	NA	NA	NA
Th	0.29	4.06	0.55	1	5.83	0.56	0.33	1.68	0.70	0.63	3.24	7.67	1.30	0.65	0.24	0.54
Tl	<0.5	NA	<0.5	<0.5	<0.5	NA	<0.5	<0.02	0.03	0.03	0.58	0.19	0.04	<0.02	<0.02	0.12
U	0.48	6.82	0.32	0.36	1.23	0.42	0.29	0.12	0.26	0.31	7.34	3.52	0.86	0.34	1.26	0.25
V	295	260	346	213	149	169	318	5	297	211	222	215	52	15	<5	325
W	<1	3	1	<1	1	2	2	<1	4	1	1	4	<1	<1	1	<1
Y	19.0	11.7	23.3	13.5	18.4	10.8	20.5	3.8	20.8	13.4	23.8	35.1	11.0	3.5	1.2	31.5
Zn**	16	20	46	107	43	18	27	3	142	176	13	8	15	7	5	66
Zr	54	121	78	78	142	79	54	34	66	106	74	154	34	10	3	77
La	7.7	12.5	4.6	2.5	20.0	3.9	4.5	5.7	4.3	7.1	24.7	17.3	9.8	3.9	1.6	5.0
Ce	16.1	24.9	12.1	18.6	44.4	9.2	10.2	11.8	10.6	18.7	44.3	35.5	24.1	6.7	2.2	11.7
Pr	2.04	2.81	1.80	2.75	5.22	1.29	1.42	1.04	1.5	2.9	4.7	4.2	2.3	0.8	0.2	1.8
Nd	8.7	10.3	9.0	13	21.3	6.3	7.1	4	7.5	13.0	18.7	19.1	9.2	2.9	1.2	9.0
Sm	2.53	2.06	2.89	3.64	4.38	1.68	2.27	0.61	2.50	3.15	3.59	4.20	2.08	0.59	0.21	3.11
Eu	0.88	0.61	1.08	1.17	1.15	0.64	0.87	0.17	0.87	1.32	1.02	1.21	0.51	0.17	0.23	1.23
Gd	3.13	2.03	3.70	3.17	4.03	2.18	2.99	0.49	3.18	3.20	3.87	4.86	2.08	0.55	0.12	4.18
Tb	0.51	0.33	0.66	0.48	0.59	0.37	0.54	0.07	0.58	0.51	0.62	0.77	0.28	0.09	0.03	0.79
Dy	3.36	1.93	4.31	2.8	3.54	2.27	3.53	0.59	3.71	2.75	3.99	5.23	1.77	0.44	0.16	5.18
Ho	0.70	0.39	0.90	0.5	0.73	0.43	0.75	0.11	0.78	0.50	0.72	1.02	0.38	0.10	0.03	1.16
Er	2.06	1.23	2.64	1.43	2.22	1.30	2.26	0.35	2.29	1.42	2.03	3.46	1.01	0.25	0.05	3.47
Tm	0.31	0.17	0.39	0.15	0.30	0.20	0.31	0.04	0.33	0.18	0.30	0.47	0.12	0.03	0.01	0.49
Yb	1.96	1.12	2.42	1.06	1.98	1.20	2.06	0.36	2.21	0.96	2.18	3.38	0.89	0.31	0.08	3.74
Lu	0.28	0.18	0.37	0.17	0.32	0.16	0.31	0.05	0.30	0.14	0.29	0.43	0.08	0.02	0.01	0.48

Major elements analysed by ICP-AES following lithium metaborate fusion and two-acid dissolution.
S occuring as S^{2-} and total C analysed using a Leco infrared analyser. Cl analysed by KOH fusion and ion chromatography.
Trace elements analysed by ICP-AES or ICP-MS following lithium metaborate fusion and two-acid dissolution, except * = aqua regia dissolution, and ** = four- acid dissolution.

< = concentration is less than detection limit as shown. NA = not analysed.
LGF = Lower greenstone formation, LSF = Lower sedimentary formation, UGF = Upper greenstone formation, TGF = Tuorevaara greenstone formation, SF = Suinavaara formation, MF = Masugnsbyn formation.

Based on the classification diagram of Jensen (1976) for sub-alkali volcanic rocks, mafic metavolcanic and metadolerite samples plot in the high-Fe and high-Mg tholeiite basalt fields, although most of the data fall in the former (Fig. 17C; cf. Lager & Loberg 1990, pp. 4–7). One relatively magnetite-rich metadolerite sample from Masugnsbyn plots above the main group, closer to the Fe^T + Ti apex. Both meta-ultramafic samples plot in the komatiitic basalt field, consistent with their relatively high MgO concentrations (approximately 16.3 & 20.0 wt. %, Table 3). These samples also contain relatively high TiO_2 values (1.34 and 1.56 wt. %) and LREE/HREE ratios (cf. Fig. 17E). Based on the classification scheme of LeMaitre et al. (2002, p. 34), they classify as picrite and meimechite, respectively. The metatuff samples have similar compositional distributions to the basaltic metavolcanic and metadolerite rocks (i.e. mainly high-Fe tholeiite, subordinate high-Mg tholeiite), and highlight the compositional similarity between the Masugnsbyn and Nunasvaara samples (Fig. 17D).

Chondrite-normalised (Boynton 1984, subscript CN) rare earth element (REE) patterns for (1) the coherent meta-igneous rocks; and (2) combined metavolcaniclastic and metasedimentary rocks are presented in Figure 17E–F, respectively. The patterns represent the mean values from Table 3, except for those from single-value determinations (as indicated).

In general, basaltic (tholeiitic) metavolcanic and metadolerite rocks from both areas form a coherent group, with enriched REE concentrations (10–25 times chondritic) and show flat to weakly $LREE_{CN}$-enriched patterns (mean $[La/Yb]_{CN}$ = 0.9–2.7, Fig. 17E). In contrast, the meta-ultramafic units (high-Mg basalts) have identical steeply sloping patterns, showing $HREE_{CN}$-depletion relative to the other meta-igneous samples and weak positive Eu_{CN} anomalies ($[La/Yb]_{CN}$ = 4.5 & 5.0, Eu/Eu* = approximately 1.1 & 1.3, respectively, Fig. 17E). These features are consistent with incompatible element source enrichment, relatively deeper or higher temperature (asthenospheric) melting, lower-degree crystal fractionation and continental contamination of true komatiitic melts (e.g. Wilson 1989, Cattell & Taylor 1990). For comparison, mean REE_{CN} patterns for N-MORB and E-MORB oceanic crust are also plotted on Figure 17E.

For the metavolcaniclastic and metasedimentary rocks (Fig. 17F), REE relative abundances (approximately 0.5 to 80 times chondritic) and chondrite-normalised patterns are more variable. For example, mafic metatuff from both areas has identical REE_{CN} patterns (flat to very weakly $LREE_{CN}$-enriched) that broadly match the patterns for basaltic metavolcanic and metadolerite rocks shown in Figure 17E. In contrast, mafic pelite to schist at Nunasvaara and graphitic schist horizons in both study areas are LREE-enriched and have weak negative Eu anomalies (mean $[La/Yb]_{CN}$ = 3.5–7.6, mean Eu/Eu* = approximately 0.8–0.9, respectively, Fig. 17E). Likewise, skarn-altered metachert and quartzite units from Masugnsbyn have similar REE systematics (though the latter has lower abundances), which are consistent with an overall continental provenance (Fig. 17F, e.g. Taylor & McLennan 1985). Finally, metacarbonate rocks from both areas (calcitic and dolomitic marbles, metalimestone to marl) show the most variability in terms of their REE abundances and normalisation patterns. In particular, the overall lower abundances and positive europium anomaly (Eu/Eu* = approximately 4.4) seen in the dolomitic marble from Masugnsbyn is not present in a calcitic marble from the same stratigraphic unit (Masugnsbyn formation). These features may reflect local-scale primary variation of the REE budget during carbonate deposition (e.g. open marine, estuarine water or hydrothermal vent fluid inputs), or represent the effects of later hydrothermal (metasomatic) fluids overprinting a higher permeability dolomitic horizon (e.g. Kamber & Webb 2001).

In summary, igneous classification plots utilising relatively immobile major and trace elements (e.g. Rollinson 1993) highlight the basaltic, predominantly Fe-tholeiitic nature of the Palaeoproterozoic metavolcanic, metadoleritic and meta-ultramafic greenstone units. This signature is underlined by the relative abundances of other major elements, such as lower values of SiO_2 and K_2O, and elevated values of MgO, total iron and CaO, compared with intercalated metasedimentary rocks (Table 3). Mafic metavolcaniclastic rocks (metatuff) are also predominantly basaltic (Fe-tholeiitic) and compositionally

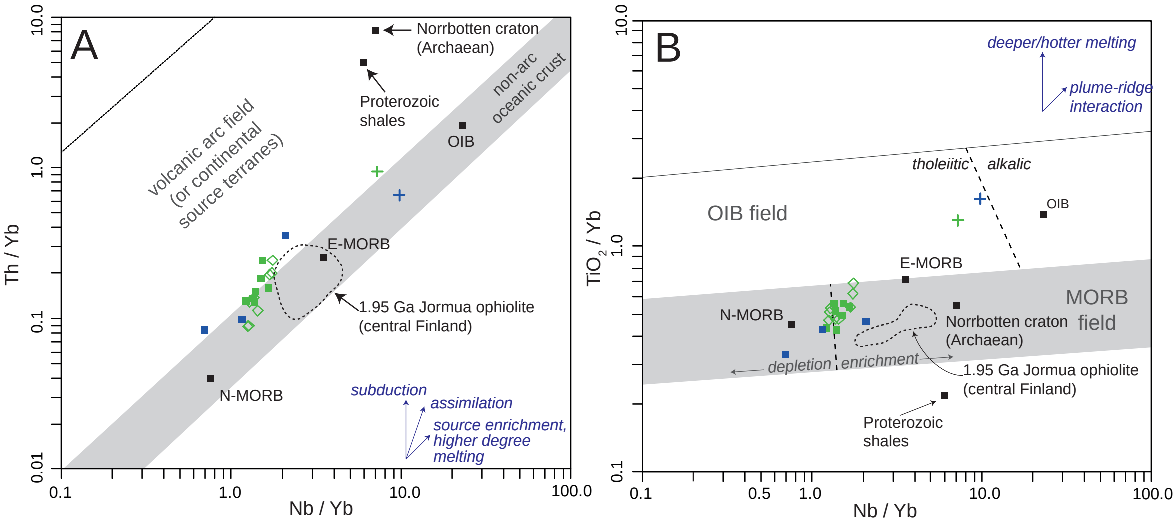

Figure 18. Nunasvaara and Masugnsbyn mafic-ultramafic meta-igneous rocks plotted on the basalt discrimination diagrams of Pearce (2008). **A.** Th/Yb versus Nb/Yb plot discriminating volcanic arc (continental) from non-arc (oceanic) basalts. See main text for discussion. **B.** TiO_2/Yb versus Nb/Yb plot discriminating spreading ridge (MORB) basalts from plume-related (OIB) basalts. See main text for discussion. Rock symbols are the same as in Figure 15. Average N-MORB, E-MORB and OIB data points are based on trace element values listed in Sun & McDonough (1989) and the TiO_2 values of Condie (1993). Average global Proterozoic shale value is from Condie (1993). Average Archaean Norrbotten craton value is based on data presented by Öhlander et al. (1987b). The dashed field for mafic rocks belonging to the 1.95 Ga Jormua ophilite (central Finland) is based on data presented by Peltonen et al. (1996).

overlap basaltic lava at Nunasvaara and the metadoleritic bodies in both study areas (e.g. Fig. 17A–B). Likewise, the weak to moderate $LREE_{CN}$-enriched REE_{CN} patterns underscore the compositional similarity between the various meta-igneous units. Given the general lithostratigraphy, the lithogeochemical results also suggest meta-igneous units in both greenstone successions may partially or wholly represent a comagmatic suite derived from a basaltic (Fe-tholeiitic) magmatic system with subordinate Mg-tholeiitic and komatiitic components (Fig. 17C–D).

Given the prevailing tectonic setting of Karelian 2.5–2.0 Ga metasupracrustal rocks in northern Fennoscandia (e.g. Laajoki 2005, Hanski 2012, Melezhik & Hanski 2012), the Pearce (2008) discrimination plot provides a means of assessing the inferred tectonic environment of the greenstone units by making a comparative assessment with major oceanic and continental crustal reservoirs (Fig. 18). In particular, the Th/Yb versus Nb/Yb plot acts as a useful first-order discriminator between compositionally variable oceanic realm (non-arc) basalts and subduction-related (arc) volcanic suites (Fig. 18A). It may also allow for less ambiguous inferences when compared with other tectonic discrimination diagrams containing superimposed or overlapping oceanic ("MORB") and volcanic arc fields (e.g. Pearce & Cann 1973, Meschede 1986; cf. Martinsson 2004).

Data points for greenstone-related basaltic metavolcanic and metadoleritic rocks mainly fall within the non-arc oceanic field between average N-MORB and E-MORB values, while a subset trends diagonally into the volcanic arc field (Fig. 18A). These data also plot close to the circular field for c. 1.95 Ga Jormua ophiolitic rocks in central Finland, which have general E-MORB geochemical signatures (Peltonen et al. 1996). If extended to the top of the diagram, the diagonal trend for the Norrbotten greenstone units intersects with the approximate positions of average Proterozoic shale and the Archaean Norrbotten craton. The latter value is a proxy for a major continental terrane underlying northern Norrbotten metasupracrustal successions. Unlike the metavolcanic and metadoleritic rocks, the meta-ultramafic samples plot within or close to the boundary of the oceanic field between average E-MORB and OIB values.

Pearce (2008) equates diagonal trends in the Th/Yb-Nb/Yb plot (Fig. 18A), extending from the oceanic to volcanic arc fields, to bulk assimilation (or contamination) by continental crustal material, primarily reflected by variable Th (and LREE) enrichment. Such assimilation may chiefly develop either when viscous magma ascends through attenuated continental lithosphere or within subduction zones. In the absence of petrological and geochemical proxies for subduction systems (e.g. general absence of calc-alkaline-type volcanic and plutonic rocks, subordinate to absent intermediate to felsic suites, no strong negative Nb or Th geochemical anomalies), and given the general tectonic regime of the Fennoscandian Shield at c. 2.1 Ga, rifting-related crustal contamination is considered a feasible explanation for the observed trend.

Figure 18B shows that data points for basaltic metavolcanic and metadoleritic rocks all fall within the oceanic (MORB) field, mostly with an enriched (E-MORB) signature close to that from Jormua ophiolite-related basaltic rocks. In contrast, both meta-ultramafic samples plot in the OIB array defined by ridge-distal oceanic island volcanism (Pearce 2008) consistent with their ultrabasic (low silica, high-Mg) geochemical signatures (cf. Fig. 17C). A weakly developed diagonal trend between all the data points is also evident. Pearce (2008) suggests that such diagonal trends in TiO_2/Yb-Nb/Yb space may result when rocks have formed during plume-ridge interactions.

Sm-Nd isotopic analysis

Whole-rock Sm-Nd isotopic analysis of 18 greenstone-related samples was conducted at the Geological Survey of Finland (GTK), Espoo, Finland. Trace element concentrations and Sm-Nd isotopic ratios were determined using the ID-TIMS method and followed the analytical procedure outlined in Huhma et al. (2012). Initial εNd values (relative to present day CHUR; Jacobsen & Wasserburg 1980) have been calculated at 2.14 Ga for the Nunasvaara samples (*n* = 11) and 2.14 Ga for the Masugnsbyn samples (*n* = 7; see Table 4, footnote No. 5). Initial εNd values are based on $^{147}Sm/^{144}Nd$ = 0.1966, $^{143}Nd/^{144}Nd$ = 0.512640 for present day CHUR (Jacobsen & Wasserburg 1980) and the decay constant $\lambda^{147}Sm = 6.54 \times 10^{-12} yr^{-1}$ (Lugmair & Marti 1978). Estimated precision for initial εNd values is ± 0.4 ε-units (2σ), except for the altered sample ELH130023D (± 2.0 ε-units, Table 4). Where listed, depleted mantle model ages (T_{DM}) utilise the Nd evolution curve of DePaolo (1981).

The results of the Sm-Nd isotopic analysis are listed in Table 4. For the Nunasvaara samples (*n* = 11), $\varepsilon Nd_{(2.14\ Ga)}$ values range from +0.4 to +4.0, with the majority (*n* = 9) falling between +1.4 and +4.0. Based on rock type, the range of $\varepsilon Nd_{(2.14\ Ga)}$ values are: basaltic metavolcanic rocks (Lower greenstone formation) = +1.4 to +4.0 (*n* = 4); basaltic metatuff (Upper greenstone formation) = +2.3 to +2.9 (*n* = 3); a sodic-altered metatuff (Upper greenstone formation) = +0.4 (n = 1); and metadolerite = +0.5 to +3.8 (*n* = 3). Four Nunasvaara samples with relatively high Sm/Nd values (0.26–0.30) yielded depleted mantle model ages (T_{DM}) ranging from 2.8–2.4 Ga (Table 4). For the Masugnsbyn samples (*n* = 7), $\varepsilon Nd_{(2.14\ Ga)}$ values range from +0.4 to +3.7. The range of values by rock type are: basaltic metatuff (Veikkavaara upper greenstone formation) = +0.4 to +3.7 (*n* = 5); metadolerite = +1.6 (*n* = 1); and meta-ultramafic rock = +2.2 (*n* = 1). Two Masugnsbyn samples with lower Sm/Nd yielded T_{DM} ages of c. 2.2 and 2.3 Ga (Table 4).

Overall, the Sm-Nd results indicate that greenstone-related units have consistently positive initial εNd signatures lying between the CHUR reference value (εNd = 0) and a LREE-depleted mantle model (εNd = approximately +3 to +4.5 at c. 2.14 Ga, Fig. 19). These signatures are characteristic of lithologic material derived from "juvenile" melts (either directly or indirectly), with a relatively short crustal residence time (e.g. Faure & Mensing 2005). However, the spread in the data and trend toward less positive initial εNd values may partly reflect the influence of overprinting metasomatic fluids, as evidenced by an $\varepsilon Nd_{(2.14\ Ga)}$ value of +0.4 for a moderate to intensely sodic-altered metatuff at Nunasvaara (Table 4).

Table 4. Whole-rock Sm-Nd results for greenstone rocks at Nunasvaara (n = 11) and Masugnsbyn (n = 7).

Sample[1]	Rock type (and unit)[2]	Sm (ppm)	Nd (ppm)	Sm/Nd	$^{147}Sm/^{144}Nd$[3]	$^{143}Nd/^{144}Nd$[4]	$\varepsilon Nd_{(t = 0\ Ga)}$	$\varepsilon Nd_{(t = 2.14)}$	T_{DM} (Ga)[5]
Nunasvaara area (t = 2.14 Ga)									
ELH130016A	Metabasalt (VGG, LGF)	2.36	6.81	0.347	0.2096 (± 8)	0.512994 (± 10)	6.9	3.4	n/a
ELH130011A	Metabasalt (VGG, LGF)	2.02	6.24	0.334	0.1962 (± 8)	0.512839 (± 25)	3.9	4.0	n/a
ELH130014D	Metabasalt (VGG, LGF)	2.74	9.02	0.303	0.1834 (± 7)	0.512601 (± 10)	-0.8	2.9	2.75
ELH130061C	Metabasalt (VGG, LGF)	2.8	10.69	0.262	0.1581 (± 6)	0.512167 (± 10)	-9.2	1.4	2.68
ELH130030A	Metatuff (VGG, UGF)	3.76	12.7	0.296	0.1793 (± 7)	0.512531 (± 10)	-2.1	2.7	2.73
ELH130010A	Metatuff (VGG, UGF)	2.93	8.2	0.245	0.2205 (± 9)	0.513092 (± 10)	8.8	2.3	n/a
ELH130006A	Metatuff (VGG, UGF)	2.82	8.53	0.331	0.2000 (± 8)	0.512838 (± 10)	3.9	2.9	n/a
ELH130023D	Metatuff (VGG, UGF)	2	6.65	0.301	0.1820 (± 7)	0.512455 (± 72)	-3.6	0.4	3.32
ELH130020D	Metadolerite	2.61	7.98	0.327	0.1981 (± 8)	0.512686 (± 10)	0.9	0.5	n/a
ELH130121A	Metadolerite	5.33	18.4	0.29	0.1750 (± 7)	0.512530 (± 10)	-2.2	3.8	2.43
ELH130025A	Metadolerite	2.11	5.31	0.397	0.2409 (± 10)	0.513434 (± 10)	15.5	3.3	n/a
Masugnsbyn area (t = 2.14 Ga)									
FHM140001B	Metatuff (VeiGG, TGF)	5.54	24.71	0.224	0.1355 (± 8)	0.511908 (± 10)	-14.3	2.5	2.21
FHM140008A	Metatuff (VeiGG, TGF)	3.5	9.27	0.379	0.2290 (± 14)	0.513115 (± 28)	9.3	0.4	n/a
FHM140009A	Metatuff (VeiGG, TGF)	2.97	8.73	0.34	0.2058 (± 12)	0.512810 (± 18)	3.3	0.8	n/a
FHM140011A	Metatuff (VeiGG, TGF)	1.73	5.23	0.332	0.2007 (± 12)	0.512873 (± 11)	4.5	3.4	n/a
FHM140018A	Metatuff (VeiGG, TGF)	2.23	7.54	0.295	0.1786 (± 11)	0.512576 (± 26)	-1.2	3.7	n/a
FHM140006A	Metadolerite	2.85	8.02	0.355	0.2147 (± 20)	0.512978 (± 16)	6.6	1.6	n/a
FHM140007A	Meta-ultra-mafic rock	3.25	12.94	0.251	0.1520 (± 9)	0.512123 (± 10)	-10.1	2.2	2.27

[1]Sample ELH130023D is an intensely scapolite-altered metatuff and the precision of the calculated $\varepsilon Nd_{2.14\ Ga}$ value is ± 2 ε-units (see main text for discussion).
[2]VGG, LGF = Vittangi greenstone group, Lower greenstone formation. VGG, UGF = Vittangi greenstone group, Upper greenstone formation. VeiGG, TGF = Veikkavaara greenstone group, Tuorevaara greenstone formation
[3]Uncertainty refers to the last digit at 2σ level.
[4]Uncertainty refers to the last two digits at 2σ level.
[5]T_{DM} = Depleted mantle model age (based on general assumptions outlined in Murphy & Nance 2002). Where n/a is shown, the evolution path does not intersect the DePaolo (1981) depleted mantle model curve. No uncertainties are reported for T_{DM} values, and any interpretation should be tentative.

Figure 19 shows initial εNd values versus $^{147}Sm/^{144}Nd$ for the greenstone units analysed (cf. Table 4). In general, the former parameter is a proxy for crustal (continental) signature, with increasing negative values (and by extension increasing crustal residence time), whereas the latter may highlight LREE enrichment or depletion characteristics of source region(s), relative degrees of fractionation in comagmatic suites, potential influence of crustal assimilation and effects of metasomatism (e.g. Beck & Murthy 1991). Figure 19 also shows Sm-Nd characteristics (shaded fields) for the depleted mantle (DM) and Archaean Norrbotten craton (ANC) calculated at c. 2.14 Ga (cf. Fig. 20). These domains represent potential source end-members for Palaeoproterozoic mafic magmatism in the northern Fennoscandian Shield.

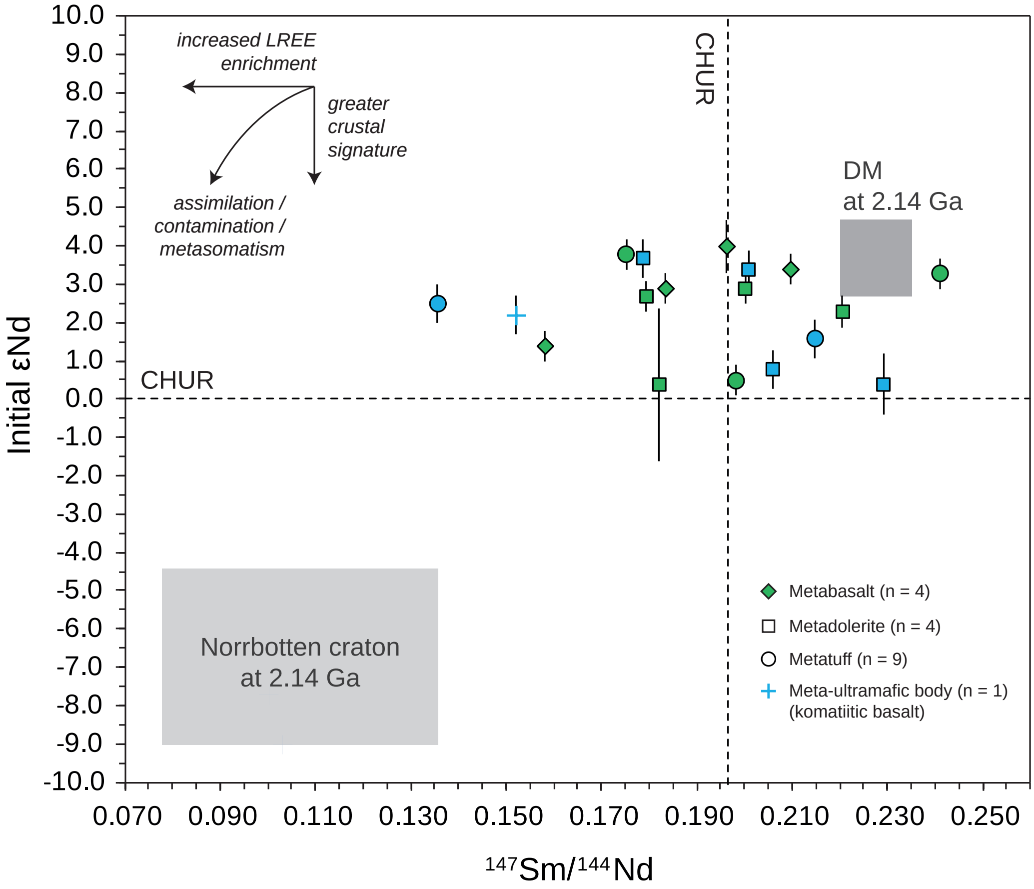

Figure 19. Initial εNd versus $^{147}Sm/^{144}Nd$ for greenstone units at Nunasvaara (green symbols) and Masugnsbyn (blue symbols). Error bars for $^{147}Sm/^{144}Nd$ not visible at the plot scale. Shaded data range (2σ spread) for a depleted mantle (DM) reservoir at c. 2.14 Ga is from Huang et al. (2013). Shaded data range for a Norrbotten craton reservoir is based on initial εNd values for Archaean orthogneisses and metagranitoids from Öhlander et al. (1987b) and Mellqvist (1999), recalculated for 2.14 Ga. The CHUR reference lines are based on $^{147}Sm/^{144}Nd$ = 0.1967 (Jacobsen & Wasserburg 1980) and εNd = 0.

Greenstone-related units generally plot as a fairly coherent group, with the majority (12) having initial εNd values that overlap the εNd signature of the DM at 2.14 Ga (Fig. 19). The remainder (6) plot between the DM and CHUR reference values. The dataset displays a broader spread in terms of $^{147}Sm/^{144}Nd$, which mainly falls between the DM range and the least evolved margin of the ANC (i.e. the higher $^{147}Sm/^{144}Nd$ margin). Overall, a somewhat indistinct mixing trend or zone of assimilation/contamination between the DM and ANC source regions is apparent. A clearer delineation of such a feature (if geologically valid) may be limited by the small number of samples, a degree of sampling bias (i.e. lack of metasedimentary units), and the relatively inadequate geochemical and isotopic constraints for the Norrbotten craton in northernmost Sweden.

In general, geological factors that may account for the observed Sm-Nd systematics of the greenstone units include (1) magma source region and corresponding LREE abundance variability (e.g. asthenospheric mantle versus sub-continental lithospheric mantle); (2) single-source LREE heterogeneity (e.g. along-axis E-MORB versus N-MORB variants); (3) melt contamination during ascent and crystallisation (i.e. assimilation of Archaean continental material); (4) magma series differentiation (affecting Sm/Nd), and (5) overprinting metasomatic-hydrothermal events, leading to LREE variability or mobility and potential disturbance of the Sm-Nd isotopic systematics (cf. Huhma et al. 1990).

The effects of metasomatic-hydrothermal fluids in the Nunasvaara and Masugnsbyn areas have been documented in this study and elsewhere (e.g. Smith et al. 2009). The ability of such overprinting events

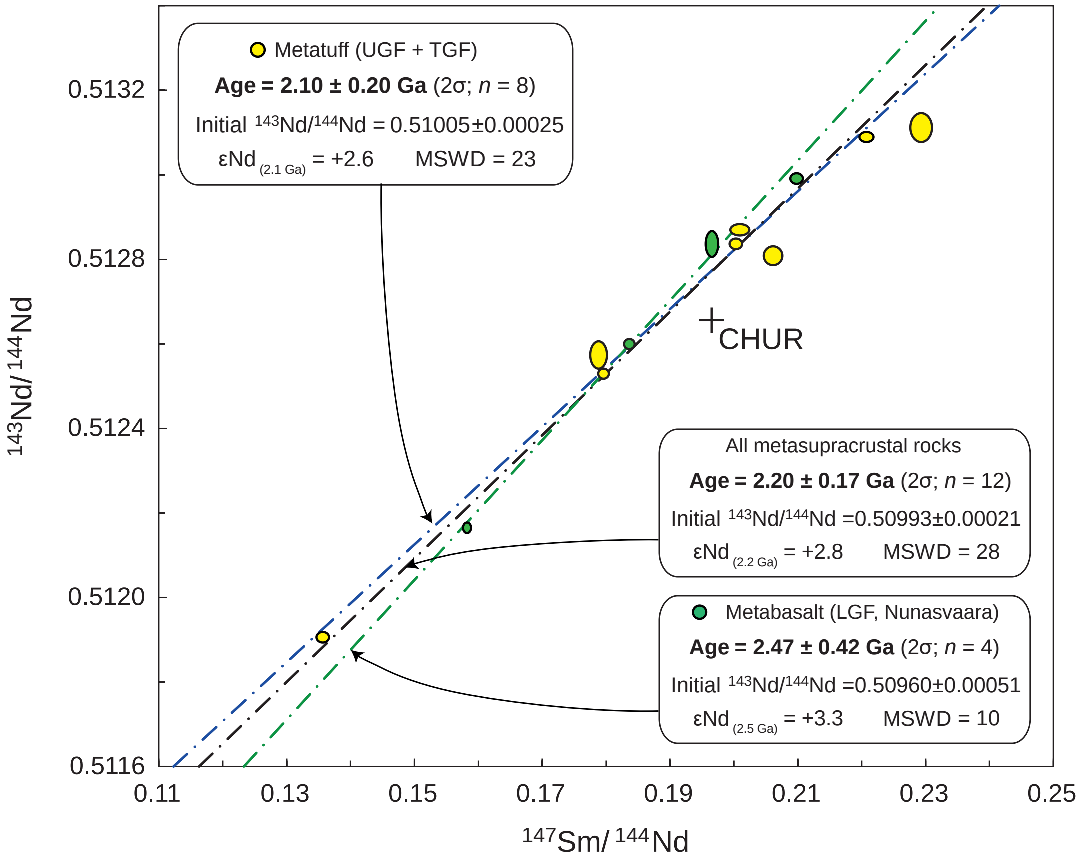

Figure 20. Sm-Nd "errorchrons" for greenstone-related metasupracrustal rocks at Nunasvaara and Masugnsbyn. The regressed ages should be regarded as statistically non-robust reference ages only, due to the large mean squares of weighted deviate (MSWD) values, narrow $^{147}Sm/^{144}Nd$ range of the samples and low precision at the 2σ level. The errorchron "age" of 2.10 ± 0.20 Ga is based on Sm-Nd results for metatuff samples from both study areas, but excludes altered metatuff sample ELH130023D (see Table 4). The errorchron "age" of 2.47 ± 0.42 Ga is for Nunasvaara metabasalt only. The errorchron "age" of 2.20 ± 0.17 Ga is for all samples. CHUR represents the present-day value for a bulk silicate Earth (Jacobson & Wasserburg 1980). Plot created in Isoplot 4.16 (Ludwig 2012). LGF = Lower greenstone formation (at Nunasvaara), TGF = Tuorevaara greenstone formation (Veikkavaara greenstone group, Masugnsbyn).

to disturb the Sm-Nd systematics of the greenstones may be partly assessed using a whole-rock Sm-Nd isochron plot as shown in Figure 20. In this plot, the slopes of three "errorchron" regression lines yield imprecise "reference ages" of c. 2.45 Ga (Nunasvaara metabasalt only), c. 2.10 Ga (metatuff from Nunasvaara and Masugnsbyn) and c. 2.20 Ga (i.e. all metasupracrustal units from both areas). Additionally, the regressed data provide $^{143}Nd/^{144}Nd$ intercepts, corresponding to initial εNd values of approximately +2.6, +3.3 and +2.8 for the three reference ages, respectively.

While the imprecise reference ages preclude any meaningful interpretation, either individually or as a whole, the age of c. 2.20 Ga through all the greenstone metasupracrustal rocks is relatively consistent with the minimum formational age of c. 2.14 Ga determined by U-Pb zircon dating. Likewise, the $\varepsilon Nd_{(2.2\ Ga)}$ value of +2.8 based on the equivalent $^{143}Nd/^{144}Nd$ intercept generally conforms to the spread of initial εNd values determined for the individual metasupracrustal samples (Table 4, Fig. 19). Thus, while some variation may be attributed to secondary metasomatic effects, on the whole the Sm-Nd systematics appear to have remained relatively robust during subsequent tectonothermal events, since a younger Sm-Nd age (i.e. < c. 2.0 Ga) is not preserved. This confirms that LREE variability as illustrated in Figure 19 may best be explained by primary geological factors as previously described.

One such factor may be melt fractionation during ascent and crystallisation, leading to a differentiated magma series. However, the predominantly tholeiitic basaltic nature of both greenstone successions and the apparent absence of intercalated intermediate and felsic units suggest that the greenstones represent a relatively homogenous geochemical suite. Likewise, the compositional overlap between the basaltic metasupracrustal units and the metadoleritic bodies suggests that a phase of relatively consistent mafic magmatism may have occurred. Thus, any local differentiation effects during magma ascent and storage cannot account for the LREE variability seen in the greenstone units. Consequently, source region variability and the assimilation of older continental material (i.e. the Norrbotten craton) were probably major factors in determining the generally positive εNd character and the relatively LREE-enriched geochemical composition of the greenstones.

A preliminary petrogenetic model

Potential source regions and precursor material for Palaeoproterozoic greenstone-type magmatism in northern Norrbotten include (1) a REE-depleted asthenospheric mantle (e.g. DM curve, Fig. 21); (2) a REE-enriched (plume-modified?) asthenospheric mantle (e.g. CHUR line, Fig. 21); (3) a REE-enriched sub-continental lithospheric mantle (e.g. adjacent to the CHUR line); (4) a depleted mantle plus assimilated Norrbotten craton mixed source; (5) a depleted mantle plus assimilated older supracrustal rocks mixed source (e.g. rift-related *Kovo group* in northern Norrbotten); and (6) a combination of 1 to 5. The initial εNd versus time plot shown in Figure 21 provides a means of assessing the contribution of potential source terranes and crustal assimilation effects, and summarises the petrogenesis of the greenstone successions as part of the broader tectonic evolution of northern Norrbotten.

In Figure 21, initial εNd values of the c. 2.14 Ga greenstone units are plotted relative to values for (1) 2.83–2.67 Ga basement rocks of the Norrbotten craton (and their projected Nd evolution field); (2) 1.90–1.80 Ga syn- to late-orogenic volcanic and plutonic rocks located in the interior part of the craton (i.e. distal from the Knaften-Skellefte arc to the south; cf. Weihed et al. 2005, Lahtinen et al. 2009); and (3) 1.92–1.78 Ga syn- to late-orogenic plutonic rocks located at the southern margin of the craton (i.e. proximal to the Knaften-Skellefte arc). Vertical time lines highlight the beginning of key tectonothermal events affecting the northern Fennoscandian Shield. These include plume-induced break-up of composite Fennoscandia at c. 2.45 Ga, eventually leading to separation of the Karelian and Norrbotten cratons (e.g. Walker et al. 1997, Melezhik & Hanski 2012), and initial subduction-related magmatism at c. 2.02 and c. 1.95–1.89 Ga on the eastern and southern margins of the Norrbotten craton, forming the Kittilä and Knaften-Skellefte arcs, respectively (Hanski & Huhma 2005, Wasström 2005, Lahtinen et al. 2009).

Based on its spatial distribution and projected Nd evolution characteristics (Fig. 21), the Meso- to Neoarchaean Norrbotten craton represents a major continental source terrane for Palaeoproterozoic magmatism in northernmost Sweden (cf. Witschard 1984). For example, studies of Svecokarelian plutonic and volcanic rocks formed within the thick interior of the craton (i.e. Knaften–Skellefte retroarc hinterland) indicate that continental anatexis contributed to syn-orogenic melt generation, producing extensive calc-alkaline to alkaline, mafic to felsic volcanic-plutonic suites with negative initial εNd values (approximately -1 to -9, Fig. 21, e.g. Öhlander et al. 1987a, Skiöld et al. 1988, Mellqvist et al. 1999). This signature partly reflects a REE budget inherited from the cratonic reservoir, which by c. 1.9 Ga had acquired a distinctly negative εNd character of between approximately -7 and -12 (Fig. 21). Conversely, contemporaneous syn-orogenic mafic to intermediate plutonic suites emplaced along the southern margin of the craton (Knaften–Skellefte arc foreland) have markedly more juvenile εNd characteristics (approximately -2 to +4), reflecting increased slab or mantle wedge-derived inputs and a lesser contribution from isotopically mature, continental source rocks. Thus, the REE budget of the arc-proximal magmas was less influenced by a relatively thinner basement margin, which by c. 1.9 Ga formed part of the upper plate of the north-directed subduction zone (Fig. 21, e.g. Nironen 1997, Lahtinen et al. 2005, Weihed et al. 2005).

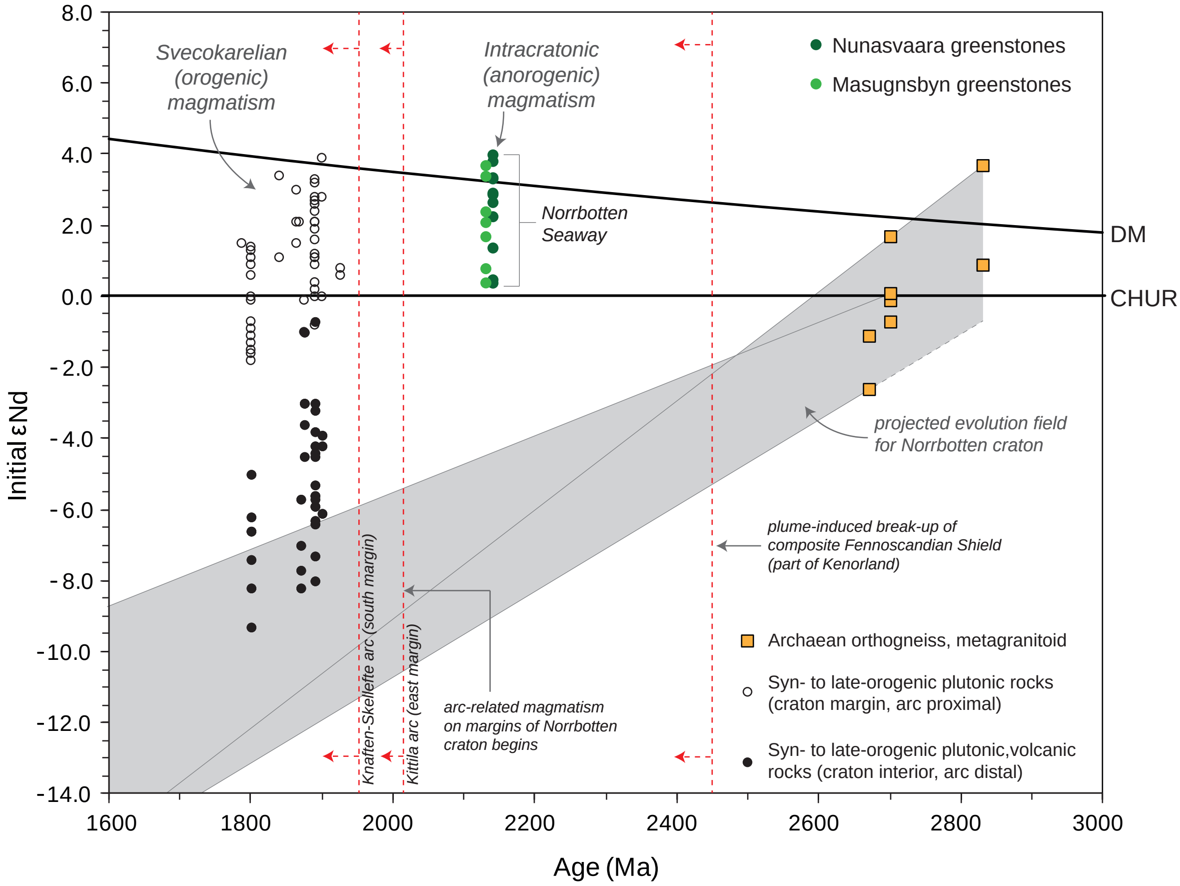

Figure 21. Initial εNd versus time plot for greenstone units at Nunasvaara and Masugnsbyn (green dots) in relation to other Norrbotten craton and Svecokarelian-related rocks. Initial εNd values are calculated at 2.14 Ga (Nunasvaara) and 2.13 Ga (Masugnsbyn) to aid data visualisation in figure and do not alter the geological interpretation from that which would have been made if all values had been calculated at 2.14 Ga. See main text for discussion. DM = depleted mantle model curve (DePaolo 1981), CHUR = chondrite uniform reservoir (e.g. DePaolo & Wasserburg 1976). Archaean data points (squares) are from Öhlander et al. 1987b, Mellqvist 1999 and Mellqvist et al. 1999. Svecokarelian-related data points (black dots and circles) are from Wilson et al. 1985, Öhlander et al. 1987a, Öhlander et al. 1987b, Skiöld et al. 1988, Cliff et al. 1990, Öhlander et al. 1993, Öhlander & Skiöld 1994, Mellqvist et al. 1999 and Mellqvist et al. 2003. Major time lines (broken red lines) are from Hanski & Huhma (2005) and Wasström (2005).

In general, the Nd isotopic characteristics of the c. 2.14 Ga greenstones indicate a mainly juvenile, depleted to enriched mantle-like signature that extends from the DM model towards the CHUR reference (Fig. 21). By c. 2.14 Ga, the bulk εNd signature of the Norrbotten craton had evolved to moderately negative εNd values of between approximately -4 and -9 (Fig. 21). Thus, the distinct continental crustal signature of the cratonic terrane is not strongly reflected in the εNd values of the greenstones and suggests that the assimilation of continental material had a minor modifying effect during primitive melt ascent and storage. Moreover, if crustal assimilation had played a significant role, a mixed initial εNd signature similar to that for Svecokarelian igneous rocks formed in the craton interior (i.e. arc distal setting) may be expected for the greenstone units formed in the same cratonic setting (Fig. 21).

The involvement of a depleted asthenospheric mantle in the petrogenesis of the greenstones is somewhat contradicted by the trace element systematics. Specifically, the chondrite-normalised REE patterns and Th/Nb ratios reveal a relatively enriched signature, more consistent with E-MORB-type oceanic crust (cf. Fig. 18). Given the regional tectonic setting at c. 2.14 Ga (e.g. Melezhik & Hanski 2012), three preferred petrogenetic scenarios may account for the geochemical and isotopic characteristics: (1) deeply sourced light REE-enriched asthenospheric melts (plume-modified?) ascended through the continental lithosphere during regional rifting and extension; (2) relatively enriched sub-continental lithospheric mantle melts ascended through the continental lithosphere during rifting and extension; or (3) N-MORB-like depleted mantle magmas partially assimilated continental material, resulting in a "mixed" light REE-enriched plus isotopically juvenile (positive initial εNd) signature. All three scenarios presuppose some degree of assimilation of continental crust.

Regional geological and tectonic reconstructions of northern Fennoscandia 2.5–2.0 Ga emphasise a major phase of lithospheric-scale continental rifting and dispersion (e.g. Smolkin 1997, Hanski & Huhma 2005, Hanski 2012, Melezhik & Hanski 2012). The c. 2.14 Ga greenstone successions at Nunasvaara and Masugnsbyn developed as part of this protracted rift-to-drift episode. In north-central Norrbotten, volcanosedimentary depocentres developed within an epieric sea, which we here name the *Norrbotten Seaway* (cf. Fig. 21). Deposition and extrusion of sedimentary and volcanic material was probably controlled by extensional tectonics and half-graben structures during relatively high rates of sedimentation and volcanism (e.g. Melezhik & Fallick 2010).

The apparent lack of Svecokarelian-cycle arc-type magmatism in the Norrbotten craton interior with juvenile Nd isotope characteristics (i.e. equivalent to arc-proximal rocks along its southern margin; cf. Fig. 21) suggests that the Norrbotten Seaway remained a relatively narrow, aulacogen-type, intracontinental basin, and did not mature into a wide oceanic plateau. Thus, the greenstone successions at Nunasvaara and Masugnsbyn probably represent authothonous or parautothonous fragments of this fully or partially closed marginal sea. By c. 2.14 Ga the Norrbotten Seaway lay adjacent to a developing oceanic basin to the northeast (Kittilä Ocean), which was spreading and maturing at that time (e.g. Melezhik & Hanski 2012).

SUMMARY AND CONCLUSIONS

New field mapping, U-Pb SIMS zircon geochronology, lithogeochemistry and Sm-Nd isotopic analysis have been integrated to investigate two Palaeoproterozoic greenstone successions in north-central Norrbotten, northern Sweden. The conclusions from this work are:

1. The greenstone succession at Nunasvaara (*Vittangi greenstone group*) consists of a partly conformable, polydeformed sequence divisible into four formations, with a minimum total thickness of approximately 2.4 km. The basal *Lower greenstone formation* (LGF) contains effusive basaltic metavolcanic rocks that locally display amygdaloidal and pillowed forms. The overlying *Lower sedimentary formation* contains a distinctive black schist horizon at the top (Nunasvaara member, NM), which locally contains significant disseminated and vein graphite mineralisation (Nunasvaara deposit). Pyrite and pyrrhotite associated with the graphite suggest a relatively reduced (anoxic to euxinic) depositional environment. The overlying *Upper greenstone formation* (UGF) comprises laminated basaltic metatuff. The uppermost unit, called the *Upper sedimentary formation* (USF), consists of pelite, black schist, minor intercalated metacarbonate layers and rare meta-ironstone and komatiitic metabasalt horizons. Locally, the USF hosts stratiform–stratabound iron mineralisation associated with variable sodic-calcic (skarn-type) alteration and sulphides.

2. At Masugnsbyn (*Veikkavaara greenstone group*), the greenstones form a relatively conformable sequence divisible into four formations, with a minimum total thickness of 3.4 km. The lowermost *Tuorevaara greenstone formation* is poorly exposed and is inferred to consist mainly of effusive basaltic metavolcanic rocks similar to the LGF at Nunasvaara. The overlying *Suinavaara formation* (SF) is a relatively thin horizon consisting of intercalated quartzite, graphitic pelite and metacarbonate rocks. The stratigraphic position of the SF remains uncertain, and correlation with a Nunasvaara unit is not proposed. The Tuorevaara greenstone formation (TGF) mainly consists of laminated basaltic metatuff.

A correlation between the TGF and the UGF at Nunasvaara is permissible based on petrographic and geochemical comparisons. Additionally, an approximately 50 m thick graphitic schist horizon at the base of the NGF correlates with the *Nunasvaara member* and further supports a stratigraphic link between the NGF and UGF (i.e. both metatuff sequences conformably overlie a distinctive black schist horizon). The uppermost *Masugnsbyn formation* (MF) consists of skarn-banded metachert (ironstone), graphitic schist and metacarbonate layers. The MF correlates with the USF at Nunasvaara and contains abundant skarn-style Fe mineralisation (e.g. the Junosuando deposit).

3. At Nunasvaara and Masugnsbyn new U-Pb SIMS zircon ages of 2144 ± 5 Ma and 2139 ± 4 Ma, respectively, obtained for metadolerite bodies intruding the greenstone successions constrain the timing of sub-volcanic mafic magmatism and provide a new minimum age of c. 2.14 Ga for the deposition of both greenstone sequences. The geochronology results identify a new c. 2.14 Ga episode of tholeiitic mafic magmatism in this sector of the Fennoscandian Shield and provide a temporal framework for greenstone-type volcanic-sedimentary depositional processes in north-central Norrbotten.

4. Major and trace element systematics in greenstone-related meta-igneous units indicate predominantly sub-alkali basaltic compositions corresponding to high-Fe and high-Mg tholeiitic rocks. Rare meta-ultramafic horizons have low silica, high-Mg (picritic to meimechitic) compositions. Metasedimentary units have mainly mafic to intermediate compositions. Chondrite-normalised rare earth element (REE) patterns for the mafic meta-igneous units are flat to light REE-enriched. Metabasalts at Nunasvaara (LGF) have REE patterns that overlap those of average E-MORB signatures. The patterns also overlap those for the metatuff and metadolerite, suggesting a potential comagmatic suite. Metasedimentary units from both areas display moderately light REE-enrichment patterns indicating evolved, upper continental crust-type signatures (cf. Taylor & McLennan 1985).

5. Sm-Nd isotopic results show initial εNd values between +0.4 and +4.0 for the greenstone units that fall between the depleted mantle and CHUR reference models. While metasomatic overprinting may partly account for some of the variation, these data, combined with the trace element systematics, suggest that juvenile melts from a geochemically enriched mantle were a major source component for the greenstones. Assimilation of older continental crust (e.g. the Norrbotten craton) may also have played a minor role.

6. The greenstone successions are interpreted to have formed within a rifted continental setting, in which crustal extension facilitated upwelling of tholeiitic magmas and provided sub-aqueous depositional sites for volcanic and sedimentary material. From a broader perspective, the Norrbotten greenstone belts evolved within an immature marginal sea or oceanic basin named the Norrbotten Seaway.

7. Overprinting geological processes recorded at Nunasvaara and Masugnsbyn, including amphibolite facies metamorphism, polyphase ductile-brittle deformation, graphitisation and hydrothermal metasomatism are attributed to subsequent tectonothermal events at 1.90–1.78 Ga.

ACKNOWLEDGEMENTS

We thank James Kilgannon for able field assistance at Nunasvaara, and Cecilia Jönsson for conducting ground geophysical measurements at Masugnbyn. Laboratory assistance by Leena Järvinen and Arto Pulkkinen at the Geological Survey of Finland (GTK) is gratefully acknowledged. U-Pb zircon dating at the Nordsim facility was performed in cooperation with the Laboratory for Isotope Geology, Swedish Museum of Natural History (NRM), Stockholm. We express our gratitude to Martin Whitehouse, Lev Ilyinsky and Kerstin Lindén at Nordsim for their analytical support. Martin Whitehouse reduced the zircon analytical data, Lev Ilyinsky assisted during SIMS analyses, while Kerstin Lindén prepared the zircon mounts and assisted with zircon imaging. Jaroslaw Majka at the Department of Earth Sciences, Uppsala University, is also thanked for his assistance during zircon imaging.

REFERENCES

Ahl, M., Bergman, S., Bergström, U., Eliasson, T., Ripa, M. & Weihed, P., 2001: Geochemical classification of plutonic rocks in central and northern Sweden. *Sveriges geologiska undersökning Rapporter och meddelanden 106*, Uppsala, 86 p.

Ambros, M., 1980: Description of the geological maps Laanavaara NV, NO, SV, SO and Karesuando SV, SO with geophysical interpretation by Herbert Henkel. *Sveriges geologiska undersökning Af 25–30*, 111 pp.

Beck, W. & Murthy, V.R., 1991: Evidence for continental crustal assimilation in the Hemlock Formation flood basalts of the early Proterozoic Penokean Orogen, Lake Superior Region. *In:* P.K. Sims & L.M.H. Carter (eds.) Contributions to Precambrian Geology of the Lake Superior Region. *United States Geological Survey Bulletin 1904-1*, 13–125.

Bergman, S., Kübler, L. & Martinsson, O., 2001: Description of regional geological and geophysical maps of northern Norbotten County. *Sveriges geologiska undersökning Ba 56*, 110 pp.

Bergman, S., Billström, K., Persson, P.-O., Skiöld, T. & Evins, P., 2006: U-Pb age evidence for repeated Paleoproterozoic metamorphism and deformation near the Pajala shear zone in the northern Fennoscandian Shield. *GFF 128*, 7–20.

Bergman, S., Stephens, M.B., Andersson, J., Kathol, B. & Bergman, T., 2012: Bedrock map of Sweden, 1:1 000 000 scale. *Sveriges geologiska undersökning K 423*.

Bergström, R., 1987. Nunasvaara grafitfyndinghet. Unpublished company report for LKAB, *K 87-4,* 98 p.

Bida, J., 1979: Hietajoki dolomitförekomst. Slutrapport. *Sveriges geologiska undersökning PRO79-38*, 19 pp.

Billström, K., Bergman, S. & Martinsson, O., 2002: Post-1.9 Ga metamorphic, mineralization and hydrothermal events in northern Sweden. *GFF 124*, p. 228.

Billström, K., Eilu, P., Martinsson, O., Niiranen, T., Broman, C., Weihed, P., Wanhainen, C. & Ojala, J., 2010: IOCG and related mineral deposits of the northern Fennoscandian Shield. *In:* T.M. Porter (ed.): *Hydrothermal iron oxide–copper–gold & related deposits: a global perspective, vol. 3*. Advances in the Understanding of IOCG deposits. PGC Publishing, Adelaide, 381–414.

Bingen, B., Solli, A., Viola, G., Torgersen, E., Sandstad, J.-S., Whitehouse, M.J., Røhr, T.S., Ganerød, M. & Nasuti, A. 2016: Geochronology of the Palaeoproterozoic Kautokeino Greenstone Belt, Finnmark, Norway: Tectonic implications in a Fennoscandia context. *Norwegian Journal of Geology 95,* 1–32.

Blake, K., 1990. *The petrology, geochemistry and association to ore formation of the host rocks of the Kiirunavaara magnetite-apatite deposit, northern Sweden*. Ph.D. thesis, University of Wales, Cardiff, UK.

Boynton, W.V., 1984. Geochemistry of the rare earth elements: meteorite studies. *In:* P. Henderson (ed.) *Rare earth element geochemistry*. Elsevier, 63–114.

Buseck, P.R. & Beyssac, O., 2014: From organic matter to graphite: Graphitization. *Elements 10*, 421–426.

Cattell, A.C. & Taylor, R.N., 1990: Archaean basic magmas. *In:* R.P. Hall & D.J. Hughes (eds) *Early Precambrian Basic Magmatism*. Blackie, Glasgow, UK, 11–39.

Cliff, R.A., Rickard, D. & Blake, K., 1990: Isotope systematics of the Kiruna magnetite ores, Sweden: Part 1. Age of the ore. *Economic Geology 85*, 1770–1776.

Condie, K.C., 1993: Chemical composition and evolution of the upper continental crust: contrasting results from surface samples and shales. *Chemical Geology 104,* 1–37.

Condie, K.C., Des Marais, D.J. & Abbott, D., 2001: Precambrian superplumes and supercontinents: a record in black shales, carbon isotopes, and paleoclimates? *Precambrian Research 106*, 239–260.

Damberg, K., Nylund, B. & Mannström, B., 1974: Tornefors järnmalmsfyndighet. Rapport rörande resultaten av Sveriges geologiska undersökning: undersökningar 1949, 1966, 1970. *Sveriges geologiska undersökning BRAP 736*, 24 pp.

DePaolo, D.J., 1981: Neodymium isotopes in the Colorado Front Range and crust-mantle evolution in the Proterozoic. *Nature 291*, 684–687.

DePaolo, D.J. & Wasserburg, G.J., 1976: Nd isotopic variations and petrogenetic models. *Geophysical Research Letters 3*, 249–252.

Edfelt, Å., Armstrong, R.N., Smith, M. & Martinsson, O., 2005: Alteration paragenesis and mineral chemistry of the Tjårrojåkka apatite–iron and Cu (-Au) occurrences, Kiruna area, northern Sweden. *Mineralium Deposita 40*, 409–434.

Edfelt, Å., Sandrin, A., Evins, P., Jeffries, T., Storey C., Elming, S.-Å. & Martinsson, O., 2006: Stratigraphy and tectonic setting of the host rocks at the Tjårrojåkka Fe-oxide Cu-Au deposits. *GFF 128,* 221–232.

Eilu, P. (ed.) 2012: Mineral deposits and metallogeny of Fennoscandia. *Geological Survey of Finland, Special Paper 53*. 401 pp.

Eriksson, B., 1969: Berggrunden inom det central Vittangifältet, dess petrografi, stratigrafi och tektonisk. *Sveriges geologiska undersökning Brap 881*, 181 pp.

Eriksson, B. & Hallgren, U., 1975: Beskrivning till berggrundskartbladen Vittangi NV, NO, SV, SO. *Sveriges geologiska undersökning Af 13–16*, 203 pp. (with summary in English).

Faure, G. & Mensing, T.M., 2005: *Isotopes. Principles and Applications*. John Wiley & Sons, Inc., Hoboken, NJ, USA. 897 pp.

Frietsch, R., 1984: Petrochemistry of the iron ore-bearing metavolcanics in Norrbotten County northern Sweden. *Sveriges geologiska undersökning C 802,* 62 pp.

Frietsch, R., 1997: The iron ore inventory programme 1963 to 1972 in Norrbotten County. *Sveriges geologiska undersökning Rapporter och meddelanden 92*, 77 pp.

Frietsch, R., Tuisku, P., Martinsson, O. & Perdahl, J-A., 1997: Early Proterozoic Cu-(Au) and Fe ore deposits associated with regional Na–Cl metasomatism in northern Fennoscandia. *Ore Geology Reviews 12*, 1–34.

Gavelin, S., 1957: Variations in isotopic composition of carbon from metamorphic rocks in northern Sweden and their geological significance. *Geochimica et Cosmochimica Acta 12*, 297–314.

Geijer, P., 1929: Masugnsbyfältens geologi. *Sveriges geologiska undersökning C 351*, 39 pp.

Gerdin, P., Johansson, L., Hansson, K.E., Holmqvist, A. & Ottosson, D., 1990: Grafit uppslagsgenerering i Norrbotten 1990. *Sveriges geologiska undersökning Prap 90068*, 100 pp.

Grigull, S., Berggren, R., Jönberger, J., Jönsson, C., Hellström, F.A. & Luth, S., 2018: Folding observed in Palaeoproterozoic supracrustal rocks in northern Sweden. *In:* Bergman, S. (ed): Geology of the Northern Norrbotten ore province, northern Sweden. *Rapporter och Meddelanden 141,* Sveriges geologiska undersökning. This volume pp 205–257.

Grip, E. & Frietsch, R., 1973: *Malm i Sverige 2. Norra Sverige*. Almqvist & Wiksell, 295 pp.

Gustafsson, B., 1993. *The Swedish Norrbotten greenstone belt. A compilation of available information concerning exploration*. Unpublished company report for the State Mining Property Commission (NSG). 52 pp.

Hanski, E.J. & Huhma, H., 2005: Central Lapland greenstone belt. *In:* R. Lehtinen, P.A. Nurmi, O.T. Rämö (eds.) *Precambrian Geology of Finland – key to the evolution of the Fennoscandian Shield*. Elsevier, Amsterdam, 139–194.

Hanski, E.J., 2012: Evolution of the Paleoproterozoic (2.5–1.95 Ga) non-orogenic magmatism in the eastern part of the Fennoscandian Shield. *In:* V.A. Melezhik, A.R. Prave, E.J. Hanski, A.E. Fallick, A. Lepland, L.R. Kump & H. Strauss (eds.) *Reading the archive of Earth's oxygenation*, Volume 1, Springer, Berlin, 179–245.

Hellström, F. & Jönsson, C., 2014: Barents project 2014: Summary of geological and geophysical information of the Masugnsbyn key area. *Sveriges geologiska undersökning 2014:21, 84 pp.*

Hellström, F. & Jönsson C., 2015: Summary of geological and geophysical field investigations in the Masugnsbyn key area, northern Norrbotten. *Sveriges geologiska undersökning 2015:04*, 31 pp.

Hellström, F.A., Kumpulainen, R., Jönsson, C., Thomsen, T.B., Huhma, H. & Martinsson, O., 2018: Age and lithostratigraphy of Svecofennian volcanosedimentary rocks at Masugnsbyn, northernmost Sweden – host rocks to Zn-Pb-Cu- and Cu ±Au sulphide mineralisations. *In:* Bergman, S. (ed): Geology of the Northern Norrbotten ore province, northern Sweden. *Rapporter och Meddelanden 141,* Sveriges geologiska undersökning. This volume pp 151–203.

Hellström, F.A., 2018: Early Svecokarelian migmatisation west of the Pajala Deformation Belt, northeastern Norrbotten Province, northern Sweden. *In:* Bergman, S. (ed): Geology of the Northern Norrbotten ore province, northern Sweden. *Rapporter och Meddelanden 141,* Sveriges geologiska undersökning. This volume pp 361–379.

Henderson, I. & Kendrik, M., 2003: Structural controls on graphite mineralisation, Senja, Troms. *Norges geologiske undersökelse (NGU) Report 2003.011*, 105 pp.
Huang, S, Jacobsen, S.B. & Mukhopadhyay, S., 2013: ^{147}Sm-^{143}Nd systematics of Earth are inconsistent with a superchondritic Sm/Nd ratio. *Proceedings of the National Academy of Sciences 110*, 4929–4934.
Huhma, H., Cliff, R.A., Perttunen, V. & Sakko, M., 1990: Sm-Nd and Pb isotopic study of mafic rocks associated with early Proterozoic continental rifting: the Peräpohja schist belt in northern Finalnd. *Contributions to Mineralogy and Petrology 104*, 369–379.
Huhma, H., Kontinen, A., Mikkola, P., Halkoaho, T., Hokkanen, T., Hölttä, P., Juopperi, H., Konnunaho, J., Luukkonen, E., Mutanen, T., Peltonen, P., Pietikäinen,K. & Pulkkinen, A. 2012: Nd isotopic evidence for Archaean crustal growth in Finland. *In*: P. Hölttä (ed.) *The Archaean of the Karelia Province in Finland*. *Geological Survey of Finland (GTK) Special Paper 54*, 176–213.
Huhma, H., Hanski, E., Vuollo, J., Kontinen, A. & Mutanen, T., 2013: Sm-Nd isotopes and age of Paleoproterozoic mafic rocks in Finland – evidence for rifting of Archaean lithosphere and multiple mantle sources. *Geological Survey of Finland (GTK) Report 198*, 45–48.
Huhma, H., Hanski, E., Vuollo, J. & Kontinen, A., 2016: Age and Sm-Nd isotopes of Paleoproterozoic mafic rocks in Finland – evidence for rifting stages and magma sources. *Bulletin of the Geological Society of Finland Special Volume 1*, p. 155
Jacobsen S.B. & Wasserburg G.J., 1980: Sm-Nd isotopic evolution of chondrites. *Earth and Planetary Science Letters* 50, 139–155.
Janoušek, V., Farrow, C.M. & Erban, V., 2006: Interpretation of whole-rock geochemical data in igneous geochemistry: introducing Geochemical Data Toolkit (GCDkit). *Journal of Petrology 47*, 1255–1259.
Jensen, L.S., 1976: A new cation plot for classifying subalkalic volcanic rocks. *Ontario Division of Mines Miscellaneous Paper 66*, 22 pp.
Kamber, B.S. & Webb, G.E., 2001: The geochemistry of late Archaean microbial carbonate: implications for ocean chemistry and continental erosion history. *Geochimica et Cosmochimica Acta 65*, 2509–2525.
Klein, C. & Beukes, N.J., 1992: Proterozoic iron formations. *In:* K.C. Condie (ed.) *Proterozoic Crustal Evolution*. *Developments in Precambrian Geology 10*, Elsevier, 383–418.
Koistinen, T., Stephens, M.B., Bogatchev, V., Nordgulen, O., Wenneström, M. & Korhonen, J., 2001: *Geology of the Fennoscandian Shield. 1:2 000 000-scale map*. Geological Survey of Finland (GTK), Geological Survey of Sweden (SGU), Geological Survey of Norway (NGU), DNRR.
Kumpulainen, R.A., 2000: *The Paleoproterozoic sedimentary record of northernmost Norrbotten, Sweden*. Unpublished report for the Geological Survey of Sweden (SGU). 45 pp.
Laajoki, K., 2005: Karelian supracrustal rocks. *In:* M. Lehtinen, P.A. Nurmi, O.T. Rämö (eds.), *Precambrian Geology of Finland – key to the evolution of the Fennoscandian Shield*. Elsevier, Amsterdam, 279–341.
Ladenberger, A., Andersson, M., Gonzalez, J., Lax, K., Carlsson, M., Olsson, S-Å. & Jelinek, C., 2012: Till geochemistry in northern Norrbotten. *Sveriges geologiska undersökning K410*, 112 pp (In Swedish).
Lager, I. & Loberg, B., 1990: *Sedimentologisk bassänganalytisk malmprospekteringsmetodik inom norrbottniska grönstensbälten*. Unpublished report for STU project 86-03967P, Luleå College, Luleå, 131 pp.
Lahtinen, R., Korja, A. & Nironen, M., 2005: Proterozoic tectonic evolution. *In:* R. Lehtinen, P.A. Nurmi, O.T. Rämö (eds.) *Precambrian Geology of Finland – key to the evolution of the Fennoscandian Shield*. Elsevier, Amsterdam, 481–532.
Lahtinen, R., Garde, A.A. & Melezhik, V.A., 2008: Paleoproterozoic evolution of Fennoscandia and Greenland. *Episodes 31*, 1–9.
Lahtinen, R., Korja, A., Nironen, M. & Heikkinen, P., 2009: Paleoproterozoic accretionary processes in Fennoscandia. *Geological Society, London, Special Publications 318*, 237–259.
Lahtinen, R., Huhma, H., Lahaye, L., Jonsson, E., Manninen, M., Lauri, L.S., Bergman, S., Hellström, F., Niiranen, T. & Nironen, M., 2015: New geochronological and Sm-Nd constraints across the Pajala shear zone of northern Fennoscandia: reactivation of a Paleoproterozoic suture. *Precambrian Research 256*, 102–119.

Le Maitre, R.W., Streckeisen, A., Zanettin, B., Le Bas, M., Bonin, B. & Bateman, P., 2002: *Igneous rocks: a classification and glossary of terms: recommendations of the International Union of Geological Sciences Subcommission on the Systematics of Igneous Rocks*. Cambridge University Press, 236 pp.

Lugmair, G.W. & Marti, K., 1978: Lunar initial $^{143}Nd/^{144}Nd$: Differential evolution of the lunar crust and mantle. *Earth and Planetary Science Letters*, v.39, p. 349–357.

Ludwig, K.R., 2012: User's manual for Isoplot 3.75. A geochronological toolkit for Microsoft Excel. *Berkeley Geochronology Center Special Publication No. 5,* 75 pp.

Luque, F.J., Crespo-Feo, E., Barrenechea, J.F. & Ortega, L., 2012: Carbon isotopes of graphite: Implications on fluid history. *Geoscience Frontiers 3*, 197–207.

Lynch, E.P., Jönberger, J., Luth, S., Grigull, S. & Martinsson, O., 2014. Geological and geophysical studies in the Nunasvaara, Saarijärvi and Tjårrojåkka areas, northern Norrbotten. *Sveriges geologiska undersökning 2014:04*, 48 pp.

Lynch, E.P., Jönberger, J., Bauer, T.E., Sarlus, Z. & Martinsson, O., 2015: Meta-volcanosedimentary rocks in the Nautanen area, Norrbotten: Preliminary lithological and deformation characteristics. *Sveriges geologiska undersökning 2015:30*, 51 pp.

Lynch, E.P., Hellström, F., & Huhma, H., 2016: The Nunasvaara graphite deposit, northern Sweden: New geochemical and U-Pb zircon age results for the host greenstones. *Bulletin of the Geological Society of Finland Special Volume 1*, 112–113.

Martinsson, O., 1993: Stratigraphy of the greenstones in the eastern part of northern Norrbotten. *In:* Martinsson, O., Perdahl, J.-A. & Bergman, J. (eds): *Greenstone and porphyry hosted ore deposits in northern Norrbotten*. Unpublished report for PIM/NUTEK project, no. 1, 77 p.

Martinsson, O., 1997: *Tectonic setting and metallogeny of the Kiruna greenstones*. Ph.D. thesis, Luleå University of Technology, Luleå, Sweden, 165 p.

Martinsson, O., Hallberg, A., Broman, C., Godin-Jonasson, L., Kisiel, T. & Fallick, A.E., 1997: Viscaria – a syngenetic exhalative Cu-deposit in the Paleoproterozoic greenstones. *In:* Martinsson, O., 1997: *Tectonic setting and metallogeny of the Kiruna greenstones*. Ph.D. thesis, Luleå University of Technology, Luleå, Sweden. 1–57.

Martinsson, O., 2004: Geology and metallogeny of the northern Norrbotten Fe–Cu–Au province. *In:* R.L. Allen, O. Martinsson & P. Weihed (eds.): Svecofennian ore-forming environments of northern Sweden – volcanic-associated Zn-Cu-Au-Ag, intrusion-associated Cu-Au, sediment-hosted Pb-Zn, and magnetite-apatite deposits in northern Sweden. *Society of Economic Geologists, guidebook series 33*, 131–148.

Martinsson, O., Van der Stilj, I., Debras, C. & Thompson, M., 2013: Day 3. The Masugnsbyn, Gruvberget and Mertainen iron deposits. *In:* O. Martinsson & C. Wanhainen (eds.): 12th Biennial SGA Meeting, Uppsala, Sweden. *Society of Geology Applied to Mineral Deposits, excursion guidebook SWE5*, 37–44.

Martinsson, O., Billström, K., Broman C., Weihed, P. & Wanhainen C., 2016: Metallogeny of the Northern Norrbotten ore province, northern Fennoscandian Shield with emphasis on IOCG and apatite-iron ore deposits. *Ore Geology Reviews 78*, 447–492.

Masurel, Q., 2011: *Volcanic and volcano-sedimentary facies analysis of the Viscaria D-zone Fe-Cu occurrence, Kiruna District, Northern Sweden*. M.Sc. thesis, Luleå University of Technology, Luleå, Sweden. 125 pp.

McClay, K.R., 1987: *The mapping of geological structures*. Geological Society, London, Field Guide Series. John Wiley & Sons, Chichester, UK. 161 pp.

Melezhik, V.A. & Fallick, A.E., 2010: On the Lomagundi-Jatuli carbon isotopic event: The evidence from the Kalix Greenstone Belt, Sweden. *Precambrian Research 179*, 165–190.

Melezhik, V.A. & Hanski, E.J., 2012: The early Paleoproterozoic of Fennoscandia: Geological and tectonic settings. *In:* V.A. Melezhik, A.R. Prave, E.J. Hanski, A.E. Fallick, A. Lepland, L.R. Kump & H. Strauss (eds.): *Reading the archive of Earth's oxygenation*, Volume 1, Springer, Berlin. 33–38.

Melezhik, V.A., Kump, L.R., Hanski, E.J., Fallick, A.E. & Prave, A.R., 2012: Tectonic evolution and major global Earth-surface palaeoenvironmental events in the Palaeoproterozoic. *In:* V.A. Melezhik, A.R. Prave, E.J. Hanski, A.E. Fallick, A. Lepland, L.R. Kump & H. Strauss (eds.): *Reading the archive of Earth's oxygenation*, Volume 1, Springer, Berlin, 3–21.

Mellqvist, C., 1999. *Proterozoic crustal growth along the Archaean continental margin in the Luleå and Jokkmokk areas, northern Sweden*. Ph.D. thesis, Luleå University of Technology, Luleå, 140 pp.
Mellqvist, C., Öhlander, B., Skiöld, T. & Wikström, A., 1999: The Archaean-Proterozoic paleoboundary in the Luleå area, northern Sweden: field and isotope geochemical evidence for a sharp terrane boundary. *Precambrian Research 96*, 225–243.
Mellqvist, C., Öhlander, B., Weihed, P. & Schöberg, H., 2003: Some aspects on the subdivision of the Haparanda and Jörn intrusive suites in northern Sweden. *GFF 125,* 77–85.
Meschede, M., 1986: A method for discriminating between different types of mid-ocean ridge basalts and continental tholeiites with the Nb-Zr-Y diagram. *Chemical Geology 56*, 207–218.
Mitchell, C.J., 1993: Industrial Minerals Laboratory Manual: Flake graphite. *British Geological Survey Technical Report WG/92/30*, 31 pp.
Murphy, J.B. & Nance, R.D., 2002: Sm–Nd isotopic systematics as tectonic tracers: an example from West Avalonia in the Canadian Appalachians. *Earth Science Reviews 59*, 77–100.
Niiniskorpi, V., 1986: En Zn-Pb-Cu-mineralisering i norra Sverige, en case-studie. Licenciate thesis., geological department of Åba Akademi, 74 pp.
Nironen, M., 1997. The Svecofennian Orogen: a tectonic model. *Precambrian Research 86*, 21–44.
Nordstrand, J., 2012: *Mineral chemistry of gangue minerals in the Kiirunavaara iron ore*. M.Sc. thesis, Luleå University of Technology, Luleå, Sweden. 46 pp.
Öhlander, B. & Skiöld, T., 1994: Diversity of 1.8 Ga potassic granitoids along the edge of the Archaean craton in northern Scandinavia: a result of melt formation at various depths and from various sources. *Lithos 33*, 265–283.
Öhlander, B., Hamilton, P.J., Fallick, A.E. & Wilson, M.R., 1987a: Crustal reactivation in northern Sweden: the Vettasjärvi granite. *Precambrian Research 35*, 277–293.
Öhlander, B., Skiöld, T., Hamilton, P.J. & Claesson, L-Å., 1987b: The western border of the Archaean province of the Baltic Shield: evidence from northern Sweden. *Contributions to Mineralogy and Petrology 95*, 437–450.
Öhlander, B., Lager, I., Loberg, B.E.H. & Schöberg, H., 1992. Stratigraphical position and Pb-Pb age of the Lower Proterozoic carbonate rocks from the Kalix Greenstone Belt, northern Sweden. *GFF 114*, 317–322.
Öhlander, B., Skiöld, T., Elming, S.-Å., BABEL Working Group, Claesson, S., & Nisca, D.H., 1993: Delineation and character of the Archaean-Proterozoic boundary in northern Sweden. *Precambrian Research 64*, 67–84.
Öhlander, B., Mellqvist, C., & Skiöld, T., 1999: Sm–Nd isotope evidence of a collisional event in the Precambrian of northern Sweden. *Precambrian Research 93*, 105–117.
Oze C. & Winter J.D., 2005. The occurrence, vesiculation and solidification of dense blue glassy pahoehoe. *Journal of Volcanology and Geothermal Research 142***,** 285–301.
Padget, P., 1970. Description of the geological maps Tärendö NW, NE, SW, SE with an appendix on geophysical aspects by J.D. Cornwell. *Sveriges geologiska undersökning Af 5–8*, 95 pp.
Pearce, J.A., 1996: A user's guide to basalt discrimination diagrams. *In:* D.A. Wyman (ed.) Trace element geochemistry of volcanic rocks: Applications for massive sulphide exploration. Geological Association of Canada, Short Course Notes 12, 79–113.
Pearce, J.A., 2008: Geochemical fingerprinting of oceanic basalts with applications to ophiolite classification and the search for Archean oceanic crust. *Lithos 100*, 14–48.
Pearce, J.A. & Cann, J.R., 1973: Tectonic setting of basic volcanic rocks determined using trace element analysis. *Earth and Planetary Science Letters 19*, 290–300.
Pearce, M., Godel, B.M., & Thompson, M., 2015: Microstructures and mineralogy of a world-class graphite deposit. *Society of Economic Geologists, Annual Conference 2015, Hobart, Australia. Program and abstracts*.
Peltonen, P., Kontinen, A., & Huhma, H., 1996: Petrology and geochemistry of metabasalts from the 1.95 Ga Jormua ophiolite, northeastern Finland. *Journal of Petrology 37*, 1359–1383.
Pharaoh, T.C. & Brewer, T.S., 1990: Spatial and temporal diversity of early Proterozoic volcanic sequences – comparisons between the Baltic and Laurentian shields. *Precambrian Research 47*, 169–189.

Pharaoh, T.C. & Pearce, J.A., 1984: Geochemical evidence for the geotectonic setting of early Proterozoic metavolcanic sequences in Lapland. *Precambrian Research 25*, 283–308.
Pharaoh, T.C., Warren, A., & Walsh, N.J., 1987: Early Proterozoic volcanic suites of the northernmost Baltic Shield. *Geological Society, London, Special Publication 33*, 41–58.
Reddy, S.M. & Evans, D.A.D., 2009: Palaeoproterozoic supercontinents and global evolution: correlations from core to atmosphere. *In:* S.M. Reddy, R. Mazumdr, D.A.D. Evans, A.S. Collins (eds): *Paleoproterozoic supercontinents and global evolution. Geological Society, London, Special Publication 323*, 1–26.
Rollinson, H., 1993: *Using geochemical data: evaluation, presentation, interpretation*. Longman Scientific & Technical, Harlow, UK, 352 pp.
Romer, R.L. & Boundy, T.M., 1988: Interpretation of lead isotope data from the uraniferous Cu-Fe-sulfide mineralizations in the Proterozoic greenstone belt at Kopparåsen, northern Sweden. *Mineralium Deposita 23*, 256–261.
Romer, R.L., Martinsson, O., & Perdahl, J.-A., 1994: Geochronology of the Kiruna iron ores and hydrothermal alterations. *Economic Geology 89*, 1249–1261.
Salvador, A. (ed.), 1994: *International stratigraphic guide. A guide to stratigraphic classification, terminology, and procedure*. International Union of Geological Sciences and Geological Society of America, 2nd edition, 214 pp.
Sandstad, J.S., Bjerkgård, T., Boyd, R., Ihlen, P., Korneliussen, A., Nlsson, J.-A., Often, M., Eilu, P., & Hallberg, A., 2012: Metallogenic areas in Norway. *In:* P. Eilu (ed) Mineral deposits and metallogeny of Fennoscandia. *Geological Survey of Finland, Special Paper 53,* 35–138.
Sarapää, O., Lauri, L.S., Ahtola, T., Al-Ani, T., Grönholm, S., Kärkkäinen, N., Lintinen, P., Torppa, A. & Turunen, P., 2015: *Discovery potential of hi-tech metals and critical minerals in Finland. Geological Survey of Finalnd, Report of Investigation 219*, 54 pp.
Scogings, A., Chesters, J. & Shaw, B., 2015: Rank and file: Assessing graphite projects on credentials. *Industrial Minerals Magazine,* August 2015, 50–55.
Self, S., Keszthelyi, L. & Thordarson, T., 1998: The importance of pāhoehoe. *Annual Reviews in Earth and Planetary Science 26*, 81–110.
Shaikh, N.A., 1972: Sammanställning over grafitförkomsterna i det centrala Vittangifältet, Norrbottens län. *Sveriges geologiska undersökning Brap 876,* 19 pp.
Skiöld, T., 1981: Radiometric ages of plutonic and hypabyssal rocks from the Vittangi–Karesuando area, northern Sweden. *GFF 103*, 317–329.
Skiöld, T., 1986. On the age of the Kiruna Greenstones, northern Sweden. *Precambrian Research 32*, 35– 44.
Skiöld, T., 1988: Implications of new U–Pb zircon chronology to early Proterozoic crustal accretion in northern Sweden. *Precambrian Research 38*, 147–164.
Skiöld, T. & Cliff, R.A., 1984: Sm–Nd and U–Pb dating of Early Proterozoic mafic–felsic volcanism in northernmost Sweden. *Precambrian Research 26*, 1–13.
Skiöld, T., Öhlander, B., Markkula, H., Widenfalk, L., & Claesson, L.-Å., 1993: Chronology of Proterozoic orogenic processes at the Archaean continental margin in northern Sweden. *Precambrian Research 64*, 225–238.
Skiöld, T., Öhlander, B., Vocke, Jr, R.D., & Hamilton P.J., 1988: Chemistry of proterozoic orogenic processes at a continental margin in Northern Sweden. *Chemical Geology 69,* 193–207.
Smith, M., Coppard, J., Herrington, R., & Stein, H., 2007: The geology of the Rakkurijärvi Cu–(Au) prospect, Norrbotten: A new iron-oxide–copper–gold deposit in northern Sweden. *Economic Geology 102*, 393–414.
Smith, M.P., Storey, C.D., Jefferies, T.E. & Ryan, C., 2009: In situ U–Pb and trace element analysis of accessory minerals in the Kiruna district, Norrbotten, Sweden: New constraints on the timing and origin of mineralization. *Journal of Petrology 50*, 2063–2094.
Smith, M.P., Gleeson, S.A. & Yardley, B.W.D., 2013: Hydrothermal fluid evolution and metal transport in the Kiruna District, Sweden: Contrasting metal behaviour in aqueous and aqueous–carbonic brines. *Geochimica et Cosmochimica Acta 102*, 89–112.

Smolkin, V.F., 1997: The Paleoproterozoic (2.5–1.7 Ga) midcontinent rift system of the northeastern Fennoscandian Shield. *Canadian Journal of Earth Sciences 34*, 426–443.

Stacey, J.S. & Kramers, J.D., 1975: Approximation of terrestrial lead isotope evolution by a two-stage model. *Earth and Planetary Science Letters 26*, 207–221.

Steiger, R.H. & Jäger, E., 1977: Convention on the use of decay constants in geo- and cosmochronology. *Earth and Planetary Science Letters 36*, 359–362.

Sun, S.-S. & McDonough, W.F., 1989: Chemical and isotopic systematics of oceanic basalts: implication for mantle composition and processes. *Journal of the Geological Society of London Special Publication 42*, 313–345.

Talbot, C.J., 2001: Weak zones in Precambrian Sweden. *Geological Society, London, Special Publications 186*, 287–304.

Talbot, C.J., & Koyi, H., 1995: Palaeoproterozoic intraplating exposed by resultant gravity overturn near Kiruna, northern Sweden. *Precambrian Research 72*, 199–225.

Talga Resources Ltd, 2014: *Annual report to shareholders*. www.talgaresources.com. 73 pp.

Talga Resources Ltd, 2016: *Vittangi graphite resource upgrade*. Press release from Talga Resources Ltd, May 2016. www.talgaresources.com.

Taylor, H.A., Jr., 2006: Graphite. *In:* J.E. Kogel, N.C. Trivedi, J.M. Barker & S.T. Krukowski (eds.): *Industrial Minerals and Rocks*, Society for Mining, Metallurgy and Exploration, 507–518.

Taylor, S.R. & McLennan S.M., 1985: *The Continental Crust: Its Composition and Evolution*. Blackwell Scientific Publications, Oxford. 312 pp.

Thiessien, R., 1986: Two-dimensional refold interference patterns. *Journal of Structural Geology 8*, 563–573.

Tice, M.M. & Lowe, D.R., 2006: The origin of carbonaceous matter in pre-3.0 Ga greenstone terrains: A review and new evidence from the 3.42 Ga Buck Reef Chert. *Earth Science Reviews 76*, 259–300.

Walker, R.J., Morgan, J.W., Hanski, E.J. & Smolkin, V.F., 1997: Re–Os systematics of Early Proterozoic ferropicrites, Pechenga Complex, northwestern Russia: evidence for ancient ^{187}Os-enriched plumes. *Geochimica et Cosmochimica Acta 61*, 3145–3160.

Wanhainen, C., Billström, K. & Martinsson, O., 2006: Age, petrology and geochemistry of the porphyritic Aitik intrusion, and its relation to the disseminated Aitik Cu-Au-Ag deposit, northern Sweden. *GFF 128*, 273–286.

Wanhainen, C., Broman, C., Martinsson, O. & Magnor, B., 2012: Modification of a Palaeoproterozoic porphyry-like system: Integration of structural, geochemical, petrographic, and fluid inclusion data from the Aitik Cu–Au–Ag deposit, northern Sweden. *Ore Geology Reviews 48*, 306–331.

Wanke, A., & Melezhik, V., 2005: Sedimentary and volcanic facies recording the Neoarchaean continent breakup and decline of the positive $\delta^{13}C_{carb}$ excursion. *Precambrian Research 140*, 1–35.

Wasström, A., 2005: Petrology of a 1.95 Ga granite–granodiorite–tonalite–trondhjemite complex and associated extrusive rocks in the Knaften area, northern Sweden. *GFF 127*, 67–82.

Weihed, P., Arndt, N., Billström, K., Duchese, J.-C., Eilu, P., Martinsson, O., Papunen, H. & Lahtinen, R., 2005: Precambrian geodynamics and ore formation: The Fennoscandian Shield. *Ore Geology Reviews 27*, 273–322.

Welin, E., 1987: The depositional evolution of the Svecofennian supracrustal sequence in Finland and Sweden. *Precambrian Research 35*, 95–113.

Wiedenbeck, M., Allé, P., Corfu, F., Griffin, W.L., Meier, M., Oberli, F., Quadt, A.V., Roddick, J.C. & Spiegel, W., 1995: Three natural zircon standards for U-Th-Pb, Lu-Hf, trace element and REE analyses. *Geostandards Newsletter 19*, 1–23.

Wiedenbeck, M., Hanchar, J.M., Peck, W.H., Sylvester, P., Valley, J., Whitehouse, M., Kronz, A., Morishita, Y., Nasdala, L., Fiebig, J., Franchi, I., Girard, J.P., Greenwood, R.C., Hinton, R., Kita, N., Mason, P.R.D., Norman, M., Ogasawara, M., Piccoli, P.M., Rhede, D., Satoh, H., Schulz-Dobrick, B., Skår, O., Spicuzza, M.J., Terada, K., Tindle, A., Togashi, S., Vennemann, T., Xie, Q. & Zheng, Y.F., 2004: Further characterisation of the 91500 zircon crystal. *Geostandards and Geoanalytical Research 28*, 9–39.

Whitehouse, M.J., Claesson, S., Sunde, T. & Vestin, J., 1997: Ion-microprobe U–Pb zircon geochronology and correlation of Archaean gneisses from the Lewisian Complex of Gruinard Bay, north-west Scotland. *Geochimica et Cosmochimica Acta 61*, 4429–4438.

Whitehouse, M.J., Kamber, B.S. & Moorbath, S., 1999: Age significance of U–Th–Pb zircon data from Early Archaean rocks of west Greenland: a reassessment based on combined ion-microprobe and imaging studies. *Chemical Geology 160*, 201–224.

Whitehouse, M.J. & Kamber, B.S., 2005: Assigning dates to thin gneissic veins in high-grade metamorphic terranes: a cautionary tale from Akilia, southwest Greenland. *Journal of Petrology 46*, 291–318.

Wikström, A., Skiöld, T., & Öhlander, B., 1996: The relationship between 1.88 Ga old magmatism and the Baltic-Bothnian shear zone in northern Sweden. *Geological Society, London, Special Publication 112*, 249–259

Williams, I.S., 1998: U-Th-Pb geochronology by ion microprobe. *In:* M.A. McKibben, W.C. Shanks III & W.I. Ridley (eds.): Applications of microanaytical techniques to understanding mineralizing processes. *Reviews in Economic Geology 7*, 1–35.

Wilson, M., 1989: *Igneous Petrogenesis. A Global Tectonic approach*. Unwin Hyman, London, 466 pp.

Wilson, M.R., Hamilton, P.J., Fallick, A.E., Aftalion, M. & Michard, A., 1985: Granites and early Proterozoic crustal evolution in Sweden: evidence from Sm-Nd, U-Pb and O isotope systematics. *Earth and Planetary Science Letters 72*, 376–388.

Winchester, J.A. & Floyd, P.A., 1977: Geochemical discrimination of different magma series and their differentiation products using immobile elements. *Chemical Geology 20*, 325–343.

Witschard, F., Nylund, B. & Mannström, B. 1972: Masugnsbyn iron ore. Report concerning the results of Sveriges geologiska undersökning:s investigations in the years 1965-1970. *Sveriges geologiska undersökning Brap 734*, 95 pp.

Witschard, F., 1984: The geological and tectonic evolution of the Precambrian of northern Sweden – A case for basement reactivation? *Precambrian Research 23*, 273–315.

Zaki, N., 2015: Masugnsbyns dolomitbrott, redovisning av dolomittillgång. Unpublished *LKAB report 15-20003*, 30 pp.

Authors, paper 3:
Olof Martinsson
Luleå University of Technology,
Division of Geosciences and Environmental Engineering,
Luleå, Sweden

Stefan Bergman
Geological Survey of Sweden
Department of Mineral Resources
Uppsala, Sweden

Per-Olof Persson
Swedish Museum of Natural History,
Department of Geosciences,
Stockholm, Sweden

Hans Schöberg
Swedish Museum of Natural History,
Department of Geosciences,
Stockholm, Sweden

Kjell Billström
Swedish Museum of Natural History,
Department of Geosciences,
Stockholm, Sweden

Leonid Shumlyanskyy
M.P. Semenenko Institute of Geochemistry,
Mineralogy and Ore formation of the National Academy of Sciences of Ukraine,
Kyiv, Ukraine

3. Stratigraphy and ages of Palaeoproterozoic metavolcanic and metasedimentary rocks at Käymäjärvi, northern Sweden

Olof Martinsson, Stefan Bergman, Per-Olof Persson, Hans Schöberg,
Kjell Billström & Leonid Shumlyanskyy

ABSTRACT

The northern part of the Fennoscandian Shield predominantly comprises a 3.5–2.6 Ga Archaean craton, 2.5 to 2.0 Ga Karelian rocks linked to its rifting and breakup, and 1.9–1.8 Ga Svecofennian rocks related to destructive plate processes along its southwestern margin. Although the main aspects of the geological evolution during Palaeoproterozoic are fairly well constrained in northern Sweden, the chronostratigraphy of individual metavolcanic and metasedimentary units is poorly known. In this paper we define stratigraphic units within the Palaeoproterozoic supracrustal rocks at Käymäjärvi in northeastern Norrbotten that represent Karelian (inferred age c. 2.3–2.0 Ga) and Svecofennian supracrustal units (≤1.9 Ga). We also present geochronological data from three stratigraphically different volcanic units at Käymäjärvi.

The Karelian rocks studied belong to the Veikkavaara greenstone group and are subdivided into the Käymäjärvi formation, mainly consisting of pyroclastic metameimechite, and the overlying Vinsa formation, which includes mafic metatuffite, graphitic metatuffite, banded iron formation and dolomite. The local Svecofennian supracrustal rocks constitute the Sammakkovaara group, which includes the metaandesitic Muotkamaa formation in the lowest part, followed by the metasedimentary Hosiokangas formation and the uppermost metaandesitic Hosiovaara formation. U-Pb zircon data for a metameimechite from the Käymäjärvi formation were obtained using both multi-grain techniques (TIMS measurements), laser ablation and SIMS in situ methods. However, the data are difficult to interpret, probably mainly due to a heterogeneous zircon population of mixed magmatic and metamorphic origin. A preliminary interpretation of U-Pb age results, in combination with carbon isotope evidence from carbonate rocks, indicates an emplacement age close to 2.05 Ga. Two metaandesites from the Muotkamaa and Hosiovaara formations, respectively, yield similar zircon ages close to 1.88 Ga, although some evidence may point to a somewhat older magmatic age for the Muotkamaa formation. This may derive some support in the 1.89 Ga age of metaandesite in the Kalixälv formation, which is tentatively correlated with the Hosiovaara formation. In addition, several zircon fractions from these rocks record a metamorphic disturbance at c. 1.8 Ga.

The Käymäjärvi and Vinsa formations may be correlated with other greenstone units in northeastern

Norrbotten and correspond to the Jatulian–Ludikovian units in the northeastern Fennoscandian Shield. Both petrographic and geochronological data support the idea that rocks of the Sammakkovaara group can be correlated with the lower Svecofennian Porphyrite group in the Kiruna area, but also with the Muorjevaara group in the Gällivare area and other arenitic to clay-rich metasedimentary formations of Svecofennian age in northern Norrbotten.

INTRODUCTION

The northern part of the Fennoscandian Shield predominantly comprises a ~3.5–2.6 Ga Archaean craton, 2.5 to 2.0 Ga Karelian rocks linked to its rifting and breakup, and 1.9–1.8 Ga Svecofennian rocks related to destructive plate processes along its southwestern margin. Palaeoproterozoic 2.3 to 2.0 Ga ultramafic to mafic metavolcanic rocks are widely distributed in northern Finland and Norway, and these greenstone belts also extend into Norrbotten County in northernmost Sweden. Due to the remarkable similarity in stratigraphy and the predominantly tholeiitic character of the metavolcanic rocks in this region, Pharaoh (1985) suggested that they represent a major tholeiitic province. These 2.3–2.0 Ga mafic-ultramafic metavolcanic rocks were formed in response to continental rifting at ~2.06 Ga, along a line from Ladoga in the southeast to Lofoten in the northwest (Kohonen & Marmo 1992, Vuollo 1994, Martinsson 1997, Lahtinen et al. 2015), which culminated in the opening of an ocean. Subduction of oceanic crust along this continental margin started more than 100 Ma later, when juvenile crust was formed and added to reworked Archaean crust as a product of Svecofennian arc magmatism (Öhlander et al. 1993, Ekdahl 1993, Lahtinen 1994).

Although the main aspects of geological evolution during Palaeoproterozoic time are fairly well constrained in northern Sweden, the chronostratigraphy of individual metavolcanic and metasedimentary units is poorly known. This hampers detailed interpretations of the geological evolution and the correlation of these rocks with similar units in other parts of the shield. In this paper we present geochronological data from three stratigraphically distinct metavolcanic units at Käymäjärvi in northeastern Norrbotten. TIMS data on a metameimechite sample were found to be too complex to interpret, and single-grain, in situ techniques were used on that sample.

GENERAL GEOLOGY

In northern Sweden a Palaeoproterozoic succession of greenstones, porphyries and clastic metasedimentary rocks rests unconformably on a deformed 3.2–2.7 Ga old Archaean basement. Following the tectofacies concept of Laajoki (2005) and the subdivision of the Karelian cover sequence in the northeastern part of the Fennoscandian Shield proposed by Melezhik et al. (1997) and Hanski & Melezhik (2012), the Kovo group is regarded to be of Sumi–Sariolian age (2.5–2.3 Ga). Rocks of the Kovo group occupy the stratigraphically lowest position in the Kiruna area, and are overlain by the Jatulian (2.3–2.06 Ga) to Ludikovian (2.06–1.96 Ga) Kiruna greenstone group (Martinsson 1997, 1999). Karelian units are unconformably overlain by Svecofennian 1.9 Ga rocks including the Porphyrite group, the Kurravaara conglomerate, the Kiirunavaara group and the Hauki quartzite. Analogously, the Karelian greenstones in eastern Norrbotten are overlain by Svecofennian volcanic and sedimentary units (Martinsson 2004a).

Karelian greenstones in northern Sweden are best known from the Kiruna area, where a complete section of the well-preserved Kiruna greenstone group exists (Martinsson 1997). To the east, in the Masugnsbyn area, the Veikkavaara greenstone group is regarded as stratigraphic equivalent of the Kiruna greenstone group (Padget 1970, Martinsson 2004a). The Veikkavaara greenstone group is exposed in the Tärendö, Pajala and Lannavaara areas, and shows a strong consistency in lithological properties and stratigraphic relations. Compared to the greenstones in the Kiruna area, however, some differences in lithological properties can be observed. These are thought to reflect different depositional environments.

Rocks from the Veikkavaara greenstone group were deposited in a shallow marine environment, whereas rocks from the more westerly Kiruna greenstone group were formed in a failed rift arm during partly deeper water conditions (Martinsson 1997, 2004a).

The greenstones have been exposed to erosion in some areas, as evidenced by the loss of the upper part of the Kiruna greenstone group in the central Kiruna area (Martinsson 1997), before being overlain by Svecofennian successions of volcanic and clastic sedimentary rocks. The lowermost Svecofennian rocks are the Porphyrite group and the Kurravaara conglomerate, and stratigraphically equivalent units outside the Kiruna area (e.g. the Pahakurkio group, Kalixälv group and Muorjevaara group). These rocks were formed in relation to northward subduction at the southwestern margin of the Archaean palaeocontinent (Martinsson 2004a). Andesitic volcanic rocks of calc-alkaline character were formed from isolated volcanic centres separated by sedimentary basins fed by volcaniclastic material and epiclastic sediments from granite-gneiss terranes in the northeast (Martinsson 2004a). In the Kiruna area, the Porphyrite group is overlain by the Kiirunavaara group, comprising a bimodal volcanic unit formed in a back arc or intra-plate setting (Martinsson 2004a). It is mainly restricted to the Kiruna and Malmberget areas; only small and isolated occurrences are known further east. Quartzitic metasedimentary rocks constitute the youngest Svecofennian units and are represented by the Hauki and Maattavaara quartzites in the Kiruna area (Offerberg 1967, Eriksson & Hallgren 1975), and the Rissavaara quartzite in the Masugnsbyn area (Padget 1970).

The Palaeoproterozoic volcanic and sedimentary rocks were deformed and metamorphosed during the Svecokarelian orogeny (1.9–1.8 Ga). Abundant syn-orogenic 1.89–1.87 Ga intrusions of the Haparanda and Perthite monzonite suites range from gabbro to granite (Bergman et al. 2001, Martinsson 2004a). Minimum melt granites and pegmatites, represented by the Lina suite, formed c. 1.79 Ga (Skiöld et al. 1988), and are coeval with 1.80–1.78 Ga Transscandinavian igneous belt intrusions (TIB 1) of monzonitic to granitic composition (Romer et al. 1992, Martinsson 2004a). Limited data suggest the presence of at least two metamorphic and deformation events in northeastern Norrbotten at c. 1.88 and 1.80 Ga, respectively (Bergman et al. 2001), as well as a more local metamorphic event at 1.85 Ga (Bergman et al. 2006). The youngest plutonic rocks are the c. 1.71 Ga TIB 2 granitoids located in the Rombak window (Romer et al. 1992).

STRUCTURE AND STRATIGRAPHY OF THE KÄYMÄJÄRVI AREA

The geology of the Käymäjärvi area, situated 25 km northwest of Pajala, has previously been described by Eriksson (1954). The bedrock is partly well exposed with Palaeoproterozoic supracrustal rocks, including the stratigraphically upper part of the Veikkavaara greenstone group and overlying Svecofennian volcanic and sedimentary rocks. Greenstones occupy the central part of an anticline that is surrounded by younger Svecofennian units (Fig. 1). Fold axes plunge approximately 45 to 60° to the southeast, with more gently plunging dips found locally in the south. The western limb dips 30 to 60° to the southwest, whereas the eastern limb is tectonically more complex due to intersection with a shear zone running along the contact between andesitic and quartzitic units. Northeast of the deformation zone rocks are mostly overturned with a steep to moderate dip to the southwest. A second phase of deformation is recorded by locally occurring fold axes and mineral lineations plunging gently to the southwest. In the east of the area the two phases of folding have resulted in a dome and basin pattern outlined by Svecofennian metasedimentary rocks and metaandesites. In the central part of the anticline a metamorphic pressure-temperature of 2.6 kbars and 510 °C is reported (Bergman et al. 2001). Outside this core of relatively low metamorphic grade, rocks show an increasing metamorphic grade, with decreasing distance to the surrounding felsic intrusions.

The lithostratigraphy of the area (Fig. 2) has been established in the present study, based on detailed mapping of well-exposed sections in combination with interpretation of geophysical magnetic and slingram ground measurements, in which iron formations and graphitic schist show up as good marker

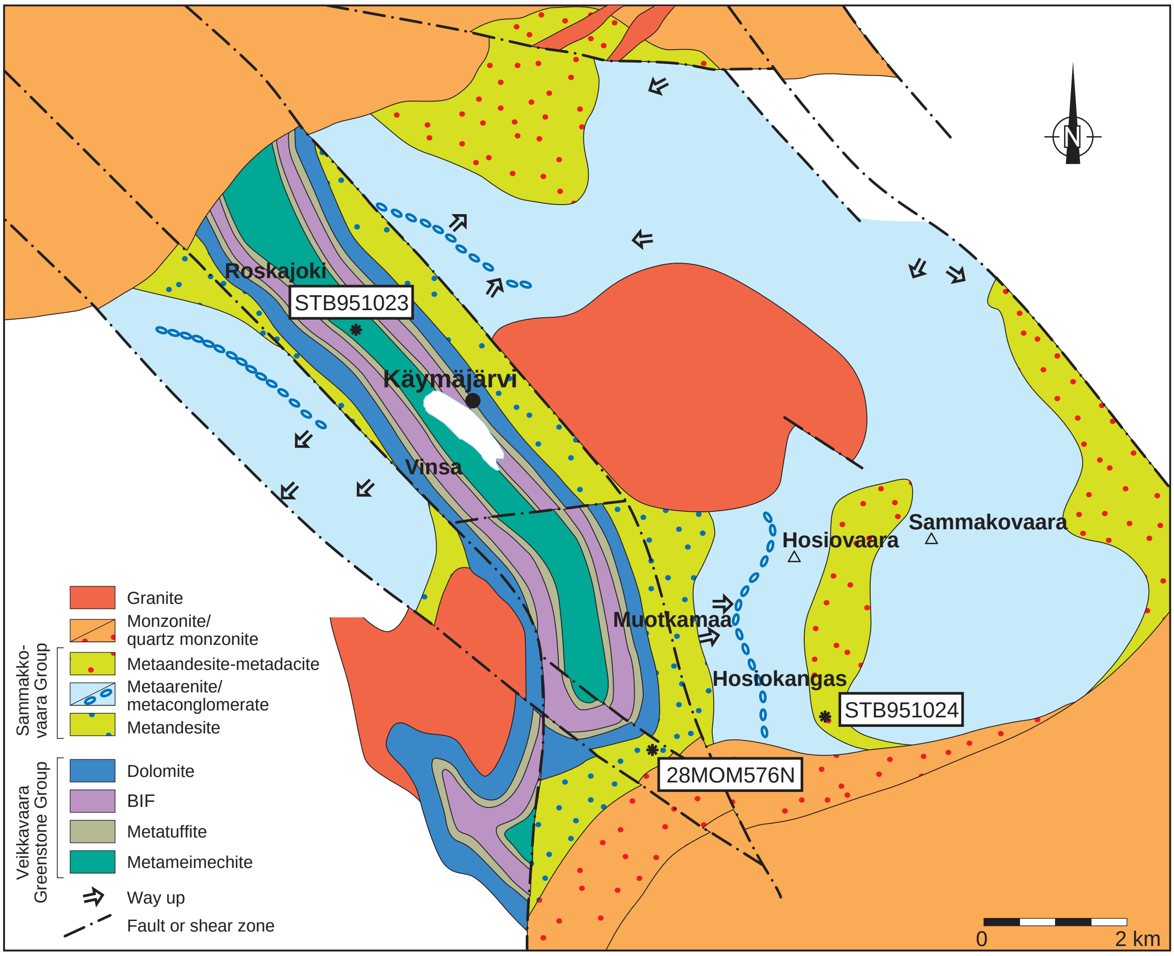

Figure 1. Bedrock map of the Käymäjärvi area with locations of samples analysed. Modified from Padget (1977).

horizons. Stratigraphic names refer to geographical names within the type areas for each unit. Lower and upper contacts are defined where possible and constitute boundaries between units having different lithological properties.

The Veikkavaara greenstone group

Metavolcanic rocks at Käymäjärvi belonging to the upper parts of the Veikkavaara greenstone group are located in the central part of an anticline and occupy an area 1.6 km wide and 10 km long. The core of the anticline consists of metameimechitic lapilli tuff constituting the Käymäjärvi formation, followed by the Vinsa formation, comprising metatuffite, graphite schist, banded iron formation (BIF), and dolomite (Fig. 1).

The Käymäjärvi formation

The Käymäjärvi formation is exposed northwest of Lake Käymäjärvi (Fig. 1). Ground geophysical measurements indicate that these rocks extend further to the southeast and northwest, thus occupying the core of the anticline in a belt approximately 400 m wide. Well-preserved metameimechite rocks occur close to the upper contact of this unit, while primary features in the central part of the anticline are largely obliterated by a strong schistosity. Within the anticline the metameimechite has an exposed thickness of about 150 m, which is taken as the minimum thickness of this unit.

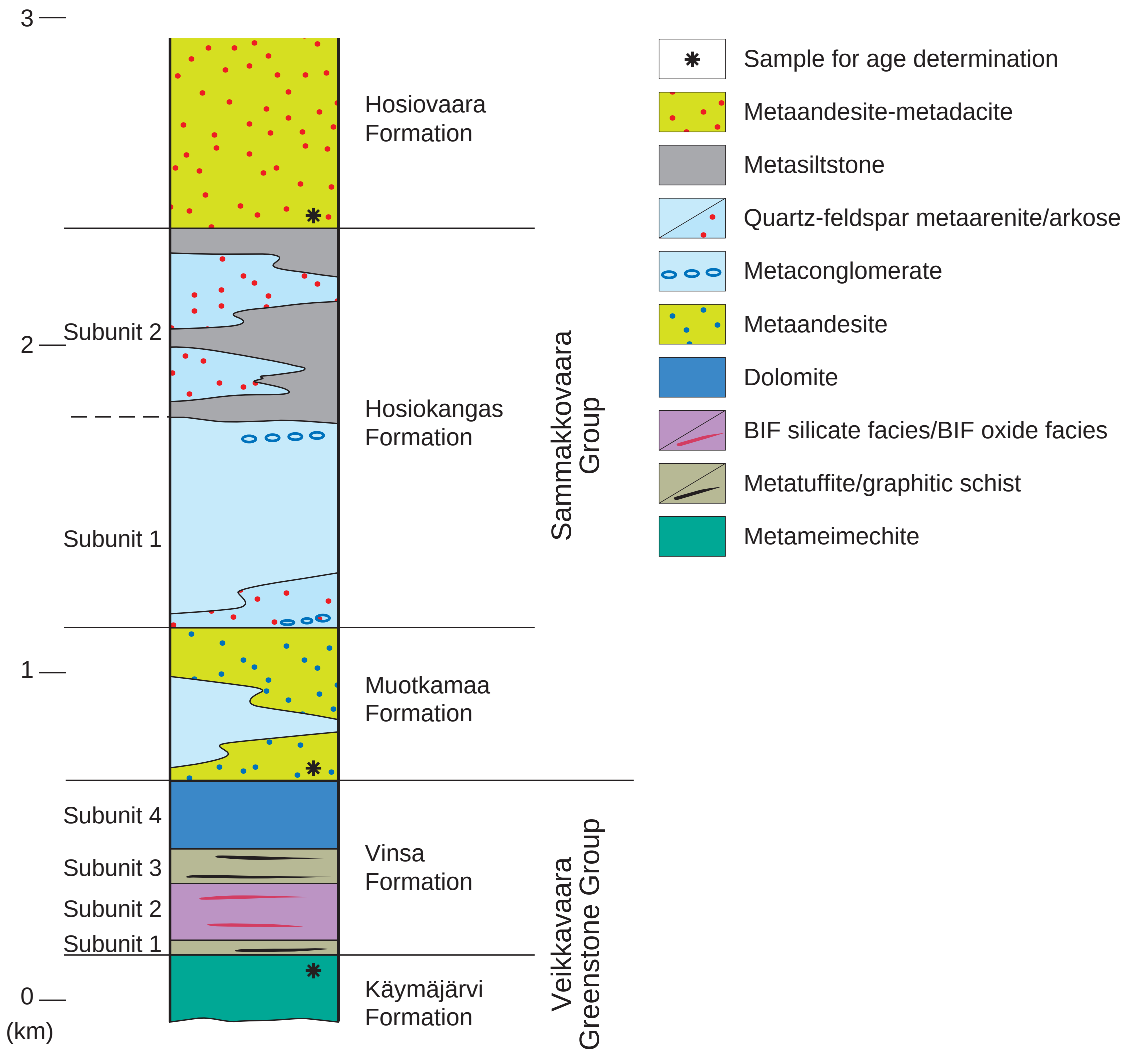

Figure 2. Lithostratigraphy of the Käymäjärvi area, including the Veikkavaara greenstone group and the Sammakkovaara group.

The metameimechite rocks have a pyroclastic character, with lapilli tuff, sometimes showing graded bedding, as a major component. Fragments are slightly vesicular, irregular in shape and mostly 5 to 30 mm in size (Fig. 3A). Lithic fragments of meimechite, with a size of up to 10 cm, are encountered locally. In thin section the rock is predominantly made up of irregularly orientated acicular actinolite porphyroblasts, occurring in a dense mass of less than 0.1 mm long needles (Fig. 3B). Slightly larger porphyroblasts of actinolite occur locally in patches or may replace the pyroclastic fragments. Coarser-grained amphibole is also present in the matrix between fragments. Chlorite, forming small rounded aggregates, and opaque minerals, are minor constituents. Ilmenite is a common accessory mineral, occurring as tabular grains up to 1.5 mm long, while magnetite is rare. The major and trace element content of two metameimechite samples are shown in Table 1. Samples are ultrabasic in composition with a MgO content varying between 19.2 and 21.1 wt %, while Cr and Ni content ranges from 1050 to 1460 and 713 to 1250 ppm, respectively. The fairly high values for Fe_2O_3 (13.2–17.1 wt %), TiO_2 (1.4–1.7 wt %), and Zr (75–96 ppm) compared with komatiites and a lower total alkali content compared with picrites is characteristic of these rocks.

The Vinsa formation

The contact between the Vinsa formation and the Käymäjärvi formation is not exposed but is arbitrarily defined as the transition from ultramafic meimechite tuff to mafic tuffite. The stratigraphic distance between the nearest exposures representing the respective formations is less than 25 m. Exposures of all units of the Vinsa formation, except those in its lowest part, crop out on Vinsa hill 1 km southwest of Lake Käymäjärvi. Most conspicuous are thick units of BIF and dolomite occupying the lower and upper part, respectively. Other lithologies are predominantly mafic tuffites and graphitic metasedimentary rocks forming the base of the Vinsa formation, and also occurring as intercalations between the BIF and the dolomite. The approximately 450 to 550 m thick Vinsa formation is divided into four lithological sub-units as follows.

The tuffites constituting the lowermost sub-unit (unit 1) have a mafic composition and are locally graphite-bearing. Fe-sulphide content is high in places, whereas the amount of graphite rarely exceeds a few per cent by weight. Layers rich in garnet porphyroblasts occur locally in the middle part, whereas scapolite may be common close to the upper contact. The total thickness of this unit is 40 to 50 m.

The next sub-unit (unit 2) is a 150 to 200 m thick silicate facies BIF with locally developed oxide facies. It can be followed along strike in scattered outcrops and by magnetic ground measurements for a distance of approximately 18 km around the core of the anticline. It is best exposed at Ylijoki, northwest of Vinsa (close to sample site STB 9510124, Fig. 1). The BIF exhibits a distinct mesobanding with 5 to 30 cm thick bands of recrystallised chert alternating with silicate bands containing mainly pyroxene, amphibole, garnet and fayalite in different proportions (Fig. 3C). Grünerite is the predominant mineral in most silicate bands (Geijer 1925). Magnetite occurs locally as microbands within silicate bands, and as low-grade dissemination in some silicate and chert bands. The occurrence of rounded aggregates rich in disseminated magnetite was interpreted as former greenalite oolites by Geijer (1925), and indicates temporary deposition above the wave base. Some iron-poor parts of the unit differ in character only by their lack of iron-rich silicates and magnetite. Calc-silicate layered dolomite occurs locally as thick intercalations up to several metres thick. The iron content varies between 14 and 25 wt % Fe in silicate facies BIF, but in oxide facies it may reach 30 to 40 wt % over some metres of stratigraphic thickness. Both the silicate and oxide facies contain between 2.3 and 3.4 wt % MnO, and Ba may be enriched up to 1 wt % in the oxide facies BIF. The BIF records a minimum of clastic sedimentation (i.e. very low content of Al and Ti).

The BIF is overlain by an approximately 100-metre-thick unit (unit 3), which contains mafic tuffites with intercalated graphitic and calc-silicate-bearing beds. Rocks are partially laminated at a mm to cm scale. Scapolite is common and, together with diopside, constitutes a major component in some of the beds. The occurrence of finely laminated and almost monomineralic diopside rocks that grade into tuffitic rocks mainly consisting of diopside, scapolite and biotite is a prominent feature of these beds. Disseminated graphite and Fe-sulphides are locally common but the amount of graphite and sulphur is generally less than 10 and 3 wt %, respectively. This unit is geochemically anomalous with a particularly pronounced enrichment of Ca, Mg, K, Ba, Cl, and Br. Other elements showing elevated concentrations compared to mafic tuff-tuffite in other stratigraphical positions in the Veikkavaara greenstone group are Mn, P, Y, Cu, Zn, As, Sb, Mo, and V.

The uppermost unit (unit 4) of the Vinsa formation is a 150 to 200 m thick dolomite that is best exposed at Muotkamaa, 5 km southeast of Käymäjärvi. The dolomite has intercalations of tuffite early in the sequence. However, most of this unit consists of a fairly pure dolomite with 22.0–22.5 wt % MgO, 29.1–29.8 wt % CaO and 2.3–5.0 wt % SiO_2. Calc-silicates are found in small quantities and are predominantly actinolite, although humite minerals may be locally abundant. Calc-silicates become more common in the upper 20–50 metres, forming more massive calc-silicate units consisting mainly of amphibole and pyroxene in different proportions, but locally also knebelite.

The Sammakkovaara group

The Veikkavaara greenstone group is followed by metamorphosed Svecofennian volcaniclastic and clastic sedimentary rocks constituting the Sammakkovaara group. This unit is best exposed at Sammakkovaara hill, about 6 km east of Käymäjärvi (Fig. 1), which is the type locality for the Sammakkovaara group. Similar rock sequences are found overlying the greenstones in other parts of northeastern Norrbotten, suggesting that the Sammakkovaara group is of regional importance. The contact with the underlying Vinsa formation is rarely exposed, but layering within the Sammakkovaara group is mainly conformable to its substratum, indicating no major angular unconformity between these units at Käymäjärvi.

Based upon lithological properties, the Sammakkovaara group may be further divided into three formations: the Muotkamaa formation, comprising a lower andesitic metavolcanic unit together with minor intercalated clastic metasedimentary rocks; the Hosiokangas formation, which is predominantly made up of arenitic to clay-rich metasedimentary rocks; and an upper andesitic metavolcanic-dominated unit, which constitutes the Hosiovaara formation.

The Muotkamaa formation

The Muotkamaa formation is exposed at Muotkamaa, about 5 km southeast of Käymäjärvi and has also been intersected in drillholes at Roskajokki, 3 km northwest of Käymäjärvi (Lundmark 1985). The total thickness of this unit is approximately 400 to 550 m. It predominantly comprises andesitic rocks but also includes minor clastic metasedimentary units of arenitic composition.

Primary structures are poorly preserved in the metaandesite, and the nature of the rock is mostly unclear. But its fine-grained character and the common presence of a porphyritic texture indicate an extrusive origin. Phenocrysts of plagioclase are up to 3 mm in size. Aggregates of amphibole 1 to 3 mm in size constitute 5–10% and probably represent relicts of pyroxene or amphibole phenocrysts (Fig. 3D). The texture is mostly granoblastic to poikiloblastic with 0.05 to 0.2 mm large grains of plagioclase, hornblende and biotite enclosed within aggregates of hornblende and diopside. Minor constituents are microcline, quartz and calcite. Scapolite may be abundant occurring as poikiloblasts and in patches. The chemical composition of metaandesites from the Muotkamaa formation is shown in Table 1.

Metaarenite with varying feldspar content occurs as a 50 to 100 m thick intercalation at Muotkamaa. The contact to the metaandesite is not exposed. Arenitic metasedimentary rocks also occur in a drillcore at Roskajokki, close to the lower contact of the Muotkamaa formation.

The Hosiokangas formation

The Hosiokangas formation is well exposed at Hosiokangas, 6 km southeast of Käymäjärvi, and is a clastic unit of arenitic to more fine-grained sediments that has a total thickness of 1100 to 1300 m. The lower and upper contacts are gradual over a distance of some metres, with epiclastic rocks that grade into metaandesite. Metaconglomerate beds and tuffitic intercalations of andesitic composition occur as minor constituents.

Based on lithological properties, the Hosiokangas formation may be divided into two sub-units. The lower unit predominantly comprises feldspar-rich quartzite that partly grades into meta-arkose. Intercalations of metaconglomerate occur in its lower and upper part. The upper unit shows rapid lithological changes, with beds consisting of subarkose, arkose, clay-rich rocks and tuffite.

An approximately 1 m thick metaconglomerate at the base of the lower sub-unit contains gravel-sized clasts, mainly of quartz or quartzite (Padget 1977), and is associated with arkosic arenite. Most of the lower unit has fairly low feldspar content and displays a reddish to light grey colour. These arenitic metasedimentary rocks often show heavy-mineral laminae and cross-bedding. In its upper part, a 5 to

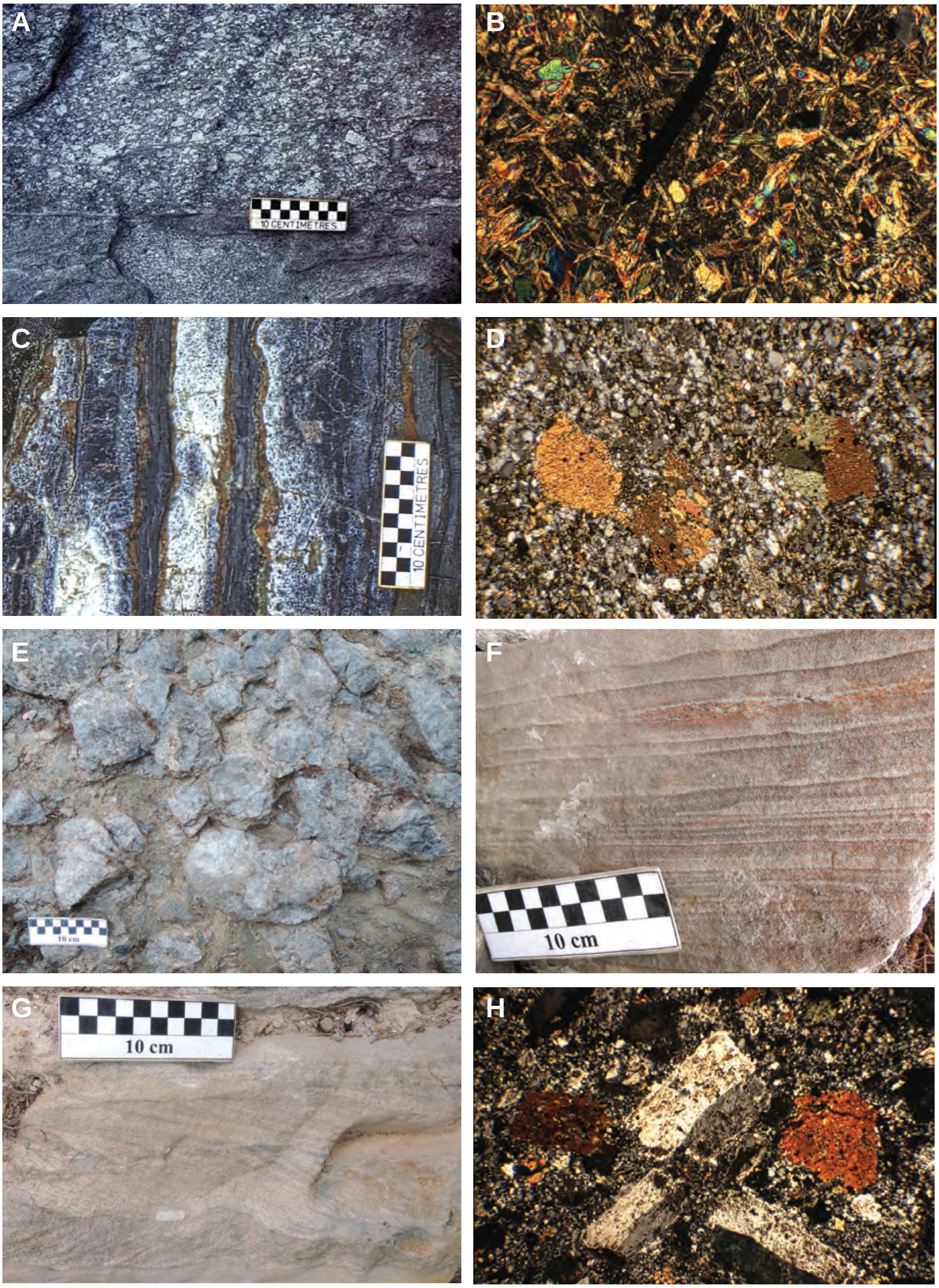

Figure 3. Photographs and photomicrographs of rocks from the Käymäjärvi area. **A** Meimechitic lapilli tuff from the Käymäjärvi formation. **B** Microphotograph of meimechitic lapilli tuff with tabular grains of ilmenite, sample STB951023, crossed nicols. **C** Silicate facies BIF from the Vinsa formation. **D** Photomicrograph of metaandesite with relict phenocrysts of amphibole or pyroxene, Muotkamaa formation, crossed nicols. **E** Quartz pebble conglomerate from the middle part of the Hosiokangas formation. **F** Graded bedding in andesitic volcaniclastitic metasandstone, upper part of Hosiokangas formation. **G** Herringbone cross-stratification from the upper part of the Hosiokangas formation. **H** Photomicrograph of plagioclase porphyritic metaandesite with relict pyroxene phenocrysts from the Hosiovaara formation, crossed nicols. Photos: Olof Martinsson.

30 m thick monomict metaconglomerate forms a laterally extensive intercalation. It contains up to 30 cm, well-rounded to more angular clasts of almost pure quartz (Fig. 3E). Minor constituents are pebbles of schist and magnetite ore. The metaconglomerate is mostly clast-supported, with a matrix consisting of quartz arenite. Quartz clasts are partly dusted by hematite, which also occurs as larger flakes in the matrix and within veinlets. Feldspar is very rare and mainly confined to the matrix. Small clasts with high iron oxides content are present in minor amounts.

In the upper sub-unit of the Hosiokangas formation, arenitic metasedimentary rocks are interlayered with more clay-rich rocks. Metaarenites are generally reddish in colour and have a feldspar content ranging from 20 to 40%. They grade into dark grey, smaller-grained and more clay-rich metasedimentary rocks with 20 to 30% biotite, which locally contain porphyroblasts of andalusite. Clay-rich rocks are partly migmatitic in character. Tuffitic units of andesitic composition occur locally as up to 50 m thick intercalations (Fig. 3F). Cross-bedding is common in the arenitic units and locally shows herringbone cross-stratification (Fig. 3G). In some beds, actinolite occurs disseminated or enriched in layers and may be the metamorphic expression of calcareous material.

The Hosiovaara formation

The Hosiovaara formation is poorly exposed. Only a few small outcrops occur close to its lower contact. However, andesite occurs in local boulders and in outcrops strongly affected by frost wedging, which are extensively distributed on the eastern slope of Hosiovaara hill, 5 km east of Käymäjärvi. At this locality, metavolcanic rocks constitute the core of a narrow syncline plunging to the south. The lower contact is gradual, with clay-rich metasedimentary rocks grading into volcaniclastic rocks of andesitic composition over a distance of several metres. Rocks are mostly porphyritic, and veins and patches of epidote-pyroxene-amphibole are locally common. The upper contact of the Hosiovaara formation is not preserved, and its total thickness is therefore unknown, but estimated to be at least 1 km.

At Hosiovaara the metaandesites are fairly well preserved and mostly porphyritic. Plagioclase phenocrysts form 10 to 40% in a matrix with a grain size of 0.02 to 0.04 mm (Fig. 3H). Phenocrysts commonly show Karlsbad twinning in combination with albite twinning and are 0.5 to 3 mm long. Larger grains and aggregates of hornblende, representing altered amphibole or pyroxene phenocrysts, are less abundant. The matrix has a granoblastic texture consisting of plagioclase together with smaller amounts of hornblende, microcline, diopside and epidote. Scapolite may occur as porphyroblasts, whereas titanite and calcite occur as accessory components. South of Hosiovaara outcrops of metaandesite are found close to the lower contact of the Hosiovaara formation. Here the rock shows a higher degree of alteration, recrystallisation, and skarn veining. The porphyritic texture is almost obliterated and scapolite is a common secondary mineral. The scapolite porphyroblasts are partly altered and replaced by epidote, hornblende, and biotite. A large granitoid intrusion exists 600 m to the south, and the volcanic rocks show migmatitic veining close to this contact. The chemical composition of metaandesites from the Hosiovaara formation is shown in Table 1. Compared to metaandesites from the Muotkamaa formation samples, they have a slightly more fractionated and silica-rich character, with higher concentrations of Si, Th, Zr, and REEs, and lower concentrations of Fe, Mg, Ca, Sc, and V. The Zr-Ti diagram (Pearce 1982) is used to compare the metaandesites from the Muotkamaa and Hosiovaara formations with other rocks, and shows them to occupy the same area as metaandesitic rocks from the Porphyrite group in the Kiruna area (Fig. 4).

Table 1. Chemical analysis of metavolcanic rocks from the Käymäjärvi area. Samples 28MOM544, 28MOM576 and 28MOM583 were analysed by ICP-AES and INAA. The other samples were analysed by ICP-AES and ICP-MS.

Sample	**28MOM544**	**STB951023**	**28MOM576N**	**28MOM583**	**STB951024**	**BOM950047B**
	Meta-meimechite	**Meta-meimechite**	**Meta-andesite**	**Meta-andesite**	**Meta-andesite**	**Meta-andesite**
Formation	**Käymäjärvi Fm**	**Käymäjärvi Fm**	**Muotkamaa Fm**	**Muotkamaa Fm**	**Hosiovaara Fm**	**Hosiovaara Fm**
wt %						
SiO_2	43.50	44.50	56.30	57.50	61.30	62.70
TiO_2	1.49	1.39	0.73	0.76	0.72	0.74
Al_2O_3	7.55	7.48	14.90	15.50	16.00	15.50
Fe_2O_3	13.80	17.10	8.28	8.55	6.02	6.44
MnO	0.25	0.49	0.38	0.13	0.09	0.08
MgO	21.10	19.20	3.89	4.08	2.42	2.18
CaO	8.99	5.39	8.15	6.94	5.45	4.55
Na_2O	0.69	0.67	2.96	4.05	5.07	4.85
K_2O	0.11	0.36	3.63	2.44	2.50	3.47
P_2O_5	0.15	0.13	0.31	0.33	0.29	0.30
LOI	3.40	2.90	1.20	0.80	0.40	0.40
SUM	**101.10**	**99.60**	**100.70**	**101.10**	**100.30**	**101.20**
ppm						
Sr	58	42	310	897	1230	1020
Ba	47	280	1060	1130	1630	1560
Rb	ND	15.1	97.0	87.0	49.5	88.5
Nb	NA	6.3	NA	NA	12.3	13.1
Ta	ND	0.63	1.40	ND	0.97	1.05
U	ND	0.38	1.80	1.80	2.73	3.60
Th	1.10	0.94	7.90	7.80	15.10	15.10
Zr	84	83	124	130	230	239
Hf	3.0	2.8	4.0	3.0	7.8	8.4
La	9.2	6.6	41.0	36.0	52.5	53.8
Ce	29.0	19.2	80.0	67.0	108.0	111.0
Nd	14.0	13.3	32.0	28.0	43.1	46.2
Sm	4.10	2.57	4.50	4.30	6.53	6.58
Eu	1.30	0.69	1.50	1.50	0.82	1.50
Gd	NA	3.45	NA	NA	4.39	4.84
Tb	ND	0.54	ND	ND	0.59	0.59
Dy	NA	2.81	NA	NA	2.90	3.09
Ho	NA	0.46	NA	NA	0.51	0.52
Er	NA	1.64	NA	NA	1.45	1.64
Tm	NA	0.19	NA	NA	0.17	0.19
Yb	1.90	1.38	1.70	1.80	1.49	1.40
Lu	0.30	0.25	0.29	0.30	0.17	0.18
Y	13.2	11.8	13.0	14.6	13.7	13.8
Sc	23.9	22.9	17.6	18.2	8.5	8.1
V	207	231	161	162	119	119
Cr	1270	1300	103	100	43	49
Ni	713	1090	29	27	30	26
Co	87.1	90.5	12.4	24.2	12.8	15.0
Cu	80	167	27	50	ND	ND
Zn	168	718	55	29	108	183
Ga	NA	12.3	NA	NA	17.8	17.4

NA = not analysed, ND = not detected

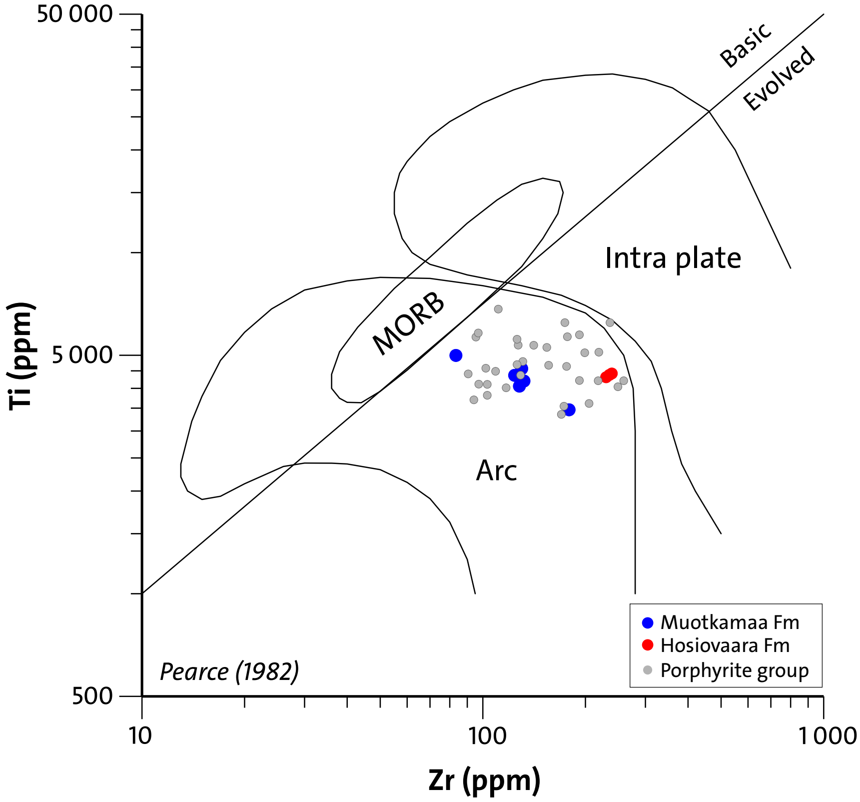

Figure 4. Geochemical comparison of metavolcanic rocks from the Sammakkovaara group with Porphyrite group metavolcanic rocks from the Kiruna area (Martinsson, unpublished data) using the Zr-Ti diagram from Pearce (1982).

SAMPLE DESCRIPTION

Sample STB951023, metameimechite from the Käymäjärvi formation

(coordinates in the Swedish National Grid SWEREF99 TM: 7497684/839675)

A sample was taken from the uppermost part of the meimechitic unit (approximately 10–20 metres from the contact with the overlying Vinsa formation). Graded bedding is seen in the outcrop, with decreasing grain size stratigraphically upwards. The meimechitic lapilli tuff has a greenish colour and consists of up to 2 cm sized fragments with a rounded shape and vesicular texture. Amphibole is the major mineral (about 95%), with ilmenite as the most important accessory mineral (about 5%). Grain size is mainly 0.05 to 0.1 mm, although porphyroblasts, clots and schlieren of actinolite with a grain size of up to 0.3 mm have partly replaced the more fine-grained matrix. Chlorite occurs in rounded aggregates that are partly replaced by amphibole. The rock is foliated; two directions of foliation are outlined by platy ilmenite and acicular amphibole.

Sample 28MOM576N, metaandesite from the Muotkamaa formation

(coordinates in the Swedish National Grid SWEREF99 TM: 7492691/843243)

The metaandesite was sampled close to the contact with the underlying dolomite within the Vinsa formation. The sample has a greenish-grey colour, is massive in character and has a granoblastic to crystalloblastic texture with a 0.05 to 0.1 mm grain size. Sparse phenocrysts of pyroxene and plagioclase occur as 0.5 to 2 mm sized relicts composed of amphibole-biotite and scapolite-biotite, respectively. Amphibole and diopside occur (approximately 15%) in a matrix of plagioclase and varying amounts of microcline. Biotite is locally abundant and scapolite is common as poikiloblasts and patches. Carbonate is found as an accessory mineral irregularly distributed in the rock. Scapolite is partly replaced by biotite, and amphibole may be replaced by diopside.

Sample STB951024, metaandesite from the Hosiovaara formation
(coordinates in the Swedish National Grid SWEREF99 TM: 7493092/845668)
The metaandesite from the Hosiovaara formation was sampled close to its lower contact. Veinlets and patches of epidote-pyroxene are common, and granitic veins are locally present in the surrounding outcrops of metaandesite. The rock has a pale grey colour and is slightly banded, locally with a diffuse clastic structure. Phenocrysts of plagioclase 0.5 to 3 mm in size consititute 10 to 30% of the sample. Amphibole pseudomorphs after pyroxene phenocrysts are sparse. The texture is granoblastic to poikiloblastic and, due to strong recrystallisation, the primary porphyritic texture is only locally well preserved (Fig. 3H). The matrix grain size is 0.05 to 0.2 mm, mainly consisting of plagioclase with some microcline. Amphibole, diopside, and scapolite occur in poikiloblastic aggregates. Epidote is a paragenetic late mineral that replaces both scapolite and amphibole. Titanite is a common accessory mineral forming part of the metamorphic assemblage. Small and rounded grains of zircon are less abundant.

ANALYTICAL METHODS

The zircons were separated using standard magnetic and heavy liquid techniques, and examined using optical microscopy. Samples were analysed using the conventional (multi-grain TIMS) technique at the Department of Geosciences at the Swedish Museum of Natural History; and for the metameimechite, also by in situ (SIMS and LA-ICP-MS) analyses. CL imaging was conducted on some grains.

Most zircon fractions selected for TIMS were abraded according to the method used by Krogh (1982). After decomposition (Krogh 1973) and aliquoting, a mixed ^{208}Pb-$^{233-235}$U tracer was added to the ID aliquots. The sample aliquots were loaded onto anion exchange columns for extraction of Pb and U. These were later loaded onto Re single filaments with silica gel and H_3PO_4. Most samples were measured in static mode using a MAT 261 mass spectrometer. Small Pb and U amounts, yielding low signals, were measured in peak jumping mode on a secondary electron multiplier. The total Pb blank was 4–7 pg and the U blank less than 2 pg. Titanite was processed using HBr chemistry to achieve better purification of lead and uranium.

The preparation of zircon grains for in situ analyses was the same for SIMS and LA-ICP-MS. Individual zircon grains, remaining after the TIMS session, were mounted in epoxy, along with the 91500 standard zircon (Wiedenbeck *et al.* 1995) and polished to approximately half their thickness. Polished grains were investigated by SEM (Scanning Electron Microscope) equipped with a CL (cathodeluminescence) detector. Images were used for choosing areas suitable for U-Pb dating. U-Th-Pb SIMS geochronological data were obtained using the Cameca 1280 ion microprobe at the Nordsim facility, at the Swedish Museum of Natural History. The analytical method follows that described by Whitehouse & Kamber (2005). A Thermo-Scientific Element 2 XR sector field ICP-MS coupled to a New Wave UP-193 Excimer Laser System, at the Museum für Mineralogie und Geologie (GeoPlasma Lab, Senckenberg Naturhistorische Sammlungen Dresden, Germany), was used for the LA-ICP-MS data set. For further details on the analytical protocol and data processing, see Gerdes & Zeh (2006).

The procedure used for calculating corrected isotope ratios and error propagation, was the same for all types of analytical protocol (using the PBDAT program of Ludwig (1991a) for TIMS data, and described elsewhere for the other types of analysis (Whitehouse and Kamber 2005, Gerdes & Zeh 2006). The decay constants recommended by Steiger & Jäger (1977) were used. Calculation of intercept ages and drawing of concordia plots were carried out using Ludwig's (1991b, 2012) ISOPLOT program. The total Pb blank was 4–10 pg and the U blank less than 2 pg. The assigned composition of common Pb was calculated according to the Pb evolution model of Stacey & Kramers (1975), which is a sufficient approximation for analyses with high ^{206}Pb/^{204}Pb (>~1000). For samples with low ^{206}Pb/^{204}Pb, the uncertainty in the common Pb correction will result in large error ellipses. The mass fractionation for Pb is 0.10 ±0.04% per a.m.u. U mass fractionation was monitored and corrected for by means of the $^{233-235}$U ratio of the spike.

ANALYTICAL RESULTS

STB951023, metameimechite from the Käymäjärvi formation

Very few zircons were recovered from this rock. The majority are small with distinct, prismatic zircon shape and are generally severely fractured. They constitute a heterogeneous population and some have visible cores. A second group of grains are very small and anhedral. Their length/width ratio is approxmately 1. Both types were analysed using the multi-grain TIMS method. Due to the small size of the crystals, none of the analysed fractions were abraded. Fractions 1, 4 and 5 have prismatic shapes, whereas 2, 3 and 6 are small and anhedral or rounded with a length/width ratio of around 1.

Analytical results are shown in Table 2 and Figure 5. The small grains are low in U and Pb, and two out of three fractions are strongly discordant. Due to the low Pb content and small sample size the total Pb concentration is only 17 and 30 pg for fractions 2 and 3, respectively. The corrected ratios are therefore very sensitive to the chosen blank concentration and composition, as well as to the chosen composition of the initial Pb. Consequently, the analyses of fractions 2 and 3 are uncertain. Fraction 1 has a higher total Pb concentration but a high common Pb content, causing great uncertainty. Only fraction 4, with a higher U and Pb concentration and low common Pb, gives a small error ellipse.

The concordia diagram shows a large scatter, indicating that the zircon population is highly heterogeneous. A discordia is calculated from fractions 2, 3, 4 and 5, giving intercept ages of 2 055 ±130 and 445 ±230 Ma, and an MSWD of 43. This result is similar to the 2 038 ±6 Ma $^{207}Pb/^{206}Pb$ age of fraction 4. However, due to the strong discordance and different morphology, it is doubtful whether fractions 2 and 3 belong to the same generation as the other fractions. A regression made using fractions 4 and 5 only yields intercept ages of 2 236 ±52 and 1 059 ±103 Ma. Fraction 6, which consists of anhedral, clear, colourless to pale brown crystals has a very low $^{206}Pb/^{204}Pb$ due to low Pb content, small sample size and high initial Pb. The data point is concordant at c. 1800 Ma and the zircons clearly belong to a later generation. It is possible that fraction 6 belongs to the same generation as fraction 1, which has a similar $^{207}Pb/^{206}Pb$ age.

Table 2. TIMS U-Pb isotopic data for samples STB951023, 28MOM576N and STB951024.

Analysis No.	Weight (µg)	No. of crystals	U (ppm)	Pb tot. (ppm)	Common Pb (ppm)	$^{206}Pb^{a}/^{204}Pb$	^{206}Pb-^{207}Pb-^{208}Pb Radiog. (atom %)[b]	$^{206}Pb^{b}/^{238}U$	$^{207}Pb^{b}/^{235}U$	$^{207}Pb/^{206}Pb$ age (Ma)
STB951023	**Metameimechite from the Käymäjärvi formation**									
1	2	4	244.0	80.7	9.17	331	82.6-9.1-8.3	0.2814±19	4.258±55	1795±19
2	2	7	49.9	10.1	0.97	154	71.2-7.4-21.4	0.1516±53	2.181±130	1703±92
3	2	25	71.9	10.3	0.57	242	77.7-7.1-15.2	0.1224±13	1.538±26	1449±32
4	12	5	214.5	72.5	0.43	4176	81.5-10.2-8.3	0.3184±15	5.514±31	2 038±6
5	5	7	451.0	145.3	0.81	532	78.3-9.4-12.3	0.2917±15	4.812±31	1 951±11
6	2	4	34.5	27.2	13.90	65.6	75.2–8.0–19.5	0.3251±46	4.937±289	1802±96
28MOM576N	**Metaandesite from the Muotkamaa formation**									
1 < 74	123		368	102	3.0	1600	72.7–8.4–18.9	0.2266±59	3.615±95	1890±6
2 74-100	223		175	69	0.24	12000	72.4–8.3–19.3	0.3315±70	5.262±12	1881±2
3 100-150	60		107	7.4	0.48	345	73.1–8.4–18.5	0.0554±48	0.877±11	1878±16
4 > 150	10		1244	202	4.7	1200	71.1–8.2–20.7	0.1310±52	2.083±13	1884±8
5 100-150 ab	40		137	48	2.4	675	72.0–8.3–19.7	0.2274±12	4.409±34	1884±11
STB951024	**Metaandesite from the Hosiovaara formation**									
Zircon 1	34	5	222.1	74.3	0.54	4614	77.0-8.5-14.5	0.2968±14	4.5439±23	1817±3
Zircon 2	16	8	99.0	40.4	0.25	3594	70.5-8.1-21.4	0.3328±18	5.2694±33	1877±5
Zircon 3	16	12	135.0	53.4	0.34	2691	70.8-8.2-21.0	0.3231±18	5.1314±33	1883±5
Zircon 4	22	15	173.9	66.8	0.57	3267	74.3-8.5-17.2	0.3288±12	5.2113±23	1879±5
Titanite 1	98	30	23.9	11.8	1.42	255	53.1-6.1-40.8	0.2672±37	4.2190±91	1872±27
Titanite 2	143	25	153.5	34.8	1.86	665	61.0-0.7-38.3	0.1429±6	2.2238±17	1846±10

a) corrected for mass fractionation (0.1% per a.m.u) and spike.
b) corrected for mass fractionation, spike, blank and common Pb.

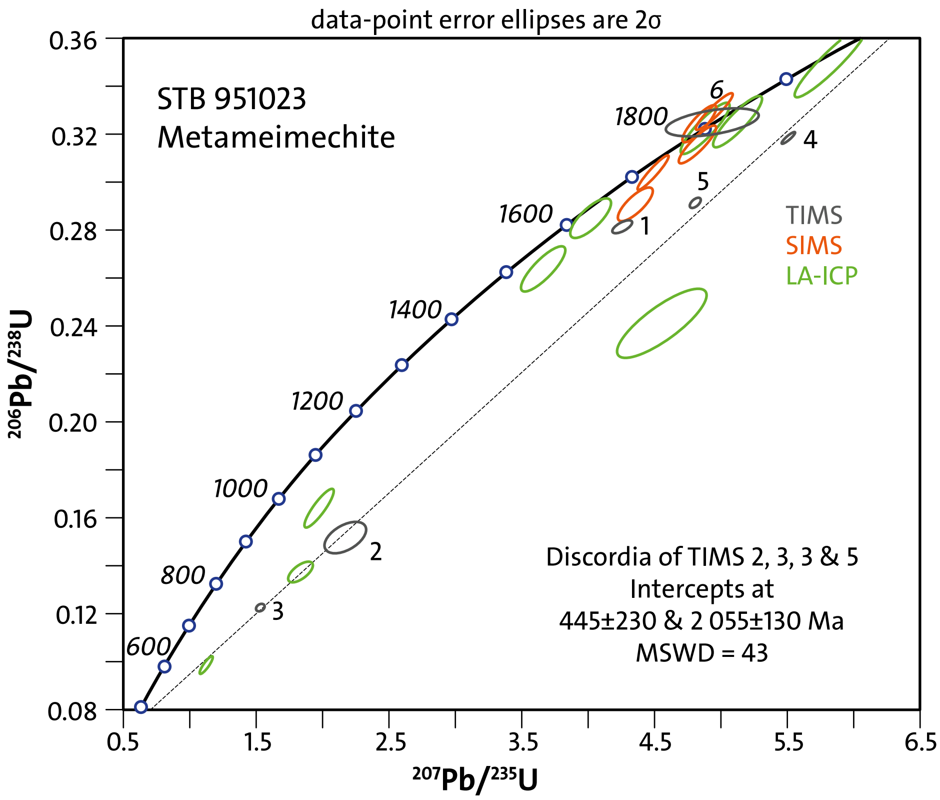

Figure 5. Concordia diagram, combining TIMS. SIMS and LA-ICP-MS data, for analysed zircon fractions from a metameimechite (sample STB951023) from the Käymäjärvi formation.

SIMS data (6 points, Fig. 6A) have produced a different analytical picture, where data show little scatter, and fit a discordia that yields a relatively well-constrained event at c. 1770 Ma, and near concordant ages of c. 1790 Ma (Table 3, Fig. 5). An averaged $^{207}Pb/^{206}Pb$ age for the concordant spots 1, 2 and 5a yields 1781 ±9.5 Ma. LA-ICP-MS data (n=10) shows a highly diverse age spread, however. One spot is concordant at c. 3.0 Ga (not shown in the diagram), and the remainder record a series of near-concordant ages defined at c. 1.97 Ga, 1.81 Ga, 1.65 Ga (Table 4, Fig. 5). A few other discordant to highly discordant analyses suggest an apparent age of around 0.4 Ga.

28MOM576N, metaandesite from the Muotkamaa formation

The heavy mineral concentrate from the metaandesite predominantly comprises pyrite; the zircon content was low. Most of the zircon crystals have irregular shape or form subhedral prisms with rounded edges and pitted or irregular surfaces. Zircons are translucent with a pale brown colour and show a length/width ratio of approximately 1–3. Inclusions and fractures are rare and no visible cores or overgrowths were observed. Based on size distribution, four fractions were obtained. Clear and well-formed crystals grains were selected for analysis from the predominant 74–100 µm fraction. Some of the zircons from fraction 100–150 µm were abraded before analysis.

Analytical results are presented in Table 2 and Figure 7. The single zircon crystal in fraction >150 µm shows higher uranium content compared to the other fractions, while fraction 100–150 µm has an abnormally low lead content. A regression line based on all fractions defines a discordia with intercept ages of 1 884 ±7 and -1 ±19 Ma, with a MSWD of 3.1. Excluding the fraction <74 µm, where the control of zircon quality is poorer, the upper and lower intercept ages are 1 882 ±2 and 0.3 ±5.4 Ma, respectively, with a MSWD of 0.5. The two least discordant fractions define a similar upper intercept age of 1 881 ±2 Ma.

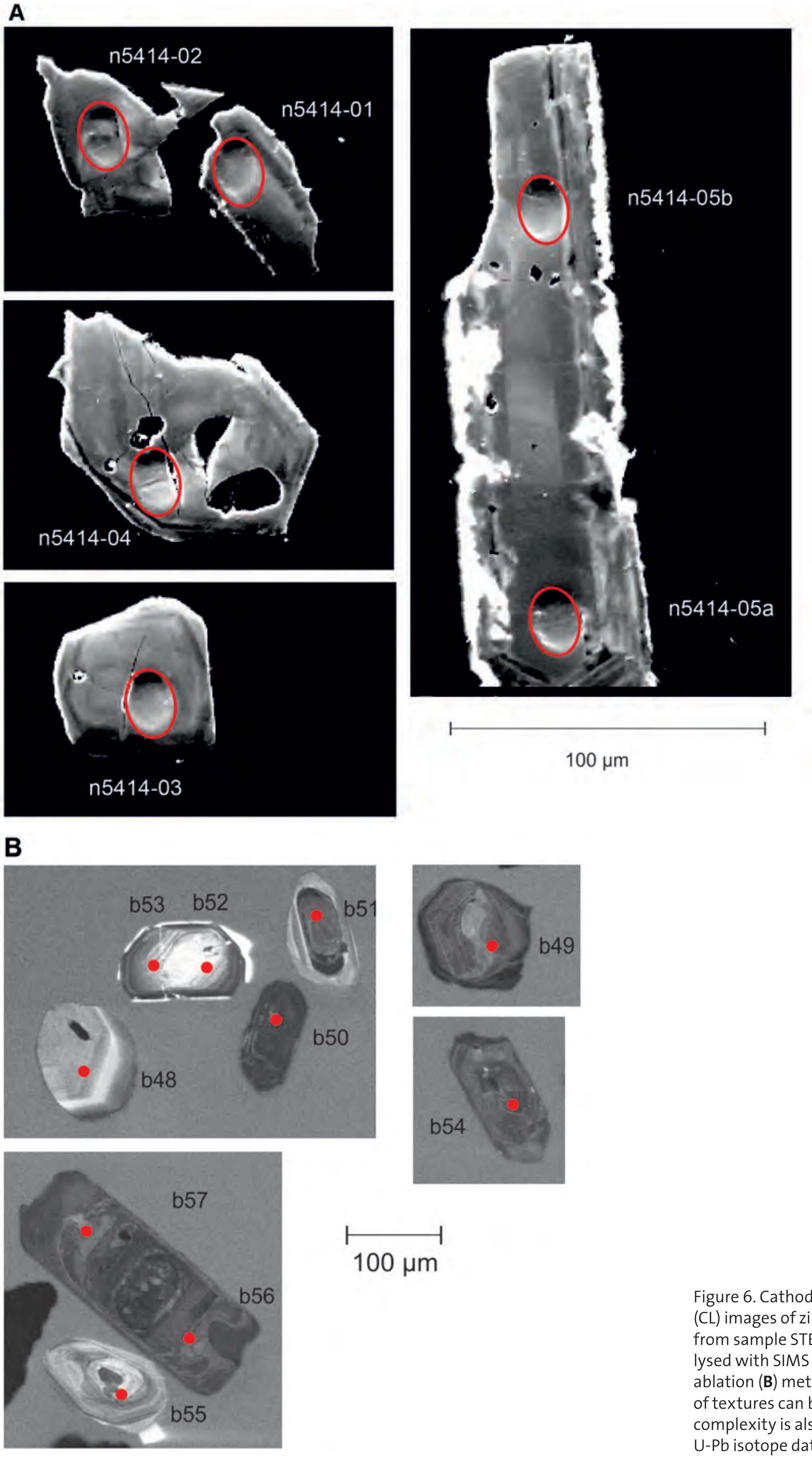

Figure 6. Cathodoluminescence (CL) images of zircon crystals from sample STB951023 analysed with SIMS (**A**) and laser ablation (**B**) methods. A variety of textures can be seen and this complexity is also noted in the U-Pb isotope data obtained.

Table 3. Ion microprobe (SIMS) U-Th-Pb zircon data for the metameimechite (STB 951023).

spot	$^{207}Pb/^{206}Pb$	1σ	$^{206}Pb/^{238}U$	1σ	$^{207}Pb/^{235}U$	1σ	$^{206}Pb/^{204}Pb$ (meas)	f206 (%)[a]	Disc.[b]	$^{207}Pb/^{206}Pb$ age	$^{206}Pb/^{238}U$ age	U (ppm)	Pb (ppm)	Th/ Ucalc[c]
n5414-01	0.1083	0.53	0.3247	0.91	4.846	1.05	8 029	0.23	2.7	1770	1812	277	112	0.50
n5414-02	0.1089	0.46	0.3238	0.91	4.860	1.02	48 710	0.04	1.8	1780	1808	323	128	0.40
n5414-03	0.1108	0.62	0.3153	0.95	4.819	1.13	5 912	0.32	-2.9	1813	1767	247	96	0.38
n5414-04	0.1087	0.73	0.2907	0.98	4.356	1.22	2 124	0.88	-8.4	1777	1645	283	100	0.33
n5413-05a	0.1093	0.39	0.3295	0.96	4.966	1.04	8 559	0.22	3.1	1788	1836	749	302	0.40
n5413-05b	0.1073	0.32	0.3039	0.90	4.494	0.95	3 871	0.48	-2.8	1753	1711	811	310	0.50

All errors are 1 sigma (%); ages in million years (Ma).
[a] fraction (percentage) of common Pb detected. Calculated from measured ^{204}Pb assuming t=0 Ma in the Stacey and Kramers (1975) model.
[b] degree of discordance as a percentage
[c] calculated from measured ThO intensity

Table 4. Laser ablation (ICP-MS) U-Pb zircon data for the metameimechite (STB 951023).

spot	$^{207}Pb/^{206}Pb$	1σ	$^{206}Pb/^{238}U$	1σ	$^{207}Pb/^{235}U$	1σ	$^{206}Pb/^{204}Pb$ (meas)	Rho[a]	$^{207}Pb/^{206}Pb$ age	$^{206}Pb/^{238}U$ age	U (ppm)	Pb (ppm)	Th/U
b48	0.2180	1.3	0.6031	2.2	18.131	2.6	36 471	0.87	2 966	3 042	39	28	0.39
b49	0.1146	1.3	0.3245	2.6	5.128	2.9	12 705	0.90	1874	1812	121	40	0.13
b50	0.1374	3.3	0.2407	5.0	4.560	6.0	889	0.83	2 194	1390	264	82	0.51
b51	0.0879	2.2	0.1638	4.1	1.985	4.6	43 467	0.88	1380	978	272	50	0.27
b52	0.1022	2.1	0.2850	2.5	4.015	3.3	49 807	0.77	1664	1616	51	16	0.35
b53	0.1008	2.1	0.2634	2.9	3.662	3.6	9 505	0.80	1639	1507	52	15	0.42
b54	0.1099	1.6	0.3224	2.8	4.884	3.2	2 787	0.87	1797	1801	122	44	0.48
b55	0.1206	1.4	0.3489	3.1	5.800	3.4	20 077	0.91	1965	1929	70	29	0.60
b56	0.0975	3.3	0.1372	2.4	1.845	4.0	8 824	0.59	1577	829	232	32	0.13
b57	0.0830	1.1	0.0982	2.7	1.125	2.9	7 211	0.93	1270	604	272	26	0.15

All errors are 1 sigma (%); ages in million years (Ma).
Isotope ratios are corrected for background, mass bias, laser induced U-Pb fractionation, and common Pb (if detectable) using Stacey & Kramers (1975) model Pb composition. Errors are propagated by quadratic addition of within-run errors (2SE) and the reproducibility of GJ-1 (2SD).
[a] correlation coefficient; defined as error206Pb/238U/error207Pb/235U.

STB951024, metaandesite from the Hosiovaara formation

The metaandesite had a very low zircon yield. The colour of the zircons varies from light brown to pink, but colourless crystals were also found. Most of the crystals are short prismatic with length/width ratios of 1–3. The shape may be either euhedral, rounded or anhedral. Some colourless, elongate (length/width ratios of approximately 4–6) zircons are also found, along with a small number of dark brown short grains with length/width ratios of approximately 1–2. Cores or overgrowths were not observed. All analysed grains were thoroughly abraded. Fraction 1 consists of large, pink grains, while in fractions 2–4 the zircons are small and colourless to light brown.

The sample also contains titanite, the colour of which may be pale yellow, brown or reddish-brown. Yellow and brown crystals were selected for analysis. The reddish-brown titanites are turbid and inclusion-rich, and were therefore rejected. Many titanite grains are anhedral or fragmented, but euhedral crystals are found among the yellow and brown ones. Both fractions were abraded.

TIMS results are shown in Table 2 and Figure 8. With the exception of one fraction (Zr 1 with a Pb-Pb age of 1 817 ±3 Ma), the remaining titanite and zircons fractions define a discordia with intercept ages of 1 880 ±3 and 49 ±5 Ma and an MSWD of 1.1. Using the three zircon and the two titanite fractions separately gives intercept ages of 1 874 ±11 for zircon fractions and 1 879 ±62 Ma

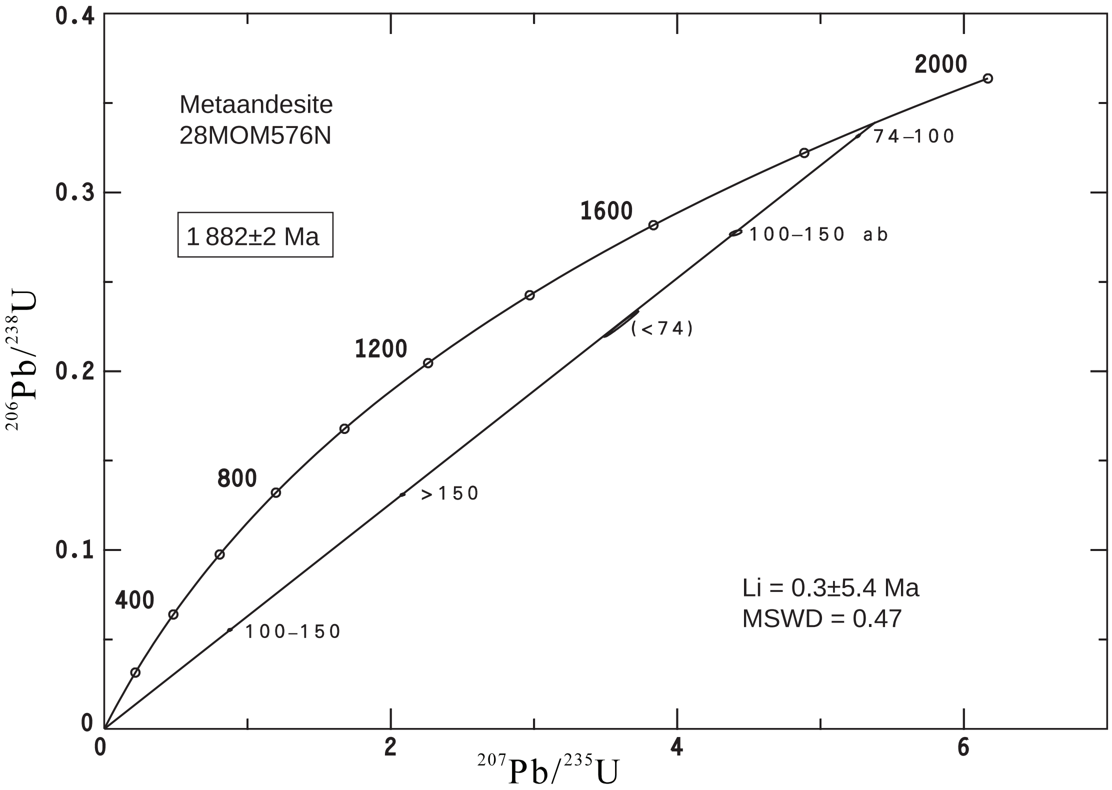

Figure 7. Concordia diagram for (TIMS) analysed zircon fractions from a metaandesite (sample 28MOM576N) from the Muotkamaa formation.

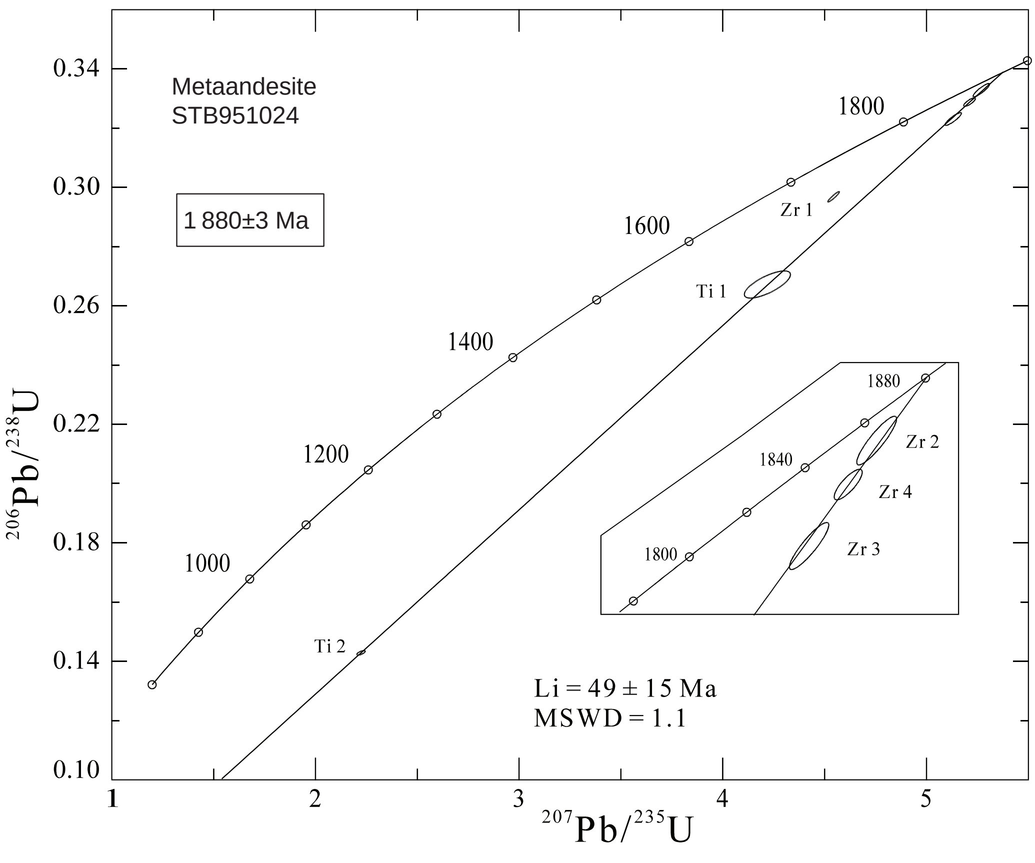

Figure 8. Concordia diagram for (TIMS) analysed titanite and zircon fractions from a metaandesite (sample STB951024) from the Hosiovaara formation.

for titanite fractions. This may indicate that titanite and zircon crystallised during the same event. Zircon fractions 2, 3 and 4 are only slightly discordant, so their age is considered to be well defined. The diverging zircon fraction 1 has the lowest ^{208}Pb and highest U content and a somewhat differing appearance (see above). It may thus contain zircon grains of a different generation than the other three fractions. The titanite fractions, especially the brown crystals, are strongly discordant. No obvious explanation for the discordance can be found. Titanite fraction 2 has a Pb-Pb age of 1 846 ±10 that is within an error range similar to titanite fraction 1.

DISCUSSION

Depositional environment of the Käymäjärvi formation and the Vinsa formation

The metameimechite within the Käymäjärvi formation consists of pyroclastic material, sometimes showing graded bedding, with fragments varying from 3 to less than 1 cm. These units of pyroclastic rocks probably formed as subaqueous pyroclastic flows fed by phreatomagmatic eruptions, occurring in fairly shallow water. The younger Vinsa formation reflects calmer conditions, with deposition of tuffitic sediments of mainly basaltic composition and partly mixed with organic material within units 1 and 3. Unit 3 also often contains abundant scapolite in partly laminated diopside-rich beds. The Vinsa formation also contains thick units of chemical sedimentary rocks, with silicate facies BIF in unit 2 and dolomite in unit 4.

The geochemical composition of the Vinsa formation indicates deposition in an evaporitic environment and slightly anoxic conditions resulting in enrichment of Cl and the occurrence of graphite, respectively. It is suggested that the BIF in unit 2 is of Algoma-type and formed as a distal exhalite in response to more local and high temperature hydrothermal input to the basin (Martinsson et al. 2016). The enrichment of Ba, Mn, Cu, Zn, As, and Sb in unit 3 was probably caused by such hydrothermal activity. Dolomite in unit 4 is suggested to have formed on a shallow marine carbonate platform similar to the dolomites in the Kalix area (Wanke & Melezhik 2005), with dolomite formed at elevated water temperatures or during evaporitic conditions (Machel & Mountjoy 1986, Warren 2000).

Depositional environment for the Sammakkovaara group

The rocks constituting the Sammakkovaara group probably formed in a shallow water environment with contemporaneous andesitic volcanism and clastic sedimentation. Rapid facies changes are recorded by different proportions of metavolcanic and metasedimentary rocks in the Muotkamaa formation and variations in grain size and composition of the metasedimentary rocks within the Hosiokangas formation. Herringbone cross-lamination occurring locally in the upper part of the Hosiokangas formation indicates a tidal depositional environment. An evolution from shallow water to terrestrial deposition is indicated in the Hosiovaara formation, and may be related to the growth of volcanic cones above sea level.

Age of metameimechite from the Käymäjärvi formation and stratigraphic correlations

The only previous chronological data from the Greenstone successions in Sweden come from the Kiruna area (Skiöld & Cliff 1984, Skiöld 1986) and indicate an age of deposition between c. 2.2 and 2.0 Ga for the Kiruna greenstone group (Martinsson 1997). The TIMS zircon age 2 055 ±130 Ma (using four fractions) of meimechitic lapilli tuff from the Käymäjärvi formation suffers from large errors and does not contribute to a more accurate age for the Veikkavaara greenstone group. However, the analysed zircons constitute a heterogeneous population; some have visible cores, while others are very small and anhedral (cf. CL images in Fig. 6). Zircons also exhibit large variation in common Pb content and in ^{206}Pb/^{204}Pb ratio, suggesting that they represent different generations. Additional results from the SIMS and LA-ICP-MS analysis add further complexities. Unfortunately, only crystals of lesser quality were available for microanalysis after completion of the TIMS multi-grain analyses.

However, the minimum age of the Käymäjärvi formation is given by fraction 4, consisting of euhedral zircon grains with the lowest content of common Pb and the highest $^{206}Pb/^{204}Pb$ ratio, giving a Pb-Pb age of 2 038 ±6 Ma. This age is probably close to the depositional age of the Kämyäjärvi formation and is supported by the carbon isotope signature of carbonate rocks in the Veikkavaara greenstone group in the Pajala area (Martinsson 2004b). Carbonate rocks in the Vinsa formation vary from -2.9 to +2.3‰, whereas carbonate rocks in the Pajala area, situated stratigraphically below metavolcanic rocks corresponding to the Käymäjärvi formation, return ratios of between +7.1 and +7.6‰ (Martinsson, unpublished data). Since the global Lomagundi-Jatuli excursion from positive values to more normal marine carbon isotope signatures for carbonate rocks ended at 2 056.6 ±0.8 Ma (Martin et al. 2013), the Käymäjärvi formation should have an age of around 2.05 Ga. Based on these data, the Vinsa formation is of Ludikovian age, whereas the Käymäjärvi formation is possibly older and of Jatulian age.

Taken together, and including a comparison with similar rocks in Finland (see below), an approximate 2.05 Ga emplacement age is suggested for the metameimechite. However, this rock has undergone a complex geological evolution. First, the old 3.0 Ga LA-ICP-MS age (point b48, Table 4) indicates assimilation of older crustal rocks. Further, this age is among the oldest zircon ages known for rocks from Sweden, with previously reported ages from northern Norrbotten falling within the range 2.7 to 3.2 Ga (Martinsson et al. 1999, Lauri et al. 2016). But even older detrital zircons with ages of 3.29, 3.38 and 3.58 Ga have been reported from metaarenites from the Pahakurkio and Kalixälv groups (Hellström et al. 2018). At least two stages of metamorphic growth or metamorphic resetting of the metameimechite, at c. 1.8 Ga and 1.65 Ga, respectively, are indicated from the zircon age data. The 1.8 Ga event is regionally well constrained (Bergman et al. 2001, Martinsson 2004a), but no significant 1.65 Ga geological event has previously been documented in northern Norrbotten. It is worth noting that certain laser spots are related to highly discordant data, suggesting a disturbance of the U-Pb system at around 0.4 Ga. A similar young age, implying a Caledonian event, was also obtained for the lower intercept of the TIMS regression, yielding an imprecise upper intercept age close of 2.05 Ga. A few 400 Ma zircons, interpreted to be of metamorphic origin, have recently been analysed from Svecofennian rocks close to Kiruna, demonstrating the impact of the Caledonian event (Billström et al., in prep.).

Stratigraphic comparisons on a local and a more regional scale help to place the approximate 2.05 Ga metameimechite age in a geological context (Fig. 9). Rocks stratigraphically equivalent to the Käymäjärvi and Vinsa formations also exist east of Käymäjärvi in the Kaunisvaara area, and at Veikkavaara in the Masungsbyn area, west of Käymäjärvi. In these areas, rocks corresponding to the Käymäjärvi formation mainly consist of volcanoclastic rocks of basaltic character, with meimechite occurring as a minor constituent, whereas rocks corresponding to the Vinsa formation generally show great similarities (Martinsson et al. 2013a,b). The Vinsa formation may also correlate with the Linkaluoppal formation in the uppermost part of the Kiruna greenstone group (Martinsson 1997). At Masugnsbyn a mafic sill intruding volcaniclastic rocks belonging to the Veikkavaara greenstone group in a stratigraphic position below the Vinsa formation returns an age of 2 131 ±5 Ma (Lynch et al. 2018b), giving an upper age limit for these rocks.

High quality geochronological data from extrusive rocks are fairly limited for Jatulian to Ludikovian greenstones in other parts of the Fennoscandian Shield. Zircon ages of metabasaltic rocks from Finland yield ages of 2 105 ±15, 2 106 ±7 and 2 115 ±6 Ma (Huhma 1986, Pekkarinen & Lukkarinen 1991, Karhu et al. 2007). Felsic metavolcanic rocks from the Koivusaari formation in the Kuopio-Siilinjärvi area occur interlayered with metabasaltic pillow lavas and have an age of 2 062 ±2 Ma (Lukkarinen 1990, Pekkarinen & Lukkarinen 1991). A similar age of 2 050 ±8 Ma is recorded for a felsic porphyry from the upper part of the Peräpohja Belt (Pertunen & Vaasjoki 2001). Metarhyolite intercalated with metabasaltic lava in the Vesmajärvi formation from the upper part of the Kittilä group is significantly younger, with a U-Pb zircon age of 2 012±3 Ma (Lehtonen et al. 1998). Sm-Nd ages of

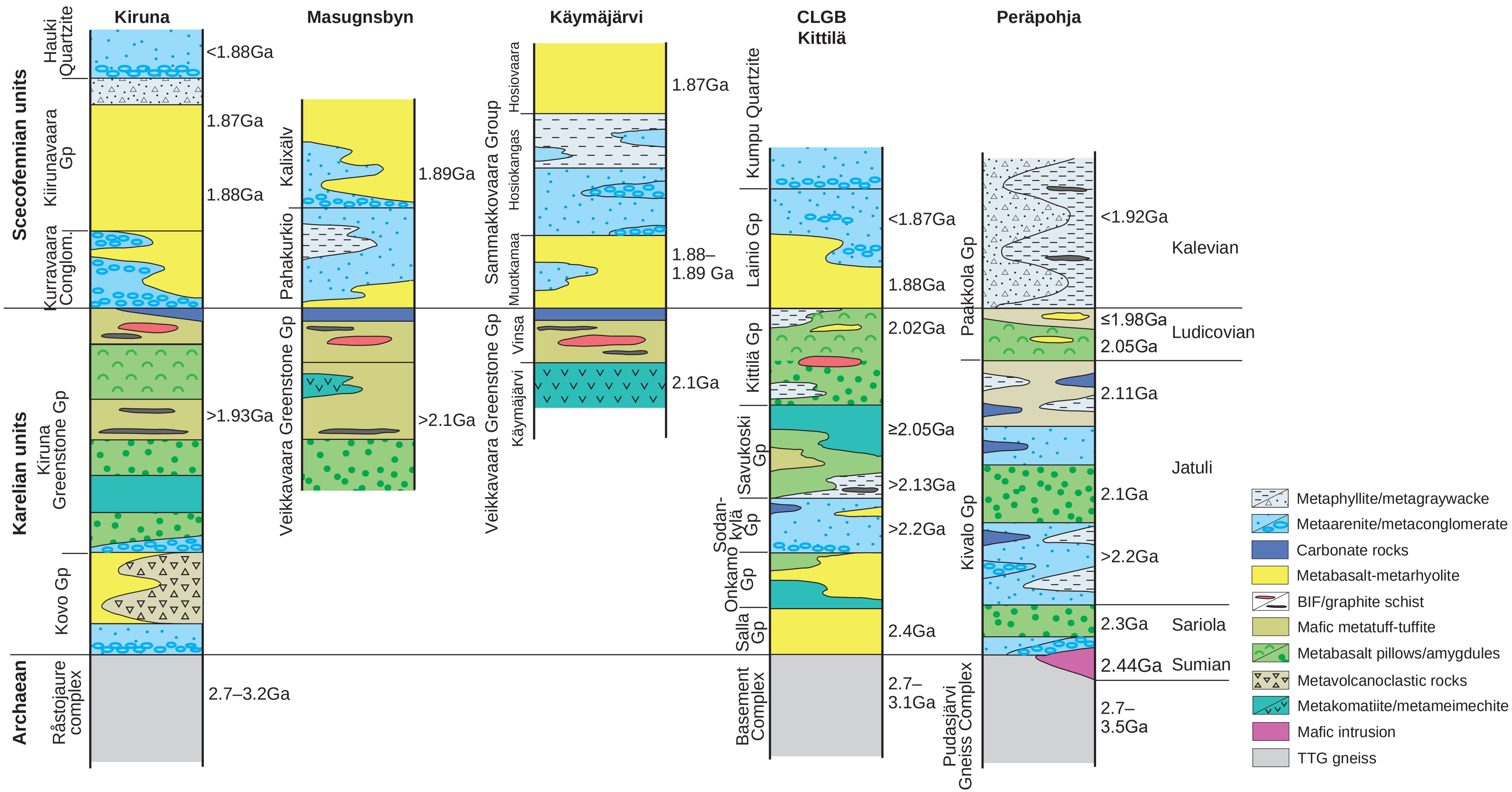

Figure 9. Stratigraphic correlation of Karelian and Svecofennian units in northern Sweden and Finland. Data for the Kiruna area from Skiöld (1979, 1986), Skiöld & Page (1998) Martinsson et al. (1999), Martinsson (2004), Bergman et al. (2000), and Westhues et al. (2016). Data for the Masugnsbyn area from Padget (1970), Martinsson (1995), Martinsson et al. (2013a), Hellström et al. (2018), and Lynch et al. (2018b). Data for the Käymäjärvi area from Martinsson (1995), Martinsson et al. (2013b) and this study. Data for the Central Lapland Greenstone Belt (CLGB) from Lehtonen et al. (1998), Rastas et al. (2001), Manninen et al. (2001), Hanski et al. (2001a, 2001b). Data for the Peräpohja Belt from Huhma et al. (1990), Perttunen & Vaasjoki (2001), Hanski et al. (2001b), Mutanen & Huhma (2003), Hanski et al. (2005), Karhu et al. (2007), and Ranta et al. (2015).

metabasaltic to metakomatiitic rocks in Finland and northern Norway give less precise ages: around 2.3 and 2.1 Ga (Krill et al. 1985, Huhma 1986, Huhma et al. 1990, Pekkarinen & Lukkarinen 1991, Hanski et al. 2001a, Perttunen & Vaasjoki 2001).

Intrusions associated with the Jatulian-Ludikovian evolution occur as dyke swarms in the Archaean granite-gneiss basement and as gabbroic plutons and sills in Karelian cover units (Gorbatschev et al. 1987, Vuollo 1994). These more precise isotopic ages indicate magmatic peaks at c. 2.3, 2.2, 2.1, 2.05 and 2.0 Ga (Vuollo et al. 2000, Hanski et al. 2001b), supporting the 2.3 and 2.1 to 2.0 Ga ages of the metavolcanic rocks. Metasedimentary rocks from the upper part of the greenstone successions give Pb-Pb ages of 2 080 ±45 Ma for an iron formation from Kainuu (Sakko & Laajoki 1975), and 2 119 ±243 Ma for a dolomite at Kalix (Öhlander et al. 1992). These fairly limited and often imprecise geochronological data, including those from the current study, indicate an age of 2.1–2.0 Ga for most of the mafic-ultramafic volcanism forming the Jatulian to Ludikovian greenstones in Finland, northern Norway and Sweden.

Age of andesites from the Sammakkovaara group and stratigraphic correlations

Within the margins of error, zircon and titanite in sample STB951024 from the Hosiovaara formation give similar ages, but with a much larger error for the titanite fractions. The three zircon fractions alone give an age of 1 874 ±11 Ma and, combined with the titanite fractions, an age of 1 880 ±3 Ma, identical, within the margin of error, to the 1 882 ±2 Ma age of sample 28MOM576N from the Muotkamaa formation. Based on the texture of the STB951024 metaandesite, the titanite is probably of metamorphic origin, supported by the rare occurrence of titanite as a primary igneous mineral in extrusive rocks. This implies that either both extrusion and metamorphism of the andesitic rocks occurred within a short time interval close to 1 880 Ma, or that the zircons also record a metamorphic event. As both of the studied andesitic rocks are fairly strongly recrystallised under middle-upper amphibolite facies conditions, and are partly affected by strong scapolitisation, a metamorphic growth of zircons or a resetting of pre-existing magmatic zircons during metamorphism should be considered. That might be reflected in the morphology of certain zircon grains that either have an irregular shape or occur as subhedral prisms with rounded edges and pitted or irregular surfaces. The 1 890 ±6 Ma Pb-Pb age of the <74 µm zircon fraction from sample 28MOM576N from the Muotkamaa formation may be evidence of an older magmatic age.

In Finland, an early Svecofennian 1.93–1.91 Ga arc magmatic event is documented from the Savo Schist Belt (Ekdahl 1993, Lahtinen 1994). The existence of c. 1.93 Ga intrusive rocks of tonalitic-granodioritic composition in the Jokkmokk and Rombak areas (Skiöld et al. 1993, Romer et al. 1992, Hellström 2015) indicates that this arc magmatism extended further to the northwest for a distance of at least 500 km along the margin of the Karelian domain. If the 1 882 ±2 Ma age for the metaandesite from the Muotkamaa formation is of metamorphic origin, this lower volcanic unit may belong to the earliest 1.93–1.91 Ga, or slightly younger 1.89 Ga, Svecofennian magmatism. If not, the metavolcanic and metasedimentary units (Muotkamaa Fm, Hosiokangas Fm and Hosiovaara Fm) constituting the Sammakkovaara group must have been deposited and subsequently metamorphosed within a few million years.

Similar ages (1 883 ±5 Ma) have been reported from volcanic rocks within the Latvajärvi formation, which belongs to the Lainio group in northern Finland (Lehtonen et al. 1998). Although the Latvajärvi metavolcanics are geochemically slightly different from the Sammakkovaara metaandesites, the Sammakkovaara group is regarded as stratigraphically equivalent to the Lainio group (Lahtinen et al. 2015).

It is suggested that the Sammakkovaara group is stratigraphically correlated to the Porphyrite group in the Kiruna area (Martinsson 2004a, Martinsson et al. 2016), supported by chemical similarity (Fig. 4). No age determinations exist from the Porphyrite group at Kiruna, but the 1 884

±4 Ma age of the Hopukka formation in the lower part of the overlying Kiirunavaara group (Westhues et al. 2016) gives it a minimum age. Consequently, the upper age limit for the Porphyrite group must be 1880 Ma, which accords with the 1 878 ±7 Ma minimum age for a "Porphyry group" metaandesite at Tjårrojåkka, west of Kiruna (Edfelt et al. 2006). Similar 1.88 Ga ages are recorded for the Muorjevaara group in the Gällivare area (Claeson & Antal Lundin 2012, Lynch et al. 2018a), suggested to correlate with the Porphyrite group (Martinsson & Wanhainen 2004). Metavolcanic rocks at Sakkarinpalo in the Masungsbyn area correlated with the Porphyrite group and have a zircon age of 1 890 ±5 Ma (Hellström et al. 2018). A similar age (1 887 ±5 Ma) is recorded from the metaandesite rocks within the Kalixälv formation (Hellström et al. 2018), which may be correlated with the Hosiovaara formation. These two zircon ages close to 1.89 Ga support a possible older 1.89 Ga depositional age of the Muotkamaa formation, indicated by the 1 890 ±6 Ma Pb-Pb age.

In a regional context, the Sammakkovaara group is regarded as stratigraphically equivalent to Svecofennian clay-rich to ruditic metasedimentary rocks in the Kiruna area (i.e. the Kurravaara conglomerate and the metasedimentary rocks at Vuotnavare and Väkkerijärvi; Offerberg 1967), and to metasedimentary rocks within the Muorjevaara group in the Gällivare area (Martinsson & Wanhainen 2004). In eastern Norrbotten, it is suggested that the Hosiokangas formation and the Hosiovaara formation correlate with the Pahakurkio and Kalixälv groups, respectively, in the Masugnsbyn area (Padget 1970; Fig. 9). These latter two groups consist of arenitic to clay-rich metasedimentary rocks with minor intercalations of quartz-pebble conglomerate and metavolcanic rocks similar to the Sammakkovaara group, and have maximum depositional ages of 1.91 and 1.88 Ga, respectively (Hellström et al. 2018).

The 1 879 ±62 Ma metamorphic titanite in sample STB951024 may relate to the suggested c. 1.88 Ga syn-magmatic metamorphic and deformation event in northern Norrbotten (Bergman et al. 2001), or to the younger, c. 1.85 Ga metamorphic event, in eastern Norrbotten (Bergman et al. 2006). An even younger, c. 1.81-1.78 Ga, metamorphic event has been documented by chronological data from the Pajala area (Bergman & Skiöld 1998, Bergman et al. 2001). This later metamorphism is probably seen in the c. 1.81 Ga zircons in sample STB951023 and the 1.82 Ga Pb-Pb age of one zircon fraction in sample STB951024. In contrast, the c. 1.65 Ga age recorded in sample STB951023 cannot be related to any known event in northern Norrbotten.

CONCLUSIONS

Petrographic, stratigraphic and geochronological data from Käymäjärvi in eastern Norrbotten are presented for 2.1–2.0 Ga Karelian and 1.9 Ga Svecofennian supracrustal units. The Karelian rocks are subdivided into the Käymäjärvi formation and overlying Vinsa formation. The Svecofennian supracrustal rocks constitute the Sammakkovaara group, which includes the Muotkamaa formation in the lowest part, followed by the Hosiokangas formation and, at the top, the Hosiovaara formation.

Zircon age determinations indicates that pyroclastic metameimechite from the Käymäjärvi formation was deposited at c. 2.1–2.0 Ga, and in combination with carbon isotope evidence this age can be narrowed down to close to 2.05 Ga. Metaandesites from the Muotkamaa and Hosiovaara formations both give zircon ages close to 1.87–1.88 Ga. But the metaandesites from the Muotkamaa formation have a zircon fraction with a Pb-Pb age of 1.89 Ga, possibly suggesting a slightly older age for this rock. Zircon evidence from the analysed samples also records a metamorphic disturbance at c. 1.8 Ga.

The Käymäjärvi and Vinsa formations can be correlated with other greenstone units in northern Norrbotten and correspond to the Jatulian-Ludikovian units in the northeastern Fennoscandian Shield. The Sammakkovaara group is correlated with the lower Svecofennian Porphyrite group in the Kiruna area, with the Muorjevaara group in the Gällivare area and other arenitic to clay-rich metasedimentary formations in northern Norrbotten.

ACKNOWLEDGEMENTS

This paper is based on age determinations financed by Sveriges geologiska undersökning and ULIG and geological research at CTMG (Centre for applied ore studies at the Luleå University of Technology) sponsored by Outokumpu Co and Boliden AB. We would like to thank Victor Melezhik, Eero Hanski, Dick Claeson, and George Morris for their valuable comments on, and corrections to, the manuscript, and Milan Vnuk who made the drawings. U-Pb SIMS and TIMS isotopic zircon and titanite data were obtained from a beneficial co-operation with the Laboratory for Isotope Geology of the Swedish Museum of Natural History in Stockholm. The Nordsim facility (SIMS analysis) is operated under an agreement between the research funding agencies of Denmark, Norway and Sweden, the Geological Survey of Finland and the Swedish Museum of Natural History. Martin Whitehouse, Kerstin Lindén and George Morris are thanked for their assistance at the Nordsim facility. This is Nordsim contribution #468.

REFERENCES

Bergman, S. & Skiöld, T., 1998: Implications of ca 1.8 Ga metamorphic ages in the Pajala area, northernmost Sweden. *23. Nordiske Geologiske Vintermøde, Århus 1998, Abstract Volume,* 32.

Bergman, S., Martinsson O. & Persson P.-O., 2002: U-Pb zircon age of a metadiorite of the Haparanda suite, northern Sweden. *Sveriges geologiska undersökning C 834*, 6–11.

Bergman, S., Kübler, L. & Martinsson, O., 2001: Description of regional geological and geophysical maps of northern Norrbotten County (east of the Caledonian orogen). *Sveriges geologiska undersökning Ba 56*, 110 pp.

Bergman, S., Billström, K., Persson, P.-O., Skiöld, T. & Evins, P., 2006: U-Pb age evidence for repeated Paleoproterozoic metamorphism and deformation near the Pajala shear zone in the northern Fennoscandian shield. *GFF 128*, 7–20.

Billström, K., Evins., P., Storey, C., Martinsson, O. & Whitehouse, M. J., In prep: Conflicting zircon vs. titanite U-Pb age systematics and the deposition of the host volcanic sequence to Kiruna-type and IOCG deposits in northern Sweden, Fennoscandian shield.

Claeson, D. & Antal Lundin, I., 2012: Beskrivning till berggrundskartorna 27K Nattavaara NV, NO, SV & SO. *Sveriges geologiska undersökning K 383–386*, 22 pp.

Edfelt, Å., Sandrin, A., Evins, P., Jeffries, T., Storey, C., Elming, S.-Å. & Martinsson, O., 2006: Stratigraphy and tectonic setting of the host rocks to the Tjårrojåkka Fe-oxide Cu-Au deposits, Kiruna area, northern Sweden. *GFF 128*, 221–232.

Ekdahl, E., 1993: Early Proterozoic Karelian and Svecofennian formations and evolution of the Raahe-Ladoga ore zone, based on the Pielavesi area, central Finland. *Geological Survey of Finland, Bulletin 373*, 137 pp.

Eriksson, T., 1954: Pre-Cambrian geology of the Pajala district, northern Sweden. *Sveriges geologiska undersökning C 522*, 38 pp.

Eriksson, B., & Hallgren, U., 1975: Beskrivning till berggrundskartbladen Vittangi NV, NO, SV, SO. *Sveriges geologiska undersökning Af 13–16*, 203 pp.

Geijer, P., 1925: Eulysitic iron ores in northern Sweden. *Sveriges geologiska undersökning C 324*, 15 pp.

Gerdes, A. & Zeh, A., 2006: Combined U-Pb and Hf isotope LA-(MC-)ICP-MS analyses of detrital zircons: Comparison with SHRIMP and new constraints for the provenance and age of an Armorican metasediment in Central Germany. *Earth and Planetary Science Letters 249*, 47–61.

Gorbatschev, R., Lindh, A., Solyom, Z., Laitakari, I., Aro, K., Lobach-Zhuchenko, S.B., Markov, M.S., Ivliev, A.I. & Bryhni, I., 1987: Mafic dyke swarms of the Baltic Shield. *In*: H.C. Halls and W.F. Fahrig (Eds.), Mafic Dyke Swarms. *Geological Association of Canada Special Paper 34,* 361–372.

Hanski, E., Huhma, H., Rastas, P. & Kamenetsky, V.S., 2001a: The Palaeoproterozoic komatiite-picrite association of Finnish Lapland. *Journal of Petrology 42*, 855–876.

Hanski, E, Huhma, H. & Vaasjoki, M., 2001b: Geochronology of northern Finnland: a summary and discussion. *In*: M. Vaasjoki (Ed.), Radiometric age determinations from Finnish Lapland and their bearing on the timing of Precambrian volcano-sedimentary sequences. *Geological Survey of Finland, Special Paper 33*, 255–279.

Hanski, E., Huhma, H. & Perttunen, V., 2005: SIMS, Sm–Nd isotopic and geochemical study of an arkosite-amphibolite suite, Peräpohja Schist Belt: evidence for1.98 Ga A-type felsic magmatism in northern Finland. *Bulletin Geological Society of Finland 77*, 5–29.

Hanski, E.J. & Melezhik, V.A., 2012: Litho- and chronostratigraphy of the Karelian formations. *In*: V.A, Melezhik, A.R. Prave, E.J. Hanski, and A.E. Fallick, A. Lepland, L.R. Kump, H. Strauss (Eds.), Reading the Archive of Earth's Oxygenation. Volume 1: The Palaeoproterozoic of Fennoscandia as Context for the Fennoscandian Arctic Russia – Drilling Early Earth Project. *Springer-Verlag, Berlin/Heidelberg*, 39–110.

Hellström, F., 2015: SIMS geochronology of a 1.93 Ga basement metagranitoid at Norvijaur west of Jokkmokk, northern Sweden. *SGU-rapport 2015:01*, 18 pp.

Hellström, F.A., Kumpulainen, R., Jönsson, C., Thomsen, T.B., Huhma, H. & Martinsson, O., 2018: Age and lithostratigraphy of Svecofennian volcanosedimentary rocks at Masugnsbyn, northernmost Sweden – host rocks to Zn-Pb-Cu- and Cu ±Au sulphide mineralisations. *In:* Bergman, S. (ed): Geology of the Northern Norrbotten ore province, northern Sweden. *Rapporter och Meddelanden 141,* Sveriges geologiska undersökning. This volume pp 151–203.

Huhma, H., 1986: Sm-Nd, U-Pb and Pb-Pb isotopic evidence for the origin of the early Proterozoic Svecokarelian crust in Finland. *Geological Survey of Finland Bulletin 337,* 48 pp.

Huhma, H., Cliff, R.A., Perttunen, V. & Sakko, M., 1990: Sm-Nd and Pb isotopic study of mafic rocks associated with early Proterozoic continental rifting: the Peräpohja schist belt in northern Finland. *Contribution to Mineralogy and Petrology 104*, 369–379.

Karhu, J., Kortelainen, N., Huhma, H., Perttunen, V. & Sergeev, S., 2007: New time constraints for the end of the Paleoproteroozoic carbon isotope excursion. *In: 7th Symposium on Applied Isotope Geochemistry, Steelenbosch, South Africa, 10th–14th September, 2007, Abstracts*, 76–77.

Kohonen, J., & Marmo, J., 1992: Proterozoic lithostratigraphy and sedimentation of Sariolan and Jatulian-type rocks in the Nunnanlahti-Koli-Kaltimo area, eastern Finland; implications for regional basin evolution models. *Geological Survey of Finland, Bulletin 364*, 67 pp.

Krill, A.G., Bergh, S., Lindahl, I., Mearns, E.W., Often, M., Olerud, S., Olesen, O., Sandstad, J.S., Siedlecka, A. & Solli, A., 1985: Rb-Sr, U-Pb and Sm-Nd isotopic dates from Precambrian rocks of Finnmark. *Bulletin, Norges geologiske Undersøkelse 403*, 37–54.

Krogh, T.E., 1973: A low-contamination method for hydrothermal decomposition of zircon and extraction of U and Pb for isotopic age determination. *Geochimica et Cosmochimica Acta 37*, 485–494.

Krogh, T.E., 1982: Improved accuracy of U-Pb zircon ages by the creation of more concordant systems using an air abrasion technique. *Geochimica et Cosmochimica Acta 46*, 637–649.

Laajoki, K., 2005: Karelian supracrustal rocks. *In,* M, Lehtinen, P.A., Nurmi, O.T., Rämö (Eds.), *Precambrian geology of Finland – Key to evolution of the Fennoscandian Shield. Elsevier, Amsterdam,* 279–342.

Lahtinen, R., 1994: Crustal evolution of the Svecofennian and Karelian domains during 2.1–1.79 Ga, with special emphasis on the geochemistry and origin of 1.93-1.91 Ga gneissic tonalites and associated supracrustal rocks in the Rautalampi area, central Finland. *Geological Survey of Finland, Bulletin 378*, 128 pp.

Lahtinen, R., Huhma, H., Lahaye, Y., Jonsson, E., Manninen, T., Lauri, L.S., Bergman, S., Hellström, F., Niiranen, T. & Nironen, M., 2015: New geochronological and Sm-Nd constraints across the Pajala shear zone of northern Fennoscandia: Reactivation of a Paleoproterozoic suture. *Precambrian Research 256*, 102–119.

Lauri, L.S., Hellström, F., Bergman, S., Huhma, H. & Lepistö, S., 2016: New insights into the geological evolution of the Archaean Norrbotten province, Fennoscandian shield. *32nd Nordic Geological Winter Meeting, Helsingfors*.

Lehtonen, M., Airo, M.-L., Eilu, P., Hanski, E., Kortelainen, V., Lanne, E., Manninen, T., Rastas, P., Räsänen, J. & Virransalo, P., 1998: The stratigraphy, petrology and geochemistry of the Kittilä greenstone area, northern Finland. *Geological Survey of Finland, Report of Investigation 140*, 144 pp.

Ludwig, K.R., 1991a: PBDAT: A computer program for processing Pb-U-Th isotope data. Version 1.20. *United States Geological Survey, Open File Report 88-542*.

Ludwig, K.R., 1991b: ISOPLOT: A plotting and regression program for radiogenic-isotope data. Version 2.53. *United States Geological Survey, Open File Report 91*.

Ludwig, K.R., 2012: User's manual for Isoplot 3.75. A Geochronological Toolkit for Microsoft Excel. Berkeley *Geochronology Center Special Publication No. 5*, 75 pp.

Lundmark, C., 1985: Käymäjärviområdet, diamantborrning 1984: *Sveriges geologiska AB, Unpublished report PRAP 85028*, 8 pp.

Lukkarinen, H., 1990: Petrography, geochemistry and tectonic setting of the Paleoproterozoic metavolcanic rocks of the Kuopio and Siilinjärvi areas, mid-Finland. *In*: Y. Kähkönen (Ed.), Proterozoic Geochemistry. *Abstracts, IGCP Project 217, Symposium, December, 13-14, 1990, Helsinki,* 39-40.

Lynch, E.P., Bauer, T.E., Jönberger, J., Sarlus, Z., Morris, G.A. & Persson, P.-O., 2018a: Petrology and deformation of c. 1.88 Ga meta-volcanosedimentary rocks hosting iron oxide-copper-gold and related mineralisation in the Nautanen-Gällivare area, northern Sweden. *In:* Bergman, S. (ed): Geology of the Northern Norrbotten ore province, northern Sweden. *Rapporter och Meddelanden 141,* Sveriges geologiska undersökning. This volume pp 107–149.

Lynch, E.P., Hellström, F.A., Huhma, H., Jönberger, J., Persson, P.-O. & Morris, G.A, 2018b: Geology, lithostratigraphy and petrogenesis of c. 2.14 Ga greenstones in the Nunasvaara and Masugnsbyn areas, northernmost Sweden. *In:* Bergman, S. (ed): Geology of the Northern Norrbotten ore province, northern Sweden. *Rapporter och Meddelanden 141,* Sveriges geologiska undersökning. This volume pp 19–77.

Machel, H.-G. & Mountjoy, E.W., 1986: Chemical and environments of dolomitization – A reappraisal. *Earth-Science reviews 23*, 175–222.

Manninen, T., Pihlaja, P. & Huhma, H., 2001: U-Pb geochronology of the Peurasuvanto area, northern Finland. *In*: M. Vaasjoki (Ed.), Radiometric age determinations from Finnish Lapland and their bearing on the timing of Precambrian volcano-sedimentary sequences. *Geological Survey of Finland, Special Paper 33*, 189–198.

Martin, A.P., Condon, D.J., Prave, A.R., Melezhik, V.A., Lepland, A. & Fallick, A.E., 2013: Dating the termination of the Palaeoproterozoic Lomagundi-Jatuli carbon isotopic event in the North Transfennoscandian Greenstone Belt. *Precambrian Research 224*, 160–168.

Martinsson, O., 1995: Greenstone and Porphyry Hosted Ore Deposits in Northern Norrbotten. *Unpublished report, NUTEK Project nr 92-00752P. Division of Applied Geology, Luleå Univiversity of Technology*, 58 pp.

Martinsson, O., 1997: Tectonic setting and metallogeny of the Kiruna greenstones. *Doctoral thesis 1997:19.* Luleå University of Technology.

Martinsson, O., 1999: Berggrundskartan 30J Rensjön SO, 1:50 000. *Sveriges geologiska undersökning Ai 133*.

Martinsson, O., Vaasjoki, M. & Persson, P.-O., 1999: U-Pb zircon ages of Archaean to Palaeoproterozoic granitoids in the Torneträsk-Råstojaure area, northern Sweden. *Geological Survey of Sweden C 831*, 70–90.

Martinsson, O., 2004a: Geology and metallogeny of the northern Norrbotten Fe-Cu-Au province. *In:* R.L Allen, O. Martinsson & P. Weihed (Eds.), Svecofennian Ore-Forming Environments: Volcanic-associated Zn-Cu-Au-Ag, intrusion associated Cu-Au, sediment-hosted Pb-Zn, and magnetite-apatite deposits in northern Sweden. *Society of Economic Geology, Guidebooks Series 33*, 131–148.

Martinsson O., 2004b: Carbon isotopes as a tool for stratigraphic correlation within the Palaeoproterozoic Kiruna Greenstones, northern Sweden. *In*, J. Mansfeld (Ed.), The 26th Nordic Geological Winter Meeting, *Abstract volume, GFF 126*, 30.

Martinsson, O. & Wanhainen, C., 2004: Field trip day five, Cu-Au deposits in the Gällivare area. *In:* R.L. Allen, O. Martinsson and P. Weihed (eds.), Svecofennian Ore-Forming Environments: Volcanic-associated Zn-Cu-Au-Ag, intrusion associated Cu-Au, sediment-hosted Pb-Zn, and magnetite-apatite deposits in northern Sweden. *Society of Economic Geoology, Guidebooks Series 33*, 159–162.

Martinsson, O. & Wanhainen, C., 2013: Fe oxide and Cu-Au deposits in the Northern Norrbotten ore district. *Geological Survey of Sweden, Excursion Guidebook SWE5,* 70 pp.

Martinsson, O., Van der Stijl, I., Debras, C. & Thompson, M., 2013a: Day 3. The Masugnsbyn, Gruvberget and Mertainen iron deposits. *In*, O. Martinsson & C. Wanhainen (Eds.), Fe oxide and Cu-Au deposits in the Northern Norrbotten ore district. *Geological Survey of Sweden, Excursion Guidebook SWE5,* 37–44.

Martinsson, O., Allan, Å. & Denisová, N., 2013b: Day 2. Skarn iron ores in the Pajala area. *In*, O. Martinsson & C. Wanhainen (Eds.), Fe oxide and Cu-Au deposits in the Northern Norrbotten ore district. *Geological Survey of Sweden, Excursion Guidebook SWE5,* 31–36.

Martinsson, O., Billström, K., Broman, C., Weihed, P. & Wanhainen C., 2016: Metallogeny of the Northern Norrbotten Ore Province, northern Fennoscandian Shield with emphasis on IOCG and apatite-iron ore deposits. *Ore Geology Reviews 78,* 447–492.

Melezhik, V.A., Fallick, A.E., Makarikhin, V.V. & Lyubtsov, V.V., 1997: Links between Palaeoproterozoic palaeogeography and rise and decline of stromatolites: Fennoscandian Shield. *Precambrian Research 82*, 311–348.

Mutanen, T. & Huhma, H., 2001: U–Pb geochronology of the Koitelainen, Akanvaaraand Keivitsa mafic layered intrusions and related rocks. *Bulletin Geological Society of Finland 33*, 229–246.

Offerberg, J., 1967: Beskrivning till bergrundskartbalden Kiruna NV, NO, SV, SO. *Sveriges geologiska undersökning Af 1–4*, 146 pp (with English summary).

Öhlander, B., Lager, I., Loberg, B.E.H. & Schöberg, H., 1992: Stratigraphical position and Pb-Pb age of Lower Proterozoic carbonate rocks from the Kalix greenstone belt, northern Sweden. *Geologiska Föreningens i Stockholm Förhandlingar* 114, 317–322.

Öhlander, B., Skiöld, T., Elming, S-Å., BABEL Working group, Claesson, S. & Nisca D.H., 1993: Delineation and character of the Archaean-Proterozoic boundary in northern Sweden. *Precambrian Research 64*, 67–84.

Padget, P., 1970: Beskrivning till berggrundskartbladen Tärendö NV, NO, SV, SO. *Sveriges geologiska undersökning Af 5–8*, 95 pp.

Padget, P., 1977: Beskrivning till berggrundskartbladen Pajala NV, NO, SV, SO. *Sveriges geologiska undersökning Af 21–24*, 73 pp.

Pearce, J.A., 1982: Trace element characteristics of lava from destructive plate boundaries. *In:* R.S. Thorpe (ed.): *Andesites, Wiley*, 525–548.

Pekkarinen, L.J. & Lukkarinen H., 1991: Paleoproterozoic volcanism in the Kiihtelysvaara-Tohmajärvi district, eastern Finland. *Geological Survey of Finland Bulletin 357,* 30 pp.

Perttunen, V. & Vaasjoki, M., 2001: U–Pb geochronology of the Peräpohja Schist Belt,northwestern Finland. *Bulletin Geological Society of Finland 33*, 45–84.

Pharaoh, T., 1985: Volcanic and geochemical stratigraphy of the Nussir group of Arctic Norway - an early Proterozoic greenstone suite. *Journal of Geological Society of London 142,* 259–278.

Ranta, J.-P., Lauri, L.S., Hanski, E., Huhma, H., Lahaye, Y. & Vanhanen, E., 2015: U-Pb and Sm-Nd isotopic constraints on the evolution of the Paleoproterozoic Peräpohja Belt, northern Finland. *Precambrian Research 266*, 246–259.

Rastas, P., Huhma, H., Hanski, E., Lehtonen, M.I., Härkönen, V., Mänttäri, I. & Paakkola, J., 2001: U-Pb isotopic studies on the Kittilä greenstone area, central Lapland, Finland. *In*: M. Vaasjoki (Ed.), Radiometric age determinations from Finnish Lapland and their bearing on the timing of Precambrian volcano-sedimentary sequences. *Geological Survey of Finland, Special Paper 33*, 95–130.

Romer, R.L., Kjösnes, B., Korneliussen, A., Lindahl, I., Skysseth, T., Stendal, H. & Sundvoll, B., 1992: The Archaean-Proterozoic boundary beneath the Caledonides of northern Norway and Sweden: U-Pb, Rb-Sr and Nd isotopic data from the Rombak-Tysfjord area. *Norges Geologiske Undersøkelse, Rapport 91.225,* 67 pp.

Romer, R.L., Martinsson, O. & Perdahl, J.-A., 1994: Geochronology of the Kiruna iron ores and hydrothermal alterations. *Economic Geology 89,* 1249–1261.

Sakko, M. & Laajoki, K., 1975: Whole rock Pb-Pb isochron age for the Pääkkö iron formation in Väyrylänkylä, south Puolanka area, Finland. *Geological Society of Finland Bulletin 47*, 113–116.

Skiöld, T., 1979: Zircon ages from an Archean gneiss province in northern Sweden. *Geologiska Föreningens i Stockholm Förhandlingar 101*, 169–171.
Skiöld, T., 1986: On the age of the Kiruna Greenstones, northern Sweden. *Precambrian Research 32*, 35–44.
Skiöld, T. & Cliff, R.A., 1984: Sm-Nd and U-Pb dating of Early Proterozoic mafic-felsic volcanism in northernmost Sweden. *Precambrian Research 26*, 1–13.
Skiöld, T. & Page, R., 1998: SHRIMP and isotope dilution zircon ages on Archaean basement-cover rocks in northern Sweden. 23. *Nordiske geologiske vintermøde, Århus 13-16 January 1998, Abstracts*, 273.
Skiöld, T., Öhlander, B., Vocke, R.D. & Hamilton, P.J., 1988: Chemistry of Proterozoic orogenic processes at a continental margin in northern Sweden. *Chemical Geology 69*, 193–207.
Skiöld T., Öhlander, B., Markkula, H, Widenfalk, L. & Claesson, L.-Å., 1993: Chronology of Proterozoic orogenic processes at the Archaean continental margin in northern Sweden. *Precambrian Research 64*, 225–238.
Stacey, J.S. & Kramers, J.D., 1975: Approximation of terrestrial lead isotope evolution by a two-stage model. *Earth and Planetary Science Letters 26*, 207–221.
Steiger, R.H. & Jäger, E., 1977: Convention on the use of decay constants in geo- and cosmochronology. *Earth and Planetary Science Letters 36*, 359–362.
Vuollo, J., 1994: Paleoproterozoic basic igneous events in eastern Fennoscandian Shield between 2.45 and 1.97 Ga. *Ph.D. thesis, Acta Universitatis Ouluensis, Ser A no 250*, 47 pp.
Vuollo, J., Huhma, H. & Pesonen, L., 2000: Mafic dyke swarms – geological evolution of the Palaeoproterozoic in the Fennoscandian Shield. *In:* L.J. Pesonen, A. Korja (Eds.), Lithosphere 2000 – A symposium on the structure, composition and evolution of the lithosphere in Finland. *Program and extended abstracts, Espoo, Finland, October 4-4, 2000, Helsinki: Institute of Seismology, University of Helsinki, Report S-41*, 107–111.
Wanke, A. & Melezhik, V.A., 2005: Palaeoproterozoic sedimentation and stromatolite growth in an advanced intracontinental rift associated with the marine realm: a record of the Neoarchaean continent breakup? *Precambrian Research 140*, 1–35.
Warren, J., 2000: Dolomite: occurrence, evolution and economically important associations. *Earth-Science Reviews 52*, 1–81.
Westhues, A., Hanchar, J.M., Whitehouse, M.J. & Martinsson, O., 2016: New constraints on the timing of host rock emplacement, hydrothermal alteration, and iron oxide-apatite mineralization in the Kiruna district, Norbotten, Sweden. *Economic Geology 111,* 1595–1618.
Whitehouse, M. J. & Kamber, B. S., 2005: Assigning Dates to Thin Gneissic Veins in High-Grade Metamorphic Terranes: A Cautionary Tale from Akilia, Southwest Greenland. *Journal of Petrology 46*, 291–318.
Wiedenbeck, M., Alle, P., Corfu, F., Griffin, W. L., Meier, M., Oberli, F., Vonquadt, A., Roddick, J. C. & Speigel, W., 1995: 3 natural zircon standards for U-Th-Pb, Lu-Hf, trace-element and REE analyses. *Geostandards Newsletter 19*, 1–23.

Authors, paper 4:
Edward P. Lynch
Geological Survey of Sweden
Department of Mineral Resources
Uppsala, Sweden

Tobias E. Bauer
Luleå University of Technology,
Division of Geosciences and Environmental Engineering,
Luleå, Sweden

Johan Jönberger
Geological Survey of Sweden
Department of Mineral Resources
Uppsala, Sweden

Zmar Sarlus
Luleå University of Technology,
Division of Geosciences and Environmental Engineering,
Luleå, Sweden

George A. Morris
Geological Survey of Sweden
Department of Mineral Resources
Uppsala, Sweden

Per-Olof Persson
Swedish Museum of Natural History,
Department of Geosciences,
Stockholm, Sweden

4. Petrological and structural character of c. 1.88 Ga meta-volcanosedimentary rocks hosting iron oxide-copper-gold and related mineralisation in the Nautanen–Aitik area, northern Sweden

Edward P. Lynch, Tobias E. Bauer, Johan Jönberger, Zmar Sarlus,
George A. Morris & Per-Olof Persson

ABSTRACT

The petrological and deformation characteristics of a Palaeoproterozoic meta-volcanosedimentary sequence in the Nautanen–Aitik area (near Gällivare, northern Sweden) are presented. The investigated sequence (part of the *Muorjevaara group*) predominantly comprises metavolcaniclastic rocks displaying variable grain size, textural and syn-depositional features (e.g. grading, cross-laminae, compositional banding). Locally, poorly sorted agglomerate-like horizons with coarser clasts (lapilli- to block-size) occur. Interbedded sections of mainly fine-grained, volcanogenic (epiclastic) metasedimentary rocks contain syn-depositional features that suggest a sub-aqueous, relatively shallow depositional environment. Locally preserved cross-laminae in this unit provide evidence of way-up and paleocurrent directions. Intercalations of pelite, mica schist and amphibolitic schist also occur throughout the sequence. In general, least altered samples indicate a predominantly intermediate (basaltic andesitic to andesitic), calc-alkaline composition for the sequence.

U-Pb SIMS zircon dating of a meta-andesite horizon, intercalated within the sequence, has yielded a precise U-Pb concordia age of 1 878 ± 7 Ma (2σ, n = 12). This date constrains the timing of intermediate volcanism and the deposition of syn-volcanic epiclastic material. By inference, it also provides an estimate for the age of *Muorjevaara group* rocks hosting the Nautanen Cu-Au and Aitik Cu-Au-Ag deposits. When combined with lithogeochemical signatures, the new age also confirms a genetic link between the metavolcaniclastic package and gabbroic to dioritic intrusions in the area (e.g. the c. 1.88 Ga Aitik stock). Additionally, several zircon cores record $^{207}Pb/^{206}Pb$ apparent ages between c. 1.90 and 1.89 Ga, suggesting inheritance of marginally older volcanic ± plutonic material not exposed at the present erosion level.

The Nautanen–Aitik area contains the roughly north-northwest-trending *Nautanen deformation zone* (NDZ), a major composite brittle-ductile structure hosting hydrothermal iron oxide-Cu-Au (IOCG)-style mineralisation (e.g. the Nautanen deposit). Here, the bedrock is relatively intensely altered and sheared, and has been transposed into a sub-parallel high-strain zone predominantly consisting of a composite planar penetrative fabric. Outside the high-strain zone, relatively large-scale approximately North-northwest-aligned folds and discordant brittle structures occur. Magnetic susceptibility and VLF-resistivity modelling of the NDZ confirm that composite planar structures mainly dip steeply to the west-southwest and continue at depth.

INTRODUCTION

The composite Svecokarelian orogeny (the name Svecofennian is also used) is recognised as a major period of crustal reworking and growth on the margins of the Fennoscandian Shield during the Palaeoproterozoic (e.g. Nironen 1997, Korja et al. 2006, Lahtinen et al. 2009). In northernmost Sweden (Norrbotten), c. 1.95–1.78 Ga volcanic, sedimentary and intrusive rocks (and their related structures) record a protracted and episodic phase of accretionary orogenesis and crustal amalgamation during a major phase of tectonic convergence, metamorphism and magmatism (e.g. Bergman et al. 2001, Weihed et al. 2005, Bergman et al. 2006).

Regional assessments of Paleoproterozoic metasupracrustal rocks across Norrbotten (i.e. metamorphosed volcanosedimentary cover sequences) have helped establish a lithostratigraphic framework for the area and provide a lithotectonic context for its metallogenic evolution (e.g. Bergman et al. 2001, Martinsson 2004, Martinsson et al. 2016). However, detailed, local-scale investigations of specific sequences and associated structures at key stratigraphic intervals are generally lacking (cf. Monro 1988, Edfelt et al. 2006, Wanhainen et al. 2006). Such investigations are warranted in Norrbotten, given the association of volcanosedimentary basins and transecting ductile-brittle deformation zones with hydrothermal base and precious metal mineralisation (e.g. Smith et al. 2007, Smith et al. 2009, Wanhainen et al. 2012, Smith et al. 2013).

In this study, we present the results of a targeted investigation of Paleoproterozoic (Orosirian) metasupracrustal rocks occurring in the Nautanen–Aitik area near Gällivare in northern Norrbotten (Fig. 1). The study area contains a partly conformable and polydeformed meta-volcanosedimentary succession (part of the *Muorjevaara group*), transected by a major deformation zone hosting iron oxide-copper-gold (IOCG)-style mineralisation. Bedrock and structural mapping, ground geophysical data, lithogeochemistry and U-Pb SIMS zircon geochronology are integrated to provide an assessment of the petrological, deformation and mineralisation characteristics of the area. The results presented here complement an earlier account of the geology of the study area reported by Lynch et al. (2015).

In this account, the "Nautanen area" corresponds to the study area outlined in Figure 2 and extends beyond the historical Nautanen Cu-Au mine and the Nautanen deformation zone. For practical, descriptive and geological reasons, we have subdivided the main study area into three lithological-structural domains (Fig. 2). From east to west they are (1) the eastern volcanosedimentary domain (EVD, Muorjevaara to Linaälven area); (2) the central Nautanen deformation zone domain (NDZ domain); and (3), the western volcanosedimentary domain (WVD, Pahtavaara-Huivijokki area).

REGIONAL SETTING

The oldest rocks in northern Norrbotten are Meso- to Neoarchaean gneisses and metagranitoids, which constitute a partially hidden basement complex extending roughly from Luleå in the south to Sweden's northern border (Fig. 1, Öhlander et al. 1987, Martinsson et al. 1999, Mellqvist et al. 1999). The Archaean basement forms part of the larger *Norrbotten craton* (Lahtinen et al. 2005, Lauri et al. 2016), a continental terrane, which at c. 2.5 Ga formed part of a composite supercontinent called *Kenorland* (e.g. Reddy & Evans 2009, Melezhik et al. 2012). The Norrbotten craton subsequently broke away from Kenorland during lithospheric-scale rifting and continental dispersal commencing at c. 2.45 Ga (e.g. Hanski & Huhma 2005, Lahtinen et al. 2008, Melezhik & Hanski 2012).

Intracontinental rifting and extension of the Norrbotten craton between c. 2.4 and 2.1 Ga resulted in the deposition of Karelian supracrustal rocks onto the Archaean basement (e.g. Bergman et al. 2001). Early rift-related Karelian successions mainly consist of clastic metasedimentary rocks (meta-conglomerate, quartzite) and subordinate mafic to intermediate metavolcanic rocks. Later-stage Karelian successions consist of abundant mafic metavolcanic and intrusive rocks (tholeiitic to minor komatiitic varieties), and intercalated metasedimentary rocks (black schist, marble, meta-ironstone, pelite, metachert).These later successions combine to form the northern Norrbotten greenstone belts, part of a Palaeoproterozoic large igneous province occurring across Fennoscandia (Fig. 1, Martinsson 1997, Melezhik & Fallick 2010, Lynch et al., 2018b; cf. Hanski 2012).

Metavolcanic and metasedimentary successions formed between c. 1.9 and 1.8 Ga during the composite Svecokarelian orogeny are the most abundant Palaeoproterozoic metasupracrustal rocks in northern Norrbotten (Fig. 1). Svecofennian successions mainly consist of calc-alkaline to alkaline, intermediate to felsic metavolcanic rocks and associated epiclastic and metasedimentary sequences (Martinsson 2004). In general, these syn-orogenic rocks are considered to have been deposited, deformed and metamorphosed (up to middle amphibolite facies) within an evolving continental arc-type setting during northward-directed subduction, arc-continent accretion and continent-continent collision (e.g. Lahtinen et al. 2005, Lahtinen et al. 2009, Melezehik et al. 2012).

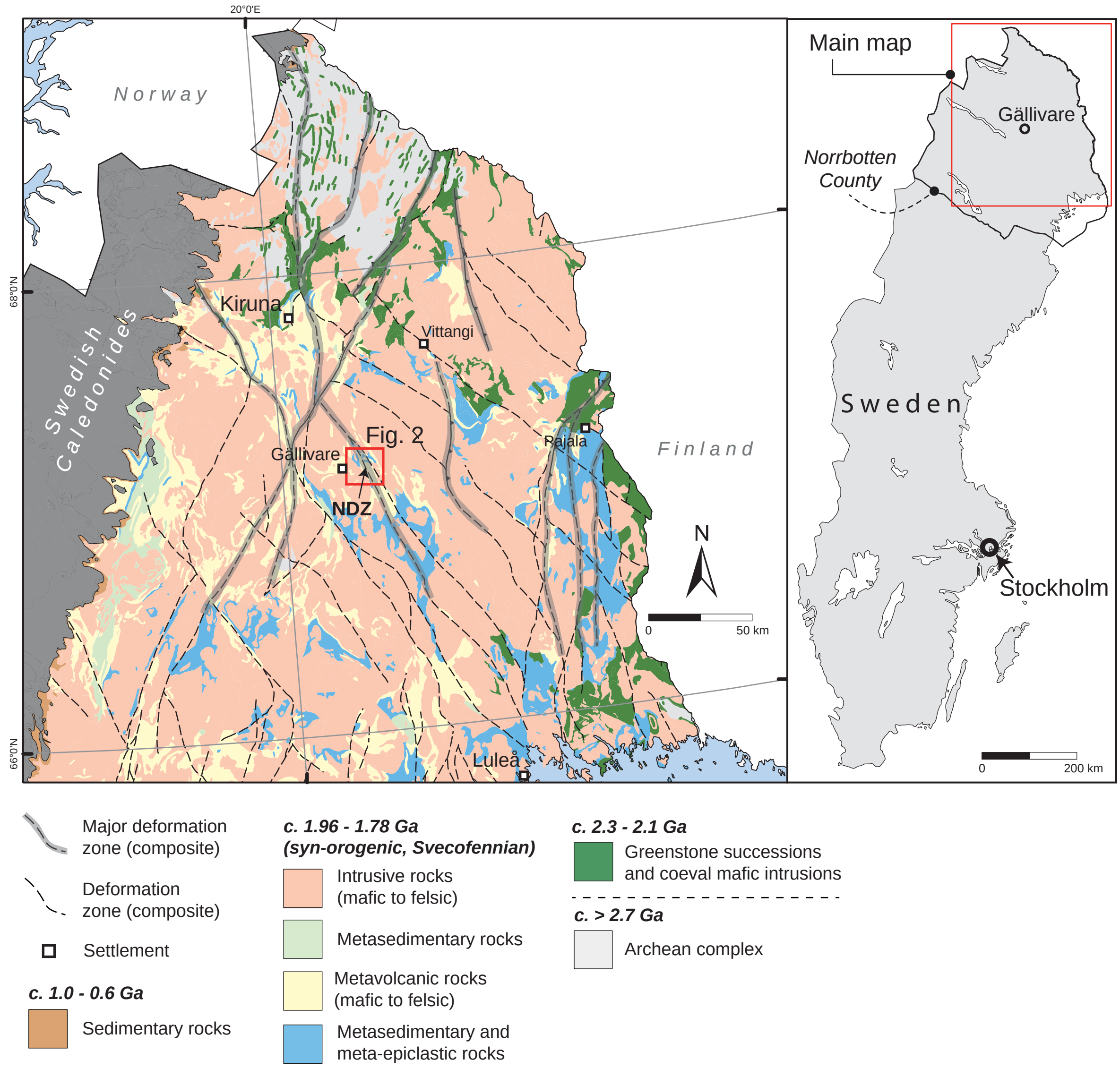

Figure 1. Regional geology of northernmost Sweden (Norrbotten). The red rectangle in the main map represents the Nautanen–Aitik area, corresponding to Figure 2. NDZ = Nautanen deformation zone. Base geology is from Bergman et al. (2012). Major deformation zones are from Bergman et al. (2001).

Across northern Norrbotten, Palaeoproterozoic metasupracrustal successions are surrounded and enclosed by voluminous, syn- to late-orogenic intrusive rocks (Fig. 1). In general, five main intrusive suites or associations are recognised (cf. Ahl et al. 2001, Bergman et al. 2001). These are (1) c. 1.89–1.86 Ga gabbros and dioritoids assigned to the *Haparanda* suite; (2) c. 1.88–1.86 Ga gabbros, syenitoids and granitoids assigned to the *Perthite monzonite* suite; (3) c. 1.86–1.84 Ga granitoids; (4) c. 1.81–1.78 Ga granitic rocks of the *Lina* suite; and (5) c. 1.80 Ga and possibly younger gabbro-dolerite intrusions (cf. Sarlus 2016).

The westernmost margin of northern Norrbotten is marked by Neoproterozoic sedimentary cover rocks and the approximately northeast-trending, low-angle nappe stacks of the Swedish Caledonides, which rest unconformably on the Archaean to Palaeoproterozoic shield area (e.g. Corfu et al. 2014).

GEOLOGY OF THE NAUTANEN–AITIK AREA

The Nautanen–Aitik area is centred on a partly conformable succession of syn-orogenic, Palaeoproterozoic meta-volcanosedimentary rocks (Fig. 2; Witschard 1996). The metasupracrustal sequence is generally of calc-alkaline, basaltic andesite to andesite composition and has undergone extensive deformation, metamorphism, recrystallisation and hydrothermal alteration (McGimpsey 2010, Waara 2015, Lynch et al. 2015).

A variety of intrusive rocks occur across the area, including deformed gabbroic, syenitic and dioritic bodies and younger, deformed to massive granitic and gabbroic-doleritic plutons and dykes (e.g. Wanhainen et al. 2006, Sarlus 2016). Two fairly large, sub-rounded, mafic-ultramafic intrusions named the Dundret and Vasaravaara complexes occur further east near Gällivare. These rocks exhibit distinct cumulate zones defining a primary magmatic layering consisting of olivine, pyroxene and plagioclase in varying proportions (Sarlus 2016).

Metasupracrustal rocks in the general Gällivare area host the Malmberget iron mine, Sweden's second largest iron resource after the Kiirunavaara deposit in Kiruna, and the Aitik Cu-Au-Ag deposit, one of Europe's largest copper mines (Fig. 2, e.g. Lund 2009, Wanhainen et al. 2012). Additionally, several hydrothermal Cu-Au occurrences assigned to the "iron oxide-copper-gold (IOCG)" mineral deposit class occur within a major approximately north-northwest-trending composite shear zone termed the Nautanen deformation zone (cf. Smith et al. 2013, Drejing-Carroll et al. 2015). Episodic deformation along this zone probably enhanced permeability and hydrothermal fluid flow, resulting in a relatively focused, linear zone of alteration and mineralisation (cf. Witschard 1996).

Metamorphic mineral assemblages and pressure-temperature (PT) estimates suggest the area reached middle amphibolite facies conditions during peak regional metamorphism. Bergman et al. (2001) noted a major metamorphic grade boundary in the area, with rocks east of the Nautanen deformation zone having a lower grade than those within the zone and to the west. Tollefsen (2014) reported PT estimates for regional metamorphism from approximately 550 to 660°C and 2 to 5 kbar (i.e. lower to middle amphibolite facies), contact metamorphism adjacent to Lina-type granite (forming a sillimanite-biotite-muscovite assemblage) between approximately 630 and 710°C and 2.0 to 4.4 kbar, and retrograde conditions between approximately 430 and 570°C, and 3.0 to 3.5 kbar. Additionally, Waara (2015) obtained PT estimates of approximately 630–680°C and 6.5 kbars for metasomatic garnet growth associated with potassic-ferroan alteration and Cu-Au mineralisation at the Nautanen deposit (equivalent to middle amphibolite facies conditions).

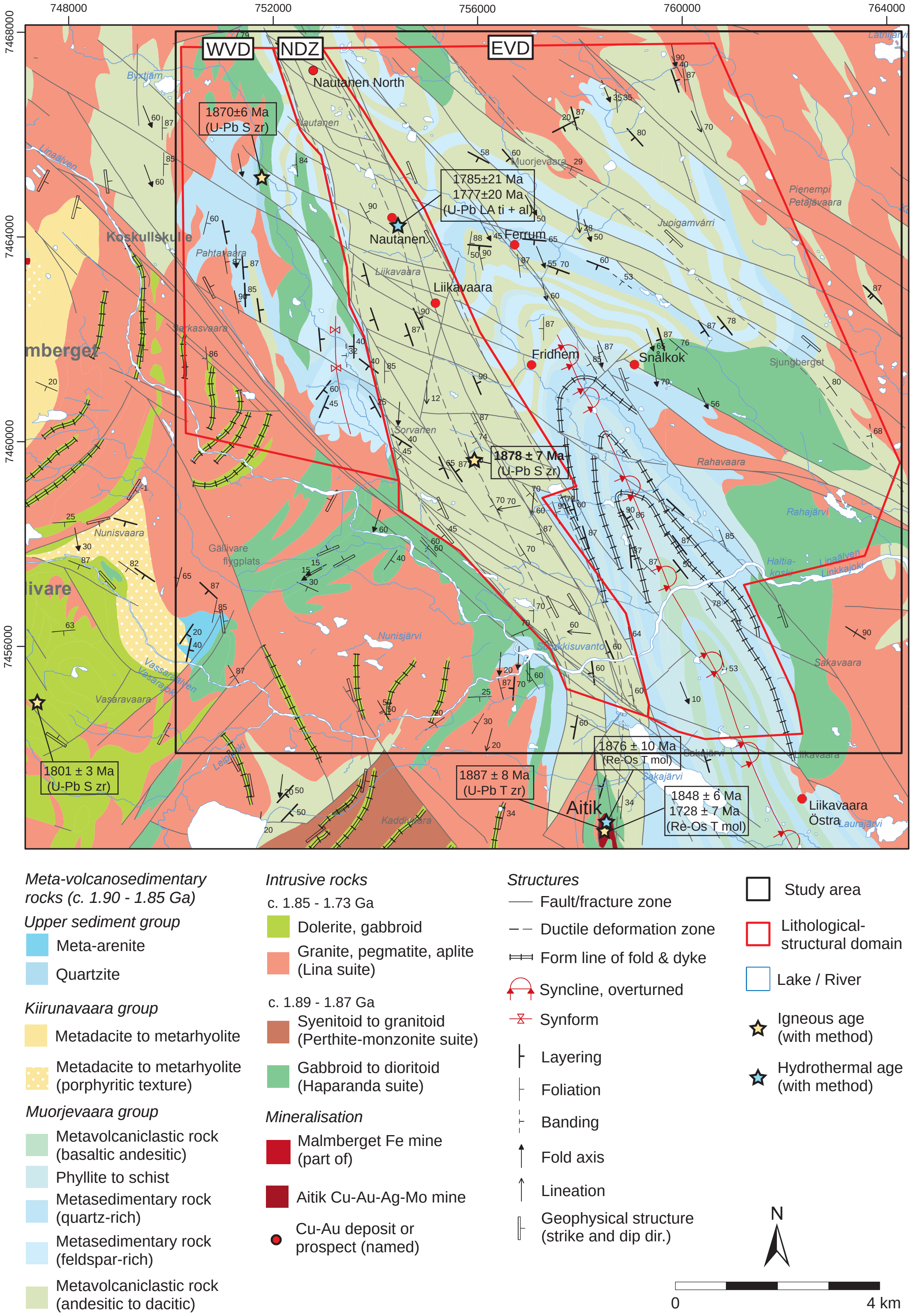

Figure 2. Geology of the Aitik–Gällivare area (modified after Witschard 1996). Abbreviations: EVD = eastern volcanosedimentary domain; NDZ = Nautanen deformation zone (domain); WVD = western volcanosedimentary domain. Geochronology abbreviations and sources: U-Pb S zr = U-Pb SIMS zircon dating (Sarlus 2016, and this study = highlighted bold text in NDZ), U-Pb T zr = U-Pb TIMS zircon dating (Wanhainen et al. 2006), Re-Os T mol = Re-Os TIMS molybdenite dating (Wanhainen et al. 2005), U-Pb T ti = U-Pb TIMS titanite dating (Wanhainen et al. 2005), U-Pb LA ti + al = U-Pb laser ablation-inductively coupled-mass spectrometry titanite and allanite dating (Smith et al. 2009).

Stratigraphy and correlations with other Svecofennian successions

A schematic stratigraphy of the Gällivare area is presented in Figure 3 and follows the system outlined in Lynch et al. (2015) and references therein. The informal stratigraphic units *Muorjevaara group, Kiirunavaara group* and *Upper sediment group* are retained here.

Stratigraphically, the *Muorjevaara group* represents a basal, mainly calc-alkaline volcanosedimentary sequence. This is overlain by the *Kiirunavaara group*, comprising alkalic (trachyitic) intermediate to acidic metavolcanic rocks (Martinsson & Wanhainen 2004). This unit hosts the iron oxide-apatite deposit at Malmberget (e.g. Lund 2009). Finally, local quartzite outliers of the *Upper sediment group* represent the uppermost stratigraphic unit. In the absence of outcropping transitional contacts, the major stratigraphic units are inferred to be separated by unconformities. The *Muorjevaara* and *Kiirunavaara* groups partly correspond to the regional *Porphyrite* and *Porphyry groups* of Bergman et al. (2001), respectively (Fig. 3). Traditionally, these regional stratigraphic units have been considered broadly coeval and have mainly been divided on the basis of petrographic and geochemical considerations (cf. Perdahl 1995).

Regional correlations between Muorjevaara group rocks and equivalent meta-volcanosedimentary successions elsewhere in northern Norrbotten are permissible based on broad lithological criteria (e.g. Ros 1980, Martinsson 1995). Inferred correlative successions include (roughly from west to east, Fig. 3) (1) Kilavaara Group schist, amphibolite and quartzite in the Svapavaara-Vittangi area (Eriksson & Hallgren 1975); (2) Ruutivaara and Haaravaara Group paragneiss and amphibolite in the Lainio area (Witschard 1970); (3) Pahakurkio Group schist, amphibolite and quartzite in the Tärendö area (Padget 1970); and (4) Sammakkovaara Group schist and metavolcaniclastic rocks in the Pajala area (Padget 1977, Martinsson 2004). In the last-mentioned case, correlation with the Sammakkovaara Group and related metavolcaniclastic rocks is supported by similar lithogeochemical signatures (cf. Luth et al. 2015). A correlation between the Muorjevaara group and rocks of the Kurravaara conglomerate unit in the Kiruna area has also been proposed (Ros 1980; cf. Offerberg 1967).

The Nautanen Deformation Zone and related iron oxide-copper-gold mineralisation

The Nautanen–Aitik area contains a regionally significant, roughly north-northwest-trending ductile-brittle shear zone named the Nautanen deformation zone (NDZ; Witschard 1996). It represents the most conspicuous structural feature in the area and is clearly delineated on magnetic anomaly maps as a somewhat dilational, linear zone of sub-parallel and tightly banded magnetic susceptibility anomalies (see *Geophysical modelling* section). The coupling of high-strain deformation and magnetic banding reflects episodic metasomatic-hydrothermal fluid flow, probably enhanced by increased permeability associated with protracted and focused deformation (e.g. Pitkänen 1997, Smith et al. 2013).

Based on regional structural and magnetic lineament geometries, Bergman et al. (2001) assigned a dextral-oblique shear sense to the NDZ, with a southwest-side up reverse component. Earlier geological mapping and geophysical measurements within the shear zone also identified several sub-parallel, north-northwest-orientated, moderately plunging folds (e.g. Gustafsson 1986, Pitkänen 1997). Internally, the deformation zone is characterised by moderate to intense shearing, mylonitisation, structural transposition and pervasive metasomatic-hydrothermal alteration (see further discussion in the *Structural geology and deformation* section).

Meta-volcanosedimentary rocks within and adjacent to the NDZ host several replacement and vein-related (epigenetic-style) Cu ± Au deposits and prospects (see reviews by Martinsson & Wanhainen 2004, Martinsson & Wanhainen 2013). Important examples include the Nautanen, Liikavaara and Ferrum prospects (Fig. 2). Two general styles of mineralisation are recognised (e.g. Gustafsson 1985, Martinsson & Wanhainen 2004): (1) an inferred older phase of disseminated to semi-massive (replacement-style) sulphide mineralisation forming sub-vertical, lenses and linear zones mainly within the

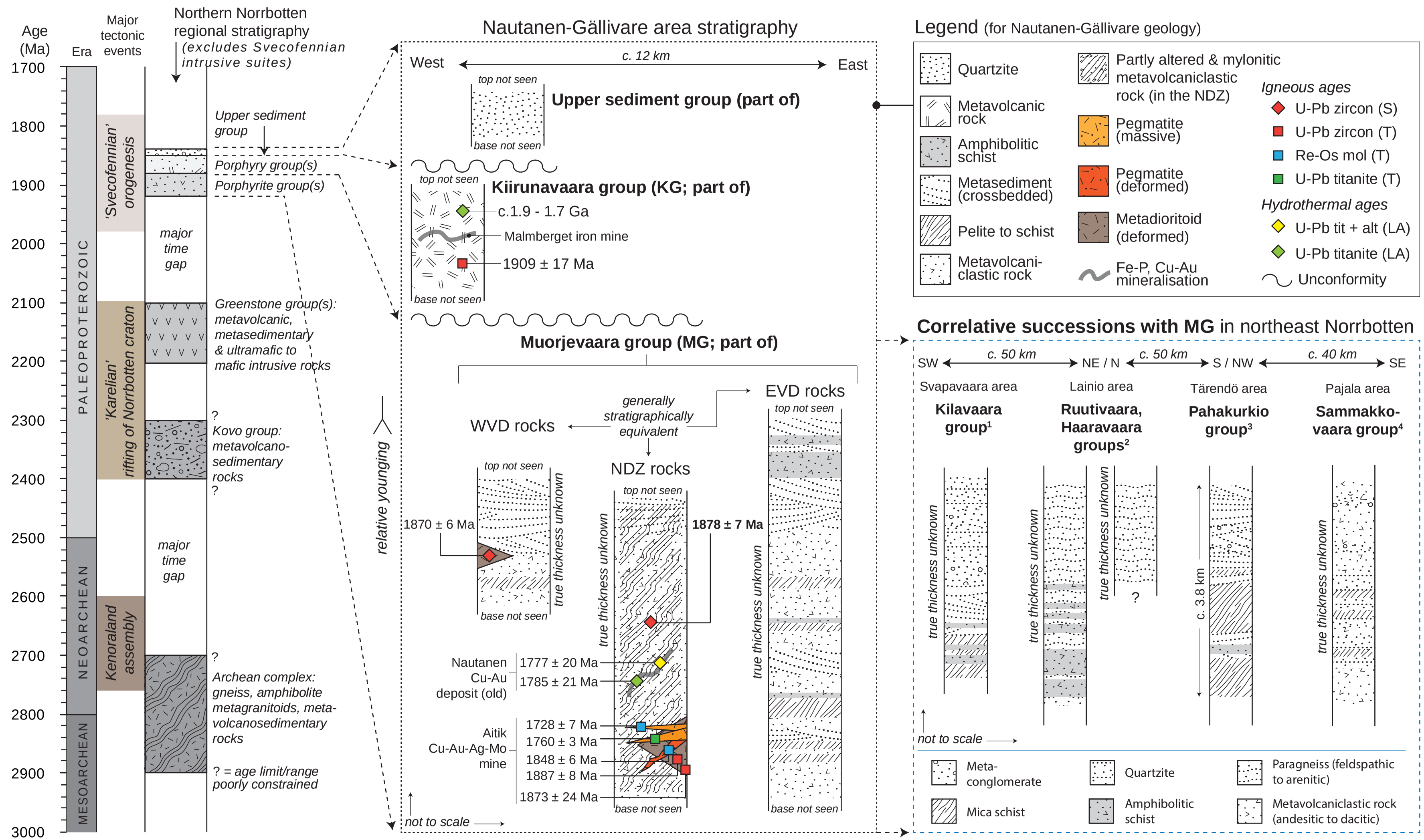

Figure 3. Outline stratigraphy of northern Norrbotten and the Gällivare area (based on descriptions by Witschard 1996, Bergman et al. 2001 and Martinsson & Wanhainen 2004). Abbreviations: EVD = eastern volcanosedimentary domain, KG = Kiirunavaara group, MG = Muorjevaara group, NDZ = Nautanen deformation zone domain, WVD = western volcanosedimentary domain. Geochronology abbreviations and sources: U-Pb SIMS (S) zircon ages = Sarlus 2016, and this study (bold text); U-Pb TIMS (T) zircon ages = Sköld & Cliff (1984), Wanhainen et al. (2006); Re-Os TIMS (T) molybdenite (mol) ages = Wanhainen et al. (2005); U-Pb TIMS (T) and laser ablation mass spectrometry (LA) titanite (tit) and allanite (alt) ages = Wanhainen et al. (2005), Storey et al. (2007), Smith et al. (2009). Schematic stratigraphy of correlative northeast Norrbotten successions is based on: 1 = Eriksson and Hallgren 1975; 2 = Witschard 1970; 3 = Padget 1970, 1977; 4 = Martinsson 2004.

NDZ (e.g. Nautanen deposit, Danielsson 1985); and (2) mineralisation associated with quartz ± tourmaline ± amphibole veins occurring mainly east of the NDZ (e.g. Ferrum prospect, Gustafsson & Johnsson 1984), or as a late-stage brittle overprint within the high-strain zone (e.g. at the Nautanen deposit).

The area around the Nautanen deposit in the northern NDZ domain is a historical mining location that has experienced intermittent exploration for over 100 years. Copper mineralisation was first discovered in 1898, and approximately 72 000 tonnes of copper and iron ore were extracted between 1902 and 1907 (Geijer 1918). Gold was not mined at that time, however. Further exploration in the 1970s and 80s produced a pre-regulatory total resource estimate for the "old" Nautanen deposit of approximately 2.94 Mt grading 0.78% Cu and 0.52 ppm Au (values derived from Danielson 1985). Present-day exploration has resulted in the discovery of additional Cu-Au mineralisation approximately 1.6 km north-northwest of the old Nautanen mine along the trend of the NDZ (Fig. 2). This "Nautanen North" deposit has an indicated resource of 9.6 Mt grading 1.7% Cu, 0.8 ppm Au, 5.5 ppm Ag and 73 ppm Mo, with an additional inferred resource of 6.4 Mt grading 1.0% Cu, 0.4 ppm Au, 4.6 ppm Ag and 41 ppm Mo (New Boliden 2016).

According to criteria presented by Grooves et al. (2010), the geological characteristics of the Nautanen Cu-Au deposit are consistent with the restricted definition of a *bona fide* iron oxide-copper-gold (IOCG) system. These include (1) enrichment of Cu and Au, with both elements representing potential economic commodities; (2) a spatial and genetic association between the mineralisation and iron silicate and iron oxide gangue minerals (i.e. *not* an iron oxide or iron oxide-apatite deposit with anomalous Cu and Au; cf. Williams 2010); (3) hydrothermal mineralisation style (i.e. replacement lenses, zones and veins); (4) sulphur mainly present in the S^{2-} oxidation state; (5) clear structural controls on the mineralisation; and (6) a temporal association with magmatism and deformation, but no obvious causative intrusion.

Pervasive and vein-related potassic-ferroan ± calcic alteration occurs variably in the NDZ domain and adjacent areas, and is associated with IOCG and related mineralisation (cf. McGimpsey 2010, Lynch et al. 2015; see also *Lithological characteristics* section). At the "old" Nautanen deposit (Fig. 2), characteristic almandine porphyroblasts are associated with amphibole + biotite + magnetite + sericite ± K-feldspar ± sulphide and tourmaline ± quartz ± sulphide banding, patches and veins (Fig. 4A–D). Textural relationships suggest garnet growth slightly predates the main-stage alteration and mineralisation event (cf. Waara 2015). Late-stage epidote ± quartz ± carbonate alteration also occurs (Fig. 4B–C). Chalcopyrite with lesser bornite and chalcocite are the main Cu-bearing minerals and are typically associated with pyrite, pyrrhotite, magnetite and tourmaline (Fig. 4D–E). Quartz-amphibole ± tourmaline veins containing pyrite and minor chalcopyrite post-date the main-stage disseminated and microfracture type sulphide mineralisation (e.g. Fig. 4F). Gold generally occurs as inclusions and segregations in pyrite, chalcopyrite, Bi-bearing phases and locally galena (e.g. Sammelin 2011, Bark et al. 2013).

At deformation zone- or belt-scale, particularly with respect to the NDZ, metal enrichment and depletion patterns are evident, reflecting bulk geochemical mobility in the area (Tollefsen 2014, Lynch et al. 2015). For example, comparison of "least altered" meta-volcanosedimentary rocks from the eastern volcanosedimentary domain with NDZ-hosted samples (pervasively altered, mylonitic) shows that the latter are relatively enriched in Cu, Ag, Au, Fe, Mo, Ba, Mn and W. Likewise, the tendency for K/Na ratios to increase when stepping into the NDZ domain reflects the association between potassic alteration and Cu-Au-Fe enrichment (cf. Lynch et al. 2015). These features are diagnostic of typical geochemical affinities and metal abundance correlations associated with IOCG-style mineralisation, particularly deposits hosted by intermediate to felsic igneous rocks in continental settings (cf. Barton 2014).

Smith et al. (2009) reported U-Pb LA-ICP-MS titanite and allanite ages ranging from c. 1.79 to 1.78 Ga for hydrothermal alteration at the Nautanen Cu-Au deposit (cf. Figs. 2 & 3). These dates provide a temporal and inferred genetic link between the mineralisation and deformation, fluid mobilisa-

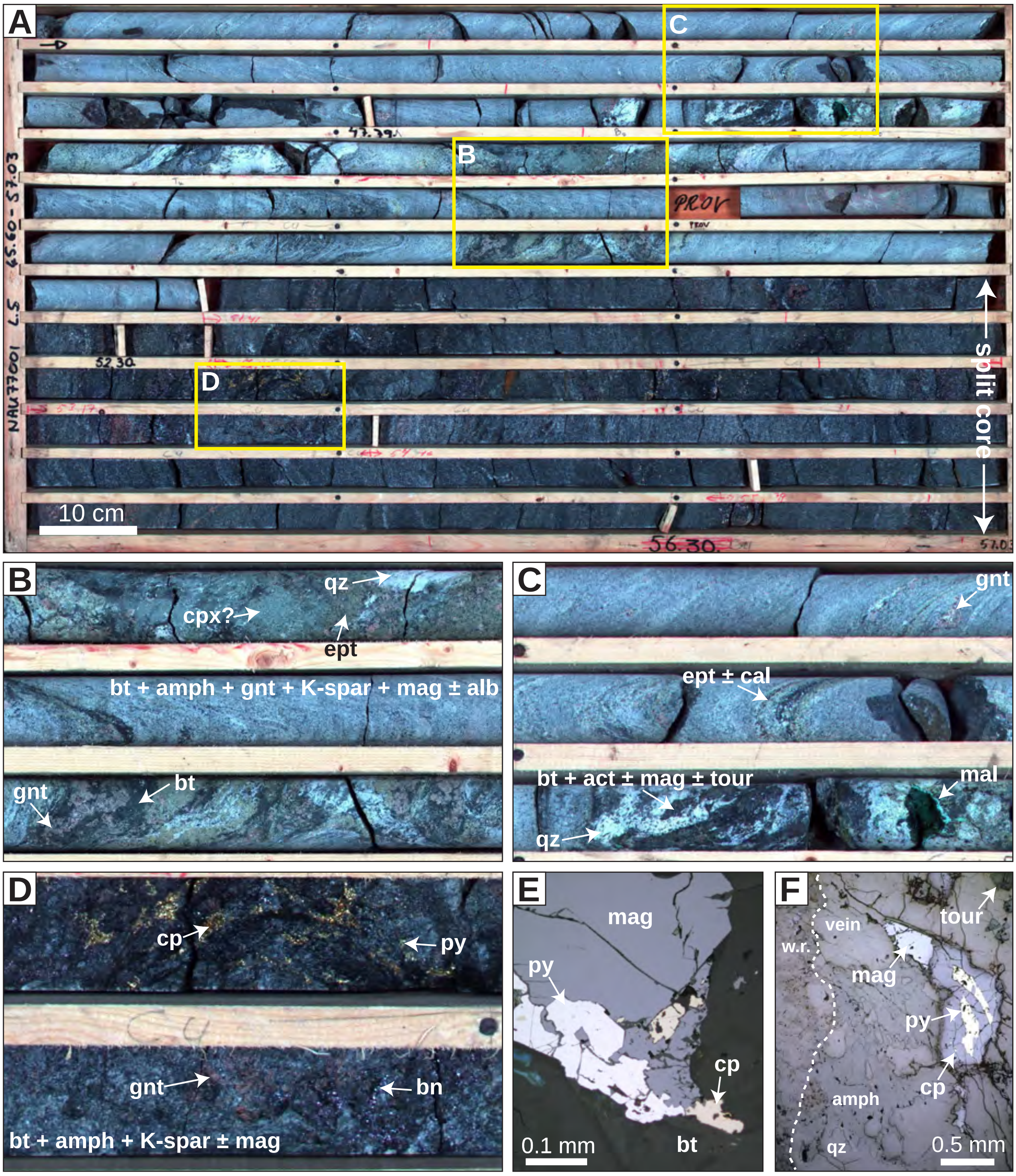

Figure 4. Alteration and mineralisation characteristics of the Nautanen IOCG deposit. **A.** True-colour image of an approximately 11.4 m section of altered and mineralised drill core (drill hole NAU77001). The lower six rungs contain split core. **B.** Foliated biotite-amphibole schist showing patchy and vein style, moderate to intense, biotite + garnet + K-feldspar ± albite ± magnetite alteration. A late-stage epidote ± calcite assemblage is also present. **C.** Foliated biotite-amphibole schist with disseminated garnet porphyroblasts associated with a possible early sodic-calcic (albite + scapolite) alteration (top rung). Some thin epidote + calcite veinlets also occur. The lower rung contains a replacement zone of biotite + chalcopyrite + bornite ± magnetite ± tourmaline and late-stage carbonate. **D.** Disseminated and irregular patches of chalcopyrite + pyrite + bornite associated with biotite + amphibole + garnet ± K-feldspar ± magnetite alteration. **E.** Thin section reflected light (RL) view of disseminated chalcopyrite and pyrite associated with magnetite. **F.** Thin section RL view of a quartz-amphibole-tourmaline vein containing pyrite, magnetite and rare chalcopyrite. W.r. = wall rock. Mineral abbreviations: act = actinolite, alb = albite, amph = amphibole, bn = bornite, bt = biotite, cal = calcite, cp = chalcopyrite, cpx = clinopyroxene, ept = epidote, gnt = garnet, K-spar = K-feldspar, mag = magnetite, mal = malachite, py = pyrite, qz = quartz, tour = tourmaline.

tion and late-orogenic granitic magmatism (cf. Fig. 3). Given the protracted and episodic nature of magmatic-hydrothermal processes and Cu-Au mineralisation at the Aitik deposit, south of Nautanen (e.g. Wanhainen et al. 2005), it is likely that coupled deformation-hydrothermal processes within the NDZ may have been active over a similarly protracted period.

Lithological characteristics of Muorjevaara group rocks

Petrographic descriptions presented in this section complement previous accounts by Zweifel (1976), Ros (1980), Monro (1988) and Lynch et al. (2015).

In general, four lithological units are recognised. They are (1) predominantly intermediate metavolcaniclastic rocks; (2) volcanogenic (epiclastic) metasedimentary rocks; (3) mica schist horizons; and (4) amphibolitic schist (mafic metavolcaniclastic rocks). Units 1 and 2 are the most common units across the Nautanen area.

Units 1, 2 and 3 represent compositionally similar lithologies (mainly basaltic andesitic to andesitic) and are primarily distinguished on the basis of textural, structural and deformation intensity criteria. In the Nautanen deformation zone domain, deformed and altered feldspar-biotite-amphibole schist (locally gneiss) is inferred to represent a composite intermediate metavolcaniclastic unit, probably consisting of a combination of units 1 to 3 (unit no. 5, Table 1).

Intermediate metavolcaniclastic rocks

In the central eastern volcanosedimentary domain, the predominant rock type is a medium to dark grey, fine- to medium-grained (approximately 0.1–3 mm), laminated and locally compositionally banded, metavolcaniclastic rock (Fig. 5). It forms planar to weakly wavy, generally sub-parallel, medium to very thick (approximately 0.1 to 1 m), laterally continuous beds (Fig. 5A–B). Inter-bed contacts are narrowly gradational to sharp. Internal textural and compositional consistency is somewhat variable and includes generally homogenous, well-sorted and granular units (fine to coarse tuff), and banded, layered and laminated sequences (Fig. 5C–E). Locally, the tuffaceous granular sections grade into somewhat irregular and wavy weathering beds consisting of mica-rich schist or relatively coarse (approximately 1–4 mm), feldspathic-rich bands and seams (Fig. 5B; cf. Fig. 7). The former tend to have a strongly developed micaceous sheen, whereas the latter may in part represent more compositionally felsic horizons or aplitic veins. Locally, tuffaceous sections display multiple, repeat grading sequences that alternate between very coarse tuff at the base (sometimes containing somewhat pumaceous, felsic clasts, Fig. 5F) to fine tuff at the top (thus, possible reverse density grading?, Fig. 5E). In addition, local horizons display cross-laminae that indicate general younging towards the southwest (Fig. 5F).

► Figure 5. Metavolcaniclastic rocks in the Nautanen area. **A.** Along-strike view (to the south-east) of medium- to thickly-bedded, intermediate, fine to coarse tuff. **B.** Bedding view to the southwest of thin- to medium-bedded, compositionally and texturally banded, intermediate metavolcaniclastic rock. **C.** View to the east-southeast of recrystallised, intermediate fine to coarse tuff. **D.** View to the northeast of intermediate metavolcaniclastic unit (tuff) with steeply dipping, sub-parallel amphibole-magnetite veinlets. **E.** Bedding view (to the northeast) of thinly laminated, well-sorted, fine to coarse tuff. Slightly coarser, epidote-altered, layers (arrows) with rare sub-rounded clasts indicate possible normal grading to the NE. **F.** Bedding view (to the southwest) of finely laminated, well-sorted, intermediate tuff with remnant elongate (feldspathic) clast. Broken lines indicate orientation of laminae (cross-lamination), indicating younging direction. **G.** Bedding view (to the southwest) of variably biotite-magnetite-altered and schistose, fine to coarse, lithic tuff. Two types of deformed clasts are visible; aggregated granular clasts (dashed outline), and relatively homogenous felsic clasts (arrows). **H.** Bedding view (to the west-southwest) of poorly sorted and foliated volcaniclastic (agglomeritic) unit, containing a mixture of deformed, angular to sub-rounded coarse (lapilli and block-sized) granular (intrusive?) and fine-grained felsic clasts. All photographs by Edward Lynch.


A
S0
S0
B
C
D
Sense Allround Permanent
E
grading
F
way-up
G
5 cm
H
BOLIDEN

The metavolcaniclastic rock mainly consists of feldspar, amphibole, biotite and minor quartz and muscovite within a fine-grained, intergranular (granoblastic) to foliated (lepidoblastic) matrix. Feldspar is anhedral, tabular to sub-rounded (platy) and is generally sericitised. Locally, feldspar also forms remnant, medium-grained (approximately 3–5 mm) phenocrysts (approximately 5–8 vol. %). Anhedral prismatic amphibole (hornblende) is intergrown with biotite and feldspar as irregular, matted, elongate and cleaved grains. Local magnetite disseminations or thin bands and veinlets (< 1 cm) occur, and prismatic and tabular grains tend to exhibit a preferred sub-parallel alignment (generally parallel to primary structures and foliations). Generally, biotite and feldspar occur in approximately equal proportions (approximately 30–45 vol. %). However, biotite ± sericite are locally predominant (up to approximately 60–70 vol. %), thus imparting a more obvious mica schist appearance to the rock (see unit 3 below). These latter intercalations may represent more altered horizons.

Locally, metavolcaniclastic sections contain coarser clastic material (> 3 mm) forming fine- to medium-grained lapilli-tuff horizons. In addition, poorly-sorted sections containing coarse, blocky clasts form local agglomeritic (volcanic breccia-like) horizons (Fig. 5G–H). Two broad clast types are recognised: fine-grained (< 0.5 mm), sub-rounded to elongate or flattened, compositionally uniform felsic clasts (possible juvenile volcanic clasts, Fig. 5G), and medium to coarse (approximately 0.1–10 cm), aggregated granular types (probably lithic clasts, Fig. 5H). In poorly-sorted sections, the latter clasts are locally up to 8 cm in size (Fig. 5H).

Overall, metavolcaniclastic rocks display a degree of compositional and textural variability across the sequence that reflects the generally interbedded nature of the eastern volcanosedimentary domain and the magnetic anomaly patterns across the area.

Volcanogenic (epiclastic) metasedimentary rocks

Throughout the eastern volcanosedimentary domain, interbedded sections of medium-grey, well-sorted, fine- to medium-grained (approximately 0.1–3 mm), generally arkosic metasedimentary rocks occur (Fig. 6). Locally, the interbedded sections transition into relatively thick sequences (approximately 500–800 m apparent thickness).

In the Muorjevaara area (northern part of the eastern volcanosedimentary domain, Fig. 2), a relatively well-exposed approximately 150 m long stratified metasedimentary sequence occurs (Fig. 6A). Here, the rocks form planar, parallel to locally non-parallel, thin to thick (approximately 0.03–0.4 m) and generally laterally continuous beds (Fig. 6A–D). Inter-bed contacts are either narrow diffuse (over approximately 0.1 m) or distinctive and sharp (e.g. Fig. 6C). Internally, the beds contain planar to locally wavy, generally parallel and laterally continuous, thin to medium (approximately 0.1–0.3 cm) laminae. Locally, however, parallel and lenticular non-parallel beds exhibit inclined cross-laminae (tabular to trough-style, respectively, Fig. 6E–F). Local co-sets display bi-directional, herringbone-type cross-lamination (Fig. 6F). In general, topset laminae and bedding contacts truncate low-angle ripple foresets towards the southwest, constraining way-up and younging direction. Likewise, in the central and southeastern volcanosedimentary domain, on the eastern limb of a large synform, cross-stratification suggests general younging towards the southwest (i.e. towards the hinge zone of the fold). These way-up indicators are locally supported by rare, normal-graded sequences (Fig. 6C). Ripple foreset patterns indicate paleocurrent directions mainly towards the north-northwest, or occasionally towards the south-southeast, while in general the cross-bedding structures suggest an above wave-base, subaqueous depositional setting.

At outcrop scale, metasedimentary rocks appear relatively homogenous and more lithologically consistent than other volcaniclastic and schistose sections, consisting of intergranular (granoblastic) feldspar and quartz with minor amphibole and rare muscovite. Locally, some beds are affected by patchy to banded biotite + amphibole + magnetite and epidote ± carbonate alteration. The latter assemblage is generally more prevalent and appears to preferentially overprint coarser (coarse to very coarse

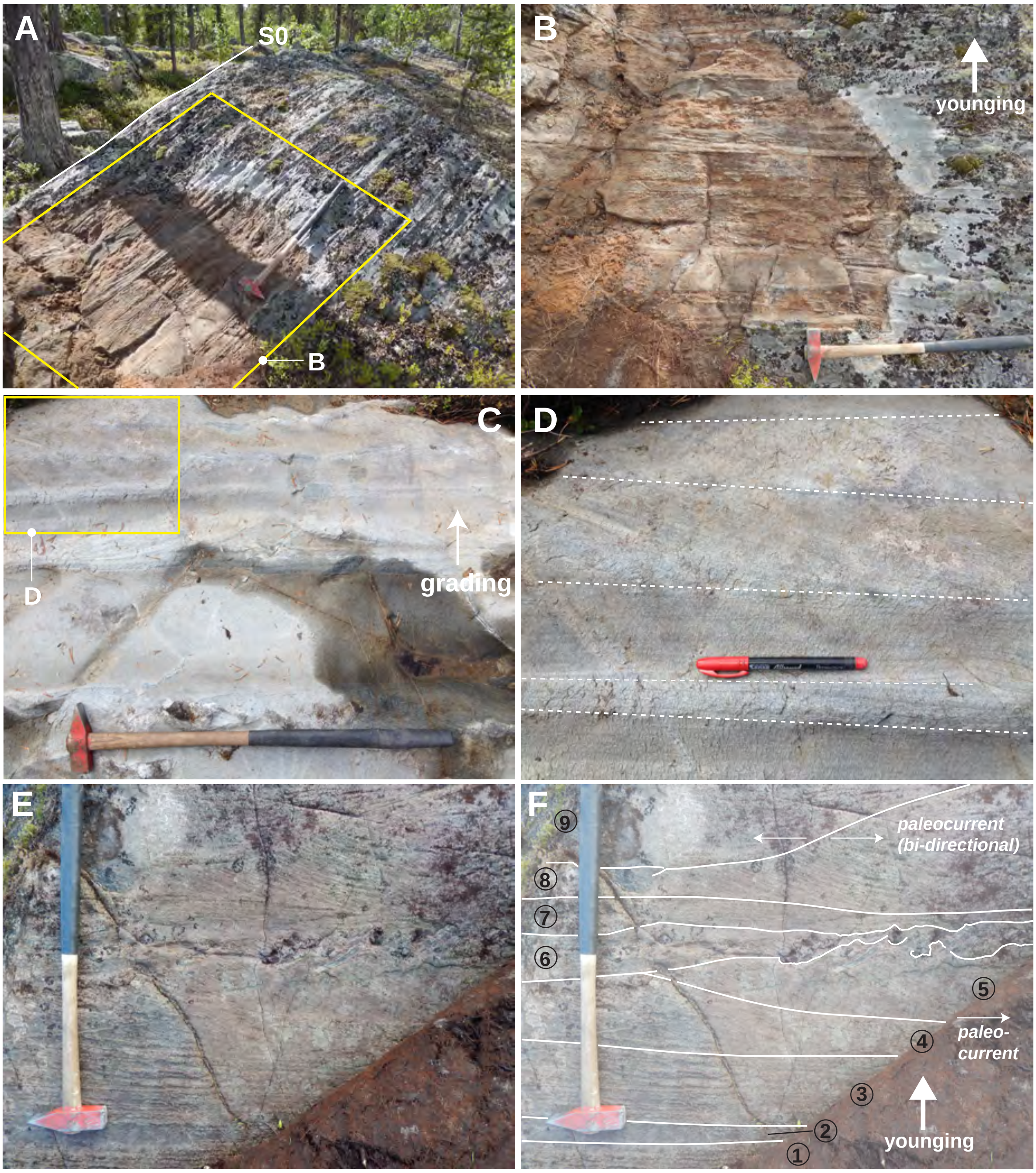

Figure 6. Volcanogenic (epiclastic) metasedimentary rocks in the Nautanen area. **A.** View to the west of planar, sub-parallel and laterally continuous, thin- to medium-bedded, arkosic metasedimentary rock (volcanic siltstone to sandstone). **B.** Detail from A with younging direction towards the southwest. **C.** Bedding view (to the southwest) of fine-grained, medium- to thickly-bedded metasedimentary rock. **D.** Detail from C showing sub-parallel, planar beds. **E.** Bedding view (to the southwest) of thin-to thickly-bedded, planar to curved (non-parallel) metasedimentary rock. **F.** Interpretive sketch of E showing nine bedding co-sets. Sets 4, 5, 8 and 9 contain inclined (ripple) foresets, indicating low-angle trough cross-lamination (sets 4 and 5) and herringbone cross-lamination (sets 8 and 9). All photographs by Edward Lynch.

sand) horizons. In general, a typical stratified sequence (approximately 0.5–2 m thick) consists of alternating very fine to coarse sand (approximately 0.1–1 mm) within planar and parallel laminated beds (Fig. 6C–F). These grade locally into wavy and cross-laminated horizons, more typically consisting of coarse to very coarse sand (approximately 1–2 mm) These general depositional characteristics are relatively consistent with medium-grained turbidite sequences (cf. Tucker 1991). Other minor features within rocks include siliceous, sub-rounded concretions (approximately 3–5 cm) locally developed at bedding contacts, and amphibole, epidote and quartz veins.

In general, the observed sedimentary structures are consistent with a sub-aqueous depositional environment. The preserved cross-bedding and herringbone-type cross laminae suggest above-wave-base or intertidal depositional environments. In terms of source material provenance and processes, the metasedimentary rocks probably represent either volcaniclastic material re-deposited within an active volcanosedimentary basin (i.e. syn-eruptive redeposition as defined by McPhie et al. 1993), primary unconsolidated volcaniclastic material, redeposited during volcanically quiescent periods ("immature" epiclastic rocks described by Cas & Wright (1988), or equate to the volcanogenic sedimentary deposits of McPhie et al. 1993). Older, detrital material (volcanic ± plutonic) most likely also contributed source material. Further petrographic and geochemical evidence for a predominantly volcanogenic source of the metasedimentary rocks includes the interbedded and gradational nature of this unit with other metavolcaniclastic rocks, the abundance of plagioclase feldspar in the matrix, and its general intermediate (andesitic) geochemical composition, similar to the metavolcaniclastic units within the sequence (see *Lithogeochemistry* section).

Pelite or mica schist

Intercalations of mica schist occur locally throughout the main meta-volcanosedimentary package and are preserved in both the eastern and western volcanosedimentary domains (Fig. 7). They typically form approximately 0.3 to 1.5 m thick, planar to laterally dilational units, with generally narrow, gradational contacts. At outcrop scale, they are recognised as texturally distinctive horizons that typically exhibit a more micaceous (lustrous), weathering-proud and schistose appearance than more granoblastic and recrystallised metavolcaniclastic and metasedimentary rocks. Locally, cross-bedding or climbing ripple-type structures are preserved, suggesting clastic depositional processes (Fig. 7A). Other horizons have a laminated, pelitic appearance (Fig. 7B). Metamorphic or fabric intensity ranges from phyllitic to schistose types, with the latter consisting of thinly spaced (approximately 0.5–2 mm), compositionally variable (mesocratic-melanocratic) banding (Fig. 7C). This textural variation probably reflects local contrasts in grain size, deformation intensity, mineralogy and composition, and somewhat mimics the broader lithological variability seen throughout the meta-volcanosedimentary sequence.

Mica schist horizons consist of fine-grained (<1 mm), intergranular biotite and feldspar, with lesser muscovite, amphibole and quartz (Fig. 7A–B). Mica grains are aligned and flattened parallel to the main schistosity and sub-parallel to inferred bedding, while medium-grained (approximately 3–5 mm) garnet porphyroblasts also occur locally (Fig. 7B). Typically, where garnet and andalusite occur, secondary hematite-goethite is exposed on weathered surfaces. Pervasive, weak to moderately intense sericite weathering is locally developed. Thin seams and veinlets of feldspathic material are also locally developed, are typically orientated parallel to the main schistosity, and are sometimes tightly folded.

Amphibolite schist (mafic metavolcaniclastic rock)

A prominent amphibolitic schist unit occurs in the southeastern volcanosedimentary domain (river Linaälven area) within the hinge zone of a major S-SE-plunging synform (Fig. 7D–F). The rock is dark grey to dark greenish-grey and is generally aphanitic to locally amphibole-porphyritic (approximately 3–7 vol. % phenocrysts). It consists of medium- to coarse-grained (approximately 1–8 mm), generally sub-rounded, anhedral platy to elongate (subhedral prismatic) amphibole (approximately 40–50 vol. %) within a fine-grained (<1 mm), plagioclase-amphibole-biotite ± magnetite matrix (approximately 35–45%). Recrystallisation of plagioclase and secondary phases such as biotite and chlorite (replacing amphibole) are common. Locally, scapolite appears to replace plagioclase.

Figure 7. Lesser intercalated rock units in the Nautanen area. **A.** View to the west-southwest of mica schist with possible cross-bedding structures. The pencil is about 15 cm long. **B.** Sub-horizontal surface view to the east-northeast of mica schist with garnet porphyroblasts. The pencil is 1 cm wide. **C**. Sub-horizontal surface view to the southwest of muscovite schist unit with a wavy and strongly foliated texture. **D.** Sub-vertical surface view to the north-northwest of amphibole-feldspar schist. **E.** Sub-horizontal surface view to the west-northwest of amphibolite schist near the river Linaälven, containing elongate or stretched lithic clasts (arrows). **F.** Sub-horizontal surface view to the east-southeast of foliated amphibolitic schist with weakly developed dextral shear planes. All photographs by Edward Lynch, except D by Zmar Sarlus.

The rock has a relatively intense deformation fabric, which imparts an overall schistose appearance (Fig. 7D). The schistosity is typically sub-vertical, north-northwest-orientated and steeply dipping. Weakly developed asymmetric shear bands also occur and suggest dextral oblique movements (Fig. 7F). Locally, thin feldspathic lenses and veinlets occur, sub-parallel to the main fabric. Additionally, elongate and stretched clasts are present. These display mainly remnant igneous (dioritic) textures (Fig. 7E). Clasts are typically aligned parallel to the main fabric in the rock (Fig. 7E).

Analogous amphibolitic units occur locally throughout the study area as fairly thin (< 1 m) intercalations within the main metavolcaniclastic package. Similar rocks have been observed in the central part of the Nautanen deformation zone and at the Salmijärvi Cu-Au prospect, approximately 2 km south-southeast of the Aitik mine (Sarlus 2013).

Biotite-amphibole schist to gneiss (Nautanen deformation zone)

The bedrock in the Nautanen deformation zone (NDZ) domain is affected by relatively intense shearing, transposition and metasomatic-hydrothermal alteration (Fig. 8). Thus, primary lithological characteristics are commonly obscured or masked by overprinting processes and remain somewhat equivocal (cf. Witschard 1996). Nevertheless, local low-strain and "least altered" zones provide some petrographic insights into the primary nature of the rocks in this area and facilitate comparisons with the rocks in the other two lithological-structural domains.

The predominant lithology is a medium to dark grey, fine- to medium-grained (approximately 0.1–3 mm), well-sorted and internally laminated, feldspar-biotite ± amphibole schist to gneiss (Fig. 8A). Locally, more weakly laminated varieties have a recrystallised, granoblastic appearance and appear more feldspar-rich (up to approximately 40 to 50 vol. %). Inferred bed forms (although rarely preserved) are approximately 0.1–0.5 m thick and are generally laterally continuous, sub-parallel and planar. In general, anhedral and platy biotite and lesser amphibole grains (approximately 15–20 and 5–10 vol. %, respectively) are aligned parallel to the dominant penetrative cleavage and intergrown with feldspar. Local horizons containing coarser (felsic) clasts (approximately 5–15 mm), elongate and stretched lensoidal patches (remnant clasts?), and composite, aggregated fragments (lithic clasts?) occur throughout the area. These features are consistent with a possible volcaniclastic derivation (cf. Fig. 5G–H). Locally, the schist grades into more quartz-rich sections consisting of fine-grained (< 1 mm), granular and anhedral quartz (approximately 10–20 vol. %), forming banded zones and aggregated, irregular to sub-rounded, lithic (?) clasts.

Throughout the Nautanen deformation zone domain the bedrock displays moderate to intense penetrative foliation and shows variable degrees of metasomatic-hydrothermal alteration (see *Structural geology and deformation* section). Distinctive dark red to pinkish-red, medium- to coarse-grained (typically approximately 1–10 mm) garnet porphyroblasts occur locally (approximately 3–12 vol. %). These appear to pre-date the main alteration assemblage and copper mineralisation event (Fig. 8C–D, e.g. Waara 2015). Locally, the garnets form quite large crystals up to 10 cm in diameter or aggregated clusters (cf. Fig. 13C). The garnets are typically of the spessartine-almandine variety, appear to be mainly syn-kinematic, and form disseminated grains or clusters associated with amphibole + biotite + magnetite veins and patches (Fig. 8C–D). Waara (2015) has suggested a link between garnet growth and early stage IOCG-related alteration, and constrained their formation at approximately 630–680°C by Thermocalc modelling.

The most important belt- to deposit-scale alteration assemblage affecting Nautanen deformation zone rocks is a moderate to intense amphibole + biotite + K-feldspar + magnetite ± garnet ± sericite ± pyrite ± chalcopyrite assemblage. Typically, it has developed along seams, linear zones and irregular veins trending parallel to the transposed foliation (Fig. 8B–C). This inferred "syn-mineralisation" assemblage overprints an earlier pervasive scapolite ± albite assemblage (Fig. 8B). Zones and bands of tourmaline ± quartz alteration represent a paragenetically later assemblage.

Syn-mineralisation magnetite typically occurs as fine- to medium-grained (approximately 0.1–2 mm), anhedral tabular and elongate platy grains within foliation planes. It also forms fracture-filling inclusions and patchy rims around garnet porphyroblasts. Consequently, the bedrock throughout the domain is magnetically anomalous (cf. Fig. 14; see *Structural geology and deformation* section). Locally,

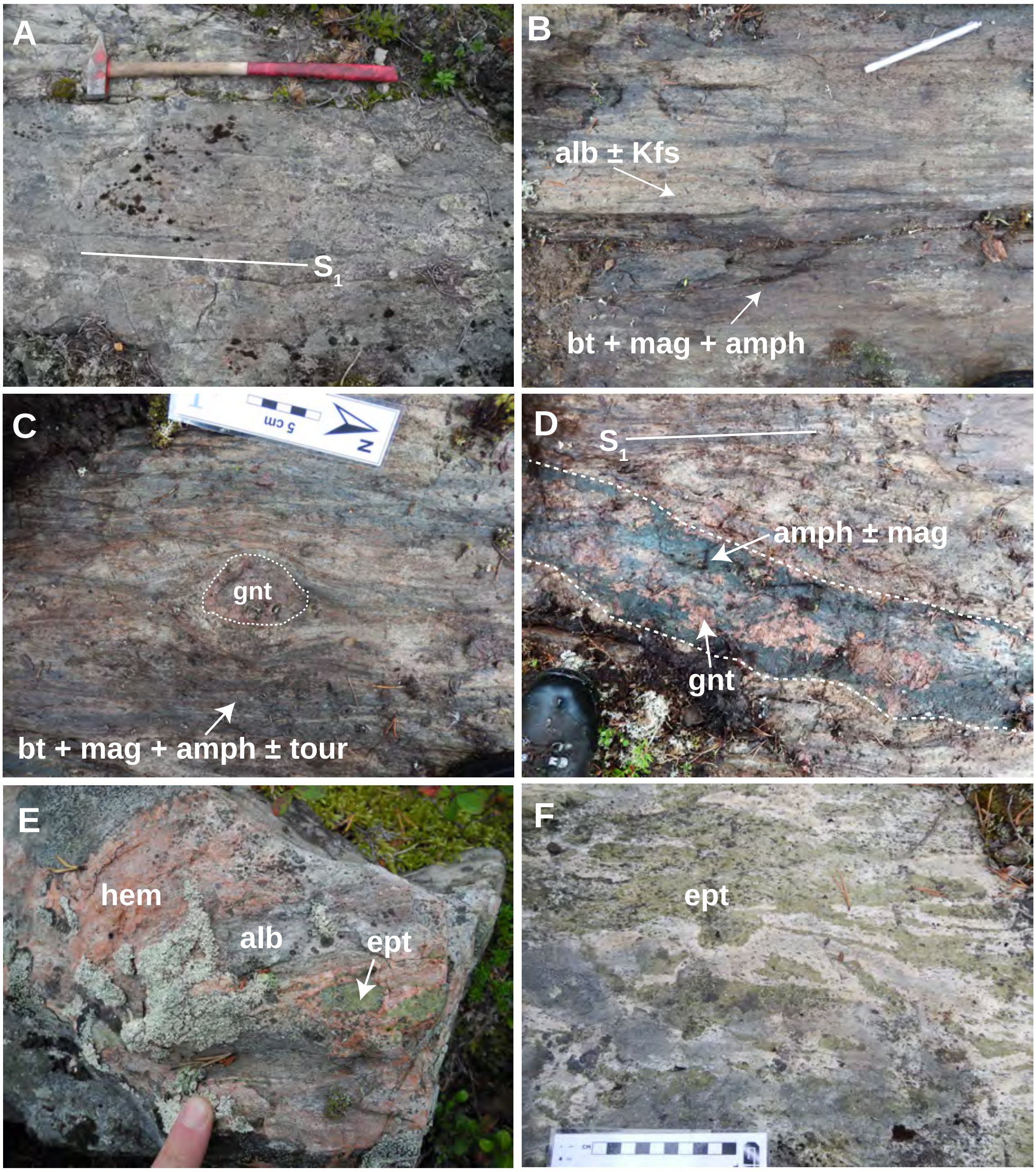

Figure 8. Variably altered biotite-amphibole-feldspar schist in the Nautanen deformation zone (inferred metavolcaniclastic unit). **A.** Relatively weakly altered. **B.** Banded metavolcaniclastic rock. **C.** Moderate to intensely altered rock. **D.** Moderate to intensely altered rock cut by an amphibole-garnet zone or vein. **E.** Feldspar-rich metavolcaniclastic rock showing pervasive "red rock" type hematite staining of feldspar (cf. Carlon 2000). Late-stage patchy epidote also developed. **F.** Late-stage epidote alteration of metavolcaniclastic rock. Abbreviations: alb = albite, amph = amphibole, bt = biotite, ept = epidote, gnt = garnet, hem = hematite, Kfs = K-feldspar, mag = magnetite, tour = tourmaline. All photographs by Edward Lynch.

feldspar-rich metavolcaniclastic rocks display reddish-pink patches and irregular zones indicative of "red rock"-type hematite staining and iron exsolution affecting alkali feldspar (Fig. 8E; cf. Carlon 2000). A late-stage epidote ± quartz ± carbonate alteration assemblage is also present and more typically overprints red rock (K-feldspar-altered) zones (Fig. 8E–F). Secondary hematite-goethite commonly replaces magnetite, while chlorite replaces biotite and is associated with epidote.

Lithogeochemistry of Muorjevaara group rocks

Preliminary lithogeochemistry results for meta-volcanosedimentary rocks from the eastern volcanosedimentary domain (EVD) are shown in Figure 9. Although the Nautanen area is affected by varying degrees of hydrothermal alteration (see above section), rocks in the EVD are generally less pervasively altered than those in the Nautanen deformation zone domain. Likewise, the inferred metamorphic grade (mid to upper greenschist facies) in the EVD is lower than that in the Nautanen deformation zone (cf. Bergman et al. 2001).

From a total of 32 analyses, a subset ($n = 24$) of relatively fresh or "least altered" eastern volcanosedimenatry domain samples were selected to geochemically characterise the meta-volcanosedimenatry rocks (Fig. 9A, shaded area). The subset includes scapolite + albite + sericite-altered samples of fine- to medium-grained, plagioclase-phyric, metavolcaniclastic rock with an elevated Na_2O concentration of approximately 7 wt. %.

Based on the classification plot of Winchester & Floyd (1977), least altered EVD meta-volcanosedimentary rocks generally have a basaltic andesitic to andesitic signature (Fig. 9B), while high-field strength element bivariate plots indicate a predominantly calc-alkaline composition (Fig. 9C–D). Metavolcaniclastic, meta-epiclastic, mica schist and amphibolitic schist samples have similar calc-alkaline, intermediate compositions, suggesting a possibly similar volcanic provenance and petrogenetic history. The altered feldspar-phyric metavolcaniclastic sample plots close to the andesite-dacite boundary and has broadly similar trace element systematics to the other samples (Fig. 9A–B).

The geochemical signatures of the meta-volcanosedimentary rocks from the eastern volcanosedimentary domain partly overlap the compositions of altered and mylonitic metavolcaniclastic rocks in the Nautanen deformation zone domain hosting the Nautanen Cu-Au deposit (Fig. 9B; cf. McGimpsey 2010). The latter units have a broader compositional range that includes dacitic, rhyodacitic and trachyandesitic (shoshonitic) varieties. However, the presence of (apparently) alkaline rocks within the Nautanen deformation zone domain may partly reflect a higher degree of potassic ± sodic alteration and "skarn" banding there (cf. Fig. 8B–C). Similar apparent alkaline enrichment is reported for metavolcaniclastic rocks hosting the Aitik Cu-Au-Ag deposit (Monro 1988, McGimpsey 2010), which also compositionally overlap both the eastern volcanosedimentary domain and Nautanen deformation zone domain metasupracrustal rocks (Fig. 9B).

Overall, the preliminary lithogeochemistry results confirm that NDZ domain rocks represent a more intensely deformed and hydrothermally altered variety of the units occurring in the eastern domain, and that the Muorjevaara group sequence in the Nautanen area is compositionally similar to the metavolcaniclastic rocks (biotite-amphibole-feldspar gneiss) hosting Cu-Ag-Au mineralisation at Aitik (cf. Monro 1988, Martinsson & Wanhainen 2004).

The lithogeochemistry results support lithostratigraphic correlations between Muorjevaara group rocks in the Nautanen area and meta-volcanosedimentary successions in northeastern Norrbotten (Pajala shear zone). For example, Luth et al. (2015) report sub-alkaline, mainly andesitic to rhyodacitic compositions for metavolcanic and metavolcaniclastic rocks assigned to the *Suorsa group* in the Pajala area. Certain units within this local group may be equivalent to the *Pahakurkio* and *Sammakkovaara groups* in adjacent areas and are inferred to belong to the regional Porphyrite group of Bergman et al. (2001).

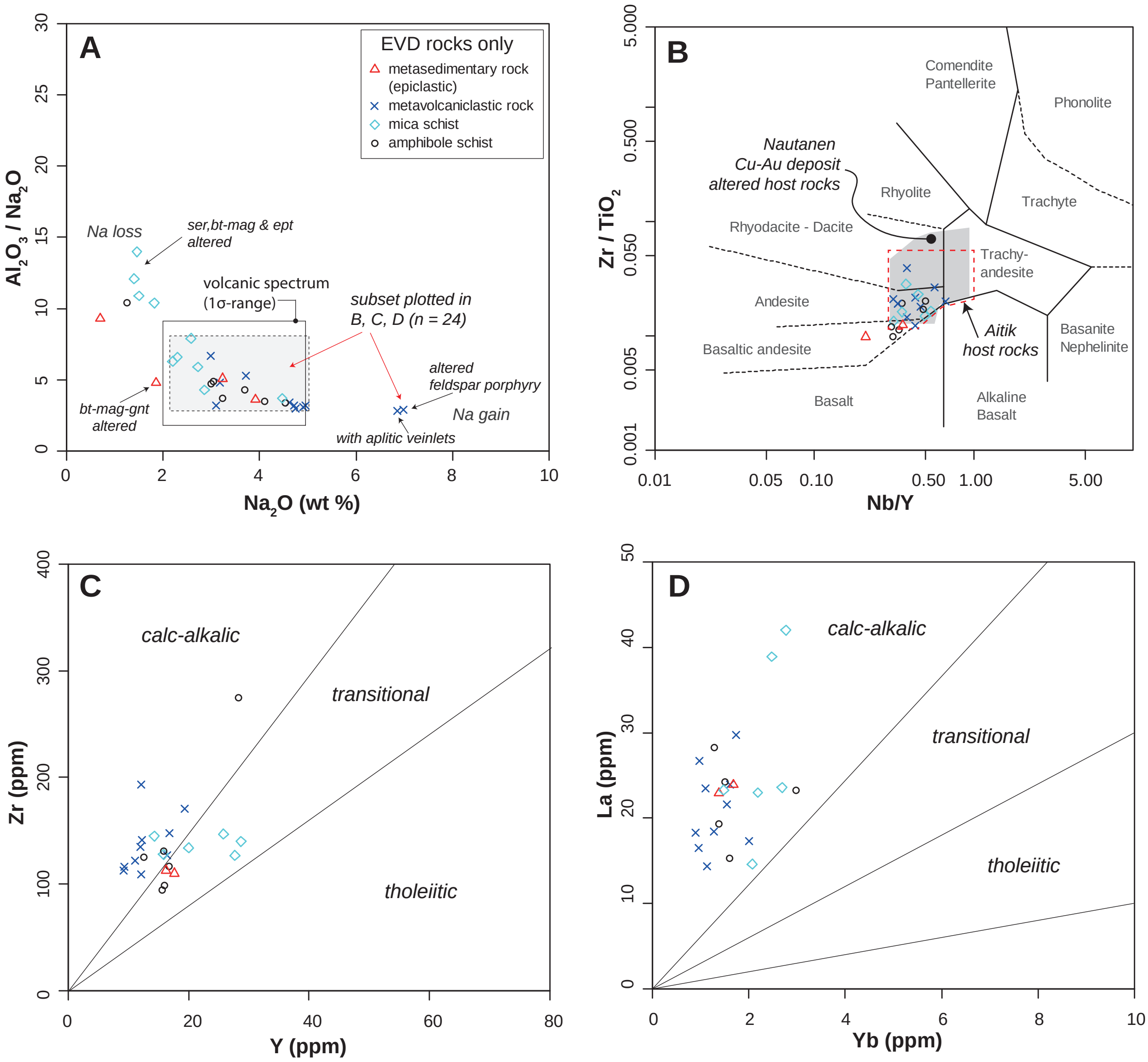

Figure 9. Geochemical classification of Muorjevaara Group meta-volcanosedimenatry rocks from the EVD, Nautanen area. **A.** Spitz-Darling type plot (Spitz & Darling 1978), delineating weakly altered samples used for the other classification plots shown in B, C and D. The spectrum for fresh volcanic rocks (basalt to rhyolite) is derived from the average and 1σ-range of 6 491 analyses reported by Le Maitre (1976). **B.** Incompatible-HFSE classification plot (Winchester & Floyd 1977) showing lithologic-compositional range of EVD meta-volcanosedimentary rocks. The shaded area represents the range reported by McGimpsey (2010) for altered metavolcaniclastic rocks hosting the Nautanen Cu-Au deposit. The broken red line represents the approximate range for metavolcaniclastic rocks hosting the Aitik Cu-Au-Ag deposit (cf. Monro 1988). **C–D.** Incompatible-HFSE bivariate plots (Barrett & MacClean 1999), indicating a predominantly calc-alkalic signature (i.e. equivalent to medium to high K, low to medium Fe, intermediate rocks).

Summary of Muorjevaara group rock units

A summary of Muorjevaara group lithologies is presented in Table 1. It includes a comparison between historical terms used for each unit and the field and protolith terms derived from this study.

Table 1: Outline description of Muorjevaara group rock units

Field term (with textural or metamorphic qualifiers, and inter-unit relationships)	Protolith term (with textural or compositional qualifiers)[1]	Historical, literature term (with reference)
In the eastern and western volcanosedimentary domains (Fig. 2)		
1. Metavolcaniclastic rock (tuffaceous, recrystallised, locally schistose; local volcanic and lithic clasts; compositionally banded, laminated; transitional or interbedded with 2, 3 and 4)	Andesitic to dacitic (intermediate), well-sorted, fine to very coarse tuff, to lapilli-tuff. Locally poorly sorted lithic tuff with agglomeritic (volcanic breccia) horizons.	Leptite (Geijer 1918) Biotite gneiss (Ros 1980) Basic to intermediate, calc-alkaline to alkaline, metavolcanic rock, tuff (Witschard 1996) Metaandesite (Bergman et al. 2001)
2. Metasedimentary rock (recrystallised appearance, laminated, locally cross-bedded, more texturally and compositionally uniform than 1, interbedded with 1)	Basaltic andesitic to andesitic (intermediate) volcanogenic epiclastic rock <u>or</u> volcanogenic siltstone to sandstone.	Meta-arenite (Zweifel 1976) Metaarkose (Ros 1980) Meta-arenite (Witschard 1996) Meta-arenite, quartzite (Bergman et al. 2001)
3. Pelite or mica schist (weathers proud, micaceous sheen, may be sericitised, generally intercalated or transitional with 1 and 2, possible textural or compositional variant of 1)	Basaltic andesitic to andesitic (basic to intermediate) fine to very coarse tuff.	Mica schist (Geijer 1918) Pelitic intercalation (Ros 1980) Phyllite to biotite schist (Witschard 1996) Pelite (Martinsson & Wanhainen 2004)
4. Amphibolitic schist (dark greenish grey, foliated, aligned grains, intercalated with 1 and 2, major unit in Linaälven synform hinge area)	Basaltic andesitic (basic to intermediate) fine to very coarse tuff, to fine lapilli-tuff. Locally contains lithic clasts (rare lithic tuff).	Amphibolitic rock (Zweifel 1976) Greenstone intercalation (Ros 1980) Amphibolitised andesite, dacite, trachyandesite (Witschard 1996) Metabasalt (Bergman et al. 2001)
In the Nautanen deformation zone domain (Fig. 2)		
5. Biotite-amphibole schist to gneiss (conspicuous garnet porphyroblasts, pervasively sericite ± scapolite and K-feldspar-altered, with local biotite-amphibole-magnetite and tourmaline banding. Locally mylonitic. NDZ-hosted equivalent to 1, 3 and possibly 2)	Andesitic to dacitic (intermediate) fine to very coarse tuff, locally agglomeritic tuff (volcanic breccia). Variably sheared, transposed, metasomatised and altered.	High magnetic, biotite-garnet ± amphibole schist to gneiss (Zweifel 1976) Biotite-muscovite-garnet gneiss (Ros 1980) Variably magnetic, basic to intermediate, calc-alkaline to alkaline metavolcanic rock, tuff (Witschard 1996) Metaandesite (Bergman et al. 2001) Shoshonitic metavolcanic rock (McGimpsey 2010)

[1] Protolith volcaniclastic terms based on White & Houghton (2006)

U-Pb SIMS zircon dating of a metavolcaniclastic rock (Nautanen deformation zone)

U-Pb SIMS zircon dating of a feldspar-phyric, intermediate (andesitic) metavolcaniclastic rock from the Nautanen deformation zone was performed to constrain the formational age of the meta-volcano-sedimentary sequence. The dated sample (ELH1500085C) was collected from a well-exposed road-cut section that forms part of a variably altered, roughly north-northwest-striking and steeply west-south-west-dipping metavolcaniclastic sequence (cf. Fig. 2).

An outline description of the dated sample and its associated zircon fraction is presented in Table 2. The results of U-Pb SIMS zircon dating are presented in Table 3 (along with an outline of the analytical method). Representative cathodoluminesance (CL) images of the dated zircons and U-Pb concordia and mean $^{207}Pb/^{206}Pb$ weighted age plots are shown in Figure 10.

In total, ten zircons were analysed, including three crystals with two spots each (i.e. core and rim), giving a total of 13 analyses (Table 3). All of the analyses are concordant or close to concordant, contain

Table 2: Brief description of the metavolcaniclastic rock used for U-Pb SIMS zircon dating

Sample	Setting	Brief sample description	Zircon characteristics
ELH150085C Sweref99 coordinates: E0755910 N7459501	Part of a metavolcaniclastic sequence *(Muorjevaara group)* within the Nautanen deformation zone (NDZ). The sample area represents a less deformed and altered zone than other parts of the NDZ (consistent with magnetic susceptibility data).	Medium grey, fine- to medium-grained (0.05–3 mm), feldspar-phyric, intermediate (andesitic) metavolcaniclastic rock. Displays weak pervasive sericite ± K-feldspar ± magnetite ± sulphide alteration. Local amphibole-magnetite and quartz veins also occur in the sample area.	Zircons are clear, mostly short (about 30–100 μm), colourless and rounded (subhedral to anhedral). Cores or overgrowths were not visible under binocular microscope observation. However, CL imaging shows distinct oscillatory zoning in most of the grains, with several containing cores or overgrowths (Fig. 10A).

Table 3. SIMS U-Pb-Th zircon data for the dated meta-andesite sample.

Spot #	U (ppm)	Th (ppm)	Pb (ppm)	Th/U calc*1	$^{238}U/^{206}Pb$	± 1σ (%)	$^{207}Pb/^{206}Pb$	± 1σ (%)	Disc. % conv.*2	$^{207}Pb/^{206}Pb$	± 2σ	$^{206}Pb/^{238}U$	± 2σ	$^{206}Pb/^{204}Pb$ measured	f_{206}%*3
Sample ELH150085C (meta-andesite, Nautanen area)															
n5397-01a	121.8	75.2	52.9	0.60	2.9595	1.21	0.114052	1.02	0.7	1864.9	36.6	1876.5	39.4	8 558	0.22
n5397-01b	93.8	52.6	41.2	0.59	2.9045	1.23	0.112785	1.36	3.9	1844.8	48.8	1907.3	40.8	8 781	0.21
n5397-02a	142.2	115.4	65.4	0.81	2.9326	1.19	0.115998	0.88	-0.2	1895.4	31.4	1891.5	39	21 997	{0.09}
n5397-02b	120.3	62.4	51.8	0.56	2.9592	1.18	0.113430	1.08	1.3	1855.1	38.8	1876.7	38.6	20 507	{0.09}
n5397-03	200.5	158.4	92.0	0.80	2.9324	1.08	0.115623	0.73	0.1	1889.6	26.0	1891.5	35.4	46 695	{0.04}
n5397-04	91.5	65.6	40.1	0.68	3.0037	1.28	0.115496	1.08	-2.1	1887.6	38.6	1852.6	41.2	15 722	{0.12}
n5397-05	191.9	156.5	88.3	0.83	2.9337	1.09	0.113559	0.78	2.1	1857.1	28.0	1890.8	35.8	12 960	0.14
n5397-06	70.7	39.2	30.5	0.55	2.9653	1.29	0.116561	1.21	-1.9	1904.1	43.4	1873.3	42.2	15 010	{0.12}
~~n5397-07~~	~~104.4~~	~~66.7~~	~~42.2~~	~~0.61~~	~~3.1822~~	~~1.19~~	~~0.108535~~	~~1.21~~	~~-0.9~~	~~1775.0~~	~~44.0~~	~~1761.6~~	~~36.8~~	~~5463~~	~~0.34~~
n5397-08	250.2	260.7	121.1	1.06	2.9089	1.05	0.113059	0.68	3.5	1849.2	24.4	1904.8	34.6	13 601	0.14
n5397-09	131.0	87.9	58.2	0.69	2.9478	1.19	0.113900	0.93	1.3	1862.5	33.4	1883.0	38.8	13 604	0.14
n5397-10a	159.2	129.1	73.7	0.83	2.9148	1.10	0.114464	0.86	1.9	1871.5	30.8	1901.5	36.4	11 157	0.17
n5397-10b	129.2	103.7	58.9	0.80	2.9434	1.18	0.114416	1.10	0.9	1870.7	39.2	1885.4	38.6	15 564	0.12

Isotope values are common Pb-corrected using modern common Pb composition (Stacey & Kramers 1975) and measured ^{204}Pb.
Data row with strikethrough text was not used in the concordia or mean weighted age determinations
*1 Th/U ratios calculated from $^{208}Pb/^{206}Pb$ and $^{207}Pb/^{206}Pb$ ratios, assuming a single stage of closed U-Th-Pb evolution
*2 Age discordance in conventional concordia space. Positive numbers are reverse discordant.
*3 Common Pb fraction. Figures in parentheses are given when no correction has been made, and indicate a value calculated assuming present-day Stacey-Kramers common Pb.

relatively low concentrations of U (approximately 71–250 ppm), and have Th/U ratios of 0.55–1.06. The spread in $^{207}Pb/^{206}Pb$ apparent ages for the 13 analyses (c. 1.90 to 1.78 Ga) and their corresponding standard deviations (2σ) are relatively large, probably due to low total Pb concentrations (approximately 31–121 ppm, Table 3). One concordant analysis (spot n5394-07, Fig. 10A, Table 3) has a distinctly younger $^{207}Pb/^{206}Pb$ apparent age of 1775 ± 44 Ma (2σ) and was not included in the final age determination. The remaining 12 analyses have $^{207}Pb/^{206}Pb$ ages that overlap at the 2σ-level (Fig. 10C).

U-Pb SIMS dating method: Zircons were obtained from a density separate of a crushed rock sample using a Wilfley water table. Magnetic minerals were removed using a hand magnet. Handpicked zircons

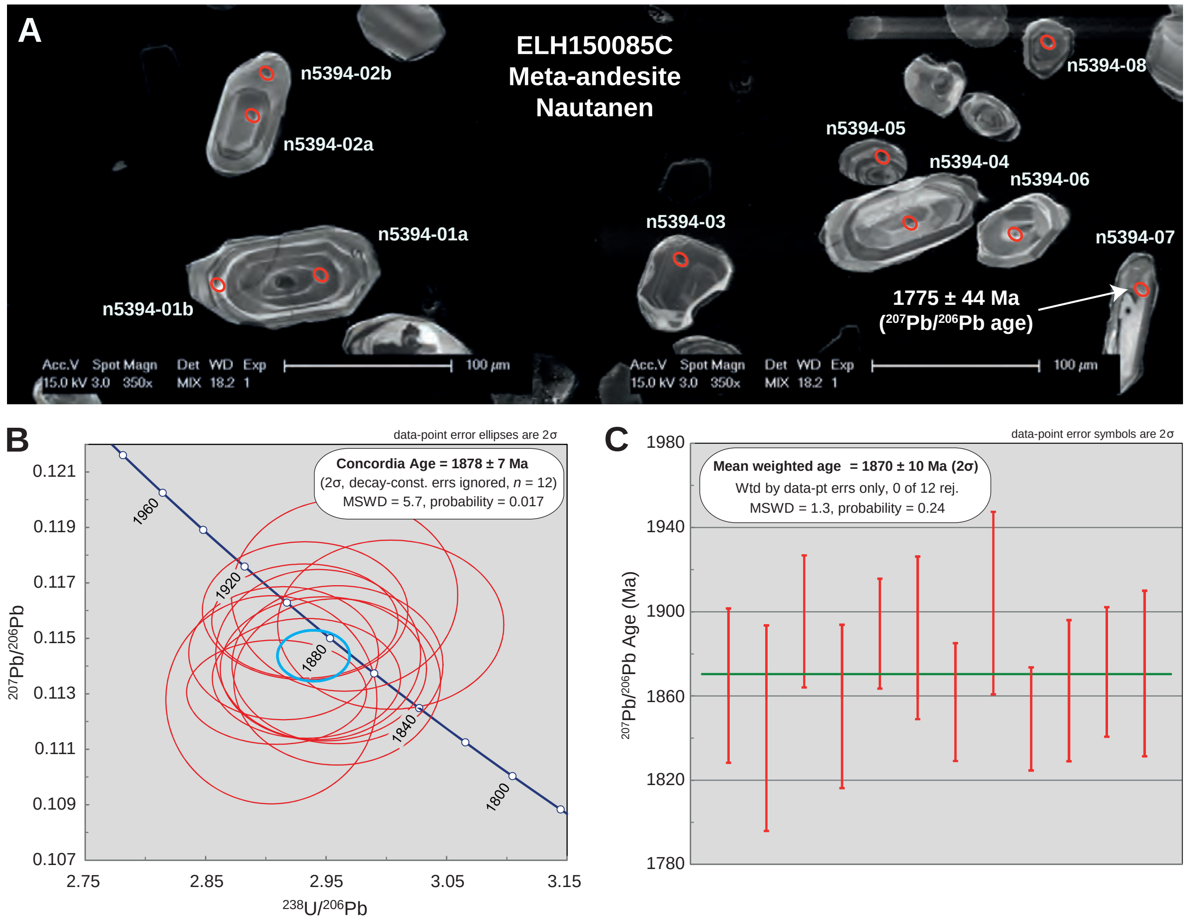

Figure 10. U-Pb SIMS zircon geochronology results for metavolcaniclastic rock sample ELH150085C (meta-andesite) from the Nautanen area (see Fig. 2). **A.** Cathodoluminescence images of representative zircons obtained from the sample. Red ovals and corresponding labels represent analytical dating spots. The zircon containing analytical spot n5394-07 yielded a significantly younger concordant ^{207}Pb/^{206}Pb age of 1775 ± 44 Ma (2σ), and was excluded from the final calculated age (Table 3). **B.** Tera-Wasserburg plot for the zircon population (n = 12). The blue oval represents the calculated concordia age of 1878 ± 7 Ma (2σ). **C.** Mean weighted ^{207}Pb/^{206}Pb age plot for the zircon population.

were mounted in transparent epoxy resin together with chips of reference zircon 91500. The zircon mounts were polished, gold coated and examined by cathodoluminescence imaging at the Swedish Museum of Natural History (NRM), Stockholm. High-spatial resolution secondary ion mass spectrometer (SIMS) analysis was carried out using a Cameca IMS 1280 at the Nordsim facility at the NRM. Detailed descriptions of the analytical procedures are given in Whitehouse et al. (1997, 1999), and Whitehouse & Kamber (2005). An approximately 6 nA O^{2-} primary ion beam was used, yielding spot sizes of approximately 15 µm. U/Pb ratios, elemental concentrations and Th/U ratios were calibrated relative to the zircon 91 500 reference, which has an age of c. 1 065 Ma (Wiedenbeck et al. 1995, 2004). Common Pb-corrected isotope values were calculated using modern common Pb composition (Stacey & Kramers 1975) and measured ^{204}Pb values in cases where the ^{204}Pb count rate was above the detection limit. U and Th decay constants follow the recommendations of Steiger & Jäger (1977). Diagrams and age calculations of isotopic data were made using Isoplot 4.15 software (Ludwig 2012). All age uncertainties are presented at the 2σ or 95% confidence level.

On a Tera-Wasserburg plot (Fig. 10B), 12 analyses plot as an overlapping concordant to near-concordant group, and yield a concordia age of 1 878 ± 7 Ma (2σ, n = 12, MSWD = 5.7, probability of concordance = 0.017). A degree of reverse discordance, where several points plot to the left of the concordia line, may account for the relatively high MSWD value. The corresponding mean weighted $^{207}Pb/^{206}Pb$ age of these 12 points is 1 870 ± 10 Ma (2σ, MSWD = 1.3, probability = 0.24; Fig. 10C). The U-Pb concordia age and the mean weighted age overlap at the 2σ-level and the former is chosen as the best estimate for the crystallisation age of the metavolcaniclastic sample (i.e. c. 1.88 Ga).

Several zircons display textural characteristics suggesting core-mantle overgrowth relationships, and have corresponding $^{207}Pb/^{206}Pb$ ages, indicating possible age heterogeneity (Fig. 10A, Table 3). For example, the core domain of zircon 2 (spot 02a) has a $^{207}Pb/^{206}Pb$ age of 1 895 ± 31 Ma (2σ), whereas the mantle domain (spot 02b) has an age of 1 855 ± 39 Ma (2σ). While both ages overlap at the 2σ-level, it is possible that the core is inherited (i.e. represents c. 1.90 Ga inherited material). The presence of older inherited material is further evidenced by a single analysis of the core domain of crystal 6 (spot 06), which yielded a $^{207}Pb/^{206}Pb$ age of 1 904 ± 43 Ma (2σ). For zircon 1 (Fig. 10A), which displays both oscillatory and core-overgrowth characteristics (e.g. curved zone boundaries in the latter case), the age difference between the inner and outer domains is smaller, with spot 01a (closer to the core) yielding a $^{207}Pb/^{206}Pb$ age of 1 865 ± 36 Ma (2σ), and spot 01b (outer mantle domain) giving 1 845 ± 48 Ma (1σ). While these ages again overlap at the 2σ-level, a real age difference between the central and peripheral parts of the crystal is possible, similar to that obtained for zircon 2.

The new U-Pb SIMS zircon age of 1 878 ± 7 Ma for the metavolcaniclastic unit from the Nautanen deformation zone constrains the timing of the Svecofennian intermediate (andesitic) volcanism that deposited the Muorjevaara group sequence and represents the first robust formational age for volcaniclastic- and epiclastic-type deposits in the broader Nautanen–Gällivare area. Additionally, given the general petrographic and lithogeochemical similarities across the meta-volcanosedimentary sequence from the Aitik area in the south to the northern part of the study area (see *Lithogeochemistry section* above; cf. Monro 1988), the new U-Pb date provides the most precise constraint on the age of metavolcaniclastic wall rocks hosting the Nautanen IOCG and Aitik Cu-Au-Ag deposits.

The U-Pb age of 1 878 ± 7 Ma for the Nautanen meta-andesite overlaps other ages determined for a variety of rock units in the Nautanen–Aitik and adjacent areas. The new date is identical to a U-Pb LA-ICP-MS zircon "minimum age" of 1 878 ± 7 Ma for a meta-andesite located approximately 100 km northwest of Gällivare, hosting the Fe-Cu ± Au system at Tjårrojåkka (Edfelt et al. 2006). The Nautanen meta-andesite age also overlaps new U-Pb SIMS zircon dates of 1 883 ± 4 Ma for the mafic-ultramafic Dundret complex (southwest of the study area), and 1 870 ± 4 Ma for a dioritic intrusion west of the Nautanen deposit (Fig. 2; Sarlus 2016). Moreover, the c. 1.88 Ga age overlaps c. 1.89–1.88 Ga igneous ages reported for dioritoid and granitoid intrusions in the Aitik area (Wanhainen et al. 2006, Sarlus 2016) and suggests that the dioritic bodies are the intrusive equivalent of the mainly intermediate meta-volcanosedimentary sequence (cf. Witschard 1996, Wanhainen et al. 2012). Additionally, the oldest sulphide mineralisation at Aitik, constrained at c. 1.88 Ga by Re-Os molybdenite dating, and inferred to relate to an initial "porphyry Cu" mineralisation event (Wanhainen et al. 2005, 2006), coincides with the c. 1.88 Ga phase of intermediate magmatism dated in this study.

Overall, the geochronology results reported here, combined with additional petrographic, geochemical and geochronological data, confirm a temporal and probable genetic link between Muorjevaara group metasupracrustal rocks and compositionally similar dioritic to granitic intrusions in the area, and highlight an important phase of syn-orogenic, mafic to intermediate magmatism at c. 1.88 Ga. Additionally, several zircon cores record $^{207}Pb/^{206}Pb$ ages from c. 1.90 to 1.89 Ga, suggesting inheritance of marginally older volcanic ± plutonic material not exposed at the present erosion level. These data partly affirm tentative U-Pb LA-ICP-MS ages of c. 1.90 Ga for the core domains of titanite crystals obtained from altered metavolcanic rocks hosting the Malmberget iron mine (Storey et al. 2007), which suggest those rocks are older than the Nautanen package investigated in this study (cf. Fig. 3). Combined, the older temporal signatures imply that a substrate of c. 1.90 to 1.89 Ga rocks may have been recycled during the c. 1.88 Ga tectonothermal event.

Intrusive rocks and their relationship to the Muorjevaara group

To the north, east and west of the Nautanen area, the Muorjevaara group is intruded by relatively abundant plutonic and hypabyssal rocks (Fig. 2). These consist of (1) generally foliated and locally folded, medium to coarse-grained, c. 1.88 to 1.87 Ga dioritic to granodioritic plutons (Fig. 11A & E–F); (2) c. 1.81 to 1.80 Ga gabbroic to doleritic and syenitic intrusions (Fig. 11H); and (3) voluminous, weakly deformed to massive, c. 1.79 to 1.78 Ga granitic intrusions (Fig. 11C & G, e.g. Witschard 1996, Sarlus 2016). The older c. 1.88 Ga dioritic intrusions were emplaced at approximately the same time as the c. 1.88 Ga mafic-ultramafic Dundret complex to the southwest (cf. Sarlus 2016). Thus, two broad episodes of bimodal plutonism at c. 1.88 Ga and c. 1.80 Ga are recognised in the general Gällivare area (see also Sarlus et al. 2017).

Locally exposed intrusive contacts in the Nautanen area provide rare field evidence of the temporal relationship between intrusive rocks and Muorjevaara group units, and help establish the number and sequence of intrusive events (Fig. 11). Dioritic and granitic bodies of varying size intrude the sequence, typically parallel to primary bedding and dominant foliations (i.e. sills), or as discordant veins or dykes with moderate to high angles relative to planar fabrics (Figs. 11B–D).

In the Eastern volcanosedimentary domain, fine- to medium-grained (approximately 0.5–3 mm), dioritic dykes and veins intrude metavolcaniclastic rocks with sharp contacts (Fig. 11B). These minor intrusions resemble larger-scale, medium- to coarse-grained (approximately 1–8 mm), diorite to quartz monzodiorite bodies in the area (e.g. c. 1.89 Ga Aitik stock), and contain similar textural and lithological features (e.g. mafic enclaves, Fig. 11A).

Granitic rocks also crosscut the meta-volcanosedimentary sequence with sharp, igneous contacts and typically intrude parallel to primary and overprinting structures (Fig. 11C–D). They occur as fairly abundant, approximately 1–15 m thick, medium- to coarse-grained (approximately 1–10 mm), granitic to locally pegmatitic, sills and minor, approximately 1–5-cm-thick, fine- to medium-grained (approximately 0.5–5 mm) aplite veins and segregations (Fig. 11C–D). Where present, granitic veins consistently crosscut dioritic bodies (Fig. 11A), and thus reflect the absolute ages of these intrusive suites in the general Gällivare area (cf. Sarlus 2016).

► Figure 11. Intrusive rocks and field relationships. **A.** View to the southwest of weak to moderately foliated monzodiorite (Haparanda suite) with mafic microgranular enclave (arrow). Crosscutting northwest-aligned aplite vein is seen near the top. **B.** Bedding view (to the northeast) of well-sorted, laminated, intermediate metavolcaniclastic rock cut by west-northwest-aligned, dioritic veins. Note elongate mafic enclaves in the veins (arrows), which are compositionally similar to the enclave shown in A. **C.** View to the north-northeast of contact (broken line) between reddish-pink, massive granite sill and biotite schist. **D.** Bedding view (to the southwest) of northwest-aligned, laminae-parallel, aplite veins crosscutting magnetite-bearing biotite schist. **E.** Intermediate, medium-grained dioritic rock predominantly comprising amphibole and plagioclase (Haparanda suite). **F.** Example of a moderately deformed (foliated), pale pink Lina-type granite. **G.** Undeformed, coarse-grained, Lina-type granite with distinct pinkish colour. **H.** Reddish-pink, K-feldspar-rich syenitic intrusion (possibly Perthite monzonite suite). Photographs A–D by Edward Lynch. Photographs E–H by Zmar Sarlus.

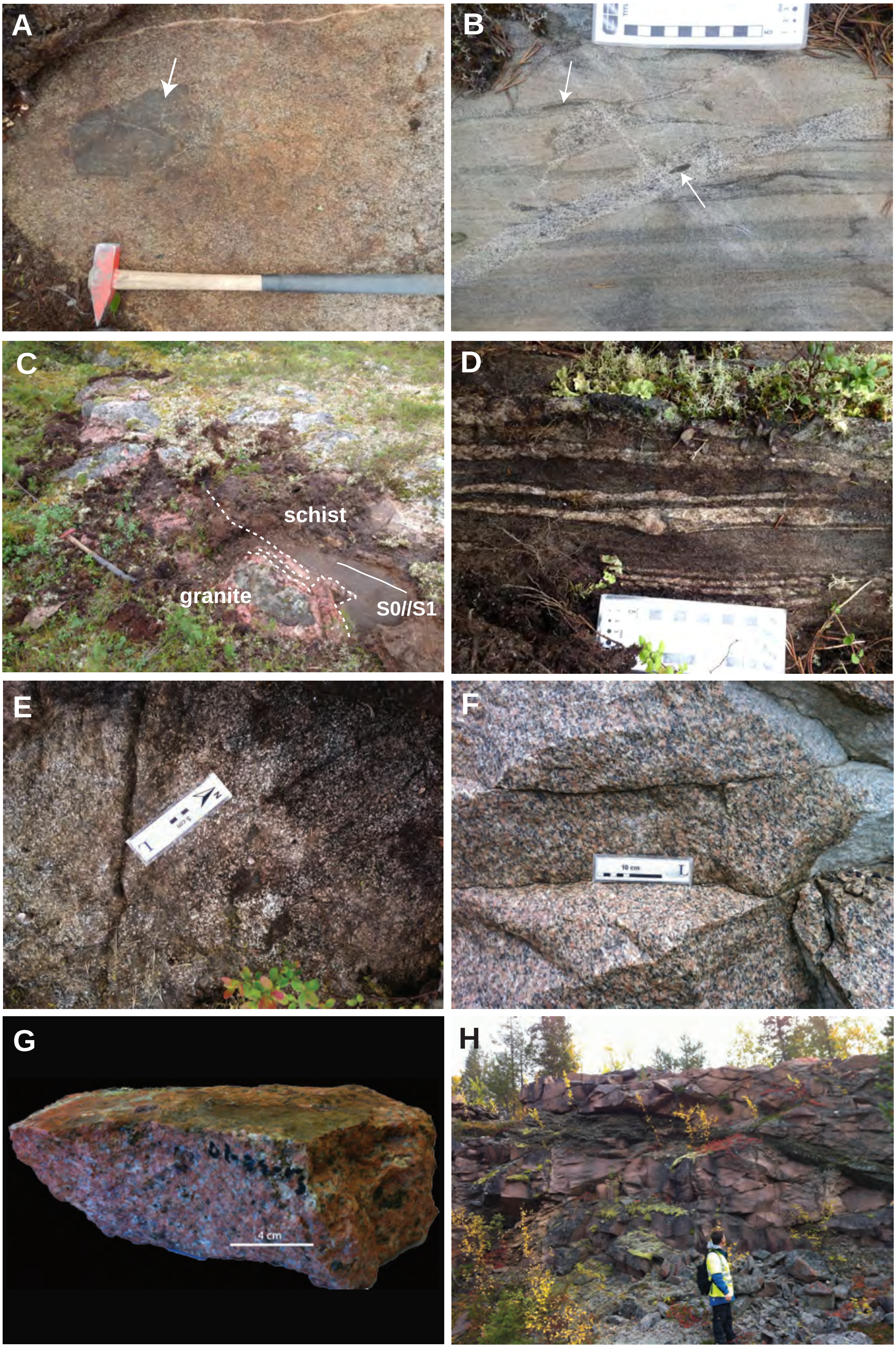
A
B
C
schist
granite
S0//S1
D
E
F
G
4 cm
H

STRUCTURAL GEOLOGY AND DEFORMATION

Structures in the eastern volcanosedimentary domain

The eastern volcanosedimentary domain (EVD) contains a variety of superimposed ductile and brittle structures recording a protracted, multiphase deformation history. The most commonly observed fabric is a variably intense, planar penetrative foliation, here designated S1 (Figs. 12A–B). This foliation is generally roughly northwest to north-northwest-aligned, moderate to steeply southwest to west-southwest-dipping, and tends to parallel primary bedding, laminae and compositional banding. S1 has a similar orientation to planar foliations in EVD-hosted dioritic intrusions. The intensity of S1 varies between outcrop and lithology, and where it forms a schistose to gneissic texture, S1 may represent a composite transposed foliation (cf. Fig. 5). Locally, S1 is axial planar to tight to isoclinal, asymmetric, intrafolial F1 folds (Fig. 12B).

The EVD is also characterised by tight to isoclinal folding of primary bedding, compositional banding, alteration banding and foliations. To the immediate east of the Nautanen deformation zone (i.e. southern EVD) the predominant structure is a distinct, large-scale, asymmetrical and overturned syncline (cf. Fig. 2). The western limb appears to be truncated roughly north-northwest-trending, shear zones and faults related to the Nautanen deformation zone. Fold vergence is typically eastward, with axial surfaces roughly north to north-northwest-aligned (sub-parallel to the Nautanen deformation zone) and generally dips steeply towards the west. The fold shapes are non-cylindrical and fold axes are locally curvilinear. The larger-scale fold structures are accompanied by parasitic, asymmetric small-scale folding. In the southern part of the EVD, parasitic fold axes commonly plunge at moderate angles towards the south-southwest, whereas in the north fold axes have doubly plunging geometries (typically roughly northwest and southeast). Mineral lineations are gently plunging and have varying orientations.

A discordant c. bedding plane-orthogonal crenulation cleavage, here designated S2, also occurs in the EVD (Fig. 10C–D). It is generally roughly north to north-northeast-aligned, sub-vertical and is axial planar to gentle, upright, moderate roughly south to south-southeast-plunging F2 folds (Fig. 10C). The S2 cleavage is associated with L2 intersection lineations that typically have a moderate plunge to the south and south-southeast, similar to F2 fold axes. Locally, near the hinge zones of larger-scale folds, fairly intense S2–L2 deformation has developed elongate and stretched L-tectonites, which form mullion-like features along bedding surfaces (Fig. 10E). In eastern limb areas local bedding plane surfaces with L2 lineations contain slicken-side notches, indicating top-block reverse movement towards the north and north-northwest (Fig. 10F).

Brittle deformation in the EVD consists of (1) locally developed spaced cleavage and fracture sets that tend to follow earlier planar structures; (2) numerous roughly north-northwest- and east-aligned, generally sub-vertical, amphibole and quartz vein sets, of which the latter are locally sulphide-bearing (e.g. Ferrum Cu-Au prospect); and (3) joint sets developed in intrusive rocks. Additionally, discordant roughly north to north-northeast-aligned brittle deformation zones are inferred from aeromagnetic data (cf. Fig. 2). These crosscutting, locally NDZ-related high-strain zones segment the EVD into several localised blocks (see below).

Structures in the Nautanen Deformation Zone

The Nautanen deformation zone (NDZ) is an important regional-scale, composite shear zone in northern Norrbotten and is the most prominent large-scale structural feature in the study area (e.g. Bergman et al. 2001). Here, it occurs as a somewhat dilational, approximately 300 m to 2 km wide high-strain deformation zone, characteristically delineated on aeromagnetic maps by planar, sub-parallel, roughly north-northwest-aligned magnetic anomalies (cf. Fig. 14).

Structurally, the NDZ is characterised by a conspicuous roughly north-northwest to northwest-

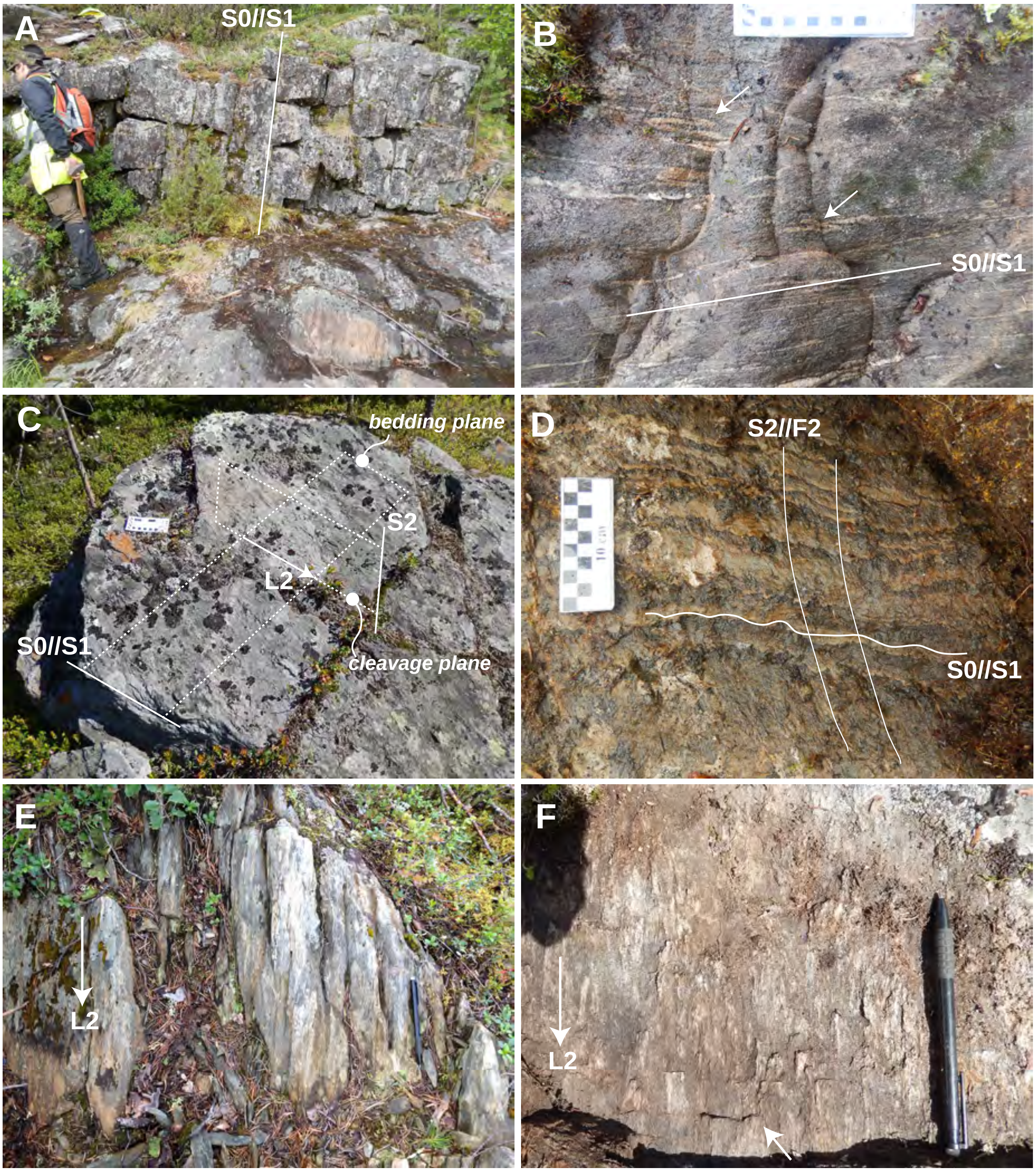

Figure 12. Examples of structures in the eastern volcanosedimentary domain. **A.** North-northeast view of steeply west-south-west-dipping, medium-bedded metavolcaniclastic rocks with bedding-parallel S1 foliation. Zmar Sarlus for scale. **B.** Side surface view (to the east-northeast) of laminated and compositionally banded mica schist with dominant bedding-parallel S1 foliation. Arrows indicate tight to isoclinal, recumbent, interfolial folding (F1) of feldspathic bands and veins. **C.** View to the northeast of mica schist showing bedding-cleavage relationship and related south-southeast-plunging L2 intersection lineations. **D.** Top surface view (to north-northeast) of compositionally banded metasedimentary rock, showing bedding-parallel S1 foliation affected by steep S2 cleavage, axial planar to gentle, upright, south-southeast-plunging F2 folds. **E.** Top surface view (to the north-northwest) of mica schist with stretched south-southeast-plunging L2 intersection lineation associated with mullion-like features. **F.** Bedding surface view (to the north) showing moderate, south to south-southeast-plunging L2 intersection lineations. Arrow marks slicken-side notches, which suggest top block movement towards the north. All photographs by Edward Lynch.

aligned, steep to locally moderate roughly west-dipping, penetrative foliation (S1), with varying but generally strong intensity (Fig. 13A–B). Locally, inferred primary bedding, compositional banding and alteration banding are typically transposed into steep orientations parallel to the dominant foliation, and locally produce a composite fabric that may represent several generations of ductile deformation. The dominant shearing direction strikes roughly north-northwest and shows mainly western-block up reverse kinematics and most commonly oblique dextral and less common sinistral components, recorded by asymmetric foliation deflections around garnet porphyroblasts and local asymmetric kink bands (Fig. 13C–E).

The predominant north-northwest-trending reverse shear zones within the NDZ are interconnected by roughly north-trending, sub-vertical high-strain zones with mainly dextral kinematics. In general, these secondary zones are interpreted as Riedel shears that formed in the oblique, dextral-reverse shear zone (Fig. 14). Additionally, local tensional features such as quartz-filled tension gashes and en-echelon quartz veins occur along the western margin of the NDZ, and are mainly orientated north to north-northeast.

Minor asymmetric folding related to shearing is mainly evident from asymmetrically folded hornblende-, magnetite- and epidote-filled veinlets (Fig. 13F). To the south of the study area, at the Aitik deposit (Fig. 14), the reverse shear zones are more N–S orientated and dip moderately towards the west, with distinct roughly west-plunging mineral lineations. Additionally, a set of sub-vertical, north-northeast-trending high-strain zones is observable. It has been suggested that it controls the distribution of gold in the Aitik deposit (Sammelin 2011).

Mineral lineations in the NDZ are defined by stretching of minerals, and their orientations are variable. In general, lineations plunge moderately towards the south and southwest. Local variations, with gentle to horizontal plunges, were also observed.

Structures in the western volcanosedimentary domain

The western volcanosedimentary domain (WVD) is characterised by alternating layers of metasedimentary and meta-volcanosedimentary rocks, with a distinct bedding (S0) and parallel foliation (S1) forming a composite S0-1 fabric. Both bedding and the S1 foliation are folded into inclined to overturned asymmetric folds, with open to close interlimb angles. The predominant large-scale structure in the WVD is a repetition of anticlines and synclines, with non-cylindrical, curvilinear fold axis (see Fig. 2). The overall orientation of fold axes is southward with gentle to moderate plunges. Fold axes in the northwest of the WVD appear to be doubly-plunging.

Typically, an axial planar parallel fabric is not observed across the WVD. Nevertheless, a weak foliation or weak-spaced cleavage, here designated S2, could be observed in several outcrops, especially in the vicinity of the NDZ. This S2 fabric clearly overprints the S0-1 foliation obliquely (Fig. 15A).

► Figure 13. Examples of structures in the Nautanen deformation zone domain. **A.** Top surface view (to the west-south-west) of dominant, steeply west-southwest-dipping, penetrative S1 schistosity affecting biotite-magnetite-altered metavolcaniclastic rocks. Arrow indicates altered and stretched clast replaced by biotite. **B.** Along-strike side view (to the south-southeast) showing localised high-strain shearing (broken lines) of altered schist. **C.** Top surface view (to the west) of garnet porphyroblast partly deflecting S1 fabrics in schist. Deflection pattern and garnet growth tails indicate possible dextral rotation. **D.** Top surface view (to the west-southwest) of elongate (stretched?) garnet porphyroblast (arrow) in biotite-magnetite-altered schist. **E.** View to the southwest of small-scale dextral kink bands (arrow) in mica schist. **F.** View to the south-southeast (along strike) of asymmetric folding of magnetite-filled veinlets in mica-amphibole schist. All photographs by Edward Lynch, except E and F by Tobias Bauer.


A
B
C
D
E
F
S1
5 cm
5 cm
N
5 cm
N

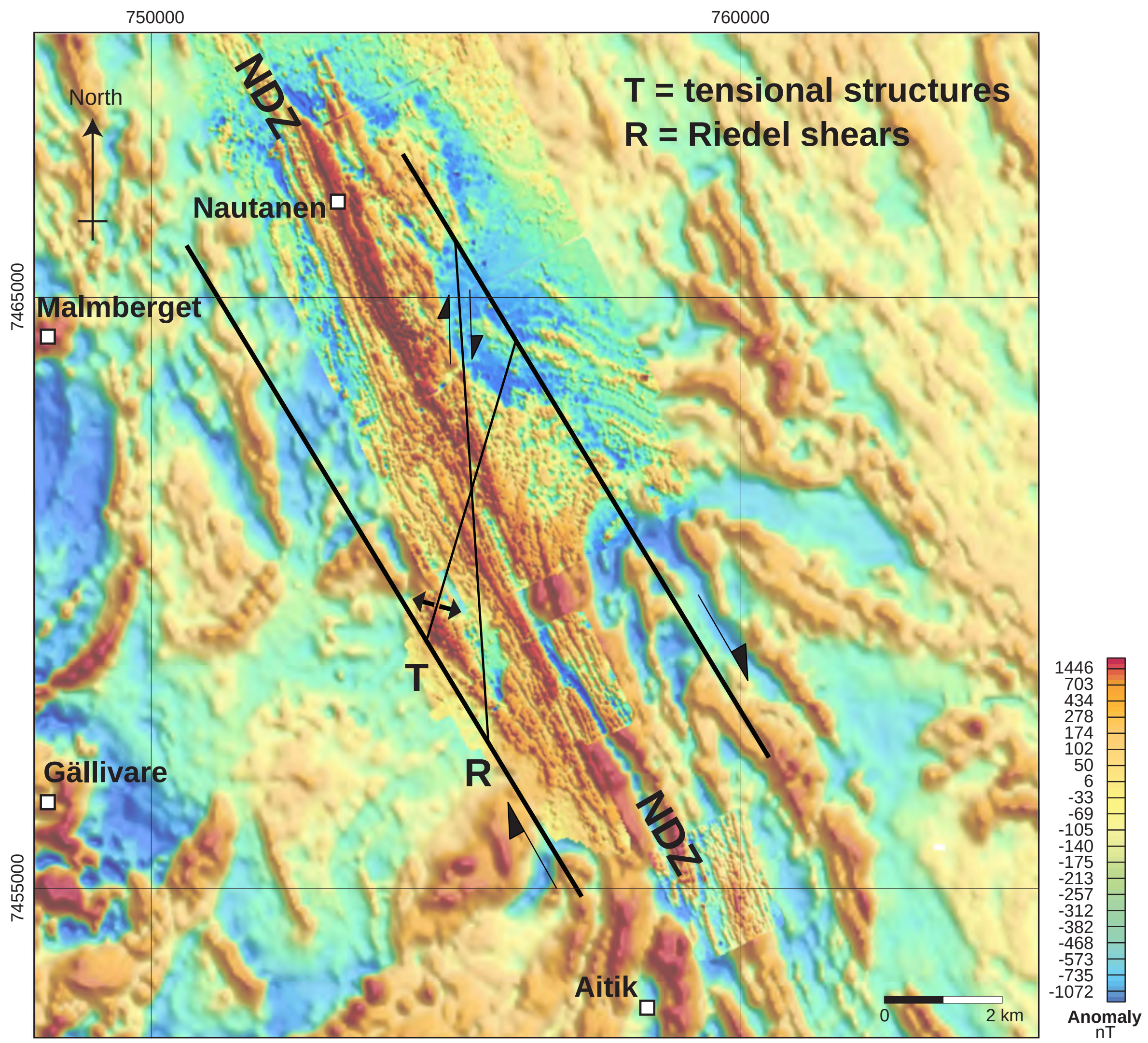

Figure 14. Conceptual model of primary, secondary and tertiary structures along the Nautanen deformation zone (NDZ). The background image is merged data from airborne and ground magnetic measurements.

Local crenulation lineations, small-scale fold axes and mineral-stretching lineations are orientated sub-parallel to the larger-scale fold axes (Fig. 15B–D).

Brittle deformation in the WVD is dominated by a large-scale, northwest-striking fault zone that divides the foliated and folded metavolcanic and metasedimentary rocks to the north from mainly undeformed granites to the south (Fig. 2). The fault zone is characterised by intense fracturing forming distinct topographic depressions.

Structures associated with intrusive rocks

Intrusive rocks in the area have varying strain intensities that reflect their relative ages and emplacement histories. A general penetrative foliation is seen in Haparanda-type dioritic to granodioritic intrusions (Fig. 16A). In the eastern domain, it is predominantly north-northwest to northwest-aligned, steeply southwest-dipping, and tends to follow the orientation of the predominant S1 foliations seen in the country rocks. Locally, dioritic dykes intruding metavolcaniclastic rocks display evidence of dextral-oblique emplacement associated with folding (e.g. Fig. 16B), while high-strain zones cutting

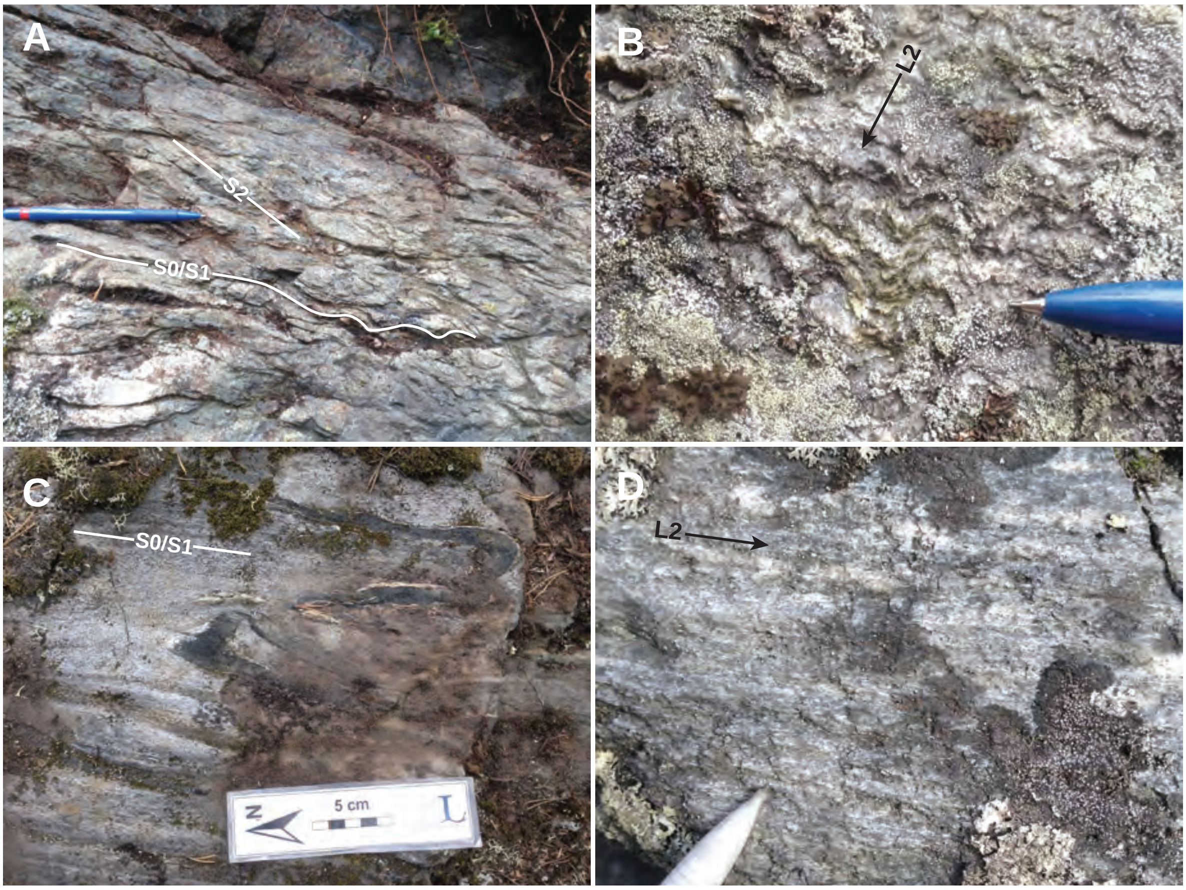

Figure 15. Examples of structures in the western volcanosedimentary domain. **A.** Mica schist, showing schistosity-cleavage relationship (S0-1 and S2, respectively). View to the east. **B.** Smale-scale folds, with L2 crenulation lineations parallel to axial planes. View to the east-northeast. **C.** View to the east of metavolcaniclastic rock and folded vein. **D.** View to the east of L2 intersection lineation in an intermediate metavolcaniclastic rock. All photographs by Tobias Bauer.

through the dioritic intrusions can cause a strong transposition of the penetrative foliation, suggesting local pre-shearing emplacement. Along the western margin of the Nautanen deformation zone, dioritic intrusions occur as narrow, elongate, north-northwest-aligned bodies that are orientated subparallel to, and deflected by, folding and Nautanen deformation zone-related shearing (cf. Fig. 2). Overall, the foliated character of the dioritic rocks, combined with their general orientation and intrusive patterns, suggests a probable syn-kinematic emplacement (cf. Witschard 1996).

Lina-type granitic rocks and subordinate aplite-pegmatite bodies typically occur as sheet-like intrusions, sills and veins intruding parallel to planar structures (cf. Fig. 11). A varying degree of strain is observable in these granitic rocks, ranging from penetratively foliated to non-foliated (cf. Fig. 11F–G). This suggests episodic emplacement of several generations of granitic rocks in the area and indicates that not all granitic intrusions may strictly belong to the Lina suite association (cf. Bergman et al. 2001).

Variably deformed granitic rocks are also known from the broader Gällivare area. For example, Wanhainen et al. (2005) report radiometric ages for both deformed and undeformed pegmatitic dykes occurring at the Aitik deposit, south of Nautanen. A deformed pegmatite dyke yielded an age of c. 1.85 Ga, while undeformed dykes have ages from c. 1.76 to 1.73 Ga. In addition, Bergman et al. (2002) obtained an age of c. 1.77 Ga from a weakly foliated, Lina granite roughly 30 km NW of the Nautanen area. These data, combined with observations presented here, support the contention that both syn- and post kinematic granite magmatism occurred in the general Gällivare area.

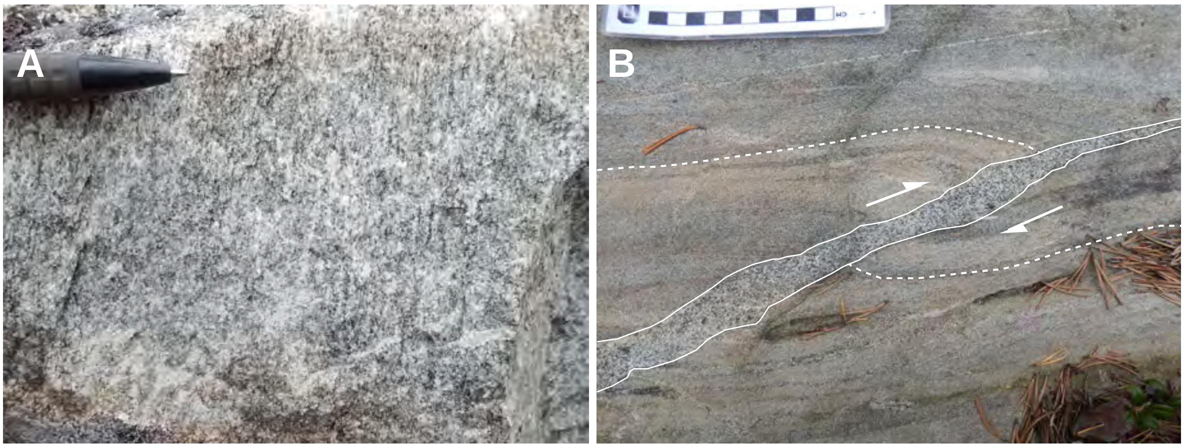

Figure 16. **A.** Sub-vertical surface view to the north-northwest of sub-vertical foliation in medium-grained, monzodioritic intrusion. **B.** Sub-horizontal surface view to the southwest of dioritic dyke crosscutting steeply south-southwest-dipping, thinly laminated, metavolcaniclastic rock. Laminae appear dextrally offset and associated with possible syn-emplacement drag fold (broken lines). All photographs by Edward Lynch.

Geophysical modelling of the Nautanen Deformation Zone

The study area was investigated in five separate airborne geophysical campaigns between the early 1960s and the mid-1990s, which resulted in the acquisition of magnetic, radiometric and electromagnetic data (slingram and VLF). Additionally, regional-scale ground gravity measurements have been conducted using approximately 1.5 km station spacing. Petrophysical sampling, ground magnetic and ground slingram measurements have also been made (cf. Lynch & Jönberger 2014).

From a magnetic anomaly perspective, the western volcanosedimentary domain (WVD) is relatively heterogeneous, with a banded pattern (Fig. 17). The low-magnetic parts of the area mainly consist of metasedimentary or felsic metavolcaniclastic rocks, while the high-magnetic bands are caused by mafic to intermediate metavolcaniclastic rocks. Mafic intrusive rocks also have relatively high magnetisation values (Table 4). On the gravity map a regional trend dipping towards the west indicates that granitic intrusions in this area have a deeper depth extent (Fig. 18).

The NDZ domain has been the target of both ground magnetic and ground slingram surveys in the past (cf. Lynch & Jönberger 2014). The magnetic anomaly map shows historical ground magnetic measurements overlaying airborne magnetic data, and displays a zone of tight, sub-parallel magnetic bands corresponding to the NDZ (Fig. 17). On the gravity map, the NDZ correlates with a broad positive gravity anomaly, implying that more mafic lithologies (higher density) underlie the NDZ than in surrounding areas (Fig. 18). The positive gravity anomaly extends eastwards from the central NDZ towards gabbroic rocks at Snålkok (cf. Fig. 2).

The eastern volcanosedimentary domain (EVD) mainly consists of intercalated metavolcanoclastic or metasedimentary rocks. Intrusive rocks in the area range from granite to gabbro. On the magnetic anomaly map the area resembles the pattern for the WVD, with high-magnetic bands alternating with areas with lower magnetic signatures. A synformal fold in the southern part of the EVD can also be observed on the magnetic anomaly map. The high-magnetic bands consist of mafic metavolcaniclastic rocks, whereas the lower magnetic areas are metasedimentary rocks. In the north of the EVD a granitic intrusion correlates well with a low gravity anomaly. Further south, the sequence of alternating metasedimentary and metavolcaniclastic rocks have roughly the same densities and give rise to a positive anomaly on the gravity map (Table 4). In the central and eastern part of the EVD, a homogenous low-magnetic area on the magnetic anomaly map corresponds to mafic intrusive rocks. Low-magnetic granite is seen as a gravity low in the far southeast of the EVD.

Three 3D models have been constructed of the NDZ by the inversion of gridded ground magnetic

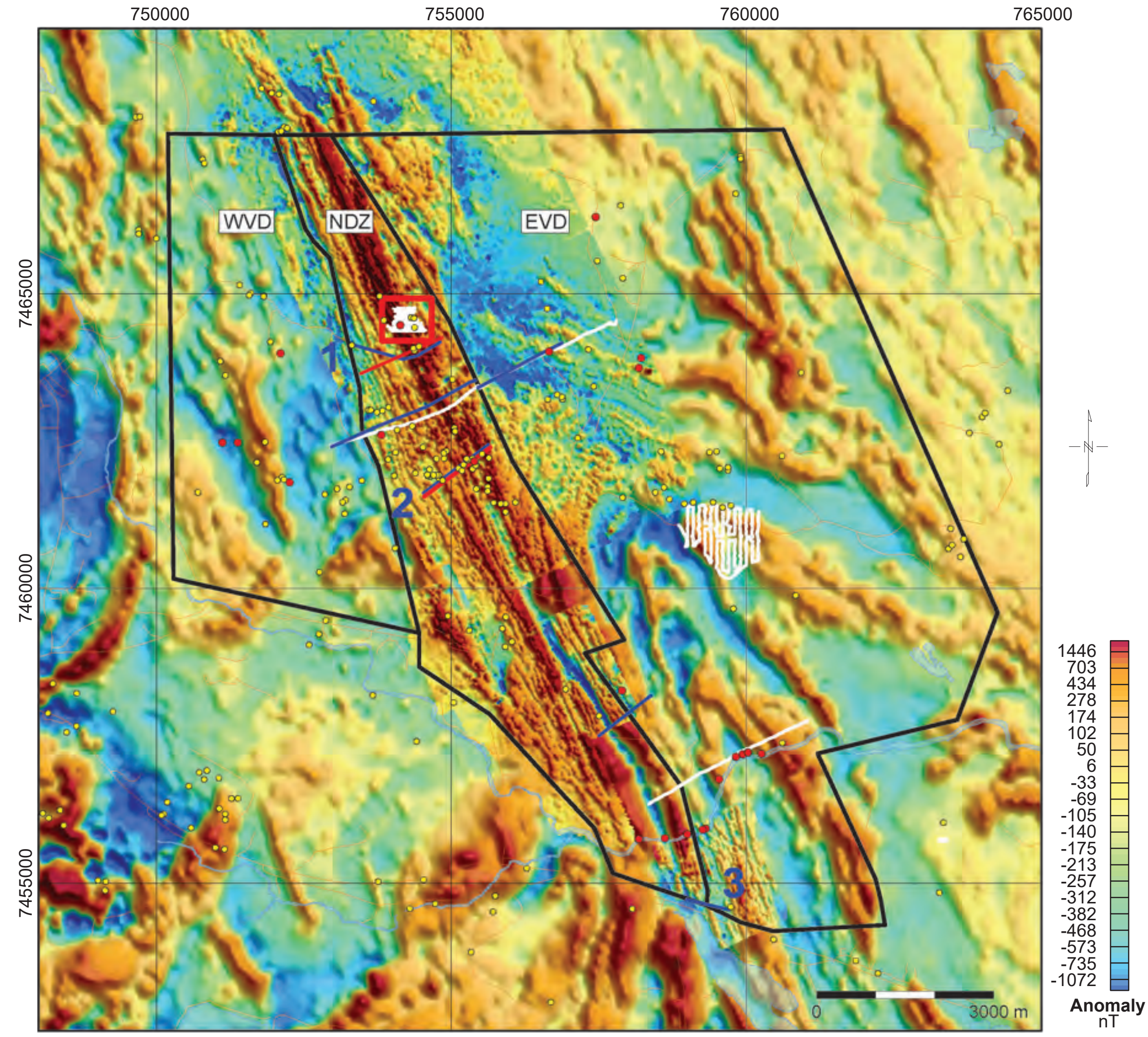

Figure 17. Magnetic anomaly map of the Nautanen area. Airborne data is overlain by ground magnetic data, acquired in previous surveys. The black polygons represent study area domains. The white and blue lines correspond to new ground magnetic and VLF measurements, respectively (this study). Petrophysical samples acquired earlier are shown as yellow dots, newer samples with red dots. The numbers "1–3" correspond to profiles discussed in the main text, and relate to Figs. 21–24. The red box surrounding the Nautanen Cu-Au deposit is presented in Figure 19. The red lines show the extent of extracted cross-sections from 3D VOXI models, shown in Figures 21 and 23.

data in the VOXI environment developed by Geosoft (Figs 20, 21 & 23). The aim of this modelling was to visualise highly magnetised structures in the sub-surface and their geometrical behaviour at shallow depth (down to approximately 200 m).

The most northerly 3D inversion model was made of the Nautanen Cu-Au deposit and surrounding area (red rectangle in Figs. 17 & 18). The input data to the model was newly acquired ground magnetic data along parallel profiles striking east-west that were collected with an individual spacing of 10 m (Fig. 19). Measurements of the magnetic field were recorded along these profiles approximately once a metre. The 3D model was confined to 300 m in an east-west direction and 400 m in a north-south direction (Fig. 19). The cell size of each volume pixel (voxel) in the model is 5 × 5 m horizontally, and a few metres vertically.

Before the data were inverted, the voxels were assigned minimum and maximum constraints for their permitted magnetic susceptibilities. Due to the occurrence of very high-magnetic bands in the area, constraints on susceptibility were set between 0 and 2 SI units. One cross-section (Fig. 20) has

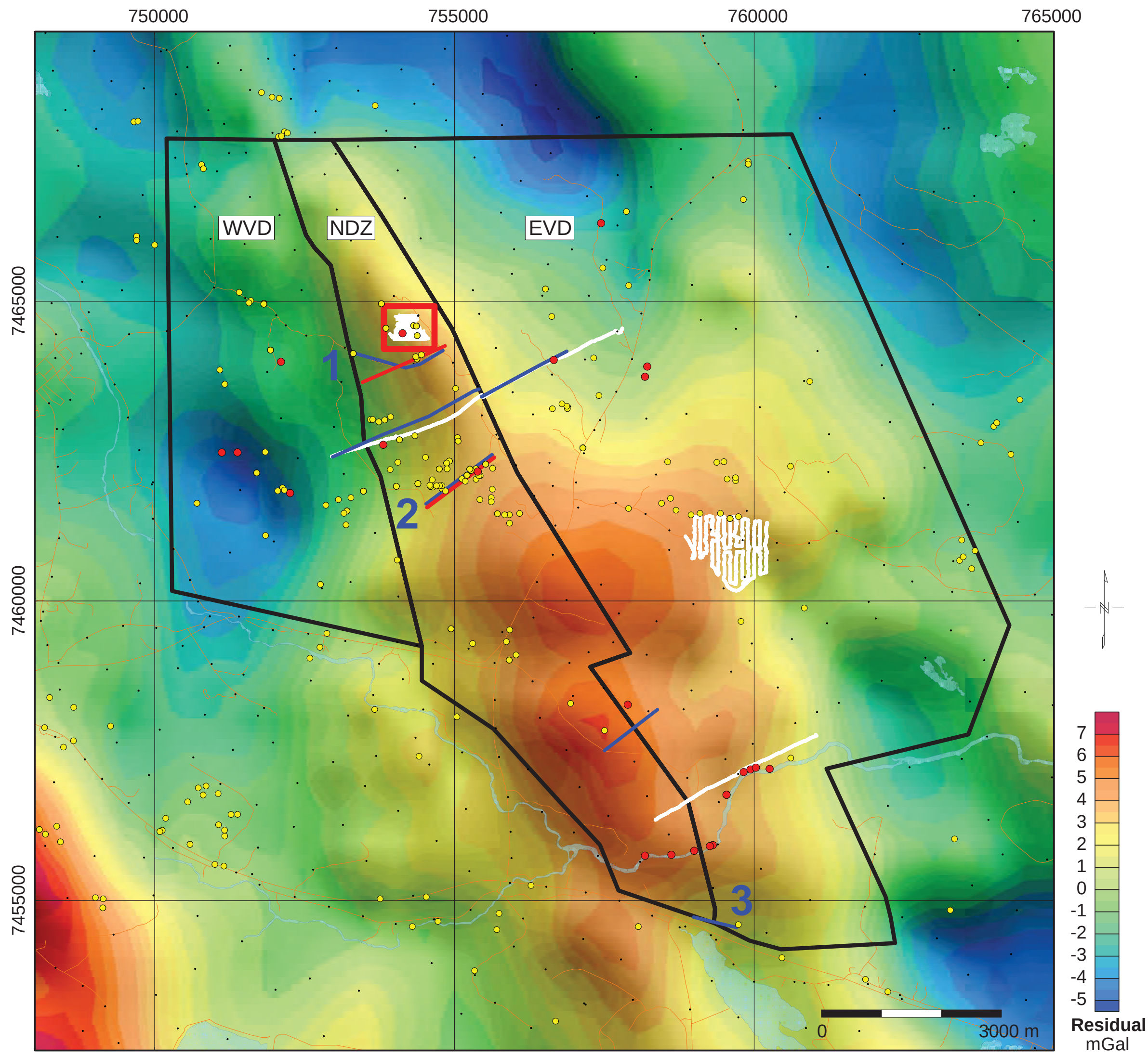

Figure 18. The residual gravity field in the Nautanen area. Black dots show the location of gravity measurements; black polygons represent study area domains. The white and blue lines represent new ground magnetic and VLF measurements, respectively (this study). The numbers "1–3" correspond to profiles discussed in the main text, and relate to Figs. 21–24. Earlier petrophysical samples are shown by yellow dots, newer samples by red dots. The red box surrounding the Nautanen deposit is presented in Figure 19; the red lines show the extent of the extracted cross-sections from 3D VOXI models shown in Figure 21 and Figure 23.

Table 4. The petrophysical properties of different rock types in the Nautanen area. The total number of petrophysical samples is 267.

Rock type	No. of samples	Density (SI) Mean	Density (SI) Std. dev.	Susceptibility x 10^{-5} (SI) min	Susceptibility x 10^{-5} (SI) max	Susceptibility x 10^{-5} (SI) median	Q-value min	Q-value max	Q-value median
Granite	13	2 612	17	0	3 691	1 544	0.00	0.87	0.07
Metasedimentary rock	16	2 836	98	18	67 510	784	0.00	89.53	0.16
Gabbro-diorite	22	2 903	50	27	19 781	70	0.00	6.81	0.01
Sandstone	24	2 768	74	12	18 660	1 850	0.00	8.37	0.45
Basalt-andesite	56	2 847	76	44	53 060	5 339	0.00	16.00	0.45
Mica schist	22	2 814	100	44	41 430	1 699	0.00	161.80	0.30
Rhyolite-dacite	18	2 708	34	21	10 933	1 801	0.01	1.76	0.26
Amphibolite	23	2 966	79	60	19 031	7 217	0.00	9.27	1.35
Greywacke	28	2 819	92	39	14 740	2 157	0.00	7.18	0.65
Granodiorite	5	2 714	53	21	3 169	1 975	0.00	1.56	0.16
Argillite	40	2 754	112	234	32 378	2 338	0.03	79.69	0.37

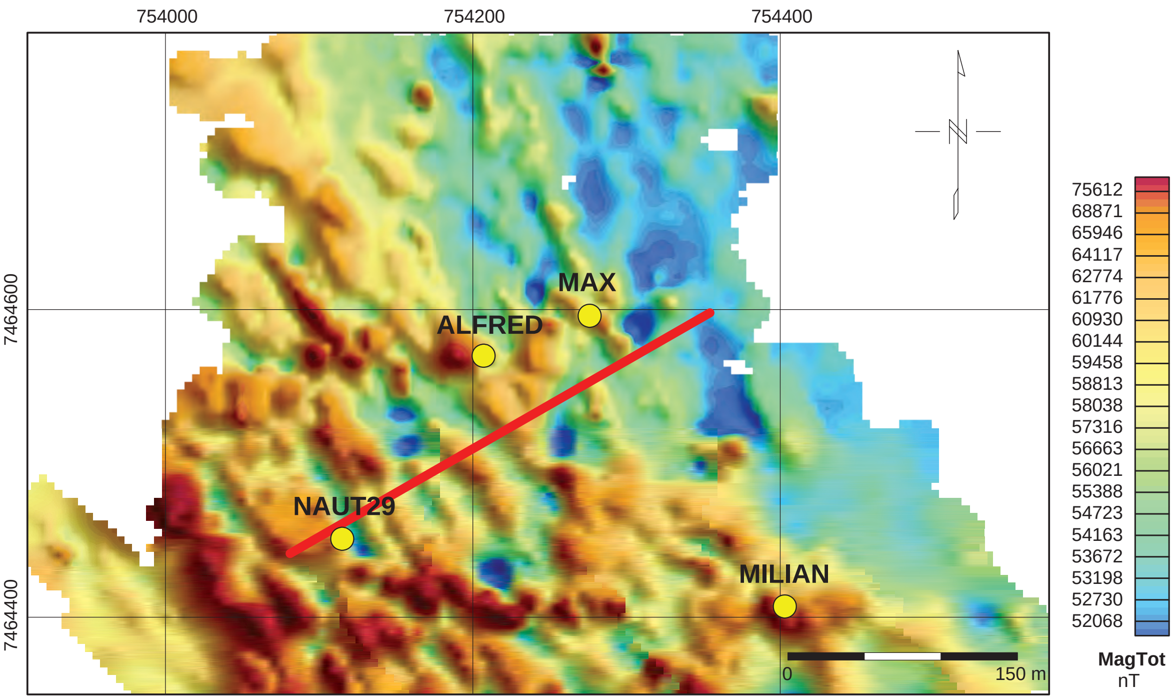

Figure 19. The total magnetic field in the area surrounding the ore deposit at Nautanen. The data is derived from ground magnetic measurements, acquired in 2014. The red profile corresponds to the cross-section from the 3D inversion shown in Figure 20.

been extracted from this 3D model, corresponding to the red profile line shown in Figure 19. The modelled cross-section shows an overturned, synformal geometry in the western part of the profile, with a southwestward-dipping axial plane, whereas the magnetic structures on the eastern side dip to the northeast (Fig. 20).

Two additional models have been made across the NDZ further south, based on ground magnetic and VLF data to visualise the geometry of the zone and interpret bedrock structures by integrating the results from both models into one comprehensive model (Figs. 21 & 22). These models correspond to the blue and red "profile 1" lines shown in Figures 17 and 18. Interpretation of resistivity cross-sections derived from VLF measurements (Figs. 22 & 24) is complicated by the fact that the measurements were made at a single frequency, and the final result is influenced by the direction of the transmitter, the signal-to-noise ratio, as well as conductors in the subsurface.

The northern part of the NDZ was the subject of ground magnetic measurements in 1977–1978. These measurements were conducted perpendicular to strike along closely spaced profiles. In general, the distance between these profiles was 80 m, but in some areas the profile spacing was reduced to 40 m. From these measurements, two 3D models have been made of shallow sub-surface conditions by inverting the gridded magnetic ground data. Results from these inversions are presented in Figure 21 and Figure 23, in which cross-sections perpendicular to the NDZ have been extracted from the 3D inversions to visualise the geometry of the magnetised sub-surface structures.

The cross-section in Figure 21 is derived from a 3D susceptibility model with an extent of 3 × 3 km. Each voxel corresponds to 25 × 25 m horizontally and 10 m vertically. 37 petrophysical samples in this area have a maximum magnetic susceptibility of 0.6 SI units. However, susceptibility is probably higher locally, so constraints on the voxels in the inversion model have been set between 0.0001 and 1 SI units.

In the cross-section shown in Figure 21 a magnetic structure in the southwest of the profile dips moderately to the southwest. A sudden break in the pattern occurs in the centre of the profile. East of this break, the highest magnetic area of the NDZ can be seen as a synformal pattern continuing towards

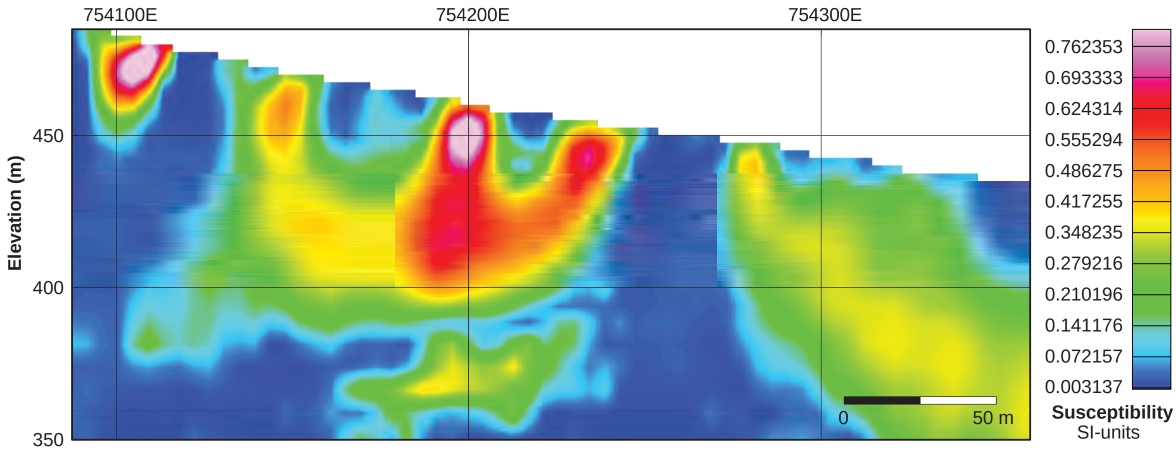

Figure 20. Susceptibility model of shallow sub-surface conditions along the cross-section shown in Figure 19. The section is derived from the 3D inversion based on ground magnetic measurements.

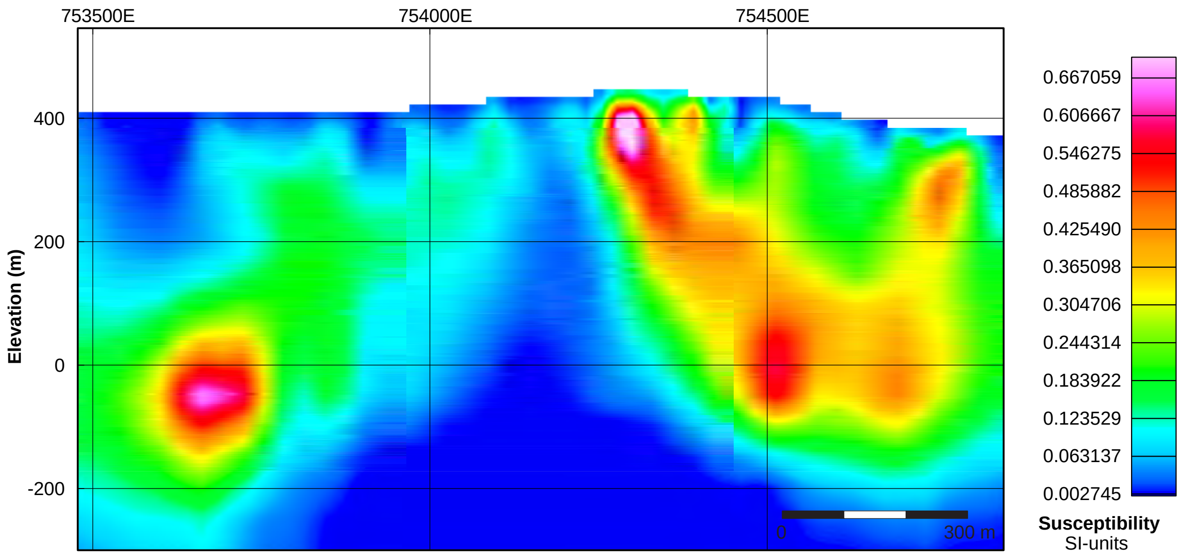

Figure 21. Cross-section from a 3D susceptibility inversion model based on gridded ground magnetic data. The lateral extent is the same as for Figure 22. Depth extent is 700 m below ground level.

the northeast. Minor magnetic structures extend up from this synformal structure towards the ground surface. These structures probably correspond to linear magnetite-rich zones.

A ground profile using a VLF instrument was carried out at roughly the same location with the aim of resolving more conductive zones in the bedrock (Fig. 22). The corresponding cross-section shows the resistivity properties of the sub-surface. Some features in the resistivity cross-section resemble those seen in the susceptibility model. For instance, more resistive west-dipping structures can be seen in the western part of the cross-section (Fig. 22). This could be a structure that has been thrust upwards from the southwest to the northeast. The structure is positioned just next to a more conductive feature, seen in the susceptibility model as a highly magnetic structure.

Another 3D susceptibility inversion model has been made of an area approximately 2 km southeast of the NDZ (Fig. 23). Its geographical extent is displayed in Figure 17 and Figure 18 as the red line marked “2”. The original model had an extent of 4 × 4 km; 116 petrophysical samples have been acquired from within that area. The maximum magnetic susceptibility value for these samples is 0.67 SI units.

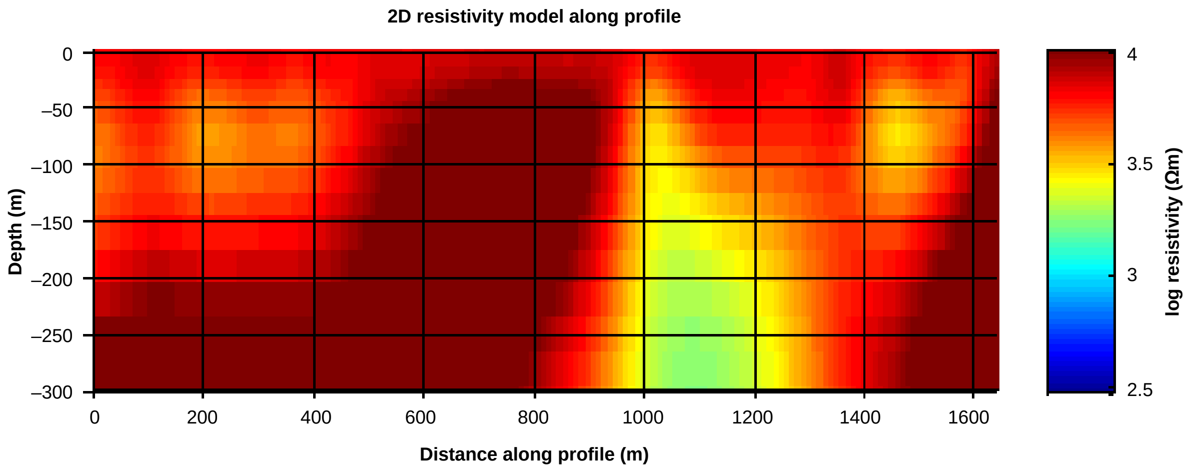

Figure 22. Inversion model based on VLF measurements along the profile labelled "1" in Figure 17 and Figure 18. It crosses the same lithological units as in Figure. 21. The model displays apparent resistivity in the ground at shallow depth.

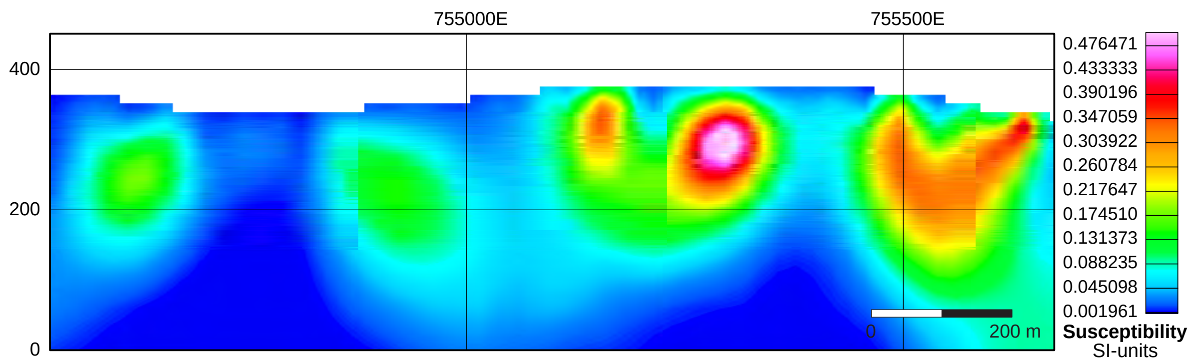

Figure 23. Cross-section derived from a 3D susceptibility inversion model based on gridded ground magnetic data. The lateral extent corresponds to profile "2" in Figure 17 and Figure 18. Depth extent is almost 400 m below ground level.

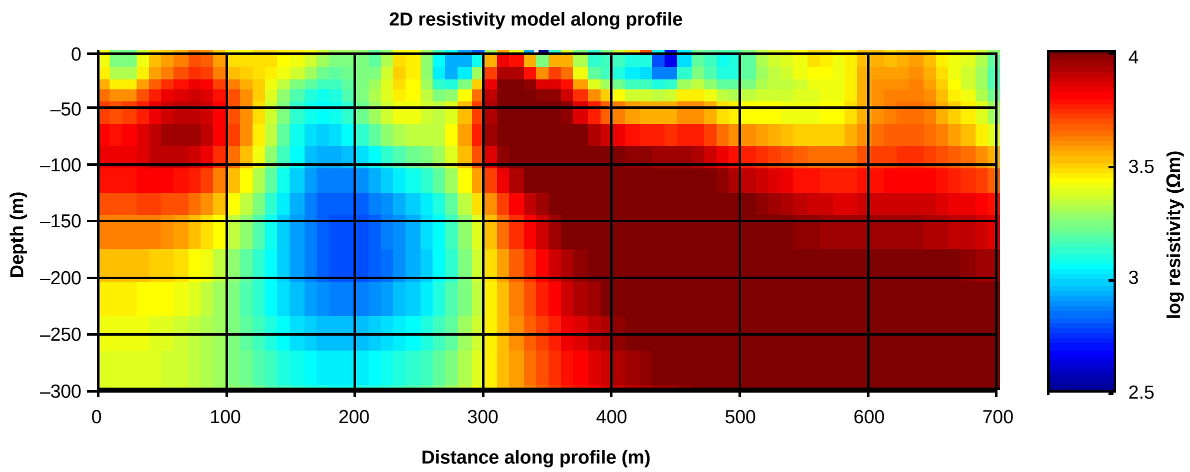

Figure 24. Resistivity cross-section derived by inverting VLF measurements along the profile labelled "3" in Figure 17 and Figure 18. The model displays apparent resistivity in the ground at shallow depth.

Thus, constraints on the voxels in the inversion model have been set between 0.0001 and 0.7 SI units. Due to the relatively small geographical extent of the model, each voxel has been given the size of 25 × 25 m laterally and approximately 10 m vertically at ground surface. In the eastern part of this cross-section, a magnetic anomaly with an inferred synformal shape occurs, resembling the anomaly structure seen in Figure 21.

The most southerly VLF profile was made a further 8 km to the S-SE along the NDZ (Fig. 24). The profile was made predominantly on the eastern side of the NDZ; its extent is marked with the blue profile line "3" in Figure 17 and Figure 18. A fairly broad conductive zone can be seen in the western part of this cross-section, corresponding to a low-magnetic area. In the east, a resistive feature with a relatively shallow south-eastward dip occurs (approximately 45°). This feature correlates to high-magnetic bands seen on the magnetic anomaly map (Figure. 17).

SUMMARY AND CONCLUSIONS

Bedrock and structural mapping, lithogeochemistry, U-Pb geochronology and geophysical modelling have been integrated to characterise a package of polydeformed and variably altered c. 1.88 Ga metavolcanosedimentary rocks in the Nautanen area of northern Norrbotten. The summary and conclusions from this work are:

(1) The investigated sequence, the Muorjevaara group, consists of calc-alkaline, basaltic andesitic to mainly andesitic metavolcaniclastic and volcanogenic (epiclastic) metasedimentary rocks. Lesser intercalated and interbedded pelite, mica schist and amphibolite units occur, and gradational and layered compositional and textural variation is relatively common throughout the sequence. Locally, granitic and dioritic rocks intrude the meta-volcanosedimentary sequence. Metasomatic-hydrothermal alteration (mainly potassic-ferroan ± calcic) variably affects the meta-volcanosedimentary sequence across the study area and is most intensely developed in high-strain shear zones.

(2) U-Pb SIMS zircon dating of a meta-andesite has yielded a relatively precise U-Pb concordia age of 1 878 ± 7 Ma (2σ). This date constrains the timing of syn-orogenic intermediate magmatism and provides the first absolute age for the metasupracrustal sequence hosting the Nautanen IOCG and Aitik Cu-Au-Ag deposits. The c. 1.88 Ga magmatic event coincides with regional, continental arc-related basic to intermediate magmatism occurring across northern Norrbotten. Such a setting is also supported by preliminary initial εNd values ranging from -4.5 to -0.3 reported by Lynch et al. (2018a) for Nautanen-Aitik supracrustal rocks.

(3) The Nautanen area contains a variety of superimposed ductile and brittle structures formed by at least two major deformation events. The predominant structures in the area are large-amplitude folds and the composite, north-northwest-striking Nautanen deformation zone (NDZ). Locally, the NDZ transects and truncates the western limbs of the large-amplitude, moderate to tight folds consistent with a phase of late-stage shearing (cf. Luth et al. 2016).

(4) Magnetic susceptibility and VLF resistivity modelling along the Nautanen deformation zone confirm the complex nature of this composite structure. Profile 1 indicates a relatively shallow dip of the lithologies in the west of the NDZ to the southwest. In the central part of the NDZ magnetic data indicates tight folding, forming synclinal structures. These features can be seen in all cross-sections derived from the 3D models in the north of the NDZ. Further south, VLF resistivity data indicate different geometries of the resistive layers in the eastern part of the NDZ.

ACKNOWLEDGEMENTS

We thank David Drejing-Carroll (Boliden) and Dave Collar for their encouragement of this study and for interesting discussions on the geology of the Nautanen–Aitik area. Martin Whitehouse, Lev Ilyinsky and Kerstin Lindén at Nordsim (Stockholm) are gratefully acknowledged for their analytical support during SIMS analysis. Nikolaos Arvanitidis (SGU) is thanked for reviewing the manuscript.

REFERENCES

Bark, G., Wanhainen, C. & Pålsson, B.I., 2013: Textural setting of gold and its implications on mineral processing: preliminary results from three gold deposits in northern Sweden. *Proceedings of the 12th SGA Biennial Meeting, Uppsala 1*, 302–305.

Barton, M.D., 2014: Iron oxide (-Cu-Au-REE-P-Ag-U-Co) systems. *In:* H. Holland & K. Turekian (eds.): *Treatise on Geochemistry*. Elsevier, 2nd edition, volume 13, 515–541.

Barrett, T.J. & MacLean, W.H., 1999: Volcanic sequences, lithogeochemistry, and hydrothermal alteration in some bimodal volcanic-associated massive sulfide systems. *In:* C.T. Barrie & M.D. Hannington (eds.): Volcanic-associated massive sulfide deposits: processes and examples in modern and ancient environments. *Reviews in Economic Geology 8*, 101–131.

Bergman, S., Kübler, L. & Martinsson, O., 2001: Description of regional geological and geophysical maps of northern Norbotten County. *Sveriges geologiska undersökning Ba 56*, 110 pp.

Bergman, S., Persson P.-O. & Kübler, L., 2002: U-Pb titanite and zircon ages of the Lina granite at the type locality NW of Gällivare, northern Sweden. *Sveriges geologiska undersökning C 834,* 12–17.

Bergman, S., Billström, K., Persson, P.-O., Skiöld, T. & Evins, P., 2006: U-Pb age evidence for repeated Palaeoproterozoic metamorphism and deformation near the Pajala shear zone in the northern Fennoscandian shield. *GFF 128*, 7–20.

Bergman, S., Stephens, M.B., Andersson, J., Kathol, B. & Bergman, T., 2012: Sveriges berggrund. 1:1 miljon. *Sveriges geologiska undersökning K 423*.

Carlon, C.J., 2000: Iron oxide systems and base metal mineralisation in northern Sweden. *In:* T.M. Porter (ed.): *Hydrothermal iron oxide copper–gold and related deposits: a global perspective*. Australian Mining Foundation, Glenside, Australia, 283–296.

Corfu, F., Anderssen, T.B. & Gasser, D., 2014: The Scandinavian Caledonides: main features, conceptual advances and critical questions. *In:* F. Corfu, D. Gasser & D.M. Chew (eds.) *New perspectives on the Caledonides of Scandinavia and related areas. Geological Society, London, Special Publication 390*, 9–43.

Danielsson, S., 1985: Nautanen. Borrhålsprotokoll och analysintyg från 1985-års arbeten. *Sveriges geologiska undersökning Prap 85090*, 241 pp.

Drejing-Carroll, D, Bauer, T., Karlsson, P., Coller, D., Nordin, R., Hitzman, M. & Allen, R., 2015: New Insight into the links between major porphyry copper, IOCG, and magnetite-apatite deposits from the Gällivare area, Northern Sweden. Society of Economic Geologists, Annual Conference 2015, Hobart, Tasmania. Program and abstracts.

Edfelt, Å., Sandrin, A., Evins, P., Jeffries, T., Storey, C., Elming, S.A. & Martinsson, O., 2006: Stratigraphy and tectonic setting of the host rocks to the Tjårrojåkka Fe-oxide Cu–Au deposits, Kiruna area, northern Sweden. *GFF 128*, 221–232.

Geijer, P., 1918: Nautanenområdet. En malmgeologisk undersökning. *Sveriges geologiska undersökning C 283*, 103 pp.

Grooves, D.I., Bierlein, F.P., Meinert, L.D. & Hitzman, M.W., 2010: Iron oxide copper-gold (IOCG) deposits through Earth history: Implications for origin, lithospheric setting, and distinction from other epigenetic iron oxide deposits. *Economic Geology 105*, 641–654.

Gustafsson, B., 1985: Fältarbeten 1984 inom delprojektområde Gällivare J Gällivare SV och SO. Slutrapport. *Sveriges geologiska undersökning Prap 85005*, 125 pp.

Gustafsson, B., 1986: Projekt 5515 Malmberget. Prospekteringsarbeten 1985. Rekommendationer för 1986. Lägesrapport 1986-01-15. *Sveriges geologiska undersökning Prap 86004*, 220 pp.

Gustafsson, B. & Johansson, L., 1984: Ferrum kopparfyndighet geofysik och geologi 1984. *Sveriges geologiska undersökning Prap 84158*, 18 pp.

Hanski, E.J., 2012: Evolution of the Palaeoproterozoic (2.50–1.95) non-orogenic magmatism in the eastern part of the Fennoscandian Shield. *In:* V.A. Melezhik, A.R. Prave, E.J. Hanski, A.E. Fallick, A. Lepland, L.R. Kump & H. Strauss (eds.): *Reading the archive of Earth's oxygenation*, Volume 1, Springer, Berlin, 179–245.

Hanski, E.J. & Huhma, H., 2005: Central Lapland greenstone belt. *In:* R. Lehtinen, P.A. Nurmi, O.T. Rämö (eds.) *Precambrian Geology of Finland – key to the evolution of the Fennoscandian Shield*. Elsevier, Amsterdam, 139–194.

Korja, A., Lahtinen, R. & Nironen, M., 2006: The Svecofennian orogen: a collage of microcontinents and island arcs. *In:* D.G. Gee & R.A. Stephenson (eds.): European lithosphere dynamics. *Geological Society, London, Memoirs 32*, 561–578.

Lahtinen, R., Korja, A. & Nironen, M., 2005: Paleoproterozoic tectonic evolution. *In:* M. Lehtinen, P.A. Nurmi & O.T. Rämö (eds.): *Precambrian geology of Finland – key to the evolution of the Fennoscandian Shield*. Elsevier, Amsterdam, 481–532.

Lahtinen, R., Garde, A.A. & Melezhik, V.A., 2008: Paleoproterozoic evolution of Fennoscandia and Greenland. *Episodes 31*, 1–9.

Lahtinen, R., Korja, A., Nironen, M. & Heikkinen, P., 2009: Paleoproterozoic accretionary processes in Fennoscandia. *Geological Society, London, Special Publications 318*, 237–259.

Lauri, L.S., Hellström, F., Bergman, S., Huhma, H. & Lepistö, S., 2016. New insights into the geological evolution of the Archean Norrbotten province, Fennoscandian Shield. *Bulletin of the Geological Society of Finland Special Volume 1*, p. 151.

Le Maitre, R.W., 1976: The chemical variability of some common igneous rocks. *Journal of Petrology 17*, 589–637.

Ludwig, K.R., 2012: User's manual for Isoplot 3.75. A geochronological toolkit for Microsoft Excel. *Berkeley Geochronology Center Special Publication No. 5,* 75 pp.

Lund, C., 2009. *Mineralogical, chemical and textural properties of the Malmberget iron deposit. A process mineralogically characterisation.* M.Sc. thesis, Luleå University of Technology, Luleå, Sweden, 98 p.

Luth, S., Jönsson C. & Jönberger J., 2015: Integrated geological and geophysical field studies in the Liviöjärvi key area, Pajala region. *Sveriges geologiska undersökning report 2015:12*, 29 pp.

Luth, S., Jönsson C., Hellström, F., Jönberger J., Djuly, T., van Assema, B. & Smoor, W., 2016: Structural and geochronological studies on the crustal-scale Pajala deformation zone, northern Sweden. *Bulletin of the Geological Society of Finland Special Volume 1*, p. 263.

Lynch, E.P. & Jönberger, J., 2014: Summary report on available geological, geochemical and geophysical information for the Nautanen key area, Norrbotten. *Sveriges geologiska undersökning report 2014:34,* 40 pp.

Lynch, E.P., Jönberger, J., Bauer, T.E., Sarlus, Z. & Martinsson, O., 2015: Meta-volcanosedimentary rocks in the Nautanen area, Norrbotten: Preliminary lithological and deformation characteristics. *Sveriges geologiska undersökning report 2015:30,* 51 pp.

Lynch, E.P., Bauer, T.E., Huhma, H., Drejling-Caroll, D., 2018a: Petrogenesis of c. 1.9 Ga meta-volcanosedimentary rocks in the Nautanen-Aitik area, northern Sweden: Geological, lithogeochemical and Sm-Nd isotopic constraints. Proceedings of the 33rd Nordic Geological Winter Meeting, Copenhagen. Program and abstracts.

Lynch, E.P., Hellström, F.A., Huhma, H., Jönberger, J., Persson, P-O. & Morris, G., 2018b: Geology, lithostratigraphy and petrogenesis of c. 2.14 Ga greenstone successions in the Nunasvaara and Masugnsbyn areas, northernmost Sweden. *In:* Bergman, S. (ed): Geology of the Northern Norrbotten ore province, northern Sweden. *Rapporter och Meddelanden 141,* Sveriges geologiska undersökning. This volume pp 19–77.

Martinsson, O., 1995: Greenstone and porphyry hosted ore deposits in northern Norrbotten. *PIM/NUTEK report #3*, 58 pp.

Martinsson, O., 1997. *Tectonic Setting and Metallogeny of the Kiruna Greenstones*. Ph.D. thesis, Luleå University of Technology, Luleå, Sweden.

Martinsson, O., 2004: Geology and metallogeny of the northern Norrbotten Fe–Cu–Au province. *In:* R.L. Allen, O. Martinsson & P. Weihed (eds.): Svecofennian ore-forming environments of northern Sweden – volcanic-associated Zn-Cu-Au-Ag, intrusion-associated Cu-Au, sediment-hosted Pb-Zn, and magnetite-apatite deposits in northern Sweden. *Society of Economic Geologists, guidebook series 33*, 131–148.

Martinsson, O. & Wanhainen, C., 2004: Character of Cu-Au mineralisation and related hydrothermal alteration along the Nautanen deformation zone, Gällivare area, northern Sweden. *In:* R.L. Allen, O. Martinsson & P. Weihed (eds.): Svecofennian ore-forming environments of northern Sweden – volcanic-associated Zn-Cu-Au-Ag, intrusion-associated Cu-Au, sediment-hosted Pb-Zn, and magnetite-apatite deposits in northern Sweden. *Society of Economic Geologists, guidebook series 33*, 149–160.

Martinsson, O. & Wanhainen, C., 2013: Fe oxide and Cu-Au deposits in the northern Norrbotten ore district. *Society of Geology Applied to Mineral Deposits (SGA) excursion guidebook SWE5*, 74 pp.

Martinsson, O., Vaasjoki, M., Persson, P.-O., 1999: U-Pb zircon ages of Archaean to Palaeoproterozoic granitoids in the Torneträsk-Råstojaure area, northern Sweden. *Sveriges geologiska undersökning C831,* 70–90.

Martinsson, O., Billström, K., Broman C., Weihed, P. & Wanhainen C., 2016: Metallogeny of the Northern Norrbotten ore province, northern Fennoscandian Shield with emphasis on IOCG and apatite-iron ore deposits. *Ore Geology Reviews 78*, 447–492.

McGimpsey, I., 2010: *Petrology and lithogeochemistry of the host rocks to the Nautanen Cu-Au deposit, Gällivare area, northern Sweden*. M.Sc. thesis, Lund University, Lund, Sweden, 82 pp.

McPhie, J., Doyle, M. & Allen, R., 1993: *Volcanic textures: A guide to the interpretation of volcanic textures in volcanic rocks*. CODES Key Centre, University of Tasmania, 198 pp.

Melezhik, V.A. & Fallick, A.E., 2010: On the Lomagundi-Jatuli carbon isotopic event: The evidence from the Kalix Greenstone Belt, Sweden. *Precambrian Research 179*, 165–190.

Melezhik, V.A. & Hanski, E.J., 2012: The early Paleoproterozoic of Fennoscandia: Geological and tectonic settings. *In:* V.A. Melezhik, A.R. Prave, E.J. Hanski, A.E. Fallick, A. Lepland, L.R. Kump & H. Strauss (eds.): *Reading the archive of Earth's oxygenation*, Volume 1, Springer, Berlin. 33–38.

Melezhik, V.A., Kump, L.R., Hanski, E.J., Fallick, A.E. & Prave, A.R., 2012. Tectonic evolution and major global Earth-surface palaeoenvironmental events in the Palaeoproterozoic. *In:* V.A. Melezhik, A.R. Prave, E.J. Hanski, A.E. Fallick, A. Lepland, L.R. Kump & H. Strauss (eds.): *Reading the archive of Earth's oxygenation*, Volume 1, Springer, Berlin, 3–21.

Mellqvist, C., Öhlander, B., Skiöld, T. & Wickström, A., 1999: The Archean-Proterozoic paleoboundary in the Luleå area, northern Sweden: field and isotope geochemical evidence for a sharp terrane boundary. *Precambrian Research 96*, 225–243.

Monro, D., 1988: *The geology and genesis of the Aitik Cu-Au deposit, arctic Sweden*. Ph.D. thesis, University College Cardiff, UK, 386 pp.

New Boliden, 2016. *Nautanen copper-mineralization in northern Sweden*. Company press release, 05-02-2016. <www.boliden.com>

Nironen, M., 1997: The Svecofennian orogen: a tectonic model. *Precambrian Research 86*, 21–44.

Öhlander, B., Skiöld, T., Hamilton, P.J. & Claesson, L.-Å., 1987: The western border of the Archaean province of the Baltic Shield evidence from northern Sweden. *Contributions to Mineralogy & Petrology 95*, 437–450.

Perdahl, J.A., 1995: *Svecofennian volcanism in northernmost Sweden*. Ph.D. thesis, Luleå University of Technology, Luleå, Sweden.

Pitkänen, T., 1997: *Anisotropy of magnetic susceptibility of mylonites from the Kolkonjoki and Nautanen deformation zones in Norrbotten, Sweden*. M.Sc. thesis, Luleå University of Technology, Luleå, Sweden, 64 pp.

Reddy, S.M. & Evans, D.A.D., 2009: Palaeoproterozoic supercontinents and global evolution: correlations from core to atmosphere. *In:* S.M. Reddy, R. Mazumdr, D.A.D. Evans, A.S. Collins (eds): *Paleoproterozoic supercontinents and global evolution. Geological Society, London, Special Publication 323*, 1–26.

Ros, F., 1980: Nautanenområdet. Rapport över SGU:s arbeten utförda under 1966–1979. *Sveriges geologiska undersökning Brap 81530*, 33 pp.

Sammelin, M., 2011. *The Nature of Gold in the Aitik Cu-Au Deposit. Implications for Mineral Processing and Mine Planning.* Licentiate thesis, Luleå University of Technology, Luleå, Sweden, 67 pp.

Sarlus, Z., 2013: *Geology of the Salmijärvi Cu-Au deposit*. M.Sc. thesis, Luleå University of Technology, Luleå, Sweden, 75 pp.

Sarlus, Z., 2016: *Geochemical and geochronological constraints on 1.88 and 1.80 Ga magmatic events in the Gällivare area, northern Sweden*. Licentiate thesis, Luleå University of Technology, Luleå, Sweden, 106 pp.

Sarlus, Z., Andersson, U.B., Bauer T.E., Wanhainen, C., Martinsson, O., Nordin, R., Andersson, J.B.H., 2017: Timing of plutonism in the Gällivare area: implications for Proterozoic crustal development in the northern Norrbotten ore district, Sweden. *Geological Magazine 154,* 1–26.

Skiöld, T. & Cliff, R.A., 1984: Sm–Nd and U–Pb dating of Early Proterozoic mafic–felsic volcanism in northernmost Sweden. *Precambrian Research 26*, 1–13.

Smith, M., Coppard J., Herrington R. & Stein H., 2007: The geology of the Rakkurijärvi Cu–(Au) prospect, Norrbotten: A new iron-oxide–copper–gold deposit in northern Sweden. *Economic Geology 102*, 393–414.

Smith, M.P., Storey, C.D., Jefferies, T.E. & Ryan, C., 2009: In situ U–Pb and trace element analysis of accessory minerals in the Kiruna district, Norrbotten, Sweden: New constraints on the timing and origin of mineralisation. *Journal of Petrology 50*, 2063–2094.

Smith, M.P., Gleeson S. A. & Yardley B. W. D., 2013: Hydrothermal fluid evolution and metal transport in the Kiruna District, Sweden: Contrasting metal behaviour in aqueous and aqueous–carbonic brines. *Geochimica et Cosmochimica Acta 102*, 89–112.

Spitz, G. & Darling, R., 1978: Major and minor element lithogeochemical anomalies surrounding the Louvem copper deposit, Val d'Or, Quebec. *Canadian Journal of Earth Sciences 15*, 1161–1169.

Stacey, J.S. & Kramers, J.D., 1975: Approximation of terrestrial lead isotope evolution by a two-stage model. *Earth and Planetary Science Letters 26*, 207–221.

Steiger, R.H. & Jäger, E., 1977: Convention on the use of decay constants in geo- and cosmochronology. *Earth and Planetary Science Letters 36*, 359–362.

Storey, C.D., Smith M.P. & Jefferies T.E., 2007: In situ LA-ICP-MS U–Pb dating of metavolcanics of Norrbotten, Sweden: Records of extended geological histories in complex titanite grains. *Chemical Geology 240*, 163–181.

Tollefsen, E., 2014: *Thermal and chemical variations in metamorphic rocks in Nautanen, Gällivare, Sweden*. M.Sc. thesis, Stockholm University, Stockholm, Sweden, 50 pp.

Tucker, M.E., 1991: *Sedimentary petrology: An introduction to the origin of sedimentary rocks*. Blackwell Science, Oxford, 260 pp.

Waara, S., 2016. *Garnet occurrence and its relationship to mineralization at the Nautanen deposit, northern Sweden.* M.Sc. thesis, Luleå University of Technology, Luleå, Sweden.

Wanhainen, C., Billström, K., Stein, H., Martinsson, O. & Nordin, R., 2005. 160 Ma of magmatic/hydrothermal and metamorphic activity in the Gällivare area: Re-Os dating of molybdenite and U–Pb dating of titanite from the Aitik Cu-Au-Ag deposit, northern Sweden. *Mineralium Deposita 40*, 435–447.

Wanhainen, C., Billström, K. & Martinsson, O., 2006. Age, petrology and geochemistry of the porphyritic Aitik intrusion, and its relation to the disseminated Aitik Cu-Au-Ag deposit, northern Sweden. *GFF 128*, 273–286.

Wanhainen, C., Broman, C., Martinsson, O. & Magnor, B., 2012: Modification of a Palaeoproterozoic porphyry-like system: Integration of structural, geochemical, petrographic, and fluid inclusion data from the Aitik Cu–Au–Ag deposit, northern Sweden. *Ore Geology Reviews 48*, 306–331.

Weihed, P., Arndt, N., Billström, K., Duchesne, J.-C., Eilu, P., Martinsson, O., Papunen, H. & Lahtinen, R., 2005: Precambrian geodynamics and ore formation: The Fennoscandian Shield. *Ore Geology Reviews 27*, 273.

White, J.D.L. & Houghton, B.F., 2006: Primary volcaniclastic rocks. *Geology 34*, 677–680.

Whitehouse, M.J. & Kamber, B.S., 2005: Assigning dates to thin gneissic veins in high-grade metamorphic terranes: a cautionary tale from Akilia, southwest Greenland. *Journal of Petrology 46*, 291–318.

Whitehouse, M.J., Claesson, S., Sunde, T. & Vestin, J., 1997: Ion-microprobe U–Pb zircon geochronology and correlation of Archaean gneisses from the Lewisian Complex of Gruinard Bay, north-west Scotland. *Geochimica et Cosmochimica Acta 61*, 4429–4438.

Whitehouse, M.J., Kamber, B.S. & Moorbath, S., 1999: Age significance of U–Th–Pb zircon data from Early Archaean rocks of west Greenland: a reassessment based on combined ion-microprobe and imaging studies. *Chemical Geology 160*, 201–224.

Wiedenbeck, M., Alle, P., Corfu, F., Griffin, W.L., Meier, M., Oberli, F., Quadt, A.V., Roddick, J.C. & Spiegel, W., 1995: Three natural zircon standards for U–Th–Pb, Lu–Hf, trace element and REE analysis. *Geostandards Newsletter 19*, 1–23.

Wiedenbeck, M., Hanchar, J.M., Peck, W.H., Sylvester, P., Valley, J., Whitehouse, M., Kronz, A., Morishita, Y., Nasdala, L., Fiebig, J., Franchi, I., Girard, J.P., Greenwood, R.C., Hinton, R., Kita, N., Mason, P.R.D., Norman, M., Ogasawara, M., Piccoli, P.M., Rhede, D., Satoh, H., Schulz-Dobrick, B., Skår, O., Spicuzza, M.J., Terada, K., Tindle, A., Togashi, S., Vennemann, T., Xie, Q. & Zheng, Y.F., 2004: Further characterisation of the 91500 zircon crystal. *Geostandards and Geoanalytical Research 28*, 9–39.

Williams, P.J., 2010: ”Magnetite-group” IOCGs with special reference to Cloncurry (NW Queensland) and northern Sweden: settings, alteration, deposit characteristics, fluid sources, and their relationship to apatite-rich iron ores. *In:* L. Corriveau & H. Mumin (eds.): *Exploring for iron oxide copper-gold deposits: Canada and global analogues*. Geological Association of Canada Short Course 20, 23–38.

Winchester, J.A. & Floyd, P.A., 1977: Geochemical discrimination of different magma series and their differentiation products using immobile elements. *Chemical Geology 20*, 325–343.

Witschard, F., 1970: Description of the geological maps Lainio NV, NO, SV, SO with an appendix by P. Niskanen the aeromagnetic maps Lainio NV, NO, SV, SO. *Sveriges geologiska undersökning Af 9–12*, 116 p.

Witschard, F., 1996: Berggrundskartan 28K Gällivare NO, NV, SO, SV. 1:50 000-scale maps. *Sveriges geologiska undersökning Ai 98–101.* (With a description in English).

Zweifel, H., 1976: Aitik. Geological documentation of a disseminated copper deposit. *Sveriges geologiska undersökning C 720*, 80 pp.

Authors, paper 5:
Fredrik A. Hellström
Geological Survey of Sweden
Department of Mineral Resources
Uppsala, Sweden

Risto Kumpulainen
Stockholm University,
Department of Geological Sciences,
Stockholm, Sweden

Cecilia Jönsson
Geological Survey of Sweden
Department of Mineral Resources
Uppsala, Sweden

Tonny B. Thomsen
Geological Survey of Denmark & Greenland,
Department of Petrology & Economic Geology,
Copenhagen, Denmark

Hannu Huhma
Geological Survey of Finland,
Espoo, Finland

Olof Martinsson
Luleå University of Technology,
Division of Geosciences and Environmental Engineering,
Luleå, Sweden

5. Age and lithostratigraphy of Svecofennian volcanosedimentary rocks at Masugnsbyn, northernmost Sweden – host rocks to Zn-Pb-Cu- and Cu ±Au sulphide mineralisations

Fredrik A. Hellström, Risto Kumpulainen, Cecilia Jönsson, Tonny B. Thomsen, Hannu Huhma, Olof Martinsson

ABSTRACT

This study focuses on the Svecofennian volcanosedimentary rock units of the Pahakurkio and Kalixälv groups in the Masugnsbyn area, approximately 90 km to the S-SE of Kiruna in northeasternmost Sweden, with the aim of constraining their depositional timing and environment. The Pahakurkio group comprises pelitic to arenitic metasedimentary rocks lying on top of the Karelian Veikkavaara greenstone group. It is divided into four subunits, two sandstones and two shale units. The sandstones are immature arkoses to subarkoses, originating predominantly from rocks in the upper continental crust. The overlying Kalixälv group consists of similar metasedimentary rocks, i.e. originally shales and sandstone, now sillimanite-bearing mica schist, migmatitic paragneisses and quartzites. Both successions were deposited in a marine coastal environment with the presence of wave activity and change in vertical facies from shallow to deeper water where, in part, graphite-bearing shales represent deposition in stagnant waters beneath the storm wave base. The Kalixälv group differs from the Pahakurkio group in that it contains a much greater abundance of volcanic and volcanogenic sedimentary rocks. Extensive volcanism is a potentially important heat source driving hydrothermal alteration and generation of the minor Zn-Pb-Cu and Cu ±Au sulphide mineralisations that occur along the border zone between the Pahakurkio and Kalixälv groups, but the partly vein-hosted nature of the ore deposits suggests a later, epigenetic, hydrothermal origin, with mineralisations formed from boron-rich fluids. Sandstones from the Pahakurkio and Kalixälv group record similar negative $\varepsilon_{Nd(1.89Ga)}$ values at -3.0 and -3.9, respectively, consistent with mixing of debris from predominantly 2.2–1.9 Ga and 3.0–2.6 Ga-old rocks, a theory supported by U-Pb provenance zircon dating. The lower sandstone in the Pahakurkio group shows a zircon age distribution pattern dominated by 2.15–1.90 Ga (66%) and 2.95–2.62 Ga ages (30%), with a maximum depositional age of approximately 1.91 Ga, similar to age data from the upper sandstone unit with a maximum depositional age of approximately 1.90 Ga. A sandstone of intermediate composition in the Kalixälv group is dominated by 2.15–1.86 Ga (81%) and 2.96–2.55 Ga zircon ages (11%), and deposition is suggested to have occurred at approximately 1.89–1.88 Ga, contemporaneous with emplacement of andesitic rock within the same group. Overall, the zircon age distribution patterns are consistent with the Kalixälv group being younger than the

Pahakurkio group, according with way-up determinations. The lower quantity of Archaean zircons in the Kalixälv group sample suggests that the Archaean basement was covered by Svecofennian rocks as the Svecokarelian orogeny progressed, and thus erosion and deposition of debris from the latter was the main source. The Sakarinpalo intermediate to felsic metavolcanic rocks occur north of, and spatially associated with, rocks of the Veikkavaara greenstone group. However, U-Pb SIMS zircon data of a meta-andesite give a Svecofennian age of 1 890 ±5 Ma, and possibly indicate inverted younging of the stratigraphy in this area due to poly-phase folding. Strongly scapolite-biotite-altered intermediate rocks of the Pahakurkio group show a similar trace element pattern to volcanic rocks in the Sakarinpalo suite, suggesting that these units can be correlated. One sample from the Kalixälv group intermediate metavolcanic rocks is dated at 1 887 ±5 Ma and is thus similar in age to the Sakarinpalo suite. In a regional context, the metavolcanic rocks in the Masugnsbyn area are of a similar age to, or are possibly slightly older than, similar intermediate metavolcanic rocks in northernmost Sweden, i.e. possibly correlated with the Porphyrite group in the Kiruna–Tjårrojokka area, the Sammakkovaara group in the Pajala area and the Muorjevaara group in the Gällivare area. It is suggested that overall negative initial ε_{Nd} signatures of metavolcanic rocks from the Sakarinpalo and Kalixälv groups ($\varepsilon_{Nd(1.89Ga)}$ at -3.9 and -2.2) are a result of juvenile arc-generated melts mixed with variable amounts of anatexis and assimilated older Archaean continental crust, and related to partial melting above a subduction zone dipping underneath the Archaean Norrbotten craton.

INTRODUCTION

Northern Sweden is one of the most important mining regions in Europe, with world-class mineral deposits such as the Kiruna and Malmberget iron ores and the Aitik copper ore. Apart from the major deposits, a large number of sub-economic to economic deposits containing Fe and Cu ±Au are known (e.g. Weihed et al. 2005, Martinsson & Wanhainen 2013, Martinsson et al. 2016). Nearly all mineralisations are hosted by supracrustal rocks and, in SGU's Barents Project, key areas were selected to cover the complete supracrustal stratigraphy with the aim of characterising and improving the understanding of the stratigraphy, geochemical signature and age of these rocks.

This chapter focuses on Svecofennian supracrustal successions at Masugnsbyn in the northeast of the Norrbotten ore province (Figs. 1–3), an area with abundant mineralisations, including stratiform quartz-banded iron ores, skarn iron ores, graphite, dolomite, Cu-Zn-Pb ±Au sulphide mineralisations (see summary review in Hellström & Jönsson 2014, Bergman et al. 2015). The lower part of the stratigraphy in Masugnsbyn, including the Veikkavaara greenstone group, is presented in Lynch et al. (2018b, Fig. 2). The upper, Svecofennian, part presented here includes pelitic to arenitic metasedimentary rocks and subordinate intermediate metavolcanic rocks. Age and geochemical data for the volcanosedimentary units in the Pahakurkio and Kalixälv groups, as well as for metavolcanic rocks of the Sakarinpalo suite (Padget 1970, Witschard 1970, Niiniskorpi 1986) put constraints on depositional timing, environment and provenance of sedimentary units and petrogenesis of the volcanic rocks, and enable comparison and correlation with similar rocks across the Norrbotten ore province. These data also increase knowledge of the stratigraphy and the geological evolution of the region, which is also of importance for further mineral exploration.

GEOLOGICAL OVERVIEW

Precambrian bedrock in northern Sweden includes a 3.2–2.6 Ga Archaean granitoid-gneiss basement, which is non-conformably overlain by Palaeoproterozoic volcanic and sedimentary successions (e.g. Ödman 1957, Witschard 1984, Bergman et al. 2001, Martinsson 2004, Kathol & Weihed 2005, Weihed et al. 2005, Martinsson & Wanhainen 2013, Lauri et al. 2016). Sm-Nd isotopic analyses of Proterozoic granitoids and metavolcanic rocks approximately delineate the Archaean palaeoboundary zone between the reworked Archaean craton in the north and more juvenile Palaeoproterozoic domains to the south, along the Luleå–Jokkmokk zone in Sweden and along the Raahe–Ladoga zone in Finland (Fig. 1, e.g. Huhma 1986, Vaasjoki & Sakko 1988, Öhlander et al. 1993, Mellqvist et al. 1999, Nironen 1997). This approximate boundary zone defines the border between the Norrbotten and the Bothnia–Skellefteå lithotectonic provinces (Stephens, pers. comm). In Norrbotten County rift-related 2.5–2.0 Ga Karelian basic metavolcanic rocks and associated metasedimentary rocks of the Kovo and Greenstone groups rest on the Archaean basement. These are overlain by terrestrial to shallow water, approximately 1.90–1.87 Ga arc-related Svecofennian successions, represented by the calc-alkaline, andesite-dominated Porphyrite group, the mildly alkaline volcanic rocks of the Kiirunavaara group (Martinsson 2004) and, in the uppermost stratigraphic level, younger clastic sedimentary rocks. The Greenstone group contains stratiform–stratabound base metal and iron deposits in the middle and upper parts (Martinsson & Wanhainen 2013), whereas the Kiirunavaara group hosts economically important apatite iron ores, e.g. the Kiirunavaara and Malmberget deposits. Sub-aerial volcanic rocks extend south of the Archaean palaeoboundary in the predominantly volcanic 1.88–1.87 Ga Arvidsjaur group (Skiöld et al. 1993, Kathol & Triumf 2004, Kathol & Weihed 2005, Kathol & Persson 2007). The volcanic rocks of the Arvidsjaur group are commonly grouped together with similar volcanic rocks north of the Archaean palaeoboundary, such as the Kiruna–Arvidsjaur porphyry group (Perdahl & Frietsch 1993). Palaeoproterozoic supracrustal rocks are intruded by the calc-alkaline 1.89–1.88 Ga Haparanda suite and the alkali-calcic 1.88–1.86 Ga Perthite monzonite suite, considered to be comagmatic with the Svecofennian volcanic rocks of the Porphyrite and Kiirunavaara–Arvidsjaur groups, respectively (Witschard 1984, Bergman et al. 2001). It has been suggested that the Aitik Cu-Au-Ag deposit is a porphyry copper system related to a 1.89 Ga quartz monzodiorite that was later modified by hydrothermal and metamorphic events (Wanhainen et al. 2012). Minimum-melt granites and pegmatites, referred to as Lina granite, intruded at 1.80–1.79 Ga and occupy large areas of Norrbotten (Öhlander et al. 1987a). Coeval with the S-type rocks of the Lina suite are approximately 1.80 Ga I- to A-type GSDG-type (Granite-syenite-diorite-gabbro) magmatic rocks in Norrbotten belonging to the Edefors suite. These rocks are related to the Transscandinavian igneous belt that forms a 1 500 km long, north–south-trending belt along the western part of the Svecokarelian orogen (Högdahl et al. 2004).

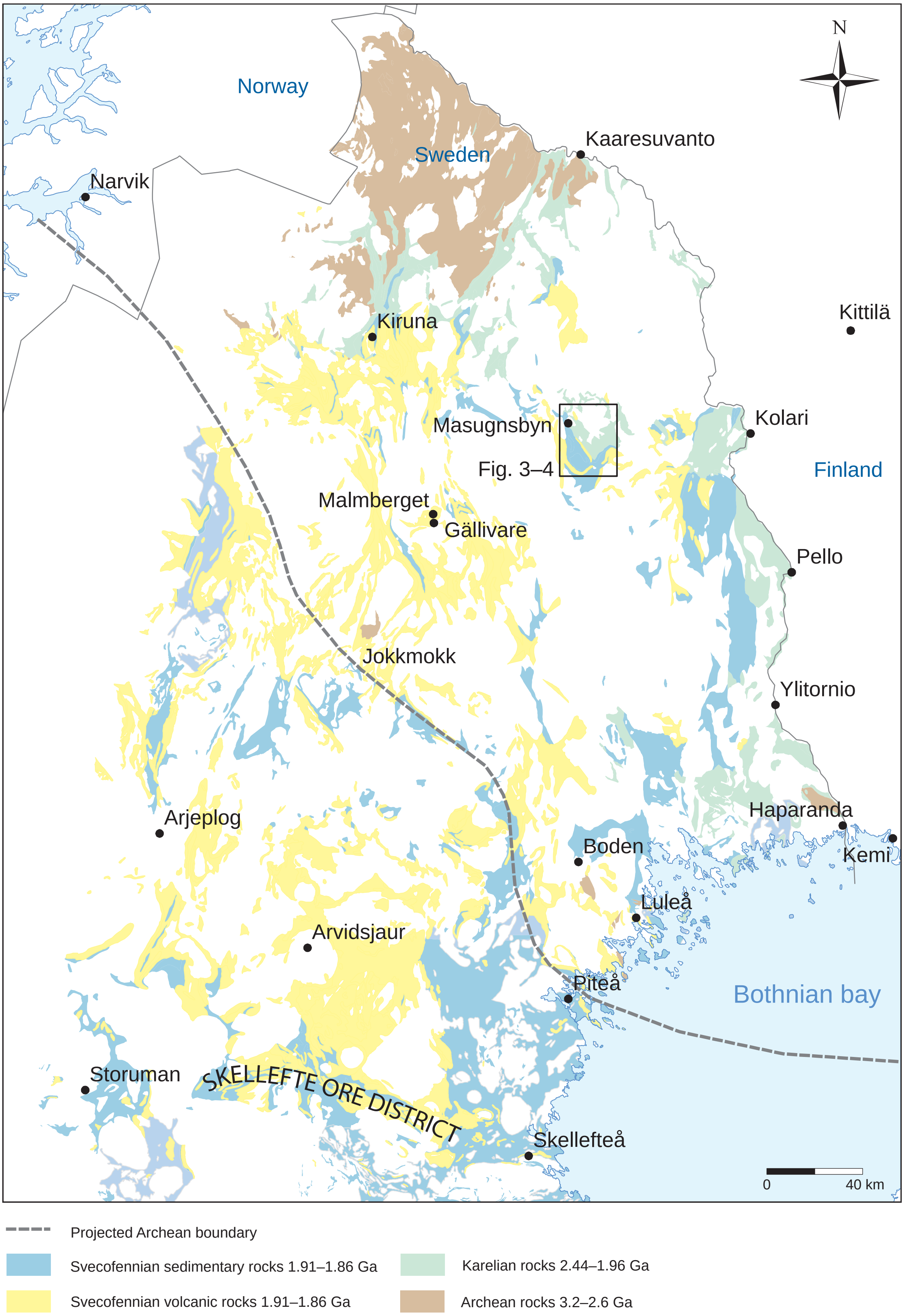

Figure 1. Geological outline of northern Sweden, showing selected lithological units (from SGU bedrock 1:M bedrock database).

Super-unit	Unit	Sub-unit	Rock units	(m)
Svecofennian supracrustal rocks	Rissavaara quartzite	4	Quartz sandstone (quartzite)	
	Kalixälv grp	3b	Semipelitic,-pelitic-, basic schists, migmatitic paragneiss	
		3a	Conglomerate, meta-sandstone, intermediate metavolcanic rocks	
	Sakarinpalo suite		Intermediate-felsic metavolcanic rocks	
	Pahakurkio grp	upper sandstone (2d)	Subarkosic metasandstone	1800
		upper shale (2c)	Pelitic micaschist, graphite schist, marble	1000
		lower sandstone (2b)	Subarkosic-arkosic metasandstone, greenshist	430
		lower shale (2a)	Pelitic micaschist	600
Karelian supracrustal rocks	Veikkavaara greenstone grp	Masugnsbyn fm (1c)	Graphite schist, skarnbanded chert (BIF), marble	370
		Tuorevaara greenstone fm (1c)	Metabasaltic tuff, graphite schist, metadolerite sills	1000
		Suinavaara fm (1b)	Pelitic schist and quartzite (Suinavaara quartzite)	100
		Nokkokorvanrova greenstone fm (1a)	Basaltic greenstone	2000

Figure 2. Schematic stratigraphy of the Masugnsbyn area, modified from Padget (1970) & Witschard (1970). The names used in Padget (1970) have been partly modified, and new informal names have been added. The alphanumerical names for the sub-units used by Padget (1970) are within brackets. Names of units within the Veikkavaara group follow Lynch et al. (2018b); grp = group, fm = formation.

Geology of the Masugnsbyn area

In the Masugnsbyn area, approximately 90 km east-southeast of Kiruna, Karelian greenstones of the Veikkavaara greenstone group are overlain by Svecofennian supracrustal rocks of the Pahakurkio and Kalixälv groups (Figs. 1–4; Padget 1970). The Veikkavaara greenstones constitute the upper part of the Greenstone group, whereas the Pahakurkio and Kalixälv groups have been included in the Middle sediment group of Witschard (1984). Intermediate volcanic rocks north of, and spatially associated with, the Veikkavaara greenstone are referred to as the Sakarinpalo suite (Witschard 1970).

The Veikkavaara greenstones form a V-shaped area in the eastern part of the Masugnsbyn area and predominantly consist of mafic volcaniclastic rocks (Fig. 3, Padget 1970, Lynch et al. 2018b). Metadoleritic sills appear to be concordant with the basaltic tuffs and are considered to have intruded shortly after the deposition of the basaltic sandstones, possibly representing near-surface intrusions related to the contemporary volcanism. A 40 m wide dolerite sill was dated by U-Pb in zircon at 2 139 ±4 Ma (2σ), and is also suggested to constrain the age of the Veikkavaara greenstone group (Lynch et al. 2018b). The uppermost part of the Veikkavaara greenstone group is referred to as the Masugnsbyn formation and consists of chemically deposited metasediments, including skarn-banded chert (silicate facies banded iron formation), graphite schist and calcitic to dolomitic marble (see Lynch et al. 2018b). Martinsson et al. (2013) used the name Vinsa formation for the uppermost part of the Veikkavaara greenstone group, defined in the Käymäjärvi area to the east (see Martinsson et al. 2018b).

The Sakarinpalo suite consists of altered acid to intermediate metavolcanic rocks and occurs immediately north of the Veikkavaara greenstones (Fig. 3, Witschard 1970). The magnetic anomaly pattern suggests that the Sakarinpalo metavolcanic rocks are spatially related to rocks of the Greenstone group (Fig. 4), and can possibly be correlated with units within the Viscaria formation in the Kiruna Greenstone group (cf. Martinsson 1997). But the area is poorly exposed and no contacts have been observed between the Veikkavaara greenstones and the Sakarinpalo suite.

The Pahakurkio group comprises arenitic to pelitic metasedimentary rocks, west of, and concordantly on top of, the Veikkavaara greenstone group (Fig. 3). Cross-bedding is common in the metasandstones, and numerous way-up determinations consistently show younging to the west (Padget 1970).

Layers of strongly scapolite-altered rocks of basic to intermediate composition occur within the meta-sandstones and may represent volcanic material. Graphite-bearing schists and carbonate rocks occur within the metapelites of the Pahakurkio group (Niiniskorpi 1986).

The *Kalixälv group* has a basal conglomerate, suggesting an unconformable contact with the Pahakurkio group. Distinct cross-bedding shows that the steeply dipping beds in meta-sandstones young to the west, and the Kalixälv group therefore overlies the Pahakurkio group (Padget 1970). In part, the contact between the groups is tectonic, i.e. along the Kalixälv fault. Niiniskorpi (1986) noted that both the Pahakurkio and the Kalixälv groups consist of similar types of metasedimentary rocks, metapelites and quartzites. However, metavolcanic rocks are much more frequent in the Kalixälv group than the Pahakurkio group (Niiniskorpi 1986). To the west and south, migmatisation increases and no natural, upper stratigraphic limit for the group is known.

Structures

The supracrustal sequence in the Masugnsbyn area is deformed into large-scale fold structures and cut by faults. Structures have northeast or northwest trends, thereby intersecting at high angles. Main tectonic features include the Kalixälv dome, the Masugnsbyn syncline, the Saittajärvi anticline and the Oriasvaara syncline with the associated Kalixälv fault (Fig. 3, Padget 1970). Fold axial planes strike northwest–southeast, except for the Oriasvaara syncline, which has a northeast–southwest trend, parallel to the Kalixälv fault. The Oriasvaara syncline is bounded to the northwest by the northeasterly-oriented Kalixälv fault. Movements along that fault have down-thrown the southeastern block, creating the tectonic contact between the Pahakurkio and Kalixälv groups. The dip of the beds in the Kalixälv dome is low to moderate but increases away from the centre of the dome, and must have resulted from combining at least two fold phases. The magnetic anomaly map reveals the complexly folded internal structure of the Veikkavaara greenstones and the presence of a possible earlier phase of isoclinal folding with a north-northwest-oriented axial plane in addition to the north-oriented axial plane of the Saitajärvi anticlinal. The fold structures in the Masugnsbyn area are evaluated by Grigull et al. (2018). Geophysical modelling supports the interpretation of the Saittajärvi fold as a synform structure.

Metamorphic constraints

Metamorphic mineral associations in the metapelitic rocks, with andalusite, sillimanite and cordierite, and the absence of kyanite, indicate amphibolite facies conditions of relatively high temperature and low to moderate pressures (Padget 1970). The composition of the plagioclase (An_{10-50}) and the presence of hornblende together with almandine suggest the rocks of the Veikkavaara greenstones are in the garnet amphibolite facies of regional metamorphism (Padget 1970). Partial melting in the migmatitic paragneisses in the south of the area suggests even upper amphibolites facies grade of metamorphism have been reached. Migmatisation in the paragneiss is dated at 1878 ±3 Ma and is suggested to be caused by heat from large volumes of contemporaneous early orogenic Svecokarelian intrusions (Hellström 2018).

Contact metamorphic alterations of the upper part of the Veikkavaara greenstones containing banded iron formations and carbonate rocks also resulted in skarn formation and remobilisation of iron to higher grades to form the Masugnsbyn skarn iron ores. Later metamorphic/hydrothermal events are possible, as recorded by a U-Pb monazite age of approximately 1.86 Ga of an andalusite bearing mica schist (Bergman et al. 2006), as well as U-Pb analyses of a single fractions of titanite plotting weakly discordant at approximately 1.80 Ga (Veikkavaara Cu-sulphide mineralisation), at approximately 1.78 Ga (Sakarinpalo, metadacite) and at 1.76 Ga (Tiankijoki, pyroxene skarn in metasedimentary rock, Martinsson et al. 2016). This is supported by the presence of deformation and high-grade metamorphism within the Pajala deformation belt to the west, which occurred in the 1.83–1.78 Ga interval (Bergman et al. 2006, Luth et al. 2016, Hellström & Bergman 2016, Luth et al. 2018), possibly overprinting earlier structures.

Mineralisations

Mineralisations of economic interest in the Masugnsbyn area include layers of iron and dolomite between the greenstones and metasedimentary rocks, and graphite layers and base-metal sulphide mineralisations within the volcaniclastic greenstones as well as in the Svecofennian supracrustal rocks (Fig. 3, Geijer 1929, Padget 1970, Witschard et al. 1972, Grip & Frietsch 1973, Niiniskorpi 1986, Frietsch 1997, Martinsson et al. 2013, 2016, Hellström & Jönsson 2014, Bergman et al. 2015). Greenstone-hosted mineralisations are described in Lynch et al. (2018b); a short summary of the mineralisations hosted by rocks in the Pahakurkio and Kalixälv groups is given below.

The Kurkkionvaara Zn-Pb-Cu mineralisation is located approximately 15 km south of Masugnsbyn at the contact between metasedimentary rocks of the Pahakurkio group and metasedimentary and intermediate metavolcanic rocks of the Kalixälv group (Fig. 3; Niiniskorpi, 1986, summarised below). The mineralisations occur as scattered sulphide veins or fracture fillings with sphalerite and galena, mainly in the metasedimentary rocks of the Pahakurkio groups but also in the overlying conglomerate. Locally, richer mineralisations occur in some fracture zones, with total Zn-Pb content up to a few per cent over 0.4–2.0 m. Impregnations of pyrrhotite and pyrite occur in metre-wide zones, where the highest concentrations of Fe-sulphides occur in the 10–20 m wide conglomerate horizon above the Pahakurkio group as an impregnation within the matrix. Veins of pyrrhotite generally occur parallel to bedding in the metasedimentary rocks, whereas the Pb-Zn-filled fractures usually dip steeply and crosscut bedding. There is a positive correlation between B and Zn + Pb content in lithochemical analyses, suggesting a hydrothermal system with boron-rich fluids containing base metals (Niiniskorpi 1986). At Kurkkionvaara, tourmaline-rich layers (tourmalinites) occur in the pelitic metasedimentary rocks, but tourmaline-rich pegmatites are also seen. Boron-rich fluids probably have a source in the metapelites, originally deposited as marine sediments. The sulphide mineralisations may have resulted from boron-rich fluids formed during migmatisation of the pelitic sediments, but the fracture style of Zn-Pb mineralisation suggests that this type of mineralisation post-dates migmatisation and ductile deformation. The age of migmatisation at 1.88 Ga thus provides a maximum age of the fracture-type Pb-Zb mineralisation at Kurkkionvaara (Hellström 2018).

The Maunuvaara Cu-Au quartz-veined-hosted mineralisations (also named Magnovaara, Geijer 1918, Hermelin 1804, Tegengren 1924) occur in a more than 5 km long north–south-trending zone located in the western part of the Masugnsbyn area (Fig. 3). The small scattered mineralisations consist of chalcocite, with small amounts of bornite and chalcopyrite in veins, together with quartz and amphibole in a fine-grained, gneissic andesite. Malachite and azurite are present, as well as zeolites, including aggregates of stilbite (desmin) and chabazite. Copper concentrations in mineralised rocks are generally low, but may reach a few per cent. Gold content is generally below 2 ppm, but one sample contained 6.5 ppm. Anomalously high molybdenum (200 ppm) and tungsten (2 900 ppm) are seen in a few rock samples (Niiniskorpi 1982).

The Rappukoski copper mineralisation occurs approximately 18 km south-southeast of Masugnsbyn in metasedimentary rocks of the Pahakurkio group, mainly quartzitic mica schist, that are cut by granite and pegmatite (Fig. 3, Ödman 1939, Grip & Frietsch 1973, Padget 1970). The mineralisation is located in a layer of calcareous skarn in outcrops on both sides of the river Kalixälven. A system of tension fractures created during folding is filled with quartz, calcite, hornblende, chalcopyrite, bornite and molybdenite. To some extent, chalcopyrite is also disseminated within the wall rock. The width of the mineralised zones is usually 0.1–0.3 m, but may reach 2 m in conjunction with folding. The mineralisation contains 1–2% copper and traces of molybdenum.

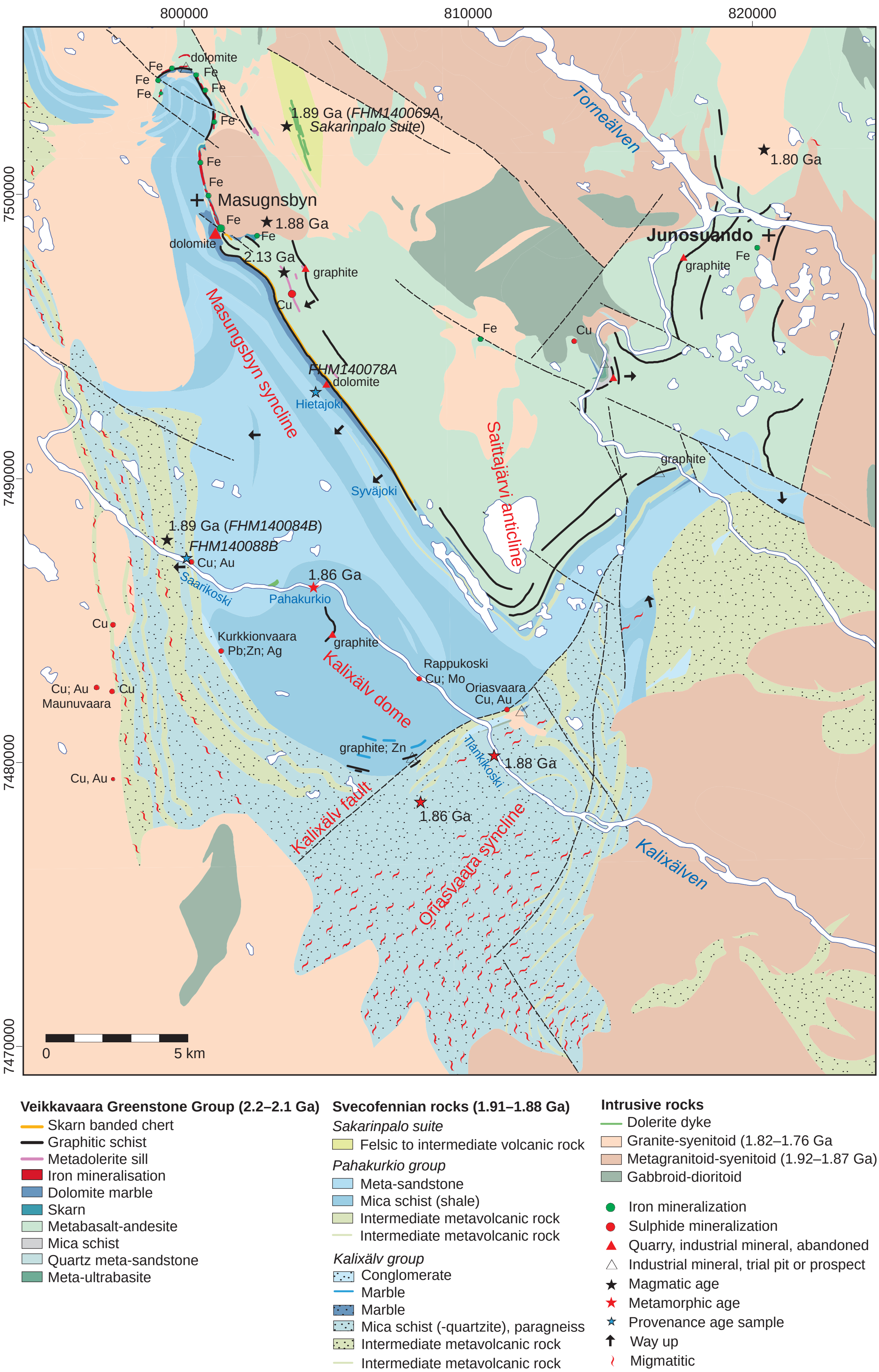
800000
810000
820000
7500000
7490000
7480000
7470000
dolomite
Fe
1.89 Ga (FHM140069A, Sakarinpalo suite)
Torneälven
1.80 Ga
Masugnsbyn
1.88 Ga
dolomite
2.13 Ga
graphite
Junosuando
Cu
Masungsbyn syncline
Fe
Cu
FHM140078A
dolomite
Hietajoki
Saittajärvi anticline
Syväjoki
graphite
1.89 Ga (FHM140084B)
FHM140088B
Cu; Au
Saarikoski
1.86 Ga
Pahakurkio
Kurkkionvaara
Pb;Zn; Ag
Kalixälv dome
Rappukoski
Cu; Mo
Oriasvaara
Cu, Au
Cu; Au
Maunuvaara
graphite; Zn
Tiankikoski
1.88 Ga
Cu, Au
1.86 Ga
Kalixälv fault
Oriasvaara syncline
Kalixälven
0
5 km
Veikkavaara Greenstone Group (2.2–2.1 Ga)
Skarn banded chert
Graphitic schist
Metadolerite sill
Iron mineralisation
Dolomite marble
Skarn
Metabasalt-andesite
Mica schist
Quartz meta-sandstone
Meta-ultrabasite
Svecofennian rocks (1.91–1.88 Ga)
Sakarinpalo suite
Felsic to intermediate volcanic rock
Pahakurkio group
Meta-sandstone
Mica schist (shale)
Intermediate metavolcanic rock
Intermediate metavolcanic rock
Kalixälv group
Conglomerate
Marble
Marble
Mica schist (-quartzite), paragneiss
Intermediate metavolcanic rock
Intermediate metavolcanic rock
Intrusive rocks
Dolerite dyke
Granite-syenitoid (1.82–1.76 Ga
Metagranitoid-syenitoid (1.92–1.87 Ga)
Gabbroid-dioritoid
Iron mineralization
Sulphide mineralization
Quarry, industrial mineral, abandoned
Industrial mineral, trial pit or prospect
Magmatic age
Metamorphic age
Provenance age sample
Way up
Migmatitic

◄ Figure 3. Bedrock geological map of the Masugnsbyn area (modified from Padget 1970, Niiniskorpi 1986). Age determinations are from Bergman et al. (2006), Hellström (2018), Lynch et al. (2018b), Martinsson et al. (2018a) and this study (FHM140069A, FHM140078A, FHM140084B, FHM140088B).

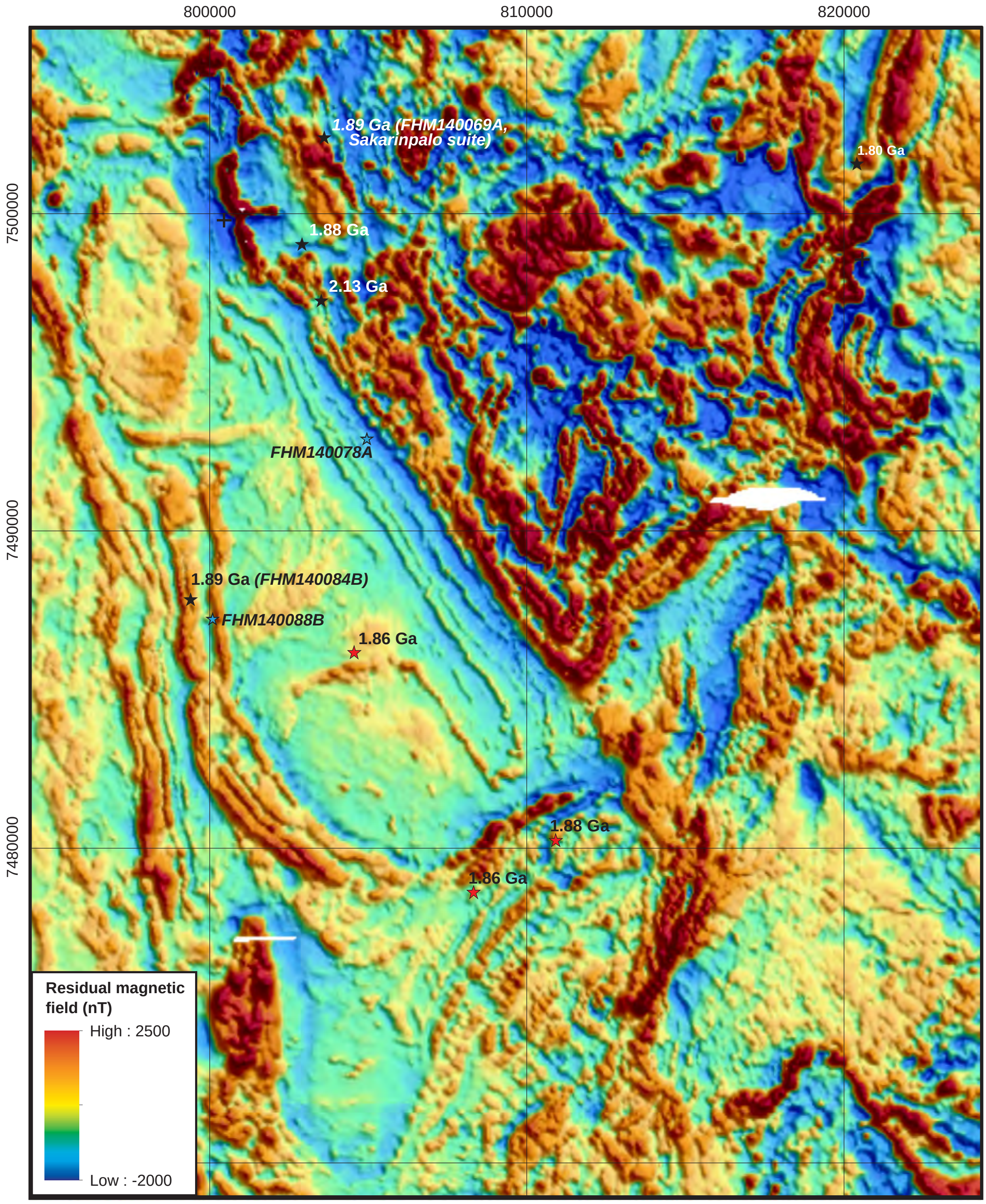

Figure 4. Magnetic anomaly map of the Masugnsbyn area with same extent as in Figure 3. Map is gridded from SGU data.

The Oriasvaara copper-gold mineralisation is located approximately 20 km south-southeast of Masugnsbyn, just east of the road to Tärendö and approximately 1 km north of the mountain Oriasvaara (Fig. 3). The Cu-Au mineralisation is spatially associated with a deformation zone: the Kalixälv fault. Two zones of mineralisation have been recognised in supracrustal rocks that have been assigned to the lower part of the Kalixälv group (Quezada 1976, Carlson 1982a, Carlson 1982b). The eastern mineralisation contains an irregular and fine-grained impregnation of pyrrhotite, chalcopyrite and pyrite in limestone. The mineralisation is locally richer in skarn-altered parts, occurring as impregnations or in bands. The western mineralisation occurs in a greenstone with zones of strong silicification and has an impregnation of sulphides, including pyrrhotite, pyrite, chalcopyrite and traces of bornite. The scapolite-altered rocks form an approximately 180 m thick unit, which generally strikes southwest–northeast and is bounded by mica schist to the north and east, and by pegmatite to the south. The richest section contains 0.5 wt. % Cu and 0.64 ppm Au over 4 m, as obtained from geochemical assays in an exploration trench in the western part (Petersson 1986).

The Sakarinpalo suite

Northeast of Masugnsbyn, at Pahtajänkkä, intermediate-felsic metavolcanic rocks referred to as the Sakarinpalo suite occur, which on a regional scale lie within the Veikkavaara greenstones (Figs. 3–5, Witschard 1970). The area is, however, poorly exposed and no contacts have been observed between the Veikkavaara greenstones and the Sakarinpalo suite. Felsic to intermediate metavolcanic rocks form a north–south-striking, steeply west-dipping unit and appear to be surrounded by granites of the Lina suite. In the west, metavolcanic rocks are bordered by a few outcrops of granite and pegmatite, but a high magnetic anomaly pattern further west cannot be explained by the low-magnetic granite (Fig. 4). The high magnetic anomaly pattern instead resembles that of the Veikkavaara greenstones, which outcrop along strike to the south, suggesting that the Sakarinpalo suite occurs within the greenstone package. Newly discovered outcrops confirm the presence of mafic rocks to the west, including dolerite and layered basaltic tuff. The metavolcanic rocks are sodium and potassium-altered and, in part, also scapolite-altered with net veining of amphibole and epidote (Fig. 5). The volcanic rocks are commonly feldspar porphyric, but volcaniclastic tuffs with alternating beds of different composition are also observed (Fig. 5).

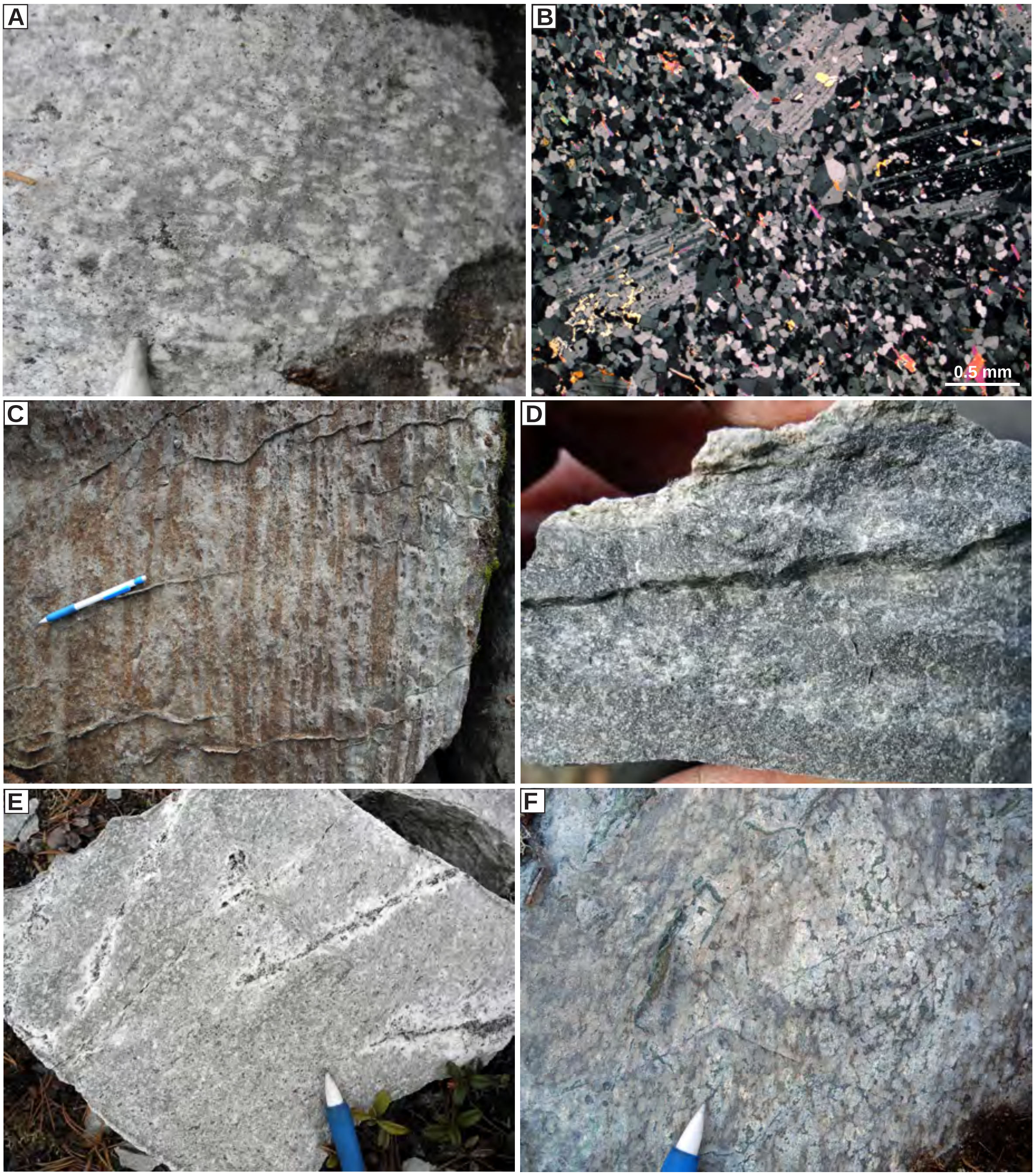

Figure 5. Metavolcanic rocks of the Sakarinpalo suite. **A.** Plagioclase porphyric meta-trachyte. (7502355 / 803715) **B.** Thin-section cross-polarised light views of plagioclase porphyric meta-trachyte. The plagioclase is sericite- and epidote-altered (7502300 / 803745). **C.** Layered volcaniclastic tuff with alternating beds of different composition (weathered outcrop surface; 7502060 / 804478). **D.** Sample of layered volcanoclastic tuff (same as in C but fresh surface; 7502060 / 804478). **E.** Albite alteration seen as bleaching next to amphibole veins in metadacite. **F.** Strongly scapolite-epidote-amphibole-altered meta-andesite (7502154 / 804535). Coordinates are given in SWEREF 99TM. All photographs by Fredrik Hellström.

The Pahakurkio group

The Pahakurkio group comprises pelitic to arenitic metasedimentary rocks to the west and on top of the Veikkavaara greenstone group (Figs. 2, 3, 7, Geijer 1930, Eriksson 1954, Padget 1970, Niiniskorpi 1986, Kumpulainen 2000). Shales have been metamorphosed to biotite-andalusite (±sillimanite) mica schists and sandstones have been recrystallised into quartzites and carry metamorphic biotite (Fig. 7E–F). The lowermost beds of the Pahakurkio group are poorly exposed, but no indications of conglomerates or any marked discordance to the uppermost unit of marble in the Veikkavaara greenstones have been observed. The magnetic anomaly pattern suggests that the Pahakurkio and Veikkavaara groups are concordant (Fig. 4). Padget (1970) studied the succession in the area between Masungsbyn and Pahakurkio along the Kalixälven river. He divided that succession into a lower shale, a lower sandstone, an upper shale and an upper sandstone. Kumpulainen (2000) later studied the sedimentological aspects of the succession; some of them are included in the text below. The Pahakurkio group is best exposed along Kalixälven between Pahakurkio and Saarikoski and at Syväjoki and Hietajoki, south-southeast of Masungsbyn (Fig. 3).

In the *Hietajoki area*, the poorly exposed, grey, *lower shale* is succeeded by the grey, *lower sandstone*, which is further sub-divided into a horizontally-bedded, grey lower arkose (~ 150m) and a grey, low-angle to hummocky cross-bedded upper arkose (approximately 300 m, Fig. 6). Dark bands in cross-bedded quartzites contain heavy minerals such as rutile, tourmaline, zircon, ilmenite and apatite, but are not significantly magnetic. This upper arkose unit contains a poorly stratified (<2.5 m thick) conglomerate unit approximately 75 m above its base. The conglomerate clasts are predominantly quartzite; a few jasper clasts are also found. In the upper part of the upper arkose, cross-bedding is

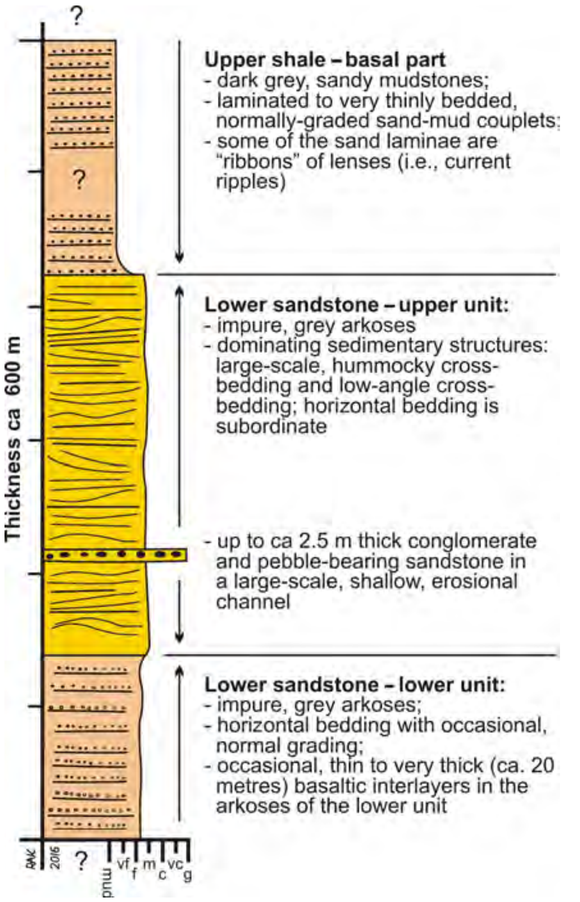

Figure 6. Stratigraphic section of the Pahakurkio group at Hietajoki, south of Masugnsbyn.

► Figure 7. Rocks of the Pahakurkio group. **A.** Trough cross-bedding in meta-sandstone at Syväjoki (7489841/806895). **B.** Cross bedding in arkosic meta-sandstone at Hietajoki (7492866/804620). **C.** Alternating beds of meta-sandstone and mica schist, originally sandy and pelitic beds at Hietajoki (7492325/804671) **D.** Wave ripples in flat dipping beds of meta-sandstone at Pahakurkio (7486133 / 803332). **E.** Deformed and folded andalusite porphyryblasts in mica schist at Hietajoki (7492168/804653). **F.** Photomicrograph in cross-polarised light of mica schist with fibrolitic sillimanite aggregate at Pahakurkio (7486176/804583). **G.** Strongly scapolite-altered intermediate rock at Syväjoki (7489838 / 806809). **H.** Photomicrograph in plane polarised light of scapolite-altered intermediate rock (7489838/806809). Coordinates are given in SWEREF 99TM. All photographs by Fredrik Hellström.

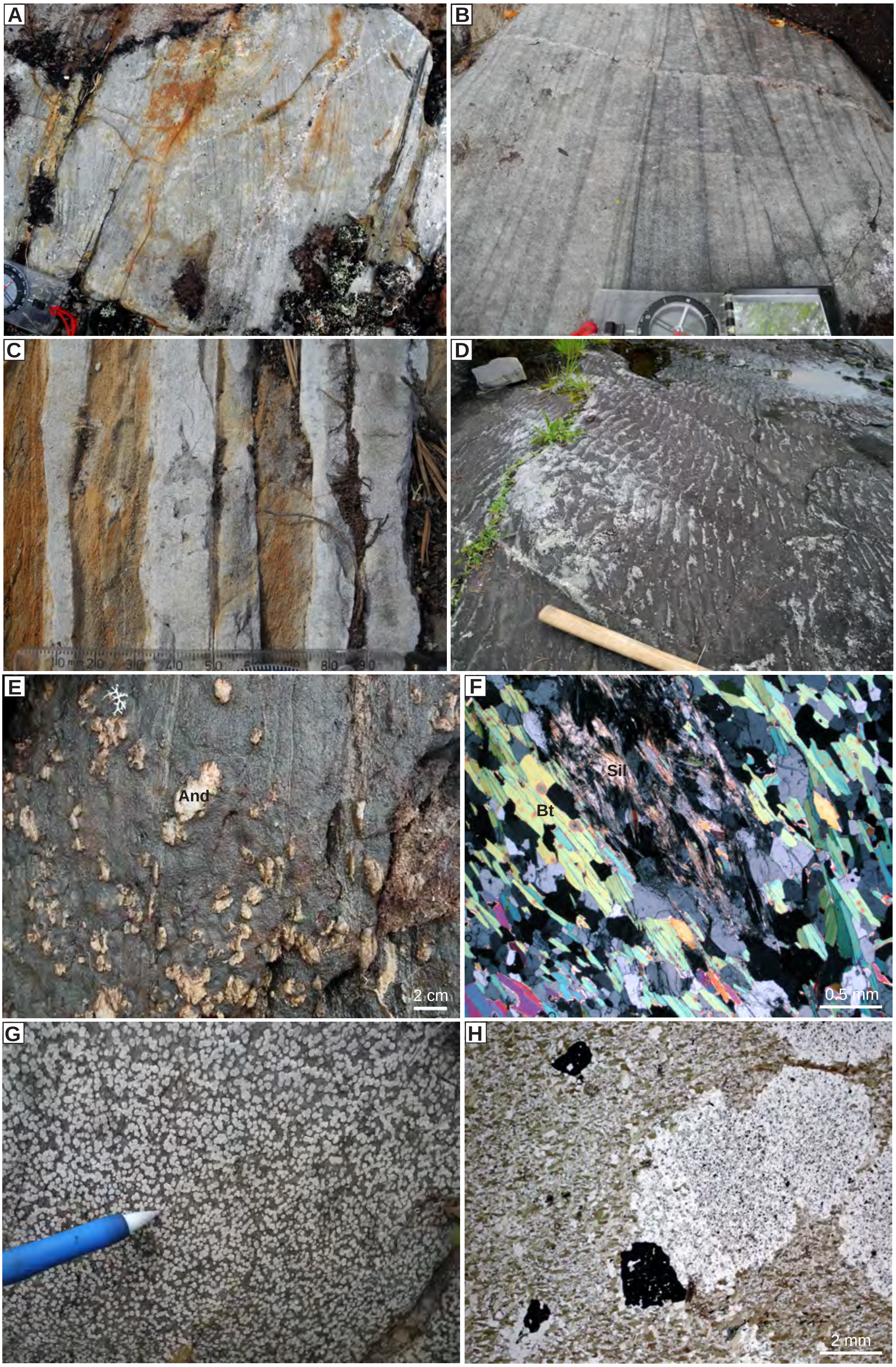
A
B
C
D
E
And
2 cm
F
Sil
Bt
0.5 mm
G
H
2 mm

gradually replaced by horizontal bedding and laminations give way-up to the grey, *upper shale* unit (Figs. 2, 7E–F). The upper shale unit is predominantly horizontally laminated and contains very thin beds and lenses of sandstone (Fig. 7C). Some of these sand lenses are normally graded.

Strongly scapolite-altered, probably basic-intermediate volcanic rocks (Fig. 7G–H, "greenschist" of Padget 1970), occur within the lower sandstone unit, and seem to have a considerable lateral extent, as is evident from the aeromagnetic map (Figs. 3–4). Similar magnetic bands occur in the upper shale unit. *The Syväjoki section* is located 3.5 km southeast of Hietajoki at the corresponding stratigraphic level and there exposes a similar stratigraphic succession (Padget 1970). Trough cross-bedding is observed locally in the arkose below the basaltic-andesitic unit (Fig. 7A).

Further south, the *Pahakurkio Canyon* of the river Kalixälven (Pahakurkio, *bad rapids* – i.e. not easy to negotiate by boat) exposes a gradual transition from the uppermost part of the grey, *upper shale* (andalusite-sillimanite-bearing mica schist) into the pale grey, *upper sandstone* (quartzite). Some very thin beds and laminas display normal grading in the transition zone. Further up the section, horizontal bedding and rare low-angle cross-bedding is encountered, and further up still, wave ripples and lunate current ripple structures are observed (Fig. 7D). The upper shale is locally graphite bearing, and layers of carbonate rocks also occur (Ödman 1939, Niiniskorpi 1986).

The Kalixälv group

Structurally and stratigraphically above the Pahakurkio group is the Kalixälv group, which is poorly exposed west and south of the former group (Fig. 3; Ödman 1939, Eriksson 1954. Padget 1970, Niiniskorpi 1986). The aeromagnetic map reveals alternating high-magnetic and low-magnetic bands, in contrast to the overall low-magnetic intensity of the Pahakurkio group (Fig. 4). These high-magnetic bands consist of intermediate volcanic or volcanogenic sedimentary rocks, and seem to alternate with low-magnetic arenitic to pelitic rocks (Fig. 8). An increasing degree of migmatisation is observed to the west and south, and no natural, upper stratigraphic limit for the group is known.

The base of the Kalixälv group is marked by an 20–30 m thick conglomerate that crops out along the river Kalixälven at Saarikoski and 13 km downstream at Tiankikoski. The conglomerate is also seen in drill core at the Kurkkionvaara Zn-Pb-Cu sulphide mineralisation (Niiniskorpi 1986). The rounded pebbles in the conglomerate consist of chert (quartz) or quartzite, and intermediate to basic volcanic rocks in a dark matrix (Fig. 8A). Ödman (1939) also noted pebbles of gabbro, syenite, granite, felsic volcanic rocks in the Tiankijoki conglomerate; thus it is indeed polymict. In the western part at Saarikoski (Fig. 3) the conglomerate grades into a dark hornblende-bearing sandstone of intermediate composition, probably consisting in part of volcanogenic material (Fig. 8B). Locally, a planar lamination with alternating laminas enriched in magnetite and light-coloured laminas is seen (Fig. 8C). The dark sandstone displays cross-bedding (Fig. 8B) similar to the structures in the underlying Pahakurkio group, which shows that both groups young westwards in this area (Padget 1970).

About 1 km above the basal conglomerate at Saarikoski, an outcrop area coincides with a positive north–south-trending magnetic anomaly band, which can be correlated with a plagioclase porphyric meta-andesite with high-magnetic susceptibility (Fig. 4). Volcanoclastic or volcanogenic sandstones,

► Figure 8. Rocks of the Kalixälv group. **A.** Polymict conglomerate at Tiankikoski, with clasts mainly of chert and mafic-intermediate rocks (7481257 / 810646) **B.** Steeply dipping, cross-bedded and amphibole-bearing meta-sandstone at Saarikoski showing way-up to the west. **C.** Photomicrograph in plane polarised light of amphibole-bearing meta-sandstone with alternating laminas enriched in magnetite. **D.** Migmatitic meta-sandstone at Tiankikoski. **E.** Photomicrograph in cross-polarised light of sillimanite-cordierite-bearing paragneiss at Tiankijoki (7480253 / 810919) **F.** Photomicrograph in plane polarised light of sillimanite-cordierite-bearing paragneiss at Tiankijoki (7480253 / 810919). **G.** Volcanoclastic, meta-andesitic tuff constitutes the host rock to the Maunuvaara Cu-Au quartz vein-hosted mineralisations (7482513 / 797469) **H.** Plagioclase porphyric meta-andesite north of Saarikoski (7487854 / 799400). Coordinates are given in SWEREF 99 TM. All photographs by Fredrik Hellström except B by Veikko Niiniskorpi.

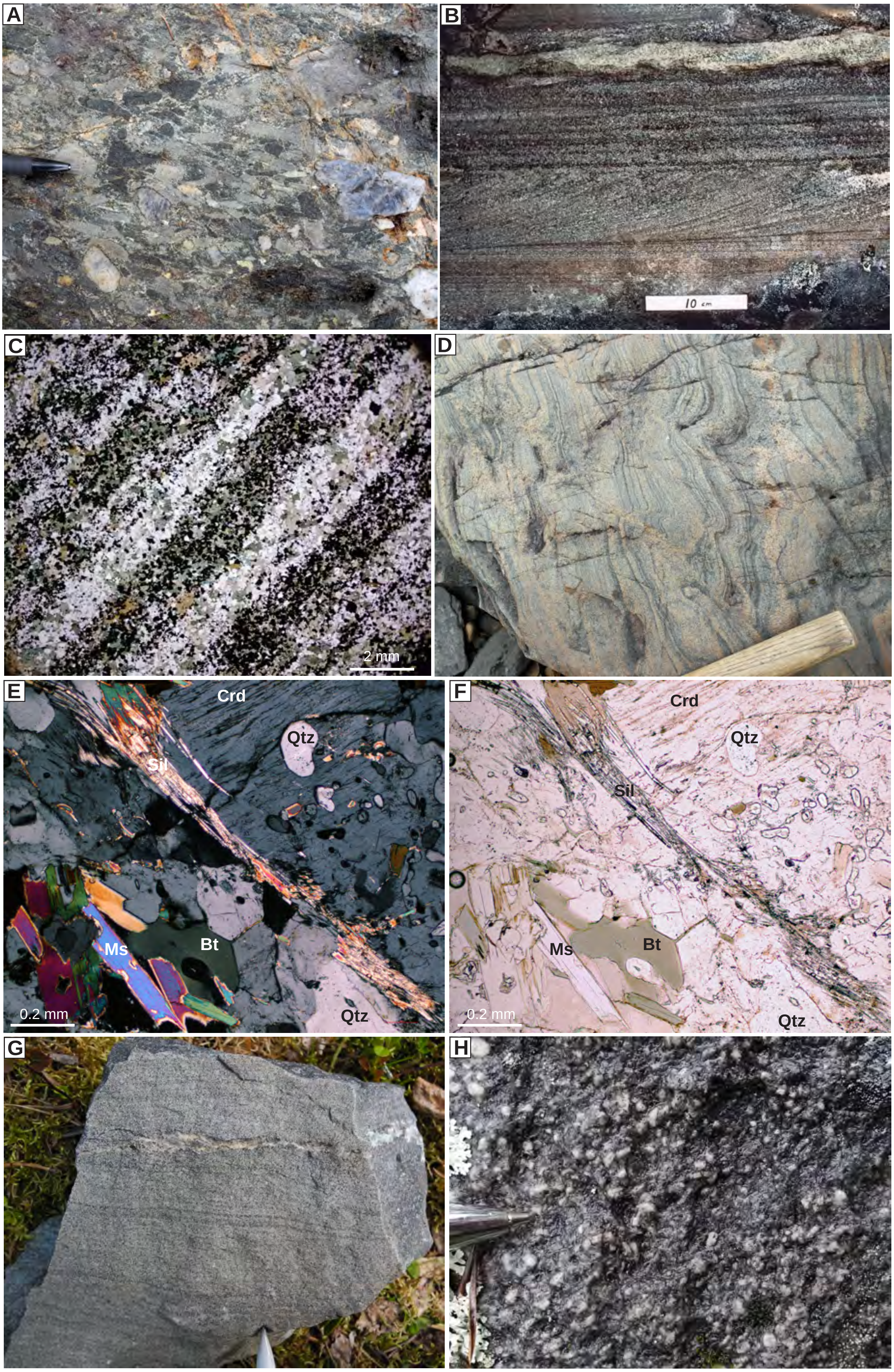
A
B
10 cm
C
2 mm
D
E
Crd
Qtz
Sil
Ms
Bt
0.2 mm
Qtz
F
Crd
Qtz
Sil
Ms
Bt
0.2 mm
Qtz
G
H

with common skarn alteration bands, and conglomeratic layers with pebbles of chert and intermediate volcanic rock occur (Niiniskorpi 1986). Modelling of magnetic data suggests that units have a steep, near vertical dip corroborating field observations of bedding (Jönberger et al. 2018).

In the south of the area (Fig. 3), sillimanite- and andalusite-bearing mica schists or migmatitic paragneisses with interlayers of quartzic sandstones are found (Fig. 8D). Niiniskorpi (1986) noted that both the Pahakurkio and the Kalixälv groups consist of similar types of metasedimentary rocks, metapelites and quartzites, which makes it difficult to distinguish between these units. Occurrences of graphite-bearing schists and carbonate rocks within the Pahakurkio group also complicate the distinction between the Pahakurkio and Veikkavaara groups.

Lithogeochemistry

Methods

Sample preparation was carried out by ALS Minerals in Piteå (Sweden) and subsequent analytical work performed at ALS Minerals lab in Vancouver (Canada). Preparation involved crushing samples and pulverising to a powder using low-chrome steel grinding mills. The lithogeochemical analysis at ALS was conducted using the whole-rock major and trace element package CCP-PKG01, a combination of different methods. Lithium metaborate fusion ICP-AES (ME-ICP06) was used for major elements. Total carbon and sulphur was analysed using a LECO analyser (ME-IR08), where the sample (0.01 to 0.1 g) is heated to approximately 1350°C in an induction furnace while passing a stream of oxygen through the sample. Total sulphur and carbon is measured by an IR detection system. Trace elements, including the full rare earth element suite, are reported from three types of sample digestion with either ICP-AES or ICP-MS analysis: lithium borate fusion for the resistive elements (ME-MS81), four-acid digestion for the base metals (ME-4ACD81), and aqua regia digestion for the volatile gold-related trace elements (ME-MS42). In addition to the new data, some old chemical analyses (SGU data & Niiniskorpi 1986) were used, in which major and trace elements were analysed by XRF, ICP-AES and ICP-MS. Geochemical diagrams were made using GCD kit software (Janoušek et al. 2006).

Metavolcanic rocks

Many metavolcanic rock samples are sodium- or potassium-altered according to the diagram by Hughes (1973, Fig. 9A), but immobile trace element, mantle-normalised spider plots show nearly identical patterns between averaged values of altered and unaltered samples within the groups (Fig. 9F). Strongly scapolite- and biotite-altered rocks within the Pahakurkio group are strongly potassium enriched, but show a trace element signature similar to volcanic rocks in the Kalixälv group. Most samples contain 52–66% SiO_2, and are thus intermediate to weakly acid in composition (Table 1, Fig. 9C). Rocks of the Sakarinpalo suite are generally more silica rich (54.0–72.6% SiO_2), than volcanic rocks in the Pahakurkio and Kalixälv groups (48.6–63.5% SiO_2,); the latter even includes a few samples of basic composition (Fig. 9C). Using the Nb/Y – Zr/TiO_2 classification plot of Pearce (1996), most samples classify as andesite, with a few samples as basalt, trachy-andesite, trachyte and rhyolite-dacite (Fig. 9B). Based on the Al – Fe_t + Ti – Mg ternary classification diagram of Jensen (1976), most samples plot in the basalt-andesite fields and a few samples in the dacite-rhyolite fields, along a low Fe-Ti, calc-alkaline trend. The TiO_2 content of the volcanic rocks in the Masugnsbyn area is relatively low, averaging 0.74% (±0.16, 1σ, n = 26, Fig. 9E) and similar to the volcanic rocks in Norrbotten classified as belonging to the "Porphyrite group" (Offerberg 1967, Martinsson & Perdahl 1995, Bergman et al. 2001). The stratigraphically higher Kiirunavaara group rocks are generally more evolved, with higher values for Ti and Zr (e.g. Bergman et al. 2001).

Volcanic rocks in the Masugnsbyn area record similar chondrite-normalised (Boynton 1984) rare earth element (REE) patterns, enriched in light REEs over heavy REEs, $(La/Yb)_N = 10.5$ ±3.3

(Fig. 9H, 1σ, n = 26). The La-Sm section has a steeper slope ($(La/Sm)_N$ = 3.8 ±0.67 (1σ)) than the Gd-Lu section, which shows an almost flat profile $(Gd/Lu)_N$ = 1.6 ±0.38 (1σ). Volcanic rocks from the Sakarinpalo and Pahakurkio groups generally have a weak negative Eu anomaly (Eu/Eu* = 0.78 ±0.17 (1σ, n = 13)), in contrast to the volcanic rocks of the Kalixälv group, which have no significant Eu anomaly.

The primitive mantle-normalised (McDonough & Sun 1995) spider diagram shows enrichment in the large ion lithophile elements, with a pronounced negative Nb-Ta anomaly, but also negative anomalies in Ti and P (Fig. 9G). The patterns for the averaged values of the different groups are similar, but rocks in the Sakarinpalo suite and Pahakurkio groups show a strong negative anomaly in Sr compared with rocks in the Kalixälv group. Although very similar element patterns are seen for all rocks, the volcanic rocks from the southeastern part of the Masugnsbyn area can be grouped with the Kalixälv group, and the highly altered rocks in the Pahakurkio group with Sakarinpalo suite. The spider diagram pattern shows a typical upper continental crustal signature, except for the low amounts of Sr, which may be due to post-depositional alteration.

Metasedimentary rocks

Sediment maturity can be expressed by SiO_2 content and the SiO_2/Al_2O_3 ratio, reflecting the abundance of quartz, clay (mica) and feldspar. Herron (1988) proposed a geochemical classification diagram of terrigenous sands and shales using log (Fe_2O_3/K_2O) versus log (SiO_2/Al_2O_3). The SiO_2/Al_2O_3 ratio separates Si-rich quartz-arenites from Al-rich shales, with other sand types showing intermediate values. The Fe_2O_3t/K_2O ratio separates lithic sands (litharenites and sublitharenites) from feldspathic sands (arkoses and subarkoses). Shale is identified on the basis of a very low SiO_2/Al_2O_3 ratio. Sandstones from the Pahakurkio group are classified as arkoses to mainly subarkoses, whereas mica schists from the same group are classified as shales to wackes, except one sample that falls in the arkose field (Fig. 10A). The amphibole-bearing dark sandstone and conglomerate from the Kalixälv group also classify as wackes, except for one more quartz-rich leucocratic sandstone that classifies as arkose (Fig. 10A).

Another useful index of chemical maturity is the alkali content (Na_2O+K_2O), which corresponds to the feldspar and clay (mica) content. The K_2O/Na_2O ratio reflects the relative abundance of potassic feldspar and mica versus plagioclase, but is also affected by the compositions of the feldspars present. In a K_2O/Na_2O versus SiO_2 plot (Fig. 10B), the dark, amphibole-bearing sandstone and conglomerate samples in the Kalixälv group have lower K_2O/Na_2O ratios (0.31–0.59) and SiO_2 (58.9–61.5%, Table 2) content than the more mature, quartz-rich sandstones within the Kalixälv and Pahakurkio groups (SiO_2: 75.6–85.4 % and K_2O/Na_2O ratios: 0.90–29.1). The difference in sodium and potassium content is also seen in a triangular Na_2O–$MgO+Fe_2O_3t$–K_2O diagram (Fig. 10E). This shows that the dark Kalixälv sandstone has a more plagioclase-rich, intermediate composition, similar to that of the meta-andesitic volcanic rocks, suggesting these contain a significant proportion of volcanoclastic or volcanogenic sedimentary material. The more mafic character of the dark sandstone is also reflected in the elevated magnesium and iron content illustrated in Figure 10E or in a bivariate plot of Al_2O_3/SiO_2 versus ($MgO+Fe_2O_3t$; Fig. 10C); the latter has also been used to discriminate sandstone from different tectonic settings (Bathia 1983). The "arc-setting" of the dark Kalixälv sandstones possibly reflects their volcanogenic nature, also seen in Figure 10B. Mica schist samples also have elevated K_2O/Na_2O ratios, as well as fairly high magnesium and iron content, reflecting their biotite (muscovite)- rich nature. A discriminate function diagram for provenance signatures of sandstone-mudstone suites using major element ratios has been proposed by Roser & Korsch (1988, Fig. 10D). The dark Kalixälv group sandstone and conglomerate samples have intermediate or mafic igneous signatures, whereas the remaining samples have a felsic igneous or quartzose signature. A trace element plot using, e.g., Sc, Th and Zr (Fig. 10F) also highlights the difference between the sandstones from the Kalixälv and Pahakurkio groups, with the more mafic sandstones showing higher Sc and lower Zr content.

Table. 1. Lithochemistry of selected metavolcanic rock samples.

Sample	Unit	Method	FHM140069A	FHM140070A	FHM140071A	FHM140074A	FHM140075A	FHM150021A	FHM140065A	FHM140065B	FHM140079A	FHM140028A	FHM140084B	FHM150018A
N		ALS-code	7502412	7502355	7502300	7502253	7502154	7502060	7489838	7489838	7493028	7482513	7487854	7485723
E			803618	803715	803745	804278	804535	804478	806809	806809	804661	797469	799400	816571
Rock			Trachy-andesite	Trachyte	Trachyte	Dacite (Ab)	Andesite (Scp)	Andesite	Andesite (Scp)	Andesite (Scp)	Andesite (Scp)	Andesite (Cu)	Andesite	Andesite
Stratigra-phic unit			Sakarinpalo suite	Sakarinpalo suite	Sakarinpalo suite	Sakarinpalo suite	Sakarinpalo suite	Sakarinpalo suite	Pahakurkio group	Pahakurkio group	Pahakurkio group	Kalixälv group	Kalixälv group	Kalixälv group
SiO_2	%	ME-ICP06	61.60	63.30	62.50	72.60	56.20	61.00	57.70	53.30	55.70	63.10	60.40	59.70
Al_2O_3	%	ME-ICP06	17.00	19.20	19.70	13.70	15.40	14.90	15.20	17.10	15.95	17.45	15.45	16.10
Fe_2O_3t	%	ME-ICP06	7.85	3.25	3.12	0.69	7.37	5.19	8.38	8.71	11.05	4.82	7.30	7.20
CaO	%	ME-ICP06	1.72	2.93	4.71	2.54	6.19	5.53	1.61	3.84	0.72	6.05	2.89	4.21
MgO	%	ME-ICP06	1.62	0.55	0.48	2.80	5.34	3.81	5.22	6.87	5.44	2.40	2.53	3.69
Na_2O	%	ME-ICP06	1.53	2.57	3.39	7.48	2.37	4.73	1.42	1.05	1.40	4.07	6.05	4.47
K2O	%	ME-ICP06	5.85	7.60	3.96	0.17	4.80	2.56	7.00	6.03	7.82	0.96	2.41	3.00
Cr_2O_3	%	ME-ICP06	0.01	<0.01	<0.01	0.01	0.02	0.02	0.04	0.04	0.04	0.02	0.01	0.01
TiO_2	%	ME-ICP06	0.73	0.54	0.54	0.34	0.92	0.62	0.76	0.87	0.82	0.67	0.66	0.70
MnO	%	ME-ICP06	0.11	0.10	0.08	0.04	0.19	0.13	0.07	0.08	0.04	0.08	0.06	0.12
P_2O_5	%	ME-ICP06	0.22	0.17	0.16	0.09	0.11	0.08	0.15	0.13	0.15	0.19	0.24	0.22
SrO	%	ME-ICP06	<0.01	<0.01	<0.01	<0.01	<0.01	<0.01	<0.01	<0.01	<0.01	0.04	0.02	0.06
BaO	%	ME-ICP06	0.13	0.31	0.25	<0.01	0.03	0.03	0.15	0.20	0.10	0.05	0.05	0.09
LOI	%	OA-GRA05	1.40	0.77	0.53	0.78	1.88	1.57	0.79	0.99	0.88	0.52	0.65	1.29
Total	%	TOT-ICP06	99.77	101.29	99.42	101.24	100.82	100.17	98.49	99.21	100.11	100.42	98.72	100.86
C	%	C-IR07	0.01	<0.01	<0.01	0.10	0.37	0.21	<0.01	0.05	0.01	0.02	0.09	<0.01
S	%	S-IR08	<0.01	<0.01	<0.01	<0.01	<0.01	0.02	<0.01	0.02	<0.01	0.06	0.01	0.01
Ba	ppm	ME-MS81	1150	2640	2180	13.3	250	234	1390	1745	902	449	473	987
Ce	ppm	ME-MS81	77.4	69.2	79.2	48.0	42.0	48.9	32.1	83.0	50.6	34.0	52.7	63.7
Cr	ppm	ME-MS81	80	10	10	70	150	110	270	310	300	100	70	90
Cs	ppm	ME-MS81	7.08	7.71	4.49	0.03	2.09	0.81	10.6	10.55	10.35	1.18	1.34	1.67
Dy	ppm	ME-MS81	3.03	2.34	2.94	2.6	3.31	2.53	3.16	3.51	3.72	2.69	3.5	3.41
Er	ppm	ME-MS81	1.85	1.31	1.67	1.36	1.92	1.54	2.21	1.76	2.1	1.6	2.05	1.89
Eu	ppm	ME-MS81	1.14	0.94	1.14	0.96	0.92	0.95	0.73	1.39	0.93	1.35	1.15	1.28
Ga	ppm	ME-MS81	24.6	20.4	18.1	15.1	19.6	20.2	21.2	23.6	23.4	19.5	19.1	22.6
Gd	ppm	ME-MS81	3.93	2.92	3.7	1.96	3.33	3.17	2.9	4.89	3.52	3.21	4.09	3.72
Hf	ppm	ME-MS81	4.7	7.7	7.4	5.3	4.9	5.7	3.5	3.3	3.8	3.0	4.4	4.6
Ho	ppm	ME-MS81	0.65	0.48	0.58	0.52	0.70	0.49	0.69	0.60	0.70	0.59	0.61	0.70
La	ppm	ME-MS81	36.3	34.7	41.2	21.7	22.1	24.8	13.7	44.0	26.9	15.6	26.6	36.6
Lu	ppm	ME-MS81	0.25	0.19	0.24	0.18	0.23	0.24	0.27	0.19	0.27	0.19	0.24	0.29
Nb	ppm	ME-MS81	12.2	13.4	14.3	4.8	8.0	5.8	9.2	9.9	9.4	5.9	9.6	10.8
Nd	ppm	ME-MS81	31.7	26.1	30.9	20.4	18.5	22.0	13.1	35.4	21.6	19.3	24.6	30.1
Pr	ppm	ME-MS81	8.55	7.49	8.86	5.45	4.75	5.15	3.56	9.58	5.75	4.84	6.11	7.62

Table. 1 continues

Sample	Unit	Method	FHM140069A	FHM140070A	FHM140071A	FHM140074A	FHM140075A	FHM150021A	FHM140065A	FHM140065B	FHM140079A	FHM140028A	FHM140084B	FHM150018A
N		ALS-code	7502412	7502355	7502300	7502253	7502154	7502060	7489838	7489838	7493028	7482513	7487854	7485723
E			803618	803715	803745	804278	804535	804478	806809	806809	804661	797469	799400	816571
Rock			Trachy-andesite	Trachyte	Trachyte	Dacite (Ab)	Andesite (Scp)	Andesite	Andesite (Scp)	Andesite (Scp)	Andesite (Scp)	Andesite (Cu)	Andesite	Andesite
Stratigra-phic unit			Sakarinpalo suite	Sakarinpalo suite	Sakarinpalo suite	Sakarinpalo suite	Sakarinpalo suite	Sakarinpalo suite	Pahakurkio group	Pahakurkio group	Pahakurkio group	Kalixälv group	Kalixälv group	Kalixälv group
Rb	ppm	ME-MS81	231	305	198	1.3	152.5	69.5	201	233	200	25.5	79.8	109
Sm	ppm	ME-MS81	5.50	4.28	4.86	3.84	3.54	3.48	2.84	6.27	4.10	3.72	4.38	6.24
Sn	ppm	ME-MS81	2	<1	<1	<1	1	1	1	2	2	1	2	4
Sr	ppm	ME-MS81	35.4	154	180	16	45.1	56.8	90.6	115	33.3	580	140.5	485
Ta	ppm	ME-MS81	0.7	0.8	0.8	0.3	0.9	0.6	0.7	0.7	1	0.3	0.7	0.7
Tb	ppm	ME-MS81	0.61	0.42	0.46	0.46	0.54	0.38	0.47	0.60	0.56	0.50	0.53	0.56
Th	ppm	ME-MS81	12.50	12.75	13.40	7.34	10.50	9.00	8.28	9.14	9.11	4.94	9.93	10.75
Tm	ppm	ME-MS81	0.24	0.20	0.25	0.17	0.27	0.24	0.29	0.25	0.29	0.18	0.29	0.29
U	ppm	ME-MS81	1.50	2.50	3.89	0.92	2.34	2.25	2.31	2.30	2.06	4.23	2.98	3.60
V	ppm	ME-MS81	81	40	29	14	129	86	145	183	171	134	150	165
W	ppm	ME-MS81	4	1	3	<1	<1	1	<1	<1	1	2	2	1
Y	ppm	ME-MS81	18.2	13.6	15.5	13.9	17.5	14.9	17.9	18.2	19.4	14.8	17.1	21.5
Yb	ppm	ME-MS81	1.99	1.51	1.99	1.28	1.88	1.59	2.14	1.96	2.08	1.58	1.77	2.07
Zr	ppm	ME-MS81	175	299	307	206	169	210	125	116	124	129	158	195
As	ppm	ME-MS42	1	3.1	3.5	<0.1	1	1.1	0.4	0.7	0.2	1.1	1.2	2
Bi	ppm	ME-MS42	<0.01	0.01	0.01	<0.01	0.04	<0.01	0.02	0.06	0.05	4.04	0.01	0.06
Hg	ppm	ME-MS42	0.007	<0.005	<0.005	<0.005	<0.005	0.006	<0.005	<0.005	<0.005	<0.005	0.005	<0.005
Sb	ppm	ME-MS42	0.06	0.09	0.11	0.08	0.28	0.29	0.14	0.11	0.45	0.17	0.2	0.31
Se	ppm	ME-MS42	0.4	0.2	0.2	0.3	0.3	<0.2	0.5	0.6	0.3	1.5	0.3	0.3
Te	ppm	ME-MS42	<0.01	<0.01	<0.01	0.03	0.01	<0.01	0.01	0.01	0.01	0.11	<0.01	0.02
Ag	ppm	ME-4ACD81	<0.5	<0.5	<0.5	<0.5	<0.5	<0.5	<0.5	<0.5	<0.5	1.9	<0.5	<0.5
Cd	ppm	ME-4ACD81	<0.5	<0.5	<0.5	<0.5	<0.5	<0.5	<0.5	<0.5	<0.5	0.8	<0.5	<0.5
Co	ppm	ME-4ACD81	9	4	4	3	14	9	30	40	34	13	14	19
Cu	ppm	ME-4ACD81	1	<1	1	1	<1	2	2	1	82	3600	9	17
Li	ppm	ME-4ACD81	40	40	30	<10	10	<10	70	70	90	20	10	10
Mo	ppm	ME-4ACD81	1	<1	<1	<1	<1	<1	<1	<1	<1	<1	<1	<1
Ni	ppm	ME-4ACD81	16	2	2	11	45	31	148	167	152	16	20	19
Pb	ppm	ME-4ACD81	<2	<2	<2	<2	<2	<2	<2	<2	2	3	3	3
Sc	ppm	ME-4ACD81	16	4	5	4	15	10	21	27	23	14	16	17
Zn	ppm	ME-4ACD81	4	6	6	4	16	9	30	37	120	31	21	117
Au	ppm	PGM-ICP23	<0.001	<0.001	<0.001	<0.001	<0.001	<0.001	<0.001	<0.001	<0.001	0.023	<0.001	<0.001
Cl	ppm	Cl-IC881	<50	<50	<50	<50	6090	na	880	2050	530	140	340	na

Lithogeochemical analysis were conducted at ALS Minerals in 2014 & 2015 using analytical packages referred to as CCP-PKG01, PGM-ICP23, Cl-IC881.

ALS method code refers to analytical method used for each element and is described in ALS methodology factsheets at www.alsglobal.com; see also the main text.

All rocks are metamorphic, with prefix meta- to be added to the rock names. Ab = albite altered, Scp = Scapolite altered, Cu = Cu-sulphide mineralised. Am = Amphibole bearing

Table. 2. Lithochemistry of meta-sandstone samples.

Sample	Unit	Method code	FHM140080A	FHM140078A	FHM140090A	FHM140087A	FHM140088A	FHM140088B
N			**7492866**	**7493033**	**7486133**	**7487718**	**7487141**	**7487141**
E			**804620**	**804679**	**803332**	**799248**	**800148**	**800148**
Rock			**Sandstone**	**Sandstone**	**Sandstone**	**Sandstone**	**Sandstone**	**Sandstone**
Stratigraphic unit			**Pahakurkio group**	**Pahakurkio group**	**Pahakurkio group**	**Kalixälv group**	**Kalixälv group**	**Kalixälv group**
SiO_2	%	ME-ICP06	85.40	85.90	77.70	75.90	61.50	63.70
Al_2O_3	%	ME-ICP06	6.56	5.66	11.35	8.13	15.55	15.35
Fe_2O_3t	%	ME-ICP06	2.23	3.65	2.24	5.09	7.63	5.88
CaO	%	ME-ICP06	0.08	0.07	0.86	3.52	3.76	5.44
MgO	%	ME-ICP06	1.30	0.67	0.90	1.39	3.30	2.08
Na_2O	%	ME-ICP06	0.08	1.22	3.46	1.47	4.54	4.54
K_2O	%	ME-ICP06	2.33	2.65	3.12	2.10	2.68	1.52
Cr_2O_3	%	ME-ICP06	0.01	0.03	0.01	0.01	0.01	0.01
TiO_2	%	ME-ICP06	0.28	0.59	0.39	0.46	0.65	0.63
MnO	%	ME-ICP06	0.02	0.01	0.03	0.16	0.08	0.09
P_2O_5	%	ME-ICP06	0.05	0.04	0.13	0.13	0.20	0.18
SrO	%	ME-ICP06	<0.01	<0.01	0.02	0.01	0.05	0.06
BaO	%	ME-ICP06	0.04	0.10	0.09	0.03	0.08	0.09
LOI	%	OA-GRA05	1.10	0.41	0.36	1.50	0.62	1.14
Total	%	TOT-ICP06	99.48	101.00	100.66	99.90	100.65	100.71
C	%	C-IR07	<0.01	<0.01	0.04	0.31	0.01	0.12
S	%	S-IR08	0.01	0.01	<0.01	0.02	0.01	<0.01
Ba	ppm	ME-MS81	434	919	825	234	662	755
Ce	ppm	ME-MS81	11.8	30.4	70.4	29.0	45.9	46.4
Cr	ppm	ME-MS81	80	210	70	90	80	100
Cs	ppm	ME-MS81	2.43	0.77	1.96	1.86	6.18	0.37
Dy	ppm	ME-MS81	1.95	2.54	3.88	2.37	2.41	2.83
Er	ppm	ME-MS81	1.48	1.33	2.23	1.34	1.45	1.72
Eu	ppm	ME-MS81	0.36	0.74	1.18	0.64	0.95	1.15
Ga	ppm	ME-MS81	8.1	6.6	11.8	9.2	16.7	16.1
Gd	ppm	ME-MS81	1.44	2.65	4.87	2.55	3.25	3.57
Hf	ppm	ME-MS81	2.7	4.5	7.8	3.2	2.4	3.7
Ho	ppm	ME-MS81	0.47	0.46	0.74	0.52	0.49	0.55
La	ppm	ME-MS81	4.3	13.3	35.3	13.7	23.3	23.3
Lu	ppm	ME-MS81	0.19	0.20	0.30	0.19	0.20	0.23
Nb	ppm	ME-MS81	4.6	4.4	6.1	4.0	5.6	5.0
Nd	ppm	ME-MS81	4.7	15.8	32.3	14.0	21.8	23.5
Pr	ppm	ME-MS81	1.32	3.75	8.33	3.45	5.45	5.56
Rb	ppm	ME-MS81	80.7	47.6	85	75.1	125	26.1
Sm	ppm	ME-MS81	1.18	3.27	5.89	2.81	3.94	4.56
Sn	ppm	ME-MS81	2	1	1	1	1	4
Sr	ppm	ME-MS81	7.5	14.4	136.5	49.1	406	524
Ta	ppm	ME-MS81	0.4	0.4	0.6	0.3	0.4	0.4
Tb	ppm	ME-MS81	0.25	0.32	0.60	0.43	0.45	0.50
Th	ppm	ME-MS81	6.01	3.71	9.55	4.92	4.30	4.59
Tm	ppm	ME-MS81	0.19	0.18	0.29	0.19	0.19	0.26
U	ppm	ME-MS81	0.76	1.28	1.93	1.47	1.08	1.64
V	ppm	ME-MS81	65	100	45	109	125	117
W	ppm	ME-MS81	2	2	2	4	2	2
Y	ppm	ME-MS81	12.9	11.4	21.2	12.6	14	15.9
Yb	ppm	ME-MS81	1.48	1.19	2.17	1.35	1.4	1.62
Zr	ppm	ME-MS81	98	169	294	123	94	130
As	ppm	ME-MS42	0.4	0.2	0.1	0.9	0.6	0.9
Bi	ppm	ME-MS42	0.03	0.02	0.06	0.04	0.01	0.05
Hg	ppm	ME-MS42	<0.005	<0.005	0.005	<0.005	<0.005	<0.005
Sb	ppm	ME-MS42	0.05	0.07	<0.05	0.25	0.05	0.17
Se	ppm	ME-MS42	<0.2	<0.2	0.3	0.2	0.2	0.3
Te	ppm	ME-MS42	<0.01	<0.01	<0.01	0.01	<0.01	<0.01
Ag	ppm	ME-4ACD81	<0.5	<0.5	<0.5	<0.5	<0.5	<0.5

Table. 2 continues

Sample	Unit	Method code	FHM140080A	FHM140078A	FHM140090A	FHM140087A	FHM140088A	FHM140088B
N			**7492866**	**7493033**	**7486133**	**7487718**	**7487141**	**7487141**
E			**804620**	**804679**	**803332**	**799248**	**800148**	**800148**
Rock			**Sandstone**	**Sandstone**	**Sandstone**	**Sandstone**	**Sandstone**	**Sandstone**
Stratigraphic unit			**Pahakurkio group**	**Pahakurkio group**	**Pahakurkio group**	**Kalixälv group**	**Kalixälv group**	**Kalixälv group**
Cd	ppm	ME-4ACD81	<0.5	<0.5	<0.5	<0.5	<0.5	<0.5
Co	ppm	ME-4ACD81	8	14	6	10	19	21
Cu	ppm	ME-4ACD81	2	5	<1	12	4	21
Li	ppm	ME-4ACD81	20	10	20	20	30	10
Mo	ppm	ME-4ACD81	<1	1	<1	<1	<1	<1
Ni	ppm	ME-4ACD81	32	36	18	23	28	23
Pb	ppm	ME-4ACD81	<2	<2	4	<2	2	<2
Sc	ppm	ME-4ACD81	5	4	7	10	14	16
Zn	ppm	ME-4ACD81	15	9	31	16	36	35
Au	ppm	PGM-ICP23	<0.001	<0.001	<0.001	0.001	<0.001	<0.001
Cl	ppm	Cl-IC881	110	160	50	1310	690	940

Lithogeochemical analysis were conducted at ALS Minerals in 2014 & 2015 using analytical packages referred to as CCP-PKG01, PGM-ICP23, Cl-IC881.

ALS method code refers to analytical method used for each element and is described in ALS methodology factsheets at www.alsglobal.com, see also the main text.

All rocks are metamorphic, with prefix meta- to be added to the rock names.

The metasedimentary rocks record similar chondrite-normalised rare earth element (REE) patterns, enriched in light REEs over heavy REEs (Fig. 11A), with averaged values very similar to mean values for volcanic rocks in the Masugnsbyn area (Fig. 11C). A primitive mantle-normalised spider diagram shows a typical upper continental crustal signature, except for the low amounts of Sr, which are seen in both sedimentary and volcanic rocks of the Pahakurkio group (Fig. 11B, D). The normalised element pattern is characterised by enrichment in the large ion lithophile elements with a pronounced negative Nb-Ta anomaly, but also negative anomalies in Ti and P, in addition to the negative Sr anomaly in the Pahakurkio group rocks. In contrast, basalts of the Veikkavaara greenstone group show a flat REE profile, and an enriched MORB trace element signature (Fig. 11E, Lynch et al. 2018b). However, graphite schist and skarn-banded chert in the Veikkavaara group show an LREE-enriched pattern and a negative Nb-Ta anomaly, suggesting an upper continental crustal source for these sediments (Fig. 11E–F).

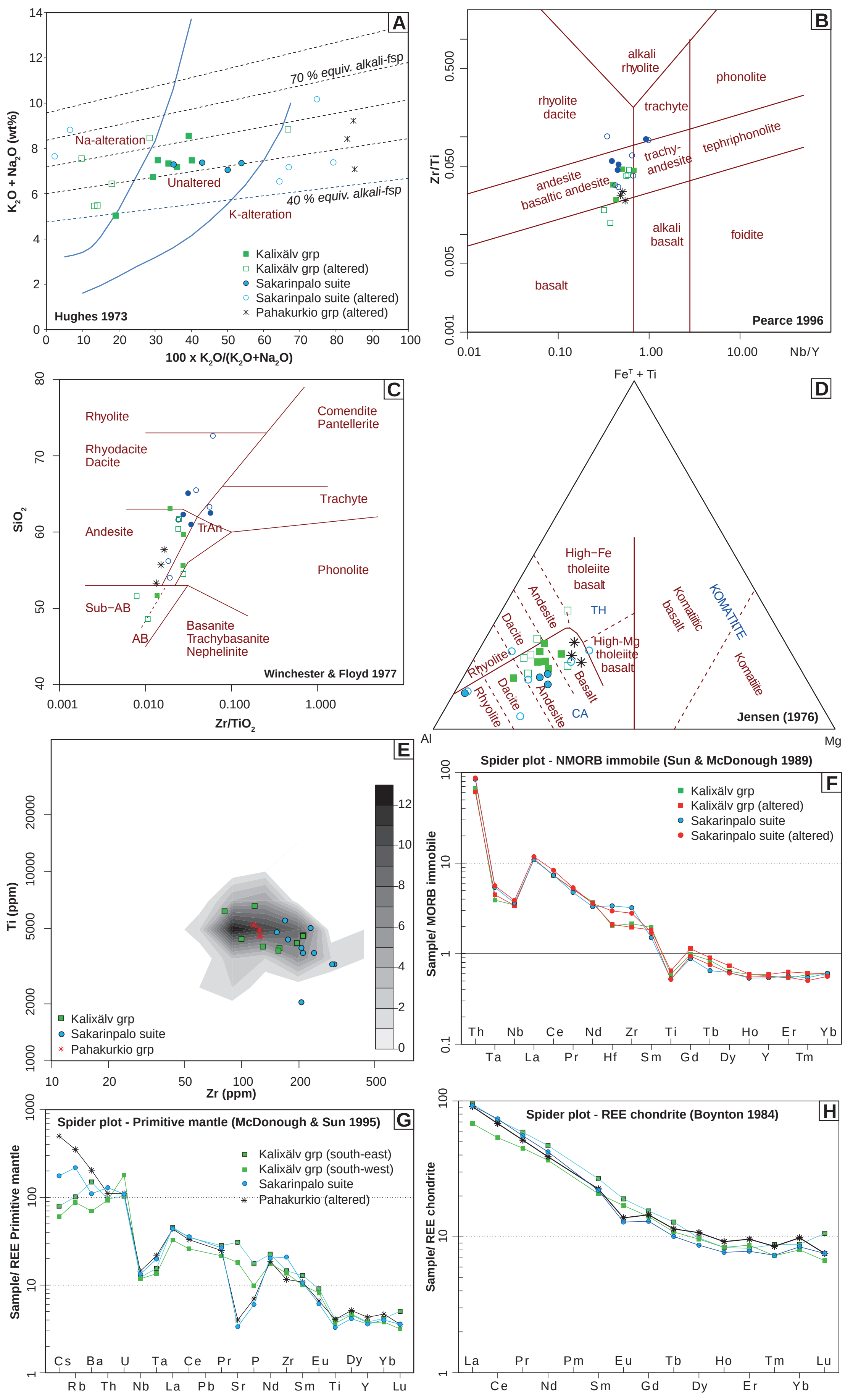
A
Na-alteration
Unaltered
K-alteration
70 % equiv. alkali-fsp
40 % equiv. alkali-fsp
Kalixälv grp
Kalixälv grp (altered)
Sakarinpalo suite
Sakarinpalo suite (altered)
Pahakurkio grp (altered)
Hughes 1973
$K_2O + Na_2O$ (wt%)
100 x $K_2O/(K_2O+Na_2O)$
B
alkali rhyolite
rhyolite dacite
trachyte
phonolite
trachy-andesite
tephriphonolite
andesite basaltic andesite
alkali basalt
foidite
basalt
Pearce 1996
Zr/Ti
Nb/Y
C
Rhyolite
Rhyodacite Dacite
Comendite Pantellerite
Trachyte
Andesite
TrAn
Phonolite
Sub-AB
AB
Basanite Trachybasanite Nephelinite
Winchester & Floyd 1977
SiO_2
Zr/TiO_2
D
Fe^T + Ti
High-Fe tholeiite basalt
TH
High-Mg tholeiite basalt
Komatiitic basalt
KOMATIITE
Komatiite
Andesite
Dacite
Rhyolite
Basalt
CA
Al
Mg
Jensen (1976)
E
Kalixälv grp
Sakarinpalo suite
Pahakurkio grp
Ti (ppm)
Zr (ppm)
F
Spider plot - NMORB immobile (Sun & McDonough 1989)
Kalixälv grp
Kalixälv grp (altered)
Sakarinpalo suite
Sakarinpalo suite (altered)
Sample/ MORB immobile
G
Spider plot - Primitive mantle (McDonough & Sun 1995)
Kalixälv grp (south-east)
Kalixälv grp (south-west)
Sakarinpalo suite
Pahakurkio (altered)
Sample/ REE Primitive mantle
H
Spider plot - REE chondrite (Boynton 1984)
Sample/ REE chondrite

◀ Figure 9. Geochemistry of metavolcanic rocks. **A.** Hughes igneous spectrum. **B.** Nb/Y – Zr/Ti classification diagram (Pearce 1996, based on Winchester and Floyd 1977). **C.** Zr/TiO_2 – SiO_2 classification diagram (Winchester & Floyd 1977). **D.** (Fe^T + Ti) – Al – Mg classification diagram (Jensen 1976). **E.** Zr – Ti diagram. Data from metavolcanic rocks classified as "Porphyrite group" in the Norrbotten ore province are shown as grey, contoured background (n = 67, SGU database). **F.** Spider plot with data normalised to normal mid-ocean ridge basalt (N-MORB, Sun & McDonough 1989), comparing averaged data from unaltered versus altered rocks of the Kalixälv group and the Sakarinpalo suite, respectively. **G.** Spider plot with mean data of groups normalised to primitive mantle (McDonough & Sun 1995). **H.** REE spider plot with averaged data of groups normalised to chondrite (Boynton 1984).

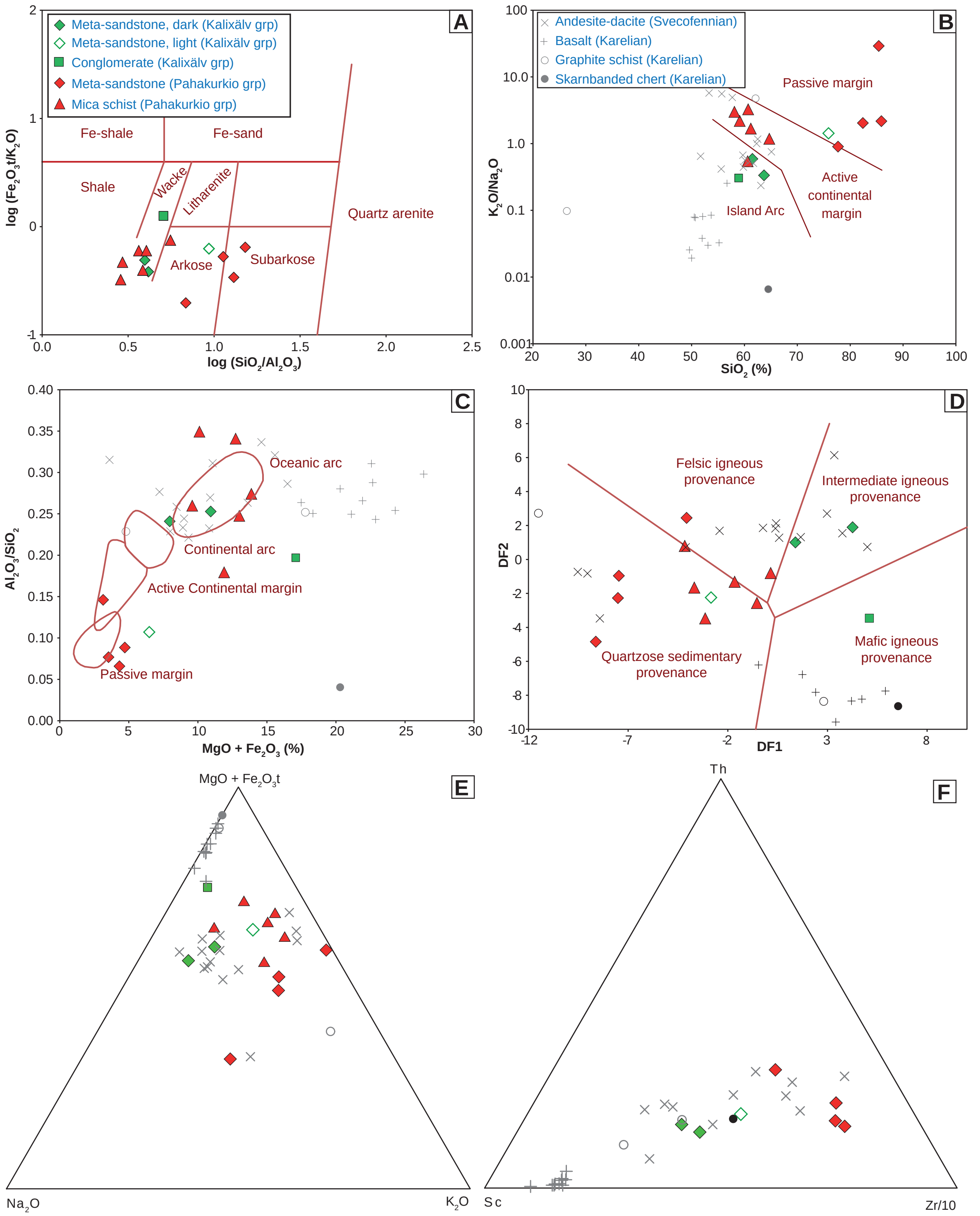

Figure 10. Geochemistry of sedimentary rocks in the Masugnsbyn area. **A.** Log(Fe_2O_3/K_2O) – log(SiO_2/Al_2O_3) classification diagram of terrigenous sandstones and shales (Herron 1988). **B.** Log(K_2O/Na_2O) – SiO_2 discrimination diagram for sandstone-mudstone suites (Roser & Korsch 1986). **C.** Al_2O_3/SiO_2 – MgO + Fe_2O_3t discrimination diagram for sandstones (Bathia 1983). **D.** DF2 – DF1 discrimination function diagram for sandstone-mudstone suites. DF1 = -1.773*TiO2+0.607*Al_2O_3+0.76*Fe_2O_3t- 1.5*MgO+0.616*CaO +0.509* Na_2O-1.224*K_2O-9.09). DF2 = 0.445*TiO_2+0.07*Al_2O_3-0.25*Fe_2O_3- 1.142*MgO+0.438*CaO +1.475*Na_2O+ 1.426*K_2O-6.861 (Roser & Korsch 1988). **E.** Na_2O – MgO+Fe_2O_3t – K_2O. F. Sc – La– Zr/10.

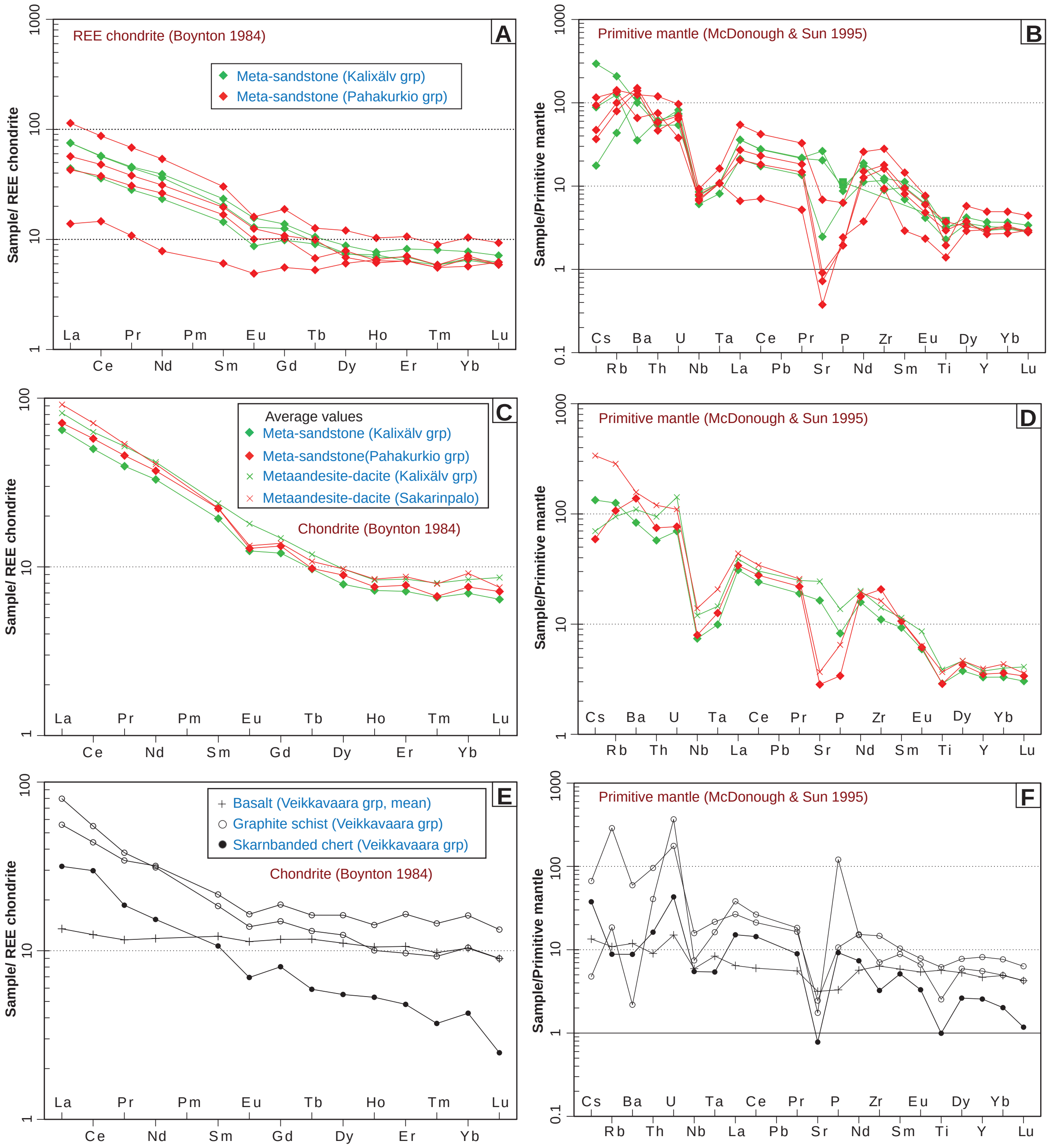

Figure 11. Trace element spider diagrams showing data on sedimentary rocks in the Masugnsbyn area. **A–B.** Spider diagram with data from meta-sandstones in the Pahakurkio and Kalixälv groups normalised to chondrite (A) and primitive mantle (B), respectively. **C–D.** Spider diagrams with averaged data from meta-sandstones in the Pahakurkio and Kalixälv groups normalised to chondrite (C) and primitive mantle (D), respectively. Averaged values of Svecofennian volcanic rocks from Masugnsbyn are shown for comparison. **E–F.** Spider diagrams with data on the Veikkavaara greenstone group rocks normalised to chondrite (E) and primitive mantle (F), respectively, for comparison of trace element patterns with the Svecofennian rocks above.

Geochronology

Methods

SIMS analysis

Zircons were obtained from a density separate of a crushed rock sample using a Wilfley water table. Magnetic minerals were removed with a hand magnet. Handpicked crystals were mounted in transparent epoxy resin together with chips of the reference zircon 91500. The zircon mounts were polished and, after gold coating, examined by Back Scattered Electron (BSE) and Cathodoluminescence (CL) imaging using electron microscopy at EBC, Uppsala University and at the Swedish Museum of Natural History in Stockholm. High-spatial resolution secondary ion mass spectrometer (SIMS) analysis was carried out in November and December 2014 using a Cameca IMS 1280 at the Nordsim facility at the Swedish Museum of Natural History in Stockholm. Detailed descriptions of the analytical procedures are given in Whitehouse et al. (1997, 1999), and Whitehouse & Kamber (2005). An approximately 6 nA O^{2-} primary ion beam was used, yielding spot sizes of approximately 15 µm. Pb/U ratios, elemental concentrations and Th/U ratios were calibrated relative to the Geostandards zircon 91500 reference, which has an age of approximately 1065 Ma (Wiedenbeck et al. 1995, 2004). Common Pb-corrected isotope values were calculated using modern common Pb composition (Stacey & Kramers 1975), and measured ^{204}Pb where the ^{204}Pb count exceeded the detection limit. Decay constants follow the recommendations of Steiger & Jäger (1977). Diagrams and age calculations of isotopic data were made using Isoplot 4.15 software (Ludwig 2012). CL imaging using electron microscopy was also carried out after the SIMS analysis at the Swedish Museum of Natural History in Stockholm to confirm the location of analysed spots.

Laser ablation ICP-MS analysis

Zircon U-Pb geochronology was carried out on mineral separates embedded in epoxy mounts by laser ablation inductively coupled plasma mass spectrometry (LA-ICP-MS) at the Geological Survey of Denmark and Greenland (GEUS). An NWR213 frequency-quintupled solid state Nd:YAG laser system from New Wave Research/ESI mounted with a TV2 ablation cell was coupled to an ELEMENT 2 double-focusing single-collector magnetic sector-field ICPMS from Thermo-Fisher Scientific. The mass spectrometer was equipped with a Fassel-type quartz torch shielded with a grounded Pt electrode and a quartz bonnet. To ensure stable laser output energy, a laser warm-up time of ~15 minutes was used before operation, providing stable laser power and flat ablation craters from a "resonator-flat" laser beam. The mass spectrometer was run for at least one hour before analyses to stabilise the background signal. Before loading, samples and standards were carefully cleaned with ethanol to remove surface contamination. After insertion, the ablation cell was flushed with helium gas to minimise gas blank level. The ablated material was swept by the helium carrier gas and mixed with argon (sample) gas of the spectrometer approximately 0.5 m before entering the plasma in the mass spectrometer. Immediately before the analyses, the ICP-MS was optimised for dry plasma conditions by continuous linear ablation of the GJ-1 zircon standard. The signal-to-noise ratios for the heavy mass range of interest (i.e. from ^{202}Hg to ^{238}U), emphasising ^{238}U and ^{206}Pb, were maximised, while opting for low element-oxide production levels by minimising the $^{254}UO_2/^{238}U$ ratio. To minimise instrumental drift, a standard-sample-standard analysis protocol was followed, bracketing eight sample analyses by six measurements of the Geostandards zircon 91500 reference. The GJ-1 (Jackson et al. 2004) and Plesovice (Slama et al. 2008) reference zircons were used for quality control of the standard analyses, and yield average age accuracies and precisions of < 3%. Data were acquired from single spot analysis of 25 µm, using nominal laser fluence of ~10 J/cm^2 and a pulse rate of 10 Hz. Total acquisition time for a single analysis was maximum 1.5 minutes, including 30-second gas blank measurement followed by laser ablation for 30 seconds and washout for 20 seconds. Factory-supplied software was used to acquire transient data, obtained through automated running mode of pre-set analytical locations. Data reduction and calculation of ratios and ages were performed offline using Iolite software (Hellstrom et al. 2008, Paton et al. 2011), using the Iolite-integral VizualAge DRS data reduction scheme (Petrus & Kamber 2012). This DRS includes a correction routine for down-hole isotopic fractionation (Paton et al. 2010), and provides procedures for data requiring correction for common Pb.

Sample description and analytical results

Geochronology sample data are summarised in Table 3.

Feldspar porphyric, intermediate metavolcanic rock (FHM140069), Sakarinpalo suite

The rock sampled for dating is a sparsely feldspar porphyric, intermediate metavolcanic rock with 1–2 mm feldspar phenocrysts in a fine-grained matrix (Fig. 3, 12A). The thin section shows a recrystallised, granular, polygonal texture, in which phenocrysts are partly recrystallised to aggregates (Fig. 12C). Parallel-oriented, dispersed grains of biotite define a foliation. The groundmass is dominated by K-feldspar, plagioclase, quartz and biotite, with subordinate amounts of opaques and muscovite, the latter also occurring as veins. There are trace amounts of apatite, zircon and tourmaline. The heavy mineral separate is rich in transparent zircon, mostly with subhedral, prismatic crystal shapes. CL imaging shows a well-developed oscillatory zonation, in some grains apparently forming as different generations (Fig. 12E). However, analyses reveal no age difference between different textural domains. A total of 13 zircon analyses were performed. These contain 81–207 ppm uranium and have rather uniform Th/U ratios of 0.42–0.85 (Table 4). All analyses are concordant and record a concordia age of 1 890 ±5 Ma (Fig. 12G, 2σ, n = 13, MSWD of concordance. + equivalence = 1.2, probability of concordance + equivalence = 0.22).

The $^{207}Pb/^{206}Pb$-weighted mean age is 1 887 ±6 Ma (2σ, MSWD = 1.4, probability = 0.18, n = 13), i.e. within error the same age as the concordia age. The Concordia age is chosen as the best age estimate, interpreted to date igneous crystallisation of the metavolcanic rocks of the Sakarinpalo suite at approximately 1.89 Ga.

Feldspar porphyritic meta-andesite (FHM140084B), Kalixälv group

A feldspar porphyritic meta-andesite was sampled approximately 1 km up-section to the basal conglomerate in the Kalixälv group. The meta-andesite has a high magnetic susceptibility and the outcrop spatially coincides with a north–south-trending, positive magnetic anomaly that continues southwards beyond the river. The rock is grey and contains 1–2 mm plagioclase phenocrysts in a fine-grained matrix of plagioclase, microcline and quartz, with subordinate amounts of magnetite, biotite, green pleochroic hornblende and titanite with traces of zircon (Fig. 12B, D). The plagioclase is partly sericite-altered and contains calcite and very fine opaques.

Table 3. Summary of geochronology sample data.

Sample	Lab-id	Rock type	Stratigraphic unit	N	S	Locality	U-Pb dating	Nd
FHM140069A	n5164	Andesite	Sakarinpalo suite	7502412	803618	Pahtajänkkä	Nordsim, NRM	x
FHM140084B	n5174	Andesite	Kalixälv group	7487854	799400	Sarikoski	Nordsim, NRM	x
FHM140078A		Sandstone (sub-arkose)	Pahakurkio group	7493033	804679	Hietajoki	LA ICP-MS; GEUS	x
FHM140088B		Sandstone (intermediate)	Kalixälv group	7487141	800148	Sarikoski	LA ICP-MS; GEUS	x
RR96128	n1383	Sandstone (sub-arkose)	Pahakurkio group	7486200	803000	Pahakurkio	Nordsim, NRM	

Nd = Sm-Nd isotopic analyses performed at GTK lab, Espoo, Finland.

All rocks are metamorphic with prefix meta- to be added to rock name.

► Figure 12. Geochronology of metavolcanic rocks from the Sakarinpalo suite and the Kalixälv groups. **A.** Dated sample of feldspar porphyric meta-andesite from the Sakarinpalo suite northeast of Masugnsbyn (FHM140069A; (7502412 / 803618). **B.** Dated sample of feldspar porphyric meta-andesite from the Kalixälv group (FHM140084B; 7487854 / 799400). **C–D.** Thin section cross-polarised light views of dated volcanic samples. **E–F.** Cathodoluminescence (CL) images of dated zircons from sample FHM140069A and Back-scattered electron (BSE) images of analysed zircon from FHM140084B. Ellipses mark the locations of analyses. Numbers refer to analytical spot number in Table 4. **G–H.** Tera Wasserburg diagram showing U-Pb SIMS data of zircon. Error ellipse of calculated weighted mean age is shown in red. Coordinates are given in SWEREF 99TM.

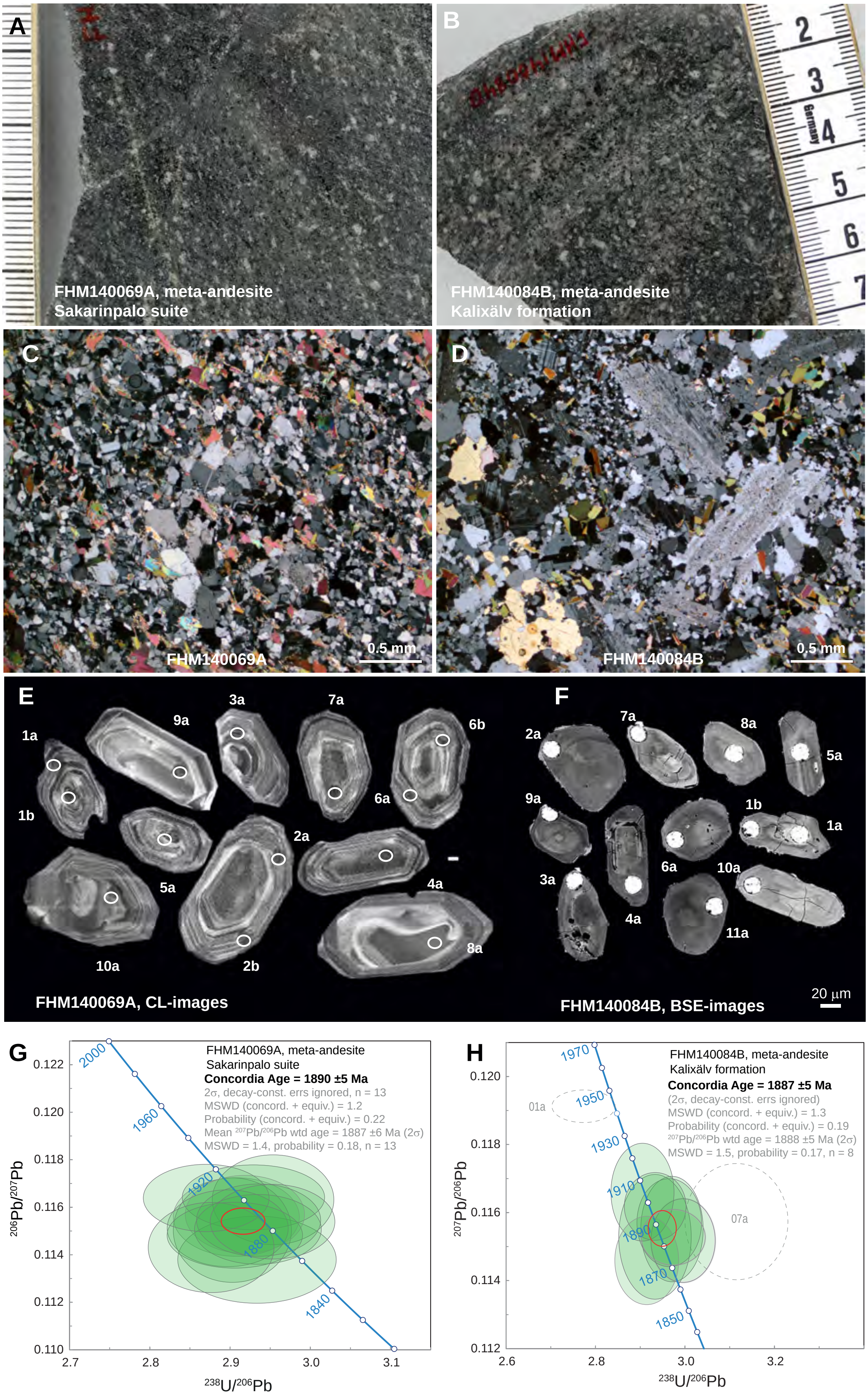
A
FHM140069A, meta-andesite
Sakarinpalo suite
B
FHM140084B, meta-andesite
Kalixälv formation
C
FHM140069A
0.5 mm
D
FHM140084B
0,5 mm
E
FHM140069A, CL-images
F
FHM140084B, BSE-images
20 µm
G
FHM140069A, meta-andesite
Sakarinpalo suite
Concordia Age = 1890 ±5 Ma
2σ, decay-const. errs ignored, n = 13
MSWD (concord. + equiv.) = 1.2
Probability (concord. + equiv.) = 0.22
Mean 207Pb/206Pb wtd age = 1887 ±6 Ma (2σ)
MSWD = 1.4, probability = 0.18, n = 13
206Pb/207Pb
238U/206Pb
H
FHM140084B, meta-andesite
Kalixälv formation
Concordia Age = 1887 ±5 Ma
(2σ, decay-const. errs ignored)
MSWD (concord. + equiv.) = 1.3
Probability (concord. + equiv.) = 0.19
207Pb/206Pb wtd age = 1888 ±5 Ma (2σ)
MSWD = 1.5, probability = 0.17, n = 8
01a
07a
207Pb/206Pb
238U/206Pb

Table 4. SIMS U-Pb-Th zircon data meta-andesite samples (FHM140069A, laboratory id n5164; FHM140084B, laboratory id n5174).

Sample/ spot #	U ppm	Th ppm	Pb ppm	Th/U calc *1	$^{207}Pb/^{235}U$	±σ %	$^{208}Pb/^{232}Th$	±σ %	$^{238}U/^{206}Pb$	±σ %	$^{207}Pb/^{206}Pb$	±σ %	ρ *2	Disc. % conv. *3	Disc. % 2σ lim. *4	$^{207}Pb/^{206}Pb$	±σ Ma	$^{206}Pb/^{238}U$	±σ Ma	$^{206}Pb/^{204}Pb$ measured	f_{206}% *5
FHM140069A, meta-andesite, Sakarinpalo suite																					
n5164_01a	163	73	69	0.45	5.431	1.24	0.0988	2.18	2.954	1.05	0.1163	0.66	0.84	-1.3		1901	12	1880	17	100393	{0.02}
n5164_01b	164	127	75	0.80	5.424	1.20	0.1014	3.34	2.935	1.08	0.1155	0.54	0.89	0.2		1887	10	1890	18	38105	{0.05}
n5164_10a	137	59	59	0.45	5.592	1.22	0.1048	2.22	2.870	1.12	0.1164	0.50	0.91	1.5		1902	9	1927	19	>1e6	{0.00}
n5164_2a	111	50	48	0.47	5.465	1.30	0.1008	2.32	2.903	1.04	0.1151	0.78	0.80	1.7		1881	14	1908	17	313475	{0.01}
n5164_2b	123	53	52	0.44	5.389	1.21	0.1002	2.37	2.953	1.07	0.1154	0.56	0.89	-0.4		1886	10	1880	18	95390	{0.02}
n5164_3a	82	43	36	0.55	5.480	1.30	0.1010	2.32	2.876	1.11	0.1143	0.68	0.85	3.4		1869	12	1923	19	29637	{0.06}
n5164_4a	207	168	96	0.85	5.481	1.33	0.1031	2.39	2.929	1.24	0.1164	0.48	0.93	-0.5		1902	9	1893	20	76620	{0.02}
n5164_5a	108	70	48	0.67	5.467	1.19	0.1018	2.29	2.918	1.04	0.1157	0.58	0.87	0.5		1891	10	1899	17	769102	{0.00}
n5164_6a	131	58	56	0.45	5.407	1.22	0.0999	2.28	2.935	1.10	0.1151	0.52	0.90	0.6		1881	9	1890	18	>1e6	{0.00}
n5164_6b	133	55	57	0.42	5.479	1.21	0.0991	2.37	2.897	1.06	0.1151	0.57	0.88	1.8		1882	10	1912	18	110242	{0.02}
n5164_7a	148	92	66	0.64	5.449	1.28	0.1007	2.47	2.906	1.19	0.1148	0.49	0.92	1.8		1877	9	1907	20	>1e6	{0.00}
n5164_8a	104	46	44	0.44	5.482	1.25	0.0979	2.32	2.908	1.10	0.1156	0.58	0.88	1.0		1889	10	1905	18	41467	{0.05}
n5164_9a	81	55	36	0.72	5.349	1.52	0.1011	3.99	2.933	1.37	0.1138	0.66	0.90	1.9		1861	12	1891	23	215686	{0.01}
FHM140084B, meta-andesite, Kalixälv formation																					
n5174_01b	206	101	88	0.52	5.362	1.10	0.1044	2.24	2.971	0.96	0.1155	0.55	0.87	-1.1		1888	10	1870	16	43645	{0.04}
n5174_02a	99	54	43	0.59	5.420	1.30	0.1056	2.30	2.933	1.13	0.1153	0.65	0.87	0.4		1885	12	1891	19	97302	{0.02}
n5174_03a	151	82	64	0.53	5.301	1.07	0.0947	2.24	2.996	0.98	0.1152	0.44	0.91	-1.6		1883	8	1857	16	12176	0.15
n5174_04a	159	73	67	0.47	5.382	1.10	0.1003	2.16	2.965	1.00	0.1157	0.46	0.91	-1.1		1891	8	1874	16	>1e6	{0.00}
n5174_05a	157	103	71	0.68	5.535	1.11	0.1020	2.07	2.905	0.99	0.1166	0.50	0.89	0.1		1905	9	1907	16	262349	{0.01}
n5174_06a	138	64	60	0.51	5.422	1.10	0.1064	2.13	2.914	1.00	0.1146	0.46	0.91	1.7		1874	8	1902	16	57614	{0.03}
n5174_07a	296	53	108	0.09	5.123	1.63	0.0485	5.55	3.115	1.51	0.1157	0.60	0.93	-5.9	-1.9	1891	11	1795	24	6314	0.30
n5174_08a	211	140	95	0.68	5.461	1.02	0.1015	2.07	2.933	0.96	0.1162	0.35	0.94	-0.4		1898	6	1891	16	>1e6	{0.00}
n5174_09a	287	521	92	0.39	3.894	2.96	0.0201	4.31	3.943	2.87	0.1114	0.73	0.97	-22.3	-16.8	1822	13	1457	38	2655	0.70
n5174_10a	188	145	74	0.51	4.943	1.13	0.0647	2.45	3.231	1.01	0.1158	0.51	0.89	-9.3	-6.4	1893	9	1738	15	4565	0.41
n5174_11a	294	161	126	0.54	5.345	1.02	0.0972	2.12	2.974	0.98	0.1153	0.29	0.96	-0.9		1884	5	1869	16	>1e6	{0.00}

Isotope values are common Pb corrected using modern common Pb composition (Stacey & Kramers 1975) and measured ^{204}Pb.

*1 Th/U ratios calculated from $^{208}Pb/^{206}Pb$ and $^{207}Pb/^{206}Pb$ ratios, assuming a single stage of closed U-Th-Pb evolution

*2 Error correlation in conventional concordia space. Do not use for Tera-Wasserburg plots.

*3 Age discordance in conventional concordia space. Positive numbers are reverse discordant.

*4 Age discordance at closest approach of error ellipse to concordia (2σ level).

*5 Figures in parentheses are given when no correction has been applied, and indicate a value calculated assuming present-day Stacey-Kramers common Pb.

The heavy mineral concentrate is rich in titanite, but there are also small amounts of weakly coloured, greyish and transparent zircon with subhedral to euhedral crystal shapes. Microfractures and inclusions are common. Back-scattered (BSE) imaging shows an internal oscillatory zonation in the zircon, and textural older cores are evident in some grains (Fig. 12F). Altogether, 11 zircon analyses were performed. These contain 99–296 ppm uranium and have rather uniform Th/U ratios of 0.39–0.68, except analysis 7a, which has a ratio of 0.09 (Table 4). Two discordant analyses (9a, 10a) have high values for common lead and are excluded from the age calculations. One analysis (1a) located in an textural older core, records an older age of approximately 1.91 Ga, compared with the other analyses, and is interpreted as inherited. Eight analyses are concordant and record a concordia age of 1 887 ±5 Ma (Fig. 12H, 2σ, MSWD of concord. + equiv. = 1.3, probability (concord. + equiv.) = 0.19, n = 8). The $^{207}Pb/^{206}Pb$-weighted mean age is 1 888 ±5 Ma (2σ, MSWD = 1.5, probability = 0.17, n = 8) or 1 889 ±5 Ma including the discordant analysis 7a (MSWD = 1.3, probability = 0.2, n = 9). The concordia age of 1 887 ±5 Ma is chosen as the best age estimate and is interpreted to date igneous crystallisation of the meta-andesite.

Meta-sandstone (FHM140078A), lower sandstone unit Pahakurkio group
A subarkosic meta-sandstone was sampled from the lower sandstone unit in the Pahakurkio group (Fig. 2), approximately 300 m west of the contact with the dolomite of the Veikkavaara greenstone group (Fig. 3). The outcrop at the sampled locality shows a planar bedded meta-arkose, with thin, 1-mm-wide laminas enriched in heavy minerals. The bedding dips steeply eastwards with cross-bedding in the unit showing way-up towards the east. 20 metres above (west of) the sampled rock is a approximately 20 m wide, highly magnetic, skarn-banded rock unit of intermediate composition, possibly of volcanic origin, as suggested by its similar chemical composition to volcanic rocks in Masugnsbyn. The meta-subarkose is dominated by quartz, usually with finer-grained feldspar (microcline and plagioclase). Biotite occurs between the quartz grains in a polygonal to seriate recrystallised texture (Fig. 13A, C). Some feldspar grains are of a similar size to the quartz grains. Parallel-oriented, dispersed grains of biotite define a foliation. There are larger grains of ilmenite enriched in laminas, together with other heavy minerals, rutile (?) and zircon.

The heavy mineral concentrate is rich in zircon, rounded, anhedral to subhedral, colourless transparent to brownish turbid. Ilmenite, rutile, tourmaline, and possibly garnet were also recovered. BSE images show zircons to have variable internal structures, many grains with oscillatory or patchy zonation (Fig. 14A). Some grains contain clearly xenocrystic cores and some have homogenous BSE-bright outer domains. Microcracks in the zircon are common and many grains show irregular BSE-dark, probably metamict domains. Altogether, 149 zircon analyses were carried out. 104 of these were less than 5% discordant and selected for plotting in the age distribution diagram (Table 5, Fig. 14C–D). The zircon age population is dominated by 2.15–1.90 Ga Karelian–Svecofennian ages (66% of the entire zircon population) and 2.95–2.62 Ga Archaean ages (30%), with a few results outside these ranges. Two analyses have ages at 2.44 & 2.50 Ga (2%) and a single analysis is dated at approximately 3.29 Ga (1%). The younger age group peaks at 2.04 Ga, with a smaller peak at 1.92 Ga (Fig. 14C). The nine youngest zircons give a $^{207}Pb/^{206}Pb$-weighted mean age of 1 911 ±10 Ma (Fig. 14F, MSWD = 0.14, probability = 0.997), suggesting a maximum depositional age of Pahakurkio group sedimentary rocks of approximately 1.91 Ga.

Meta-sandstone (RR96128), upper sandstone unit, Pahakurkio group
A meta-sandstone was previously sampled by Roy Rutland in the upper sandstone unit of the Pahakurkio group, upstream of the Pahakurkio rapids on the river Kalixälven. The locality contains flat-lying ripple- and rill-marked meta-sandstones of subarkosic composition. Zircons from this sample were previously dated at Nordsim in 2004. 13 analyses from 8 zircon grains were carried out. These contain 101–793 ppm U and Th/U ratios of 0.26–0.99, except two CL-dark rim analyses, which have Th/U

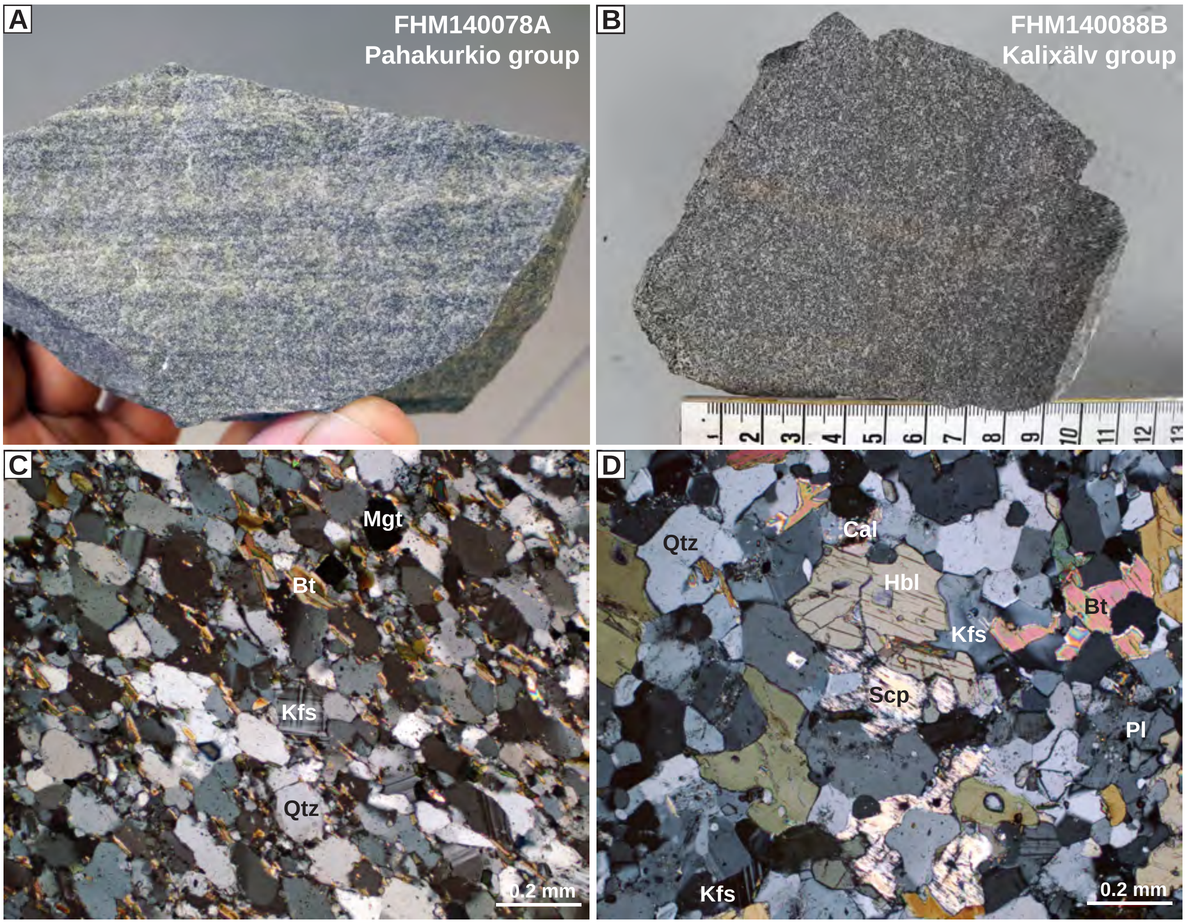

Figure 13. Provenance geochronology of meta-sandstones of the Pahakurkio and the Kalixälv groups. **A–B.** Dated samples of meta-sandstone from the Pahakurkio group (A, sub-arkose) and Kalixälv group (B, intermediate amphibole-bearing). **C–D.** Photomicrographs in cross-polarised light of dated samples of meta-sandstones from the Pahakurkio group (C) and the Kalixälv group (D).

ratios of 0.06 and 0.09 (Table 6). The analyses are concordant or weakly discordant at the two-sigma error level, with low amounts of common lead. Although a very limited number of analyses were made, these give similar age results to the dated sample from the lower sandstone unit. The $^{207}Pb/^{206}Pb$ zircon ages range from 1.89 to 2.09 Ga, with one analysis at 2.65 Ga (Fig. 15). The three youngest zircons give a $^{207}Pb/^{206}Pb$-weighted mean age of 1896 ±10 Ma (Fig. 15), suggesting a maximum depositional age of approximately 1.90 Ga, i.e. similar to the lower Pahakurkio sandstone unit.

► Figure 14. Provenance geochronology of meta-sandstones of the Pahakurkio and Kalixälv groups. **A–B.** Selection of BSE-images of dated zircons from the two provenance samples. **C.** Probability density diagram showing $^{207}Pb/^{206}Pb$ zircon age spectra (<5% discordant) from the Pahakurkio group sample (red) and Kalixälv group sample (green). n = number of zircon analyses measured in each sample used to construct the curves in the diagram. >5% discordant analyses are excluded; see Table 5. **D–E.** Diagrams showing <5% discordant $^{207}Pb/^{206}Pb$ zircon ages from the Pahakurkio group sample(D) and the Kalixälv group sample (E). **F–G.** Estimated maximum depositional ages from the youngest group of zircon analyses from the Pahakurkio meta-sandstone (F) and the Kalixälv meta-sandstone (G). The three youngest ages from the Kalixälv group sample were excluded from the maximum depositional age calculation, assuming secondary partial resetting of the U-Pb isotopic system in these.

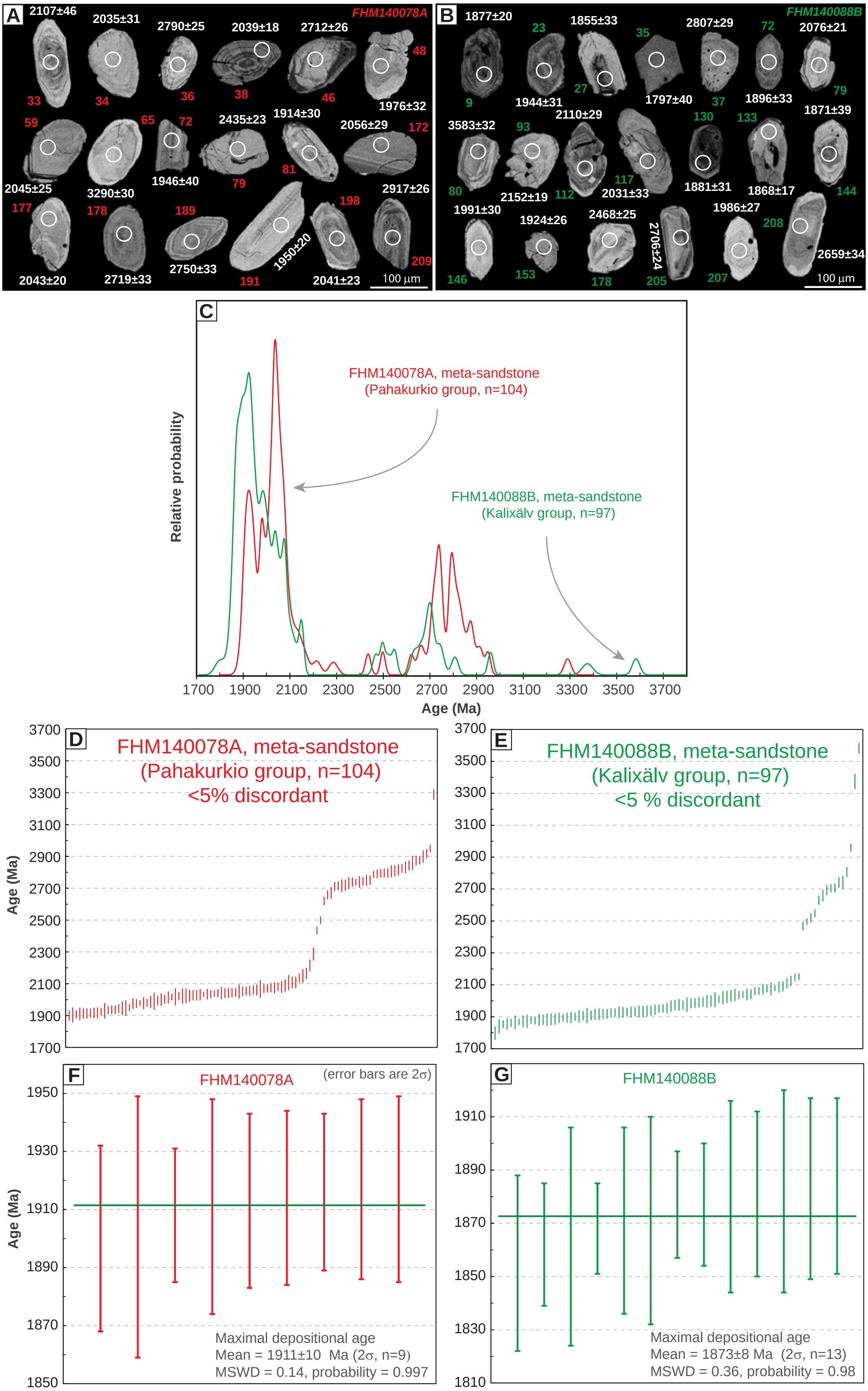
A
FHM140078A
B
FHM140088B
C
Relative probability
FHM140078A, meta-sandstone
(Pahakurkio group, n=104)
FHM140088B, meta-sandstone
(Kalixälv group, n=97)
Age (Ma)
D
FHM140078A, meta-sandstone
(Pahakurkio group, n=104)
<5% discordant
E
FHM140088B, meta-sandstone
(Kalixälv group, n=97)
<5 % discordant
F
FHM140078A
(error bars are 2σ)
Maximal depositional age
Mean = 1911±10 Ma (2σ, n=9)
MSWD = 0.14, probability = 0.997
G
FHM140088B
Maximal depositional age
Mean = 1873±8 Ma (2σ, n=13)
MSWD = 0.36, probability = 0.98

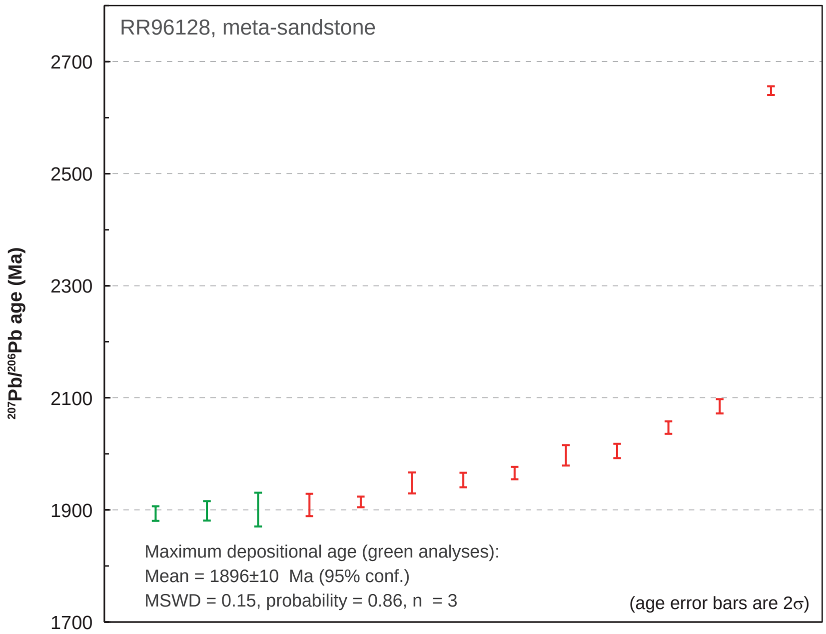

Figure 15. Diagram showing U-Pb SIMS data on a meta-sandstone sample from the upper part of Pahakurkio group. A maximum depositional age is calculated from the three youngest zircons (in green).

Meta-sandstone (FHM140088B), Kalixälv group

A cross-bedded, amphibole-bearing meta-sandstone was sampled immediately above the basal conglomerate, approximately 250 m west of the contact with the Pahakurkio group (Fig. 2–3, 13B). The rock is fine-grained with a recrystallised evenly-grained, polygonal texture, but grains of hornblende tend to be slightly larger (Fig. 13D). The main minerals are quartz, K-feldspar, plagioclase, green hornblende and biotite, with subordinate amounts of cordierite and calcite, the latter interstitial between quartz grains. Accessory phases are epidote, monazite, zircon, magnetite and fluorite. A few metres above the sampled rock is a laminated (1–10 mm) cordierite, quartz, and hornblende meta-sandstone, where magnetite-rich laminas alternate with laminates with subordinate amounts of opaques (Fig. 8C). Other layers consist of larger proportions of quartz, K-feldspar and amphibole, with subordinate amounts of biotite and cordierite.

The heavy mineral concentrate is rich in zircon, with subhedral to rounded, anhedral crystal shapes, generally with better developed crystal shapes than in the Pahakurkio group sample. Some grains of monazite, amphibole and magnetite are also seen. BSE images show variable internal structures, many grains showing oscillatory or patchy zonation (Fig. 14B). Some grains have clearly xenocrystic cores. Microcracks in the zircons are common and many grains show BSE-dark, probably metamict domains. 149 zircon analyses were carried out. 92 analyses of these were less than 5% discordant and selected for plotting in the age distribution diagram (Table 5, Fig. 14C, E). This sample shows a similar age distribution to the Pahakurkio meta-sandstone sample (FHM140078), but generally trends towards somewhat younger ages (Fig. 14C). The zircon age population is dominated by 2.15–1.86 Ga ages (81%) and 2.96–2.55 Ga ages (11%), with a few analyses outside these ranges. Two analyses have ages of approximately 3.38 and 3.58 Ga (2%), three analyses of 2.52–2.47 Ga (3%) and three of approximately 1.85–1.84 and 1.80 Ga (3%). The significance of young ages is uncertain, but they may reflect secondary partial resetting of the U-Pb isotopic system, or lab contamination. The youngest zircon (no 35, Fig. 14B) is homogenous BSE-dark. Excluding this, the second and third-youngest zircons (no 63, 111), the $^{207}Pb/^{206}Pb$-weighted mean age of the 13 youngest analyses is 1 873 ±8 Ma (Fig. 14G). Including analyses 63 and 111 marginally lowers the mean age to 1 870 ±7 Ma. The maximum depositional age is estimated to be approximately 1.87 Ga.

Table 5. Laser ICP-MS U-Pb zircon provenance data of Pahakurkio group, lower sandstone sample (FHM140078A), and Kalixälv group intermediate sandstone sample (FHM140088B).

Analysis	Concentrations (ppm)[a]						Ratios								Ages (Ma)						CONC.
No	U	2 σ	Th	2 σ	Pb	2 σ	U/Th[a]	$^{207}Pb/^{235}U$[b]	2 σ[d]	$^{206}Pb/^{238}U$[b]	2 σ[d]	rho[c]	$^{207}Pb/^{206}Pb$[e]	2 σ[d]	$^{207}Pb/^{235}U$[b]	2 σ[d]	$^{206}Pb/^{238}U$[b]	2 σ[d]	$^{207}Pb/^{206}Pb$[e]	2 σ[d]	%
FHM140078A, meta-sandstone, Pahakurkio group																					
7	150	12	35	3	444	30	4.4	17.110	0.420	0.602	0.015	0.733	0.2086	0.0047	2940	24	3038	61	2892	37	105
8	272	47	58	8	418	53	5.3	5.960	0.110	0.368	0.009	0.847	0.1173	0.0016	1970	15	2018	40	1915	24	105
10	218	6	245	12	2210	140	0.9	6.550	0.210	0.369	0.016	0.858	0.1308	0.0026	2052	28	2024	75	2108	34	96
11	710	160	245	31	1800	330	3.1	6.060	0.160	0.356	0.011	0.915	0.1233	0.0019	1983	23	1964	52	2003	27	98
12	472	70	157	11	1120	140	3.1	6.030	0.150	0.373	0.009	0.882	0.1173	0.0010	1980	21	2041	42	1915	16	107
13	773	52	177	18	1830	190	4.7	11.780	0.300	0.465	0.014	0.815	0.1817	0.0028	2585	24	2458	62	2667	26	92
14	294	16	17	1	162	12	17.1	6.420	0.130	0.358	0.007	0.717	0.1283	0.0019	2034	18	1973	32	2074	26	95
15	919	64	283	31	2220	200	3.4	5.575	0.084	0.344	0.011	0.740	0.1167	0.0029	1912	13	1903	54	1904	45	100
16	590	100	166	34	1790	330	3.6	11.260	0.240	0.494	0.015	0.808	0.1641	0.0020	2544	20	2588	63	2498	21	104
20	700	130	287	70	2730	690	2.5	9.320	0.750	0.418	0.031	0.973	0.1606	0.0041	2354	84	2240	150	2459	43	91
21	259	15	17	2	203	27	15.5	14.980	0.200	0.540	0.013	0.706	0.1989	0.0040	2814	13	2797	50	2815	32	99
24	193	34	162	33	610	63	1.5	13.410	0.410	0.492	0.017	0.800	0.1922	0.0043	2707	29	2576	75	2776	36	93
25	348	24	23	1	280	18	14.6	14.860	0.390	0.536	0.017	0.818	0.2023	0.0034	2805	25	2763	72	2843	28	97
26	442	57	72	7	645	54	6.0	7.260	0.260	0.406	0.015	0.929	0.1286	0.0013	2142	33	2194	70	2079	17	106
27	607	64	59	11	499	99	11.3	6.480	0.110	0.364	0.007	0.719	0.1280	0.0019	2047	14	1998	34	2070	25	97
28	331	38	73	8	571	75	4.3	6.550	0.240	0.365	0.013	0.897	0.1294	0.0027	2051	32	2003	61	2088	36	96
33	193	29	18	3	151	20	11.4	7.150	0.240	0.395	0.016	0.587	0.1309	0.0034	2127	31	2144	75	2107	46	102
34	383	24	58	2	473	15	6.7	6.530	0.150	0.377	0.010	0.721	0.1256	0.0022	2050	20	2060	49	2035	31	101
35	263	35	107	8	797	44	2.5	5.440	0.130	0.329	0.012	0.866	0.1199	0.0025	1890	21	1832	57	1962	35	93
36	384	52	105	10	1080	140	3.7	13.820	0.440	0.514	0.017	0.913	0.1958	0.0030	2735	31	2673	71	2790	25	96
37	312	31	117	13	829	92	2.6	6.670	0.130	0.385	0.009	0.910	0.1253	0.0010	2068	17	2099	39	2033	14	103
38	397	33	59	4	418	36	7.0	6.360	0.180	0.361	0.010	0.960	0.1258	0.0013	2025	24	1985	47	2039	18	97
40	347	39	103	19	1060	200	3.9	13.880	0.390	0.527	0.015	0.805	0.1894	0.0030	2740	27	2727	62	2751	27	99
41	186	16	65	3	491	25	2.9	5.480	0.220	0.340	0.015	0.871	0.1177	0.0033	1895	35	1886	74	1931	47	98
42	393	44	73	9	546	61	5.6	6.900	0.230	0.392	0.015	0.947	0.1283	0.0023	2097	29	2129	69	2074	32	103
46	458	52	108	13	1310	150	3.9	13.100	0.470	0.509	0.018	0.868	0.1867	0.0029	2684	34	2649	79	2712	26	98
48	133	18	25	4	207	31	5.0	5.800	0.190	0.347	0.013	0.875	0.1215	0.0022	1944	30	1919	61	1976	32	97
49	295	33	86	6	974	52	3.2	12.430	0.480	0.497	0.019	0.901	0.1806	0.0030	2634	37	2599	81	2658	27	98
52	1400	140	469	91	6100	1500	3.2	11.270	0.380	0.432	0.016	0.892	0.1874	0.0043	2544	31	2313	71	2717	38	85
53	129	10	45	4	372	47	2.8	7.510	0.530	0.339	0.028	0.935	0.1614	0.0038	2169	64	1880	140	2468	40	76
59	259	17	26	3	211	17	10.8	6.540	0.190	0.372	0.011	0.865	0.1262	0.0018	2050	26	2036	52	2045	25	100
60	436	46	205	28	2260	330	2.3	14.350	0.390	0.537	0.016	0.848	0.1955	0.0032	2771	26	2771	67	2794	25	99
61	209	20	100	8	1086	95	2.2	13.510	0.300	0.521	0.014	0.762	0.1896	0.0031	2715	21	2700	60	2738	27	99
62	141	20	69	9	606	82	2.2	7.320	0.160	0.391	0.009	0.624	0.1353	0.0026	2150	19	2128	40	2165	34	98
63	255	35	35	7	285	46	7.2	6.430	0.290	0.378	0.018	0.902	0.1245	0.0019	2041	43	2083	81	2028	30	103
64	630	160	177	54	1080	340	4.1	5.750	0.310	0.351	0.018	0.994	0.1187	0.0016	1935	49	1939	87	1937	25	100

Table 5 continues

Analysis	Concentrations (ppm)[a]						Ratios								Ages (Ma)						CONC.
No	U	2 σ	Th	2 σ	Pb	2 σ	U/Th[a]	$^{207}Pb/^{235}U$[b]	2 σ[d]	$^{206}Pb/^{238}U$[b]	2 σ[d]	rho[c]	$^{207}Pb/^{206}Pb$[e]	2 σ[d]	$^{207}Pb/^{235}U$[b]	2 σ[d]	$^{206}Pb/^{238}U$[b]	2 σ[d]	$^{207}Pb/^{206}Pb$[e]	2 σ[d]	%
FHM140078A, meta-sandstone, Pahakurkio group																					
65	351	15	41	2	530	40	8.9	25.130	0.550	0.679	0.020	0.828	0.2674	0.0050	3312	21	3338	76	3290	30	101
66	194	20	76	13	599	80	2.9	6.850	0.300	0.387	0.016	0.887	0.1268	0.0020	2088	39	2107	72	2053	28	103
67	260	14	115	7	874	56	2.3	5.860	0.160	0.363	0.012	0.941	0.1157	0.0019	1954	23	1995	57	1896	27	105
68	847	56	300	17	3180	180	2.8	13.830	0.620	0.511	0.022	0.989	0.1954	0.0023	2734	42	2660	94	2787	19	95
72	216	12	75	4	580	33	2.8	5.920	0.170	0.357	0.012	0.809	0.1195	0.0027	1962	25	1967	59	1946	40	101
74	255	7	15	2	208	31	19.3	14.940	0.360	0.521	0.012	0.778	0.2047	0.0028	2810	23	2703	49	2863	23	94
75	474	30	216	17	2350	200	2.2	13.490	0.320	0.523	0.010	0.739	0.1896	0.0022	2720	25	2712	43	2738	19	99
77	624	35	130	12	983	51	4.9	5.480	0.120	0.324	0.009	0.710	0.1242	0.0016	1897	19	1808	44	2017	22	90
79	736	50	103	8	907	57	7.3	10.540	0.180	0.474	0.012	0.830	0.1581	0.0021	2484	15	2502	53	2435	23	103
80	738	66	447	28	3700	300	1.6	6.130	0.100	0.357	0.008	0.478	0.1222	0.0024	1995	14	1968	40	1986	35	99
81	529	14	279	14	2084	91	1.9	5.340	0.150	0.329	0.005	0.911	0.1173	0.0020	1875	23	1834	25	1914	30	96
85	309	17	20	2	259	22	15.1	13.770	0.280	0.504	0.011	0.617	0.1959	0.0031	2733	19	2629	49	2791	26	94
87	334	34	63	8	718	93	5.4	12.020	0.320	0.485	0.015	0.917	0.1765	0.0025	2605	25	2546	63	2620	24	97
88	910	57	231	8	1958	93	4.1	6.400	0.120	0.375	0.010	0.638	0.1232	0.0026	2031	16	2052	46	2001	37	103
89	404	34	106	24	1260	300	4.8	13.200	0.490	0.501	0.018	0.919	0.1903	0.0028	2691	35	2617	76	2744	24	95
90	448	38	25	1	261	11	19.5	14.620	0.210	0.539	0.011	0.653	0.1963	0.0032	2790	14	2778	44	2795	26	99
91	1710	170	259	25	1940	220	7.0	5.020	0.230	0.302	0.011	0.735	0.1211	0.0027	1821	39	1701	54	1970	40	86
92	86	8	11	2	127	20	9.0	15.600	0.350	0.566	0.018	0.891	0.1999	0.0031	2852	21	2888	76	2824	25	102
93	951	90	198	25	1530	210	5.3	5.590	0.130	0.343	0.008	0.791	0.1169	0.0015	1914	20	1903	37	1908	23	100
98	1070	120	260	25	2470	300	4.2	7.510	0.240	0.396	0.010	0.789	0.1392	0.0028	2172	29	2150	45	2215	35	97
99	1266	49	232	24	1957	94	5.7	5.800	0.120	0.331	0.011	0.760	0.1251	0.0021	1946	18	1842	54	2029	29	91
100	962	76	223	10	1950	130	4.3	6.090	0.110	0.369	0.009	0.687	0.1241	0.0025	1988	17	2026	42	2014	36	101
101	356	30	49	6	548	47	7.6	5.690	0.210	0.354	0.012	0.709	0.1172	0.0020	1935	34	1964	53	1913	30	103
103	297	22	49	3	487	22	5.9	7.330	0.240	0.395	0.015	0.717	0.1339	0.0030	2151	30	2144	68	2148	40	100
104	486	31	71	3	561	46	6.7	5.555	0.087	0.343	0.006	0.603	0.1164	0.0021	1909	13	1901	29	1900	32	100
112	557	50	152	13	1310	130	3.8	6.120	0.160	0.355	0.013	0.692	0.1249	0.0031	1991	22	1956	60	2024	44	97
114	432	41	126	11	1370	150	3.6	12.140	0.290	0.481	0.013	0.904	0.1830	0.0017	2614	22	2532	57	2680	15	94
115	234	29	163	31	1830	380	1.6	14.390	0.490	0.524	0.013	0.794	0.1979	0.0043	2773	33	2717	55	2807	36	97
116	1080	140	343	43	2760	370	3.4	6.330	0.120	0.368	0.007	0.478	0.1269	0.0018	2022	16	2019	33	2054	24	98
117	559	31	154	14	1224	47	3.7	7.410	0.170	0.398	0.009	0.717	0.1329	0.0021	2161	21	2159	43	2136	27	101
118	888	91	35	4	330	34	27.7	6.670	0.200	0.378	0.014	0.889	0.1288	0.0017	2073	29	2063	67	2080	23	99
119	234	49	52	12	570	120	4.9	13.280	0.490	0.492	0.017	0.895	0.1963	0.0035	2696	35	2576	72	2794	29	92
120	583	59	30	2	336	18	20.4	12.260	0.290	0.486	0.014	0.731	0.1822	0.0037	2623	22	2553	63	2671	34	96
124	550	110	135	41	1090	310	4.8	5.920	0.200	0.359	0.015	0.834	0.1196	0.0031	1962	31	1976	70	1947	47	101
125	549	41	3	1	70	7	146.0	14.510	0.390	0.525	0.013	0.782	0.1982	0.0040	2782	26	2721	54	2809	33	97
127	579	26	122	6	1036	65	4.6	6.190	0.130	0.361	0.011	0.718	0.1253	0.0023	2002	19	1987	53	2031	33	98
128	90	19	19	5	280	44	4.8	15.770	0.590	0.608	0.024	0.921	0.1917	0.0021	2872	31	3062	95	2756	18	111

Table 5 continues

Analysis	Concentrations (ppm)[a]						Ratios								Ages (Ma)						CONC.
No	U	2 σ	Th	2 σ	Pb	2 σ	U/Th[a]	$^{207}Pb/^{235}U$[b]	2 σ[d]	$^{206}Pb/^{238}U$[b]	2 σ[d]	rho[c]	$^{207}Pb/^{206}Pb$[e]	2 σ[d]	$^{207}Pb/^{235}U$[b]	2 σ[d]	$^{206}Pb/^{238}U$[b]	2 σ[d]	$^{207}Pb/^{206}Pb$[e]	2 σ[d]	%
FHM140078A, meta-sandstone, Pahakurkio group																					
129	140	11	84	7	686	69	1.6	6.320	0.078	0.360	0.007	0.713	0.1273	0.0020	2021	11	1980	34	2061	28	96
131	482	44	92	32	1020	390	6.5	13.210	0.230	0.518	0.013	0.491	0.1872	0.0041	2694	17	2691	57	2716	37	99
132	313	13	119	3	969	50	2.6	6.270	0.170	0.362	0.012	0.765	0.1274	0.0023	2013	24	1989	59	2061	32	97
133	480	110	193	51	1910	540	2.6	10.870	0.530	0.452	0.016	0.649	0.1804	0.0058	2509	46	2404	71	2654	54	91
137	240	13	59	3	497	25	4.1	6.460	0.230	0.384	0.019	0.917	0.1246	0.0016	2039	32	2093	87	2022	23	104
140	334	32	119	26	990	220	3.0	9.540	0.420	0.417	0.023	0.817	0.1675	0.0039	2389	41	2240	110	2531	40	89
141	253	29	115	6	746	97	2.3	6.000	0.160	0.353	0.014	0.654	0.1216	0.0024	1974	24	1948	67	1978	35	98
142	141	10	42	6	454	68	3.5	15.830	0.350	0.557	0.014	0.888	0.2061	0.0029	2865	21	2853	59	2875	23	99
143	134	52	34	6	255	26	3.9	6.770	0.310	0.383	0.022	0.679	0.1260	0.0020	2088	45	2090	110	2041	28	102
144	181	21	56	8	629	72	3.3	16.060	0.370	0.564	0.017	0.610	0.2094	0.0047	2879	22	2880	69	2899	36	99
145	740	100	455	75	2970	500	1.8	5.390	0.370	0.337	0.025	0.988	0.1179	0.0014	1876	65	1870	120	1924	22	97
146	147	12	58	4	470	29	2.6	6.030	0.170	0.353	0.013	0.816	0.1250	0.0021	1978	24	1948	61	2028	30	96
150	116	5	46	2	562	32	2.6	16.930	0.420	0.568	0.016	0.923	0.2158	0.0029	2930	24	2900	65	2949	22	98
151	145	9	43	6	348	42	3.6	6.440	0.130	0.371	0.015	0.794	0.1261	0.0032	2037	19	2034	70	2052	42	99
152	285	16	111	3	935	31	2.6	6.490	0.160	0.379	0.012	0.835	0.1243	0.0026	2044	22	2086	60	2025	35	103
153	48	3	36	3	404	23	1.3	13.790	0.500	0.530	0.021	0.816	0.1891	0.0041	2742	31	2761	96	2732	36	101
154	361	25	55	9	450	52	6.5	6.270	0.190	0.376	0.012	0.845	0.1217	0.0016	2013	25	2055	57	1980	23	104
155	255	19	63	3	472	31	4.1	5.890	0.190	0.369	0.015	0.865	0.1189	0.0017	1958	29	2023	71	1938	25	104
156	70	4	24	2	285	18	2.8	14.780	0.360	0.552	0.017	0.796	0.1964	0.0032	2800	24	2833	71	2795	27	101
157	147	20	69	17	900	230	2.4	19.980	0.800	0.580	0.022	0.932	0.2530	0.0035	3096	36	2946	89	3203	22	92
163	147	8	34	1	275	9	4.4	6.510	0.140	0.377	0.008	0.766	0.1256	0.0016	2046	19	2063	36	2036	23	101
164	398	23	93	6	744	56	4.3	5.570	0.100	0.348	0.009	0.572	0.1170	0.0019	1911	16	1923	44	1916	27	100
165	344	13	58	2	469	13	5.8	5.660	0.150	0.354	0.013	0.886	0.1170	0.0019	1924	23	1953	60	1917	32	102
166	240	17	72	3	810	71	3.4	15.260	0.500	0.549	0.023	0.829	0.2061	0.0035	2829	31	2817	95	2874	28	98
167	207	29	47	8	390	70	4.2	6.500	0.220	0.383	0.015	0.909	0.1242	0.0014	2044	30	2087	71	2017	19	103
168	126	5	43	2	343	15	2.9	5.860	0.140	0.372	0.007	0.665	0.1162	0.0017	1954	21	2039	31	1897	26	107
169	257	14	50	3	409	19	5.0	6.310	0.150	0.368	0.010	0.646	0.1260	0.0025	2020	21	2018	49	2041	36	99
170	193	8	49	4	377	39	3.9	6.440	0.140	0.390	0.012	0.626	0.1217	0.0020	2036	19	2123	56	1980	29	107
171	419	58	179	24	1300	180	2.3	5.540	0.170	0.343	0.010	0.920	0.1186	0.0015	1916	32	1900	48	1934	23	98
172	167	11	45	2	380	22	3.5	6.410	0.290	0.375	0.011	0.920	0.1270	0.0020	2031	43	2051	51	2056	29	100
176	162	12	75	8	805	84	2.2	13.150	0.270	0.515	0.018	0.767	0.1870	0.0029	2690	19	2678	77	2716	26	99
177	176	14	66	3	536	23	2.6	6.340	0.150	0.363	0.009	0.773	0.1261	0.0019	2024	20	1996	45	2043	27	98
178	350	22	77	7	882	70	4.7	14.330	0.620	0.556	0.024	0.901	0.1875	0.0038	2768	42	2848	98	2719	33	105
179	315	80	93	32	570	140	4.0	6.490	0.280	0.376	0.017	0.899	0.1260	0.0021	2041	38	2058	77	2042	29	101
181	293	83	190	59	2010	650	1.8	13.500	0.730	0.506	0.028	0.776	0.1941	0.0056	2721	58	2630	120	2773	47	95
182	706	55	109	5	834	51	6.7	5.974	0.090	0.361	0.007	0.551	0.1227	0.0019	1972	13	1984	32	1995	27	99
183	880	190	28	6	192	57	30.7	5.790	0.520	0.345	0.031	0.988	0.1215	0.0011	1935	80	1900	150	1978	16	96
185	137	28	30	5	231	27	4.9	6.910	0.550	0.368	0.023	0.958	0.1362	0.0032	2091	74	2020	110	2178	41	93

Table 5 continues

Analysis	Concentrations (ppm)[a]						Ratios								Ages (Ma)						CONC.
No	U	2 σ	Th	2 σ	Pb	2 σ	U/Th[a]	$^{207}Pb/^{235}U$[b]	2 σ[d]	$^{206}Pb/^{238}U$[b]	2 σ[d]	rho[c]	$^{207}Pb/^{206}Pb$[e]	2 σ[d]	$^{207}Pb/^{235}U$[b]	2 σ[d]	$^{206}Pb/^{238}U$[b]	2 σ[d]	$^{207}Pb/^{206}Pb$[e]	2 σ[d]	%
FHM140078A, meta-sandstone, Pahakurkio group																					
189	163	6	81	5	923	57	2.0	13.260	0.340	0.504	0.015	0.800	0.1911	0.0038	2697	24	2631	64	2750	33	96
190	359	28	131	7	1450	160	2.8	15.140	0.330	0.550	0.015	0.759	0.2009	0.0042	2823	21	2825	62	2831	34	100
191	454	40	184	19	1340	120	2.6	5.800	0.100	0.357	0.008	0.728	0.1196	0.0013	1946	15	1967	36	1950	20	101
193	252	69	74	16	650	120	3.5	7.200	0.210	0.403	0.014	0.800	0.1289	0.0025	2134	26	2182	66	2080	35	105
194	243	19	61	7	458	63	4.2	5.630	0.160	0.348	0.012	0.910	0.1170	0.0019	1919	26	1925	56	1917	31	100
196	308	27	53	5	405	43	5.9	5.580	0.140	0.346	0.009	0.740	0.1171	0.0024	1912	22	1933	53	1911	37	101
198	186	13	26	2	208	17	6.9	6.250	0.150	0.363	0.010	0.697	0.1259	0.0016	2010	21	1995	46	2041	23	98
202	53	4	30	3	346	31	1.7	14.120	0.490	0.541	0.019	0.846	0.1900	0.0040	2756	33	2785	78	2740	35	102
203	714	62	218	37	1870	350	3.6	8.480	0.290	0.426	0.012	0.759	0.1451	0.0033	2281	31	2287	53	2286	38	100
204	440	41	209	24	1680	270	2.2	6.080	0.130	0.367	0.008	0.798	0.1214	0.0017	1987	19	2014	39	1976	25	102
205	187	7	23	0	182	6	8.0	5.610	0.130	0.341	0.009	0.822	0.1193	0.0017	1917	20	1892	45	1944	25	97
206	375	41	107	13	1157	73	3.6	11.040	0.980	0.453	0.034	0.943	0.1787	0.0037	2513	81	2400	150	2639	35	91
207	195	8	45	1	353	11	4.4	6.125	0.098	0.358	0.011	0.518	0.1248	0.0032	1993	14	1971	55	2023	45	97
208	307	41	111	19	840	190	2.9	6.230	0.220	0.349	0.014	0.864	0.1299	0.0028	2006	31	1927	66	2095	38	92
209	186	14	51	4	637	49	3.8	16.560	0.480	0.570	0.018	0.871	0.2116	0.0034	2908	28	2907	72	2917	26	100
Common-Pb corrected[f]																					
9	800	170	215	52	1410	340	3.9	5.000	0.160	0.314	0.010	0.794	0.1160	0.0022	1818	28	1759	49	1902	30	92
22	1000	67	294	18	1880	250	3.4	5.050	0.160	0.316	0.011	0.895	0.1138	0.0017	1826	26	1770	54	1871	20	95
23	658	64	199	9	1410	110	3.3	4.790	0.260	0.296	0.015	0.915	0.1167	0.0031	1779	45	1672	75	1902	48	88
39	396	41	116	22	900	210	3.7	5.570	0.310	0.315	0.018	0.929	0.1275	0.0026	1917	46	1762	90	2061	36	85
47	787	85	121	17	1200	190	6.7	7.480	0.280	0.368	0.012	0.840	0.1464	0.0029	2168	33	2021	56	2302	34	88
50	1112	47	207	15	1261	86	5.3	4.530	0.190	0.280	0.013	0.927	0.1177	0.0019	1733	35	1589	67	1921	29	83
51	934	53	114	24	1000	210	9.1	5.250	0.200	0.319	0.012	0.880	0.1186	0.0020	1858	32	1785	57	1934	31	92
76	259	24	45	6	430	62	5.5	11.450	0.580	0.465	0.021	0.933	0.1759	0.0028	2566	45	2458	93	2614	27	94
78	321	9	126	5	1135	63	2.6	9.930	0.320	0.398	0.017	0.745	0.1751	0.0045	2428	30	2157	80	2606	43	83
86	900	100	141	38	1240	200	6.1	6.420	0.330	0.359	0.013	0.899	0.1283	0.0037	2032	46	1978	65	2071	24	96
94	2600	130	790	81	5060	370	3.7	4.510	0.250	0.276	0.016	0.933	0.1195	0.0021	1730	47	1570	80	1948	31	81
105	317	24	79	3	709	46	4.1	6.520	0.180	0.368	0.014	0.749	0.1281	0.0038	2047	24	2019	64	2067	53	98
111	2640	330	296	87	1930	520	11.1	3.800	0.340	0.201	0.013	0.954	0.1372	0.0042	1582	72	1181	67	2188	53	54
113	324	15	74	7	631	40	4.8	11.600	0.370	0.460	0.017	0.862	0.1828	0.0032	2571	30	2439	76	2677	29	91
126	1130	230	278	74	1800	340	3.7	4.91	0.21	0.305	0.014	0.94775	0.1156	0.0017	1802	38	1717	70	1888	26	91
130	1850	190	403	33	3200	340	4.5	7.54	0.21	0.339	0.016	0.86893	0.1604	0.0039	2176	25	1882	76	2443	27	77
138	591	56	151	15	827	86	4.0	5.350	0.170	0.325	0.010	0.835	0.1185	0.0025	1876	27	1814	51	1932	37	94
139	371	22	86	8	597	53	4.4	5.130	0.180	0.323	0.015	0.716	0.1169	0.0031	1839	30	1801	71	1906	49	94
180	210	34	83	13	581	95	3.0	5.990	0.330	0.355	0.016	0.874	0.1244	0.0036	1971	49	1958	78	2018	52	97
184	690	140	111	8	810	130	6.4	3.670	0.600	0.233	0.036	0.982	0.1151	0.0023	1580	150	1340	190	1879	36	71
192	330	22	71	11	694	39	4.9	15.4	0.61	0.544	0.03	0.74176	0.2042	0.0053	2838	38	2800	120	2859	42	98
195	432	62	121	19	1000	260	3.7	6.750	0.260	0.379	0.015	0.894	0.1300	0.0028	2077	34	2071	72	2108	34	98
197	240	15	184	19	1560	140	1.3	6.340	0.270	0.378	0.017	0.775	0.1226	0.0036	2021	38	2062	81	1990	52	104

Table 5 continues

Analysis	Concentrations (ppm)[a]						Ratios								Ages (Ma)						CONC.
No	U	2 σ	Th	2 σ	Pb	2 σ	U/Th[a]	$^{207}Pb/^{235}U$[b]	2 σ[d]	$^{206}Pb/^{238}U$[b]	2 σ[d]	rho[c]	$^{207}Pb/^{206}Pb$[e]	2 σ[d]	$^{207}Pb/^{235}U$[b]	2 σ[d]	$^{206}Pb/^{238}U$[b]	2 σ[d]	$^{207}Pb/^{206}Pb$[e]	2 σ[d]	%
FHM140088B, meta-sandstone, Kalixälv group																					
7	339	17	123	7	912	39	2.8	5.446	0.097	0.339	0.008	0.902	0.1159	0.0013	1892	15	1879	39	1894	21	99
8	579	32	237	11	1693	79	2.6	5.480	0.130	0.344	0.009	0.943	0.1148	0.0014	1897	21	1906	44	1877	23	102
9	228	9	78	1	590	12	2.9	5.510	0.140	0.342	0.009	0.898	0.1149	0.0013	1901	23	1896	44	1877	20	101
10	236	39	29	7	158	20	8.8	6.020	0.250	0.378	0.018	0.966	0.1177	0.0016	1976	37	2064	82	1921	24	107
12	143	20	25	2	199	18	6.1	5.860	0.230	0.370	0.016	0.780	0.1174	0.0025	1953	34	2029	75	1915	39	106
13	391	34	100	26	720	180	4.8	6.230	0.250	0.377	0.014	0.887	0.1207	0.0023	2006	36	2073	60	1965	33	105
14	501	25	356	17	2570	150	1.4	5.542	0.091	0.350	0.009	0.739	0.1160	0.0018	1907	14	1932	41	1894	29	102
15	155	9	36	5	232	11	4.7	5.910	0.160	0.367	0.009	0.763	0.1176	0.0018	1962	23	2013	43	1919	28	105
16	228	18	89	9	860	110	2.6	14.190	0.350	0.542	0.013	0.630	0.1904	0.0044	2761	24	2790	56	2743	38	102
21	310	13	189	11	2041	72	1.7	13.270	0.290	0.509	0.013	0.508	0.1862	0.0030	2698	21	2651	57	2707	26	98
23	339	28	98	6	781	63	3.6	5.760	0.110	0.339	0.009	0.645	0.1193	0.0021	1939	17	1906	35	1944	31	98
24	420	32	160	13	1224	90	2.9	5.180	0.140	0.315	0.009	0.933	0.1189	0.0017	1848	23	1767	45	1940	25	91
25	334	27	108	4	911	50	3.2	6.020	0.170	0.343	0.009	0.894	0.1268	0.0019	1978	25	1900	45	2061	24	92
26	204	10	86	4	649	31	2.5	5.150	0.120	0.325	0.009	0.661	0.1154	0.0021	1848	21	1813	41	1884	33	96
27	384	88	210	37	1300	170	1.9	5.330	0.400	0.341	0.026	0.980	0.1135	0.0021	1889	54	1890	130	1855	33	102
28	180	57	40	11	500	110	5.2	17.630	0.880	0.660	0.036	0.917	0.1978	0.0027	2965	49	3260	140	2808	22	116
29	900	130	229	34	2280	430	4.1	11.620	0.240	0.456	0.014	0.706	0.1860	0.0034	2574	19	2422	60	2706	30	90
33	1368	81	56	17	460	140	29.7	5.620	0.130	0.329	0.011	0.747	0.1220	0.0021	1919	20	1831	52	1985	31	92
35	486	16	16	2	121	16	32.2	4.900	0.130	0.323	0.009	0.724	0.1100	0.0024	1802	22	1804	44	1797	40	100
36	754	51	236	14	1710	140	3.1	5.354	0.092	0.333	0.007	0.787	0.1168	0.0017	1882	17	1854	32	1907	27	97
37	334	61	18	8	142	65	25.6	15.900	0.250	0.574	0.014	0.690	0.1968	0.0031	2870	15	2923	57	2807	29	104
38	193	17	32	2	301	25	6.3	9.500	0.300	0.475	0.015	0.770	0.1447	0.0027	2385	30	2502	68	2282	31	110
39	227	12	115	8	1251	67	1.9	14.330	0.230	0.551	0.010	0.691	0.1843	0.0028	2771	15	2829	43	2691	25	105
40	832	36	128	4	1533	72	6.4	16.720	0.290	0.565	0.013	0.780	0.2173	0.0031	2918	17	2884	53	2960	23	97
41	350	25	108	9	802	49	3.4	6.810	0.340	0.406	0.022	0.947	0.1217	0.0019	2083	45	2190	100	1980	28	111
42	412	45	12	5	84	29	66.0	5.610	0.120	0.352	0.008	0.415	0.1139	0.0014	1917	19	1942	39	1862	23	104
46	1276	64	378	49	2830	230	3.6	5.190	0.160	0.319	0.010	0.930	0.1194	0.0015	1849	26	1782	50	1946	22	92
51	987	94	269	51	3300	590	3.9	12.670	0.360	0.485	0.020	0.907	0.1923	0.0053	2655	27	2549	85	2760	45	92
52	657	90	347	25	2530	230	1.8	5.049	0.075	0.316	0.008	0.418	0.1178	0.0025	1827	13	1777	33	1920	38	93
53	360	33	78	3	898	59	4.6	11.830	0.260	0.485	0.014	0.861	0.1777	0.0030	2590	21	2547	62	2630	27	97
59	340	40	209	18	2100	150	1.6	10.540	0.280	0.494	0.018	0.872	0.1514	0.0027	2482	25	2584	78	2360	31	109
60	357	65	54	6	360	17	6.5	13.390	0.460	0.508	0.019	0.895	0.1901	0.0036	2705	33	2646	82	2741	31	97
61	418	72	119	23	700	110	3.8	5.450	0.190	0.340	0.010	0.848	0.1152	0.0023	1891	30	1884	48	1880	36	100
62	551	23	146	13	951	70	4.0	5.180	0.091	0.324	0.009	0.543	0.1140	0.0019	1849	15	1807	42	1882	38	96
64	701	21	180	7	1444	64	4.0	6.660	0.120	0.392	0.011	0.846	0.1216	0.0020	2067	16	2132	51	1979	29	108
65	451	37	156	15	1290	130	2.8	5.730	0.180	0.354	0.012	0.824	0.1170	0.0030	1934	28	1953	59	1907	45	102

Table 5 continues

Analysis	Concentrations (ppm)[a]						Ratios								Ages (Ma)						CONC.
No	U	2 σ	Th	2 σ	Pb	2 σ	U/Th[a]	$^{207}Pb/^{235}U$[b]	2 σ[d]	$^{206}Pb/^{238}U$[b]	2 σ[d]	rho[c]	$^{207}Pb/^{206}Pb$[e]	2 σ[d]	$^{207}Pb/^{235}U$[b]	2 σ[d]	$^{206}Pb/^{238}U$[b]	2 σ[d]	$^{207}Pb/^{206}Pb$[e]	2 σ[d]	%
FHM140088B, meta-sandstone, Kalixälv group																					
66	956	50	395	53	3100	480	2.5	5.810	0.150	0.353	0.009	0.777	0.1189	0.0019	1947	21	1949	43	1938	30	101
67	288	8	144	5	1284	63	2.0	7.020	0.190	0.398	0.009	0.837	0.1286	0.0011	2114	24	2158	41	2078	15	104
72	544	39	130	16	919	60	4.1	5.080	0.140	0.324	0.011	0.764	0.1156	0.0019	1831	22	1808	52	1896	33	95
74	237	49	74	14	710	120	3.8	8.950	0.320	0.450	0.018	0.923	0.1414	0.0024	2331	34	2395	83	2243	29	107
75	555	68	218	34	2190	350	2.6	11.430	0.670	0.456	0.021	0.906	0.1818	0.0044	2552	53	2421	90	2667	40	91
77	377	55	162	34	1170	200	2.3	6.070	0.200	0.354	0.012	0.758	0.1256	0.0025	1984	29	1952	59	2036	36	96
79	545	64	145	26	1230	200	4.0	6.796	0.083	0.380	0.006	0.579	0.1284	0.0015	2085	11	2078	28	2076	21	100
80	209	29	98	18	1370	260	2.3	33.380	0.660	0.753	0.014	0.510	0.3231	0.0067	3591	20	3617	50	3583	32	101
81	301	26	9	2	93	14	36.4	13.630	0.320	0.548	0.014	0.748	0.1820	0.0039	2723	22	2817	60	2668	35	106
85	236	34	73	15	740	200	3.0	6.720	0.170	0.380	0.009	0.361	0.1267	0.0035	2074	22	2085	44	2076	38	100
87	335	23	90	8	746	76	3.5	5.687	0.090	0.338	0.006	0.400	0.1225	0.0025	1932	13	1875	29	1991	36	94
88	233	14	61	3	454	15	3.5	5.960	0.140	0.360	0.007	0.748	0.1174	0.0021	1968	21	1980	34	1915	32	103
89	93	6	43	3	335	20	2.1	6.010	0.140	0.348	0.008	0.494	0.1215	0.0030	1977	21	1925	37	1975	43	97
91	513	69	67	15	397	91	6.5	5.760	0.150	0.347	0.011	0.822	0.1182	0.0017	1938	23	1919	53	1929	25	99
92	362	85	71	14	450	110	4.9	6.140	0.190	0.362	0.015	0.872	0.1246	0.0028	2002	30	1989	70	2020	39	98
93	479	17	64	3	597	29	7.3	7.580	0.150	0.405	0.011	0.758	0.1341	0.0014	2182	18	2193	53	2152	19	102
94	530	36	44	7	420	55	12.2	6.100	0.140	0.357	0.012	0.684	0.1234	0.0030	1989	20	1966	55	2024	36	97
98	765	67	335	60	4060	690	2.5	19.560	0.470	0.576	0.016	0.701	0.2465	0.0036	3069	23	2931	66	3161	23	93
99	425	70	148	24	1210	210	2.8	5.480	0.140	0.343	0.011	0.744	0.1166	0.0024	1897	21	1899	53	1903	37	100
101	660	110	214	46	1880	370	3.3	9.710	0.200	0.425	0.012	0.779	0.1639	0.0027	2407	19	2281	52	2501	30	91
102	1440	190	530	130	3500	1000	2.8	5.030	0.210	0.304	0.014	0.892	0.1161	0.0019	1822	36	1711	69	1895	30	90
103	1164	80	381	28	3430	240	2.8	5.800	0.110	0.338	0.010	0.802	0.1238	0.0020	1951	19	1878	47	2011	28	93
104	501	18	173	11	2060	130	2.6	13.250	0.250	0.495	0.015	0.682	0.1938	0.0032	2697	18	2589	64	2773	28	93
105	143	10	65	10	480	31	2.2	5.530	0.120	0.334	0.008	0.857	0.1182	0.0015	1904	18	1857	36	1928	23	96
111	341	28	75	9	398	31	4.8	4.730	0.140	0.301	0.010	0.771	0.1164	0.0026	1772	24	1694	50	1909	36	89
112	210	11	96	3	738	23	2.3	6.780	0.120	0.395	0.008	0.618	0.1310	0.0022	2083	16	2147	37	2110	29	102
115	277	23	155	13	1032	97	2.0	5.490	0.110	0.351	0.008	0.744	0.1182	0.0021	1898	17	1940	37	1928	31	101
116	913	47	691	62	4620	510	1.5	6.150	0.110	0.369	0.007	0.552	0.1260	0.0020	1997	15	2025	35	2042	28	99
117	470	35	221	13	1499	70	2.2	5.900	0.100	0.349	0.007	0.675	0.1252	0.0023	1965	17	1932	32	2031	33	95
118	1569	51	465	84	3130	550	3.7	5.510	0.130	0.349	0.009	0.826	0.1170	0.0018	1901	20	1929	45	1909	28	101
119	416	29	168	28	933	93	2.8	5.400	0.120	0.344	0.010	0.767	0.1175	0.0019	1883	20	1905	47	1918	29	99
120	524	70	177	13	1398	90	2.9	6.550	0.120	0.377	0.009	0.870	0.1274	0.0016	2053	16	2063	43	2062	22	100
124	804	27	512	44	4610	390	1.5	10.470	0.230	0.461	0.011	0.822	0.1633	0.0022	2476	21	2442	50	2496	19	98
127	992	60	158	12	1270	120	6.2	6.590	0.110	0.381	0.009	0.203	0.1249	0.0031	2057	15	2081	41	2040	35	102
128	358	10	122	4	1010	43	2.9	5.790	0.110	0.343	0.009	0.771	0.1230	0.0026	1945	16	1901	45	1998	38	95
129	708	78	236	81	1650	520	3.3	5.640	0.180	0.343	0.013	0.852	0.1184	0.0018	1920	28	1901	62	1932	27	98
130	154	10	49	3	382	26	3.1	5.170	0.110	0.322	0.008	0.721	0.1152	0.0019	1846	17	1798	38	1881	31	96

Table 5 continues

Analysis	Concentrations (ppm)[a]						Ratios								Ages (Ma)						CONC.
No	U	2 σ	Th	2 σ	Pb	2 σ	U/Th[a]	$^{207}Pb/^{235}U$[b]	2 σ[d]	$^{206}Pb/^{238}U$[b]	2 σ[d]	rho[c]	$^{207}Pb/^{206}Pb$[e]	2 σ[d]	$^{207}Pb/^{235}U$[b]	2 σ[d]	$^{206}Pb/^{238}U$[b]	2 σ[d]	$^{207}Pb/^{206}Pb$[e]	2 σ[d]	%
FHM140088B, meta-sandstone, Kalixälv group																					
131	725	89	137	25	1110	210	5.8	5.800	0.210	0.332	0.010	0.752	0.1269	0.0026	1944	31	1847	48	2053	37	90
132	331	28	262	44	1970	310	1.4	6.070	0.120	0.338	0.012	0.866	0.1308	0.0025	1985	18	1877	58	2107	34	89
133	354	38	255	40	1920	330	1.4	5.370	0.110	0.340	0.006	0.733	0.1142	0.0011	1879	18	1887	30	1868	17	101
138	548	93	199	59	1380	400	3.3	5.075	0.088	0.310	0.008	0.848	0.1164	0.0017	1831	15	1742	41	1900	27	92
139	433	53	32	4	246	35	14.7	5.720	0.160	0.343	0.010	0.912	0.1196	0.0015	1933	24	1902	49	1950	22	98
140	221	25	101	3	749	24	2.3	5.820	0.140	0.352	0.009	0.689	0.1198	0.0016	1949	21	1943	44	1952	24	100
141	948	61	217	10	2510	130	4.5	12.720	0.390	0.473	0.019	0.806	0.1928	0.0045	2658	29	2493	83	2765	38	90
144	325	16	31	3	226	15	11.3	5.640	0.210	0.347	0.013	0.644	0.1145	0.0024	1921	33	1920	61	1871	39	103
145	396	44	165	35	1300	280	2.3	7.120	0.180	0.386	0.010	0.725	0.1337	0.0016	2126	22	2104	46	2147	21	98
146	377	27	70	8	490	39	5.7	6.240	0.200	0.362	0.010	0.876	0.1225	0.0020	2008	29	2003	51	1991	30	101
150	316	52	65	9	477	80	4.7	5.884	0.093	0.351	0.007	0.591	0.1220	0.0021	1958	14	1941	32	1985	30	98
151	640	130	152	26	1180	210	3.9	5.740	0.130	0.350	0.009	0.736	0.1199	0.0021	1936	20	1935	43	1954	31	99
152	260	33	61	5	507	40	4.1	6.190	0.140	0.368	0.011	0.905	0.1237	0.0014	2003	20	2018	50	2010	20	100
153	550	150	148	37	910	250	3.3	5.590	0.170	0.352	0.010	0.927	0.1171	0.0017	1913	26	1944	50	1924	26	101
154	623	80	113	27	930	210	5.7	6.760	0.260	0.366	0.014	0.903	0.1352	0.0023	2078	34	2010	65	2165	30	93
155	185	37	150	19	1010	180	1.2	5.840	0.260	0.355	0.013	0.945	0.1212	0.0017	1951	38	1956	62	1974	26	99
156	151	15	87	18	664	92	1.8	7.140	0.110	0.402	0.011	0.804	0.1296	0.0021	2129	14	2178	49	2091	29	104
157	1780	190	384	35	2880	260	4.5	5.270	0.140	0.311	0.011	0.840	0.1236	0.0016	1864	23	1746	53	2008	23	87
163	630	120	143	22	1230	170	4.5	6.720	0.170	0.381	0.012	0.934	0.1283	0.0023	2073	24	2078	57	2073	31	100
164	548	46	59	6	669	73	9.9	12.930	0.440	0.507	0.019	0.889	0.1846	0.0033	2681	28	2639	83	2693	30	98
165	242	20	125	16	1150	150	2.0	7.400	0.190	0.403	0.014	0.828	0.1321	0.0022	2159	23	2182	63	2125	30	103
166	609	19	105	5	723	41	5.9	5.220	0.140	0.332	0.010	0.877	0.1145	0.0022	1855	22	1845	46	1871	35	99
167	278	42	34	3	258	30	8.3	5.820	0.160	0.357	0.007	0.691	0.1188	0.0022	1947	23	1967	34	1936	33	102
168	728	21	268	21	2460	140	2.8	8.690	0.230	0.407	0.012	0.803	0.1529	0.0021	2305	24	2199	54	2378	23	92
169	876	79	293	24	2400	190	3.0	6.710	0.150	0.382	0.011	0.906	0.1255	0.0017	2073	20	2084	53	2036	24	102
170	678	45	166	49	2370	450	3.8	25.400	2.300	0.652	0.046	0.964	0.2825	0.0082	3317	78	3230	170	3375	46	96
171	807	37	135	6	800	28	6.0	5.322	0.091	0.331	0.005	0.662	0.1160	0.0013	1872	15	1842	26	1900	23	97
172	520	140	143	44	1070	400	3.5	6.250	0.200	0.360	0.015	0.922	0.1273	0.0017	2017	24	1982	70	2060	23	96
176	377	95	320	110	3000	1100	1.6	11.320	0.450	0.495	0.020	0.919	0.1663	0.0027	2556	34	2588	87	2520	27	103
177	1424	75	278	41	1980	280	5.1	5.450	0.120	0.328	0.006	0.654	0.1190	0.0018	1892	18	1826	28	1941	27	94
178	576	94	291	66	2640	600	2.2	10.490	0.270	0.475	0.016	0.910	0.1613	0.0024	2478	23	2504	70	2468	25	101
179	286	28	121	17	740	120	3.0	5.670	0.170	0.346	0.011	0.906	0.1186	0.0021	1925	27	1916	53	1933	33	99
180	365	19	108	5	813	32	3.5	6.120	0.160	0.370	0.010	0.689	0.1230	0.0024	1991	22	2028	48	1999	34	101
181	298	28	149	23	1200	240	2.0	6.970	0.270	0.399	0.016	0.842	0.1292	0.0023	2105	35	2163	74	2086	31	104
182	299	28	104	9	756	61	2.9	5.790	0.190	0.365	0.013	0.847	0.1164	0.0024	1942	29	2003	63	1899	37	105
183	820	180	460	140	2420	510	2.0	6.090	0.430	0.353	0.024	0.960	0.1265	0.0024	1995	59	1950	120	2057	31	95
184	344	20	144	9	1026	81	2.4	6.010	0.160	0.364	0.008	0.841	0.1212	0.0020	1975	23	2001	36	1973	30	101

Table 5 continues

Analysis	Concentrations (ppm)[a]						Ratios								Ages (Ma)						CONC.
No	U	2 σ	Th	2 σ	Pb	2 σ	U/Th[a]	$^{207}Pb/^{235}U$[b]	2 σ[d]	$^{206}Pb/^{238}U$[b]	2 σ[d]	rho[c]	$^{207}Pb/^{206}Pb$[e]	2 σ[d]	$^{207}Pb/^{235}U$[b]	2 σ[d]	$^{206}Pb/^{238}U$[b]	2 σ[d]	$^{207}Pb/^{206}Pb$[e]	2 σ[d]	%
FHM140088B, meta-sandstone, Kalixälv group																					
185	1400	110	316	10	2228	63	4.5	5.560	0.110	0.335	0.008	0.334	0.1207	0.0027	1909	16	1862	39	1963	39	95
190	140	11	47	4	352	30	2.9	5.270	0.130	0.326	0.007	0.683	0.1183	0.0020	1863	21	1816	35	1929	31	94
191	510	110	132	28	780	180	3.8	5.770	0.180	0.334	0.010	0.732	0.1220	0.0028	1940	27	1855	49	1984	40	93
192	330	22	84	4	609	34	3.8	5.660	0.110	0.345	0.009	0.792	0.1186	0.0023	1925	17	1912	43	1933	35	99
193	159	10	97	4	707	22	1.7	6.250	0.140	0.375	0.010	0.595	0.1194	0.0023	2011	19	2064	44	1967	34	105
194	297	27	130	11	971	90	2.2	5.530	0.150	0.339	0.011	0.925	0.1184	0.0021	1904	23	1880	55	1930	32	97
195	238	30	24	1	177	12	9.4	6.170	0.120	0.360	0.008	0.845	0.1226	0.0019	1999	17	1983	37	1993	28	99
196	189	17	49	8	263	18	4.4	6.490	0.150	0.371	0.009	0.942	0.1258	0.0014	2044	20	2031	40	2039	20	100
197	694	44	279	8	1791	55	2.5	5.360	0.120	0.333	0.005	0.591	0.1153	0.0022	1877	19	1851	25	1883	34	98
202	950	120	193	47	1310	330	5.2	5.220	0.130	0.324	0.008	0.798	0.1155	0.0019	1854	21	1810	38	1893	31	96
203	289	24	94	7	677	44	3.1	5.620	0.110	0.335	0.010	0.740	0.1214	0.0023	1919	18	1863	50	1975	33	94
204	209	11	67	2	623	29	3.2	10.770	0.170	0.474	0.008	0.545	0.1692	0.0022	2503	14	2500	35	2549	22	98
205	200	11	23	4	344	58	9.2	13.270	0.290	0.525	0.015	0.260	0.1850	0.0030	2698	21	2721	64	2706	24	101
206	127	6	26	1	186	7	5.0	5.140	0.100	0.324	0.007	0.531	0.1165	0.0024	1845	16	1809	34	1909	39	95
207	235	5	63	3	498	30	3.9	5.960	0.110	0.359	0.008	0.695	0.1221	0.0018	1970	16	1977	37	1986	27	100
208	223	7	129	4	1320	75	1.8	12.470	0.300	0.509	0.012	0.587	0.1793	0.0044	2640	23	2653	51	2659	34	100
209	106	9	43	4	293	22	2.6	5.140	0.110	0.334	0.011	0.603	0.1142	0.0026	1842	19	1859	51	1865	41	100
Common-Pb corrected[f]																					
11	415	71	195	22	1690	110	2.2	8.320	0.440	0.391	0.020	0.914	0.1551	0.0031	2263	49	2124	92	2402	34	88
20	1558	88	799	38	5510	290	2.0	4.890	0.120	0.284	0.011	0.709	0.1258	0.0028	1800	21	1609	53	2039	40	79
22	970	240	322	84	3330	900	3.2	12.040	0.340	0.427	0.031	0.564	0.1990	0.0120	2607	26	2280	140	2804	96	81
34	1200	380	248	61	1090	330	4.5	5.120	0.500	0.317	0.031	0.975	0.1154	0.0018	1831	80	1770	150	1886	28	94
47	318	22	46	3	930	160	7.2	6.310	0.250	0.370	0.015	0.785	0.1237	0.0030	2016	35	2048	64	2007	44	102
48	382	29	115	11	348	58	3.4	4.810	0.130	0.298	0.009	0.781	0.1167	0.0018	1785	23	1682	42	1906	27	88
49	1036	78	308	27	2280	200	3.6	5.163	0.076	0.317	0.009	0.779	0.1182	0.0021	1850	14	1773	45	1934	34	92
50	740	140	363	58	2570	550	1.9	5.760	0.160	0.342	0.012	0.896	0.1229	0.0020	1939	24	1897	59	1997	29	95
63	381	60	470	160	1360	220	1.3	5.420	0.550	0.339	0.028	0.967	0.1126	0.0026	1876	83	1880	130	1840	42	102
68	251	12	117	10	954	63	2.1	6.380	0.120	0.390	0.015	0.776	0.1175	0.0032	2029	16	2121	71	1914	49	111
73	1930	480	580	140	2530	530	3.2	3.130	0.310	0.211	0.018	0.988	0.1081	0.0016	1454	85	1231	99	1767	26	70
76	393	28	66	14	585	87	6.4	5.570	0.130	0.350	0.007	0.754	0.1183	0.0023	1910	21	1935	34	1928	35	100
78	560	95	248	44	1420	300	2.3	12.070	0.430	0.463	0.015	0.777	0.1913	0.0032	2607	33	2450	68	2752	28	89
86	865	83	190	24	1820	300	4.2	9.19	0.24	0.417	0.017	0.92872	0.159	0.0023	2357	24	2246	76	2444	25	92
90	1220	210	497	81	3280	740	2.5	5.06	0.29	0.305	0.018	0.96848	0.1193	0.0013	1826	50	1712	92	1945	20	88
113	700	160	255	74	1220	290	3.4	5.060	0.410	0.335	0.027	0.988	0.1134	0.0014	1818	70	1860	130	1854	23	100
114	552	49	168	11	1240	100	3.5	5.610	0.110	0.358	0.006	0.587	0.1175	0.0022	1917	17	1974	30	1916	34	103
126	668	30	831	33	7150	260	0.8	8.060	0.160	0.392	0.008	0.908	0.1476	0.0022	2237	18	2133	38	2323	28	92
137	468	76	220	41	1230	250	2.2	5.740	0.200	0.344	0.009	0.900	0.1208	0.0025	1935	31	1903	43	1974	34	96

Table 5 continues

Analysis	Concentrations (ppm)[a]						Ratios								Ages (Ma)						CONC.
No	U	2σ	Th	2σ	Pb	2σ	U/Th[a]	$^{207}Pb/^{235}U$[b]	2σ[d]	$^{206}Pb/^{238}U$[b]	2σ[d]	rho[c]	$^{207}Pb/^{206}Pb$[e]	2σ[d]	$^{207}Pb/^{235}U$[b]	2σ[d]	$^{206}Pb/^{238}U$[b]	2σ[d]	$^{207}Pb/^{206}Pb$[e]	2σ[d]	%
FHM140088B, meta-sandstone, Kalixälv group																					
142	414.9	9.1	388	48	3330	200	1.1	10.73	0.27	0.431	0.012	0.67121	0.1765	0.004	2498	24	2309	56	2627	41	88
143	160	7	60	3	439	21	2.8	5.320	0.150	0.323	0.007	0.698	0.1187	0.0026	1871	24	1804	35	1935	39	93
198	2580	100	860	35	30900	1200	3.1	4.940	0.180	0.283	0.011	0.933	0.1264	0.0028	1808	32	1605	54	2046	39	78

CONC. = Concorcance (Tera Wasserburg)

[a]U, Th and Pb concentrations with errors (2SE) and U/Th ratios are calculated relative to the GJ-1 reference zircon

[b]Corrected for background, downhole and within-run Pb/U fractionation. Normalised to the reference zircon GJ-1 (TIMS/measured values)

The $^{207}Pb/^{235}U$ is calculated through: $(^{207}Pb/^{206}Pb)/(^{238}U/^{206}Pb * 1/137.88)$

[c]Rho is the error correlation defined as the quotient of the propagated errors of the $^{206}Pb/^{238}U$ and $^{207}/^{235}U$ ratios

[d]Quadratic addition of within-run errors (2 SE) and the all-session reproducibility of GJ-1 (2 SE)

[e]Normalised to the GJ-1 reference zircon (~0.6 per atomic mass unit)

[f]Common Pb correction through measured Pb^{204} (corrected for Hg^{204} using natural abundance Hg isotopic ratios) and the model Pb composition of Stacey & Kramers (1975)

Table 6. SIMS U-Pb-Th zircon data on Pahakurkio upper sandstone sample (RR96128, laboratory id n1383).

Sample/ spot #	Comment	U ppm	Th ppm	Pb ppm	Th/U calc [*1]	^{238}U / ^{206}Pb	±σ %	^{207}Pb / ^{206}Pb	±σ %	Disc. % conv. [*2]	Disc. % 2σ lim. [*3]	^{207}Pb / ^{206}Pb	±σ Ma	^{206}Pb / ^{238}U	±σ Ma	$^{206}Pb/^{204}Pb$ meas.	f_{206}% [*4]
n1383-01a	CL-grey, margin	349	187	164	0.55	2.732	1.29	0.3661	1.29	0.3		2005	6	2011	22	43304	0.04
n1383-01b	CL-grey, central	185	136	89	0.69	2.768	1.31	0.3613	1.31	-0.5		1997	9	1988	22	49945	{0.04}
n1383-02a	CL-dark grey, margin	793	61	301	0.06	2.986	1.29	0.3349	1.29	-3.1	-0.4	1914	5	1862	21	22821	0.08
n1383-02b	CL-light-grey, osc zon, central	327	339	173	0.99	2.673	1.29	0.3742	1.29	-2.0		2085	6	2049	23	85644	{0.02}
n1383-03a	CL-dark grey, margin	476	46	198	0.09	2.752	1.29	0.3634	1.29	1.9		1966	6	1998	22	29054	0.06
n1383-04a	CL-grey, margin	473	197	218	0.40	2.685	1.29	0.3724	1.29	-0.4		2047	6	2041	23	39121	0.05
n1383-05a	CL-grey, margin	256	126	107	0.43	2.966	1.29	0.3371	1.29	-1.5		1898	9	1873	21	13017	0.14
n1383-05b	CL-dark grey, central	366	140	157	0.40	2.863	1.29	0.3493	1.29	2.3		1894	7	1931	22	21331	0.09
n1383-06a	CL-dark grey, osc. zon., margin	482	147	206	0.26	2.794	1.29	0.3579	1.29	1.1		1953	6	1972	22	35459	0.05
n1383-06b	CL-grey, central	181	118	78	0.49	2.946	1.29	0.3395	1.29	-3.8	-0.4	1948	9	1884	21	19157	0.1
n1383-07a	CL-darkgrey	491	243	329	0.49	1.957	1.29	0.5110	1.29	0.6		2648	4	2661	28	104433	0.02
n1383-08a	CL-grey, margin	173	139	76	0.75	3.043	1.29	0.3286	1.29	-4.6	-1.1	1909	10	1832	21	16729	0.11
n1383-08b	CL-grey, osc. zon, central	101	58	44	0.55	2.926	1.29	0.3417	1.29	-0.3		1901	15	1895	21	17843	{0.10}

CL = Cathodoluminescence, osc. Zon = oscillatory zoned (Roye Rutland, pers. com)

Isotope values are common Pb corrected using modern common Pb composition (Stacey & Kramers 1975) and measured ^{204}Pb.

[*1] Th/U ratios calculated from $^{208}Pb/^{206}Pb$ and $^{207}Pb/^{206}Pb$ ratios, assuming a single stage of closed U-Th-Pb evolution

[*2] Age discordance in conventional concordia space. Positive numbers are reverse discordant.

[*3] Age discordance at closest approach of error ellipse to concordia (2σ level).

[*4] Figures in parentheses are given when no correction has been applied, and indicate a value calculated assuming present-day Stacey-Kramers common Pb.

Sm-Nd isotopic analysis

Method

For whole-rock Sm-Nd analysis, 120–200 mg of powdered sample was spiked with a ^{149}Sm-^{150}Nd tracer. The sample-spike mixture was dissolved in HF-HNO_3 in sealed Teflon bombs in an oven at 180°C (felsic rocks) or in Savillex screw-cap beakers on a hot plate (mafic rocks) for 48 hours. Before dissolving the residue in 6.2 N HCl, the fluorides were gently evaporated using HNO_3. Conventional cation exchange chromatography was used to separate the light rare earth elements and Sm and Nd were further separated by a modified Teflon-HDEHP (hydrogen di-ethylhexyl phosphate) method (Richard et al. 1976). Total procedural blank was <0.5 ng for Nd. Isotope ratios were measured on a VG Sector 54 TIMS using Ta-Re triple filaments. Nd isotope ratios were measured in dynamic mode and Sm isotopes in static mode. Nd ratios are normalised to $^{146}Nd/^{144}Nd = 0.7219$. Based on several duplicate analyses, the error of the $^{147}Sm/^{144}Nd$ is estimated to be better than 0.6%. The long-term average $^{143}Nd/^{144}Nd$ for the La Jolla standard is 0.511850 ±0.000010 (standard deviation for 220 measurements during 1996–2010). Recent analysis on BCR-1 yielded Sm = 6.63 ppm, Nd = 28.88 ppm, $^{143}Nd/^{144}Nd = 0.512640 \pm 0.000010$. The ε_{Nd} was calculated using $\lambda 147Sm = 6.54 \times 10^{-12}\ a^{-1}$, $^{147}Sm/^{144}Nd = 0.1966$, and $^{143}Nd/^{144}Nd = 0.512640$ for the present CHUR (Jacobsen & Wasserburg 1980). TDM was calculated after DePaolo (1981). Plotting and calculations of isotope data were performed using Isoplot software (Ludwig 2012).

Results and interpretation of data

Sm-Nd isotopic analysis was performed on the same samples as selected for geochronology (see previous section). Two meta-andesitic samples from the Sakarinpalo suite and the Kalixälv group, record $\varepsilon_{Nd(1.89Ga)}$ -3.9 and -2.2 values, and depleted mantle model ages of approximately 2.4 Ga, respectively (Table 7). Volcanic rocks of the Kiirunavaara group as well as early Svecokarelian intrusive rocks record overall negative initial ε_{Nd} signatures (i.e. lie below the CHUR reference value (Fig. 16). This is suggested to be a result of variable anatexis of the Archaean basement rocks, which by approximately 1.9 Ga had acquired distinctly negative ε_{Nd} values (< -10; Fig. 16). Sm-Nd isotopic analyses of Palaeoproterozoic granitoids and metavolcanic rocks approximately delineate the Archaean palaeoboundary zone between the reworked Archaean craton in the north and more juvenile Palaeoproterozoic domains to the south along the Luleå–Jokkmokk zone in Sweden and along the Raahe–Ladoga zone in Finland (Fig. 1, Huhma 1986, Öhlander et al. 1993, Mellqvist et al. 1999, Vaasjoki & Sakko 1988, Nironen 1997). In contrast, Svecofennian arc volcanism in the Skellefte field south of the Norrbotten ore province records positive initial ε_{Nd} signatures ($\varepsilon_{Nd(1.89Ga)}$ 2.7 and 4.0) close to the depleted mantle model line. It is suggested that this is the result of 'juvenile' melts above a north-dipping subduction zone at the continental margin or possibly in an island arc accreted to the craton (Hietanen 1975, Nironen 1997, Weihed et al. 2005). The Veikkavaara greenstones, which are part of Karelian, approximately 2.1 Ga rift-related magmatism in Norrbotten, have whole-rock initial ε_{Nd} values from 0.4 to +3.7 (Fig. 16), indicating juvenile depleted to partly-enriched tholeiitic mantle melts with minor assimilation of older continental crust of the Archaean Norrbotten craton during magma ascent or storage (Lynch et al. 2018b).

Meta-sandstones from the Pahakurkio and Kalixälv groups record similar $\varepsilon_{Nd(1.89Ga)}$ values at -3.0 and -3.9, respectively, consistent with a mixture of debris from predominantly 2.2–1.9 Ga and 3.0–2.6 Ga-old rocks, as suggested by U-Pb provenance zircon dating of these samples.

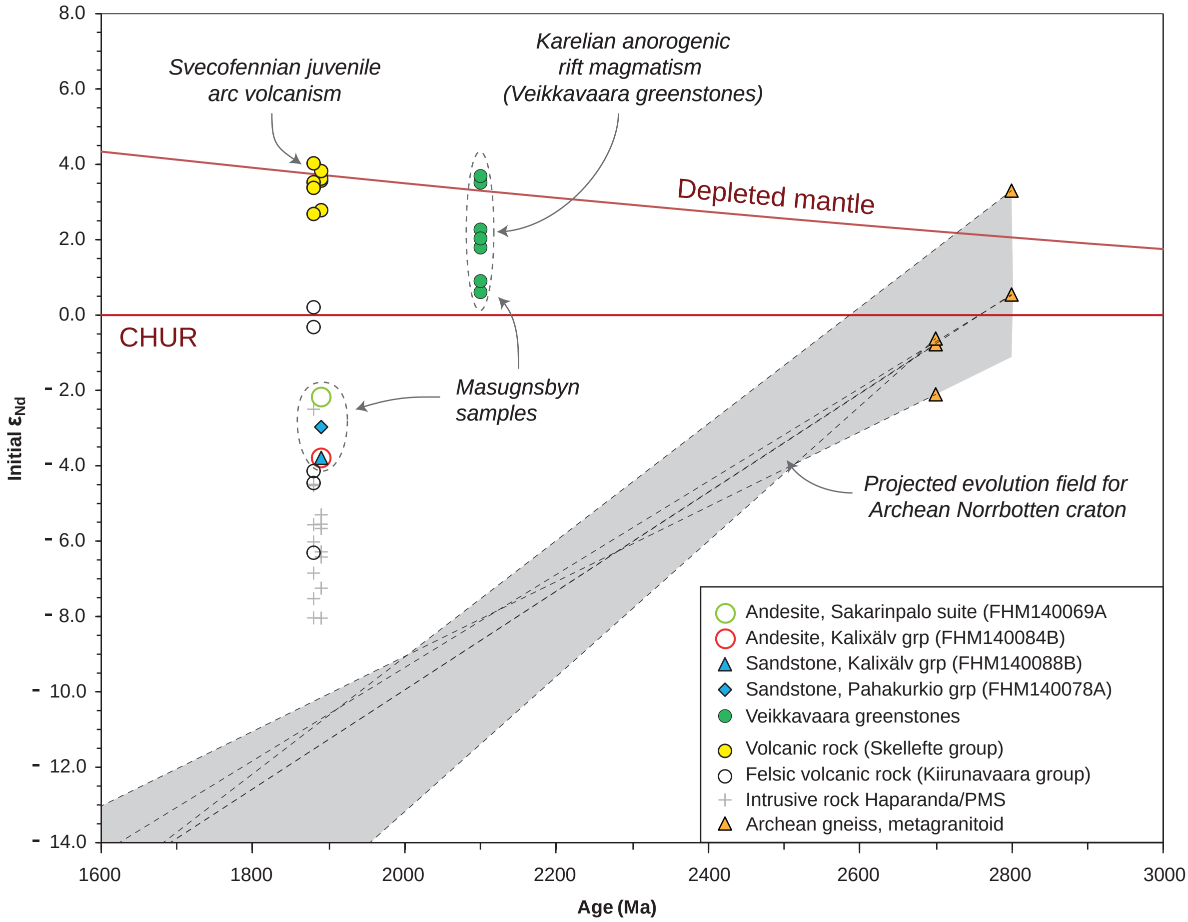

Figure 16. Initial ε_{Nd} versus time plot for rock samples from Masugnsbyn. Data from selected age groups and rock types from northern Norrbotten are shown for comparison, as well as data from the Skellefte group volcanic rocks. DM = depleted mantle model curve, based on DePaolo (1981), CHUR = chondrite uniform reservoir (e.g., DePaolo & Wasserburg 1976). The rocks are metamorphic with the prefix meta- to be added to rock names. References to data: Öhlander et al. (1987a, b, 1993), Skiöld et al. (1988), Kathol & Weihed (2005), Lynch et al. (2018b).

Table 7. Sm-Nd-isotopic data from Svecofennian supracrustal rocks in the Masugnsbyn area. Sm-Nd data from the Veikkavaara greenstones are presented in Lynch et al. (2018b).

Sample	N Sweref	E Sweref	Rock type	Unit	Sm (ppm)	Nd (ppm)	Sm/Nd	$^{147}Sm/^{144}Nd$	Error ±2σ	$^{143}Nd/^{144}Nd$	Error ±2σ	ε_{Nd} 1890 Ma	T-DM (Ma)
FHM140069A	7502412	803618	Andesite	Sakarinpalo suite	4.5	27.5	0.16	0.0991	0.0006	0.511231	0.000010	-3.9	2409
FHM140078A	7493033	804679	Sandstone	Pahakurkio grp	3.9	19.5	0.20	0.1194	0.0007	0.511525	0.000012	-3.0	2455
FHM140084B	7487854	799400	Andesite	Kalixälv grp	8.0	40.0	0.20	0.1204	0.0007	0.511578	0.000010	-2.2	2392
FHM140088B	7487141	800148	Sandstone	Kalixälv grp	4.3	22.4	0.19	0.1150	0.0007	0.511429	0.000010	-3.9	2495

Laboratory assistance by Leena Järvinen and Arto Pulkkinen are acknowledged.
For methods see Huhma et al (2012).
Measurements were made on VG Sector 54 mass-spectrometer.
Error in $^{147}Sm/^{144}Nd$ is 0.6% (spiked Sm and $^{150}/^{144}Nd$ was measured using single collector mode).
$^{143}Nd/^{144}Nd$ ratio is normalized to $^{146}Nd/^{144}Nd$=0.7219.
Long-term average $^{143}Nd/^{144}Nd$ for the La Jolla standard at GTK is 0.511851±0.00008 (standard deviation for 60 measurements during 2012).
Depleted mantle model age (T-DM) was calculated after DePaolo (1981).
Rocks are metamorphic with prefix meta- to be added to rock names.

DISCUSSION AND PRELIMINARY CONCLUSIONS

Interpretation of the depositional environment for supracrustal rocks in the Pahakurkio and Kalixälv groups is given below and mainly follows Padget (1970), Niiniskorpi (1986) and Kumpulainen (2000). Heavy mineral layers and cross-bedding are common in the lower and upper sandstone units of the Pahakurkio group, and ripple and rill marks are found locally, suggesting a coastal marine depositional environment affected by wave and possibly storm activity. The interval of pebbly conglomerates may represent a storm event resulting in erosion on the shelf and transport of pebbly debris from the shoreline setting. The gradual facies change from the deposition characterised by hummocky cross-stratification and low-angle cross-bedding of the lower sandstone unit into the normally graded and ripple-laminated sandy mudstones of the upper shale suggests a gradual increase in relative water depth, where the locally graphite-bearing shales represent deposition in stagnant waters beneath the storm wave base. There appears to be a gradual transition from the upper shale unit to the upper sandstone unit, with localised normally graded bedding in the transition zone. Sandstone deposition gradually takes over and the upper sandstone unit is characterised by horizontal lamination and low-angle cross-bedding, which, together with common wave ripples, indicate a shallow water coastal depositional environment, similar to the lower sandstone unit. Thus, the whole Pahakurkio group represents two consecutive cycles of deepening and shallowing related to corresponding relative sea level changes. The changes in relative water depth could depend on: (a) real sea level changes; (b) changes in input of clastic material; (c) subsidence of the basin floor; or (d) a combination of these factors.

The sandstones of the Pahakurkio group are immature arkoses to subarkoses, and major and trace element chemistry suggests predominantly continental crust source rocks. According to Boggs (2009), feldspar-rich sandstones typically come from rapid erosion of feldspar-rich felsic to intermediate crystalline plutonic or metamorphic rocks, where chemical weathering is subordinate to physical weathering. Transportation of the arkosic material results in better sorting and various degrees of grain rounding, especially when further transported into marine environments, where feldspar-rich sandstone may be inter-bedded with a variety of marine deposits including shales, limestones, and evaporates. A marine depositional environment for the Pahakurkio group sediments is further supported by the presence of tourmaline as a common boron-bearing accessory phase in the sedimentary rocks. Carbonate layers may represent chemically deposited sediments, whereas scapolite-rich rocks may have an evaporitic origin.

The stratigraphically higher Kalixälv group consists of similar types of metasedimentary rocks to the Pahakurkio group, i.e. originally shales and sandstone, but with a generally higher grade of metamorphic alteration and less preserved primary structures. Cross-bedding and wave-ripples can be seen locally in quartzitic rocks, suggesting shallow water deposition. Thus, the depositional environment appears similar to the Pahakurkio group, with vertical facies changes into relatively deeper water where, in part, graphite-bearing shales represent deposition in stagnant waters beneath the storm wave base. A distinct difference is the much greater abundance of volcanic and volcanogenic sedimentary rocks in the Kalixälv group than in the Pahakurkio group. Extensive volcanism is a potentially important heat source driving both hydrothermal alteration and the generation of minor Zn-Pb-Cu and Cu ±Au sulphide mineralisations that occur in the border zone between the Pahakurkio and Kalixälv groups. However, the partly vein-hosted character suggests a later, epigenetic origin. A positive correlation exists between B and Zn + Pb content in lithochemical analyses from the Kurkkionvaara Zn-Pb-Cu mineralisation, suggesting a hydrothermal system with boron-rich fluids containing base metals (Niiniskorpi 1986). Boron-rich fluids probably have a source in the metapelites, originally deposited as marine sediments, and tourmaline-rich rocks could potentially be used as an exploration tool.

A maximum depositional age of the Kalixälv group of approximately 1.87 Ga, as suggested by U-Pb zircon provenance age data, is somewhat lower than the 1 887 ±5 Ma U-Pb zircon age obtained from the plagioclase porphyric meta-andesite within the same group, and the migmatisation age of

1 878 ±3 Ma obtained from the high-grade southern part of the Masugnsbyn area (Hellström 2018). The latter age must constrain the deposition of sediments as older than approximately 1.88 Ga. A limited amount of SIMS analyses on zircon core domains from a migmatitic paragneiss record an age distribution similar to the meta-arenite sample in this study, with the majority of ages in the 2.02–1.92 Ga and 2.97–2.75 Ga intervals (Hellström 2018).

The lower sandstone sample (FHM140078A) in the Pahakurkio group shows a zircon age distribution pattern dominated by 2.15–1.90 Ga (66%) and 2.95–2.62 Ga ages (30%), similar to the intermediate sandstone in the Kalixälv group, dominated by 2.15–1.86 Ga ages (81%) and 2.96–2.55 Ga ages (11%). The younger age interval of the Pahakurkio group, however, has slightly older ages, peaking at 2.04 Ga and with a maximum depositional age estimated at approximately 1.91 Ga from the youngest zircons. Zircon age data from the Pahakurkio upper sandstone unit (sample RR96128) show a similar age distribution pattern to the lower sandstone unit, although based on a very limited number of analyses (n = 13) of the former. The maximum depositional age is calculated from the three youngest zircon grains at approximately 1.90 Ga, and is similar or slightly younger than the maximum depositional age from the lower Pahakurkio sandstone unit.

Overall, the zircon age distribution patterns are consistent with the Kalixälv group being younger than the Pahakurkio group, according with field-based way-up determinations. The lower quantity of Archaean zircons in the Kalixälv group sample (13%) compared with the Pahakurkio group sample (31%), suggests that the Archaean basement was covered by Svecofennian rocks as the Svecokarelian orogeny progressed, and thus erosion and deposition of debris from the latter were more predominant. This scenario could explain the peak offset seen in the 2.2–1.9 Ga age interval between the Pahakurkio and Kalixälv groups, with maximum peaks shifting from 2.04 to 1.93 Ga, although the Pahakurkio sample does have a pronounced peak at approximately 1.92 Ga. Archaean rocks are exposed in the Råstojaure complex in northernmost Sweden (Martinsson et al. 1999, Lauri et al. 2016). Sm-Nd isotopic analyses of Proterozoic granitoids and metavolcanic rocks suggest a covered Archaean basement south of the Råstojaure complex (Öhlander et al. 1993, Mellqvist et al. 1999). So far, there are few age determinations from felsic to intermediate igneous rocks in the 2.2–1.92 Ga interval, but some do exist from the Savo schist belt within the Raahe–Ladoga zone in Finland, at Norvijaur in the Jokkmokk area and in the Rombak–Sjangeli basement window of the Caledonides, all along the Archaean–Palaeoproterozoic boundary (Helovuori 1979, Korsman et al. 1984, Vaasjoki & Sakko 1988, Kousa et al. 1994, Lahtinen & Huhma 1997, Vaasjoki et al. 2003, Kousa et al. 2013, Skiöld et al. 1993, Romer et al. 1992; Hellström 2015). In addition, 1.96–1.94 Ga calc-alkaline rocks with island arc affinity occur in the northern part of the Bothnian basin, south of the Skellefte district (Wasström 1993, 1996, Lundqvist et al. 1998, Eliasson et al. 2001, Skiöld & Rutland 2006). It can be concluded from zircon age provenance data that 2.2–1.9 Ga felsic to intermediate rocks can be expected to be present to a far greater extent than is known from present age determination of the rocks within the Svecokarelian orogen, or suggest the presence of a still unlocated major continental block that must have existed somewhere nearby to supply the abundant detritus material. This pattern is observed in several other provenance studies of Svecofennian sedimentary rocks (e.g. Huhma et al. 1991, Claeson et al. 1993, Huhma et al. 2011, Lahtinen et al. 2015). The 2.5–2.2 Ga age interval seems to have been a “quiet” period with no major rock-forming events, except for minor mafic magmatism (see compilation in Huhma et al. 2011). Meta-sandstones from the Pahakurkio and Kalixälv group record similar $\varepsilon_{Nd(1.89Ga)}$ values at -3.0 and -3.9, respectively, which are consistent with mixture of debris from predominantly 2.2–1.9 Ga and 3.0–2.6 Ga old rocks, as suggested by U-Pb provenance zircon dating of these samples (cf. Huhma 1987).

It is suggested that deposition of epiclastic material occurred contemporaneously with volcanism at approximately 1.89–1.88 Ga, with erosion and redeposition of volcanic material to form mixed epiclastic and volcanoclastic sediments of the Kalixälv group. Sub-arkosic sandstone of the Pahakurkio group has a more mature, quartz-rich composition than the amphibole-bearing sandstones of the Kalixälv group. Volcanic rocks seem to be much less abundant in the Pahakurkio group, except for the correlated Sakarinpalo suite

The Sakarinpalo metavolcanic rocks occur spatially with rocks of the Veikkavaara greenstone group, and are tentatively correlated with units within the Viscaria formation in the Kiruna Greenstone group (cf. Martinsson 1997). However, U-Pb SIMS zircon geochronology dates an intermediate metavolcanic rock sample of the Sakarinpalo suite at 1 890 ±5 Ma, a Svecofennian age. Magnetic anomaly patterns reveal a complexly folded internal structure for the Veikkavaara greenstones. Poly-phase deformation and folding, together with the very low rock exposure complicates interpretation of way-up in the stratigraphic succession. The Svecofennian age of the Sakarinpalo suite may even suggest inverted younging, with way-up towards the core of the V-shaped Veikkavaara greenstone structure.

Strongly scapolite-biotite-altered intermediate rocks of the Pahakurkio group show an identical trace element pattern to volcanic rocks in the Sakarinpalo suite, suggesting these units may be correlated. The meta-andesite in the Kalixälv group is dated at 1 887 ±5 Ma and is thus of a similar age to the rocks in the Sakarinpalo suite. In a regional context, the metavolcanic rocks in the Masugnsbyn area are of a similar or possibly slightly older age to the intermediate metavolcanic rocks in the Sammakkovaara group in the Pajala area of northeastern Norrbotten, dated at 1 882 ±3 and 1 880 ±3 Ma (Martinsson et al. 2018b), as well as intermediate volcanic rocks of the "Porphyrite group" in the Kiruna area, dated at 1 878 ±7 Ma (minimum age; Edfelt et al. 2006), intermediate metavolcanic rocks of the Muorjevaara group in the Gällivare area, dated at 1 882 ±6 Ma and 1 878 ±7 Ma (Claeson & Antal Lundin 2012, Lynch et al. 2018a) and felsic metavolcanic rocks in the Boden area, dated at 1 886 ±4 and 1 884 ±5 Ma (Sadeghi & Hellström 2015).

Chemically, the metavolcanic rocks in the Masugnsbyn area are intermediate to weakly felsic, low-Fe-Ti and calc-alkaline, thus of similar composition to "Porphyrite group" rocks in Norrbotten. A detailed, regional comparison of data from volcanic rocks in Norrbotten has not been carried out here, however. Most samples from Masugnsbyn are classified as andesite according to the Nb/Y –Zr/Ti classification diagram (Pearce 1996), but basalts, trachy-andesites, trachytes and dacites-rhyolites also occur. Volcanic rocks record similar chondrite-normalised rare earth element (REE) patterns, enriched in light REE over heavy REE, $(La/Yb)_N = 10.5 \pm 3.3$ (1σ, n = 26), but with a relatively flat pattern in the HREE end ($(Gd/Lu)_N = 1.6 \pm 0.38$ (1σ)). Primitive mantle-normalised spider diagrams show enrichment in the large ion lithophile elements, with a pronounced negative Nb-Ta anomaly, as well as negative anomalies in Ti and P. The normalised element patterns thus show a typical subduction zone signature, but also a typical upper continental crustal signature. Alternatively, this signature could be inherited from partial melting of crustal source rock. Although they have very similar averaged normalised element patterns, the volcanic rocks from the southeastern part of the Masugnsbyn area can be grouped with the Kalixälv group, and the highly altered rocks in the Pahakurkio group with the Sakarinpalo suite, only distinguished by a strong negative anomaly in Sr in the latter groups. In part, strong potassium or sodium alteration of the volcanic rocks in the Sakarinpalo suite suggest that this poorly exposed area could have potential for hydrothermal sulphide mineralisations.

Overall, negative initial ε_{Nd} signatures of metavolcanic rocks from the Sakarinpalo and Kalixälv groups ($\varepsilon_{Nd(1.89Ga)}$ at -3.9 and -2.2), metavolcanic rocks of the Kiirunavaara Group, as well as early Svecokarelian intrusive rocks in the Northern Norrbotten ore province suggest a source of juvenile arc-generated melts mixed with variable amounts of assimilated older continental crust of the Archaean craton, which by approximately 1.9 Ga had acquired distinctly negative ε_{Nd} values (< -10). Svecofennian igneous activity was related to partial melting above a subduction zone dipping under the older continental crust of the Archaean Norrbotten craton.

ACKNOWLEDGEMENTS

Our sincere thanks go to George Morris, Nikolaos Arvanitidis, Stefan Bergman and Veikko Niiniskorpi for their comments on the manuscript. Roy Rutland and Martin Whitehouse are gratefully acknowledged for providing unpublished SIMS zircon data from a meta-sandstone sample (RR96128) of the Pahakurkio group. U-Pb isotopic zircon data were obtained from fruitful cooperation with the Laboratory for Isotope Geology of the Swedish Museum of Natural History (NRM) in Stockholm. The Nordsim facility is operated under an agreement between the research funding agencies of Denmark, Norway and Sweden, the Geological Survey of Finland and the Swedish Museum of Natural History. Martin Whitehouse, Lev Ilyinsky and Kerstin Lindén at the Nordsim analytical facility are gratefully acknowledged for their first-class analytical support with SIMS analyses. Martin Whitehouse reduced the zircon analytical data, Lev Ilyinsky assisted during ion probe analyses and Kerstin Lindén prepared the zircon mounts. Milos Bartol at the Evolutionary Biology Centre and Jaroslaw Majka at the Department of Geology, Uppsala University, along with Kerstin Lindén at NRM are all warmly thanked for their support during BSE/CL imaging of zircons. Laboratory assistance with Sm-Nd isotopic analyses by Leena Järvinen and Arto Pulkkinen at GTK is gratefully acknowledged. Magnetic data from areas adjacent to northern Sweden used in Figure 1 were supplied by the geological surveys of Norway (ngu.no), and Finland (gtk.fi). Veikko Niiniskorpi is thanked for permission to use his photo of cross-bedding at Saarikoski in Figure 8B. Tone Gellerstedt and Maxwell Arding are much thanked for editing and proofreading.

REFERENCES

Bhatia, M.R., 1983: Plate Tectonics and Geochemical Composition of Sandstones. *The Journal of Geology 91*, 611–627.

Bergman, S., Billström, K., Persson, P.-O., Skiöld, T. & Evins, P., 2006: U-Pb age evidence for repeated Palaeoproterozoic metamorphism and deformation near the Pajala shear zone in the northern Fennoscandian shield. *GFF 128*, 7–20.

Bergman, S., Kübler, L. & Martinsson, O., 2001: Description of Regional Geological and Geophysical Maps of Northern Norrbotten County (east of the Caledonian Orogen). *Sveriges geologiska undersökning Ba 56*, 110 pp.

Bergman, T., Hellström, F. & Ripa, M., 2015: Verksamhetsrapport 2014: Norrbottens malm och mineral. *SGU-rapport 2015:08,* Sveriges geologiska undersökning. 20 pp.

Boggs, S., 2009: *Petrology of Sedimentary Rocks.* Cambridge University Press, 600 pp.

Boynton, W., 1984: Cosmochemistry of the rare earth elements: meteorite studies. Rare Earth Element Geochemistry.-Developments in Geochemistry 2 (Henderson, R., ed.), 89-92. Elsevier, Amsterdam.

Carlson, L., 1982a: Guld i Norrbotten del 1. *Sveriges geologiska undersökning BRAP 82039*, 140 pp.

Carlson, L., 1982b: Guld i Norrbotten. Del 2. *Sveriges geologiska undersökning BRAP 82040*, 133 pp.

Claeson, D. & Lundin, I.A., 2012: Beskrivning till berggrundskartorna 27K Nattavaara NV, NO, SV & SO. *Sveriges geologiska undersökning K383–386*, 22 pp.

Claesson, S., Huhma, H., Kinny, P.D. & Williams, I.S., 1993: The Baltic Shield Svecofennian detrital zircon ages—implications for the Precambrian evolution of the Baltic Shield. *Precambrian Research 64,* 109–130.

DePaolo, D.J., 1981: Neodymium isotopes in the Colorado Front Range and crust-mantle evolution in the Proterozoic. *Nature 291*, 684–687.

DePaolo, D.J. & Wasserburg, G.J., 1976: Nd isotopic variations and petrogenetic models. *Geophysical Research Letters 3*, 249–252.

Eliasson, T., Greiling, R., Sträng, T. & Triumf, C., 2001: Bedrock map 23H Stensele NV, scale 1:50 000. *Sveriges geologiska undersökning Ai 126*.

Edfelt, Å., Sandrin, A., Evins, P., Jeffries, T., Storey, C., Elming, S.-Å. & Martinsson, O., 2006: Stratigraphy and tectonic setting of the host rocks to the Tjårrojåkka Fe-oxide Cu-Au deposits, Kiruna area, northern Sweden. *GFF 128*, 221–232.

Eriksson, T., 1954: Pre-Cambrian Geology of the Pajala District, Northern Sweden. *Sveriges geologiska undersökning C 522*, 38 pp.

Frietsch, R., 1997: The iron ore inventory program 1963-1972 in Norrbotten County. *Sveriges geologiska undersökning Rapporter och meddelanden 92*, 77 pp.

Geijer, P., 1918: Nautanenområdet. En malmgeologisk undersökning. *Sveriges geologiska undersökning C 283*, 105 pp.

Geijer, P., 1929: Masugnsbyfältens geologi. *Sveriges geologiska undersökning C 351*, 39 pp.

Geijer, P., 1930: Pre-Cambrian geology of the iron bearing region Kiruna Gällivare Pajala. *Sveriges geologiska undersökning C 366*, 225 pp.

Grigull, S., Berggren, R., Jönberger, J., Jönsson, C., Hellström, F.A. & Luth, S., 2018: Folding observed in Palaeoproterozoic supracrustal rocks in northern Sweden. *In:* Bergman, S. (ed): Geology of the Northern Norrbotten ore province, northern Sweden. *Rapporter och Meddelanden 141,* Sveriges geologiska undersökning. This volume pp 205–257.

Grip, E. & Frietsch, R., 1973: *Malm i Sverige 2. Norra Sverige*. Almqvist & Wiksell, 295 pp.

Hellström, F., 2015: SIMS geochronology of a 1.93 Ga basement metagranitoid at Norvijaur west of Jokkmokk, northern Sweden. *SGU-rapport 2015:01*, Sveriges geologiska undersökning. 18 pp.

Hellström, F.A., 2018: Early Svecokarelian migmatisation west of the Pajala Shear Zone in the northeastern part of the Norrbotten Province, northern Sweden. *In:* Bergman, S. (ed): Geology of the Northern Norrbotten ore province, northern Sweden. *Rapporter och Meddelanden 141,* Sveriges geologiska undersökning. This volume pp 361–379.

Hellström, F.A. & Bergman, S., 2016: Is there a 1.85 Ga magmatic event in northern Norrbotten? – U-Pb SIMS zircon dating of the Pingisvaara metagranodiorite and the Jyryjoki granite, northern Sweden. *GFF 138, 526–532.*

Hellström, F. & Jönsson, C., 2014: Barents project 2014: Summary of geological and geophysical information of the Masugnsbyn key area. *SGU-rapport 2014:21*, Sveriges geologiska undersökning. 84 pp.

Hellström, F., Carlsäter Ekdahl, M. & Kero, L., 2012: Beskrivning till berggrundskartorna 27L Lansjärv NV, NO, SV & SO. *Sveriges geologiska undersökning K 387–390*, 27 pp.

Hellstrom, J., Paton, C, Woodhead, J. & Hergt, J., 2008: Iolite: Software for spatially resolved LA- (quad and MC) ICPMS analysis. *In:* Sylvester P (Ed.): *Laser Ablation ICP–MS in the Earth Sciences: Current Practices and Outstanding Issues*. Mineral. Assoc. of Canada, Quebec, Canada., 343–348.

Helovuori, O., 1979: Geology of the Pyhäsalmi ore deposit, Finland. *Economic Geology 74*, 1 084–1 101.

Hermelin, S.G., 1804: *Försök till mineral historia öfver Lappmarken och Vesterbotten; af friherre S.G. Hermelin. Stockholm, tryckt hos Carl Delén, 1804.* Stockholm.

Herron, M.M., 1988: Geochemical classification of terrigenous sands and shales from core or log data. *Journal of Sedimentary Research 58*, 820-829.

Hietanen, A., 1975: Generation of potassium-poor magmas in the northern Sierra Nevada and the Svecofennian of Finland. *J. Res. US Geol. Surv 3*, 631–645.

Högdahl, K., Andersson, U.B. & Eklund, O., 2004: The Transscandinavian Igneous Belt (TIB) in Sweden: a review of its character and evolution. *Geological Survey of Finland, Special Paper 37*, 123 pp.

Hughes, C.J., 1973: Spilites, keratophyres, and the igneous spectrum. *Geological Magazine 109*, 513–527.

Huhma, H., 1986: Sm-Nd, U-Pb and Pb-Pb isotopic evidence for the origin of the Early Proterozoic Svecokarelian crust in Finland. *Geologian survey of Finland Bulletin 337,* 48 pp.

Huhma, H., 1987: Precambrian Geology and Evolution of the Cental Baltic Shield Provenance of early proterozoic and archaean metasediments in Finland: a Sm-Nd isotopic study. *Precambrian Research 35*, 127–143.

Huhma, H., Claesson, S., Kinny, P. & Williams, I., 1991: The growth of Early Proterozoic crust: new evidence from Svecofennian detrital zircons. *Terra Nova 3*, 175–178.

Huhma, H., O'Brien, H., Lahaye, Y. & Mänttäri, I. 2011. Isotope geology and Fennoscandian lithosphere evolution. *Geological Survey of Finland, Special Paper 49,* 35–48

Huhma, H., Kontinen, A., Mikkola, P., Halkoaho, T., Hokkanen, T., Hölttä, P., Juopperi, H., Konnunaho, J., Luukkonen, E., Mutanen, T., Peltonen, P., Pietikäinen,K. & Pulkkinen, A. 2012: Nd isotopic evidence for Archaean crustal growth in Finland. *In*: P. Hölttä (ed.) *The Archaean of the Karelia Province in Finland*. *Geological Survey of Finland (GTK) Special Paper 54*, 176–213.

Jacobsen S.B. & Wasserburg G.J., 1980. Sm-Nd isotopic evolution of chondrites. *Earth and Planetary Science Letters, 50,* 139–155.

Jackson S.E., Pearson, N.J., Griffin W.L., Belousova E.A., 2004: The application of laser ablation-inductively coupled plasma-mass spectrometry to in situ U–Pb zircon geochronology. *Chemical Geology 211*, 47–69.

Janoušek, V., Farrow, C.M. & Erban, V., 2006: Interpretation of whole-rock geochemical data in igneous geochemistry: introducing Geochemical Data Toolkit (GCDkit). *Journal of Petrology 47,* 1255–1259.

Jensen, L.S., 1976: A new cation plot for classifying subakalic volcanic rocks. *Ontario Division of Mines Miscellaneous Paper 66,* 22 pp.

Jönberger, J., Jönsson, C., & Luth, S., 2018: Geophysical 2D and 3D modeling in the areas around Nunasvaara and Masugnsbyn, northern Sweden. *In:* Bergman, S. (ed): Geology of the Northern Norrbotten ore province, northern Sweden. *Rapporter och Meddelanden 141,* Sveriges geologiska undersökning. This volume pp 311–339.

Kathol, B. & Persson, P.-O., 2007: U-Pb zircon age of an ignimbritic rhyolite from Benbryteforsen in the area between Moskosel and Vidsel, southern Norrbotten County, Sweden. *In:* F. Hellström & J. Andersson (eds.): Results from radiometric datings and other isotope analyses 1. *SGU-rapport 2007:28*, Sveriges geologiska undersökning, 17–19.

Kathol, B. & Triumf, C.-A., 2004: Bedrock map 24J Arvidsjaur SO, scale 1:50 000. *Sveriges geologiska undersökning Ai 151.*

Kathol, B. & Weihed, P., (eds.) 2005: Description of regional geological and geophysical maps of the Skellefte District and surrounding areas. *Sveriges geologiska undersökning Ba 57*, 197 pp.

Korsman, K., Hölttä, P., Hautala, T. & Wasenius, P., 1984: Metamorphism as indicator of evolution and structure of the crust in eastern Finland. *Geological Survey of Finland Bulletin 328*, 40 pp.

Kousa, J., Luukas, J., Huhma, H. & Mänttäri, I., 2013: Palaeoproterozoic 1.93–1.92 Ga Svecofennian rock units in the northwestern part of the Raahe–Ladoga zone, central Finland. *In:* P. Hölttä (ed.): Current research: GTK Mineral potential workshop, Kuopio, May 2012. *Geological Survey of Finland Report of Investigation 198*, 91–96.

Kousa, J., Marttila, E. & Vaasjoki, M., 1994: Petrology, geochemistry and dating of Palaeoproterozoic metavolcanic rocks in the Pyhäjärvi area, central Finland. *In:* M. Nironen & Y. Kähkönen (eds.): Geochemistry of Proterozoic supracrustal rocks in Finland. *Geological Survey of Finland, Special Paper 19*, 7–27.

Kumpulainen, R.A., 2000: The Palaeoproterozoic sedimentary record of northernmost Norrbotten, Sweden. Unpublished report. *Sveriges geologiska undersökning BRAP 200030*, 45 pp.

Lahtinen, R. & Huhma, H., 1997: Isotopic and geochemical constraints on the evolution of the 1.93–1.79 Ga Svecofennian crust and mantle. *Precambrian Research 82*, 13–34.

Lahtinen, R., Huhma, H., Lahaye, Y., Jonsson, E., Manninen, T., Lauri, L.S., Bergman, S., Hellström, F., Niiranen, T. & Nironen, M., 2015: New geochronological and Sm–Nd constraints across the Pajala shear zone of northern Fennoscandia: Reactivation of a Paleoproterozoic suture. *Precambrian Research 256*, 102–119.

Lauri, L.S., Hellström, F., Bergman, S., Huhma, H. & Lepistö, S., 2016: New insights into the geological evolution of the Archaean Norrbotten province, Fennoscandian shield. *32nd Nordic Geological Winter Meeting, Helsingfors.*

LKAB Prospektering K-8656, 74 pp.

Ludwig, K.R., 2012: User's manual for Isoplot 3.75. A Geochronological Toolkit for Microsoft Excel. *Berkeley Geochronology Center Special Publication No. 5*, 75 pp.

Lundqvist, T., Vaasjoki, M. & Persson, P.-O., 1998: U-Pb ages of plutonic and volcanic rocks in the Svecofennian Bothnian Basin, central Sweden, and their implications for the Palaeoproterozoic evolution of the basin. *GFF 120*, 357–363.

Luth, S., Jönsson, C., Hellström, F., Jönberger, J., Djuly, T., Van Assema, B., Smoor, W., 2016: Structural and geochronological studies of the crustal-scale Pajala Deformation Zone, northern Sweden. *32nd Nordic Geological Winter Meeting, Helsingfors.*

Luth, S., Jönsson, C., Jönberger, J., Grigull, S., Berggren, R., van Assema, B., Smoor, W. & Djuly, T., 2018: The Pajala deformation belt in northeast Sweden: Structural geological mapping and 3D modelling around Pajala. *In:* Bergman, S. (ed): Geology of the Northern Norrbotten ore province, northern Sweden. *Rapporter och Meddelanden 141,* Sveriges geologiska undersökning. This volume pp 259–285.

Lynch, E.P., Bauer, T.E., Jönberger, J., Sarlus, Z., Morris, G.A. & Persson, P.-O., 2018a: Lithological and deformation characteristics of c. 1.88 Ga meta-volcanosedimentary rocks hosting iron oxide-copper-gold (IOCG) and related mineralisation in the Nautanen-Gällivare area, northern Sweden. *In:* Bergman, S. (ed): Geology of the Northern Norrbotten ore province, northern Sweden. *Rapporter och Meddelanden 141,* Sveriges geologiska undersökning. This volume pp 107–149.

Lynch, E.P., Hellström, F.A., Huhma, H., Jönberger, J., Persson, P.-O.& Morris, G.A., 2018b: Geology, lithostratigraphy and petrogenesis of c. 2.14 Ga greenstones in the Nunasvaara and Masugnsbyn areas, northernmost Sweden. *In:* Bergman, S. (ed): Geology of the Northern Norrbotten ore province, northern Sweden. *Rapporter och Meddelanden 141,* Sveriges geologiska undersökning. This volume pp 19–77.

Martinsson, O., 2004: Geology and Metallogeny of the Northern Norrbotten Fe-Cu-Au Province. *In:* R.L Allen, O. Martinsson & P. Weihed (eds.): Svecofennian ore-forming environments: volcanic-associated Zn-Cu-Au- Ag, intrusion associated Cu-Au, sedimenthostedPb-Zn, and magnetite-apatite deposits in northern Sweden. *Economic Geology Guidebook series 33*, 131–148.

Martinsson, O., 1997: Tectonic setting and metallogeny of the Kiruna greenstones. *Doctoral thesis, Luleå University of Technology*, 19 pp.
Martinsson, O. & Wanhainen, C., 2013: Fe oxide and Cu-Au deposits in the northern Norrbotten ore district: excursion held 16–20 August 2013. 12th Biennial SGA Meeting. Excursion guidebook SWE5, 70 pp.
Martinsson, O. & Perdahl, J.-A., 1995: Paleoproterozoic extensional and compressional magmatism in northern Sweden. *In:* J.-A. Perdahl: *Svecofennian volcanism in northern Sweden, Doctoral thesis 1995:169D, Paper II,* 1–13. Luleå University of Technology.
Martinsson, O., Vaasjoki, M. & Persson, P.-O., 1999: U-Pb ages of Archaean to Palaeoproterozoic granitoids in the Torneträsk-Råstojaure area, northern Sweden. *In:* S. Bergman (ed.): Radiometric dating results 4. *Sveriges geologiska undersökning C 831*, 70–90.
Martinsson, O., Van der Stilj, I., Debras, C. & Thompson, M., 2013: Day 3. The Masugnsbyn, Gruvberget and Mertainen iron deposits. *In:* O. Martinsson & C. Wanhainen (eds.): *12th Biennial SGA Meeting, Uppsala, Sweden. Excursion guidebook SWE5*, 37–44.
Martinsson, O., Billström, K., Broman, C., Weihed, P. & Wanhainen, C., 2016: Metallogeny of the Northern Norrbotten Ore Province, northern Fennoscandian Shield with emphasis on IOCG and apatite-iron ore deposits. *Ore Geology Reviews 78*, 447–492.
Martinsson, O., Bergman, S., Persson, P.-O. & Hellström, F.A., 2018a: Age and character of late-Svecokarelian monzonitic intrusions in north-eastern Norrbotten, northern Sweden. *In:* Bergman, S. (ed): Geology of the Northern Norrbotten ore province, northern Sweden. *Rapporter och Meddelanden 141,* Sveriges geologiska undersökning. This volume pp 381–399.
Martinsson, O., Bergman, S., Persson, P.-O., Schöberg, H., Billström, K. & Shumlyanskyy, L., 2018b: Stratigraphy and ages of Palaeoproterozoic metavolcanic and metasedimentary rocks at Käymäjärvi, northern Sweden. *In:* Bergman, S. (ed): Geology of the Northern Norrbotten ore province, northern Sweden. *Rapporter och Meddelanden 141,* Sveriges geologiska undersökning. This volume pp 79–105.
McDonough, W.F. & Sun, S.s., 1995: The composition of the Earth. *Chemical Geology 120*, 223–253.
Mellqvist, C., Öhlander, B. & Skiöld, T., 1999: Traces of Archaean crust in the Jokkmokk area, northern Sweden: a way of defining the Archaean-Proterozoic boundary. *In:* C. Mellqvist: *Proterozoic crustal growth along the Archaean continental margin in the Luleå and Jokkmokk areas, northern Sweden.* Doctoral thesis, Luleå University, 24 pp.
Niiniskorpi, V., 1982: Kurkkionvaara. Årsrapport 1981. *LKAB Ki 8207*, 5 pp.
Niiniskorpi, V., 1986: *En Zn-Pb-Cu-mineralisering i norra Sverige, en case-studie.* Licenciate thesis., geological department of Åba Akademi, 74 pp.
Nironen, M., 1997: The Svecofennian orogen: a tectonic model. *Precambrian Research 86*, 21–44.
Ödman, O.H., 1939: Urbergsgeologiska undersökningar inom Norrbottens län. *Sveriges geologiska undersökning C 426*, 100 pp.
Ödman, O.H., 1957: Beskrivning till berggrundskarta över urberget i Norrbottens län. *Sveriges geologiska undersökning Ca 41*, 151 pp.
Offerberg, J., 1967: Beskrivning till berggrundskartbladen Kiruna NV, NO, SV, SO. *Sveriges geologiska undersökning Af 1–4,* 147 pp.
Öhlander, B., Hamilton, P.J., Fallick, A.E. & Wilson, M.R., 1987a: Crustal reactivation in northern Sweden: the Vettasjärvi granite. *Precambrian Research 35*, 277–293.
Öhlander, B., Skiöld, T., Elming, S.Å., Claesson, S. & Nisca, D.H., 1993: Delineation and character of the Archaean-Proterozoic boundary in northern Sweden. *Precambrian Research 64*, 67–84.
Öhlander, B., Skiöld, T., Hamilton, P.J. & Claesson, L.-Å., 1987b: The western border of the Archaean province of the Baltic shield: evidence from northern Sweden. *Contributions to Mineralogy and Petrology 95*, 437–450.
Padget, P., 1970: Beskrivning till berggrundskartbladen Tärendö NV, NO, SV, SO. *Sveriges geologiska undersökning Af 5–8*, 95 pp.

Paton, C., Hellstrom, J.C., Paul P., Woodhead J.D. & Hergt J.M., 2011: Iolite: Freeware for the visualisation and processing of mass spectrometric data. *Journal of Analytical Atomic Spectrometry 26*, 2508–2518.
Paton C., Woodhead J.D., Hellstrom J.C., Hergt J.M., Greig A. & Maas R., 2010: Improved laser ablation U-Pb zircon geochronology through robust downhole fractionation correction. *Geochemistry Geophysics Geosystems 11*, 1–36.
Pearce, J.A., 1996: A user's guide to basalt discrimination diagrams. *Trace element geochemistry of volcanic rocks: applications for massive sulphide exploration. Geological Association of Canada, Short Course Notes 12*, 113.
Perdahl, J.-A. & Frietsch, R., 1993: Petrochemical and petrological characteristics of 1.9 Ga old volcanics in northern Sweden. *Precambrian Research 64*, 239–252.
Petersson, G., 1986: Projektet Nordöstra Norrbotten. Delprojektet Tärendö Ö:a. Årsrapport 1985. Studsvik Analytica AB. *Sveriges geologiska undersökning MINK 97043,* 40 pp.
Petrus, J.A. & Kamber, B.S., 2012: VizualAge: A Novel Approach to Laser Ablation ICP-MS U-Pb Geochronology Data Reduction. *Geostandards and Geoanalytical Research 36*, 247–270.
Quezada, R., 1976: Oriasvaara Kopparmalmsfyndighet: Rapport rörande resultat av SGUs undersökningar under åren 1974-1976. *Sveriges geologiska undersökning Mink 97010*, 15 pp.
Richard, P., Shimizu, N. & Allégre, C.J., 1976: ^{134}Nd/^{146}Nd, a natural tracer: an application to oceanic basalts. *Earth Planetary Science Letter 31*, 269–278.
Romer, R.L., Kjösnes, B., Korneliussen, A., Lindahl, I., Skyseth, T., Stendahl, M. & Sundvoll, B., 1992: The Archaean–Proterozoic boundary beneath the Caledonides of northern Norway and Sweden: U-Pb, Rb-Sr, and εNd isotope data from the Rombak-Tysfjord area. *NGU rapport 91.225*, 67 pp.
Roser, B. & Korsch, R., 1988: Provenance signatures of sandstone-mudstone suites determined using discriminant function analysis of major-element data. *Chemical Geology 67*, 119–139.
Sadeghi, M. & Hellström, F., 2015: U-Pb zircon ages of ignimbritic and porphyritic metarhyolites in the Boden area, northern Sweden. *SGU-rapport 2015:15,* Sveriges geologiska undersökning. 15 pp.
Skiöld, T., 1988: Implications of new U-Pb zircon chronology to early proterozoic crustal accretion in northern Sweden. *Precambrian Research 38*, 147–164.
Skiöld, T. & Rutland, R.W.R., 2006: Successive ~1.94 Ga plutonism and ~1.92 Ga deformation and metamorphism south of the Skellefte district, northern Sweden: Substantiation of the marginal basin accretion hypothesis of Svecofennian evolution. *Precambrian Research 148*, 181–204.
Skiöld, T., Öhlander, B., Markkula, H., Widenfalk, L. & Claesson, L.-Å., 1993: Chronology of Proterozoic orogenic processes at the Archaean continental margin in northern Sweden. *Precambrian Research 64*, 225–238.
Sláma, J., Košler, J., Condon, D.J., Crowley, J.L., Gerdes, A., Hanchar, J.M., Horstwood, M.S.A., Morris, G.A., Nasdala, L., Norberg, N., Schaltegger, U., Schoene, B., Tubrett, M.N. & Whitehouse, M.J., 2008: Plešovice zircon – A new natural reference material for U–Pb and Hf isotopic microanalysis. *Chemical Geology 249*, 1–35.
Stacey, J.S. & Kramers, J.D., 1975: Approximation of terrestrial lead isotope evolution by a two-stage model. *Earth and Planetary Science Letters 26*, 207–221.
Steiger, R.H. & Jäger, E., 1977: Convention on the use of decay constants in geo- and cosmochronology. *Earth and Planetary Science Letters 36*, 359–362.
Sun, S.S. & McDonough, W.F., 1989: Chemical and isotopic systematics of oceanic basalts: implications for mantle composition and processes. *In:* A.D. Saunders, M. Norry (eds.). Magmatism in Ocean Basins. *Geological Society of London Special Publications 42,* 313–345.
Tegengren, F.R., 1924: Sveriges ädlare malmer och bergverk. *Sveriges geologiska undersökning Ca 17*, 406 pp.
Vaasjoki, M. & Sakko, M., 1988: The evolution of the Raahe-Ladoga zone in Finland: isotopic constraints. *In:* K. Korsman (ed.): Tectono-metamorphic evolution of the Raahe Ladoga zone. *Geological Survey of Finland Bulletin 343*, 7–32.
Vaasjoki, M., Huhma, H., Lahtinen, R. & Vestin, J., 2003: Sources of Svecofennian granitoids in the light of ion probe U-Pb measurements on their zircons. *Precambrian Research 121*, 251–262.

Wanhainen, C., Broman, C., Martinsson, O. & Magnor, B., 2012: Modification of a Palaeoproterozoic porphyry-like system: Integration of structural, geochemical, petrographic, and fluid inclusion data from the Aitik Cu–Au–Ag deposit, northern Sweden. *Ore Geology Reviews 48*, 306–331.
Wasström, A., 1993: U-Pb zircon dating of a quartz-feldspar porphyritic dyke in the Knaften area; Västerbotten County; northern Sweden. *In:* T. Lundqvist (ed.): Radiometric dating results 2. *Sveriges geologiska undersökning C 82*8, 34–40.
Wasström, A., 1996: The Knaften granitoids of Västerbotten County, northern Sweden. *In:* T. Lundqvist (Ed.): Radiometric dating results. *Sveriges geologiska undersökning C 823*, 60–64.
Weihed, P., Arndt, N., Billström, K., Duchesne, J.-C., Eilu, P., Martinsson, O., Papunen, H. & Lahtinen, R., 2005: 8: Precambrian geodynamics and ore formation: The Fennoscandian Shield. *Ore Geology Reviews 27*, 273–322.
Wiedenbeck, M., Allé, P., Corfu, F., Griffin, W.L., Meier, M., Oberli, F., Quadt, A.V., Roddick, J.C. & Spiegel, W., 1995: Three natural zircon standards for U-Th-Pb, Lu-Hf, trace element and REE analyses. *Geostandards Newsletter 19*, 1–23.
Wiedenbeck, M., Hanchar, J.M., Peck, W.H., Sylvester, P., Valley, J., Whitehouse, M., Kronz, A., Morishita, Y., Nasdala, L., Fiebig, J., Franchi, I., Girard, J.P., Greenwood, R.C., Hinton, R., Kita, N., Mason, P.R.D., Norman, M., Ogasawara, M., Piccoli, P.M., Rhede, D., Satoh, H., Schulz-Dobrick, B., Skår, O., Spicuzza, M.J., Terada, K., Tindle, A., Togashi, S., Vennemann, T., Xie, Q. & Zheng, Y.F., 2004: Further characterisation of the 91500 zircon crystal. *Geostandards and Geoanalytical Research 28*, 9–39.
Whitehouse, M.J., Claesson, S., Sunde, T. & Vestin, J., 1997: Ion-microprobe U–Pb zircon geochronology and correlation of Archaean gneisses from the Lewisian Complex of Gruinard Bay, northwestern Scotland. *Geochimica et Cosmochimica Acta 61*, 4 429–4 438.
Whitehouse, M.J., Kamber, B.S. & Moorbath, S., 1999: Age significance of U–Th–Pb zircon data from Early Archaean rocks of west Greenland: a reassessment based on combined ion-microprobe and imaging studies. *Chemical Geology (Isotope Geoscience Section) 160*, 201–224.
Whitehouse, M., J. & Kamber, B.S., 2005: Assigning Dates to Thin Gneissic Veins in High-Grade Metamorphic Terranes: A Cautionary Tale from Akilia, Southwest Greenland. *Journal of Petrology 46*, 291–318.
Winchester, J. & Floyd, P., 1977: Geochemical discrimination of different magma series and their differentiation products using immobile elements. *Chemical Geology 20*, 325–343.
Witschard, F., 1970: Description of the geological maps Lainio NV, NO, SV, SO. *Sveriges geologiska undersökning Af 9–12*, 102 pp.
Witschard, F., 1984: The geological and tectonic evolution of the precambrian of northern Sweden – A case for basement reactivation? *Precambrian Research 23*, 273–315.
Witschard, F., Nylund, B. & Mannström, B., 1972: Masugnsbyn iron ore. Report concerning the results of Sveriges geologiska undersökning:s investigations in the years 1965–1970. *Sveriges geologiska undersökning BRAP 734,* 95 pp.

Authors, paper 6:
Susanne Grigull
Geological Survey of Sweden,
Department of Physical Planning,
Uppsala, Sweden

Robert Berggren
Geological Survey of Sweden,
Department of Mineral Resources,
Uppsala, Sweden

Johan Jönberger
Geological Survey of Sweden,
Department of Mineral Resources,
Uppsala, Sweden

Cecilia Jönsson
Geological Survey of Sweden,
Department of Mineral Resources,
Uppsala, Sweden

Fredrik Hellström
Geological Survey of Sweden,
Department of Mineral Resources,
Uppsala, Sweden

Stefan Luth
Geological Survey of Sweden,
Department of Mineral Resources,
Uppsala, Sweden

6. Folding observed in Palaeoproterozoic supracrustal rocks in northern Sweden

Susanne Grigull, Robert Berggren, Johan Jönberger,
Cecilia Jönsson, Fredrik Hellström & Stefan Luth

ABSTRACT

Despite the abundance of iron ore and sulphide deposits in the northern Fennoscandian Shield and a long history of mining in northern Sweden, the structural geological development of the area is poorly understood. In this paper, available and newly acquired geological and geophysical data are integrated and interpreted with particular emphasis on characterising the folding history in supracrustal rocks in these parts of the northern Fennoscandian Shield. The collection and integration of geological and geophysical data concentrate on key areas north of Kiruna, south of Masugnsbyn and north of Pajala. The Kiruna key area lies to the west of a major dextral-reverse shear zone: the Karesuando–Arjeplog deformation zone (KADZ), while the other areas lie to the east of the zone. A comparison of the folding history between these areas shows that the rocks to the west have been subject to fewer folding phases than those to the east.

INTRODUCTION

During the late Palaeoproterozoic (2.0–1.8 Ga), the Fennoscandian Shield was subject to the polycyclic Svecokarelian (or Svecofennian) orogeny. During the orogeny strain in the northern Fennoscandian Shield was partitioned into localised deformation zones and zones occupying the space between these shear zones (Fig. 1).

Structural geological studies of the northern Fennoscandian Shield addressing deformation in the Kiruna area and within the Kiruna–Naimakka deformation zone (KNDZ) were mainly undertaken by, e.g., Vollmer et al. (1984), Witschard (1984), Forsell (1987), Wright (1988), Talbot & Koyi (1995) and Bergman et al. (2001). Work specifically addressing deformation in the Pajala area and within the Pajala deformation belt was carried out by, e.g. Berthelsen & Marker (1986), Henkel (1991), Kärki et al. (1993), Olesen & Sandstad (1993), Bergman et al. (2006), Niiranen et al. (2007) and Luth et al. (2015).

Bergh et al. (2010, 2012) studied the deformation history in tectonic windows exposing Palaeoproterozoic deformation zones in Norway. Lahtinen et al. (2015a) present a new model for the tectonic evolution of Fennoscandia from detailed structural studies in the Palaeoproterozoic Martimo belt in Finland.

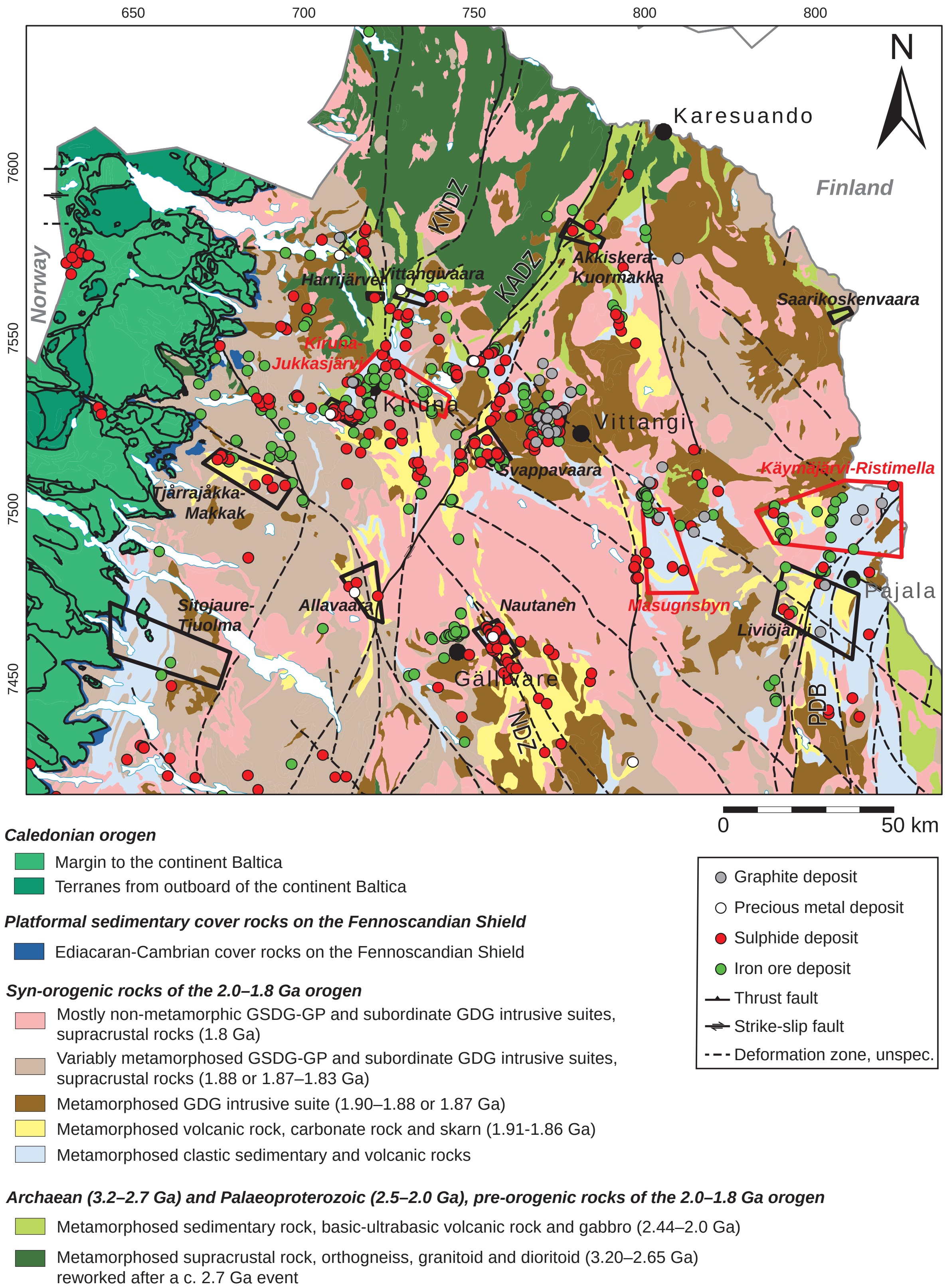

Figure 1. Simplified geological map of northern Norrbotten, modified from the 1:1 000 000 bedrock geological map of Sweden (Bergman et al. 2012). The black and red polygons show the key areas that were studied during the Barents project. The key areas marked in red are those from which the majority of the information on folding was derived for this study. KNDZ: Kiruna–Naimakka deformation zone, KADZ: Karesuando–Arjeplog deformation zone, NDZ: Nautanen deformation zone, PDB: Pajala deformation belt, GSDG: Granite-syenitoid-dioritoid-gabbroid, GP: Granite-pegmatite, GDG: Granitoid-dioritoid-gabbroid.

Bergman et al. (2001) and Lahtinen et al. (2015b) conclude that rocks of the Fennoscandian Shield have been affected by at least two, and locally three or four, folding phases. However, the timing between them is poorly constrained and it is difficult to interpret the relationships between ductile folding phases and localised deformation observed in major crustal scale shear zones such as the Kiruna–Naimakka deformation zone, the Karesuando–Arjeplog deformation zone, the Nautanen deformation zone, and the Pajala deformation belt (Fig. 1). But it is important to understand the relationship between various deformation phases in order to establish the structural architecture and tectonic evolution of the northern Fennoscandian Shield. Where possible, the work carried out for this paper aims to clarify the ductile deformation history of the Palaeoproterozoic rocks before formation of the high strain deformation belts. Integrating available data with newly acquired geophysical and geological data, this paper focuses on unravelling the folding patterns and phases observed in the Kiruna–Jukkasjärvi, Masugnsbyn, and Käymäjärvi–Ristimella key areas.

GEOLOGICAL SETTING

The supracrustal rocks of northern Norrbotten can be divided into rocks that were deposited before or during the approximately 2.0–1.8 Ga orogeny (Fig. 1; see also Bergman 2018). Pre-orogenic rocks include deformed Archaean basement rocks and overlying younger, predominantly mafic volcanic and volcaniclastic-sedimentary successions as well as carbonate rocks collectively known as the Karelian greenstone group (e.g. Martinsson et al. 2016). In the key areas west of the Karesuando–Arjeplog deformation zone (KADZ in Fig. 1) the greenstones are assigned to the Kiruna greenstone group, whereas in the eastern key areas greenstones are defined as the Veikkavaara greenstone group. The Kiruna greenstone group is thought to have been deposited in a failed rift setting (Martinsson 2004), whereas the Veikkavaara greenstone group was more likely deposited at the margins of a rift (Martinsson et al. 2016).

Younger, syn-orogenic, supracrustal rocks overlie the Karelian greenstones and consist of intermediate to felsic volcanic rocks, and (epi)clastic sediment successions (e.g. Kurravaara conglomerate, Porphyrite group, Pahakurkio group, Kalixälv group, Sammakkovaara group, Kiirunavaara group). These rocks are assumed to have formed along an active continental margin during a period of NE-directed subduction under the Archaean craton, and related accretion of volcanic arc complexes (Nironen 1997, Korja et al. 2006, Lahtinen et al. 2009, Martinsson et al. 2016 and references therein).

Both pre- and syn-orogenic rocks are intruded by numerous syn- and post-orogenic magmatic suites, which locally led to contact metamorphism and metasomatic alterations within the intruded rocks. All supracrustal rocks have undergone metamorphism, and metamorphic grades range from greenschist to upper amphibolite facies, seemingly increasing in grade from west to east. Where the protolith to the metamorphic rocks is still discernible, the prefix "meta" is included when referring to the rock type. Metamorphic terminology is used for the metamorphic rock types where the protolith is unknown.

The stratigraphy of the key areas addressed in this paper has been described in various SGU reports. Grigull & Antal Lundin (2013) and Grigull & Jönberger (2014) provide a summary for the Kiruna area; Hellström & Jönsson (2014) for the Masugnsbyn area; and Luth & Jönsson (2014), Luth et al. (2015), Grigull et al. (2014), Grigull & Berggren (2015) for the areas south and north of Pajala. Figure 2 illustrates the generalised, correlated lithostratigraphy for the key areas in relation to each other (Martinsson 1995). The lithostratigraphic sequences used for the Kiruna, Masugnsbyn, and Käymäjärvi–Ristimella key areas are described in more detail in the respective sections below.

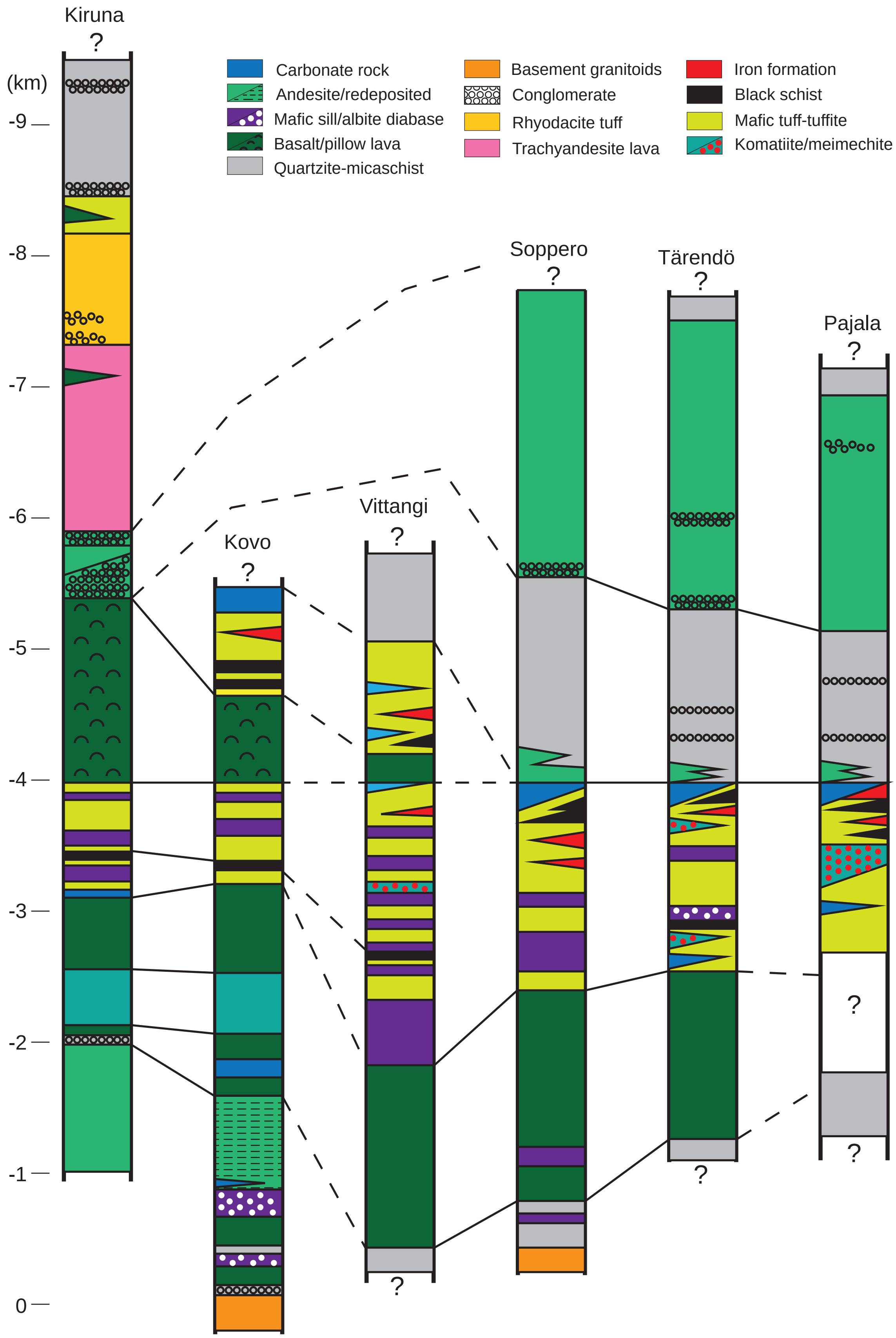

Figure 2. Correlated lithostratigraphic columns for Palaeoproterozoic supracrustal rocks in northern Norrbotten. After Martinsson (1995).

STRUCTURAL GEOLOGICAL MODELS

Kiruna–Jukkasjärvi key area and Pussijärvi

Lithostratigraphy

The current understanding of the geological units and lithostratigraphy in the Kiruna–Jukkasjärvi key area is largely based on Geijer (1910), Offerberg (1967), Witschard (1984), Forsell (1987), Martinsson (1997), Bergman et al. (2001), Martinsson (2004), and Martinsson et al. (2016). Martinsson et al. (2016) provide the most recent stratigraphic overview of the supracrustal and intrusive rocks in northern Norrbotten. In this report the stratigraphic sequence and terminology proposed by Martinsson et al. (2016) are adapted specifically for the rocks in the Kiruna key area. In the Kiruna area, and up to Kurravaara village, the entire stratigraphic succession from the Kovo group through to the Hauki quartzite can be observed. A simplified stratigraphic column is shown in Figure 3.

To the northeast of lake Mikonjärvi, the oldest supracrustal rocks in the Kiruna area occur as a thin sliver of conglomerate belonging to the Kovo group and unconformably overlying an Archaean granite intrusion. This conglomerate is overlain by most of the Kiruna greenstone group, starting with predominantly amygdaloidal basalts and conglomerates belonging to the Såkevaratjah formation (200–400 m), followed by ultrabasic rocks of the Ädnamvare formation (500 m), and a thick package of amygdaloidal basaltic lava flows of the Pikse formation (500–1000 m). The Pikse formation is overlain by the economically important, sulphide-bearing Viscaria formation (600 m), which predominantly consists of graphite-bearing tuffites, mafic sills, and some carbonate rocks. For the sake of simplicity, the reinterpreted map for the Kiruna area in Figure 3 does not display rocks older than the Viscaria formation. The reader is referred to Martinsson (1997) for a description of those rocks. The Viscaria formation is followed by an approximately 1 500 m thick sequence of basaltic pillow lavas interrupted by thinner tuffitic units belonging to the Peuravaara formation. From Lake Kirkkoväärtijärvi up to Lake Linkaluoppal, the Peuravaara formation is followed by graphitic schists, iron-rich metasedimentary rocks, and dolomitic rocks of the Linkaluoppal formation (min. 700 m). The Linkaluoppal formation is missing in the Kiruna area and up to Kurravaara township. Here, conglomeratic to sandy metasedimentary rocks belonging to the Kurravaara conglomerate (see below) directly overlay pillow lavas of the Peuravaara formation, indicating at least a local unconformity between the pre-orogenic Kiruna greenstone group and the overlying syn-orogenic units (see also Martinsson 1997).

The Kurravaara conglomerate is clast-supported with a sandy matrix. The clasts are well–rounded, and the concentration of Kiruna greenstone group-derived clasts is high at the bottom. Towards the top most clasts are derived from volcanic rocks of the Porphyrite group (e.g. Martinsson & Perdahl, 1995). The Porphyrite group predominantly occurs east of Kiruna, and it is suggested that it was deposited contemporaneously with the Kurravaara conglomerate (Martinsson & Perdahl 1995, Kumpulainen 2000, Martinsson 2004, Martinsson et al. 2016). The volcanic rocks of the Porphyrite group do not occur in the Kiruna key area.

The Kurravaara conglomerate is mainly covered by metavolcanic rocks of the Kiirunavaara group, which is divided into three formations (Martinsson 2004). The Hopukka formation mainly consists of andesitic to trachyandesitic metavolcanic rocks, followed by rhyodacitic rocks and occasionally conglomerates of the Luossavaara formation. The Luossavaara formation forms the hanging wall to the Kiirunavaara and Luossavaara magnetite ore deposits. It is followed by the Matojärvi formation which predominantly consists of felsic tuffite, basalt, reworked volcaniclastic metasedimentary rocks and clastic metasedimentary rocks such as metagreywacke and phyllite. The Matojärvi formation forms the hanging wall to hematite ore deposits such as Rektorn, Henry and Nukutus. It is also the hanging wall to the Lappmalmen ore body that does not crop out, but can be interpreted as a displaced part of the Rektorn ore body due to late horst and graben type brittle faulting (Parák 1975).

Although the lower part of the Kiirunavaara group is lithologically similar to the rocks of the Por-

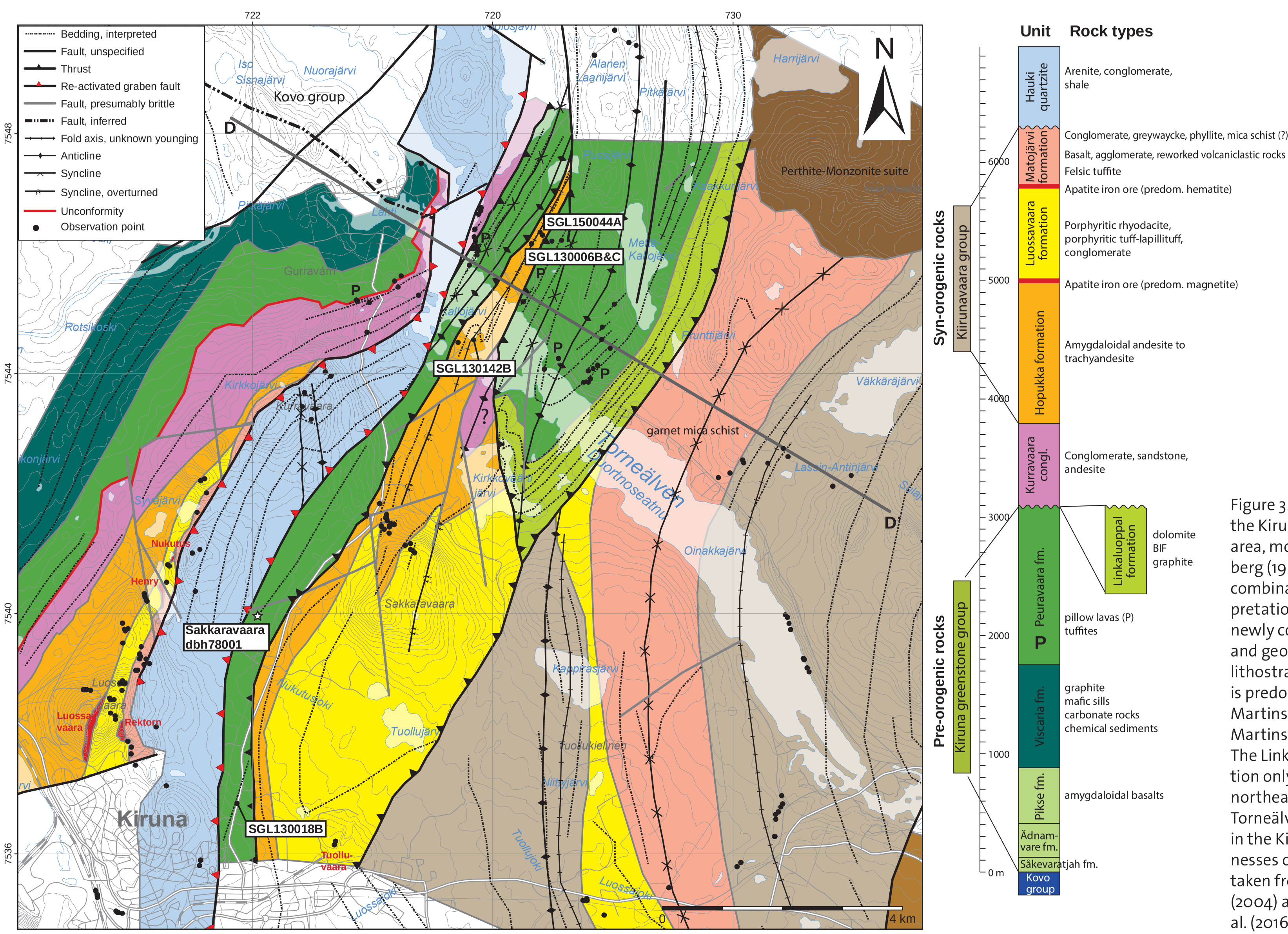

Figure 3. Geological map of the Kiruna–Jukkasjärvi key area, modified from Offerberg (1967), based on the combination and reinterpretation of available and newly collected geological and geophysical data. The lithostratigraphic column is predominantly based on Martinsson (1995) and Martinsson et al. (2016). The Linkaluoppal formation only occurs to the northeast of the river Torneälven and is eroded in the Kiruna area. Thicknesses of formations are taken from Martinsson (2004) and Martinsson et al. (2016).

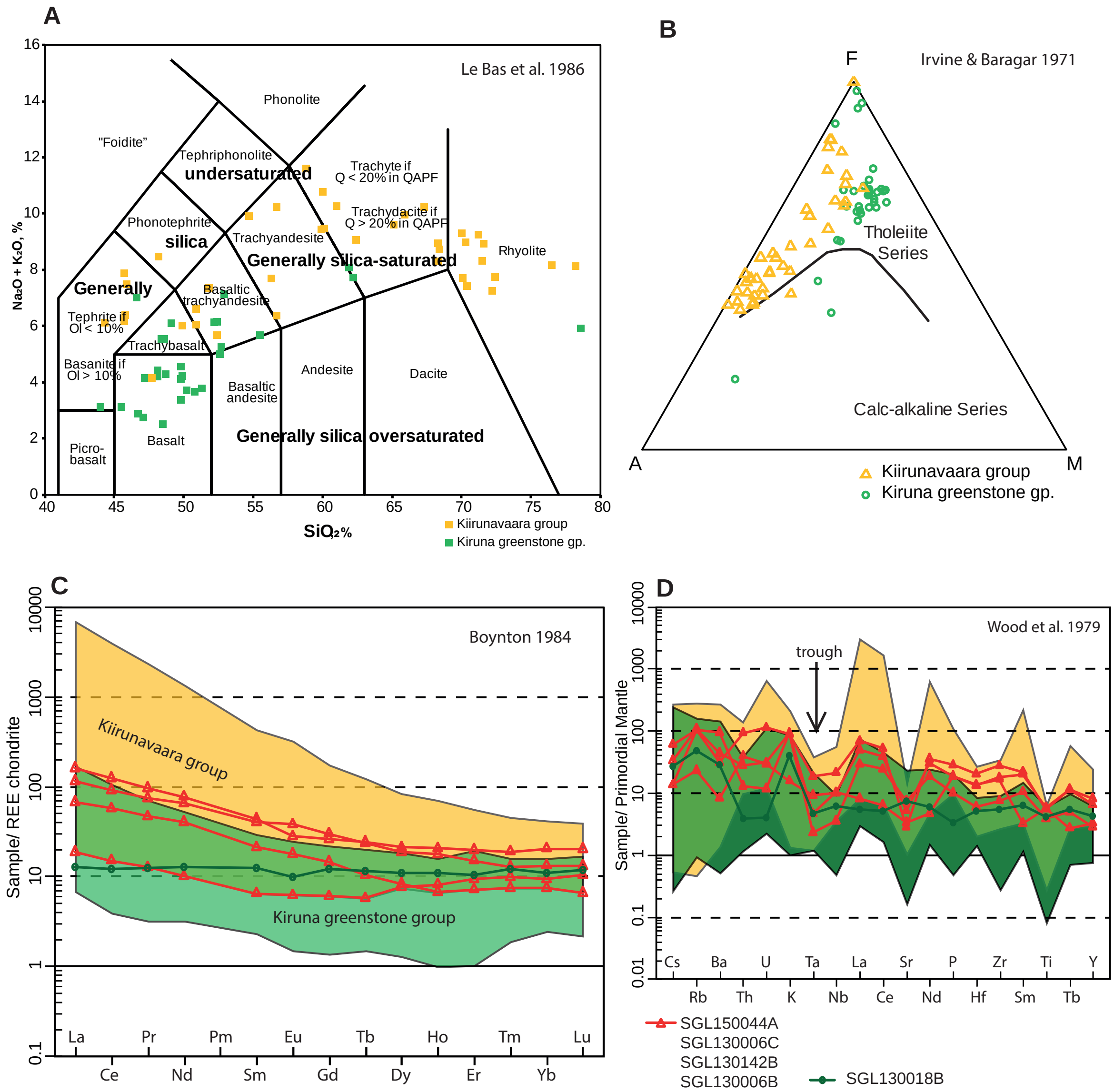

Figure 4. Whole-rock geochemistry results for rocks from the Kiruna greenstone group (KGG) compared with the syn-orogenic rocks of the younger Kiirunavaara group. **A.** TAS classification diagram after Le Bas et al. (1986). **B.** AFM discrimination diagram after Irvine & Barager (1971). **C.** REE from mafic rocks normalised to chondrite (Boynton 1984). **D.** Spider diagram of incompatible trace elements from mafic rocks normalised to primordial mantle (Wood et al. 1979).

phyrite group, they are chemically distinct. The Kiirunavaara group rocks exhibit a tholeiitic or slightly alkaline and partly bimodal geochemical character, whereas the Porphyrite group rocks have a calc-alkaline chemical composition (e.g. Martinsson & Perdahl, 1995).

Unconformably overlying the Kiirunavaara group are quartzites, metaarenites and, locally, conglomerate lenses of the Hauki quartzite extending in a long band at least from Kiruna up to the Vittangivaara key area (cf. Luth et al. 2018a). The clasts of the conglomerate predominantly consist of Kiirunavaara group material (Martinsson 2004), suggesting a local source. The contact with the underlying units is presumed to be tectonic.

Lithogeochemically, the rocks of the Kiruna greenstone group and the younger syn-orogenic rocks are distinctly different (Martinsson & Perdahl 1995). Figure 4 shows the lithogeochemical characteristics of pre-orogenic mafic rocks of the Kiruna greenstone group and the syn-orogenic rocks of the

Kiirunavaara group in the Kiruna area. The rocks of the Kiirunavaara group are generally trachy-andesitic to rhyolitic. Basalts occur very rarely, whereas the Kiruna greenstone group rocks are of a predominantly basaltic composition (Fig. 4A). The metavolcanic rocks of the Kiirunavaara group plot in the tholeiitic field in an AFM diagram (Fig. 4B). This distinguishes them from the predominantly calc-alkaline metavolcanic rocks of the Porphyrite group (Martinsson et al. 2016, Martinsson et al. 2018). One of the characteristics that can be used to distinguish between these two groups is the steep negative slope towards heavier rare earth elements in the Kiirunavaara group, whereas the Kiruna greenstone group exhibits a relatively shallow slope (Fig. 4C). An additional characteristic of the Kiirunavaara group is a depletion of high field strength elements (HFS elements) Ta and Nb compared with other incompatible elements. This depletion is not observed in the Kiruna greenstone group (Fig. 4D).

GEOPHYSICAL DATA

Introduction

The area was investigated by airborne geophysical surveys made by LKAB in 1960, 1973 and 1983. The airborne geophysical information includes magnetic, radiometric and electromagnetic data (both slingram and VLF). Ground gravity measurements have been acquired over the area with regional coverage of approximately 1–1.5 km station spacing. A compilation of the petrophysical properties of the rocks in the area is presented in Figure 5 and Table 1. Several parts of the area have also been surveyed with ground magnetic or slingram measurements. More information on these previous geophysical investigations is found in Grigull & Antal Lundin (2013).

Figure 5. Petrophysical properties of the lithologies in the area, expressed graphically as magnetic susceptibility (SI unit) v density (kg/m³). The total number of petrophysical samples is 131.

Intrusive rocks in the northwestern part of the area shown in Figure 6–8 are Archaean basement. These intrusions vary between granites and gabbros. On the gravity map (Fig. 6) the area is seen as a low anomaly, which indicates that the more felsic intrusive rocks predominate. In the north-central part of the area there is a low-gravity anomaly that coincides with a low magnetic anomaly (Fig. 6 and 7). This area coincides with the Hauki quartzite, extending in a north-south direction. According to the gravity map, the low anomaly is also relatively pronounced between the two major positive anomalies on both sides of the river Torneälven (Fig. 6). Thus, it is possible that the quartzite is coherent throughout this low-gravity anomaly.

Table 1. Petrophysical information on the rock types in the area.

Rock type	No. of samples	Density (SI) mean	Density (SI) Std. dev.	Susceptibility x 10^{-5} (SI) min	Susceptibility x 10^{-5} (SI) max	Susceptibility x 10^{-5} (SI) median	Q-value min	Q-value max	Q-value median
Basalt-andesite	50	2893	93	36	23206	5403	0.00	29.61	0.45
Gabbro-diorite	12	2916	64	77	12860	3915	0.01	2.31	0.86
Mica schist	2	2784	*	49	106	*	0.02	0.02	*
Granite	4	2609	10	40	1694	1184	0.01	0.66	0.37
Conglomerate	4	2725	139	3	80	58	0.02	0.10	0.04
Quartzite	24	2647	32	1	94	12	0.00	0.03	0.00
Rhyolite-dacite	35	2671	39	40	16780	1025	0.02	16.73	0.34

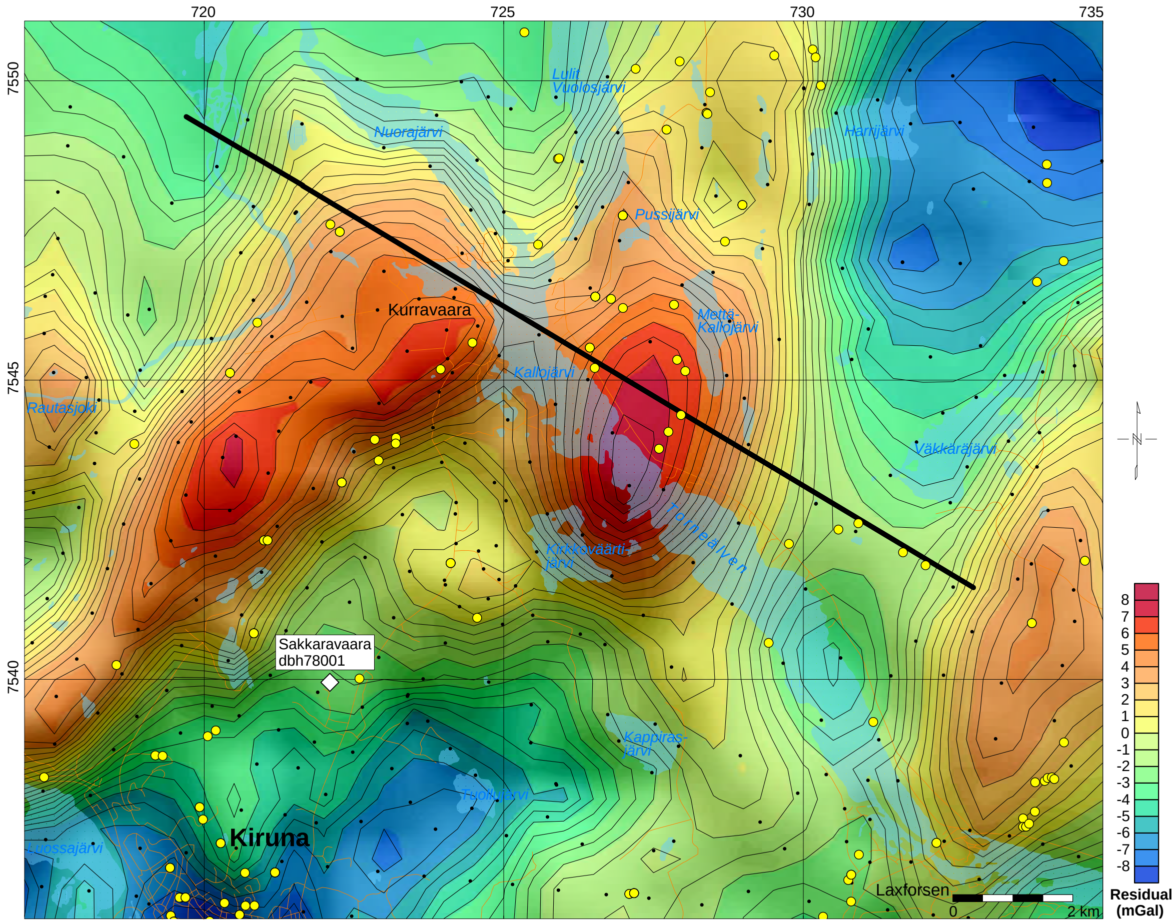

Figure 6. Residual gravity field, expressed as the difference between the Bouguer anomaly and an analytical continuation upwards to 3 km. The black dots represent measurement points. The yellow circles represent acquired petrophysical samples. The black line represents the extent of the regional interpreted geological profile presented in Figure 14A.

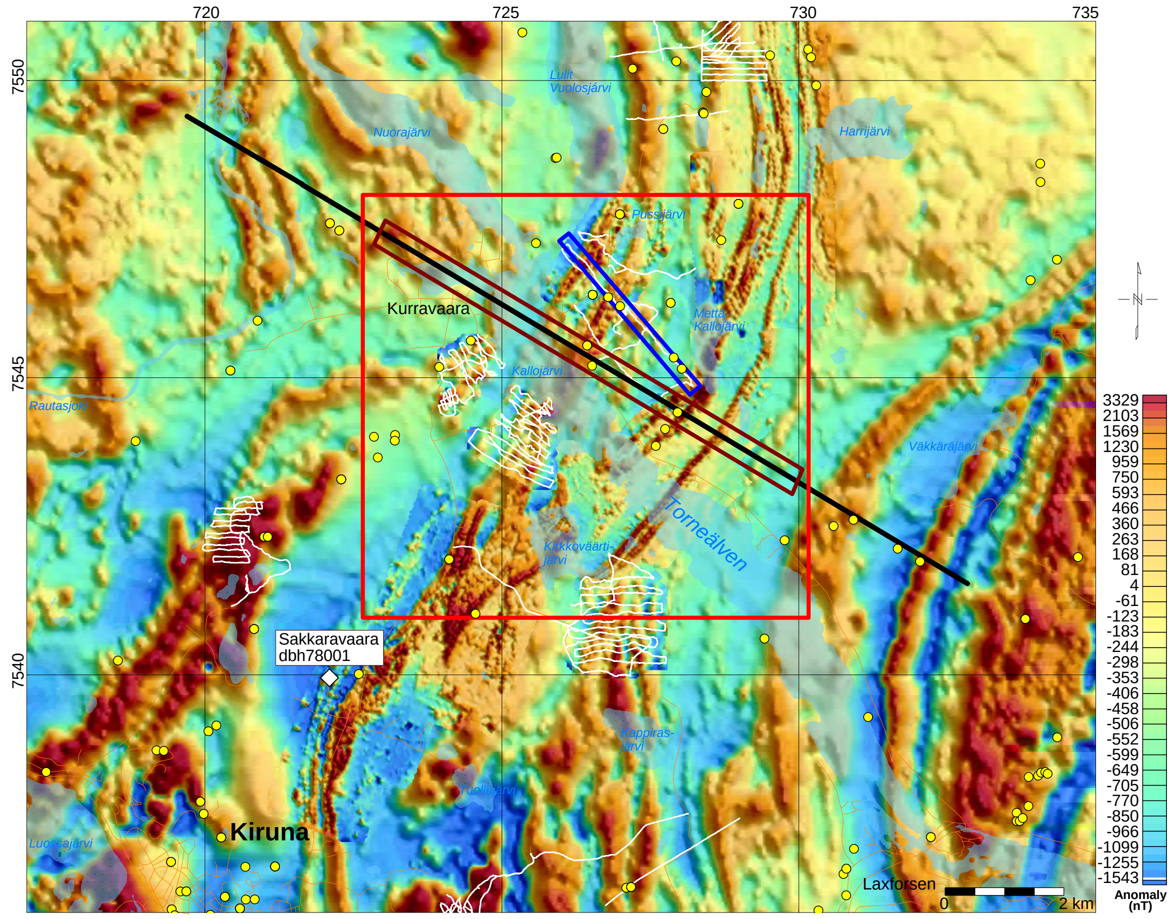

Figure 7. Magnetic anomaly map. The data from the airborne measurements are overlain by data from ground magnetic surveys. The yellow circles represent acquired petrophysical samples. The white lines represent newly acquired ground profiles by magnetometer. The black line represents the extent of the interpreted regional geological profile, shown in Figure 14A. The red polygon shows the extent of a 3D VOXI model and the brown box surrounding the central part of the regional profile represents the extent of the cross-section derived from that 3D VOXI model, and shown in Figure 15. The blue box marks the interpreted ground magnetic profile presented in Figure 16.

A rock sequence dominated by greenstones belonging to the Kiruna greenstone group occurs east of the Hauki quartzite. This gives rise to a positive anomaly in the gravity data. Sharp variations in the content of magnetic minerals are visible in the banded magnetic signature obtained from previously acquired ground magnetic surveys. Strong conductive horizons in the eastern part of the greenstone sequence, which consist of graphite horizons, are seen in the slingram data (Fig. 8). Intercalated within the greenstones are intermediate metavolcanic rocks belonging to the Kiirunavaara group, which produce a generally high-magnetic pattern, continuing to the south. A granite intrusion occurs in the northeastern part of the area, which is seen as a relatively homogeneous, low-magnetic area corresponding to a pronounced gravity low (Fig. 6).

The gravity low continues to the south and coincides with both relatively high-magnetic and low-magnetic areas. The lithology of this area is dominated by felsic metavolcanic rocks with relatively low densities. The felsic metavolcanic rocks are situated between mica schist to the west, and mafic to intermediate metavolcanic rocks to the east. The mica schist continues to the south, where it gives rise to a moderate gravity high. Several high-magnetic bands, striking in a north-south direction, occur in the central-southern part of the area. The bands are produced by alternating sequences of felsic metavolcanic rocks of rhyolitic to dacitic composition. Further west is an area with a lower magnetic signature. This area coincides with a pronounced gravity low, and the lithology in this part is metavolcanic rock

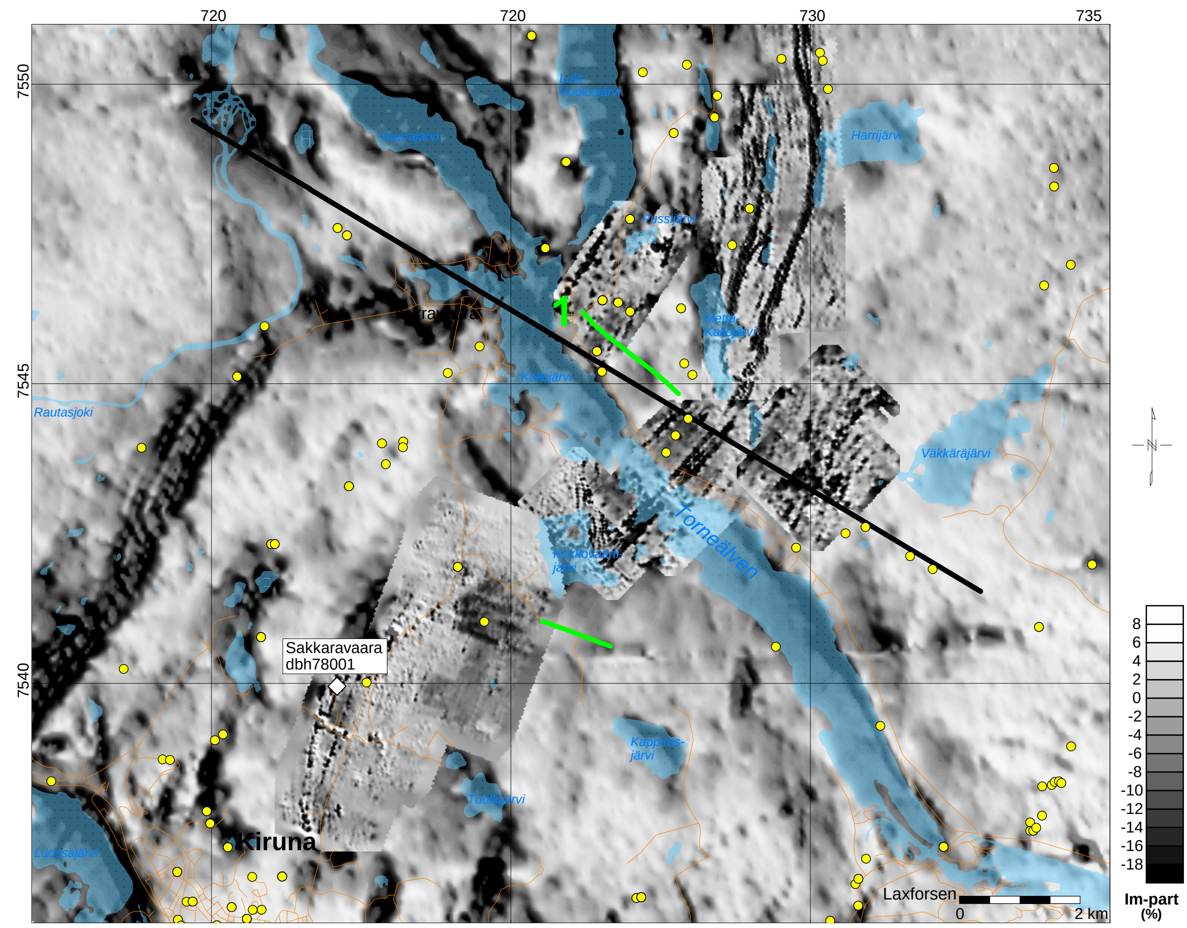

Figure 8. Slingram data from airborne measurements, overlain by data from ground-measured slingram surveys. The data displayed is the quadrature portion of the slingram data. The yellow circles represent acquired petrophysical samples. The green lines represent the extent of ground profiles with VLF instruments and the result from the profile labelled "1" is presented in Figure 17. The black line represents the extent of the regional interpreted geological profile, shown in Figure 14A.

of a rhyolitic composition. West of this area is a high-magnetic structure, oriented north-south, which consists of intermediate metavolcanic rock. The relatively broad, low-magnetic area to the west consists of Hauki quartzite.

A positive gravity anomaly occurs west of Torneälven, extending to the southwest and coinciding with a low-magnetic area. The lithology is dominated by mafic metavolcanic rocks, while to the southeast there is a strong high-magnetic area caused by felsic to intermediate metavolcanic rocks.

Structural inventory

Although several studies of the tectonic development of the Kiruna area exist (e.g. Vollmer et al. 1984, Witschard 1984, Forsell 1987, Wright 1988, Talbot and Koyi 1995), there is no generally accepted structural model. Moreover, the structural framework around Kurravaara township and Lake Pussijärvi (Fig. 3) to the northeast of Kiruna is poorly understood. Here, the rocks have been affected by deformation within the Kiruna–Naimakka deformation zone (Bergman et al. 2001, Fig. 1), and the structures by which the Kiirunavaara group and the Kiruna greenstone group are connected with the rocks north and northeast of Torneälven are unclear (see also Luth et al. 2018a). A new structural geological model has therefore been developed with particular emphasis on the area around Kurravaara township and Pussijärvi, linking the model to the relatively well-understood Kiruna area.

Between Mt Luossavaara and Kurravaara township, bedding planes dip moderately to steeply mainly to the east to southeast and younging is consistently to the east for rocks both of the Kiirunavaara group and the Kurravaara conglomerate (Fig. 9A, B; cf. Martinsson et al. 2016, Wright 1988). Axial-planar cleavage and foliation planes are generally subvertical or dip steeply to the east-southeast. Cleavage and foliation dip is steeper than, or similar to, bedding in most locations (Fig. 9A). Bedding/cleavage intersection lineations and mineral lineations plunge steeply to moderately and usually trend roughly southwards. Other lineation orientations also occur and are not easily explained (Fig. 9A, B). A possible cause is non-cylindrical folding, resulting in warped fold axes with depressions and culminations.The foliation density in the Kurravaara conglomerate increases and steepens close to the contact with the Hauki quartzite. Wherever a strong foliation in the Kurravaara conglomerate could be observed, the clasts are strongly stretched into a prolate geometry and sometimes even boudinaged parallel to the bedding/cleavage intersection lineations. This may indicate shearing parallel to the foliation, but needs further investigation.

Direct evidence of folding was observed at very few locations. In a tephrite of the Matojärvi formation in the hanging wall of the Rektorn iron ore deposit, mineralised veins are folded into west-vergent, overturned meso-scale folds (Fig. 10A). These folds are interpreted to be parasitic to the regional fold structure. Bedding/cleavage intersection lineations at the Rektorn quarry plunge approximately 60 degrees to the south and south-southeast. Close to the contact with the Hauki quartzite, quartz veins cutting through sheet silicate-rich metavolcanic rocks belonging to the Matojärvi formation were folded ptygmatically (Fig. 10B). A clear foliation has developed parallel to the axial plane of the ptygmatic folds. The metavolcanic rock contains many circular quartz blasts which may be quartz-filled amygdyles. Strain shadows around the quartz blasts are symmetrical, and the rock is affected by pressure solution enhancing the foliation. The axial plane of the ptygmatic folds dips 65 degrees to the southeast. A mineral lineation was measured at 107/70, a more or less plunging dip of the axial planar foliation and parallel to the plunge of the fold axis. Folds were also observed in rocks of the Kiirunavaara group at Sakkaravaara (Fig. 9C) and in quartzites of the Hauki quartzite on Mt. Kurravaara (Fig. 9D). The Hauki quartzite is folded into upright, open folds plunging approximately 45 degrees to the southwest.

The rocks of the Kiirunavaara group are cut off by an east-dipping fault and brought into contact with the Hauki quartzite (Fig. 3). Mafic rocks to the east of the Hauki quartzite have been interpreted as belonging to the Kiirunavaara group on some maps (Offerberg 1967, Bergman et al. 2001), and as belonging to the Kiruna greenstone group on others (Forsell 1987). No isotope dates are available for these rocks, however. During this project, a sample of a mafic metavolcanic rock was taken (SGL130018A in Fig. 3) that exhibits a lithogeochemical signature matching other mafic rocks belonging to the Kiruna greenstone group (Fig. 4C and 4D). Additionally, graphite-bearing schist is reported from a drill hole at Sakkaravaara, west of the road to Kurravaara (dbh 78001 in Fig. 3). In the Kiruna area, graphite has so far only been described as occurring in the greenstones. The graphite layer is a good electrical conductor, creating a relatively clear electromagnetic anomaly on the slingram anomaly map (Fig. 8). In the geological model presented here, a strip of rocks up to 900 m wide to the east of the Hauki quartzite is therefore attributed to the Kiruna greenstone group.

The rocks between Kiruna and Kurravaara to the west of the fault between the Kiirunavaara group and the Hauki quartzite occupy the upright western limb of a regional-scale, west-vergent, probably overturned syncline. It is unclear whether the folds observed in the Hauki quartzite were formed synchronously with this syncline or post-date this folding event.

To the northeast of Kurravaara township on the northeastern side of the river Torneälven, previous geological maps show only greenstones, cut off by a major NW–SE striking fault running more or less parallel to Torneälven (e.g. Offerberg 1967). However, based on work carried out for the Barents Project, several observations indicate that both the Kurravaara conglomerate and the Kiirunavaara group extend

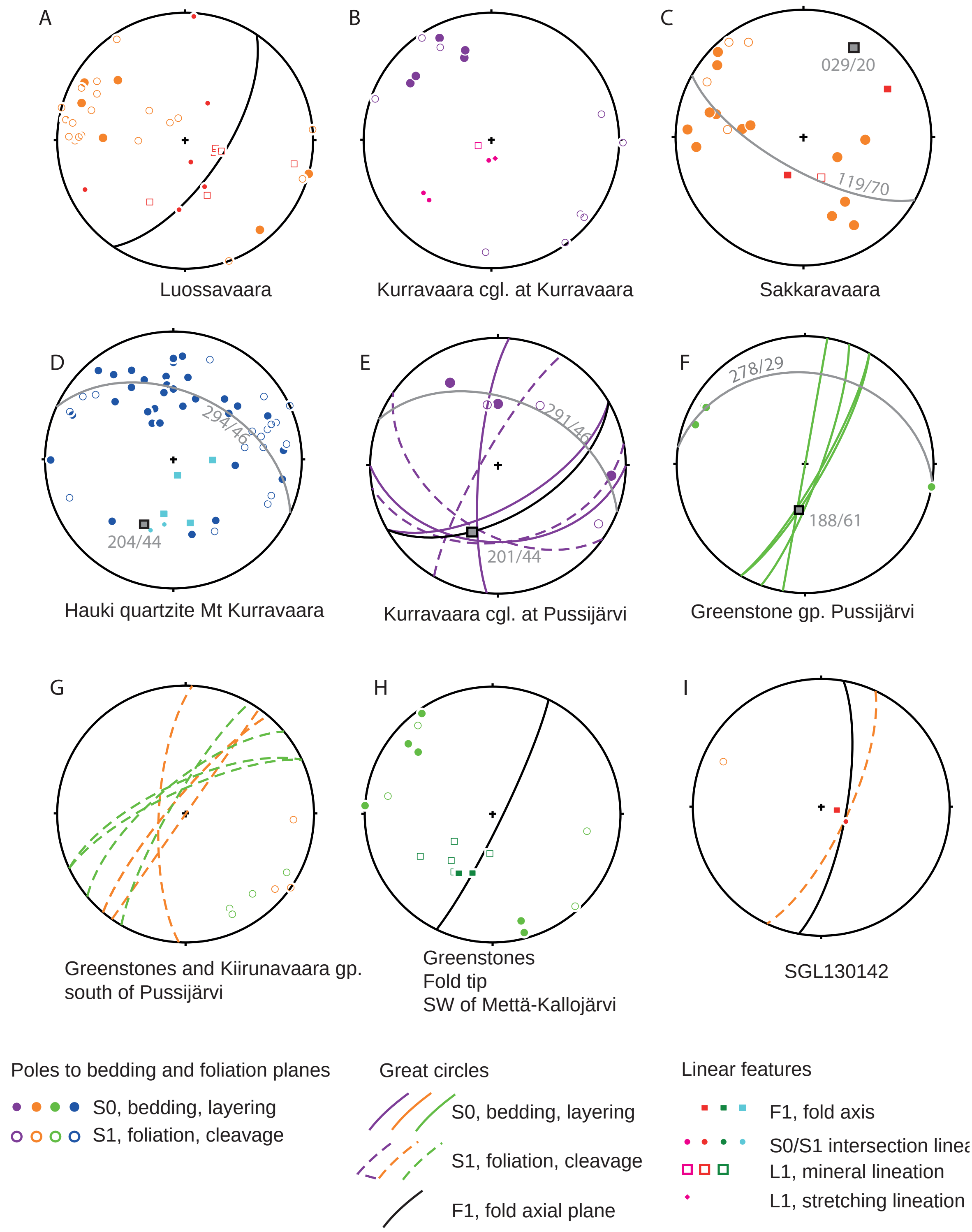

Figure 9. Stereographic projections (lower hemisphere) of structural geology data in the Kiruna–Pussijärvi area. Green: Kiruna greenstone group. Purple and pink: Kurravaara conglomerate. Red and orange: Kiirunavaara group. Blue: Hauki quartzite. Grey: Cylindrical best-fit great circles and poles to these.

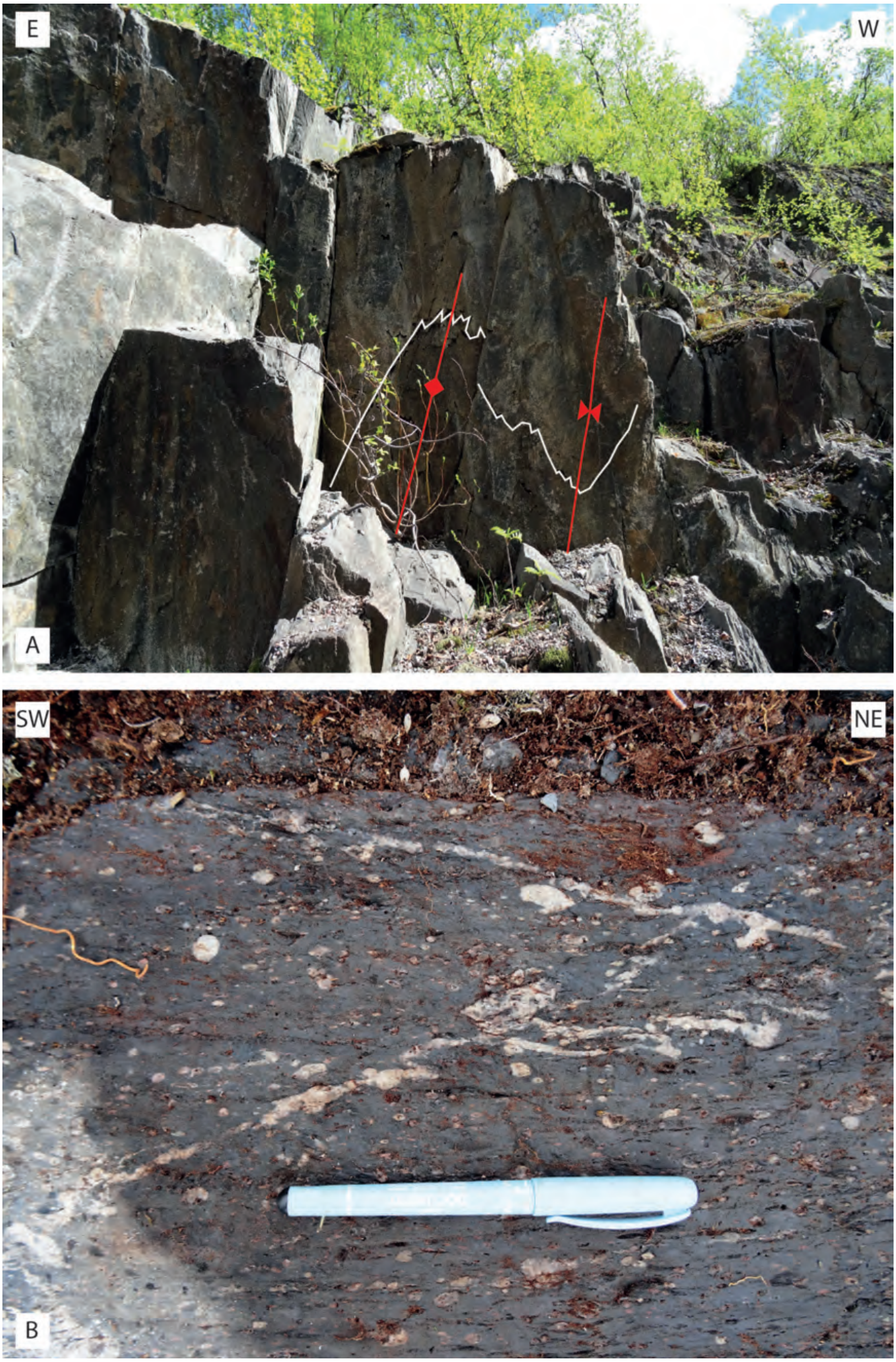

Figure 10. **A.** West-vergent parasitic folds observed in the hanging wall to the Rektorn iron ore deposit. (SWEREF99 TM: N7537660, E719979). **B.** Ptygmatically folded quartz vein in amygdaloidal metavolcanic rock of the Matojärvi formation close to the contact with the Hauki quartzite. The axial plane to the fold dips approximately 65 degrees to the southeast and a mineral lineation plunges approximately 70 degrees to the E-SE. (SWEREF99 TM: N7539147, E720193).

Figure 11. Conglomerate attributed to the Kurravaara conglomerate (SWEREF99 TM: N7546700, E725797). **A.** The conglomerate is clast-supported and contains sandy layers. **B.** Porphyritic clast with large plagioclase phenocrysts, probably belonging to the Porphyrite group (same location as A.). **C.** Kink fold in strongly-foliated and migmatised paragneiss, thought originally to have been Kurravaara conglomerate (SWEREF99 TM: N7546253, E725711). **D.** Stereographic projection (lower hemisphere) of structural data collected from the kink folds in C.

further to the north of Torneälven. A conglomerate was found along the northern shore (Fig. 3) and could be followed in small outcrops downstream for at least 200 metres. It is a clast-supported conglomerate with a sandy matrix and intercalated sandy layers (Fig. 11A). The conglomerate mainly contains mafic to intermediate volcanic clasts, but also chert clasts. One clast exhibits large plagioclase phenocrysts (Fig. 11B), typical of metavolcanic rocks from the Porphyrite group. This conglomerate was therefore attributed to the Kurravaara conglomerate. About 100 m to the east of that relatively well-preserved conglomerate, a rapid increase in deformation and metamorphic grade is marked by a penetrative, closely-spaced foliation grading into a mica-rich paragneiss even further east. The protolith of the paragneiss is unclear, but is here interpreted as belonging to the Kurravaara conglomerate. At a later stage the gneissic foliation has been affected by lower grade kink folds (Fig. 11C). The same gneissic band may thereby exhibit both Z- and S-shaped kink folds, indicating that the rocks were shortened in parallel with the gneissic foliation. The axial planes to the kink folds dip moderately to steeply to the east and north, i.e. they are nearly perpendicular to each other (Fig. 11D). But this was the only location where such kink folds were observed, and they are therefore difficult to interpret without further field work.

Approximately 50 m east of where the kink folds were observed, near-pristine pillow lavas of the Kiruna greenstone group occur and are thought to belong to the Peuravaara formation. Bedding planes and foliations in both the pillow lavas and the strongly-foliated part of the conglomerate dip moderately to steeply to the southeast (Fig. 9F and 11). The greenstones, consisting of pillow lavas and intercalated

Figure 12. Basaltic trachyandesite attributed to the Kiirunavaara group (SWEREF99 TM: N7546305, E726830). Samples SGL150044A, SGL130006C, SGL130006B were retrieved from this area. For exact localities refer to the map in Figure 3.

tuffite layers, can be followed towards the east for approximately 750 metres. Further to the east, the rock type changes into a strongly-foliated intermediate metavolcanic rock with a strong positive magnetic anomaly (cf. Fig. 7). This rock is characterised by round quartz-filled nodules and feldspar porphyroclasts (Fig. 12).

The lithostratigraphic position of this rock is unclear. However, lithogeochemical analyses of three samples taken several hundred metres apart (cf. Fig. 3) indicate that these rocks are basaltic trachyandesites with a REE and trace element signature typical of the syn-orogenic rocks of the Kiirunavaara group (Fig. 4C and 4D). Hence, the rock may not be a part of the Kiruna greenstone group, but may instead belong to the Kiirunavaara group. Axial length ratios of what is interpreted as flattened pumice pieces were measured on both a horizontal and a vertical surface, and resulted in a maximum flattening strain of approximately 10 on both surfaces, assuming the pumice pieces were originally spheroidal. Despite the development of a penetrative foliation, and the relatively high strain, no stretching or mineral lineations were observed, and strain shadows formed around round quartz nodules are symmetrical. It is therefore assumed that the foliation is due to strong co-axial deformation. To the east of these strongly foliated rocks, further pristine pillow lavas occur as part of the Peuravaara formation. These pillow lavas can be traced approximately 2.3 km eastwards. The new geological model of the Kurravaara–Pussijärvi area suggests an extension of the Kurravaara conglomerate and the Kiirunavaara group further to the north. The northwest–southeast-striking deformation zone proposed in older maps (e.g. Offerberg 1967) probably does not exist. This conclusion is supported by newly acquired ground magnetic data southeast of Lake Kirkkoväärtijärvi showing no displacement of highly magnetic anomalies (Fig. 7).

The Kiruna greenstone group contains rock types that can be used as geophysical markers, such as

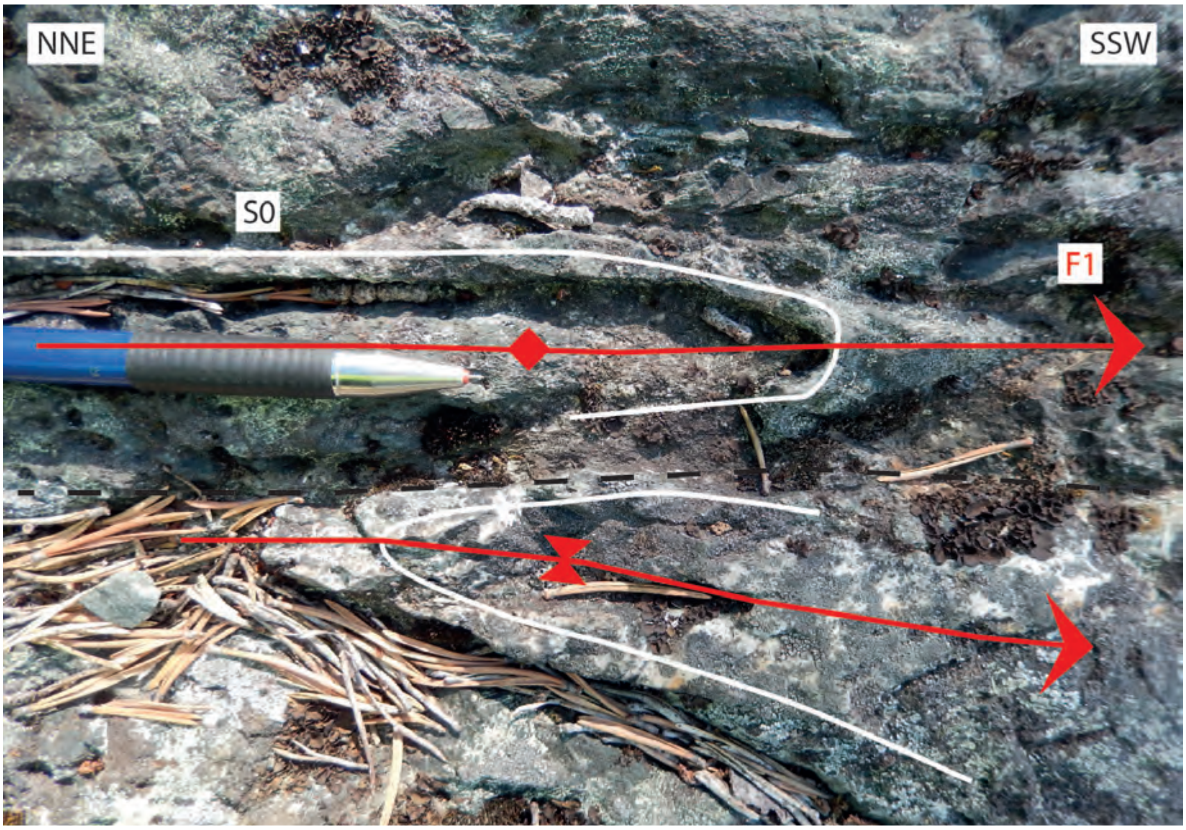

Figure 13. Small-scale folding observed in pillow basalts belonging to the Peuravaara formation of the Kiruna greenstone group. Top section. (SWEREF99 TM: N7544069, E726864).

graphite horizons in the Viscaria formation, and also laterally continuous graphite horizons and a banded iron formation (BIF) in the upper part of the Linkaluoppal formation. The graphite horizons and the BIF belonging to the Linkaluoppal formation can be traced on magnetic and electromagnetic maps (Fig. 7 and 8) and are interpreted to occur in the western limb of an approximately north–south-trending syncline ranging approximately from Vittangivaara in the north (cf. Luth et al. 2018a; not included in Fig. 3) to approximately 1.5 km north of lake Harrijärvi in the south (Fig. 3), where the core of the syncline is cut off to the east by an intrusion belonging to the Perthite monzonite suite. North of Torneälven, the corresponding anticline to the west is cored by pillow lava basalts of the Peuravaara formation. Further north, diorites and graphite layers of the Viscaria formation crop out (e.g. Martinsson 1999), indicating that, regionally speaking, younging is to the east and south, and that one of the major structures in the area is a slightly west-vergent, locally overturned, south–southwest-plunging anticline ranging at least from Alanen Laanijärvi in the north to Lake Kirkkovaartijärvi in the south. Meso-scale folding close to the hinge of that anticline in the south has been observed in drill cores during an excessive drilling program to the northeast of Lake Kirkkovaartijärvi (Gustafsson & Carlson 1992, Kallosalmi drilling project, prospecting report PRAP92013), and in pillow lavas belonging to the Peuravaara formation on the northeastern shore of Torneälven (Fig. 13). Here, a fold axial plane was measured dipping steeply towards the southeast. Fold axes and mineral lineations plunge approximately 65 degrees towards the southwest (Fig. 9H). In the eastern limb of the anticline, bedding mainly dips steeply towards the southeast, and only locally towards the northwest. In a very few outcrops younging is reliably indicated by chert fillings between some pillows or by the shape of the pillows themselves. However, younging in both directions was observed within the eastern limb of the anticline, and this is interpreted as representing parasitic folding within the actual fold limb.

2D modelling based on magnetic and gravity data

In order to resolve the folding patterns in the area, a geological cross-section marked D-D' in Figure 3 was developed, based on geophysical modelling and geological data. Several ground measurements were made, primarily by magnetometer, at a number of key locations to achieve a more detailed picture of the geometries of the bedrock structures. The coverage of these newly acquired magnetometer profiles is shown in Figure 7.

The area mainly consists of greenstones; the magnetic properties of these rocks differ significantly over small distances. On the gravity map the centre of the fold gives rise to a strong positive anomaly (Fig. 6). Petrophysical analyses of samples from this area show that the densities of these lithologies are mainly between 2 900 and 3 100 kg/m3.

The interpreted regional geological model in Figure 14A is based on geophysical information from ground gravity data and airborne magnetic measurements. Figure 14B shows the geological model for the Kovo and Vakko zones described in Luth et al. (2016, 2018a). The model has been constructed by forward modelling with "Potent" software, using the potential field data together with petrophysical information on the various rock types to constrain the model. In areas with sparse petrophysical information, especially in the northwestern part of the profile, the rocks have been assigned the properties shown in Table 1. The background properties for the density and magnetic susceptibility of the subsurface have been specified at 2 700 kg/m^3 and 100 × 10^{-5} SI units.

In the west the profile starts within the Archaean granitoid. The petrophysical samples available from this lithology have an average density of 2 670 kg/m^3 and susceptibility of 1 000 × 10^{-5} SI units. East of the granitoid is a vast area of mainly mafic to intermediate rocks. The low- to moderate-magnetised rocks in this area have been visualised in Figure 14A in light green, while the higher magnetised rocks are shown in darker green. Closest to the granitoid is an elliptical magnetic structure on the magnetic anomaly map (Fig.7). No petrophysical information is available from this structure, so density and magnetic susceptibility have been assumed to be 2 860 kg/m^3 and 10 000 × 10^{-5} SI units, respectively. In order to fit the observed magnetic data with the modelled data, the structure could be represented as a near-isoclinal syncline. The behaviour of the gravity field indicates that the granitoid dips under the more dense mafic to intermediate rocks.

Very little petrophysical information is available between 2 000 m and 5 000 m along the profile. One sample was obtained from the low-magnetic metavolcanic rocks with a density of 2 860 kg/m^3 and a susceptibility of 200 × 10^{-5} SI units. Four samples were analysed from the more highly magnetised metavolcanic rocks whose average properties are 2 900 kg/m^3 and 12 400 × 10^{-5} SI units. These properties have been assigned to the lithologies and, based on the shape of the magnetic field, it is possible that the highly magnetised lithologies are folded across the outline of the profile. No petrophysical data exists between 5 000 m and 6 000 m along the profile. To achieve a good fit between observed data and calculated response, density and susceptibility values of 2 900 kg/m^3 and 2 000 × 10^{-5} SI units have here been assigned to the subsurface.

Just west of the Hauki quartzite, at 6 000 m along the profile, one petrophysical sample from the metavolcanic rock was obtained, having a density of 2 970 kg/m^3 and a susceptibility of 6 500 × 10^{-5} SI units. Based on the shape of the magnetic field curve, it is likely that the metavolcanic rock dips beneath the quartzite. The quartzite is not exposed at the extent of the profile, but its existence is indicated by both the magnetic and gravity data. On the magnetic map, a smooth, low-anomaly area and a local gravity low between the positive anomalies to the northwest and southeast indicate less dense bedrock. Petrophysical samples from the quartzite in the vicinity have an average density of 2 650 kg/m^3 and susceptibility of 20 × 10^{-5} SI units. By applying these physical properties to the quartzite, the modelled depth extent is roughly 300 m at the eastern side.

A highly magnetised metavolcanic rock occurs east of the quartzite. Both in situ measurements of susceptibility and petrophysical laboratory measurements have been carried out and give densities in

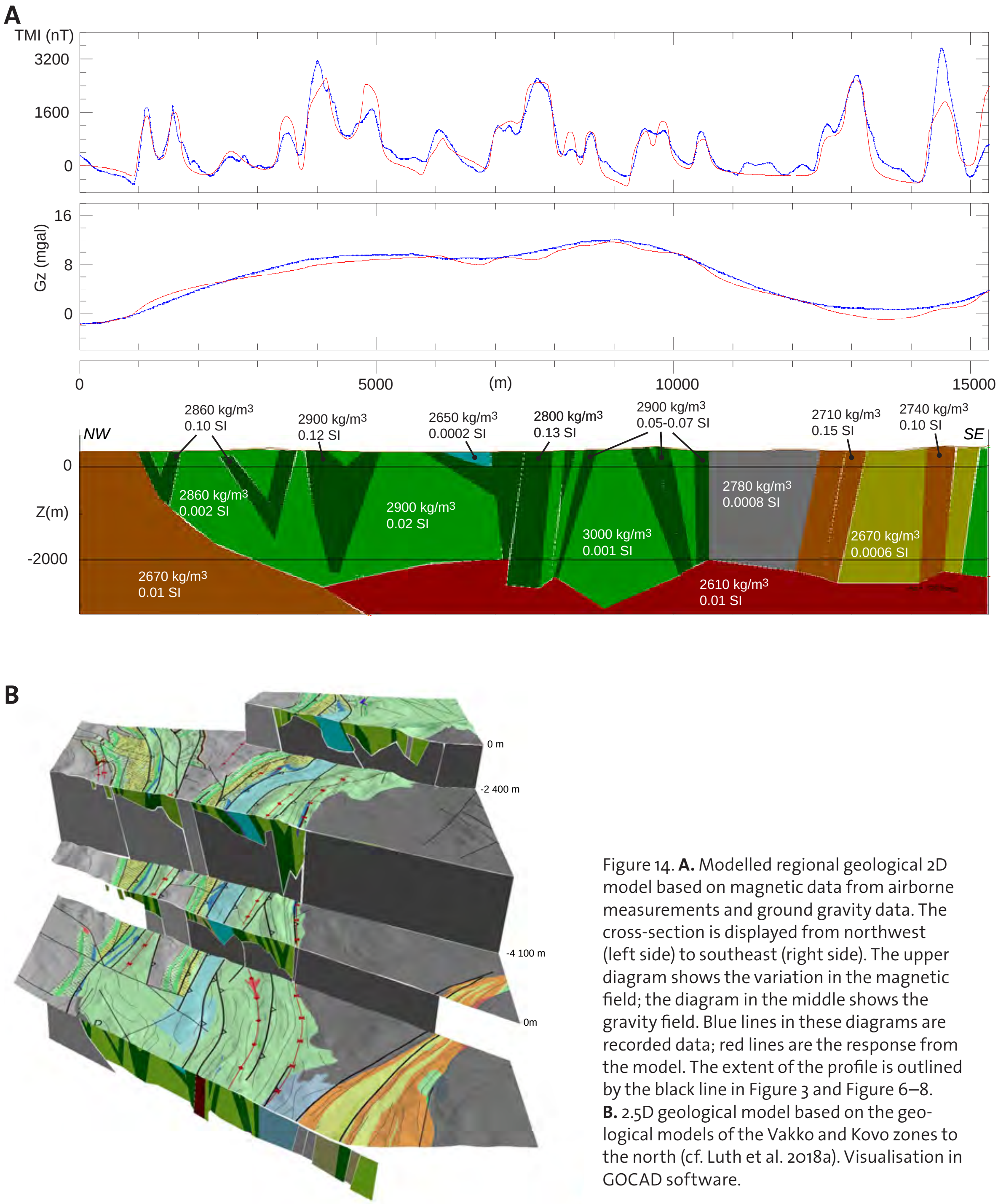

Figure 14. **A.** Modelled regional geological 2D model based on magnetic data from airborne measurements and ground gravity data. The cross-section is displayed from northwest (left side) to southeast (right side). The upper diagram shows the variation in the magnetic field; the diagram in the middle shows the gravity field. Blue lines in these diagrams are recorded data; red lines are the response from the model. The extent of the profile is outlined by the black line in Figure 3 and Figure 6–8. **B.** 2.5D geological model based on the geological models of the Vakko and Kovo zones to the north (cf. Luth et al. 2018a). Visualisation in GOCAD software.

the range of 2 800–2 900 kg/m^3 and susceptibilities in the range of 8 000–12 900 × 10^{-5} SI units. The highest magnetised lithology dips towards the northwest, and can be seen in the cross-section from the VOXI model (Fig. 15). A low-magnetic mafic metavolcanic rock occurs to the east. This has been sampled at two locations, giving an average density of 3 000 kg/m^3 and susceptibility of 120 × 10^{-5} SI units.

Narrow high-magnetic bands surrounding the low-magnetic core can be observed in the vicinity of the anticline. Samples have been obtained on the eastern side and these have an average density and susceptibility of 2 900 kg/m^3 and 7 000 × 10^{-5} SI units, values that have also been assigned to the high-

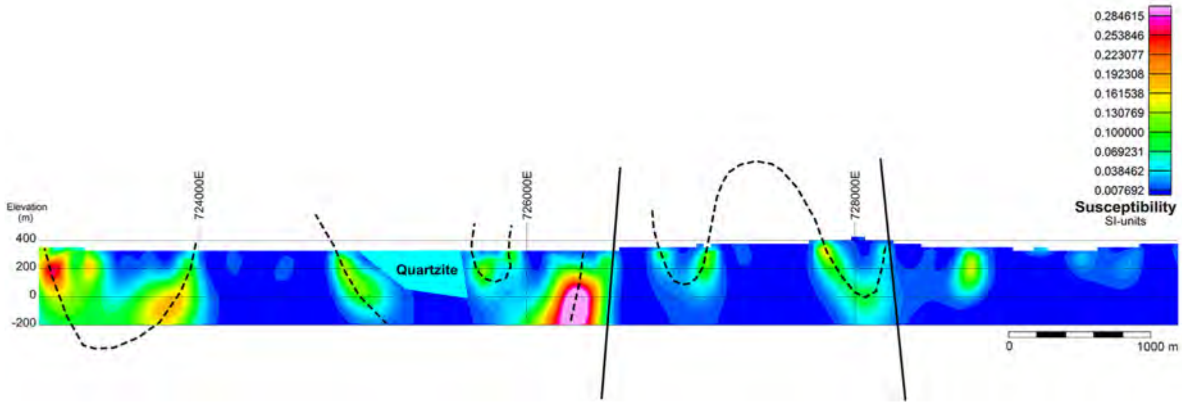

Figure 15. Cross-section derived from a 3D VOXI model along the central part of the regional 2D model in Figure 7. This model is based on data from airborne magnetic measurements.

magnetic bands on the western side of the low-magnetic core. The centre of the anticline consists of low-magnetic mafic metavolcanic rock with a higher density of 3 000 kg/m^3. The susceptibility of the low-magnetic metavolcanic rocks in this area is approximately 100×10^{-5} SI units.

A mica schist occurs east of the anticline, shown in light grey in the profile in Figure 14A. This rock is thought to belong to the Matojärvi formation and is seen as a orange-coloured area on the bedrock map (Fig. 3). It has an average density of 2 780 kg/m^3. The less dense rock is reflected in the gravity data, which is lower in the mica schist than in the core of the anticline. The gravity field continues to decrease to the east over the felsic metavolcanic rocks, which have densities in the range 2 670–2 740 kg/m^3. When comparing the gravity and magnetic signatures, the more rhyolitic sequences (yellow in Fig. 14A) coincide with low-magnetic areas, whereas the dacitic rocks (orange in Fig. 14A) are heterogeneously magnetised and give rise to high magnetic anomalies. This is supported by both field observations and petrophysical analysis, which state that the susceptibilities for the rhyolite are less than 100×10^{-5} SI units, while the susceptibility for the dacitic rocks is in the range 5 000–15 000 $\times 10^{-5}$ SI units. According to the geophysical data, these metavolcanic rocks dip quite steeply. To the east lies a highly magnetised andesite which has been sampled for petrophysical analysis at several locations. These samples have an average density of 2 910 kg/m^3 and susceptibility of 14 000 $\times 10^{-5}$ SI units.

Both granitic and gabbroic intrusive rocks occur to the east of these metavolcanic rocks, with granite predominating north of them. Petrophysical samples acquired from this granite have an average density of 2 610 kg/m^3. In the central and eastern part of the profile, it is assumed that the felsic intrusions underlie the supracrustal rocks.

3D modelling based on airborne magnetic data

Several 3D models have been made of the area. The data input was primarily magnetic data from airborne measurements, but modelling was also based on ground gravity data and data from ground magnetic measurements. 3D models have been constructed by inversion in the VOXI module, an extension of the Geosoft package. The main aim was to achieve an image of the geometries at depth of the various lithologies. One result of the 3D modelling is presented as a cross-section (Fig. 15). It is based on magnetic data from airborne measurements and shows the variations in magnetic susceptibility in the sub-surface down to 200 m below sea level. The 3D model, from which this cross-section is derived, covers an area of 7 km × 7 km surrounding the anticline at Pussijärvi (Fig. 7). The cell size of the volume pixels (voxels) is 50 m × 50 m in the horizontal direction and 25 m in the vertical direction. The voxels gradually increase in size with depth, causing decreased resolution. The lateral extent of the cross-section represents the central part of the regional profile in Figure 14A and is marked as a brown box in the magnetic anomaly map (Fig. 7).

Before the model was inverted, the magnetic susceptibilities of the sub-surface were constrained to keep the inversion within pre-defined boundaries. Available susceptibility information from previous and newly acquired petrophysical samples was used to constrain the model, along with in situ measurements of susceptibilities on outcrops. 19 petrophysical samples from this area, which have a magnetic susceptibility span in the range 30–13000 × 10^{-5} SI units, were used. In situ measurements of susceptibility on outcrops were conducted at 16 locations; eight measurements are normally made for each rock type and at each location. As the maximum value from these in situ measurements is 33 000 × 10^{-5} SI units, the constraints for the 3D model were set from -10 × 10^{-5} to 35 000 × 10^{-5} SI units so as to include the paramagnetic properties that could occur, particularly due to quartzite.

A high-magnetic structure, which can be interpreted as a syncline, occurs in the western part of the cross-section (Fig. 15). A highly magnetic structure dips towards the southeast just west of the quartzite. In the middle of the cross-section is a strong, highly magnetic structure that dips to the northwest. The latter corresponds well with the structural measurements in this area, which show that the dip of the foliation is approximately 70–80 degrees to the northwest. Further east, on the eastern flank of the anticline, is a relatively highly magnetic feature, the orientation of which corresponds well to structural information measured on outcrops. The structural measurements show that the foliation dips towards the southeast, at approximately 65–85 degrees, and becomes steeper to the southeast.

2D modelling based on ground magnetic data

The interpreted geological cross-section (Fig. 16) is based on the ground magnetic profile highlighted with a blue box in the magnetic anomaly map (Fig. 7). The main aim was to achieve an image of the geometrical properties of the highly magnetised structures along the extent of the profile. The model is constrained by either the magnetic properties of the petrophysical samples acquired along the profile, or in situ susceptibility measurements on outcrops. The depth extent of the lithologies is adopted from the regional geological profile shown in Figure 14A.

In the geological model in Figure 16, the less magnetised rocks are shown in light green and the higher magnetised rocks in dark green. It is evident from the ground magnetic data that the supracrustal rocks in the Kiruna greenstone group are heterogeneously magnetised.

In situ measurements of magnetic susceptibilities in the northwestern part of the profile show that the magnetisation of metavolcanic rocks varies from 40 to 13 000 × 10^{-5} SI units. The behaviour of measured magnetic data in the area indicates that the geometries of these magnetised layers dip to the southeast beneath a broader low-magnetic portion of metavolcanic rock with a susceptibility of less than 100 × 10^{-5} SI units.

To the southeast is an area of roughly 1 km showing rapid variations in magnetic field. Field observations show that the magnetic susceptibility of the more magnetised layers is around 12 000 × 10^{-5} SI units, so the thin layers giving rise to the positive magnetic anomalies have been assigned susceptibilities of between 10 000 and 15 000 × 10^{-5} SI units. Between these are lithologies with considerably lower magnetisation; measurements of 100 × 10^{-5} SI units have been recorded on the greenstones in this area. The geometries of the greenstones are steep, dipping to the northwest. Considering the geometries observed to the northwest, this observation suggests the presence of a syncline.

The lithologies continue to show this steep, northwestward dip until the relatively large, low-magnetic area in the southeastern part of the profile. Both in situ measurements and petrophysical sampling show this area to have a susceptibility of 100 × 10^{-5} SI units.

Lithologies are more magnetised at the southeastern end of the profile. Field observations close to the profile show magnetic susceptibility values of up to 7 000 × 10^{-5} SI units. But to fit the model to the magnetic measurements, the greenstones must be assigned values of 8 000–10 000 × 10^{-5} SI units. Signature

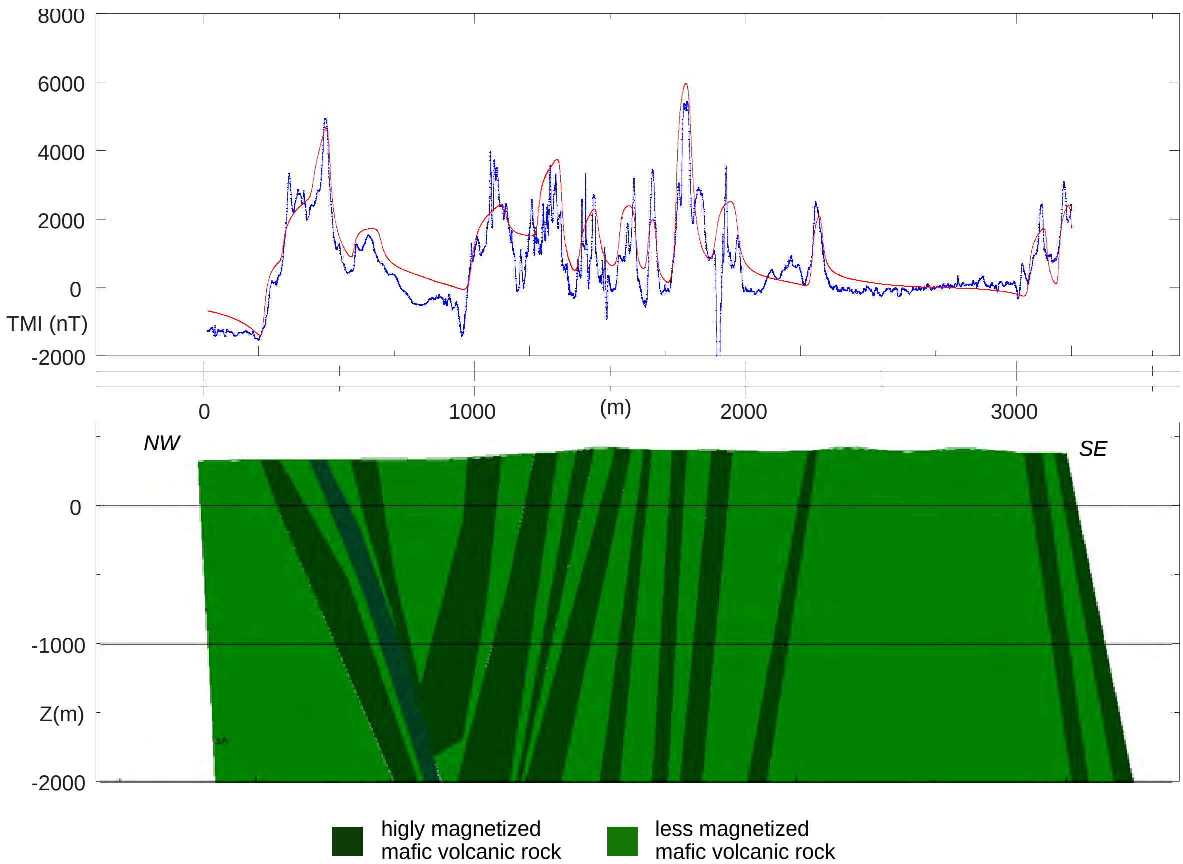

Figure 16. Forward modelled geological cross-section based on ground magnetic measurements along the profile marked in Figure 7 by the blue box. A syncline to the west and an anticline to the east are indicated in the model.

of the magnetic field shows that these highly magnetised greenstones dip to the southeast, indicating that they make up the eastern limb of an anticline.

Ground measurements along a profile with a VLF instrument have also been carried out in the area. The extent of this profile is marked in Figure 8 as the green line labelled "1". The result of this measurement is displayed as a resistivity cross-section in Figure 17. The VLF profile is located a short distance southwest of the profile measured by magnetometer (the geological interpretation is presented in Fig. 16). The majority of the lithologies seen in Figure 16 were crossed by this VLF profile.

The most striking feature in the resistivity cross-section is a narrow conductive zone, roughly 600–700 m from the western end. This could represent a brittle fault just east of the syncline interpreted from the magnetic data in Figure 16.

On a regional scale, the rocks of the Kiruna greenstone group, the Kurravaara conglomerate, and the Kiirunavaara group are all deformed into a series of synclines and anticlines with large amplitudes (~600 m) and wavelengths of hundreds of metres to 1–2 kilometres. Fold axes plunge predominantly to the south to southwest (Fig. 9), although north-plunging folds also occur. Fold axial traces can be followed for several kilometres, deflected slightly around younger and older magmatic intrusions due to rheology differences between the usually coarse-grained intrusive rocks and the finer-grained volcanic-metasedimentary rocks. Cleavage has developed in most rocks, but varies distinctly between rocks that appear nearly pristine and rocks that are pervasively foliated, and even partially migmatised. Foliation planes are usually lined with chlorite or biotite. With the exception of small-scale, subordinate kink folds in migmatitic mica-rich paragneiss south of Pussijärvi, no evidence of more than one folding event was found. Grigull & Lundin (2014), Talbot & Koyi (1995) and Forsell (1987) suggest that an

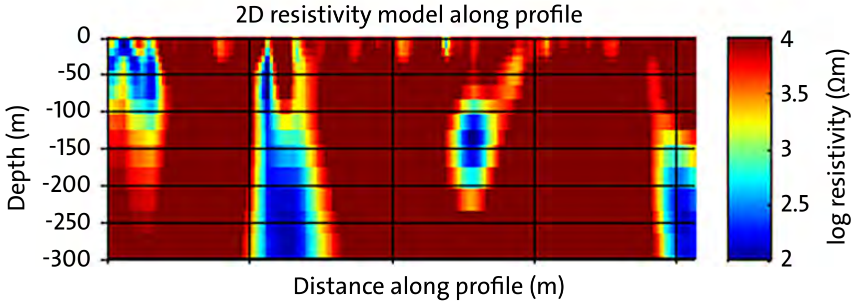

Figure 17. Inversion model based on VLF measurements along the profile labelled "1" (Fig. 8). The cross-section displays the apparent resistivity in the ground at shallow depth.

(isoclinal) folding phase preceded the folding described above. After thorough interpretation of existing and newly collected geoscientific data, no convincing evidence of this event could be detected, however. The structural model derived from the results of the Barents Project therefore predicts only one folding phase due to NW–SE to E–W-directed shortening and later or contemporaneous displacement of these folds along several thrusts and brittle faults. This model is supported by the studies of Vollmer et al. (1984) and Wright (1988). In the present geological model (Fig. 3 and 14), it is suggested that the Hauki quartzite was deposited into a graben that formed during a period of extension, cutting into the underlying rocks and partially reusing old structures, locally cutting them at an acute angle. Regional-scale folding of the Hauki quartzite is inferred from outcrop-scale open folds and cleavage-bedding relationships, indicating continued E–W compression and graben inversion after sediment deposition. Although direct evidence of thrusting was not observed in the field, placement of stratigraphically older rocks onto younger rock units requires westward-directed thrusting, corresponding to an overall east–west-directed compressional stress regime (cf. Luth et al. 2018a).

Masugnsbyn key area

Lithostratigraphy

The Masugnsbyn area features metavolcanic and metasedimentary rocks of predominantly basaltic composition corresponding to the Veikkavaara greenstone group (VGG) to the east, and metasedimentary, partially migmatised rocks of the Pahakurkio (PHG) and Kalixälv group (KÄG) to the west and south (Padget 1970, Niiniskorpi 1986; Fig. 18A). A simplified lithostratigraphic column is shown in Figure 18B. For a detailed description of the lithostratigraphic units, the reader is referred to Lynch et al. (2018) and Hellström et al. (2018); see also summary review of geological and geophysical information of the Masungsbyn area by Hellström & Jönsson (2014). The following brief description of lithological units of the Masugnsbyn area mainly follows Padget (1970) and Niiniskorpi (1986).

The Veikkavaara greenstone group (VGG) contains predominantly basaltic greenstone at the base, a thin middle unit of pelitic schists and quartzite, and at the top volcaniclastic, basaltic tuffs with laterally extensive graphite horizons. The upper part of the VGG contains a banded iron formation and at the top lenses of marble that are locally dolomitic, e.g. the Masugnsbyn dolomite, which is currently quarried. The Veikkavaara greenstones have an overall high-magnetic signature and form a V-shaped fold, which can also be observed in the gravity data (Fig. 19 and 20). The greenstone sequence is clearly outlined as a high-magnetic, banded sequence, where alternating high and low magnetic anomalies probably reflect depositional features. Graphite-bearing layers in the upper part of the Veikkavaara greenstones are good electrical conductors and can therefore be traced from electromagnetic

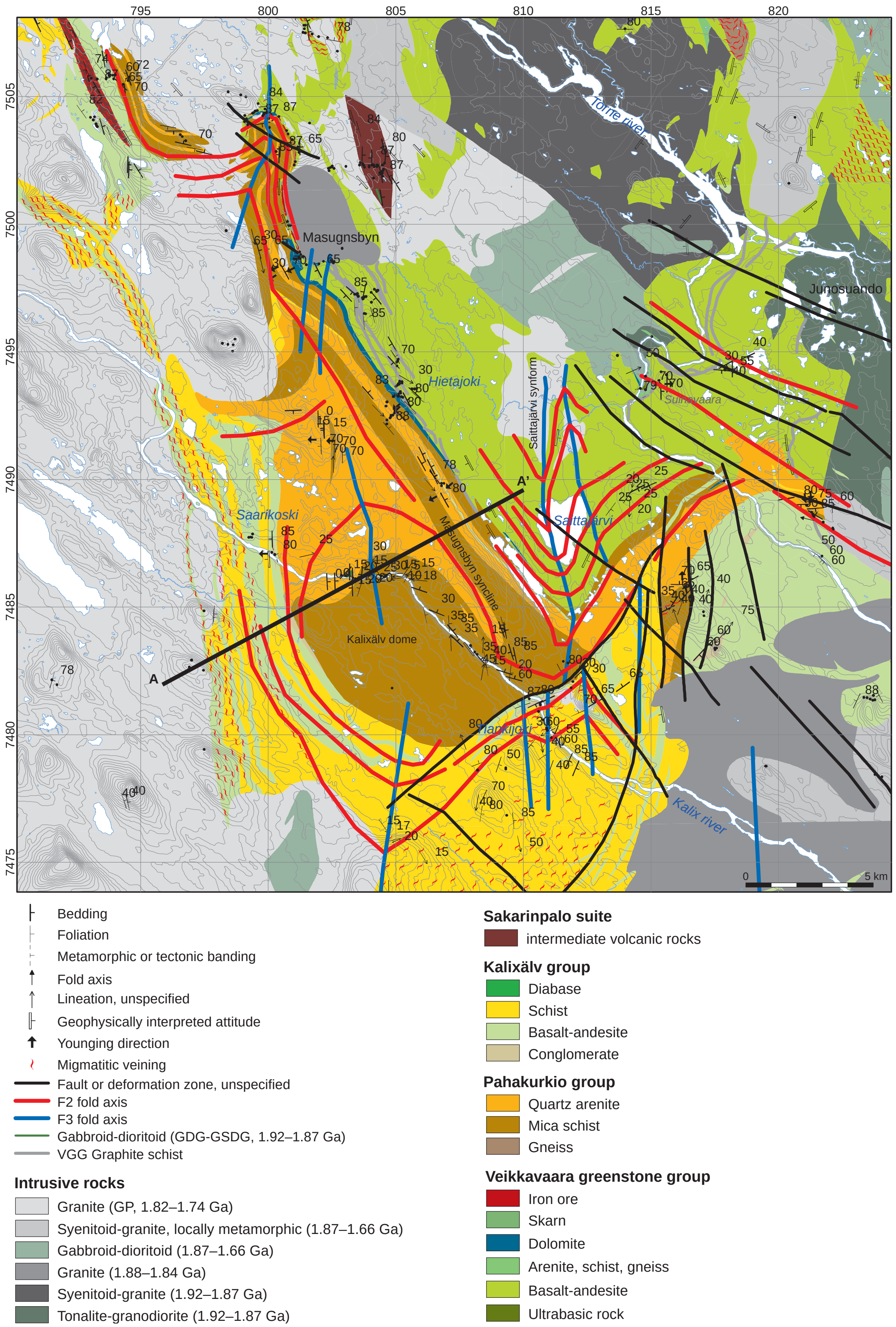

Figure 18. **A.** Geological map of the southern part of the Masugnsbyn key area (see also Hellström et al., 2018). Profile A-A' refers to a qualitative cross-section presented in Figure 28. Fold axial traces of the folding phase F2 are marked in red; F3 fold axial traces are marked in blue. Small black dots mark recent outcrop observations.

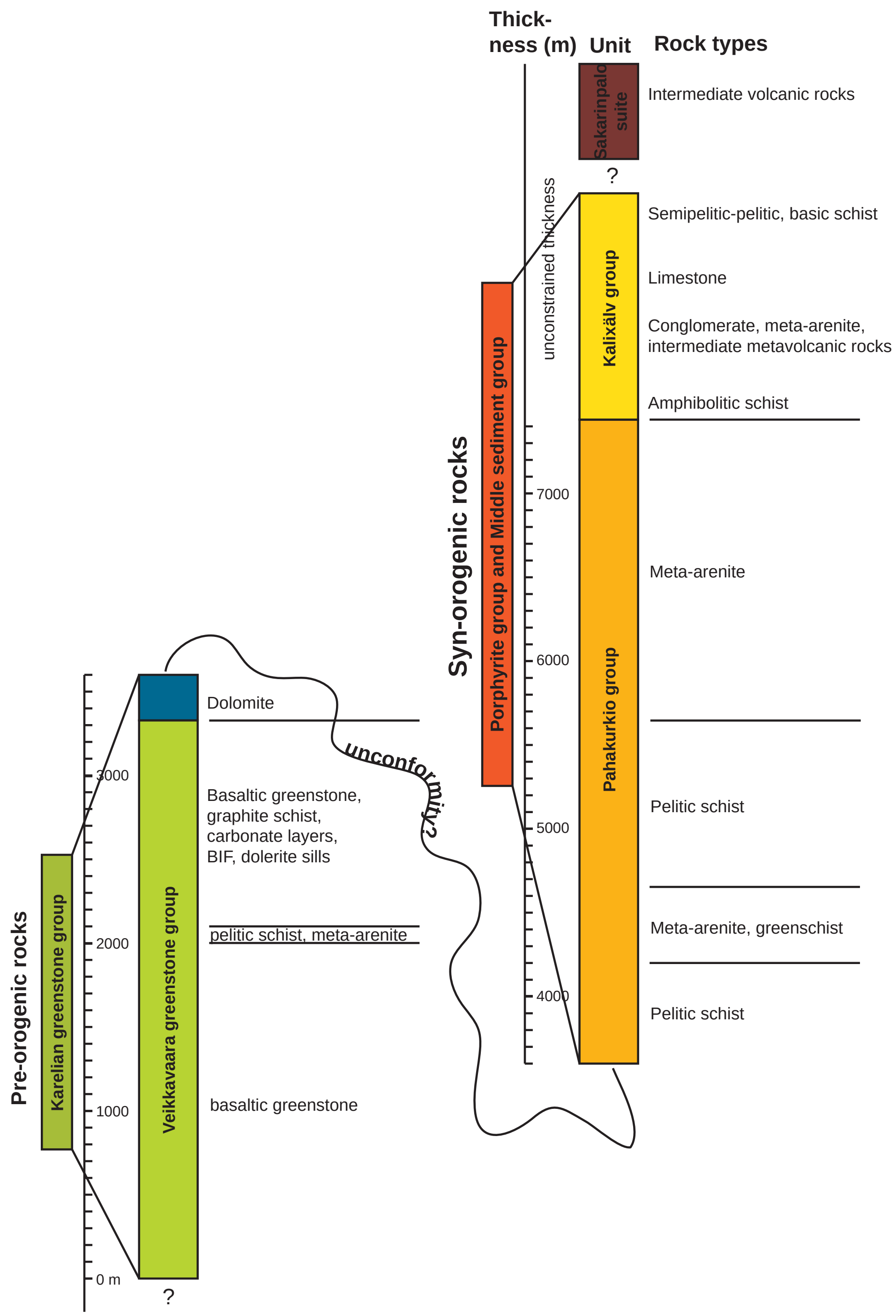

Figure 18. **B.** Simplified lithostratigraphic column of the southern Masugnsbyn area based on a combination of geological data from Padget (1970), Niiniskorpi (1986) and Hellström & Jönsson (2014).

maps such as VLF (Very Low Frequency) and slingram maps over approximately the same distance (Fig. 21, cf. Hellström & Jönsson 2014).

The Pahakurkio group overlies the rocks of the Veikkavaara greenstone group. The contact between these two units is not exposed, so it is unclear whether the contact is conformable. The Pahakurkio group consists of a sequence of clastic metasedimentary rocks and has been divided into four lithological units. From bottom to top, these are pelitic schist, metaarenite (arkosic sandstone), andalusite-

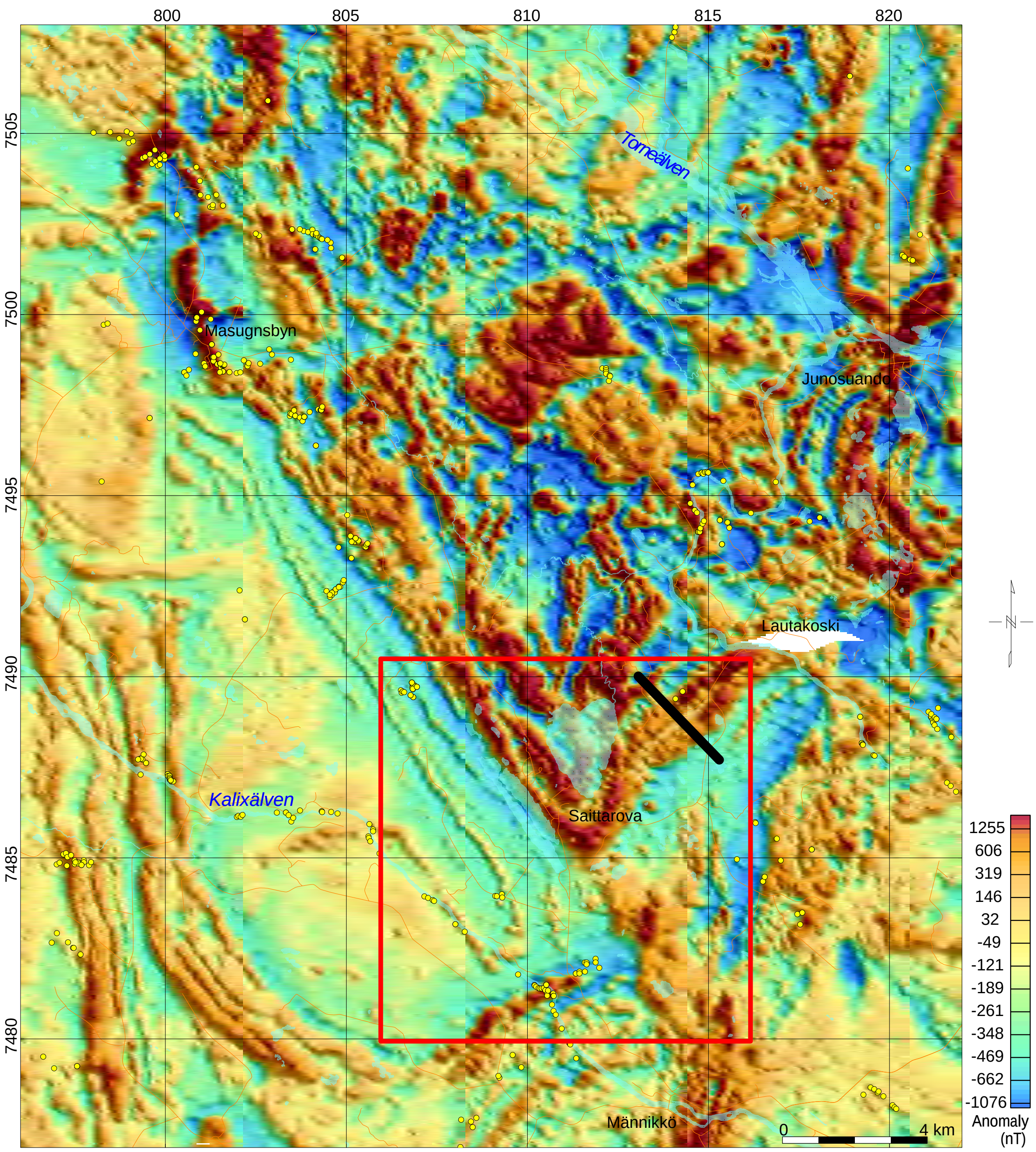

Figure 19. Residual magnetic anomaly map based on data from airborne measurements. Yellow circles represent acquired petrophysical samples. The red polygon outlines the area of the 3D VOXI model and the black line in its upper right-hand corner shows the extent of the cross-section derived from it (Fig. 27). Note the high-magnetic signature of the mafic rocks of the greenstone group.

bearing pelitic schist and a second unit of metaarenite. The arenites are often cross-bedded, allowing the determination of younging directions, which are consistently to the west. The rocks of the Pahakurkio group have an overall low magnetic signature, but there are higher-magnetic conformable layers consisting of strongly scapolite-altered intermediate rocks, which, judging from the aeromagnetic map, have a considerable lateral extent (Fig. 19). Graphite schists and carbonate rocks may also occur within the Pahakurkio group, which makes it difficult to distinguish these rocks from the VGG.

Rocks of the Kalixälv group are exposed to the west and south of the Pahakurkio group sedimentary pile. On the aeromagnetic map, the unit is characterised by alternating high and low-magnetic

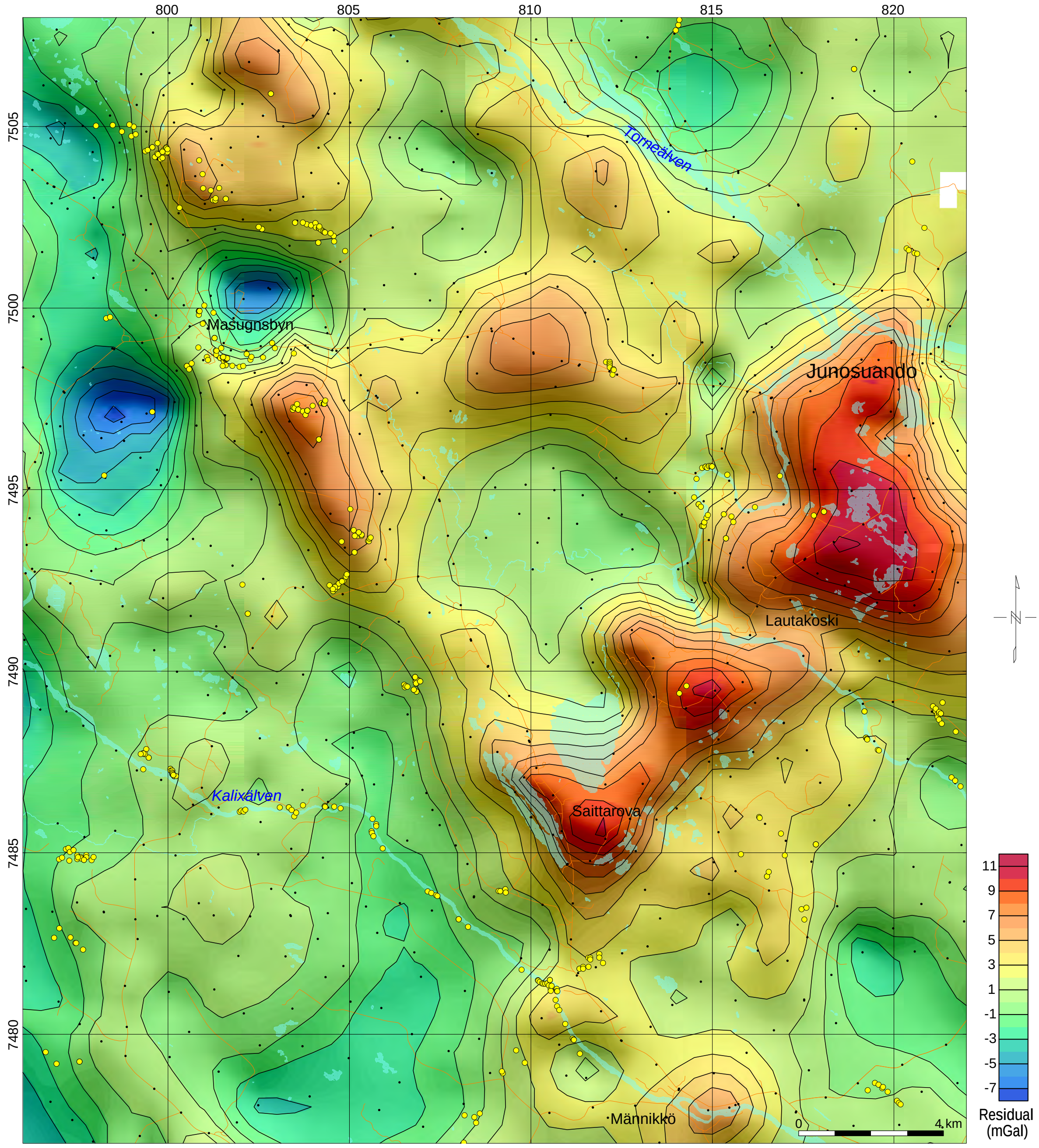

Figure 20. Residual gravity anomaly. Yellow circles represent acquired petrophysical samples and black dots are measurement sites. The dense mafic rocks of the greenstone group generate positive gravity anomalies, while the lighter metasedimentary rocks of the Pahakurkio and Kalixälv group are negative features on the gravity map

bands caused by alternating layers of metavolcanic rocks and pelitic to arenitic metasedimentary rocks, respectively. An approximately 20–30 m thick basal conglomerate is overlain by amphibole-bearing metaarenite, followed by mica schist, quartzites and layers of meta-andesite, but the bedrock crops out poorly. To the west and southwest, an increasing degree of migmatisation affects the metasedimentary rocks, so the natural, upper stratigraphic limit for the group is not known. The transition from the Pahakurkio to Kalixälv group is not well understood, and an interpretation of structures is difficult, due not least to the similar lithologies of both groups (pelitic and arenitic metasedimentary rocks).

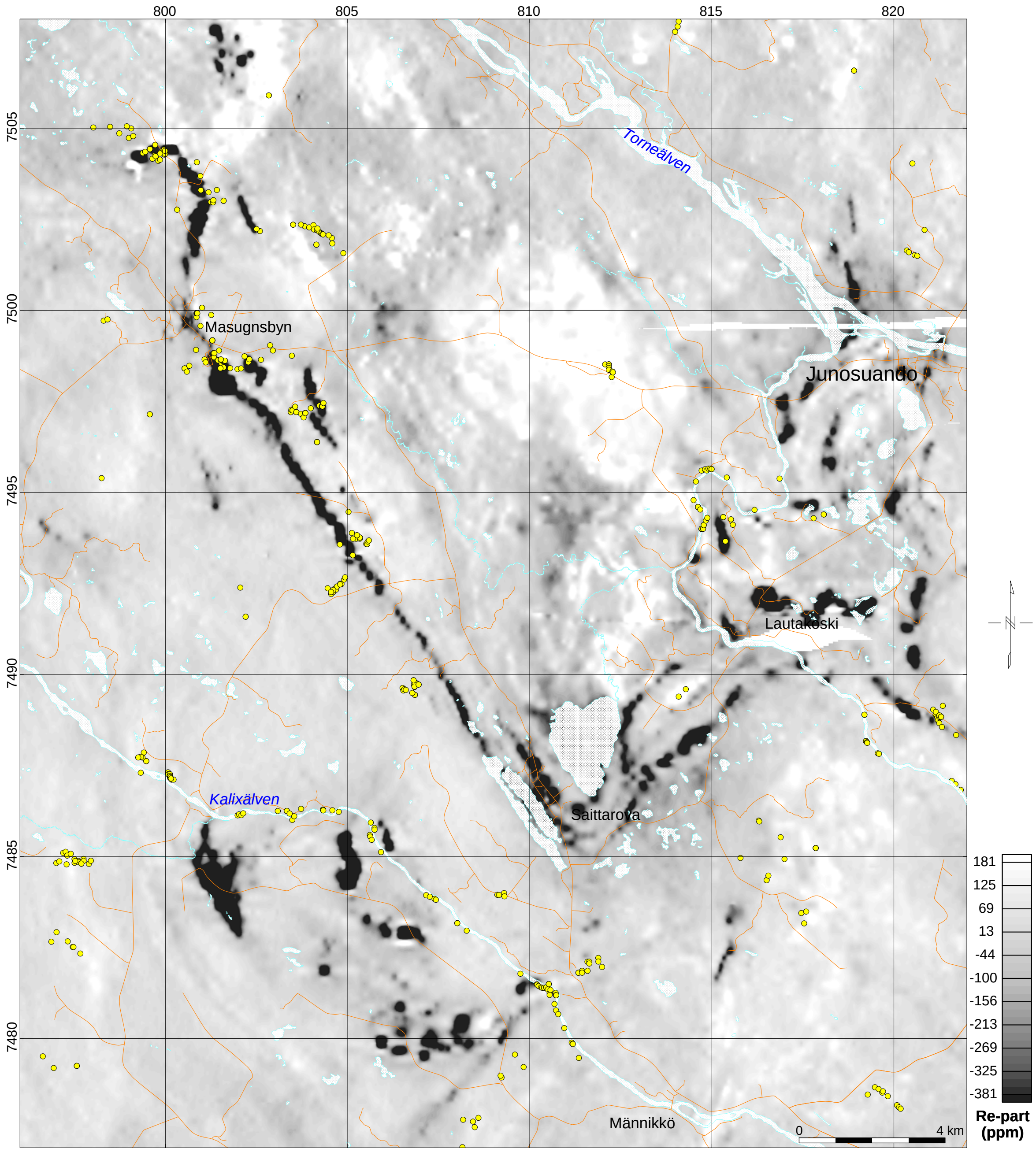

Figure 21. Slingram anomaly map based on data from airborne measurements. In-phase component. Yellow circles represent acquired petrophysical samples. The darker colours show metasedimentary rocks that are rich in graphite and therefore good electrical conductors.

Structural inventory

The deformational record is best preserved in sedimentary rocks of the Pahakurkio group. During a first deformation phase (D1), a gneissic foliation (S1) with foliation-parallel migmatitic veins formed locally in these rocks. It is therefore assumed that all rocks in the area were deformed to some extent during D1. It is, however, unclear whether folding occurred during D1. The first observed folds F2 are attributed to a second deformation event D2, since they fold the migmatitic foliation S1.

Structural geological data from Lake Saittajärvi (cf. Fig. 18A) northwestwards to at least Masugnsbyn show that both metasedimentary rocks of the Pahakurkio group and graphite and dolomite layers

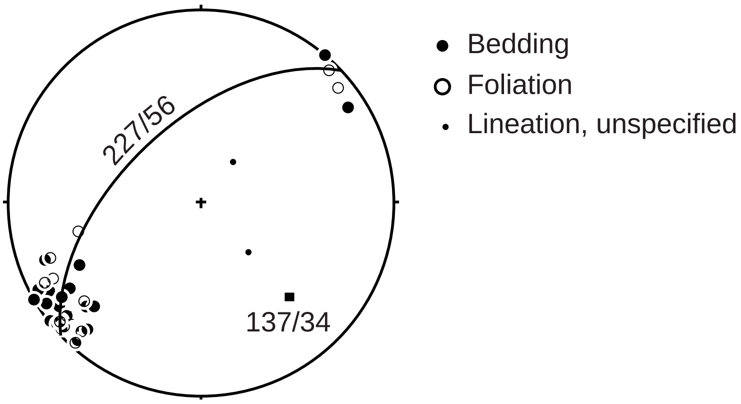

Figure 22. Stereographic projection (lower hemisphere) of structural data at Hietajoki. Note that both bedding and foliation dip steeply to the northeast. However, younging is consistently to the southwest (see text).

of the Veikkavaara greenstone group dip steeply towards the northeast (Fig. 22), whilst younging is consistently to the southwest, i.e. positioning younger under older rocks (Fig. 18A; see also Kumpulainen 2000). These structural data suggest that the rocks in this approximately 16 km long NW–SE oriented band from Masugnsbyn to Saittajärvi occupy an overturned F2 fold limb formed during a second deformation phase D2.

At Suinavaara (cf. Fig.18A), rocks of the Veikkavaara greenstone group crop out and display a hinge zone of an F2 fold. Here, fold axes plunge 40 degrees towards the southeast. Folding is disharmonic and a well-developed axial planar foliation striking northwest–southeast truncates the original layering (Fig. 23A). The truncation is interpreted to be a consequence of dissolution along the foliation planes perpendicular to the original shortening direction. On a regional scale, this process creates pinnate fold hinges and apparent offsets of the greenstone layers visible on outcrop scale (Fig. 23A) and as magnetic lows on the aeromagnetic map (Fig. 19).

Strong coaxial deformation during F2 is also inferred from, e.g., chocolate tablet boudinage of competent layers in siltstones of the Pahakurkio group at Hietajoki (Fig. 23B, cf. Fig. 18A) and isoclinal F2 folding of greenstone layers observed just south of Masugnsbyn (Fig. 23B).

Direct geological evidence of a second folding phase (F2) affecting the rocks at least in the southern part of the Masugnsbyn key area can be found in outcrops along the river Kalixälven near the estuary of the Tiankijoki river (cf. Fig. 18A). Here, fold interference patterns can be observed in arenitic to pelitic metasedimentary rocks of the Kalixälv group. A gneissic foliation (S1) developed in these rocks during D1. At some locations, the original bedding (S0) is still discernible, and S1 crosscuts S0. Migmatite veins run parallel to this gneissic foliation and were tightly to isoclinally folded during folding phase F2, belonging to a second deformation phase D2. Parasitic folds belonging to the F2 folding phase are locally discernible (Fig. 24A–C). During folding phase F2, compression was oriented N–S, and an axial planar foliation S2 developed locally.

Sillimanite platelets grew parallel to S2 and were folded by a later folding event (F3) during a third deformation phase (D3). Some of the F3 fold hinges are infilled by migmatitic veins (Fig. 24B) and a non-pervasive, spaced cleavage (S3) developed parallel to the kink fold axial planes (Fig. 24B & C).

Recent radiometric isotope dating of the migmatitic rocks along the river Kalixälven yielded metamorphic ages of 1.88–1.86 Ga (Bergman et al. 2006, Hellström 2018). U-Pb SIMS analyses of metamorphic, low-Th/U zircon rims from a sillimanite-cordierite-bearing migmatite (cf. Fig. 24C), were dated at 1878 ±3 Ma (Hellström 2018). This age is interpreted to date migmatitisation and also puts constraints on the age of folding of supracrustal rocks. The 20 Ma age difference between the zircon rim age obtained and the monazite age of Bergman et al. (2006) possibly reflects resetting of the U-Pb isotopic system in monazite, i.e. 20 million years after the migmatisation event dated by U-Pb in zircon.

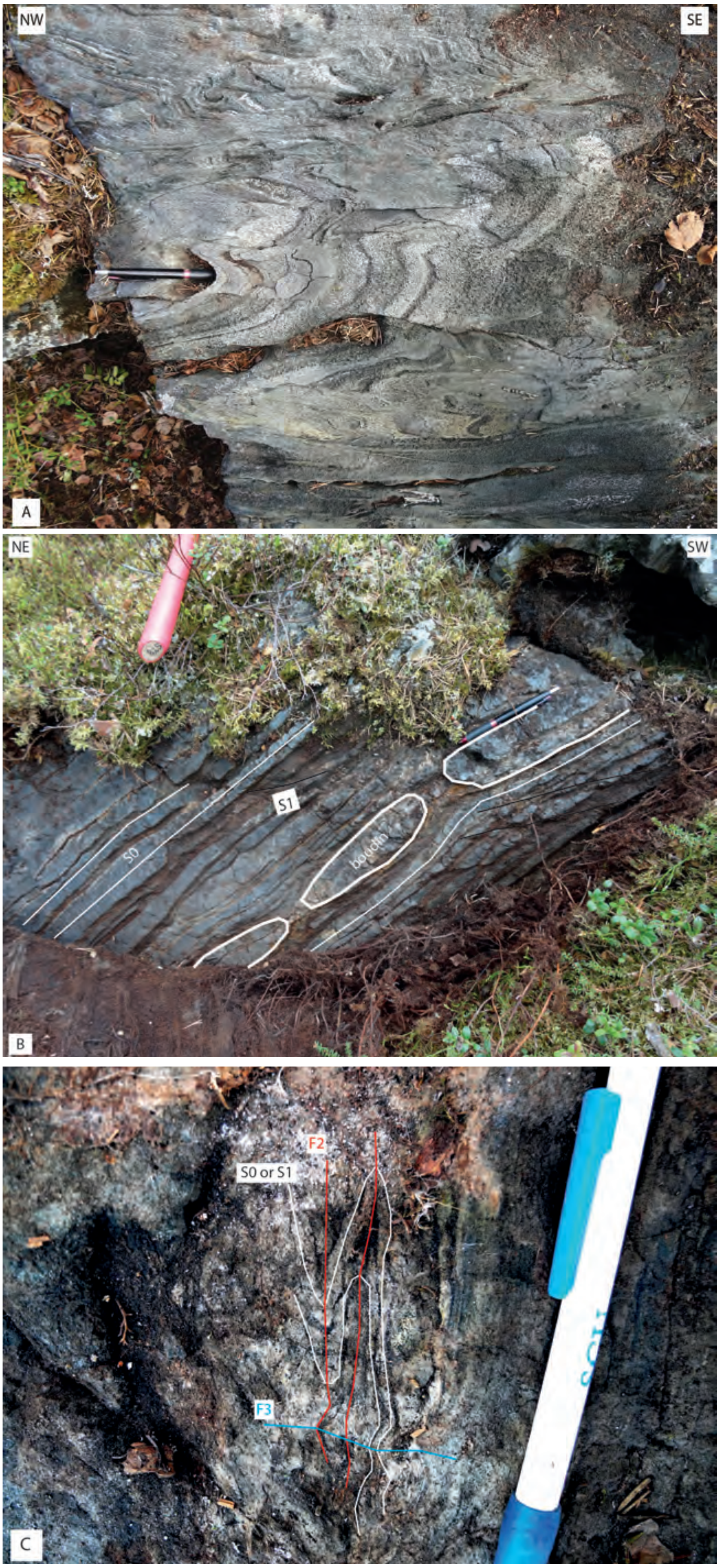

Figure 23. **A.** Disharmonic folds in basaltic volcaniclastic metasedimentary rocks of the Veikkavaara greenstone group at Suinavaara (SWEREF99 TM: N7494097, E815614). A southeast-plunging fold axis is marked by the pencil. Note the thinning of the fold limbs in the top left-hand corner of the photograph and the truncation of original bedding by the axial planar cleavage. **B.** Boudinage of competent layers parallel to S0 in siltstones of the Pahakurkio group. The interboudin space is filled with quartz. S1 is recognisable in the finer-grained layers, shallowly dipping to the northeast. Hietajoki (SWEREF99 TM: N7492325, E804671). **C.** Isoclinal folds (F2) in mafic volcaniclastic metasedimentary rocks of the Veikkavaara greenstones. Kink folds (F3) occur orthogonal to F2. Pahtajoki (SWEREF99 TM: N7502177, E802368).

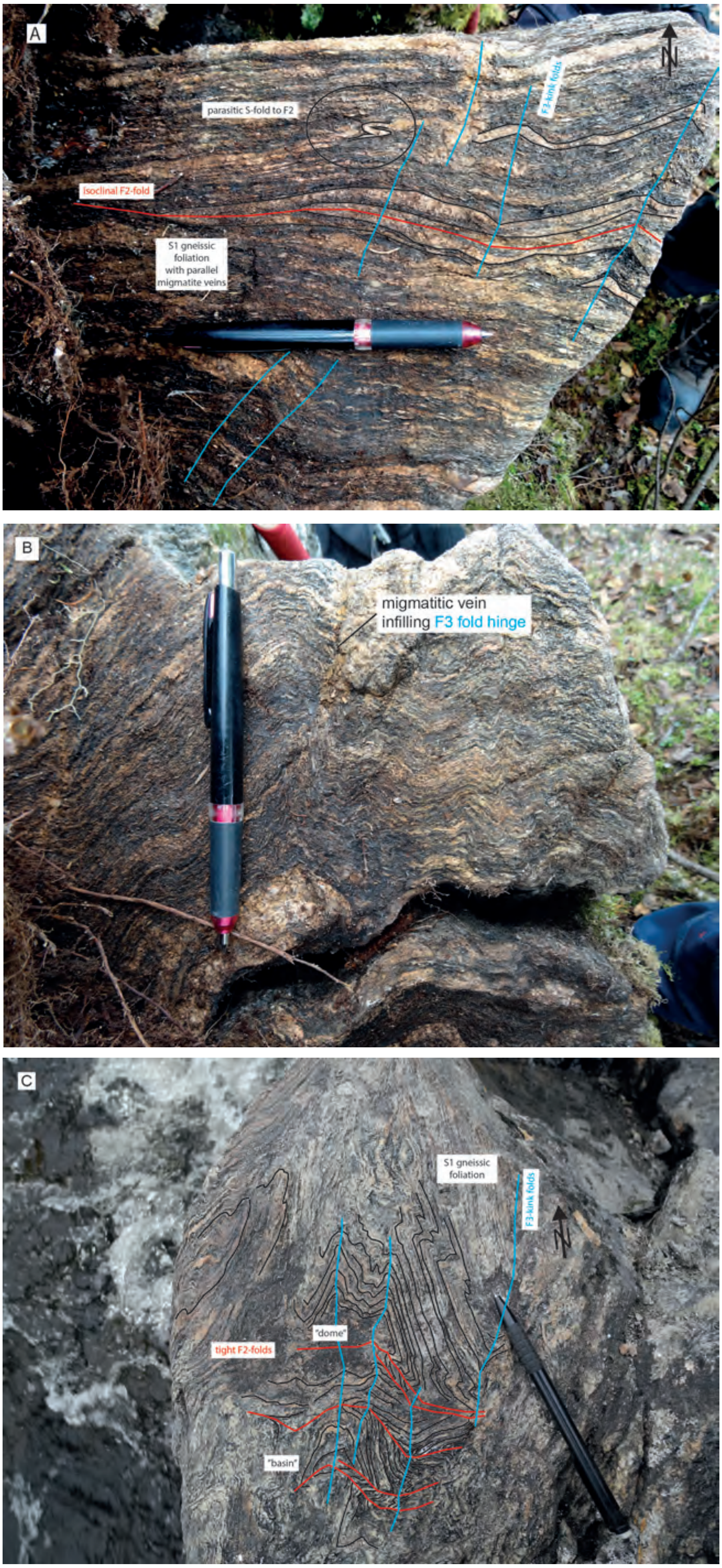

Figure 24. Fold interference patterns in migmatitic pelitic rocks of the Kalixälv group on the shore of the river Kalixälven (SWEREF99 TM: N7480220, E810924). Tight to isoclinal F2 folds are refolded by open kink folds (F3). **A.** Note the small S fold, which is incompatible with the F3 folding and must therefore be a parasitic fold to F2. **B.** Increased amplitude and decreased wavelength of F3 folds. The F3 fold hinge is infilled by a migmatitic vein. North is up. **C.** Small-scale "basin and dome" structure created by depressions and culminations of the F3 folds. This fold interference pattern is thought to roughly represent the regional-scale structural pattern in the Masugnsbyn area.

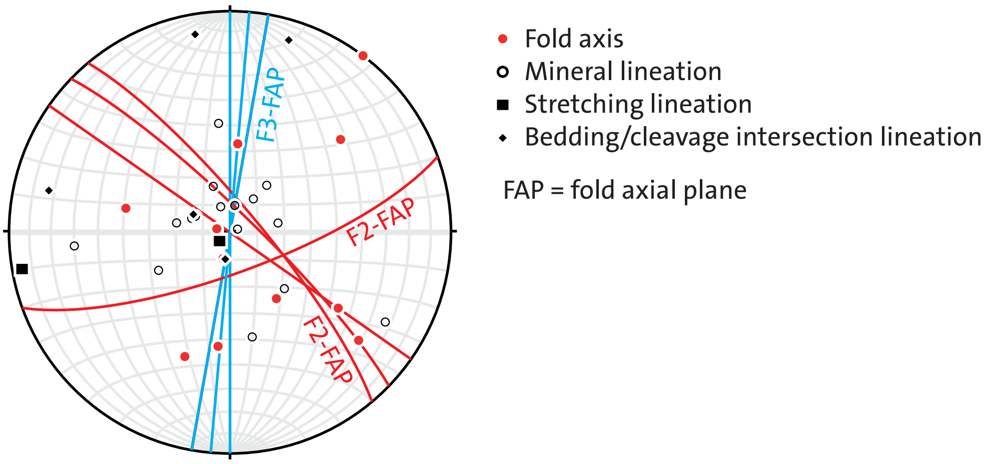

Figure 25. Stereographic projection (lower hemisphere) of fold axial planes, fold axes, and related lineations for the Masugnsbyn area. Three predominant fold orientations can be seen. The two fold axial plane orientations of F2 are interpreted as being due to reorientation of F2 folds during F3 kink folding around vertically or steeply dipping fold axes. No distinction was drawn between greenstones and syn-orogenic rocks.

Plotting axial planes and fold axes for the entire Masugnsbyn key area in a stereographic projection shows three main fold axial plane orientations (Fig. 25).

The relationship between F2 and F3 folding can be seen impressively in high-resolution magnetic data available for an area just north of Masugnsbyn (Fig. 26). Here, the magnetic banding created by the different lithologies in the Pahakurkio group can be used to trace entire layers. The fold interference pattern is evident immediately and matches the proposed two more or less orthogonal folding events that have affected the area.

On the current bedrock map at a scale of 1:50 000 (Padget 1970), the large-scale, V-shaped structure at Lake Saittajärvi in the centre of Figure 18A is interpreted to be an anticline cored by greenstones. However, a 3D model of airborne magnetic data on that area reveals that the limbs of this structure dip towards each other (Fig. 27,) suggesting that the structure is instead a north-plunging synformal anticline. The eastern limb and the core of the synform are poorly exposed and it is difficult to verify the proposed structural model. A cross-section across the eastern part of the 3D model supports the theory that the rocks in the eastern limb of the synform had been folded prior to its formation (Fig. 22B). This is consistent with the structural data collected from the western limb of the V-shaped structure near Hietajoki and Masugnsbyn.

Both the structural observations and the geophysical modelling results suggest two phases of folding. During F2 compression was oriented N–S, resulting in isoclinal to tight E-W trending folds. During F3 compression was oriented E–W and resulted in open kink or crenulation folds with steeply to shallowly north and south-plunging fold axes. F3 fold axial planes dip steeply. Fold interference patterns were created by refolding of the F2 fold axial planes (Fig. 24 A–C). F3 folds are less pervasive and have somewhat more variable amplitudes and wavelengths than the F2 folds. Their effect is mostly observed in the hinge zones of what has been interpreted as regional-scale F3 folds. The dominant large-scale synform mentioned earlier is therefore a synform that folds bedding (S0), migmatitic banding (S1) and F2 folds around a steeply north-plunging fold axis. The hinge of this regional-scale F3 synform lies close to lake Saittajärvi. Here, a large positive slingram anomaly can be observed (Fig. 21), but it is unclear whether this relates to the water body of the lake or to a potential enrichment in graphite. Although some of the F3 fold hinges are infilled by migmatitic veins, the kink folding style during F3 indicates colder metamorphic conditions during the second folding phase than during the isoclinal F2 folding.

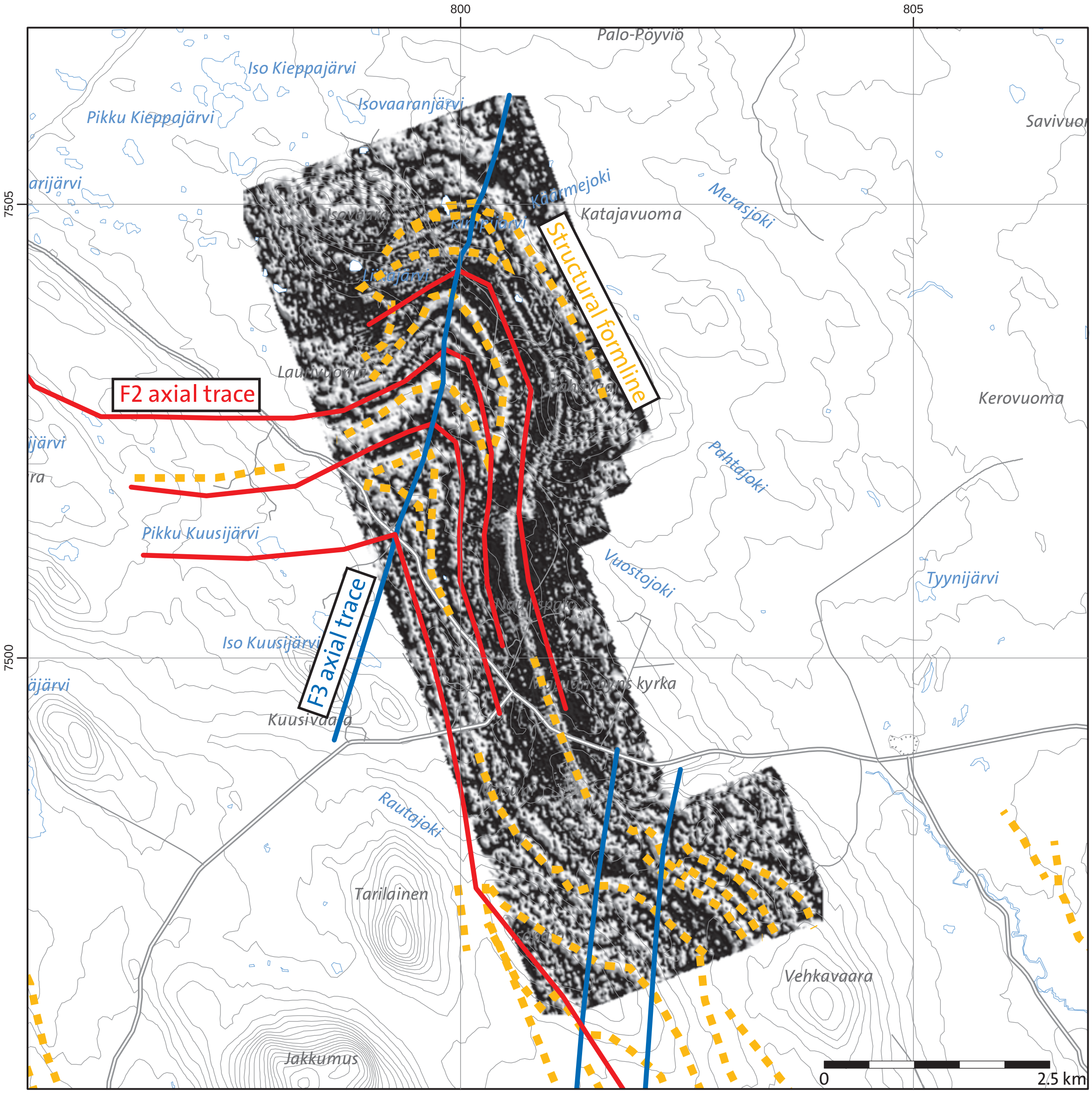

Figure 26. Fold interference created by originally E–W-striking F2 folds (red lines), being refolded by F3 folds (blue lines). The yellow lines mark magnetic connections corresponding roughly to original bedding S0 and S1 foliation.

Unresolved questions

A major break in the orientation of magnetic markers occurs at Saarikoski (cf. Fig. 18A) at the boundary between shallowly dipping rocks of the Pahakurkio group and steeply dipping rocks of the Kalixälv group. Along the east–west-oriented part of the Kalixälven shore, mica schists and metarenites of the Pahakurkio group dip shallowly, and predominantly to the west. Stretching lineations also plunge to the west. Following these units along the river, however, it becomes clear that these rocks are folded into open, north–south-trending, doubly plunging folds, which are attributed to the F3 folding phase in this report. The "Kalixälv dome" (Padget 1970; cf. Fig. 18A) is therefore interpreted here to correspond to a culmination of a doubly plunging antiform refolding of the "Masugnsbyn syncline" (Padget, 1970). But it is unclear whether the Kalixälv dome and the Saittajärvi synform formed during the same folding

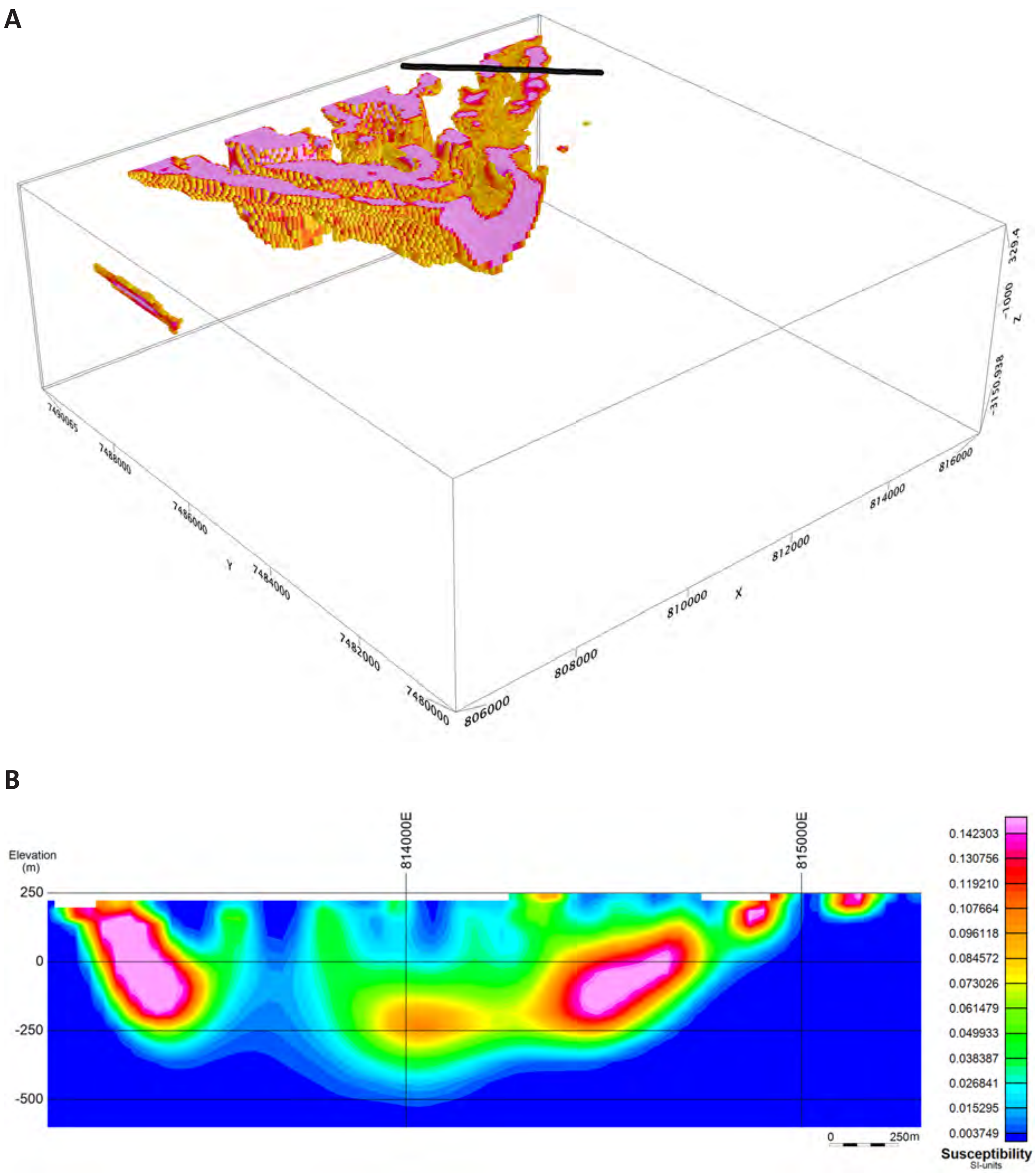

Figure 27. **A.** 3D model of the V-shaped structure at Saittajärvi using VOXEL modelling of the magnetic field. The synformal shape of the greenstone succession becomes clear when looking obliquely at the model from above towards the NE. **B.** Vertical section derived from the 3D VOXI model across the eastern limb of the Saittajärvi synform. This profile suggests that the rocks in the limb had been folded prior to formation of the synform.

event. Alternatively, the open, gently plunging folds at Kalixälven may be the result of a fourth, late folding phase F4. It is relatively unlikely though, that these flat-lying rocks reflect early thrusting in the area as was suggested by R. Rutland (pers. comm.). More detailed structural work is necessary to answer this question. A conceptual cross-section from Saarikoski to Hietajoki is presented in Figure 28.

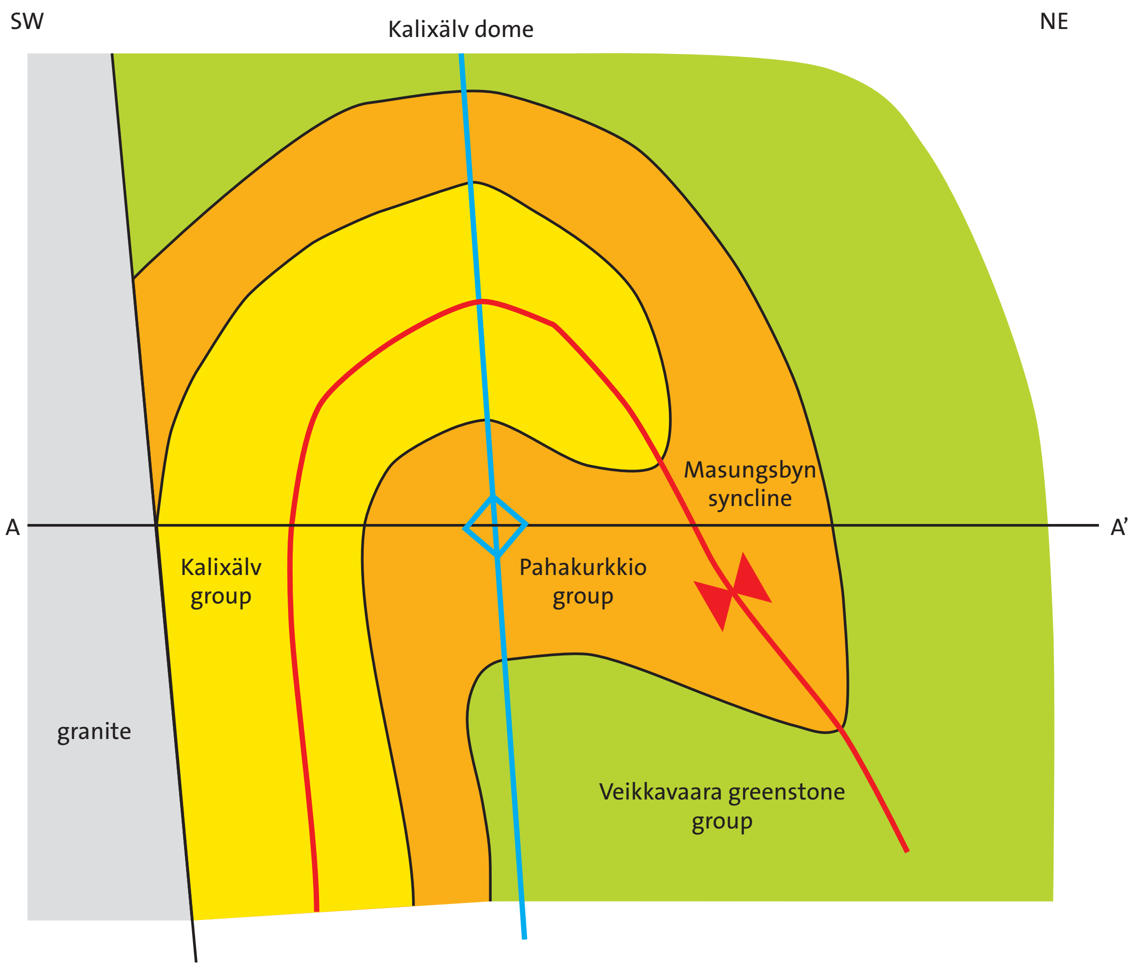

Figure 28. Conceptual cross-section (not to scale) across the Kalixälv dome. Profile line A-A' refers to the ground surface; structures above are thought to be eroded. For approximate location of the profile line see Fig. 18A.

Käymäjärvi–Ristimella key area

Lithostratigraphy

The inferred lithostratigraphy for the Käymäjärvi–Ristimella key area is predominantly based on map descriptions by Padget (1977), Lindroos & Henkel (1981) and Martinsson et al. (2013). More detailed descriptions of the lithostratigraphic sequences are given in Grigull et al. (2014), Grigull & Berggren (2015) and Martinsson et al. (2018). A simplified geological map and lithostratigraphic column are shown in Figure 29.

The oldest rocks in the area occur close to Käymäjärvi township (Fig. 29A) and consist of high-Mg, meimechitic lapilli tuffs, probably of pyroclastic origin. Meimechite belonging to the Käymäjärvi formation (Fig. 29B) of the Veikkavaara greenstone group occupies the core of an overturned anticline addressed later. The Käymäjärvi formation is overlain by rocks belonging to the Vinsa formation, a mixed unit of mafic metavolcanic and metavolcaniclastic rocks, calc-silicate rocks, dolomite, graphite-bearing schists, skarn-hosted iron ore and a banded iron formation. It is subdivided into four sub-units (Fig. 29B, cf. Martinsson et al. 2013, 2018). The lowest sub-unit of the Vinsa formation occurs within the core of the Käymäjärvi anticline and, possibly, in the far northeastern corner of the key area. Grey, fine- to medium-grained tuffites of basic composition, along with grey, fine-grained basalts, comprise the main part of the lowest sub-unit of the formation. Dark grey, very fine-grained graphite-bearing

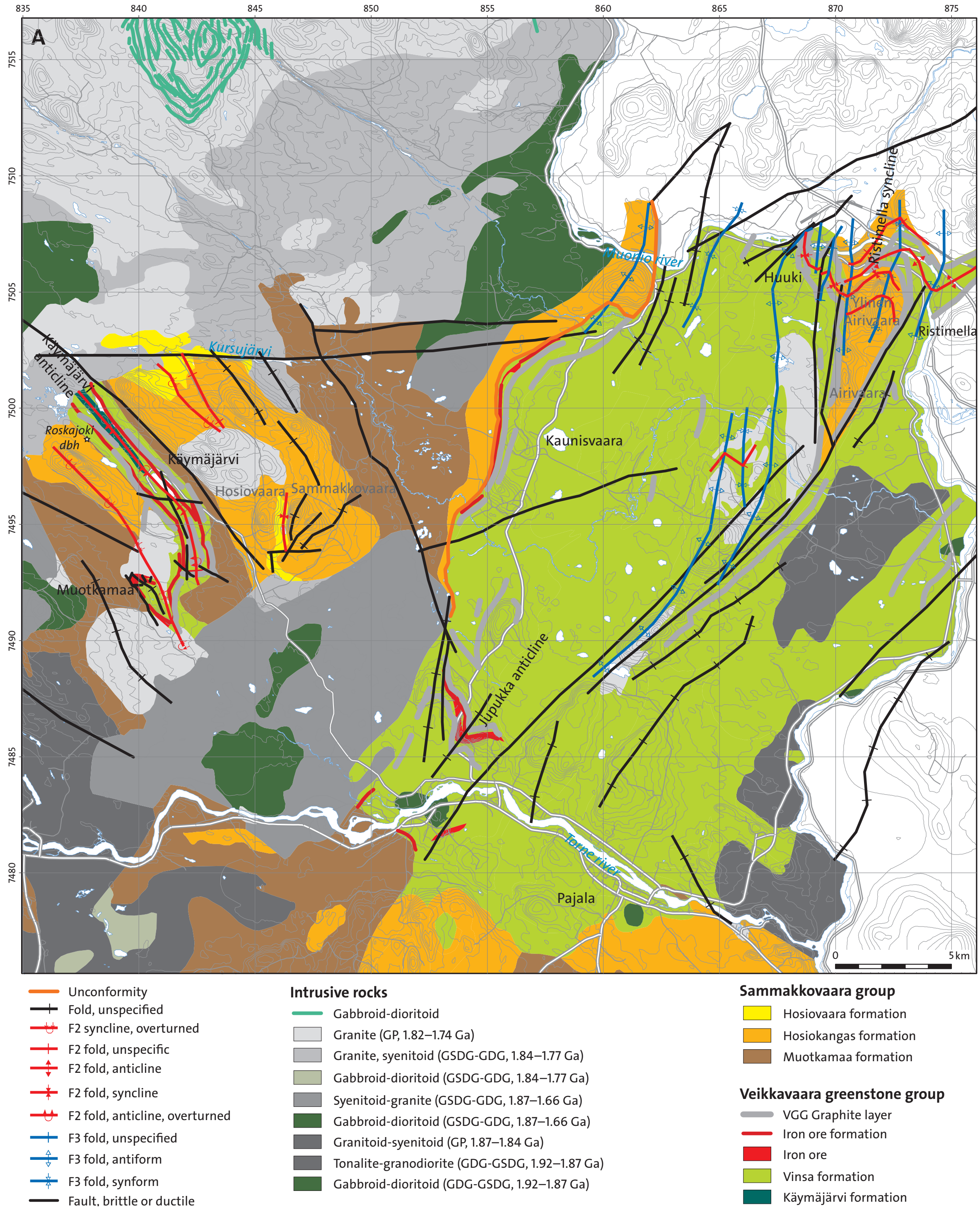

Figure 29. **A.** Simplified geological map of the Käymäjärvi–Ristimella area.

schists are intercalated with the tuffites. Schists contain sulphide mineralisations such as pyrite, chalcopyrite and pyrrhotite, leading to typical rusty weathering.

The second sub-unit of the Vinsa formation consists of a banded iron formation (BIF) with a locally developed oxide facies. These rocks are banded with 10–20 cm thick layers of recrystallised chert and silicates. The BIF occurs in limbs of both the Käymäjärvi anticline and the Jupukka anticline. Where it is magnetite-bearing, it has a strong magnetic susceptibility, which is prominent in magnetic field

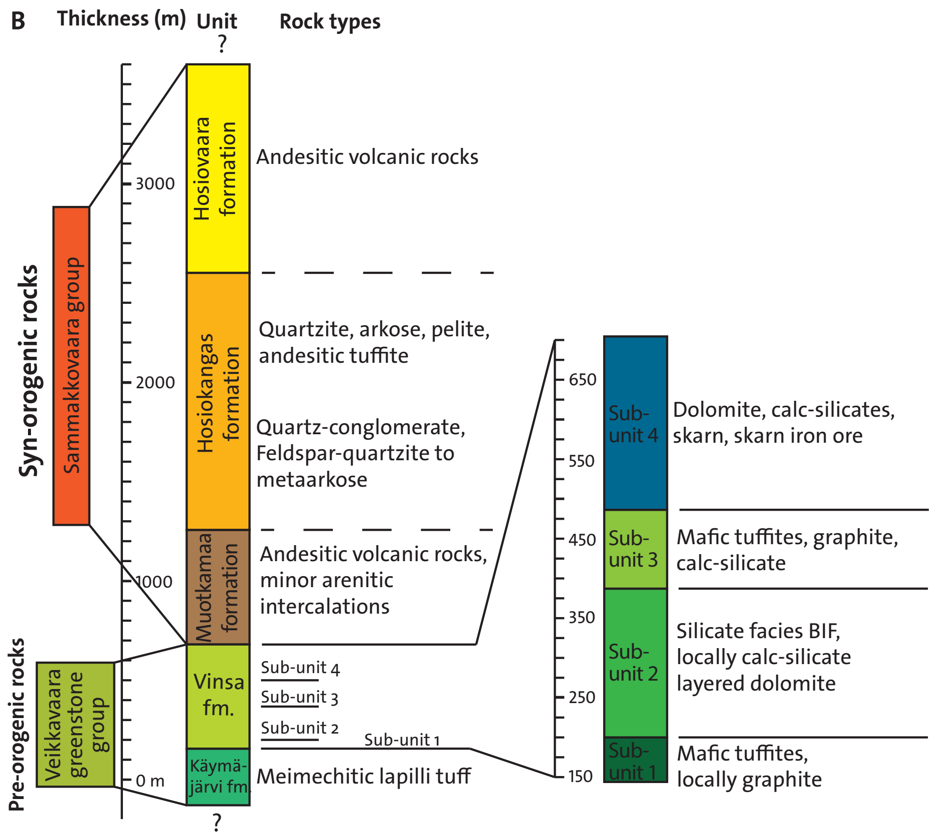

Figure 29. **B.** Simplified stratigraphic column for the Käymäjärvi–Ristimella key area.

(Fig. 30). The third sub-unit of the Vinsa formation consists of mafic tuffites, graphite-bearing schists and impure limestone intercalations. These rocks occur mainly to the east of the Kaunisvaara ore belt and to a lesser extent in the Käymäjärvi anticline.

Grey to green, fine-grained to very fine-grained tuffites make up the main rock volume of sub-unit 3 and are often laminated on a millimetre scale. Graded bedding and soft-sediment deformation structures, including decimetre-scale faults, slumping structures and sedimentary collapse structures, are locally preserved in the laminated tuffites. The presence of soft-sediment structures indicates that the laminated tuffites were deposited under water, either as primary volcanic metasedimentary rocks or redeposited as epiclastic metasedimentary rocks. Locally, the tuffites contain layers of massive, unbedded mafic rocks. It is unclear whether these are basaltic layers or basic sills, as the contact between the massive layers and the tuffites has not been observed in situ. Both the tuffites and the massive layers can be slightly magnetic. The impure limestones are light grey and usually coarse-grained. The limestone intercalations can reach significant thickness of approximately 100 m or more, for example in Finland just north of the river Muonioälven (Fig. 29A), where the limestone has been quarried in two open pits. Within the key area, impure limestones were observed on the shore of Muonioälven between Aareavaara and Huuki and in both limbs of the Käymäjärvi anticline. The graphite-bearing schists are probably basic tuffites enriched in graphite. These rocks are mostly very fine-grained and show typically rusty to orange weathering due to a high content of iron sulphides. Pyrite, for example, occurs disseminated throughout the graphite-bearing schist. The latter and the impure limestone intercalations usually occur close to one another.

A coarse-grained, light grey, locally calcitic dolomite forms the top of the Vinsa formation. The dolomite contains layers of more competent material (silicates?). In an outcrop near Käymäjärvi, the dolomite contains lenses and nodules of actinolite or tremolite crystals, indicating skarn alteration. A

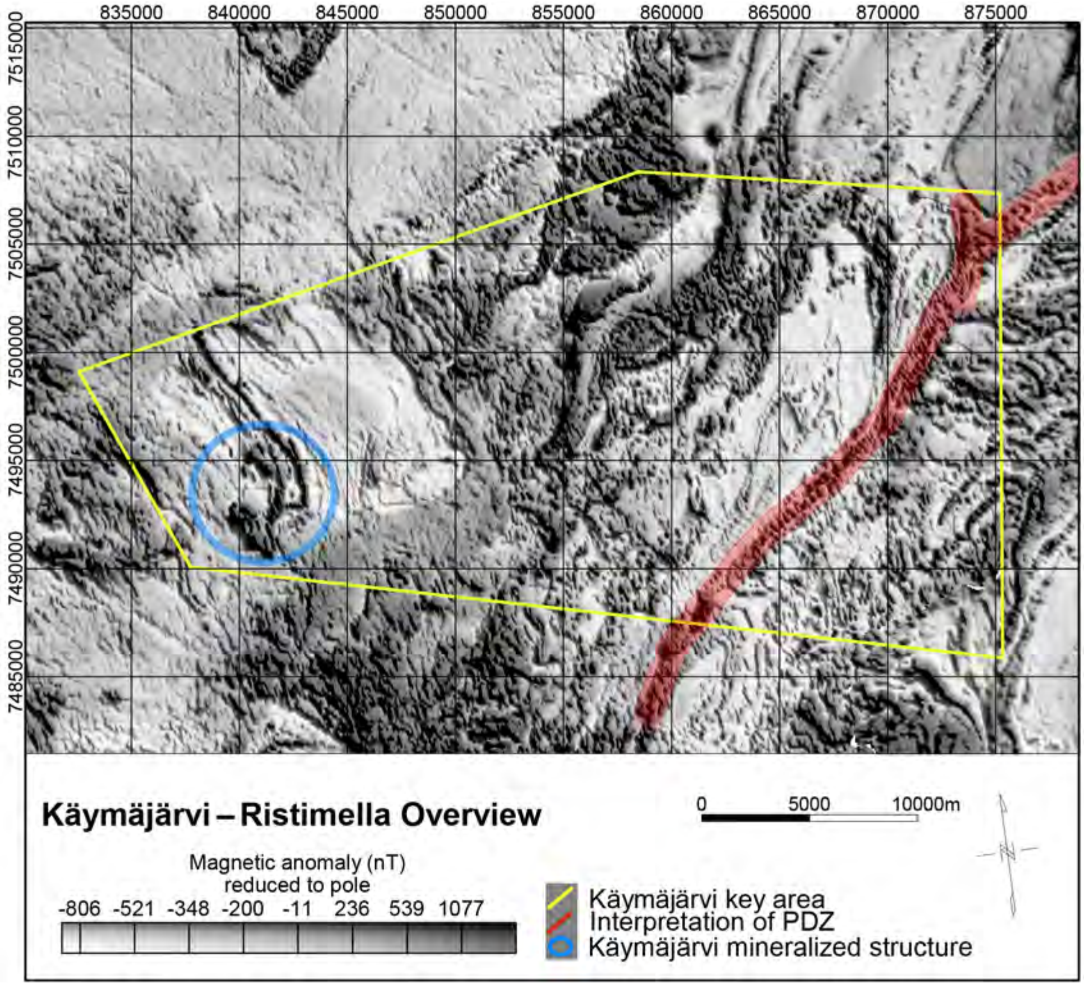

Figure 30. Magnetic anomaly map of the Käymäjärvi–Ristimella key area (yellow), based on data from airborne measurements. The blue circle marks an area modelled in 3D. The red area marks the approximate extent of the Pajala deformation belt, which is further described in the text.

banded skarn horizon underlies the dolomite lens here. At this location, the dolomite has a magnetic susceptibility ten times higher than elsewhere, indicating a higher magnetite content. The dolomite hosts the skarn iron ores in the Kaunisvaara ore belt (e.g. Tapuli and Sahavaara), which is clearly visible on the magnetic anomaly maps.

The rocks of the Veikkavaara greenstone group are overlain by syn-orogenic rocks belonging to the Sammakkovaara group (Martinsson 2004, Martinsson et al. 2018). The Sammakkovaara group mainly occurs in the western part of the key area, west of the Kaunisvaara ore belt. In the eastern part of the key area the group is exposed in the core of the Ristimella syncline, addressed later in the text. In Finland, immediately to the north of the key area, large amounts of clastic metasedimentary rocks occur, along with a body of an intermediate metavolcanic rock (Väänänen 1984, GTK map sheet 2713, Kolari). To the south of the key area, in the Liviöjärvi key area (Luth & Jönsson 2014), clastic metasedimentary rocks and metavolcanic rocks belonging to the Sammakkovaara group are both abundant. The Sammakkovaara group is divided into the Muotkamaa, Hosiokangas and Hosiovaara formations (Fig. 29B, Martinsson et al. 2018).

Andesitic metavolcanic rocks observed just east of the dolomites at Muotkamaa are interpreted as belonging to the Muotkamaa formation. The formation is poorly exposed, and other rocks belonging to it were only observed in one outcrop. However, andesitic rocks occur between a sub-unit 4 dolomite and clastic metasedimentary rocks of the Hosiokangas formation in a borehole at Roskajoki (cf. Fig. 29A). A thin band of Muotkamaa formation is therefore included to the west of the Käymäjärvi anticline (Fig. 29A).

Rocks of the Hosiokangas formation are predominantly of clastic sedimentary origin. To the east of Käymäjärvi, the Hosiokangas formation occupies the western, overturned limb of a syncline. Light grey to pink quartzitic to arkosic and sublithic arenites occur at the bottom of the depositional succession. Heavy mineral layers in these beds trace cross-bedding on the centimetre to decimetre scale as well as horizontal lamination on the millimetre to centimetre scale. Magnetite layers occur locally and the rock has been migmatised in places. A clast-supported conglomerate has been deposited on top of the arenites or occurs as lenses. More than 95% of the clasts consist of quartz or quartzite, and the pebbles can be up to 30 cm in diameter. Less than 5% of the pebbles consist of basic volcanic rock; these are generally smaller than the quartz pebbles. The conglomerate matrix is coarse-grained. The conglomerate probably occurs as lenses within the arenites rather than as continuous layers. Arenites are overlain by sublitharenitic sandstones and siltstones with distinct hummocky cross-bedding, indicating sedimentation under tidal conditions. Pelitic siltstones were deposited on top of the arenitic sandstones and are locally laminated; ripple marks have been observed. The siltstones become richer in mafic material towards the top, and biotite content increases. White quartzites without any recognisable sedimentary structures occur as intercalations within the pelitic rocks. Migmatisation of these pelites can be observed at Sammakkovaara and in the Ristimella syncline (cf. Fig. 29A).

Andesitic to dacitic metavolcanic rocks of the Hosiovaara formation (Martinsson 2004) were observed in situ along the shoulders of the Kursujärvi valley in the northwest of the key area. Metavolcanic rocks with andesitic to dacitic composition are also reported to occur in the valley between Hosiovaara and Sammakkovaara (Martinsson 2004).

The majority of observed intrusive rocks in the key area belong to the Granite-pegmatite association. These rocks are light red to red, locally porphyritic granites and pegmatites of variable grain size and composition. The granites locally contain magnetite patches.

A white, quartz-poor, albite-rich granite to syenite occurs in the centre of the key area. This rock usually exhibits a ductile foliation and lineation, indicating significant deformation. It may be crosscut by coarse-grained pegmatites. The lineation and parts of the foliation are sometimes traced with amphibole and biotite patches. It is unclear which magmatic suite these rocks belong to.

Structural inventory

Although the rocks of the Kaunisvaara ore belt and the Käymäjärvi anticline belong to the same lithostratigraphic units, it is still unclear which structures actually connect them. A several kilometre-wide body with a relatively irregular but highly magnetic pattern, interpreted as an andesite belonging to the Sammakkovaara group, separates these two ore belts (Fig. 29A and 30). No outcrop or drill core information is available for this area. Information on folding in the Kaunisvaara ore belt is particularly scarce, although small-scale folding was reported from a few drill cores near Sahavaara. Due to poor background data, this report focuses on two sub-areas: the Käymäjärvi anticline and the Ristimella syncline.

Käymäjärvi anticline

The Käymäjärvi anticline is the most noticeable structure in the Käymäjärvi area (Fig. 31A, Padget 1977, Grigull et al. 2014). It contains ultramafic metavolcanic rocks (meimechite) of the Käymäjärvi formation in the core and rocks of the Vinsa formation and Sammakkovaara groups in both limbs (Martinsson et al. 2013). The banded iron formation of the Vinsa formation sub-unit 2 creates a relatively continuous high magnetic anomaly, and detailed ground magnetic data make it easy to trace the BIF (Fig. 31A). The same goes for the graphitic schist of sub-unit 3, which shows up well on electromagnetic slingram maps (Fig. 31B).

A

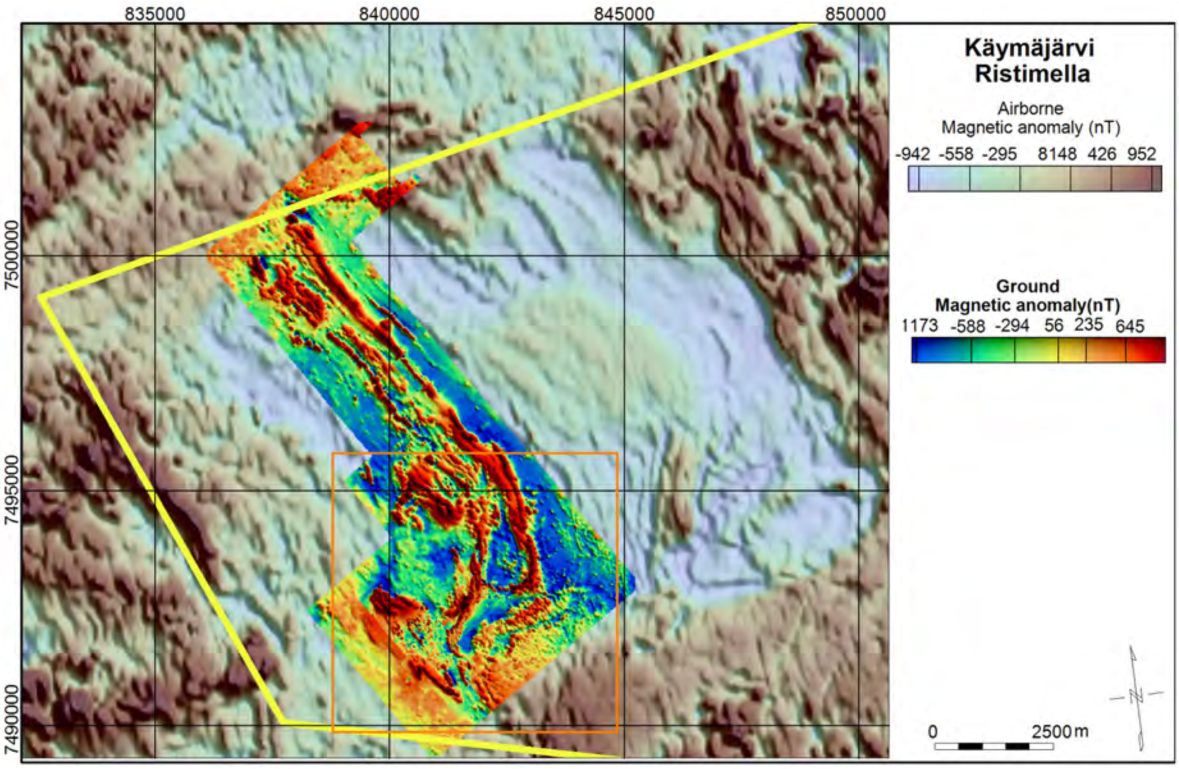

B

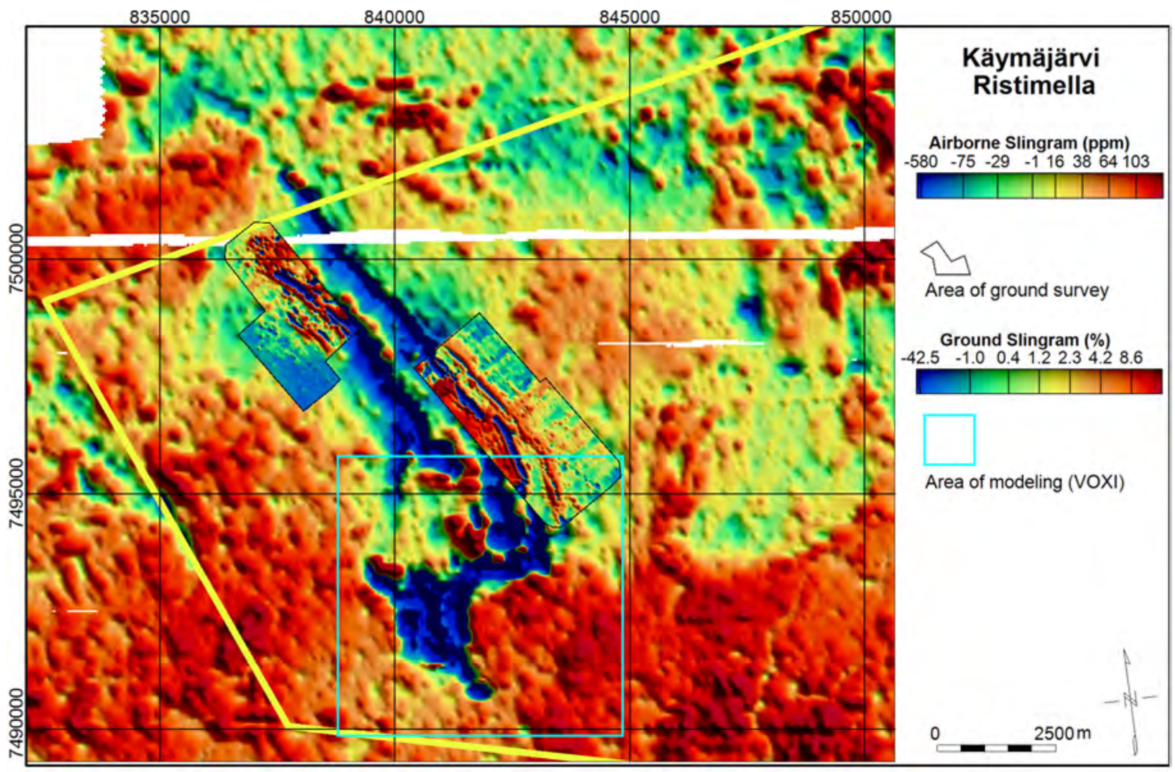

Figure 31. **A.** Airborne magnetic anomaly map of the Käymäjärvi area, based on airborne measurements with overlying ground magnetic map. The BIF and iron-rich skarn horizons of the Vinsa formation clearly stand out. The orange quadrangle refers to a 3D VOXI model of the geophysical ground data. **B.** Airborne slingram anomaly map with superposed ground slingram data. The blue areas are conducting layers and are here attributed to graphite-bearing tuffites of the Vinsa formation.

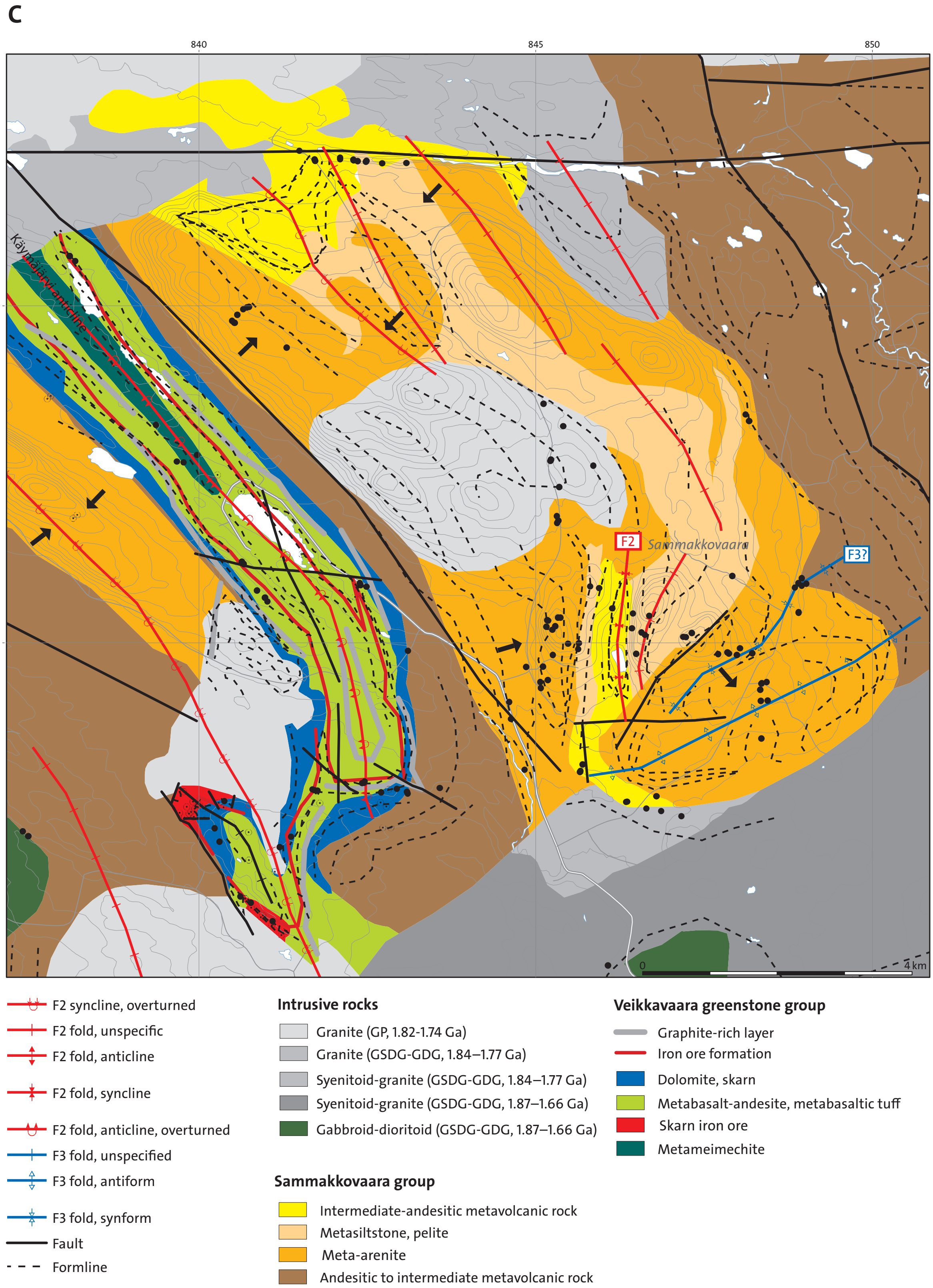

Figure 31. **C.** Simplified geological map of the area around Käymäjärvi and Sammakkovaara. The black arrows indicate younging directions. The black dots show the locations of recent outcrop observations.

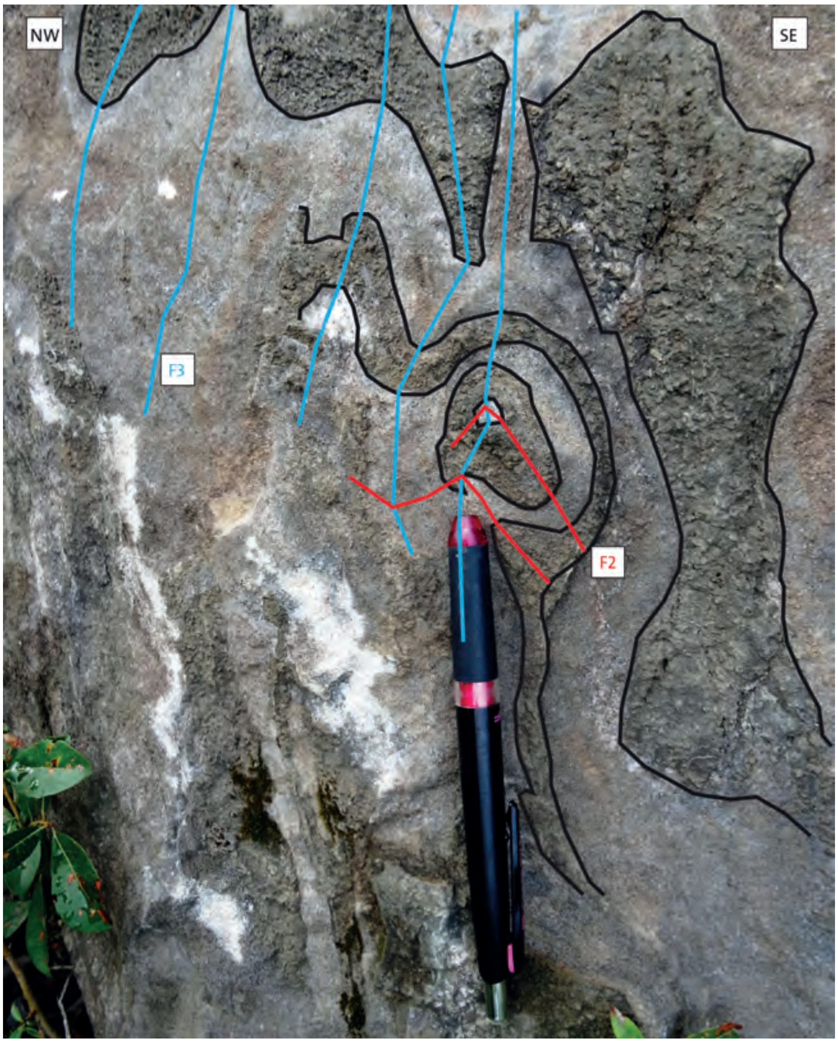

Figure 32. Potentially doubly folded impure marble belonging to the Vinsa formation sub-unit 4. Southeast of Käymäjärvi (SWEREF99 TM: N7495828, E842492).

The northern part of the anticline strikes northwest–southeast (Fig. 31C) and here the eastern limb of the anticline appears to be upright. As bedding measured in the BIF dips steeply towards the northeast, younging direction is also towards the northeast. Towards the southern part of the anticline, bedding planes in both the Veikkavaara greenstones and the Sammakkovaara group rocks dip steeply to moderately to the west. The rocks become younger towards the east, indicating that the fold axial trace changes direction from southeast to south and the eastern fold limb is overturned.

Although the lithologies strongly resemble those in the Masugnsbyn area, indicators of multiple folding phases are hard to find in the Käymäjärvi area. An impure limestone marble in the eastern limb of the Käymäjärvi anticline has been interpreted as refolded. This was tentatively deduced from fold interference patterns in the impure layers of the marble (Fig. 32). It is questionable, however, whether this observation is representative of the larger-scale structures.

Folding of the clastic metasedimentary rocks of the Sammakkovaara group (Hosiokangas formation) is more evident than in the greenstones, particularly on Sammakkovaara hill (cf. Fig. 31C). Here, metapsammitic rocks of silty origin show gneissic banding (S1) that is tightly folded (F2). In other outcrops at Sammakkovaara hill the migmatitic banding forms open folds (F3) with S-asymmetry on the western side of Sammakkovaara hill and into Z folds further to the east. However, the outcrops where these fold shapes were observed lie too far apart to allow an interpretation of a larger-scale fold structure.

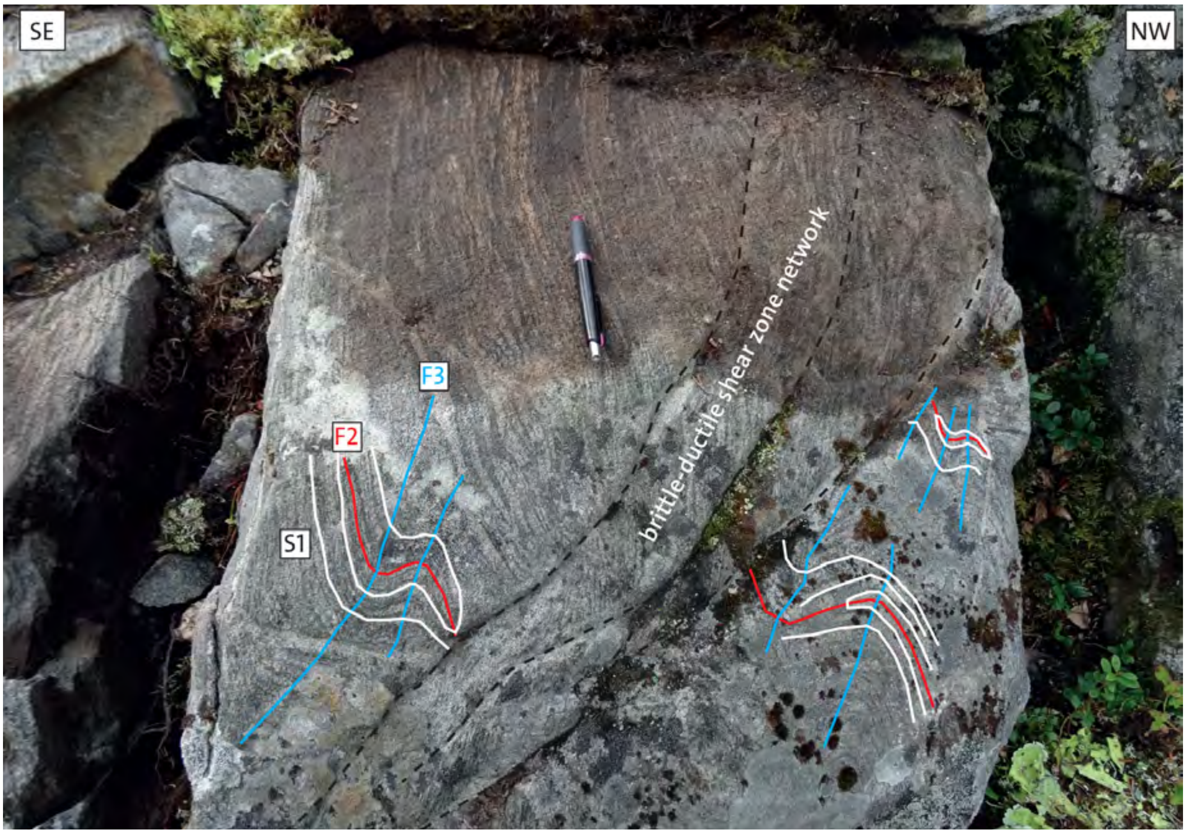

Figure 33. Isoclinal folding (F2) of migmatitic banding (S1) observed in metapelites of the Hosiokangas formation. The banding and the F2 folds are folded into open S folds (F3). Brittle-ductile shear zones cut through the banding sub-parallel to the fold axial planes of the S folds. Sammakkovaara hill (SWEREF99 TM: N7495144, E847317).

The pelitic layers in the Sammakkovaara group produce a slightly stronger magnetic signal and can therefore be used to draw form lines from the magnetic anomaly map. The form line traces, and the relatively abrupt change in strike of both bedding and foliation in the Sammakkovaara group also indicate a possible second, northeast–southwest-trending, set of folds (Fig. 31C). Migmatitic leucosomes that were isoclinally folded during F2 were observed in pelitic metasedimentary rocks at Sammakkovaara (Fig. 33). The F2 folds were refolded into open S folds (F3) with southeast-dipping axial planes (Fig. 33). These folds could be related to the development of a brittle-ductile shear zone system roughly parallel to the orientation of the F3 folds. Although further work is necessary to fully understand the structural framework, it may generally be concluded that, at least locally, the rocks in the Käymäjärvi area underwent two folding events.

The predominant structural grain in the area, seen in both geological and geophysical data, runs northwest–southeast to north–south. When projecting the area's structural data onto a stereonet, however, many lineations and fold axes plunge steeply to moderately to the south and southwest (Fig. 34A), i.e. down-dip on the predominant foliation planes (Fig. 34B). Moreover, poles to the best-fit great circles to bedding of all units and to migmatitic banding also plunge to the south and southwest. This may indicate that the rocks were affected by a second folding event, resulting in a transposition of pre-existing linear and planar structures.

The possibility that the Käymäjärvi anticline could in fact be a synformal anticline can be discounted on the basis of 3D geophysical modelling of the ground geophysical data that is available on the southern part of the Käymäjärvi anticline (Fig. 35). The model does not show convergence of the two limbs of the fold, but instead supports an anticlinal geometry with steeply dipping fold limbs.

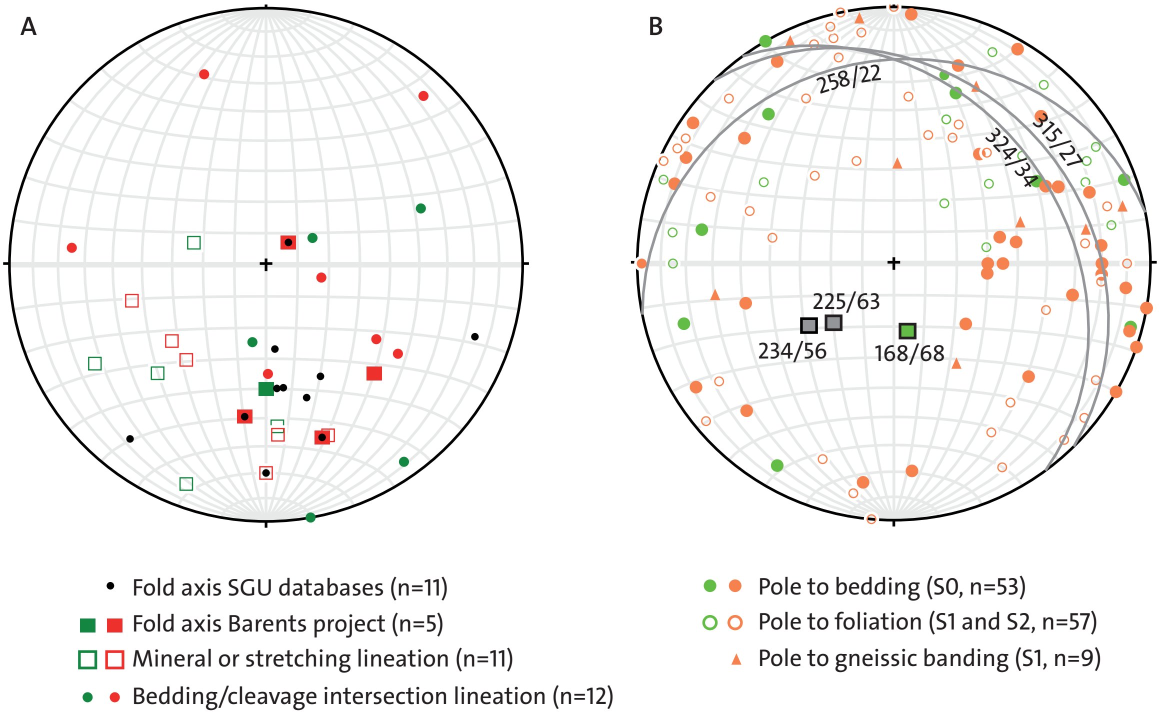

Figure 34. Stereographic projections of structural geological data from the Käymäjärvi and Sammakkovaara area. Green: Veikkavaara greenstone group. Red and orange: Sammakkovaara group. **A.** Linear data. **B.** Planar data.

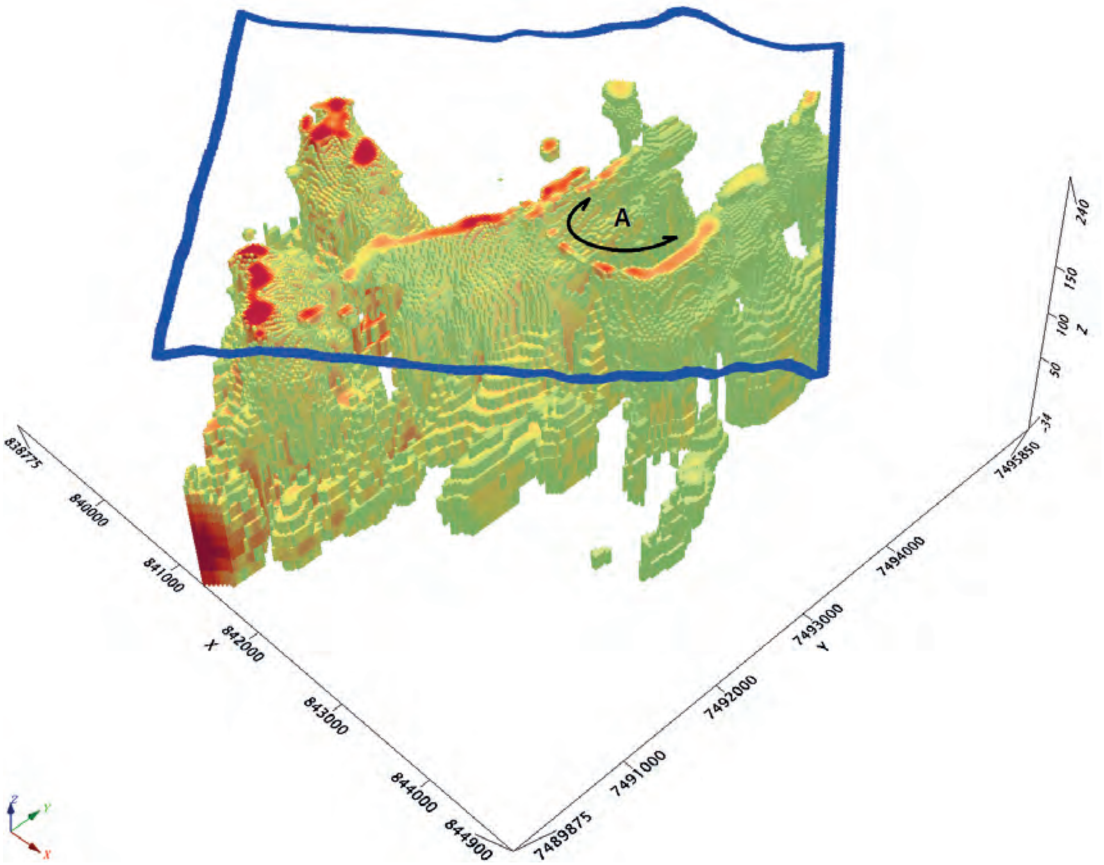

Figure 35. 3D Voxel model of ground magnetic data south of Käymäjärvi. Only high susceptibilities are plotted. Note that the steeply dipping limbs at A do not converge at depth but instead seem to diverge, indicating an anticlinal structure. For modelling area, see Figure 31A.

Ristimella

The rocks in the area between Huuki and Ristimella, and their continuation into Finland are affected by deformation within the north–south trending Pajala deformation belt (Fig. 36, cf. Luth et al. 2018b). It is therefore important to distinguish between structures that formed before and during this event.

The most noticeable fold structure is the "Ristimella synform", trending approximately north–south and located to the west of Ristimella (cf. Fig. 36; Grigull & Berggren 2015). The core contains pelitic and psammitic metasedimentary rocks, and is bounded by mafic metavolcanic and graphite-bearing rocks of the Veikkavaara greenstone group in both limbs. While it is not clear whether the metasedimentary rocks belong to the Sammakkovaara group, they are assumed to be younger than the greenstones. The large difference in susceptibility between the metasedimentary rocks and the metamorphic mafic rocks of the greenstone group helps to make the synform visible in a Voxel model of aeromagnetic data (Fig. 37). A subvertical fault bounding the Ristimella syncline to the east can also be inferred from this model.

Despite regional migmatisation of the metasedimentary rocks, the original bedding (S0) is often still discernible. On Airivaara and Ylinen Airivaara (Fig. 36), a first foliation (S1) developed parallel to the original bedding (S0). Locally, quartz veins are folded isoclinally with what were interpreted to be F1 fold axial planes parallel to the original bedding (Fig. 38A). A second deformation phase (D2) resulted in tight folds (F2), refolding the older structures. Locally, andalusite and sillimanite have grown parallel to the S2 foliation. A younger foliation cuts the first foliation at a high angle (Fig. 38B). It is not clear whether the younger foliation is a cleavage, indicating a second folding event that may not be easily recognisable in the field, or whether the development of this foliation is related to the northeast–southwest-trending Pajala deformation belt, in which case the surfaces would represent small-scale shear bands. Dextral movement along this foliation was mainly observed on Airivaara (Fig. 38C; cf. Grigull & Berggren 2015), where shear bands and asymmetric andalusite blasts indicate dextral kinematics. But shearing can of course also occur along cleavage planes. Since the nature of this foliation could not be determined, it is referred to here as Sx.

Direct evidence of several folding phases was documented in the area around the Ristimella synform. In a quarry in Finland, north of the river Muonioälven (cf. Fig. 36), fold interference patterns were observed in a locally derived block of impure limestone marble (Fig. 39).

Fold interference and crenulation of an earlier foliation was observed in the centre of the key area, north of the Kaunisjoki river. This outcrop lies in the core of a regional F3 antiform (cf. Fig. 36). Here, migmatitic, mica-rich (para?)gneiss shows evidence of at least three deformation events, including at least two folding events, best observed in a hand specimen (Fig. 40).

A first biotite foliation S1 developed during D1. It is possible that this foliation was originally parallel to bedding S0. During the second deformation event D2, S1 was folded about isoclinal to very tight F2 folds, and an axial planar, biotite-lined foliation S2 developed. During a third deformation event D3, the F2 folds, and both the S1 and S2 foliations were folded into open kink folds (F3). The D3 foliation is not pervasive and locally forms a spaced crenulation cleavage. The folds observed in the hand specimen are assumed to represent the large-scale structural architecture in the central part of the key area. The F3 folds are interpreted to be the result of E–W compression during dextral transpression in the Pajala deformation belt. Closer to the main northeast–southwest-striking part of the Pajala deformation belt, the F3 fold axial traces appear to have been dragged into parallelism, with the strike of the deformation zone indicating they formed before or contemporaneously with the development of this deformation zone.

Projecting all structural data from the area around Ristimella and Airivaara into a stereonet shows that bedding as well as foliations strike predominantly NE–SW (Fig. 41). The majority of mineral lineations plunge moderately to the southwest and may have formed during dextral shearing along Sx. South and southwest-plunging fold axes and crenulation lineations are probably the result of F3. The

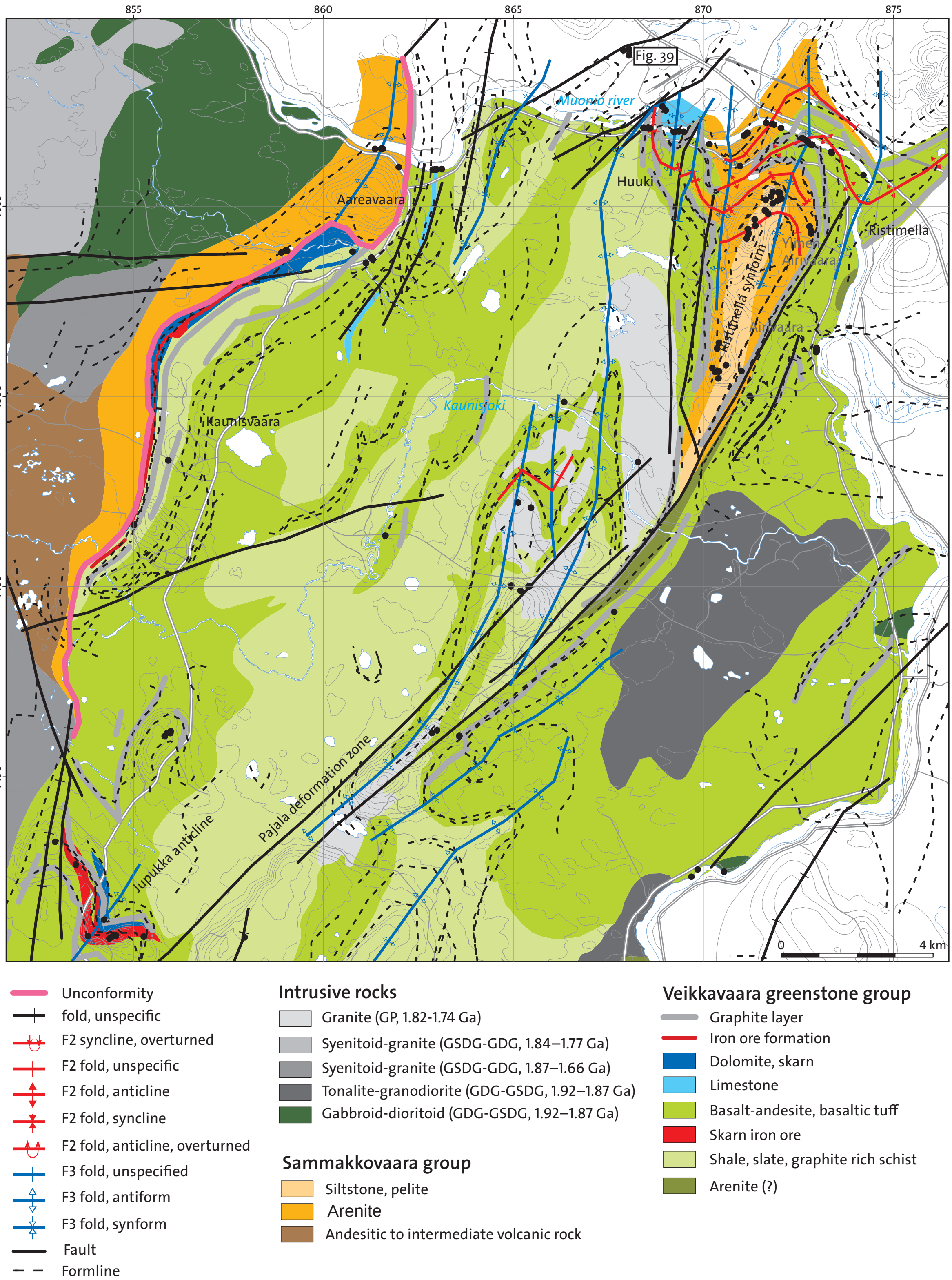

Figure 36. Simplified geological map of the area between Kaunisvaara and Ristimella. The form lines and all fold axial traces are based on a combination of geophysical lineaments and geological field observations. The black dots show locations of field observations.

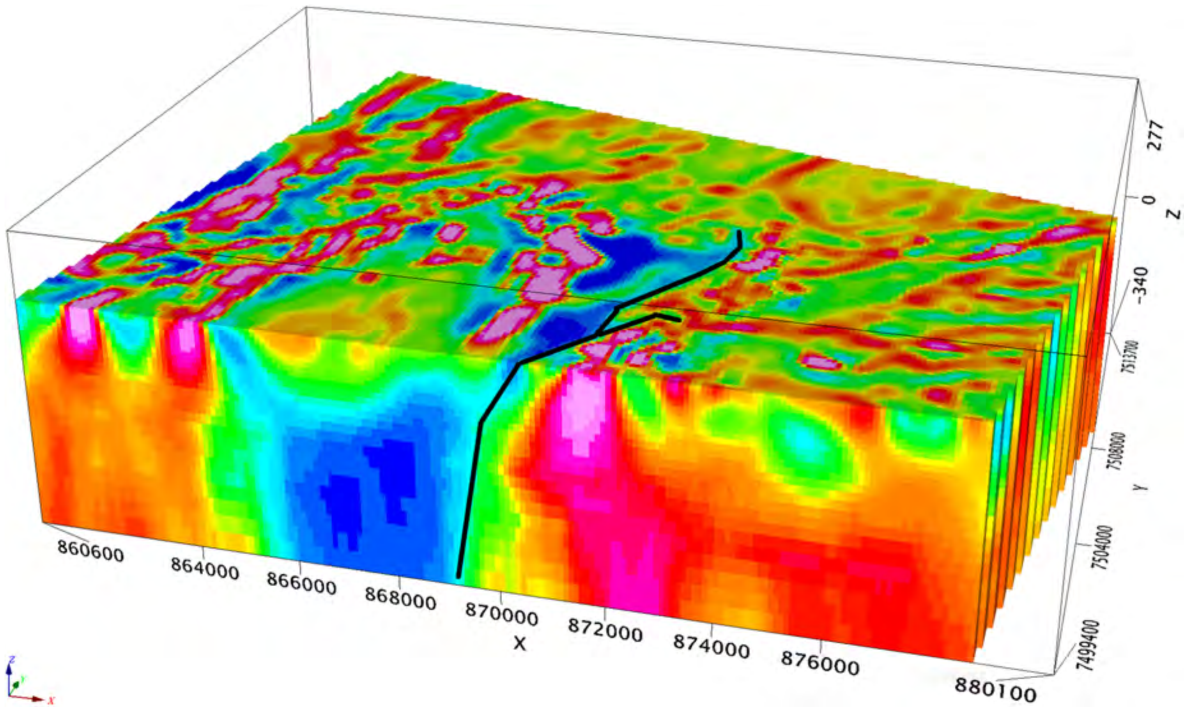

Figure 37. Voxel model based on aeromagnetic data of the Ristimella syncline. Blue represents low-magnetic rocks (e.g. metasedimentary rocks), red represents highly magnetic rocks.

Voxi model in Figure 37 also indicates regional-scale south to southwest-plunging antiforms and synforms for the area around the Ristimella synform.

The supracrustal rocks around Ristimella and Huuki have been folded into tight east–west-trending folds with vertical axial planes (F2), indicating north–south compression. Before or synchronously with the development of the northeast–southwest-trending step-over of the Pajala deformation belt, the rocks were folded into open, south to southwest-plunging kink folds (F3) and sheared dextrally. The sketch in Figure 42 illustrates the suggested geological model for the rocks around Ristimella.

DISCUSSION AND CONCLUSIONS

New geological and geophysical information from key areas in the northern Fennoscandian Shield show that both pre- and syn-orogenic supracrustal rocks were affected by the same folding phases during the orogeny. But the results also indicate that deformation styles and folding phases differ distinctively from west to east. Only one folding event, probably related to contemporaneous thrusting, could be identified in the Kiruna area. The rocks in the Kiruna area are folded into a series of west-verging tight folds. Graben inversion after the deposition of the Hauki quartzite is thought to have led to a minor amount of kink folding in the Kurravaara area. However, more work is needed to support this theory. The Masugnsbyn area has undergone at least three deformation events, of which two, possibly three, are folding events. The second deformation event produced approximately E–W-trending upright, tight folds with horizontal or moderately plunging fold axes (F2) that were kinked around subvertical to moderately plunging fold axes (F3) during the third folding event, resulting in a transposition of F2 fold axial traces now trending both northwest–southeast and northeast–southwest. The Kalixälv dome, while not easily interpreted, may be part of the F3 folding event or correspond to a fourth folding phase that domed the older fold structures. The folding patterns in the Käymäjärvi area are comparable to those in the Masugnsbyn key area. Evidence for vertical fold axes in Käymäjärvi is

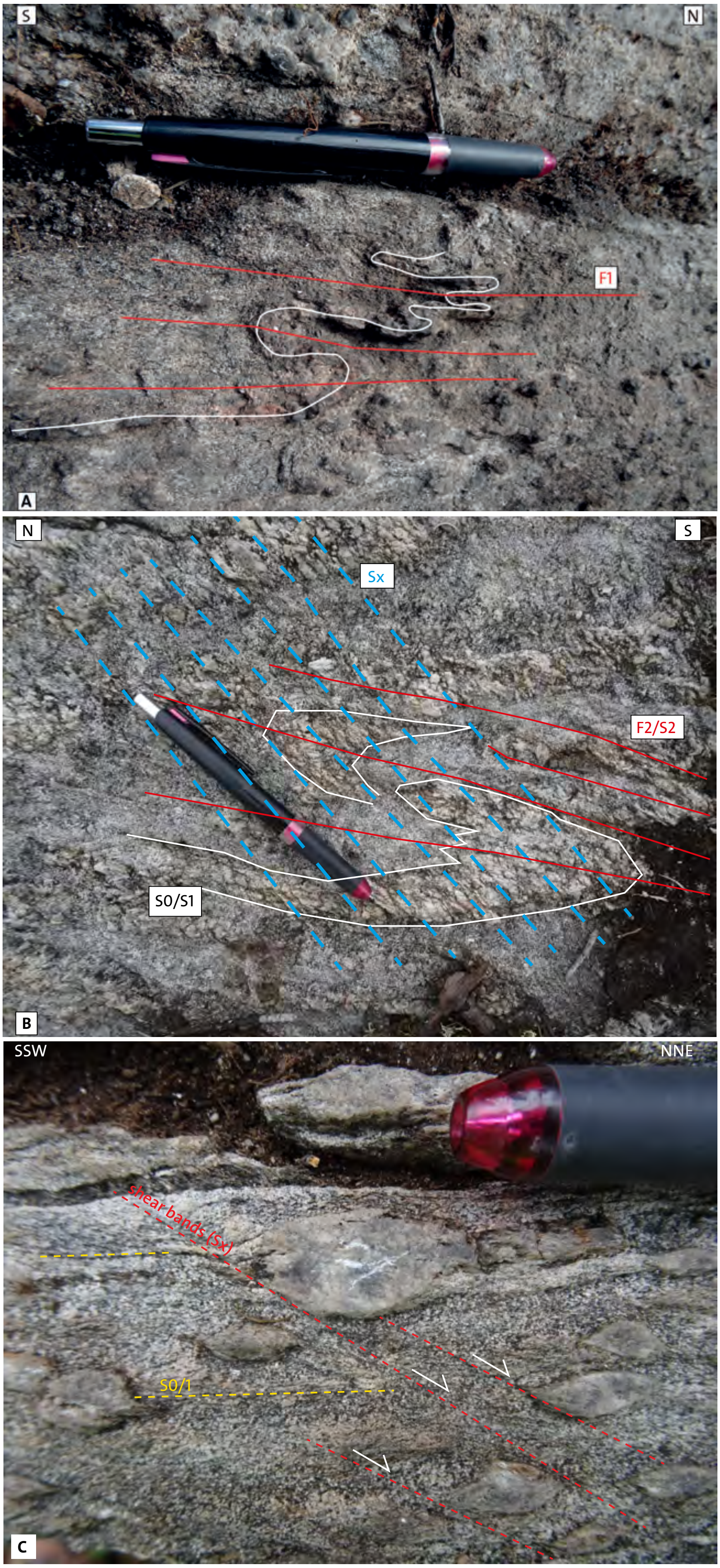

Figure 38. **A.** Migmatite vein asymmetrically folded during F1 in pelitic to psammitic metasedimentary rocks (Sammakkovaara group?). Airivaara (SWEREF99 TM: N7501253, E870365).**B.** Asymmetric F2 folds are intersected by another foliation (Sx) at a high angle. It is unclear whether this foliation is related to the F3 folding or whether it formed due to later dextral shearing within the Pajala deformation belt. Ylinen Airivaara (SWEREF99 TM: N7504142, E871137). **C.** Dextral kinematics observed along shear bands parallel to Sx. Airivaara (SWEREF99 TM: N7500640, E870405).

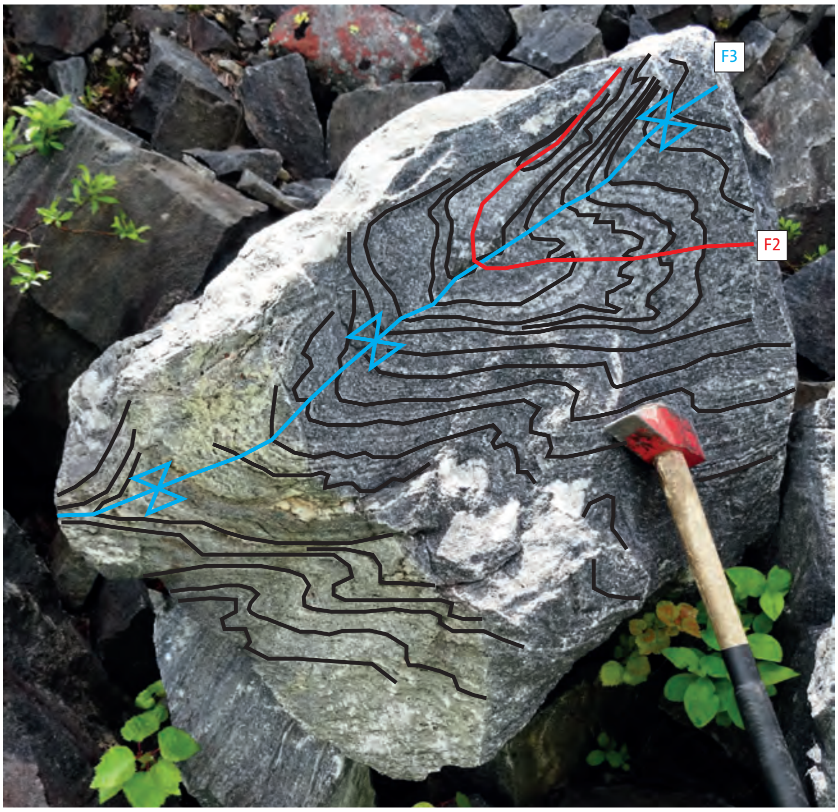

Figure 39. Fold interference observed in a block of impure limestone in a quarry in Finland (SWEREF99 TM: N7509079, E867902). Red: F2 axial trace. Blue: F3 axial trace. Black: metamorphic banding (S1).

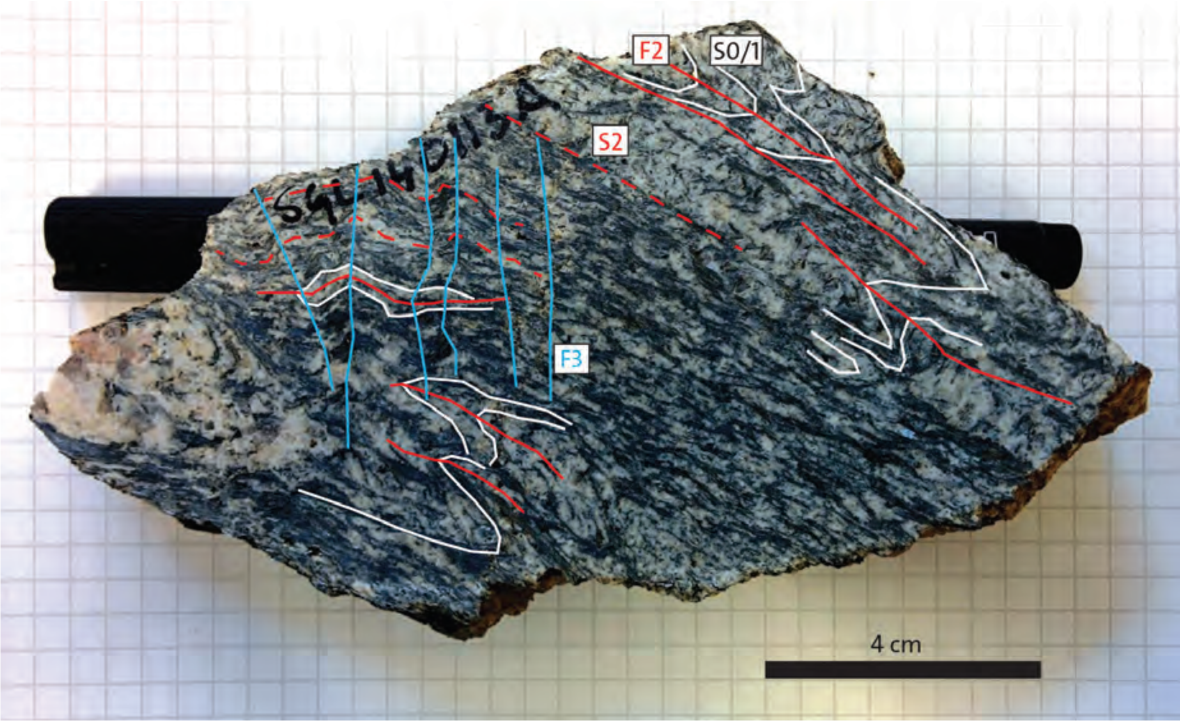

Figure 40. (Para?)gneiss from the central part of the key area (SWEREF99 TM: N7499850, E866343). F3 kink folds crenulate F2 isoclinal folds and older foliations S1 and S2.

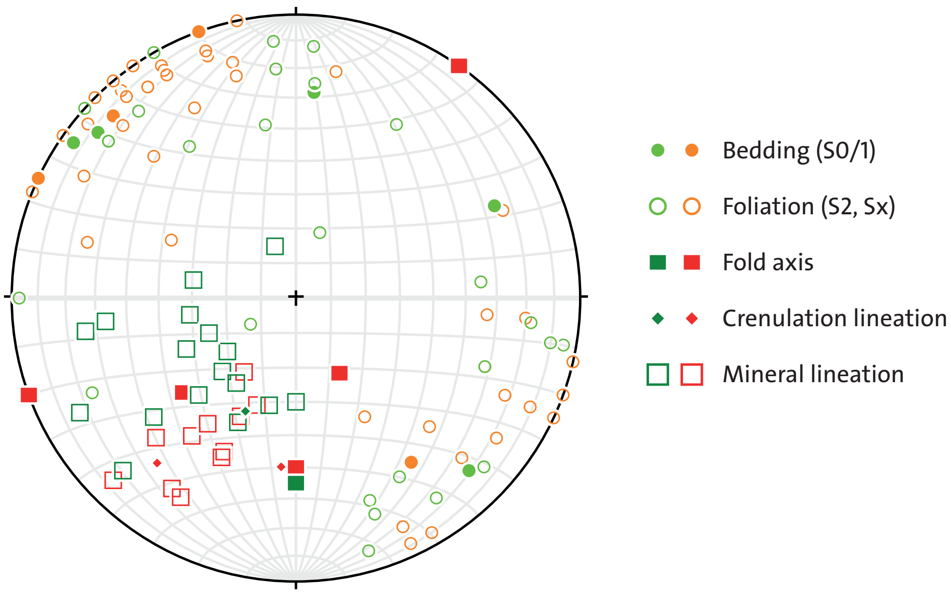

Figure 41. Stereographic projection of structural data collected in the Ristimella area. Green: Veikkavaara greenstone group. Red and orange: metasedimentary rocks, probably Sammakkovaara group.

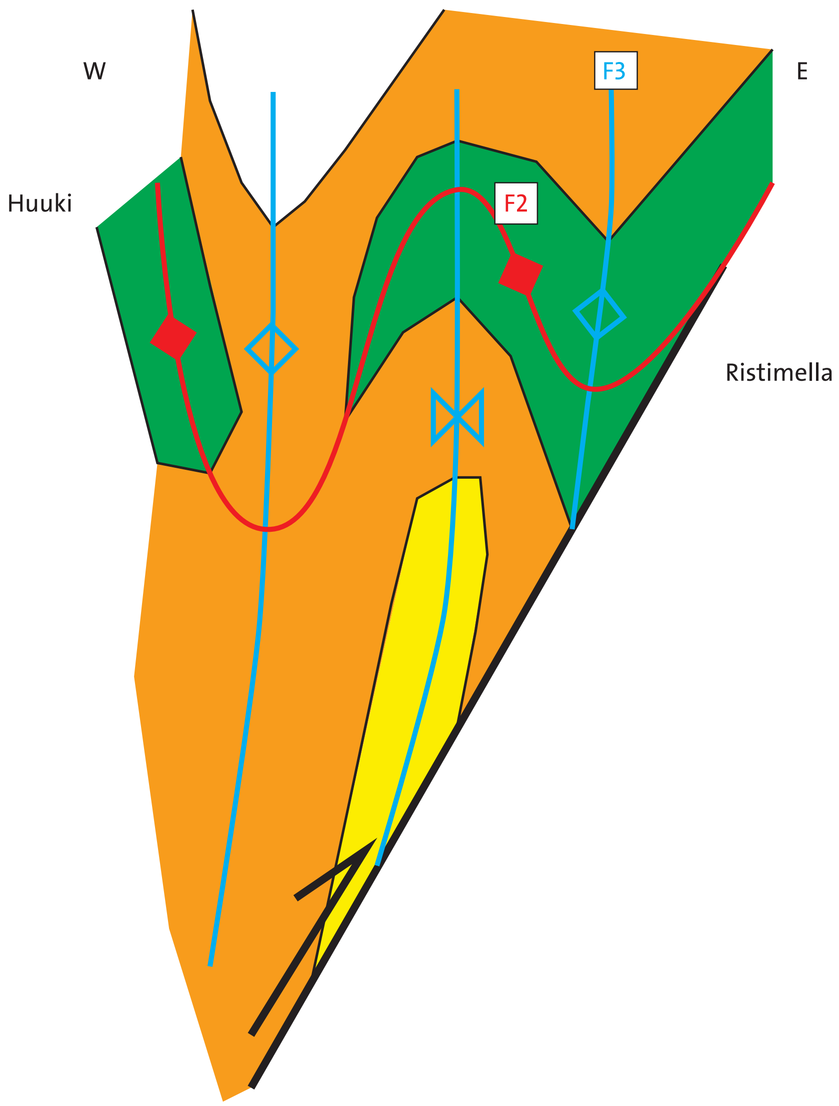

Figure 42. Geological model (map view, not to scale) of the folding pattern between Ristimella and Huuki. Green: Veikkavaara greenstone group, Orange and yellow: metasediments, possibly Sammakkovaara group younger than the greenstones.

scarce, however. Crenulation folding, indicating a third folding event, is predominantly found along the shore of the river Muonioälven near Huuki, but open S and Z-F3 folds also exist around Sammakkovaara. At Muonioälven, F2, and F3 axial traces can be drawn from slingram and magnetic anomaly maps. On a regional scale, F3 folds dominate the structural architecture. However, axial traces appear transposed due to dextral shearing along a NE–SW-striking step-over in the Pajala deformation belt. This may be a structure that is younger than all the previously described folding events (cf. Luth et al., 2018).

The observation of folding patterns in several key areas indicates that the rocks to the east of the Karesuando–Arjeplog deformation zone have undergone more phases of deformation than those to the west. The other key areas to the east of the Karesuando–Arjeplog deformation zone, such as Nunasvaara (Lynch et al., 2018), Svappavaara (Grigull & Jönberger 2014) and Liviöjärvi (Luth et al. 2018b), also feature a minimum of two, but potentially more folding phases. In contrast, the rocks in the key areas around Kiruna have been subjected to a single folding event.

REFERENCES

Bergh, S.G., Kullerud, K., Armitage, P.E.B., Zwaan, K.B., Corfu, F., Ravna, E.J.K. & Myhre, P.I. 2010: Neoarchaean to Svecofennian tectono-magmatic evolution of the West Troms Basement Complex, North Norway. *Norwegian Journal of Geology 90*, 21–48.

Bergh, S.G., Corfu, F., Myhre, P.I., Kullerud, K., Armitage, P.E.B., Zwaan, K.B., Ravna, E.K., Holdsworth, R.E., Chattopadhya, A., 2012: Was the Precambrian Basement of Western Troms and Lofoten-Vesterålen in Northern Norway Linked to the Lewisian of Scotland? A Comparison of Crustal Components, Tectonic Evolution and Amalgamation History. *In:* Sharkov, E. (ed.): Tectonics – Recent Advances. Earth and Planetary Sciences, Geology and Geophysics, 283–330.

Bergman, S., Kübler, L. & Martinsson, O., 2001: Description of regional geological and geophysical maps of northern Norrbotten County (east of the Caledonian orogen). S*veriges geologiska undersökning Ba 56*, 110 pp.

Bergman, S., Billström, K., Persson, P.-O., Skiöld, T., Evins, P., 2006: U-Pb age evidence for repeated Palaeoproterozoic metamorphism and deformation near the Pajala shear zone in the northern Fennoscandian Shield. *GFF 128*, 7–20.

Bergman, S., Stephens, M.B., Andersson, J., Kathol, B., Bergman, T., 2012: Sveriges berggrund 1:1 miljon. *Sveriges geologiska undersökning K 423*.

Berthelsen, A., Marker, M. 1986: 1.9-1.8 Ga old strike-slip megashears in the Baltic shield, and their plate tectonic implications. *Tectonophysics 128*, 163–181.

Boynton, W.V., 1984: Cosmochemistry of the rare earth elements: meteorite studies. *In:* Henderson, P. (ed.): Rare Earth Element Geochemistry. Elsevier, Amsterdam, 63–114.

Forsell, P., 1987: The stratigraphy of the Precambrian rocks of the Kiruna district, Northern Sweden. *Sveriges geologiska undersökning C 812*, 36 pp.

Geijer, P., 1910: Igneous rocks and iron ores of Kiirunavaara, Luossavaara and Tuolluvaara. *Economic Geology 5*, 699–718.

Grigull, S. & Antal Lundin, I., 2013: Kartering Barents. Background information Kiruna-Jukkasjärvi key area. *SGU-rapport 2013:08*, Sveriges geologiska undersökning. 43 pp.

Grigull, S. & Jönberger, J., 2014: Geological and geophysical field work in the Kiruna-Jukkasjärvi and Svappavaara key areas, Norrbotten. *Sveriges geologiska undersökning SGU-rapport 2014:10*, 30 pp.

Grigull, S., Berggren, R. & Jönsson, C., 2014: Background information Käymäjärvi-Ristimella key area. *SGU-rapport 2014:30*, Sveriges geologiska undersökning. 37 pp.

Grigull, S. & Berggren, R., 2015: Geological and geophysical field work in the Käymäjärvi-Ristimella key area. Sveriges geologiska undersökning SGU-rapport 2015:29, 31 pp.

Gustafsson, B. & Carlson, L., 1992: Kallosalmi Diamantborrning 1992. Sveriges Geologiska AB Prospekteringsrapport, PRAP92013, 93 pp.

Hellström, F.A., 2018: Early Svecokarelian migmatisation west of the Pajala Deformation Belt, northeastern Norrbotten Province, northern Sweden. *In:* Bergman, S. (ed): Geology of the Northern Norrbotten ore province, northern Sweden. *Rapporter och Meddelanden 141,* Sveriges geologiska undersökning. This volume pp 361–379.

Hellström, F. & Jönsson, C., 2014: Summary of geological and geophysical information of the Masugnsbyn key area. *SGU-rapport 2014:21*, Sveriges geologiska undersökning. 84 pp.

Hellström, F.A., Kumpulainen, R., Jönsson, C., Thomsen, T.B., Huhma, H. & Martinsson, O., 2018: Age and lithostratigraphy of Svecofennian volcanosedimentary rocks at Masugnsbyn, northernmost Sweden – host rocks to Zn-Pb-Cu- and Cu ±Au sulphide mineralisations. *In:* Bergman, S. (ed): Geology of the Northern Norrbotten ore province, northern Sweden. *Rapporter och Meddelanden 141,* Sveriges geologiska undersökning. This volume pp 151–203.

Henkel, H., 1991: Magnetic crustal structures in northern Fennoscandia. *Tectonophysics 192*, 57–79.

Irvine, T. N. & Baragar, W. R. A., 1971: A guide to the chemical classification of the common volcanic rocks. *Canadian Journal of Earth Sciences 8*, 523–548.

Korja, A., Lahtinen, R. & Nironen, M., 2006: The Svecofennian orogen: a collage of microcontinents and island arcs. *In:* Gee, D.G. & Stephenson, R.A. (eds.): European Lithosphere Dynamics. Geological Society, London, Memoirs, 32, 561–578.

Kumpulainen, R., 2000: The Palaeoproterozoic sedimentary record of northernmost Norrbotten, Sweden. Unpublished report. *Sveriges geologiska undersökning BRAP 200030*, 45 pp.

Kärki, A., Laajoki, K. & Luukas, J., 1993: Major Paleoproterozoic shear zones of the central Fennoscandian Shield. *Precambrian Research 64*, 207–223.

Lahtinen, R., Korja, A., Nironen, M. & Heikkinen, P., 2009: Paleoproterozoic accretionary processes in Fennoscandia. *In:* Cawood, P.A., Kröner, A. (eds.) Earth Accretionary Systems in Space and Time. Geol. Soc. London Special Publication, 318, 237–256.

Lahtinen, R., Huhma, H., Lahaye, Y., Jonsson, E., Manninen, T., Lauri, L.S., Bergman, S., Hellström, F., Niiranen, T. & Nironen, M., 2015a: New geochronological and Sm-Nd constraints across the Pajala shear zone of northern Fennoscandia: Reactivation of a Paleoproterozoic suture. *Precambrian Research 256*, 102–119.

Lahtinen, R., Sayab, M. & Karell, F., 2015b: Near-orthogonal deformation successions in the poly-deformed Paleoproterozoic Martimo belt: Implications for the tectonic evolution of Northern Fennoscandia. *Precambrian Research 270*, 22–28.

LeBas, M.J., LeMaitre, R.W., Streckeisen, A. & Zanettin, B., 1986: A chemical classification of volcanic rocks based on the total alkali-silica diagram. *Journal of Petrology 27*, 745–750.

Lindroos, H., Henkel, H. & 1981: Beskrivning till berggrundsgkartorna och geofysiska kartorna Huuki NV/NO, SV, SO och Muonionalusta NV, SV/SO. *Sveriges geologiska undersökning Af 35–39*.

Luth, S. & Jönsson, C., 2014: Summary report on the geological and geophysical characteristics of the Liviöjärvi key area. *SGU rapport 2014:29*, Sveriges geologiska undersökning. 34 pp.

Luth, S., Jönsson, C. & Jönberger, J., 2015: Integrated geological and geophysical studies in the Liviöjärvi key area, Pajala region. *SGU rapport 2015:12*, Sveriges geologiska undersökning. 29 pp.

Luth, S., Jönberger, J. & Grigull, S., 2018a: The Vakko and Kovo greenstone belts north of Kiruna: Integrating structural geological mapping and geophysical modelling. *In:* Bergman, S. (ed): Geology of the Northern Norrbotten ore province, northern Sweden. *Rapporter och Meddelanden 141,* Sveriges geologiska undersökning. This volume pp 287–309.

Luth, S., Jönsson, C., Jönberger, J., Grigull, S., Berggren, R., van Assema, B., Smoor, W. & Djuly, T., 2018b: The Pajala Deformation Belt in northeast Sweden: Structural geological mapping and 3D modelling around Pajala. *In:* Bergman, S. (ed): Geology of the Northern Norrbotten ore province, northern Sweden. *Rapporter och Meddelanden 141,* Sveriges geologiska undersökning. This volume pp 259–285.

Lynch, E.P., Hellström, F.A., Huhma, H., Jönberger, J., Persson, P.-O. & Morris, G.A, 2018: Geology, lithostratigraphy and petrogenesis of c. 2.14 Ga greenstones in the Nunasvaara and Masugnsbyn areas, northernmost Sweden. *In:* Bergman, S. (ed): Geology of the Northern Norrbotten ore province, northern Sweden. *Rapporter och Meddelanden 141,* Sveriges geologiska undersökning. This volume pp 19–77.

Martinsson, O., 1995: Greenstone and porphyry hosted ore deposits in northern Norrbotten. Report, NUTEK, Project nr. 9200752-3, Div. of Applied Geology, Luleå University of Technology.
Martinsson, O., 1997: Tectonic setting and metallogeny of the Kiruna greenstones. *Doctoral thesis 1997:19*. Luleå University of Technology.
Martinsson, O., 1999: Berggrundskartan 30J Rensjön SO. *Sveriges geologiska undersökning Ai 133*.
Martinsson, O., 2004: Geology and Metallogeny of the Northern Norrbotten Fe-Cu-Au Province. *In:* R.L. Allen, O. Martinsson & P. Weihed (eds.): Svecofennian ore-forming environments. Volcanic-Associated Zn-Cu-Au-Ag, Intrusion-Associated Cu-Au, Sediment-Hosted Pb-Zn, and Magnetite-Apatite Deposits of Northern Sweden. *Society of Economic Geologists Guidebook Series 33*, 131–148.
Martinsson, O. & Perdahl, J.-A., 1995: Paleoproterozoic extensional and compressional magmatism in northern Sweden. *In:* J.-A. Perdahl: Svecofennian volcanism in northern Sweden, *Doctoral thesis 1995:169D, Paper II*, 1–13. Luleå University of Technology.
Martinsson, O., Allan, Å. & Denisová, N., 2013: Day 2. Skarn iron ores in the Pajala area. *In:* O. Martinsson & C. Wanhainen (Eds.): Fe oxide and Cu-Au deposits in the northern Norrbotten ore district. Excursion guidebook SWE5, 12th Biennial SGA Meeting, Uppsala, Sweden.
Martinsson, O. Billström, K., Broman, C., Weihed, P., Wanhainen, C., 2016: Metallogeny of the Northern Norrbotten Ore Province, northern Fennoscandian Shield with emphasis on IOCG and apatite-iron ore deposits. *Ore Geology Reviews 78*, 447–492.
Martinsson, O., Bergman, S., Persson, P.-O., Schöberg, H., Billström, K. & Shumlyanskyy, L., 2018: Stratigraphy and ages of Palaeoproterozoic metavolcanic and metasedimentary rocks at Käymäjärvi, northern Sweden. *In:* Bergman, S. (ed): Geology of the Northern Norrbotten ore province, northern Sweden. *Rapporter och Meddelanden 141,* Sveriges geologiska undersökning. This volume pp 79–105.
Niiniskorpi, V., 1986: Kurkkionvaara – En Zn-Pb-Cu-mineralisering i norra Sverige en case-studie. LKAB Prospektering, K 86–56, 90 pp.
Niiranen, T., Poutianen, M. & Mänttäri, I., 2007: Geology, geochemistry, fluid inclusion characteristics, and U–Pb age studies on iron oxide–Cu–Au deposits in the Kolari region, northern Finland. *Ore Geology Reviews 30*, 75–105.
Nironen, M., 1997: The Svecofennian Orogen: a tectonic model. *Precambrian Research 86*, 21–44.
Offerberg, J., 1967: Beskrivning till Berggrundskartbladen Kiruna NV, NO, SV, SO. *Sveriges geologiska undersökning Af 1–4*, 147 pp.
Olesen, O. & Sandstad, J.S., 1993: Interpretation of the Proterozoic Kautokeino Greenstone Belt, Finnmark, Norway from combined geophysical and geological data. *NGU Bulletin 425*, 43–64.
Padget, P., 1970: Beskrivning till berggrundskartbladen Tärendö NV, NO, SV, SO. *Sveriges geologiska undersökning Af 5–8*, 95 pp.
Padget, P., 1977: Beskrivning till berggrundskartbladen Pajala NV, NO, SV, SO. *Sveriges geologiska undersökning Af 21–24*, 73 pp.
Parák, T., 1975: The origin of the Kiruna iron ores. *Sveriges geologiska undersökning C 709*, 209 pp.
Talbot, C.J. & Koyi, H., 1995: Paleoproterozoic intraplating exposed by resultant gravity overturn near Kiruna, northern Sweden. *Precambrian Research 72*, 199–225.
Vollmer, F.W., Wright, S.F. & Hudleston, P.J., 1984: Early deformation in the Svecokarelian greenstone belt of the Kiruna iron district, northern Sweden. *GFF 106*, 109–118.
Väänänen, J., 1984: Kolari. Kallioperäkartta 1:100 000 – Maps of Pre-Quaternary Rocks. Geological survey of Finland GTK Map sheet 2713, Kolari.
Witschard, F., 1984: The geological and tectonic evolution of the Precambrian of northern Sweden – a case for basement reactivation? *Precambrian Research 23*, 273–315.
Wood, D.A., Joron, J.-L., Treuil, M., Norry, M. & Tarney, J., 1979: Elemental and Sr isotope variations in basic lavas from Iceland and the surrounding ocean floor. *Contributions to Mineralogy and Petrology 70*, 319–339.
Wright, S.F., 1988: Early Proterozoic deformational history of the Kiruna district, northern Sweden. *Unpublished PhD thesis, University of Minnesota*, 170 pp.

Authors, paper 7:
Stefan Luth
Geological Survey of Sweden,
Department of Mineral Resources,
Uppsala, Sweden

Cecilia Jönsson
Geological Survey of Sweden,
Department of Mineral Resources,
Uppsala, Sweden

Johan Jönberger
Geological Survey of Sweden,
Department of Mineral Resources,
Uppsala, Sweden

Susanne Grigull
Geological Survey of Sweden,
Department of Physical Planning,
Uppsala, Sweden

Robert Berggren
Geological Survey of Sweden,
Department of Mineral Resources,
Uppsala, Sweden

Bart van Assema
VU University Amsterdam,
Amsterdam, the Netherlands

Willem Smoor
VU University Amsterdam,
Amsterdam, the Netherlands

Thomas Djuly
VU University Amsterdam,
Amsterdam, the Netherlands

7. The Pajala deformation belt in northeast Sweden: Structural geological mapping and 3D modelling around Pajala

Stefan Luth, Cecilia Jönsson, Johan Jönberger, Susanne Grigull, Robert Berggren, Bart van Assema, Willem Smoor & Thomas Djuly

ABSTRACT

Results from structural geological mapping and 3D geological subsurface modelling of the Palaeoproterozoic Pajala deformation belt (PDB) in northeast Sweden are presented. The structural geological map is based on integration between detailed geological field observations and interpreted geophysical datasets (magnetic, electromagnetics and gravity). The deformation pattern obtained reveals a complex network of several parallel and intersecting shear zones striking mainly N–S and bounding tightly-folded domains. Strike and dip measurements and sense of shear determinations on these mapped structures were then combined with the subsurface geometries obtained from 2D and 3D models based on gravity, magnetic and electromagnetic data. The resulting 3D geological interpretation yields a wedge-shaped subsurface geometry for the Pajala deformation, belt with steeply east-dipping shear zones along its western border and steeply west-dipping shear zones towards the east. Internally, the wedge is folded into multiple ellipsoidal dome structures bounded by a network of N–S-striking shear zones. The folded domes appear strongly elongated in a N–S direction, suggesting E–W flattening and possible vertical extrusion as the main deformation mechanisms. Tectonically, the PDB is now interpreted as a 60 to 80 km wide transpressive wedge formed during NE–SW transpressive shortening (D1), followed by E–W shortening (D2). An eastward offset of the PDB along the intersecting NE–SW-striking Kolari shear zone north of Pajala probably occurred during D2. Relatively young metamorphic ages (1.8 Ga) recorded in the PDB in relation to its surroundings (1.84 Ga) indicate that D2, which (re)folded the main metamorphic fabric in the PDB, must have occurred after 1.8 Ga. Finally, deformation by NNW–SSE shortening (D3) caused discrete faulting and sinistral brittle-ductile reactivation, mainly along the western boundary of the PDB.

GEOLOGICAL SETTING

The Pajala deformation belt

The Pajala deformation belt (PDB) is a large N–S-trending high-strain belt transecting the Fennoscandian Shield from the Baltic Sea into northern Sweden, Finland and Norway. The belt was formerly named the Baltic–Bothnian megashear by Berthelsen & Marker (1986), and was interpreted to have resulted from large intraplate strike-slip movements. Kärki et al. (1993) renamed the belt the Pajala Shear Zone and assigned a prominent dextral strike-slip component to it. More recently, contrasting plate kinematic models were proposed by Nironen et al. (1997) and Lahtinen et al. (2005, 2015), suggesting the PDB was formed during continental rifting, or was a suture zone, respectively. In both scenarios the PDB accommodated dextral and sinistral movements during stages of subsequent reactivation. The evidence for these tectonic interpretations is primarily based on large-scale geophysical patterns as well as geochronological data derived from the major lithotectonic units surrounding the PDB (Lahtinen et al. 2015). However, no detailed structural geological study has been carried out along the Swedish part of the PDB, nor have any attempts been made to unravel its subsurface geometries in 3D. The existing tectonic models must therefore be examined in light of the outcomes from an integrated, structurally-orientated, geological study along the PDB.

This study focuses on the Swedish part of the PDB, striking along the border with Finland (Fig. 1). To the south of the small town of Pajala, the belt is up to 60 km wide and comprises several N–S-striking parallel shear zones mainly interpreted from airborne magnetic and gravity surveys (Fig. 2). North of Pajala, however, the PDB is intersected by the NE–SW-striking Kolari shear zone, causing an apparent eastward bending of the PDB into Finland (Väisänen 2002, Niiranen et al. 2007). As such, the PDB and Kolari shear zone were lumped together as the Kolari–Pajala Shear Zone in studies focusing on the Finnish side (e.g. Niiranen et al. 2009, Niiranen 2011). Detailed investigations in Finland based on mapping and depth interpretations along a seismic profile crossing the Kolari–Pajala shear zone (Fig. 4B) revealed several shear zones with different orientations (Niiranen 2011). It is evident from these studies that the observed deformation pattern reflects multiple phases of deformation. Earlier geological studies and mapping projects focusing on the Swedish section also recognised that deformation within, as well as outside, the PDB was polyphase, resulting in superimposed and interfering folding patterns (Eriksson 1954, Padget 1977, Grigull et al. 2018). It has been suggested by the same authors that major northwest–southeast-trending folds (F1) became refolded by north–south-trending F2 folds. Refolding by F2 was most intense within the PDB and intimately associated with shearing along the N–S-orientated shear zones, resulting in the formation of tectonic lenses composed of folded gneisses, migmatites or more massive granitoids. Eastern-side-up sense of shear documented along the western boundary of the PDB was proposed in previous studies to explain major east–west jump in the grade and timing of metamorphism (Bergman et al. 2001, 2006, Jonsson and Kero 2013). West of this boundary, upper greenschist facies metamorphism is recorded at 1.85 Ga, whereas units inside the PDB underwent upper amphibolite facies metamorphism between 1.82 and 1.78 Ga. Apart from observations at one locality (Bergman et al. 2001), structural geological evidence to support eastern-side-up movements is still lacking, but was one of the aims of this study. Moreover, the PDB largely overlaps the Fe-Cu-Au Pajala–Kolari metallogenic area. Studies on deposits located on the Finnish side of the PDB indicated an iron oxide-copper-gold (IOCG) affinity as well as large structural control by major shear zones and more locally by second to fourth-order shear zones and faults (e.g. Niiranen et al. 2007). An improved understanding of deformation history and the resulting structural pattern in the bedrock around the town of Pajala is therefore crucial to better constrain the region's ore potential.

Lithostratigraphy and deformation in the Pajala area

The Pajala region is predominantly made up of Palaeoproterozoic supracrustal rocks (2.4–1.86 Ga) and intrusive rocks related to several magmatic suites (1.96–1.75 Ga, Fig. 1). Most of the rocks were formed in a volcanic arc setting and were deformed and metamorphosed during the Svecokarelian orogeny (Bergman et al. 2001). The study area is subdivided into three domains based on distinctive lithology, deformation pattern or metamorphic grade (Fig. 1). The *greenstone domain* north of Pajala is composed of rocks mainly belonging to the Karelian greenstone group (2.3–1.96 Ga); the *migmatite domain,*

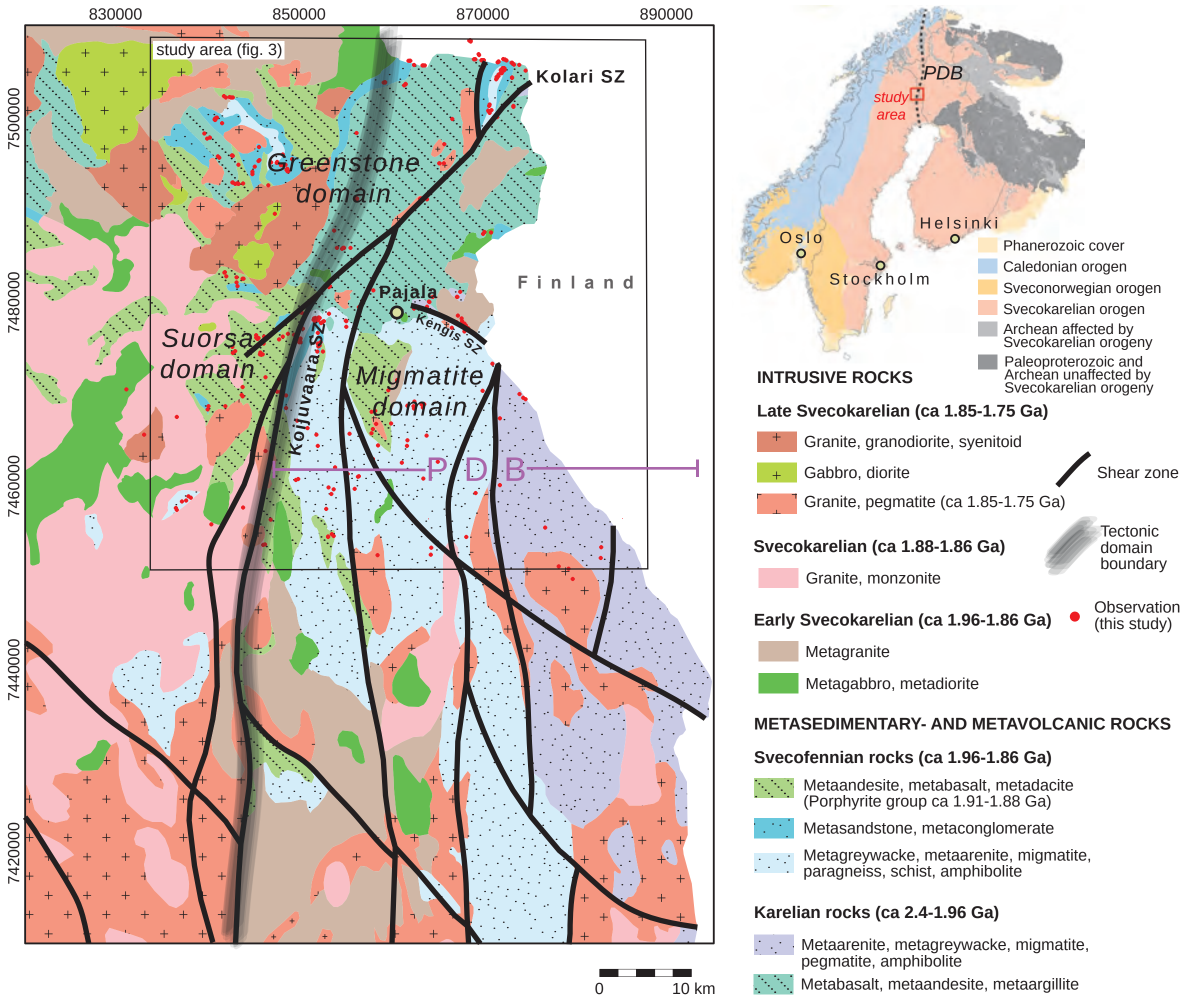

Figure 1. Geological map of the Pajala area. PDB: Pajala deformation belt, SZ: shear zone. Only the major shear zones are displayed on this map and are derived mainly from geophysical data. The tectonic domain boundary (thick black line) is based on Bergman et al. (2006). Figure 3 shows a more detailed and complete structural map of the study area. Insert map shows the main geological domains of the Fennoscandian shield.

south of Pajala, is characterised by strongly deformed metasedimentary rocks of Svecofennian age (1.96–1.88 Ga); and the *Suorsa Domain,* directly west of the PDB, is composed of weakly deformed mafic to intermediate metavolcanic rocks of roughly the same age as the metasedimentary rocks.

The predominant rock types in the greenstone domain are mafic and ultramafic pyroclastic and volcaniclastic rocks. Higher up in the stratigraphy, mafic tuffites intercalated by graphitic layers, carbonates and iron-rich sedimentary rocks (BIF) occur. The overlying 200 m thick dolomite unit hosts economically important skarn iron ore deposits: Stora Sahavaara, Runtijärvi, Tapuli and Palotieva. Based on the abundance of garnet and diopside, the metamorphic grade in the greenstone domain reached at least amphibolite facies. Scapolite alteration affecting mafic rocks is common and locally very strong (Grigull & Berggren 2015). Due to very limited bedrock exposures, structural data north of Pajala was mainly obtained for this study from the Ristimilla and Käymäjärvi areas. For a more detailed description of the Karelian greenstone group the reader is referred to Padget (1977), Martinsson & Wanhainen (2013) and Martinsson et al. (2018).

The Migmatite domain is characterised by metaarenites, metagreywackes and banded gneisses, which are mostly migmatitic. Detrital zircon studies on the metaarenite yield mostly 1.91 Ga inherited grains (Bergman et al. 2001, Lahtinen et al. 2015, Ladenberger et al., 2018). These rocks underwent amphibolite facies metamorphism with peak temperatures of between 510–615 °C at 4–6 kbar around 1.8 Ga (Bergman et al. 2006). Some common metamorphic minerals present include sillimanite, cordierite and garnet. Despite the high-grade metamorphism, sedimentary structures such as cross-bedding are locally well preserved. In the western part of the Migmatite domain in particular, the metamorphic grade is highly variable. Within the well-preserved sedimentary rocks, Martinsson et al. (2004) documented ripple marks, indicating a shallow marine depositional environment for the Sammakkovaara group. In contrast, areas with predominantly diatexitic migmatites show an enrichment of granitic and pegmatitic material. Locally, granitic intrusions occur as elongated bodies aligned with shear zones. These rocks are weakly foliated to massive pinkish granite, pegmatite or aplites, and are characterised by a relatively high radium index (0.8). Foliated units are commonly intruded or brecciated by pegmatite, indicating multiple injection events along the PDB.

The Suorsa domain is predominantly composed of mafic to intermediate metavolcanic rocks, which were also included in the Sammakkovaara group by Martinsson et al. (2004), albeit occurring on a higher stratigraphic level than the metasedimentary rocks from the Migmatite domain. The metavolcanic rocks are generally fine-grained and contain hornblende and plagioclase phenocrysts with some pyrite, epidote and magnetite. Laminated tuffs and volcanic breccias occur locally. The volcanic rocks are of an andesitic to trachyandesitic composition and a calc-alkaline signature, interpreted as reflecting arc-volcanism during northeastward subduction of oceanic crust below an Archaean palaeocontinent (Martinsson et al. 2004). The deformation imprint varies from very weakly deformed rocks to locally intensively sheared mylonites and associated discrete shear zones. The metamorphic grade in the Suorsa domain is predominantly lower to upper greenschist facies, but reaches amphibolite facies in a few areas with predominantly by metasedimentary rocks. The volcanic rocks are dated at 1.88 Ga by Martinsson et al. (2018).

Geophysical characterisation

The Pajala region is well covered by geophysical measurements, with a complete coverage of gravity, airborne magnetic, gamma-ray spectrometry and electromagnetic measurements (VLF and slingram) (Fig. 2A, B and Luth & Jönsson (2014), Grigull et. al (2014)). The spatial distribution of gravity measurements is approximately one point per 1.5 km^2, but measurement locations are locally more closely spaced. For a detailed overview on the different types and coverage of the geophysical datasets in the study area the reader is referred to Luth & Jönsson (2014).

Within the study area, the gravitational field shows two distinctive negative anomalies (Fig. 2A). One correlates with the low density quartz-feldspar rich paragneiss in the Migmatite domain; the other is found in the northwestern corner of the study area. Positive Bouguer anomalies correlate with rocks with basaltic to andesitic composition in the Suorsa and Migmatite domains. The Migmatite domain shows a homogeneous low-magnetic pattern in the west and somewhat higher magnetism in the east. Low magnetic anomalies were identified with an N–S ellipsoidal-shaped outline, some of which have been subject to structural and 3D modelling studies. The Migmatite domain can also be distinguished in the electromagnetic anomaly pattern, in which increased electrical conductivity is observed in the in-phase component. The magnetic pattern for the Suorsa domain varies considerably, with areas of high or low-magnetic signature, anomalies reflecting fold patterns, as well as disrupted anomalies due to intense deformation and shearing within the PDB.

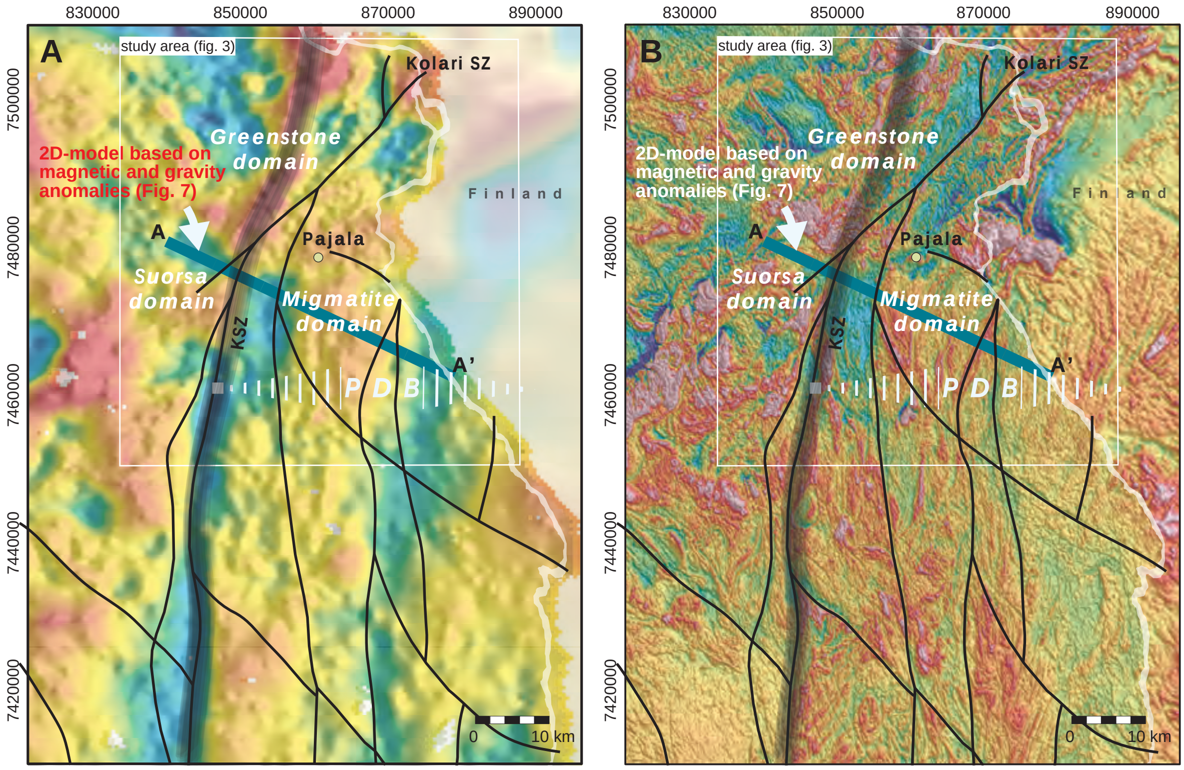

Figure. 2. Geophysical anomaly maps of the Pajala area. **A.** Bouguer gravity anomaly map. Blue indicates low gravity anomaly and red indicates high gravity anomaly. **B.** Airborne magnetic anomaly map. Blue indicates low magnetic anomaly and red indicates high magnetic anomaly. Profile line A-A' shown refers to the modelled profile displayed in Figure 7. Shear zones (lines); see the legend in Figure 1. PDB: Pajala deformation belt, KSZ: Koijuvaara shear zone.

STRUCTURAL ANALYSIS

Shear sense indicators and inferred direction of regional shortening

Several directions of shortening were deduced from the analyses of shear sense indicators in the field and in thin section. Figure 3 and Table 1 include the most representative kinematic indicators observed, as well as the inferred directions of shortening under which they may have been formed. Most of the analyses were carried out along shear zones where deformation and shearing were observed in most rock types. However, shear indicators such as asymmetric shear folds, shear bands, mica-fish and sigmoids are generally best developed within banded paragneiss, mica-schist and migmatite, which are the most common rock types in the Migmatite domain. Virtually all shear indicators are observed in a metamorphic fabric (banding, porphyroblasts etc.), and therefore record deformation that most likely post-dates peak metamorphism and migmatitisation.

The structural fabrics seen in outcrops and thin sections often reveal deformation by dextral shearing along N–S-striking and sub-vertically-dipping foliations. In the Migmatite domain in particular, dextral shearing was most commonly observed and is often associated with a medium-grade mylonitic fabric (Fig. 4). The documented dextral shear along a N–S-striking fabric mostly likely developed during NE–SW transpression. Some other shear indicators observed throughout the study area are more consistent with E–W-directed shortening. Additional evidence for E–W shortening in the Migmatite domain is inferred from the pattern of upright folds along N–S-trending fold axes. In the Suorsa domain, E–W shortening was primarily deduced from the predominantly dextral shear sense associated with the NE–SW-striking Kolari Shear Zone. Whether the inferred NE–SW and E–W directions of shortening reflect two separate shortening events or may be considered the result of local strain partitioning is discussed later in this chapter. A third direction of shortening is orientated

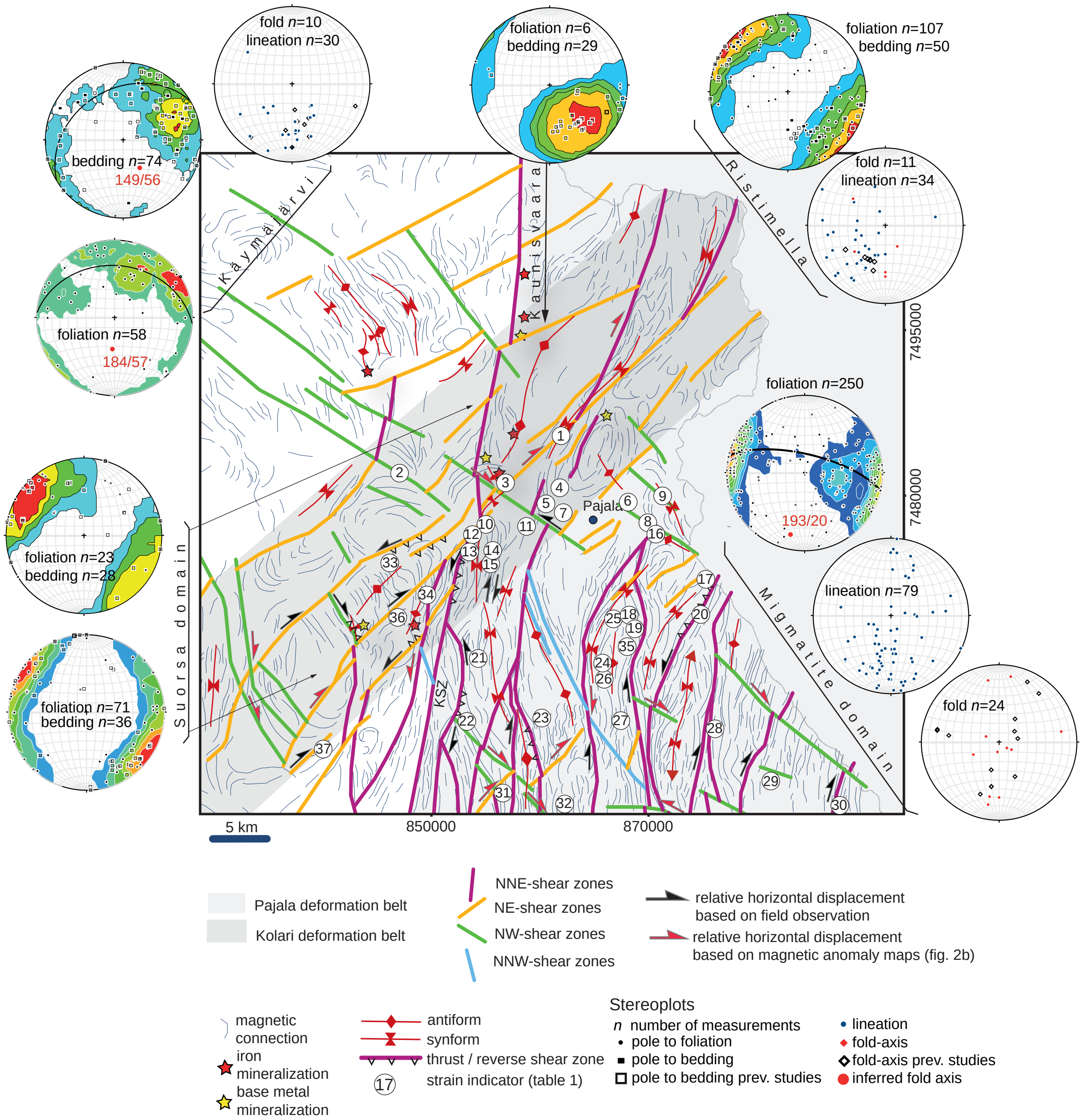

Figure 3: Structural geological map of the Pajala area based on new and existing field data. Numbers refer to the locations of strain indicators observed in outcrops and thin sections (see also Table 1). Notice the distinction made between two intersecting deformation belts as the main difference when compared with previous published maps (Fig. 1).

Table 1. Location and type of observed strain indicators as displayed in Figure 3.

Nr (Fig. 3)	North (Sweref 99)	Easting (Sweref 99)	Domain	Lithology	Strain indicator	Kinematics	Inferred direction of shortening
1	7485784	857942	Greenstone	paragneiss	drag fold	sinstral	NW-SE
2	7482491	843671	Greenstone	igneous rock	rotated clast	reverse, top-to-the-NNW	NW-SE
3	7481670	853029	Greenstone	BIF	upright fold		ENE-WSW
4	7481191	857787	Greenstone	migmatite	fold (F2)		E-W
5	7479358	856206	Greenstone	paragneiss	fault	sinistral	ENE-WSW
5	7479358	856206	Greenstone	paragneiss	fold (F1)		NE-SW
6	7479944	863843	Greenstone	paragneiss	garnet porphyroblast	dextral	NE-SW
7	7479250	856318	Greenstone	paragneiss	sigmoid	sinistral	ENE-WSW
8	7478158	865552	Greenstone	paragneiss	fold (F1)		NE-SW
8	7478158	865552	Greenstone	paragneiss	fold (F2)		E-W

Table 1 continues

Nr (Fig. 3)	North (Sweref 99)	Easting (Sweref 99)	Domain	Lithology	Strain indicator	Kinematics	Inferred direction of shortening
9	7480482	866899	Greenstone	paragneiss	shear band	dextral	NW-SE
10	7477973	851256	Migmatite	micaschist	CS, mica fish	sinistral	NNW-SSE
10	7477973	851256	Migmatite	micaschist	CS, mica fish	dextral-reverse	NE-SW
11	7477835	854824	Migmatite	paragneiss	drag fold	dextral	N-S
12	7477054	850102	Migmatite	paragneiss	drag fold	sinistral	N-S
13	7475601	849810	Migmatite	paragneiss	CS, mica-fish	reverse	E-W
14	7475422	851744	Migmatite	paragneiss	CS, mica-fish	dextral	NE-SW
15	7475138	851810	Migmatite	paragneiss	shear band	dextral	NE-SW
16	7477150	866319	Migmatite	paragneiss	fold (F1)		NE-SW
17	7473207	870709	Migmatite	paragneiss	mica-fish	dextral	NE-SW
17	7473207	870709	Migmatite	paragneiss	mica-fish	reverse (top-to-the-ESE)	E-W
18	7468812	863312	Migmatite	migmatite	fold (F2)		E-W
19	7468820	863008	Migmatite	migmatite	thrust	reverse (top-to-the-NNE)	NNE-SSW
20	7470069	870243	Migmatite	paragneiss	drag fold	sinistral	NW-SE
21	7466229	850611	Migmatite	migmatite	drag fold	sinistral	NW-SE
22	7460694	849576	Migmatite	paragneiss	rotated clast	dextral	NE-SW
22	7460694	849576	Migmatite	paragneiss	sigmoid	reverse (top-to-the-W)	NE-SW
23	7460963	856205	Migmatite	paragneiss	drag fold	sinistral	NW-SE
24	7464914	861486	Migmatite	paragneiss	fold (F2)		E-W
25	7468477	863131	Migmatite	paragneiss	garnet porphy-roblast	dextral	NE-SW
26	7464301	861444	Migmatite	migmatite	drag fold	dextral	NE-SW
27	7460711	863213	Migmatite	paragneiss	sigmoid	reverse (top-to-the-E)	E-W
28	7460016	871530	Migmatite	paragneiss	sigmoid	sinistral	NW-SE
29	7455418	876425	Migmatite	paragneiss	sigmoid	dextral	NE-SW
30	7453245	882560	Migmatite	paragneiss	drag fold	sinistral	NE-SW
31	7454418	852819	Migmatite	metagranite	fold		E-W
32	7452408	858216	Migmatite	paragneiss	drag fold	dextral	NE-SW
33	7474601	842747	Suorsa	andesite	sigmoid	dextral	E-W
33	7474601	842747	Suorsa	andesite	conjugate faults		NNW-SSE
34	7471759	846047	Suorsa	andesite	drag fold	dextral	E-W
35	7468477	863131	Suorsa	biotite gneiss	drag fold	dextral	NE-SW
35	7468477	863131	Suorsa	biotite gneiss	reverse fault	reverse (top-to-the-W)	E-W
36	7469807	843451	Suorsa	altered rock	sigmoid	dextral	ENE-WSW
37	7458252	836943	Suorsa	paragneiss	sigmoid	dextral	WNW-ESE

NNW–SSE and is inferred from shear sense indicators along brittle-ductile shear zones in the Migmatite domain and conjugates faults in the Suorsa domain. Typically, the NW–SE-orientated brittle-ductile shear zones and faults accommodated dextral slip, while the intersecting NE–SW-orientated zones generally record sinistral slip. Moreover, only a few shear indicators were observed in vertical sections and mostly indicated E–W flattening or reverse shearing. As such, eastern-side-up shearing along a steeply eastward-dipping fabric was recorded southwest of Pajala, whereas in the eastern part of the Migmatite domain western-side-up shearing along steeply westward-dipping structures was observed.

Structural geological map of the Pajala area

Integration between new field observations with pre-existing data resulted in a new structural geological map of the Pajala region (Fig. 3). Geophysical lineaments, mostly derived from earlier geophysical studies (magnetics, VLF, slingram), were reinterpreted and grouped by orientation into four main groups: 1) N–S to NNE–SSW, 2) NE–SW, 3) NW–SE and NNW–SSE-striking lineaments. Observations on shear sense indicators and strike-dip measurements on strongly deformed rocks were then linked to nearby geophysical lineaments. As a result, many lineaments displayed in Figure 3 could be "translated" into shear zones. Relative movements accommodated by these shear zones were derived from shear sense indicators or from displaced geophysical markers. Relative timing of shearing was determined for some shear zones based on the displacement or intersection by other shear zones. From this analysis we obtained the following sequence of shear zone activation: 1) Dextral shearing along N–S to NNE–SSW-orientated shear zones, 2) Dextral shearing along NE–SW-orientated shear zones, 3) Dextral shearing along NW–SE-orientated shear zones, 4) Sinistral reactivation along N–S to NNE–SSW-orientated shear zones.

The mapped folding pattern displayed in Figure 3 was derived from a combination of new and pre-existing strike-dip measurements of foliations and lineations (see stereographic plots). Magnetic anomaly maps were also used to determine the map trace of the fold hinges. The resulting pattern largely accords with earlier maps of the area (e.g. Bergman et al. 2001), but some more N–S and NW–SE-striking upright folds were recognised southeast of Pajala. Many of the folds in the Pajala region are aligned to shear zones, which may indicate a spatial and temporal relationship between the two structures. As such, the folds can be grouped according to the strike of axial planes into groups resembling the geophysical lineaments: 1) N–S, 2) NE–SW and 3) NW–SE-trending. With a subdivision of structural features based on orientation, two major deformation zones or belts can now be distinguished in the Pajala region: the Pajala deformation belt (PDB), in which shear zones, folds and main foliation predominantly strike N–S; and the Kolari shear zone, along which associated shear zones and folds strike mainly NE–SW. Both shear zones are shown on the structural geological map as large shear zones (belts) with a considerable width, i.e. tens of kilometres (Fig. 3). The Kolari shear zone clearly overprints the PDB, causing an eastward displacement of the PDB into Finland.

The migmatite domain

Folding patterns

The Migmatite domain is characterised by a predominantly N–S-orientated folding pattern. The scale of the observed folds varies from centimetres in outcrops to more than 4 km outlined by magnetic anomalies. Most mesoscopic folds observed in outcrops are upright folds with N–S-striking fold axes, and fold the main metamorphic fabrics (S1). Fold axes are typically shallow-plunging towards the south, but may also be doubly–plunging, producing dome shapes in outcrop and on a map scale. The absence of two intersecting foliations in outcrops suggests that the domes may not have resulted from fold interferences. However, superimposed folding as a dome-forming mechanism should not be excluded (see discussion in this chapter). On a map scale, many of the km-sized N–S-trending folds in the Migmatite domain appear as doubly-plunging folds resembling large dome geometries. The domes are ellipsoidal in an N–S direction and typically bounded by shear zones. Hinge zones characterised by shallow-dipping migmatitic fabric (S1) were observed in the core of some dome interiors (Fig. 4B). Apart from metamorphic banding, no axial plane cleavage was observed in these hinge zones. NW–SE-striking folds are generally obscured by N–S-striking folds and shear zones, and were only recognised in some outcrops (Fig. 4C). Directly east of Pajala, a series of folds with moderately southwest-dipping axial planes and sub-horizontally NE–SW-orientated fold axes strike parallel to the NW–SE-striking Kengis shear zone (Fig. 1, Fig. 4C). Like the N–S-striking folds, the NE–SW-striking folds clearly fold a migmatitic banding and should therefore post-date peak metamorphism.

Shear zones and tectonic lenses

The larger and dominant N–S-striking folds are typically bounded by 5–100 m wide shear zones characterised by low- to medium-grade protomylonites as well as pegmatites forming large vein networks. A simple shear component is often recorded together with predominantly dextral-slip indicators, but sinistral slip was also observed (Fig. 4D–E). The shear zones acted as zones of weakness, along which progressive deformation was localised. Consequently, the folded domains embedded into the braided pattern of shear zones eventually behaved as tectonic lenses and were less affected by late ductile deformation.

The Koijuvaara shear zone

The Koijuvaara shear zone defines the western boundary of the PDB and is named after the type locality at Koijuvaara hill, southwest of Pajala. The shear zone includes the discrete Koijuvaara brittle-ductile shear zone, which stands out as a geophysical lineament (magnetics, VLF and slingram), as well as the higher-grade Koijuvaara mylonite zone, which extends 1 km east of the fault (Fig. 4).

The metasedimentary rocks along the Koijuvaara brittle-ductile shear zone contain a prominent N–S-striking spaced cleavage, along which bedding and metamorphic banding are folded (Fig. 4H). In the Koijuvaara area, primary bedding is well preserved inside the fold hinge and represents an alternation between quartz-feldspar layers and mica-rich layers. Mica-rich layers contain anhedral andalusite overgrown by euhedral staurolite. Biotite, muscovite and ilmenite inclusions in the staurolite are aligned, but not parallel to the main fabric, suggesting mineral growth between a first and second phase of deformation. The spaced cleavage usually strikes parallel to the axial planes of the minor folds, whereas in other cases it clearly crosscuts the folding pattern (Fig. 4G–J). Locally, these folds form ellipsoidal domes, typically with N–S to NW–SE-orientated axial traces (Fig. 4G). In addition, a fold interference pattern of N–S-orientated "heart-shapes" suggests multi-phase folding during NE–SW shortening and E–W shortening. To the south of Koijuvaara, horizontal dextral shearing overprinted by later sinistral shearing was inferred from microstructures, confirming Bergman et al. (2006), who described well-developed shear bands, indicating dextral movements in the Koijuvaara area. Metamorphic temperature and pressure were determined from a garnet-bearing sample by the same authors, recording up to 515 °C at 4.1 kbar.

Less than one kilometre east of Koijuvaara, paragneisses and mica schists are migmatitic and contain a penetrative, mainly N–S-striking, mylonitic fabric. The mylonitic foliation dips steeply eastward and strikes parallel to the migmatitic banding. Shear sense indicators, such as C-S fabric, imbricated clasts and mica-fish, are consistent with predominantly dextral shear, but sinistral shear was also observed. There are only a few observations on vertical sections, but they generally indicate eastern-side-up sense of shear. Moreover, quartz ribbons appear elongated, particularly in a vertical direction (L>S tectonite), suggesting that vertical movements were more intensive than strike-slip movement (Fig. 4M). The mylonitic fabric is best developed in biotite-rich paragneisses. Stratigraphic levels comprising layers of quartz-arenites are only weakly foliated and have preserved sedimentary structures. However, some local occurrences of weakly deformed quartz-arenites as boudins do indicate deformation. Another indicator of intense deformation in the mylonite zone is the strongly ellipsoidal outline of a large N–S-striking fold interpreted from the magnetic anomaly (Rasi syncline). Detailed studies and 3D modelling of the structure indicate that the fold is a steeply eastward-dipping, doubly-plunging syncline, which was probably formed by a combination of vertical shearing during NE–SW transpression and later flattening during E–W shortening (Luth et al. 2015, and section 5.5). The fact that the Rasi syncline is more elongated than the domes located further to the east suggests relatively high deformation in the Koijuvaara shear zone. In a few observations located around the fold hinge zone the mylonic fabric appears folded, and the inferred mylonitic fabric is overprinted at an angle of 45 ° by a N–S-orientated spaced cleavage composed of unstrained micas (Figs. 4K–L). In most observations, however, the spaced cleavage strikes parallel to the mylonitic fabric and may be associated with brittle-ductile reactivation along the Koijuvaara shear zone.

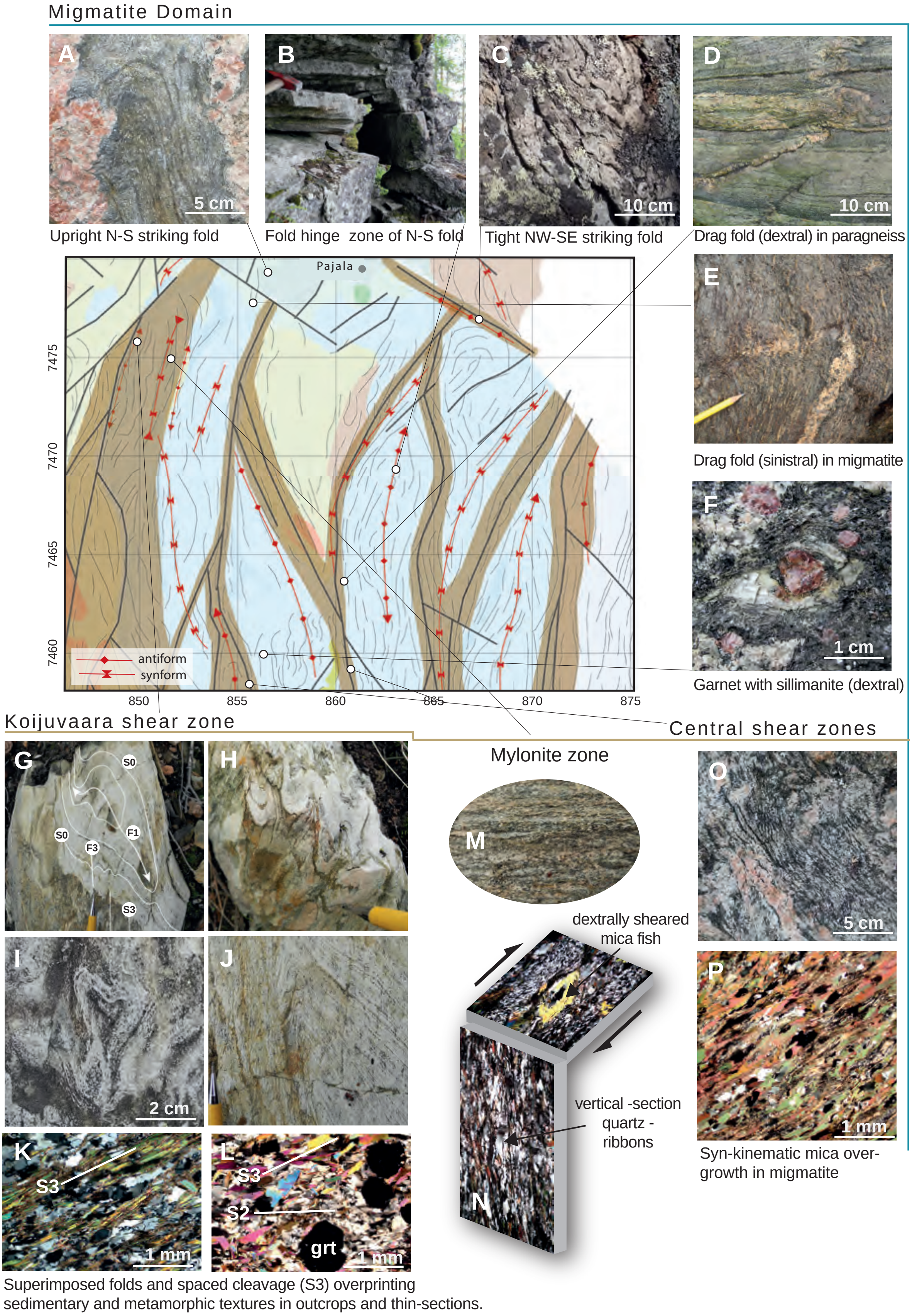

Figure 4. Observations and interpretations of structural features present in outcrops and thin sections from the Migmatite domain. Brown zones on the map indicate an estimated width of the major shear zones. For explanations of the other colours see legend in Figure 1.

Suorsa domain and Kolari shear zone

The Suorsa domain lies west of the Koijuvaara shear zone and predominantly consists of weakly deformed intermediate volcanic and volcaniclastic rocks. Despite some alteration (scapolite, K-fsp, epidote), an andesitic composition was deduced from geochemical analyses (Luth et al. 2015). Deformation in the Suorsa domain is heterogeneous and mainly restricted to discrete NE–SW-striking ductile shear zones and faults. These deformation zones are interpreted from lineaments derived from magnetic and VLF anomaly maps (Figs. 2, 5 and 6). It is clear from the apparent resistivity map that the NE–SW-striking lineaments crosscut the N–S-striking lineaments associated with the Koijuvaara shear zone further east. Geological observations along some of the NE–SW-striking lineaments reveal altered mylonites as well as strongly deformed fault rocks (Fig. 5A–E). Kinematic indicators in the mylonites are mostly consistent with dextral strike-slip (Fig. 5), but sinistral strike-slip has also been observed. Typically, a few tens of metres away from the deformation zones, the rocks are only weakly deformed and often lack foliation or metamorphic banding (Fig. 5F–G). Consequently, the NE–SW-striking lineaments should be treated as narrow, localised deformation zones. Based primarily on their orientation and continuation towards the northeast (Finland), we consider the deformation zones to represent the southwestern segment of the Kolari shear zone (see also Figs. 1, 3 and discussion). In addition, subsurface geometries of the zones were obtained from 2D resistivity models based on new VLF data (Fig. 6). The resulting models reveal sub-vertically dipping deformation zones corresponding to low-resistivity domains (Fig. 6). Along strike the low-resistivity domain widens towards the NE from 300 m to 1 km (see sections 1 and 7). This transition from a narrow to a wider system coincides with the intersection between the Kolari shear zone and the Koijuvaara shear zone. The exact dip of the deformation zones remains difficult to interpret from the modelling results; however, a steeply eastward dip can be deduced from some sections (e.g. 1, 5 and 8).

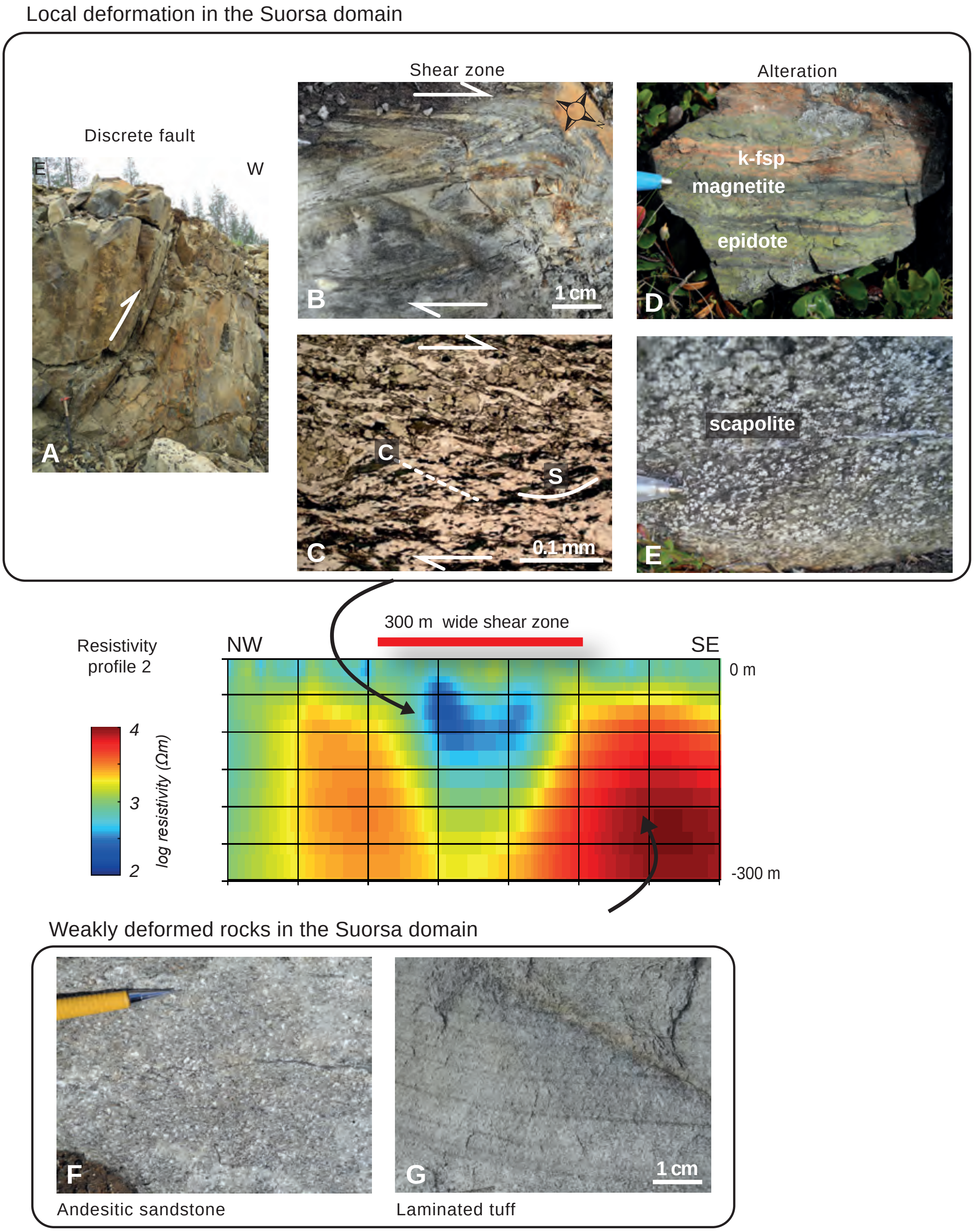

Figure 5. Examples of deformation in the Suorsa domain. Discrete faults and shear zones with associated potassium alteration and mineralisation (iron-oxides and sulphides) (**A–E**). The zones separate areas of weakly deformed rocks, with primary textures often well preserved **(F–G)** The resistivity profile, derived from ground measurements of electromagnetics, defines the shear zones as domains of low resistivity. Location of profile 2 is shown in Figure 6.

► Figure 6. Resistivity 2D models of the Koijuvaara and Kolari shear zones based on data from electromagnetic ground measurements. **A.** VLF anomaly map with locations of numbered profiles as red lines. **B–C.** Profiles of resistivity 2D models. The results can be grouped according to the width and geometry of the interpreted faults or shear zones into a "wide shear zone system" and a "narrow shear zone system". Note that the wider system coincides with the region of intersection between the Koijuvaara shear zone and the Kolari shear zone. The black arrow points to the shear zone in map view.

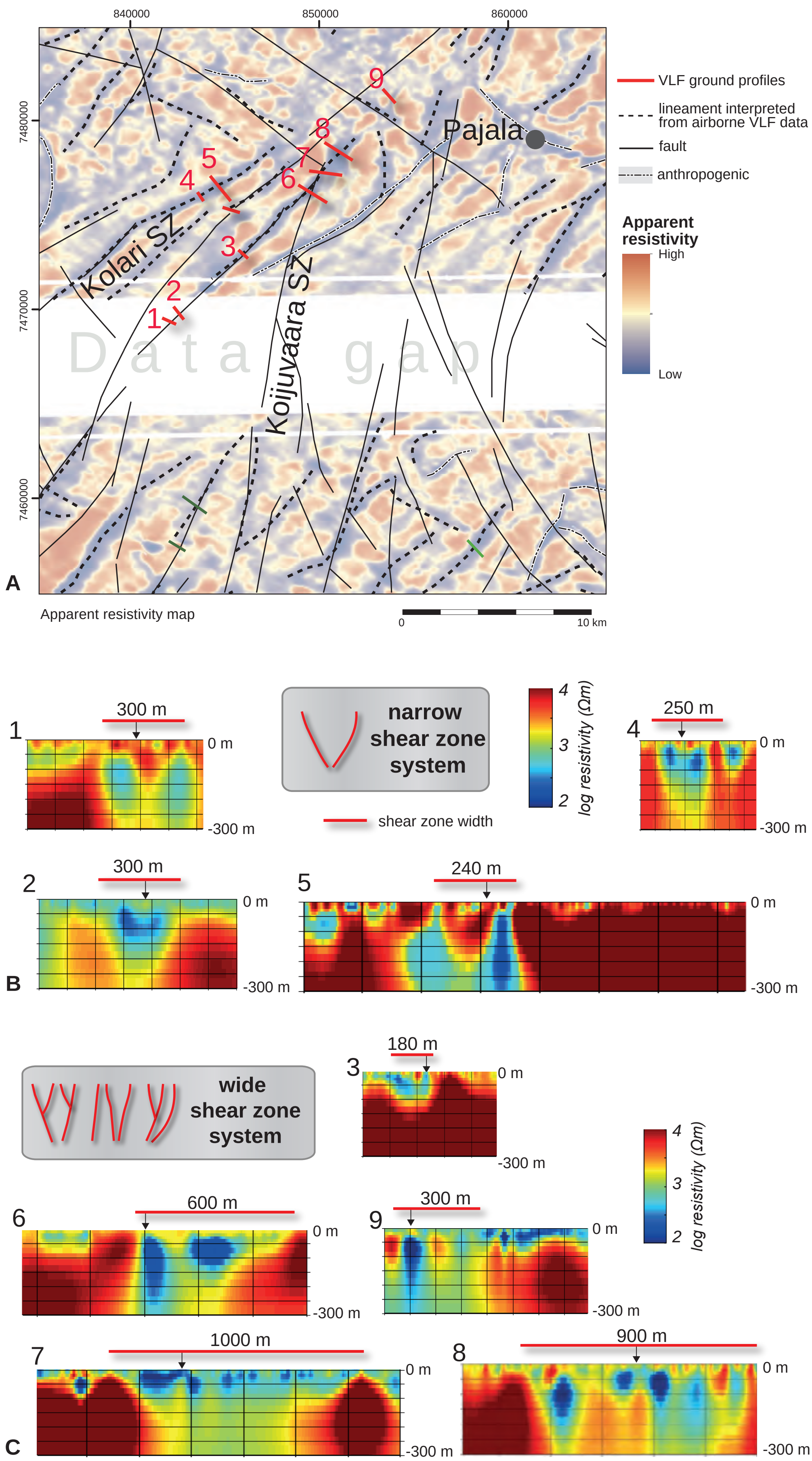
840000
850000
860000
7480000
7470000
7460000
VLF ground profiles
lineament interpreted from airborne VLF data
fault
anthropogenic
Apparent resistivity
High
Low
Pajala
Kolari SZ
Koijuvaara SZ
Data gap
1
2
3
4
5
6
7
8
9
A
Apparent resistivity map
0
10 km
narrow shear zone system
shear zone width
log resistivity (Ωm)
300 m
300 m
250 m
240 m
0 m
-300 m
B
wide shear zone system
180 m
600 m
300 m
1000 m
900 m
C

2D REGIONAL GEOPHYSICAL MODELLING AND GEOLOGICAL INTERPRETATION

2D forward modelling of gravity and magnetic data along a WNW-ESE-striking profile (Fig. 2) allowed for a better constraint on the geometry of the major boundaries within the PDB at depth. Petrophysical parameters from samples combined with in situ measurements of magnetic susceptibility along the profile were acquired to constrain the model. The subsurface geometries obtained are interpreted geologically as a large crustal wedge-shape bounded by steeply opposing dipping shear zones (Fig. 7). The Koijuvaara shear zone is modelled as a steeply eastward-dipping shear zone. Shear zones in the central part of the PDB dip sub-vertically towards the west. Also the Kolari shear zone in the Suorsa domain appears as a narrow crustal wedge with steeply opposing dipping shear zones.

Construction of the 2D geophysical model

Tonalitic-granodioritic rock occurs in the western part of the profile and is visualised as the brown body in Figure 7. 22 petrophysical samples were acquired from this lithology, yielding an average density of 2.73 g/cm^3. The median magnetic susceptibility of these samples is $3\,000 \times 10^{-5}$ SI units. East of the tonalite-granodiorite a granite outcrops at the surface (red in Fig. 7) and was sampled at 14 locations. Its average density is 2.63 g/cm^3 and its modelled depth extent is approximately 1 500 m below the surface. The granite has a relatively low content of magnetic minerals, resulting in an average susceptibility of 500×10^{-5} SI units. There are some strong positive magnetic anomalies within the granite caused by dolerites. The dolerites have been sampled at one location; the density for that sample is 3.11 g/cm^3. The content of magnetic minerals is quite high in the dolerite, with a susceptibility of almost $50\,000 \times 10^{-5}$ SI units. The in situ measurements with a susceptibility meter on the dolerite give an average value of $29\,000 \times 10^{-5}$ SI units. The bodies in the model that represent the dolerite (shallow purple bodies in Fig. 7) have therefore been assigned a magnetisation value of $40\,000 \times 10^{-5}$ SI units. This corresponds fairly well with the observed data and also indicates that the dolerites dip to the northwest. There is a sharp, positive gravity anomaly east of the granite, corresponding to intermediate volcanic rock (light green in Fig. 7). Seven petrophysical samples from this lithology give an average density of 2.8 g/cm^3. In situ measurements of magnetic susceptibility on outcrops give an average value of $4\,000 \times 10^{-5}$ SU units. The modelled depth extent of the volcanic rock is around 2 000 m below ground surface and is wedged between the intrusions in the west and the sedimentary rock in the east.

A meta-arenitic rock borders the intermediate volcanic rocks to the east (light blue in Fig. 7). It is seen in the geophysical data as a low-magnetic and low-gravity area, which accords well with the petrophysical samples analysed from this lithology. Three petrophysical samples give an average density of 2.63 g/cm^3, and a very small quantity of magnetic minerals yield a susceptibility of around 10×10^{-5} SI units. According to the observed magnetic field, however, there are some high magnetic anomalies within the meta-arenite, although these have not been taken into account in the model. The meta-arenite is bordered to the east by a thin sliver of granite (red in Fig. 7), which is considerably more magnetised than the metasedimentary rock. Five petrophysical samples of the granite have been collected roughly seven km south of the profile. The average density is 2.65 g/cm^3. In situ measurements of magnetic susceptibility on outcrops give a median value of $7\,000 \times 10^{-5}$ SI units. Taken together, the magnetic and gravity data indicate that the contact between the granite and the metasedimentary rock dips fairly steeply. The relatively high magnetic field continues further east, where the gravity field is also high. This corresponds to the intermediate metavolcanic rock (light green in Fig. 7). However, no petrophysical samples have been collected from this lithology close to the profile, so the modelled body has been given the same physical properties as the intermediate metavolcanic rock further to the west, i.e. 2.8 g/cm^3 and $4\,000 \times 10^{-5}$ SI units for the density and magnetic susceptibility, respectively. A large area of paragneiss occurs east of the metavolcanic rock, visualised as a light blue body in Figure 7. The magnetic field is relatively heterogeneous and the gravity field is quite high. In the vicinity of the profile, within 5 km on both sides, 13 petrophysical samples have an average density of 2.80 g/cm^3 and a median magnetic susceptibility of 6 000 × 10^{-5} SI units. The heterogeneity in the magnetic field has not been addressed in this model. The main geometry of the paragneiss is the dip to northwest and the thinning out at depth to the southeast. An area of considerably higher magnetisation occurs within the paragneiss close to the southeastern boundary with the granite. There are no ground observations in this magnetised lithology, however, so it has been assigned the same density as the surrounding paragneiss (2.80 g/cm^3), but with a higher magnetic susceptibility of 11 000 × 10^{-5} SI units. It is seen in Figure 7 as a darker blue body. The profile ends in the southeast in a granitic rock (red in Fig. 7). Three petrophysical samples have been collected from this granite within less than 1 km from the profile. The average density is 2.61 g/cm^3, and a relatively moderate magnetic susceptibility of approximately 1 000 × 10^{-5} SI units was obtained. The gravity field over the granite and the adjacent paragneiss indicates that the granite dips under the more dense metasedimentary rock.

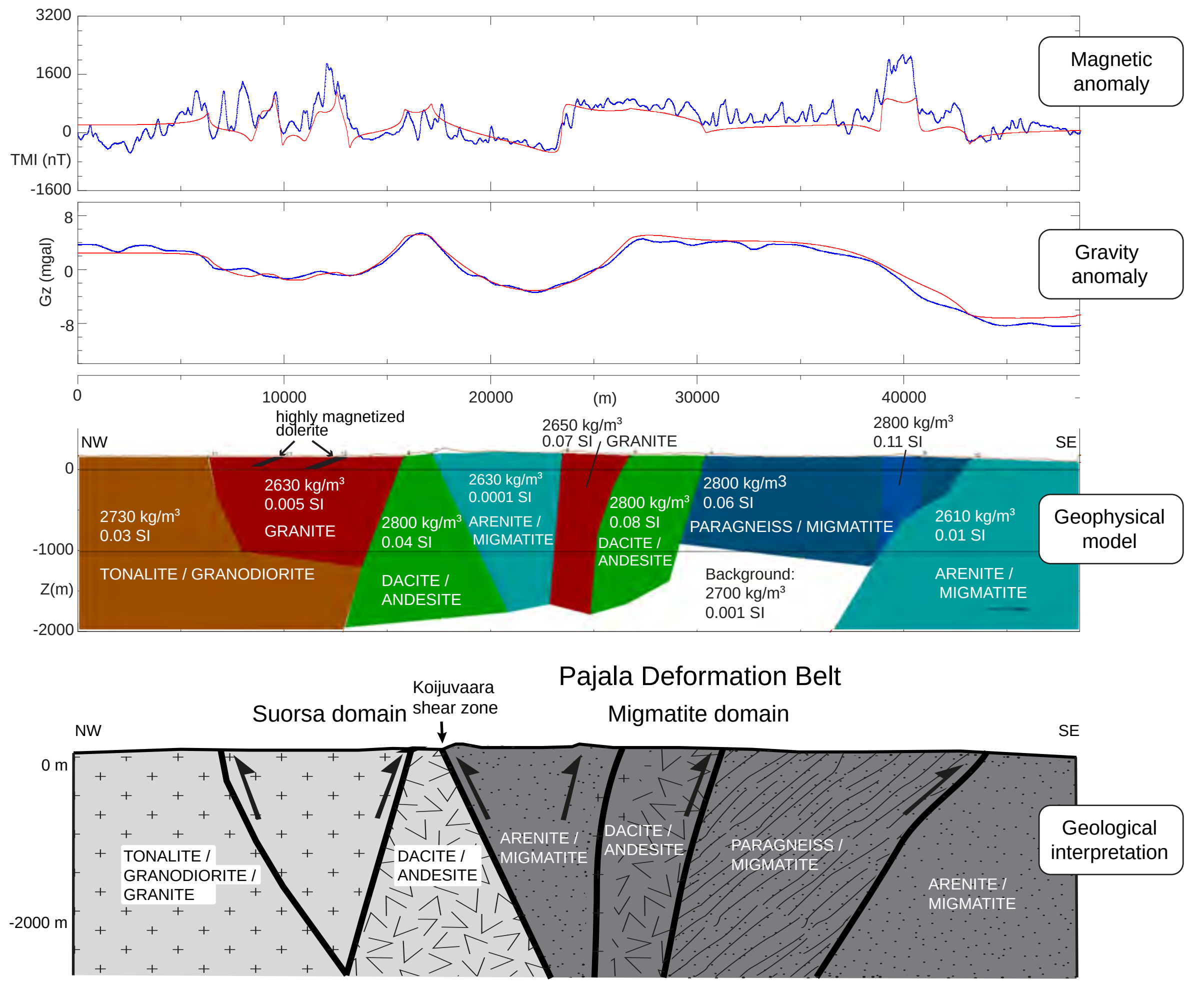

Figure 7. 2D geophysical model and geological interpretation of the PDB (profile location is shown in Figs. 2A–B). The model (bottom view) is based on airborne magnetic (top view) and gravity data (middle view). Blue and red lines represent the measured and calculated values, respectively. See text for more detailed explanations.

LOCAL AND SEMI-REGIONAL 3D MODELS

Input data and methodology

Local and semi-regional 3D models were constructed primarily to constrain subsurface geometries of structural features shown on the geological and geophysical anomaly maps (Figs. 2, 3). The resulting 3D geometries provided the framework for the conceptual regional-scale model presented in section 6.2 (Fig. 12). Input data for the local 3D models were geological field observations and structural measurements, geophysical potential field data and, for the Liviövaara model, drill core data as well. Geophysical potential field data were processed using Geosoft, Voxi and ModelVision modelling software packages. These modelling results were then compiled and visualised in combination with geological data using Gocad Paradigm.

Eastern folds model

The Eastern folds model is located in the east of the Migmatite domain (Fig. 8). Its dimensions are approximately 9 km east–west by 18 km north–south. The model was selected to resolve the subsurface geometry of a series of N–S-striking folds. The model reaches down to 4 km, but the depth extent of the interpreted bodies does not exceed 2 km. The cell size of each volume pixel (voxel) in the model is 100 × 100 m laterally and 50 m vertically. Before the data were inverted, voxels were assigned minimum and maximum magnetic susceptibility constraints. These constraints were provided by available petrophysical data from the area, along with in situ susceptibility measurements on outcrops. Based on a total of 42 petrophysical samples, the constraints on the model have been set within 0 and 0.2 SI units. The grid obtained was then imported into Gocad, where N–S and E–W-orientated sections were extracted from the grid volume. Each section was then interpreted manually, focusing primarily on the large-scale folding pattern. An interpolation between the sections was made, resulting in an undulating surface that reflects the overall 3D folding style within the domes.

A remarkable result from the Eastern folds model is an internal structure characterised by multiple aligned "domes and basins". As such, relatively long wavelength folds are interpreted from the N–S-orientated section, whereas folding is tight in the E–W-orientated sections. In addition, section 1 reveals a pattern of steeply west-dipping folds, bounded and intersected by moderately west-dipping zones. The combination of observations on sense of shear in outcrops and the geometry deduced from the geophysical models implies tectonic transportation was directed to the east in this part of the Pajala deformation belt.

Central model

The model area measures 9 by 16 km and is located in the centre of the Migmatite domain. The lithology of the selected area was mapped as intermediate metavolcanic rocks, but this interpretation is based on only a few field observations. Contrastingly, new field observations made for the present study reveal a gneissic to metagranodioritic lithology. It may be assumed that the coinciding relatively high magnetic and gravity responses may actually have a deeper source. The model depth is 2 km and the cell size of each volume pixel (voxel) in the model is 100 × 100 m laterally and 50 m vertically. Before the data were inverted, voxels were assigned minimum and maximum values ranging between 0 and 0.15 SI units for magnetic susceptibility constrained by petrophysical data. N–S and E–W-orientated sections were extracted from the resulting grid volume. Interpretation of and interpolation between the sections resulted in an undulating surface representing the base of the high anomaly body. In addition, a high anomaly body with a relatively high magnetic susceptibility was constrained by isosurfaces.

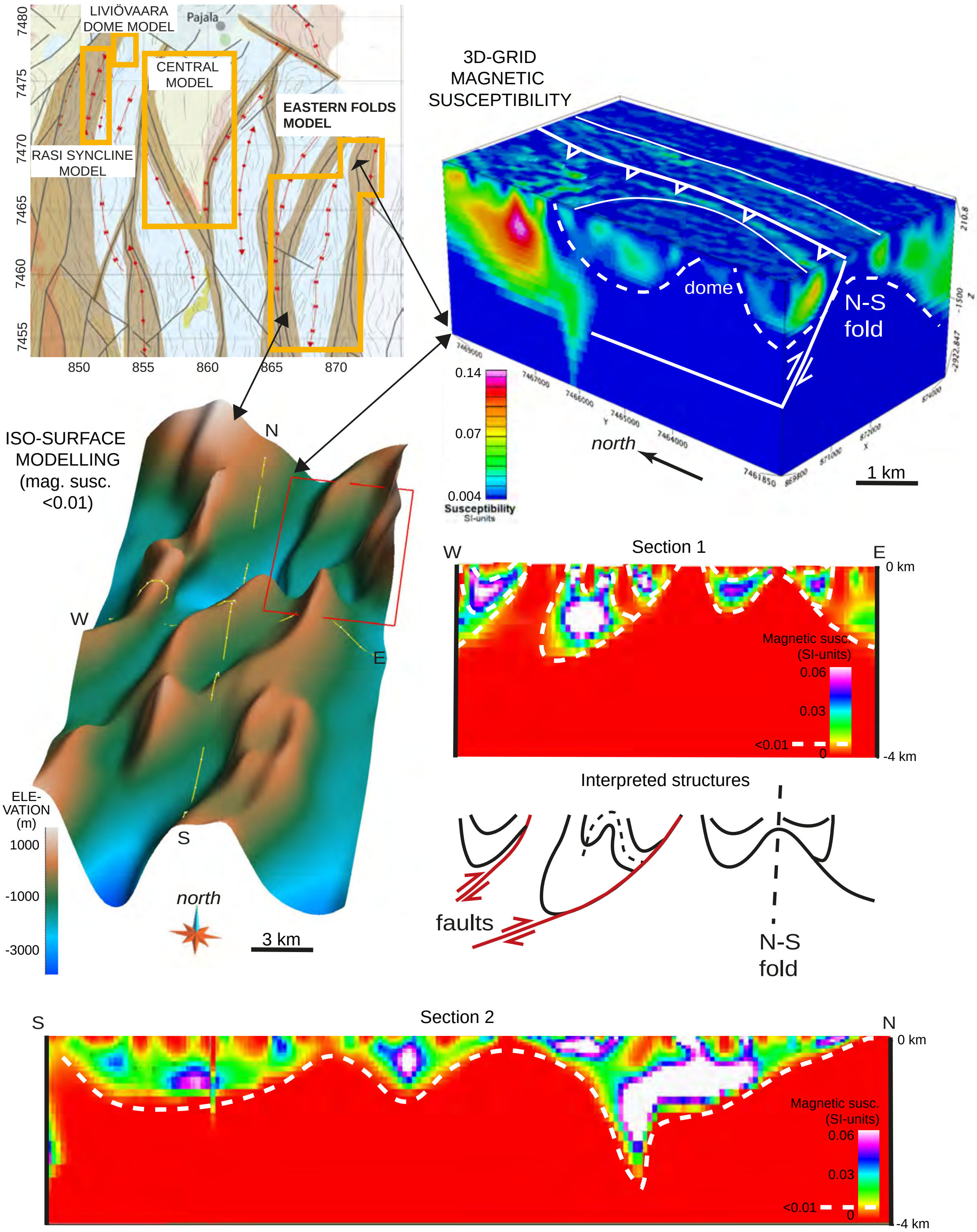

Figure 8. 3D model and interpreted cross-sections of the Eastern folds (see map insert for location). Several folds associated with shear zones are interpreted from the 3D magnetic susceptibility model (upper right). The undulating surface represents the lower limits of magnetic susceptibility and was extracted from the 3D model (middle left). Two sections through the model with an interpreted folding pattern are displayed to the right and below.

The resulting 3D model reveals a high-magnetic planar body underlying the area at a depth between 500 and 2 000 m (Fig. 9). The body is heart-shaped and dips moderately towards the south. The body appears to be folded in a similar style to the "Eastern dome model", with long wavelength, relatively open E–W folds and shorter-wavelength folds striking N–S. Whereas only low magnetic rocks were found at the surface, the modelled body may explain the region's relatively high and constant magnetic anomaly. The rock type of the modelled high magnetic anomaly body remains unknown. However, the relatively high gravity anomaly in the area may be consistent with gabbro or basalt.

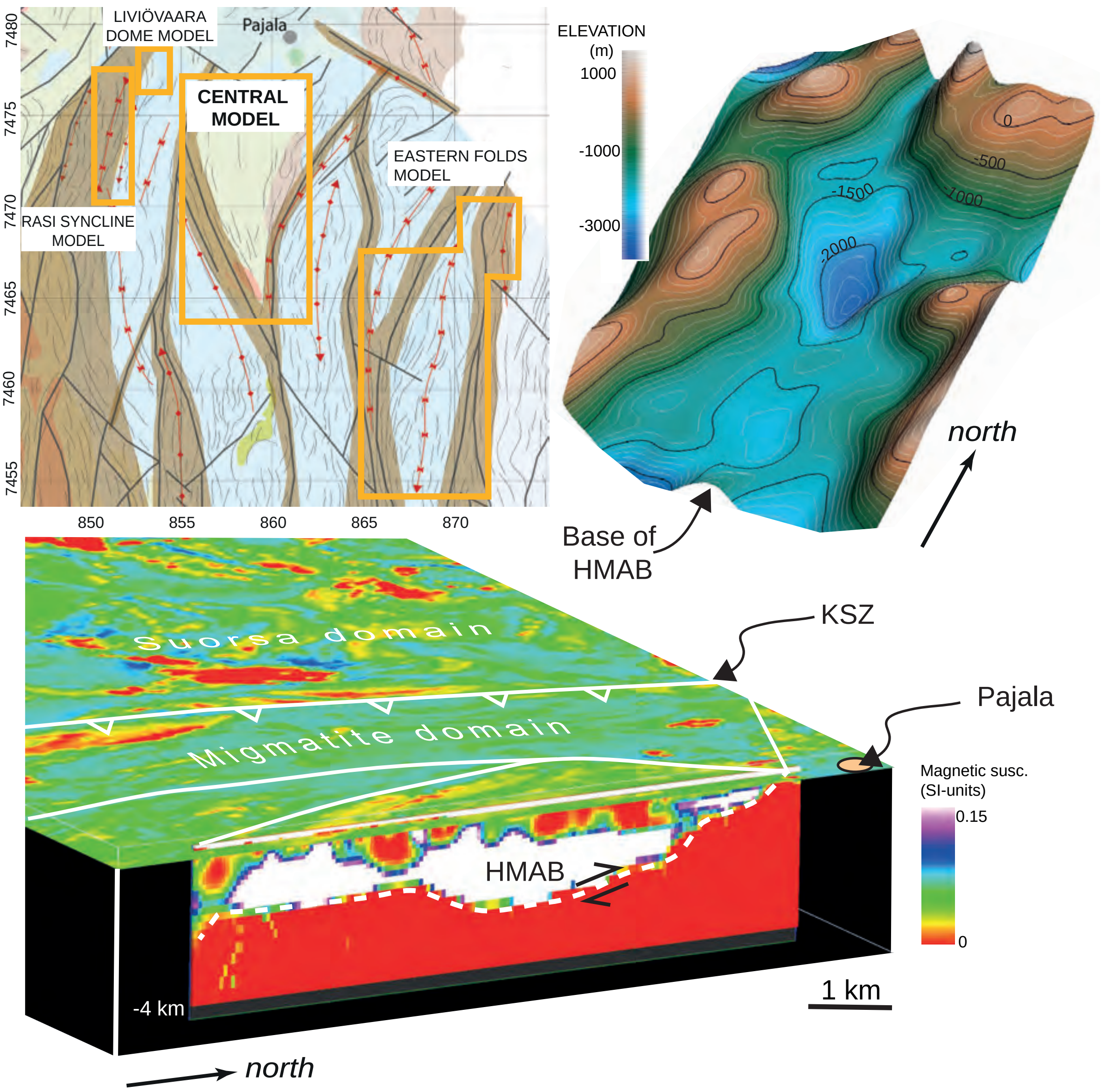

Figure 9. 3D local model of the central part of the Migmatite domain. A large tabular body with high magnetic susceptibility (HMAB) is hidden directly below the surface (magnetic anomaly map). The broken white line is the interpreted lower base of the body (lower view). The surface created in Gocad represents the lower base of the tabular body (upper view).

Liviövaara dome model

This model is mainly constrained by ground magnetic data, slingram and drill core data (see also Johansson 1985). No outcrops were located in the modelled area, which measures only 2 by 2 km (Fig. 10). Drill core data have shown that the area is underlain by metasedimentary and metavolcanic rocks, and also by gabbroic and monzonitic intrusive rocks. Some drill cores contained graphite schist and several limestone horizons were drilled, some of which were ore-bearing (Gerdin et al. 1990). Three

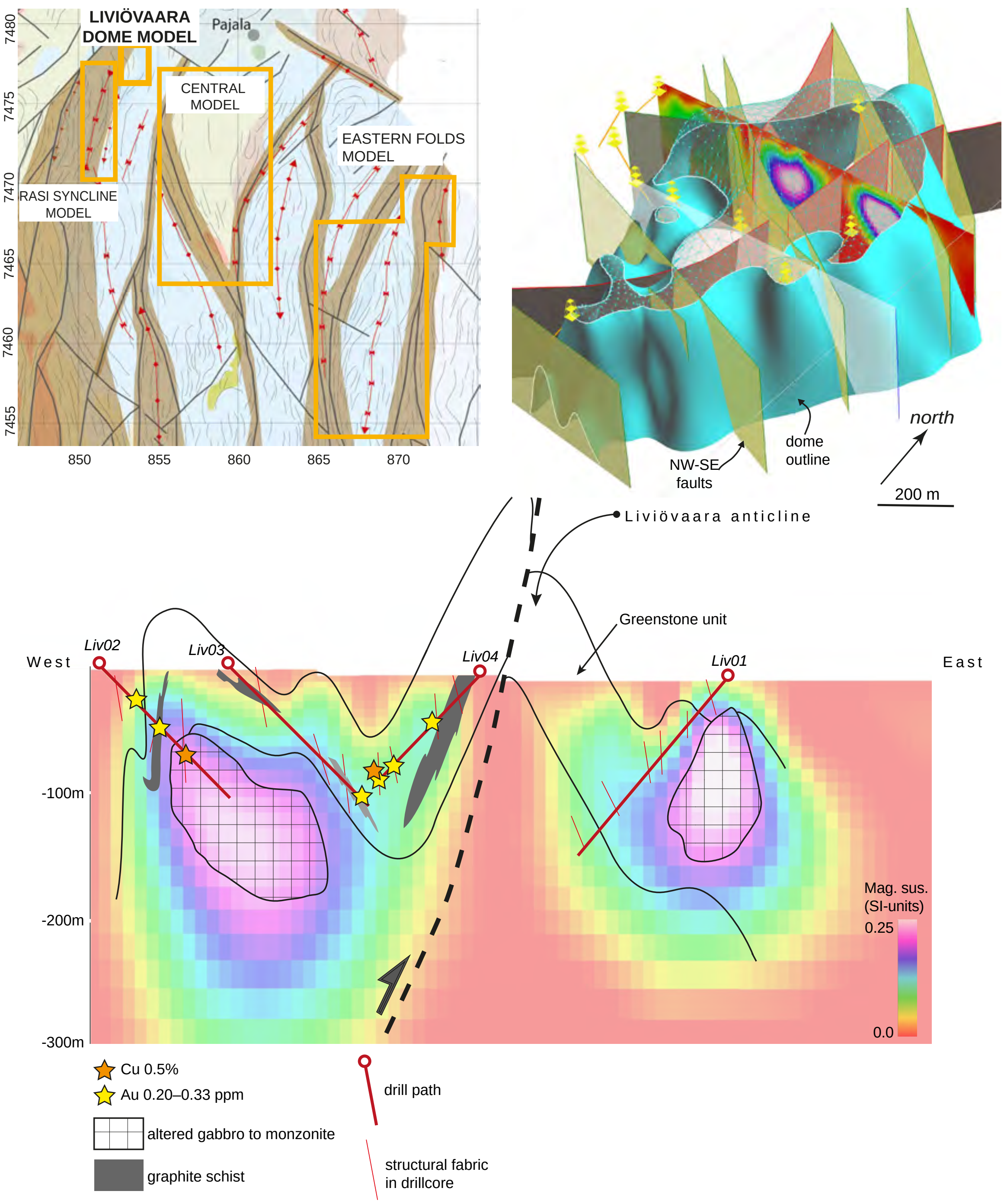

Figure 10. 3D local model of the Liviövaara dome (upper right). Interpreted cross-section through the dome, based on magnetic inversion modelling results and drill core data, is shown in the lower view.

types of ore were identified: 1) Cu-Au in altered rhyolites; 2) Cu-Au in altered limestone; and 3) Cu-(Ni-Au) in intrusive rocks (Gerdin et al. 1990).

The purpose of this model is twofold: to visualise in high-resolution local folding and faulting patterns in 3D, and to relate drill core data to the modelling results based on geophysical data. The model was constructed by the following steps: 1) Unconstrained inversion of ground magnetic data using VOXI. The cell size of each volume pixel (voxel) in the model is 10 × 10 m laterally and 5 m vertically; 2) import of inversion results, Lidar, drill holes, geophysical maps (ground magnetics and slingram) and lineaments into Gocad; 3) digitising of fault and fold outlines; 4) Creation of iso-surfaces surrounding domains with equal values for magnetic susceptibility derived from the inversion; 5) creation of a fault network constrained by map traces and iso-surfaces; and 6) interpretation of folding pattern based on magnetic inversion and drill core data.

The 3D model reveals a large antiformal dome, including several smaller sub-domes (Fig. 10). A NNE–SSW-striking deformation zone dipping steeply towards the west curves into the modelled area and offsets the antiform in a reverse sense. This deformation zone is displaced dextrally by a series of steeply dipping NW–SE-striking faults, which also accommodate a vertical slip component inferred from staircase stepping of the dome's map trace. Both the northern and southern boundaries of the dome are abrupt due to this late faulting. The high-magnetic bodies located on both fold limbs correlate with intrusive rocks, which were drilled only on the dome's western limb. The structural fabrics derived from drill cores consistently dip steeply to the east, which, together with the asymmetric parasitic fold located on the western limb, may suggest westward tectonic transportation.

Rasi syncline model

In the westernmost part of the PDB an elongated fold structure has been outlined (Fig. 11) and its deeper geometry investigated (see also Luth et al. 2015). Additional measurements have been carried out, and a refined model of the northern part of the fold is presented below, based primarily on new ground magnetic measurements. The total length of acquired ground magnetic measurements is approximately 20.5 km. In areas where ground measurements were lacking the model is based on magnetic anomaly data from airborne measurements, with a line separation of 200 m and point distance of approximately 35 m. A forward modelling procedure has been used. Other available data restricting the parameters have been used to limit the degree of freedom in creating the bodies. These data include structural measurements and laboratory measurement of the magnetic susceptibility and remnant magnetisation. In general, the bodies have a simple tabular geometry, assumed to represent elevated magnetic susceptibility layers embedded into a sequence of metasedimentary rocks. All bodies have been assigned an approximate depth extent of 500 m. For the sake of simplicity, the surrounding rocks are set to have a magnetic susceptibility value of zero. Physical properties of two samples collected from the magnetic layer were used to set further boundary conditions for the model (Fig. 11). In general, the magnetic horizons consist of two layers of higher magnetite content, but one and three layers are also observed in the data. The width of these layers varies between 4 and 40 m.

The resulting subsurface geometries of the strongly ellipsoidal Rasi syncline are shown in Figure 11. The fold appears entirely closed with the fold axis dipping towards the centre of the structure. In the northern half of the model, both folds limbs dip steeply to the east, whereas in the southern half the eastern limb dips steeply inwards to the west. The latter implies that the fold should be considered a doubly-plunging syncline, which is consistent with geological observations of cross-bedding, indicating stratigraphically younger rocks towards the centre of the fold.

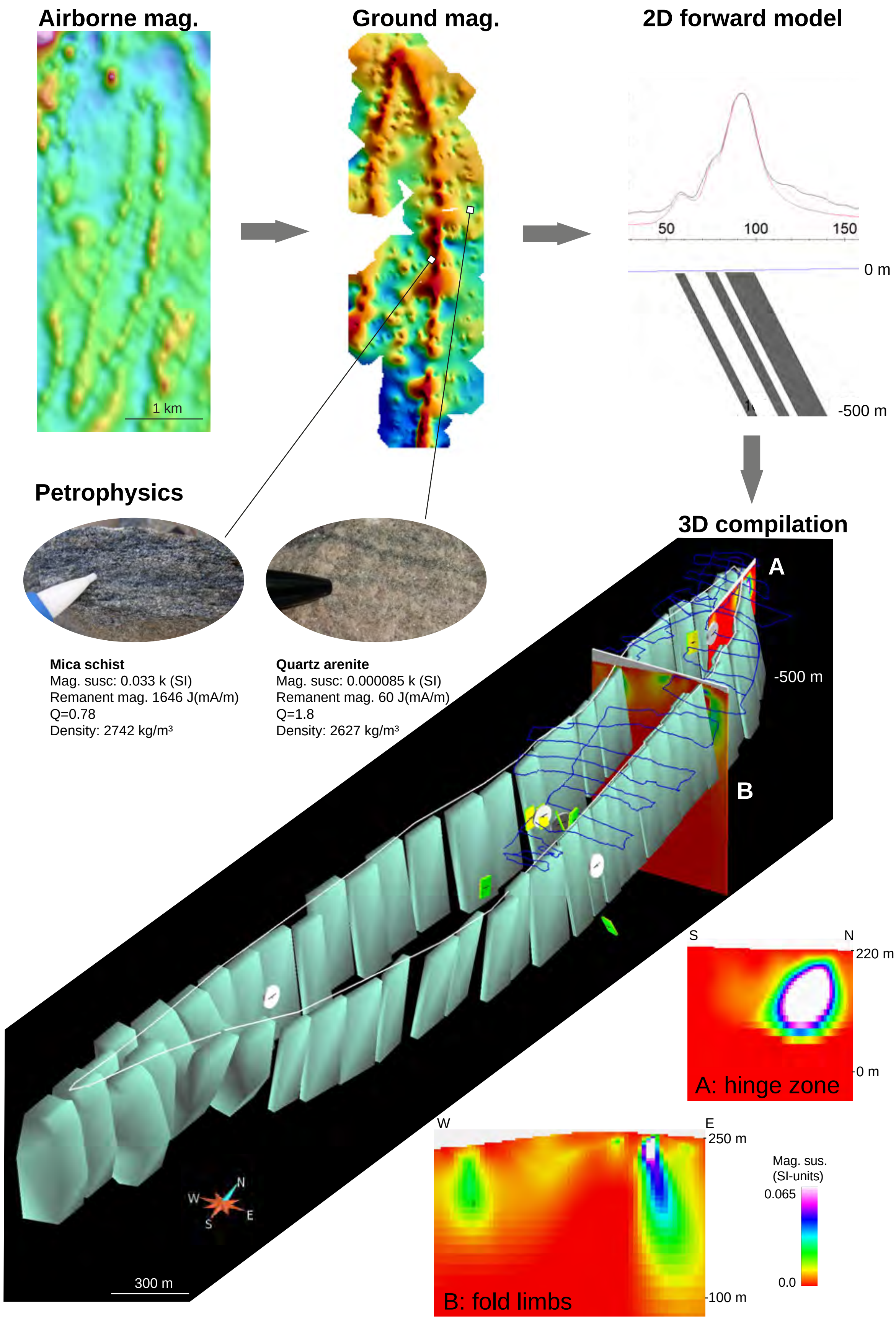

Figure 11. Construction chart of the 3D model of the Rasi syncline (see map insert in Fig. 10 for location). A combination of new ground magnetic data, sampling for physical rock properties and geological mapping was used to constrain the subsurface outline of the syncline.

DISCUSSION

On the origin of folds and domes

Earlier studies in the Pajala area postulated that major northwest–southeast-trending folds (F1) became refolded along north–south-trending F2 folds (Eriksson 1954, Padget 1977; see also Grigull et al., 2018). Following their interpretations, some of the smaller and larger dome patterns observed within the PDB in this study can be explained as the result of interference between NW–SE-orientated F1 folds and N–S-orientated F2 folds. Examples of some large-scale superimposed folds within the PDB may be represented by the modelled undulating surfaces underlying the eastern fold (see previous section and Fig. 8). In outcrop, superimposed folds were clearly observed along the Koijuvaara shear zone, marking the western border of the PDB (Fig. 4). In addition, heart-shaped patterns outlined on various scales (outcrop and 3D modelled surfaces) may also be considered the expression of F2 refolding F1. As such, the F1 axial planes may initially have dipped moderately to the southwest, whereas the superimposed F2 folds were more upright.

Another mechanism that could have produced the observed dome geometries, or "doubly-plunging-folds", within the PDB is vertical shearing or extrusion. Vertical extrusion is the upward flow of material, and can be promoted by intensive shortening of rock units bounded by more competent units along steeply dipping boundaries. Most of the domes and larger folds within the PDB are indeed associated with steeply dipping shear zones, which often form the contact between domains of intensively folded migmatite and domains of more massive, weakly deformed intrusive or volcanic rocks (Fig. 12). In addition, a predominant component of vertical shearing is inferred from shear indicators observed in outcrops and thin sections (Fig. 4). An important tectonic implication of assigning a role to vertical extrusion is that the domes observed within the PDB can be explained by a single shortening event and therefore may not necessarily be considered the result of F1-F2 fold interference.

4D tectonic evolution of the Pajala region

Based on new observations and insights obtained from the modelling results, we propose three distinct phases of shortening that explain most of the structural features observed within the PDB and its immediate surroundings (Fig. 13). Most of these structures, including the predominant foliation and metamorphic banding, formed as a result of NE–SW transpressive bulk shortening (D1). During this stage the PDB evolved into a N–S-striking transpressional ductile wedge bounded by major shear zones, such as the Koijuvaara shear zone to the west (Fig. 12). Shearing along the N–S-orientated shear zones was oblique, or may also have been partitioned into vertical and dextral components among the different shear zones. The folding pattern observed between the shear zones of the PDB most likely formed during D1 NE–SW transpressive bulk shortening. As such, NW–SE-trending folds (previously considered F1 by Eriksson (1954) and Padget (1977)), as well as N–S-orientated folds (previously considered F2) may both have resulted from strain partitioning operating on several scales. It has been shown by Tikoff and Peterson (1998), among others, that in transpression, folds may form obliquely to the tectonic transport direction at an angle of 40–50 °. In addition, rotation caused by non-coaxial strain within the PDB could have rotated some of the earlier formed NW–SE-trending folds into a N–S orientation (Figs. 12 and 13). With ongoing NE–SW transpression, the PDB may have finally reached a kinematic stage of full-strain partitioning between strike-slip in the central part (Migmatite domain) and reverse displacements, with folding and thrusting along the margins (Koijuvaara shear zone). This stage is the final distinct kinematic stage observed in analogue experiments on transpressive wedges presented by Leever et al. (2011). Large vertical displacement along steeply dipping major shear zones promoted vertical extrusion and the formation of several domes and doubly-plunging folds adjacent to the shear zones. With ongoing shortening and exhumation of the wedge, deformation became more localised along discrete shear zones, and NE–SW-striking Riedel shears were likely to form. In analogue experiments where the shortening direction is at an angle of

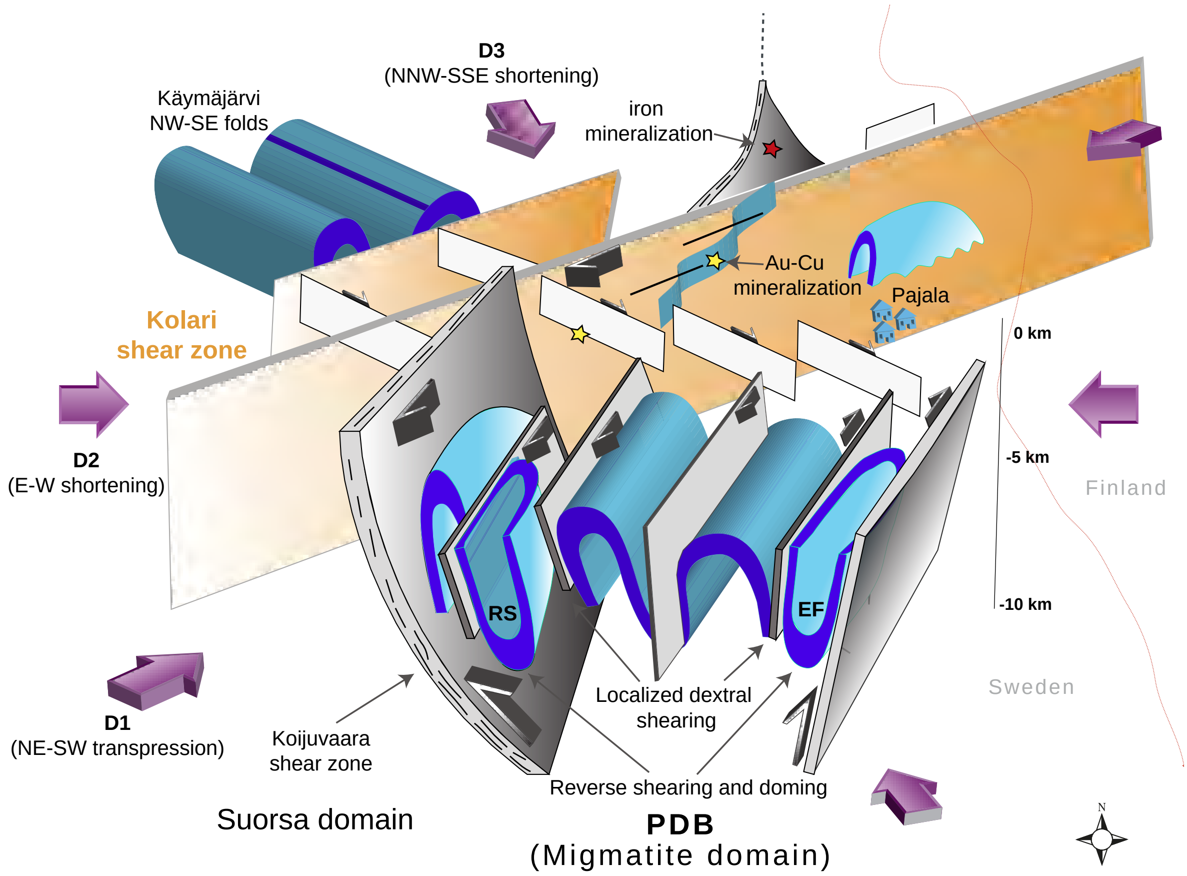

Figure 12. 3D conceptual model of the Pajala deformation belt (PDB) and the Kolari shear zone in the Pajala area (not to scale). The PDB is represented by a transpressional wedge outlined by major shear zones accommodating both vertical and dextral movements. Within the wedge, strain partitioning during D1 NE–SW shortening resulted in upright, cylindrical and non-cylindrical, N–S-trending folds, which became intersected by parallel striking, mainly dextral, shear zones. North of Pajala, the wedge is disrupted by the NE–SW-striking Kolari shear zone as well as by a set of en-echelon W-NW–E-SE-orientated faults and shear zones, formed during D2 E-W and D3 N-NW–S-SE crustal shortening, respectively (see also Fig.13). RS: Rasi syncline (Fig. 11), EF: Eastern folds (Fig. 8). Purple arrows indicate direction of regional shortening. The thin red line marks the national border between Sweden and Finland.

15 ° to the plate boundary, NE–SW-striking structures formed, mimicking the orientation of the shear zones observed in the Suorsa domain. It is therefore very possible that a precursor of the Kolari shear zone had already formed at this stage. The Kolari shear zone did not, however, develop into a major shear zone accommodating dextral displacements before stage D2 (E–W shortening), which finally resulted in an eastward offset of the entire PDB north of Pajala. Consequently, the Kolari shear zone should be treated as a separate shear zone system, rather than part of the PDB, as was proposed in earlier studies (e.g. Niiranen 2011). We suggest that during D2 E–W shortening the central Lapland granitoid complex located directly east of the PDB acted as a large rigid unit, along which deformation in the surrounding supracrustal rocks became localised, and structural features were reshaped towards parallelism along its contact (Fig. 13). E–W shortening was then primarily accommodated by reverse shearing, fold amplification and flattening. The larger folds eventually evolved into tectonic lenses, and deformation became localised along the limbs. A relatively high elongation (length/width ratio = 9/1) of the Rasi doubly-plunging fold may indicate that E–W flattening was most severe along the PDB's western border (Koijuvaara shear zone). Deformation finally became brittle during the last shortening stage D3 (N-NW–S-SE shortening). Conjugate faults, of which the WNW–ESE-orientated dextral faults are often the best developed, crosscut all other fabrics observed within and outside the PDB. At some localities, such as Liviövaara, the individual faults also accommodate tens of metres of vertical displacements, as inferred from a few brittle-ductile kinematic indicators.

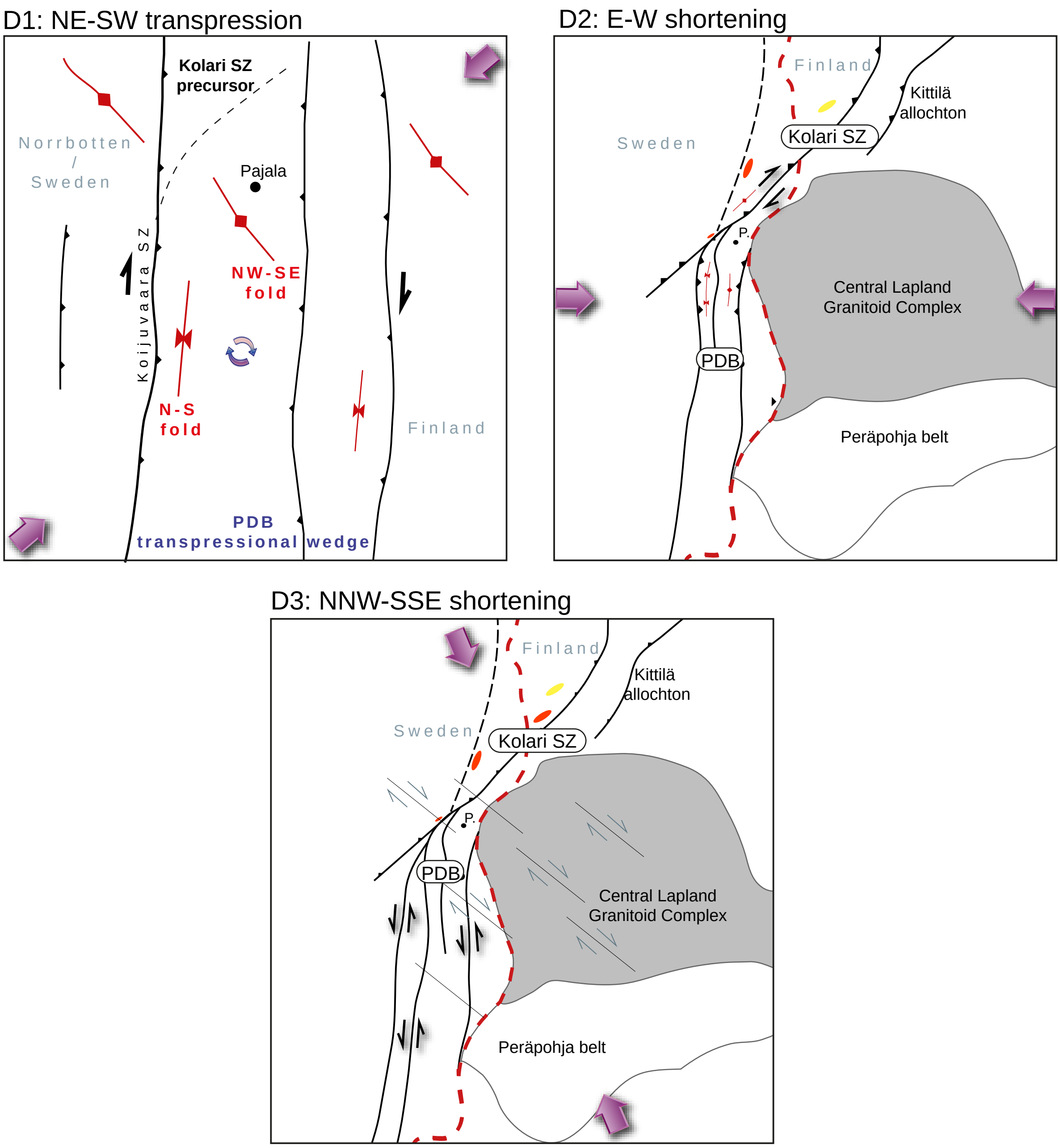

Figure 13. Map sketches of the three main deformation stages affecting the Pajala deformation belt (PDB) and the Kolari shear zone (Kolari SZ). Purple arrows indicate direction of crustal shortening. Red and yellow ellipsoids indicate Fe and Cu-Au deposits, respectively. Red dashed line indicate national border.

CONCLUSIONS

Structural geological mapping combined with 3D geological modelling in the Pajala area has provided insights into the complex deformation pattern associated with the Pajala deformation belt (PDB) and the Kolari shear zone. Several major shear zones related to the PDB were accurately mapped and their sense of shearing determined. Strike and dip measurements were then combined with subsurface geometries obtained from gravity and resistivity models. The overall interpretations reveal a wedge-shaped subsurface geometry for the Pajala Deformation Belt directly south of Pajala with steeply east-dipping shear zones along its western border (Koijuvaara shear zone) and steeply west-dipping shear zones towards the east. Mylonites associated with these shear zones record multi-reactivations, accommodating reverse, dextral, oblique and sinistral movements. The internal part of the wedge is folded, resulting in multiple ellipsoidal dome structures, often surrounded by a network of N–S-striking shear zones. The larger domes were possibly formed by interference of NW–SE-orientated F1 folds and N–S-orientated F2 folds, or resulted from vertical extrusion operating during a single deformation event. Fold interference patterns occur to the west of the PDB (e.g. Nunasvaara and Masugnsbyn areas; see Lynch et al., 2018, Grigull et al., 2018), forming large-scale, oblate or sub-circular dome-like structures. Within the PDB, however, most domes appear strongly elongated in a N–S direction, suggesting E–W flattening and possible vertical extrusion as important deformation mechanisms. Consequently, the PDB is interpreted as a 60 to 80 km wide transpressive wedge formed during NE–SW transpressive shortening (D1), followed by E–W shortening (D2). D2 eventually resulted in an eastward offset of the PDB along the NE–SW-striking Kolari Shear zone north of Pajala. These shear zones should therefore not be treated as part of the same shear systems. Time constraints on D2 are based on the relatively young metamorphic ages (1.8 Ga) recorded in the PDB in comparison with its surroundings (1.84 Ga). Folding of the metamorphic fabrics during D2 must therefore have occurred after 1.8 Ga. Finally, deformation by NNW–SSE shortening (D3) caused discrete faulting and sinistral brittle-ductile reactivation along the PDB's western boundary.

REFERENCES

Bergman, S., Kübler, L. & Martinsson, O., 2001: Description of regional geological and geophysical maps of northern Norrbotten County (east of the Caledonian orogen). *Sveriges geologiska undersökning Ba 56*, 110 pp.

Bergman, S., Billström, K., Persson, P.-O., Skiöld, T. & Evins, P., 2006: U-Pb age evidence for repeated Palaeoproterozoic metamorphism and deformation near the Pajala shear zone in the northern Fennoscandian shield. *GFF 128*, 7–20.

Berthelsen, A. & Marker, M., 1986: 1.9-1.8 Ga old strike-slip megashears in the Baltic Shield, and their plate tectonic implications. *Tectonophysics 128*, 163–181.

Eriksson, T., 1954: Pre-Cambrian geology of the Pajala district, northern Sweden. *Sveriges geologiska undersökning C 522,* 38 pp.

Gerdin, P., Johansson, L., Hansson, K.-E., Holmqvist, A. & Ottosson, D., 1990: Grafit-uppslagsgenerering i Norrbotten. *Unpublished report, SGAB PRAP 90068,* 77 pp.

Grigull, S., Berggren, R. & Jönsson, C., 2014: Summary report on the geological and geophysical characteristics of the Käymäjärvi-Ristimella key area. *Sveriges geologiska undersökning SGU-rapport 2014:30.*

Grigull, S. & Berggren, R., 2015: Geological and geophysical fieldwork in the Käymäjärvi-Ristimella key area. *SGU-rapport 2015:29.* Sveriges geologiska undersökning.

Grigull, S., Berggren, R., Jönberger, J., Jönsson, C., Hellström, F.A. & Luth, S., 2018: Folding observed in Palaeoproterozoic supracrustal rocks in northern Sweden. *In:* Bergman, S. (ed): Geology of the Northern Norrbotten ore province, northern Sweden. *Rapporter och Meddelanden 141,* Sveriges geologiska undersökning. This volume pp 205–257.

Johansson, L., 1985: Liviövaara, geofysisk tolkning, *SGAB Prospekteringsrapport PRAP 85092,* 3 pp.

Jonsson, E. & Kero, L., 2013: Beskrivning till berggrundskartorna 27M Korpilombolo NV, NO, SV, SO och 27N Svanstein NV, SV. *Sveriges geologiska undersökning K 391–394*, 20 pp.

Kärki, A., Laajoki, K. & Luukas, J., 1993: Major Palaeoproterozoic shear zones of the central Fennoscandian Shield. *Precambrian Research 64,* 207–223.

Ladenberger, A., Andersson, M., Smith, C. & Carlsson, M., 2018: Till geochemistry in northern Norrbotten – regional trends and local signature in the key areas. *In:* Bergman, S. (ed): Geology of the Northern Norrbotten ore province, northern Sweden. *Rapporter och Meddelanden 141,* Sveriges geologiska undersökning. This volume pp 401–428.

Lahtinen, R., Korja, A., & Nironen, M., 2005: Paleoproterozoic tectonic evolution. *Developments in Precambrian Geology*, *14*, 481–531.

Lahtinen, R., Huhma, H., Lahaye, Y., Jonsson, E., Manninen, T., Lauri, L.S., Bergman, S., Hellström, F., Niiranen, T. & Nironen, M., 2015: New geochronological and Sm–Nd constraints across the Pajala shear zone of northern Fennoscandia: Reactivation of a Paleoproterozoic suture. *Precambrian Research 256, 102–119.*

Leever, K., Gabrielsen, R., Sokoutis, D. & Willingshofer, E., 2011: The effect of convergence angle on the kinematic evolution of strain partitioning in transpressional brittle wedges: Insight from analog modelling and high-resolution digital image analysis. *Tectonics 30, TC2013, doi:10.1029/2010TC002823.*

Luth, S. & Jönsson, C., 2014: Barents Project 2014: Summary report on the geological and geophysical characteristics of the Liviöjärvi key area. *SGU-rapport 2014:29*, Sveriges geologiska undersökning. 34 pp.

Luth, S., Jönsson, C. & Jönberger, J., 2015: Barents Project 2014: Integrated geological and geophysical field studies in the Liviöjärvi key area, Pajala region. *SGU-rapport 2015:12*, Sveriges geologiska undersökning. 29 pp.

Lynch, E.P., Hellström, F.A., Huhma, H., Jönberger, J., Persson, P.-O. & Morris, G.A, 2018: Geology, lithostratigraphy and petrogenesis of c. 2.14 Ga greenstones in the Nunasvaara and Masugnsbyn areas, northernmost Sweden.*In:* Bergman, S. (ed): Geology of the Northern Norrbotten ore province, northern Sweden. *Rapporter och Meddelanden 141,* Sveriges geologiska undersökning. This volume pp 19–77.

Martinsson, O., 2004: Geology and metallogeny of the northern Norrbotten Fe-Cu-Au Province. *Society of Economic Geologists Guidebook Series 33, 131–148.*

Martinsson, O. & Wanhainen, C., 2013: The northern Norrbotten ore district. *In:* O. Martinsson & C. Wanhainen (eds.): Fe oxide and Cu-Au deposits in the northern Norrbotten ore district. Excursion guidebook SWE5, 12th Biennial SGA Meeting, Uppsala, Sweden, 19–28.

Martinsson, O., Bergman, S., Persson, P.-O., Schöberg, H., Billström, K. & Shumlyanskyy, L., 2018: Stratigraphy and ages of Palaeoproterozoic metavolcanic and metasedimentary rocks at Käymäjärvi, northern Sweden. *In:* Bergman, S. (ed): Geology of the Northern Norrbotten ore province, northern Sweden. *Rapporter och Meddelanden 141,* Sveriges geologiska undersökning. This volume pp 79–105.

Niiranen, T., Poutiainen, M. & Mänttäri, I., 2007: Geology, geochemistry, fluid inclusion characteristics, and U–Pb age studies on iron oxide–Cu–Au deposits in the Kolari region, northern Finland. *Ore Geology Reviews 30, 75–105.*

Niiranen, T., Nykänen V., Lahti, I. & Karinen, T., 2009: Geological interpretation of the upper crust along the FIRE 4A and 4B seismic profiles. *Geologian tutkimuskeskus, arkistoraportti, K 31.4/2009/78*

Niiranen, T., 2011: IOCG and Porphyry-Cu deposits in northern Finland and Sweden. *Excursion guide, 25th International Applied Geochemistry Symposium* 22-26 August 2011 Rovaniemi, Finland.

Nironen, M., 1997: The Svecofennian Orogen: a tectonic model. *Precambrian Research 86,* 21–44.

Padget, P., 1977: Beskrivning till berggrundskartbladen Pajala NV, NO, SV, SO. *Sveriges geologiska undersökning Af 21–24*, 73 pp.

Tikoff, B. & Peterson, K., 1998: Physical experiments of transpressional folding. *Journal of Structural Geology Vol. 20 nr. 6, 661–672.*

Väisänen, M., 2002: Structural features in the central Lapland greenstone belt, northern Finland. 20 s. *Geologian tutkimuskeskus, arkistoraportti, K 21.42/2002/3.*

Authors, paper 8:
Stefan Luth
Geological Survey of Sweden,
Department of Mineral Resources,
Uppsala, Sweden

Johan Jönberger
Geological Survey of Sweden,
Department of Mineral Resources,
Uppsala, Sweden

Susanne Grigull
Geological Survey of Sweden,
Department of Physical Planning,
Uppsala, Sweden

8. The Vakko and Kovo greenstone belts north of Kiruna: Integrating structural geological mapping and geophysical modelling

Stefan Luth, Johan Jönberger & Susanne Grigull

ABSTRACT

A geological structural framework has been constructed for the early Palaeoproterozoic Vakko and Kovo greenstone belts, located north of Kiruna. The framework is based on a new structural geological map and a series of NW–SE-oriented profiles that show a series of N–S-striking folds and shear zones. These structures are correlated with subsurface interpretations derived from models based on gravity, magnetic and petrophysical data. The resulting model reveals a shallow to moderate southeastward-dipping Archaean basement below metasupracrustal units. Predominantly steeply eastward-dipping shear zones bound and intersect the basement and the overlying units. A variety of shear sense indicators record formation and deformation of the belts by E–W crustal extension followed by NE–SW to E–W-directed crustal shortening, respectively. As such, the parallel-striking Vakko and Kovo belts, whose stratigraphy is almost identical, may initially have formed as separate basins or may represent a tectonic repetition. A rapid southward deepening of the Archaean basement from 2 to 3 km is apparent from the southernmost profiles. NW–SE-trending fault systems possibly accommodate part of the vertical movements causing basement deepening, but more geological and geophysical investigations are needed to confirm this hypothesis.

INTRODUCTION

Just north of Kiruna, the Vakko and Kovo belts consist of two narrow, N–S-trending greenstone belts predominantly comprising early Palaeoproterozoic sedimentary and volcanic rocks (Fig. 1). The belts are bounded by the Råstojaure Archaean basement complex to the west and north, whereas the eastern border of the Kovo belt is a contact with an oval granitic pluton intruding into the supracrustal rocks. All the rocks have been deformed and metamorphosed under low to medium-grade conditions (e.g. Bergman et al. 2001). Earlier mapping projects have assigned differing tectonic interpretations based on the observed deformational features within the belts. Vollmer et al. (1984) associated the bulk deformation with the emplacement of granitic bodies, whereas Wright (1988) and Talbot & Koyi (1995) assigned a major role to regional-scale thrusting and the formation of duplexes. More recently, Bergman et al. (2001) included the Kovo belt as a segment of the crustal-scale Kiruna–Naimakka deforma-

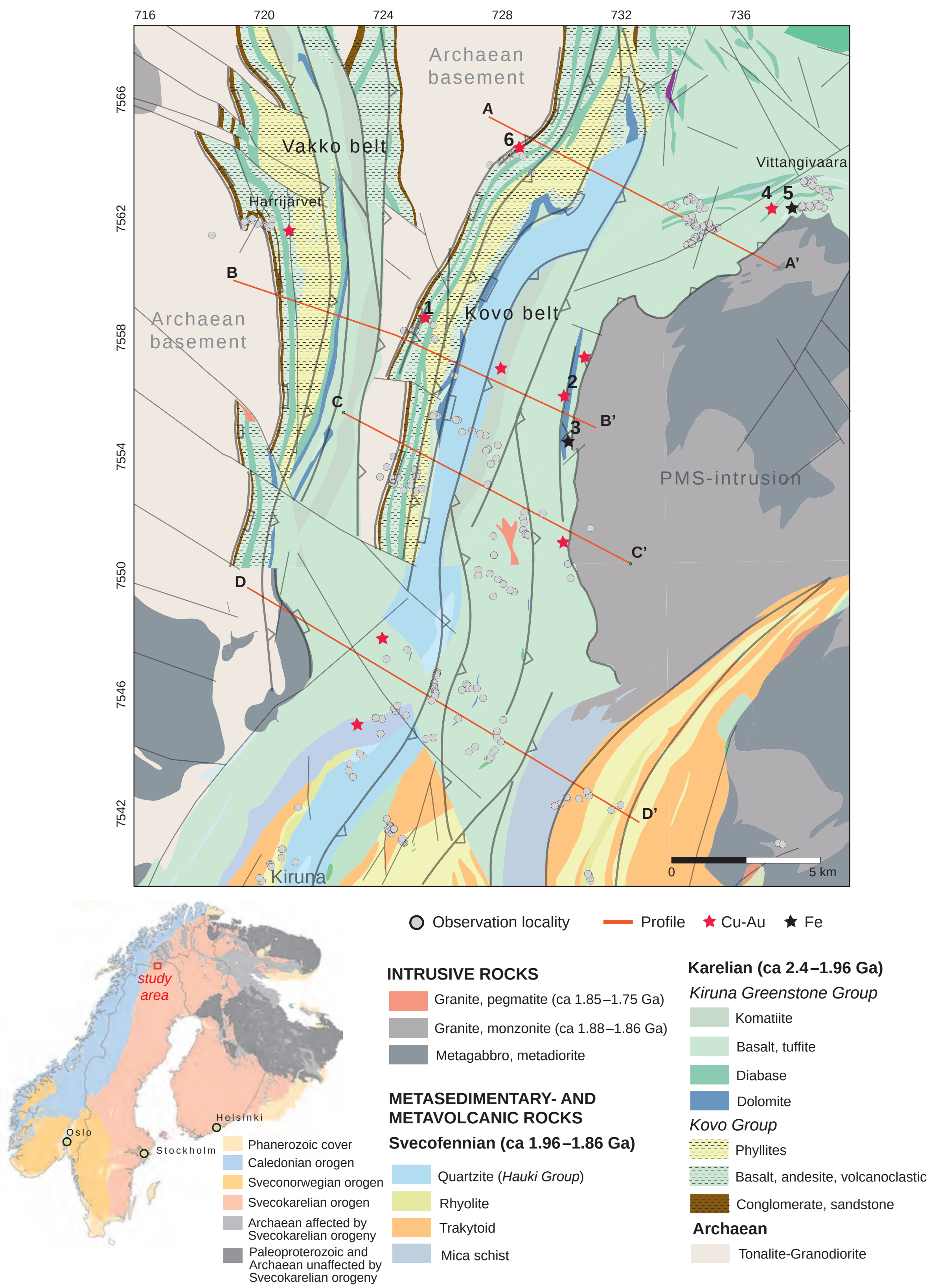

Figure 1. Geological map of the Vakko and Kovo belts. Lithological boundaries and structural features are modified after Martinsson (1999). Indicated profiles are shown in Figure 7. Structural elements are explained in the legend for Figure 3. Numbers refer to abandoned mines, trial pits or mineralised outcrops discussed in the text: 1: Kovogruvan, 2: Linkaluoppal, 3: Tjärro, 4: Mount Vittangivaara, 5: ORED00329, 6: Kruuvivaara. Insert map shows the main geological domains of the Fennoscandian shield.

tion zone, which accommodated dextral strike-slip movements. However, the amount of structural data obtained in these published studies is limited, rendering the above interpretations of deformation history ambiguous. On the most recent regional geological map of the area (Martinsson 1999), the extent and attitude of rock unit boundaries and shear zones were primarily derived from geophysical data, with very few constraints on deformation style and relative movements. No reliable constraints can be derived from the 3D geometry of the belt, and correlation with the Kiruna area further south is not straightforward (see Grigull et al., 2018). The latter is of major interest considering the crustal-scale structures observed in reflection seismic and audiomagnetotellurics (AMT) studies recently published by Holmgren (2013) and Bastani et al. (2015). In this study we present a new structural map of the Vakko and Kovo belts, which is the result of structural field mapping, thin-section analysis and (re)interpretation of existing and new geophysical data. Geological interpretations of 2D geophysical profiles were constructed along four lines transecting both belts and adjacent units. The results were used to interpret the 3D internal geometry of the Vakko and Kovo belts and the depth of the underlying Archaean basement. The chapter concludes with a brief discussion of regional deformation history in the context of this new information, as well as a correlation of subsurface structures with the Kiruna area.

GEOLOGICAL SETTING

The Vakko and Kovo belts comprise late Archaean to early Palaeoproterozoic metasedimentary rocks, described by Geijer (1927, 1931), Ödman (1957) and later by Martinsson (1999) and Kumpulainen (2000, 2003). A review of those earlier studies is presented in Luth & Antal Lundin (2013) and is briefly summarised below.

Archaean basement

The oldest rocks in the region form part of the Råstojaure complex, primarily consisting of 2.8 Ga-old, moderately-foliated metatonalite to metagranodiorite (Welin et al. 1971, Skiöld 1979, Martinsson et al. 1999). Biotite gneiss, reddish metagranite, metavolcanic rocks and quartzite also occur in significant quantities. However, the distribution and age of these lithologies are poorly constrained.

Kovo group

The Kovo group overlies the Archaean basement and consists of metamorphosed volcanic and sedimentary rocks subdivided into two formations. The Rautojaure formation (Martinsson 1999, Vakko unit in Kumpulainen 2000) consists of an up to 200 m thick package of metaconglomerate, containing a variety of clasts between 0.5 and 20 cm in diameter. Stream current indicators are locally well preserved in the pebble-poor interlayers of quartzite and metaarkose, indicating alluvial and fluvial deposits sourced from the Archaean terrain in the west (Kumpulainen 2000). The main part of the Kovo group consists of the 1 to 2-km-thick Harrejaure formation (Martinsson 1999), comprising volcaniclastic metasedimentary rocks interlayered with meta-tholeiitic basalt. The lavas can reach a thickness up to 200 m and often contain amygdules, commonly filled with quartz or carbonate. The interbedded layers of metavolcaniclastic rocks consist of metavolcanic siltstones and tuffites, including sizeable feldspar and quartz grains in a matrix also containing carbonate. In the Kovo belt, the upper 300–500 m (Harrejaure formation in Martinsson 1999) consists of a phyllitic unit, characterised by well-developed schistosity. The Rautojaure and Harrejaure formations are separated by an albite-bearing metadolerite dated at 2.2 Ga (Skiöld 1986), considered to be the minimum age of the Kovo group.

Kiruna greenstone group

The Kovo group is overlain by the Kiruna greenstone group (KGG), described in detail in the Kiruna region by Martinsson (1997). The predominant rock types are mafic to ultramafic metavolcanic rocks, probably formed during a phase of intensive rifting (e.g. Kumpulainen 2000). Martinsson (1997) subdivided the Kiruna greenstone group into six formations, primarily based on differences in lithology or chemistry (Table 1). For a more detailed description the reader is referred to Martinsson (1997, 1999).

The stratigraphic sequence of the upper three formations is well exposed at Mount Vittangivaara (Fig. 1), predominantly comprising greenstone facies effusive pillow basalts, fine-grained lavas and tuffaceous rocks. Locally, the volcanic sequence alternates between metasedimentary rocks of various types, e.g. impure carbonaceous skarn to pure dolomite marble, graphite-bearing sedimentary rocks and quartz-rich schists. Quartz-banded iron-rich layers are found between pillow lava beds and between beds of massive (meta)basalt. The thin beds have an iron content of approximately 30–33 per cent and consist mainly of magnetite and hematite in equal amounts. The banded iron-rich sedimentary rocks are strongly recrystallised and alternate with thin garnet (andradite)-bearing layers.

The Kiruna greenstone group is overlain by the Kurravaara conglomerate, consisting of a basal conglomerate overlain by intermediate metavolcanic rocks. This formation is mainly exposed to the south in the Kiruna region and is described in more detail in Grigull et al. (2018).

Hauki quartzite

The youngest supracrustal unit exposed in the area is Hauki quartzite, consisting of cross-bedded feldspar metaarenite, intercalations of metasedimentary breccia and conglomerates mostly at the base of the unit. An erosional unconformity separates Hauki quartzite from the underlying Kiirunavaara group (Grigull et al., 2018). Witschard (1984) shows that the contact with the underlying rocks is often tectonic and proposes deposition of Hauki sediments in small, tectonically active grabens.

Alteration, iron, copper and gold mineralisations

Several kinds of alteration have affected the rocks of the Kovo and Vakko belts. Along shear and fault zones, extensive albite and ankerite alteration appears locally, while quartz and carbonate dykes and breccias may contain chalcopyrite. Scapolite appears as porphyroblasts in the Kiruna greenstones along the eastern border of the Kovo belt, but also occasionally in low-grade metamorphic mafic intrusions and dolerites. Epidotisation of amygdule-rich basalts is common in the Kovo belt, particularly in the lower part of the Kiruna greenstone group.

Mineralisations of copper and iron in particular have been found in the Vakko and Kovo belts (Fig. 1) but currently have no economic value. Some abandoned quarries can be found, dating back to the 16th–17th centuries, e.g. "Kovogruvan" (ORED00295), where the mineralisation consists of small concentrations of chalcopyrite, pyrite and barite in quartz veins. The veins occur in albite-bearing metadolerite and are associated with faulting in the lower part of the Kovo group. Most of the miner-

Table 1. Formations of the Kiruna greenstone group after Martinsson (1997). Youngest formation at the top.

Formation	Dominant lithology	Thickness range or maximum thickness
Linkaluoppal	Tholeiitic volcaniclastics, with layers of graphite schists, magnetite skarn, and dolomite (up to 50 m)	> 50 m
Peuravaara	Tholeiitic pillow basalts	500–1500 m
Viscaria	Basaltic tuff and thin layers of graphite schist	600 m
Pikse	Tholeiitic basalt	500–1000 m
Ädnamvare	Peridotitic and basaltic komatiite	500 m
Såkevaratjah	Dolomite (up to 200 m) and basaltic lava	200–400 m

alisations were discovered by prospecting carried out in the 1970s. The highest concentrations of copper (1.23%, Godin et al. 1979) were found at Linkaluoppal (ORED00900), and are associated with a skarn-altered metadolerite-intruding dolomitic marble, characteristic of the upper parts of the Linkaluoppal formation. The dolomitic marble has been locally altered to a skarn and contains high concentrations of barite. To the south of Linkaluoppal, iron mineralisation at Tjärro (ORED00112) was found by drilling, following geophysical measurements, and occurs as accumulations of magnetite within skarn-altered, biotite-rich tuffs of the Kiruna greenstone group. The mineralisation is the cause of a high magnetic anomaly that can be followed in magnetic survey data along a trace of approximately 9 km. The map trace of this magnetic anomaly reveals a tight syncline wrapping along the boundary, between the eastern border of the Kovo belt and the quartz-monzonite intrusion belonging to the Perthite monzonite suite (PMS) to the east.

Immediately northeast of Mount Vittangivaara a sulphide deposit was discovered based on drilling by Redmond, a prospecting company, in 1998 (ORED15581) (Fig. 1). The drill cores reveal several accumulations of pyrite, pyrrhotite and chalcopyrite associated with skarn-altered metapelites. Concentrations of copper within these 2–5-metre-intervals never exceed 2%. The iron deposit ORED00329 on Mount Vittangivaara is described by Folcker (1974) as a thin layer of altered tuff, containing the iron-rich minerals ilmenite, hematite and goethite. The graphite-bearing metapelites and schists in the area are generally fine-grained and have only a low graphite content.

Deformation and metamorphism

Earlier studies interpret the Vakko and Kovo belts as a series of synformal structures separated by shear zones (e.g. Martinsson et al. 1999). Axial planes generally trend in a north–south direction, with gently south-plunging fold axes. The area is affected by several major shear zones trending parallel to lithological contacts. The rocks in these zones display pervasive foliation and are often mylonitic. Several brittle faults have been identified, mainly interpreted from airborne magnetic data, displacing the N–S trending anomalies and appearing as linear low magnetic anomalies. Metamorphic grade varies between upper greenschist facies and lower amphibolite facies (Bergman et al. 2001). The central parts of the Kovo and Vakko belts are characterised by a relatively low metamorphic grade, which increases into the amphibolite facies along the eastern boundary of the Kovo belt with the PMS intrusions. Contact metamorphism resulted in the formation of garnet porphyroblasts within the mafic tuffs of the KGG (Martinsson et al. 1999).

GEOPHYSICAL SURVEYS

Gravity, airborne magnetic and electromagnetic (slingram) data on the Vakko and Kovo belts are presented in Figure 2. Several airborne geophysical campaigns have been carried out over the area. SGU measured the airborne total magnetic field in the early 1960s and LKAB carried out airborne measurements between 1973 and 1985, when total magnetic field, gamma radiation and electromagnetic field (both VLF and slingram) data were acquired. In addition, several ground geophysical surveys have been conducted in different parts of the area, in which magnetic or electromagnetic information has been acquired and petrophysical samples collected (Fig. 2A–B, Table 2). More information on these earlier ground geophysical surveys is presented in Luth & Antal Lundin (2013). In 2013 Bell Geospace Ltd. conducted an airborne fixed-wing campaign to collect magnetic field and gravity gradiometer FTG (Full Tensor Gradient) data over a large area of northern Sweden, including the central and northern part of the Vakko and Kovo belts. This survey was conducted at an altitude of 100–300 m, along east–west flight lines with 500 m line separation. Perpendicular tie-lines were made with a spacing of 5 km. Also in 2013 the same area was the subject of an airborne TEM (time domain electromagnetic) survey by Geotech Ltd. These measurements were made by a helicopter-based system with

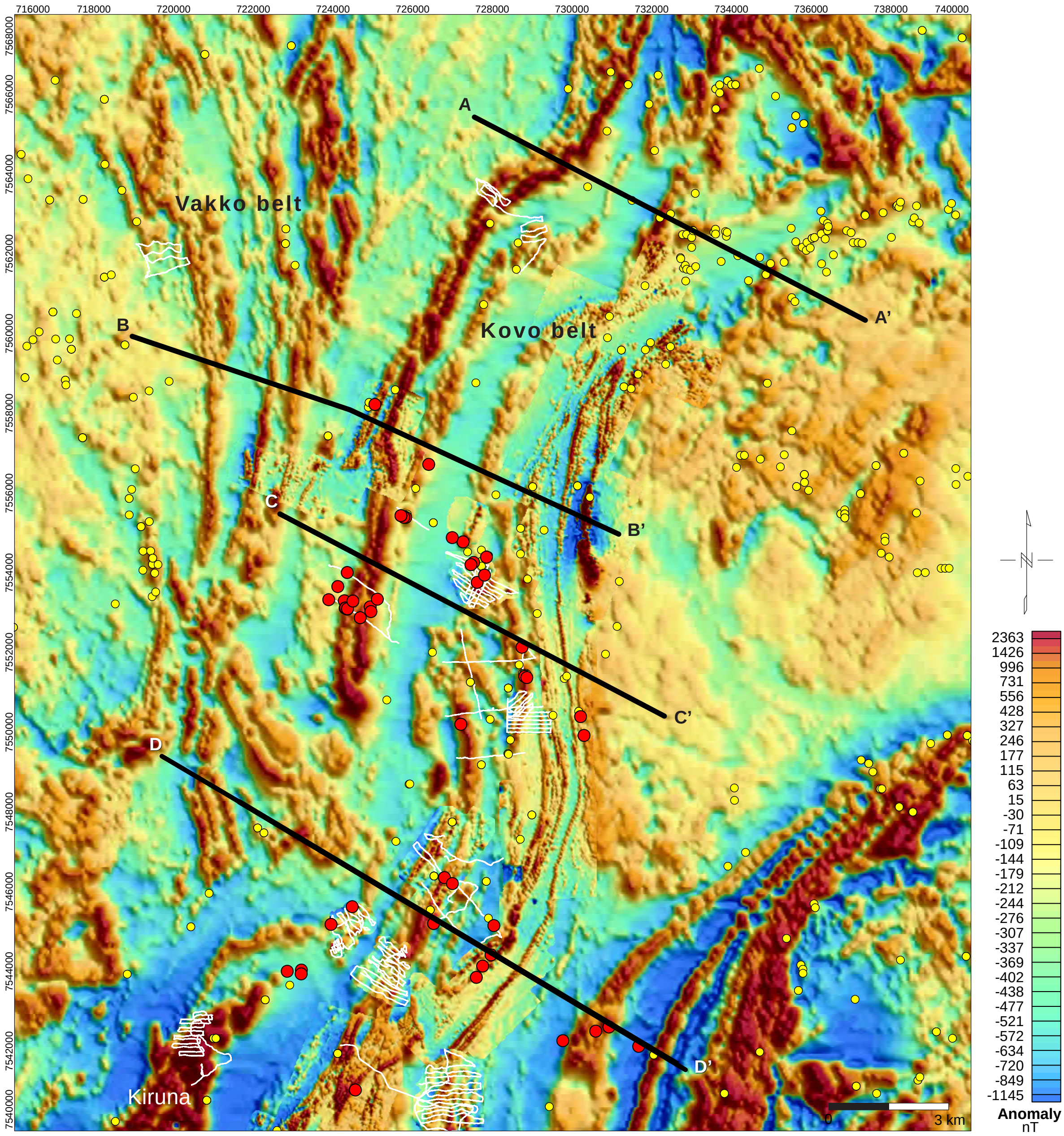

Figure 2A. Magnetic anomaly map of the Vakko and Kovo belts and adjacent areas. The magnetic data from the airborne campaigns are overlain by earlier ground magnetic surveys. Older petrophysical sample localities are displayed as yellow dots; those acquired in this project are marked with red dots. White lines represent ground magnetic profiles conducted within this project and the black lines outline the regional interpretation profiles.

the transmitter/receiver loops 56 m above the ground. The magnetic field was also measured, and the survey was carried out along east–west flight lines with 500 m line separation.

Geophysical characterisation

In the west, the Archaean basement (Råstojaure complex) is mainly composed of metamorphosed granitic to granodioritic rocks. On the magnetic anomaly map it appears as a relatively homogenous low-magnetic unit, and as a gravity low in the FTG data (Figs. 2A–B). Petrophysical samples have an average density of 2 667 kg/m^3 (n = 17). The contact with the adjacent Vakko belt has been investi-

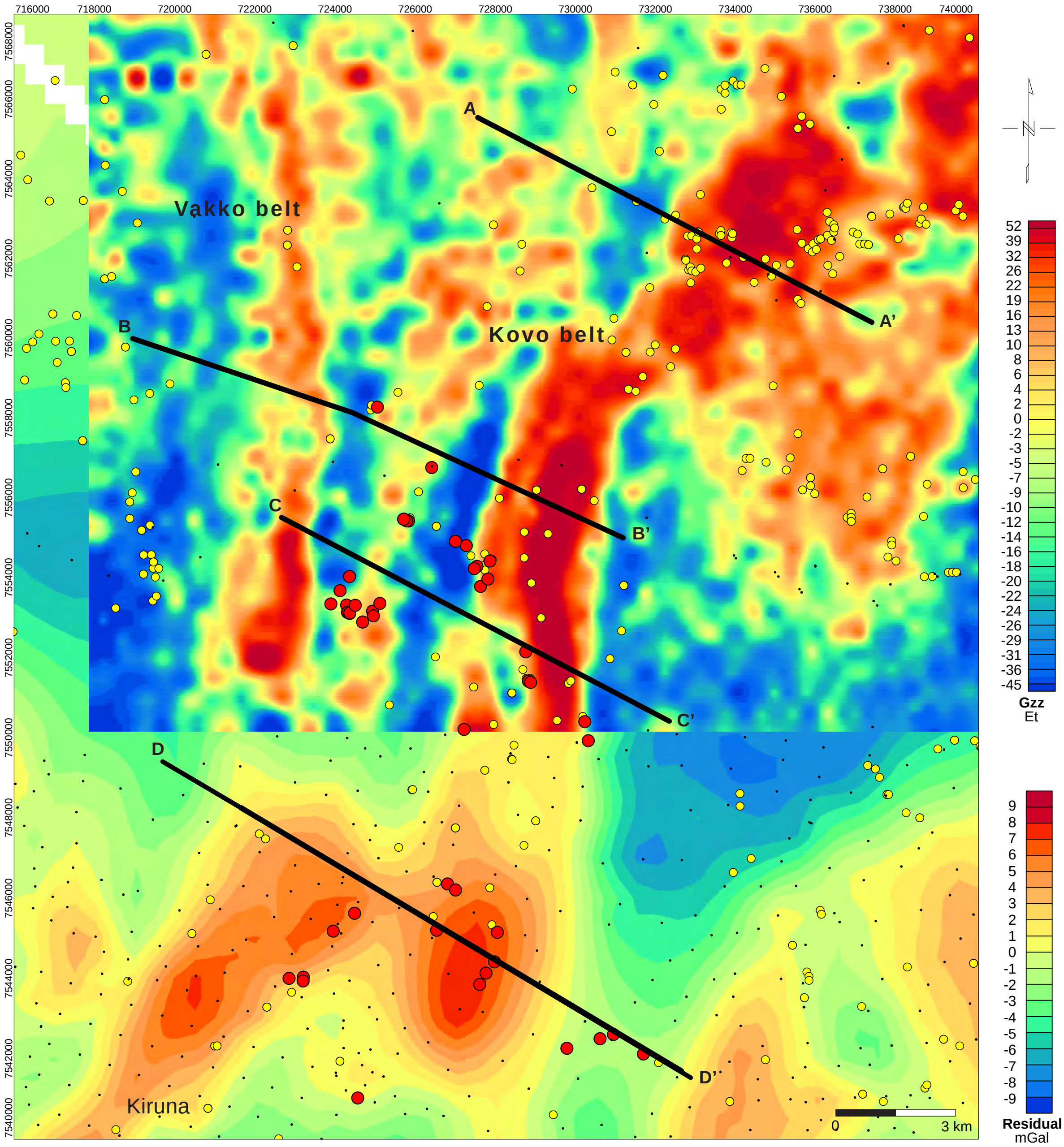

Figure 2B. Gravity anomaly map of the Vakko and Kovo belts and adjacent areas. Gravity data on the south of the area are based on ground measurements; in the north they are based on airborne FTG measurements. Black dots show the location of pre-existing ground gravity measurements. Older petrophysical sample localities are displayed as yellow dots; the red dots show the location for samples acquired in this project. The black lines outline the regional interpretation profiles.

gated by ground magnetic measurements. The Vakko belt mainly consists of metabasites, which explains the high magnetic anomalies (Fig. 2A). Petrophysical samples have densities between 2 850 and 2 950 kg/m^3 but there is no profound positive gravity anomaly over the western part of the Vakko belt, indicating a relatively moderate depth extent of the denser rocks. However, a strong positive gravity anomaly is present over the eastern part of the Vakko belt, especially over the southernmost part, where an ultramafic volcanic rock is present. East of the Vakko belt is an Archaean basement high, which separates the Vakko belt from the Kovo belt. The Kovo belt is predominantly mafic metavolcanic rock and metadolerite, which the gravity data suggest only extends to a shallow depth. In the centre of the Kovo belt is an area of Hauki quartzite, seen on the FTG map as an elongated gravity low. Analysed

Table 2. Density and magnetic properties of the petrophysical samples from the main lithological units in the Kovozone area and its closest surroundings.

Rock type	No. of samples	Density (SI) Mean	Density (SI) Std. dev.	Susceptibility x 10^{-5} (SI) min	Susceptibility x 10^{-5} (SI) max	Susceptibility x 10^{-5} (SI) median	Q-value min	Q-value max	Q-value median
Rhyolite	10	2643	32	18	1173	271	0.14	23.76	0.36
Dacite-rhyolite	3	2719	17	3570	9011	5580	0.07	3.50	0.35
Basalt-andesite	195	2951	101	4	173300	109	0.02	81.46	0.37
Mafic rock	7	2896	47	22	5358	99	0.04	2.37	0.38
Granite	32	2618	22	5	4284	664	0.08	4.71	0.31
Tonalite-granodiorite	35	2712	36	0	14230	74	0.05	3.12	0.28
Syenite	10	2639	45	23	15851	2500	0.10	1.77	0.25
Gabbro-diorite	39	2906	48	70	18560	5138	0.14	5.48	0.90
Dolerite	34	2958	123	61	32060	6111	0.08	82.45	0.45
Conglomerate	7	2693	117	3	80	51	0.29	22.07	2.07
Quartzite	20	2644	48	1	94	6	0.29	11.99	1.12
Phyllite	9	2724	66	12	5444	20	0.32	9.32	1.83
Schist	5	2730	51	14	2001	49	0.17	1.27	0.86

petrophysical samples (n = 20) show the quartzite has a relatively low density, averaging 2 644 kg/m^3. The quartzite has a low content of magnetic minerals, reflected in a median susceptibility value of 6×10^{-5} SI units. As such, the quartzite can be followed on the magnetic anomaly map as a magnetic low. East of the quartzite, the mafic metavolcanic rocks of the KGG stand out on the gravity map as a positive anomaly, indicating, in combination with constraints derived from petrophysical measurements, that the unit has a substantial depth extent, in contrast to the "shallower" western part of the zone (see also the section *Construction of geophysical profiles*). A series of high and low magnetic anomalies within the KKG reveals a tight, N–S-striking folding pattern in the easternmost part of the Kovo belt. Strong variations in magnetic properties within the KKG are also evident in the analysed petrophysical samples (Fig. 2C, Table 2). Further north, in the Mount Vittangivaara area, a significant positive gravity anomaly correlates well with a low magnetic anomaly. Ten petrophysical samples from outcrops within this anomaly have an average density and susceptibility of 2 980 kg/m^3 and 80×10^{-5} SI units, respectively. The lithologies dominating this area are mafic metavolcanic rocks and metadolerite. Furthest to the east, the PMS intrusion adjacent to the Kovo belt has a low density, with an average of 2 613 kg/m^3 (n = 14). But the presence of metagabbro in the northern part of the intrusion gives rise to a positive gravity anomaly and a slightly higher magnetic anomaly.

Construction of geophysical profiles

The geophysical survey conducted for this study has focused on better constraining the structural and lithological relationships at a number of key locations (Fig. 2A). The resulting datasets include ground-based total field magnetic and electromagnetic profiles, along with measurements of the physical properties of most lithologies. These datasets, together with the airborne magnetic, FTG data or ground gravity data were then used to construct 2D geophysical subsurface models along 4 NW–SE-striking profiles. The profiles are the result of 2D modelling of geophysical potential field data (airborne or ground magnetic and gravity data). The three most northerly profiles shown in Figures 2A–C are located in an area that was part of a FTG survey conducted by Bell Geospace in 2013. The FTG survey was carried out at an altitude of 100–300 m, along east–west flight lines with an internal spacing of 500 m. Although magnetic field was also measured, the data used in the models originate from the SGU airborne survey, since that was conducted at an altitude of 30 m, the lower altitude giving considerably more information. "Potent" modelling software was used to construct these models. Background properties in the models were set at 2 700 kg/m^3 for density and 100×10^{-5} SI units for magnetic

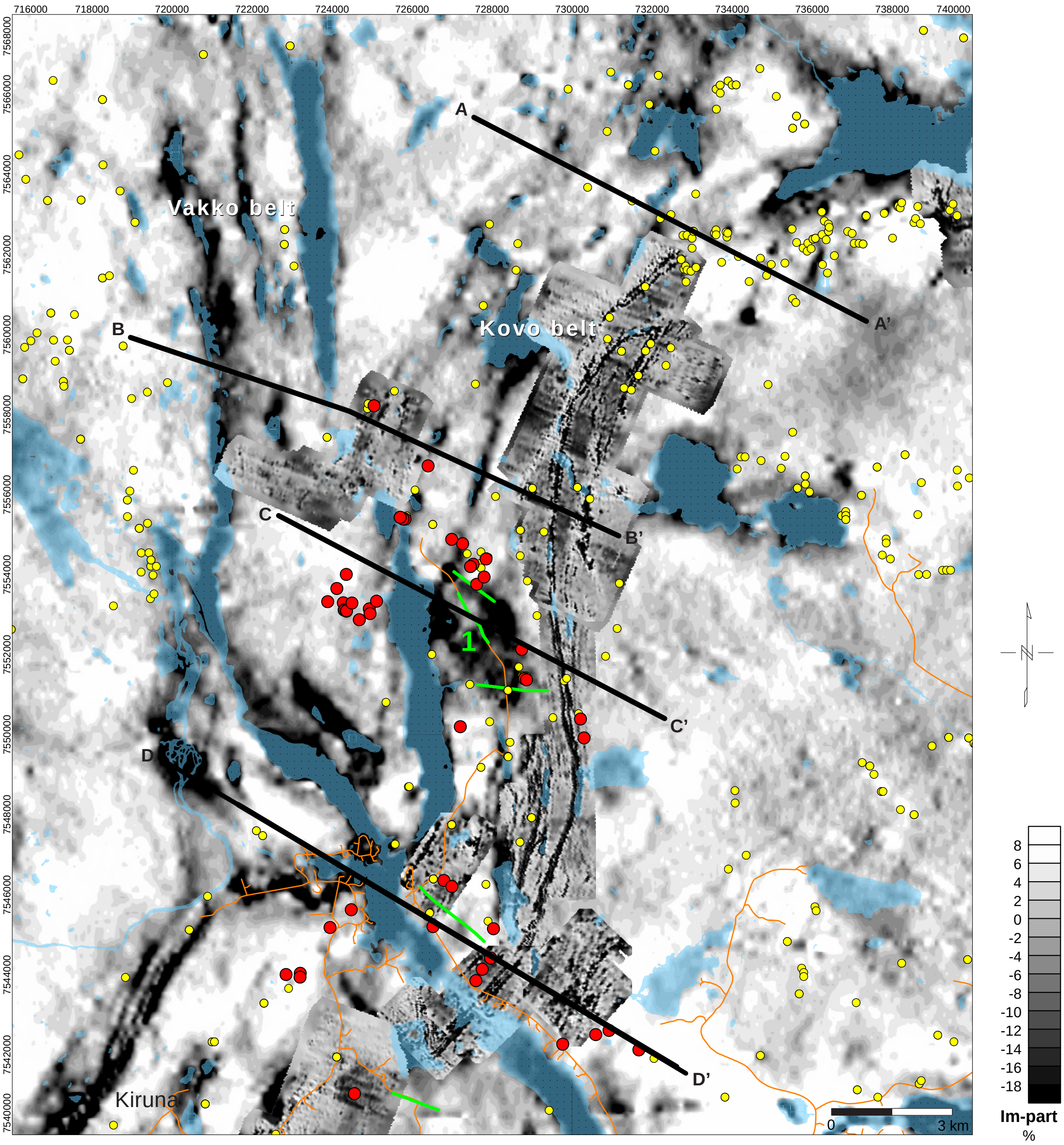

Figure 2C. Airborne slingram map of the Kovo and Vakko belts and adjacent areas. Older petrophysical sample localities are displayed as yellow dots; the red dots show the location for samples acquired in this project. Green lines show the location of ground profiles using a VLF instrument under this project, and the black lines outline the modelled profiles.

susceptibility. The magnetic and gravity data were used to constrain the depth extent of the various lithologies traversed by the profiles. The results from ground measurements using a magnetometer or VLF instrument carried out for this study were adopted in the modelling work. Densities and magnetic properties obtained from petrophysical samples and in situ measurements of magnetic susceptibilities on outcrops provided additional constraints on the modelled geometries (Fig. 2D).

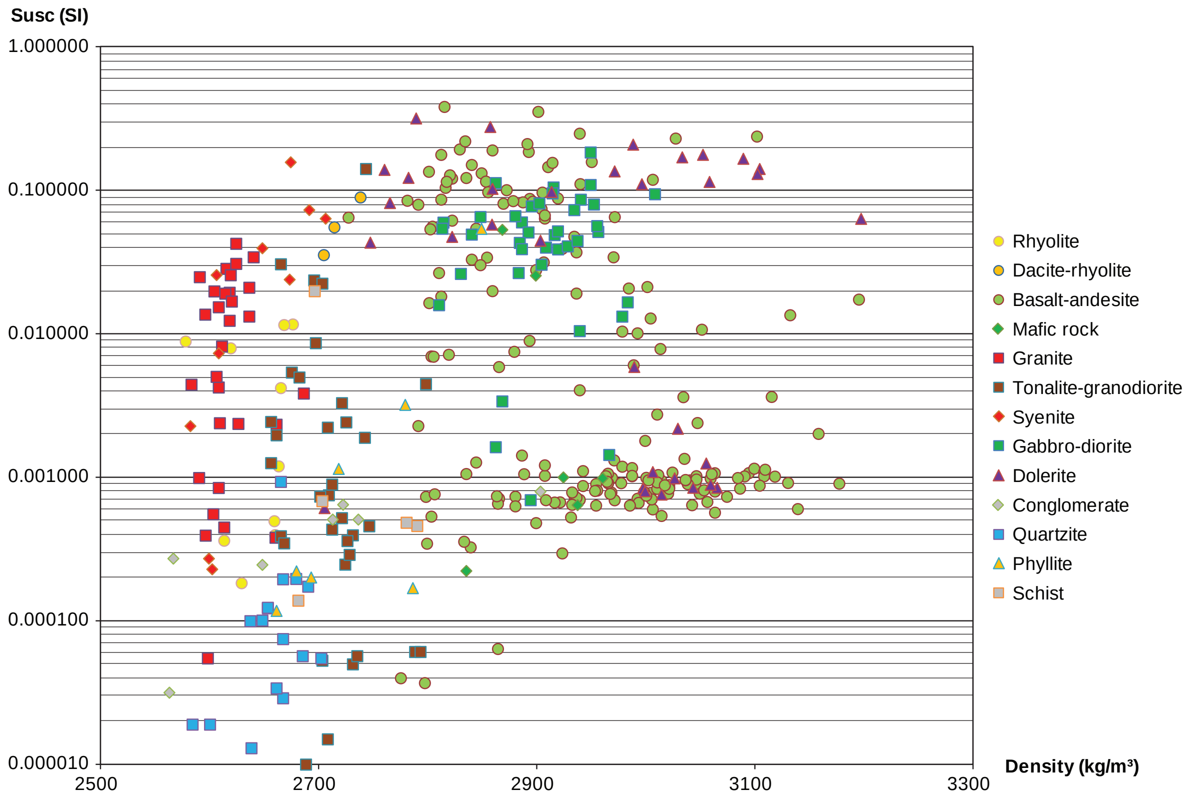

Figure 2D. Magnetic susceptibility vs. density of the petrophysical samples from the main lithological units in the Kovo belt and its immediate surroundings.

RESULTS

New structural geology map

The large-scale structural pattern of the Vakko and Kovo belts is highlighted in the new structural geology map (Fig. 3). Form lines were primarily derived from the airborne magnetic and electromagnetic anomaly maps and represent continuous lithological horizons or deformational features. Traces of the major shear zones were mainly derived from interpretations of the geophysical anomaly maps, but direct geological evidence has now been provided for most zones and is elaborated on in the following section. Kinematic symbols are based on geological observations, with the exception of some strike-slip indicators, which are only apparent from the magnetic anomaly patterns. The map trace and types of folds displayed on the structural map were constructed using a combination of geophysical and geological data, respectively. The constructed profiles provide further constraints on the mapped features in terms of dip direction and sometimes, kinematics. The new structural geological map is therefore a result of combining interpretations of surface and subsurface data.

Main deformation features

The Vakko and Kovo belts are both characterised by series of narrowly-spaced, N–S-striking folds and shear zones (Fig. 3). Many of the observed shear zones are several metres wide, strongly sheared contact zones between lithological units (e.g. Hauki quartzite). It appears from field observations that most shear zones dip steeply to moderately east, and have accommodated mainly dip-slip reverse movements in combination with a minor component of dextral strike-slip. Normal shearing has been recorded along locally folded tectonic contacts between the Kovo group and the Archaean basement, and also

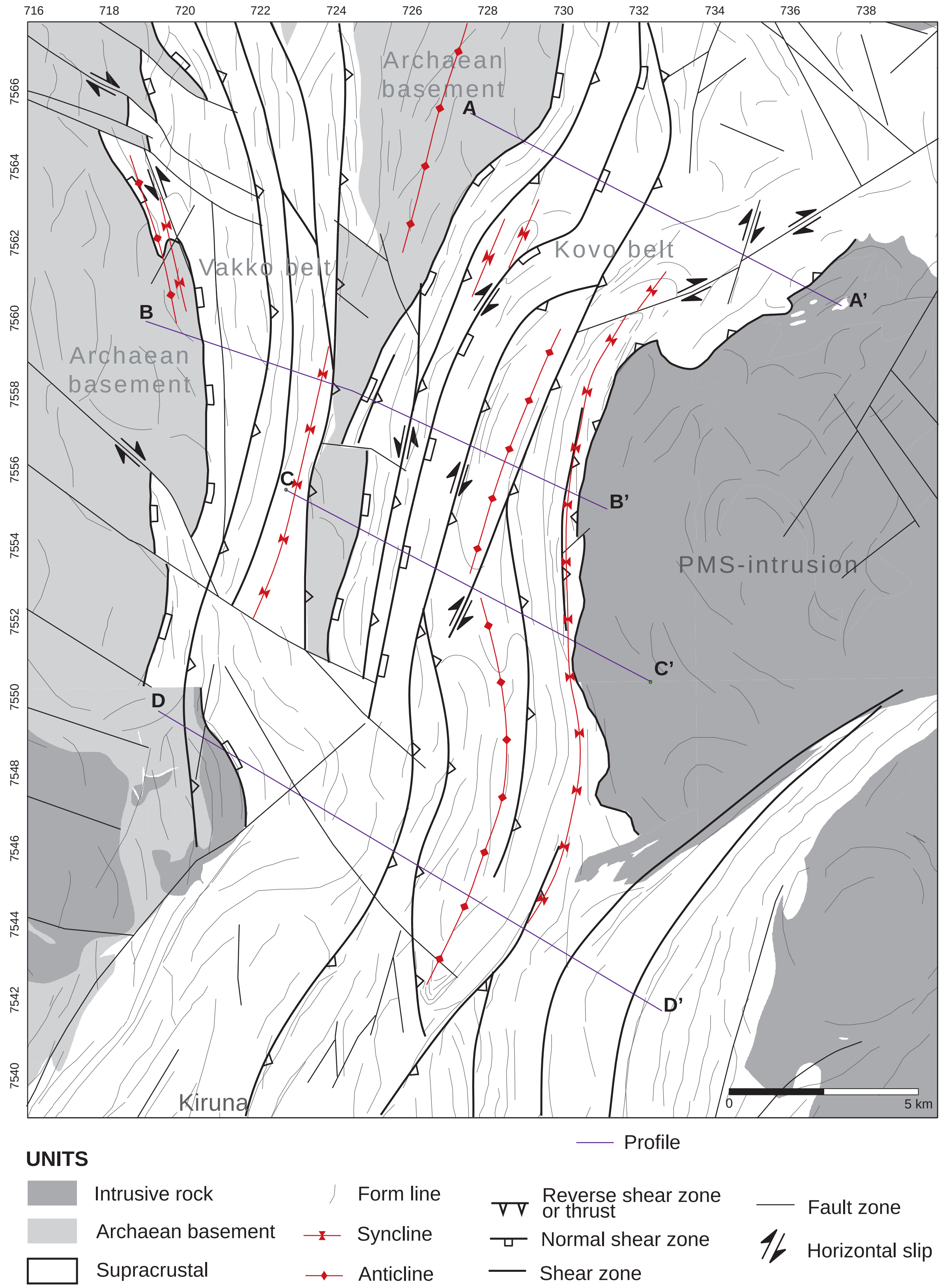

Figure 3. Compiled structural map of the Vakko and Kovo belts. The form lines were primarily derived from magnetic and slingram anomaly maps (Fig. 2a, c) and may represent continuous lithological horizons or deformational features such as tectonic foliation. Shear zones and associated kinematics are based on new field observations and Martinsson (1999), and also on geophysical anomaly maps and subsurface models presented in this study (see text for more detail). Profiles indicated are displayed in Figure 7.

along the western border between the Kovo group and the Hauki quartzite. In contrast, the eastern borders of both the Vakko and Kovo belts are marked by major reverse shear zones and by upright isoclinal folds striking parallel to the shear zones. Within the surrounding units, the observed deformation due to folding and shearing is less pronounced than within the belts. In the interior of the PMS intrusion, deformation is weak and the concentric pattern outlined by form lines may relate to a magmatic zonation (Fig. 3). The Archaean basement is locally folded and clearly fragmented along NW–SE-striking dextral faults or shear zones interpreted from the magnetic anomaly map (Fig. 3). However, deformation in the internal part of the Archaean basement has been mainly inferred from form lines striking in a N–S direction, parallel to the contact with the Vakko and Kovo belts. No deformational features related to these form lines within the Archaean basement were analysed in this study.

Structural field data

Structural data from the Vakko and Kovo belts, collected during geological field studies, are presented in stereographic plots (Fig. 4). Plotted poles to bedding planes show clusters of steeply N-NE–S-SW-striking bedding, along with shallower (20–30 °) southward-dipping bedding. The clusters can be interpreted as reflecting N-NE–S-SW folding. The plotted poles to foliation planes show a gradual variation between sub-vertical NE–SW and NW–SE-striking planes parallel to the outline of the Vakko and Kovo belts. Based on a comparison between the bedding and foliation plots, it may be stated that the foliation represents an unfolded axial plane cleavage around which the bedding is folded. Only a single phase of folding is therefore recognised. Measured fold axes also show a NE–SW trend, and vary from moderately northward to moderately southward-plunging. It should be noted that in previous studies only southward-plunging fold axes were documented. But measured intersection lineations, which are mostly oriented parallel to the fold axis, do usually plunge to the south. Stretching lineations, rarely documented in earlier studies, appear mainly to plunge steeply to the southeast, or moderately towards the southwest. Associated kinematic indicators are most consistent with an east-side-up sense of shear, but an additional component of dextral strike-slip has been derived from several horizontal outcrops and from thin sections. The type of stretching lineation depends very much on the lithology. Pencil and cigar-type lineations are often well developed in dolomitic marbles (Fig. 5C) and metaconglomerates, whereas mineral lineations defined by calcite or chlorite are more abundant in phyllitic, metavolcaniclastic siltstones (Fig. 6A–D). However, the competent basaltic units contain very few deformational features. A moderate degree of deformation is locally indicated by possibly flattened, ellipsoidal pillow metabasalts (Fig. 5D), while thin sections reveal local development of a spaced cleavage (Fig. 6E, G, H). In the eastern part of the Kovo belt along the contact with the PMS intrusion in particular, the cleavage is oriented parallel to the main foliation and is defined by mica overgrowing a partly recrystallised fabric composed of quartz and feldspar (Fig. 6E–F). Drag folds with an overall S asymmetry, indicating an eastern-side-up sense of shear. Tectonic vergence towards the west is typical of those outcrops located along or within shear zones (Figs. 5B, 6G). In contrast, away from the shear zones, mesoscopic open, upright folds were observed within the Hauki quartzite (Fig. 5E). A number of small-scale, moderately-dipping thrusts overprint the main foliation (Fig. 5F). Based on retrograde assemblages (chlorite, mica, quartz) as well as brittle-ductile microstructures, we interpret these thrusts to be relatively young features.

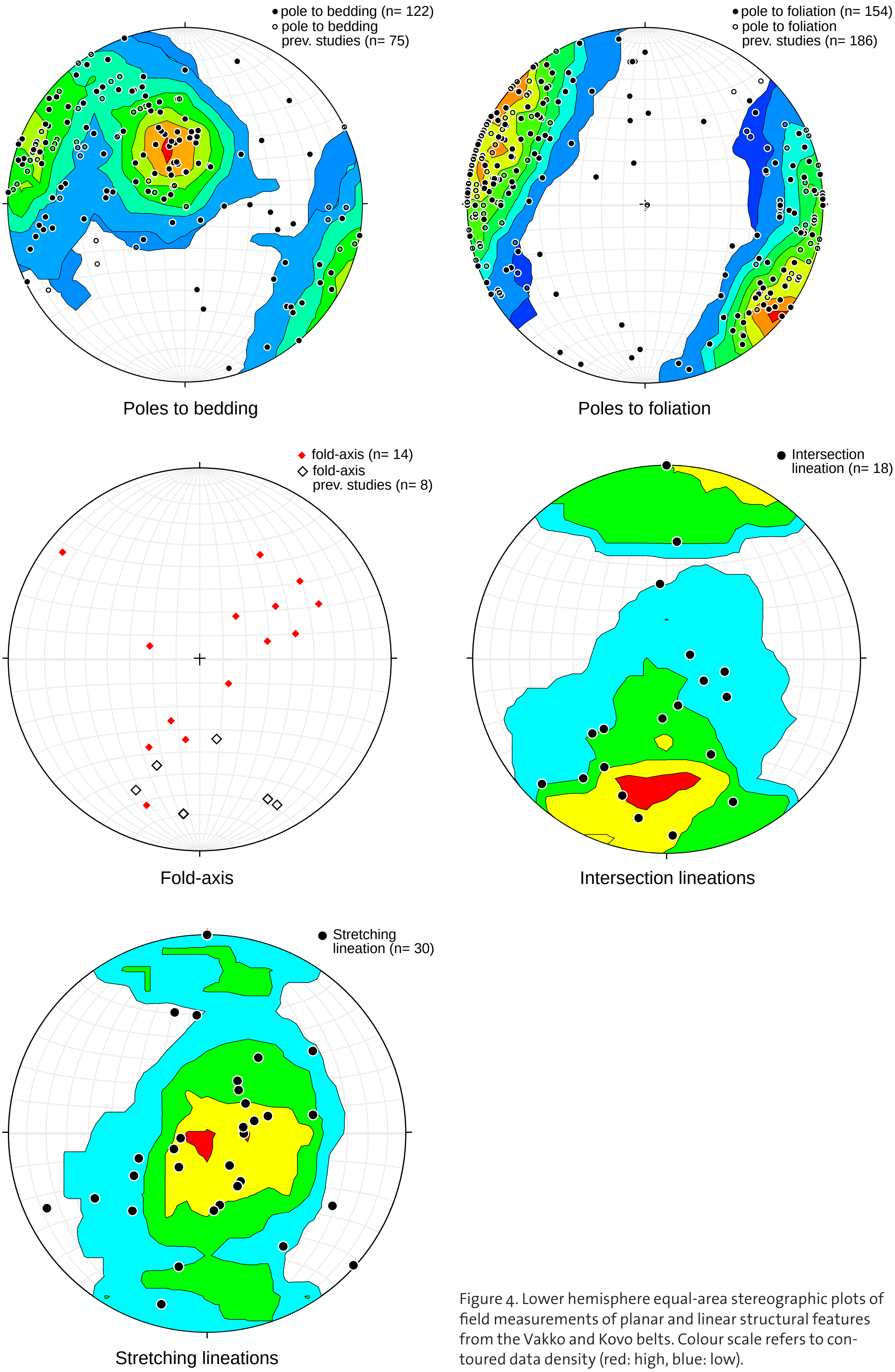

Figure 4. Lower hemisphere equal-area stereographic plots of field measurements of planar and linear structural features from the Vakko and Kovo belts. Colour scale refers to contoured data density (red: high, blue: low).

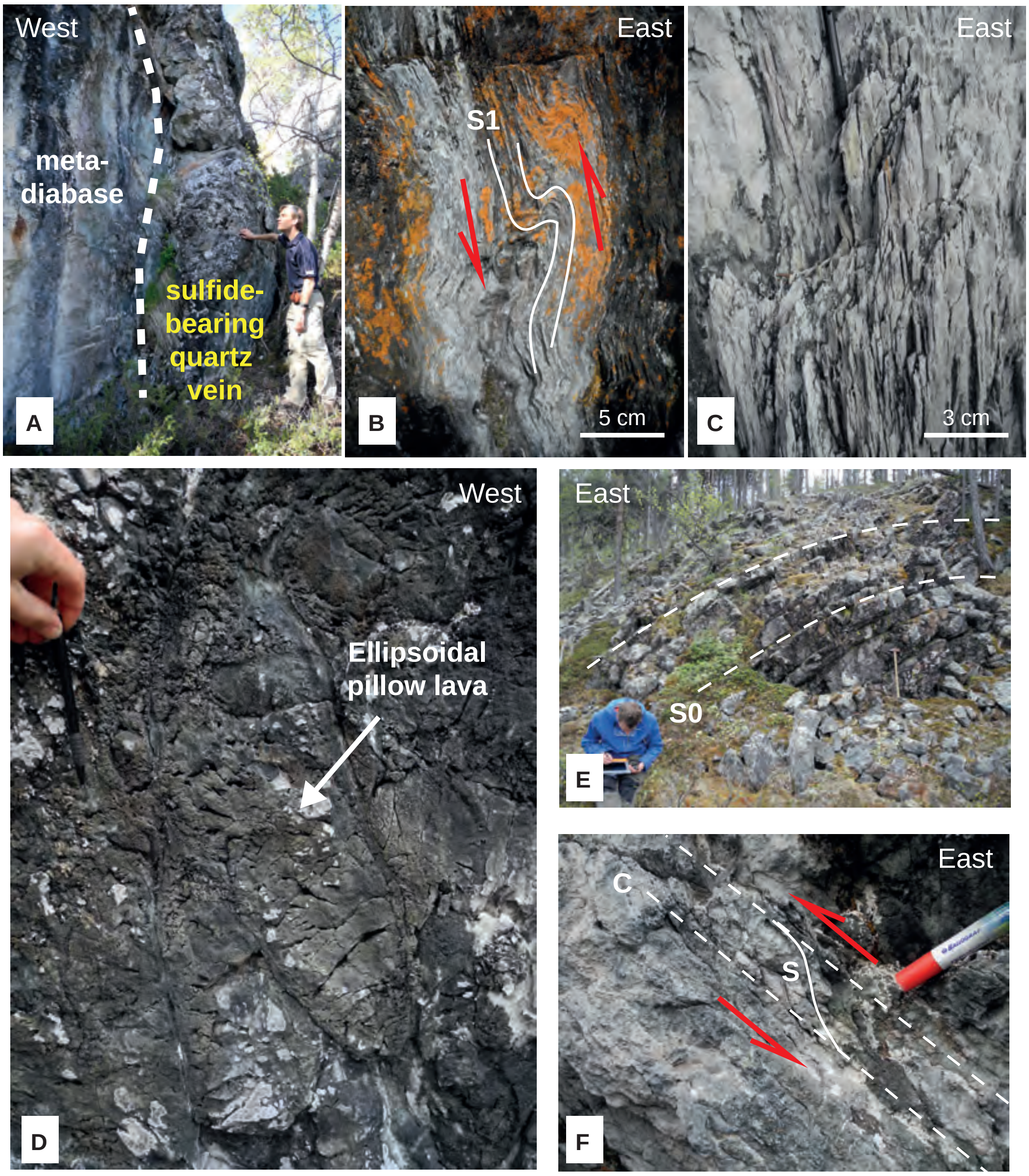

Figure 5. Outcrop photos and interpretations from the Kovo belt. **A.** Kovogruvan (see Fig. 1). A large sulphide-bearing (mainly pyrite) quartz vein along a fault plane juxtaposing metadolerite with strongly-foliated mafic metavolcaniclastic siltstone to the east (not visible in picture). **B.** A strongly-folded phyllitic unit in the upper part of the Kovo group (Harrejaure formation). S-shaped asymmetry indicates tectonic vergence towards the west. **C.** Steeply east-plunging pencil lineations in dolomitic marble (lower Kiruna greenstone group). **D.** Ellipsoidal pillow basalt from the KGG. **E.** Gentle folding of meta-arenites from the Hauki quartzite. **F.** Moderately east-dipping, low-grade shear zone with top-to-the-west sense of shear.

► Figure 6. Microstructures from the Kovo belt. **A.** Rock sample of metavolcanic L>S tectonite from the lower part of the Harrejaure formation (Kovo group). **B.** Microscopic view (crossed polars) from the same sample as in (A). The rods parallel to the mylonitic foliation in the volcaniclastic siltstone indicate eastern-side-down sense of shear (sinistral) and are mainly composed of calcite in the core and quartz in the rims. **C.** East-side-up sense of shear already interpreted from observations on outcrops are confirmed by this asymmetrically-sheared calcite clast. The sample is taken from the upper Kovo group. **D.** Horizontal section from the same outcrop revealing additionally dextral shearing, but with lower strain intensity than the vertical section. **E.** Medium-grade mylonite from the KGG along the contact with the PMS intrusion in the east. Sub-rounded feldspar porphyroclasts recrystallised into polygonal crystalloblastic aggregates. Deviation of the foliation around the porphyroclasts is symmetric and no shear indictors are observed. **F.** Scapolite clast with eye-shaped rim indicates E–W flattening. The sample was taken from a layered basaltic tuff in the upper part of the KGG a few hundred metres from the PMS intrusion. **G.** Folded cleavage in a phyllite from the upper Kovo group indicates E–W shortening with tectonic vergence towards the west. **H.** Fracturing and faulting of lithoclasts (mainly feldspar) surrounded by chlorite indicates shearing parallel to cleavage at relatively low temperatures (>350 °C). The sample was taken from a low-grade shear zone along the eastern contact between the Hauki Quartzite and the KGG.

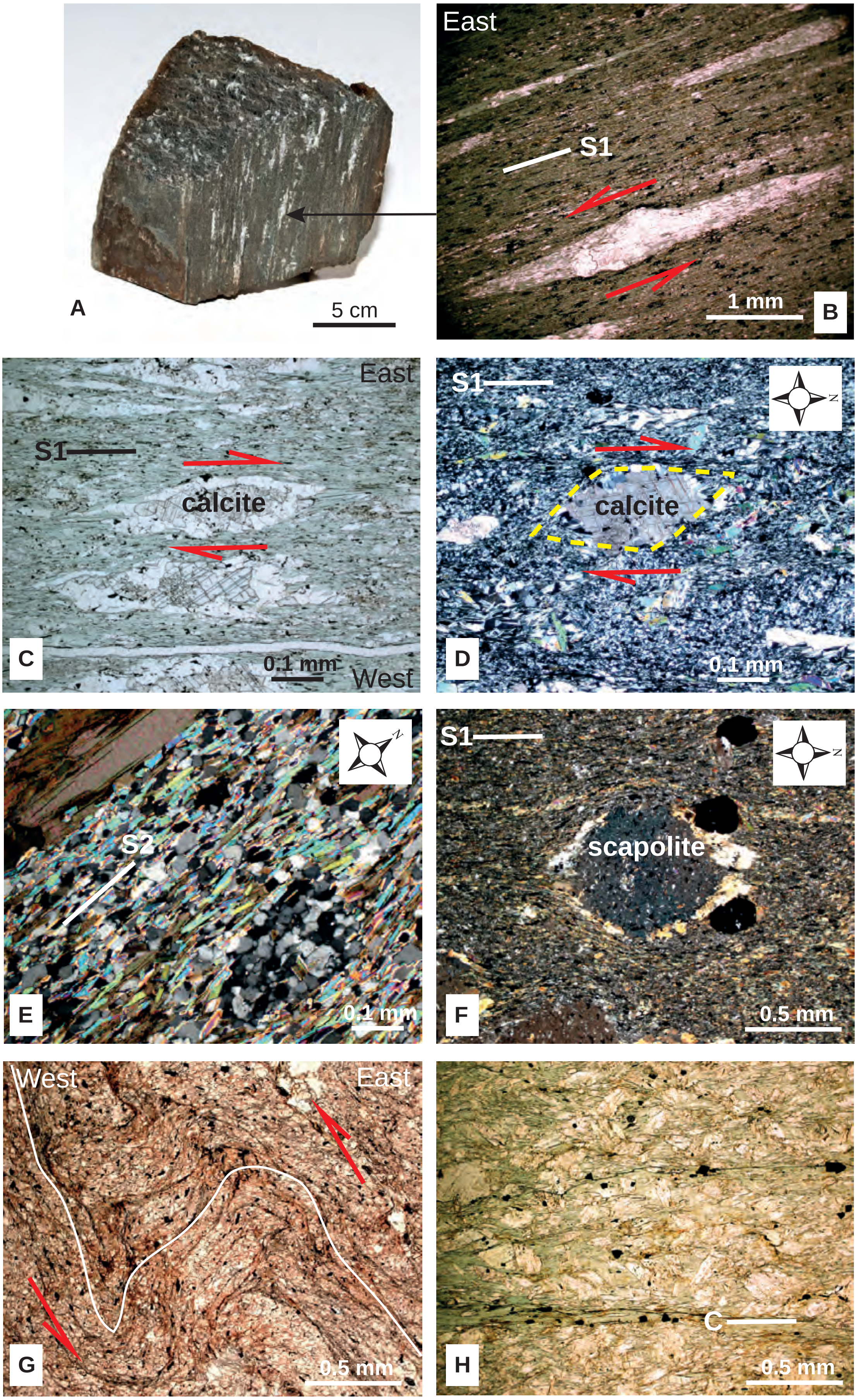
A
5 cm
East
S1
1 mm
B
East
S1
calcite
0.1 mm
West
C
S1
calcite
0.1 mm
D
S2
0.1 mm
E
S1
scapolite
0.5 mm
F
West
East
0.5 mm
G
C
0.5 mm
H

Geophysical and Geological profiles

Four profiles were constructed to resolve subsurface geometries in the Vakko and Kovo belts (Fig. 7A–D). With a NW–SE orientation, all profiles are oriented roughly orthogonally to the main contacts and structural fabrics. Profile locations were based on the best concentration of available geological and geophysical data. A horizontal projection distance of 200 m of geological data on both sides of the profile was applied, and interpretation depths range between 2 and 3.5 km.

Profile AA'

An additional ground magnetic survey was conducted along the westernmost part of the profile to investigate the nature of the contact between the Archaean basement and the overlying Kovo group (Fig. 7A). Geological evidence for a tectonic contact is derived from moderately foliated and intensively fractured metatonalites, which are locally intersected by metre-wide quartz veins as well as by low-grade, strongly-altered and gold-bearing mylonite zones (see also Luth et al. 2014). Mylonite zones are mostly N–S to N-NE–S-SW-striking and are up to 2 m wide. Mylonitic fabrics consistently indicate an eastern-side-down sense of shear. Based on the interpreted geophysical model, however, a steep eastward-dipping normal shear zone was defined as the main contact between the Archaean basement and the Kovo group. Moreover, within the Kovo group itself, a series of steeply eastward-dipping metadolerites is seen in outcrop as well as in the geophysical modelling results. To the east, a coinciding magnetic and gravity low fits well with the surface expression of the Hauki quartzite. The asym-

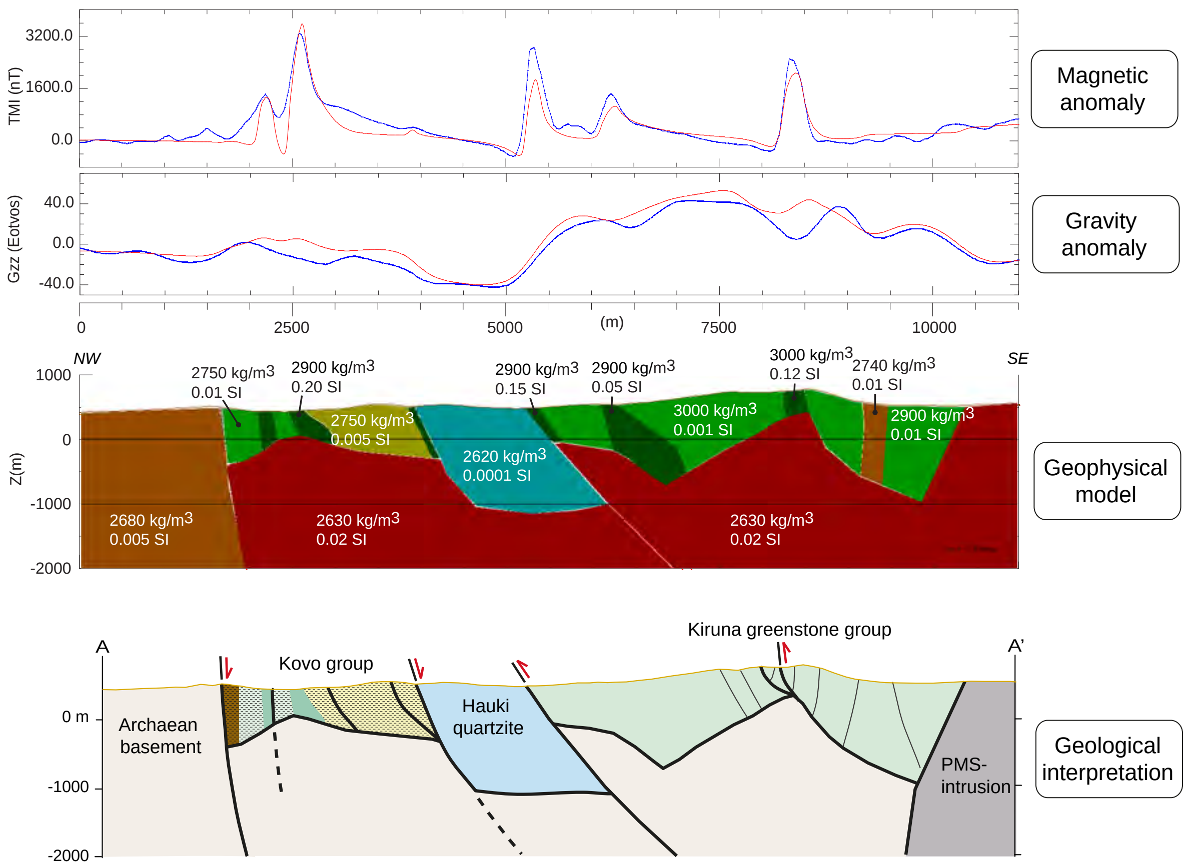

Figure 7A. Profile AA'. The geophysical model is based on airborne magnetic anomalies (upper), gravity (FTG) data (lower) and measured physical rock properties (Table 2). The blue and red graphs plot the measured and calculated values, respectively Colouring refers to specified physical rock properties highlighted in Table 2. The geological interpretation is based on the geophysical model and geological field observations. Bold lines represent tectonic contacts along shear zones. For colour explanation see the legend in Figure 1.

metric shape of both anomalies indicates that the unit dips to the east and extends to a greater depth (-1100 m) than surrounding units. The western boundary of the Hauki quartzite unit is marked by a shear zone accommodating normal movement as well as a deepening of the underlying basement to the east. In contrast, a relative basement high east of the Hauki quartzite unit should indicate reverse shearing along the contact with the Kiruna greenstone group. Field evidence for both shear zones is lacking due to the absence of exposure along this part of the profile. However, a "look-alike" interpretation of the subsurface outline of the Hauki quartzite unit along profile CC' does include kinematic field constraints. Further to the east, large depth variations of the Archaean basement underlying the Kiruna greenstone group may be associated with major shear zones and with folding. Large-scale upright folding of the Kiruna greenstone group along profile AA' near the contact with the PMS intrusion is evident from the pattern seen on magnetic and electromagnetic ground anomaly maps (see also Luth & Antal-Lundin 2013 and Luth et al. 2014).

Profile BB'

The profile intersects the Vakko and Kovo belts and is an extension of a profile published earlier by Martinsson (1999) (Fig. 7B). A large-scale interpretation reveals a moderately southeastward-dipping Archaean basement overlain by supracrustal rock units intersected and bounded by steeply-dipping

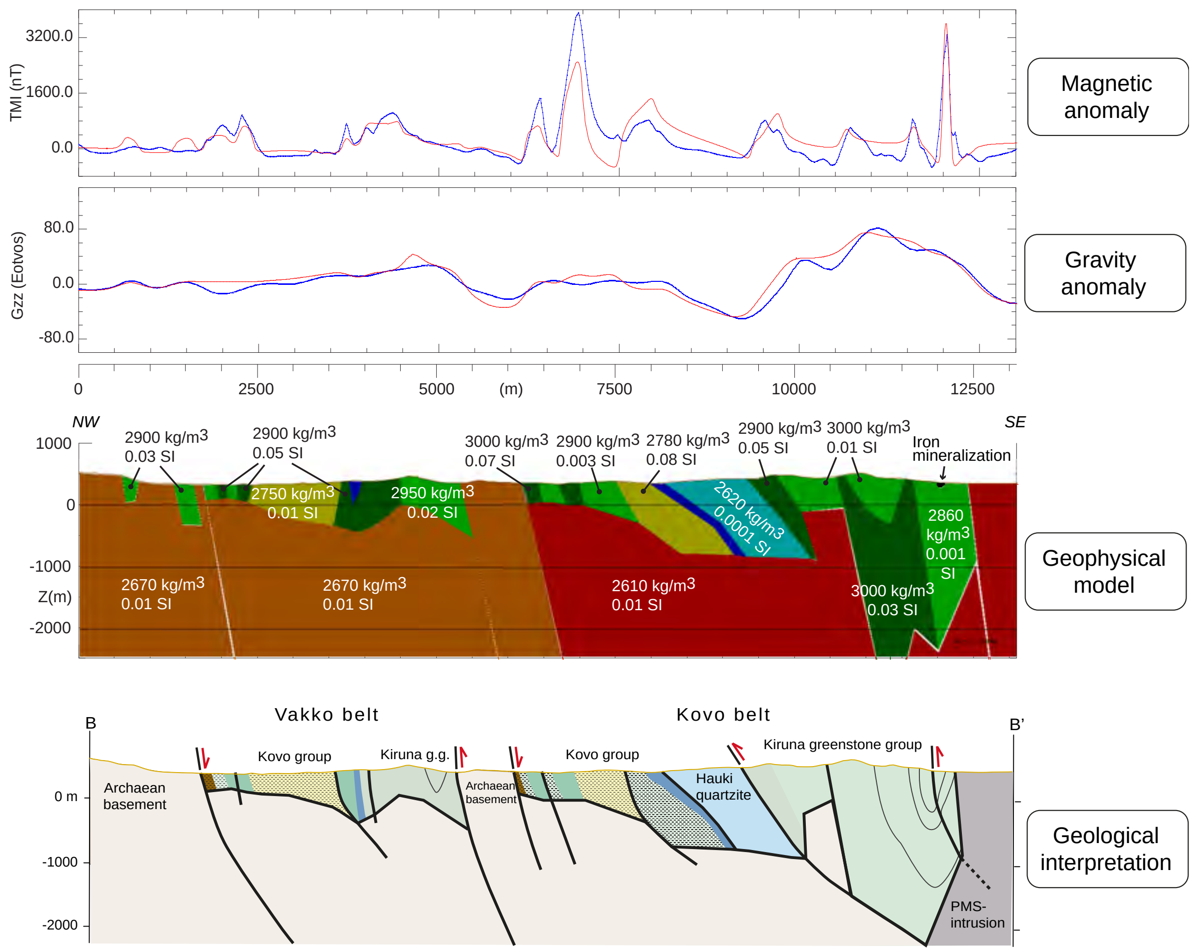

Figure 7B. Profile BB'. The geophysical model is based on airborne magnetic anomalies (upper), gravity (FTG) data (lower) and measured physical rock properties (Table 2). The blue and red graphs plot the measured and calculated values, respectively Colouring refers to specified physical rock properties highlighted in Table 2. The geological interpretation is based on the geophysical model and geological field observations. Bold lines represent tectonic contacts along shear zones. For colour explanation see the legend in Figure 1.

shear zones. As with profile AA', the tectonic contact between the Archaean basement and the overlying Kovo group dips steeply to the east. A deeper continuation of the shear zone within the Archaean basement is most likely, but evidence is lacking. Field observations along the western border of the Vakko belt indicate tight folding of both the Archaean basement unit and the Kovo group (see also Luth et al. 2014). Foliations and fold axial planes steepen towards vertical in the central and eastern part of the Vakko belt. Underlying local variations in basement depth may be due to folding or faulting. However, a basement high, separating the Vakko and Kovo belts, is bounded by major, steeply southeast-dipping shear zones. As with the Kovo belt, the deepest and easternmost part of the Vakko belt is characterised by a large isoclinal syncline, bounded and possibly intersected to the east by a major shear zone. This shear zone may have accommodated a large amount of east-side-up movement, causing a relative uplift of the Archaean basement, but field constraints on the shear zone's kinematics are lacking. To the east, the part of the profile intersecting the Kovo belt is largely comparable to the corresponding section in profile AA' (Fig. 7A), with the notable exception that the Hauki quartzite unit has a vertical thickness equal to its surrounding units. Normal shearing is localised within the Kovo group to the east of the Hauki quartzite unit, and was inferred from a rapid deepening of the Archaean basement. In contrast, east of the Hauki quartzite, shortening is evident from the tectonic wedge bounding the Kiruna greenstone group. Here, the FTG data show a strong positive anomaly, which can be explained by an abrupt deepening of the basement. In combination with the folding pattern seen on magnetic and slingram anomaly maps, as well as structural field measurements, basement deepening coincides with a large synform, bounded and probably disrupted by the PMS intrusion to the east.

Profile CC'

In comparison with the other profiles, geological interpretations along profile CC' are constrained by a greater number of field observations, and also by several geophysical ground surveys (Fig. 7C). The result portrays a large-scale subsurface structure that has been taken as an example in less well-constrained interpretations of the other profiles. Profile CC' reveals supracrustal units bounded and intersected by major shear zones rooted in the Archaean basement, which deepens to the southeast. The nature of the contact between the Archaean basement and the Kovo group is somewhat ambiguous and appears as a nonconformity where Archaean metatonalites are in contact with conglomerates. Nonetheless, the conglomerates display weak foliation with pebbles that are modestly elongated; no indications of intense shearing were observed. In contrast, intense shearing and a variety of kinematic indicators were observed further to the east of the contact. Here, metavolcanic siltstones directly overlying the basal conglomerates record intense normal shearing in L>S tectonites. 1 to 2 km further east and stratigraphically higher in the Kovo group, reverse shearing in combination with dextral shearing predominates (Fig. 6). Normal shear indicators again become abundant along the contact between the Hauki quartzite and the Kiruna greenstone group. It should be noted in Figure 7C that normal shearing does not accord with subsurface interpretations of the geophysical model, which conversely suggests reverse shearing, causing a vertical offset within the Hauki quartzite. Further east, the Kiruna greenstone group is internally folded along N–S to NE–SW-striking and steeply-dipping axial planes. A slight asymmetry in the folding pattern combined with steeply eastward-dipping shear zones suggests tectonic transportation directed to the northwest. As with profiles AA' and BB', the eastern border of the Kovo belt is characterised by a rapid deepening of the Archaean basement, reaching -2000 m below ground level. The basement is overlain by the Kiruna greenstone group, which is folded into a large syncline. The small gravity increment near the end of the profile is probably due to underlying gabbroic rocks belonging to the PMS intrusion.

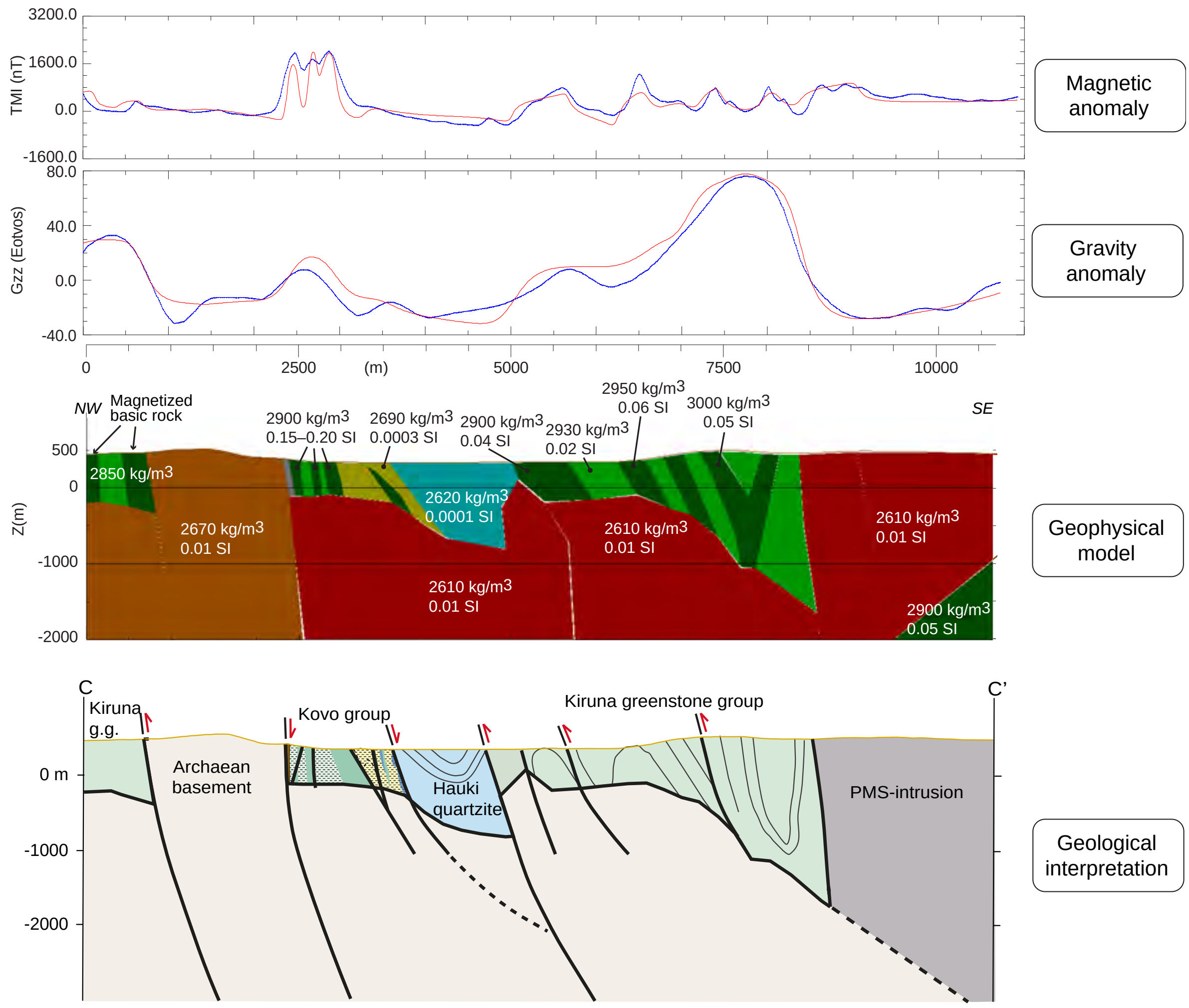

Figure 7C. Profile CC'. The geophysical model is based on airborne magnetic anomalies (upper), gravity (FTG) data (lower) and measured physical rock properties (Table 2). The blue and red graphs plot the measured and calculated values, respectively Colouring refers to specified physical rock properties highlighted in Table 2. The geological interpretation is based on the geophysical model and geological field observations. Bold lines represent tectonic contacts along shear zones. For colour explanation see the legend in Figure 1.

Profile DD'

Profile DD' is the southernmost profile and aims to connect between subsurface interpretations from the Vakko and Kovo belts and the Kiruna region (Fig. 7D). The profile differs from the northern profiles mainly in the absence of an Archaean basement high separating the Vakko and Kovo belts and the presence of Svecofennian units in place of the PMS intrusion. The resulting geological interpretation highlights the greater depth (3 000 m) of the Archaean basement as the most outstanding feature. A rapid but gradual northwest to southeast deepening of the basement is inferred mainly from the gradually increasing gravity anomaly derived from ground measurements. There are few additional constraints from measured physical properties and geological field data along this part of the profile. Within the Kiruna greenstone group, the magnetic response shows strong variation, allowing interpretations of the subsurface folding pattern. A narrow band of relatively low magnetic anomalies, together with a local gravity low, corresponds to the Hauki quartzite. The unit is wedge-shaped with a maximum depth of only 300 m along its eastern border. East of the Hauki quartzite, the inclusion of northwest-dipping shear zones is primarily based on surface mapping, and the depth extent is uncertain (see Grigull et al., 2018). Further to the east, two narrow magnetic bands surrounding a low

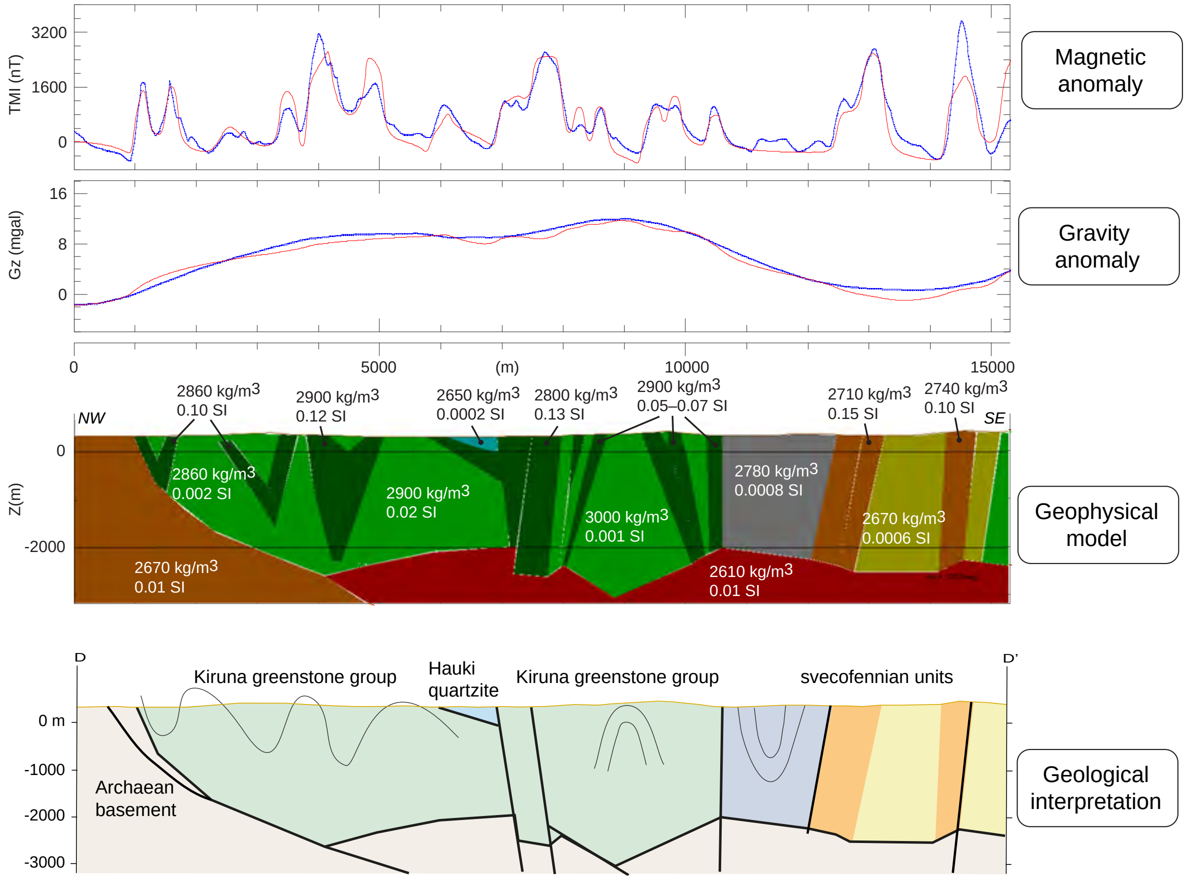

Figure 7D. Profile DD'. The geophysical model is based on airborne magnetic anomalies (upper), gravity (FTG) data (lower) and measured physical rock properties (Table 2). The blue and red graphs plot the measured and calculated values, respectively. Colouring refers to specified physical rock properties highlighted in Table 2. The geological interpretation is based on the geophysical model and geological field observations. Bold lines represent tectonic contacts along shear zones. For colour explanation see the legend in Figure 1.

magnetic core indicate an isoclinal antiform. East of the antiform the Svecofennian units are mainly composed of mica schist and felsic volcanic rocks. Both lithologies have relatively low densities, which is reflected by correspondingly low gravity. The presence of somewhat more dacitic rocks corresponds well with higher magnetic anomalies. Modelling results suggest sub-vertically-oriented units, and is consistent with the steep foliation measured in the field.

DISCUSSION

Tectonic models for the Vakko and Kovo belts

The deformation pattern observed in the Vakko and Kovo belts is most likely the result of a combination of early E–W extension and later NE–SW to E–W-directed shortening. Early extension led to thinning and finally fragmentation of the Archaean basement into separate fault blocks and basins, which then became filled with sediments (see also Kumpulainen 2000). Normal shearing, observed along the major shear zones bounding the Vakko and Kovo belts to the east, may date back to this period of extension. In contrast, and taking into account the 400 Ma time window between the rocks from the Kovo group and the Hauki quartzite, normal shearing observed along the contacts with the Hauki quartzite may be associated with a younger extensional event. Subsequently, crustal shortening inverted the basins and was accommodated by folding, flattening and reverse and dextral shearing along moderately to steeply southeast-dipping shear zones. The resulting crustal stack mainly comprises supracrustal units, but the Archaean basement was also affected by shortening as it became folded and fragmented.

The PMS intrusion, composed of weakly foliated granite to monzonite and located in the east of the study area, probably formed during or slightly after the main stage of crustal shortening. However, tight, upright folds within the Kiruna greenstone group are warping around the PMS intrusion and may reflect a high amount of shortening in front of a rigid and more competent unit. Likewise, the large syncline marking the eastern border of the Vakko belt may have a comparable origin, where the more competent Archaean basement caused strain localisation. The interpreted tectonic wedge bounded by reverse shear zones within the Kiruna greenstone group in the eastern Kovo belt (profile BB') may also represent crustal "pop-ups" forming directly in front of an indenter in analogue and numerical models (e.g. Davis et al. 1983, Ellis et al. 2004). In the central part of the Kovo belt shortening resulted in predominantly E–W flattening, as well as reverse and dextral shearing. In the northern part of the Kovo belt E–W shortening resulted in local dextral strike-slip along N to NE-striking shear zones. At a later stage the deformed units were intersected by more discrete NW–SE-striking faults accommodating dextral slip as well as vertical, southern-block-up movement.

Deformation resulting from predominantly NE–SW to E–W shortening is largely consistent with the results of earlier geological studies in the Kiruna area (e.g. Wright 1988, Vollmer et al. 1984, Talbot & Koyi 1994). Wright (1988), however, states that all structural features were formed before the intrusion of granite batholiths and that the surrounding supracrustal rocks were not affected by the intrusions. Conversely, Vollmer et al. (1984) concludes that diapirism is a likely explanation for the observed deformation patterns in the area. More recently He et al. (2009) presented an emplacement model for the Fangshan pluton in China, where some structural features are comparable to the PMS intrusion and the eastern part of the Kovo belt, such as a concentric internal pattern of the pluton as well as the presence of an outer rim syncline directly along the contact. However, some other features favouring an emplacement model, such as a high-temperature shear aureole with pluton-side-up kinematic indicators do not accord with our observations.

The depth of the Archaean basement and correlation with the Kiruna area

In the profiles presented, the depth to the Archaean basement varies below the Vakko and Kovo belts from only a few hundred metres in the northwest to more than 2 km in the southeast. A further southward deepening of the Archaean basement is inferred from a comparison between profiles CC' and DD', where the basement reaches a depth of 3 km below the surface (Fig. 8). In line with our observations, recent results from modelling of a seismic reflection survey near Kiruna by Holmgren (2013) and Bastani et al. (2018) have revealed eastward-dipping reflectors originating from lithological boundaries to a depth of approximately 3.5 km. A deepening of the Archaean basement from 2 to 3.5 km over a distance of 6 km probably requires a southward-dipping basement combined with a significant amount of vertical displacement along major shear zones located between the Kovo belt and the Kiruna area. The main candidate along which vertical movements could be accommodated is a series of NW–SE-striking faults interpreted from magnetic anomaly maps northwest of profile DD' (Figs. 1 and 3). Fault zones with a similar orientation crosscutting both the Archaean basement and the overlying Palaeoproterozoic units were mapped earlier throughout the study area, primarily based on geophysical data (e.g. Martinsson 1999), but good geological field observations on those structures are lacking.

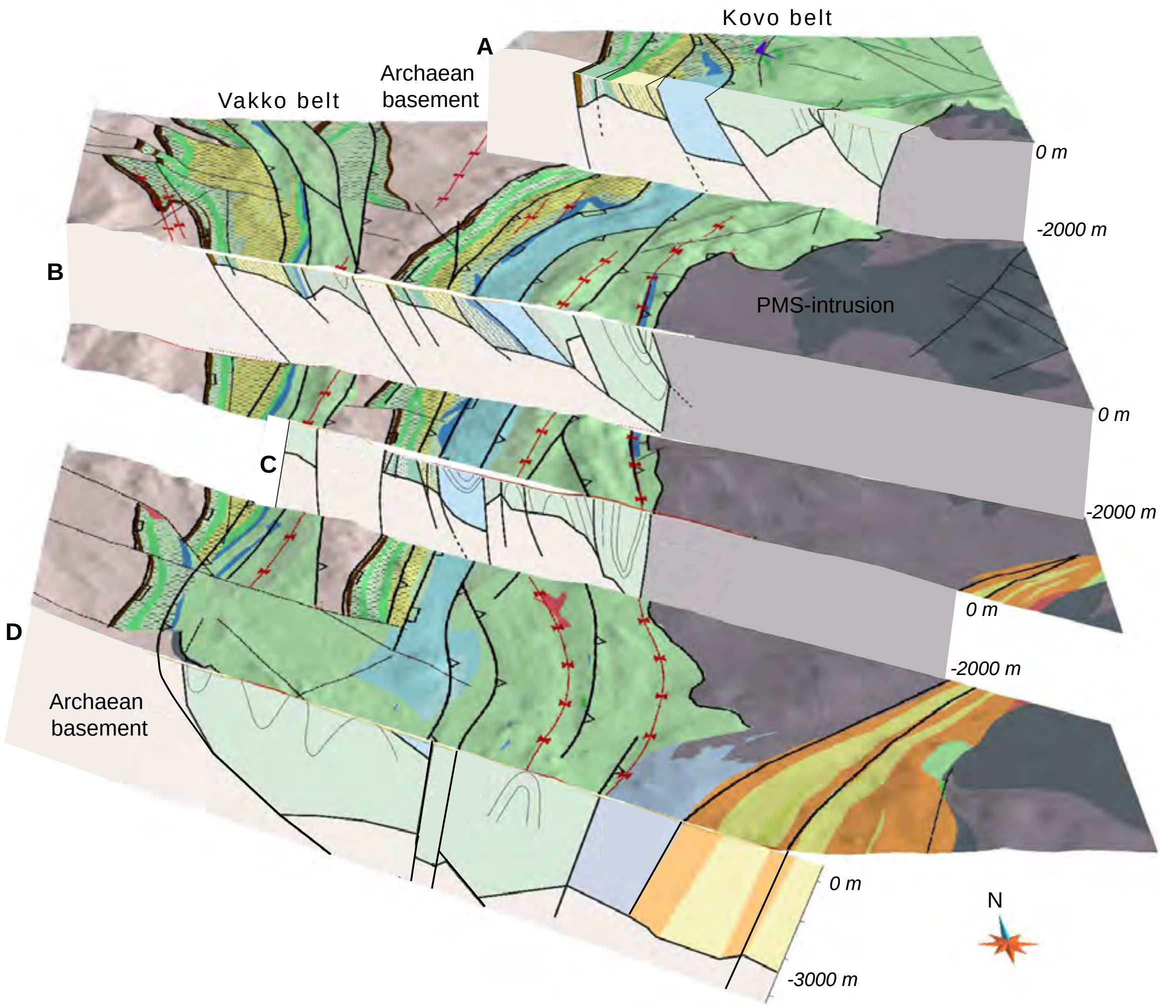

Figure 8. Regional block model for the Vakko and Kovo belts based on a combination of structural geology mapping and geophysical modelling (gravity and magnetic) along 4 transects (Figs. 1 and 3). The area is sliced and translated vertically along each profile to highlight the subsurface structures below the transposed geological map. Map colours are as in Figure 1 and line symbols as in Figure 3.

CONCLUSIONS

Structural geological field investigations combined with geophysical modelling have revealed the 3D structure of the Palaeoproterozoic Vakko–Kovo greenstone belts north of Kiruna. Predominantly steep eastward-dipping shear zones bound and intersect both the Archaean basement and the overlying metasupracrustal units. Shear sense indicators associated with the major shear zones reveal that formation and deformation of the belts occurred during E–W crustal extension, followed by NE–SW to E–W shortening. As such, several major shear zones are thought to have started out as normal shear zones, becoming reactivated and steeped during shortening by reverse shearing or dextral strike-slip. Deformation by shortening also resulted in upright isoclinal folding of both the Archaean basement and the metasupracrustal units. Based on the high amplitude of folds and the recognition of a tectonic wedge, we suggest that some shortening became localised in the eastern parts of the both belts. Localisation of shortening can be attributed to indentation of the adjacent highly competent rocks of the Archaean basement and of the PMS intrusions into the Vakko and Kovo belts, respectively. A 3D correlation between the profiles presented indicates that the shallow to moderately-dipping Archaean basement extends towards the southeast. A rapid southward deepening of the basement from 2 to 3.5 km below Kiruna may be assigned to vertical movements along NW–SE striking fault systems but requires further investigation.

REFERENCES

Bastani, M., Antal Lundin, I., Savvaidis, A., Kamm, J. & Wang, S., 2015: Barentsprojektet 2014: audiomagnetotelluriska (AMT) mätningar i Kiruna- och Lannavaraområdet, preliminära resultat. *Sveriges geologiska undersökning SGU-rapport 2015:10*, 16 s.

Bergman, S., Kübler, L. & Martinsson, O., 2001: Description of regional geological and geophysical maps of northern Norrbotten County. *Sveriges geologiska undersökning Ba 56*. 110 pp.

Davis, D., Suppe, J. & Dahlen, F. A., 1983: Mechanics of fold-and-thrust belts and accretionary wedges. *Journal of Geophysical Research: Solid Earth*, *88*(B2), 1153–1172.

Ellis, S., Schreurs, G. & Panien, M., 2004: Comparisons between analogue and numerical models of thrust wedge development. *Journal of Structural Geology*, *26*(9), 1659–1675.

Folcker, G., 1974: Urbergsstratigrafisk studie över Vittangivaara, Norrbottens län. *Sveriges geologiska undersökning C 697. 20 pp.*

Geijer, P., 1927: Vakkojärvidiskordansens stratigrafiska ställning. Geol. Fören. Förh. 49, s. 483.

Geijer, P., 1931: Berggrunden inom malmtrakten Kiruna–Gällivare–Pajala. *Sveriges geologiska undersökning C 366,* 225 pp.

Godin, L., Parák, T., Espersen, J. & Forsell, P., 1979: Cu i Kirunagrönsten. Slutrapport. LKAB Prospekteringsrapport Ki-04-79, 58 pp.

Grigull, S., Berggren, R., Jönberger, J., Jönsson, C., Hellström, F.A. & Luth, S., 2018: Folding observed in Palaeoproterozoic supracrustal rocks in northern Sweden. *In:* Bergman, S. (ed): Geology of the Northern Norrbotten ore province, northern Sweden. *Rapporter och Meddelanden 141,* Sveriges geologiska undersökning. This volume pp 205–257.

He, B., Xu, Y.-G. & Paterson, S., 2009: Magmatic diapirism of the Fangshan pluton, southwest of Beijing, China. Journal of Structural Geology 31: 615–626

Holmgren J., 2013: Seismic modeling of reflection survey near Kiruna. Bachelor thesis, Luleå University, 41 pp.

Kumpulainen, R., 2000: The Palaeoproterozoic sedimentary record of northernmost Norrbotten, Sweden. Final report. Stockholm University, Department of geology and geochemistry.

Kumpulainen, R. A., 2003: Svecofennian sedimentary record of northern Sweden. Unpublished report, Sveriges geologiska undersökning, 20 pp.

Luth, S. & Antal-Lundin, I., 2013: Summary report on the geological and geophysical characteristics of the Harrijärvet-Vittangivaara key areas. *Sveriges geologiska undersökning Report S1313.*

Luth, S., Lynch, E.P., Grigull S., Thörnelöf, M., Berggren, R. & Jönberger, J., 2014: Geological and geophysical studies in the Harrijärvet, Vittangivaara and Akkiskera-Kuormakka key areas. *Sveriges geologiska undersökning SGU-rapport 2014:09,* 24 s.

Martinsson O., 1997: Paleoproterozoic greenstones at Kiruna in northern Sweden: a product of continental rifting and associated mafic-ultramafic volcanism. *In:* O. Martinsson: *Tectonic setting and metallogeny of the Kiruna greenstones. Doctoral thesis 1997:19, Paper I,* 1–49. Luleå University of technology.

Martinsson, O., 1999: Bedrock map 30J Rensjön NO, scale 1:50 000. *Sveriges geologiska undersökning Ai 131.*

Martinsson, O., Vaasjoki, M. & Persson, P.-O., 1999: U-Pb ages of Archaean to Palaeoproterozoic granitoids in the Torneträsk-Råstojaure area, northern Sweden. *In:* S. Bergman (ed.): Radiometric dating results 4. *Sveriges geologiska undersökning C 831*, 70–90.

Ödman, O.H., 1957: Beskrivning till berggrundskarta över urberget i Norrbottens län. *Sveriges geologiska undersökning Ca 41*, 151 pp.

Offerberg, J., 1967. Beskrivning till Berggrundskartbladen Kiruna NV, NO, SV, SO. *Sveriges geologiska undersökning Af 1–4,* 147 pp.

Skiöld, T., 1979. Zircon ages from an Archean gneiss province in northern Sweden. *Geologiska Föreningens i Stockholm Förhandlingar 103*, 169–171.

Skiöld, T., 1986: On the age of the Kiruna Greenstones, northern Sweden. *Precambrian Research 32*, 35–44.

Talbot, C.J. & Koyi, H., 1995: Paleoproterozoic intraplating exposed by resultant gravity overturn near Kiruna, northern Sweden. Precambrian Research 72, 199–225.

Vollmer, F.W., Wright, S.F. & Huddleston, P.J., 1984: Early deformation in the Svecokarelian greenstone belt of the Kiruna district, northern Sweden. *Geologiska Föreningens i Stockholm Förhandlingar 106*, 109–118.

Welin, E., Christiansson, K. & Nilsson, Ö., 1971: Rb-Sr radiometric ages of extrusive and intrusive rocks in Northern Sweden. *Sveriges geologiska undersökning C 666 1-38* 40.

Witschard, F., 1984: The geological and tectonic evolution of the Precambrian of northern Sweden – a case for basement reactivation? *Precambrian Research 23,* 273–315.

Wright, S.F., 1988: Early Proterozoic deformational history of the Kiruna district, northern Sweden. Unpublished Ph.D. thesis. University of Minnesota, 170 pp.

Authors, paper 9:
Johan Jönberger
Geological Survey of Sweden
Department of Mineral Resources,
Uppsala, Sweden

Cecilia Jönsson
Geological Survey of Sweden
Department of Mineral Resources,
Uppsala, Sweden

Stefan Luth
Geological Survey of Sweden
Department of Mineral Resources,
Uppsala, Sweden

9. Geophysical 2D and 3D modelling in the areas around Nunasvaara and Masugnsbyn, northern Sweden

Johan Jönberger, Cecilia Jönsson & Stefan Luth

ABSTRACT

This chapter focuses on the geophysical aspects of two key areas in northern Sweden with the emphasis on modelling the subsurface conditions primarily using magnetic and gravity data. The areas dealt with here are Nunasvaara, located 10 km west of the village of Vittangi, and Masugnsbyn, located 60 km northwest of Pajala. The areas surrounding both Nunasvaara and Masugnsbyn are well covered by pre-existing magnetic, electromagnetic and gravity geophysical data. Moreover, there is good coverage of petrophysical samples that have been analysed for density and magnetic properties. Using these data sets together with newly acquired geophysical and petrophysical information, 2D and 3D models have been constructed for a number of strategic locations to provide more information about subsurface conditions and ore-bearing lithologies. In Nunasvaara two 2D geophysical models, based on ground magnetic, gravity and petrophysical information, have been made across the greenstones. One profile is regional with a length of 11 km, whereas the other is a relatively short 2 km profile. An inversion model based on VLF data has been generated along the shorter profile, which crossed several known graphite-bearing black schist horizons. The modelling results show consistently east-dipping geometries in the northeastern part of Nunasvaara, while the regional model shows mostly vertical or west-dipping structures. The regional model suggests that the greenstones in the central part have a dome-shaped structure, surrounding an area with local magnetic and gravity minima. In the area around Masugnsbyn 3D models of the Masugnsbyn iron ore deposit have been made, based on dense gravity data and correlated to borehole information. The model shows a width between 50 and 150 m of the mineralised skarn, represented by a vertical slab (central model). This correlates well with the ore zone presented in Witschard et al. (1972). A forward 3D regional model over a large part of the area, based primarily on airborne magnetic data and petrophysical information, was also constructed. Newly acquired geophysical data have also provided important input to improve interpretation of the lithological and stratigraphic relationships along this regional profile. This new model gives new insight into the geometries of the volcanic rocks in the western part of the profile. It was found that these rocks dip to the east, unlike the older profile from Padget (1970), which shows west-dipping structures.

NUNASVAARA

Geological introduction

The bedrock in the Nunasvaara area consists predominantly of metavolcanic and metavolcaniclastic rocks of basaltic to andesitic composition, metasedimentary rocks including graphite-bearing black schist, and metadolerites (Fig. 1). These rocks are part of the *Vittangi greenstone group (VGG)*, which has a lateral extent of approximately 9 × 11 km extending N–NE (Eriksson & Hallgren 1975). The VGG in this area is surrounded by intrusions ranging from gabbro to granite belonging to the *Haparanda, Perthite monzonite* and *Lina* suites. Several mineralisations occur, including skarn iron and graphite deposits. For a more detailed description of the geology and lithostratigraphy around Nunasvaara, the reader is referred to Lynch et al. (2018).

Geophysical interpretation in the Nunasvaara area

A considerable amount of geophysical information is available for the Nunasvaara area. Airborne surveys have been conducted by SGU and LKAB on several occasions on which different geophysical data sets have been acquired, including magnetic, radiometric and electromagnetic data (slingram and VLF). In addition, dense ground magnetic, slingram and gravity measurements have been made over the entire area, together with extensive sampling for petrophysical analysis. More information about these previous geophysical investigations can be found in Lynch & Jönberger (2013).

The overall pattern of the magnetic and gravity field, along with the electromagnetic map (slingram data) represents lithological units in the area. The bedrock mainly consists of basaltic to andesitic metavolcanic rocks (tuffs) and metadolerites. The magnetic properties vary considerably, reflected in the statistics on the petrophysical samples in Figure 2 and Table 1. These variations can be seen on the magnetic anomaly map (Fig. 3) of the western part of the area, where tuffs generate both a banded pattern of relatively narrow, high-magnetic anomalies along with areas of considerably lower magnetic signature. Sequences of skarn iron ores, mainly in the west of the area, cause the strongest anomalies

Table 1. Tabular presentation of the petrophysical properties in the area, subdivided into the main lithologies.

Rock type	No. of samples	Density (SI), mean	Density (SI) Std. dev.	Susceptibility x 10^{-5} (SI) min	Susceptibility x 10^{-5} (SI) max	Susceptibility x 10^{-5} (SI) median	Q-value min	Q-value max	Q-value median
Basalt-andesite	205	2 958	117	9	44 850	165	0.03	94.77	0.54
Granite	31	2 632	30	6	4 315	902	0.01	1.06	0.13
Gabbro-diorite	54	2 954	95	7	49 730	4 501	0.05	29.00	0.29
Dolerite	118	2 979	93	13	117 200	279	0.02	37.42	0.79
Carbonate	8	2 779	74	16	1 074	38	0.09	4.26	0.35
Schist	22	2 765	134	-22	1 910	82	-0.87	180.62	0.83
Skarn	7	3 597	225	834	408 500	214 900	1.79	37.55	6.59

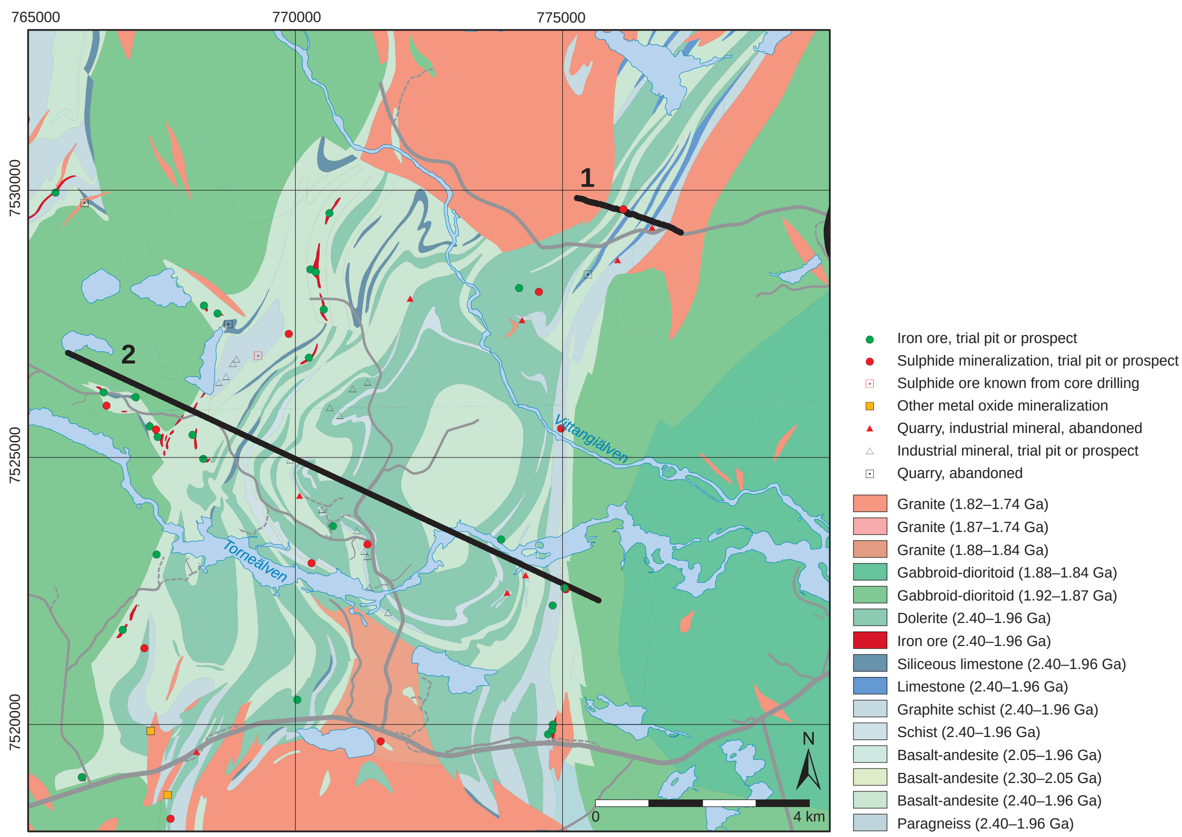

Figure 1. Bedrock map of the area around Nunasvaara (after Bergman et al. 2012). The mineralisation occurrences are shown on the map. Black lines represent the extent of profiles that have been modelled using geophysical data.

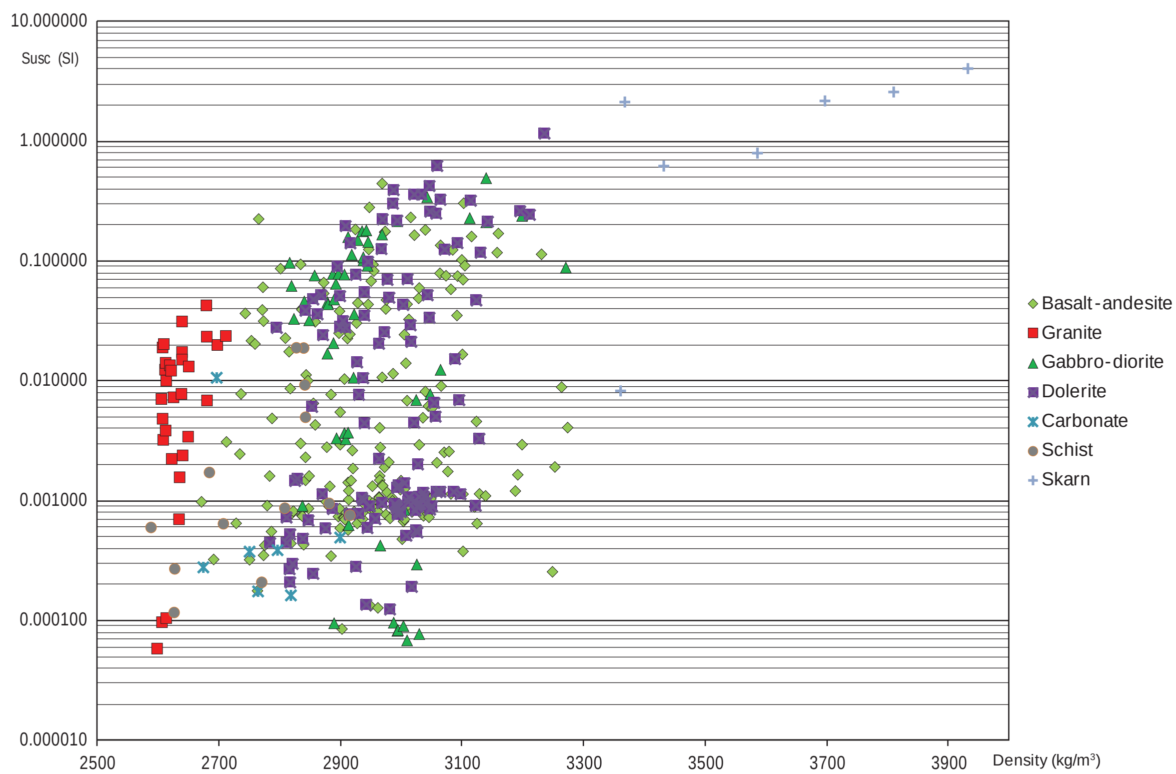

Figure 2. Petrophysical properties of the different lithologies in the area. Magnetic susceptibility (SI unit) v density (kg/m³). The total number of petrophysical samples is 445.

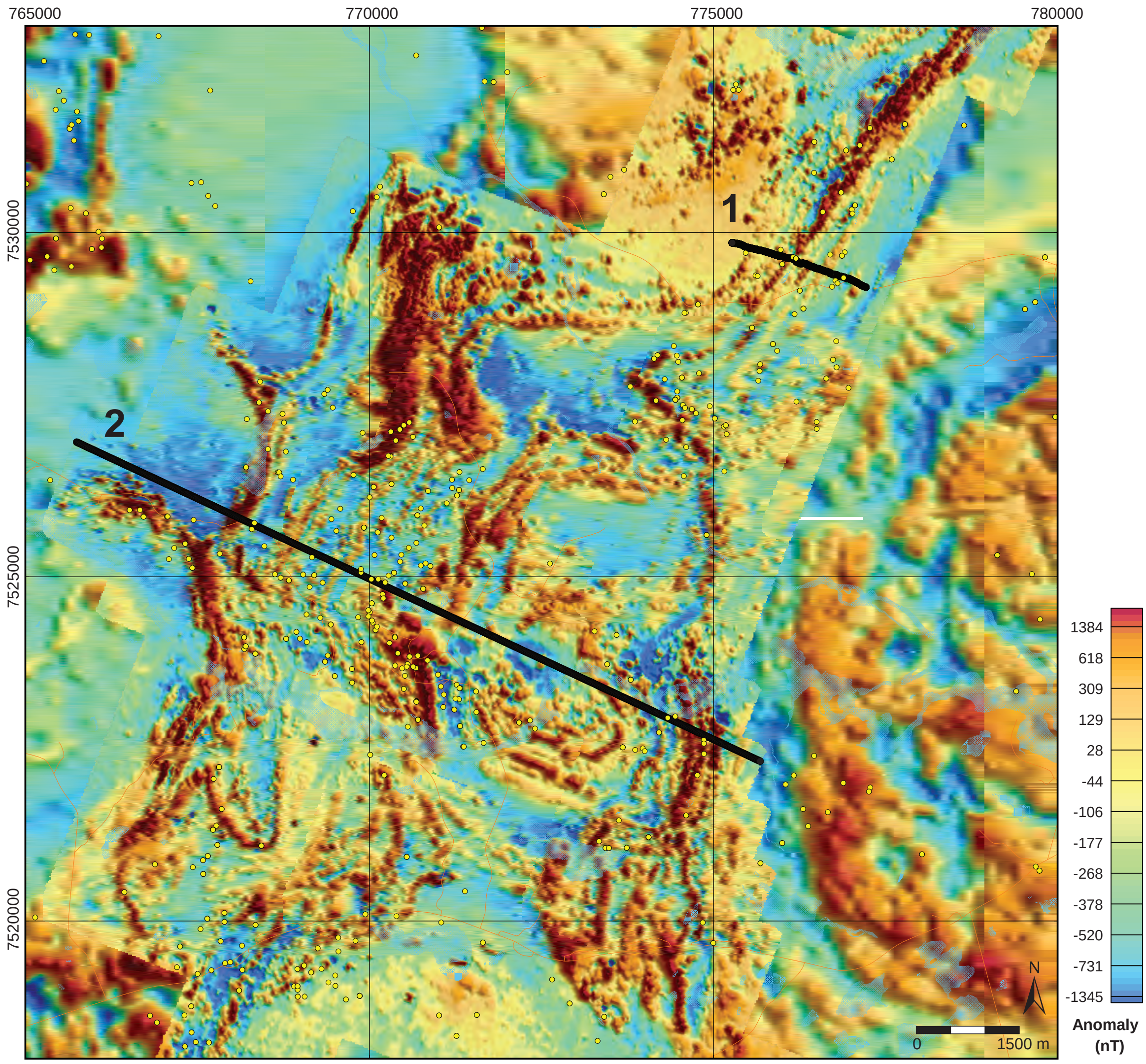

Figure 3. Magnetic anomaly map of the Nunasvaara area. Airborne data are overlain by ground-measured data. Yellow circles show the location of analysed petrophysical samples. Black lines show the extent of the 2D geological profiles that were interpreted from geophysical data.

in the magnetic map. The ground magnetic data also show the various folding events that the area has been subjected to. The high densities of the metavolcanic rocks and metadolerites (on average 2 958 kg/m^3 and 2 979 kg/m^3, respectively) give rise to a predominant gravity high in the area (Fig. 4). However, to generate such a pronounced gravity high, the dense rock must have a substantial depth. This is discussed further in the section on modelling aspects.

In the centre of the area, a few semicircular structures appear as local low anomalies on the gravity map. These gravity lows correlate with low-magnetic signatures and are shown on the bedrock map as

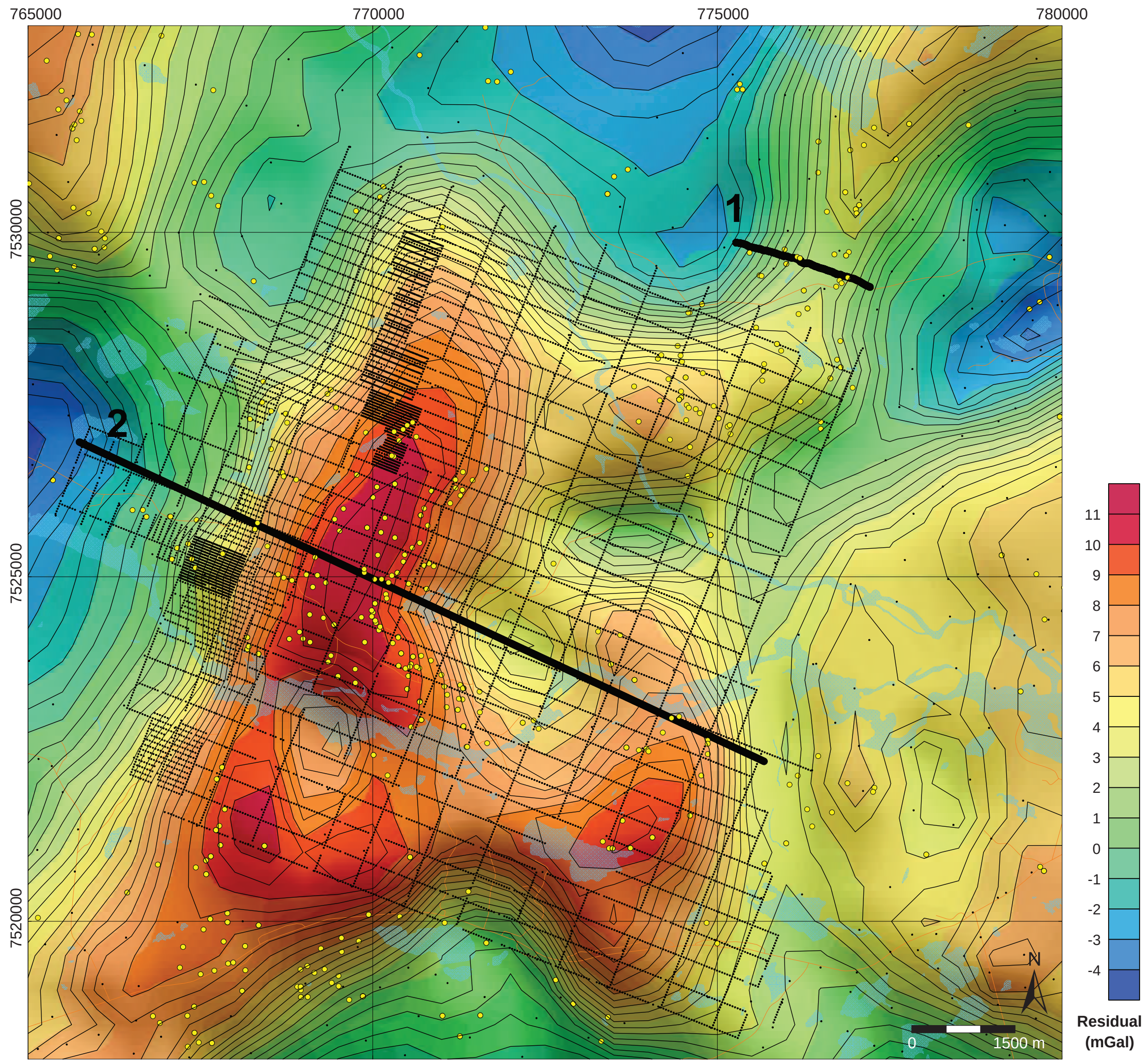

Figure 4. Residual gravity anomaly map of the Nunasvaara area. The grid of black dots represents measurement sites. Yellow circles show the location of analysed petrophysical samples. Black lines show the extent of the 2D geological profiles that were interpreted from geophysical data.

basic volcanic rocks. This appears to be an assumption, since there are no outcrops within these gravity lows, leading to considerable uncertainty about the geographical extent of this lithology. Assuming the presence of basic volcanic rocks in these gravity lows implies a shallower depth extent, underlain by less dense rocks for this lithology. Tuffs and metadolerites are present on all adjacent sides of the low-magnetic basic volcanic rock. The graphite schist horizons and their fold patterns around the central dome structure in the area are seen as narrow, conductive zones in the ground slingram data (Fig. 5).

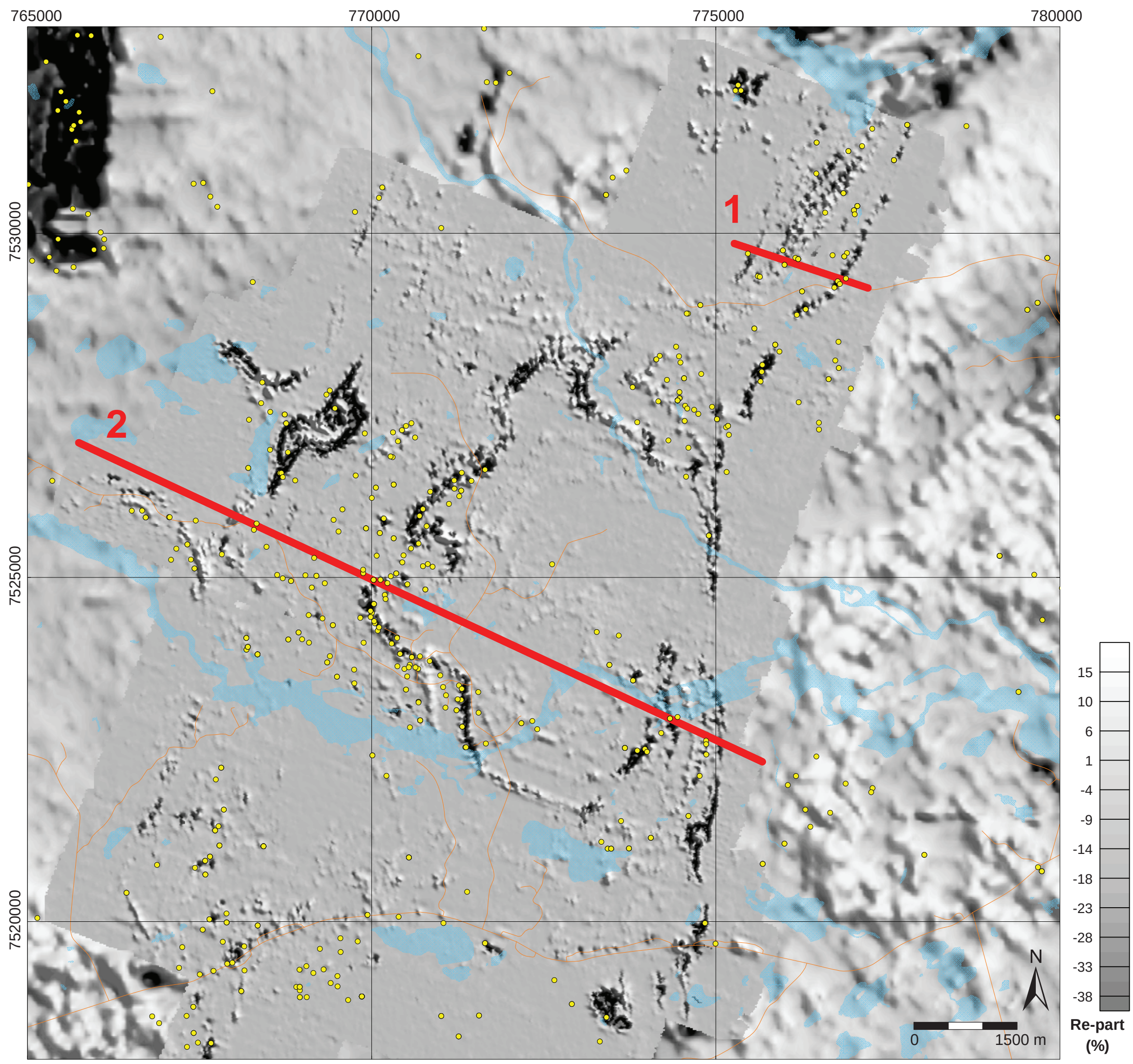

Figure 5. Slingram map of the Nunasvaara area, showing the in-phase component (Re-part). Airborne data are overlain by ground-measured data. Yellow circles show the location of analysed petrophysical samples. Red lines show the extent of the 2D geological profiles that were interpreted from geophysical data. Ground-measured VLF data were also acquired along profile "1"; results shown in Figure 7.

2D MODELLING OF PROFILE 1 AND 2

Modelling was carried out using Potent software. Background density and susceptibility have been set at 2 700 kg/m^3 and 100×10^{-5} SI, respectively.

Profile 1

Profile line "1" in Figure 1 and Figures 3–5 has been forward modelled based on information from newly acquired ground magnetic and pre-existing gravity measurements, together with data from analysed petrophysical samples close to the profile. This is an area where the different lithologies of the greenstones are tightly pinched between intrusive rocks on either side. VLF data were also acquired along the same profile, the extent of which crosses several black schist horizons. The results of the model are displayed in Figure 6, clearly showing the greenstones between the intrusions on either side. To gain a better understanding of the depth extent of the intrusions, the profile was extended during the modelling stage both to the northwest and the southeast to make use of regional gravity field data.

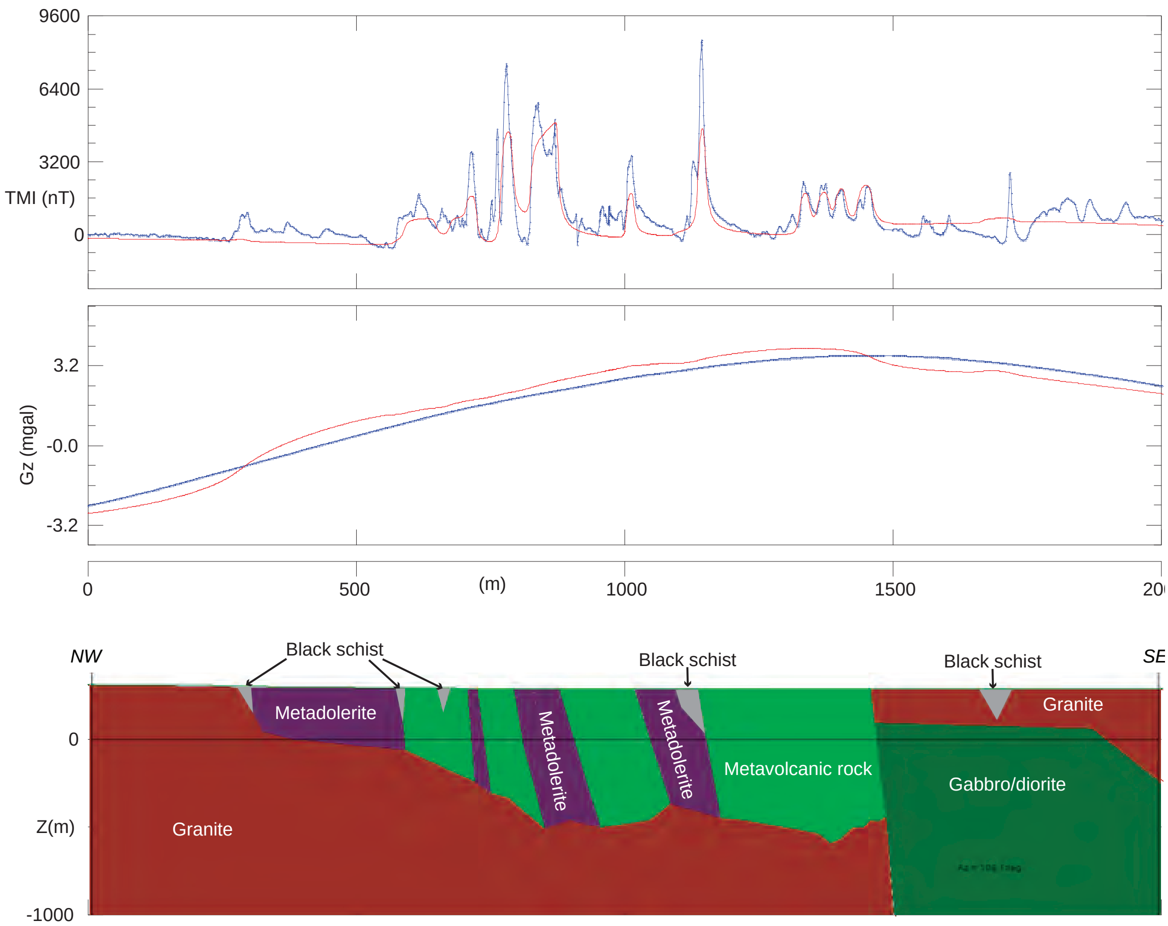

Figure 6. The modelled geological cross-section of profile "1", based on geophysical data. The cross-section is displayed from northwest (left side) to southeast (right side). The lateral extent of the profile is shown in Figure 1 and Figures 3–5. Upper: variations in the magnetic field. Middle: the gravity field. Blue lines in these boxes are observed data; red lines are the response from the model.

Model description and discussion

The gravity anomaly map (Fig. 4) shows that the profile is located across a gravity high, which strikes in a southwest–northeast direction and coincides relatively well with the basic volcanic rocks and metadolerites. The northwestern and southeastern part of the profile lie within granite intrusions from which petrophysical samples have been acquired close to the profile (red body in Fig. 6). These samples have an average density of 2 620 kg/m^3 (n = 2). Petrophysical samples acquired from the metadolerites (purple bodies in Fig. 6) and metavolcanic rocks (light green bodies in Fig. 6) in the vicinity of the profile have densities ranging from 2 800–3 200 kg/m^3 (n = 48), with an average density of 2 970 kg/m^3. This is quite uniform over the area as a whole (Table 1), with the metadolerites and the metavolcanic rocks having almost the same average densities. The assumption has been that the granite intrusion in the west continues under the greenstones, which deepen towards the east down to 800 m below ground level in the centre and east of the sequence. However, the maximum gravity anomaly along the profile is reached in the east, close to the contact with the granite intrusion. To compensate for this, a body with mafic properties has been added to the model (dark green body in Fig. 6), underlying the granite. A gabbroic to dioritic intrusive rock occurs east of the granite (Fig. 1), from which petrophysical samples have been acquired, approximately 2.5 km from the eastern end of the profile. These samples have an average density of 2 910 kg/m^3 (n = 3), which has been assigned to the mafic body. To satisfy the observed gravity data, the depth extent of the mafic body is approximately 3 km.

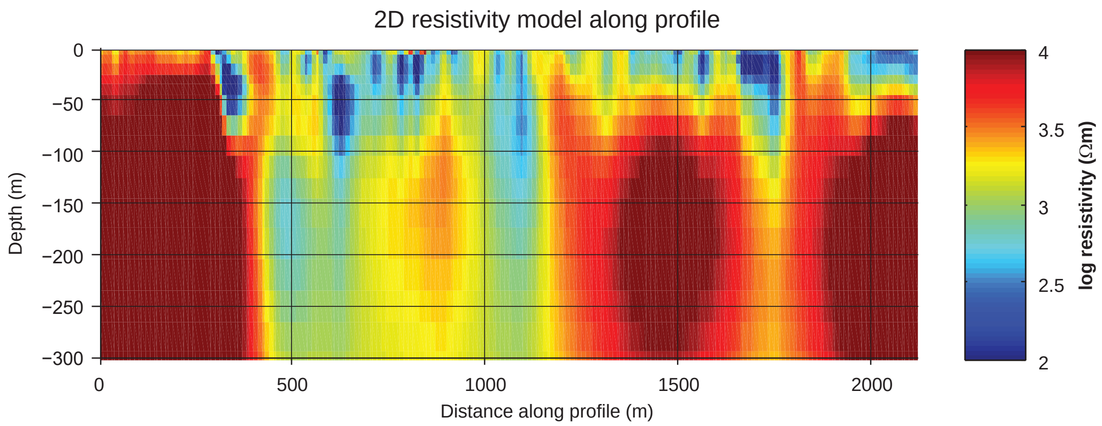

Figure 7. Resistivity cross-section along profile "1" (Fig. 1 and Figs. 3–5). The cross-section displays the resistivity properties of the shallow subsurface and is derived by inversion of VLF data.

The magnetic susceptibilities of metadolerites and metavolcanic rocks vary within a broad range over small distances, as seen in the ground magnetic data in Figure 6. The metadolerites, for instance, have magnetic susceptibilities ranging from 60×10^{-5} SI to $20\,000 \times 10^{-5}$ SI, according to data from both petrophysical samples and in situ measurements of magnetic susceptibility on outcrops close to the profile. The modelled magnetic data show that the lithologies of the greenstones dip steeply towards the east by approximately 80 degrees. The grey bodies in Figure 6 represent black schist horizons and have been adapted from the interpretation of the VLF profile, presented below.

Slingram anomalies are caused by narrow (50–100 m) black schist horizons and are aligned in the same strike direction as the magnetic anomalies. To evaluate the geometry of the black schist horizons, ground VLF measurements have been made along the profile shown in Figure 6. The results of these measurements are presented in Figure 7 as a resistivity cross-section, where the properties of the shallow subsurface are displayed. However, the exact dip and depth extents of the horizons are difficult to determine from this cross–section, since the measurements were made at only one frequency. Other factors influencing the result are the direction to the transmitter and its signal-to-noise ratio.

Several strong conductive features appear close to the surface in the resistivity cross-section (Fig. 7). Starting from the west (left side), a narrow conductive feature is located 350 m from the western end of the profile. The dip of this feature is steep towards the east and has a depth extent of approximately 100 m. This is probably the westernmost horizon of the black schist, situated at the contact between the granite intrusion and the greenstones. Continuing further east, additional conductive, vertical horizons are visible at distances of 650 m, 1 100 m and 1 750 m along the profile.

A relatively conductive segment occurs between 400–1 200 m down to 300 m below ground level. According to the slingram map (Fig. 5), this part of the profile is an area with several closely-spaced conductive horizons. It is possible that this area of multiple conductive black schist horizons causes the single broad low resistivity zone seen in the resistivity cross-section.

Profile 2

An interpreted geological 2D profile based on magnetic data (primarily ground data), gravity data and information from petrophysical samples has been created along a section crosscutting the area roughly in the middle. The geographical extent of this profile is drawn in Figure 1 and Figures 3–5 and labelled "2". The profile covers the area from the intrusion in the west, through the volcanoclastic metasedimentary rocks, basic metavolcanic rocks and metadolerites of the greenstone group to the eastern side, where it ends in intrusive rock. The resulting model is shown in Figure 8.

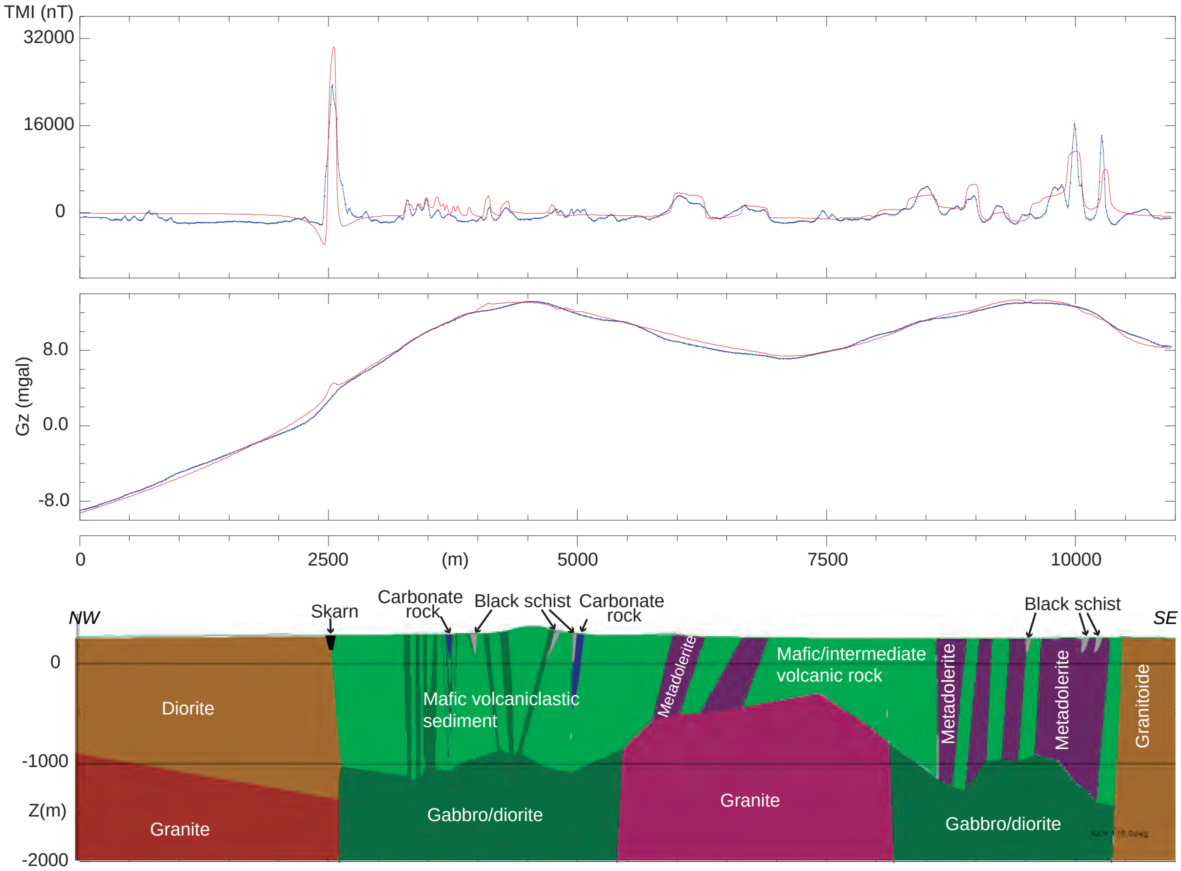

Figure 8. Forward-modelled geological cross-section of profile "2". The cross-section is displayed from northwest (left side) to southeast (right side). Upper: variations in the magnetic field. Middle: gravity field. Blue lines in these boxes are observed data; red lines are the response from the model.

Model description and discussion

The western part of the cross-section (Fig. 8) lies in an intrusion of dioritic composition, visualised as the shallower brown body. Petrophysical samples acquired from the diorite have an average density of 2 800 kg/m^3. The red body beneath the diorite is Lina granite, which has been sampled west of the profile. The samples have low densities, averaging 2 610 kg/m^3. The granite has a significant depth extent, indicated by the pronounced gravity low in the western part of the profile.

A skarn iron formation occurring at the contact between the diorite and the greenstones is clearly seen in the magnetic anomaly data. Petrophysical samples from this skarn horizon have an average density of 3 600 kg/m^3 and, for this particular location, susceptibility has been assumed to be 50 000 $\times 10^{-5}$ SI in order to fit the response from the observed magnetic field. Two samples were collected from this high-magnetic structure and have susceptibilities of 40 000 and 70 000 $\times 10^{-5}$ SI, so the assigned susceptibility is realistic. To fit the modelled response from the skarn horizon to the observed field, the structure must dip steeply to the east.

East of the skarn is a package of alternating volcaniclastic sediments of predominantly mafic composition. These lithologies are tightly stacked and folded with rapid variations in magnetic mineral content. The bulk densities of these layers are roughly similar, however, with an average density of 2 950 kg/m^3 (n = 61). This whole package is seen in the ground magnetic data as an area with short spatial distance in the east–west direction between each magnetised horizon. In Figure 8 the low-magnetic parts of the volcaniclastics are shown in light green, and the higher magnetised horizons in darker green. The high-magnetic horizons have been assigned susceptibilities in the range of

$10\,000–17\,000 \times 10^{-5}$ SI. The geometry of the magnetic layers is steep, and several have a synclinal shape. A carbonate rock occurs within the sequence (blue in Fig. 8), at approximately 3 750 m along the profile. A possible interpretation from the model could be that the magnetic layers surrounding the carbonate form a syncline around it. A pronounced gravity high can be seen in this area (Fig. 4) and, for the model to satisfy it, there must be dense rocks continuing down to substantial depth. The assumption has been that the supracrustal rocks have a depth extent of approximately 1 km, which corresponds relatively well with the shorter-waved anomalies seen in the ground magnetic data. At greater depth, a mafic intrusive (dark green in Fig. 8) has been adopted in the model, which, to satisfy the gravity high, continues down several km. The average density of the petrophysical samples analysed from the gabbro/diorite is 2 954 kg/m^3 (n = 54; Table 1), so this value has been assigned to this deep-seated lithology.

Highly magnetised metadolerites (purple colour in Fig. 8) occur between 6 000–7 000 m along the profile, which can be clearly seen on the magnetic anomaly map (Fig. 3). In situ measurements on outcrops show the average magnetic susceptibility of the metadolerites to be $28\,000 \times 10^{-5}$ SI (n = 24).

East of the metadolerites is an area of low-magnetic mafic to intermediate volcanic rock (light green in Fig. 8). This area has low exposure of outcrops. These lithologies are therefore assigned the average density value of all analysed petrophysical samples acquired from volcanic rocks in the model: 2 960 kg/m^3 (Table 1). On the gravity map (Fig. 4), this part of the profile corresponds to an area with a local, semicircular low-gravity anomaly. To achieve a model that is relatively consistent with the observed gravity field, there must be a less dense lithology underlying both the highly magnetic metadolerites and the dense volcanic rocks between 5 500–8 000 m along the profile. The assumption during the modelling process has been that the underlying rock is a granitic intrusion (pink in Fig. 8), with the same physical properties as the one closest to the southern border of the greenstone package (Fig. 1). The deep-seated granitic intrusion has thus been assigned a density of 2 650 kg/m^3 and a susceptibility of 100×10^{-5} SI. In the model, the shallower metadolerites and volcanic rocks extend approximately 600–1 100 m below the surface, while the intrusion continues down to a depth of several km to satisfy the observed gravity field.

East of the low-magnetic volcanic rock is another area with banded magnetic structures making up a semicircular pattern around the low-magnetic volcanic rocks. These high-magnetic bands are mainly caused by metadolerites (purple in Fig. 8), with magnetic susceptibilities up to $40\,000 \times 10^{-5}$ SI, and appear to have a steep dip closest to the low-magnetic volcanic rock, with a tendency to dip more to the west closest to the eastern rim of the greenstone package. There are also strongly conductive horizons in the area, clearly seen in the slingram data (Fig. 5), caused by black schist horizons. A high-gravity anomaly is associated with this area (Fig. 4); the amplitude indicates a substantial depth extent of the dense rocks. Available petrophysical information shows the densities of the shallower greenstones are within the range 2 900–3 000 kg/m^3 in the area. By applying magnetic and density properties derived from samples to the shallow bodies in the model that represent the greenstones, a good fit is achieved to the shorter-waved ground magnetic data, suggesting a depth extent of the metadolerites and metavolcanic rocks of approximately 1 km below ground level. Ending the greenstones at this depth, however, creates a mass deficiency in the gravity response compared with the observed data. A mafic intrusive (dark green in Fig. 8) has therefore been adopted in the model below the greenstones to compensate for this. Using a density of 2 954 kg/m^3 for this body, which is the average density for gabbro/diorite in the area (Table 1), the mafic intrusive has a depth extent of several km below ground level.

The bedrock east of the greenstones consists of intrusions. Closest to the greenstones is an intrusion with relatively low average density, 2 750 kg/m^3 (brown in Fig. 8).

MASUGNSBYN

Geological introduction

The bedrock in the Masugnsbyn area consists of basaltic metatuff belonging to the *Veikkavaara greenstone group*, overlain by metavolcanic and metasedimentary units (chert, mafic schist and marbles) belonging to the *Kalixälv* and *Pahakurkio groups* (Padget, 1970). Metadolerite and graphitic black schist occur in the metatuffs. Intrusive rocks of mainly granitic to syenitic composition have intruded the supracrustal rocks, and gabbroic rock is also present (Fig. 9). Skarn iron, dolomite, Cu-Zn-Pb, Cu-Au, and graphite mineralisations occur in the area. A more detailed description of the geology and lithostratigraphy around Masugnsbyn is found in Lynch et al. (2018).

Geophysical interpretations in the Masugnsbyn area

Geophysical data coverage is extensive around Masugnsbyn. Airborne magnetic, radiometric, VLF and slingram data all exist, as well as regional ground gravity data. The area is well covered by various ground geophysical measurements targeting, mainly, exploration objects in previous campaigns. For more information on airborne and ground geophysical data the reader is referred to the report by Hellström & Jönsson (2014).

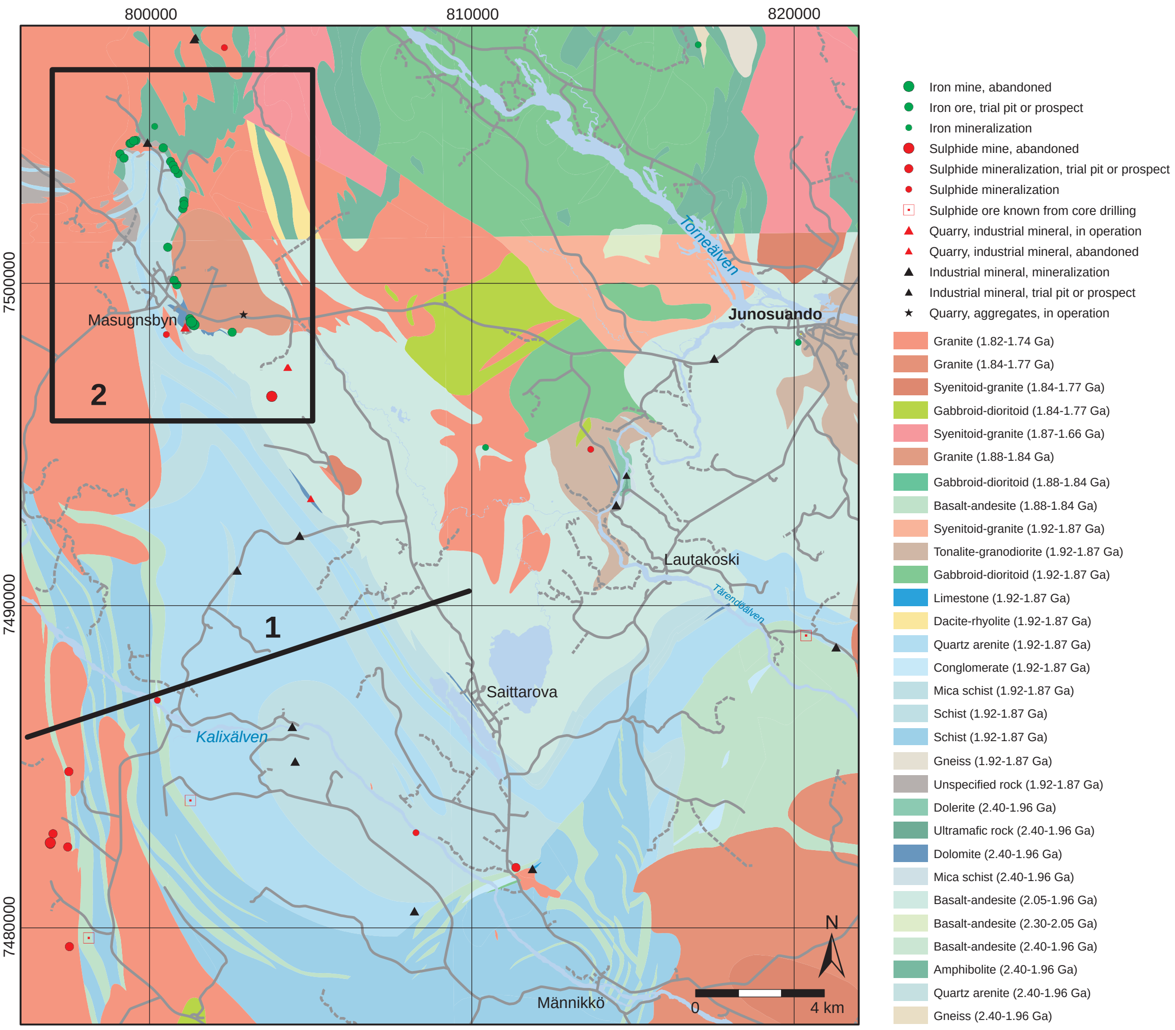

Figure 9. Bedrock map of the area around Masugnsbyn, after Bergman et al. (2012). The mineralisation occurrences are shown on the map. The areas targeted for modelling lie along the profile "1" and within the polygon "2".

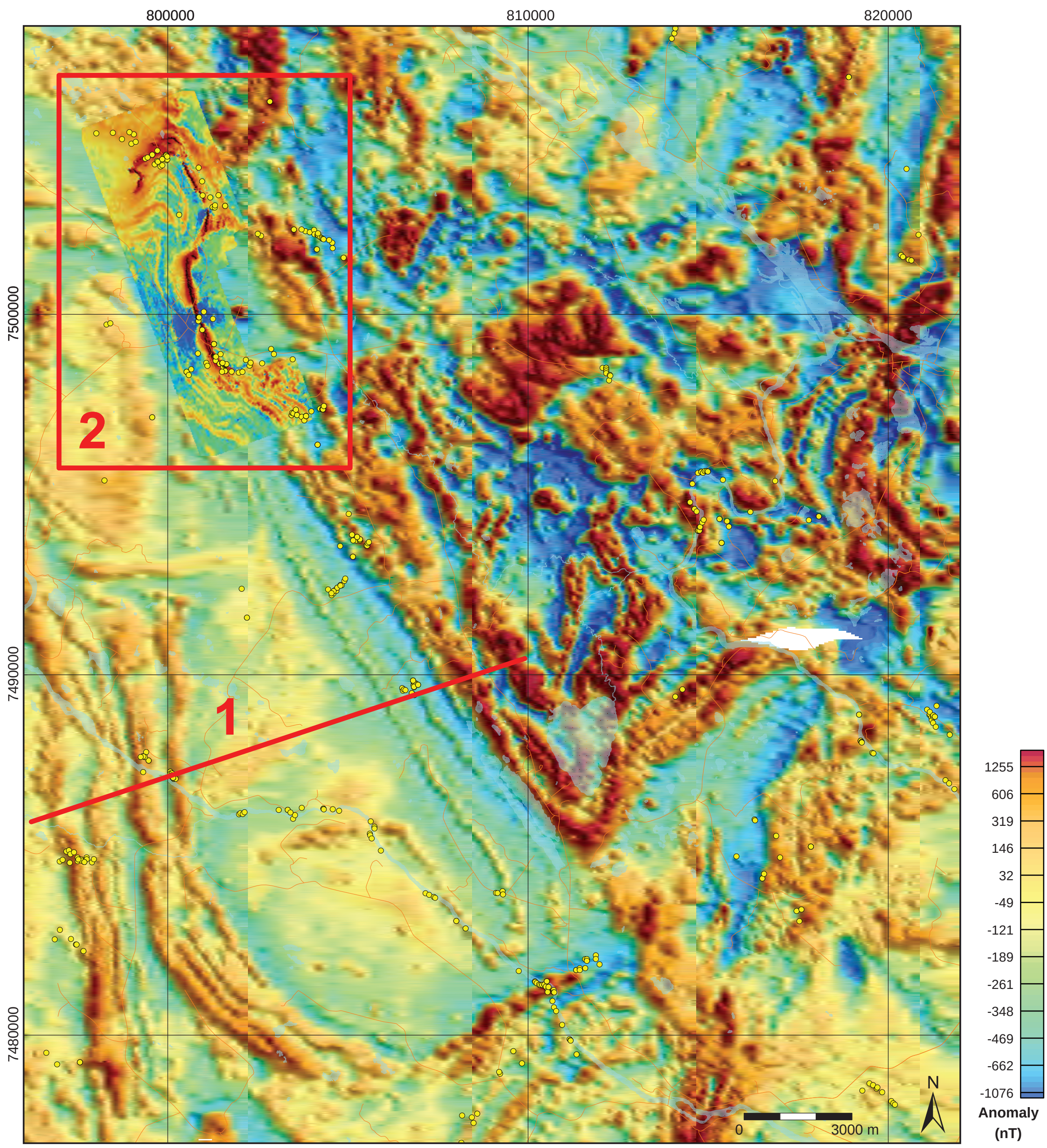

Figure 10. Magnetic anomaly map of the Masugnsbyn area. Data from ground magnetic surveys around the Masugnsbyn ore deposit are transposed onto the airborne data. Yellow circles show the location of analysed petrophysical samples. The areas targeted for modelling lie along the profile "1" and within the polygon "2".

The overall pattern of magnetic (Fig. 10) and gravity field data (Fig. 11) represents the lithological units in the area. In the most westerly part, the bedrock predominantly consists of metasedimentary rocks of the *Kalixälv* group, with intercalations of basaltic to andesitic metavolcanic rocks. The metavolcanic rocks have a higher magnetic susceptibility and can be outlined with the aid of the magnetic field pattern. The metasedimentary *Pahakurkio* group predominates in the central parts of the area. These rocks are characterised by low magnetic susceptibility and low to intermediate density. Several long, narrow and weakly positive magnetic anomalies within this sedimentary unit may represent original layering. The eastern part of the area has a high-magnetic signature and an obvious V-shaped

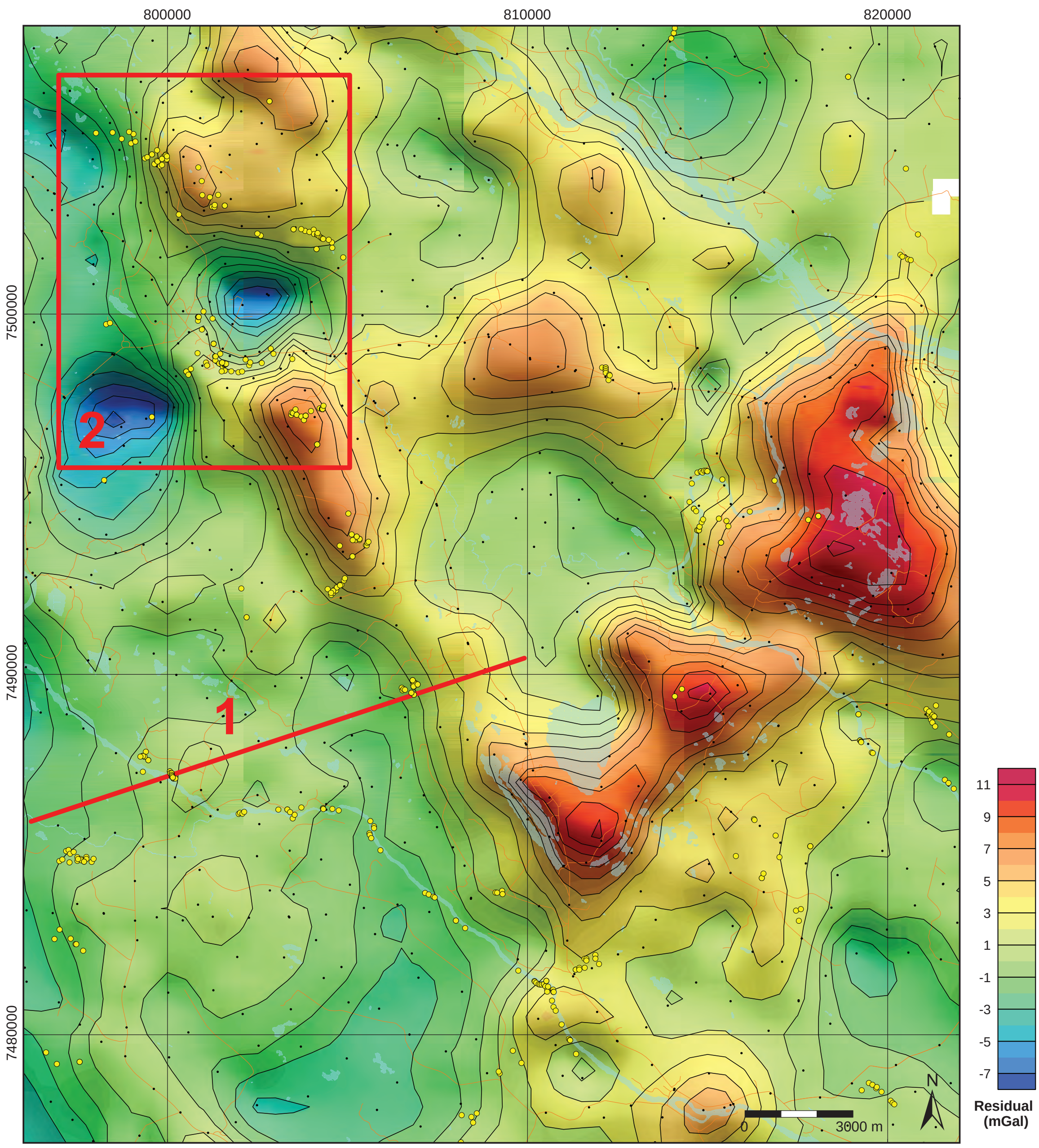

Figure 11. Residual gravity map of the Masugnsbyn area. Yellow circles show the location of analysed petrophysical samples. Black dots represent regional measurement sites. The areas targeted for modelling lie along the profile "1" and within the polygon "2".

fold, which can also be observed in the gravity and slingram data. The observed patterns are due to the Veikkavaara greenstone group consisting of basaltic greenstone with graphitic schist and carbonate horizons. The graphitic schist horizon is evident in the electromagnetic geophysical data (VLF and slingram), which outline the conducting horizon well (Fig. 12). The geophysical and petrophysical data is further presented and described in Hellström & Jönsson (2015).

Geophysical modelling in the Masugnsbyn area has been carried out in two areas; see Figures 9–12. The first area of interest is the Masugnsbyn iron ore, where dense sampled gravity data, together with information from petrophysical samples and boreholes, have been used as input data to construct 3D models of the anomalies hosting the mineralisation. Ground magnetic and slingram data have been used to quantify the dip of these lithologies at depth. The second area of interest is the regional geological setting across the sedimentary basin, which is surrounded by granite in the southwest and mafic volcanic rocks in the northeast. In this regional model, airborne magnetic data were primarily used as input data, along with information from petrophysical samples. At some locations, newly acquired geophysical data were also used during the modelling stage to resolve more details in the subsurface conditions.

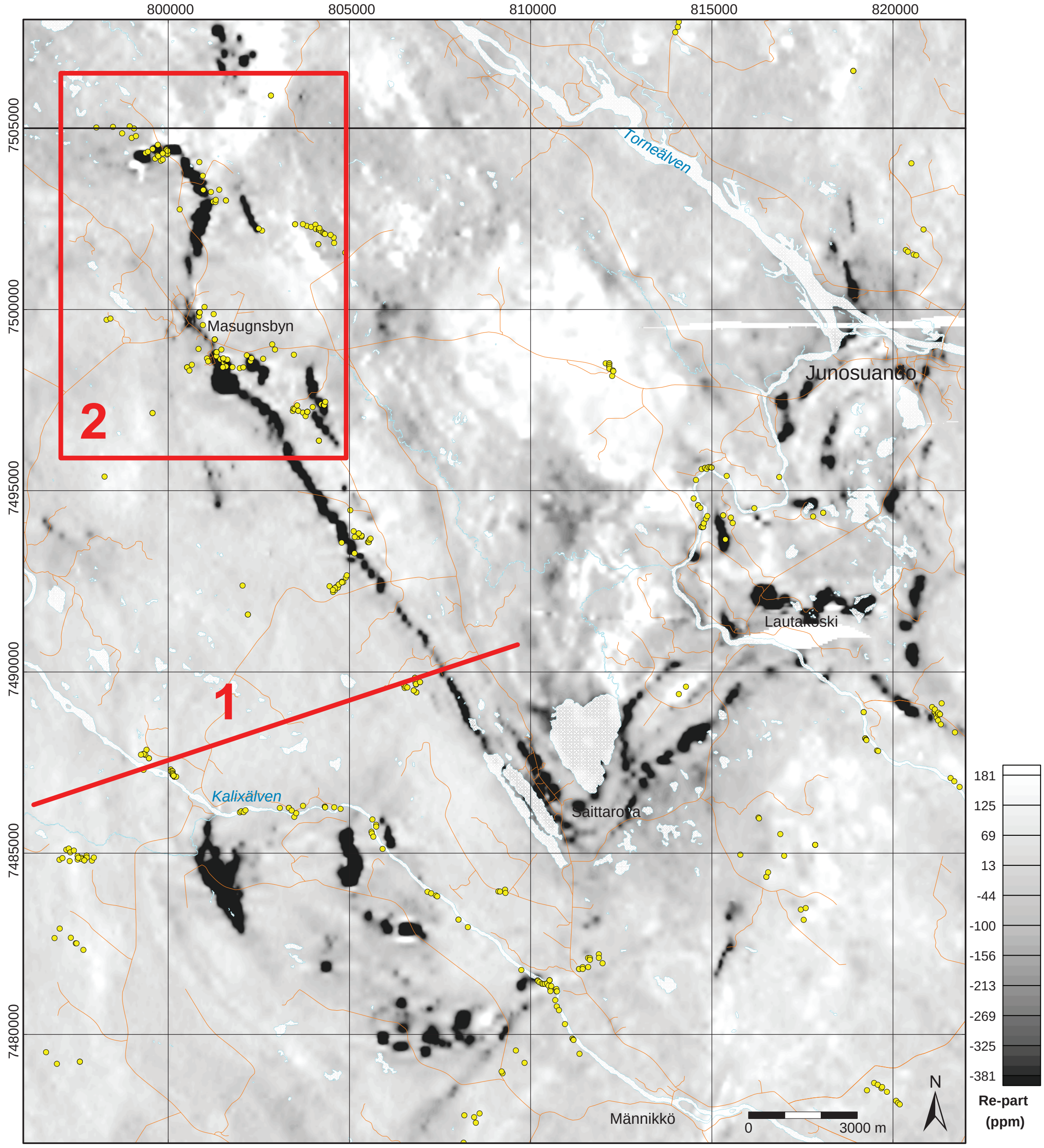

Figure 12. Slingram map of the Masugnsbyn area showing the in-phase component, based on airborne measurements. Yellow circles show the location of analysed petrophysical samples. The areas targeted for modelling lie along the profile “1” and within the polygon “2”.

3D modelling of the Masugnsbyn iron ore

Geophysical modelling of the Masugnsbyn iron ore deposit was carried out with the aim of visualising the ore body in 3D. The final model was then compared with the results from the numerous boreholes in the area to build a 3D geological model. The Masungsbyn iron ore is a well-known and well-explored area. A historical and geological description of the area and references to earlier publications are presented in Hellström & Jönsson (2014). Detailed gravity and magnetic surveys were conducted between 1963 and 1967; slingram measurements were carried out in 1974.

Model description

The model was constructed from inverse modelling of gravity field data and has been generated in the VOXI environment, an extension of the Geosoft software package. The gravity data used as input data for the model were acquired by SGU in 1964–1965 and consist of terrain-corrected Bouguer anomaly data. The line/point distances vary within the area: from 320 m/40 m to 40 m/20 m over the ore body. The densest sampled areas have been modelled separately to maximize the model resolution (called North and Central part in Fig. 13). The different modelled areas are shown in Figure 14, the southern

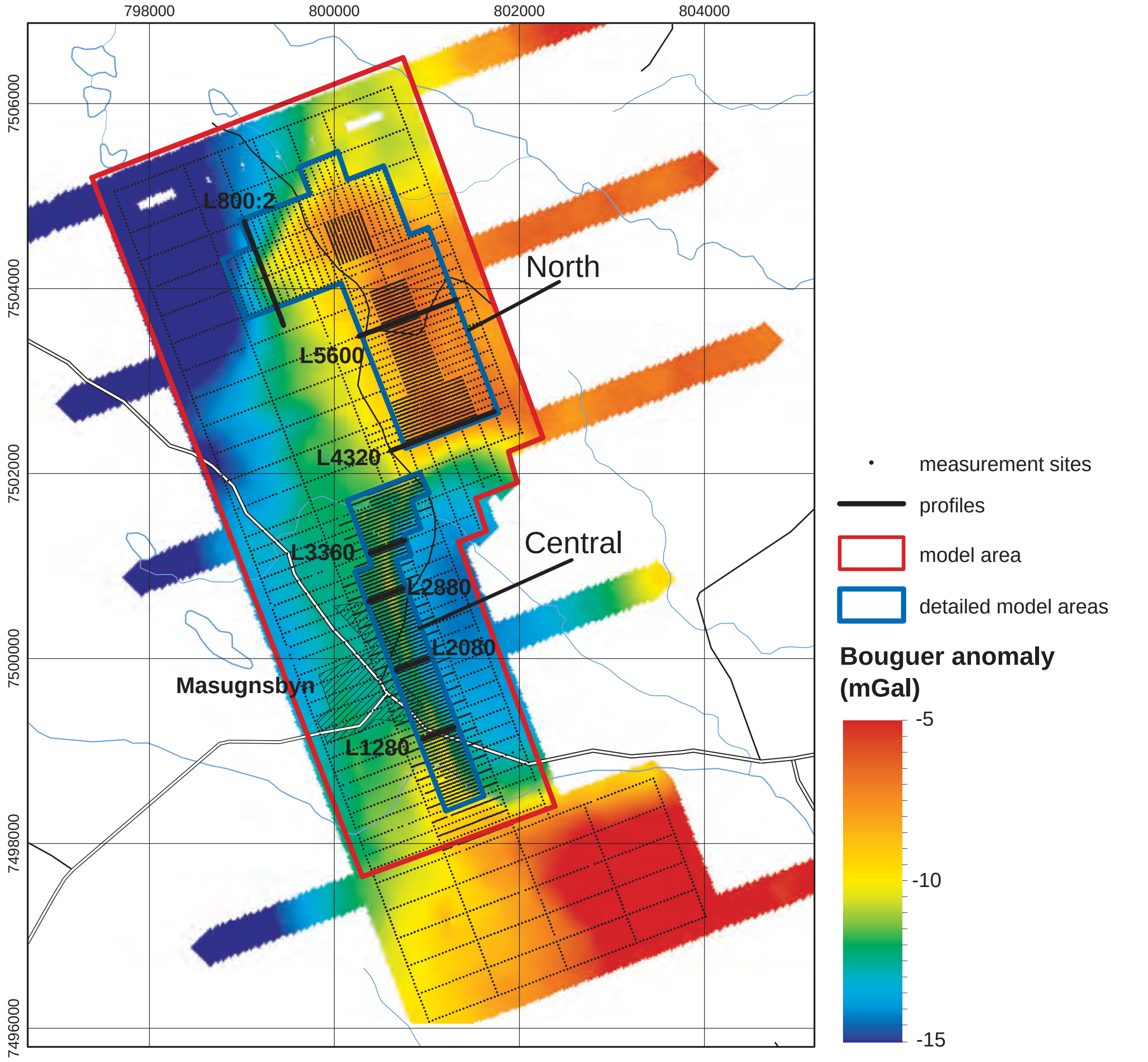

Figure 13. Dense gravity measurements in the Masugnsbyn iron ore area. The map extent corresponds to polygon "2" in Figures 9–12.

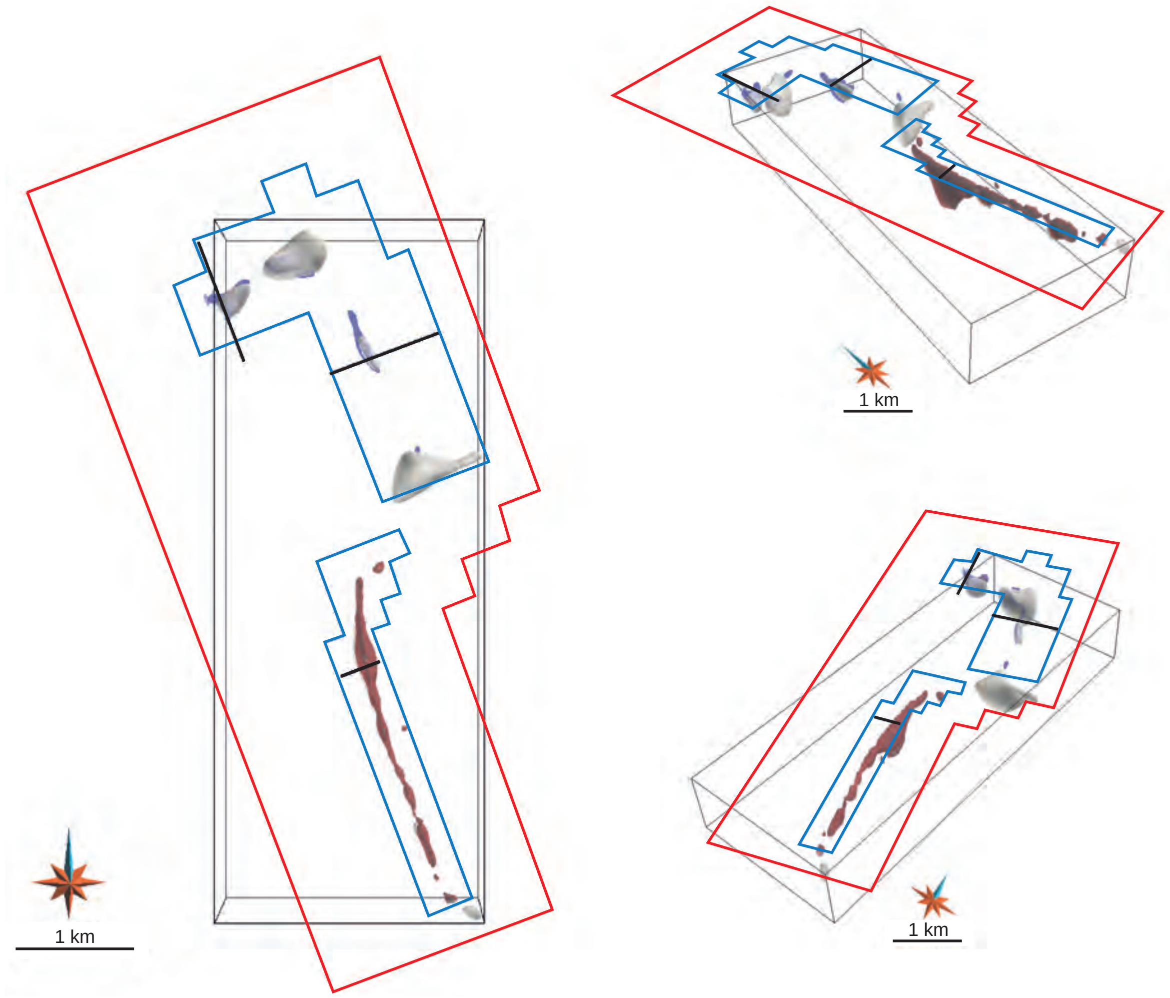

Figure 14. The modelled density distribution seen from different perspectives. The red polygon defines the area modelled, with the two subsidiary modelled areas North and Central (blue). The black lines show the location of the profiles in Figure 16. The grey isosurface represents a density value of 3 000 kg/m³, the blue 3 020 kg/m³ and the red 3 100 kg/m³. The dimensions of the black box are: x: 2 600 m, y: 6 700 m and z: 1 200 m. Visualisation in GOCAD software.

part covering the Junosuando field and the northern area including Vähävaara, Välivaara, Vuoma and Isovaara. The models are restricted to values between 2 200–3 700 kg/m^3, as the background density is attributed to 2 700 kg/m^3. Petrophysical samples acquired and analysed in 2015 show that the skarn iron ore has a density range of 3 300–4 500 kg/m^3.

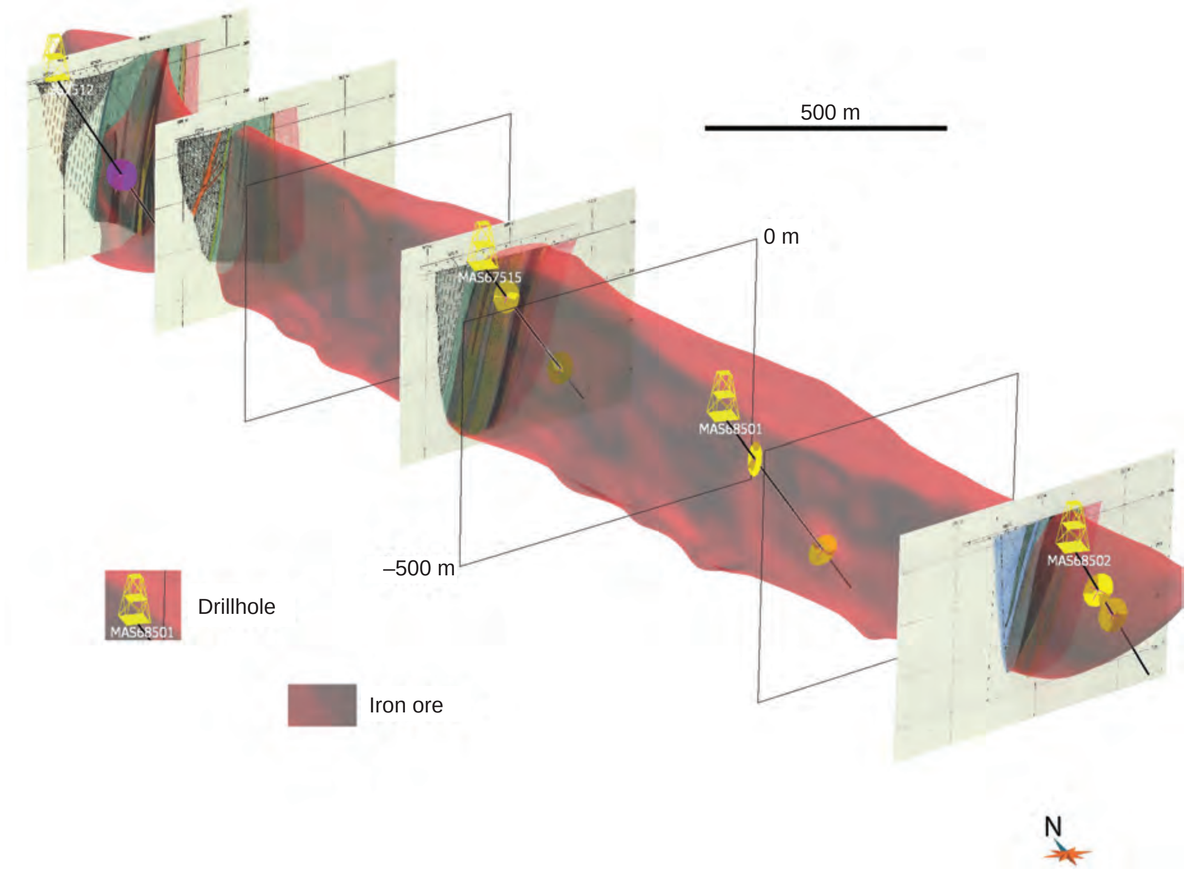

Figure 15. Established southern part of the Masugnsbyn iron ore body based on surface modelling using a series of geological profiles and drill core data. The profiles were published earlier by Witschard et al. (1972). Note the similarity between the geometries of the mineralised skarn and thin ore body obtained in this model and the geometries of the density isosurfaces displayed in Figure 14. Hollow frames refer to the locations of the non-displayed profiles, which were also used to constrain the outline of the ore body. Drill markers (yellow discs) indicate the outer contact with the ore body. Visualisation in GOCAD software.

Result

The result of the modelling is shown in Figure 14, where three isosurfaces visualise a possible density distribution that would yield the observed gravity field. The surfaces are constructed from the three model areas (Fig. 13) and have the same data but different resolutions, yielding a slightly different result. These surfaces correlate well with earlier interpretations of the subsurface density distribution. According to Witschard et al. (1972), the ore zone in the Junosuando field is between 70 and 100 m wide and dips steeply to the west (Fig. 15). The model shows a width between 50 and 150 m for the mineralised skarn, represented by a vertical slab (central model). In Figure 16 the gravity response along three profiles is shown to illustrate the result of the model, as well as the correlation between the observed gravity data and response from the modelled density distribution.

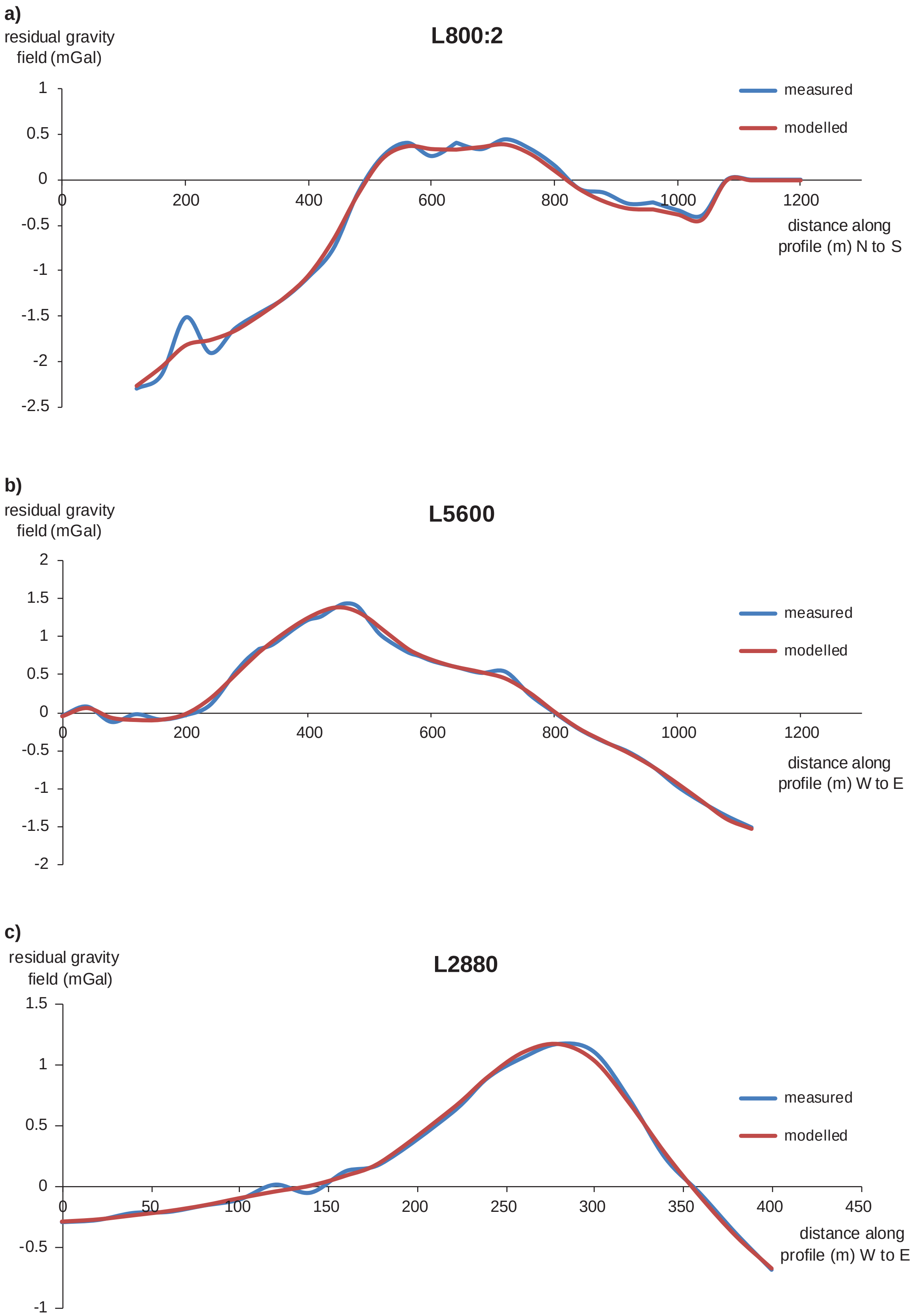

Figure 16. Comparison between measured gravity data and response from the model along three profiles. The profiles L800:2 (a), L5600 (b), and L2880 (c) correspond to those displayed in Figure 13.

REGIONAL MODELLING

Introduction

The structural domain in which the Masugnsbyn area is located shows variable foliations and complexly folded rocks. A detailed description of the geological setting can be found in Lynch et al. (2018) and Grigull et al. (2018). The bedrock map from Padget (1970) uses four cross-sections to illustrate different structural, tectonic and lithological relationships. The extent to which geophysical information was used during the modelling stages to produce these profiles is not known. Profile I (Figs. 9–12 and 17) is of two of the main tectonic features in the area; the *Kalixälv dome* and the *Masungsbyn syncline*.

A regional geological model, based on geophysical data and petrophysical information, has been constructed along Profile I and its closest surroundings. Both previously and newly acquired geophysical data have served as input data to develop a structural and lithological interpretation of the area. Airborne magnetic data are primarily used together with magnetic properties of analysed petrophysical samples or in situ measurements of magnetic susceptibility on outcrops. The model has been further refined in those areas where new ground magnetic or VLF data have been acquired.

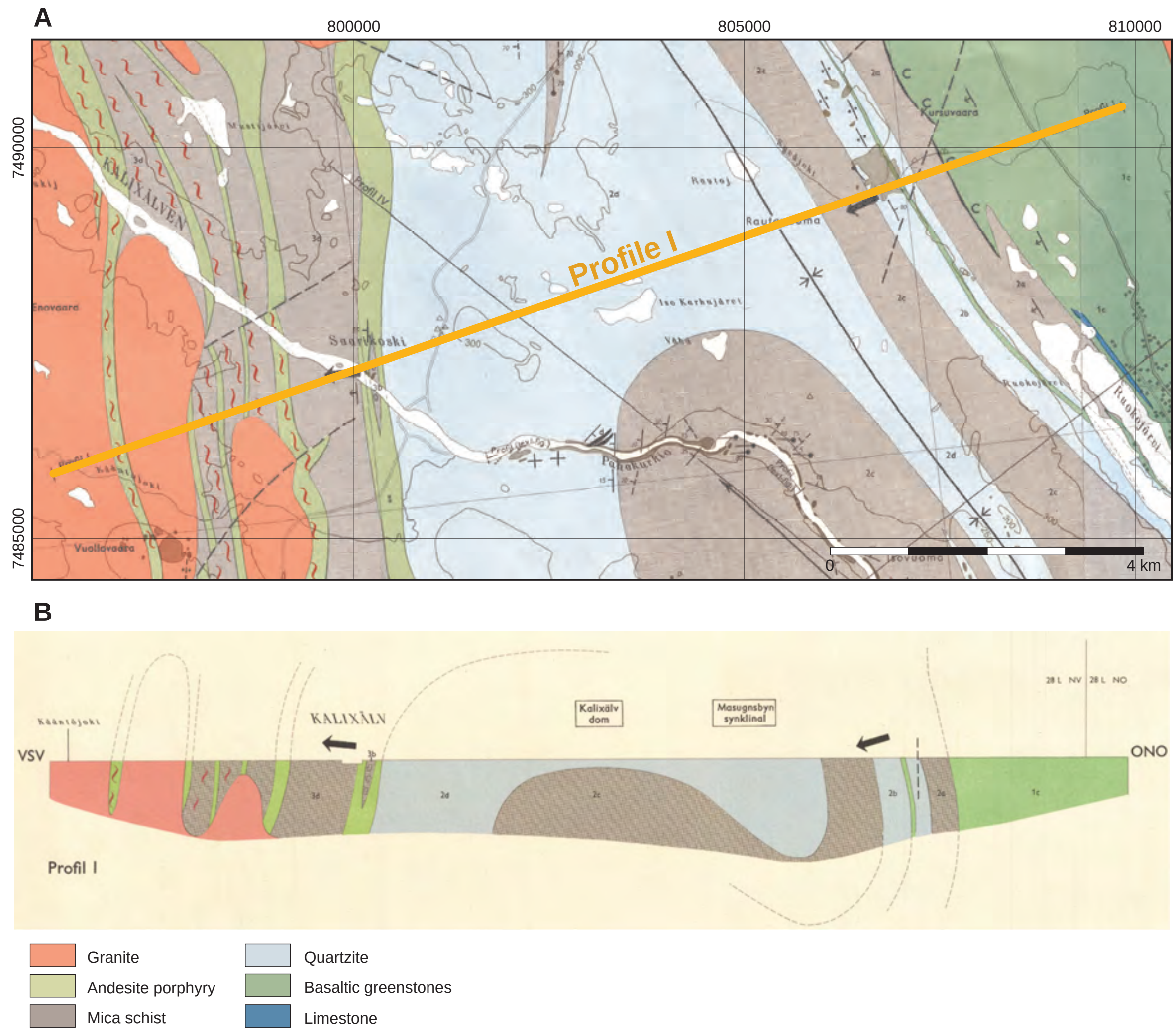

Figure 17. The location of Profile I on the bedrock map (A) and its vertical section (B), both from Padget (1970). The length of the profile is 14.6 km and the depth extent of the cross-section is approximately 1 km.

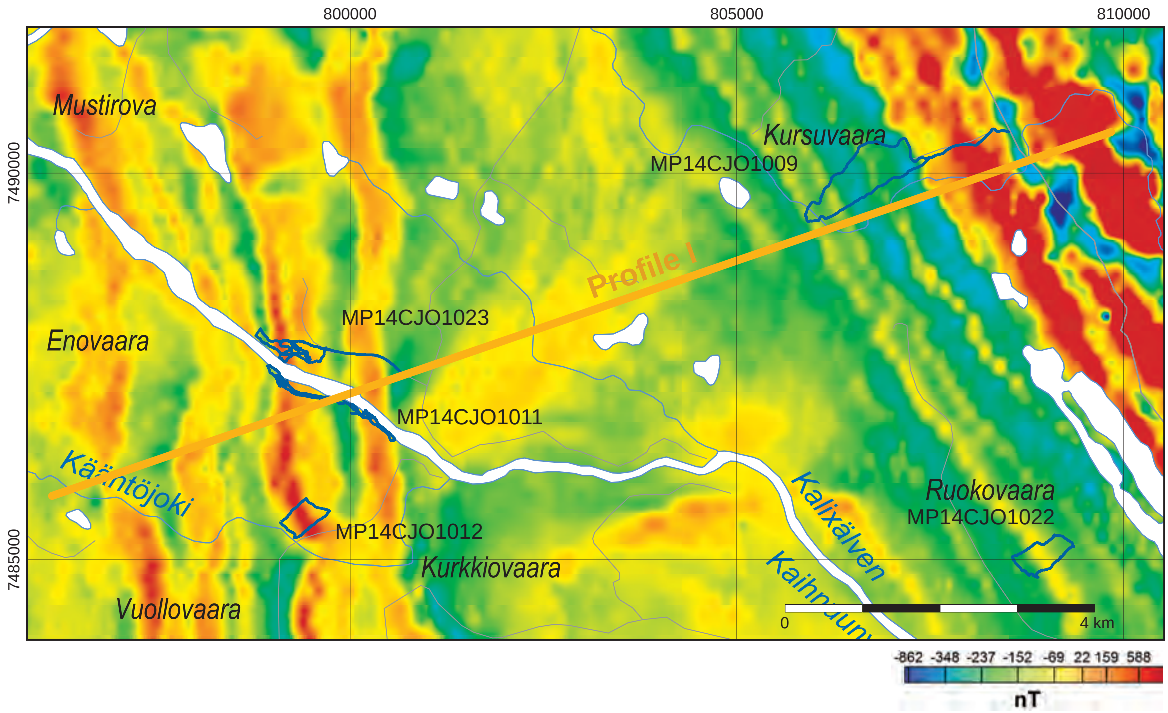

Figure 18. The magnetic anomaly field together with the location of newly acquired ground magnetic profiles (blue) and the extent of the profile (Profile I) along which the model is presented.

Model description

The modelling procedure is a forward modelling concept, where bodies have been created and assigned parameters that would yield a similar response compared to the observed magnetic data. To limit the degree of freedom when creating the model, other available data have been used to restrict parameters. The model bodies generally have simple tabular geometry, assumed to represent layers or dikes within the area. Other limiting data include structural measurements and automated strike and dip calculations of the magnetic anomaly field, which provide an indication of the dip of the bodies (Bastani & Pedersen 2001). Information on magnetic susceptibility, either from in situ measurements or from analysed petrophysical samples, is of most importance in limiting the range of possible values and, together with measurements of remnant magnetisation, if prominent, its direction.

The magnetic susceptibility of the background (i.e. where there are no bodies) is set at zero. Thus, magnetic susceptibility values for the bodies presented are relative values compared with the surrounding rocks. The depth extent for all bodies is set at approximately 1 km. Bodies have been grouped according to the anomaly in the magnetic field pattern to which they belong. This may correlate to different bedrock types or different magnetic characteristics within a bedrock type (Figs. 18 and 19a).

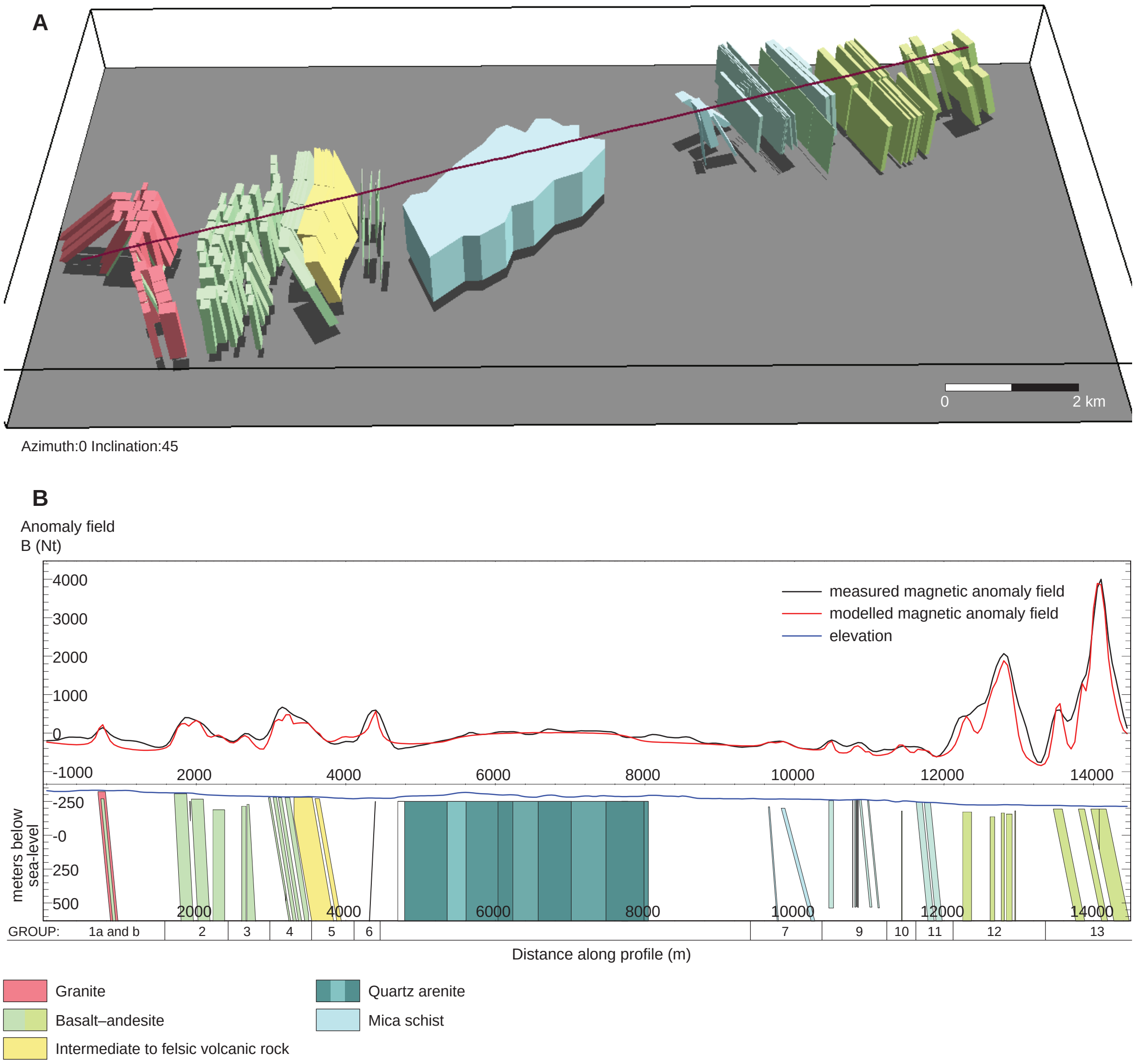

Figure 19. The results from the forward model based on geophysical data. **A.** shows the bodies in perspective with the modelled profile outlined, and **B.** shows the modelled response (red) compared with the measured magnetic anomaly field (black) and the cross-section of the bodies below. Note the different horizontal and vertical scales in B.

Results

The spatial geometry and distribution of bodies are shown in Figure 19a). The measured and the modelled response from the bodies are shown in cross-section in Figure 19b). The outline of the modelled bodies at the surface is shown in Figures 20a) and b). The bodies have been divided into different groups, depending on which anomaly and assumed lithology they represent. The magnetic susceptibility distribution for the different groups is shown in Figure 21.

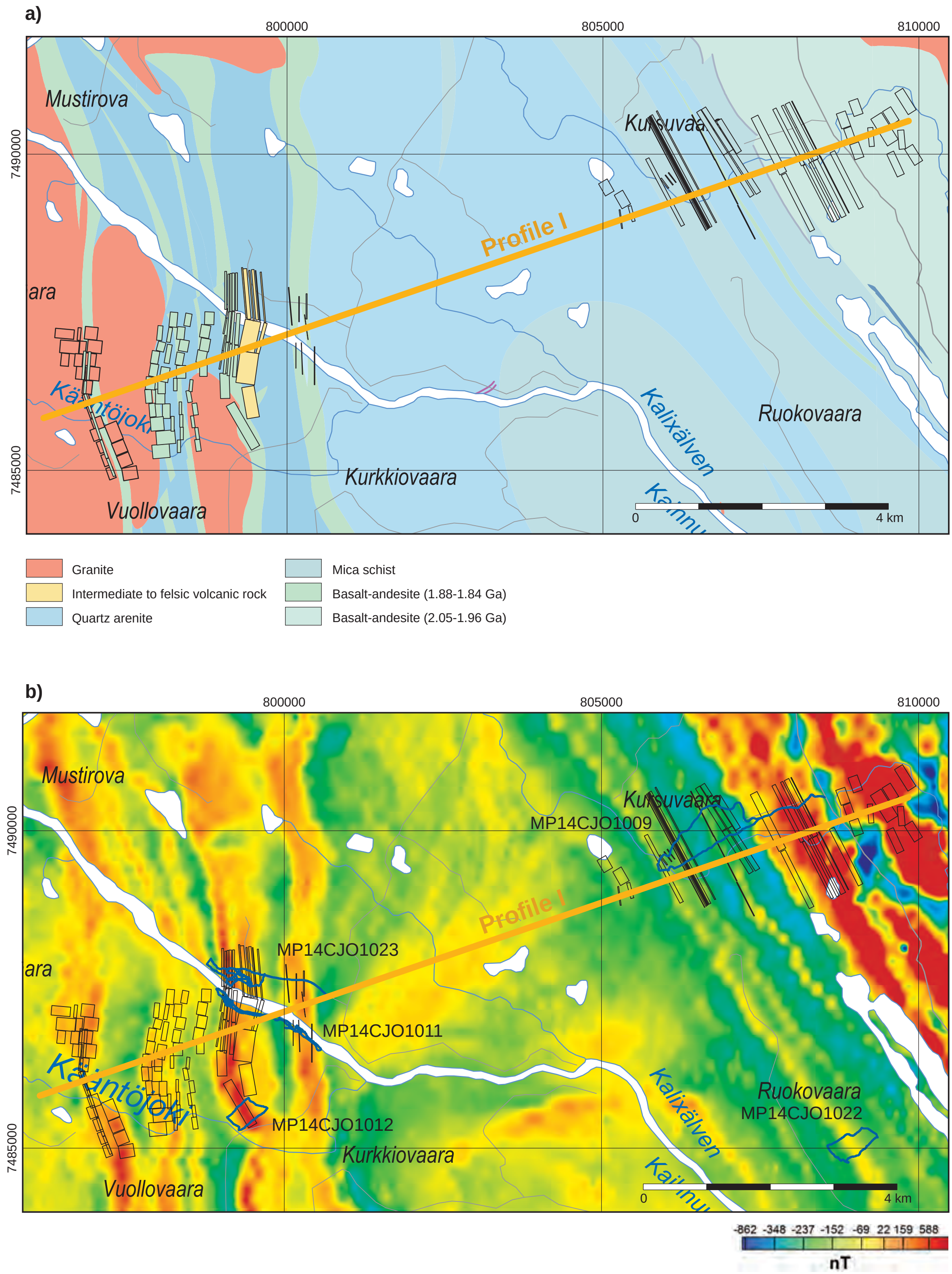

Figure 20. The location of the modelled bodies at the surface compared with the bedrock map a) and the magnetic anomaly map b). The bedrock map is from Bergman et al. (2012).

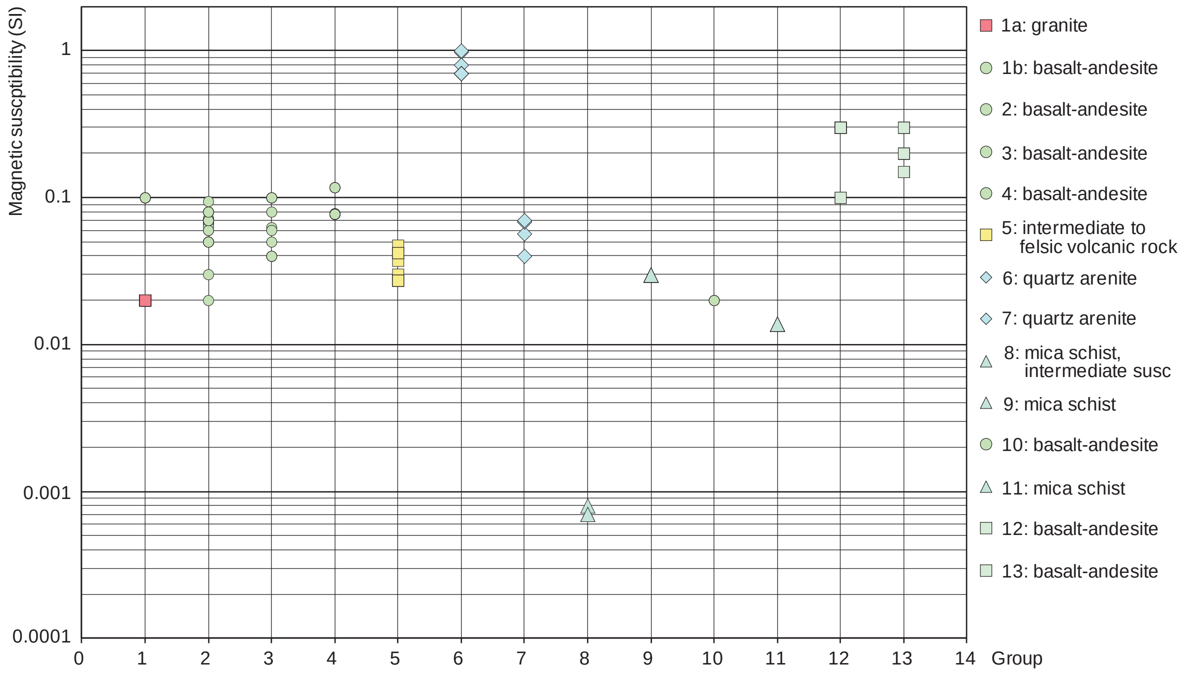

Figure 21. Magnetic susceptibility distribution within the different groups of bodies corresponding to those in Figure 19.

Description of the model and discussion

Field observations and petrophysical analysis of the granite in *Group 1* show there is a significant variation of the magnetite content, with increasing magnetic susceptibility adjacent to andesitic horizons. Three petrophysical samples from the granite gave a susceptibility range of 0.0016–0.021 SI while one sample from the copper mineralised andesite has 0.15 SI. On this basis, and compared with the observed magnetic field, the horizon must have a dip close to vertical.

There is considerable uncertainty about the physical and geometric properties of *Groups 2 and 3* due to the lack of field data or geophysical constraints. Instead, the assumption has been that the magnetic anomalies are caused by similar andesite to *Group 1*, but intercalated in low-magnetic sedimentary bedrock. A VLF profile of this area shows two distinct vertical horizons with high electrical conductivity (blue areas in the profile in Fig. 22B).

The basic volcanic rocks in *Group 4* are modelled on the basis of newly acquired ground magnetic data (Fig. 23), whose geographical extent in shown in Figure 20b). The data indicate that magnetic anomalies are caused by several thin, 20–60 m, tightly spaced slabs dipping 75 degrees to the east. The total width of this package is approximately 150 m.

Group 5 consists of volcanic rocks whose composition ranges from intermediate to felsic (Fig. 24A). The ground magnetic data indicate that magnetic horizons are 10–60 m wide, with a total width of 200–300 m for the entire unit of volcanic rocks. The geometry of these horizons is assumed to be concordant with group 4, i.e. an approximate dip of 75 degrees to the east (yellow bodies in Fig. 23).

Field observations of lithologies in *Group 6* show that this part of the profile consists of fine-layered arenite with highly variable magnetic susceptibility (Fig. 24B), which in itself may explain the enhanced magnetic anomalies in the area. Locally, susceptibility values over 1 SI have been observed in outcrops. The geometry of the highly magnetised horizons is determined by automated calculations on the magnetic anomaly pattern which yield a dip of 80–85 degrees to the west.

Bodies within *Group 7* are constructed on the basis of airborne measurements alone. There is considerable uncertainty, but the shape of the magnetic anomaly indicates a dip towards the east.

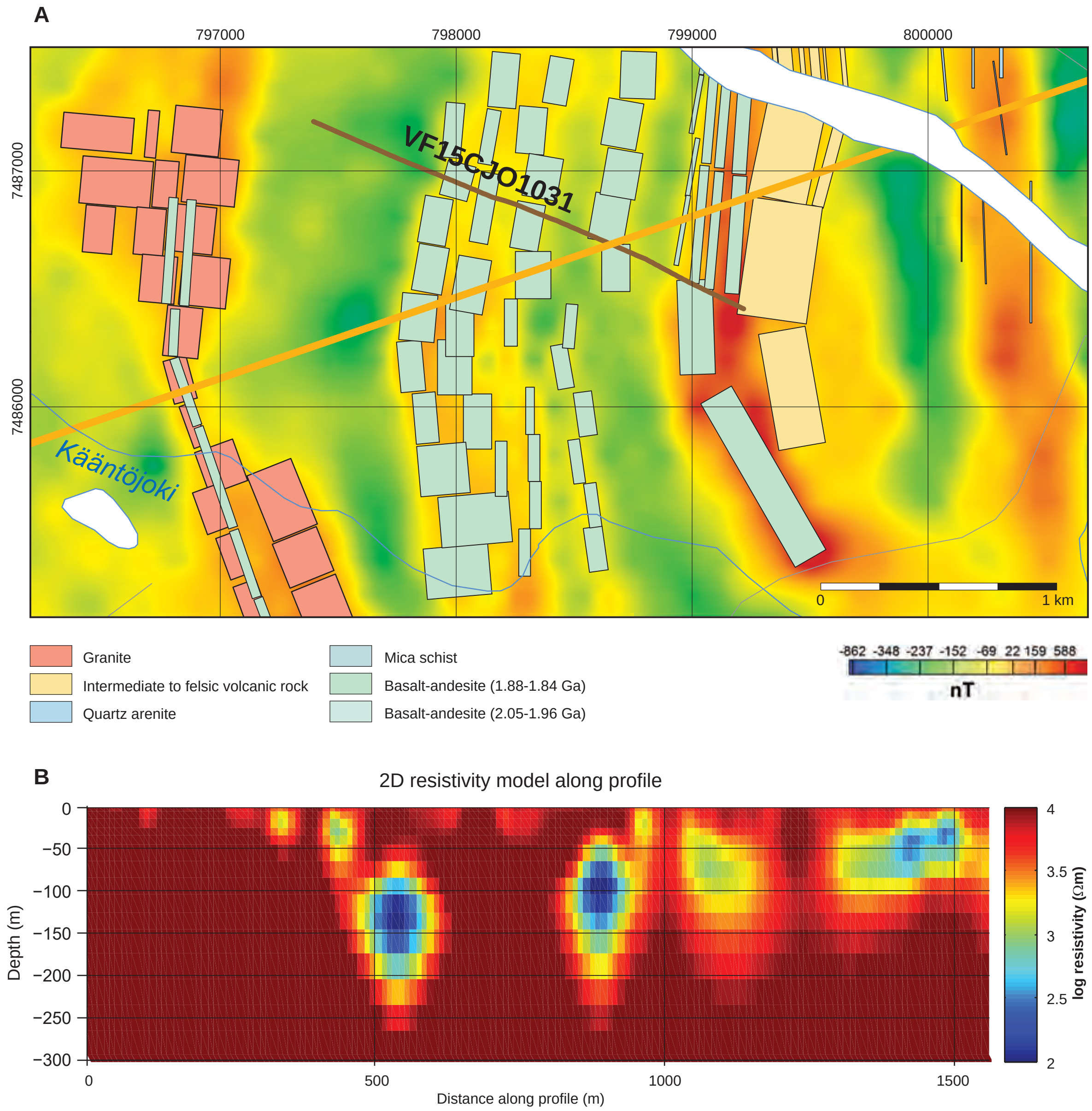

Figure 22. The location (A) and result (B) of the VLF profile "VF15CJO1031" in relation to modelled bodies. The resistivity cross-section shows the subsurface conditions down to 300 m below the ground surface.

Mica schist makes up *Groups 8, 9 and 11*, the lateral extent of which is covered by ground magnetic data. The bodies in *Group 8* have very low susceptibility, whereas the anomalies associated with *Group 9 and 11* are also clearly outlined in the airborne magnetic data. The bodies in *Group 9* are thin, 5–50 m, and are vertical or dip steeply towards the east. Figure 24C shows a sample of mica schist with a magnetic susceptibility of 0.03 SI. The bodies in *Group 9* are assumed to represent this rock. The bodies in *Group 11* are approximately 80 m wide and dip steeply towards the east (Fig. 25). No outcrops are present in the modelled area, but further north, along the same anomaly, there are numerous observations and sampling sites constraining the geometry and susceptibility values of the groups.

On the current bedrock map, a thin horizon of basic volcanic rock (Figs. 9 and 17a) is intercalated with the quartz arenite sedimentary package. This horizon has been assigned the name *Group 10* in the model. Observations and sampling show that this is a basaltic horizon approximately 10 m wide with a susceptibility of 0.02–0.03 SI and vertical dip. The basaltic horizon is altered and heterogeneous (Figs. 26A–C), locally banded at cm scale.

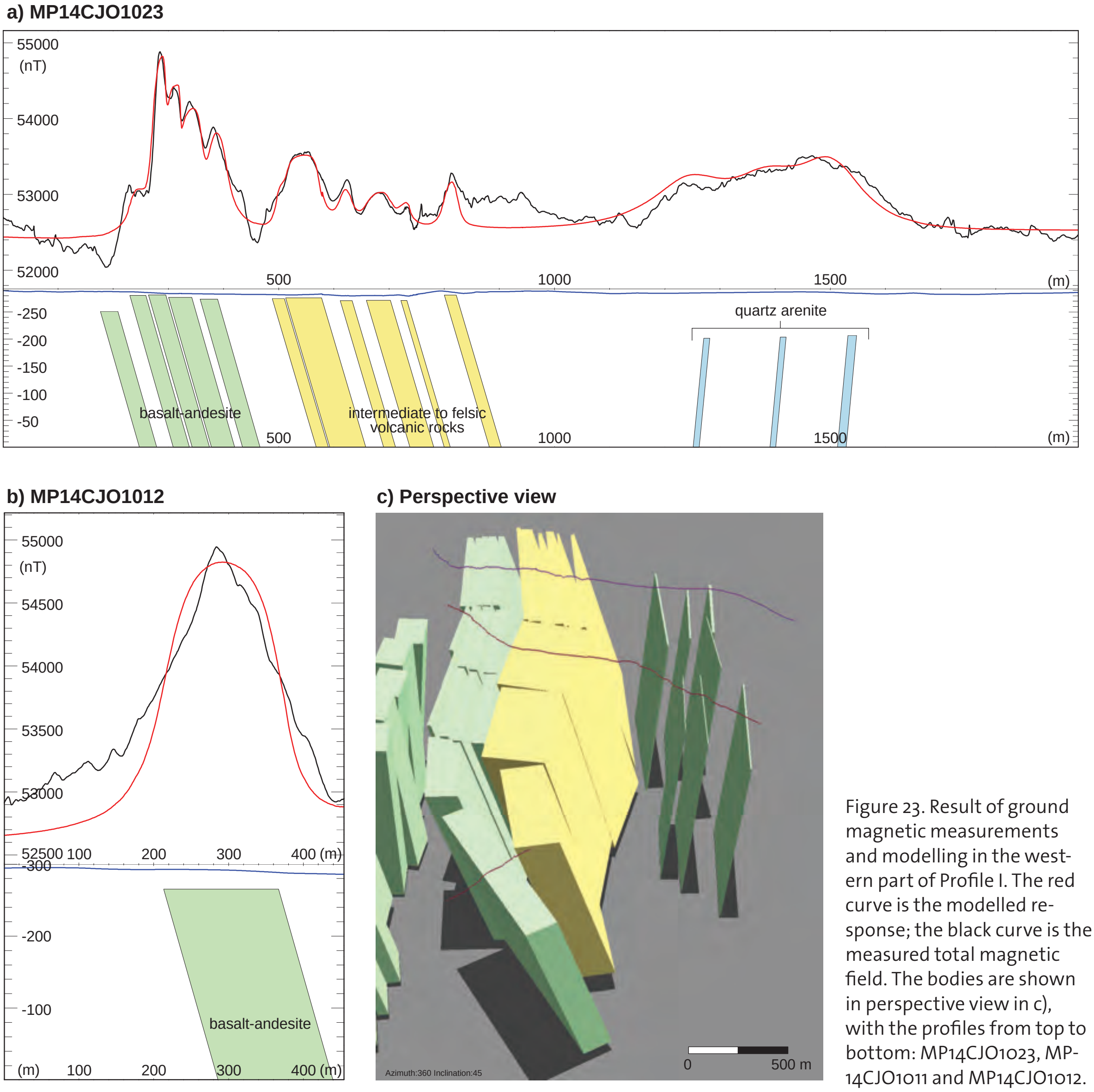

Figure 23. Result of ground magnetic measurements and modelling in the western part of Profile I. The red curve is the modelled response; the black curve is the measured total magnetic field. The bodies are shown in perspective view in c), with the profiles from top to bottom: MP14CJO1023, MP-14CJO1011 and MP14CJO1012.

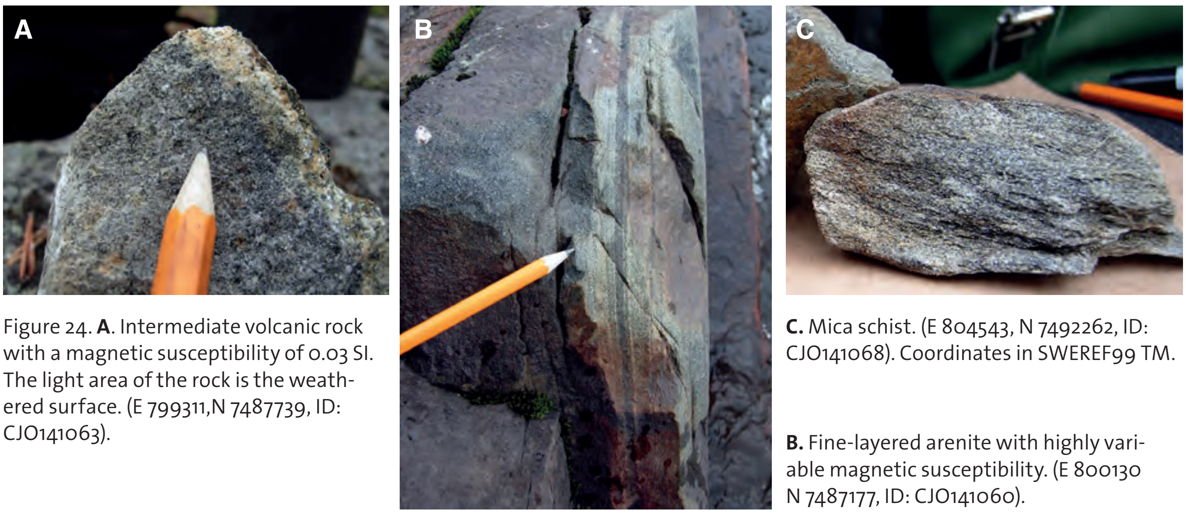

Figure 24. **A**. Intermediate volcanic rock with a magnetic susceptibility of 0.03 SI. The light area of the rock is the weathered surface. (E 799311,N 7487739, ID: CJO141063).

C. Mica schist. (E 804543, N 7492262, ID: CJO141068). Coordinates in SWEREF99 TM.

B. Fine-layered arenite with highly variable magnetic susceptibility. (E 800130 N 7487177, ID: CJO141060).

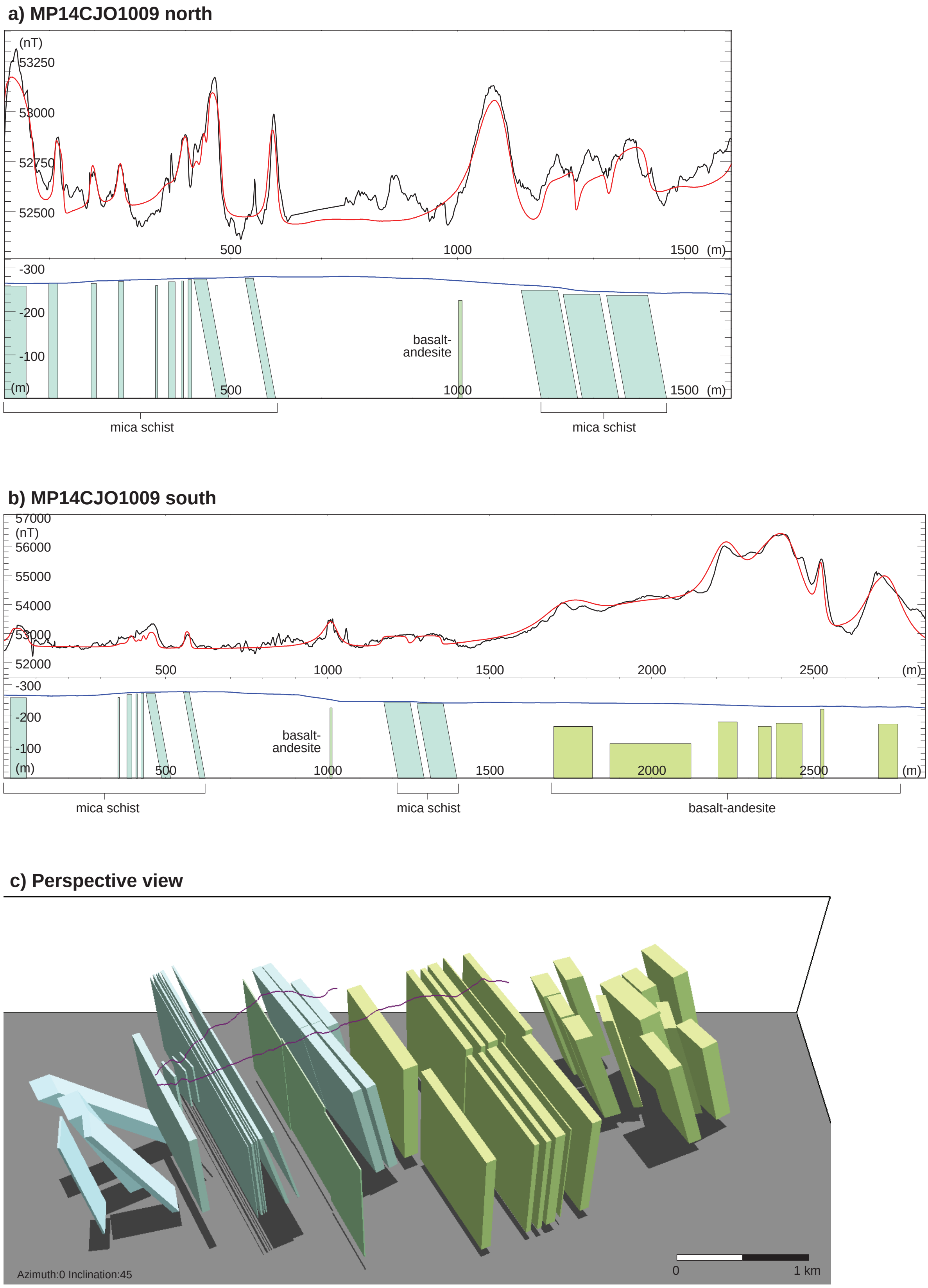

Figure 25. Results of ground magnetic measurements and modelling in the eastern part of Profile I. The red curve is the modelled response; the black curve is the measured total magnetic field. The bodies are shown in perspective view in c), with the profile MP14CJO1009, north and south parts.

Figure 26. A–C shows different appearances of the basaltic rock intercalated in a sedimentary rock unit. The samples were taken within 10 m of each other (SWEREF99 TM: E 806837, N 7489784. ID: CJO151073).

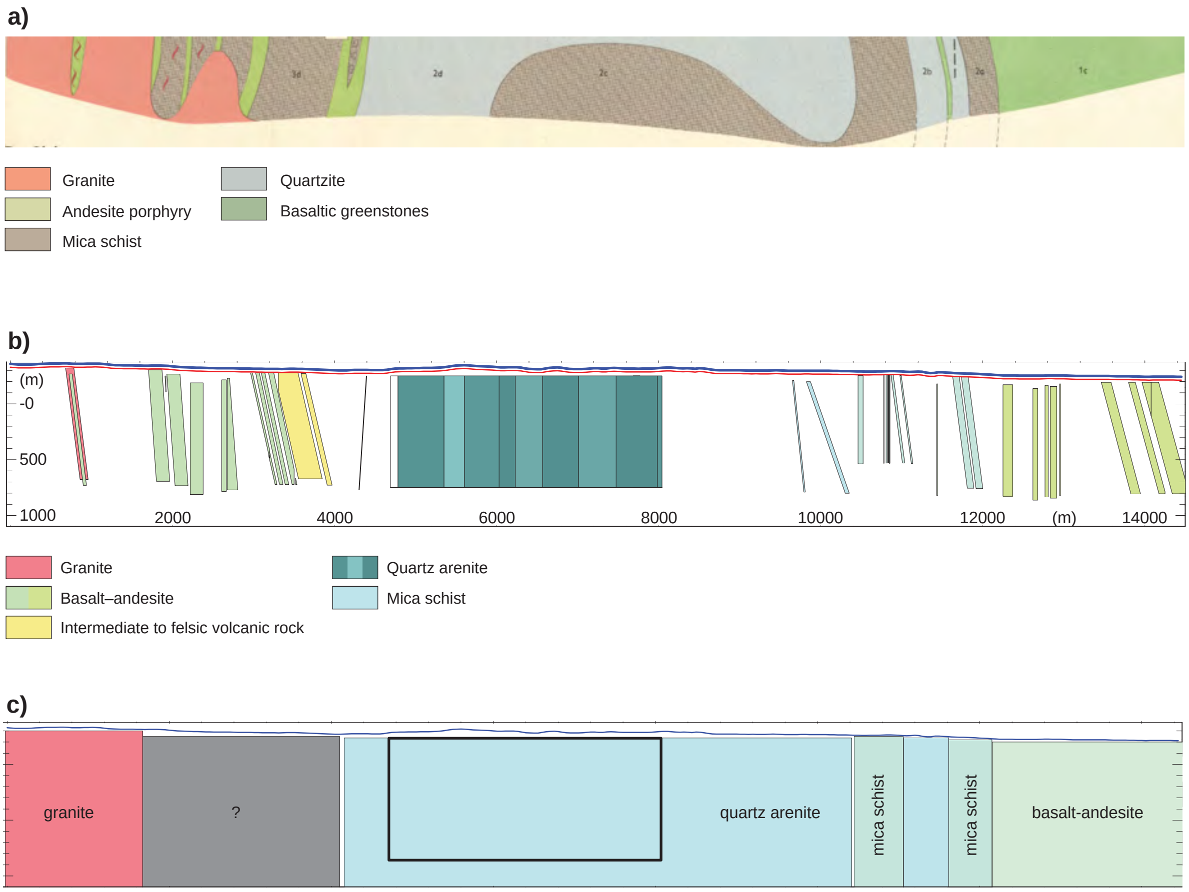

Figure 27. Comparison between the old (a) and new (b) models. c) shows the background bedrock type in the new model.

Groups 12 and 13 consist of the *Veikavaara greenstone group*, whose high magnetite content causes a high-magnetic pattern on a regional scale (Fig. 10) folded to a V shape in the southern part. These rocks cover an extensive area, but with few outcrops and thus observations and samples. *Group 12* is covered by ground magnetic measurements by profile MP14CJO1009 (Fig. 25) Observations and samples north of the profile in association with another ground magnetic profile have been used to increase the reliability of the model. This assumes that the rocks do not change much along the horizon on which they are found. The model gives upright horizons of varying width (10 to 120 m) for *Group 12* and easterly-dipping horizons for *Group 13*. Magnetic susceptibility is very high: between 0.1 and 0.3 SI.

CONCLUSION

The geological and the geophysical models generated in this study are compared with each other in Figure 27. The "background" bedrock types in the different areas are also included. The grey area in the western part of Figure 27c) is not named, since it is not certain whether it is mica schist, according to Padget (1970), or basic volcanic rock, according to Bergman et al (2001).

It is evident that several areas match between the two models but that there are also some discrepancies. The largest discrepancies between the models are found in the areas for *Groups 4 and 5*, basaltic and intermediate to felsic volcanic rocks. The new model shows that layers dip approximately 75 degrees towards the east, while the older model shows westward dips. An eastward dip is supported both by newly acquired ground magnetic data and by automated strike/dip calculations, so this is stated with confidence.

Another area where the structures differ occurs in the western part of the profile, but here there are far fewer structural indications to resolve the differences. In the eastern part of the profile, the old and new models show a similar character, but the new model resolves the different horizons to a higher degree. It also provides the link between the magnetic susceptibilities of the rocks and the magnetic anomalies observed.

REFERENCES

Bastani, M. & Pedersen, L. B., 2001: Automatic interpretation of magnetic dike parameters using the analytical signal technique, *Geophysics 66*, 551–561.

Bergman, S., Kübler, L. & Martinsson, O., 2001: Description of regional geological and geophysical maps of northern Norbotten County. *Sveriges geologiska undersökning Ba 56*, 110 pp.

Bergman, S., Stephens, M.B., Andersson, J., Kathol, B. & Bergman, T., 2012: Bedrock map of Sweden, 1:1 000 000 scale. *Sveriges geologiska undersökning K 423*.

Eriksson, B. & Hallgren, U., 1975: Description of the geological maps Vittangi NV, NO, SV, SO. *Sveriges geologiska undersökning Af 13–16*, 203 pp. (in Swedish with summary in English).

Grigull, S., Berggren, R., Jönberger, J., Jönsson, C., Hellström, F. & Luth, S., 2018: Folding observed in Palaeoproterozoic supracrustal rocks in northern Sweden. *In:* Bergman, S. (ed): Geology of the Northern Norrbotten ore province, northern Sweden. *Rapporter och Meddelanden 141,* Sveriges geologiska undersökning. This volume pp 205–257.

Hellström, F. & Jönsson, C., 2014: Barents project 2014, Summary of geological and geophysical information of the Masugnsbyn key area. *Sveriges geologiska undersökning SGU-rapport 2014:21,* 84 pp.

Hellström, F. & Jönsson, C., 2015: Summary of geological and geophysical field investigations in the Masugnsbyn key area, northern Norrbotten. *Sveriges geologiska undersökning 2015:04*, 31 pp.

Lynch, E.P. & Jönberger, J., 2013: Kartering Barents 2013, Summary report on the geological and geophysical characteristics of the Nunasvaara key area. *Sveriges geologiska undersökning SGU-rapport 2013:11,* 35 pp.

Lynch, E.P., Hellström, F.A., Huhma, H., Jönberger, J., Persson, P.-O. & Morris, G.A, 2018: Geology, lithostratigraphy and petrogenesis of c. 2.14 Ga greenstones in the Nunasvaara and Masugnsbyn areas, northernmost Sweden. *In:* Bergman, S. (ed): Geology of the Northern Norrbotten ore province, northern Sweden. *Rapporter och Meddelanden 141,* Sveriges geologiska undersökning. This volume pp 19–77.

Padget, P., 1970: Description of the geological maps Tärendö NW, NE, SW, SE with an appendix on geophysical aspects by J.D. Cornwell. *Sveriges geologiska undersökning Af 5–8*, 95 pp.

Witschard, F., Nylund, B. & Mannström, B., 1972: Masugnsbyn iron ore. Report concerning the results of Sveriges geologiska undersökning:s investigations in the years 1965–1970. *Sveriges geologiska undersökning BRAP 734,* 96 pp.

Authors, paper 10:
Mehrdad Bastani
Geological Survey of Sweden
Department of Mineral Resources,
Uppsala, Sweden

Ildiko Antal Lundin
Geological Survey of Sweden
Department of Mineral Resources,
Uppsala, Sweden

Shunguo Wang
Uppsala University,
Department of Earth Sciences,
Uppsala, Sweden

Stefan Bergman
Geological Survey of Sweden
Department of Mineral Resources,
Uppsala, Sweden

10. Imaging deeper crustal structures by 2D and 3D modelling of geophysical data. Examples from northern Norrbotten

Mehrdad Bastani, Ildiko Antal Lundin, Shunguo Wang & Stefan Bergman

ABSTRACT

Geophysical measurements were carried out by SGU in an area between Kiruna and Vittangi in northern Norrbotten, Sweden. The purpose of this study is to improve knowledge of the geology using modern methods, thereby creating supporting material for the exploration and mining industry in the region. In the summer of 2012 a 74 km long reflection seismic profile was acquired between Kiruna and Vittangi with the objective of imaging bedrock contacts and the geometry of structures at depth. In 2014 the seismic profile was followed up with magnetotelluric (MT) measurements aimed at modelling the variation in electrical resistivity of the upper crustal structures. In this study we present models from the 3D inversions of MT, magnetic and gravity field data. We compare the results with those from the reflection seismic data to reveal some of the details of the physical properties, the geometry of upper crustal structures and the bedrock in the study area. The analysis of the models to a depth of 5 km along five selected sections demonstrates a reasonable correlation between the modelled physical properties, although some differences are observed. The reflection seismic and susceptibility models have better resolution in imaging shallower structures such as folds and smaller-scale structures, due to denser data sampling and higher sensitivity. However, the deeper structures (>2 km) seen in the reflection seismic image correlate better with the density and resistivity models. Towards the eastern part of the area very low-electrical resistivity structures seen in the resistivity model coincide with a zone dominated by sulphide and graphite mineralisation. We propose a more detailed ground and airborne survey to identify potential areas for exploration.

INTRODUCTION

Over the past few decades 2D and 3D modelling of geophysical data, such as gravity, magnetic, reflection seismic and electromagnetic data, has played a key role in imaging crustal structures as deep as tens of kilometres (England & Ebbing 2012, Arora et al. 2012, Hedin et al. 2014, Cherevatova et al. 2015, Kamm et al. 2015). The geophysical models are generated by either forward or inverse techniques. Forward modelling uses *a priori* knowledge of the physical properties of the bedrock in the study area, for example, in the case of gravity field, density. The *a priori* knowledge is usually gained from laboratory measurements on the physical properties of rock samples or, in some cases, known values extracted from other surveys with similar geological settings. Forward modelling is therefore parameter driven: it assumes a property and finds the geometry of structures to fit the measured data. In inverse modelling, measured data determine the geometry and physical properties of the geological structures. There are two main inversion techniques: Finite Difference (FD) and Finite Element (FE). In FD modelling, the space is divided into cells of known geometry and the physical properties of each cell are estimated using an iterative mathematical method (Aster et al. 2005). In the FE method, the cells have irregular forms and both the geometry and physical properties are modelled. In this report we present the results from 3D modelling of gravity, magnetic and electromagnetic data collected by SGU in the vicinity of the town of Kiruna in northern Norrbotten County in Sweden. The main aim of this study is to produce a more detailed understanding of the depth extent of known geological units and structures. The reflection seismic data collected by SGU along a 74 km long profile (Juhojuntti et al. 2014) is used to check the validity of the models.

METHODOLOGY

Existing data in SGU databases were compiled and mapped using GIS tools. These include ground gravity, airborne and ground magnetics, electromagnetic (VLF), natural gamma radiation, petrophysical and ground geological observation data. The data in the study area were then extracted and imported into geophysical software for further analyses. At several locations ground geophysical measurements were carried out to fill in gaps in the existing data. New geophysical data, such as reflection seismic and magnetotelluric (MT) data with reasonably great penetration depth (> 5 km), were also obtained. The geophysical data were then processed and modelled in 2D and 3D using an FD approach.

GEOLOGICAL SETTING

The bedrock (Fig. 1A) represents part of the Svecokarlian orogen, formed 1.9–1.8 Ga ago, and includes Archaean and early Palaeoproterozoic rocks. The Råstojaure complex, north of Kiruna, consists of metagranitoids and subordinate metasupracrustal rocks formed, deformed and metamorphosed in the Archaean. These rocks are unconformably overlain by metaconglomerate, quartzite and metaandesitemetabasalt of the 12 km thick Kovo group (Martinsson 1999). The overlying Kiruna greenstone group (Martinsson 1997) is 14 km thick, consisting mainly of metabasalt with lesser amounts of metaultramafic rocks, graphite schist, iron formation and marble. This unit hosts the Viscaria copper deposit as well as a number of iron mineralisations. Mafic dyke swarms cut the Råstojaure complex, and mafic sills are common in the Kovo and Kiruna greenstone groups. The Svecofennian supracrustal rocks and several suites of intrusive rocks were formed during the Svecokarelian orogeny. The Svecofennian supracrustal rocks unconformably overlie the Kiruna greenstone group, and consist of acidic, intermediate and basic metavolcanic, and clastic metasedimentary rocks with a total thickness greater than 3 km. Kiirunavaara iron ore and several other iron deposits occur within these metavolcanic rocks.

The youngest Svecofennian supracrustal rock in the area is a quartz-rich metasandstone (Hauki quartzite). Except for the youngest intrusive suite (Lina granite), all rocks in the area were affected by ductile deformation, hydrothermal alteration and greenschist to amphibolite facies metamorphism during the Svecokarelian orogeny.

Nd isotopic studies have shown that Archaean rock is probably present in the subsurface north of a line between Luleå and Jokkmokk (Öhlander et al. 1993). It is therefore highly probable that Archaean rocks can be found at depth in the Kiruna area. The outcrop pattern suggests that the general dip of the units is to the south (Juhojuntti et al. 2014). During ductile deformation large folds with wavelengths of up to several kilometres were formed, with steep axial planes and south-plunging fold

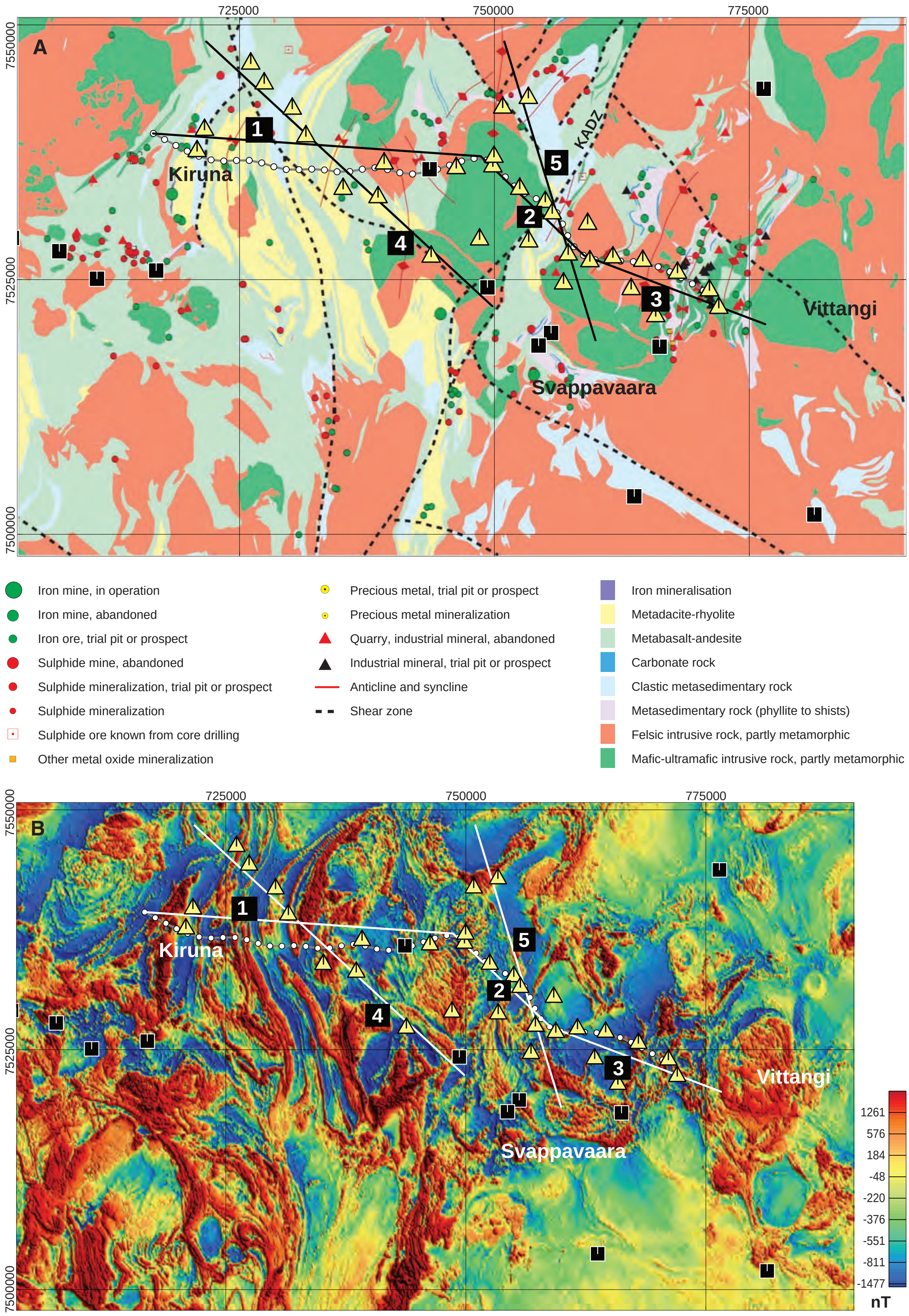

Figure 1. **A.** Simplified regional bedrock map of the study area (after Bergman et al. 2000). **B.** Map of total magnetic field anomaly.

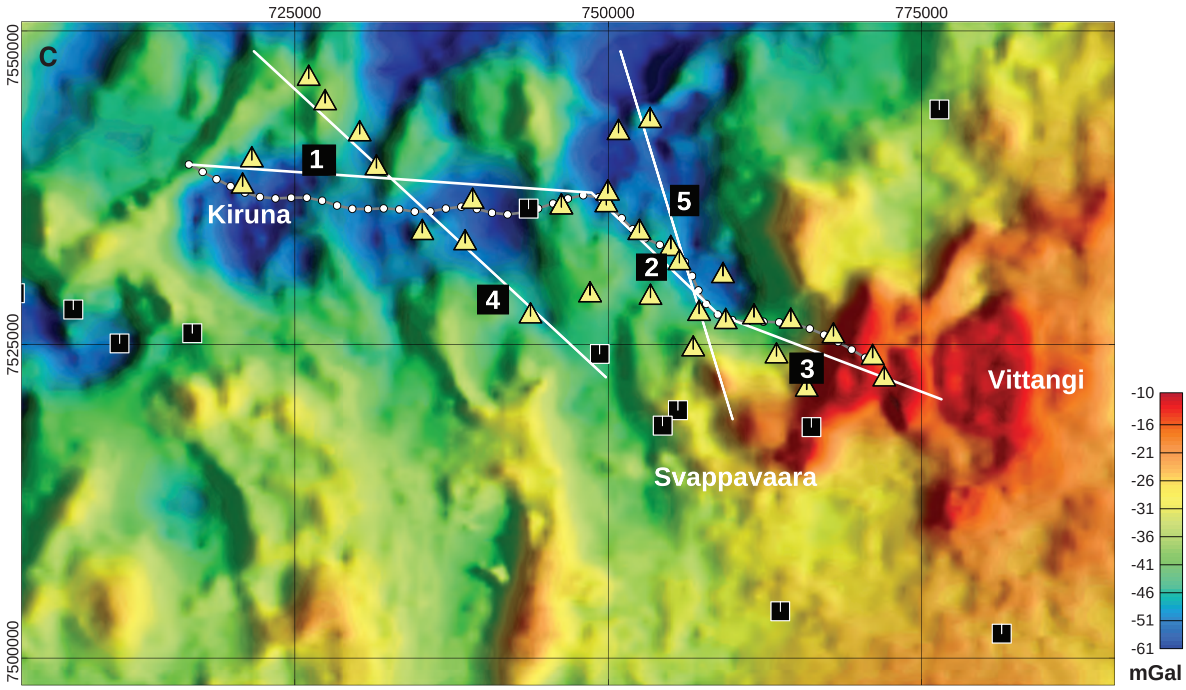

Figure 1. **C.** Bouguer anomaly map from ground measurements. The legends to the right in A show the bedrock and mineralisations in the area. The reflection seismic line is shown as a white line with white circles. The yellow triangles and the black squares are MT stations measured by SGU and Oulu University, respectively (see Bastani et al. 2015). The white lines with black squares (numbered in white) are the selected directions to show model sections from the 3D models (see Fig. 2D).

axes. In the eastern part of the area the structure is more complicated, with several folding phases in different orientations. Foliations developed with strongly variable intensity. Ductile shear zones separate more weakly deformed domains. The two most important shear zones are the Karesuando–Arjeplog deformation zone in the east and the Kiruna–Naimakka deformation zone in the west (Bergman et al. 2001), with widths of 810 km, including less deformed lenses. Ductile shear zones are commonly reactivated in the brittle regime. Some copper and gold mineralisations can be found along the Karesuando–Arjeplog deformation zone.

At the eastern end of the seismic profile (Fig. 1A) the Vittangi greenstone group (VGG), which forms the central part of the Nunasvaara key area, contains 61 mineral deposits, prospects or showings (Lynch & Jönberger 2013), the main commodity being graphite-bearing schists (e.g. Nunasvaara).

Geophysical data

Airborne geophysical measurements were carried out by SGU during 1960–1964. The magnetic field was measured as a part of the iron inventory programme. Loussavaara–Kiirunavaara AB (LKAB) collected airborne data during 1979–1984. LKAB carried out airborne magnetic field, electromagnetic (both VLF and Slingram) and gamma ray radiation data acquisition. The survey direction was east–west. All airborne surveys in the area were made with a line separation of 200 m, a point distance of 40 m and a ground clearance of 30 m. The magnetic anomaly map (Fig. 1B) of the same area shown in Fig. 1A) reveals complicated patterns, such as banded, folded and circular features caused by supracrustal and intrusive rocks. Those data contain valuable information about the deformation history of the rocks.

Regional gravity measurements were made by SGU and LMV during different periods, most intensively between 1960 and 1985. The distance between the measurement points varies between 300 and

3 000 metres. Gravity data (Fig. 1C) are usually shown in the form of Bouguer anomaly maps. The gravity highs can usually be related to mafic magmatic rocks at depth. Gravity lows coincide with the distribution of supracrustal rocks with felsic compositions. In summer 2012 a reflection seismic profile approximately 74 km long was acquired by SGU in the Kiruna area (shown by white circles in Figs. 1A–C). The main aim of the seismic measurements was to better understand the upper crustal structure in the Kiruna area, e.g. by imaging bedrock contacts and deformation zones. The western end of the seismic profile is only a few kilometres from the Kirunavaara mine, and close to the profile are several known mineralisation zones, some of which are active exploration targets. For more details of the data acquisition parameters the reader is referred to the report by Juhojuntti et al. (2014).

Magnetotelluric (MT) measurements were conducted in two areas (A and B) in northern Norrbotten during the summer of 2014 (Figs. 1A–C). The survey objectives were to model the variation of electrical resistivity of the upper crustal structures along the reflection seismic profile collected in the summer of 2012 (Juhojuntti et al. 2014) and to study the depth extent of known mineralisations. The collected MT signals cover a wide frequency band, from 10^{-2} to 300 Hz. 2D and 3D modelling of the collected data images the variation of electrical resistivity down to depths > 30 km. Bastani et al. (2015) give a detailed account of the results from 2D modelling of collected MT data along two selected directions in two areas. Here we show the results from the 3D modelling of MT data in area A and, where necessary, compare them with the 2D modelling results.

RESULTS

The VOXI program, a 3D finite difference inversion module supplied by Geosoft Company in the Oasis montaj software package was used for the 3D inversion of the potential field data. We tested several inversions using different parameter settings to obtain models as close as possible to the field and laboratory observations and measurements. The models resulting from 3D inversions of the gravity and magnetic field data are shown as density contrast and magnetic susceptibility in Figures 2A and 2B, respectively. The 3D inversion of the magnetic field and gravity data were made using model cells of 500 m × 500 m × 250 m in x, y and z directions, respectively. We used petrophysical data and constrained model susceptibility within the range of 0.00001 to 2.0 SI units. The unusually high-upper susceptibility limit of 2 was imposed to enable the inversion to take into account the several known iron ores in the area, of which the world-class Kiruna iron ore is best known. A density contrast of between –0.12 and 0.9 was used to constrain the density model.

We used the inversion code WSINV3DMT by Siripunvaraporn et al. (2005) to carry out 3D modelling of the data using a smoothing regularisation. The resulting 3D resistivity model is shown in Figure 2C. Note that the model is presented in the inversion's local coordinate system.

The MT data do not have sufficient resolution at the surface due to the low-frequency content of the signal. The susceptibility model shows higher frequency variations, which are mainly due to denser sampling and partly to the higher sensitivity of the method compared with gravity and MT.

Selected susceptibility, resistivity and density sections from 3D models

Five portions of models numbered 1–5 that cross a few known geological structures and mineralised zones are selected to present more detailed results in the form of depth sections. The selected portions are shown on the density model in Figure 2A. The density contrast depth sections (here called sections) from the 3D models are shown in Figures 2A–2C. Sections 1 to 3 are collocated with three portions of the reflection seismic profile (Fig. 1) reported by Juhojuntti et al. (2014). The density contrast sections are shown in Figure 2D as an example. Along each direction we present model sections showing susceptibility, resistivity and density contrast. In each resistivity section we superimposed the contours of estimated susceptibilities and, on the upper part of the section, the bedrock geology. The location and type of known mineralisations are shown to facilitate comparison and interpretation.

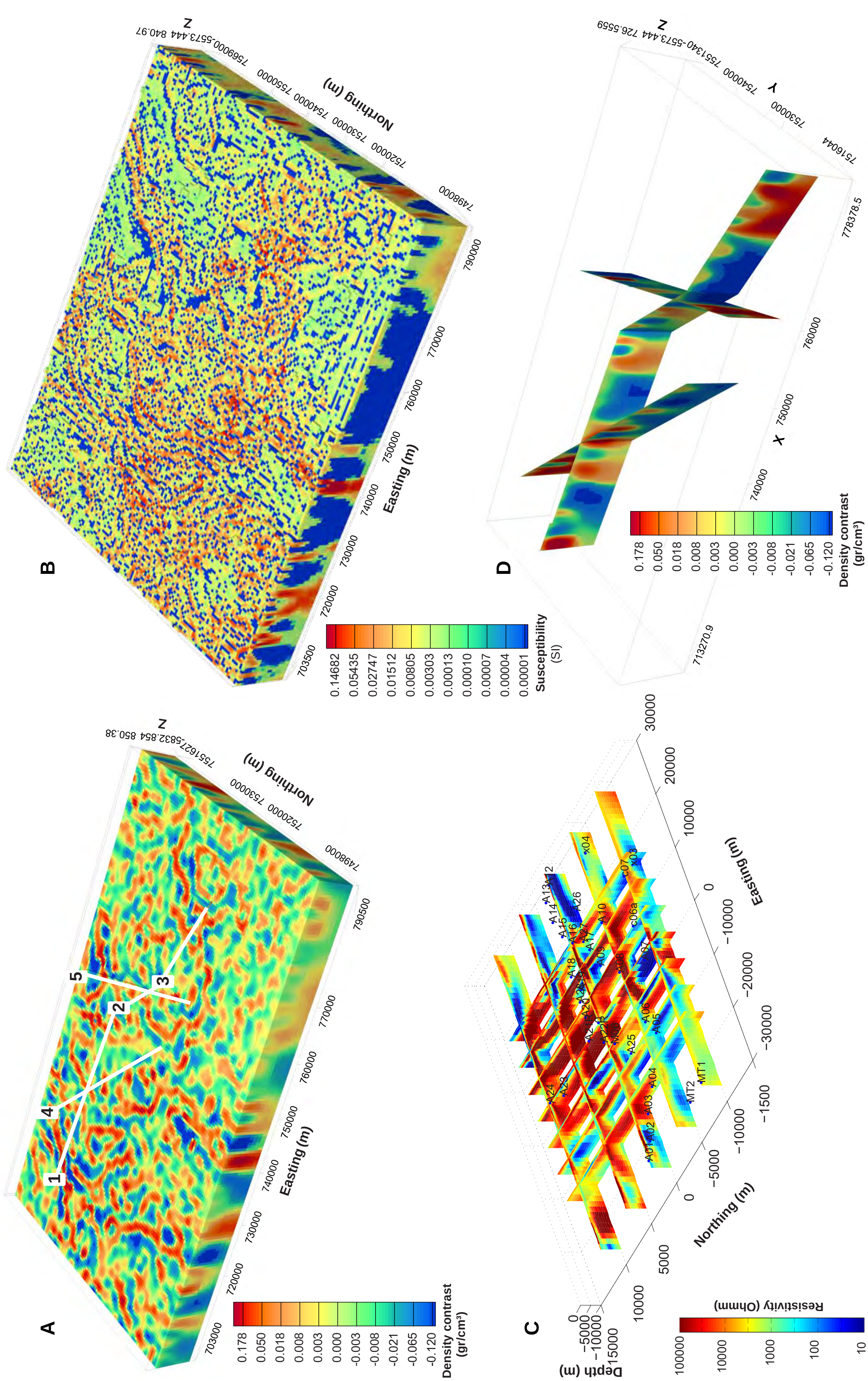

A
B
C
D
Density contrast (gr/cm³)
0.178
0.050
0.018
0.008
0.003
0.000
-0.003
-0.008
-0.021
-0.065
-0.120
Easting (m)
Northing (m)
Z
Susceptibility (SI)
0.14682
0.05435
0.02747
0.01512
0.00805
0.00303
0.00013
0.00010
0.00007
0.00004
0.00001
Resistivity (Ohmm)
100000
10000
1000
100
10
Depth (m)
X
Y

◀ Figure 2. **A.** 3D density contrast model from the inversion of Bouguer anomaly data in the area. The selected section lines are shown in white. **B.** The 3D susceptibility model from the inversion of magnetic field anomaly data shown in Figure 1 B. **C.** Resistivity model from the 3D inversion of MT data. **D.** Density contrast sections taken from the model shown in a) along the selected sections (see Figure 1).

Comparison of the 3D models with the information in the reflection seismic data was rather difficult, mainly because of the weak reflection patterns seen in the seismic data. In a separate section we compare the seismic images with the 3D models, where a clear reflection pattern could be extracted to interpret regional structures in a more integrated manner.

Section 1

This section is 32 km long and runs approximately west–east. Although distribution of the MT stations is sparse along section 1 (see Fig. 1) the 3D inversion model reveals valuable information along this section (Fig. 3). To make the comparison easier the modelled physical properties of various geological structures and units are summarised in Table 1.

The susceptibility model shows more details and resolves structures resembling major folds with varying dips that contain minor/smaller folds (higher frequency near surface susceptibility variations). The white and black arrows indicate the apparent average dips of major high- and low-magnetic susceptibility structures, respectively. The arrows are also shown on the resistivity and density contrast sections. For example, a few zones with susceptibilities > 0.05 (5000×10^{-5} SI units) dip almost vertically in the mid-western part of the section. An easterly-dipping structure in the western part of the model and a steeply east-dipping structure in the middle of the model (close to 730000E) demonstrate variations in the dips of the modelled susceptibilities/structures, indicating folding structures present in the study area. The western to central part of the resistivity model is dominated by a low-resistivity zone with very faint high-resistivity structures. However, the lowest resistivity zones correlate very well with the lowest susceptibility zones (shown by black arrows) that reach very close to the surface. A good example coincides with a mapped shear zone in the middle part of the model. Towards the western end of section 1 Juhojuntti et al. (2014) reported an east-dipping structure in the seismic data at CDP 500, which may be associated with Hauki quartzite, which forms the eastern contact of the east-dipping high-susceptibility structure. This dip is not observed in the resistivity model, but corresponds with a low-density zone in the density model. It should be noted that dips from the high-magnetic structures (white) shown on the density model are reasonably collocated with the high-density zones. The resistivity and density contrast models seem to have a better depth penetration and resolve structures at depths > 2.5 km that are not resolved in the susceptibility model. The west-dipping low resistivity and low/intermediate density at the western end of the section (west of 740000E) and the low-density and high-resistivity features (Figs. 3B and 3C) to the east of this structure (east of 720000E) are two examples. The high-resistivity structure at depths below 3000 m, east of 720000E may be caused by intrusive rocks which, due to the density contrasts, are probably felsic intrusions.

Table 1: Summary of the estimated physical properties of various geological units and structures along section 1.

Structure/unit	Magnetic susceptibility (SI $\times 10^{-5}$)	Resistivity (Ohmm)	Density contrast (kg/m^3)
Sedimentary rocks	Low (<100)	Low (< 1000)	Low/intermediate (-0.07–0.00)
Felsic volcanic rocks	Low	Intermediate (1000–4000)	Low (<–0.07)
Mafic volcanic rocks	High (>5000)	Not resolved	High (>0.06)
Shear zones	Low	Low	Low
Granitoids	Low–intermediate	High (> 4000)	Low
Mafic intrusions	High	Very high (> 10000)	High (>0.06)

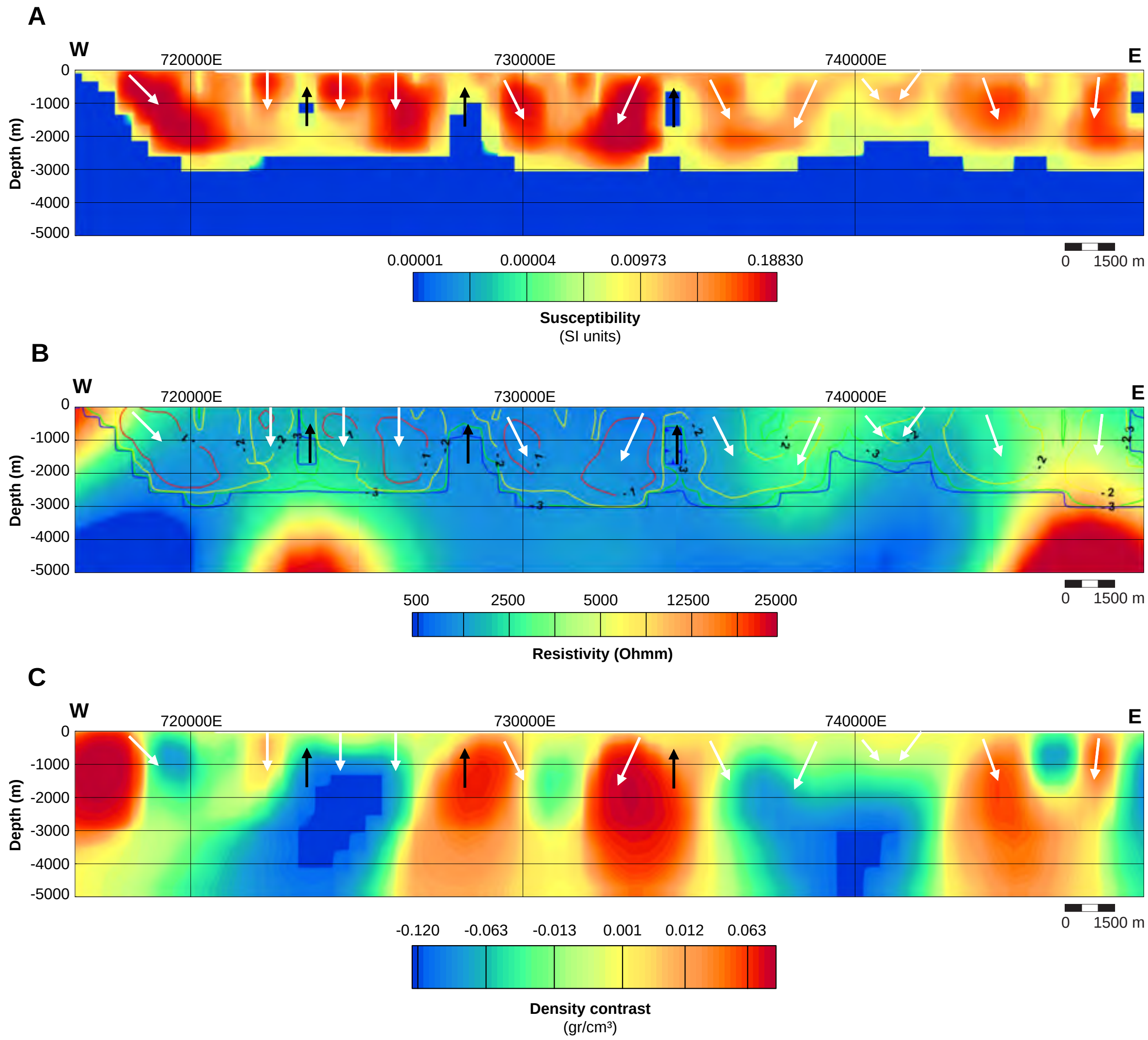

Figure 3. Sections from 3D models along section 1 shown in Figures 1 and 2. **A.** Susceptibility. **B.** Resistivity. **C.** Density contrast. In B the resistivity model is in the background and the contours with different colours represent the estimated magnetic susceptibility in logarithmic scale. The mapped bedrock and known mineralisations along each direction are shown on top of the resistivity section. The white and black arrows indicate the interpreted dips of high- and low-susceptibility zones, respectively.

Section 2 and 3

Figure 4 shows the models along sections 2 and 3. The MT data along the nearly 15 km long section 2 has a better coverage than section 1. Table 2 shows the modelled physical properties of geological units and structures along sections 2 and 3.

Along section 2 (Figs. 3A–C) extremely high-resistivity (> 20 000 Ohm) and relatively high-susceptibility and high-density zones are resolved (west of 756000E). The high-resistivity zone continues down to a depth of approximately 4 km with a northwest-dipping trend. The same dip is observed in the susceptibility and density model. However, the magnetic model estimates a maximum depth of 3 km, and the density model a depth of approximately 3.5 km. On the geological map the first 4 km of the section in the west is marked as a gabbro intrusion with some inclusion of a granitoid. At the point of granitoid inclusion modelled resistivity decreases towards the west, and susceptibility shows some slight changes. The density model indicates low values in this interval that do not match the geological information and indicate intrusions of a more felsic nature. Towards the east of the Karesuando–Arjeplog

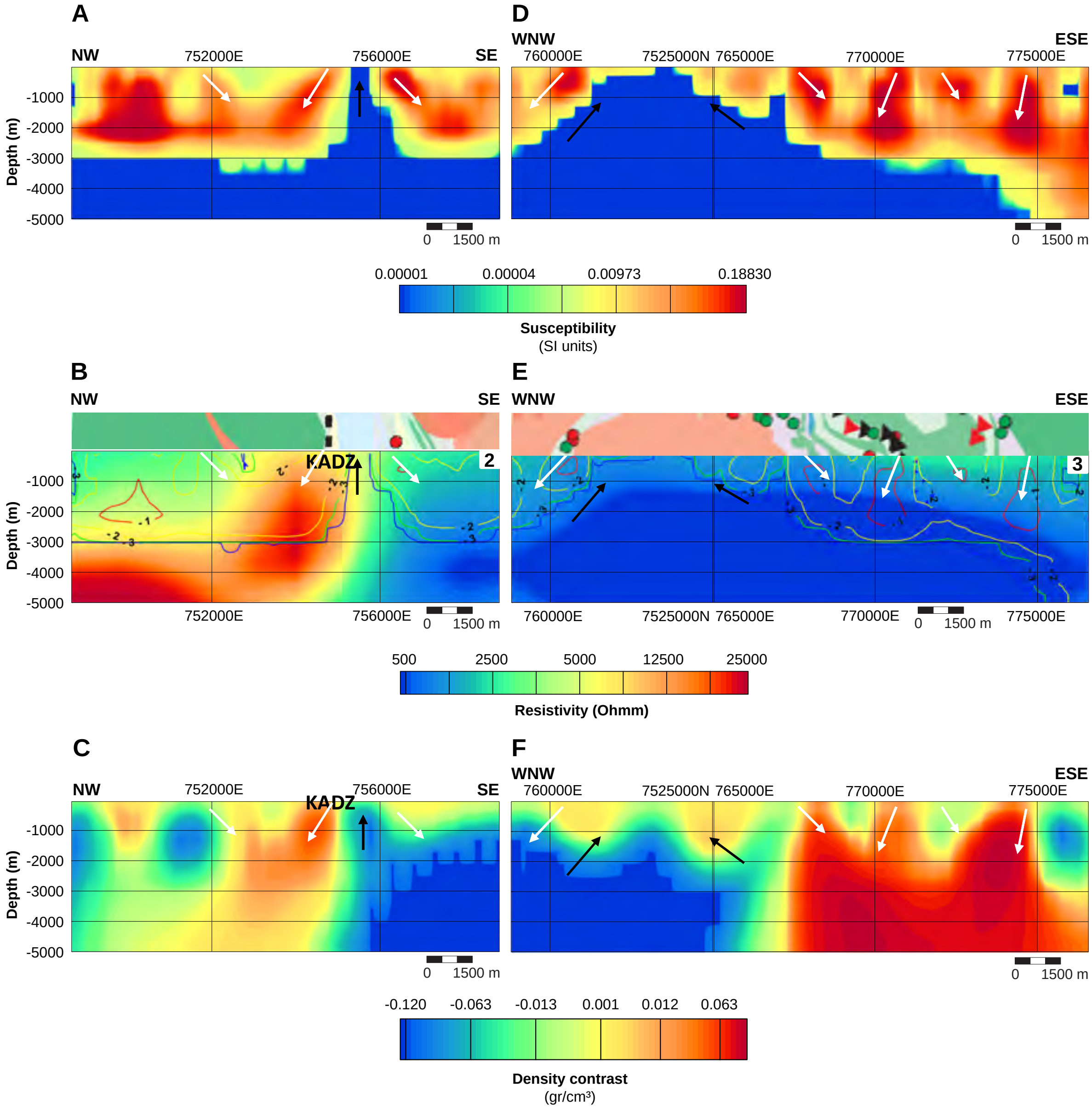

Figure 4. Sections from 3D models along portion 2 and 3 shown in Figure 1 and 2. **A.** Susceptibility. **B.** Resistivity. **C.** Density contrast along direction 2. **D.** Susceptibility. **E.** Resistivity. **F.** Density contrast along direction 3. In B and E the resistivity model is in the background and the contours with different colours represent the estimated magnetic susceptibility in logarithmic scale. The mapped bedrock and known mineralisations along each direction are shown on top of the resistivity section. The white and black arrows indicate the interpreted dips of high and low-susceptibility zones, respectively.

deformation zone (KADZ) the resistivity and density models show a dramatic change, with decreasing values, especially at deeper levels (resistivities < 500 Ohmm and density contrasts < –0.12 kg/m^3). Close to this contact a few sulphide mineralisations are reported in the SGU mineral resource database. A folded structure can be seen on the magnetic anomaly map (Fig. 1B) and modelled susceptibility also suggests a folded structure in the form of a syncline that continues to a depth of approximately 2 km. It is obvious that the folded structure within the KADZ is more like an anticline fold, with a northwest-dipping, high-susceptibility structure most likely caused by highly magnetic volcanic rocks.

Section 3 is 19 km long and has a W-NW–E-SE orientation. A high-susceptibility structure dipping northwest shows up at the W-NW end of the section. Further east, the profile crosses granitic rocks

Table 2. Summary of the estimated physical properties of various geological units and structures along sections 2 and 3

Structure/unit	Magnetic susceptibility ($\times 10^{-5}$)	Resistivity (Ohmm)	Density contrast (kg/m^3)
Sedimentary rocks	Low (<100)	Low (< 1000)	Intermediate (0.00–0.02)
Felsic volcanic rocks	Low	Not resolved	Low (<-0.07)
Mafic volcanic rocks	High (>5000)	Intermediate (1000–4000)	High (>0.06)
Karesuando–Arjeplog deformation zone (KADZ)	Low	Low	Low
Granitoids	Low–intermediate	Intermediate (1000–4000)	Low-intermediate (-0.07–0.01)
Mafic intrusions	High	Intermediate–high	High (>0.06)

with low-susceptibility contrasts. Occurrence of low-density, quartz monzodioritic rocks at the eastern gradient of the gravity low was mapped by Lynch & Jönberger (2013). Our data suggest that the intrusives here are predominantly rocks of mainly felsic composition at depth, which is confirmed by the forward modelling presented by Juhojuntti et al. (2014). At coordinates SWEREF99 TM 767971/7523890 the profile cuts the Nunasvaara area with known graphite, iron and sulphide mineralisations, the host rock being the Vittangi greenstone group. The group is dominated by volcanic, volcanoclastic and sedimentary rocks, and cut by doleritic sills. (Lynch & Jönberger 2013). The susceptibility model suggests steeply dipping, folded structures that deepen to the southeast. There is good correlation with the 2D interpretation of the gravity and magnetic data made by Juhojuntti et al. 2013. The resolution of the 3D models is 500 metres, but there are high-frequency changes in the lithology data to consider for more detailed interpretation of this specific area. The resistivity section is mainly dominated by a very low-resistivity feature east of KADZ. Resistivity decreases considerably with depth, reaching values < 500 Ohmm. Based on various reports (e.g. Lynch & Jönbeger 2013, Martinsson 2011 and references therein), this area is dominated by graphite and sulphide mineralisations and, in the most easterly part, is best known for schist-hosted graphite deposits (e.g. Nunasvaara), which represent the largest known graphite resource in Sweden. The susceptibility model also indicates the presence of an extremely low-susceptibility zone at a depth > 2 km. The density section depicts a huge contrast in the middle part in which a very high-density zone that continues to depths > 5 km is resolved in the eastern part of the section. Shallower density variations indicate folded structures with dips that correlate well with those predicted by the susceptibility model. High densities and high susceptibilities may be directly related to the mafic volcanics and intrusions mapped in the area. The very low-density zone at depth in the western part of the density model may be caused by a granitic intrusion observed in the area. Two scenarios are suggested for the deep and very low-resistivity feature that starts at 756000E and continues to the end of section 3: a) the highly conductive mineralisations observed in the area (Martinsson 1993); or b) a deep-seated rock type with low resistivity, susceptibility and density. The latter is considered more likely due to the geometry and extent, although the extremely low resistivity is hard to explain. This is a scientific question to be answered by future research.

Section 4

This is the longest section (38 km) and crosses a variety of geological units and structures (Figure 5 A–C). Table 3 summarises the physical properties of various rock types and structures along section 4.

Although the low-susceptibility feature/zone at depth (> 2 km) correlates well with another low-resistivity zone in the northwestern part of the section, the density model suggests that this zone has a very high-density material at depth. The sole explanation for this may be the presence of highly conductive, low-susceptibility and high-density sulphide mineralisations.

In the density model the low-density felsic volcanic rocks (e.g. at 7540000N) affect the model due

Table 3. Summary of the estimated physical properties of various geological units and structures along section 4

Structure/unit	Magnetic susceptibility (SI × 10^{-5})	Resistivity (Ohmm)	Density contrast (kg/m³)
Sedimentary rocks	Low (<100)	Low (< 1000)	Intermediate (0.00–0.02)
Felsic volcanic rocks	Low	Not resolved	Low (<-0.07)
Mafic volcanic rocks	High (>5000)	Intermediate (1000–4000)	High (>0.06)
Karesuando–Arjeplog deformation zone (KADZ)	Low	Low	Low
Granitoids	Low–intermediate	Intermediate (1000–4000)	Low–intermediate (-0.07–0.01)
Mafic intrusions	High	Intermediate–high	Intermediate to high (0.03–0.06)

to coarser data sampling than in the susceptibility model. This affects the comparison between the apparent estimated dips for the high-susceptibility structures that are superimposed on the density model along this section. There are a few cases where the high-susceptibility dips are collocated with low-density zones in the density model. The rhyolitic low-density rocks at SWEREF99 TM 739527/7531904 appear to dip below the mafic basaltic rocks to the northwest, which could explain the low-density contrast.

High-density basalts and andesites of considerable depth appear in the northwest of the profile. It is not clear what rocks are responsible for the density low within the high-density area at SWEREF99 TM 725475/7544910, due to the lack of outcrop, but they are probably the quartz-rich sedimentary rocks to the southwest continuing to the northeast. In the susceptibility models, and to some extent in the density contrast model, mafic volcanic rocks appear folded and have deeper roots than the felsic volcanic rocks. Volcanic rock sequences of felsic and mafic composition follow with low and high-density areas, respectively. At coordinates SWEREF99 TM 732994/7537950 high-density and high-susceptibility structures occur but cannot be correlated with the trachyte-rhyolites on the geological map.

To the southeast, close to 740000E, all three models demonstrate a sharp contrast/change. In the susceptibility model, two distinct, rather high-susceptibility zones that continue down to depths > 3 km coincide with a resistivity zone with intermediate to high-resistivity dipping towards the north-northwest (Fig. 5B). Both zones become shallower in the most easterly parts of the sections. The density model (Fig. 5C) correlates well with the information shown on the geological map. A low-density zone is sandwiched between two higher-density zones that can be correlated to the granitic and gabbroic intrusions, respectively. The low-density zone appears to have deeper roots than the denser zones, implying that the granites might continue deeper than their gabbroic counterparts. This low-density zone relating to the granitic intrusion correlates well with the low-susceptibility zone resolved by the magnetic model (Fig. 5A).

Section 5

This section has an almost north–south orientation, is 31 km long and crosses two shear zones, as well as various felsic and mafic intrusions and volcanic rocks. A summary of the physical properties of the geological features mentioned above is given in Table 4.

In the northern part of the sections a clear low-susceptibility, intermediate resistivity (1 000–4 000 Ohmm) and very low-density (density contrast < –0.12) structure/feature that continues down to depths > 5 km is prominent (Fig. 6A–C). It dips approximately 45 degrees to the SE. At the location marked by a shear zone on the geological map, a sharp boundary can be observed in almost all sections. Towards the south of the shear zone a high-susceptibility and density zone is apparent, and appears deeper in the density model. The zone is not resolved in the resistivity model because of very poor data coverage in this area (see Fig. 1). Further to the south, a zone marked by two vertical and one horizon-

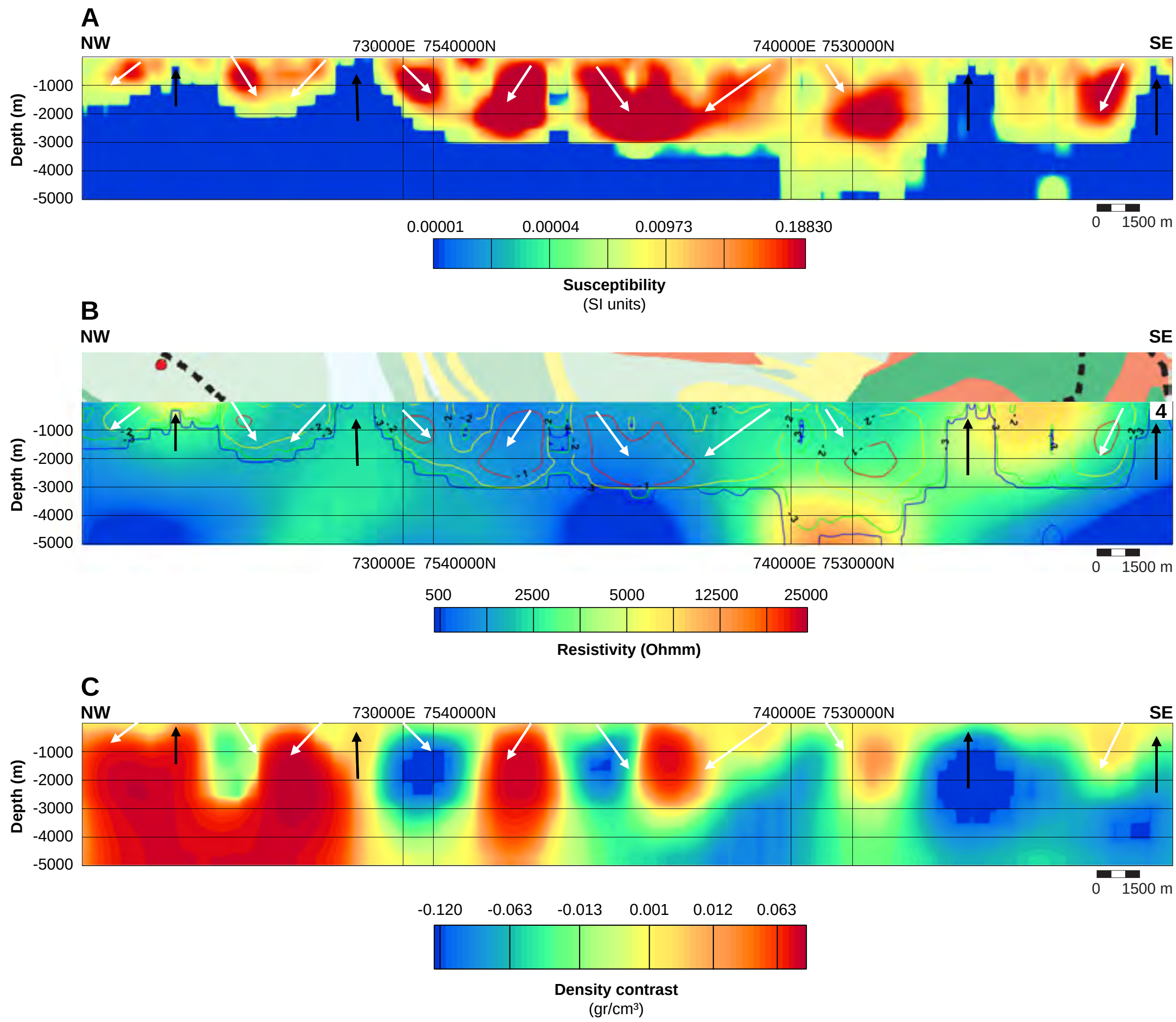

Figure 5. Sections from 3D models along portion 4 shown in Figures 1 & 2. **A.** Susceptibility. **B.** Resistivity. **C.** Density contrast. In B the resistivity model is in the background and the contours with different colours represent the estimated magnetic susceptibility in logarithmic scale. The mapped bedrock and known mineralisations along each direction are shown on top of the resistivity section. The white and black arrows indicate the interpreted dips of high and low-susceptibility zones, respectively.

Table 4: Summary of the estimated physical properties of various geological units and structures along section 5

Structure/unit	Magnetic susceptibility ($\times 10^{-5}$)	Resistivity (Ohmm)	Density contrast (kg/m^3)
Sedimentary rocks	Low (<100)	Intermediate–high	Intermediate (0.00–0.02)
Felsic volcanic rocks	Low or not resolved	Not resolved	Low or not resolved
Mafic volcanic rocks	High (>5 000)	High (> 10 000)	High (>0.06)
Karesuando–Arjeplog deformation zone (KADZ)	Low	Not resolved	Low (< -0.07)
Granitoids	Low	Intermediate (1 000–4 000)	Low to very low
Mafic intrusions	High	Low to high	Intermediate to high (0.03–0.06)

tal arrow (Figs. 6A–C) is noted. At the top a 200–300 m thick, moderately dense and magnetic layer is apparent. Below this, a very low-susceptibility (almost zero), high-resistivity (> 10 000 Ohmm) and low to intermediate density structure continues to depths > 5 km. A syncline-shaped high-susceptibility and moderately high-density structure is resolved north of KADZ. This may be associated with the mafic volcanic rocks mapped in this part of the section. The northern limb dips more gently and the folding is more pronounced in the magnetic model, probably due to better data coverage. It should be borne in mind that the section crosses the magnetic anomalies at a high angle, which may generate

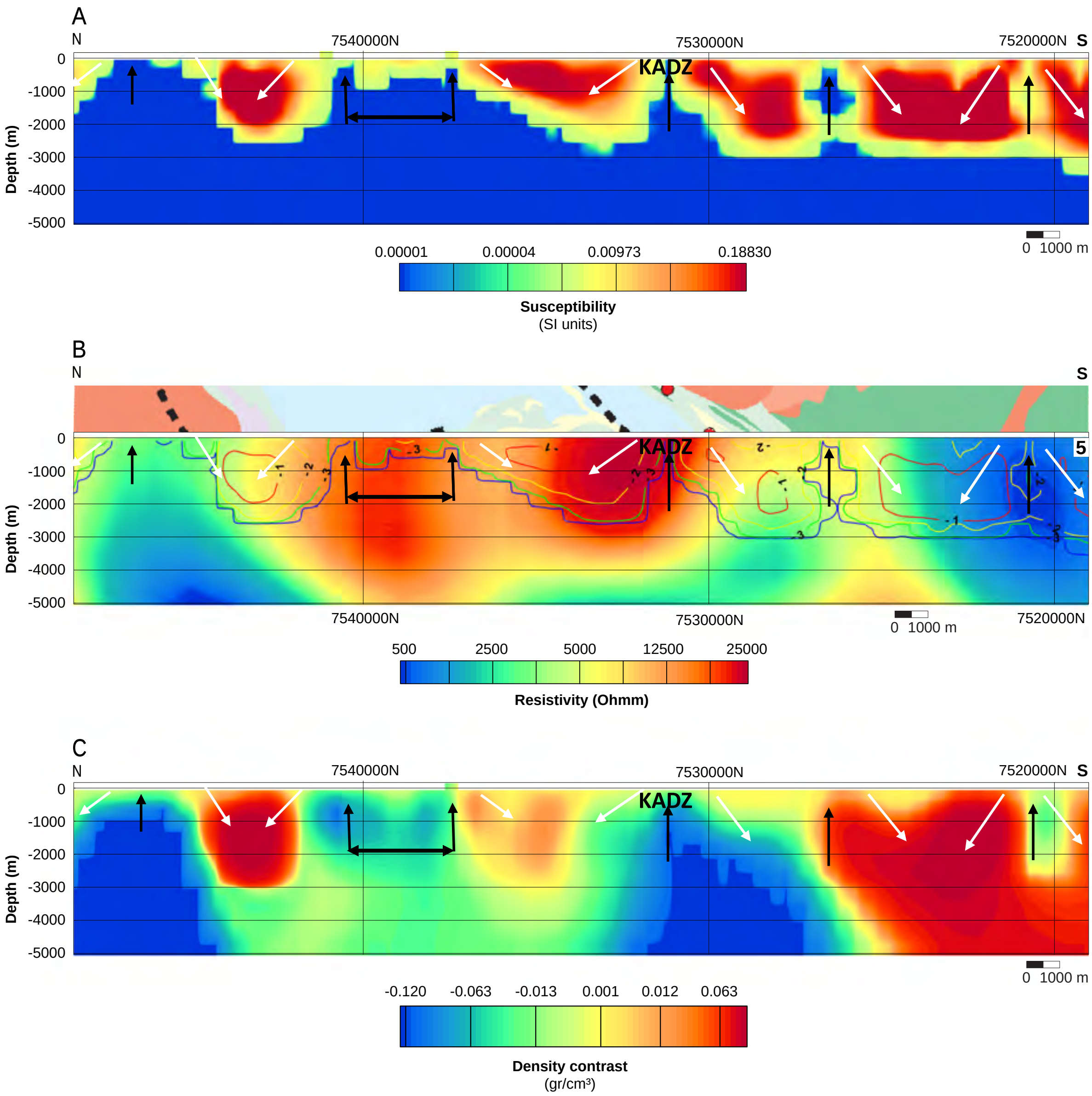

Figure 6. Sections from 3D models along section 5 shown in Figures 1 & 2. **A.** Susceptibility. **B.** Resistivity. **C.** Density contrast. In B the resistivity model is in the background and the contours with different colours represent the estimated magnetic susceptibility in logarithmic scale. The mapped bedrock and known mineralisations along each direction are shown on top of the resistivity section. The white and black arrows indicate the interpreted dips of high and low-susceptibility zones, respectively.

"false" synforms, showing instead the plunging hinge of a fold in the southeastern part of the anomaly.

As in sections 2 and 3, the KADZ is also pronounced in the susceptibility and density sections, showing sharp changes with extremely low values. However, it is not so pronounced in the resistivity model at that exact location of the KADZ, but a few kilometres towards the north a NW-dipping low to intermediate zone is seen. The susceptibility and density highs at the southern end of the section (SWEREF99 TM 748233/7525845) coincide with a mafic gabbro-diorite intrusion. Contact between the gabbro and the granites dipping to the northwest is seen in both sections. Surprisingly, a very low-resistivity zone is modelled in the last 3 km of the southern end of the section at the contact between the granite and gabbro. On the magnetic field anomaly map a highly negative lineament occurs in this zone.

Comparison with reflection seismic sections

We compare the models shown along sections 1, 2, and 3 with the migrated reflection seismic sections reported by Juhojuntti et al. (2014). Along sections 1 and 3 we compare the susceptibility and density contrast models, whereas along section 2 the resistivity model is also included. The comparison is mainly qualitative because much more detail is seen in the seismic sections due to the higher data sampling density. We show the seismic section on top of the selected models and use arrows and broken lines to indicate the most dominant reflection patterns, i.e. the stronger reflections that are clearer in the seismic sections. Figure 7 shows seismic section 1. The broken black line marks the bottom of shallower reflections above a depth of approximately 1 km, where the reflectivity is substantially higher. The smaller arrows show the apparent dip of dominant reflections. In the depth range 0–1 km, the apparent dip of shallower reflections mostly accords reasonably well with those seen in the susceptibility and density contrast models. However, dips are gentler in the seismic section (compare with those shown in Figs. 3A and 3C). Below 2 km, the susceptibility model does not resolve any contrast and the best comparison is made between the density contrast model and the reflection seismic sections. Generally speaking, below this depth the reflections are weaker and sparser. In the west, an almost horizontal high-reflectivity zone predominates at > 4 km, while to the east, after 720000E, a 45-degree west-dipping high-reflectivity zone clearly predominates until 730000E. This higher-reflectivity zone coincides very well with the low and high-density zones with approximately the same dips. Further east, the dominant dip of the high-reflectivity zone changes towards the east, coinciding with a high-density zone (Fig. 7B). We have marked with "?" two deeper reflectivity zones that seem to be artefacts dictated by the migration process. The east-dipping reflection trend predominates to the eastern end of the section and no significant correlation can be seen with either the susceptibility or the density contrast models.

Figure 8A–C shows the comparison between susceptibility, resistivity, density contrast models and the reflection seismic data along section 2. The apparent dips of shallower reflections (marked by smaller arrows) correlate well with the highs and lows seen in the susceptibility model (Fig. 8A) and to some extent with the structures seen in the density contrast model (Fig. 8C). In the depth range 1–3 km, the first third of the section in the NW, a moderately SE-dipping high-reflectivity trend (marked by a long arrow) predominates in the seismic section and coincides best with the high-susceptibility zone. Further SE the dip changes to the NW, which can be interpreted as a regional syn-

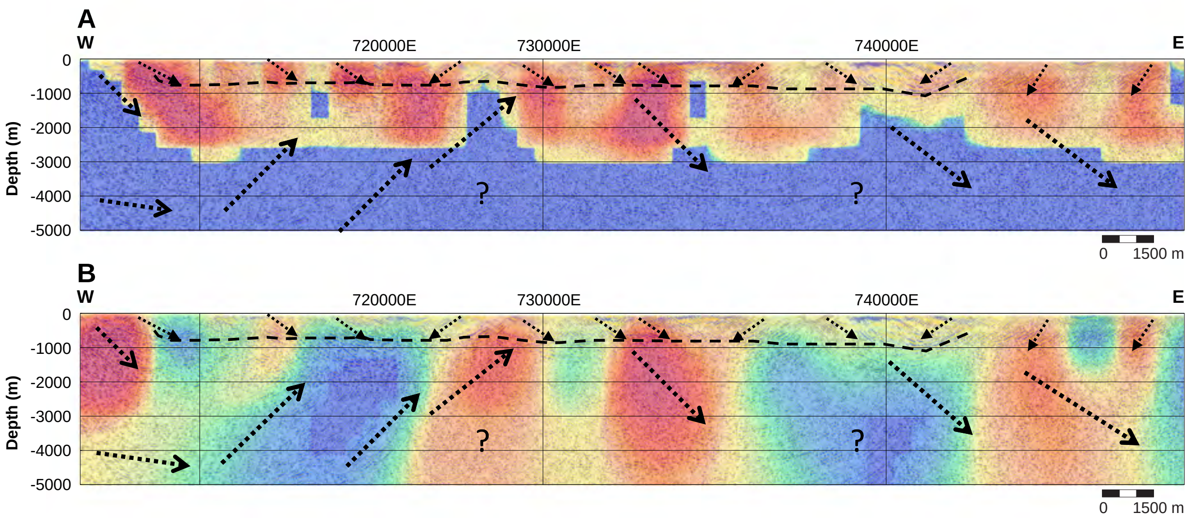

Figure 7. Comparison between the migrated seismic section with **A** the susceptibility model and **B** the density contrast model along section 1. The smaller arrows indicate shallower and more local predominant trends. The longer arrows represent deeper reflections. The broken black line marks the bottom of a shallower high-reflectivity zone in the seismic section. The "?" shows possible artefacts caused by migration.

clinal structure. NW-dipping strong positive susceptibility, positive density contrast and a high-resistivity zone are clearly observed in this part of the sections (Figs. 8A–C). With the exception of a few shallow diffractions in the seismic section, the KADZ is not resolved as clearly as in the other sections. Towards the SE of the KADZ the regional dip trend in the seismic section reverts towards the SE. It should be noted that at the deeper levels in this part of the section (> 3 km) fringe-shape reflection may have been introduced by the migration processes.

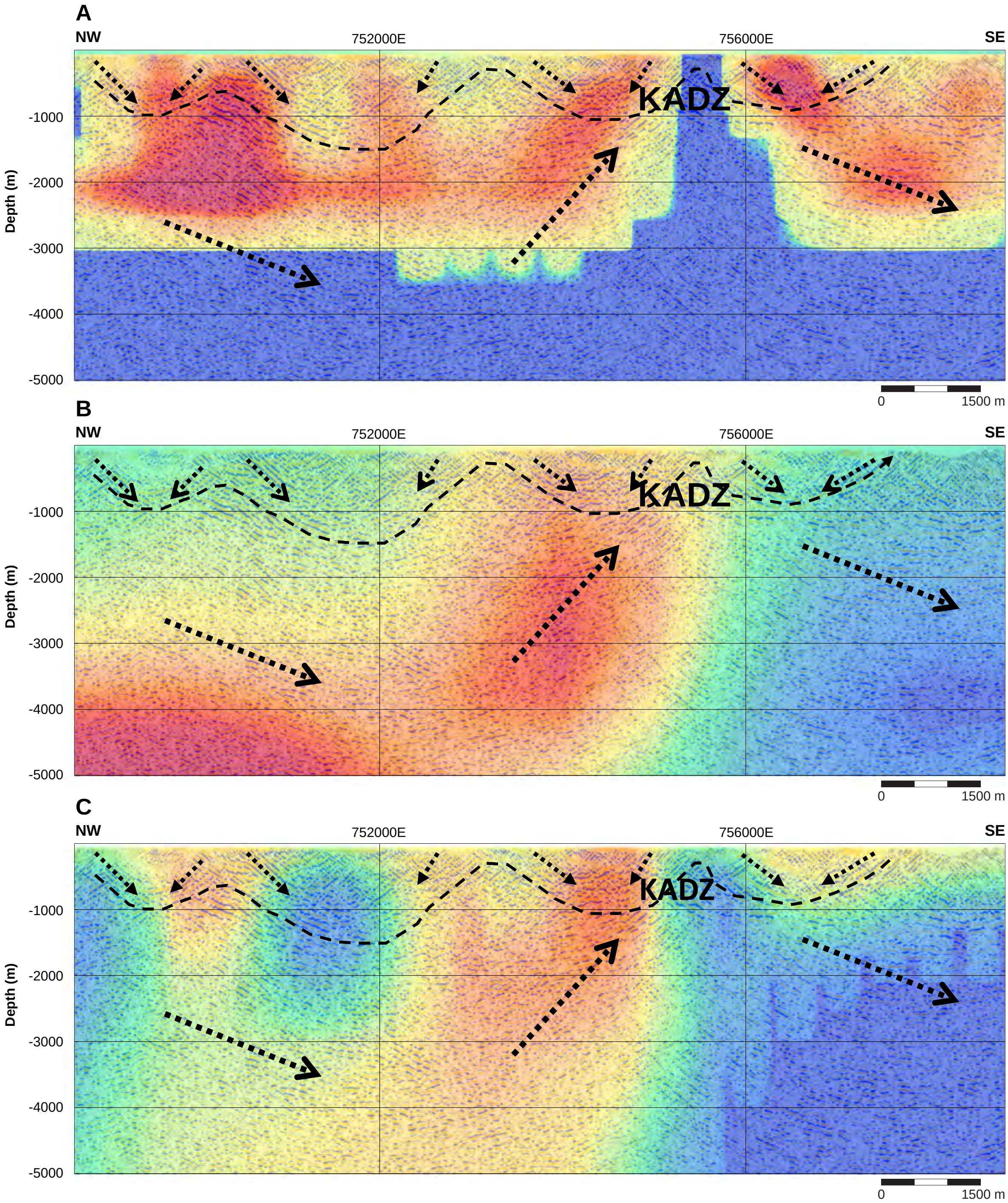

Figure 8. Comparison between the migrated seismic section with **A** susceptibility model, **B** resistivity model and **C** density contrast model along section 2. The smaller arrows indicate shallower and more local predominant trends. The longer arrows represent deeper reflections. The broken black line marks the bottom of a shallower high-reflectivity zone in the seismic section.

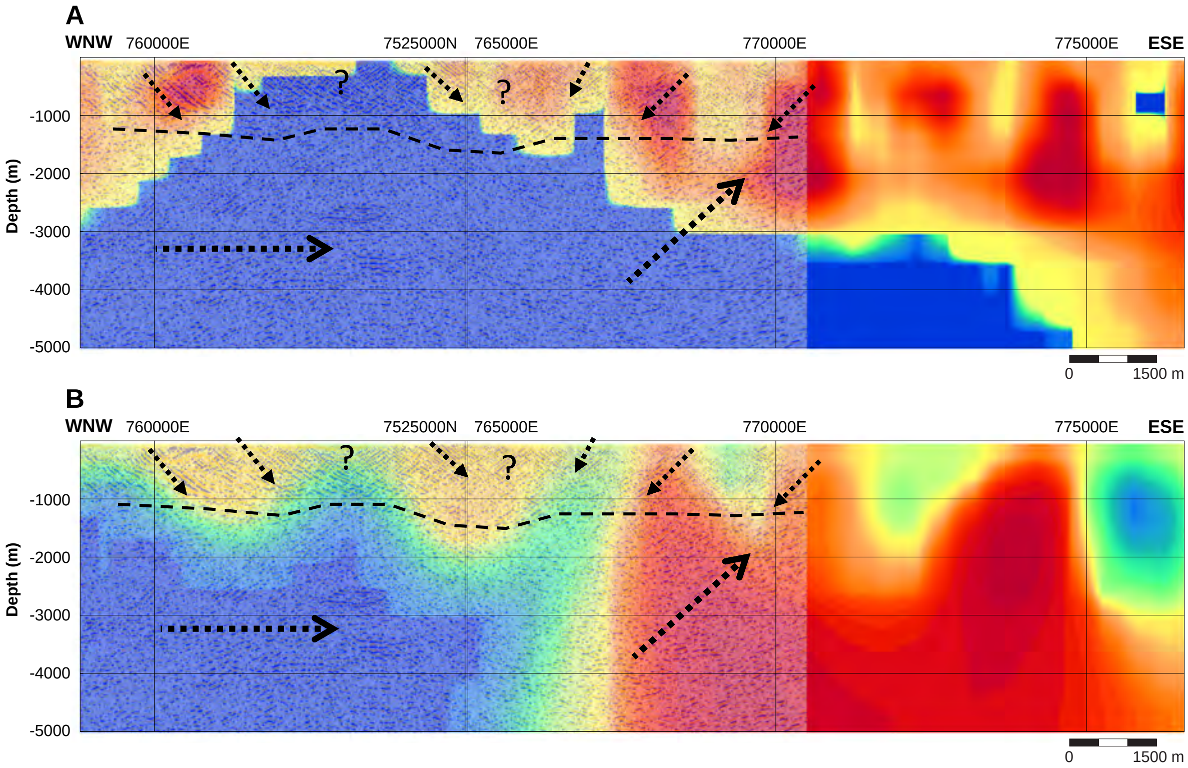

Figure 9. Comparison between the migrated seismic section with **A** susceptibility model and **B** density contrast model along section 3. The smaller arrows indicate shallower and more local predominant trends. The longer arrows represent deeper reflections. The broken black line marks the bottom of a shallower high-reflectivity zone in the seismic section. The "?" shows possible artefacts caused by migration.

The seismic data cover the first two-thirds of section 3 (Fig. 9). The apparent dip of shallower reflections is dominated by E-SE and W-NW trends in the first and second half of the section, respectively. The deeper reflections show varying dips in the first half of the section, whereas the second half is dominated by a W-NW-dipping high-reflectivity zone that starts at the position where an almost vertical high-density zone appears in the density model. High-density mafic volcanic and gabbro intrusions are mapped at this boundary. Two very distinct almost horizontal reflectors, marked by a long horizontal arrow at a depth of 2.5–3.5 km, are of great importance in the seismic section. These were interpreted as smaller mafic bodies in the forward model presented by Juhojuntti et al. (2014). Neither the magnetic nor the gravity inversion model reveals such a distinct zone, although a weak gradient in the density contrast model can be distinguished in that area.

Figure 10 shows a more regional summary of the estimated apparent dips along sections 1 to 5 taken from the magnetic susceptibility models and seismic sections (1–3) shown on the geological maps in the area. The black arrows point towards the down-dip. Note that the dips are presented for moderate to high-susceptibility structures. In our interpretations we have also taken some account of the density and the resistivity models where the dips are not well resolved by both datasets. A few arrows might represent the steeply dipping structures that are shown in the magnetic models with vertical arrows. The reader is referred to the discussions made to compare the dips with those seen in the density contrast models. The thicker broken line marked by a "?" indicates possible continuation of the shear zone mapped in the NE and crossing section 5. This approach can be applied to the entire model area to construct a more detailed image of variation of the dip direction. To verify the validity of our dip interpretations we have compared them with an analysis made by Eriksson & Hallgren (1975). The folds (anticlines and synclines) interpreted by their study are shown in Figure 10 by red

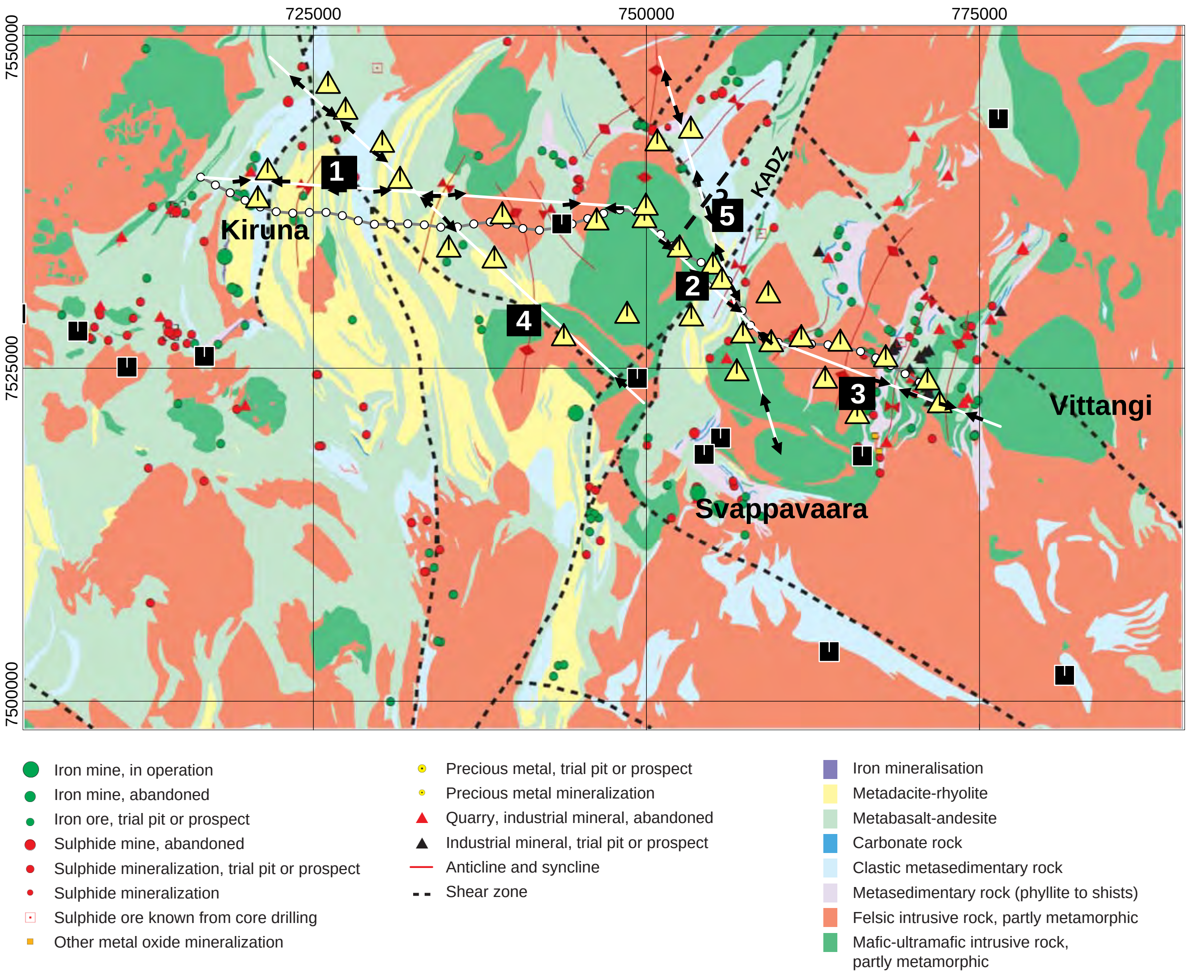

Figure 10. Regional presentation of the estimated dips of structures with moderate to high magnetic susceptibilities taken from the 3D inversion results. Most of the dips are confirmed by the reflection seismic data.

symbols. We generally find a good correlation between the geological structures presented by Eriksson & Hallgren (1975) and those derived by interpreting models from different geophysical responses. However, there are also some differences, giving us new information and insights. In the middle part of section 1, east of 730000E, the susceptibility model suggests an anticline (Fig. 3A). The same pattern (Fig. 5A) is also observed in section 4, near the intersection with section 1, while the geological observations reported by Eriksson & Hallgren (1975) show a synclinal structure (Fig. 10). This is also the case along the eastern part of KADZ (Fig. 10) where sections 2 and 5 cross each other. The susceptibility and the density sections show an anticline (Fig. 4A, C and Fig. 6A), c), whereas the geological model/interpretation shows a syncline (Fig. 10). In this case, the seismic section also suggests an anticline structure at depth (Fig. 8). It should be noted that the geological observations and geophysical models have somewhat different scales, which gives rise to different interpretations.

CONCLUSION

The models from 3D inversions of the potential field and the MT data demonstrate a reasonable correlation with geological units and mineralised zones in the area. As expected, shear zones appear as low-resistivity, low-susceptibility and low-density zones in the selected sections from the 3D models. High-susceptibility and high-density zones mark the basaltic volcanics and in most of the cases, appear as high-resistivity zones in the resistivity models. A very distinct low-resistivity and low-susceptibility zone of varying density (high and low) is observed in the eastern part of section 3, where zones of sulphide and graphite mineralisations are known. The MT method has a poor resolution at shallower depths but a reasonably deep depth penetration. The 3D resistivity models can be used to study geometry and properties of deep-seated crustal structures as deep as 50 km. The susceptibility models, on the other hand, demonstrate a very high-resolution near the surface and are best for comparison with the high-resolution reflection seismic data for the study of shallower structures and geological units. Dips estimated using the susceptibility models accord fairly well with those from seismic data. However, the smoothing regularization used in the 3D modelling and the coarser sampling of the magnetic data led to big differences in some portions of the sections. The density, resistivity and reflection seismic data correlate best in deeper parts of the models. This suggests they may be preferred when constructing a 3D model for more regional structures residing at depths >2 km. The dips interpreted from integrated use of geophysical models correlate reasonably well with previous geological interpretations made from field observations. But there are differences that might be due to the difference between the scales used in the modelling. These differences give us new information and insights thanks to the ability of geophysical models to resolve deeper information.

OUTLOOK

This study suggests that models from independent 3D inversions of the geophysical data contain valuable information that can be used for imaging and classifying geological structures in 3D. The methods used here have different sensitivities and, when inverted jointly, can produce models with even more reliable information. Joint inversion of MT and gravity data has become a common practice and can be tried on these datasets. The valuable detailed structural information found in the reflection seismic data can be applied in the inversion of magnetic field data as constraints or *a priori* information to estimate the geometry of the geological structures more accurately. We suggest a detailed electromagnetic survey with higher frequencies, such as a controlled source and radio magnetotelluric survey, to collect supplementary information to better understand the depth and lateral extent of the low-resistivity mineralised zones close to Vittangi village. The cause of a deep and extremely low-resistivity, low-density and low-susceptibility zone in the middle of section 3 is unknown and should be the subject of more scientific research.

ACKNOWLEDGEMENTS

Dr. Maxim Smirnov of Olou University (currently at Luleå University of Technology) kindly provided us with existing MT stations close to the study area.

REFERENCES

Arora, K., Tiwari, V.M., Singh, B., Mishra, D.C. & Grevemeyer, I., 2012: Three dimensional lithospheric structure of the western continental margin of India constrained from gravity modelling: implication for tectonic evolution, *Geophysical Journal International 190,* 131–150, doi:10.1111/j.1365-246X.2012.05506.x

Aster, R. C., Borchers, B. & Thurber, C.H., 2005: *Parameter estimation and inverse problems*: Academic Press.

Bastani, M., Antal Lundin, I., Savvaidis, A., Kamm, J., & Wang, S., 2015: Audiomagnetotelluriska (AMT) mätningar i Kiruna- och Lannavaraområdet, preliminära resultat. *Sveriges geologiska undersökning* SGU-rapport 2015:10, 16 p.

Bergman, S., Kübler, L. & Martinsson, O., 2000: Regional geological and geophysical maps of northern Norrbotten County: Bedrock map (east of the Caledonian orogen). *Sveriges geologiska undersökning, Ba 56:1.*

Bergman, S., Kübler, L. & Martinsson, O., 2001: Description of regional geological and geophysical maps of northern Norrbotten County (east of the Caledonian orogen). *Sveriges geologiska undersökning Ba 56,* 110 pp.

Cherevatova, M., Smirnov, M.Yu., Jones, A.G., Pedersen, L.B. & MaSca Working Group, 2015: Magnetotelluric array data analysis from north-west Fennoscandia, *Tectonophysics 653*, 1-19, doi:10.1016/j.tecto.2014.12.023

England, R. W. & Ebbing, J. 2012: Crustal structure of central Norway and Sweden from integrated modelling of teleseismic receiver functions and the gravity anomaly. *Geophysical Journal International 191 (1):* 1–11. doi:10.1111/j.1365-246X.2012.05607.x

Eriksson, B. & Hallgren, U., 1975: Berggrundsgeologiska och flygmagnetiska kartbladen Vittangi NV, NO, SV, SO. *Sveriges geologiska undersökning Af Nr 13–16*.

Hedin, P., Malehmir, A., Gee, D., Juhlin, C. & Dyrelius, D., 2014: 3D interpretation by integrating seismic and potential field data in the vicinity of the proposed COSC-1 drill site, central Swedish Caledonides. *Geological Society Special Report, Geological Society. 390,* 301–319.

Juhojuntti, N., Olsson, S., Bergman, S. & Antal Lundin, I., 2014: Reflexionsseismiska mätningar vid Kiruna – preliminär tolkning. Sveriges geologiska undersökning *SGU-rapport 2014:05*, 26 p.

Kamm, J., Antal Lundin, I., Bastani, M., Sadeghi, M. & Pedersen, L., 2015: Joint inversion of gravity, magnetic and petrophysical data – A case study from a gabbro intrusion in Boden, Sweden. *Geophysics, 80(5):* B131–B152.

Lynch, E. P., & Jönberger, J., 2013: Summary report on the geological and geophysical characteristics of the Nunasvaara key area (29K Vittangi NO & SO). Sveriges geologiska undersökning, *SGU-rapport 2013:11*, 35 p.

Martinsson, O., 1993: Greenstone and porphyry hosted ore deposits in northern Norrbotten. *PIM/NUTEK report # 1*, 77 p.

Martinsson, O., 1997: Paleoproterozoic greenstones at Kiruna in northern Sweden: a product of continental rifting and associated mafic-ultramafic volcanism. *In:* O. Martinsson: *Tectonic setting and metallogeny of the Kiruna greenstones. Doctoral thesis 1997:19, Paper I*, 1–49. Luleå University of Technology.

Martinsson, O., 1999: Berggrundskartan 30J Rensjön SO, skala 1:50 000. *Sveriges geologiska undersökning Ai 133.*

Martinsson, O., 2011: Kiskamavaara: a shear zone hosted IOCG-style of Cu-Co-Au deposit in Northern Norrbotten, Sweden: 11th Biennial SGA meeting, Antofagasta, Chile.

Öhlander, B., Skiöld, T., Elming, S.-Å., BABEL Working Group, Claesson, S. & Nisca, D.H., 1993: Delineation and character of the Archaean-Proterozoic boundary in northern Sweden. *Precambrian Research 64*, 67–84.

Siripunvaraporn, W., Egbert, G., Lenbury, Y. & Uyeshima, M., 2005: Three dimensional magnetotelluric inversion: Data-space method. *Physics of the Earth and Planetary Interiors 150*, 3–14, doi: 10.1016/j.pepi.2004.08.023.

Author, paper 11:
Fredrik A. Hellström
Geological Survey of Sweden
Department of Mineral Resources,
Uppsala, Sweden

11. Early Svecokarelian migmatisation west of the Pajala deformation belt, northeastern Norrbotten province, northern Sweden

Fredrik A. Hellström

ABSTRACT

An older phase of deformation and high-grade metamorphism is preserved in the Masugnsbyn area, west of the Pajala deformation belt, in the northeastern Norrbotten province. The Pajala deformation belt is a major high-strain belt characterised by NNE–SSW to NNW–SSE-oriented zones with high-grade metamorphic alterations, while the area west of the Pajala deformation belt is structurally heterogeneous, displaying both medium- and high-grade metamorphic alterations. High-grade metamorphism in the Pajala deformation belt was previously dated in the 1.83–1.78 Ga interval. In contrast, U-Pb SIMS analyses of metamorphic, low-Th/U zircon rims from a migmatitic, sillimanite-cordierite-bearing paragneiss in the western domain are dated here at 1878 ±3 Ma (2σ). This age is interpreted to date migmatisation and constrains the maximum age of folding of supracrustal rocks. There were possibly also later metamorphic/hydrothermal events in the Masugnsbyn area, as previously recorded by a U-Pb monazite age of approximately 1.86 Ga and by U-Pb titanite ages of 1.80–1.76 Ga. 1.88 Ga migmatisation was contemporaneous with large volumes of early orogenic intrusions, and it is suggested that heat from these intrusions caused high-grade metamorphism and partial melting in the southern part of the Masugnsbyn area. Metamorphic alteration of supracrustal rocks at 1.88 Ga has implications for the timing of skarn iron ore formation and base-metal sulphide mineralisations. Despite the limited amount of SIMS data on zircon core domains, the maximum depositional age of sediments in the Kalixälv group may be constrained by the youngest zircon core age of 1882 ±25 Ma (2σ), but must have occurred before migmatisation at 1878 ±3 Ma. 50% of the recorded zircon core ages fall in the range 2.02–1.92 Ga, suggesting that rocks of this age interval were the main source of the Kalixälv group, together with debris from 2.97–2.75 Ga Archaean rocks (29%). This suggests that 2.02–1.92 Ga felsic to intermediate rocks can be expected to be present to a greater extent than is known from available age determination of the rocks in the Svecokarelian orogen.

INTRODUCTION

Bergman et al. (2006) recognised two different structural domains in northeastern Norrbotten separated roughly along a N–S-trending structural boundary defined by the western margin of the Pajala deformation belt (Fig. 1; see Luth et al. 2018). The eastern domain occurs within the Pajala deformation belt, and is characterised by N-NE to N-NW high-strain zones with high-grade metamorphic alterations. The area west of the Pajala deformation belt is structurally heterogeneous, with both medium- and high-grade metamorphic areas and is here referred to as the Masugnsbyn structural domain (Fig. 1; Bergman et al. 2001). The latter domain is located between the N-NE-oriented Karesuando–Arjeplog deformation zone in the northwest, the N-NE to NE-oriented Pajala deformation belt in the east, and the NW-trending Nautanen deformation zone in the southwest (Fig. 1). Metamorphic monazite and titanite as well as zircon overgrowths in the Pajala deformation belt verify deformation and high-grade metamorphism in the 1.83–1.78 Ga interval, while metamorphic monazite in rocks of the Masugnsbyn structural domain records a 1.86–1.85 Ga metamorphic event (Bergman et al. 2006, Hellström & Bergman 2016).

Monazite was dated from two localities south of Masugnsbyn (Fig. 1–2), interpreted to date metamorphism at approximately 1.86 Ga (Bergman et al. 2006). One sample was taken from an andalusite-bearing meta-argillite at Pahakurkio and the other sample from a weakly migmatitic, sillimanite-bearing paragneiss at Takanenvaara, i.e. in the higher-grade area southeast of Pahakurkio (Figs. 1–2; Bergman et al. 2006). The single discordant monazite analysis from the Pahakurkio sample has an upper intercept age of 1 856 ±7 Ma, whereas the two Takanenvaara analyses record ages of 1 856 ±4 and 1 861 ±4 Ma, with regression forced through a lower intercept at 300 ±300 Ma. Based on analysis of only 1–2 monazite fractions, the calculated ages are uncertain, however. A strongly migmatitic paragneiss was sampled close to the Takanenvaara locality in order to perform U-Pb SIMS dating of possible, secondary zircon domains to improve the poorly constrained approximately 1.86 Ga metamorphic age. It has recently been suggested that the Pajala deformation belt marks an old suture zone between the continents of Norrbotten and Karelia (Lahtinen et al. 2015). One of the significant questions addressed here is: is there a preserved older metamorphic event in the Masugnsbyn domain than within the Pajala deformation belt?

GEOLOGY OF THE MASUGNSBYN AREA

The Masugnsbyn area shows variable foliations and complexly-folded supracrustal rocks (Bergman et al. 2001). Metamorphism in the Masugnsbyn key area reaches medium- to high-grade, and generally increases towards the south and west, where migmatitic paragneiss occurs next to adjacent granitic intrusions (Fig. 2). In the central part of the area, the clastic metasedimentary rocks of the Pahakurkio

► Figure 1. **A.** Metamorphic map of northern Norrbotten showing high-grade rocks in the eastern and south-central parts of the area and low-grade rocks in the Kiruna and Stora Sjöfallet areas in the west. The study area at Masugnsbyn is of medium metamorphic grade, but the southern part contains high-grade, sillimanite-bearing, migmatitic paragneisses. KADZ – the Karesuando–Arjeplog deformation zone, KNDZ – the Kiruna–Naimakka deformation zone, NDZ – the Nautanen deformation zone, PDB – the Pajala deformation belt (modified after Bergman et al. 2001). Selected metamorphic ages (U-Pb) are from: Bergman et al. (2006), Storey et al. (2007), Smith et al. (2009), Hellström & Bergman (2016), and this study (FHM140097A). **B.** Simplified map of the Fennoscandian Shield, modified from Koistinen et al. (2001) & Bergman et al. (2006). The area of northern Norrbotten County is marked with a red polygon. **C.** Magnetic anomaly map of northern Sweden, including adjacent areas of Norway and Finland. White = high magnetisation, dark grey = low magnetisation. Data from adjacent areas have been supplied by the geological surveys of Norway (ngu.no), and Finland (gtk.fi). The Pajala deformation belt is seen as an approximately north–south-trending zone along the Swedish-Finnish border, with a continuation into Norway. M – Masugnsbyn, B – Bothnian shear zone (southern part of the Pajala deformation belt), K – Kiruna, R – Rovaniemi.

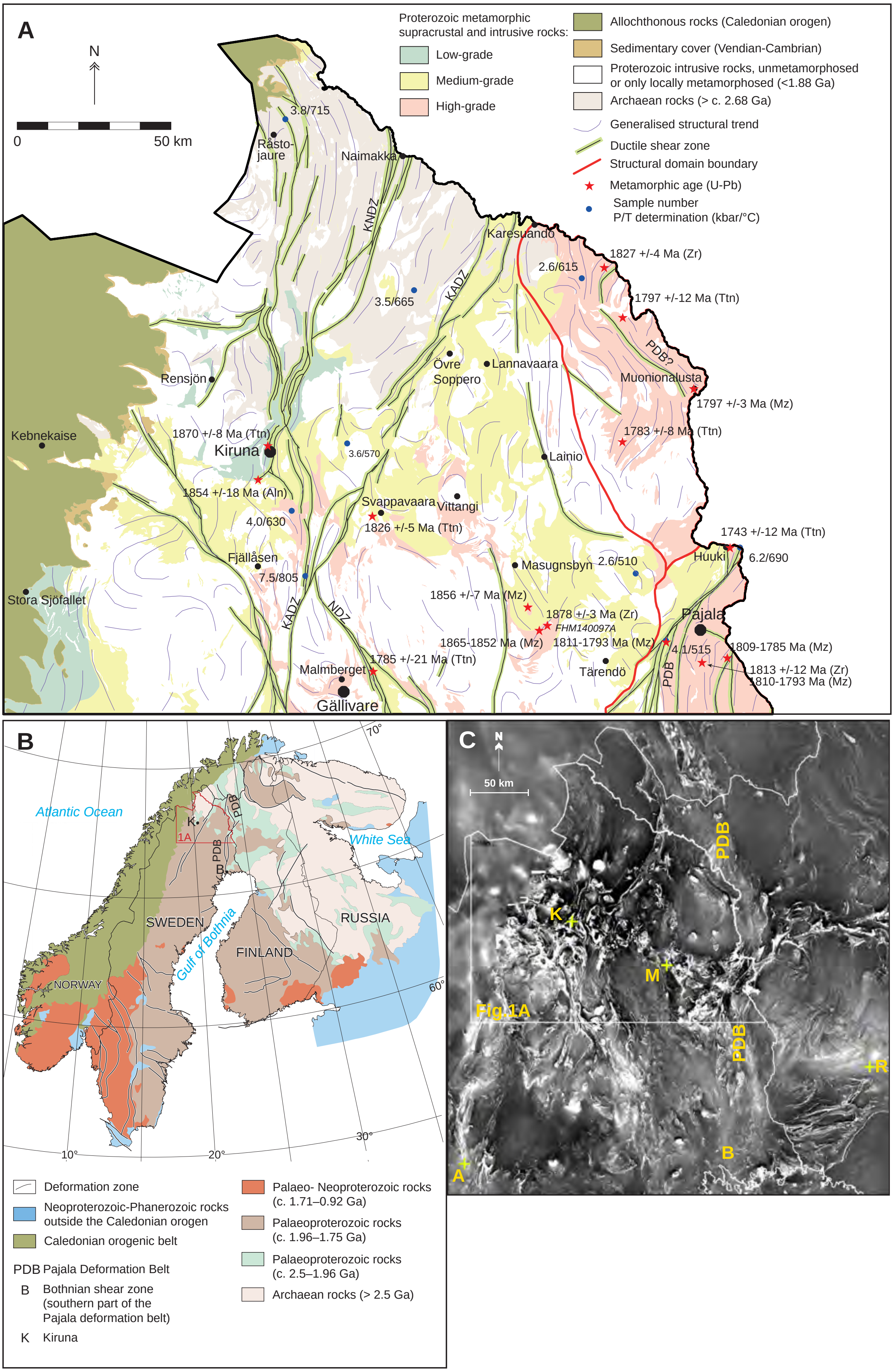
A
B
C
Proterozoic metamorphic supracrustal and intrusive rocks:
Low-grade
Medium-grade
High-grade
Allochthonous rocks (Caledonian orogen)
Sedimentary cover (Vendian-Cambrian)
Proterozoic intrusive rocks, unmetamorphosed or only locally metamorphosed (<1.88 Ga)
Archaean rocks (> c. 2.68 Ga)
Generalised structural trend
Ductile shear zone
Structural domain boundary
Metamorphic age (U-Pb)
Sample number
P/T determination (kbar/°C)
50 km
Kiruna
Gällivare
Pajala
Karesuando
Deformation zone
Neoproterozoic-Phanerozoic rocks outside the Caledonian orogen
Caledonian orogenic belt
PDB Pajala Deformation Belt
B Bothnian shear zone (southern part of the Pajala deformation belt)
K Kiruna
Palaeo- Neoproterozoic rocks (c. 1.71–0.92 Ga)
Palaeoproterozoic rocks (c. 1.96–1.75 Ga)
Palaeoproterozoic rocks (c. 2.5–1.96 Ga)
Archaean rocks (> 2.5 Ga)

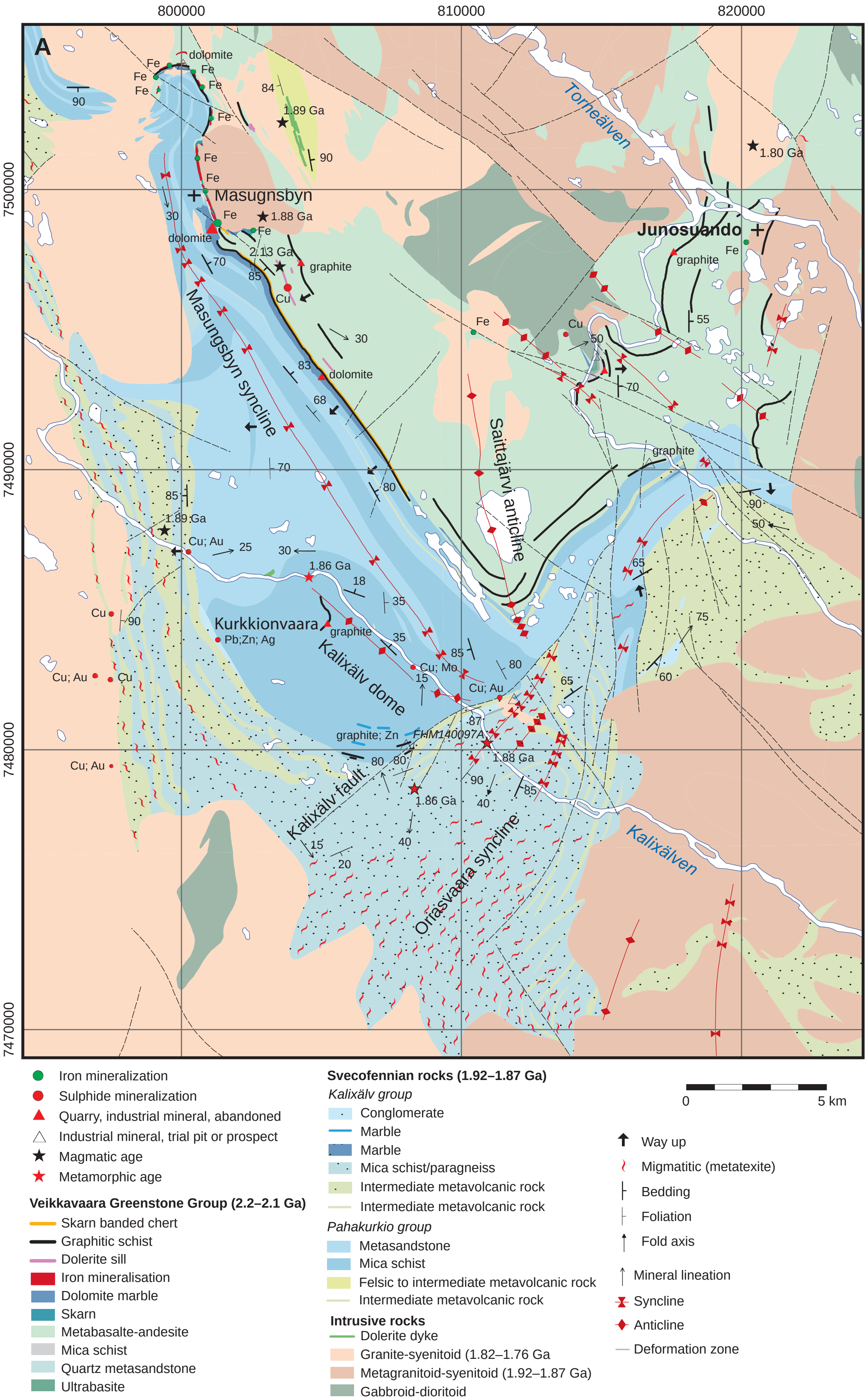
A
800000
810000
820000
7500000
7490000
7480000
7470000
Masugnsbyn
Junosuando
Torneälven
Kalixälven
Masugnsbyn syncline
Saittajärvi anticline
Kalixälv dome
Kalixälv fault
Oriasvaara syncline
Kurkkionvaara
Pb;Zn; Ag
1.89 Ga
1.88 Ga
2.13 Ga
1.80 Ga
1.86 Ga
FHM140097A
dolomite
graphite
graphite; Zn
Fe
Cu
Cu; Au
Cu; Mo
Iron mineralization
Sulphide mineralization
Quarry, industrial mineral, abandoned
Industrial mineral, trial pit or prospect
Magmatic age
Metamorphic age
Veikkavaara Greenstone Group (2.2–2.1 Ga)
Skarn banded chert
Graphitic schist
Dolerite sill
Iron mineralisation
Dolomite marble
Skarn
Metabasalte-andesite
Mica schist
Quartz metasandstone
Ultrabasite
Svecofennian rocks (1.92–1.87 Ga)
Kalixälv group
Conglomerate
Marble
Marble
Mica schist/paragneiss
Intermediate metavolcanic rock
Intermediate metavolcanic rock
Pahakurkio group
Metasandstone
Mica schist
Felsic to intermediate metavolcanic rock
Intermediate metavolcanic rock
Intrusive rocks
Dolerite dyke
Granite-syenitoid (1.82–1.76 Ga
Metagranitoid-syenitoid (1.92–1.87 Ga)
Gabbroid-dioritoid
0
5 km
Way up
Migmatitic (metatexite)
Bedding
Foliation
Fold axis
Mineral lineation
Syncline
Anticline
Deformation zone

◀ Figure 2. **A.** Bedrock geological map of the Masugnsbyn area. Age determinations are from Bergman et al. (2001, 2006) Hellström et al. (2018), Lynch et al. (2018) and this study (FHM140097A).

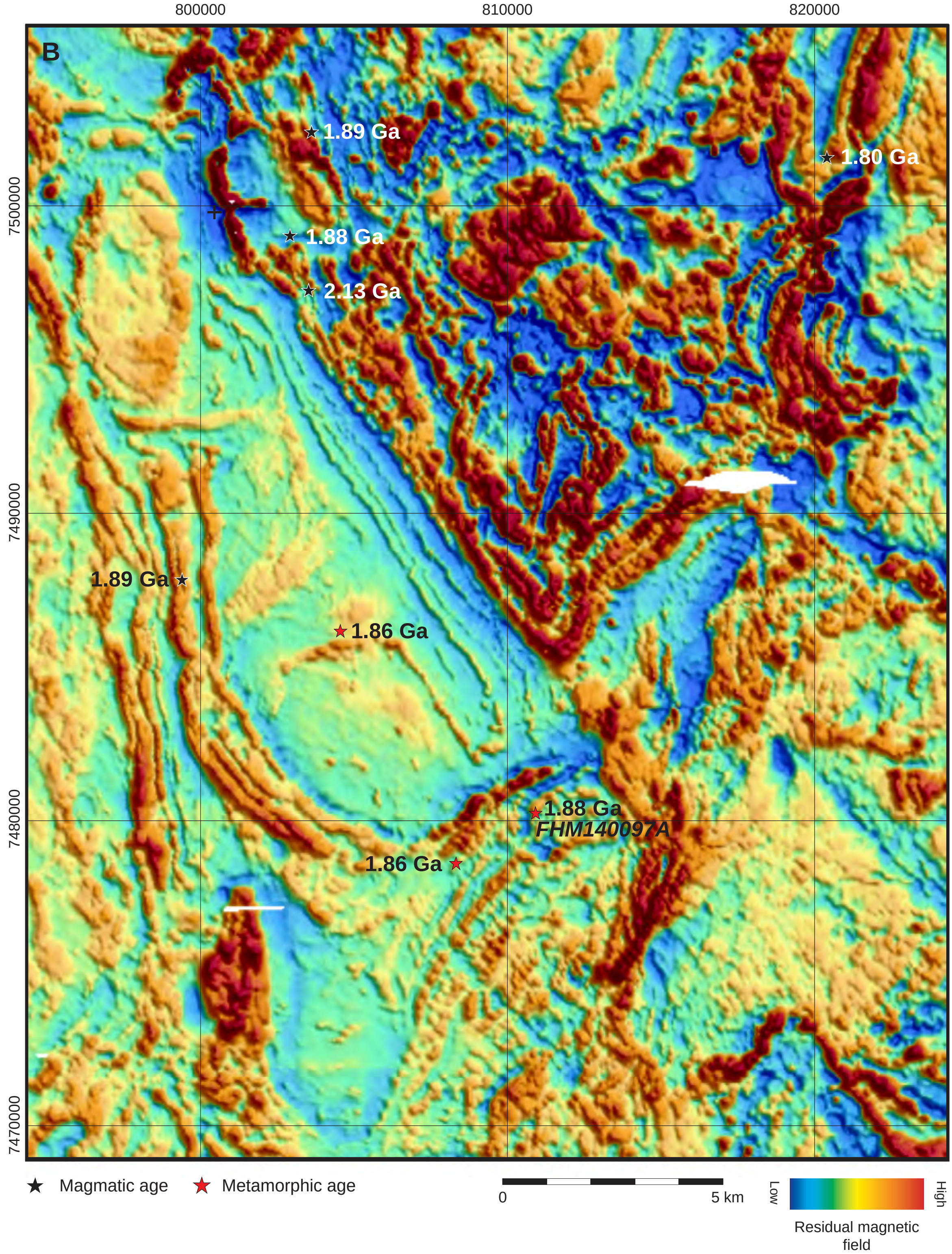

Figure 2. **B.** Magnetic anomaly map with same extent as in figure A. Map gridded from SGU data.

group still show primary sedimentary structures such as cross-bedding (Padget 1970). The sampled migmatitic paragneiss is part of the Kalixälv group, which forms the upper part of the supracrustal sequence in Masugnsbyn (Figs. 2, 3).

Karelian greenstones of the Veikkavaara greenstone group are overlain by Svecofennian metasedimentary pelitic to arenitic rocks of the Middle sediment group (Witschard 1984), which include the Pahakurkio and Kalixälv groups (Padget 1970). The latter group also contains intermediate metavolcanic rocks. Of economic interest in the Masugnsbyn area are layers of iron mineralisations and dolomite between the greenstones and metasedimentary rocks, as well as graphite schist layers and base-metal, sulphide mineralisations within the volcaniclastic greenstones and in the Svecofennian supracrustal rocks (Geijer 1929, Padget 1970, Witschard et al. 1972, Grip & Frietsch 1973, Niiniskorpi 1986, Frietsch 1997, Martinsson et al. 2013, 2016, Hellström & Jönsson 2014, Bergman et al. 2015).

The supracrustal sequence in the Masugnsbyn area is deformed into large-scale fold structures and cut by faults. The structures have NE or NW trends, thus intersecting at high angles. According to Padget (1970), the main tectonic features include the Kalixälv dome, the Masugnsbyn syncline, the Saittajärvi anticline and the Oriasvaara syncline with the associated Kalixälv fault (Fig. 2, Padget 1970). The fold structures in Masugnsbyn have recently been evaluated by Grigull et al. (2018), with the Saittajärvi fold structure now interpreted as a synform structure, supported by geophysical modelling. The fold axial planes are oriented in a northwesterly direction, except for the Oriasvaara syncline, which has a northeasterly trend, parallel to the Kalixälv fault, and the Saittajärvi synform, which has a N–NW orientation.

The Oriasvaara syncline is bounded to the NW by the northeasterly-oriented Kalixälv fault. Movements along that fault have down-thrown the southeastern block, creating a tectonic contact between the Pahakurkio and Kalixälv groups. For a description of the structural geology of the Masugnsbyn area, see Grigull et al. (2018).

The original shales of the Pahakurkio group have been metamorphosed to andalusite +/- sillimanite-bearing mica schists (Fig. 4A, C, D), and the sandstones have been recrystallised to quartzites with metamorphic biotite (Padget 1970, Kumpulainen 2000, Hellström et al. 2018). Other secondary minerals include muscovite, epidote, amphibole and scapolite, the last-named mineral showing a characteristic white spotted appearance in basic to intermediate rocks (Fig. 4B). The higher-grade gneisses in

Superunit	Unit	Subunit	Rock units
Svecofennian supracrustal rocks	Rissavaara quartzite	4	Quartz arenite
	Kalixälv grp	3b	Semipelitic,-pelitic-, basic schists, migmatitic paragneiss
		3a	Conglomerate, meta-arenite, intermediate metavolcanic rocks
	Sakarinpalo suite		Intermediate metavolcanic rocks
	Pahakurkio grp	2d	Meta-arenite
		2c	Pelitic schist, graphite schist, carbonate rocks
		2b	Meta-arenite, greenshist
		2a	Pelitic schist
Karelian supracrustal rocks	Veikkavaara greenstone grp	Masugnsbyn fm (1c)	Graphite schist, skarnbanded chert (BIF), carbonate rock
		Nokkokorvanrova greenstone fm (1c)	Basaltic tuff, graphite schist, dolerite sills
		Suinavaara fm (1b)	Pelitic schist and meta-arenite (Suinavaara quartzite)
		Tuorevaara greenstone fm (1a)	Basaltic greenstone

Figure 3. Schematic stratigraphy of the Masugnsbyn area. grp = group, fm = formation, modified from Padget (1970). The names used in Padget (1970) have been modified, and new names have been added, here used as informal names (see Lynch et al. and Hellström et al., both 2018).

the south of the area contain bundles of fibrolitic sillimanite, growing at the expense of biotite, and locally cordierite and andalusite. The rocks have been altered to migmatitic paragneisses in places (Fig. 4E). The migmatitic gneiss is interlayered with quartzitic bands, interpreted to represent a primary variation from pelitic to arenitic layers, where the former composition is more susceptible to melting during high-grade, amphibolite-facies metamorphic conditions (4F). The primary mafic minerals in the Veikkavaara greenstones have been altered to amphibole, giving the rocks their dark green colour. The amphibole is commonly a green pleochroic hornblende, but non-pleochroic, pale-coloured amphibole is also quite common (Padget 1970). Garnet porphyroblasts occur together with amphibole in certain, distinct layers in the basaltic tuffs (Fig. 4G) and seem to be late-kinematic, overgrowing the foliation in the rock (Fig. 4H). The composition of the plagioclase (An_{10-50}) and the presence of hornblende together with almandine suggest the rocks are in the garnet amphibolite facies of regional metamorphism (Padget 1970). The metamorphic mineral association in the mica schists with andalusite, sillimanite and cordierite, and the absence of kyanite also indicate amphibolite facies conditions of relatively high temperature and low to moderate pressure. Partial melting in the migmatitic paragneisses in the south suggests this area has even reached an upper amphibolite facies grade of metamorphism.

Sample description

The sampled rock for U-Pb SIMS geochronology is a sillimanite-cordierite-biotite-muscovite-bearing migmatitic paragneiss from the Kalixälv group in the southern part of the Masugnsbyn area (Fig. 4E, 5A–B, Table 1). The gneiss is rich in medium- to coarse-grained, granitic leucosome, interlayered with quartzitic bands showing less partial melting (Fig. 4F). The veining is complexly and polyphase folded, in part asymmetric with both S and Z folds. Needles of fibrolitic sillimanite have grown at the expense of biotite and cordierite, and seem to crosscut post-kinematic muscovite (Fig. 5B), suggesting that sillimanite is a late phase. Accessory mineral phases are monazite, zircon, sulphides and tourmaline.

Analytical results and interpretation of geochronological data

Zircons were obtained from a density separate of a crushed rock sample using a Wilfley water table. Magnetic minerals were removed with a hand magnet. Handpicked crystals were mounted in transparent epoxy resin together with chips of the reference zircon 91 500. Zircon mounts were polished and after gold coating examined with Back Scattered Electron (BSE) and Cathodoluminescence (CL) imaging using electron microscopy at EBC, Uppsala University and the Swedish Museum of Natural History in Stockholm. High-spatial resolution secondary ion masspectrometer (SIMS) analysis was carried out in November and December 2014 using a Cameca IMS 1280 at the Nordsim facility at the Swedish

Table 1. Summary of the sample data.

Rock type	Migmatitic paragneiss
Tectonic domain	Svecokarelian orogen
Tectonic sub-domain	Norrbotten lithotectonic unit
Stratigraphic unit	Kalixälv group
Sample number	FHM140097A
Lab ID	n5161 (Nordsim)
Coordinates	7480256 / 810923 (SWEREF 99TM)
Map sheet	28L NO (RT90)
Locality	Tiankijoki
Project	Barents

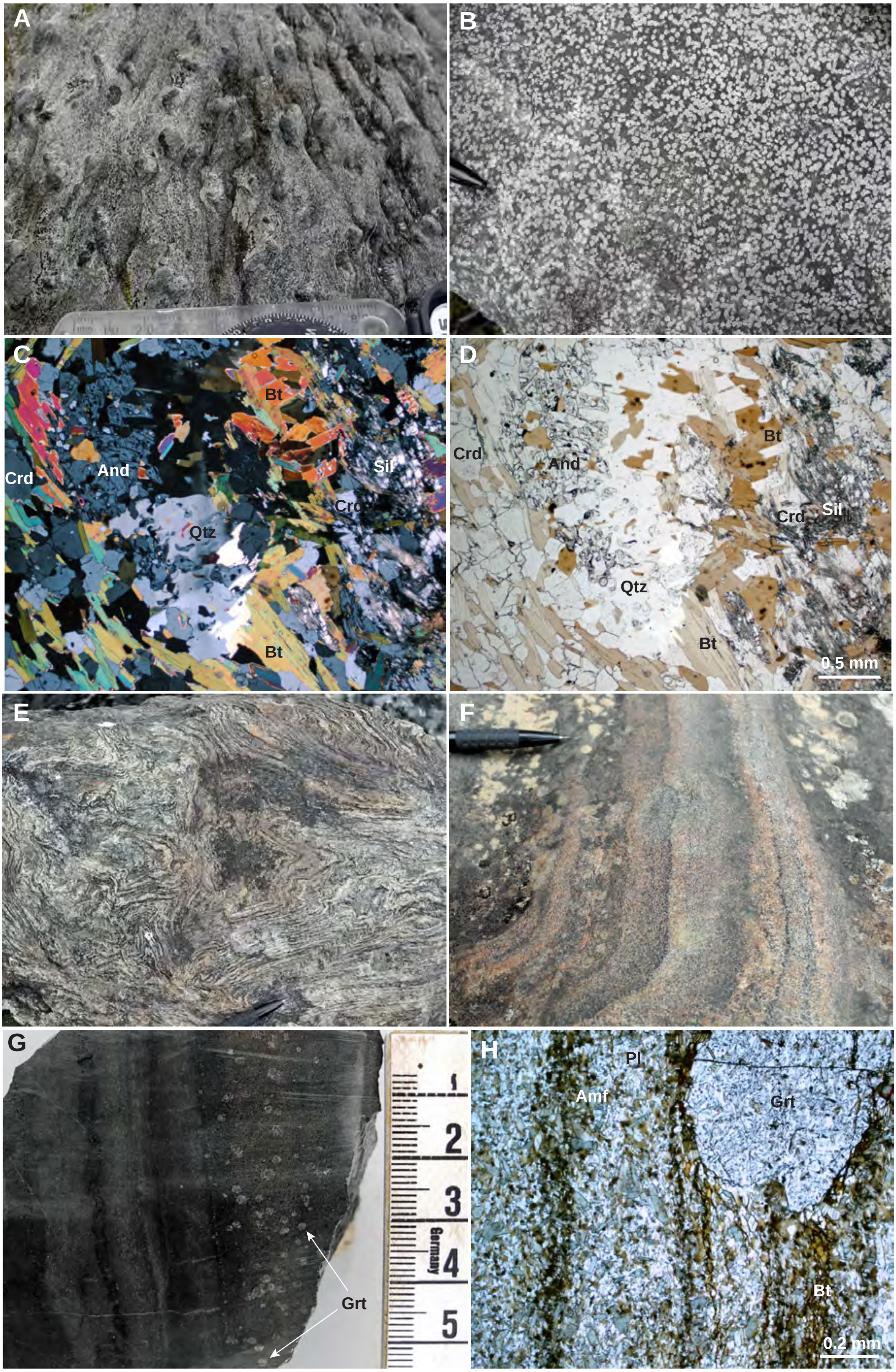
A
B
C
Bt
Crd
And
Sil
Crd
Qtz
Bt
D
Crd
And
Bt
Crd
Sil
Qtz
Bt
0.5 mm
E
F
G
Grt
1
2
3
4
5
Germany
H
Pl
Amf
Grt
Bt
0.2 mm

◀ Figure 4. **A.** Mica schist with porphyroblasts of andalusite (Pahakurkio group, unit 2b 7483486/807939. **B.** Strongly scapolite-altered meta-andesite, with characteristic whitespotted appearance of the scapolite (Pahakurkio group, unit 2c, greenschist, 7489838 / 806809). **C.** Photomicrograph in cross-polarised light of andalusite-sillimanite mica schist (same rock as in Fig. 4 A). **D.** Photomicrograph in plane-polarised light of andalusite-sillimanite mica schist (same extent as in Fig. 4C). **E.** Complexly poly-phase-folded, migmatitic paragneiss at Tiankijoki. North is to the left in the photograph (Kalixälv group, 7480253/810919). **F.** The migmatitic gneiss is interlayered with quartzitic bands, interpreted to represent a primary variation from pelitic to arenitic layers, where the pelitic layers are more susceptible to melting during the high-grade, amphibolite facies metamorphic conditions. **G.** Certain layers within the Veikkavaara greenstones contain abundant garnet porphyroblasts (7497316 / 804044). **H.** The garnet in the basaltic tuffs appears late-kinematic, overgrowing the lamination and foliation in the rock (7494442 / 805044). Coordinates are in SWEREF 99TM. All photographs by Fredrik Hellström.

Museum of Natural History. Detailed descriptions of the analytical procedures are given in Whitehouse et al. (1997, 1999), and Whitehouse & Kamber (2005). An approximately 6 nA O^{2-} primary ion beam was used, yielding spot sizes of 10–15 µm. U/Pb ratios, elemental concentrations and Th/U ratios were calibrated relative to the Geostandards zircon 91 500 reference, which has an age of approximately 1 065 Ma (Wiedenbeck et al. 1995, 2004). Common Pb-corrected isotope values were calculated using modern common Pb composition (Stacey & Kramers 1975) and measured ^{204}Pb, in cases of a ^{204}Pb count rate above the detection limit. Decay constants follow the recommendations of Steiger & Jäger (1977). Diagrams and age calculations of isotopic data were made using Isoplot 4.15 software (Ludwig 2012). BSE imaging of the dated zircons was performed using electron microscopy at the Department of Geology, Uppsala University.

The heavy mineral concentrate contains subhedral zircon with rounded edges; most are turbid. Many rounded grains of yellowish monazite are also present in the sample. BSE images of the zircon reveal oscillatory zoned cores and texturally younger, homogenous, BSE-bright rims (Fig. 5C). Two analyses (4c, 6a) show high values for common lead (f_{206}% = 4.99, 0.51), and are excluded in the description and diagrams below (see Table 2). Rims are rich in uranium (807–1 303 ppm) and are very low in Th (2.7–16.3 ppm), resulting in very low Th/U ratios, 0.00–0.01 (Fig. 5D, Table 2). In contrast, the oscillatory zoned cores have distinctly higher Th/U ratios (0.33–1.78), with 49–372 ppm uranium and 26.1–301 ppm Th. Examination of the post-analysis BSE images show that some rim analyses include some core domain material (analyses no 02, 03b, 04, 09, Fig. 5C) and these analyses record slightly higher Th/U ratios (0.03–0.06), and somewhat older (mixed) ages (Fig. 5E, Table 2).

Two rim analyses are excluded from the age calculations; analysis no 6b hits a fracture, and plots discordantly, and analysis no 01 records a rather high value for common lead (f_{206}% = 0.35), probably because the spot was placed too close to, and partly outside the margin of the grain. It also seems to include BSE-dark inclusions. The remaining seven rim analyses record a concordia age of 1880 ±5 Ma. High MSWD of concordance at 24 and zero probability of concordance, result from analyses being slightly reversely discordant, although all but two plot concordantly at the two sigma confidence level. The weighted average ^{207}Pb/^{206}Pb age is calculated at 1 878 ±3 Ma (Fig. 5, MSWD = 0.94, probability = 0.47, n = 7) and is chosen as the best age estimate, interpreted to date migmatisation at approximately 1.88 Ga.

The oscillatory zoned core analyses plot concordant or weakly reversely discordant, and show a spread in ^{207}Pb/^{206}Pb apparent ages from 2 972 ±23 Ma to 1 882 ±25 Ma (2σ). The age distribution is: 2.97 Ga (n = 1), 2.87–2.86 Ga (n = 2), 2.75 (n = 1) 2.35–2.34 Ga (n = 2), 2.02 Ga (n = 1), 1.99–1.98 Ga (n = 2), 1.96 Ga (n = 1), 1.93–1.92 (n = 3) and 1.88 Ga (n = 1). The youngest core analysis (5C) records a similar age to the BSE-bright rim (no 5) in the same grain (Table 2).

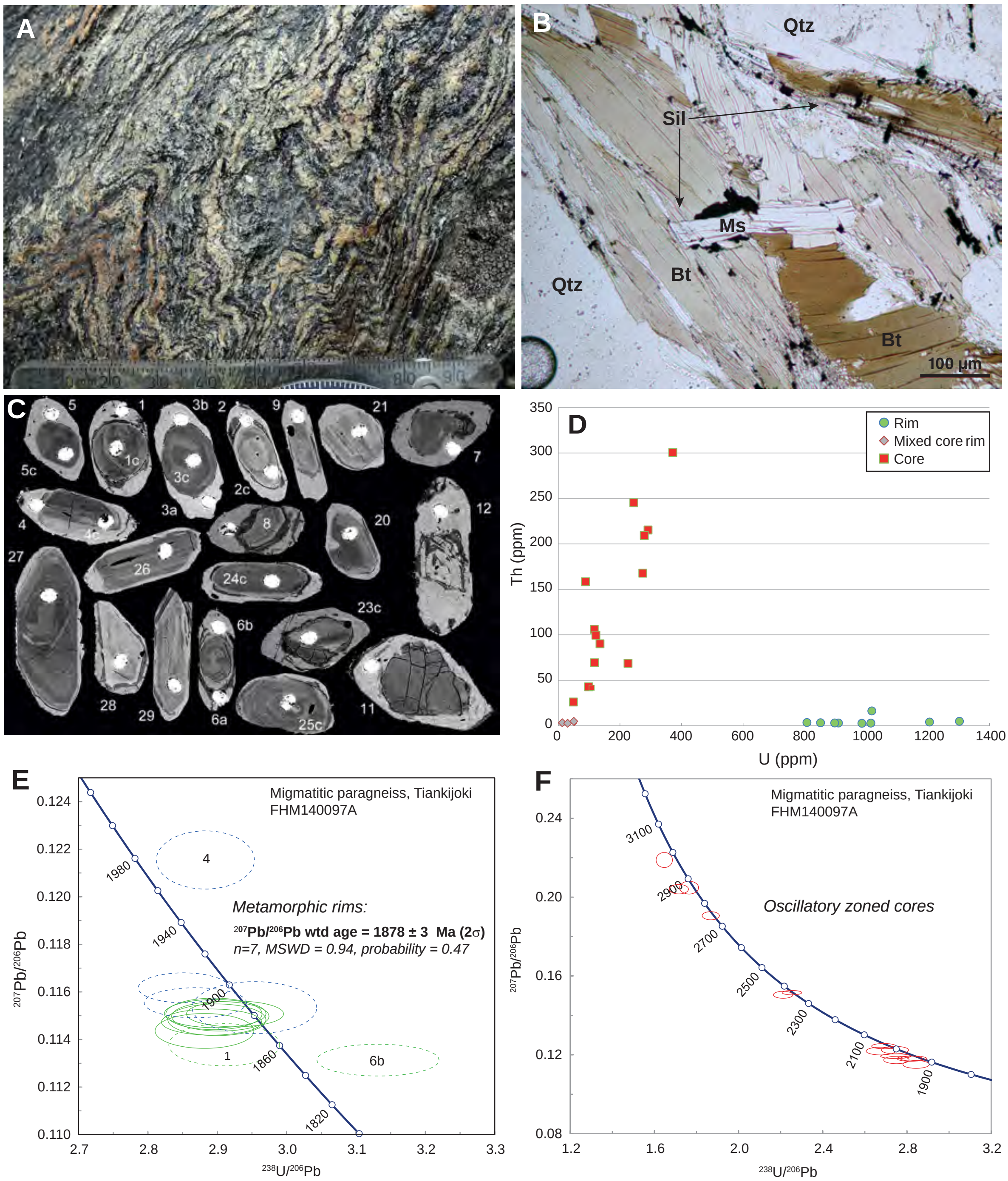

Figure 5. Geochronology of a migmatitic paragneiss from Tiankijoki, south of Masugnsbyn (FHM140097A). **A.** Complexly polyfolded migmatitic paragneiss at the sampling locality (7480253 / 810919 SWEREF 99TM). North is to the left in the photograph. **B.** Needles of fibrolitic sillimanite growing at the expense of biotite, but also crosscutting post-kinematic (?) muscovite. **C.** Backscattered electron (BSE) images of analysed zircon grains. White spots (c. 10µm) mark the locations of analyses. Numbers refer to analytical spot numbers in Table 2. **D.** Th versus U content of zircon analyses. **E.** Tera Wasserburg diagram with U-Pb SIMS data on the migmatitic paragneiss. Rim analyses are marked in green. Rim analyses partly mixed with core domain material are marked in blue. Analyses shown with broken lines are excluded from age calculation (see text for explanation). **F.** Tera Wasserburg diagram showing U-Pb SIMS data of core analyses (red). All photographs by Fredrik Hellström.

Table 2. SIMS U-Pb-Th zircon data (FHM140097A, Lab-id: n5161).

Sample/ spot #	Comment	U ppm	Th ppm	Pb ppm	Th/U calc[1]	$^{207}Pb/^{235}U$	±σ %	$^{208}Pb/^{232}Th$	±σ %	$^{238}U/^{206}Pb$	±σ %	$^{207}Pb/^{206}Pb$	±σ %	ρ [2]	Disc. % conv.[3]	Disc. % 2σ lim.[4]	$^{207}Pb/^{206}Pb$	±σ Ma	$^{206}Pb/^{238}U$	±σ Ma	$^{206}Pb/^{204}Pb$ measured	f_{206}% [5]
n5161-01	BSE-bright rim, close to margin	807	4	[310]	no data	5.391	1.17	no data	no data	2.910	1.12	0.1138	0.32	0.96	2.7		1861	6	1904	19	5375	0.35
n5161-01c	Osc zon core	88	158	85	1.78	16.389	1.19	0.1500	2.89	1.716	1.08	0.2040	0.48	0.91	4.4	1.4	2859	8	2960	26	120444	{0.02}
n5161-02	Metamict rim mixed with core	1503	51	572	0.03	5.384	1.30	0.0888	6.61	2.954	1.24	0.1153	0.39	0.95	-0.3		1885	7	1880	20	15114	0.12
n5161-02c	Osc zon core	226	69	100	0.33	6.152	1.15	0.1115	2.42	2.743	0.96	0.1224	0.63	0.84	0.7		1991	11	2004	17	29211	{0.06}
n5161-03a	BSE-bright rim, close to margin	899	3	348	0.00	5.472	1.04	0.0409	82.55	2.882	1.01	0.1144	0.26	0.97	3.1	0.7	1870	5	1920	17	15326	0.12
n5161-03b	BSE-bright rim, close to core, mix?	939	13	370	0.03	5.617	0.96	0.2058	4.89	2.851	0.94	0.1162	0.22	0.97	2.4	0.3	1898	4	1938	16	119155	{0.02}
n5161-03c	Osc zon core	98	43	80	0.45	18.320	1.20	0.1652	2.39	1.647	0.97	0.2188	0.72	0.80	3.7	0.2	2972	12	3059	24	122403	{0.02}
n5161-04	BSE-bright rim partly mixed with core	761	30	300	0.06	5.813	1.08	0.1495	5.46	2.883	1.00	0.1215	0.41	0.93	-3.5	-0.8	1979	7	1920	17	55402	0.03
n5161-04c	Osc zon core	111	78	78	0.65	12.639	10.26	0.1274	29.09	1.920	1.74	0.1760	10.11	0.17	4.1		2615	159	2703	38	375	4.99
n5161-05	BSE-bright rim	851	3	328	0.00	5.480	1.01	0.0940	4.59	2.895	0.98	0.1151	0.24	0.97	1.9		1881	4	1913	16	110883	{0.02}
n5161-05c	Osc zon core	108	42	47	0.40	5.584	1.14	0.1008	2.51	2.843	0.90	0.1151	0.70	0.79	3.7		1882	13	1943	15	24164	{0.08}
n5161-06a	Metamict-BSE-bright rim	1910	8	671	0.00	4.888	0.99	0.0757	56.31	3.172	0.96	0.1124	0.25	0.97	-4.5	-2.3	1839	4	1767	15	3670	0.51
n5161-06b	BSE-bright rim, with fracture	1018	16	363	0.01	4.981	1.17	0.0543	11.24	3.132	1.15	0.1131	0.24	0.98	-4.0	-1.5	1850	4	1786	18	15497	0.12
n5161-07	BSE-bright rim	1015	3	391	0.00	5.477	1.05	0.0462	32.51	2.897	1.03	0.1151	0.21	0.98	1.9		1881	4	1912	17	49649	0.04
n5161-08	BSE-bright rim	986	3	379	0.00	5.458	1.01	0.0809	16.55	2.904	0.99	0.1150	0.22	0.98	1.7		1879	4	1907	16	86506	0.02
n5161-09	BSE-bright rim partly mixed with core	1074	50	423	0.05	5.554	1.07	0.0995	2.58	2.868	1.05	0.1155	0.22	0.98	2.4	0.0	1888	4	1928	18	96225	0.02
n5161-10	Rim	1302	5	497	0.00	5.423	1.00	0.0730	8.89	2.926	0.98	0.1151	0.19	0.98	0.9		1881	3	1895	16	111274	0.02
n5161-11	BSE-bright rim	908	3	349	0.00	5.460	1.02	0.0645	17.73	2.899	1.00	0.1148	0.24	0.97	2.0		1877	4	1910	16	62360	0.03
n5161-12	BSE-bright rim	1205	4	465	0.00	5.470	1.04	0.0751	9.12	2.892	1.02	0.1147	0.20	0.98	2.4	0.1	1876	4	1915	17	134586	0.01
n5161-20c	Osc zon core	122	100	62	0.84	6.283	1.25	0.1055	2.36	2.675	1.06	0.1219	0.66	0.85	3.7		1985	12	2047	19	44901	{0.04}
n5161-21c	Osc zon core	291	215	141	0.76	5.990	1.14	0.1042	2.59	2.746	1.07	0.1193	0.41	0.93	3.4	0.5	1946	7	2002	18	>1e6	{0.00}
n5161-22c	Osc zon core	245	245	129	1.04	6.375	0.98	0.1093	2.46	2.690	0.88	0.1244	0.44	0.89	1.0		2020	8	2038	15	315381	{0.01}
n5161-23c	Osc zon core	372	301	228	0.83	9.272	0.90	0.1280	2.22	2.254	0.84	0.1515	0.30	0.94	0.2		2363	5	2367	17	39852	0.05
n5161-24c	Osc zon core	135	90	82	0.70	9.380	0.99	0.1290	2.24	2.211	0.86	0.1504	0.49	0.87	2.8	0.0	2351	8	2405	17	>1e6	{0.00}
n5161-25c	Osc zon core	116	106	90	0.93	14.068	1.00	0.1484	2.23	1.868	0.90	0.1906	0.44	0.90	0.8		2747	7	2764	20	44800	{0.04}
n5161-26c	Osc zon core	117	69	55	0.60	5.886	1.11	0.1012	2.35	2.750	0.90	0.1174	0.65	0.81	5.0	1.5	1917	12	2000	16	16515	{0.11}
n5161-27c	Osc zon core	49	26	37	0.51	16.001	1.23	0.1455	2.57	1.765	1.04	0.2048	0.64	0.85	1.3		2865	10	2894	24	18118	{0.10}
n5161-28c	Osc zon core	279	209	132	0.74	5.788	0.98	0.0989	2.62	2.813	0.87	0.1181	0.44	0.89	2.0		1927	8	1961	15	57629	{0.03}
n5161-29c	Osc zon core	274	168	126	0.64	5.753	1.01	0.1043	2.22	2.831	0.91	0.1181	0.44	0.90	1.3		1928	8	1950	15	420974	{0.00}

Isotope values are common Pb corrected using modern common Pb composition (Stacey & Kramers 1975) and measured ^{204}Pb.
1 Th/U ratios calculated from $^{208}Pb/^{206}Pb$ and $^{207}Pb/^{206}Pb$ ratios, assuming a single stage of closed U-Th-Pb evolution
2 Error correlation in conventional concordia space. Do not use for Tera-Wasserburg plots.
3 Age discordance in conventional concordia space. Positive numbers are reverse discordant.
4 Age discordance at closest approach of error ellipse to concordia (2σ level).
5 Figures in curly brackets are given when no correction has been applied, and indicate a value calculated assuming present-day Stacey-Kramers common Pb.

DISCUSSION

Overall, ages of metamorphism and deformational events in the Svecokarelian orogeny north of the Skellefte district are poorly constrained. Within the Pajala deformation belt in eastern Norrbotten County, deformation and high-grade metamorphism occurred in the 1.83–1.78 Ga interval (Bergman et al. 2006, Luth et al. 2016, Hellström & Bergman 2016), possibly overprinting earlier structures. In the southern part of the Pajala deformation belt, migmatisation and related emplacement of Lina granite is dated at 1783 ±3 Ma (Wikström & Persson 1997). In the central and southwestern part of Norrbotten County, 1.88–1.87 Ga metagranitoid-metasyenitoid intrusions of the Perthite-monzonite suite show variable low to high degrees of deformation and metamorphic recrystallisation, suggesting heterogeneous, post-1.87 Ga age of deformation and metamorphism also in large areas west of the Pajala deformation belt domain (Hellström et al. 2012, 2015). Granites-pegmatites of the late-orogenic 1.81–1.78 Ga Lina suite are also usually weakly foliated in central Norrbotten County. In contrast, Bergman et al. (2001) suggested there was an early orogenic event at 1.89–1.87 Ga, based on the observation of markedly different degrees of deformation between rocks of the Haparanda and the Perthite monzonite suites in the northwestern part of the Norrbotten County, although radiometric age determinations show no significant age differences between the two intrusive suites. Evidence of an older phase of migmatisation and shearing was reported from the southeastern part of the Norrbotten County, where the 1881 ±9 Ma Bläsberget felsic-mafic dykes cuts migmatites occurring immediately west of the Pajala deformation belt (at "B" in Fig. 1B; B – Baltic–Bothnian mega-shear; Wikström et al. 1996). In the northeastern part of the Skellefte ore district, 1.88 Ga old plutons also crosscut deformed metasedimentary rocks (Lundström et al. 1997, 1999).

The Masugnsbyn area, just west of the Pajala deformation belt, is an area with a preserved, older phase of early orogenic Svecokarelian migmatisation and deformation. U-Pb analyses of secondary BSE-bright rim domains are interpreted to date migmatisation in the Tiankijoki paragneiss at 1878 ±3 Ma (2σ). The rim analyses have very low Th/U ratios in contrast to core analysis, which suggests a metamorphic origin of the rims and a contemporaneous crystallisation with the coexisting monazite. Bergman et al. (2006) dated monazite from a meta-argillite at Pahakurkio and a weakly migmatitic paragneiss at Takanenvaara, both located close to Tiankijoki dating locality (Fig. 2). A weighted average $^{207}Pb/^{206}Pb$ age of the two weakly discordant fractions of Takanenvaara monazites can be calculated at 1857 ±3 Ma (2σ), suggesting an age of metamorphism of approximately 1.86 Ga. The 20 Ma age difference between the zircon rim age obtained in this study and the monazite age of Bergman et al. (2006), may reflect resetting of the U-Pb isotopic system in monazite during a later metamorphic event, i.e. 20 million years after the migmatisation event dated by U-Pb in zircon. Martinsson et al. (2016) reported single fraction, weakly discordant U-Pb titanite $^{207}Pb/^{206}Pb$ ages of 1.80–1.76 Ga, interpreted to date an even younger event of metamorphism or hydrothermal alteration in the Masugnsbyn area.

The 1.88 Ga age of migmatisation is contemporaneous with large volumes of early orogenic intrusions of the 1.88–1.86 Ga Perthite monzonite suite (Bergman et al. 2001, Hellström et al. 2015). The increase in metamorphic grade towards the adjacent intrusive rocks in the Masugnsbyn area suggests that heat from the intrusions was responsible for the metamorphic conditions. Thus, heat from these intrusions is inferred to have caused the high-grade metamorphism and partial melting. The area to the southeast of the migmatites is dominated by granites, syenites and gabbro. Padget (1970) placed the granites in the Lina suite, whereas Bergman et al. (2001) suggested that the rocks belong to the 1.8 Ga granite-syenitoid-gabbroid association. However, 30 km towards the southeast, in the Narken area, a nearly isotropic metagranite sample was dated at 1872 ±4 Ma (MSWD = 1.4, n = 4, TIMS, U-Pb zircon, Hellström et al. 2012). That granite is co-magmatic with gabbroic rocks and was assigned to the Perthite monzonite suite, which is also suggested to have an affinity with the intrusive rocks southeast of the Masugnsbyn key area. The Tärendö gabbro occupies an area of 22 × 6 km, and several smaller gabbro intrusions surrounded by granite also occur. Input of large volumes of mafic magmas would increase the temperature of the crust, possibly causing partial melting and migmatisation in the pelitic rocks south of Masugnsbyn.

Implications for mineralisations

The metamorphic alteration of supracrustal rocks at 1.88 Ga has implications for the timing of skarn iron ore formation, and remobilisation of base metals in sulphide mineralisations. The Masugnsbyn iron mineralisations form a more or less regular sheet, concordant between the Veikkavaara greenstones and the overlying quartzitic and metapelitic metasedimentary rocks of the Pahakurkio group (Figs. 2–3, Frietsch 1997, Geijer 1929, Padget 1970, Witschard et al. 1972). The southern iron deposits are classified as skarn iron ores, whereas the mineralisations to the north have characteristics of sedimentary, millimetre- to centimetre-wide, quartz-magnetite banded iron ore of an exhalative origin. A significant difference between the mineralisations is that the southern area is characterised by the presence of a rather thick dolomitic marble unit and by a perthite granite, which borders the skarn iron ores. The close spatial connection between the skarn iron ores and the perthite granite suggests that the intrusion of the granite is responsible for skarn formation and remobilisation of iron, with a higher grade and coarser grain size of the magnetite ore in the footwall next to the granite. The perthite granite was dated at 1 858 ±9 Ma using discordant U-Pb TIMS zircon data (Skiöld & Öhlander 1989). However, recent U-Pb SIMS zircon data suggest an age of 1 881 ±5 Ma (Hellström et al. in prep.), thus contemporaneous with the age of migmatisation in the high-grade southern part of the Masugnsbyn area.

The Kurkkionvaara Zn-Pb-Cu mineralisation is located approximately 15 km south of Masugnsbyn at the contact between the metasedimentary rocks of the Pahakurkio group and the metasedimentary and intermediate metavolcanic rocks of the Kalixälv group (Fig. 2, Niiniskorpi 1986). The mineralisations occur as scattered sulphide veins or fracture fillings with sphalerite and galena, mainly in the metasedimentary rocks of the Pahakurkio groups, but also in the overlying quartz-rich conglomerate. Locally, richer mineralisations in some fracture zones, with total Zn-Pb content up to a few per cent over 0.4–2.0 m occur. Impregnations of pyrrhotite and pyrite occur in metre-wide zones, where the richest concentrations of Fe-sulphides occur in the 10–20 m wide conglomerate horizon above the Pahakurkio group as an impregnation in the matrix. Veins of pyrrhotite generally occur parallel to bedding in the sedimentary rocks, whereas the Pb-Zn-filled fractures usually dip steeply and crosscut bedding. Lithochemical analyses show a positive correlation between B and Zn + Pb content, suggesting a hydrothermal system with boron-rich fluids containing base metals (Niiniskorpi 1986). At Kurkkionvaara, tourmaline-rich layers (tourmalinites) occur in the pelitic sedimentary rocks, along with tourmaline-rich pegmatites. Boron-rich fluids probably have a source in the metapelites, originally deposited as marine sediments. Sulphide mineralisations may have resulted from boron-rich fluids formed during migmatisation of these pelitic sedimentary rocks, but the fracture-style Zn-Pb mineralisation suggests that this type of mineralisation post-dates migmatisation and ductile deformation. The migmatisation age obtained thus provides a maximum age of the fracture-type Pb-Zb mineralisation at Kurkkionvaara.

Provenance

The large spread in zircon core ages suggests a detrital origin of the zircon, and therefore a sedimentary origin of the migmatitic gneiss. Despite the limited number of SIMS analyses on zircon core domains, the maximum depositional age can be constrained by the youngest core analysis (5c) at 1 882 ±25 Ma (2σ), but deposition must have occurred before migmatisation at 1 878 ±3 Ma (2σ). 50% of the recorded ages fall in the range 2.02–1.92 Ga, suggesting that rocks of this age interval were the main source, together with debris from Archaean rocks (29%). Archaean rocks are exposed in the

Råstojaure complex in northernmost Sweden (Martinsson et al. 1999, Lauri et al. 2016). Sm-Nd isotopic analyses of Proterozoic granitoids and metavolcanic rocks suggest a covered Archaean basement south of the Råstojaure Complex (Öhlander et al. 1987a, b, 1993, Skiöld et al. 1988, Lauri et al. 2016, Hellström et al., 2018).

The Archaean palaeoboundary zone between the reworked Archaean craton in the north and more juvenile Palaeoproterozoic domains to the south occurs along the Luleå–Jokkmokk zone in Sweden and along the Raahe–Ladoga zone in Finland (Öhlander et al. 1993, Mellqvist et al. 1999, Vaasjoki & Sakko 1988, Nironen 1997). To date, there are very few age determinations of igneous rocks in the interval 2.02–1.92 Ga, but some occur in the Savo schist belt within the Raahe–Ladoga zone in Finland, at Norvijaur in the Jokkmokk area and in the Rombak–Sjangeli basement window of the Caledonides, all of which lie along the Archaean–Palaeoproterozoic boundary (Helovuori 1979, Korsman et al. 1984, Vaasjoki & Sakko 1988, Kousa et al. 1994, Lahtinen & Huhma 1997, Vaasjoki et al. 2003, Kousa et al. 2013, Skiöld et al. 1993, Romer et al. 1992; Hellström 2015). In addition, 1.96–1.94 Ga calc-alkaline rocks with island arc affinity occur in the northern part of the Bothnian Basin, south of the Skellefte district (Wasström 1993, 1996, Lundqvist et al. 1998, Eliasson et al. 2001, Skiöld & Rutland 2006).

CONCLUSIONS

- Early Svecokarelian migmatisation is dated at 1 878 ±3 Ma in the Masugnsbyn structural domain, west of the Pajala deformation belt, which constrains the maximum age of folding of the supracrustal rocks.
- It is suggested that the 1.88 Ga migmatisation was caused by heat transfer from large volumes of contemporaneous early orogenic Svecokarelian intrusions.
- Intrusion of a 1.88 Ga perthite granite at Masugnsbyn caused contact metamorphic alterations of the upper part of the Veikkavaara greenstones, containing banded iron formations and carbonate rocks, resulting in skarn formation and remobilisation of iron to higher grades to form the Masugnsbyn skarn iron ores, contemporaneous with migmatisation in the higher-grade south of the Masugnsbyn area.
- The obtained migmatisation age provides a maximum age for the Kurkkionvaara fracture-type Pb-Zb mineralisation, which occurs in metapelites in the upper part of the Pahakurkio group, below the migmatitic paragneisses of the Kalixälv group.
- The maximum depositional age of the original sediments in the Kalixälv group is constrained by the youngest zircon core analysis at 1 882 ±25 Ma (2σ), but must have occurred before migmatisation at 1 878 ±3 Ma.
- The main source of the original sediments of the Kalixälv group is 2.02–1.92 Ga (50%) and 2.97–2.75 Ga rocks (29%). 2.02–1.92 Ga felsic to intermediate rocks can be expected to be present to a greater extent than is known from present age determination of rocks in the Svecokarelian orogeny.

ACKNOWLEDGEMENTS

Carl-Henric Wahlgren, George Morris and Stefan Bergman are gratefully acknowledged for their careful review, which significantly improved the manuscript. Cecilia Jönsson is much thanked for conducting ground geophysical measurements at Masugnsbyn, as well as for compilation, gridding and interpretation of geophysical data. Ildikó Antal Lundin is thanked for gridding the magnetic data on the map in Figure 1. U-Pb isotopic zircon data were obtained from beneficial cooperation with the Laboratory for Isotope Geology at the Swedish Museum of Natural History (NRM) in Stockholm. The Nordsim facility is operated under an agreement between the research funding agencies of Denmark, Norway and Sweden, the Geological Survey of Finland and the Swedish Museum of Natural History. We would like to express our gratitude to Martin Whitehouse, Lev Ilyinsky and Kerstin Lindén at the Nordsim analytical facility for their first-class analytical support with SIMS analyses. Martin Whitehouse reduced the zircon analytical data, Lev Ilyinsky assisted during ion probe analyses and Kerstin Lindén prepared the zircon mounts. Our sincere thanks also go to Milos Bartol at the Evolutionary Biology Centre and Jaroslaw Majka at the Department of Geology, Uppsala University, an also Kerstin Lindén at NRM for their support during BSE/CL imaging of zircons. Tone Gellerstedt and Maxwell Arding are much thanked for editing and proofreading.

REFERENCES

Bergman, S., Billström, K., Persson, P.-O., Skiöld, T. & Evins, P., 2006: U-Pb age evidence for repeated Palaeoproterozoic metamorphism and deformation near the Pajala shear zone in the northern Fennoscandian shield. *GFF 128*, 7–20.

Bergman, S., Kübler, L. & Martinsson, O., 2001: Description of Regional Geological and Geophysical Maps of Northern Norrbotten County (east of the Caledonian Orogen). *Sveriges geologiska undersökning Ba 56*, 110 pp.

Bergman, T., Hellström, F. & Ripa, M., 2015: Verksamhetsrapport 2014: Norrbottens malm och mineral. *Sveriges geologiska undersökning SGU-rapport 2015:08,* 20 pp.

Eliasson, T., Greiling, R., Sträng, T. & Triumf, C., 2001: Bedrock map 23H Stensele NV, scale 1:50 000. *Sveriges geologiska undersökning Ai 126*.

Frietsch, R., 1997: The iron ore inventory program 1963–1972 in Norrbotten County. *Rapporter och meddelanden 92*, Sveriges geologiska undersökning. 77 pp.

Geijer, P., 1929: Masugnsbyfältens geologi. *Sveriges geologiska undersökning C 351*, 39 pp.

Grigull, S., Berggren, R., Jönberger, J., Jönsson, C., Hellström, F.A. & Luth, S., 2018: Folding observed in Palaeoproterozoic supracrustal rocks in northern Sweden. *In:* Bergman, S. (ed): Geology of the Northern Norrbotten ore province, northern Sweden. *Rapporter och Meddelanden 141,* Sveriges geologiska undersökning. This volume pp 205–257.

Grip, E. & Frietsch, R., 1973: *Malm i Sverige 2. Norra Sverige*. Almqvist & Wiksell, 295 pp.

Hellström, F.A., 2015: SIMS geochronology of a 1.93 Ga basement metagranitoid at Norvijaur west of Jokkmokk, northern Sweden. *SGU-rapport 2015:01*, Sveriges geologiska undersökning. 18 pp.

Hellström, F. & Bergman, S., 2016: Is there a 1.85 Ga magmatic event in northern Norrbotten? − U-Pb SIMS zircon dating of the Pingisvaara metagranodiorite and the Jyryjoki granite, northern Sweden. *GFF 138, 526–532.*

Hellström, F. & Jönsson, C., 2014: Barents project 2014: Summary of geological and geophysical information of the Masugnsbyn key area. *SGU-rapport 2014:21*, Sveriges geologiska undersökning. 84 pp.

Hellström, F., Carlsäter Ekdahl, M. & Kero, L., 2012: Beskrivning till berggrundskartorna 27L Lansjärv NV, NO, SV & SO. *Sveriges geologiska undersökning K 387–390*, 27 pp.

Hellström, F., Kathol, B. & Larsson, D., 2015: Age and chemical character of the Perthite monzonite suite in south-western Norrbotten, northern Sweden. *SGU-rapport 2015:38*, Sveriges geologiska undersökning. 23 pp.

Hellström, F.A., Kumpulainen, R., Jönsson, C., Thomsen, T.B., Huhma, H. & Martinsson, O., 2018: Age and lithostratigraphy of Svecofennian volcanosedimentary rocks at Masugnsbyn, northernmost Sweden – host rocks to Zn-Pb-Cu- and Cu ±Au sulphide mineralisations. *In:* Bergman, S. (ed): Geology of the Northern Norrbotten ore province, northern Sweden. *Rapporter och Meddelanden 141,* Sveriges geologiska undersökning. This volume pp 151–203.

Helovuori, O., 1979: Geology of the Pyhäsalmi ore deposit, Finland. *Economic Geology 74*, 1084–1101.

Korsman, K., Hölttä, P., Hautala, T. & Wasenius, P., 1984: Metamorphism as indicator of evolution and structure of the crust in eastern Finland. *Geological Survey of Finland Bulletin 328*, 40 pp.

Kousa, J., Luukas, J., Huhma, H. & Mänttäri, I., 2013: Palaeoproterozoic 1.93−1.92 Ga Svecofennian rock units in the northwestern part of the Raahe–Ladoga zone, central Finland. *In:* P. Hölttä (Ed.): Current research: GTK Mineral potential workshop, Kuopio, May 2012. *Geological Survey of Finland Report of Investigation 198*, 91–96.

Kousa, J., Marttila, E. & Vaasjoki, M., 1994: Petrology, geochemistry and dating of Paleoproterozoic metavolcanic rocks in the Pyhäjärvi area, central Finland. *In:* M. Nironen & Y. Kähkönen (eds.): Geochemistry of Proterozoic supracrustal rocks in Finland. *Geological Survey of Finland, Special Paper 19*, 7–27.

Kumpulainen, R.A., 2000: The Paleoproterozoic sedimentary record of northernmost Norrbotten, Sweden. Unpublished report. *Sveriges geologiska undersökning BRAP 200030*, 45 pp.

Lahtinen, R. & Huhma, H., 1997: Isotopic and geochemical constraints on the evolution of the 1.93–1.79 Ga Svecofennian crust and mantle. *Precambrian Research 82*, 13–34.
Lahtinen, R., Huhma, H., Lahaye, Y., Jonsson, E., Manninen, T., Lauri, L.S., Bergman, S., Hellström, F., Niiranen, T. & Nironen, M., 2015: New geochronological and Sm–Nd constraints across the Pajala shear zone of northern Fennoscandia: Reactivation of a Paleoproterozoic suture. *Precambrian Research 256*, 102–119.
Lauri, L.S., Hellström, F., Bergman, S., Huhma, H. & Lepistö, S., 2016: New insights into the geological evolution of the Archean Norrbotten province, Fennoscandian shield. *32nd Nordic Geological Winter Meeting, Helsingfors*.
Ludwig, K.R., 2012: User's manual for Isoplot 3.75. A Geochronological Toolkit for Microsoft Excel. *Berkeley Geochronology Center Special Publication No. 5*, 75 pp.
Lundqvist, T., Vaasjoki, M. & Persson, P.-O., 1998: U-Pb ages of plutonic and volcanic rocks in the Svecofennian Bothnian Basin, central Sweden, and their implications for the Palaeoproterozoic evolution of the basin. *GFF 120*, 357–363.
Lundström, I., Persson P.-O. & Bergström U., 1999: Indications of early deformational events in the north-eastern part of the Skellefte field. Indirect evidence from geological and radiometric data from the Stavaträsk-Klintån area, Boliden map-sheet. *In:* S. Bergman (ed.) Radiometric dating results 4: *Sveriges geologiska undersökning C 831*, 52–69.
Lundström, I., Vaasjoki, M., Bergström, U., Antal, I. & Strandman F., 1997: Radiometric age determinations of plutonic rocks in the Boliden area: the Hobergsliden granite and the Stavaträsk diorite. *In:* T. Lundqvist (ed.) Radiometric dating results 3: *Sveriges geologiska undersökning C 830*, 20–30.
Luth, S., Jönsson, C., Hellström, F., Jönberger, J., Djuly, T., Van Assema, B. & Smoor, W., 2016: Structural and geochronological studies of the crustal-scale Pajala Deformation Zone, northern Sweden. *32nd Nordic Geological Winter Meeting, Helsingfors.*
Luth, S., Jönsson, C., Jönberger, J., Grigull, S., Berggren, R., van Assema, B., Smoor, W. & Djuly, T., 2018: The Pajala Deformation Belt in northeast Sweden: Structural geological mapping and 3D modelling around Pajala. *In:* Bergman, S. (ed): Geology of the Northern Norrbotten ore province, northern Sweden. *Rapporter och Meddelanden 141,* Sveriges geologiska undersökning. This volume pp 259–285.
Lynch, E.P., Hellström, F.A., Huhma, H., Jönberger, J., Persson, P.-O. & Morris, G.A, 2018: Geology, lithostratigraphy and petrogenesis of c. 2.14 Ga greenstones in the Nunasvaara and Masugnsbyn areas, northernmost Sweden. *In:* Bergman, S. (ed): Geology of the Northern Norrbotten ore province, northern Sweden. *Rapporter och Meddelanden 141,* Sveriges geologiska undersökning. This volume pp 19–77.
Martinsson, O., Vaasjoki, M. & Persson, P.-O., 1999: U-Pb ages of Archaean to Palaeoproterozoic granitoids in the Torneträsk-Råstojaure area, northern Sweden. *In:* S. Bergman (ed.): Radiometric dating results 4. *Sveriges geologiska undersökning C 831*, 70–90.
Martinsson, O., Van der Stilj, I., Debras, C. & Thompson, M., 2013: Day 3. The Masugnsbyn, Gruvberget and Mertainen iron deposits. *In:* O. Martinsson & C. Wanhainen (eds.): *12th Biennial SGA Meeting, Uppsala, Sweden. Excursion guidebook SWE5*, 37–44.
Martinsson, O., Billström, K., Broman, C., Weihed, P. & Wanhainen, C., 2016: Metallogeny of the Northern Norrbotten Ore Province, northern Fennoscandian Shield with emphasis on IOCG and apatite-iron ore deposits. *Ore Geology Reviews 78*, 447–492.
Martinsson, O., Bergman, S., Persson, P.-O. & Hellström, F.A., 2018: Age and character of late-Svecokarelian monzonitic intrusions in north-eastern Norrbotten, northern Sweden. *In:* Bergman, S. (ed): Geology of the Northern Norrbotten ore province, northern Sweden. *Rapporter och Meddelanden 141,* Sveriges geologiska undersökning. This volume pp 381–399.
Mellqvist, C., Öhlander, B. & Skiöld, T., 1999: Traces of Archean crust in the Jokkmokk area, northern Sweden: a way of defining the Archean-Proterozoic boundary. *In:* C. Mellqvist: Proterozoic crustal growth along the Archean continental margin in the Luleå and Jokkmokk areas, northern Sweden. Doctoral thesis, Luleå University, 24 pp.

Niiniskorpi, V., 1986: En Zn-Pb-Cu-mineralisering i norra Sverige, en case-studie. LKAB Prospektering K-8656, Licenciate thesis, geological department of Åbo Akademi, 74 pp.
Nironen, M., 1997: The Svecofennian orogen: a tectonic model. *Precambrian Research 86*, 21–44.
Öhlander, B., Hamilton, P.J., Fallick, A.E. & Wilson, M.R., 1987a: Crustal reactivation in northern Sweden: the Vettasjärvi granite. *Precambrian Research 35,* 277–293.
Öhlander, B., Skiöld, T., Hamilton, P.J. & Claesson, L.-Å., 1987b: The western border of the Archaean province of the Baltic shield: evidence from northern Sweden. *Contributions to Mineralogy and Petrology 95,* 437–450.
Öhlander, B., Skiöld, T., Elming, S.Å., Claesson, S. & Nisca, D.H., 1993: Delineation and character of the Archaean-Proterozoic boundary in northern Sweden. *Precambrian Research 64,* 67–84.
Padget, P., 1970: Beskrivning till berggrundskartbladen Tärendö NV, NO, SV, SO. *Sveriges geologiska undersökning Af 5–8*, 95 pp.
Romer, R.L., Kjösnes, B., Korneliussen, A., Lindahl, I., Skyseth, T., Stendahl, M. & Sundvoll, B., 1992: The Archean–Proterozoic boundary beneath the Caledonides of northern Norway and Sweden: U-Pb, Rb-Sr, and εNd isiotope data from the Rombak-Tysfjord area. *NGU rapport 91.225,* 67 pp.
Silvennoinen, A., 1991: Kuusamon ja Rukatunturin kartta-alueiden kallioperä. Geological map of Finland 1:100 000, *Explanation to the maps of pre-Quaternary rocks, Sheets 4524+4542 and 4616. Geological Survey of Finland,* 36 pp.
Skiöld, T. & Öhlander, B., 1989: Chronology and geochemistry of late Svecofennian processes in northern Sweden. *Geologiska Föreningen i Stockholm Förhandlingar 111*, 347–354.
Skiöld, T., Öhlander, B., Vocke Jr, R.D. & Hamilton, P.J., 1988: Chemistry of Proterozoic orogenic processes at a continental margin in northern Sweden. *Chemical Geology 69*, 193–207.
Skiöld, T. & Rutland, R.W.R., 2006: Successive ~1.94 Ga plutonism and ~1.92 Ga deformation and metamorphism south of the Skellefte district, northern Sweden: Substantiation of the marginal basin accretion hypothesis of Svecofennian evolution. *Precambrian Research 148*, 181–204.
Skiöld, T., Öhlander, B., Markkula, H., Widenfalk, L. & Claesson, L.-Å., 1993: Chronology of Proterozoic orogenic processes at the Archaean continental margin in northern Sweden. *Precambrian Research 64*, 225–238.
Smith, M.P., Storey, C.D., Jeffries, T.E. & Ryan, C., 2009: In Situ U-Pb and Trace Element Analysis of Accessory Minerals in the Kiruna District, Norrbotten, Sweden: New Constraints on the Timing and Origin of Mineralization. *Journal of Petrology 50*, 2063–2094.
Stacey, J.S. & Kramers, J.D., 1975: Approximation of terrestrial lead isotope evolution by a two-stage model. *Earth and Planetary Science Letters 26*, 207–221.
Steiger, R.H. & Jäger, E., 1977: Convention on the use of decay constants in geo- and cosmochronology. *Earth and Planetary Science Letters 36*, 359–362.
Storey, C.D., Smith, M.P. & Jeffries, T.E., 2007: In situ LA-ICP-MS U-Pb dating of metavolcanics of Norrbotten, Sweden: Records of extended geological histories in complex titanite grains. *Chemical Geology 240*, 163–181.
Vaasjoki, M. & Sakko, M., 1988: The evolution of the Raahe–Ladoga zone in Finland: isotopic constraints. *In:* K. Korsman (ed.): Tectono-metamorphic evolution of the Raahe–Ladoga zone. *Geological Survey of Finland Bulletin 343,* 7–32.
Vaasjoki, M., Huhma, H., Lahtinen, R. & Vestin, J., 2003: Sources of Svecofennian granitoids in the light of ion probe U-Pb measurements on their zircons. *Precambrian Research 121*, 251–262.
Wasström, A., 1993: U-Pb zircon dating of a quartz-feldspar porphyritic dyke in the Knaften area; Västerbotten County; northern Sweden. *In:* T. Lundqvist (ed.): Radiometric dating results 2. *Sveriges geologiska undersökning C 82*8, 34–40.
Wasström, A., 1996: The Knaften granitoids of Västerbotten County, northern Sweden. *In:* T. Lundqvist (Ed.): Radiometric dating results. *Sveriges geologiska undersökning C 823*, 60–64.

Wiedenbeck, M., Allé, P., Corfu, F., Griffin, W.L., Meier, M., Oberli, F., Quadt, A.V., Roddick, J.C. & Spiegel, W., 1995: Three natural zircon standards for U-Th-Pb, Lu-Hf, trace element and REE analyses. *Geostandards Newsletter 19*, 1–23.

Wiedenbeck, M., Hanchar, J.M., Peck, W.H., Sylvester, P., Valley, J., Whitehouse, M., Kronz, A., Morishita, Y., Nasdala, L., Fiebig, J., Franchi, I., Girard, J.P., Greenwood, R.C., Hinton, R., Kita, N., Mason, P.R.D., Norman, M., Ogasawara, M., Piccoli, P.M., Rhede, D., Satoh, H., Schulz-Dobrick, B., Skår, O., Spicuzza, M.J., Terada, K., Tindle, A., Togashi, S., Vennemann, T., Xie, Q. & Zheng, Y.F., 2004: Further characterisation of the 91500 zircon crystal. *Geostandards and Geoanalytical Research 28*, 9–39.

Whitehouse, M.J., Claesson, S., Sunde, T. & Vestin, J., 1997: Ion-microprobe U–Pb zircon geochronology and correlation of Archaean gneisses from the Lewisian Complex of Gruinard Bay, northwestern Scotland. *Geochimica et Cosmochimica Acta 61*, 4429–4438.

Whitehouse, M.J., Kamber, B.S. & Moorbath, S., 1999: Age significance of U–Th–Pb zircon data from Early Archaean rocks of west Greenland: a reassessment based on combined ion-microprobe and imaging studies. *Chemical Geology (Isotope Geoscience Section) 160*, 201–224.

Whitehouse, M.J. & Kamber, B.S., 2005: Assigning Dates to Thin Gneissic Veins in High-Grade Metamorphic Terranes: A Cautionary Tale from Akilia, Southwest Greenland. *Journal of Petrology 46*, 291–318.

Wikström, A. & Persson, P.-O., 1997: U-Pb zircon and monazite dating of a Lina-type leucogranite in northern Sweden and its relationship to the Bothnian shear zone. *In:* T. Lundqvist (ed.): Radiometric dating results 3. *Sveriges geologiska undersökning C 830*, 81–87.

Wikström, A., Skiöld, T. & Öhlander, B., 1996: The relationship between 1.88 Ga old magmatism and the Baltic–Bothnian shear zone in northern Sweden. *Geological Society, London, Special Publications 112,* 249–259.

Witschard, F., Nylund, B. & Mannström, B., 1972: The Masugnsbyn iron ore. Report concerning the results of Sveriges geologiska undersökning:s investigations in the years 1965–1970. *Sveriges geologiska undersökning BRAP 734*, 95 pp.

Authors, paper 12:
Olof Martinsson
Luleå University of Technology,
Division of Geosciences and Environmental Engineering,
Luleå, Sweden

Stefan Bergman
Geological Survey of Sweden
Department of Mineral Resources
Uppsala, Sweden

Per-Olof Persson
Swedish Museum of Natural History,
Department of Geosciences,
Stockholm, Sweden

Fredrik A. Hellström
Geological Survey of Sweden
Department of Mineral Resources
Uppsala, Sweden

12. Age and character of late-Svecokarelian monzonitic intrusions in northeastern Norrbotten, northern Sweden

Olof Martinsson, Stefan Bergman, Per-Olof Persson & Fredrik A. Hellström

ABSTRACT

Palaeoproterozoic magmatism in northern Norrbotten shows a complex evolution, with several different plutonic suites ranging in age 1.93–1.70 Ga. Here we present data for three monzonitic intrusions from different parts of the area. They are petrographically and chemically similar, consisting mainly of perthite, augite and orthopyroxene, with megacrysts of poikilitic biotite as a characteristic minor component, and with high Sr and Ba. The intrusions have been dated at 1.80 Ga and may be part of a more extensive magmatic event in northern Sweden, including other chemically similar monzonitic and gabbroic intrusions, which often occur as ring dykes at the Merasjärvi gravity high (MGH) in northeastern Norrbotten. The monzonitic intrusions have A-type signatures and chemical characteristics overlapping those of rocks in arc and within-plate settings. These intrusions may thus have formed in either a back arc setting related to eastward subduction associated with the Transscandinavian Igneous Belt further west (TIB 1), or through a separate igneous event caused by a mantle plume.

INTRODUCTION

Palaeoproterozoic magmatism in northern Norrbotten has a complex evolution, with several different plutonic suites ranging in age 1.93–1.70 Ga (Bergman et al. 2001, Martinsson et al. 1999, Romer et al. 1992, 1994, Skiöld 1988, Skiöld et al. 1988, 1993). Due to a rather limited chronological dataset and somewhat similar petrographical and geochemical characteristics of the different suites, classification of individual plutons has been rather arbitrary. However, the classification was revised during the project "Synthesis bedrock maps of northern Norrbotten", and six plutonic suites were identified by differences in age and composition (Bergman et al. 2001).

One of the results from the new geochronological data obtained during that project was the identification of 1.8 Ga ages of some monzonitic rocks in the northeastern part of northern Norrbotten. Plutonic rocks of this age and composition were previously unknown in this area, and based on this new information, it was suggested that they represent TIB-type magmatism extending far eastward from the Transscandinavian Igneous Belt proper (Bergman et al. 2001). In this paper, petrographical,

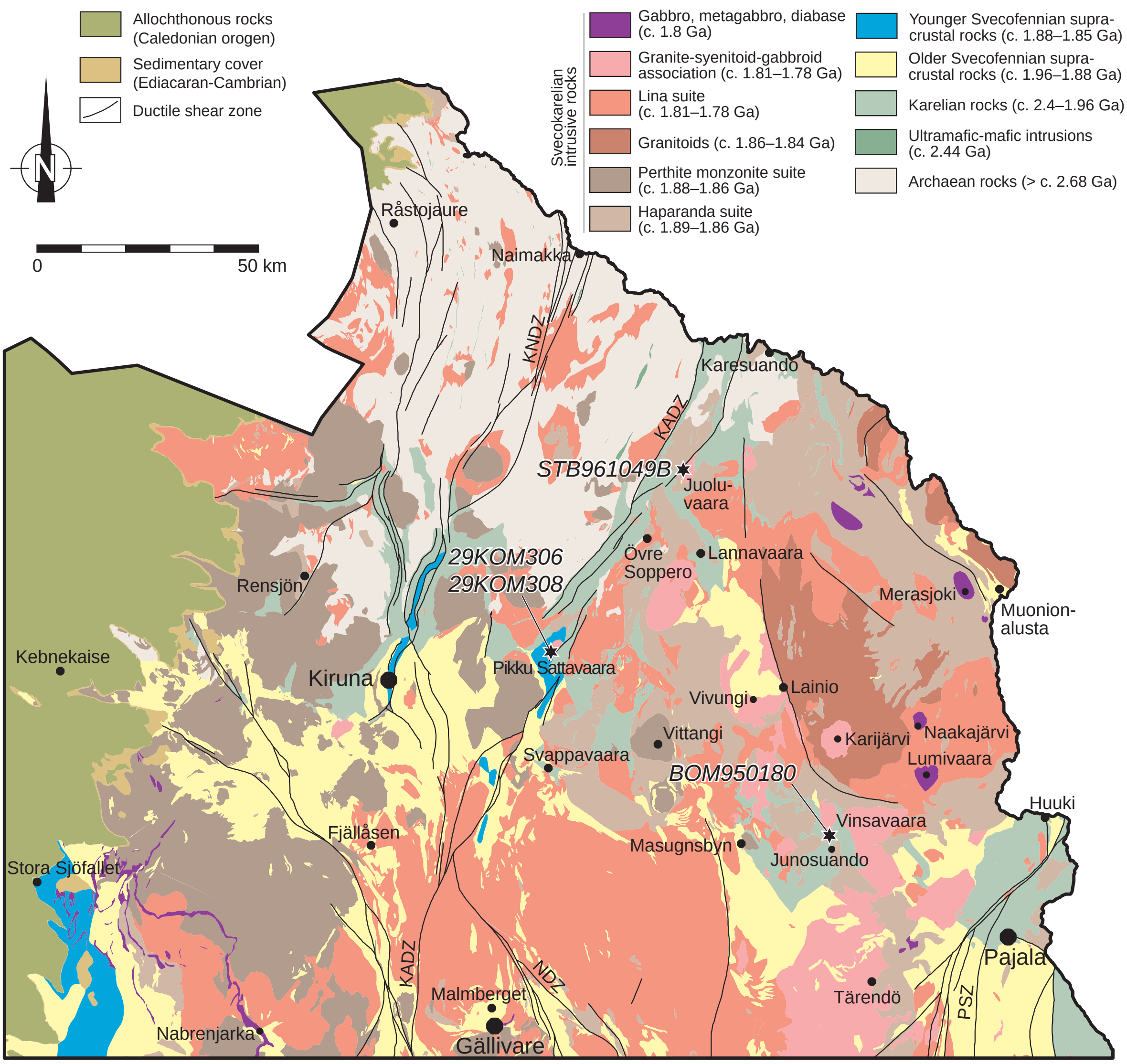

Figure 1. Bedrock map of northern Norrbotten County, modified from Bergman et al. (2001), with location of analysed samples.

geochemical and geochronological data are presented for 1.8 Ga monzonitic intrusions at Pikku Sattavaara, Juoluvaara and Vinsavaara, situated 37 km east of Kiruna, 18 km northeast of Soppero and 50 km northwest of Pajala, respectively (Fig. 1).

GEOLOGICAL SETTING

The Precambrian bedrock in northern Norrbotten includes a c. 2.8 Ga Archaean granitoid-gneiss basement, which is unconformally overlain by greenstone, porphyry and sedimentary successions of Palaeoproterozoic age. Stratigraphically lowest of these successions are rift-related 2.5–2.0 Ga Karelian units, which in the Kiruna area are represented by the Kovo Group and the overlying Kiruna Greenstone Group (Martinsson 1997). The later c. 1.9 Ga Svecofennian successions comprise the Porphyrite Group, the Kurravaara Conglomerate, the Kiirunavaara Group and the Hauki Quartzite (Martinsson 2004). Most of these Palaeoproterozoic units extend outside the Kiruna area, and may be considered to be regionally developed in northern Norrbotten (Bergman et al. 2001).

The approximately 10 km thick pile of Palaeoproterozoic volcanic and sedimentary rocks was deformed and metamorphosed during the Svecokarelian orogeny (1.9–1.8 Ga), contemporaneous with intrusions of the 1.89–1.86 Ga Haparanda and Perthite-monzonite suites. These plutonic rocks have calc-alkaline to alkali-calcic character and are comagmatic with the Svecofennian volcanic rocks (Witschard 1984, Bergman et al. 2001; Martinsson, 2004). The 1.85 Ga Jyryjoki granite occurs in northeastern Norrbotten and is mainly of granitic composition (Bergman et al. 2001; Hellström & Bergman 2016). The Lina Suite comprises 1.81–1.78 Ga minimum-melt granites, aplites and pegmatites (Skiöld et al. 1988), which are widely distributed in Norrbotten and contemporaneous with TIB 1 intrusions in the Kiruna–Narvik area (Romer et al. 1992, 1994). A second metamorphic and deformation event occurred at that time (Bergman et al. 2001). The youngest plutonic rocks are c. 1.71 Ga TIB 2 intrusive rocks along the Swedish–Norwegian border (Romer et al. 1992).

The Pikku Sattavaara monzonite

At Pikku Sattavaara, monzonite occurs as an oval intrusion extending over an area of 2 × 5 km. It is situated along the Karesuando-Arjeplog deformation zone (KADZ) and intrudes the contact between the Karelian greenstones and the unconformably overlying Maattavaara Quartzite. Exposures are rather sparse and mainly found at Pikku Sattavaara hill, situated 37 km east-northeast of Kiruna. Contacts with the surrounding rocks are not exposed. However, according to aeromagnetic data, the eastern boundary of the intrusion is partly controlled by the KADZ. The monzonite is generally undeformed, but brittle structures have developed locally in a northwesterly orientation. Brittle to ductile shearing in a NNE direction affects the monzonite in outcrops in the southeast.

The exposed parts of the monzonite show no major variation in composition or texture, and aeromagnetic data indicate that the intrusion is of a fairly homogenous nature. Texturally, it is medium-grained, with feldspar and pyroxene as the main constituents. Pyroxene constitutes 35–40% of the rock and includes both augite and hyperstene, the former being most abundant. A characteristic minor component is poikilitic megacrysts of biotite, whose colour is reddish-brown in thin section. Apatite and magnetite occur as accessory phases. The pyroxenes are partly altered to amphibole, particularly in areas affected by deformation. Close to the KADZ, the rock is greatly altered and partly veined by carbonate. Secondary biotite, chlorite and epidote have formed at the expense of pyroxene and amphibole.

Sample description

Two samples were collected from Pikku Sattavaara for age determination (sample 29KOM306, 7542444/757142 and sample 29KOM308, 7542142/757036, coordinates in SWEREF99 TM). Both are from the south-central part of the intrusion and differ slightly in mineral composition and texture. Sample 29KOM308 shows the best preserved character, while sample 29KOM306 shows significant late- to post-magmatic alteration. Both samples have a grain size of 1 to 3 mm, with biotite as sparse 7–15 mm sized poikilitic megacrysts, having a brownish colour in thin section. Apatite is the most common accessory mineral, occurring in short prismatic to rounded grains. Sample 29KOM308 is a reddish-brown colour, and contains augite and some hyperstene. Augite is partly replaced by biotite and amphibole. Sample 29KOM306 is taken from a dark brownish-coloured monzonite. Pyroxene is largely altered to amphibole and the biotite contains abundant needles of rutile and minute grains of titanite.

The Vinsavaara monzodiorite

Some intrusions of monzonitic to monzodioritic composition occur north of Junosuando in northeastern Norrbotten (Witschard 1970). They are highly magnetic structures with a rounded to oval shapes and sizes of 10 to 15 km in the longest dimension (Vinsavaara, Karijärvi and Vivungi). The best exposed intrusion occurs at Vinsavaara, 3 km north of Junosuando. The predominant rock is a medium- to coarse-grained monzodiorite, consisting of perthite (70%), amphibole (10%), pyroxene (7%) and biotite (5%). The perthite comprises a complex mixture of microcline and plagioclase, with both perthitic and antiperthitic intergrowths. Locally, the perthite grains contain irregular cores of plagioclase (albite to andesine), which are corroded to a greater or lesser extent by the surrounding microcline. Pyroxene is mostly augite, although hyperstene is found in the Vinsavaara intrusion. Amphibole occurs as primary magmatic hornblende and as a secondary replacement after pyroxene. Magnetite and apatite are the main accessory minerals. Quartz is rare and when present occurs interstitially with feldspar. Its texture is generally granular, with irregular and sutured boundaries of perthite grains as a typical feature (Witschard 1970).

Sample description

One sample of monzodiorite has been taken from the southern slope of Viiksvaara hill, situated in the southern part of the Vinsavaara intrusion (BOM950180, coordinates in SWEREF99 TM: 7501593/820409). The rock is reddish-brown in colour and medium- to coarse-grained (Fig. 2A). A characteristic feature is the occurrence of large poikilitic flakes of biotite randomly distributed in the rock. The matrix predominantly consists of perthitic feldspar, with approximately 10 and 5 per cent augite and hyperstene, respectively (Fig. 2B). A second type of biotite partly replaces inner parts of augite grains, but also occurs as secondary rims on grains of magnetite and pyroxene. Apatite is a common accessory mineral, forming short prismatic grains.

The Juoluvaara intrusion

The Juolovaara intrusion is situated 18 km northeast of Soppero, close to the Karesuando–Arjeplog deformation zone, just east of exposed Archaean rocks of the Råstojaure complex. It intrudes Haparanda-type granodiorite and Karelian greenstones. The Juolovaara intrusion is oval in shape, 5 × 3 km,

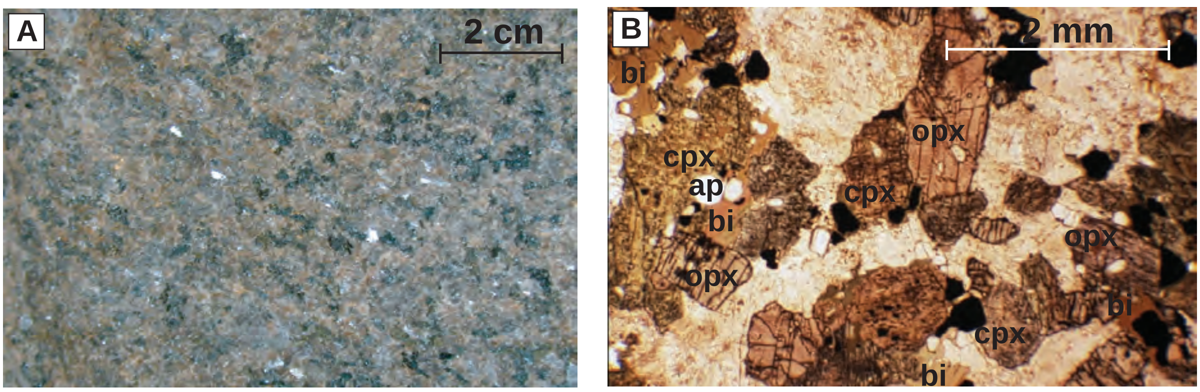

Figure 2. The Vinsavaara monzonite. **A.** Photograph of analysed sample. **B.** Photomicrograph of analysed sample showing orthopyroxene, clinopyroxene, biotite and apatite in a matrix of perthitic feldspar. opx - orthopyroxene, cpx - clinopyroxene, bi – biotite, ap - apatite. All photographs by Olof Martinsson.

with a mafic border zone up to 600 m wide and a monzonitic core. The rocks of the mafic border vary from olivine gabbro to anorthosite with a diffuse layering that conforms to the border of the intrusion. Mafic enclaves in the monzonite and mingling textures at the border zone suggest that monzonitic and gabbroic rocks are comagmatic.

The Peuravaara intrusion is situated less than 1 km to the east and is probably of similar age. It is more rounded and slightly smaller in size. Based on a few outcrops and aeromagnetic data, it has been suggested that it is predominantly gabbroic in character, including anorthosite and gabbro, locally containing up to 30% magnetite (Ambros 1980).

Sample description

At Juoluvaara a sample of monzonite was taken from the western part of the intrusion, close to the gabbroic border (STB961049B, coordinates in SWEREF99 TM: 7583891/786367). The monzonite is grey, fine- to medium-grained and isotropic, with sparse 5 mm sized phenocrysts of K-feldspar (Fig. 6A). Perthitic K-feldspar is the predominant mineral, with subordinate amounts of plagioclase, green pleochroitic hornblende, brown biotite and Fe-Ti oxides (Fig. 6B). Quartz, titanite, clinopyroxene, epidote, apatite, pyrite and zircon occur as accessory phases. Clinopyroxene is mostly replaced by hornblende, with irregular-shaped quartz inclusions. Titanite usually occurs as rims on ilmenite. According to the normative composition, the rock should contain both clino- and orthopyroxene.

Geochemistry of the sampled intrusions

Three samples from Pikku Sattavaara and one each from Vinsavaara and Juoluvaara have been chemically analysed by ICP-AES and ICP-MS using lithium borate fusion for main and trace element composition (Table 1). All samples show general chemical similarities, particularly the Pikku Saattavaara samples, which are almost identical in terms of major and trace element composition. Only one sample, 29KOM309, from Pikku Sattavaara, affected by brittle to ductile deformation and containing biotite, epidote and chlorite as alteration minerals, differs, with lower concentrations of sodium and higher values for loss of ignition (LOI). Based on normative mineral compositions, the Vinsavaara intrusion is a monzodiorite, whereas the Pikku Sattavaara and Juoluvaara intrusions are monzonites.

Chemical results (red symbols) are plotted in the R1-R2 diagram of De la Roche et al. (1980) for classification (Fig. 3A). Included in the diagram are data from other petrologically similar intrusions from northeastern Norrbotten (blue symbols) and 1.8 Ga intrusions from elsewhere in northern Sweden (black symbols). The three samples analysed from Pikku Sattavaara plot close to each other in the monzonite field, while the sample from Vinsavaara plots within the syenodiorite field, and the Juoluvaara sample at the border between syenodiorite and syenite. Together with samples of similar intrusions in northeastern Norrbotten, they describe a trend from monzodiorite to more syenitic composition, and based on the Ta/Yb-Ce/Yb diagram (Pearce 1982), they have a shoshonitic character similar to that of ring gabbro complexes in northeastern Norrbotten (Fig. 3B). In the Y-Nb classification diagram (Pearce et al. 1984; Fig. 3C) the Pikku Sattavaara and Vinsavaara samples plot together with TIB 1 intrusions from Rombak at the border between within plate granites (WPG) and volcanic arc to syn-collisional granites (VAG+SYN-COLG), while in a Zr-Ga/Al diagram (Whalen et al. 1987) samples plot in the A-type field (Fig. 3D). According to this classification, they are geochemically transitional between an intra-plate and destructive plate margin setting. A high concentration of Sr and Ba is typical of all three intrusions (Table 1).

Table 1. Chemical analysis of monzonites from Pikku Saattavaara, Vinsavaara and Juoluvaara. All elements were analysed by ICP-AES and ICP-MS for main and trace elements.

Sample	29KOM306	29KOM308	29KOM309	BOM950180	STB991049B
Locality	Pikku Saattavaara	Pikku Saattavaara	Pikku Saattavaara	Vinsavaara	Juoluvaara
wt %					
SiO_2	55.83	56.21	54.58	55.60	58.30
TiO_2	1.54	1.59	1.60	1.29	1.30
Al_2O_3	15.10	15.03	14.69	15.60	16.95
Fe_2O_3	7.19	7.45	8.01	7.77	5.70
MnO	0.13	0.10	0.12	0.13	0.09
MgO	4.57	4.67	4.66	3.63	2.05
CaO	5.59	5.80	5.58	5.58	4.21
Na_2O	3.55	3.63	2.88	4.24	4.74
K_2O	4.42	4.42	4.98	4.08	4.93
P_2O_5	1.04	1.03	1.13	0.71	0.64
LOI	0.63	0.13	1.92	0.10	0.29
SUM	99.58	100.07	100.16	98.73	99.83
ppm					
Sr	1473	1630	1161	1160	1545
Ba	3604	3534	3488	2310	4280
Rb	97.3	97.9	101.0	89.9	76.8
Nb	17.7	18.0	15.7	11.4	17.6
Ta	0.84	0.88	0.78	0.89	0.70
U	1.77	2.54	1.98	4.66	0.73
Th	7.00	7.30	6.30	13.60	1.98
Zr	337	378	338	298	272
Hf	8.27	9.19	8.07	7.75	6.30
La	101.3	98.4	91.6	93.0	84.9
Ce	148.8	186.3	140.1	190.0	188.5
Pr	24.7	26.4	24.7	22.80	20.9
Nd	91.8	90.8	85.5	86.1	84.0
Sm	14.00	13.41	13.04	12.10	13.65
Eu	3.10	3.21	3.00	2.93	3.75
Gd	10.14	10.18	10.80	8.52	7.48
Tb	1.01	1.00	0.98	1.05	0.93
Dy	4.53	4.31	4.22	4.94	4.42
Ho	0.75	0.80	0.76	0.88	0.79
Er	1.85	2.10	2.03	2.47	1.83
Tm	0.25	0.25	0.24	0.35	0.26
Yb	1.57	1.51	1.42	2.36	1.55
Lu	0.18	0.20	0.17	0.34	0.23
Y	22.0	22.0	23.0	25.4	20.3
Sc	14.0	14.0	15.0	11.2	9.0
V	123	125	126	144	93
Cr	130	126	132	75	20
Ni	23	18	18	46	7
Co	26	25	25	22	9
Cu	59	42	5	45	10
Zn	53	87	39	83	78
Mo	0.5	0.5	0.5	1.2	
W	0.2	0.2	0.9	1.0	
Sn	1.6	1.5	1.3	2.1	
Be	3.0	3.0	3.0	3.4	
Ga	21.0	20.1	18.5	14.8	

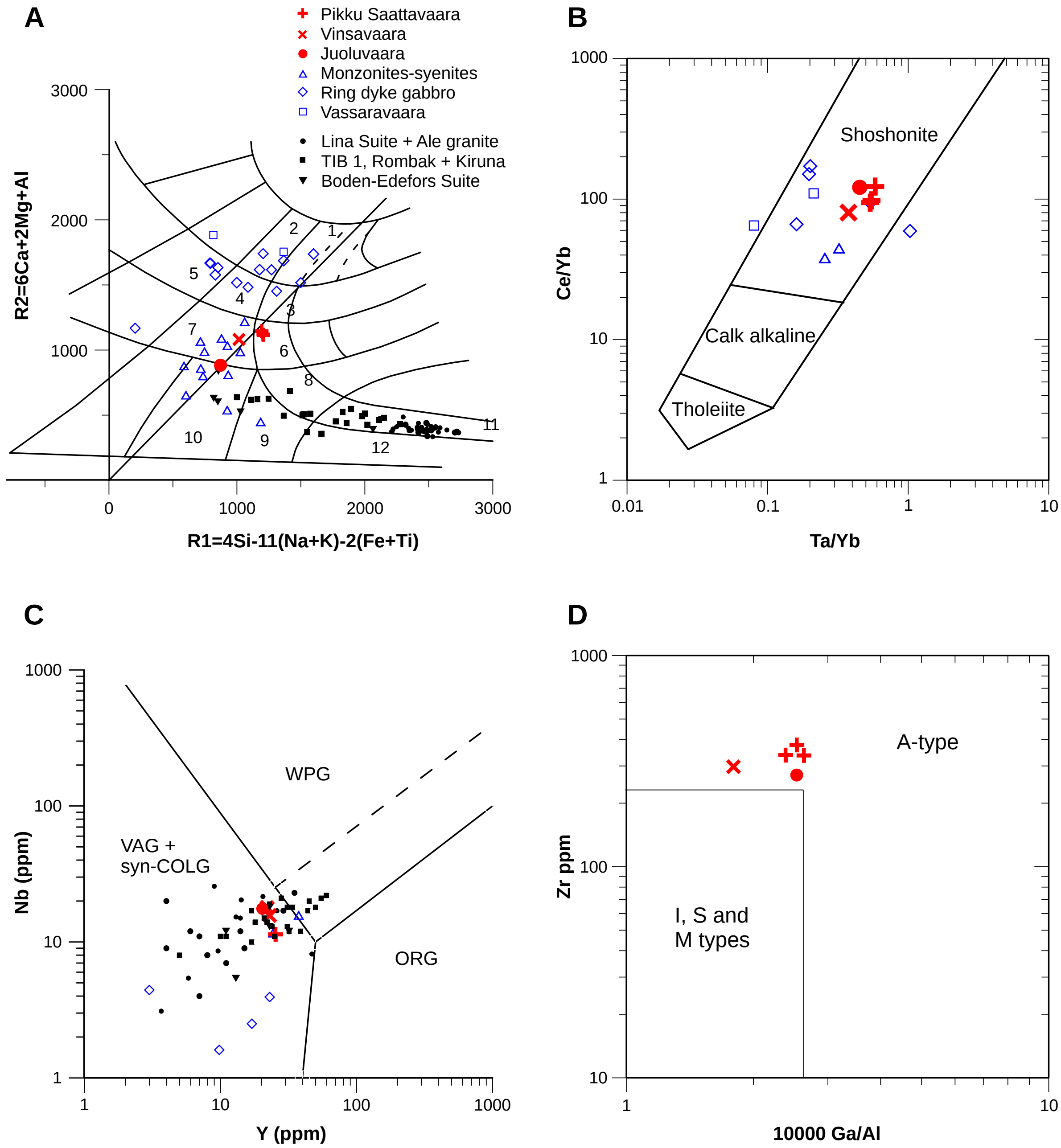

Figure 3. Chemical classification of monzonitic rocks from Pikku Sattavaara, Vinsavaara and Juoluvaara (red symbols). Included are data from petrographically similar intrusions in northeastern Norrbotten (blue symbols) and other 1.8 Ga plutonic rocks in northernmost Sweden (black symbols, data from Öhlander & Schöberg 1991, Öhlander & Skiöld 1994, Öhlander et al. 1987, Lindroos & Henkel 1981, Romer et al. 1992, Skiöld et al. 1988, Witschard 1970). **A.** R1-R2 diagram from de la Roche et al. (1980), 1-olivine gabbro, 2-alkali gabbro, 3-monzo gabbro, 4-syenogabbro, 5-essexite, 6-monzonite, 7-syenodiorite, 8-quartz monzonite, 9-quartz syenite, 10-syenite, 11-granite, 12-alkali granite. **B.** Ta/Yb-Ce/Yb diagram from Pearce (1982). **C.** Y-Nb diagram from Pearce et al. (1984). **D.** 10000*Ga/Al diagram from Whalen et al. (1987). For Figure B, C and D symbols as in Figure 3A.

ANALYTICAL METHODS

Zircons from the Vinsavaara and Pikku Sattavaara intrusions were separated using standard magnetic and heavy liquid techniques. Most fractions were abraded using the Krogh (1982) method. They were dissolved in $HF:HNO_3$ in Teflon® capsules in autoclaves using the Krogh (1973) method. After decomposition, the samples were dissolved in HCl and split into 2 aliquots. A mixed ^{208}Pb-$^{233-235}U$ tracer was added to the ID aliquots. Some of the smaller samples were spiked with a mixed ^{205}Pb-$^{233-235}U$ tracer before decomposition. The sample aliquots, dissolved in 3.1 N HCl (ID aliquots and ^{205}Pb-spiked samples) or 2 N HCl (IC aliquots), were loaded onto anion exchange columns with 50 µl resin volume for extraction of Pb and U. Pb was loaded on Re single filaments with silica gel and H_3PO_4. U was loaded on Re double filaments with HNO_3. The isotopic ratios were measured on a Finnigan MAT 261 mass spectrometer at the Laboratory for Isotope Geology (now Department of Geosciences) at the Swedish Museum of Natural History, equipped with five faraday cups. Most samples were measured in the static mode with the faraday cups. Small Pb and U amounts, yielding low signals, were measured in peak jumping mode on a secondary electron multiplier. The corrected isotope ratios and error propagation were calculated using the PBDAT program of Ludwig (1991a), with the decay constants recommended by Steiger & Jäger (1977). The intercept ages were calculated and the concordia plot drawn using the Ludwig (1991b) ISOPLOT program. The total Pb blank was 4–10 pg and the U blank less than 2 pg. The assigned composition of common Pb was calculated using the Pb evolution model of Stacey & Kramers (1975), which is a reasonable approximation for analyses with high $^{206}Pb/^{204}Pb$ (>~1000). For samples with low $^{206}Pb/^{204}Pb$, the uncertainty in the common Pb correction will result in large error ellipses. The mass fractionation for Pb is 0.10 ±0.04% per a.m.u. U mass fractionation was monitored and corrected for by means of the $^{233-235}U$ ratio of the spike. All analytical errors are given as 2σ.

Zircons from the Juoluvaara monzonite sample (STB961049B) were analysed by high-spatial resolution secondary ion mass spectrometer (SIMS) analysis in November 2013, using a Cameca IMS 1280 at the Nordsim facility at the Swedish Museum of Natural History in Stockholm. Zircons were obtained from a density separate of a crushed rock sample using a Wilfley water table. Magnetic minerals were removed using a hand magnet. Handpicked crystals were mounted in transparent epoxy resin together with chips of reference zircon 91500. The zircon mounts were polished and, after gold coating, examined by cathodoluminescence (CL) imaging using electron microscopy at the Swedish Museum of Natural History in Stockholm. Detailed descriptions of the analytical procedures are given in Whitehouse et al. (1997, 1999) and Whitehouse & Kamber (2005). An approximately 6 nA O^{2-} primary ion beam was used, yielding spot sizes of approximately 10–15 µm. U/Pb ratios, elemental concentrations and Th/U ratios were calibrated relative to the Geostandards zircon 91500 reference, which has an age of c. 1 065 Ma (Wiedenbeck et al. 1995, 2004). Common Pb-corrected isotope values were calculated using modern common Pb composition (Stacey & Kramers 1975) and measured ^{204}Pb, in cases of a ^{204}Pb count rate above the detection limit. Decay constants follow the recommendations of Steiger & Jäger (1977). Diagrams and age calculations of isotopic data were made using Isoplot 4.15 software (Ludwig 2012). All age uncertainties are presented at the 2σ or 95% confidence level. CL imaging of the dated zircons was performed using electron microscopy at the Department of Geology, Uppsala University to confirm the location of the analytical spot.

ANALYTICAL RESULTS

The Pikku Sattavaara monzonite

Zircons from the two samples of the Pikku Sattavaara monzonite have similar appearance. Most of the grains recovered are crystal fragments of larger zircon grains. They are elongate and fractured or anhedral, making it difficult to determine the original morphology. The pyramids present are all sharp. Magmatic zonation is common and both cores and overgrowths are found in some grains, but were avoided when selecting grains for analysis. Grains are either colourless to pale yellow, pink or pale brown. All grains analysed were thoroughly abraded.

The analytical data are shown in Table 2 and Figure 4. Seven of the eight data points define a discordia, with intercept ages of 1 799 ±2 and 25 ±149 Ma and an MSWD of 0.09. The eighth fraction is

Table 2. U-Pb isotopic data for samples 29KOM306, 29KOM308 and BOM950180.

Analysis. No.	Weight (µg)	No. of crystals	U (ppm)	Pb tot. (ppm)	Common Pb (ppm)	$^{206}Pb^{a}$ / ^{204}Pb	^{206}Pb - ^{207}Pb - ^{208}Pb Radiog. (atom %)^{b}	$^{206}Pb^{b}$ / ^{238}U	$^{207}Pb^{b}$ / ^{235}U	$^{207}Pb/^{206}Pb$ age (Ma)
29KOM306 Pikku Saattavaara monzonite										
1	25	4	124.3	51.0	0.04	14769	65.3 - 7.2 - 27.5	0.3109±11	4.714±19	1799±4
2	20	1	69.6	28.5	0.17	4225	66.6 - 7.3 - 26.2	0.3139±8	4.761±17	1800±5
3	21	1	69.6	28.9	0.28	3165	67.0 - 7.3 - 25.7	0.3196±20	4.823±36	1790±7
4	21	5	105.1	43.8	0.01	13508	65.4 - 7.2 - 27.4	0.3162±9	4.794±16	1799±3
29KOM308 Pikku Saattavaara monzonite										
1	18	2	74.4	28.3	0.70	1518	68.1 - 7.5 - 24.4	0.2929±11	4.438±24	1798±7
2	22	1	63.2	26.2	0.07	6088	66.1 - 7.3 - 26.6	0.3178±10	4.819±19	1799±4
3	23	1	84.5	34.8	0.14	5951	66.0 - 7.3 - 26.7	0.3146±19	4.771±31	1799±3
4	21	1	140.6	55.3	0.01	19229	69.4 - 7.6 - 23.0	0.3166±12	4.803±20	1800±3
BOM 950180 Vinsavaara monzonite										
1	31	2	1024.0	395.0	0.53	26310	67.3 - 7.4 - 25.3	0.3011±7	4.567±11	1800±1
2	30	2	269.7	94.2	0.22	12527	73.5 - 8.1 - 18.4	0.2974±7	4.498±13	1794±2
3	35	1	436.8	147.4	0.21	21815	73.7 - 8.1 - 18.2	0.2886±10	4.371±16	1797±1
4	38	1	153.6	53.6	0.17	9046	72.4 - 8.0 - 19.6	0.2925±7	4.438±12	1800±3
5	33	7	151.6	55.1	0.35	7835	72.9 - 8.0 - 19.1	0.3062±9	4.637±15	1798±2

[a] Corrected for mass fractionation (0.1% per a.m.u).
[b] Corrected for mass fractionation, blank and common Pb.

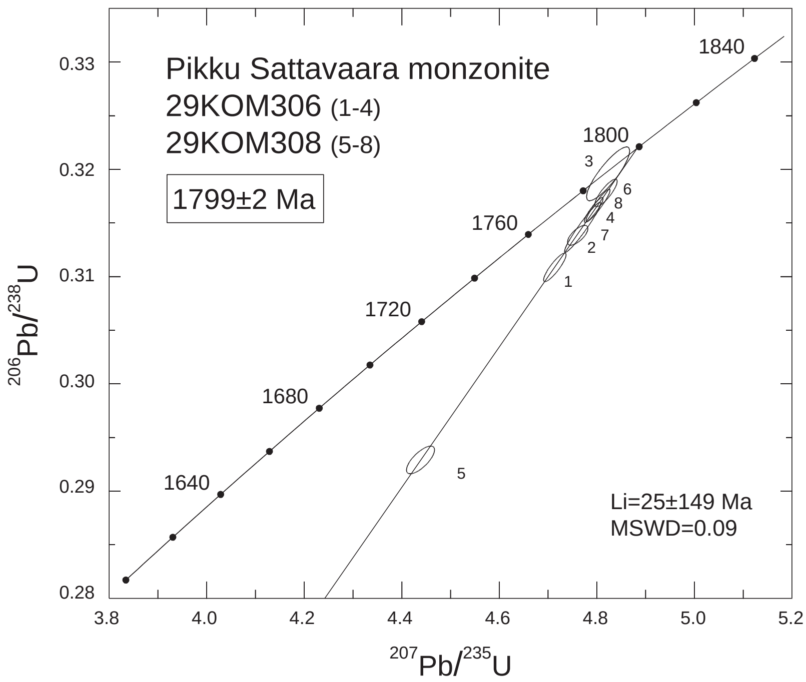

Figure 4. Concordia diagram for analysed zircon fractions from the monzonite samples 29KOM306 and 29KOM308, Pikku Sattavaara.

the least discordant and has a $^{207}Pb/^{206}Pb$ age of 1790 ±7 Ma. Since this point displays great uncertainty and diverges distinctly from the others, it is justifiable to omit it from the age calculation. There is no difference between the chemistry and morphology of the zircons from the two samples.

The Vinsavaara monzodiorite

Separated zircons were divided into five fractions, consisting mainly of crystal fragments >150 µm, implying that the original zircon grains were unusually large. However, fraction 5 consists of small, generally euhedral, non-fractured zircons. No signs of cores or overgrowths were observed and the grains are either pink, brown or colourless. Fractions 3, 4 and 5 were thoroughly abraded.

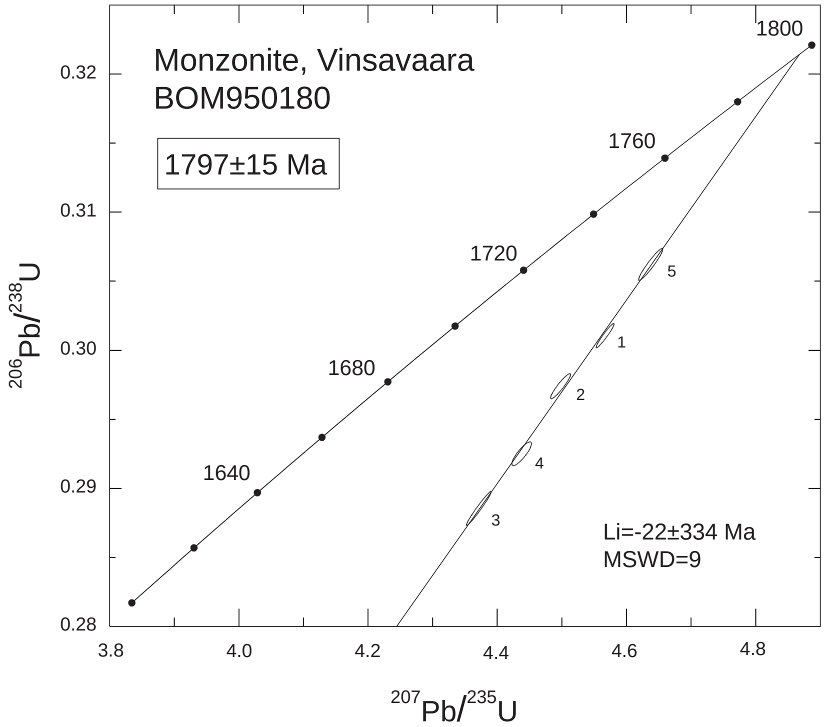

Figure 5. Concordia diagram for analysed zircon fractions from the monzodiorite sample BOM950180, Vinsavaara.

The analytical data are shown in Table 2 and Figure 5. Fractions 2, 4 and 5, which consist of colourless or pale brown grains, have lower uranium content than fractions 1 and 3, which consist of brown crystals. The discordia has concordia intercepts at 1799 ±15 and -22 ±334 Ma and an MSWD of 9. The upper intercept age is interpreted as the intrusion age of the rock.

The Juoluvaara monzonite

The heavy mineral concentrate contained euhedral, prismatic transparent and colourless zircons. Most grains were angular fragments, however. CL images of the zircon show a broad oscillatory or sector zonation, but large areas of the zircon lack zonation and show a homogenous CL intensity (Fig. 6C). The ten analyses carried out are all concordant and show low concentrations of common lead. The analyses show 22–139 ppm U and have Th/U ratios of 0.53–1.14 (Table 3). A Concordia age is calculated at 1804 ±6 Ma (Fig. 6D, 2σ, MSWD of concordance = 0.53, probability of concordance = 0.47, n = 10) and a weighted average $^{207}Pb/^{206}Pb$ age at 1803 ±8 Ma (2σ, MSWD = 0.70, probability = 0.71, n = 10). The concordia age at 1804 ±6 Ma (2σ) is chosen as the best age estimate, interpreted to date igneous crystallisation of the monzonite. This age also applies to the surrounding gabbro intrusion, since this is considered contemporaneous, evident from mingling in the contact zone.

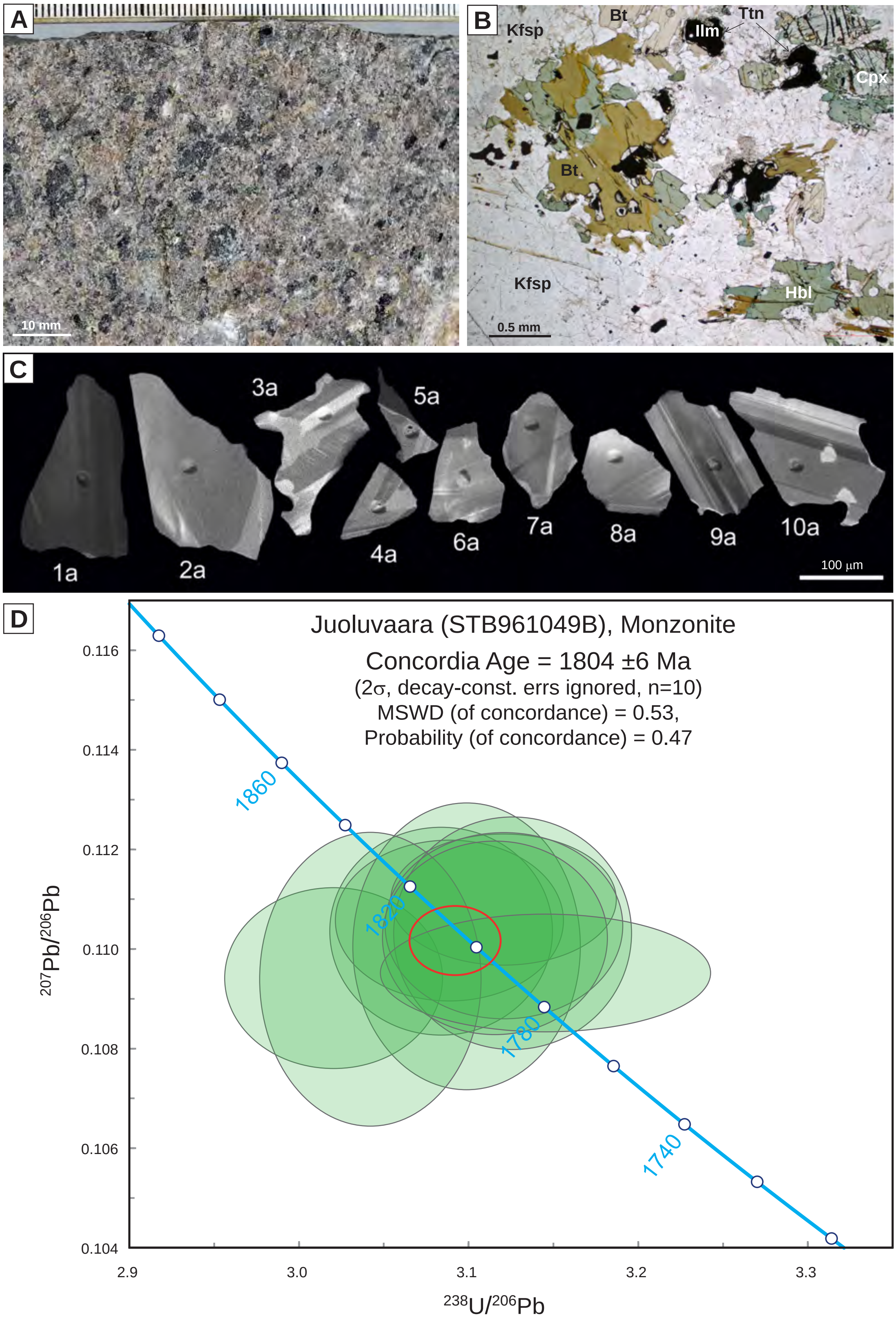

Figure 6. Geochronolgy of the Juoluvaara monzonite. **A.** The dated rock sample. **B.** Photomicrograph of dated sample. **C.** Cathodoluminescence (CL) images of analysed zircon grains. Numbers refer to analytical spot number in Table 3. **D.** Tera Wasserburg diagram showing U-Pb SIMS data of of analysed zircon from monzonite sample STB991049B, Juoluvaara. Error ellipse of calculated weighted mean age is shown in red. All photographs by Fredrik Hellström.

Table 3. U-Pb isotopic data for sample STB991049B (n4835).

Analysis	Comment	U ppm	Th ppm	Pb ppm	Th/U calc *1	^{207}Pb/ ^{235}U	±s %	^{238}U/ ^{206}Pb	±s %	^{207}Pb/ ^{206}Pb	±σ %	ρ *2	Disc. % conv.*3	^{207}Pb/^{206}Pb age (Ma)	±σ	^{206}Pb/^{238}U age (Ma)	±σ	^{206}Pb/^{204}Pb measured	f_{206}% *4
01a	Osc zon	115	74	48	0.65	4.906	1.00	3.120	0.87	0.1110	0.48	0.87	-1.5	1816	9	1792	14	213129	* 0.01
02a	CL-hom.	60	54	26	0.92	4.882	1.15	3.120	0.92	0.1105	0.69	0.80	-1.0	1807	13	1792	14	76857	{0.02}
03a	Osc zon	22	11	9	0.54	4.960	1.41	3.041	0.88	0.1094	1.10	0.62	2.8	1790	20	1833	14	76975	{0.02}
04a	Osc zon	45	27	19	0.63	4.936	1.16	3.083	0.87	0.1104	0.77	0.75	0.3	1806	14	1811	14	>1e6	* 0.00
05a	Osc zon	57	37	25	0.70	4.996	1.10	3.020	0.87	0.1094	0.68	0.79	3.5	1790	12	1844	14	120605	{0.02}
06a	Osc zon	51	32	21	0.64	4.880	1.13	3.115	0.87	0.1102	0.72	0.77	-0.5	1803	13	1795	14	193629	{0.01}
07a	Osc zon	75	65	33	0.89	4.937	1.07	3.088	0.89	0.1106	0.60	0.83	0.0	1809	11	1808	14	272646	* 0.01
08a	Osc zon	40	21	16	0.53	4.898	1.39	3.098	0.88	0.1101	1.07	0.64	0.2	1800	19	1803	14	39065	* 0.05
09a	Osc zon	139	155	63	1.14	4.803	1.34	3.145	1.26	0.1095	0.44	0.94	-0.7	1792	8	1780	20	380321	{0.00}
10a	Osc zon	69	57	30	0.82	4.867	1.26	3.125	0.92	0.1103	0.86	0.73	-1.0	1805	16	1790	14	244324	{0.01}

osc. = oscillatory, CL = Cathodoluminescence, hom. = homogenous

Isotope values are common Pb corrected using modern common Pb composition (Stacey & Kramers 1975) and measured 204Pb.

*1 Th/U ratios calculated from ^{208}Pb/^{206}Pb and ^{207}Pb/^{206}Pb ratios corrected for Pb_{com}, assuming a single stage of closed U-Th-Pb evolution

*2 Error correlation in conventional concordia space. Do not use for Tera-Wasserburg plots.

*3 Age discordance in conventional concordia space. Positive numbers are reverse discordant.

*4 % of common ^{206}Pb in measured ^{206}Pb, estimated from ^{204}Pb assuming a present day Stacey and Kramers (1975) model.

Figures in parentheses are given when no correction has been applied.

DISCUSSION

Possibly related intrusions in northeastern Norrbotten

Monzodioritic to syenitic intrusions with petrographic and geochemical similarities to the 1.8 Ga Vinsavaara, Pikku Sattavaara and Juoluvaara intrusions also occur at Karijärvi and Vivungi, north of Vinsavaara (Fig. 1). At Vivungi, a magnetic anomaly with a diameter of approximately 15 km shows a more or less concentric internal pattern. The area is poorly exposed but an approximately 500 m wide dyke of syenitic composition is found in the west of the structure, and a similar rock is reported from its northern part (Witschard 1970), suggesting that the magnetic structure is caused by syenitic ring dykes. The Karijärvi intrusion is 8 km in diameter and has a more magnetic rim in its northeastern part. Only the magnetic part is exposed, consisting of monzonite similar to that of the Vinsavaara intrusion (Witschard 1970). The unexposed parts have been investigated using geophysical methods and sampled by drilling in a profile crossing the structure. These results showed the internal part to consist mainly of Lina granite or Jyryjokki granite, with minor occurrences of peridotite and monzonite. Thus, the core predominantly comprises rocks similar to those found outside the structure. The monzonite is interpreted to form a cone sheet dipping inwards and converging at a depth of approximately 5 km (Westin 1983).

Several ring dyke complexes of gabbroic rocks are found in this part of northeastern Norrbotten, and two occur close to the Vinsavaara and Karijärvi intrusions (Fig. 1). The complexes are rounded to oval in shape and 3 to 7 km in their longest dimension. Gabbroic rocks are usually rich in Fe, Ti and P, and show an alkalic character, but locally include anorthositic varieties. Mineralogically, rocks show some variations, with amphibole as the predominant mafic mineral in most intrusions, and clinopyroxene as a minor component in several of them. The Merasjoki intrusion (Fig. 1) also contains some orthopyroxene. Geophysical interpretations indicate an inward-dipping shape and a convergence of the steeply dipping cone sheets at approximately 5 km for the Lumivaara and Nakajärvi intrusions (Fig. 1), while the Merasjoki intrusion only comprises two concentric dykes of a more lopolitic shape (Lindroos & Henkel 1981). The Juoluvaara intrusion has the characteristics of both the gabbroic ring dykes (its gabbroic outer margin) and the 1.8 Ga monzonitic intrusions (its core).

All the monzonitic-syenitic to gabbroic rocks forming composite intrusions, ring dykes or cone sheets appear to postdate the 1.89–1.86 Ga Haparanda and Perthite-monzonite suite plutons (Lindroos & Henkel 1981, Bergman et al. 2001). Gabbroic cone sheets occur within a conspicuous positive gravimetric anomaly centred close to Merasjärvi. A large mafic intrusion with an upper surface at a depth of 6 to 9 km may explain this gravimetric anomaly, as well as the high T/low P metamorphic regime in the region (Bergman et al. 2001). It is proposed that this suggested intrusion is the magmatic source of the cone sheets in its roof. The monzonitic to syenitic intrusions occur along the southern and western margin of this gravimetric anomaly. Based on similarities in petrology, intrusion character and their spatial relationship to the Merasjärvi gravity high (MGH, Fig. 7), it is suggested that these mafic to intermediate intrusions are part of the same magmatic event. This c. 1.8 Ga magmatism in northeastern Norrbotten shows a shoshonitic character, with alkaligabbro, monzonite, syenodiorite and syenite as predominant compositions (Fig. 3A).

Other 1.8 Ga intrusive rocks in the northern Fennoscandian Shield

Intrusive rocks with an age of c. 1.8 Ga are common in the Fennoscandian Shield, and in the north include the 1.77 Ga Nattanen granite (Haapala et al. 1987), 1.81–1.78 Ga Lina type granites (Öhlander et al. 1987, Bergman et al. 2001), 1.79–1.77 Ga TIB 1 intrusions (Skiöld 1988, Romer et al. 1992, 1994) and 1.80 Ga Edefors-Boden granitoids (Öhlander & Skiöld 1994).

The Lina granites are of a predominantly minimum (eutectic) melt composition, with quartz, microcline and oligoclase occurring in approximately similar proportions (Ödman 1957, Öhlander &

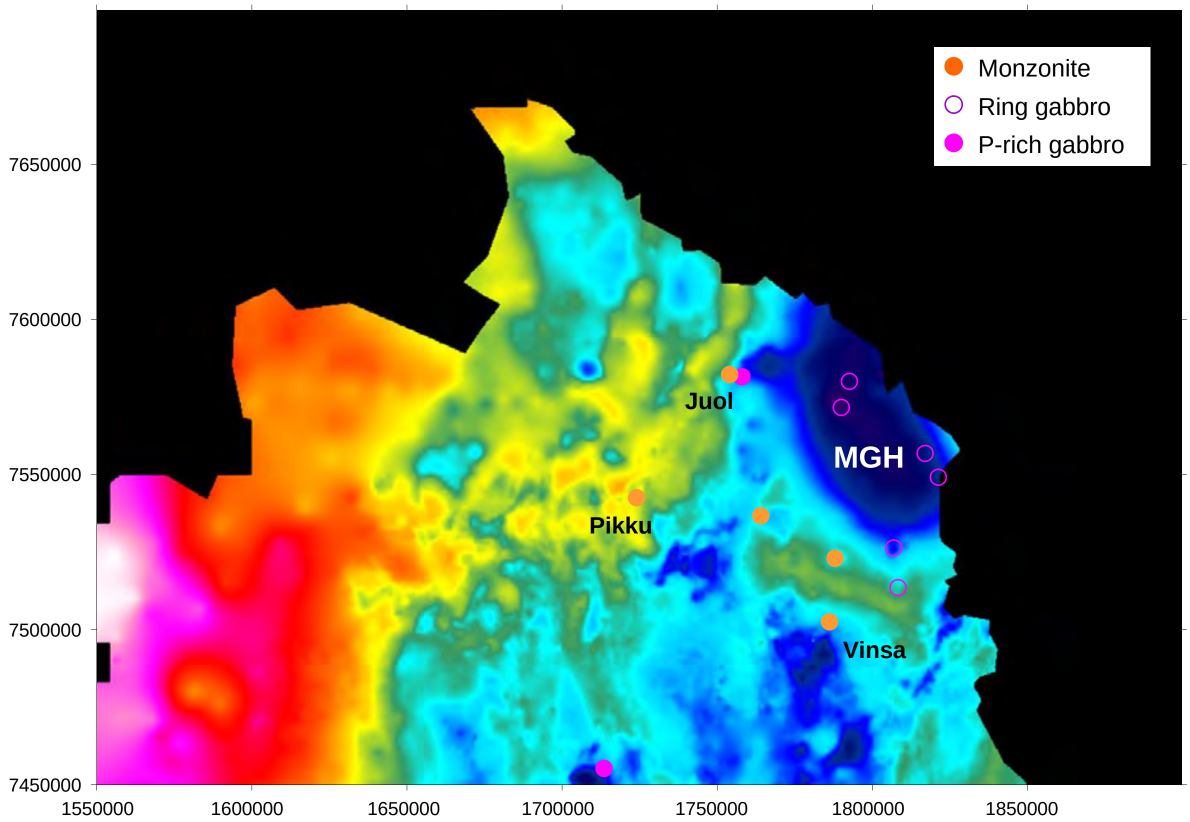

Figure 7. The regional Bouguer anomaly over the map area in Figure 1. Dark blue relates to high density rocks and red to low density rocks. Location of 1.8 Ga monzonitic intrusions (Vinsa: Vinsavaara, Juol: Juoluvaara, Pikku: Pikku Sattavaara), and geochemically similar 1.8 Ga gabbroic intrusions are indicated.

Sköld 1994). A larger compositional variation is exhibited by the Edefors intrusive rocks northwest of Luleå, and the TIB 1 intrusions occurring in the westernmost part of Norrbotten and adjacent areas of Norway. Intrusions vary from monzonitic or syenitic to quartz monzonitic and granitic composition (Romer et al. 1992, 1994, Öhlander & Sköld 1994).

The Edefors intrusions also include some gabbroic to anorthositic units (Wikström & Söderman 2000). The occurrence of clinopyroxene and, locally, olivine or orthopyroxene in felsic intrusive rocks predominantly made up of perthite is typical of the Edefors intrusions (Ödman 1957, Öhlander & Sköld 1994). In the Lofoten area, TIB 1 is represented by monzonites containing orthopyroxene and olivine (mangerite), gabbro and anorthosite (Griffin et al. 1978). Further east, in the Rombak window, quartz monzonites and granites predominate (Romer et al. 1992). A local occurrence of syenite is found in the Kiruna area (Romer et al. 1994).

The 1.8 Ga plutonic rocks in Norrbotten show geochemical similarities. In the R1–R2 diagram (Fig. 3A), intermediate and felsic members describe a shoshonitic trend from monzodiorite-syenodiorite to syenite-quartz syenite and into the granite field, represented by the Jyrijokki and Lina granites. Mafic rocks are subordinate and include alkalic gabbros from the MGH in northeastern Norrbotten. The Vassaravaara intrusion at Gällivare is chemically similar to the ring gabbros at the MGH, with an alkaline character and containing significant amounts of apatite and magnetite (Martinsson 1994). It has an age of 1 798±4 Ma (Sarlus et al. 2017), and although it occurs outside the MGH, it supports the petrogenetic relation between monzonite and gabbroic intrusions of shoshonitic to alkalic character in northern Norrbotten. Common to both types of intrusion are high concentrations of Sr and Ba.

Tectonic setting

The Transscandinavian Igneous Belt (TIB) is a major Palaeoproterozoic magmatic province in the Fennoscandian Shield. It is suggested to have formed as a result of eastward subduction (Wilson 1980, Nyström 1982, Andersson 1991, Romer et al. 1992), possibly during a period of extensional conditions (Wilson et al. 1986, Åhäll & Larsson 2000). However, the Edefors intrusive rocks are interpreted to be products of plate convergence, but related to a collision event further south caused by northward subduction. During collision, extensional conditions may have formed in response to delamination, causing melting of the astenosphere. The Edefors monzonitic to granitic rocks then formed from the juvenile mantle melts by differentiation and crustal interaction (Öhlander & Skiöld 1994). Lina-type granites are typical minimum-melt granites created by melting of 1.9 Ga granitoids during the collision event (Öhlander et al. 1987, Öhlander & Skiöld 1994).

Considering the tectonic models presented for the 1.8 Ga magmatism in northern Sweden, a complex scenario is outlined, with contemporaneous westward and northward plate convergence, including processes generating local extension. But an alternative intra-cratonic extensional setting has been suggested for the TIB magmatism, with mantle-derived melts interacting with continental crust (Wilson et al. 1985, Andersson 1997).

Geochemical approaches to deciphering the tectonic environment for the 1.8 Ga magmatism generally yield ambiguous results. This is illustrated by the Nb-Y diagram, with most samples clustering at the border between convergent to intraplate settings, except for the Lina granites that occupy the field of volcanic arc and syn-collisional granites (Fig. 3C).

Although the scattered occurrence of mafic to felsic 1.80 Ga intrusions in northern Norrbotten east of the TIB proper show temporal and petrological similarities to typical TIB 1 intrusions, they also resemble intraplate magmatic complexes related to mantle plumes in their composition and intrusion character. Examples include the Jurassic ring complexes in Nigeria, the Permian Oslo rift and the North Atlantic Tertiary igneous province. In Nigeria, ring dyke complexes have diameters of 8 to 15 km and comprise olivine- and pyroxene-bearing granitoids associated with minor anorthosite intrusions (Turner 1963, Black & Girod 1970). Ring complexes are also characteristic of the Oslo rift, with syenitic to granitic ring dykes associated with alkali-gabbroic, monzonitic and granitic plutons (Ihlen 1986). Tertiary mafic to felsic magmatic centres in east Greenland and western Scotland include classic cone sheet complexes related to mantle plume activity during the opening of the North Atlantic (Upton 1988). In Scotland these intrusions are related to a significant positive gravimetric and magnetic anomaly interpreted to be caused by an underlying dense body of mafic rocks (Bott & Tantrigoda, 1987), resembling the MGH in northeastern Norrbotten. Mafic to felsic 1.8 Ga intrusions also exist in southern Finland, and have petrographical and chemical similarities to the 1.8 Ga monzonites and related gabbroic ring dyke intrusions in northeastern Norrbotten. Some of these intrusions also occur as ring dykes and are strongly enriched in Sr and Ba. Associated mafic rocks have high concentrations of Ti and P (Eklund et al. 1998). It is suggested that they formed from melting of lithospheric mantle enriched by carbonatite metasomatism (Eklund et al. 1998).

The 1.8 Ga mafic to intermediate intrusions in northeastern Norrbotten may thus be isolated and slightly more alkaline expressions of subduction-related TIB 1 magmatism east of the main TIB belt, or may represent a separate igneous event caused by mantle plume activity. In northeastern Norrbotten there may exist a genetically related large mafic intrusion at depth within the MGH (Bergman et al. 2001), and these 1.8 Ga intrusions could be part of a major mafic magmatic event of intraplate character. A back arc setting related to TIB 1 is an alternative possibility.

CONCLUSIONS

Three monzonitic intrusions (Pikku Sattavaara, Juoluvaara and Vinsavaara) in northern Norrbotten have been dated at 1.80 Ga. They are petrographically and geochemically similar, with a shoshonitic character. The Juoluvaara intrusion is distinct in having a gabbroic border zone and a monzonitic core.

Intrusions predominantly consist of perthite, augite and hyperstene, with megacrysts of poikolitic biotite as typical minor constituents. It is suggested that other chemically similar monzonitic and gabbroic intrusions in northeastern Norrbotten, often occurring as ring dykes, are part of the same 1.8 Ga magmatic event.

Most of these intrusions occur within, or at the margin of, the Merasjärvi gravity high (MGH) and may represent higher-level intrusions related to a much larger mafic intrusion deeper in the crust. Monzonitic intrusions have A-type signatures and chemical characteristics overlapping those of rocks in arc and within plate settings. They may have formed in a back arc setting related to eastward subduction generating the Transscandinavian Igneous Belt further west (TIB 1), or may represent a separate igneous event caused by a mantle plume.

ACKNOWLEDGEMENTS

This paper is based on age determinations financed by Sveriges geologiska undersökning (SGU), geological work carried out by SGU and research at CTMG (Centre for Applied Ore Studies at Luleå University of Technology) financed by Outokumpu OY and Boliden Mineral AB. We would like to thank Olav Eklund, Anders Wikström, Magnus Ripa and George Morris for their valuable comments, which significantly improved the manuscript. All U-Pb isotopic zircon data were obtained from beneficial cooperation with the Laboratory for Isotope Geology of the Swedish Museum of Natural History (NRM) in Stockholm. The Nordsim analytical facility is operated under an agreement between the research funding agencies of Denmark, Norway and Sweden, the Geological Survey of Finland and the Swedish Museum of Natural History. Martin Whitehouse, Lev Ilyinsky and Kerstin Lindén at the Nordsim facility are gratefully acknowledged for their first-class analytical support with SIMS analyses. Martin Whitehouse reduced the zircon data, Lev Ilyinsky assisted during ion probe analyses and Kerstin Lindén prepared the zircon mount. Jarosław Majka at the Department of Geology, Uppsala University, and Kerstin Lindén at NRM are thanked for their support during CL imaging of zircons.

REFERENCES

Åhäll, K.-I. & Larsson, S.Å., 2000: Growth-related 1.85–1.55 Ga magmatism in the Baltic Shield: a review addressing the tectonic characteristics of Svecofennian, TIB 1-related Gothnian events. *GFF 122,* 193–206.

Ambros, M., 1980: Beskrivning till berggrundskartorna Lannavaara NV, NO, SV, SO och Karesuando SV, SO. *Sveriges geologiska undersökning, Af 25–30,* 109 pp.

Andersson, U.B., 1991: Granitoid episodes and mafic-felsic magma interaction in the Svecofennian of the Fennoscandian shield, with main emphasis on the ca. 1.8 Ga plutonics. *Precambrian Research 51,* 127–149.

Andersson, U.B., 1997: Petrogenesis of some Proterozoic granitoid suites and associated basic rocks in Sweden (geochemistry and isotope geology). *Sveriges geologiska undersökning Rapporter och Meddelanden 91,* 216 pp.

Bergman, S., Kübler, L. & Martinsson, O., 2001: Description of regional geological and geophysical maps of northern Norrbotten county (east of the Caledonian orogen). *Sveriges geologiska undersökning Ba 56,* 110 pp.

Black, R. & Girod, M., 1970: Late Palaezoic to Recent igneous activity in West Africa and its relationship to basement structures. *In*, T.N. Clifford & I.G. Gass (Eds.) *African magmatism and tectonics, Oliver & Boyd, Edinburgh*, 185–210.

Bott, M.H.P. & Tantrigoda, D.A., 1987: Interpretation of the gravity and magnetic anomalies over the Mull Tertiary intrusive complex, NW Scotland. *Journal of the Geological Society 144,* 17–28.

De la Roche, H., Leterrier, J., Grand Claude, P. & Marchal, M., 1980: A classification of volcanic and plutonic rocks using R1-R2 diagrams and major element analyses – its relationship with current nomenclature. *Chemical Geology 29*, 183–210.

Eklund O., Konopelko, D., Rutanen, H., Fröjdö, S. & Shebanov, A.D., 1998: 1.8 Ga Svecofennian post-collisional shoshonitic magmatism in the Fennocandian Shield. *Lithos 45*, 87–108.

Griffin, W.L., Taylor, P.N., Hakkinen, W., Heier, K.S., Iden, I.K., Krogh, E.J., Makm, O., Olesen, K.I., Ormaasen, D.E. & Tveten, E., 1978: Archaean and Proterozoic crustal evolution in Lofoten Vesterålen, N. Norway. *Journal of the Geological Society of London 135*, 629–647.

Haapala, I., Front, K., Rantala, E. & Vaarma, M., 1987: Petrology of Nattanen-type granite complexes, Northern Finland. *Precambrian Research 35*, 225–240.

Hellström, F.A, & Bergman, S., 2016: Is there a 1.85 Ga magmatic event in northern Norrbotten? – U-Pb SIMS zircon dating of the Pingisvaara metagranodiorite and the Jyryjoki granite, northern Sweden. *GFF 138,* 526–532.

Ihlen, P.M., 1986: The geological evolution and metallogeny of the Oslo paleorift. *In*, S. Olerud & P.M. Ihlen (Eds.): *Metallogeny associated with the Oslo paleorift. Sveriges geologiska undersökning Ca 59*, 5–17.

Krogh, T.E., 1973: A low-contamination method for hydrothermal decomposition of zircon and extraction of U and Pb for isotopic age determination. *Geochimica et Cosmochimica Acta 37,* 485–494.

Krogh, T.E., 1982: Improved accuracy of U-Pb zircon ages by the creation of more concordant systems using an air abrasion technique. *Geochimica et Cosmochimica Acta 46,* 637–649.

Lindroos, H. & Henkel, H., 1981: Beskrivning till berggrundskartorna och geofysiska kartorna Huuki NV/NO, SV, SO och Muonionlusta NV, SV/SO. *Sveriges geologiska undersökning Af 13–16*, 85 pp.

Ludwig, K.R., 1991a: PBDAT: A computer program for processing Pb-U-Th isotope data. Version 1.20. *United States Geological Survey, Open File Report 88–542.*

Ludwig, K.R., 1991b: ISOPLOT: A plotting and regression program for radiogenic-isotope data. Version 2.53. *United States Geological Survey, Open File Report 91.*

Ludwig, K.R., 2012: User's manual for Isoplot 3.75. A Geochronological Toolkit for Microsoft Excel. Berkeley *Geochronology Center Special Publication No. 5*, 75 pp.

Martinsson, E., 1994: Geology and geochemistry of the Dundret-Vassaravaara gabbro complex, Northern Sweden. *Abstract 21:a Nordiska Geologiska Vintermötet, Luleå 1994,* 136.

Martinsson, O., 1997: Tectonic setting and metallogeny of the Kiruna greenstones. *Doctoral thesis 1997:19, Luleå University of Technology.*

Martinsson, O., 2004: Geology and metallogeny of the northern Norrbotten Fe-Cu-Au province. In, R.L Allen, O. Martinsson & P. Weihed (Eds.): *Svecofennian Ore-Forming Environments: Volcanic-associated Zn-Cu-Au-Ag, intrusion associated Cu-Au, sediment-hosted Pb-Zn, and magnetite-apatite deposits in northern Sweden. Society of Economic Geoology, Guidebooks Series 33,* 131–148.

Martinsson, O., Vaasjoki, M. & Persson, P.-O., 1999: U-Pb ages of Archaean to Palaeoproterozoic granitoids in th e Torneträsk-Råstojaure area, northern Sweden. *In:* S. Bergman (ed.): *Radiometric dating results 4. Sveriges geologiska undersökning C 831,* 70–90.

Nyström, J.O., 1982: Post-Svecokarelian Andinotype evolution in central Sweden. *Geologische Rundschau 71,* 141–157.

Ödman, O., 1957: Beskrivning till Bergrundskarta över Norrbottens Län. *Sveriges geologiska undersökning Ca 41,* 151 pp.

Öhlander, B. & Skiöld, T., 1994: Diversity of 1.8 Ga potassic granitoids along the edge of the Archaean craton in northern Scandinavia: a result of melt formation at various depths and from various sources. *Lithos 33,* 265–283.

Öhlander, B., Hamilton, P.J., Fallick, A.E. & Wilson, M.R., 1987: Crustal reactivation in northern Sweden: the Vettasjärvi granite. *Precambrian Research 35,* 277–293.

Öhlander, B., Skiöld, T., Hamilton, P.J. & Claesson, L.-Å., 1987: The western border of the Archaean province of the Baltic Shield: evidence from northern Sweden. *Contributions to Mineralogy and Petrology 95,* 437–450.

Pearce, J.A., 1982: Trace element characteristics of lava from destructive plate boundaries. *In:* R.S. Thorpe (ed.): *Andesites, Wiley,* 525–548.

Pearce, J.A., Harris, N.B.W. & Tindle, A.G., 1984: Trace element discrimination diagrams for the tectonic interpretation of granitic rocks. *Journal of Petrology 25,* 956–983.

Romer, R.L., Kjösnes, B., Korneliussen, A., Lindahl, I., Skysseth, T., Stendal, H. & Sundvoll, B., 1992: The Archaean-Proterozoic boundary beneath the Caledonides of northern Norway and Sweden: U-Pb, Rb-Sr and Nd isotopic data from the Rombak-Tysfjord area. *Norges Geologiske Undersøkelse, Rapport 91, (225),* 67 pp.

Romer, R.L., Martinsson, O. & Perdahl, J.-A., 1994: Geochronology of the Kiruna iron ores and hydrothermal alterations. *Economic Geology 89,* 1249–1261.

Sarlus, Z., Andersson, U.B., Bauer, T.E., Wanhainen, C., Martinsson, O., Nordin, R. & Andersson, J.B.H., 2017: *Timing of plutonism in the Gällivare area: Implications for Proterozoic crustal development in the northern Norrbotten ore district, Sweden.* Geological Magazine, 1–26. doi:10.1017/S0016756817000280.

Skiöld, T., 1988: Implications of new U-Pb zircon chronology to early Proterozoic crustal accretion in northern Sweden. *Precambrian Research 38,* 147–164.

Skiöld, T., Öhlander, B., Vocke, R.D. & Hamilton, P.J., 1988: Chemistry of Proterozoic orogenic processes at a continental margin in northern Sweden. *Chemical Geology 69,* 193–207.

Skiöld, T., Öhlander, B., Markkula, H., Widenfalk, L. & Claesson, L.-Å., 1993: Chronology of Proterozoic orogenic processes at the Archaean continental margin in northern Sweden. *Precambrian Research 64,* 225–238.

Stacey, J.S. & Kramers, J.D., 1975: Approximation of terrestrial lead isotope evolution by a two-stage model. *Earth and Planetary Science Letters 26,* 207–221.

Steiger, R.H. & Jäger, E., 1977: Convention on the use of decay constants in geo- and cosmochronology. *Earth and Planetary Science Letters 36,* 359–362.

Turner, D.T., 1963: Ring-structures in the Saara-Fier younger granite complex, northern Nigeria. *Quarterly Journal of the Geological Society of London 119,* 345–366.

Upton, B.G.J., 1988: History of Tertiary igneous activity in the N Atlantic borderlands. *In:* A.C. Morton & L.M. Parson (eds.): *Early Tertiary volcanism and the opening of the NE Atlantic. Geological Society, Special Publication 39,* 429–453.

Westin, T., 1983: Slutrapport, projekt 4016, Geofysisk tolkning av Karijärvi-strukturen. *Unpublished Report, LKAB Prospektering AB, Ki 09-83,* 3 pp.

Whalen, J.B., Currie, K.L. & Chappell, B.W., 1987: A-type granites: geochemical characteristics, discrimination and petrogenesis. *Contribution to Mineralogy and Petrology 95,* 407–419.
Whitehouse, M.J., Claesson, S., Sunde, T. & Vestin, J., 1997: Ion-microprobe U–Pb zircon geochronology and correlation of Archaean gneisses from the Lewisian Complex of Gruinard Bay, north-west Scotland. *Geochimica et Cosmochimica Acta 61,* 4429–4438.
Whitehouse, M.J., Kamber, B.S. & Moorbath, S., 1999: Age significance of U–Th–Pb zircon data from Early Archaean rocks of west Greenland: a reassessment based on combined ion-microprobe and imaging studies. *Chemical Geology (Isotope Geoscience Section) 160,* 201–224.
Whitehouse, M., J. & Kamber, B.S., 2005: Assigning dates to thin gneissic veins in high-grade metamorphic terranes: A cautionary tale from Akilia, Southwest Greenland. *Journal of Petrology 46,* 291–318.
Wikström, A & Söderman J., 2000: Bedrock map 24L Luleå NV, scale 1:50 000. *Sveriges geologiska undersökning Ai 152.*
Wilson, M.R., 1980: Granite types in Sweden. *Geologiska Föreningens i Stockholm Förhandlingar 102,* 167–176.
Wilson, M.R., Hamilton, P.J., Fallick, A.E., Aftalion, M. & Michard, A., 1985: Granites and early Proterozoic crustal evolution in Sweden: evidence from Sm-Nd, U-Pb and O isotope systematics. *Earth and Planetary Science Letters 72,* 376–388.
Wilson, M.R., Fallick, A.E., Hamilton, P.J. & Persson, L., 1986: Magma sources for some mid-Proterozoic granitoids in SE Sweden: geochemical and isotope constraints. *Geologiska Föreningens i Stockholm Förhandlingar 108,* 79–91.
Wiedenbeck, M., Allé, P., Corfu, F., Griffin, W.L., Meier, M., Oberli, F., Quadt, A.V., Roddick, J.C. & Spiegel, W., 1995: Three natural zircon standards for U-Th-Pb, Lu-Hf, trace element and REE analyses. *Geostandards Newsletter 19,* 1–23.
Wiedenbeck, M., Hanchar, J.M., Peck, W.H., Sylvester, P., Valley, J., Whitehouse, M., Kronz, A., Morishita, Y., Nasdala, L., Fiebig, J., Franchi, I., Girard, J.P., Greenwood, R.C., Hinton, R., Kita, N., Mason, P.R.D., Norman, M., Ogasawara, M., Piccoli, P.M., Rhede, D., Satoh, H., Schulz-Dobrick, B., Skår, O., Spicuzza, M.J., Terada, K., Tindle, A., Togashi, S., Vennemann, T., Xie, Q. & Zheng, Y.F., 2004: Further characterisation of the 91500 zircon crystal. *Geostandards and Geoanalytical Research 28,* 9–39.
Witschard, F., 1970: Description of the geological maps Lainio NV, NO, SV, SO. *Sveriges geologiska undersökning Af 13–16,* 116 pp.
Witschard, F., 1984: The geological and tectonic evolution of the Precambrian of northern Sweden – a case for basement reactivation? *Precambrian Research 23,* 273–315.

Authors, paper 13:
Anna Ladenberger
Geological Survey of Sweden,
Department of Mineral Resources,
Uppsala, Sweden

Madelen Andersson
Geological Survey of Sweden,
Department of Mineral Resources,
Uppsala, Sweden

Colby Smith
Geological Survey of Sweden,
Department of Physical Planning,
Uppsala, Sweden

Mikael Carlsson
Geological Survey of Sweden,
Department of Mineral Resources,
Uppsala, Sweden

13. Till geochemistry in northern Norrbotten – regional trends and local signature in the key areas

Anna Ladenberger, Madelen Andersson, Colby Smith & Mikael Carlsson

ABSTRACT

2 316 new till geochemistry analyses are presented. Together with pre-existing data, they provide an overview of natural element concentrations in overburden within the Barents region. The primary influence on till geochemistry is the composition of underlying bedrock. Transport distances in Norrbotten are generally low (5–10 km maximum), allowing till composition to be used as a good analogue for the often poorly exposed bedrock. Correlation of anomalies with known ore deposits shows the value of this data as a preliminary exploration tool. Anomalies related to both glacial and post-glacial reworking can be recognised, as well as a distinct depletion of many elements in the southeast of the area due to inundation by seawater in the immediate post-glacial period. In the Key Areas additional samples were collected with higher sample density than on a regional scale. Elevated concentrations of many elements were obtained and correlated with the location of Fe, Cu and Au mineralisation, as well as zones of intense alteration.

INTRODUCTION

In addition to geological mapping and geophysical surveys, extensive till geochemical mapping was carried out in the Barents Project. Glacial till has been used as a sampling medium in geochemical surveys for decades. As a widespread Quaternary deposit in high latitudes (till covers approximately 75% of the land surface in Sweden) it usually well reflects the underlying bedrock, which is not always well exposed and cannot be accessed and studied. This chapter is devoted to till geochemistry, including sampling strategy, analytical protocol, results and their interpretation in the regional (Norrbotten) and local (key areas) contexts.

Under the Barents Project, 2 300 till samples were collected from previously unmapped areas during field campaigns in 2012 and 2013 (Fig. 1). Earlier, the southern, eastern and central parts of Norrbotten, which have better road infrastructure, were sampled and analysed during SGU's regional mapping programme (1993–1995, 1998–2003, 2005–2007, 2009 and 2011–2012). A nominal sampling density of one sample per 6.5 km^2 was maintained.

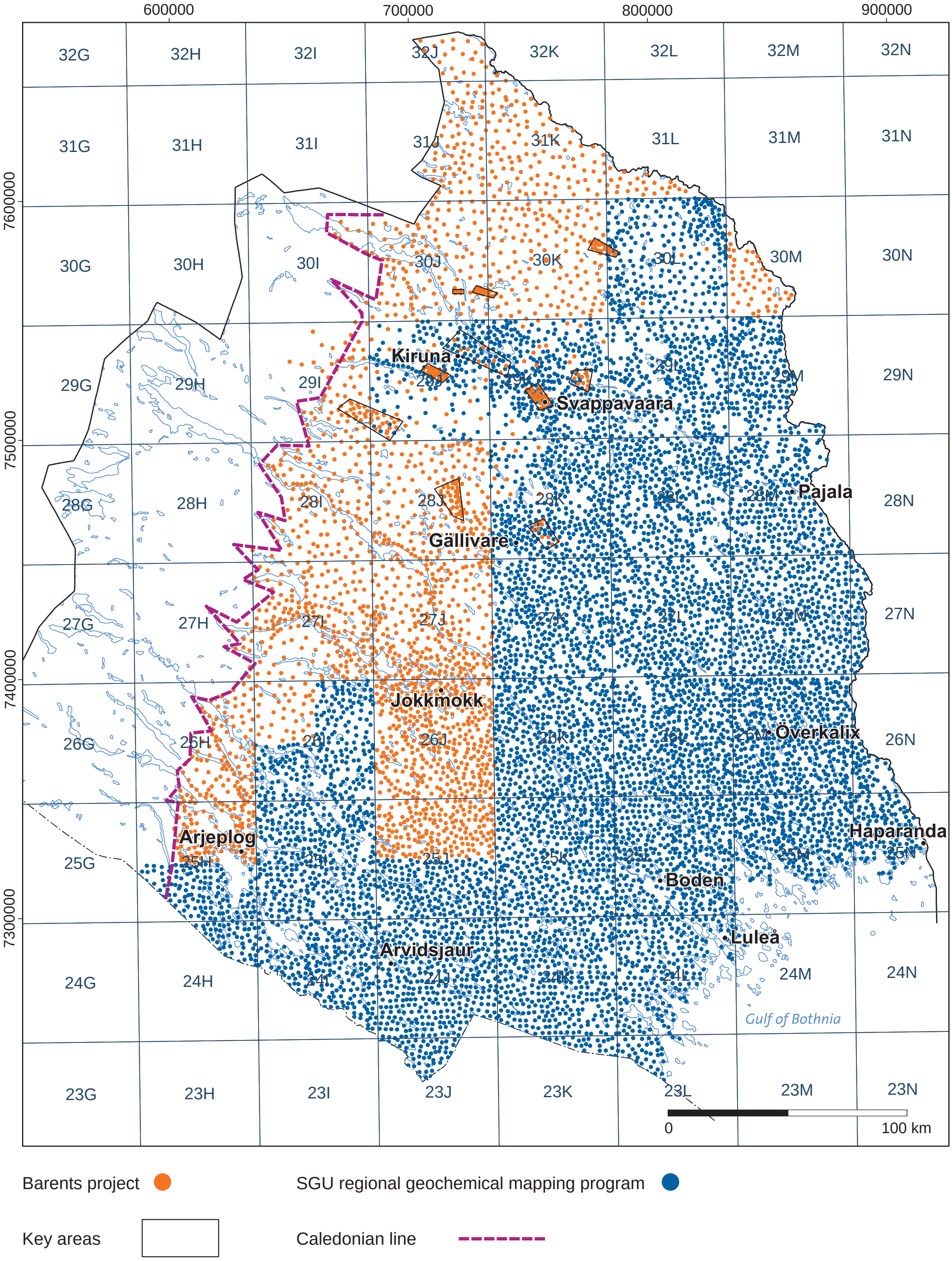

Figure 1. Sampling sites in Norrbotten from various field campaigns. Till samples collected under the Barents Project are marked in orange. Key areas (the subject of detailed geological and geochemical investigations) are outlined in black.

The results from the Nordkalott Project (sampled in 1981 and 1983; Bölviken et al. 1986) and the NSG/SGAB (Nämnden för Statens Gruvegendom/Sveriges Geologiska AB) database have also been used for regional interpretation.

The use of various methods for more than 30 years of different surveys, insufficient and varied quality control protocols and rapid improvements in analytical techniques have resulted in rather inhomogeneous datasets, thereby hampering a quantitative interpretation of the Norrbotten region. At local scale, however, the results perform satisfactorily and more quantitative methods can be used to evaluate the geochemical patterns and trends.

In general, geochemical results obtained during surveys described here show natural variation of element concentrations in till and provide reliable background levels of major and trace elements as well as pH. These can be used for evaluation of groundwater quality, availability of nutrients, for mineral exploration, for assessments of the weathering grade etc.

GLACIAL GEOMORPHOLOGY AND QUATERNARY STRATIGRAPHY OF NORRBOTTEN

Information on the Quaternary geology of northern Sweden was compiled as part of the Nordkalott Project, a collaborative effort involving the geological surveys of Finland, Norway, and Sweden. The project produced a series of five 1:1 000 000 scale maps of the Quaternary deposits, glacial geomorphology, ice flow indicators, Quaternary stratigraphy, and ice flow directions (Nordkalott Project 1986a, b, c, d). While the Nordkalott maps provide an excellent overview of the region, more detailed (1:100 000 and 1:250 000 scale) maps of Quaternary deposits have been produced by the Geological Survey of Sweden (SGU digital database). Together, these map series provide the framework to interpret the glacial geomorphology and Quaternary stratigraphy of the study area (Fig. 2A and B).

Although tills from the previous glacial cycle – the Saalian – are sometimes encountered in excavations, most of the glacial landforms in northern Sweden date from the most recent glacial cycle, the Weichselian. During the Weichselian, ice advanced across northern Sweden several times. In the early Weichselian, ice advanced from the northwest, creating well-defined streamlined glacial landforms (Lagerbäck & Robertsson 1988). During the retreat of the early Weichselian ice sheet margin, there was an extended period of ice stagnation. This led to deposition of stagnant ice and associated water-lain sediments across large portions of northern Sweden (Lagerbäck 1988a). Collectively, these deposits are known as Veiki Moraine and are best expressed in a 30–50 km wide zone of hummocky topography that extends northeast to southwest along the entire length of Norrbotten (Lagerbäck & Robertsson 1988).

Following this ice-free period, stratigraphical evidence indicates at least two (Lagerbäck 1988a, Lagerbäck 1988b, Lagerbäck & Robertsson 1988) and perhaps three (Helmens et al. 2007) subsequent periods of ice advance in Norrbotten. But large areas of southern and central Norrbotten contain little geomorphic evidence of middle and late Weichselian ice advance(s) because of largely non-erosive frozen-bed conditions at the base of the ice. This lack of glacial reworking often causes middle and late Weichselian landforms to be undifferentiated from each other (Nordkalott Project 1986a, b, c, d). Ice flow during these periods was from the west and southwest.

Frozen-based glacial conditions may not have been limited to the Weichselian. It has been suggested that a landscape in northern Norrbotten is not of glacial origin. Thus, it must predate the Quaternary Period (Hättestrand & Stroeven 2002). The widespread presence of saprolites supports this hypothesis. Subsequent work has shown that this is not an isolated case. Landscapes interpreted to contain components more than 1 million years old persist throughout the far north of Sweden (Hall et al. 2013).

Glacial stratigraphy often changes dramatically over just a few hundred lateral metres. The patchwork of frozen-based and wet-based conditions beneath Weichselian ice sheets in northern Sweden exacerbates this phenomenon. Thus, descriptions of regional stratigraphy based on relatively few point

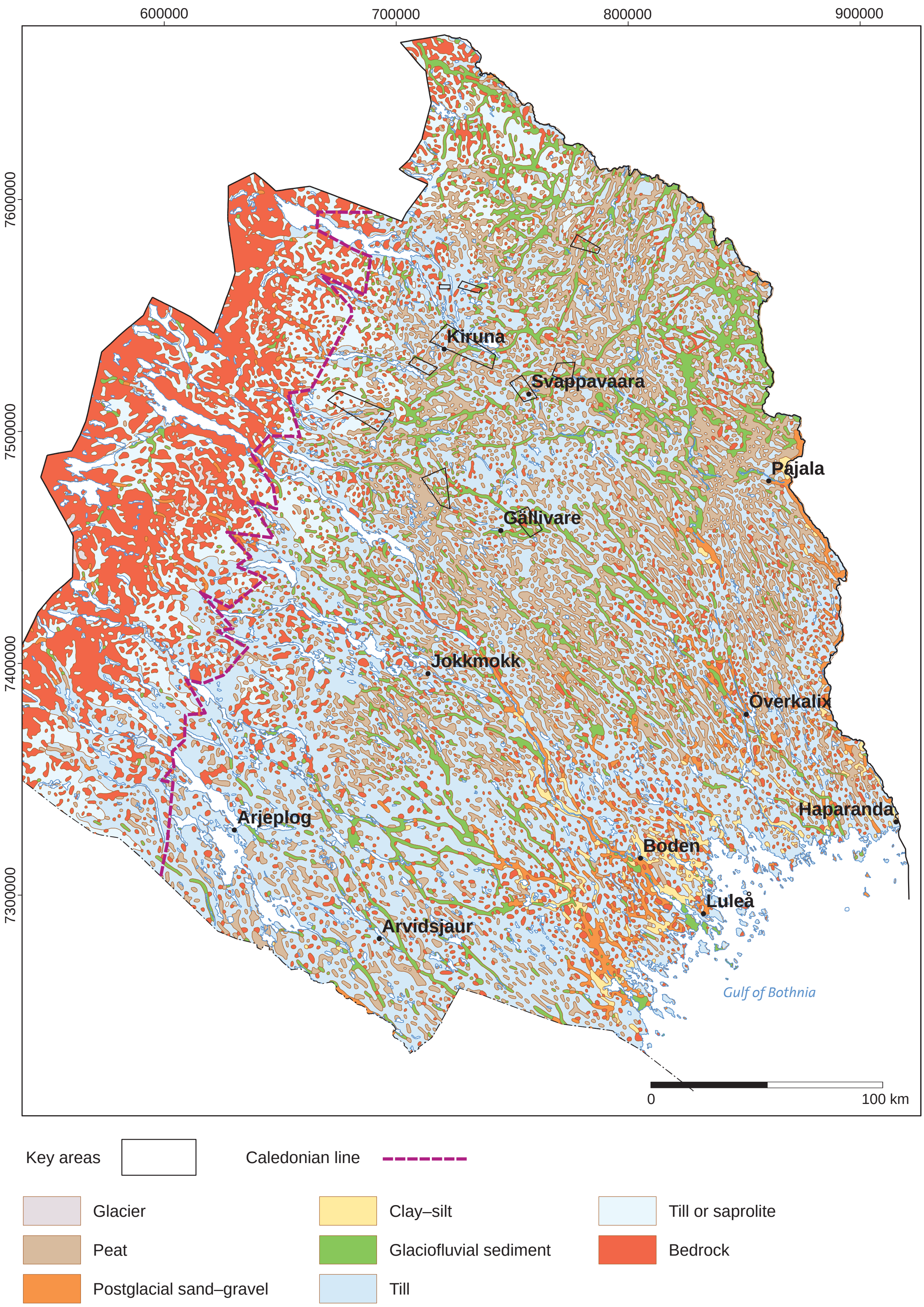

Figure 2. **A.** Quaternary map of Northern Sweden.

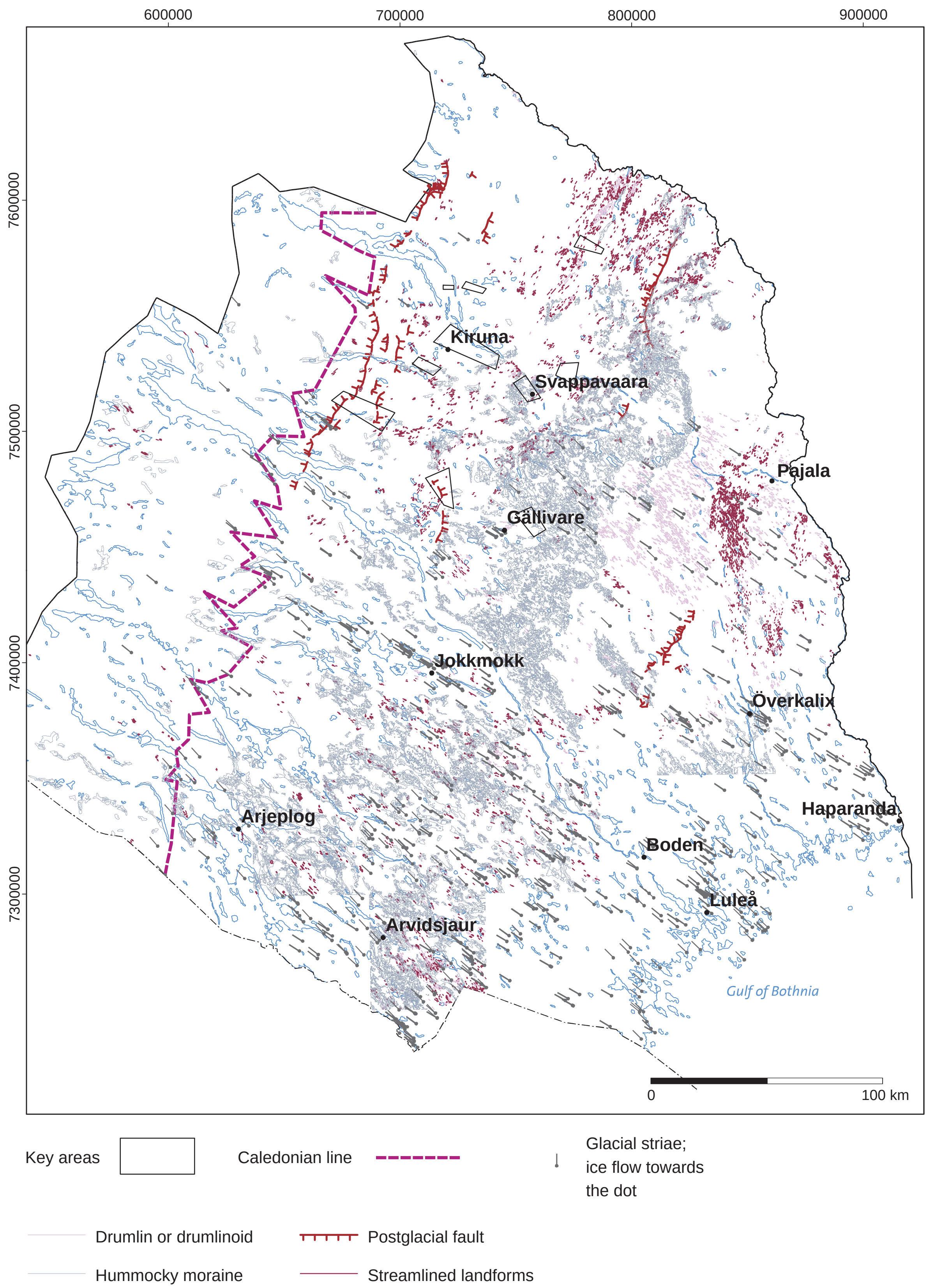

Figure 2. **B.** Major features of glacial and periglacial morphology of Northern Sweden (modified from SGU digital database).

observations should be viewed with caution. With that warning in place, an idealised stratigraphy in an excavated trench in northern Sweden may include the following units from the bottom up: saprolite, Saalian till, early Weichselian till, middle Weichselian till, and late Weichselian till. The till units are often, but not always, separated from each other by either organic or clastic water-lain sediments.

Following the retreat of the late Weichselian ice, water from the Gulf of Bothnia covered much of eastern Norrbotten due to depression of the crust caused by the mass of the ice sheet. Thick deposits of clay and silt were deposited over these submerged areas. Subsequently, the land surface rebounded, leading to a regional transgression. These large vertical displacements of the crust also contributed to reactivation of pre-existing faults immediately following deglaciation (Lagerbäck & Sundh 2008).

SAMPLES AND METHODS

Since the 1980s, several sampling campaigns have been carried out both by SGU and exploration companies in Norrbotten County. This has resulted in relatively good coverage of geochemical data for the fine fraction (<0.06 mm) of till. The Nordkalott Project (1980–1986) delivered total concentrations for 11 elements analysed using optical emission spectrometry (OES) and 16 elements using neutron activation analysis (NAA). In addition, total concentrations of 25 elements in heavy mineral fractions (>2.96 g/cm^3, 0.06–0.5 mm) from till were obtained. In this chapter, we use chlorine results from that survey (Fig. 7). Field campaigns carried out by NSG/SGAB delivered results for 34 elements obtained by aqua regia extraction, but they only cover the western part of county.

Sampling and preparation

As part of the Barents Project, 2 316 till samples were hand-dug from the C horizon at a depth of approximately 0.6–1.1 m. At this depth, till is generally not disturbed by intense weathering or anthropogenic activities (Fig. 3). The sampling grid varies, from a routine grid of 1 sample per 6.5 km^2 in areas with easy access, to 1 sample per 18 km^2 in remote areas sampled from a helicopter.

Figure 3. Typical sampling site of till C horizon in Norrbotten.

Sandy till predominates, especially in areas above the highest coastline, but till can vary from clayey to coarse-grained. Approximately 0.8 kg of sample was collected, vacuum dried (56 °C) and sieved with a nylon screen to a fine fraction of <63 µm.

Chemical analyses

Two partial-leach methods have been used for the fine fraction of till (<63 µm): nitric acid leach (2 g of the till sample) and aqua regia leach (5g of the till sample). Both leachate types were analysed by ICP-MS at the SGU geochemical laboratory. Samples were analysed in random order to avoid systematic error. Duplicates and internal standards were used for quality control and to monitor instrument drift.

The nitric acid (7M HNO_3) method provides results for 52 elements: Ag, Al, As, B, Ba, Be, Bi, Ca, Cd, Ce, Co, Cr, Cu, Dy, Er, Eu, Fe, Ge, Gd, Ho, K, La, Li, Lu, Mg, Mn, Mo, Na, Nb, Nd, Ni, P, Pb, Pr, Rb, Sc, Se, Sm, Sn, Sr, Tb, Th, Ti, Tl, Tm, U, V, W, Y, Yb, Zn and Zr; the aqua regia method provides results for 13 elements: Ag, As, Au, Bi, Cd, Cu, Mo, Rh, Sb, Sn, Ta, Te and U. In practice, the aqua regia method is specifically designed for measuring Au, Rh, Sb, Ta and Te concentrations. More details of the methodology can be found in Morris & Ladenberger (2017). Depending on the type of leachate, element analysed and mineralogy of the sample, the efficiency of the leaching procedure varies from almost 100% (e.g. Cu, As, Cd) to <1% (e.g. Na, Zr).

Alkalinity (pH) was obtained from 4 grams of till sample (<63 µm), which was mixed with 20 ml deionised water (MilliQ®). After 48 hours, pH was determined by a Radiometer CDM83 electrode on a MeterLab® pHM240 system at SGU.

Combining various datasets often results in data quality and element levelling difficulties. Regional maps presented in this chapter should thus be treated as 'trend' maps, where the accurate element concentrations may vary due to the different analytical techniques used, or longer time-span between the series analysed.

RESULTS AND DISCUSSION

Regional distribution patterns in till

Quaternary history of glaciations and deglaciations reflected in till geochemistry

Although the major geochemical signature in till originates from the parent materials, there is a substantial influence on till chemical composition due to surficial processes such as till deposition, stratigraphy, age, till fraction, water activity and resulting sorting and transport with glacial meltwater, and other factors. The general spatial distribution of geochemical anomalies is controlled by ice movement directions and till transport distances. Ice directions have a rather complex pattern in northern Sweden, with prevailing ice flow from the west and southwest during the middle and late Weichselian and ice directions from the northwest during the early Weichselian. The major shift in ice directions is indicated by the ice divide observed in the central part of the project area. The NW–SE orientation of some geochemical anomalies (e.g. Ag, Cu, Na) in Norrbotten is consistent with predominant ice directions and the shape of glacial landforms such as eskers and drumlins.

Since ice in northern Sweden was frozen to the base for most of the time during glaciations, erosion-free conditions are assumed and the transport distances in most places are insignificant (Hättestrand & Stroeven 2002, Sohlenius et al. 2009, Lagerbäck 1988a). Along river valleys and postglacial lakes stretching from the Caledonian front in the west towards the Fennoscandian Shield in the east, till could have been transported further, however, and geochemical signatures in till can be influenced by material transported from the mountains.

During ice retreat and transgression of Baltic waters, submerged land and surface deposits were intensively reworked and till chemistry was modified. In southeast Norrbotten, where the deposition of clay and silt occurred, leaching of many elements resulted in depleted concentrations of Ag, Al, Ba, Be, Co, Cu, Fe, Mg, Mn, Na, Ni, P, Pb, REEs, Sr, Th, Ti, Y and Zn in exposed till, as well as some elements traditionally considered immobile, such as Ti and Y (Fig. 4). Additionally, development

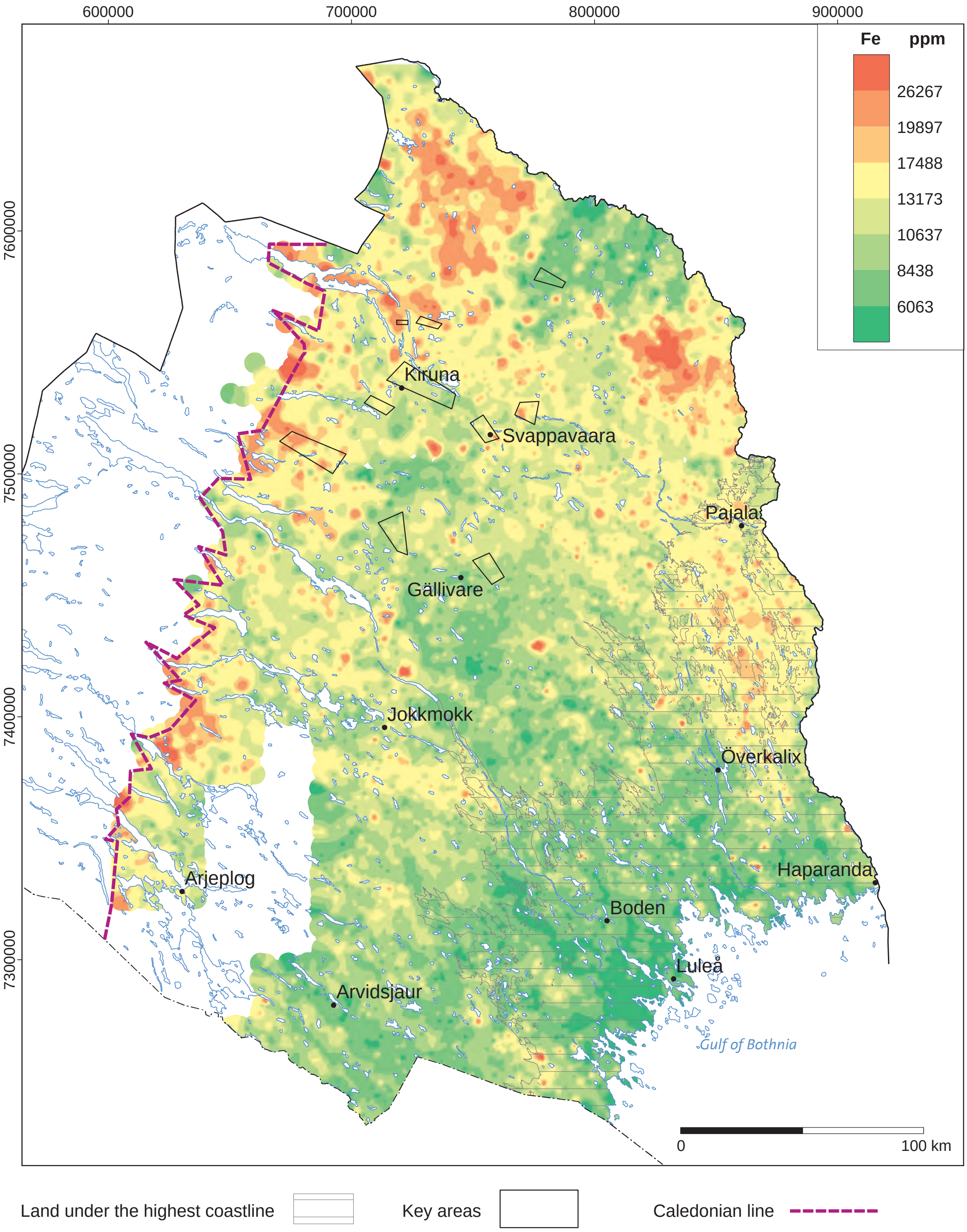

Figure 4. Fe in till (HNO_3 leach by ICP MS). The spatial distribution of Fe and several other elements reflects large morphological structures related to the Quaternary history of Norrbotten, e.g. leaching processes under the highest coastline.

of low pH (on average below 5) contributed to reduced concentrations of most metals (Ladenberger et al. 2014).

Similar depletion of many elements (Al, Ba, Be, Co, Cu, Fe, Li, Mg, Mn, Ni, Pb, REEs, Ti, Y and Zn) can be observed in NE Norrbotten (30 L map sheet Lannasvaara) within the "Kiruna fan" (Hätterstrand et al. 2004). The streamlined glacial landforms in this area date to the late Weichselian and indicate warm-based glacial conditions. The most viable explanation for the depletion of elements is intense glacial reworking of an older landscape, leading to removal and transport of elements (Fig. 4). On the SE side of the anomalous area lies the early Weichselian ablation till complex known as the Veiki moraine, and the associated end moraine known as the Lainio arc. The Lainio arc can be followed in the geochemical pattern of several elements, e.g. Ca and Na. The fact that Veiki moraine landforms have been preserved beneath at least two subsequent ice sheets confirms limited erosion and frozen-bed conditions in the area during the middle and late Weichselian. These conditions would limit reworking and transport of material from west to east.

Other areas with frozen-bed conditions and relict landforms (including drumlins and eskers transverse to the youngest ice flow direction) also experienced limited erosion beneath the late Weichselian ice sheet. For example, the geochemistry of till in the Pajala region was less affected than in areas of erosive wet-based conditions (Hätterstrand & Stroeven 2002).

To an extent, high or low metal content correlates with local pH (Fig. 5) and presence of organic matter (e.g. in peat regions). At low pH, elements like Cd, Co, Cu, Fe, Pb, Mg, Mn, Ni, P, Tl and Zn can be mobilised and redeposited to other depths or places, or released into ground and surface water.

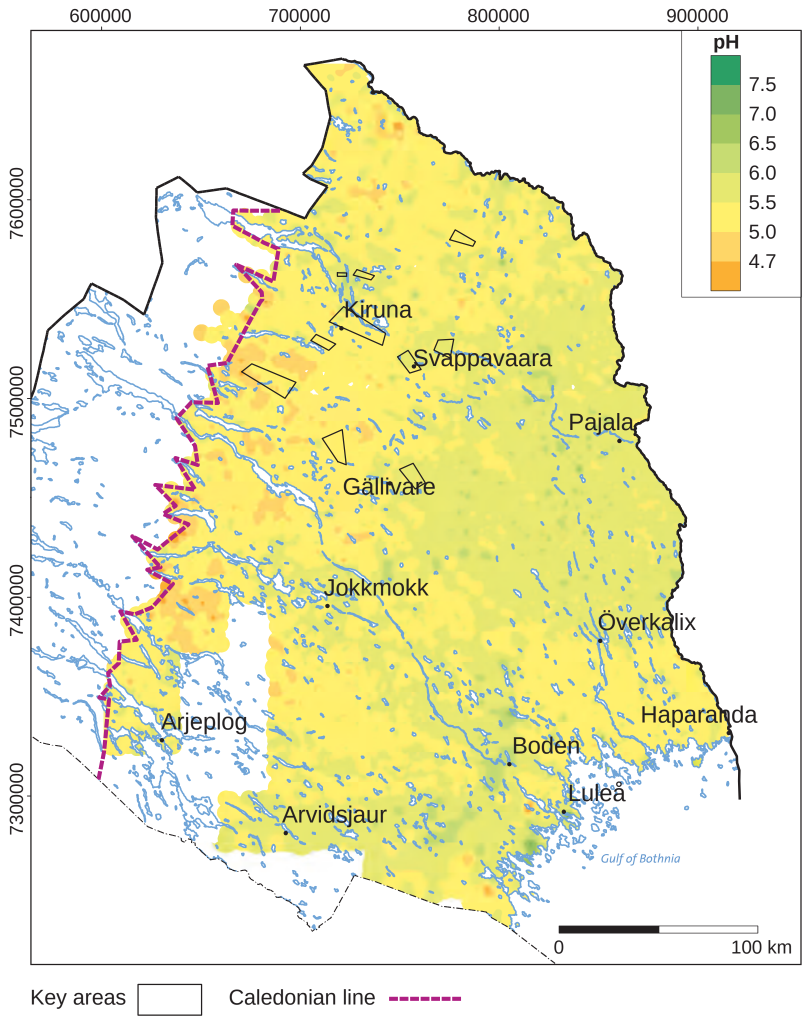

Figure 5. pH in till (source: Geochemical Atlas of Sweden).

Influence of underlying bedrock lithology, metamorphism and alteration of bedrock on till geochemical composition

The type of the parent material has the greatest influence on the geochemical composition of till, which is commonly either older till or the underlying bedrock. In most cases, when the basal till is sampled, transport of till can be ignored. In Norrbotten, ice transport distances are generally short, but can be up to 5–10 km. This distance is estimated from block train counting, a method commonly used by exploration companies (Sohlenius et al. 2009). But the fine-grained fraction of till has been shown to have greater transport distances than pebbles (Klassen, 1999). The main advantage of till sampling in glaciated areas is the opportunity to obtain indirect information about the underlying bedrock, including regions without available outcrops, and covered by large peat bogs.

In the Barents Project study area the contrast between distribution of silica-rich (e.g. granitoids, pegmatites, rhyolites) and silica-poor magmatic rocks (e.g. gabbro, basalt, peridotite) can be easily observed (Fig. 6). Silica-rich intrusive rocks are usually a source of elevated concentrations of Al, Ba, Be, K, Na, Rb, REEs, U, Th and Zr in till, whereas silica-poor (mainly mafic) rocks give high concentrations of Mg, Ca, Co, Cr, Cu, Fe, Mg, Mn, Ni, Ti and V. Minor U and Th anomalies in till usually correspond to granites and pegmatites of the Haparanda and Lina types.

Till overlying metasedimentary rocks occurs in the west (by the Caledonian front, i.e. Stora Sjöfallet region) and in the east (south of Pajala) of the mapped area. This till has a similar chemical signature to till overlying granitic rocks. Occurrences of graphite-bearing metasedimentary rocks are reflected in till geochemistry by local anomalies of B, Co, Pb and V. The geochemical signature of volcanosedimentary complexes with intercalated sediments mainly comprises the volcanic members (e.g. Cr, Co, Ni, Mg, Fe, P, Ti, V) and the presence of limestone and dolomite (e.g. Ca, high pH).

In Norrbotten's till, concentrations of elements typically associated with felsic volcanic rocks (e.g. As, Bi, Cd, K, Mo, Pb, Rb, Sb, Se, Sn, Tl, W and Zr) are lower than the country's median values. However, a handful of elements (P, Ti and V) are enriched in till, their background values being the highest in Sweden (for comparison see Geochemical Atlas of Sweden by Andersson et al. 2014).

Archaean rocks, which are exposed in the northernmost part of the project area, tend to have a distinct geochemical signature in till as compared with the area with predominantly Palaeoproterozoic parent materials. Enrichment in Ba, Mn, Ni, Pb, Rb, Sr, Tl, LREEs and Zn, and depletion in Na, Zr, HREEs, U can be observed in the Archaean terrain, for example.

Till chemistry in the west and northwest of the area is influenced by material transported from the Caledonide mountain belt.

A notable characteristic feature of Norrbotten soil geochemistry is very high chlorine concentrations in till. This large Cl anomaly extends diagonally NW to SE across the area studied and correlates with a positive sodium anomaly. It overlaps with the extent of Palaeoproterozoic metavolcanic complexes (greenstone belts). Its origin has been attributed to the widespread scapolitisation of intrusive and supracrustal rocks belonging to the greenstone belts, such as the Kiruna Greenstone Belt. Scapolite is rare in the Archaean domain (Bergman et al. 2001). In general, alterations related to metamorphism and hydrothermal processes such as scapolitisation, albitisation, carbonatisation, and skarn formation can be reflected in enrichment in Ba, Ca, Cl, K, Na, Sr, La, Rb and P (Fig. 7). Such anomalies can occur locally (Ba, Sr, K, La, As) or regionally (P, Cl and Na), and often overlap with the location of known mineralisations (Ladenberger et al. 2012).

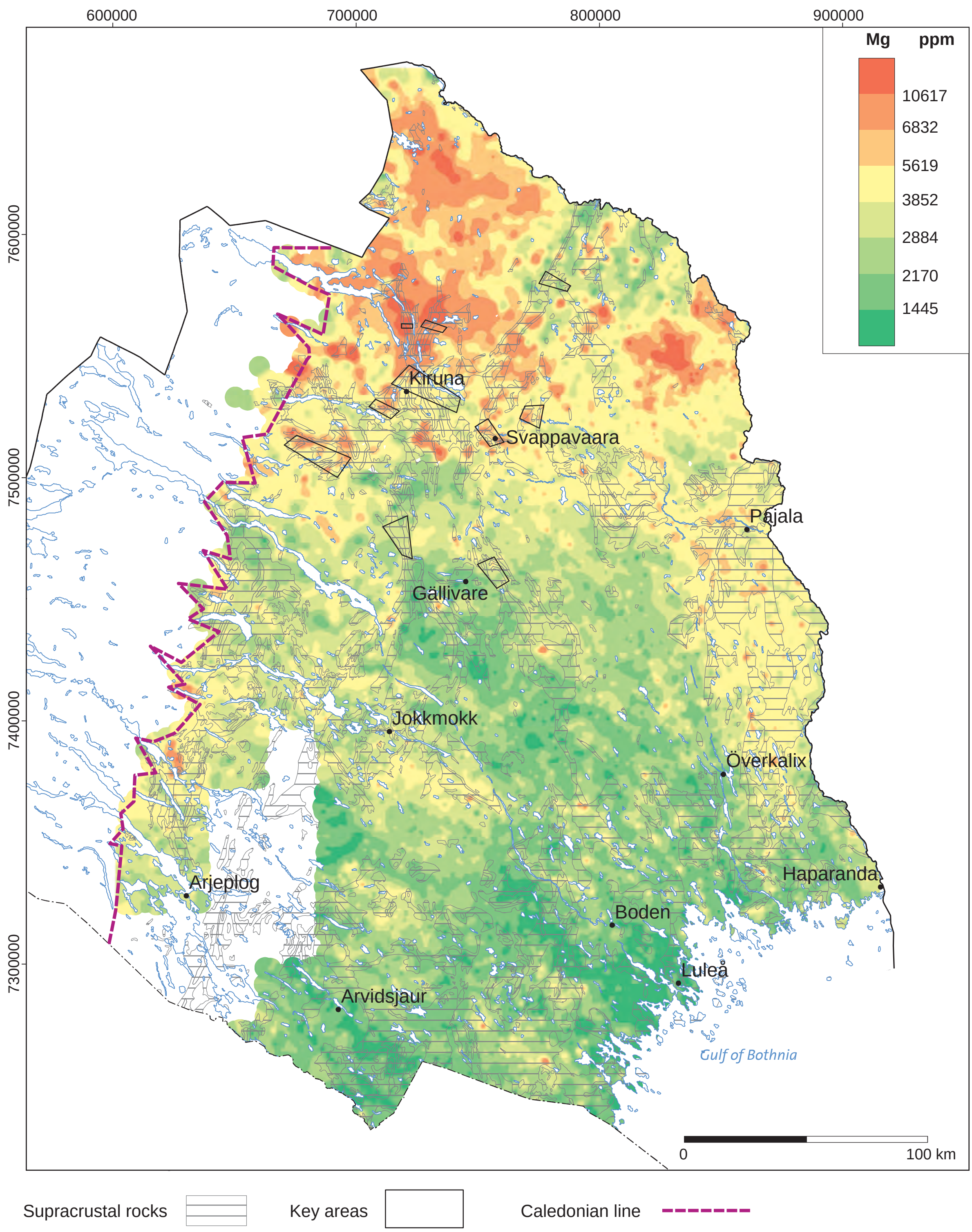

Figure 6. Major lithotectonic units reflected in Mg anomalies in till. Volcano-sedimentary units (greenstone belts) are clearly outlined by anomalously high concentrations of Fe, Ni, Co and Cu in till.

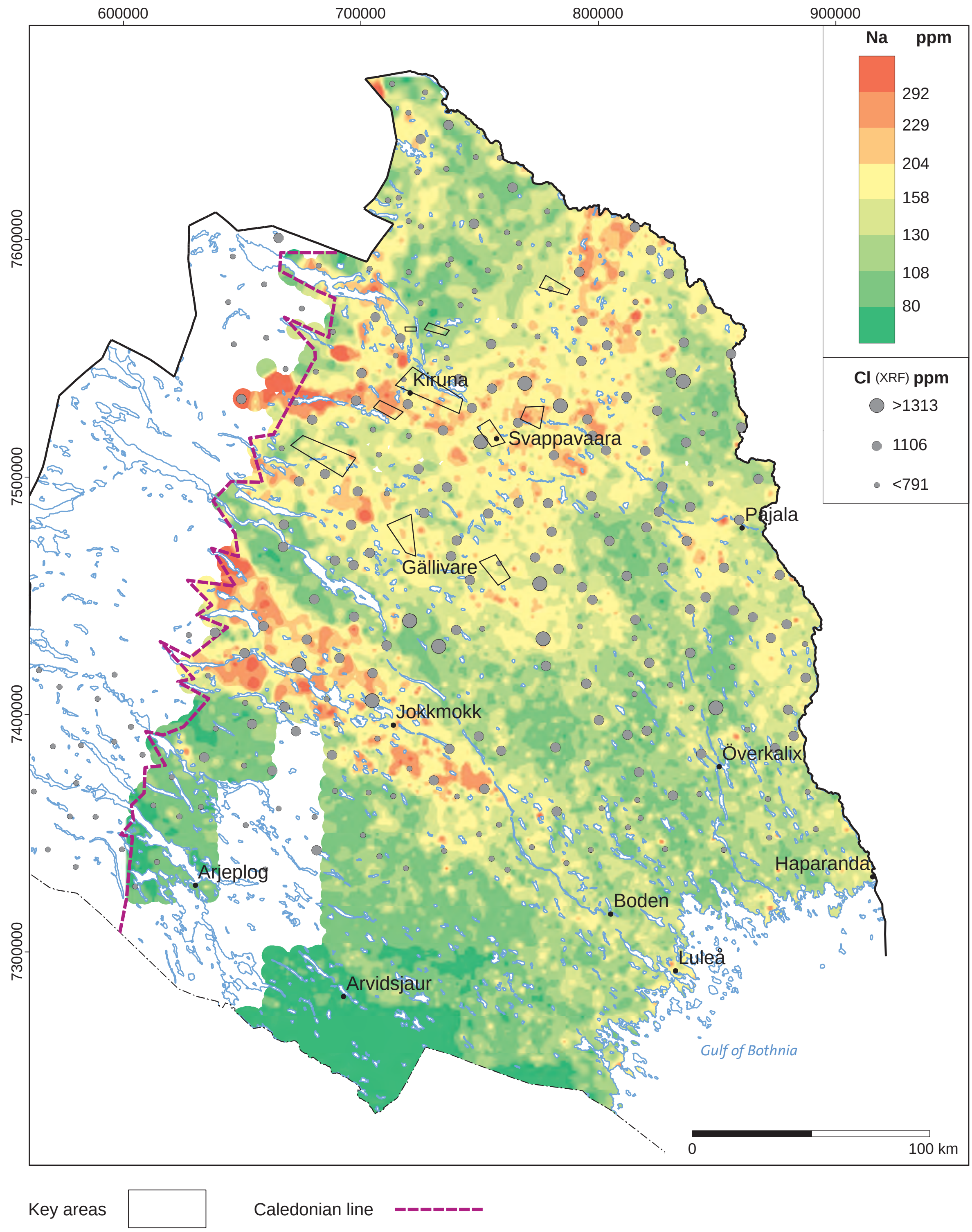

Figure 7. Na (HNO_3 leach by ICP MS) and Cl (XRF) anomalies reflect regional alteration zones with scapolitisation, which predominantly affects metavolcanic units.

Mineralisations and their impact on till geochemical anomalies

The Barents Project study area is one of Sweden's major ore districts, with active iron mines at Kiruna and Malmberget, and a copper-silver-gold mine at Aitik. Apart from these active mines, there are many deposits that have previously been mined, and a large number of mineralisations are known in the region. Most of the mineral deposits are located within metavolcanic units of the greenstone belts and represent both iron-oxide type and sulphide deposits (Martinsson & Wanhainen 2013).

Major types of deposit are loosely classified as: iron oxide copper gold types (IOCG) e.g. iron formations, including typical Banded Iron Formation deposits (BIF, e.g. Törnefors); stratiform Cu-Fe deposits (e.g. Viscaria); Kiruna-type Fe oxide-apatite ores (e.g. Kiirunavaara, Malmberget); intrusion-related Cu-Au mineralisation (e.g. Aitik); and shear- or vein-style Cu-Au deposits (e.g. Nautanen). Some minor Mo occurrences are hosted by Archaean granites (Bergman et al. 2001).

Till geochemistry has been used in mineral exploration in glaciated areas for decades and has contributed to the discovery of many ore deposits of high economic value. Till sampling and analyses are cheaper and logistically less demanding than drilling. This methodology is therefore widely used in ore prospecting, mainly in the northern hemisphere, i.e. Scandinavia, Russia, Canada and Greenland.

Since the occurrence of major ore deposits is limited to areas with mafic to intermediate metavolcanic and volcanoclastic rocks, their locations overlap with large positive regional geochemical anomalies in till for elements such as Co, Cr, Fe, Mg, Ni, V and Ti (Fig. 8). Sulphide mineralisations often coincide with copper, cobalt, molybdenum and lead anomalies in till, the largest copper anomalies being between Kiruna and Vittangi, west of Pajala, and in the Tärendö–Svanstein area.

In central Norrbotten, natural concentrations of As, Ba, Pb, Co, Cu, Cr and V are locally higher than guideline values established for contaminated soil by the Swedish Environmental Protection Agency (Naturvårdsverket). The guideline values are exceeded naturally in, for example, Svappavaara (Ba, Co, Cu and Ni), Pahtohavare (Co, Cr, Cu and Ni), west and north of Kiruna (Co, Ni and Cu), northwest and north of Vittangi (Cu and Co), and in Poulalaki (As, Cu, Cr and V). All these anomalies are situated in the vicinity of known mineralisations. In Kitkiöjärvi and Pessinki concentrations of Ba, Co, Cu, Cr, Ni and V exceed guideline values but no mineralisations have so far been found at those locations.

The spatial distribution of metals associated with mafic magmatic rocks (Co, Cu, Fe, Ni, Ti and V), which constitute the main lithological units in greenstone formations, is as follows:

- The northern part of the study area has higher Co, Ni and Cu than the south, but Co-Cu-Ni enrichment also occurs along the Caledonian front.
- Co, Cu (+Ni) enrichment occurs in greenstone formations hosting numerous Fe-apatite mineralisations, occurring particularly in mafic, silica poor metavolcanic rocks, but also in skarn-type rocks, e.g. in the Kiruna area and in Archaean rocks.
- Co and Cu enrichment can be seen in Harrijärvi, Vittangivaara, Saarijärvi (near Pahtohavare Cu mineralisation), Svappavaara (Kiilavaara Cu-Zn-Pn deposit, Cu Gruvberget, Cu-Mo-Au Särkivaara), Nunasvaara (numerous Cu and Fe mineralisations) Tjårrojåkka–Makkak (near Cu mineralisation), Nautanen (northern part) and in the Akkiskera–Kuormakka key areas.
- Cu anomalies match known Cu mineralisations of various origin, e.g. Tjårrojåkka, Gruvberget, Kallosalmi, Saivo, Pahtohavare, Isovainio, Ferrum, Puolalaki, Tornefors near Tärendo, Marjajärvi near Pajala and Masugnsbyn.
- Ni has almost the same geochemical distribution as Co, with enrichment in greenstone belts with mafic rocks (e.g. gabbro, basalt, serpentinite and amphibolites), in the Archaean rocks in the north (correlates with Fe-oxide and Fe-sulphide mineralisations) and in the SW of the area studied along the Caledonian front. High Ni content in till often occurs in conjunction with Fe-oxide and Fe-sulphide mineralisations.

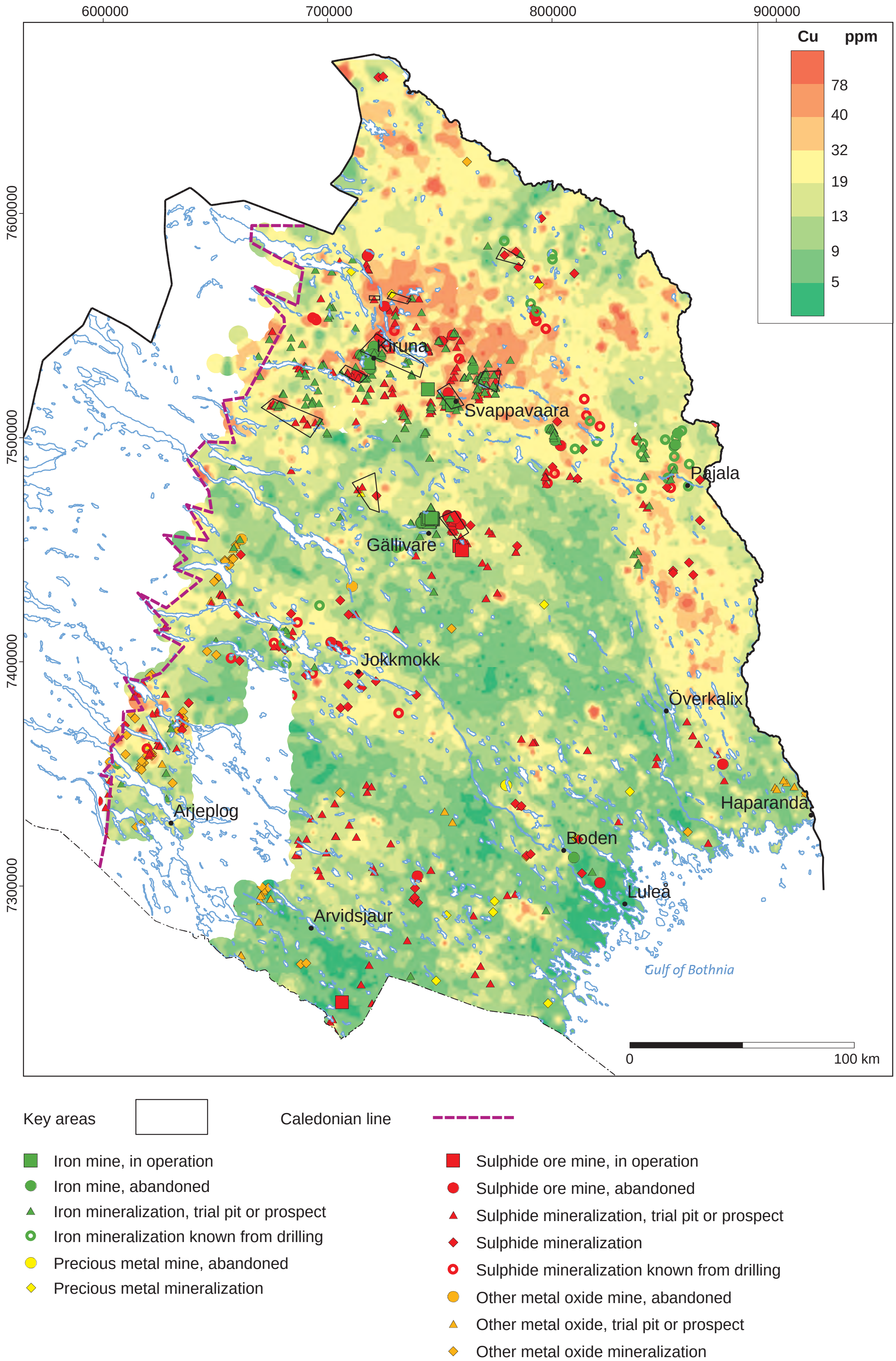

Figure 8. Example of regional trends in Cu (HNO_3 leach by ICP MS) in till pointing to major mineralisation zones in Norrbotten.

- The most prominent geochemical feature of apatite iron ore deposits is high P concentrations in overlying till.
- Ti and V are clearly enriched in Archaean rocks, in eastern and southeastern Norrbotten and in the southwest (NE part of the map sheet 26H – Jäkkvikk) by Lake Tjeggelvas.
- Ti concentrations in till are elevated in the following key areas: Harrijärvi, Tjårrojåkka–Makkak, Svappavaara and Nunasvaara, where there are known Ti mineralisations (with Fe-apatite-Ti-V mineralisations in intrusive alkaline rocks and mafic rocks)
- V content in till is high in Harrijärvi, Vittangivaara and Tjårrojåkka–Makkak key areas, and elevated concentrations occur in Svappavaara, Nunasvaara and the northern part of the Nautanen key area. A large and still unexplained Ti and V (and other metals; see text below) anomaly occurs in the NE (Lainio–Mounionalusta).

While elements characteristic of greenstone belts and related mineralisations in Norrbotten follow rather large-scale, regional trends, precious metals such as Au and Ag have a spatial outlier appearance and more local anomalies.

The geochemical distribution of gold may be summarised thus:

- Au concentrations in till are not particularly high in Norrbotten. However, several point anomalies with elevated contents can be related to known mineralisations, e.g. 5 km NE of Cu-Au Raggisvaara (north of Kiruna), 1.5 km east of Kovogruvan (Cu-Fe-Au), two anomalies east of Pahtohavare, and S of Kiruna in the vicinity of the Kallosalmi Au deposit, SW of Pajala in conjunction with known Au-sulphide mineralisations, within Harrijärvet and Vittangivaara key areas, approximately 20 km north of Övre Soppero (where a few small mineralisations containing Au are known), SW of Hakkas (accompanied by As and W anomalies) in the vicinity of the Puolalaki mineralisation with As, W, Cu and Au, approximately 12 km SE of Harrads (in the vicinity of Au anomalies in quartz veins and volcanic rocks, together with Cu, Sb, Bi, As and Ag).
- The highest Au concentrations in till occur on the map sheet 29 – Vittangi, with anomalies in the key areas studied, especially Svappavaara and Nunasavaara.
- Au anomalies commonly follow As, Cu, S, Sb and Bi anomalies west and southwest of Kiruna, southeast and northeast of Gällivare, and in the Svappavaara region.
- Examples of unexplained Au anomalies include two major Au anomalies by the border with Finland on map sheets 30L–30M (near the Saarikoskenvaara key area), and approximately 12 km SE of Junosuando, in Hakkas, 10 km SE of Nattavaara, NE of Gunnarsbyn.
- Many Au anomalies are interpreted as local, i.e. short transport by glacial drift along the main ice direction.

Ag enrichment in till correlates both with Au geochemical distribution and with the presence of sulphide mineralisations with Cu, Zn and Pb:

- Single Ag anomalies occurring within the Archaean unit in the northernmost part may be related to minor Au and Mo mineralisations.
- Examples where Ag anomalies correlate with sulphide mineralisations include Lieteksavo, Pårkajaure, Viscaria and Aitik.
- Elevated Ag concentrations in till occur in the following key areas: the Tjårrojåkka–Makkak key area (related to sulphide mineralisations with Cu, Mo, Au in andesite and quartz veins), the Kiruna and Saarijärvi key areas in conjunction with sulphide mineralisations with Cu and Au located SW and N of Kiruna.

- Silver enrichment in till occurs in the east of the project area, by the Finnish border between Kangos and Övertorneå.
- Generally higher Ag content in till occurs along the Caledonian front and along watercourses coming from the Caledonides (e.g. between Laisvall and Arjeplog, in the SW and S of the study area, the main source being felsic metavolcanic rocks and metasedimentary rocks with minor sulphide and noble metal mineralisations).
- High Ag content in till is observed south of Porjus, west of Arjeplog, west of Boden in the south of the study area, and towards the Caledonian front. Numerous precious metal and Cu-Zn-Pb (+W+As+U+Mo) sulphide mineralisations are spatially correlated with elevated or high Ag concentrations, e.g. approximately 7 km SE of Benbrytefors Cu-Au-Ag (between Vidsel and Moskosel, also accompanied by high Bi content in till).
- As and Bi anomalies often follow Ag anomalies in SW part of the study area.

As, Bi, Cd, Pb, Sb, Sn, Mo, U, W and Zn content in till is fairly low in Norrbotten, and localised anomalies with high concentrations of metals are usually associated with minor mineralisations.

High Bi concentrations occur along the Caledonian front, e.g. between Laisvall and Arjeplog, in the northern part of Stora Sjöfallet, in conjunction with the U mineralisations and Cu-Pb-Zn+Mo+Sn mineralisations in granite and metasedimentary and felsic metavolcanic rocks. Relatively high concentrations are present in the south of the study area, e.g. S of Alvsbyn, where there are known Au-Cu-As mineralisations in schist and granite, SE of Puolalaki sulphide (Cu-Zn, Ag-Pb-Zn with As-W-Au) deposit (approximately 40 km SE of Gällivare), approximately 12 km E of Niemisel (in the vicinity of the Hällkölen Sb-Bi-As-Au prospect). In Harrijärvet and Vitangivaara key area (N of Kiruna), elevated Bi concentrations in till occur in association with Cu mineralisations in quartz veins; vein and skarn Cu-Zn-Pb mineralisations occur in the Svappavaara key area (e.g. Kiilavaara), in the Nautanen key area, and Bi anomalies east of Aitik are associated with sulphide mineralisations (Cu-Au).

Molybdenum mineralisations have been reported from several localities in the area studied and molybdenum till anomalies, together with Ni, Co, Cu, Ag and Au, are often related to these mineralisations. A few Mo outliers occur near the Caledonian front (e.g. Stora Sjöfallet area, Kvikkjokk region), and NW of Boden, related to Cu (Ag+Au+Mo) deposits.

Pb outliers occur in Archaean rocks (but lack correlation to known Zn-Pb deposits) as well as in the Palaeoproterozoic rocks of the Masugnsbyn key area (approximately 5 km east of several Cu-sulphide mineralisations). Elevated Pb values occur along the Caledonian front (in the Caledonides Zn-Pb mineralisations are more common than in the Fennoscandian Shield), within the Stora Sjöfallet formation and in the SW corner of the study area, where numerous Pb-Zn+Ag mineralisations are known, mainly within the Caledonian autochthon (e.g. Laisvall, Maiva). The more prominent Pb (and Sb) anomaly in till stretches from the Caledonian front by the Laisvall Zn-Pb deposits towards the SE in the Arvidsjaur region.

The distribution pattern for Zn is similar to that of Pb, with higher concentrations in till overlying Archaean rocks in the north, enrichment in metavolcanic rocks and skarn-hosting sulphide mineralisations (Pb, Cu, Au, Ag, Mo) along the Caledonian front (east of Laisvall) and in the SW of the study area (e.g. southern part of Stora Sjöfallet). A regional-scale Zn anomaly (accompanied by Sb) stretches from Stora Sjöfallet southeast via Jokkmokk to Boden, with an outlier (343 ppm) near the Ravejaure Cu-Mo-Sn-Ti mineralisation, approximately 30 km east of Kvikkjokk. The maximum Zn concentration (1 384 ppm) has been found in the NW of the study area, approximately 30 km NW of Kiruna by lake Rensjön, near a Pb-Zn-Cu-Ag mineralisation hosted by metavolcanic and volcanoclastic rocks. Numerous Zn anomalies are found in northern part of the studied region. These correlate well with several known Zn mineralisations such as Viscaria, west of Kiruna. A single Zn outlier near Hournaisenvuoma is located near a Zn-Pb-Ag deposit enriched in Mn and Ba.

Low Sn concentrations in till dominate in the northern part of the study area. Elevated Sn concentrations occur in the SW (Jäkkvik–Jokkmokk–Arjeplog–Arvidsjaur), where they correlate with known Mo and U mineralisations in granite, felsic metavolcanic rocks and quartz veins.

Although U content in till is low, a number of exceptions exist. Elevated U concentrations can be observed between Kvikkjokk and Jokkmokk in the SW of the area, with an outlier located 5 km south of the known U mineralisation, approximately 30 km S of Kvikkjokk in the Lower Allochthon of the Swedish Caledonides. Minor uranium and thorium (together with REEs) anomalies occur south of Svappavaara (Leveäniemi). Two other uranium mineralisations are known in this area: Äijärova (together with copper and molybdenum) and Meutesvare (together with copper).

Certain local geochemical anomalies in till can be directly linked to known ore fields and mineralisations, for example:

1. In the **Kiruna area,** Cu, Co, Fe, P, REEs, Au, and V anomalies correlate with iron formations (Fe-apatite), stratiform sulphide deposits (Cu) and epigenetic sulphide deposits (Cu), e.g. Kiirunavaara, Lappmalmen, Nukutus, Henry, Rektorn, Haukivaara, Luossavaara, Pahtohavare. Na, Cl, K, Fe, Al, Ca anomalies can be related to alterations such as scapolitisation, albitisation, formation of actinolite, K-feldspar, chlorite, sericite, and carbonate. Locally, till overlying metal deposits influenced by metasomatic processes has elevated concentrations of alkaline elements (Ba and Rb) and point anomalies of metals such as As, Au, Bi, Sb, W, Tl and Sn, e.g. in till overlying the Lower Hauki series with apatite-iron deposits located north of Kiruna.
2. In the Gällivare area (Aitik and Nautanen Cu ores, Malmberget Fe-apatite ore), the best-defined anomalies in till occur north of the Nautanen ore field (Cu-Fe+Au + Ag mineralisations). Elevated concentrations of Ba, Na, Mn, Ca, Rb and K reflect the main type of alterations (scapolite, microcline, biotite, sericite, garnet, amphibole, epidote and tourmaline). Notably, neither the Aitik Cu ore nor the Malmberget apatite-Fe oxide ore is visible in the geochemical signature of local till. The most significant anomaly related to Aitik, for Bi, occurs approximately 5 km east. Elevated palladium and tellurium concentrations (obtained in an earlier survey, presented in the NSG database, occur in till in the Gällivare area and are related to the Dundret gabbro intrusion, southwest of Gällivare.
3. The **Svappavaara** and **Vittangi** areas are known for one of the largest former copper mines in Norrbotten (apatite-Fe ore and Cu deposits; e.g. Gruvberget). Till anomalies of Al, Au, Bi, Co, Cr, Cu, Fe, K, Na, Ni, P, V, and REEs can be observed here, and they are directly related to the type of local deposits whereas Al, Ca, K, and Na anomalies are explained by the types of alteration (e.g. scapolite, albite, biotite, sericite, K-feldspar).
4. In the **Pajala area,** various iron ore deposits (BIF deposits, Fe sulphides, skarn iron ore) occur, particularly north of Pajala (e.g. Tapuli skarn Fe deposits, Stora Sahavaara Fe deposit). The following geochemical anomalies have been observed in this region: Ag, Au, Co and Cu. The local alteration signature is characterised by low Na, Ba, Ca and Sr content in till.
5. The Masugnsbyn area (including the Masugnsbyn key area) is well known for its Fe ore skarn deposits such as Magnetgruvan (BIF and skarn Fe ore with magnetite), but no prominent geochemical anomalies in till have been observed in the immediate vicinity of these ore fields. The only distinct geochemical anomaly for several metals (Ag, Co, Cr, Ni, Fe, Pb, Zn) occurs in the central–western part of the Masugnsbyn key area, in conjuction to Zn, Pb and Cu mineralisation at Kurkkionvaara.

Several other unexplained anomalies can be found within the dataset, e.g. in the NE of the study area (map sheet 30M+SE of 30L+ NW 29M) many metals, such as Ni, Co, Cu, Au, Cr, Fe, P, Pb, Ti, V, and Zn, show high concentrations in till, but no mineralisations are documented in the area (Fig. 9).

The element association may imply the existence of another iron oxide-apatite deposit (with V and Ti), with associated sulphides, potentially located in an unexposed volcano-sedimentary unit.

It is notable that concentrations of elements typically associated with felsic volcanic rocks (e.g. As, Bi, Cd, K, Mo, Pb, Rb, Sb, Se, Sn, Tl, W and Zr) are low in Norrbotten's till. This contrasts with till located to the south, in the Skellefte Mining District of Västerbotten, where felsic volcanic rocks are the main host rock for sulphide deposits and a source of major metal anomalies in the till.

The southeast of the study area is almost devoid of metal anomalies. This is interpreted to result from lacustrine/marine inundation and glacial meltwater activity during deglaciation. Several mineral deposits in this area (e.g. Ni-Cu-Co-bearing layered intrusion at Notträsk) are not outlined by geochemical anomalies. This is more likely an effect of post-depositional leaching processes under relatively low pH conditions (Ladenberger et al. 2016).

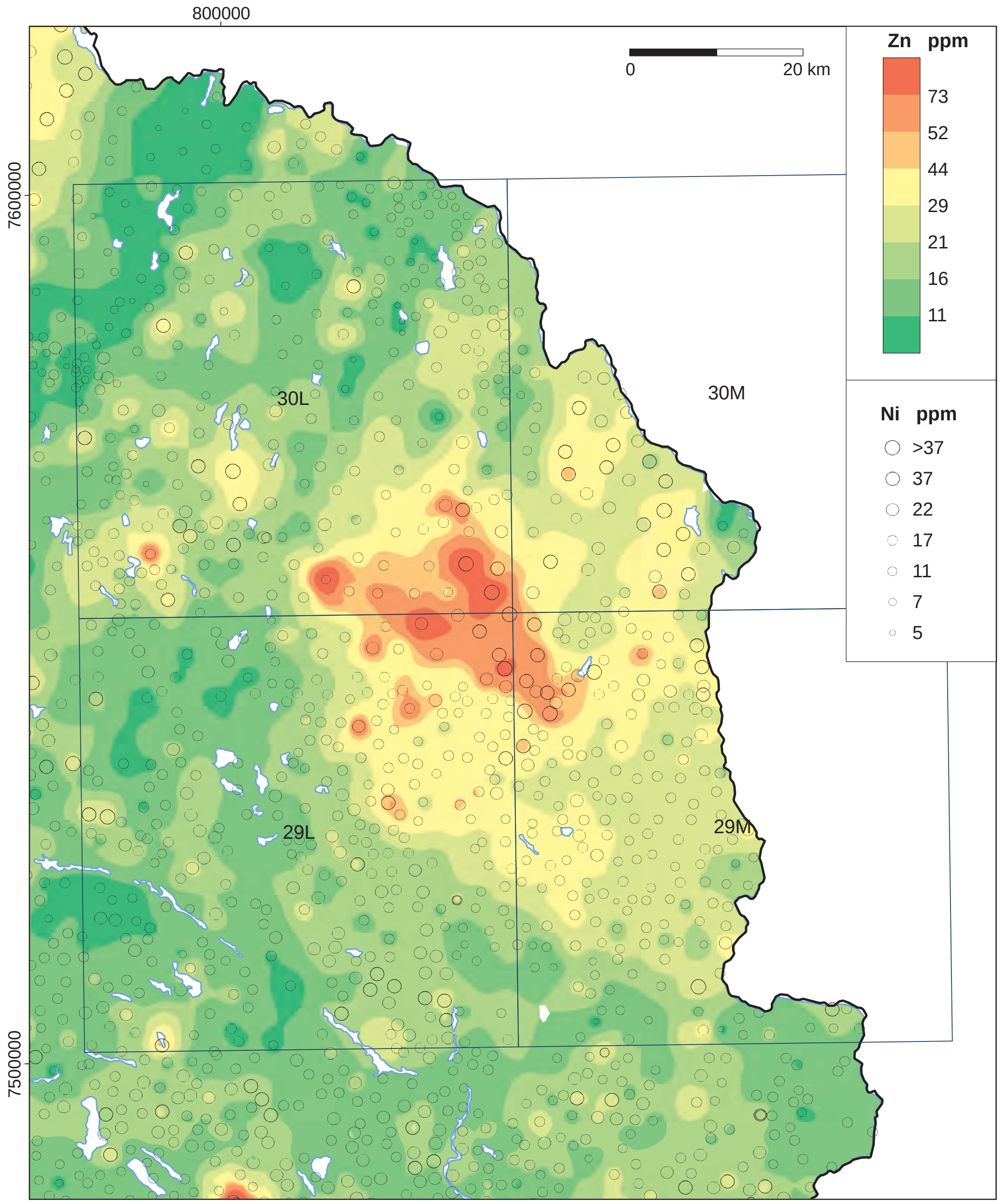

Figure 9. Zn (raster map as a background) and Ni (as dots) anomalies (HNO_3 leach by ICP MS) in the NE of the study area (map sheets 30L, 30M, 29L and 29M). Method: HNO_3 leach by ICP MS.

Till geochemistry in the key areas

Key areas described in this volume have been chosen under the Barents Project for detailed geological investigations, mainly in relation to their mineral potential and previous history of mineral exploration (Grigull & Antal Lundin 2013, Luth & Antal Lundin 2013, Luth & Berggren 2013, Lynch & Berggren 2013, Lynch & Jönberger 2013a,b, Lynch et al. 2014). Geochemical sampling followed geological mapping and geophysical surveys in ten key areas in order to better understand local geological history in relation to ore-forming processes and Quaternary development.

Sampling of till (194 samples in total) was carried out in 2012 and 2013 in the following regions: Tjårrojåkka–Makkak, Saarijärvi, Kiruna–Jukkasjärvi, Harrijärvet, Vittangivaara, Akkiskera–Kuormakka, Nunasvaara, Nautanen, Allavaara and in Svappavaara (Fig. 1). Additional samples in the key areas originate from earlier geochemical surveys (2000–2007) reported in Ladenberger et al. (2012).

Among collected till, cover moraine predominates, but approximately 20% of samples were collected from hummocky moraine. Till parent material originates from various lithologies, which are reflected in the geochemical composition of till and median values for several elements are generally higher in key areas than for the Barents dataset as a whole (e.g. Au, Ca, Co, Cr, Cu, Mg, Na, Ni, P, Rh, Te, Ti and V) (Figs. 10 and 11).

Tjårrojåkka–Makkak

The geology of this key area is described in Lynch & Berggren (2013) and in Lynch et al. (2014). The Tjårrojåkka–Makkak area is located approximately 50 km SW of Kiruna, and was chosen for detailed study mainly due to the apatite-iron (Täunatjåkka, Kuosatjvare), copper (-gold), and molybdenum (e.g. Tjårrojåkka, Hannåive) deposits, which are well documented by numerous drill cores. Local geology is predominantly represented by metamorphosed volcanic rocks (basalt, andesite, rhyolite), with minor occurrences of metasedimentary rocks (phyllite) and intrusive rocks such as gabbro, diorite, monzonite, syenite and granitoid. Most of the mineralisations are hosted in the metavolcanic units. Fe-oxide mineralisation usually occurs as banded or disseminations with magnetite, hematite and apatite as ore minerals, whereas Cu mineralisations occur as quartz veins and disseminations, with chalcopyrite and bornite as major Cu-bearing phases. Hydrothermal alterations have mainly affected metavolcanic units, with scapolitisation and epidotisation on a regional scale and local formation of sericite, tourmaline, epidote, albite, K-feldspar, hematite and carbonate.

38 till samples were collected in this area and have medium-high to high concentrations of Ag, B, Ba, Be, Li, Nb, REE, Sb, U and Zn. One of the highest silver, cobalt and Eu concentrations in till was found in the NW of the area. Elevated concentrations of Cu, Ag, Mo, Pb, Sb and Zn in the NW and SE are spatially related to known mineralisations. No Au anomalies in till have been noted in the vicinity of Cu-Au mineralisations, however. High concentrations of Ba, Be, Rb and Sr can be explained by the presence of hydrothermal alterations. The general trend for the bedrock to become increasingly felsic towards the east is reflected well in the till geochemistry, e.g. by decreasing concentrations of elements typical of mafic rocks, such as Co, Cr, Al, Fe, Mg, Mn, Ni, Sc, Ti, and V, from west to east. Elevated content of Be, Nb, Ta, Th, Y and REEs correlates well with outcrops of felsic metavolcanic rocks (andesite, rhyolite) and numerous quartz veins locally containing tourmaline.

Saarijärvi

The geology of this key area is described in Lynch & Jönberger (2013a) and Lynch et al. (2014). The major rock units belong to the volcanic rocks of the Kiruna greenstone group, of predominantly basalt-andesite composition, and the overlying porphyry group. Minor metasedimentary horizons (e.g. conglomerate, schist, phyllite, marble) occur within the various volcanic sequences (e.g. Kurravaara conglomerate). Intrusive rocks are represented by variably metamorphosed syenitoid and gabbroid types, minor doleritic, granitic and syenitic dykes. Outcropping rocks show varying degrees of hydrothermal alteration, with scapolitisation-epidotisation in metavolcanic rocks and potassic metasomatosis in alkaline intrusive rocks and metasediments. There are several mineralisations in the area, hosted exclusively by metavolcanics, with significant Fe-oxide (magnetite ± apatite), Cu-Fe sulphides (chalcopyrite, pyrrhotite, bornite) and minor gold (native Au, auriferous Cu–Fe sulphides, auriferous tellurides) mineralisations, e.g. Pahtohavare, Rakkurijärvi, Saarijärvi, Pitkäjärvi and Puoltsa.

20 new till samples have been collected in this area and used, along with six samples from a previous campaign. Elevated concentrations of Be, Ca, Cr, Ge, Na, P, Sc, Y and REE have been noted. REE content in till is among the highest obtained for all key areas studied. Single Cu anomalies correlate well with known Cu mineralisations.

Kiruna–Jukkasjärvi

The geology of this key area is described in Grigull & Antal Lundin (2013). The region belongs to the Kiruna mining district, with numerous mineralisations, including apatite-iron ores (e.g. Nukutus, Lappmalmen, Rektorn, Haukivaara, Luossavaara) and Cu sulphide ores (Viscaria type), and small precious metal deposits such as Au (e.g. Kallosalmi). The majority of mineral deposits occur in the west of the key area. The lithology predominantly comprises metavolcanic rocks with mafic to felsic compositions and associated metasediments, such as metasandstone, quartzite, conglomerate, phyllite, schist (locally with graphite) and dolomite. Plutonic rocks include gabbroid, tonalite, monzonite, granodiorite and granitoid. The prevailing alteration type is scapolitisation, epidotisation and albitisation. A detailed description of hydrothermal alterations in relation to mineralisation and till geochemistry can be found in Ladenberger et al. (2012).

Nine new till samples were collected in 2013. These complemented 42 existing samples from previous campaigns (Ladenberger et al. 2012). Elevated concentrations of several elements have been noted, particularly in the NW of the area, for example Co, Cu, Na, P and V. A signature typical of mafic lithologies (Co, Cr, Fe, Mg, Mn, Ni, Sc, Ti, V, Zn) prevails in the western part of the area, where the majority of mineralisations are located. Generally, high Na content in till can be interpreted as an indication of regional scapolitisation and albitisation, which affect metavolcanic rocks.

Harrijärvet

The geology of this key area is described in detail in Luth & Antal Lundin (2013) and Luth et al. (2014). Most of the area is underlain by mafic to intermediate rocks forming metavolcanic units, mainly of the Kovo group and Kiruna greenstone group. In the west, Archaean gneisses (tonalite-granodiorite) are overlain by metaconglomerate (composed of granite and quartzite pebbles) and metasandstone. In the east, a belt of dolomite stretches N–S as a horizon within the metavolcanic sequence. Ultramafic metavolcanite (komatiite) crops out in the NE corner of the key area. The main prospect is a Cu mineralisation (Harri), with chalcopyrite, pyrite and cubanite hosted by the metavolcanic complex in the central part of the key area.

Five till samples have been collected in the Harrijärvet key area. Elevated concentrations of Al, Au, Ba, Ca, Co, Cr, Fe, Ge, K, Mg, Mn, Ni, P, Rb, Sc and Ti, V have been observed, with concentrations generally decreasing eastwards. A single anomalous sample with high Te (144 ppb) and Bi concentrations was collected in the northeast of the area, which predominantly comprises mafic metavolcanic rock units (basalt-andesite and komatiite). Relatively high pH (>6) was encountered in this area.

Vittangivaara

The geology of this key area is presented in detail in Luth & Antal Lundin (2013). Most outcropping lithologies are volcanosedimentary sequences of basaltic and andesitic composition, intercalated with metaarenite and dolomite. A sulphide deposit, with pyrite, pyrhhotite and chalcopyrite associated with skarn, occurs in the NE of the area. Locally, iron oxide mineralisations (ilmenite, hematite, goethite) occur within an altered tuff. In the NE, a small vein mineralisation with Au in association with Fe oxide occurs in abrecciated granite.

20 till samples have been collected in the Vittangivaara key area, and they show elevated or high concentrations of several elements, including Ag, Au, Ba, Bi, Co, Cr, Cu, Fe, K, Li, Mg, Mn, Ni, Pb, Rb, REE, Te, Ti, Tl, V and Zn. The prevailing geochemical signature is typical of mafic lithologies (Co, Cr, Ni, Fe, Mg). There is no great difference between the geochemical composition of till overlying metavolcanic, mainly mafic rocks and till overlying metasedimentary rocks. Elevated content of Rb, K and Ba may indicate the presence of secondary alterations. Local occurrences of dolomite and marble (near Kåvvojaure) contribute to local basic pH values (>7).

Akkiskera–Kuormakka

The geology of this key area has previously been summarised in Luth & Berggren (2013). The Akkiskera–Kuormakka region is the northernmost area studied under the Barents Project. Apart from mineralised blocks and boulders found in the northwest of the area, there are only three known outcrop-scale deposits, which are in fact located just outside the key area itself (Cu and Au Luspavaara deposit in a quartz vein cutting basalt, the Juoluvaaranjärvi Fe deposit in skarn, and Kuormakka, a sulphide prospect within silicified greenstones, with Cu, Au, Ag, S and Zn). A significant feature in the west of this area is the NE–SW trending Karesuando–Arjeplog deformation zone (KADZ). The geology is dominated by the Kiruna greenstone group (KGG) with mafic volcanic rocks (basalt) and a thin series of clastic metasediments consisting of mica- and feldspar-rich quartzite and conglomerate of the Tjärro Quartzite group resting on the Archaean basement in the west. In addition, zones and veins of ankerite-albite rich rocks are often bounded by faults. Carbonate-rich horizons with skarn, graphite-bearing schists and tuffitic layers occur in the easternmost part of the key area. The Archaean basement and the supracrustal rocks are intruded by granite and gabbro belonging predominantly to the Haparanda suite. Mafic and ultramafic rocks have been the subject of mineral exploration for Ni and Cr.

20 new till samples were collected in 2012 and 2013. Apart from generally elevated Au, Cr, Sr, P, Na and Ca concentrations, and single anomalies (e.g. Cu with 195 ppm in the NW), no major element anomalies have been observed in this region.

Nunasvaara

Details of the geology of Nunasvaara are provided in Lynch & Jönberger (2013b) and Lynch et al. (2014). The geology predominantly comprises volcanosedimentary units of the Vittangi greenstone group, with mainly mafic volcanic and plutonic rocks, intercalated with metasedimentary units represented by quartzite, graphite-bearing schist, marble and related skarn. The main alteration types are scapotilisation, carbonitisation and albitisation of mafic rocks, with local presence of tourmaline and epidote. Several mineralisation types occur in the area, including schist-hosted graphite deposits (Nunasvaara), banded iron oxide mineralisations in skarn and copper mineralisation (e.g. Tievakoski). South of the key area itself, mineralisations with uranium, molybdenum, cobalt and gold are known.

12 new till samples have been collected in this key area, complementing eight till samples from a previous campaign. Elevated and locally high element concentrations are seen for Au, Co, Cr, Cu, Ni, P, Rh, V, Ti and Te. These present a typical geochemical signature related to the presence of mafic rocks and graphite-rich metasediments (especially in the west of the key area). In general, higher ab-

solute element concentrations occur in the west and SW than in the east. High Na content in till is related to regional scapolitisation of metavolcanic rocks and correlates with high Cl content (XRF method) in till obtained during previous campaigns (2002–2003). High Ca content correlates with high pH values and is related to local occurrences of carbonates and skarn (calc-silicate rocks).

Nautanen

The geology of the Nautanen key area is described in detail in Lynch & Jönberger (2014a) and in Lynch et al. (2015). The geology predominantly consists of Palaeoproterozoic metavolcanic (basalt, andesite, tuff) and metasedimentary (metaarenite, marble, skarn, phyllite, schist) rocks metamorphosed during the Svecokarelian orogeny (c. 1.9–1.8 Ga). Subordinate Palaeoproterozoic intrusive rocks of gabbroic, dioritic and granitic composition occur at the periphery. The area was influenced by intense hydrothermal alteration, including scapolitisation, sericitisation, potassic alteration, and the formation of tourmaline, apatite, magnetite, amphibole, garnet and epidote. The rocks at Nautanen are situated within the brittle–ductile Nautanen deformation zone. Numerous sulphide deposits with Cu, Au, Fe, Ag (Nautanen, Liikavare, Fridhem, Ferrum, Snålkok) and Pb (Muorjevaara) occur along the deformation zone, particularly in the north. Copper-gold prospects from the Nautanen area are thought to have a genetic affinity to the broad iron oxide-copper-gold (IOCG) family of hydrothermal mineral deposits. Chalcopyrite and bornite are the commonest ore minerals, associated with minor magnetite, sphalerite, galena, molybdenite and scheelite. Numerous mineralised boulders are seen in the area, which may have influenced the general composition of till.

Ten new till samples were collected in the Nautanen key area (together with 14 samples from an earlier survey; Ladenberger et al. 2012). These show elevated concentrations of Ag, As, B, Ba, Li, P, REEs, Sb, Ta, Th, U and W. Single Au (up to 9 ppb Au) and Bi (+Co, Cr, Cu, Fe, Li, Rb, Sc, Te, Ti, Tl and Zn) anomalies have been observed in the NE part, 1.5 km west of an Au-Pb mineralisation drilled at Muorjevaara, and north of several Cu-Au mineralisations, all hosted by a quartz vein. The till geochemical signature of the key area accords well with the mineralisation types and related alterations along the Nautanen deformation zone.

Allavaara

The geology of the Allavaara area is described in Lynch & Jönberger (2014b), and is predominantly made up of Palaeoproterozoic metavolcanic (basaltic andesite, andesite, dacite, rhyolite, and rare komatiite) and metasedimentary (skarn and carbonate) rocks, with minor monzonitic and granitic intrusives. The key area is cut by a broad, mainly ductile deformation zone trending N-NW–S-SE. The major types of hydrothermal alterations are sericitisation, saussuritisation and chloritisation.

Known mineralisations in the area include Cu, Au, Ag and Pt vein-type with azurite, bornite, chalcopyrite and malachite at Fjällåsen, hosted by metavolcanic rocks, and minor veins with Cu (e.g. Risbäck).

36 till samples were collected during surveys in 2012 and 2013. Apart from elevated concentrations of Ca, Cu, Na, P, REEs, Se, Sr, Ti and V, no significant element anomalies are noted in this area. A single till sample located only 1.5 km west of the Risbäck Cu mineralised vein (in the central part of the key area) has slightly anomalous W (1.6 ppm), Cu, Ce, Sb concentrations.

Svappavaara

The detailed geology of the Svappavaara key area is described in Grigull & Jönberger (2013). Palaeoproterozoic rocks in the area belong to four major units: the upper part of the Vittangi greenstone group (basaltic tuffite, schist, graphite schist and skarn), the Kilavaara quartzite group (biotite schist, quartzite and arkose), the porphyry group (basalt, andesite, rhyolite, trachyte), and younger intrusive rocks (e.g. gabbro, quartz diorite, monzonite, granite). The Svappavaara key area extends between the major SW–NE trending Karesuando–Arjeplog deformation zone (NW) and the intrusive rocks of the NW–SE oriented Luongastunturi massif. The most common mineral deposits in the area are iron ore and Cu-hosting (with Au and Mo) sulphide deposits. The most important iron ore deposits are the Tansari, Gruvberget, and Leveäniemi, the last-mentioned being recognised as the third-largest apatite iron ore deposit in Norrbotten. The commonest alteration types are scapolitisation, albitisation and skarn formation.

24 till samples were collected in 2013, together with 14 till samples from previous surveys. High or moderately elevated concentrations of several elements (Au, Ca, Co, Cu, Mg, Ni, P, Sc, Ti, V and Rh) are noted. The highest Au (44 ppb), Mn, Pb (30 ppm) and Rh (173 ppb) single-point concentrations from all key areas studied are located in this area. High Cd and Mo concentrations occur locally in till. High concentrations of Al, Ba, Ca, and Na correlate with high Cl concentrations (XRF dataset from previous campaigns) and can be interpreted as an indication of the various types of alterations, e.g. scapolitisation and albitisation. High Ca content in till overlaps with elevated pH values and indicates the presence of carbonates and skarn-type rocks. The general geochemical signature accords well with the predominantly mafic to intermediate metavolcanic rocks underlying the till.

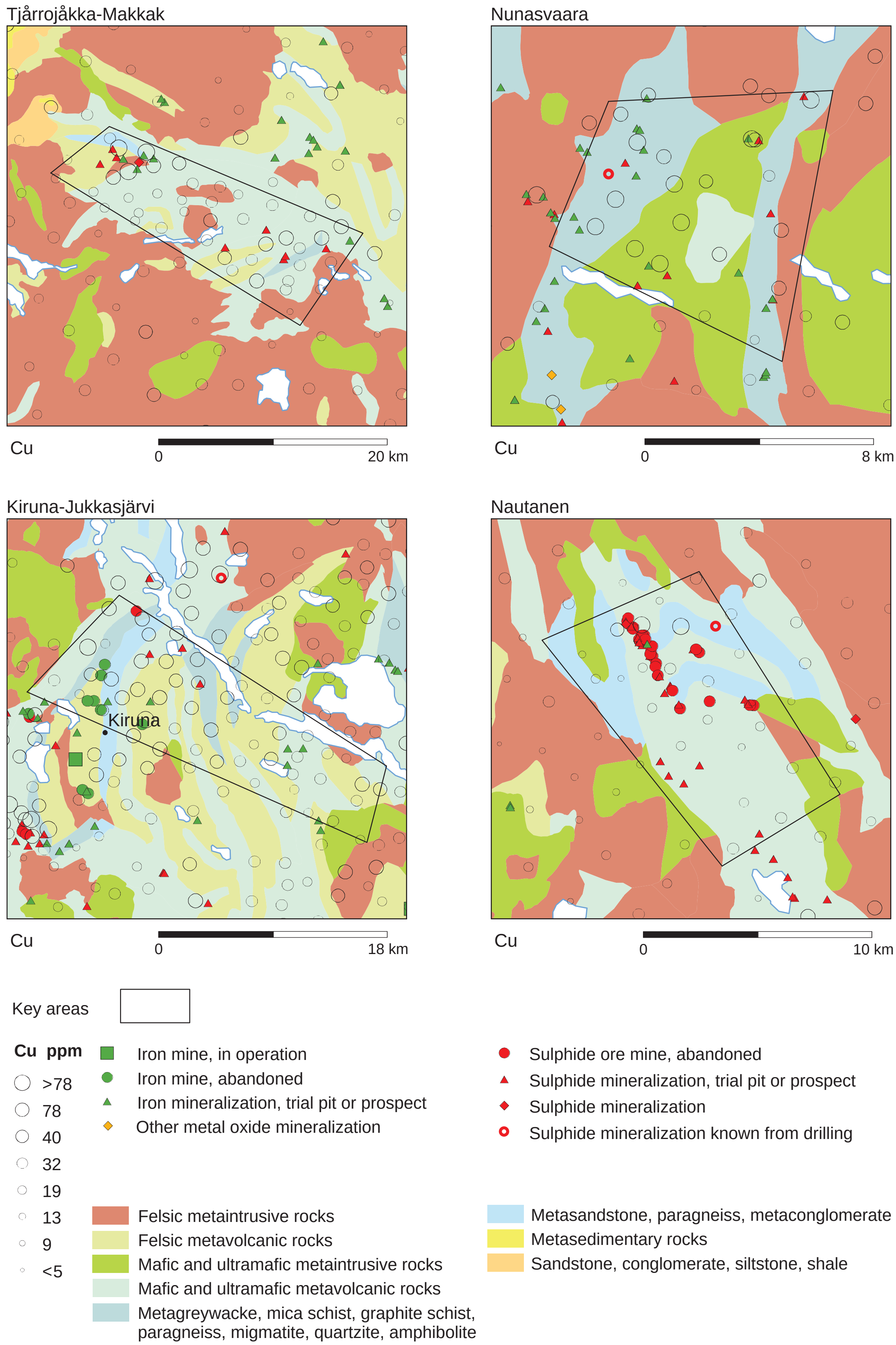

Figure 10. Cu (ppm, HNO_3 leach by ICP MS) in till in selected key areas. Bedrock map 1:1 000 000 as background layer and mineral resources according to the SGU digital database.

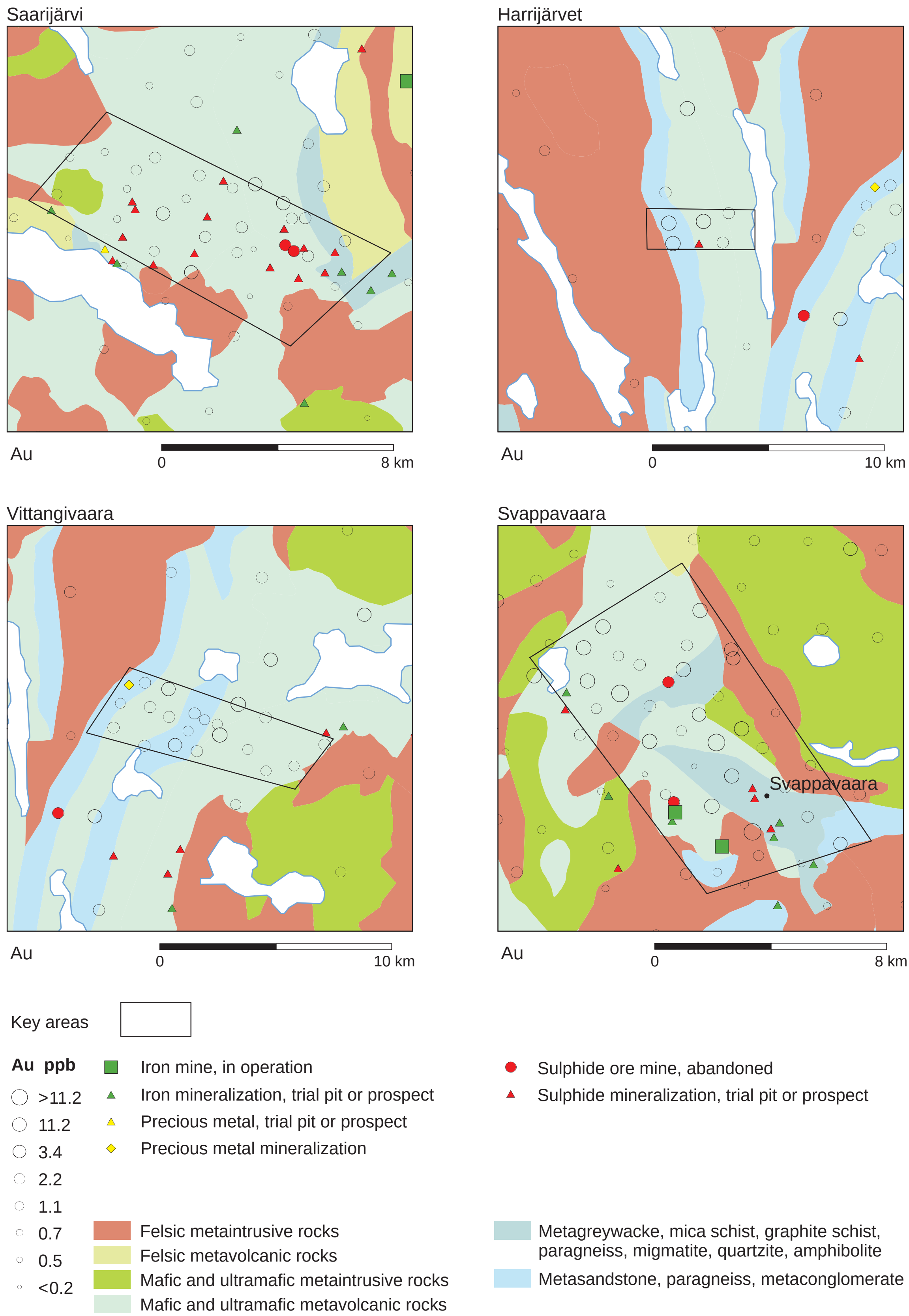

Figure 11. Au (ppb, aqua regia leach by ICP MS) in till in selected key areas. Bedrock map 1: 1 000 000 as background layer and mineral resources according to the SGU digital database.

CONCLUSIONS

The compilation of new till geochemical data obtained under the Barents Project and older datasets resulted in a large database that can be used for multipurpose interpretations of element spatial distribution in northernmost Sweden. The area studied is a well-preserved glacial landscape featuring a relatively complete glacial stratigraphy due to limited erosion during frozen-base ice conditions. The glacial geomorphology contains components from multiple stadials.

The regional till geochemistry signature is mainly governed by underlying bedrock lithology, which is defined by rock origin, its mineralogy and chemical composition. The main compositional contrast related to geology originates from the distribution of silica-rich (e.g. granitoid, pegmatite, rhyolite) and silica-poor magmatic rocks (e.g. gabbro, basalt, peridotite). Silica-rich intrusive rocks are usually a source of elevated concentrations of Al, Ba, Be, K, Na, Rb, REEs, U, Th and Zr in till. High concentrations of Mg, Ca, Co, Cr, Cu, Fe, Mg, Mn, Ni, Ti and V in till are characteristic of silica-poor parent materials (typically mafic rocks). Till resting on bedrock primarily consisting of metasedimentary rocks usually has a similar chemical signature to till overlying granitic rocks. Norrbotten bedrock has a long polymetamorphic history and was intensively deformed during orogenies and influenced by metasomatic and hydrothermal processes contributing to the formation of large ore deposits, some of high economic value. The most common alterations are scapolitisation, albitisation, carbonatisation, and skarn formation. These alterations are reflected in till geochemistry as enrichments in Ba, Ca, Cl, K, Na, Sr, La, Rb and P. Anomalies related to secondary alterations occur locally (Ba, Sr, K, La, As) or regionally (P, Cl and Na), and often overlap with known mineralisation locations.

Norrbotten County is one of the richest ore districts in Europe, and till geochemistry reflects the location of known ore deposits and minor mineralisations, and outlines areas with high mineral exploration potential. The geology of the northern part of the Barents Project is characterised by Co, Cu, Fe, Ni, Ti and V anomalies in till, typical of apatite-Fe ore deposits located in volcanosedimentary complexes of greenstone belts and associated sulphide mineralisations, mainly with Cu and Au. Au anomalies are more localised but often overlap with known Au occurrences. Silver shows enrichment in till overlying sulphide deposits (Cu, Zn, Pb, W, As, Bi, U, Mo) and in areas mainly featuring volcanic and metasedimentary rocks. As, Bi, Cd, Pb, Sb, Sn, Mo, U, W and Zn content in till is rather low in Norrbotten, and single anomalies with high concentrations of metals can usually be related to minor mineralisations.

The element distribution pattern in till geochemistry is modified by long-lasting surficial processes as well as glacial history. The shape of the anomalies has been influenced by ice movement direction and transport, formation of glacial features (e.g. drumlins, ribbed moraines) and meltwater reworking during ice retreat. These can best be observed for major elements that are evenly distributed over the area studied, such as Ca and Na. The southeastern part of the Barents Project represents an area that was below sea level during the last deglaciation, and intense water activity resulted in leaching of many elements e.g. Ag, Al, Ba, Be, Co, Cu, Fe, Mg, Mn, Na, Ni, P, Pb, REEs, Sr, Th, Ti, Y and Zn. Local till conditions, defined mainly by pH, contributed to the depletion or enrichment of elements whose mobility depends on acidity and redox conditions.

Additional till samples were taken in the key areas to investigate the specific geochemical signatures related to mineralisation and their link to the local geology. It has been noted that median concentrations of several elements (e.g. Ca, Co, Cr, Cu, Mg, Na, Ni, P, Rh, Te, Ti and V) are higher than for the whole dataset analysed under the Barents Project. Bedrock lithology, alteration type and mineralisation in the key areas (mainly Fe, Cu, Au) correlate well with elevated metal concentrations in till, e.g. Ag, Ba, Be, REE, Sb, U and Zn in Tjårrojåkka–Makkak; Be, Ca, Cr, Ge, Na, P, Sc, Y and REE in Saarijärvi; Co, Cu, P, Fe, Mg, Mn, Na, Ni, Sc, Ti, V and Zn in Kiruna; Au, Ba, Ca, Co, Cr, Fe, Ge, K, Mg, Mn, Ni, P, Ti and V in Haarijärvet; Ag, Au, Ba, Bi, Co, Cr, Cu, Fe, K, Mg, Mn, Ni, Pb, REE, Ti, V and Zn in Vittangivaara; Au, Cr, Sr, P, Na and Ca in Akkiskera–Kuormakka; Au, Co, Cr, Cu, Ni, P, Rh, V, Ti in Nunasvaara; Ag, As, Au, Ba, Bi, P, REEs, Sb, Ta, Th, U and W in Nautanen; Ca, Cu, Na, P, REEs, Se, Sr, Ti and V in Allavaara; and Au, Ca, Co, Cu, Mg, Ni, P, Sc, Ti, V and Rh in Svappavaara.

The geochemical till survey, together with bedrock mapping and geophysical measurements, proved to be a very useful tool for reconnaissance studies in glaciated areas, providing valuable information about the predominant bedrock lithology, presence of mineralisation (confirmation of existing anomalies and discoveries of new ones), as well as surface processes that may play an important role in modifying the regional and local geochemical signature.

ACKNOWLEDGEMENTS

The authors would like to thank a number of field geologists who helped to collect samples in the Barents Project. Sten-Åke Ohlsson, Alicja Kawalec-Majka, George Morris and Jo Uhlbäck are thanked for their assistance in performing analyses. Kaj Lax and George Morris are kindly acknowledged for reviewing the manuscript and for their valuable comments on the text.

REFERENCES

Andersson, M., Carlsson, M., Ladenberger, A., Morris, G., Sadeghi, M. & Uhlbäck, J., 2014: *Geokemisk Atlas över Sverige (Geochemical Atlas of Sweden).* Sveriges geologiska undersökning ISBN 978-91-7403-258-1, 208 pp.

Bergman S., Kübler, L. & Martinsson, O., 2001: Description of regional geological and geophysical maps of northern Norrbotten County (east of the Caledonian orogen). *Sveriges geologiska undersökning Ba 56*, 1–110.

Bölviken, B., Bergström, J., Björklund, A., Konti, M., Lehmuspelto, P., Lindholm, T., Magnusson, J., Ottesen, R.T., Steenfelt, A. & Volden, T., 1986: Geochemical Atlas of Northern Fennoscandia, scale 1:4 million. Geological Surveys of Finland, Norway and Sweden, 20 p., 155 maps.

Grigull, S. & Antal Lundin, I., 2013: Kartering Barents 2013: background information Kiruna-Jukkasjärvi key area. *Sveriges geologiska undersökning SGU-rapport 2013:08,* 41 pp.

Grigull, S. & Jönberger, J., 2013: Kartering Barents 2013: Background information Svappavaara key area. *Sveriges geologiska undersökning SGU-rapport 2013:9,* 39 pp.

Grigull, S. & Jönberger, J., 2014: Barents project 2013: Geological and geophysical field work in the Kiruna–Jukkasjärvi and Svappavaara key areas, Norrbotten. *Sveriges geologiska undersökning SGU-rapport 2014:10,* 30 pp.

Hall, A.M., Ebert, K. & Hättestrand, C., 2013: Pre-glacial landform inheritance in a glaciated shield landscape. Geografiska Annaler: Series A, Physical Geography, 95, 33–49.

Helmens, K.F., Johansson, P.W., Räsänen, M.E., Alexanderson, H. & Eskola, K.O., 2007: Ice-free intervals continuing into Marine Isotope Stage 3 at Sokli in the central area of the Fennoscandian glaciations. *Bulletin of the Geological Society of Finland 79,* 17–39.

Hättestrand, C., Götz, S., Näslund, J.O., Fabel, D. & Stroeven, A.P., 2004: Drumlin formation time: evidence from northern and central Sweden. Geografiska Annaler 86A, 155–167.

Hättestrand, C. & Stroeven, A.P., 2002: A relict landscape in the centre of the Fennoscandian glaciation: Geomorphological evidence of minimal Quaternary glacial erosion. *Geomorphology 44,* 127–143.

Klassen, R.A., 1999: The application of glacial dispersal models to the interpretation of till geochemistry in Labrador, Canada. *Journal of Geochemical Exploration 67*, 245–269.

Ladenberger, A., Andersson, M., Gonzalez, J., Lax, K., Carlsson, M., Ohlsson, S.Å. & Jelinek, C., 2012: Markegeokemiska kartan. Morängeokemi i norra Norrbotten. *Sveriges geologiska undersökning K410, 112 pp.*

Ladenberger A., Carlsson, M., Andersson, Bergman, S., Uhlbäck, J., Ohlsson, S.Å., Smith, C., Morris, G. & Arvanitidis, N., 2016: Morängeokemi i Södra Norrbotten. *Sveriges geologiska undersökning K561, 67 pp.*

Lagerbäck, R. & Sundh, M., 2008: Early Holocene faulting and paleoseismicity in northern Sweden, *Sveriges geologiska undersökning C 836*, 84 pp.

Lagerbäck, R., 1988a: The Veiki moraines in northern Sweden- widespread evidence of an Early Weichselian deglaciation. *Boreas 17*, 469–486.
Lagerbäck, R., 1988b: Periglacial phenomena in the wooded areas of Northern Sweden – relicts from the Tärendö Interstadial. *Boreas 17*, 487–499.
Lagerbäck, R. and Robertsson, A., 1988: Kettle holes – stratigraphical archives for Weichselian geology and palaeoenvironment in northernmost Sweden. *Boreas 17*, 439–468.
Luth, S. & Antal Lundin, I., 2013: Kartering Barents 2013: Summary report on the geological and geophysical characteristics of the Harrijärvet-Vittangivaara key areas. *Sveriges geologiska undersökning SGU-rapport 2013:13,* 36 pp.
Luth, S. & Berggren, R., 2013: Kartering Barents 2013: summary report on the geological and geophysical characteristics of the Akkiskera–Kuormakka key area. *Sveriges geologiska undersökning SGU-rapport 2013:12,* 35 pp.
Luth, S., Lynch, E.P., Grigull, S., Thörnelöf, M., Berggren, R. & Jönberger, J., 2014: Barents project 2013: Geological and geophysical studies in the Harrijärvet, Vittangivaara and Akkiskera-Kuormalla key areas. *Sveriges geologiska undersökning SGU-rapport 2014:09,* 24 pp.
Lynch, E.P. & Berggren, R., 2013: Kartering Barents 2013: Background information Tjårrojåkka key area (29I Kebnekaise SC & 29J Kiruna SV). *Sveriges geologiska undersökning SGU-rapport 2013:14,* 43 pp.
Lynch, E.P. & Jönberger, J., 2013a: Kartering Barents 2013: Summary report on the geological and geophysical characteristics of the Saarijärvi key area (29J Kiruna NO, NV, SO). *Sveriges geologiska undersökning SGU-rapport 2013:10,* 48 pp.
Lynch, E.P. & Jönberger, J., 2013b: Kartering Barents 2013: Summary report on the geological and geophysical characteristics of the Nunasvaara key area (29K Vittangi NO & SO). *Sveriges geologiska undersökning SGU-rapport 2013:11,* 35 pp.
Lynch, E.P. & Jönberger, J., 2014a: Barents project: Summary report on available geological, geochemical and geophysical information for the Nautanen key area, Norrbotten. *Sveriges geologiska undersökning SGU-rapport 2014:34,* 40 pp.
Lynch, E.P. & Jönberger, J., 2014b: Barents project: Summary report on available geological, geochemical and geophysical information for the Allavaara key area, Norrbotten. *Sveriges geologiska undersökning SGU-rapport 2014:28,* 29 pp.
Lynch, E.P., Jönberger, J., Luth, S., Grigull, S. & Martinsson, O., 2014: Barents project 2013: Geological and geophysical studies in the Nunasvaara, Saarijärvi and Tjårrojåkka areas, northern Norrbotten. *Sveriges geologiska undersökning SGU-rapport 2014:04,* 48 pp.
Lynch, E.P., Jönberger, J., Bauer, T.E., Sarlus, Z. & Martinsson, O., 2015: Meta-volcanosedimentary rocks in the Nautanen area, Norrbotten: preliminary lithological and deformation characteristics. *Sveriges geologiska undersökning SGU-rapport 2015:30,* 51 pp.
Martinson O. & Wanhainen, C., (ed), 2013: Fe oxide and Cu-Au deposits in the northern Norrbotten ore district. Excursion guidebook SWES, 12th Biennal SGA Meeting, SGU, 74 pp.
Morris, G. & Ladenberger, A., 2017: Till Geochemistry by Nitric Acid (HNO_3) partial leaching at the Geological Survey of Sweden. *Sveriges geologiska undersökning SGU-rapport 2017:14,* 12 pp.
Nordkalott Project, 1986a: Map of Quaternary geology, sheet 2: Glacial Geomorphology and Paleohydrology, Northern Fennoscandia, 1:1 mill. Geological Surveys of Finland, Norway, and Sweden.
Nordkalott Project, 1986b: Map of Quaternary geology, sheet 3: Ice Flow Indicators, Northern Fennoscandia, 1:1 mill. Geological Surveys of Finland, Norway, and Sweden.
Nordkalott Project, 1986c: Map of Quaternary geology, sheet 4: Quaternary Stratigraphy, Northern Fennoscandia, 1:1 mill. Geological Surveys of Finland, Norway, and Sweden.
Nordkalott Project, 1986d: Map of Quaternary geology, sheet 5: Ice Flow Directions, Northern Fennoscandia, 1:1 mill. Geological Surveys of Finland, Norway, and Sweden.
Sohlenius, G., Lax, K. & Ladenberger, A., 2009: Kan SGUs data användas för att uppskatta moränens transportlängd? *Sveriges geologiska undersökning SGU-rapport 2009:26*, 25 pp.
SGU database. Accessed 28 September 2015.

Geological Survey of Sweden
Box 670
SE-751 28 Uppsala
Phone: +46 18 17 90 00
Fax: +46 18 17 92 10
www.sgu.se

Uppsala 2018
ISSN 0349-2176
ISBN 978-91-7403-393-9
Tryck: Elanders Sverige AB